MCEER
EARTHQUAKE ENGINEERING TO EXTREME EVENTS

ISSN 1520-295X

# Performance-Based Assessment and Design of Squat Reinforced Concrete Shear Walls

by
Cevdet Kerem Gulec and Andrew S. Whittaker

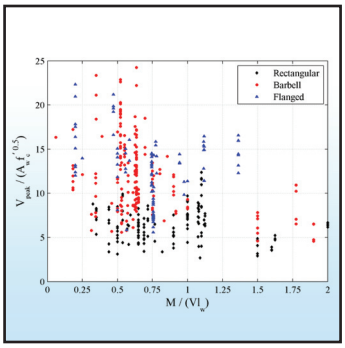


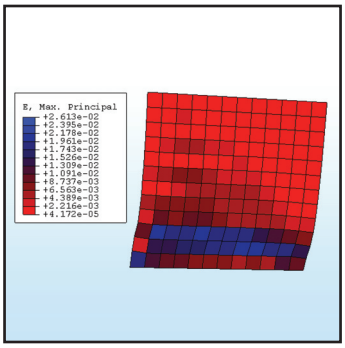


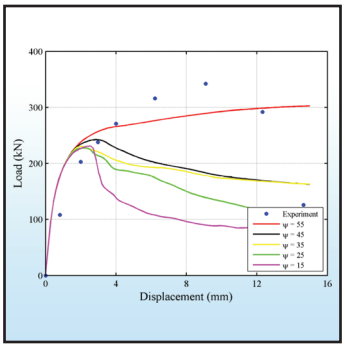


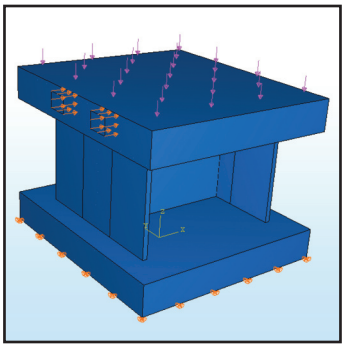

Technical Report MCEER-09-0010

September 15, 2009

This research was conducted at the University at Buffalo, State University of New York and was supported primarily by the Earthquake Engineering Research Centers Program of the National Science Foundation under award number EEC 9701471.

# NOTICE

This report was prepared by the University at Buffalo, State University of New York as a result of research sponsored by MCEER through a grant from the Earthquake Engineering Research Centers Program of the National Science Foundation under NSF award number EEC-9701471 and other sponsors. Neither MCEER, associates of MCEER, its sponsors, the University at Buffalo, State University of New York, nor any person acting on their behalf:

a. makes any warranty, express or implied, with respect to the use of any information, apparatus, method, or process disclosed in this report or that such use may not infringe upon privately owned rights; or

b. assumes any liabilities of whatsoever kind with respect to the use of, or the damage resulting from the use of, any information, apparatus, method, or process disclosed in this report.

Any opinions, findings, and conclusions or recommendations expressed in this publication are those of the author(s) and do not necessarily reflect the views of MCEER, the National Science Foundation, or other sponsors.

MCEER
EARTHQUAKE ENGINEERING TO EXTREME EVENTS

# Performance-Based Assessment and Design of Squat Reinforced Concrete Shear Walls

by

Cevdet Kerem Gulec[1] and Andrew S. Whittaker[2]

Publication Date: September 15, 2009
Submittal Date: July 20, 2009

Technical Report MCEER-09-0010

NSF Master Contract Number EEC 9701471

1 Senior Engineer, Thornton Tomasetti; Former Ph.D. Candidate, Department of Civil, Structural and Environmental Engineering, University at Buffalo, State University of New York
2 Professor, Department of Civil, Structural and Environmental Engineering, University at Buffalo, State University of New York

MCEER
University at Buffalo, State University of New York
Red Jacket Quadrangle, Buffalo, NY 14261
Phone: (716) 645-3391; Fax (716) 645-3399
E-mail: *mceer@buffalo.edu*; WWW Site: *http://mceer.buffalo.edu*

# Preface

The Multidisciplinary Center for Earthquake Engineering Research (MCEER) is a national center of excellence in advanced technology applications that is dedicated to the reduction of earthquake losses nationwide. Headquartered at the University at Buffalo, State University of New York, the Center was originally established by the National Science Foundation in 1986, as the National Center for Earthquake Engineering Research (NCEER).

Comprising a consortium of researchers from numerous disciplines and institutions throughout the United States, the Center's mission is to reduce earthquake losses through research and the application of advanced technologies that improve engineering, pre-earthquake planning and post-earthquake recovery strategies. Toward this end, the Center coordinates a nationwide program of multidisciplinary team research, education and outreach activities.

MCEER's research is conducted under the sponsorship of two major federal agencies: the National Science Foundation (NSF) and the Federal Highway Administration (FHWA), and the State of New York. Significant support is derived from the Federal Emergency Management Agency (FEMA), other state governments, academic institutions, foreign governments and private industry.

MCEER's NSF-sponsored research objectives are twofold: to increase resilience by developing seismic evaluation and rehabilitation strategies for the post-disaster facilities and systems (hospitals, electrical and water lifelines, and bridges and highways) that society expects to be operational following an earthquake; and to further enhance resilience by developing improved emergency management capabilities to ensure an effective response and recovery following the earthquake (see the figure below).

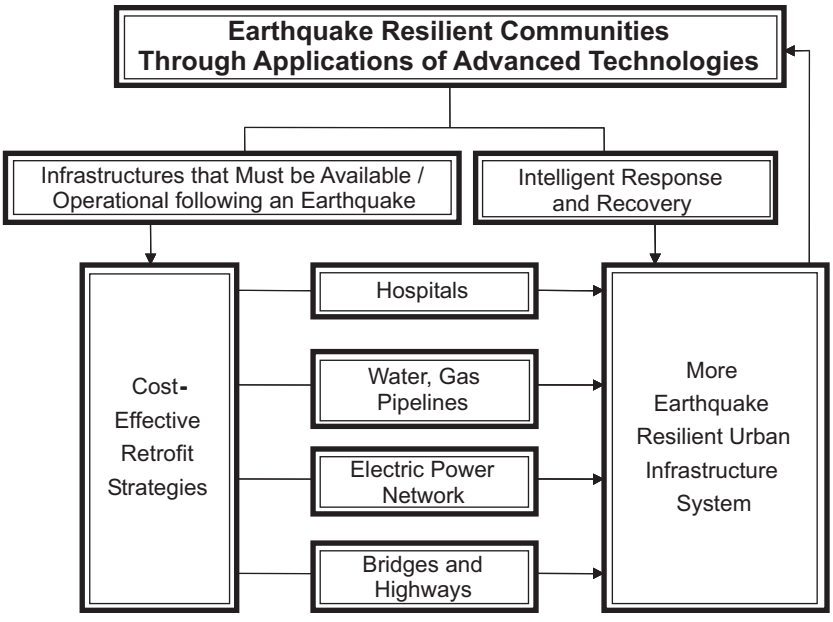

A cross-program activity focuses on the establishment of an effective experimental and analytical network to facilitate the exchange of information between researchers located in various institutions across the country. These are complemented by, and integrated with, other MCEER activities in education, outreach, technology transfer, and industry partnerships.

*This report investigates the failure mechanisms of shear-critical squat (ratio height to length of less than two) reinforced concrete walls, commonly used in many commercial buildings and nearly all safety-related nuclear structures. A database with experimental data obtained from 434 tests is assembled with the objective of improving the current state of knowledge on squat wall response. The adequateness of the peak shear strength predictive equations available in current design provisions is evaluated. Improved empirical equations are developed for peak shear strength prediction for rectangular walls and walls with boundary elements in a format suitable for inclusion in standards and codes of practice. Squat walls are modeled using finite elements to predict their monotonic and cyclic responses. Modeling decisions that are critical to predict the wall responses are explored and recommendations for finite element modeling are made. Macro-level hysteretic models are prepared for a small number of squat walls for which digital load-displacement data are available. The calibrated Ibarra-Krawinkler pinching model is used to properly capture the strength, stiffness degradation and pinching effects in the walls response. Information in the database is used to identify damage states and to develop fragility functions for buildings and safety-related nuclear structures incorporating squat reinforced concrete walls.*

# ABSTRACT

Reinforced concrete walls with a ratio of height to length of less than two are important structural components in many commercial buildings and nearly all safety-related nuclear structures. The performance of these short (squat) walls is most important during earthquake shaking because they are designed and detailed to provide most of the lateral stiffness and strength in a building or structure.

Current design provisions in codes and standards for reinforced concrete walls focus on tall (flexure-critical) walls and pay less attention to squat walls, although squat walls are far more common in practice. Squat wall failure is generally shear-related and non-ductile. Shear-critical squat walls are the focus of this report.

A database of information from tests of 434 squat walls is assembled with the objective of improving the current state of knowledge on squat wall response. The utility of predictive equations currently used in North America for the peak shear strength of squat walls is determined using the database. These equations do not provide unbiased estimates of peak shear strength with a small coefficient of variation. Improved empirical equations are developed for peak shear strength for rectangular walls and walls with boundary elements in a format suitable for inclusion in standards and codes of practice.

Squat walls are modeled using two widely used finite element codes: ABAQUS and VecTor2. These codes are used to predict the monotonic and cyclic response of squat walls. Modeling decisions that are critical to predicting response are explored and recommendations for finite element analysis are made.

Macro-level hysteretic models are prepared for a small number of squat walls for which digital load-displacement data are available. The calibrated Ibarra-Krawinkler pinching model captures well the key features of squat wall response: strength and stiffness deterioration and pinched hysteresis.

Information from the database is used to develop fragility functions, damage states, and scopes of repair for seismic performance assessment of buildings and safety-related nuclear structures incorporating squat reinforced concrete walls.

## ACKNOWLEDGMENTS

A number of expert researchers and design professionals contributed to this report: John Hooper, Laura Lowes, Jack Moehle, Nebojsa Orbovic, Alan Rabideau, Detlef Rothe, Thomas Salonikios, Maw-Shyong Sheu, Jean Francois Sidaner, Bozidar Stojadinovic, Frank Vecchio and Sharon Wood. The authors' gratefully acknowledge these contributions.

A number of the figures in the report are reproduced from reports, conference proceedings, and journal papers. Amr Elnashai, Abhinav Gupta, Pedro Hidalgo, Pierino Lestuzzi, Murat Saatcioglu, Anthony Synge, Frank J. Vecchio, John Wallace, Yan Xiao, American Concrete Institute (ACI), Architectural Institute of Japan, Elsevier, Earthquake Engineering Research Institute, Imperial College, International Association for Structural Mechanics in Reactor Technology, and the Swiss Federal Institute of Technology, Zurich, granted permission to reproduce these figures.

Financial support for these studies was provided by: (a) MCEER through grants from the Earthquake Engineering Centers Program of the National Science Foundation (NSF), Award Number EEC-9701471, and New York State; (b) the Applied Technology Council and the Federal Emergency Management Agency; and (c) the National Science Foundation NEESR Program under Grant No. CMMI-0829978.

## TABLE OF CONTENTS

## TABLE OF CONTENTS (CONT'D)

## TABLE OF CONTENTS (CONT'D)

## TABLE OF CONTENTS (CONT'D)

## TABLE OF CONTENTS (CONT'D)

## LIST OF FIGURES

## LIST OF FIGURES (CONT'D)

## LIST OF FIGURES (CONT'D)

## LIST OF FIGURES (CONT'D)

## LIST OF FIGURES (CONT'D)

## LIST OF FIGURES (CONT'D)

## LIST OF FIGURES (CONT'D)

## LIST OF FIGURES (CONT'D)

## LIST OF TABLES

## LIST OF TABLES (CONT'D)

## LIST OF TABLES (CONT'D)

# GLOSSARY

$A$ = coefficient used to calculate $\rho_{se}$

$A_c$ = area of the concrete section resisting shear per ACI 318-08

$A_{be}$ = total boundary element area

$A_{cv}$ = gross area of concrete bounded by web thickness and length of section in the direction of the shear force per ACI 318-08, Wood (1990), and Wallace (2007)

$A_{eff}$ = effective wall area

$A_g$ , $A_t$ = gross area of the wall cross section

$A_v$ = area of horizontal reinforcement within a distance $s$ per ACI 318-08

$A_{vf}$ = area of reinforcement perpendicular to the plane of the crack per ACI 318-08 and Wood (1990)

$A_w$ = area of the web cross section

= effective wall area that is equal to the product of $D$ and $t_w$ per Fukuzawa et al. (1988)

$b_{eff}$ = effective flange width

$b_f$ = boundary element width

$B$ = coefficient used to calculate $\rho_{se}$

$c$ = residual strength ratio per ASCE 41-06

= parameter that defines the rate of cyclic deterioration (see Section 7)

$d$ = drift at nominal shear strength per ASCE 41-06

= distance from the extreme compression fiber to the force centroid of the wall vertical reinforcement in tension and assumed equal to $0.8l_w$ unless a larger value is determined by a strain compatibility analysis, per ACI 318-08

= distance from the extreme compression fiber to the location of the resultant of forces in vertical reinforcement in tension, which may be determined from a strain compatibility analysis and is assumed equal to $0.6l_w$ if no analysis is performed, per ASCE 43-05

= distance from extreme tension fiber to centroid of tension reinforcement per Barda et al. (1977)

$d_1$ = distance from extreme compression fiber to the location of the resultant of forces in vertical reinforcement in tension and assumed equal to $0.8l_w$ unless a larger value is determined by a strain compatibility analysis

$d_2$ = distance from extreme compression fiber to area centroid of the wall vertical reinforcement in tension

$d_3$ = distance from the extreme compression fiber to the location of the resultant of forces in vertical reinforcement in tension, which may be determined from a strain compatibility analysis and is assumed equal to $0.6l_w$ if no analysis is performed

$D$ = wall length measured from the centers of the boundary barbells per Fukuzawa et al. (1988)

= test parameter of the K-S test (see Section 7)

$D_{crit}$ = critical test parameter for the K-S test (see Section 7)

$e$ = ultimate drift ratio per ASCE 41-06

$E_c$ = modulus of elasticity of concrete

$E_i$ = hysteretic energy dissipated in excursion *i*

$\Sigma E_j$ = sum of the hysteretic energy dissipated in excursions 1 through *i*

$E_s$ = modulus of elasticity of steel

$E_t$ = inherent hysteretic energy dissipation capacity

$f_b$ = bending stress per ASCE 43-05

$f_{cr}$ = cracking stress per ASCE 43-05

$f_c'$ = compressive strength of concrete

$f_t'$ = tensile strength of concrete

$f_X(x)$ = probability density function

$f_{ube}$ = ultimate stress of vertical boundary element reinforcement

$f_{uh}$ = ultimate stress of horizontal web reinforcement

$f_{uv}$ = ultimate stress of vertical web reinforcement

$f_y$ = yield stress of reinforcement

$f_{ybe}$ = yield stress of vertical boundary element reinforcement

$f_{yh}$ = yield stress of horizontal web reinforcement

$f_{yv}$ = yield stress of vertical web reinforcement

$f_{y1}$ = reinforcement yield stress used with $\rho_{se}$

$f_{y2}$ = reinforcement yield stress for a combination of vertical web and boundary element reinforcement used for Wood (1990)

$f_u$ = ultimate stress of reinforcement

$F_c$ = peak strength

$F_{cx}$ = horizontal component of the compression strut force

$F_{cy}$ = vertical component of the compression strut force

$F_{fri}$ = friction force associated with aggregate interlock between the two surfaces of the cracks

$F_{hw}$ = force carried by horizontal web reinforcement

$F_r$ = residual strength

$F_{vbe}$ = force carried by vertical boundary element reinforcement

$F_{vw}$ = force carried by vertical web reinforcement

$F_X(x)$ = cumulative distribution function

$F_y$ = yield strength

$g$ = drift ratio corresponding to the development of nominal shear strength per Wallace (2007)

$G_c$ = shear modulus of concrete ($=0.4E_c$)

$h$ = wall thickness per ACI 318-08 and Barda et al. (1977)

$h_f$ = boundary element thickness

$h_L$ = moment-to-shear ratio

$h_w$ = height of wall

$I_g$ = moment of inertia of gross concrete section about centroidal axis neglecting reinforcement

$l_w$ = length of wall

$L(\theta)$ = likelihood function

$k$ = shape parameter for gamma and Weibull distributions

$K_c$ = ratio of the second deviatoric stress invariant on the tensile meridian to that on the compressive meridian (see Section 5)

= post-capping stiffness (see Section 7)

$K_e$ = elastic stiffness of wall

$K_{rel\_a}$ = reloading stiffness (see Section 7)

$K_{rel\_b}$ = reloading stiffness (see Section 7)

$K_s$ = post-yielding stiffness

$K_1$ = coefficient used to calculate shear-friction strength associated with sum of the shearing of protrusions on the crack faces and the dowel action of the reinforcement (400 psi for normalweight concrete, 200 psi for all-lightweight concrete, and 250 psi for sand-lightweight concrete) per ACI 318-08

$M_u$ = factored moment

$M/QD$ = moment-to-shear ratio per Fukuzawa et al. (1988)

$M/Vl_w$ = moment-to-shear ratio

$n$ = sample size

$N_A$ = axial force per ASCE 43-05

$N_u$ = factored axial force per ACI 318-08 and Barda et al. (1977)

$P$ = axial force

$s$ = spacing of the horizontal reinforcement per ACI 318-08

$S_X(x)$ = empirical cumulative distribution function

$t_n$ = thickness of wall web per ASCE 43-05

$t_w$ = thickness of wall web

$V$ = shear force

$V_{BE}$ = predicted peak shear strength for walls with boundary elements

$V_c$ = shear strength provided by concrete per ACI 318-08 and ASCE 43-05

$V_{cr}$ = shear strength at cracking per Wallace (2007)

$V_{flex}$ = shear-flexural strength

$V_n$ = nominal shear strength per ACI 318-08 and Wallace (2007)

$V_{n1}$ = nominal shear strength per Section 21.9 of ACI 318-08

$V_{n2}$ = nominal shear strength per Section 11.9 of ACI 318-08

$V_{n3}$ = nominal shear strength per Barda et al. (1977)

$V_{n4}$ = nominal shear strength per ASCE 43-05

$V_{n5}$ = nominal shear strength per Wood (1990)

$V_{peak}$ = experimentally measured peak shear strength

$V_{peak\_FE}$ = peak shear strength predicted using finite element analysis

$V_{peak\_R}$ = predicted peak shear strength for rectangular walls

$V_{peak\_B}$ = predicted peak shear strength for walls with barbells

$V_{rec}$ = predicted peak shear strength for rectangular walls

$V_s$ = shear strength provided by horizontal web reinforcement per ACI 318-08

$V_u$ = factored shear force per ACI-318

= shear capacity per ASCE 43-05

$\alpha$ = coefficient used to calculate the contribution of concrete to peak shear strength [see Fukuzawa et al. (1988)]

= angle of inclination for the crack (see Section 6)

= shape parameter for beta distribution

$\alpha_c$ = empirical coefficient that is a function of wall aspect ratio and used to calculate the concrete contribution to peak shear strength of reinforced concrete walls per ACI 318-08 (3.0 for $h_w / l_w \le 1.5$, 2.0 for $h_w / l_w \ge 2$ and varies linearly between 1.5 and 2.0)

$\alpha\tau_c$ = shear stress contributed by concrete to peak shear strength [see Fukuzawa et al. (1988)]

$\beta$ = dispersion

= shape parameter for beta distribution

$\beta_i$ = deterioration parameter in excursion *i*

$\delta_c$ = displacement at peak strength

$\delta_y$ = displacement at yield strength

$\delta_r$ = displacement beyond which lateral strength is assumed equal to the residual strength ($F_r$)

$\varepsilon$ = eccentricity parameter for the concrete damaged plasticity model in ABAQUS

$\varepsilon_{c0}$ = axial strain corresponding to $f_c'$

$\varepsilon_t$ = axial strain in the extreme tension reinforcement per ACI 318-08

$\phi$ = strength reduction factor equal to 0.65 for compression-controlled sections ($\varepsilon_t \le 0.002$), 0.90 for tension-controlled sections ($\varepsilon_t \ge 0.005$), and varies linearly between 0.65 and 0.90 for sections with $\varepsilon_t$ values between 0.002 and 0.005 per ACI-318

= capacity reduction factor equal to 0.8 per ASCE 43-05

$\gamma$ = parameter used to calculate inherent hysteretic energy dissipation capacity ($E_t$)

$\gamma_{cr}$ = drift angle at cracking per Wallace (2007)

$\kappa_D$, $\kappa_F$ = empirical parameters associated with modeling pinching behavior (see Section 7)

$\lambda$ = coefficient per ACI 318-08 used to transform design equations for normalweight concrete to lightweight concrete

= scale parameter for gamma and Weibull distributions

$\mu$ = coefficient of friction per ACI 318-08

= mean (see Section 7)

$\mu_{\ln x}$ = mean of the natural log of the demand parameter

$\theta$ = median

$\rho_{be}$ = flexural reinforcement ratio calculated using boundary element area

$\rho_{be2}$ = flexural reinforcement ratio calculated using total wall area

$\rho_h$, $\rho_t$ = horizontal web reinforcement ratio per ASCE 43-05 and ACI 318-08

$\rho_n$, $\rho_v$, $\rho_l$ = vertical web reinforcement ratio per Barda et al. (1977), ASCE 43-05, and ACI 318-08

$\rho_{se}$ = combined reinforcement ratio per ASCE 43-05

$\rho_{vall}$ = ratio of the total area of vertical reinforcement to the wall area

$\rho_w$ = web reinforcement ratio [see Fukuzawa et al. (1988)]

$\sigma$ = standard deviation

$\sigma_{b0} / \sigma_{c0}$ = ratio of initial equibiaxial compressive yield stress to initial uniaxial compressive yield stress

$\sigma_{\ln x}$ = standard deviation of the natural log of the demand parameter

$\Sigma A_c$ = total area of barbells [see Fukuzawa et al. (1988)]

$\tau_0$ = shear stress contributed by axial force to peak shear strength [see Fukuzawa et al. (1988)]

$\tau_{peak}$ = peak shear stress [see Fukuzawa et al. (1988)]

$\tau_s$ = shear stress contributed by reinforcement to peak shear strength [see Fukuzawa et al. (1988)]

$\nu_n$, $\nu_u$ = nominal peak shear stress

$\psi$ = dilation angle

# 1 INTRODUCTION

## 1.1 General

Reinforced concrete walls with a ratio of height to length of less than or equal to two are widely used in conventional buildings and safety-related nuclear structures. The literature and design professionals describe such walls as *squat* or short.

Squat walls are generally grouped by plan geometry, namely, rectangular, barbell, and flanged. They provide much or all of a structure's lateral strength and stiffness to resist earthquake and wind loadings. Accurate modeling of the response of squat walls is important because conventional buildings are likely to experience multiple deformation cycles at or beyond yield in maximum earthquake shaking, and nuclear safety-related structures will likely be subjected to multiple cycles of loading to peak strength in safe shutdown earthquake shaking. Code provisions for seismic design of reinforced concrete walls were drafted primarily for slender walls although most reinforced concrete walls in building structures around the world are squat.

A desirable earthquake resistant design philosophy for reinforced concrete walls is to suppress shear failure in design earthquake shaking. Experimental studies have shown that well designed and detailed tall (or slender) walls will yield in flexure and not fail in shear. On the contrary, squat walls are prone to shear failure that is generally associated with rapid loss of strength and stiffness under cyclic loading.

Figure 1-1 shows first quadrant load-displacement relationship for a squat flanged wall (Wall 3) tested by Synge (1980). This wall had a vertical web reinforcement ratio of 0.37%, horizontal web reinforcement ratio of 1.61%, vertical flange reinforcement ratio of 1.81% and an aspect ratio of 0.50. This wall was tested under cyclic loading at a quasi-static rate with two cycles at each displacement amplitude. No axial force was applied to the wall. This wall achieved its peak strength during the first cycle of loading to a displacement of 6 mm (0.4% drift). The dashed line in the figure represents the shear force corresponding to the wall flexural strength calculated using a strain compatibility analysis on the wall section. Following the loading to peak shear strength, sliding displacements at the interface between the wall web and the foundation dominated the response. As seen in Figure 1-1, the wall experienced a significant loss of strength and stiffness in the displacement cycles following the cycle to the peak shear strength as the sliding deformations became more pronounced. Significant residual displacements (measured at the zero-force intercept) and modest energy dissipation that are indicators of poor seismic performance are seen in the reported experimental load-displacement relationship.

A significant number of experiments on squat reinforced concrete walls have been completed in the past 50+ years. The first experimental programs on squat walls were conducted at Massachusetts Institute of Technology and Stanford University [Galletly (1952), Benjamin and Williams (1953), Benjamin and Williams (1954), Benjamin and Williams (1956)] on barbell cross-section. These tests were performed using monotonic loading and focused mainly on evaluation of peak shear strength. In the United States, the first cyclic tests on squat walls were performed by Barda (1972). In the interim period, a substantial number of cyclic loading experiments on squat walls were conducted in Japan [Hirosawa (1975)].

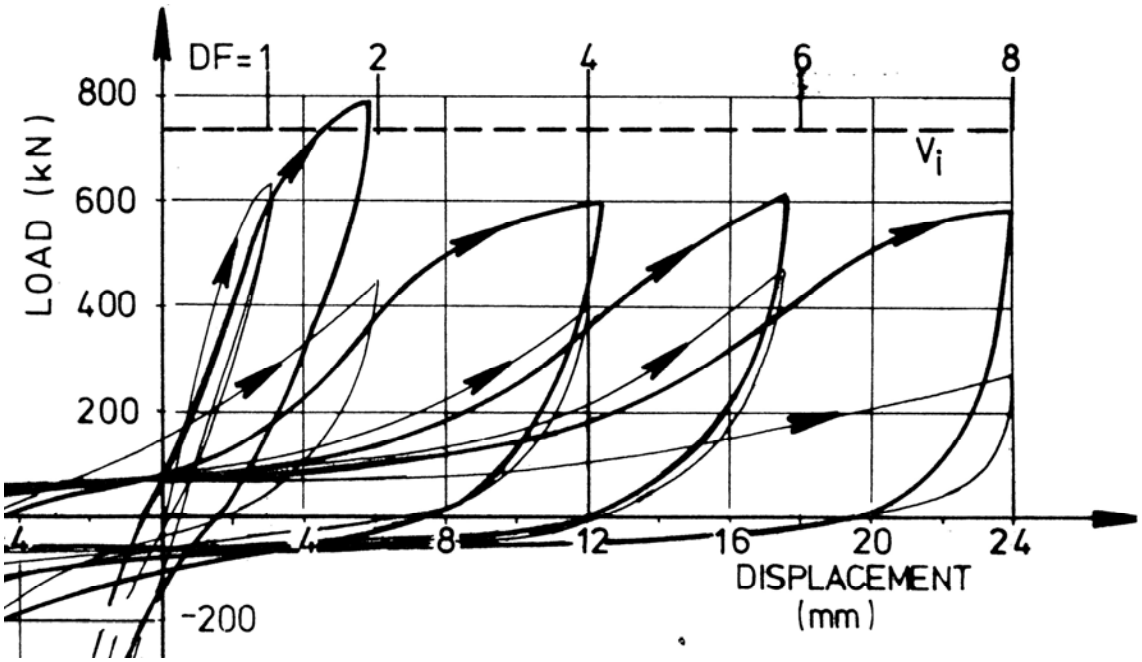


**Figure 1-1 First quadrant load-displacement relationship of Wall 3 tested by Synge (1980)**

Although there is substantial experimental data in the literature on squat walls, current design procedures have been essentially unchanged for more than 40 years. One such example is the prediction of peak shear strength, which is the key parameter in design of squat walls. The procedures available in code-provisions, building manuals and literature to calculate the peak shear strength of squat walls do not correlate well with the experiments resulting substantial scatter in the predictions [Wood (1990), Gulec (2005), Gulec et al. (2007), Gulec et al. (2008), Gulec et al. (2009)].

## 1.2 Failure Modes in Reinforced Concrete Walls

Three types of shear failure are observed in squat walls, namely, diagonal tension, diagonal compression, and sliding shear [Paulay and Priestley (1992)]. If a shear failure occurs after the wall achieves its flexural strength, the failure mode is considered mixed and termed a flexure-shear failure (e.g., flexure-diagonal tension). Flexure-shear failures occur as the shear strength of a wall, which is initially higher than the shearing force associated with flexural failure, degrades with increasing displacement cycles and drops below the flexural strength of the wall. The experimental data evaluated in this study shows that the failure of walls with aspect ratios of less than 1.0 are generally governed by shear whereas the failure of taller walls with aspect ratios of between 1.0 and 2.0 is generally governed by mixed modes. Exceptions to this classification exist since design parameters such as horizontal and vertical web reinforcement ratios, wall geometry, and axial force also affect the behavior of squat reinforced concrete walls. The following sub-sections present information on the failure modes observed in reinforced concrete walls.

### 1.2.1 Diagonal Tension Failure

Diagonal tension failure is generally observed in squat walls with light horizontal web reinforcement. This failure is characterized by one or more wide inclined cracks with respect to each loading direction. Cracking is not widespread over the wall web as the damage is concentrated in the inclined cracks. Yielding of horizontal web reinforcement is observed as the cracks widen with increasing displacement demands on the wall. The orientation of the failure plane (typically assumed to form at an angle of approximately 45 degrees) is influenced strongly by the presence of a large beam at the top of the wall (if any) and the aspect ratio of the wall. A stiff top beam and foundation contribute to the formation of a corner-to-corner crack. Figure 1-2 presents the final condition of a squat wall that failed by diagonal tension.

**Figure 1-2 Diagonal tension failure of wall 27 tested by Hidalgo et al. (2001)**

### 1.2.2 Diagonal Compression Failure

A diagonal compression failure may be triggered if a diagonal tension failure is prevented by providing adequate horizontal web reinforcement. Resistance of the concrete compression struts in the web of the wall deteriorates as the inclined cracks in two opposite directions open and close successively under cyclic loading. The crushing of the concrete struts in the web of the wall triggers a diagonal compression failure.

Walls with boundary elements (barbells or flanges) are more prone to diagonal compression failure than walls with rectangular cross sections. Flanged and barbell walls can potentially accommodate more reinforcement at the wall ends, which provides substantial flexural strength and increase the shear demands in the wall web. Axial forces will help to limit the crack widths in a squat wall, which increases peak shear strength. However, large axial forces also increase substantially the compressive stresses in the web of the wall and contribute to a diagonal compression failure. In design, the maximum shear stresses in a wall section are limited to prevent a diagonal compression failure, which is relatively more brittle than a diagonal tension

failure since it is associated with concrete crushing rather than reinforcement yielding. Figure 1-3 presents the final condition of a squat wall that failed by diagonal compression.

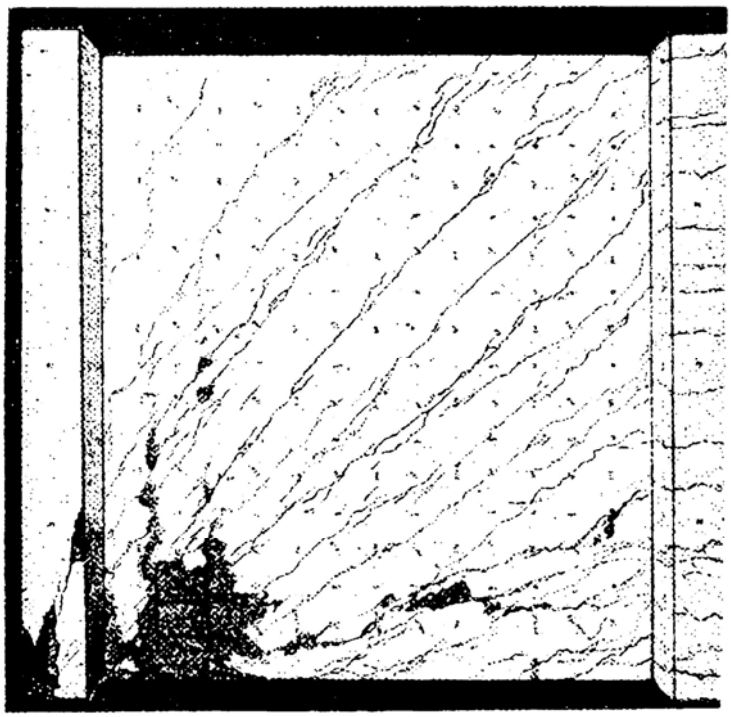

**Figure 1-3 Diagonal compression failure of wall S1 tested by Maier and Thürlimann (1985)**

### 1.2.3 Sliding Shear

Heavily reinforced walls subjected to large number of displacement cycles may be susceptible to sliding shear failure. This failure is similar to a diagonal compression failure in the sense that it is also a result of concrete crushing. Squat walls that fail in sliding shear initially experience inclined shear cracking. Inclined shear cracks that form in each direction intersect each other due to cyclic loading and the strength of the concrete between these cracks deteriorates as a result of subsequent displacement cycles at higher amplitude. Note that crack density is higher for heavily reinforced walls and the concrete struts are narrower. Concrete crushing then spreads over the wall length in a narrow band, forming a weakened horizontal plane near the base of the wall web. The upper part of the wall then starts to slide on this weakened plane and such failure is associated with sliding shear. Figure 1-4 presents the final condition of a squat wall that failed by sliding shear.

### 1.2.4 Flexural Failure

FEMA 306 [ATC (1998b)] states that walls that fail in flexure generally sustain in-plane rotations of at least 2% (0.02 rad) or displacements of eight times the yield displacement.

This failure mode is rare in squat walls but is discussed below for completeness. According to ASCE 41-06 [ASCE (2007)], slender walls with relatively high aspect ratios (3.0+) will generally fail in flexure. The response of walls that fail in flexure can be predicted accurately

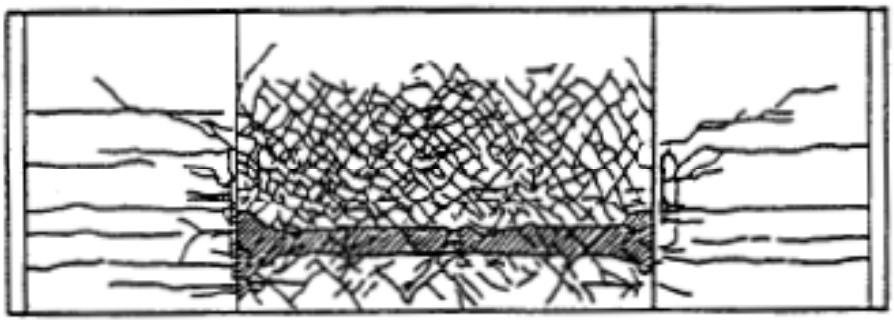

**Figure 1-4 Sliding shear failure of NUPEC wall U-1 [Kitada et al. (1997)]**

using cross-section strain-compatibility analysis.

Flexural failure is often associated with wide flexural cracks near the bottom of the wall web. Minor shear cracking, which does not significantly alter the overall response of the wall, may occur. Spalling of concrete at the extreme compression fibers near the base of the wall is often observed Vertical reinforcement at the ends of the wall near its base may fracture with increasing displacement demand on the wall. Figure 1-5 presents a representative cracking pattern for flexural failure.

### 1.2.5 Mixed Failure Modes

A mixed failure mode is shear failure at a displacement that is greater than the displacement corresponding to the peak flexural strength. Wall behavior is governed initially by flexure (i.e., flexural cracking and yielding of vertical boundary element reinforcement), which is similar to the initiation of flexural failure. For a wall that exhibits a mixed failure mode, wall shear strength is initially equal to or greater than the shear force corresponding to wall flexural strength. However, the shear resistance of the wall degrades with displacement cycles of increasing amplitude. At some level of displacement, the shear strength of the wall degrades below the

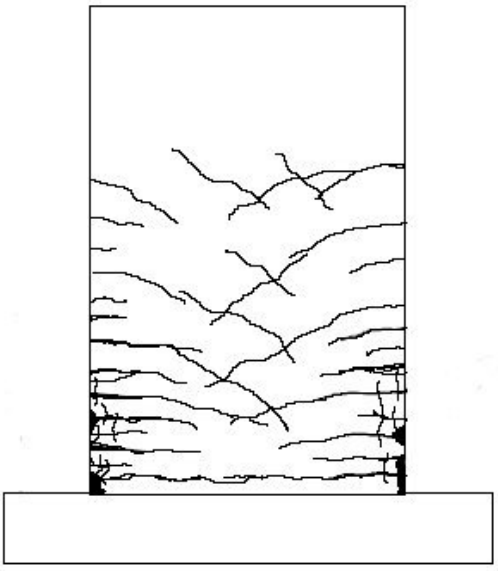

**Figure 1-5 Representative cracking pattern for flexural failure [ATC (1998b)]**

shear force associated with flexural strength and shear controls wall response thereafter. The failure of squat reinforced concrete walls with intermediate aspect ratios ($1.0 \le h_w / l_w \le 2.0$) is generally governed by mixed modes. Information on mixed failure modes, which are flexure-diagonal tension, flexure-diagonal compression, and flexure-sliding is presented next using the terminology of FEMA 306.

Flexural-diagonal tension failure is associated with the formation of wide inclined cracks after the wall achieves its flexural strength. The mechanism for this failure mode is similar to that of diagonal tension. Figure 1-6a presents a representative cracking pattern for flexure-diagonal tension failure. If a wall has sufficient horizontal reinforcement to prevent development of wide inclined cracks, a flexure-diagonal compression failure is likely to occur.

Flexure-diagonal compression failure is associated with failure of compression struts after the wall achieves its flexural strength. The mechanism associated with this failure mode is similar to that of diagonal compression. Figure 1-6b presents a representative cracking pattern for flexure-diagonal compression failure.

Flexure-sliding shear failure is associated with significant sliding after the wall achieves its flexural strength. Limiting the shear stress in the wall web and providing adequate horizontal web reinforcement can avoid failures associated with diagonal compression or tension, respectively. However, the upper portion of the wall can slide relative to the foundation along a horizontal crack at the base of a wall. Due to cyclic loading, flexural cracks form at each end of the wall near its base. These flexural cracks may propagate to the center of the wall and form a continuous crack at the base of the wall with cycles of increasing displacement amplitude. Further cycling diminishes the resistance mechanisms (aggregate interlock, shear friction) along this crack and a sliding plane forms. Thereafter, shear force is transferred primarily from the wall to the foundation by dowel action of the vertical reinforcement, which can provide only modest lateral strength and stiffness. Sliding results in a significant reduction in stiffness and strength and large residual displacements.

Figure 1-7 presents the final condition of a squat wall that failed by flexure-sliding shear [wall 1, Synge (1980)]. Walls with light vertical web reinforcement, no boundary element reinforcement, and low axial forces are susceptible to this type of failure.

## 1.3 Code Approaches to Squat Wall Design

Building codes and provisions provide limited information on the design of squat reinforced concrete walls. ACI 318-08 [ACI (2008)] procedures are applicable to all types of structural walls: squat and slender. The requirements of ACI 318-08 associated with shear design of structural walls are summarized in Section 1.3.1. The procedures of ASCE 41-06 [ASCE (2007)] for seismic rehabilitation of reinforced concrete shear walls and design requirements of ASCE 43-05 [ASCE (2005)] for squat walls in nuclear facilities are summarized in Sections 1.3.2 and 1.3.3, respectively.

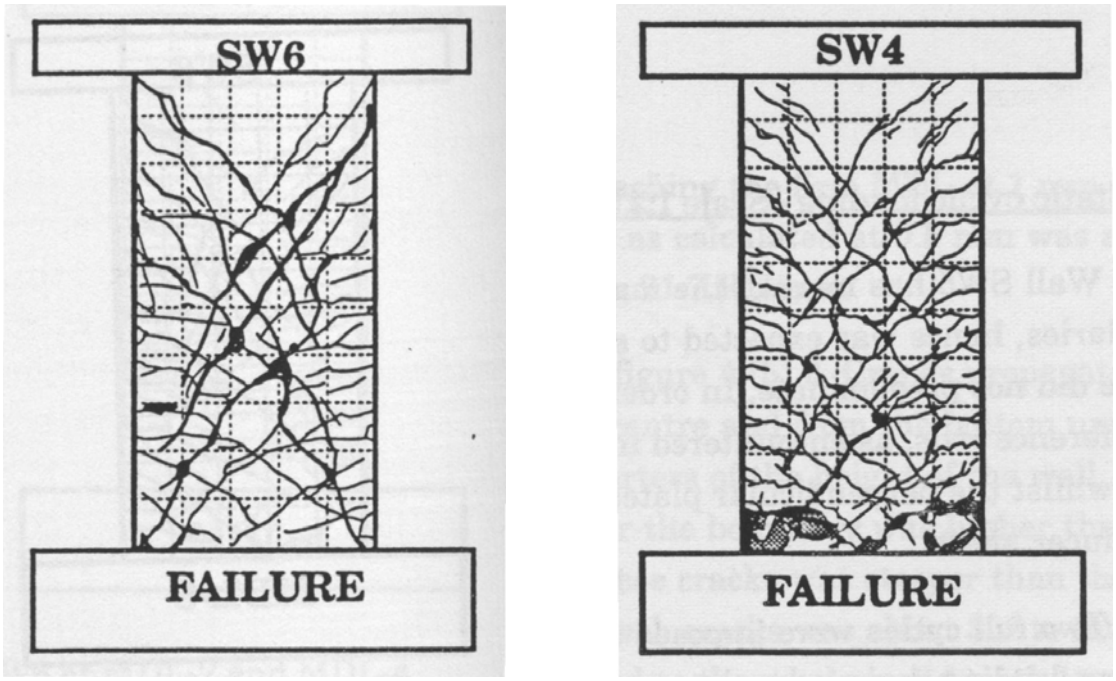


**a) Flexure-diagonal tension failure** **b) Flexure diagonal-compression failure**

**Figure 1-6 Representative cracking patterns for flexure-diagonal tension and flexure diagonal failures [Pilakoutas and Elnashai (1995)]**

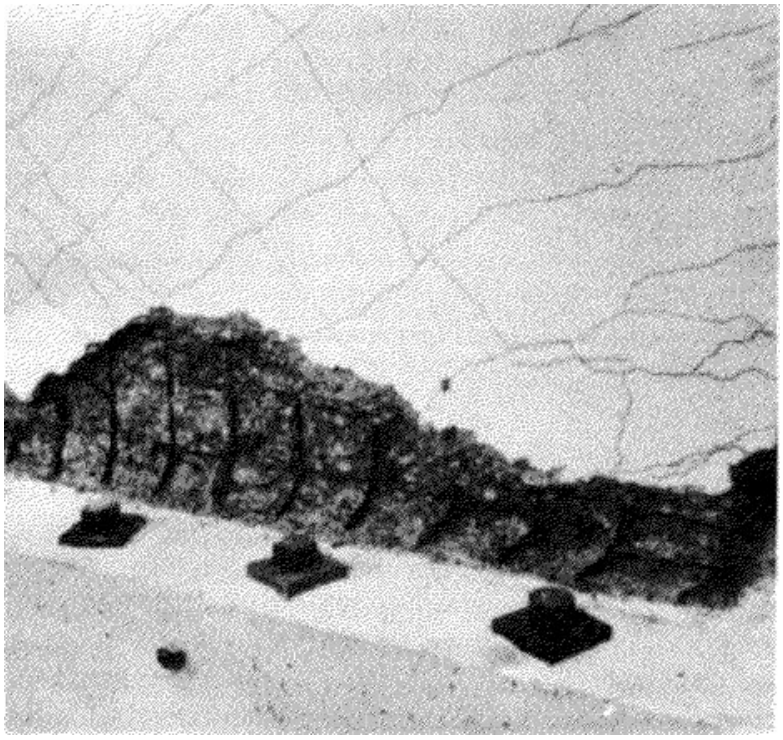

**Figure 1-7 Flexure-sliding shear failure of wall 1 tested by Synge (1980)**

### 1.3.1 ACI 318-08 [ACI (2008)]

Design procedures for shear in reinforced concrete walls are presented in Sections 11.6, 11.9, and 21.9 of ACI 318-08. Section 11.6 deals with failure mechanisms associated with shear transfer across a plane. Section 11.9 provides requirements for structural walls subjected to non-seismic lateral loadings and Section 21.9 provides requirements for the seismic design of reinforced concrete structural walls. Sections 11.9 and 21.9 assume a diagonal tension failure mechanism with a 45-degree crack to calculate wall shear strength and seek to prevent failure by diagonal compression by specifying an upper limit on the shear stress.

Section 11.6 of ACI 318-08 provides design provisions for shear transfer across a crack. Sliding shear failures along an interface between the wall web and the foundation may occur in squat walls subjected to cyclic loading. The provisions of Section 11.6 can be used to assess the sliding shear strength of squat walls. Section 11.6 provides two equations to calculate the nominal shear transferred through a crack. The first equation is based on the work of Mattock [Mattock (1976), Mattock (1977)] and is presented in Equation 1-1. In Equation 1-1, $A_{vf}$ ($in^2$) is the area of reinforcement perpendicular to the plane of the crack, $f_y$ (psi) is the yield stress of the reinforcement, $A_c$ ($in^2$) is the area of the concrete section resisting shear and $K_1 = 400$ psi for normalweight concrete, 200 psi for all-lightweight concrete, and 250 psi for sand-lightweight concrete.

$$V_n = 0.8 A_{vf} f_y + A_c K_1 \tag{1-1}$$

In Equation 1-1, the first term represents the contribution of the shear-friction force to the overall shear transfer through the crack (0.8 = coefficient of friction) and the second term represents the sum of the resistances to shearing of protrusions on the crack faces and the dowel action of the reinforcement.

The second equation in Section 11.6 of ACI 318-08 is based solely on shear-friction as presented in as Equation 1-2. In this equation $\mu$ is the coefficient of friction: for concrete placed monolithically assumed $\mu = 1.4\lambda$; for concrete placed against hardened concrete with surface intentionally roughened, $\mu = 1.0\lambda$; and for concrete placed against hardened concrete not intentionally roughened, $\mu = 0.6\lambda$; $\lambda$ is assumed to be 1.0 for normalweight concrete, 0.85 for sand-lightweight concrete and 0.75 for all lightweight concrete.

$$V_n = A_{vf} f_y \mu \tag{1-2}$$

Section 11.6 states that $V_n$ shall not be taken greater than the smaller of $0.2 f_c'$ and $800 A_c$ and the value of $f_y$ used for design of shear friction reinforcement shall not exceed 60 ksi.

The procedure to predict the peak shear strength in Section 11.9 of ACI 318-08 is given by Equations 1-3 through 1-7 for normalweight concrete. Section 11.9 limits the nominal peak shear stress in a wall to $10\sqrt{f_c'}$ and the minimum horizontal web reinforcement ratio ($\rho_t$) to 0.25%. The minimum vertical web reinforcement ratio ($\rho_l$) is assumed to be the larger of Equation 1-7 and 0.0025. Section 11.9 requires that the spacing of the horizontal web reinforcement shall not

be less than the smallest of $l_w/5$, $3h$ and 18 in., and the spacing of the vertical web reinforcement shall not be less than the smallest of $l_w/3$, $3h$ and 18 in.

$$V_n = V_c + V_s \le 10\sqrt{f_c'}hd \tag{1-3}$$

$$V_c = 3.3\sqrt{f_c'}hd + \frac{N_u d}{4l_w} \tag{1-4}$$

$$V_c = \left[ 0.6\sqrt{f_c'} + \frac{l_w\left(1.25\sqrt{f_c'} + \dfrac{0.2N_u}{l_w h}\right)}{\dfrac{M_u}{V_u} - \dfrac{l_w}{2}} \right] hd \tag{1-5}$$

$$V_s = \frac{A_v f_y d}{s} \tag{1-6}$$

$$\rho_l = 0.0025 + 0.5\left(2.5 - \frac{h_w}{l_w}\right)\left(\rho_t - 0.0025\right) \tag{1-7}$$

In Equations 1-3 through 1-7, $V_c$ (lb) is the shear strength provided by concrete, $V_s$ (lb) is the shear strength provided by shear reinforcement, $h$ (in) is the wall thickness, $d$ (in) is the distance from extreme compression fiber to the force centroid of the wall vertical reinforcement in tension and assumed equal to $0.8l_w$ unless a larger value is determined by a strain compatibility analysis, $N_u$ (lb) is the factored axial force that is negative in tension, $M_u$ (lb-in) is the factored moment, $V_u$ (lb) is the factored shear force, $s$ (in) is the spacing of the horizontal reinforcement, and $A_v$ (in$^2$) is the area of horizontal reinforcement within a distance $s$. Other variables have been defined previously.

The major difference between the procedures of Section 11.9 and 21.9 is the calculation of the contribution of concrete ($V_c$) to peak shear strength. The concrete contribution in Section 21.9 is calculated using an empirical factor ($\alpha_c$) that is as a function of wall aspect ratio. In Section 11.9, the two values for $V_c$ (see Equations 1-4 and 1-5) correspond to different cracking conditions and the smaller value of the two is used to calculate the nominal peak shear strength. Equation 1-4 was derived assuming a principal tensile stress of $4\sqrt{f_c'}$ on a section subjected to combined axial load and shear, and Equation 1-5 was derived assuming a flexural tensile stress of $6\sqrt{f_c'}$ at a section located $l_w/2$ above the section being investigated [Cardenas et al. (1973)]. In addition, an effective wall length ($d$) is used to calculate wall shear strength in Section 11.9 whereas the total wall length ($l_w$) is used in Section 21.9.

Section 21.9 of ACI 318-08 notes that both vertical and horizontal web reinforcement in structural walls should be uniformly distributed across the shear plane to limit the width of the inclined cracks. Evenly distributed vertical reinforcement along the wall section theoretically results in lower curvature ductilities and moment capacity, but this arrangement may be preferable because it results in an increased depth of the flexural compression zone and improved conditions for shear friction and dowel action, which contribute to sliding shear resistance. The minimum horizontal and vertical web reinforcement ratio is limited to 0.0025 and the maximum allowed spacing between the reinforcement is 18 in. If the aspect ratio of the walls $(h_w / l_w)$ does not exceed 2.0, the vertical web reinforcement ratio $(\rho_l)$ shall not be less than horizontal web reinforcement ratio $(\rho_t)$. Section 21.9 also requires that at least two curtains of reinforcement be placed in structural walls.

The shear strength equation of Section 21.9, presented in Equation 1-8 for normalweight concrete, is based on the modified truss analogy [Wood (1990)]. This analogy was used originally to estimate the peak shear strength of reinforced concrete beams and assumes that resistance is provided by concrete and transverse reinforcement. The nominal shear-strength calculation procedures of ACI 318-08 for structural walls and beams are closely related. In Equation 1-8, the contribution of horizontal web reinforcement to the shear strength is calculated assuming a failure plane at 45 degrees to the horizontal. The equation recognizes the higher shear strength of low aspect-ratio walls by allowing higher concrete contribution to the overall shear strength through the coefficient $\alpha_c$:

$$V_n = A_{cv}\left(\alpha_c \sqrt{f_c'} + \rho_t f_y\right) \tag{1-8}$$

In Equation 1-8, $V_n$ (lb) is the nominal shear strength, $A_{cv}$ (in$^2$) is the gross area of concrete bounded by web thickness and length of section in the direction of the shear force, $f_c'$ (psi) is the compressive strength of concrete, $\rho_t$ is the ratio of area of distributed (horizontal) reinforcement parallel to the plane of $A_{cv}$ to gross concrete area perpendicular to that reinforcement, $f_y$ (psi) is the specified yield strength of reinforcement, and $\alpha_c$ is an aspect-ratio coefficient and equal to 3.0 for $h_w / l_w \le 1.5$, 2.0 for $h_w / l_w \ge 2$ and varies linearly between 1.5 and 2.0, where $h_w$ is the height and $l_w$ is the length of the wall. To prevent diagonal compression failures, the nominal peak shear stress in horizontal wall segments is limited to $10\sqrt{f_c'}$.

Section 21.9 of ACI 318-08 requires that the concrete and longitudinal reinforcement within effective flange widths be included for the flexure and axial load design of structural walls. Unless a more detailed analysis is performed, the effective flange widths are required to be extended from the face of the web to the smaller of one-half the distance to an adjacent wall web and 25% of the total wall height. Section 21.9 refers to Chapter 10, *Flexure and Axial Loads*, for the design of structural walls under flexural and axial loads. The requirements of Chapter 10 are not presented in detail herein but a) the use of a strain compatibility analysis is allowed, b) the maximum extreme concrete compression fiber strain is taken as 0.003, c) the tensile strength of concrete is neglected, and d) a bilinear stress-strain relationship is assumed for reinforcement with a modulus elasticity of 29,000 ksi.

Note that the procedures of Section 11.9 and Chapter 21.9 of ACI 318-08 to predict the peak shear strength of walls are adopted in ACI 349-06 [ACI (2006)], *Code Requirements for Nuclear Safety-Related Concrete Structures*, without revision despite the significantly different performance expectations for conventional building structures and nuclear structures.

The design strength of members per ACI 318-08 is calculated by multiplying the calculated nominal strength by a strength reduction factor, $\phi$. The strength reduction factor for shear is 0.75 and $\phi$ is calculated as a function of the strain in extreme tension reinforcement ($\varepsilon_t$) for members subjected to flexure and axial load. For compression-controlled sections ($\varepsilon_t \le 0.002$), $\phi$ is set equal to 0.65 (0.75 for members with spiral reinforcement); for tension-controlled sections ($\varepsilon_t \ge 0.005$), $\phi$ is set equal to 0.90; and for sections with $\varepsilon_t$ values between 0.002 and 0.005, $\phi$ varies linearly between 0.65 and 0.90.

## 1.3.2 ASCE 41-06 [ASCE (2007)]

ASCE 41-06, *Seismic Rehabilitation of Existing Buildings*, categorizes the behavior of reinforced concrete walls based on aspect ratio. ASCE 41-06 states that walls with an aspect ratio of less than 1.5 (squat walls) are controlled by shear, walls with an aspect ratio of greater 3.0 (slender walls) are controlled by flexure and the walls with intermediate aspect ratios are controlled by both flexure and shear. ASCE 41-06 refers to Section 21 of ACI 318 (Equation 1-8) to calculate the nominal shear strength of reinforced concrete walls. If the horizontal web reinforcement ratio for a wall is less than 0.0015, a minimum value of 0.0015 is used for shear strength calculations. The spacing of horizontal and vertical web reinforcement is limited to 18 in. ASCE 41-06 refers to Chapter 10 requirements of ACI 318 for nominal flexural strength calculations with the exception that expected yield strength for longitudinal reinforcement can be used in lieu of specified minimum yield strength. ASCE 41-06 refers to Section 21 of ACI 318 for effective flange width calculations.

ASCE 41-06 provides default component-level load-deformation relationships for linear and non-linear analysis of reinforced concrete structures. For the linear analysis procedures, ASCE 41-06 recommends the use of component effective stiffness values that correspond to the secant value at the yield point of the component. In the absence of experimental data, the default values of Table 1-1 are permitted to be used, where $E_c$ is the modulus of elasticity of concrete, $I_g$ is the moment of inertia of gross concrete section about centroidal axis neglecting reinforcement, $A_w$ is the area of the web cross section, and $A_g$ is the gross area of the cross section.

**Table 1-1 ASCE 41-06 default values for stiffness for linear analysis of structural walls**

| Component | Flexural Rigidity | Shear Rigidity | Axial Rigidity |
|---|---|---|---|
| Walls (uncracked) | $0.8E_cI_g$ | $0.4E_cA_w$ | $E_cA_g$ |
| Walls (cracked) | $0.5E_cI_g$ | $0.4E_cA_w$ | $E_cA_g$ |

Figure 1-8 presents the general component load-deformation relationship of ASCE 41-06 for nonlinear analysis. For structural walls, the slope from point A to B can be determined using the data of Table 1-1. If the response is dominated by shear, the strength associated with points B (yield strength) and C (nominal shear strength) are taken to be the same. The nominal shear strength corresponding to points B and C can be calculated by Equation 1-8; $c$ is the residual strength ratio, given as a decimal fraction of the nominal shear strength, $d$ is the drift ratio corresponding to the nominal shear strength (point C) and $e$ is the ultimate drift ratio (point E); the default values of $c$, $d$ and $e$ are specified as 0.40, 0.75 and 2.0 respectively for walls governed by shear. ASCE 41-06 notes members with axial forces higher than $0.15A_g f_c'$ must be treated as force-controlled components.

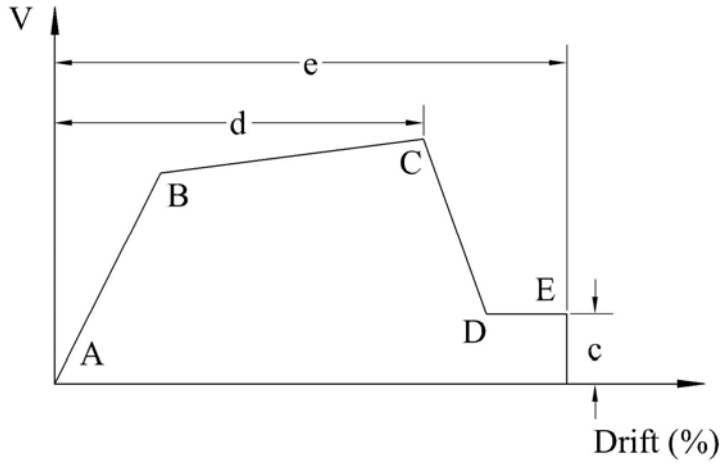


**Figure 1-8 Default load-displacement relationship in ASCE 41-06 [ASCE (2007)]**

### 1.3.3 ASCE 43-05 [ASCE (2005)]

ASCE 43-05, *Seismic Design Criteria for Structures, Systems, and Components in Nuclear Facilities and Commentary*, provides equations for the effective stiffness of reinforced concrete walls (repeated in Table 1-2) to be used in linear elastic static or dynamic analysis. In Table 1-2, $E_c$ is the modulus of elasticity of concrete per ACI 318 (=$57000\sqrt{f_c'}$ in psi or $4733\sqrt{f_c'}$ in MPa), $I_g$ is the gross moment of inertia, $A_w$ is the web area, and $A_g$ is the gross area of the concrete section, $G_c$ is the concrete shear modulus ($0.4E_c$), $V$ is the wall shear force, $V_c$ is the nominal strength of the concrete, $f_b$ is the bending stress, and $f_{cr}$ is the cracking stress.

ASCE 43-05 refers to ACI 349-01 [ACI (2001)] for the nominal shear strength calculation of reinforced concrete walls. However, ASCE 43-05 notes that the procedure of ACI 349-01 is generally too conservative and presents an alternative shear-strength calculation method, which is presented in Equations 1-9 through 1-11. The procedure is applicable for walls with barbells or flanges that have aspect ratios of less than or equal to 2.0. If the web reinforcement ratios exceed 1.0%, the combined reinforcement ratio $\rho_{se}$ (calculated using Equation 1-11) is limited to 1.0%. ASCE 43-05 procedure imposes an upper limit of $20\sqrt{f_c'}$ on peak shear stress as seen in Equation 1-10.

**Table 1-2 ASCE 43-05 effective stiffness values for reinforced concrete walls**

| Component | Flexural Rigidity | Shear Rigidity | Axial Rigidity |
|---|---|---|---|
| Walls (uncracked) | $E_c I_g$ ($f_b < f_{cr}$) | $G_c A_w$ ($V < V_c$) | $E_c A_g$ |
| Walls (cracked) | $0.5E_c I_g$ ($f_b < f_{cr}$) | $0.5G_c A_w$ ($V > V_c$) | $E_c A_g$ |

$$V_u = v_u d t_n \tag{1-9}$$

$$v_u = \phi\left(8.3\sqrt{f_c'} - 3.4\sqrt{f_c'}\left(\frac{h_w}{l_w} - 0.5\right) + \frac{N_A}{4 l_w t_n} + \rho_{se} f_y\right) \le \phi 20\sqrt{f_c'} \tag{1-10}$$

$$\rho_{se} = A\rho_v + B\rho_h \tag{1-11}$$

In Equations 1-9 through 1-11, $\phi$ is the capacity reduction factor assumed equal to 0.8, $f_c'$ (psi) is the concrete compressive strength, $h_w$ (in) is the wall height, $l_w$ (in) is the wall length, $N_A$ (lb) is the co-existing axial load, $t_n$ (in) is the wall thickness, $\rho_{se}$ is the combined reinforcement ratio calculated using $\rho_h$ (horizontal reinforcement ratio) and $\rho_v$ (vertical reinforcement ratio) and the constants $A$ and $B$ presented in Table 1-3, $f_y$ (psi) is the reinforcement yield strength, $v_u$ (psi) is the ultimate shear stress, $V_u$ (lb) is the shear capacity, and $d$ (in) is the distance from the extreme compression fiber to the center of force of all reinforcement in tension which may be determined from a strain compatibility analysis. If a strain compatibility analysis is not performed $d$ is set equal to $0.6 l_w$.

**Table 1-3 $A$ and $B$ constants used to calculate $\rho_{se}$**

| Aspect Ratio | $A$ | $B$ |
|---|---|---|
| $h_w / l_w \le 0.5$ | 1 | 0 |
| $0.5 \le h_w / l_w \le 1.5$ | $-h_w / l_w + 1.5$ | $h_w / l_w - 0.5$ |
| $h_w / l_w \ge 1.5$ | 0 | 1 |

## 1.4 Research Objectives

The objectives of the research project presented in this report are six-fold, namely,

1. To compile metadata and response data for all tests of squat reinforced concrete walls reported in the literature since the 1950s
2. To evaluate the utility of equations used in the United States to predict the shear strength of squat reinforced concrete walls of differing cross sections

3. To develop new predictive equations for peak shear strength of squat reinforced concrete walls if the existing equations prove unsatisfactory
4. To provide guidance on nonlinear finite element analysis of squat reinforced concrete walls of differing cross sections
5. To develop macro-level hysteretic models for squat reinforced concrete walls
6. To prepare fragility functions, damage states and methods of repair for squat reinforced concrete walls in a form suitable for performance assessment and loss computations.

Collectively, the goal is to improve substantially the state of knowledge on the seismic response of squat (short) reinforced concrete walls.

## 1.5 Report Outline

This report is organized in nine sections, a list of references, and five appendices. Section 1 provides introductory information on squat reinforced concrete walls. Section 2 presents a literature review, which includes a brief summary of the squat wall experiments in the literature and analytical studies that focused on predicting the behavior of squat walls. The literature presented on analytical studies includes a review of existing stiffness and peak shear-strength prediction procedures, macro models used to predict global behavior, and finite element studies. Section 3 presents summary information on a squat wall database assembled using data from tests of 434 walls. (Detailed information is presented on each wall in the database in Appendix A.) Section 4 investigates the performance of five widely used equations to predict the peak shear strength of squat reinforced concrete walls. Section 5 focuses on finite element analysis of squat walls. (Appendix B presents information on the mathematical formulations used to simulate the behavior of reinforced concrete squat walls.) Using the data presented in Section 3 and Appendix A, empirical peak shear strength equations are developed in Section 6. In Section 7, the hysteretic behavior of selected squat walls is simulated using a cyclic deterioration model developed by Ibarra et al. (2005). Fragility functions are developed in Section 8 for squat walls in building and nuclear structures. Three appendices are included to support Section 8, namely, Appendices C, D, and E. Appendix C presents a summary of the assembled damage data; Appendix D presents a discussion on total crack lengths to be repaired using epoxy injection; and Appendix E provides information on scopes of repair for squat reinforced concrete walls. Section 9 summarizes the study, identifies the key conclusions, and provides recommendations for future research. A list of references follows Section 9.

# 2 LITERATURE REVIEW

## 2.1 Overview

This section provides a review of the literature on experimental and analytical studies of squat reinforced concrete walls. The section is organized using two sub-sections: Section 2.2, which presents a summary of the experimental programs conducted on squat reinforced concrete walls; and Section 2.3, which presents a summary of analytical studies used to model squat reinforced concrete walls.

## 2.2 Review of Experimental Programs

A significant number of tests of squat reinforced concrete walls were conducted from 1950 to the time of this writing in countries including the United States, Canada, Chile, England, France, Germany, Japan, New Zealand, Switzerland, Portugal, Mexico, Australia, and Taiwan. These tests were conducted mainly at the component level and mainly on walls with three types of cross sections, namely, rectangular, barbell (rectangular section with columns at wall ends), and flanged (rectangular section with cross walls at the ends). Table 2-1 presents summary information on the experimental programs conducted on squat reinforced concrete walls without openings (solid walls).

## 2.3 Review of Studies on Analytical Modeling

The following subsections introduce studies that focused on analytical modeling of squat reinforced concrete walls. The first sub-section reviews studies on the calculation of elastic stiffness. The second sub-section reviews studies on the calculation of peak shear strength. The third sub-section introduces studies on macro models (backbone curves and fiber-based modeling) that are used to predict global response characteristics (e.g., load-displacement relationships). The last sub-section reviews studies on finite element analysis of squat walls.

### 2.3.1 Wall Stiffness

#### 2.3.1.1 Sozen and Moehle (1993)

Sozen and Moehle (1993) evaluated the utility of elastic stiffness calculation procedures for walls with moment-to-shear ratios of less than 2.0 using experimental data. They calculated the elastic stiffness using strength of materials principles accounting for both flexural and shear deformations and assuming a cantilever wall model with a fixed foundation. Gross section moment-of-inertia was used to calculate flexural deflections and an effective shear area [taken as $A_w/1.2$ for walls with rectangular sections and $A_w/1.1$ for walls with flanges; $A_w$ is the product of wall depth $(l_w)$ with wall web thickness $(t_w)$] was used to calculate shear deflections. Sozen and Moehle (1993) reported that the experimentally measured elastic stiffnesses were consistently less than those calculated using strength of materials principles. They attributed the difference to flexibility beyond the web of the wall such as deformability of base girder,

**Table 2-1 Review of experimental programs on squat reinforced concrete walls**

| Program ID / Reference | Information |
|---|---|
| Galletly / Galletly (1952) | Twelve walls with barbell cross-sections were tested. The moment-to-shear of each wall was 0.72. None of the walls was tested with coexisting axial force. All walls were loaded monotonically. |
| Benjamin / Benjamin and Williams (1953, 1954, 1956) | Walls with barbell cross-sections were tested. Wall moment-to-shear ratios ranged between 0.31 and 1.0. None of the walls was tested with coexisting axial force. All walls were loaded monotonically. |
| Antebi / Antebi et al. (1960) | Sixty walls with barbell cross-sections were tested. Wall moment-to-shear ratios ranged between 0.34 and 0.64. None of the walls was tested with coexisting axial force. Nineteen walls were subjected to blast loads; forty-one walls were loaded monotonically. The tension columns of 9 specimens were strengthened using externally attached steel bars (Walls 21 through 24 and 26 through 30). Three walls failed prematurely by the failure of the welded connection at the base of the tension column (Walls 1 through 3). No data were recorded for two walls (Walls 39 and 42). |
| Barda / Barda (1972) | Eight walls with flanged cross-sections were tested. Wall moment-to-shear ratios ranged between 0.25 and 1.0. None of the walls was tested with coexisting axial force. Two walls were loaded monotonically and six walls were loaded cyclically (quasi-static). |
| Alexander / Alexander et al. (1973) | Five walls with rectangular cross-sections were loaded cyclically (quasi-static). Wall aspect ratios ranged between 0.50 and 1.50. Three walls were tested with coexisting axial forces that ranged between $0.046 A_t f_c'$ and $0.093 A_t f_c'$. Four walls (2, 3, 4, and 5) included additional reinforcement at the interface between the wall-web and foundation. |
| Shiga / Shiga et al. (1973); Shiga et al. (1975) | Seventeen walls with barbell cross-sections were tested. The moment-to-shear ratio of each wall was 0.63. Twelve walls were tested with coexisting axial forces that ranged between $0.146 A_t f_c'$ and $0.321 A_t f_c'$. Two walls were loaded monotonically and fifteen walls were loaded cyclically (quasi-static). |

Note: Program IDs are assigned to each experimental program for identification throughout this report. Program IDs either represent the primary researchers of experiment programs or the organizations associated with test program (e.g., NUPEC).

**Table 2-1 Review of experimental programs on squat reinforced concrete walls (cont'd)**

| | |
|---|---|
| Aoyagi / Hirosawa (1975) | Five walls with barbell cross-sections were cyclically loaded (quasi-static). The moment-to-shear ratio of each wall was 0.50. None of the walls was tested with coexisting axial force. |
| Endo / Hirosawa (1975) | Three 2-story and two 1-story walls with barbell cross-sections were loaded cyclically (quasi-static). Wall moment-to-shear ratios ranged between 0.39 and 0.83. All walls were tested with coexisting axial forces that ranged between $0.053 A_t f_c'$ and $0.070 A_t f_c'$. |
| Hirosawa / Hirosawa (1975) | Fourteen walls with rectangular cross-sections were cyclically loaded (quasi-static). Wall moment-to-shear ratios ranged between 1.0 and 2.0. All walls were tested with coexisting axial forces that ranged between $0.094 A_t f_c'$ and $0.143 A_t f_c'$. |
| Ryo / Hirosawa (1975) | Three walls with barbell cross-sections were tested. Wall moment-to-shear ratios ranged between 0.58 and 0.85. None of the walls was tested with coexisting axial force. One wall was subjected to repeated loading and two walls were loaded cyclically (quasi-static). |
| Sugano / Hirosawa (1975) | Ten walls with barbell cross-sections were tested. Wall aspect ratios ranged between 0.36 and 0.52. Eight walls were tested with coexisting axial forces that ranged between $0.071 A_t f_c'$ and $0.167 A_t f_c'$. Two walls were loaded monotonically and 8 walls were loaded cyclically (quasi-static). |
| Tsuboi / Hirosawa (1975) | Six walls with barbell cross-sections were subjected to repeated loading (quasi-static). The aspect ratio of each wall was 0.50 but the moment-to-shear ratios ranged between 0.80 and 1.77. None of the walls was tested with coexisting axial force. |
| Yoshizaki / Hirosawa (1975) | Fifteen walls with rectangular cross-sections were cyclically loaded (quasi-static). Wall moment-to-shear ratios ranged between 0.54 and 1.08. None of the walls was tested with coexisting axial force. |
| Cardenas / Cardenas et al. (1980) | Seven walls with rectangular cross-sections were tested. The moment-to-shear ratio of each wall was 1.08. None of the walls was tested with coexisting axial force. Six walls were loaded monotonically and one wall was loaded cyclically (quasi-static). |
| Hernandez / Hernandez (1980) | Seven walls with rectangular, four walls with flanged, and nine walls with barbell cross-sections were tested. Moment-to-shear ratios ranged between 0.50 and 2.0. All walls were tested with coexisting axial forces that ranged between $0.058 A_t f_c'$ and $0.126 A_t f_c'$. All walls were loaded cyclically (quasi-static). |

**Table 2-1 Review of experimental programs on squat reinforced concrete walls (cont'd)**

| Program ID / Reference | Information |
|---|---|
| Synge / Synge (1980) | Two walls with flanges and two walls with rectangular cross-sections were cyclically loaded (quasi-static). The moment-to-shear ratio of each wall was 0.57. None of the walls was tested with coexisting axial force. One flanged wall and one rectangular wall included diagonal web reinforcement. |
| Endebrock / Endebrock et al. (1985) | Twelve small-scale ($t_w = 1$ in.) walls with rectangular cross-sections were tested. Eleven walls simulated single story structures ($h_w / l_w = 0.42$); one wall simulated a two-story structure ($h_w / l_w = 1.01$). The experimental program was divided into three groups with respect to testing procedure, namely, *quasi-static tests*, *sine-sweep vibration tests,* and *simulated seismic tests*. Five single story walls (No. 1 through No. 5) were loaded quasi-statically (two monotonic, three cyclic). None of the walls was tested with coexisting axial force. Three walls included additional reinforcement at the interfaces between the wall-web and foundation and wall-web and top beam. *Sine-sweep vibration tests* and *simulated seismic tests* were conducted using an earthquake simulator. Four single story walls (No. 10 through 13) were subjected to *sine-sweep vibration tests*; two single-story (No. 21 and 23) and one two-story (No. 2-2) walls were subjected to *simulated seismic tests*. Tests on earthquake simulator were conducted using 300 lb of additional weight (steel plates) per story. |
| Chiba / AIJ (1985a) | Eight walls with barbell cross-sections were tested using cyclic loading (quasi-static). Wall moment-to-shear ratios ranged between 0.35 and 0.70. All walls were tested with coexisting axial forces that ranged between $0.049 A_t f_c'$ and $0.123 A_t f_c'$. |
| Kabeyasawa / Ogata and Kabeyasawa (1984); Kabeyasawa and Somaki (1985) | Ten walls with barbell cross-sections were tested using cyclic loading (quasi-static). The aspect ratio of each wall was 0.75; the moment-to-shear ratio varied between 0.75 and 2.00 during each test. All walls were tested with coexisting axial forces that ranged between $0.072 A_t f_c'$ and $0.098 A_t f_c'$. Four walls included diagonal web reinforcement (K5, K6, K9, and K10) and one wall (K8) included 45 degree rotated orthogonal reinforcement. |

**Table 2-1 Review of experimental programs on squat reinforced concrete walls (cont'd)**

| Program ID / Reference | Information |
|---|---|
| Maier / Maier and Thürlimann (1985) | Seven walls with flanged and 3 walls with rectangular cross-sections were tested. Moment-to-shear ratios of all walls were 1.02. All walls were tested with coexisting axial forces that ranged between $0.063 A_t f_c'$ and $0.273 A_t f_c'$. Six walls were loaded monotonically and 4 walls were loaded cyclically (quasi-static). One monotonically loaded wall (S10) included additional vertical reinforcement on the tension side and one cyclically loaded wall (S8) included an opening. |
| Wiradinata / Wiradinata (1985) | Two walls with rectangular cross-sections were tested using cyclic loading (quasi-static). Moment-to-shear ratios ranged between 0.33 and 0.58. Neither wall was tested with a coexisting axial force. |
| Yagishita / AIJ (1986c) | Three walls with barbell cross-sections were tested using cyclic loading (quasi-static). The moment-to-shear ratio of each wall was 0.52. Two walls were tested with coexisting axial forces of $0.066 A_t f_c'$ and $0.067 A_t f_c'$, respectively. |
| Fukuzawa / AIJ (1985b) | Twelve walls with barbell cross-sections were tested using cyclic loading (quasi-static). Moment-to-shear ratios ranged between 0.35 and 0.70. Ten walls were tested with coexisting axial forces that ranged between $0.056 A_t f_c'$ and $0.124 A_t f_c'$. |
| Hatori / AIJ (1986b) | Six walls with barbell cross-sections were tested using cyclic loading (quasi-static). The moment-to-shear ratio of each wall was 0.52. Five walls were tested with coexisting axial forces that ranged between $0.055 A_t f_c'$ and $0.116 A_t f_c'$. |
| Taga / AIJ (1986a) | Seven walls with barbell cross-sections were tested using cyclic loading (quasi-static). The moment-to-shear ratio of each wall was 0.55. All walls were tested with coexisting axial forces that ranged between $0.034 A_t f_c'$ and $0.076 A_t f_c'$. |
| Pilette / Pilette (1987) | Two walls with rectangular cross-sections were tested using cyclic loading (quasi-static). The moment-to-shear ratio of each wall was 0.58. Neither wall was tested with a coexisting axial force. |

**Table 2-1 Review of experimental programs on squat reinforced concrete walls (cont'd)**

| Program ID / Reference | Information |
|---|---|
| Sheu / Huang and Sheu (1988, 1994), Cheng (1992), Cheng et al. (1994), Cheng and Yang (1996), Sheu (2007) | Twenty-seven walls with rectangular and 17 walls with barbell cross-sections were tested. Moment-to-shear ratios ranged between 0.65 and 1.90. Four walls with rectangular cross-sections were tested with a coexisting axial force of $0.12 A_t f_c'$ and one wall with barbell cross-section was tested with a coexisting axial force of $0.063 A_t f_c'$. Nineteen walls were loaded monotonically, 3 walls were subjected to repeated loading, and 22 walls were loaded cyclically (quasi-static). |
| Wasiewicz / Wasiewicz (1988) | Two walls with rectangular cross-sections were tested using cyclic loading (quasi-static). Moment-to-shear ratios ranged between 0.33 and 0.58. Neither wall was tested with a coexisting axial force. Additional vertical reinforcement at the interface between the wall web and foundation was placed in both walls with the intention of controlling sliding shear. |
| Saito / Saito et al. (1989) | Nine walls with flanged cross-sections were tested using cyclic loading (quasi-static). Moment-to-shear ratios ranged between 0.47 and 0.94. All walls were tested with coexisting axial forces that ranged between $0.027 A_t f_c'$ and $0.079 A_t f_c'$. |
| Sato / Sato et al. (1989) | Twenty-two walls with flanged cross-sections were tested using cyclic loading (quasi-static). Moment-to-shear ratios ranged between 0.56 and 1.12. All walls were tested with coexisting axial forces that ranged between $0.045 A_t f_c'$ and $0.082 A_t f_c'$. |
| Lefas / Lefas et al. (1990) ; Lefas and Kotsovos (1990) | Seventeen walls with rectangular cross-sections were tested. Moment-to-shear ratios ranged between 1.10 and 2.12. Seven walls were tested with coexisting axial forces that ranged between $0.087 A_t f_c'$ and $0.182 A_t f_c'$. Fourteen walls were loaded monotonically and 3 walls were loaded cyclically (quasi-static). Wall SW25 was reported to have failed prematurely due to an unintended eccentricity that formed during the test. |
| Rothe / Rothe (1992) | Six walls with barbell and 5 walls with rectangular cross-sections were tested. The moment-to-shear ratio of each wall was 1.50. Three walls were tested with coexisting axial forces that ranged between $0.065 A_t f_c'$ and $0.096 A_t f_c'$. One wall was loaded monotonically, 5 walls were loaded cyclically (quasi-static) and 5 walls were tested using an earthquake simulator. |

**Table 2-1 Review of experimental programs on squat reinforced concrete walls (cont'd)**

| Program ID / Reference | Information |
|---|---|
| Mohammadi-Doostdar / Mohammadi-Doostdar (1994) | Two walls with rectangular cross-sections were tested using cyclic loading (quasi-static). Moment-to-shear ratios ranged between 0.82 and 1.09. None of the walls was tested with a coexisting axial force. |
| Pilakoutas / Pilakoutas (1991) | Six walls with rectangular cross-sections were tested using cyclic loading (quasi-static). The moment-to-shear ratio of each wall was 2.13. None of the walls was tested with a coexisting axial force. |
| Seki / Seki et al. (1995) | Six walls with flanged cross-sections were tested using cyclic loading (pseudo-dynamic). Moment-to-shear ratios ranged between 0.59 and 0.98. Three walls were tested with coexisting axial forces that ranged between $0.034 A_t f_c'$ and $0.035 A_t f_c'$. |
| Mo / Mo and Chan (1996) | Twenty walls with flanged cross-sections were tested using cyclic loading (quasi-static). The moment-to-shear ratio of each wall was 0.76. None of the walls was tested with a coexisting axial force. |
| NUPEC / Kitada et al. (1997) | Two walls with flanged cross-sections were tested using an earthquake simulator. The moment-to-shear ratio of both walls was 0.77. Both walls were tested with coexisting axial forces ($0.039 A_t f_c'$ for wall U-1; $0.038 A_t f_c'$ for wall U-2). |
| Hidalgo / Hidalgo et al. (1998) | Twenty-six walls with rectangular cross-sections were tested using cyclic loading (quasi-static). Wall aspect ratios ranged between 0.70 and 2.0 but the corresponding moment-to-shear ratios were 0.35 and 1.0 since the lateral load was applied at the mid-height of the walls. None of the walls was tested with a coexisting axial force. |
| Salonikios / Salonikios et al. (1999) | Eleven walls with rectangular cross-sections were tested using cyclic loading (quasi-static). Moment-to-shear ratios ranged between 1.10 and 1.60. Two walls were tested with a coexisting axial force of $0.07 A_t f_c'$. Four walls included diagonal web reinforcement. One wall was reported to have failed out-of-plane buckling (MSW-2). |
| XiangDong / XiangDong (1999) | Thirteen walls with barbell cross-sections were tested using cyclic loading (quasi-static). The moment-to-shear ratio of each wall was 0.75. All walls were tested with coexisting axial forces that ranged between $0.013 A_t f_c'$ and $0.093 A_t f_c'$. Four walls (FSW-1, FSW-2, FSW-3, and FSW-11) failed prematurely. |

**Table 2-1 Review of experimental programs on squat reinforced concrete walls (cont'd)**

| Program ID / Reference | Information |
|---|---|
| Xie / Xie and Xiao (2000) | One wall with rectangular cross-section was tested using cyclic loading (quasi-static). The moment-to-shear ratio of the wall was 0.59 and the wall was tested with a coexisting axial load of $0.094 A_t f_c'$. |
| Lopes / Lopes and Elnashai (1991) | Seven walls with rectangular cross-sections were tested. The moment-to-shear ratio of each wall was 1.10 whereas the aspect ratio was 1.90. None of the walls was tested with coexisting axial forces. One wall was loaded monotonically and 6 walls were loaded cyclically (quasi-static). One wall included an embedded steel plate to simulate a pre-existing crack. |
| SAFE / Naze and Sidaner (2001) | Thirteen walls with flanged cross-sections were tested using cyclic loading (pseudo-dynamic). All walls had an aspect ratio of 0.40 but the corresponding moment-to-shear ratio was 0.20 since the lateral load was applied at the mid-height of the walls. Three walls were tested with a coexisting axial force of $0.025 A_t f_c'$. Two walls were reported to have failed prematurely (T1 and T2). One wall (T13) was strengthened on both faces of the web using CFRP (carbon fiber reinforced polymer). |
| Palermo / Palermo and Vecchio (2002a) | Two walls with flanged cross-sections were tested using cyclic loading (quasi-static). The moment-to-shear ratio of each wall was 0.76. One wall was tested with a coexisting axial force of $0.054 A_t f_c'$. |
| Bouchon / Bouchon et al. (2004) | Three walls with barbell cross-sections were tested using cyclic loading (quasi-static). All walls had an aspect ratio of 0.40 but the corresponding moment-to-shear ratio was 0.20 since the lateral load was applied at the mid-height of the walls. All walls were tested with coexisting axial forces that ranged between $0.027 A_t f_c'$ and $0.035 A_t f_c'$. Only one wall (No.3) was loaded to its peak shear strength. |
| Greifenhagen / Greifenhagen et al. (2005) | Four walls with rectangular cross-sections were tested using cyclic loading (quasi-static). Moment-to-shear ratios of all walls were 0.69. All walls were tested with coexisting axial forces that ranged between $0.022 A_t f_c'$ and $0.095 A_t f_c'$. |

**Table 2-1 Review of experimental programs on squat reinforced concrete walls (cont'd)**

| Program ID / Reference | Information |
|---|---|
| Massone / Massone (2006) | Ten walls with rectangular cross-sections were tested using cyclic loading (quasi-static). Six walls were identified as *piers* in Massone (2006) four of which were tested with coexisting axial force that ranged between $0.05 A_t f_c'$ and $0.10 A_t f_c'$. Remaining four walls were tested without axial forces [identified as *spandrels* in Massone (2006)] and included weakened joints at the mid-heights of the walls created by cutting the vertical web reinforcement and reducing the wall thickness. Aspect ratios of the *piers* were 0.89 whereas the moment-to-shear ratios were 0.44 since the load was applied at the mid-height of the walls. Aspect ratio of the *spandrels* was 1.0 and the corresponding moment-to-shear ratio was 0.50. |
| Farvashany / Farvashany et al. (2008) | Seven walls with flanged cross-sections were tested using monotonic loading. The moment-to-shear ratio of each wall was 1.36. All walls were tested with coexisting axial forces that ranged between $0.043 A_t f_c'$ and $0.216 A_t f_c'$. High-strength concrete was used for the walls in the test program with $f_c'$ ranging between 84 MPa and 104 MPa (12.2 ksi and 15.1 ksi). |
| Kuang / Kuang and Ho (2008) | Eight walls with rectangular cross-sections were tested using cyclic loading (quasi-static). Moment-to-shear ratios ranged between 1.13 and 1.63. All walls were tested with a coexisting axial force of $0.15 A_t f_c'$. One wall included crossties between the vertical web reinforcement. |

reinforcement slip, and cracks at the wall-girder junctions. Sozen and Moehle (1993) proposed a modification to the calculation of flexural stiffness that accounts for these sources of flexibility.

### 2.3.1.2 Farrar and Baker (1993)

An experimental program focusing on seismic behavior of reinforced concrete components used in nuclear power plants (The Seismic Category I Structures Program) started in 1980 at Los Alamos National Laboratory (LANL) with the sponsorship of Nuclear Regulatory Commission's Office of Nuclear Regulatory Research. The objective of the program was to investigate the response characteristics of *Category I Reinforced Concrete Structures*, which included one- and two-story isolated walls (1/30 scale, 1 in. thick walls), one- and two-story diesel generator buildings (1/10 and 1/30 scale), three-story auxiliary buildings (1/42 and 1/14 scale) and flanged walls with heavily reinforced top and bottom slabs under seismic loading. The experimental program included tests of 37 shear wall structures using quasi-static (monotonic and cyclic) and dynamic (sine sweep, random, simulated seismic and impulse) loading. The test results of isolated walls, diesel generator and auxiliary buildings indicated that the experimentally

measured elastic stiffnesses were lower than those calculated using strength-of-materials principles [Endebrock et al. (1985), Dove et al. (1987), Bennett et al. (1987a), Bennett et al. (1987b), Bennett et al. (1988)]. The focus of the program was then shifted to estimation of elastic stiffness of reinforced concrete walls. A final series of tests were performed on 15 TRG[1] walls (TRG-1 and TRG-3 through TRG-16)[2] [Farrar et al. (1989), Farrar et al. (1990a), Farrar et al. (1990b), Farrar et al. (1991), Farrar and Baker (1993)]. Based on the outcome of the tests of the TRG walls, the researchers concluded that the overestimation of the experimentally measured values of elastic lateral stiffness using strength-of-materials principles for the earlier tests and for TRG-1, TRG-3, and TRG-6 walls were due to damage that occurred during transportation, lack of adequate resolution in the instrumentation and rocking of the earthquake simulator. Farrar and Baker (1993) stated that the results of these tests were not as reliable as the subsequent tests (TRG-4, TRG-5 and TRG-7 through TRG-16) for which the experimentally measured stiffnesses were comparable to those calculated using strength-of-materials approaches or finite element models. They noted that the best estimates using strength-of-materials principles were obtained assuming that flanges were fully effective in contributing to the flexural stiffness of the walls. The study recommended that the use of stiffness reduction factors to calculate effective stiffnesses of walls be abandoned.

#### 2.3.1.3 ASCE (1994)

A report [ASCE (1994)] prepared by the working group on the stiffness of concrete shear wall structures of the ASCE dynamic analysis committee reviewed the in-plane stiffness calculation procedures for squat reinforced concrete walls used in nuclear power plants. The study recommended using two elastic stiffness estimates (lower and upper bound) to address the variation of elastic wall stiffness. Lower and upper bounds on elastic stiffness were calculated using strength-of-materials principles with the only difference being in the estimation of the modulus of elasticity and shear modulus used for the calculations. The calculated values of the modulus of elasticity (per ACI) and shear modulus (using elasticity) were both decreased by 25% to calculate the lower bound estimate on elastic stiffness whereas they were both increased by 25% to calculate the upper bound estimate. The upper bound sought to account for the probability of $f_c'$ being higher than the specified 28-day strength. The lower bound was based on experimental data and assumptions regarding variation of concrete quality in the field.

### 2.3.2 Peak Shear Equations

Peak shear strength is the major response variable in force-based design and performance assessment. The following sub-sections review four procedures used to calculate the peak shear strength of squat reinforced concrete walls.

#### 2.3.2.1 Fukuzawa et al. (1988)

Fukuzawa et al. (1988) used an empirically derived relationship, presented in Equations 2-1 through 2-6 herein, to calculate the peak shear strength of barbell walls. The procedure summed

[1] Reinforced concrete walls with flanges named after the Technical Review Group (TRG) that proposed the wall geometry for testing.
[2] TRG-2 was not tested because of cracks formed during curing.

the contributions of concrete ($\alpha\tau_c$) calculated per Equation 2-4, web reinforcement ($\tau_s$) calculated per Equation 2-5, and axial force ($\tau_0$) calculated per Equation 2-6 to estimate the peak shear strength. The contribution of concrete to peak shear strength was calculated using a parameter ($\alpha$) that was a function of the ratio of total area of barbells ($\Sigma A_c$) to effective wall area ($A_w$), therefore, the procedure explicitly accounted for the effect of (boundary) barbells on peak shear strength. The calculation of $\alpha$ is per Equation 2-3 and the effective wall area is calculated as the product of wall length measured from the centers of the boundary barbells ($D$) with wall thickness ($t_w$).

$$V_{peak} = \tau_{peak} t_w D \tag{2-1}$$

$$\tau_{peak} = \alpha\tau_c + \tau_s + \tau_o \tag{2-2}$$

$$\alpha = 0.4 + \frac{\Sigma A_c}{A_w} \quad \text{for} \quad \frac{\Sigma A_c}{A_w} \le 0.6$$
$$\alpha = 1 \quad \text{for} \quad \frac{\Sigma A_c}{A_w} > 0.6 \tag{2-3}$$

$$\tau_c = 2.7\sqrt{f_c'}\left(1.9 - 1.5\frac{M}{QD}\right) \tag{2-4}$$

$$\tau_s = \frac{\rho_w f_y}{2} \quad ; \quad \rho_w f_y \le 6\sqrt{f_c'} \quad ; \quad \rho_w \le 2.4\% \tag{2-5}$$

$$\tau_o = P / A_t \tag{2-6}$$

In Equations 2-4 through 2-6, $f_c'$ (kg/cm$^2$) is the concrete compressive strength, $M/QD$ is the moment-to-shear ratio, $\rho_w$ is the web reinforcement ratio[3], $f_y$ (kg/cm$^2$) is the corresponding yield stress, $P$ (kg) is the axial force on the section and $A_t$ (cm$^2$) is the total wall area. The applicability of the Fukuzawa et al. (1988) procedure is limited to the range of the data it was generated; the moment-to-shear ratios ($M/QD$) ranged between 0.4 and 0.8, $f_c'$ ranged between 150 kg/cm$^2$ (14.7 MPa) and 600 kg/cm$^2$ (58.9 MPa), $\tau_0$ ranged between 0 and 40 kg/cm$^2$ (3.9 MPa) and the ratio of $\Sigma A_c / A_w$ was $\ge 0.2$. Note that Fukuzawa et al. (1988) procedure requires the use of kg/cm$^2$ as the stress unit.

[3] The procedure assumes equivalent horizontal and vertical web reinforcement ratios therefore the variable $\rho_w$ refers to both.

### 2.3.2.2 Barda et al. (1977)

Barda et al. (1977) proposed Equation 2-7 to calculate the peak shear strength of squat reinforced concrete walls. The equation was derived using experimental data from tests of 8 squat walls with heavily reinforced flanges.

$$V = \left( 8\sqrt{f_c'} - 2.5\sqrt{f_c'}\frac{h_w}{l_w} + \frac{N_u}{4l_w h} + \rho_n f_y \right) hd \tag{2-7}$$

In Equation 2-7, the shear strength attributed to concrete (first two terms in parenthesis) increases with decreasing aspect ratio. In Equation 2-7, $N_u$ (lb) is the axial force, $\rho_n$ is the vertical web reinforcement ratio, $f_c'$ (psi) is the concrete compressive strength, $h_w$ (in) is the wall height, $l_w$ (in) is the wall length, $h$ (in) is the web thickness, $d$ (in) is the distance from extreme tension fiber to centroid of tension reinforcement, and $f_y$ (psi) is the yield stress for the vertical web reinforcement.

### 2.3.2.3 Wood (1990)

Wood (1990) evaluated experimental peak shear strength data obtained from 143 squat wall tests. Wood (1990) proposed a semi-empirical equation based in part on a shear-friction analogy to estimate the peak shear strength of squat walls:

$$6\sqrt{f_c'} \le \frac{A_{vf} f_y}{4A_{cv}} \le 10\sqrt{f_c'} \tag{2-8}$$

where $f_c'$ (psi) is the concrete compressive strength, $A_{vf}$ (in$^2$) is the area of total vertical reinforcement in the wall, $f_y$ (psi) is the yield stress associated with vertical reinforcement in the wall, and $A_{cv}$ (in$^2$) is effective wall area equal to the product of web thickness ($t_w$) and wall length ($l_w$).

### 2.3.2.4 Hwang et al. (2001)

Hwang et al. (2001) developed a strut-and-tie model to predict the peak shear strength of squat walls for which the governing failure mode was diagonal compression. Three strut-and-tie load paths associated with the load transfer through a diagonal concrete strut, vertical reinforcement, and horizontal reinforcement are used in the model. The lateral shear force is assigned to these resistance mechanisms on the basis of their stiffness. The behavior of cracked concrete was represented using the concrete softening model of Zhang and Hsu (1998). Reinforcement was modeled using a bilinear relationship with no strain hardening. The authors assessed the performance of their model using experimental data for 62 squat walls. The cross-sections for the selected walls were rectangular, barbell and flanged and the failure mode was diagonal compression only. The mean ratio for experimental to predicted peak shear strength was 1.18 with a coefficient of variation of 0.17. The model underestimated the peak shear strength of

walls with boundary elements whereas it accurately predicted the peak shear strength of rectangular walls.

### 2.3.3 Macro Models

Macro models are used to predict the response (e.g., load-displacement relationships) of structural components. These models have two advantages over more complex finite element models (see Section 2.3.4), namely, a) easier modeling that involves fewer analysis parameters, and b) significantly less computation time. The following sub-sections present a summary of backbone models and relatively more sophisticated fiber-based models, respectively, used to model squat reinforced concrete walls.

#### 2.3.3.1 Backbone Curves

Sozen and Moehle (1993) proposed a backbone model to predict the load-displacement response of squat reinforced concrete walls up to peak shear strength. The total wall deformation was computed as the sum of flexural, shear and slip deformations. Each source of flexibility was modeled using a spring. The flexural spring was trilinear with changes in stiffness associated with cracking and yielding. The post-yielding stiffness was positive. The shear spring was bilinear with the single break point corresponding to shear cracking. The slip spring was linear. The method showed reasonable correlation with some experimental data but the utility of the method is limited to the accurate definition of the break points and the slopes for the springs.

Wallace (2007) modified the ASCE 41-06 [ASCE (2007)] backbone curve used to model the response of reinforced concrete walls governed by shear. The ASCE 41-06 backbone curve is presented in Figure 1-8 and the backbone curve proposed by Wallace (2007) is presented in Figure 2-1.

The modification of Wallace (2007) to the ASCE 41-06 backbone curve was the inclusion of a cracking point that is denoted as *F* in Figure 2-1. The cracking point in the Wallace (2007) model corresponds to the shear strength of the component at cracking ($V_{cr}$) defined by Equation 2-9. The drift angle ($\gamma_{cr}$) at $V_{cr}$ is calculated using Equation 2-10.

$$V_{cr} = 4\sqrt{f_c'}\sqrt{1+\frac{P/A_g}{4\sqrt{f_c'}}}A_{cv} < 0.6V_n \tag{2-9}$$

$$\gamma_{cr} = \frac{V_{cr}}{0.4A_{cv}E_c} \tag{2-10}$$

In equations 2-9 and 2-10, $V_n$ (lb) is the nominal shear strength, $f_c'$ (psi) is the concrete compressive strength, $A_{cv}$ (in$^2$) is the wall area calculated using wall length and web thickness, $A_g$ (in$^2$) is the gross area of the wall cross-section, $P$ (lb) is axial force and $E_c$ (psi) is the modulus of elasticity of concrete. The nominal shear strength ($V_n$) corresponding to points *B* and *C* in Figure 2-1 is calculated using the equation of Chapter 21.9 of ACI 318-08 [ACI (2008)]. In Figure 2-1, $g$ is the drift ratio corresponding to the development of nominal shear

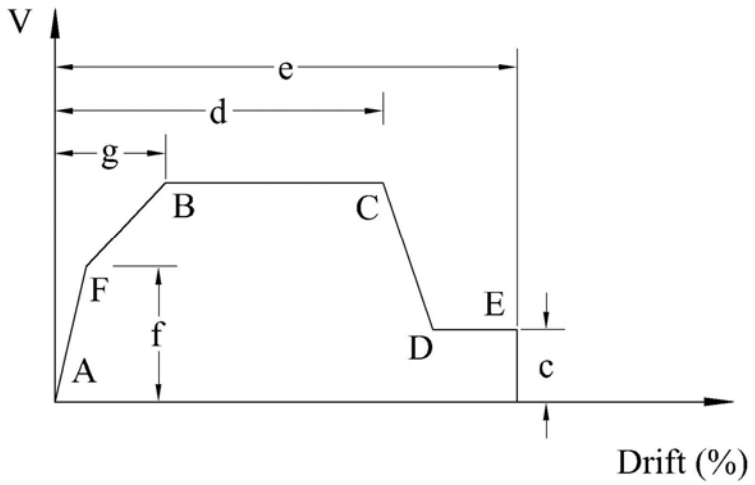


**Figure 2-1 Load-displacement relationship proposed by Wallace (2007)**

strength, $d$ is the drift ratio corresponding to the initiation of strength degradation, $e$ is the ultimate drift ratio, and $c$ is the residual strength ratio, given as a decimal fraction of the nominal shear strength. The default values of $g$, $d$, $e$, and $c$ are specified as 0.4, 1.0, 2.0 and 0.2, respectively for walls with axial forces less than or equal to $0.05A_g f_c'$ and the corresponding values for walls with axial forces higher than $0.05A_g f_c'$ are 0.4, 0.75, 1.0 and 0.0, respectively.

### 2.3.3.2 Fiber-Based Models

Following full-scale testing of a seven-story reinforced concrete building, Kabeyasawa et al. (1982) developed three vertical line element model (TVLEM) to predict the global response of reinforced concrete structural walls. TVLEM consisted of three vertical line elements surrounded by rigid beams at the top and bottom, which represented floors of a prototype structure. The outer vertical elements model the axial stiffness of boundary columns of the wall and the inner element consisted of vertical, horizontal, and rotational springs to model the behavior of wall web. The axial stiffness of the vertical elements was modeled empirically and the rotational and horizontal springs of the central element were represented using an origin-oriented hysteresis model (OOHM). Although the TVLEM formulation showed reasonable agreement with experimental results, its utility was limited by a) difficulties in defining the properties of the springs representing the panel due to their empirical structure, and b) the inherent incompatibility that exists between the wall panel and boundary columns.

Vulcano et al. (1988) modified the TVLEM formulation to include multiple vertical elements (MCPM or MVLEM) for the wall panel. In MVLEM formulation, the vertical elements were modeled using a mechanically derived axial stiffness hysteresis model and material modeling was improved using more advanced constitutive models [i.e., Menegotto and Pinto (1973) model for steel, Colotti and Vulcano (1987) model for uncracked concrete, and Bolong et al. (1980) or cracked concrete]. In this approach, the two outer vertical elements modeled the axial stiffness of the boundary columns and the inner vertical elements modeled the axial and flexural behavior of the wall web. A horizontal spring with an origin-oriented hysteresis model (OOHM) simulated the nonlinear shear response of the wall. The formulation of MVLEM addressed some of the

shortcomings of the TVLEM and produced improved predictions of the global response of slender walls. However, the relative contributions of shear and flexural deformations to overall deformations varied significantly with the selection of model parameters and did not correlate well with the experimental results, which is later attributed to the interaction between flexural and shear deformations [Orakcal et al. (2006)].

Massone and Wallace (2004) conducted experiments on slender reinforced concrete walls to investigate the nature of interaction between shear and flexural deformations. The study concluded that shear deformations are affected by flexural yielding and are not linear even for slender reinforced concrete walls whose response is dominated by bending. Orakcal et al. (2006) modified the MVLEM formulation to include coupled shear and flexural behavior. The model included horizontal springs on all vertical elements as instead of the single horizontal spring used for multiple vertical elements in the original MVLEM formulation. The interaction between shear and flexure at the fiber level is accounted for by treating each line element as a reinforcement concrete panel. A rotating angle panel constitutive model [Rotating angle softened truss model (RA-STM), Pang and Hsu (1995)] was used to represent the constitutive behavior of the panel. The Orakcal et al. (2006) model reasonably predicted the shear and flexural deformations observed in slender wall tests. However, the model had limited success in predicting the response of squat reinforced concrete walls. The accuracy of the model diminished with decreasing moment-to-shear ratio. The relatively poor performance of the model for squat walls was attributed to the use of a zero-resultant horizontal stress at every location on the wall and a uniform distribution of shearing strains along the wall length. Each of these modeling assumptions is violated in squat reinforced concrete walls.

## 2.3.4 Finite Element Modeling of Squat Reinforced Concrete Walls

A brief summary of finite element applications to reinforced concrete is presented in Section 2.3.4.1. Section 2.3.4.2 presents a review of studies on finite element modeling of squat reinforced concrete walls.

### 2.3.4.1 Background – Finite Element Modeling of Reinforced Concrete

Simplified methods, although they are in general derived empirically using experimental data, fail to provide accurate predictions of reinforced concrete behavior in many cases. This may be attributed to complex behavior of reinforced concrete that can be characterized by a) cracking, b) nonlinear time-dependent (i.e., creep, shrinkage) material behavior of concrete that is significantly affected by multiaxial loading conditions, c) interaction between concrete and reinforcement (bond characteristics), d) tension stiffening, e) aggregate interlock (friction), and f) dowel action of reinforcement. These response characteristics are also influenced by the type of the boundary conditions and loading protocol (i.e., cyclic loading), and the rate at which loading is applied to the specimen (strain rate). Finite element modeling of reinforced concrete structures began in earnest in the early 1970s to address some of these complexities. Various constitutive models and modeling techniques have been implemented to model the local and global response of reinforced concrete structures.

Ngo and Scordelis (1967) published the first study on finite element analysis of a structural reinforced concrete component: a beam subjected to two-point loading. The concrete was assumed to be linear elastic and a pre-selected cracking pattern was defined using link elements

represented the nonlinear behavior. Nilson (1968) improved the solution technique developed by Ngo and Scordelis (1967) by 1) incorporating nonlinear material properties and bond-slip relationships, and 2) tracing the tensile failure of concrete for each crack and updating the mesh topology as the cracking progressed. The studies conducted by Ngo and Scordelis (1967) and Nilson (1968) used a discrete-crack representation, which models cracks explicitly by updating the finite element mesh (separation of nodes). Another viable crack-representation method for finite element modeling is the smeared-crack approach that was developed by Rashid (1968) who analyzed prestressed concrete reactor structures using axisymmetric finite elements. The procedure introduced by Rashid represented cracked concrete as an orthotropic material. In the smeared-crack representation, an average stress-strain relationship for cracked concrete is adopted in each principal direction and the behavior of cracked concrete is defined in a continuous manner.

Although the early finite element work on reinforced concrete was based on discrete cracking, the smeared-crack approach gained popularity quickly due to its simplicity. According to Sittipunt and Wood (1993), there are three major drawbacks in using discrete crack approach: 1) cracking can occur only along element boundaries which introduces bias into the finite element solution, 2) unless the cracks in the model are pre-defined, cracking will cause continuous updating of the mesh topology as it progresses, destroying the narrow bandwidth in the structural stiffness matrix, and 3) following the separation of nodes, crack closing and reopening has to be defined using a contact algorithm that significantly complicates the problem. In contrast, the smeared-crack approach has the advantage of utilizing the same mesh topology for a given structure throughout the analysis. However, for lightly reinforced structures whose response is dictated by a few, wide cracks, the use of discrete-crack approach is a viable alternative. Application of models formulated using the smeared-crack approach is appropriate for reinforced concrete components with homogeneously distributed cracks.

The constitutive modeling of cracked concrete consists of two key components for the smeared-cracking model [Sittipunt and Wood (1993)]: 1) stress-strain relationship, and 2) crack model. ASCE (1993) identifies the stress-strain behavior of concrete under various stress states using: 1) elasticity theory, 2) plasticity theory, 3) fracture processes, and 4) endochronic theory. There are two widely used models to represent cracking, namely, the fixed-crack model and the rotating-crack model. In both models, cracks initiate in a direction perpendicular to the principal tensile stresses when the principal tensile stress in the element exceeds a limiting value that is defined by the user. The material then becomes orthotropic with different material properties normal and parallel to the cracks. In the fixed-crack model, the crack direction remains fixed throughout the analysis whereas in the rotating-crack model, the crack directions are not fixed but are continuously aligned orthogonal to the principal tensile stresses.

Originally developed for axisymmetric elements, smeared modeling of cracks along with orthotropic material properties were also widely used to model biaxial loading conditions, a load state that is appropriate for modeling squat reinforced concrete walls since their thickness is modest in comparison with their length and height. Cervenka (1970) was the first to use a smeared-crack approach with a plane stress formulation. Cervenka (1970) used results of reinforced-concrete panel experiments to evaluate numerical results. In the years that followed, smeared-crack solution techniques were further refined with the development of more advanced constitutive models for concrete and reinforcement. The reinforced concrete panel experiments conducted by Vecchio and Collins (1982) have played a key role in development of new

constitutive models for the plane stress state [ASCE (1993)]. Each panel test was analogous to a single element in homogeneous stress state. These experiments gave the finite element analysts the opportunity to improve their procedures and better match the experimental behavior of reinforced concrete.

The evolution of constitutive models, modeling and solution techniques for finite element modeling of reinforced concrete structures over the years is discussed in the *State of the Art Reports* prepared by American Society of Civil Engineers [ASCE (1982, 1986, 1993)].

### 2.3.4.2 Previous Research on Finite Element Modeling of Squat Walls

In 1991, the Nuclear Power Engineering Corporation (NUPEC) tested two squat walls with flanges to failure using an earthquake simulator to investigate their response under dynamic loading. The responses of the walls tested by NUPEC were then simulated by researchers who volunteered to participate in the *Seismic Shear Wall International Standard Problem* (SSWISP) organized by NUPEC. Forty-seven analytical simulations were made of the response of the dynamically tested walls. Thirty-one of these simulations used finite element analysis, 10 used simplified models, and 6 used lumped mass models. The finite element analyses used commercial software such as ABAQUS, ADINA, and DIANA and research-oriented software. The concrete models considered in the analyses were mostly of the smeared-crack type. Details of these simulations are reported in OECD/NEA/CSNI (1996). The finite element analysis results presented in the OECD report indicate that a) the effect of variation in the tension-stiffening models on the response was relatively modest, b) the majority of the predicted elastic stiffnesses were within 15% of the experimentally measured values, c) two 2-D models that assumed an effective flanged width of 1000 mm better simulated the lateral stiffness of the walls than a 2-D model that assumed fully effective flanges (2980 mm), d) the simulations that did not model the wall foundation performed similarly in predicting lateral stiffness to the simulations that modeled the wall foundation, e) the peak shear strengths predicted by the finite element analysis simulations varied between 65% and 115% of the experimentally measured values, f) the displacements at peak shear strength predicted by the simulations varied between 25% and 185% of the experimentally measured displacement at peak shear, and g) neither the fixed-crack nor the rotating-crack formulations performed better than the other.

Asfura and Bruin (1997) simulated the response of wall U-1 tested by NUPEC [Kitada et al. (1997)] using IDARC2D [Reinhorn et al. (1996)], FEM-I [Ewing, Kariotis, Englekirk & Hart (1990)], ADINA [ADINA R&D, Inc. (1995)]: three finite element codes. Fiber modeling was used to model the wall in IDARC2D and plane stress elements were used to model the wall in FEM-I and ADINA. An effective flange width of 24% of the total flange width as calculated per Paulay and Priestley (1992) was assumed for the analyses. Asfura and Bruin (1997) concluded that the models simulated the wall response successfully up to first yielding. The lateral stiffness of the wall was generally overestimated by the three codes following the first yielding of reinforcement. The authors concluded that assumption of an effective flange width of 24% of the total flange width was reasonable.

Ile et al. (1998) presented finite element analysis results that simulated the response of NUPEC wall U-1. The analyses were performed using a 2-D model constructed with 3-node plane stress elements and a 3-D model constructed shell elements. Reinforcement was modeled discretely using truss elements. Ottosen's four-parameter failure criterion with isotropic hardening and an

associated flow rule was used to represent the behavior of concrete. Cracks were modeled as smeared and fixed. Reinforcement was modeled as plastic with isotropic hardening. Perfect bond was assumed between reinforcement and concrete. Ile et al. (1998) concluded that a) the overall response predicted using 2-D and 3-D formulations were similar, b) the predicted crack orientation in the wall web was consistent with that of the experiment, c) the strains in the flange reinforcement were predicted more accurately using the 3-D model, and d) the experimental failure mode of the wall could not be reproduced by any of the models.

Kwak and Kim (2001) proposed an orthotropic constitutive model based on smeared rotating crack approach to predict the behavior of reinforced concrete walls subjected to in-plane monotonic loading. The formulation was later extended to simulate cyclic loading [Kwak and Kim (2004)]. The model proposed by Kwak and Kim (2001) used the compression softening relationship proposed by Vecchio and Collins (1986), which reduces the compressive strength of concrete as a function of principal tensile strains. A new tension-stiffening algorithm was implemented in the concrete model to account for the effect of reinforcement in horizontal and vertical directions. Reinforcement was smeared and its behavior was defined using a bilinear stress-strain relationship that included strain hardening. Perfect bond between the concrete and the reinforcement was assumed. The model was used to predict the behavior of six squat reinforced concrete walls (SW13, SW16, SW21, SW22, SW24, SW25) tested by Lefas et al. (1990). The analyses were conducted for two cases: with and without tension stiffening. Kwak and Kim (2001) concluded that the proposed model including tension stiffening could reasonably predict the experimental load-displacement relationships and the failure modes. The analyses conducted without tension-stiffening underestimated the experimentally measured lateral stiffnesses of the walls following the initiation of cracking.

Palermo and Vecchio (2002a) tested two squat flanged walls, which had a similar geometry to the NUPEC walls. One of the walls was tested with an additional axial compressive force of 5.4% of the product of total wall area and $f_c'$. The experimental responses of the walls were simulated using the *Modified Compression Field Theory* (MCFT) formulation [Vecchio and Collins (1986)], which uses a smeared rotating crack approach. VecTor2, an in-house finite element analysis software, developed at the University of Toronto was used to perform the analyses. The software included a 2-D implementation of the MCFT formulation and is capable of simulating cyclic loading. Rectangular 4-noded constant strain elements were used to mesh the finite element models of the walls and reinforcement was smeared. Flanges were assumed to be fully effective and defined using elements of corresponding width (3045 mm). A shrinkage strain of $-0.4 \times 10^{-3}$ was applied in the finite element analysis, which was used to account for the delay between the casting and testing. The predicted peak shear strengths were within 2% and 17% of the experimentally measured peak shears for walls DP-1 and DP-2, respectively. The failure mode for wall DP-1, which was associated with significant concrete crushing in the wall web, was successfully predicted. The failure of wall DP-2 was due to sliding between the top slab and wall web, which was unexpected. This failure mode could not be captured using the finite element model. The authors attributed the relatively inaccurate prediction of the response of wall DP-2 to lower concrete strength near the intersection between of wall web and top slab. The authors also constructed finite element models for walls SW4, SW5 and SW6 tested by Pilakoutas and Elnashai (1995). These walls had an aspect ratio of 2.0 and had mixed failure modes. The predicted responses of walls SW4 and SW6 were in good agreement with the experimentally measured responses whereas the experimental response of wall SW5 was

predicted with less accuracy. The authors attributed the difference in part to the use of smooth reinforcement in the experiments.

# 3 SQUAT WALL DATABASE

## 3.1 Introduction

Gulec (2005) reviewed and catalogued the results of tests of 352 reinforced concrete squat walls with three different cross-section types, namely, rectangular, barbell, and flanged. This database was expanded to 434 walls. Of the 434 walls in the database, 150 have a rectangular cross section and 284 have boundary elements [barbells (191), flanges (93)]. The assembled data can be used to assess the performance of existing models that are used to predict squat wall response and to develop new models. Detailed information for each wall in the database is tabulated in Appendix A. In this section, a brief summary of the assembled data is presented. The test specimens in the database are selected using the following criteria: 1) a minimum web thickness of 5 cm. (1.97 in.); 2) symmetric reinforcement layout; 3) no diagonal reinforcement or additional wall-to-foundation reinforcement to control sliding shear; and 4) aspect ratios $(h_w / l_w)$ less than or equal to 2.0. Walls that do not comply with these criteria are not included in the 434-wall database and information on these walls is not presented.

Figure 3-1 presents the variation of the experimentally measured peak shear strength ($V_{peak}$) with moment-to-shear ratio[1] ($M/Vl_w$) for the walls in the database. In the figure, the experimental peak shear strength is normalized by the product of $A_w$ and $\sqrt{f_c'}$, where $A_w$ is the web area calculated as the product of the wall length ($l_w$) and the web thickness ($t_w$), and $f_c'$ is the concrete compressive strength. The data presented in Figure 3-1 shows that the experimental peak shear strength for walls with boundary elements is generally much higher than those of the walls with rectangular cross-sections. Figure 3-1 indicates that the ranges of measured peak shear strengths for barbell and flanged walls are comparable. The normalized peak shear strengths for rectangular walls are generally smaller than $10\sqrt{f_c'}$ whereas the majority of the normalized peak shear strengths for walls with boundary elements exceed $10\sqrt{f_c'}$, which is the upper limit on the peak shear strength equation of Section 21.9 of ACI 318-08. As shown in Sections 1 and 2, the peak shear strength calculation procedures for reinforced concrete walls generally do not recognize the effects of boundary elements. For two walls, one with a rectangular cross-section and the other with boundary elements, the current procedures predict identical peak shear strengths provided that the walls have the same web area, reinforcement ratio, aspect ratio, axial force and $f_c'$. Neither wall-cross section type nor boundary element reinforcement are considered as variables for calculating peak shear strength. These issues are addressed in the following sections.

Sections 3.2, 3.3 and 3.4 present summary information on rectangular, barbell and flanged walls in the database, respectively. In these sections, monotonic loading refers to incrementally increasing the load in one direction until failure; repeated loading refers to loading in one direction, unloading to the origin, and reloading to a similar or larger displacement in the same direction; cyclic loading refers to application of lateral force alternatively in both horizontal

[1] Moment-to-shear ratio is normalized by the wall length in this study.

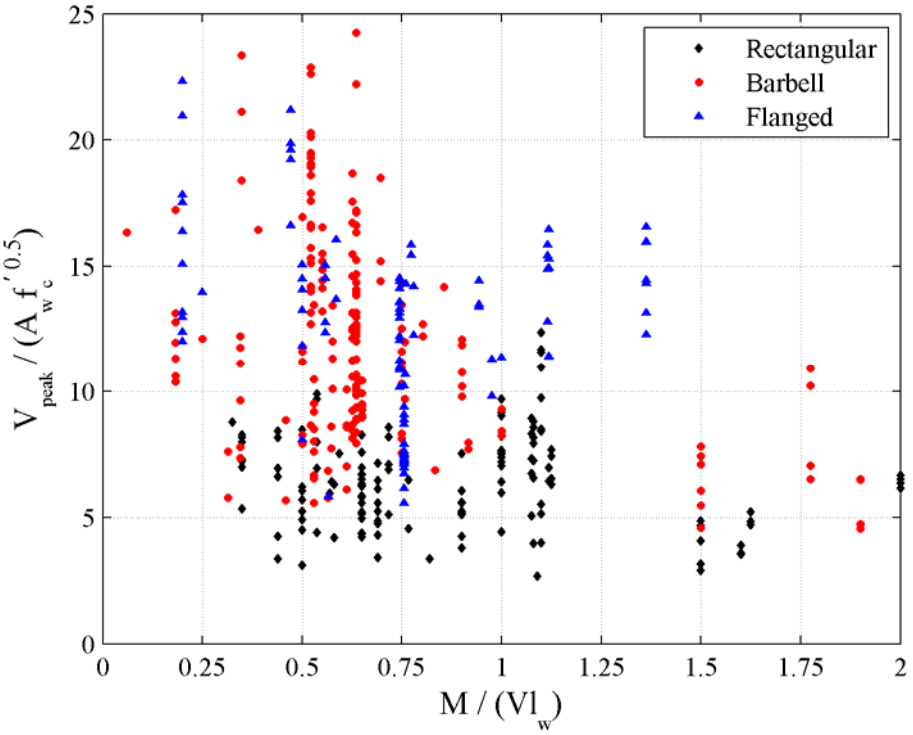


**Figure 3-1 Variation of shear stress [normalized by the product of web area ( $A_w$ ) and $\sqrt{f'_c}$ ] obtained using experimentally determined peak shear strength ( $V_{peak}$ ) with moment-to-shear ratio ( $M/Vl_w$ )**

directions with incremented force or displacement following a conventional quasi-static cyclic testing protocol; dynamic loading refers to the use of earthquake simulators; and blast loading refers to application of large amplitude dynamic pulses.

## 3.2 Walls with Rectangular Cross-Section

The rectangular-wall database included experiments of 150 specimens at various scales. The data for the 150 rectangular wall tests were obtained from Alexander et al. (1973), Hirosawa (1975), Cardenas et al. (1980), Synge (1980), Maier and Thürlimann (1985), Wiradinata (1985), Pilette (1987), Huang and Sheu (1988, 1994), Lefas and Kotsovos (1990), Lefas et al. (1990), Pilakoutas (1991), Rothe (1992), Cheng (1992), Cheng et al. (1994), Mohammadi-Doostdar (1994), Cheng and Yang (1996), Hidalgo et al. (1998), Salonikios et al. (1999), Xie and Xiao (2000), Greifenhagen et al. (2005), Massone (2006), Sheu (2007), and Kuang and Ho (2008). Figure 3-2 presents summary information on the 150 rectangular walls included in this database. Wall aspect ratios (wall height divided by wall length) ranged between 0.25 and 2.0; moment-to-shear ratios ranged between 0.33 and 2.13; web thickness ranged from 2.36 to 6.30 in. (60 to 160 mm); wall length varied between 23.6 and 118.1 in. (600 and 3000 mm); wall height varied between 19.7 and 78.7 in. (500 and 2000 mm); 45 walls were tested with coexisting axial load[2]

[2] Self-weight of the walls are not included in the axial load calculations presented in this chapter.

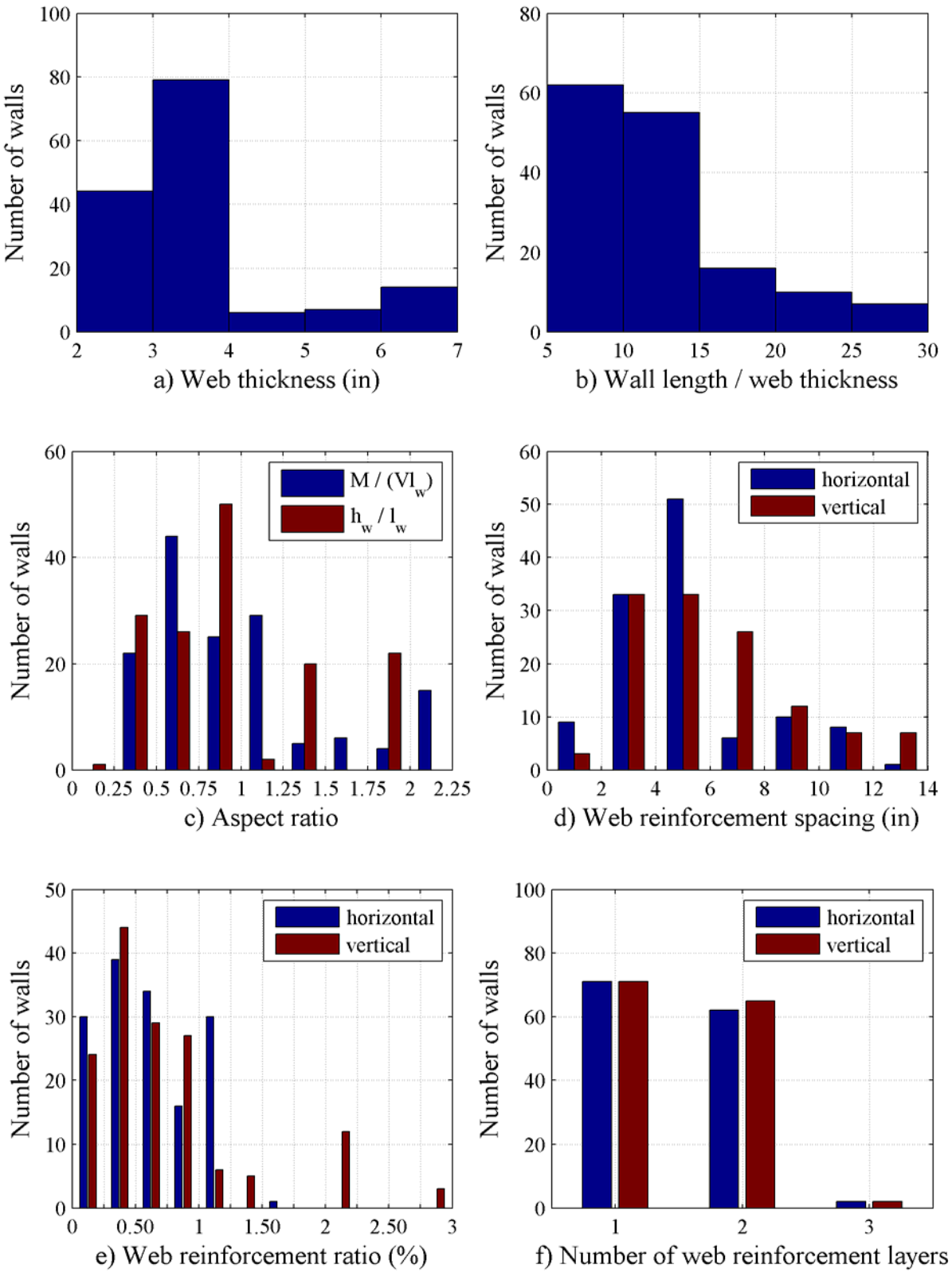


**Figure 3-2 Histograms of geometric, material, and loading properties of the 150 squat rectangular walls**

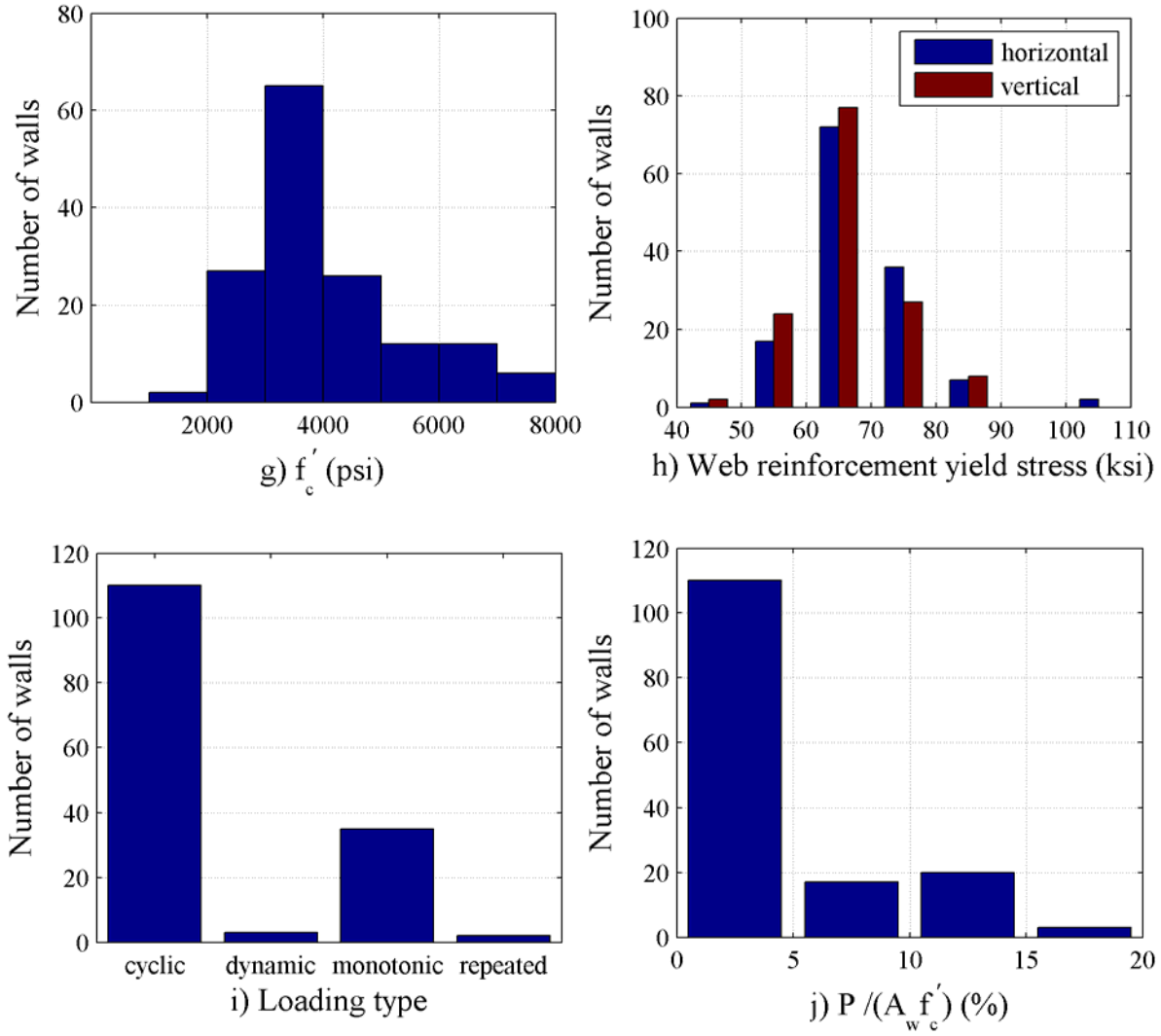


**Figure 3-2 Histograms of geometric, material, and loading properties of the 150 squat rectangular walls (cont'd)**

that ranged between $0.022\,A_w f_c'$ and $0.182\,A_w f_c'$; reported concrete compressive strength[3] varied between 1991 and 7395 psi (13.7 and 51 MPa); horizontal web reinforcement ratios ranged between 0.00 and 0.0161; and vertical web reinforcement ratios ranged between 0.00 and 0.0287. Boundary element reinforcement with ratios up to 0.128 was used in 110 of the 150 walls in addition to the uniformly distributed vertical web reinforcement. Fifteen of the 150 walls in the dataset did not have horizontal web reinforcement; 12 did not have vertical web reinforcement; 7 had neither horizontal nor vertical web reinforcement and included only boundary element reinforcement at wall ends. The reported yield stress of the wall vertical web reinforcement ranged between 43.5 and 88.5 ksi (300 and 610 MPa), and that of the horizontal web reinforcement ranged between 47.3 and 108.1 ksi (326 and 745 MPa). The reported yield stress for the boundary element reinforcement ranged between 43.5 and 84.8 ksi (300 and 585 MPa).

[3] Some authors used cube strength rather than cylinder strength to report the compressive strength of concrete; cube strengths were converted to cylinder strengths per Mindess et al. (2003).

Vertical web reinforcement was provided in a single layer for 71 of the 150 walls, in two layers for 65 walls and in three layers for 2 walls. Horizontal web reinforcement was provided in a single layer for 71 of the 150 walls, in two layers for 62 walls and in three layers for 2 walls. The maximum spacing for horizontal and vertical web reinforcement was 13.5 in. Note that Section 21.9 of ACI 318-08 [ACI (2008)] requires that web reinforcement in special structural walls be provided in two layers and with a spacing of less than 18 in.

The selected walls were tested using one of four types of loading: monotonic (quasi-static), repeated (quasi-static), cyclic (quasi-static), and dynamic. Thirty of the 150 walls were tested using monotonic loading, 2 walls were tested using repeated loading, 110 walls were tested using cyclic loading, and 3 walls were tested using dynamic loading.

## 3.3 Walls with Barbells

The data for the 191 squat barbell walls were obtained from (in chronological order), Benjamin and Williams (1953, 1954, 1956), Antebi et al. (1960), Shiga et al. (1973, 1975), Hirosawa (1975), Ogata and Kabeyasawa (1984), Kabeyasawa and Somaki (1985), AIJ (1985a, b, 1986a, b, c), Rothe (1992), XiangDong (1999), Bouchon et al. (2004), and Sheu (2007). Figure 3-3 presents summary information associated with other experimental parameters, in the form of histograms, on the 191 squat barbell walls included in the database. Wall aspect ratios (wall height divided by wall length) ranged between 0.28 and 1.60 and moment-to-shear ratios ranged between 0.06 and 1.90. The web thicknesses of the walls ranged from 1.97 to 6.30 in. (50 to 160 mm). The wall length varied between 20.0 and 155.9 in. (507 and 3960 mm) and the wall height varied between 19.7 and 70 in. (500 and 1778 mm). The ratios of the boundary element area (total barbell area, $A_{be}$) to the total area of the wall ($A_t$) varied between 0.22 and 0.60. Seventy-five walls were tested with coexisting axial load that ranged between 0.013 $A_t f'_c$ and 0.321 $A_t f'_c$; the axial forces on the remaining walls were limited to the self-weight of the wall and upper loading beam (or slab). Reported concrete compressive strength varied from 1451 to 8463 psi (10 to 58.3 MPa); 59% of the walls had compressive strengths between 3000 and 5000 psi (20.7 and 34.5 MPa). Both horizontal and vertical web reinforcements ranged between 0.00 and 0.028. Boundary element reinforcement (reinforcement restricted to the barbells) was provided in all 191 walls; reinforcement ratios ranged between 0.71 and 8.27% of each boundary element area. Ten of the 191 walls in the dataset had neither horizontal nor vertical web reinforcement and included only boundary element reinforcement. The reported yield stress of the wall vertical and horizontal web reinforcement ranged between 39.3 and 90.5 ksi (271 and 624 MPa). The reported yield stress for the boundary element reinforcement ranged between 37.8 and 81.9 ksi (261 and 565 MPa).

The selected walls were tested using one of five types of loading: monotonic (quasi-static), repeated (quasi-static), cyclic (quasi-static), blast, and dynamic. Fifty-seven of the 191 walls were tested using monotonic loading, 8 walls were tested using repeated loading, 94 walls were tested using cyclic loading, 2 walls were tested using dynamic loading and 30 walls were tested using blast loading.

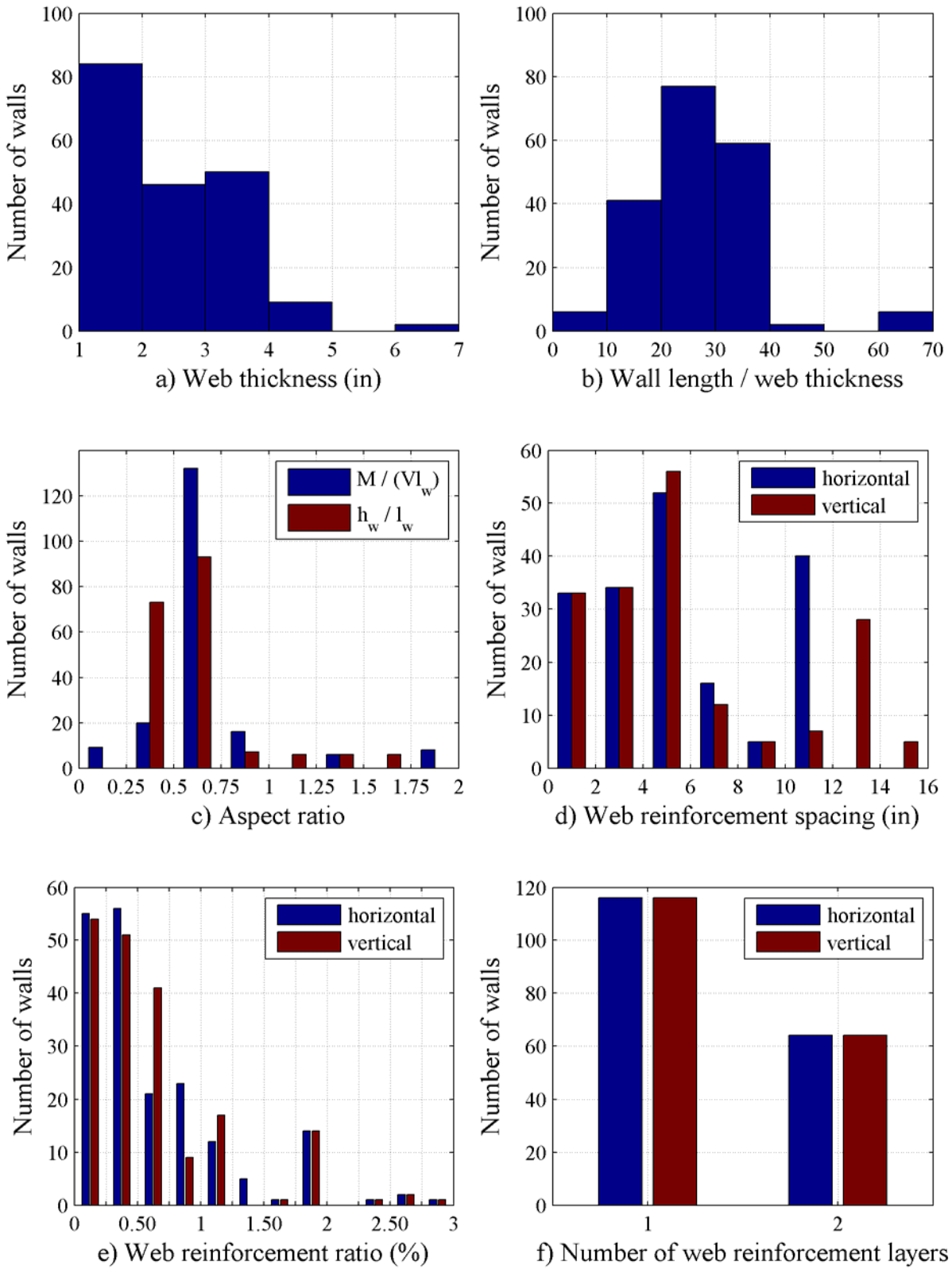


**Figure 3-3 Histograms of geometric, material, and loading properties of the 191 squat barbell walls**

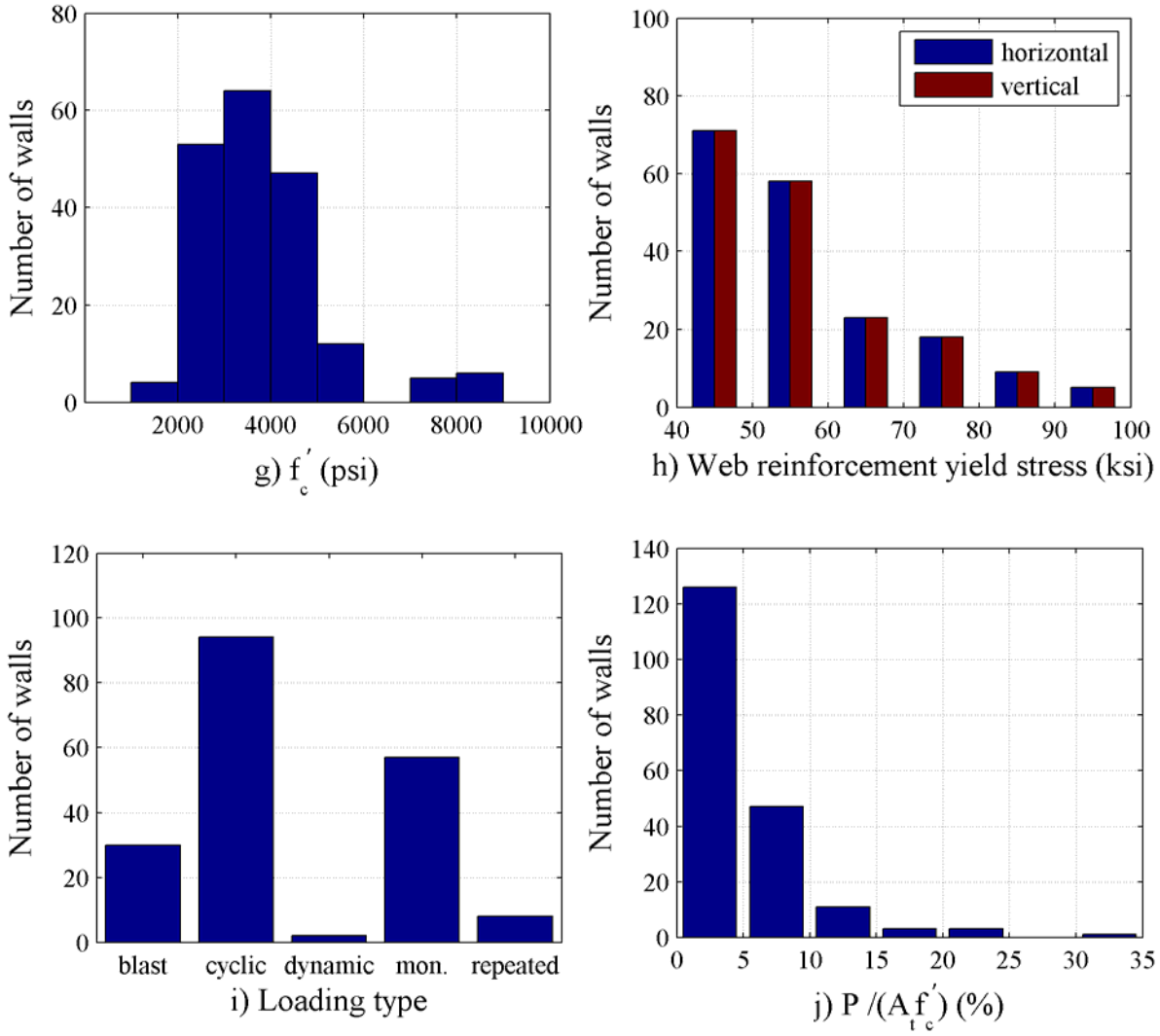


**Figure 3-3 Histograms of geometric, material, and loading properties of the 191 squat barbell walls (cont'd)**

## 3.4 Walls with Flanges

The data for the 93 squat flanged walls in the database were obtained from Barda (1972), Synge (1980), Maier and Thürlimann (1985), Saito et al. (1989), Sato et al. (1989), Seki et al. (1995), Mo and Chan (1996), Kitada et al. (1997), Naze and Sidaner (2001), Palermo and Vecchio (2002a), Farvashany et al. (2008). Figure 3-4 presents summary information associated with other experimental parameters, in the form of histograms, on these 93 squat flanged walls. For these walls, aspect ratios (wall height divided by wall length) ranged between 0.21 and 1.25 and moment-to-shear ratios ranged between 0.20 and 1.36. The web thickness of the walls ranged from 2.76 to 7.87 in. (70 to 200 mm). The wall length varied between 33.9 and 122 in. (860 and 3100 mm) and the wall height varied between 15.8 and 103.1 in. (400 and 2620 mm). The ratios of the boundary element area (total barbell area, $A_{be}$) to the total area of the wall ($A_t$) varied between 0.26 and 0.74. Fifty-six walls were tested with coexisting axial load that ranged between

$0.015 A_t f_c'$ and $0.273 A_t f_c'$; the axial forces on the remaining walls were limited to the self-weight of the wall and upper loading beam (or slab). Reported concrete compressive strength varied from 2170 to 15084 psi (16.3 to 104 MPa); 69% of the walls had compressive strengths between 4000 and 6000 psi (27.6 and 41.4 MPa). Horizontal web reinforcement ratios ranged between 0.0 and 1.69, and vertical web reinforcement ratios ranged between 0.0 and 2.54. Boundary element reinforcement (reinforcement restricted to the flanges) was provided in all 93 walls; reinforcement ratios ranged between 0.35 and 6.39% of each boundary element area. One wall was tested without horizontal web reinforcement and one wall tested without vertical web reinforcement. The reported yield stress of the vertical and horizontal web, and vertical boundary element reinforcement ranged between 42.9 and 87.7 ksi (296 and 605 MPa).

The selected walls were tested using one of three types of loading: monotonic (quasi-static), cyclic (quasi-static), and dynamic. Thirteen of the 93 walls were tested using monotonic loading, 78 walls were tested using cyclic loading, and 2 walls were tested using dynamic loading.

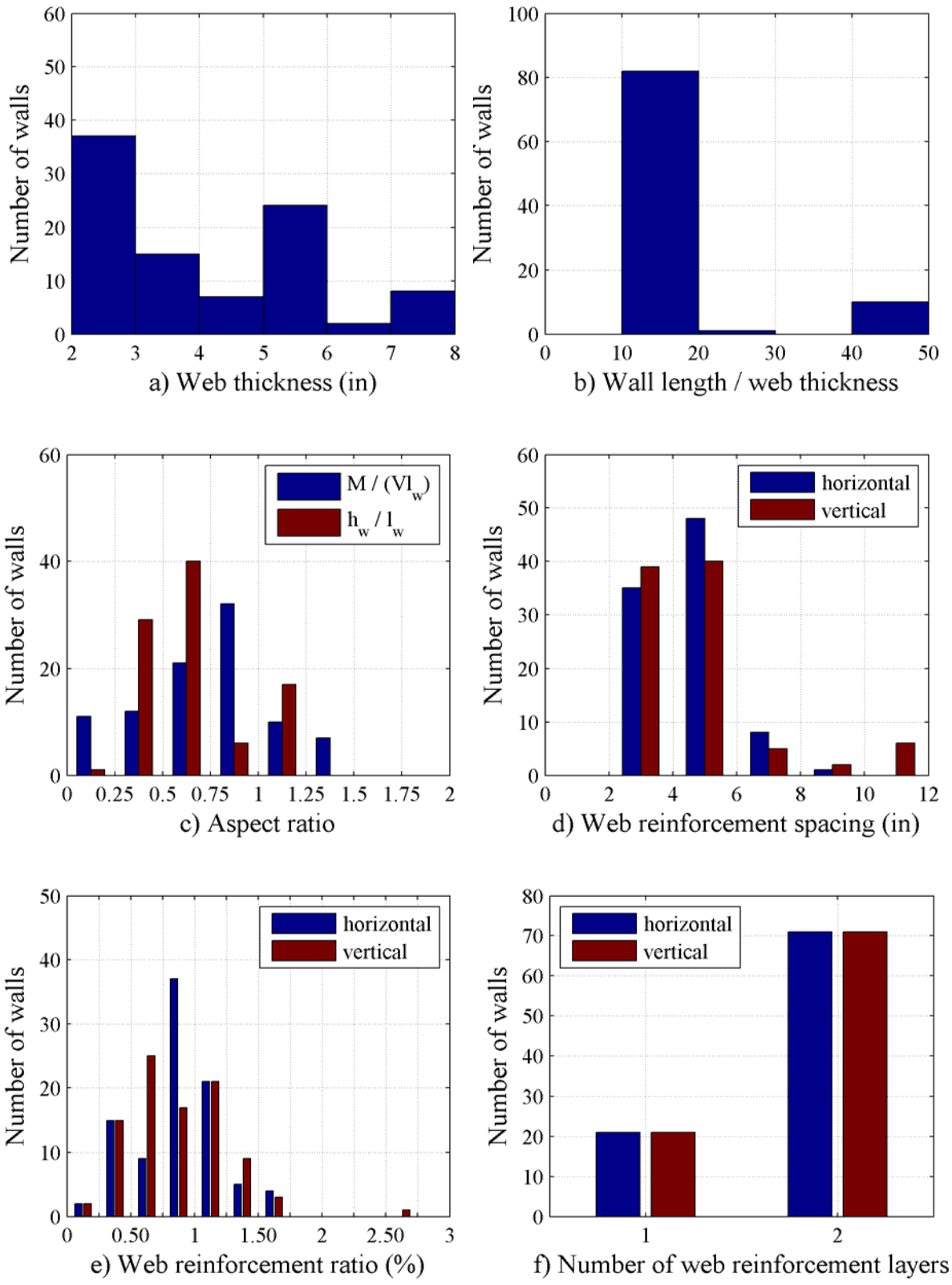


**Figure 3-4 Histograms of geometric, material, and loading properties of the 93 squat flanged walls**

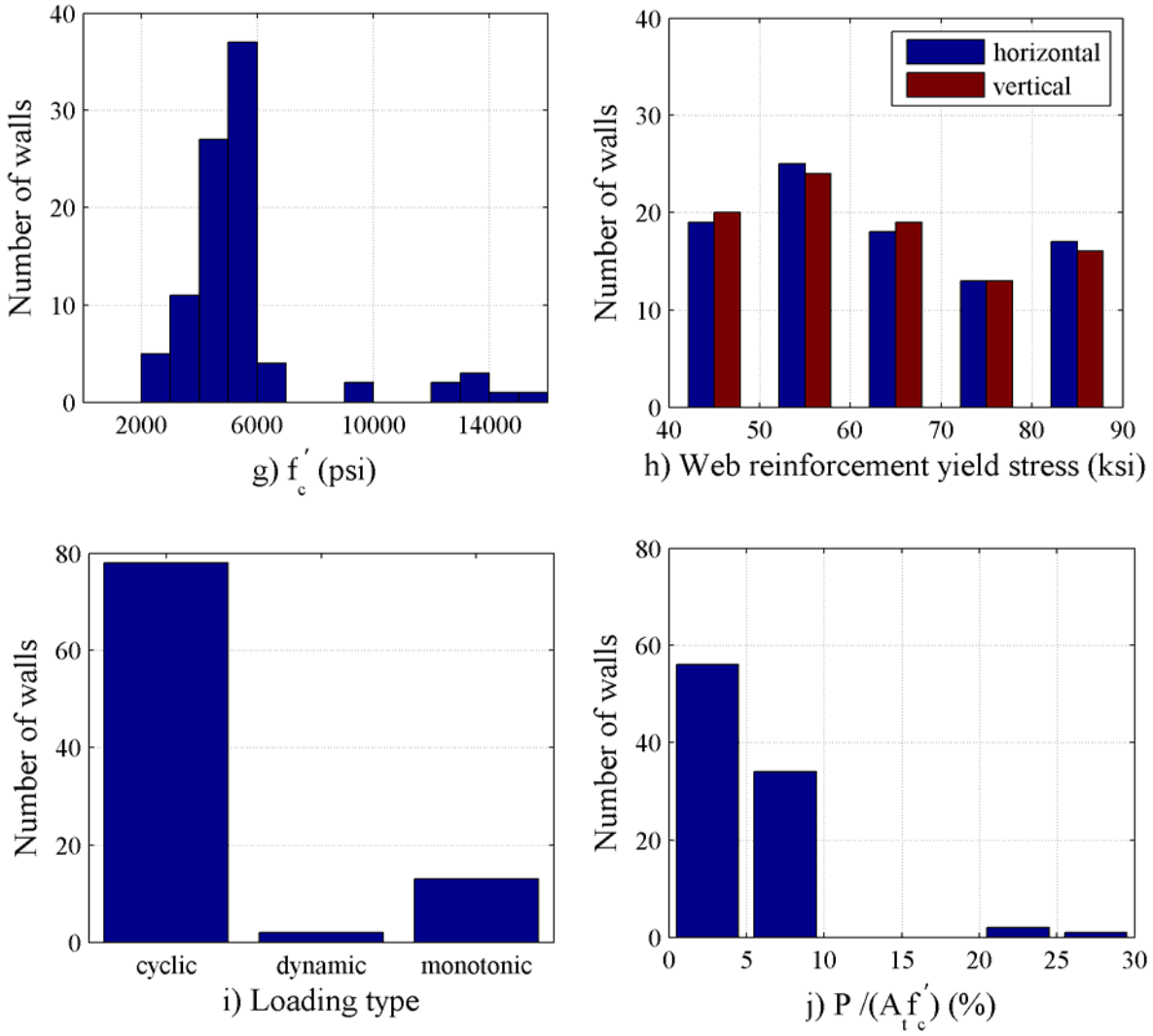


**Figure 3-4 Histograms of geometric, material, and loading properties of the 93 squat flanged walls (cont'd)**

# 4 EVALUATION OF PREDICTIVE EQUATIONS FOR PEAK SHEAR STRENGTH

## 4.1 Introduction

Peak shear strength is the key variable for force-based design and performance assessment of reinforced concrete squat walls. Accurate evaluation of the peak shear strength of squat walls is important because conventional buildings are likely to experience multiple deformation cycles well beyond yield in maximum earthquake shaking, and nuclear safety-related structures are likely to be subject to multiple cycles of loading to peak strength in safe shutdown earthquake shaking. Building codes, manuals of practice, guidelines and the literature provide a number of equations for the peak shear strength of reinforced concrete walls. However, these equations significantly vary in structure [Orbovic et al. (2007)] and there is substantial scatter in the peak shear strength predicted by these equations as indicated by prior studies [Wood (1990), Gulec (2005)]. The following sections aim to assess the performances of widely used peak shear strength equations using the 434-specimen squat wall database presented in Section 3. The experimentally measured peak shear strengths of the walls are compared with nominal shear strengths predicted by five equations: 1) Section 21.9 of ACI 318-08; 2) Section 11.9 of ACI 318-08; 3) Barda et al. (1977); 4) ASCE 43-05 [ASCE (2005)]; and 5) Wood (1990). The selected equations are those widely used in the U.S. for design and structural performance evaluation of squat walls in building and nuclear safety-related structures. Nominal rather than design strengths are used for the comparison because the strength reduction factor is not intended to account for bias in the strength equation. Reported material strengths and member dimensions are used to predict nominal strengths. The mean, median and dispersion in the ratios of the predicted to measured peak shear strengths provide insight into the utility of each strength equation and the simplified models upon which the equations are based. A preliminary investigation showed that the experimental peak shear strengths of squat walls with rectangular cross-sections and boundary elements differed significantly. Accordingly, an evaluation is performed for each wall type to judge the impact of boundary elements on the utility of each peak shear strength equation.

Section 4.2 presents the selected equations used for predicting peak shear strength of squat reinforced concrete walls. Sections 4.3 and 4.4 evaluate the performances of the selected equations for squat rectangular walls and squat walls with boundary elements, respectively.

## 4.2 Selected Peak Shear Strength Equations

Five sets of predictive equations, based on the procedures provided in Section 11.9 of ACI 318-08, Section 21.9 of ACI 318-08, Barda et al. (1977), ASCE 43-05 and Wood (1990), are used to evaluate the peak shear strength of the 434 squat walls in the database of Section 3. A unified notation is used for common variables in the predictive equations and the notation used herein may differ from that used in the referenced documents. Some equations from previous sections are repeated in this section to simplify the presentation.

ACI 318-08 provides two semi-empirical equations, both based on the modified truss analogy approach, to predict the peak shear strength of reinforced concrete walls. The modified truss

analogy approach assumes that wall peak shear strength can be approximated as the summation of shear force resisted by concrete and transverse (horizontal) web reinforcement. One equation is provided in ACI 318-08 Section 21.9 (Special structural walls and coupling beams) for seismic design. The equation in Section 11.9 (Provisions for walls) is used for general (non-seismic) design. Equation Set I (Equation 4-1 below) is from Section 21.9 of ACI 318-08. Note that the peak shear calculation procedures of ACI 318-08 are essentially the same for reinforced concrete beams and walls.

$$V_{n1} = \left(\alpha_c \sqrt{f_c'} + \rho_h f_{yh}\right) A_w \le 10\sqrt{f_c'} A_w \tag{4-1}$$

where $V_{n1}$ (lb) is the nominal shear strength per Section 21.9 of ACI 318-08, $\alpha_c$ is a function of aspect ratio, which per ACI 318-08, equal to 3.0 for $h_w / l_w \le 1.5$, 2.0 for $h_w / l_w \ge 2$ and varies linearly for $1.5 \le h_w / l_w \le 2$; $f_c'$ (psi) is the compressive strength of concrete; $\rho_h$ is the horizontal web reinforcement ratio; $f_{yh}$ (psi) is the yield stress of the horizontal web reinforcement; $A_w$ (in$^2$) is the area of the wall bounded by web thickness ($t_w$) and wall length ($l_w$); and $h_w$ (in) is the height of the wall.

Section 21.9 of ACI 318-08 imposes an upper limit of $10\sqrt{f_c'}$ on peak shear stress; this limit is intended to prevent diagonal compression failure. A lower limit of 0.25% is imposed on the horizontal and vertical web reinforcement ratios. Section 21.9 of ACI 318-08 does not account explicitly for the effect of vertical web reinforcement ratio on peak shear strength but requires the vertical web reinforcement ratio be no less than the horizontal web reinforcement ratio that for walls with aspect ratios less than or equal to 2.

The procedure to predict the peak shear strength in Section 11.9 of ACI 318-08, Equation Set II, is given by the following four equations.

$$V_{n2} = V_c + V_s \le 10\sqrt{f_c'} t_w d_1 \tag{4-2}$$

$$V_c = 3.3\sqrt{f_c'} t_w d_1 + \frac{N_u d_1}{4 l_w} \tag{4-3}$$

$$V_c = \left[ 0.6\sqrt{f_c'} + \frac{l_w \left( 1.25\sqrt{f_c'} + \dfrac{0.2 N_u}{l_w t_w} \right)}{\dfrac{M_u}{V_u} - \dfrac{l_w}{2}} \right] t_w d_1 \tag{4-4}$$

$$V_s = \frac{A_v f_{yh} d_1}{s} \tag{4-5}$$

where $V_{n2}$ (lb) is the nominal shear strength per Section 11.9 of ACI 318-08; $V_c$ (lb) is the nominal shear strength provided by the concrete; $V_s$ (lb) is the nominal shear strength provided

by horizontal reinforcement; $d_1$ (in) is the distance from extreme compression fiber to the location of the resultant of forces in vertical reinforcement in tension and assumed equal to $0.8l_w$ unless a larger value is determined by a strain compatibility analysis; $N_u$ (lb) is the factored axial load that is negative in tension; $M_u$ (lb-in) is the factored moment at the section; $V_u$ (lb) is the factored shear force at the section; and $A_v$ (in$^2$) is the area of horizontal reinforcement within a distance $s$ (in).

Per Section 11.9.6 of ACI 318-08, the shear strength provided by concrete is taken as the smaller of the values provided by Equations 4-3 and 4-4. Equation 4-4 does not apply if $M_u / V_u - l_w / 2 \le 0$. The peak shear stress is limited to $10\sqrt{f_c'}$. The minimum horizontal web reinforcement ratio is 0.25%. The minimum vertical web reinforcement ratio ($\rho_v$) is given by

$$\rho_v = 0.0025 + 0.5\left(2.5 - \frac{h_w}{l_w}\right)\left(\rho_h - 0.0025\right) \tag{4-6}$$

Section 11.9 and 21.9 of ACI 318-08 use a different effective area to calculate shear strength. The procedures of Chapter 11 and Chapter 21 of ACI 318-08 to predict the peak shear strength of squat walls are adopted in ACI 349-06 [ACI (2006)], *Code Requirements for Nuclear Safety-Related Concrete Structures*, without revision despite the significantly different performance expectations for building and nuclear structures.

Equation Set III was proposed by Barda et al. (1977) to predict the peak shear strength of walls in low-rise buildings:

$$V_{n3} = \left(8\sqrt{f_c'} - 2.5\sqrt{f_c'}\frac{h_w}{l_w} + \frac{P}{4l_w t_w} + \rho_v f_{yv}\right) t_w d_2 \tag{4-7}$$

where $V_{n3}$ (lb) is the nominal shear strength per Barda, $\rho_v$ is the vertical web reinforcement ratio, $f_{yv}$ (psi) is the yield stress of the vertical web reinforcement, $d_2$ (in) is the distance from extreme compression fiber to area centroid of the wall vertical reinforcement in tension, $P$ is the axial force, and all other variables have been defined previously.

Barda (1972) concluded that horizontal web reinforcement did not influence peak shear strength and Equation 4-7 does not consider horizontal web reinforcement ratio as a variable.

Equation Set IV is that of Equations 4.2-3 and 4.2-4 of ASCE 43-05 (Equations 4-8, 4-9 and 4-10 below) to predict the peak shear strength of squat walls with barbells or flanges. This equation is applicable for walls with aspect ratios $h_w / l_w \le 2.0$ and vertical and horizontal web reinforcement ratios less than or equal to 1%. If the reinforcement ratios exceed 1%, the combined reinforcement ratio $\rho_{se}$ (calculated using Equation 4-10) is limited to 1%. ASCE 43-05 imposes an upper limit of $20\sqrt{f_c'}$ on the peak shear stress in the web of the wall.

$$V_{n4} = v_n d_3 t_w \tag{4-8}$$

$$v_n = 8.3\sqrt{f_c'} - 3.4\sqrt{f_c'}\left(\frac{h_w}{l_w} - 0.5\right) + \frac{P}{4l_w t_w} + \rho_{se} f_{y1} \le 20\sqrt{f_c'} \tag{4-9}$$

$$\rho_{se} = A\rho_v + B\rho_h \tag{4-10}$$

where $V_{n4}$ (lb) is the nominal shear strength per ASCE 43-05; $v_n$ (psi) is the nominal peak shear stress per ASCE 43-05; $d_3$ (in) is the distance from the extreme compression fiber to the location of the resultant of forces in vertical reinforcement in tension, which may be determined from a strain compatibility analysis and is assumed equal to $0.6l_w$ if no analysis is performed; $\rho_{se}$ is the combined reinforcement ratio; $f_{y1}$ (psi) is the reinforcement yield stress used with $\rho_{se}$; $A$ and $B$ are defined in Table 1-3 as a function of aspect ratio, and all other terms have been defined previously.

Equation Set V (Equation 4-11) was proposed by Wood (1990) to calculate the peak shear strength of squat walls using data from tests of 143 squat walls. Wood's database included both rectangular walls and walls with boundary elements.

$$6\sqrt{f_c'}A_w \le V_{n5} = \frac{A_{vf} f_{y2}}{4} \le 10\sqrt{f_c'}A_w \tag{4-11}$$

where $V_{n5}$ (lb) is the nominal shear strength per Wood, $A_{vf}$ (in$^2$) is the area of total reinforcement (sum of areas of the vertical web and boundary element reinforcement) crossing the shear plane, and $f_{y2}$ (psi) is the reinforcement yield stress for a combination of vertical web and boundary element reinforcement used for Equation Set V.

## 4.3 Rectangular Walls

The accuracy of the five predictive equations presented in Section 4.2 is evaluated using the experimental peak shear strengths ($V_{peak}$) of the 150 squat rectangular walls presented in Section 3. For the cyclically loaded walls, the peak shear strength was taken as the average of the peak shear strengths obtained in the two (opposite) loading directions. The 150 squat rectangular walls were parsed into three groups: Group 1—all 150 squat walls, Group 2—shear-critical squat walls, and Group 3—ACI 318-compliant, shear-critical squat walls. Group 1 includes all 150 rectangular walls in the database. Group 2 is formed to reduce the bias, if any, introduced into the predictions by the walls in the database whose response was governed by flexure or mixed failure modes. Group 2 is formed by excluding those walls of Group 1 for which the experimental peak shear strength was greater than the shearing force associated with flexural failure (shear-flexural strength, $V_{flex}$). Group 3 is limited to walls of Group 2 that comply with the minimum web reinforcement requirements of ACI 318-08 (0.25 %). A second criterion to form this group was the requirement of ACI 318-08 that the vertical web reinforcement ratio be no less than the horizontal web reinforcement ratio for walls with aspect ratios less than 2.0.

For each wall in the database, the area centroid of the wall vertical reinforcement in tension (to calculate $d_1$ in Equations 4-2 through 4-5), the location of the resultant tensile force in the vertical reinforcement (to calculate $d_2$ in Equation 4-7 and $d_3$ in Equation 4-8) and the ultimate moment capacity (to identify flexure-critical walls in Groups 2 and 3) were computed using a commercially available cross-section analysis program [Imbsen and Associates, Inc. (2007)]. The concrete was assumed to be unconfined and a standard nonlinear stress-strain relationship with strain hardening was used to model reinforcement. The reported values of geometric (wall cross-sectional layout, reinforcement size and layout), material ( $f_c'$, yield and fracture stresses for reinforcement) and loading properties (axial force) were used for the cross-section analysis. The concrete tensile strength was set equal to zero, the compressive failure strain was assumed to be 0.003 and the modulus of elasticity was taken as $57000\sqrt{f_c'}$ (psi) per ACI 318-08. For reinforcement, the strains at the onset of hardening and the fracture strain were taken as 0.01 and 0.1, respectively.

### 4.3.1 Group 1: All 150 Rectangular Walls

A statistical summary of the ratios of the predicted to measured peak shear strength for the 150 walls in Group 1 is presented in Table 4-1 for each of the five equation sets. The ratios of predicted to measured strength tagged with an asterisk (e.g., $V_{n1*}$) present statistics for the equation set without the corresponding upper shear stress limits. Values in columns 2 (arithmetic mean) or 3 (median or 50th percentile) in Table 4-1 greater than 1.0 indicate that the predictive equation is unconservative in a mean or median sense, respectively, namely, the equation overestimates the measured peak shear strength. The last column in the table reports the percentage of unconservative predictions for the 150 specimens in the group. The standard deviation (column 4) and coefficient of variation (column 5 – COV) are also reported to provide supplemental information on the dispersion in the ratios.

Figure 4-1 presents the distributions of the ratios of the predicted peak strength to measured peak strength for the five procedures using box and whisker plots, which present the lower quartile ($Q_1$), median ($Q_2$), upper quartile ($Q_3$), and extreme values. The maximum length of a whisker was limited to 1.5 times the interquartile range ($IQR$) unless its length was governed by minimum or maximum data points. The data points larger than $Q_3 + 1.5 \times IQR$ or smaller than $Q_1 - 1.5 \times IQR$ are identified by "+" in the figure.

The mean and median values of the shear strength ratios presented in Table 4-1 and Figure 4-1 for Equation Sets I ($V_{n1}$) and II ($V_{n2}$) indicate that Set II (Section 11.9 of ACI 318-08) is the more accurate of the two because the mean and median ratios for Equation Set II are closer to 1.0. The assumption about the effective shear area of the wall is the principal reason why Equation Set II is more conservative than Equation Set I. In Equation Set I, the effective shear area is equal to the gross area of the wall, $l_w t_w$; in Equation Set II, the effective shear area of the wall is equal to $d_1 t_w$ and smaller than that for Set I. Furthermore, the scatter, as measured by coefficient of variation, is smaller for Equation Set II. The Barda and ASCE 43-05 equations, $V_{n3}$ and $V_{n4}$, respectively, overpredict the measured peak strength of 85% and 86% of the 150

**Table 4-1 Statistics of the ratio of the shear strength predicted using Equation Sets 1 through 5 to measured peak shear strength of all walls (Group 1)**

| | Mean | Median | St. Dev. | COV | Min | Max | % Over-Predictions |
|---|---|---|---|---|---|---|---|
| $V_{n1}/V_{peak}$ | 1.28 | 1.17 | 0.54 | 0.42 | 0.36 | 3.52 | 67 |
| $V_{n1*}/V_{peak}$ | 1.44 | 1.32 | 0.66 | 0.46 | 0.36 | 3.52 | 69 |
| $V_{n2}/V_{peak}$ | 1.06 | 0.97 | 0.41 | 0.39 | 0.37 | 2.74 | 49 |
| $V_{n2*}/V_{peak}$ | 1.22 | 1.17 | 0.52 | 0.43 | 0.37 | 2.74 | 59 |
| $V_{n3}/V_{peak}$ | 1.46 | 1.38 | 0.47 | 0.32 | 0.56 | 2.83 | 85 |
| $V_{n4}/V_{peak}$ | 1.52 | 1.46 | 0.48 | 0.31 | 0.75 | 3.09 | 87 |
| $V_{n4*}/V_{peak}$ | 1.52 | 1.46 | 0.48 | 0.31 | 0.75 | 3.09 | 87 |
| $V_{n5}/V_{peak}$ | 1.05 | 0.97 | 0.33 | 0.32 | 0.48 | 2.23 | 46 |

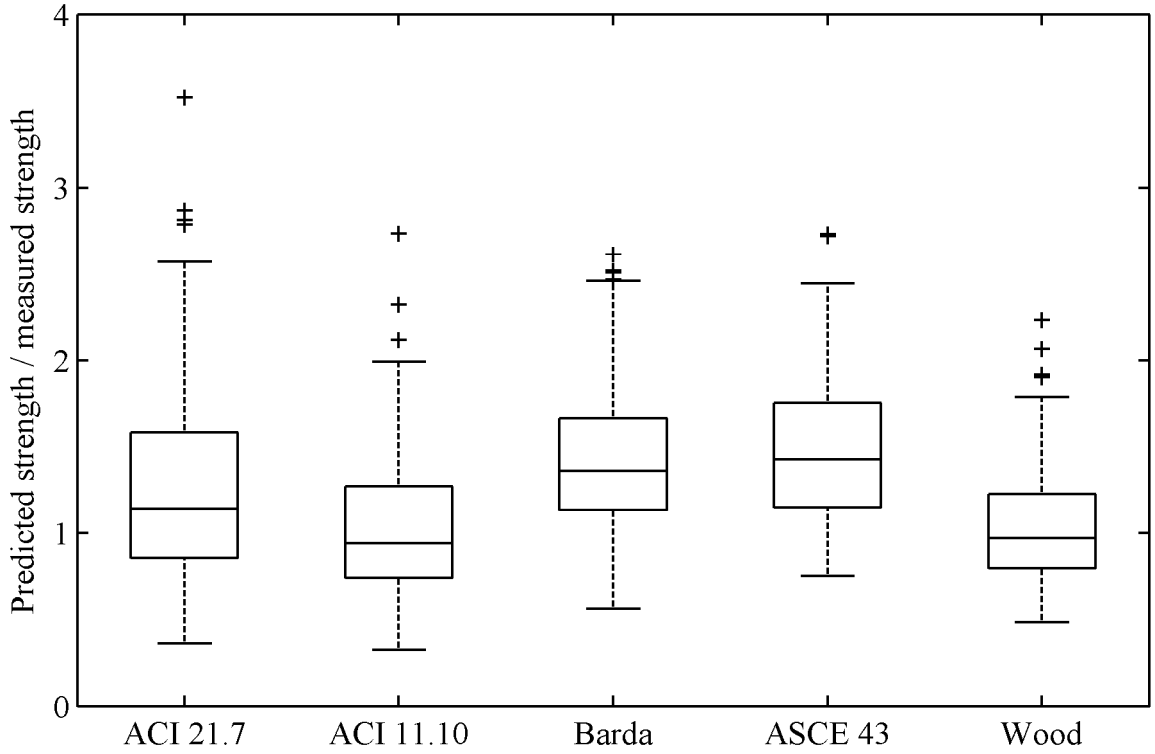


**Figure 4-1 Distribution of the ratio of the predicted shear strengths to measured peak shear strengths for all walls**

walls, respectively. Equation Set V ($V_{n5}$), developed by Wood, is accurate and reliable because the mean and median values are close to 1.0 and the standard deviation and coefficient of variation are both relatively small.

It should be noted that both ACI 318-08 equations yield more unconservative estimations (i.e., overpredict) of the peak shear strength when the upper shear stress limit on the equations sets is removed. Conversely, the upper shear stress limit on the ASCE 43-05 equation does not govern the peak shear strength of any of the walls in the rectangular wall database.

#### 4.3.1.1 ACI 318-08 Chapter 21 Equation (Equation Set I)

Equation Set I overpredicts the peak shear strength of 67% of the walls in the rectangular wall database with mean and median values of $V_{n1}/V_{peak}$ ($V_{n1*}/V_{peak}$) of 1.28 (1.44) and 1.17 (1.32), respectively. The standard deviation and coefficient of variation associated with $V_{n1}/V_{peak}$ ($V_{n1*}/V_{peak}$) are 0.54 (0.66) and 0.42 (0.46), respectively. The basic statistics associated with the predictions of Equation Set I reveal that the procedure is generally unconservative in predicting peak shear strength, and also that the predictions are highly scattered as implied by the high coefficient of variation value (0.42). The large coefficient of variation calls into question the utility of the equation.

Figure 4-2 through Figure 4-4 present the variation of $V_{n1}/V_{peak}$ with the design variables used by Equation Set I, namely, horizontal reinforcement ratio, aspect ratio (represented using moment-to-shear ratio), and the concrete compressive strength, respectively. Values of $V_{n1}/V_{peak}$ greater than 1.0 represent an overprediction (unconservative estimate) of the measured peak shear strength. Linear fits on the data are also included in all three figures. Figure 4-2 indicates that the equation set becomes more unconservative with increasing horizontal reinforcement ratio. However, for specimens with horizontal reinforcement ratios around or below the minimum limit specified by ACI 318-08 ($\rho_h f_{yh} \leq$ 150 psi for $f_{yh}$ = 60 ksi), the ratios of $V_{n1}$ to $V_{peak}$ is less than 1.0 and thus conservative. Equation Set I consistently overestimates the peak shear strength of walls with $\rho_h f_{yh}$ greater than 350 psi. Figure 4-3 shows that the procedure becomes more unconservative with increasing moment-to-shear ratio. As noted previously, the effect of moment-to-shear ratio (or aspect ratio) is addressed using $\alpha_c$, which increases the contribution of concrete to the overall shear strength with decreasing moment-to-shear ratio. The functional form of this coefficient is questionable, as $V_{n1}/V_{peak}$ tends to increase with increasing moment-to-shear ratio. Figure 4-4 indicates that $V_{n1}/V_{peak}$ increases with increasing concrete compressive strength, which shows that the form of the concrete contribution term for this equation is questionable. It should be noted that for a well-performing model, the residuals associated with the predictions of the model should be close to zero without exhibiting any trends and with small coefficient of variation. Similarly, the trend lines in Figure 4-2 through Figure 4-4 should be almost horizontal with a value equal to 1.0. The scatter as measured by the coefficient of variation should be low. Note that the substantial scatter observed in Figure 4-2 through Figure 4-4 may also indicate that the predictive equation does not account for some variables that affect the peak shear strength.

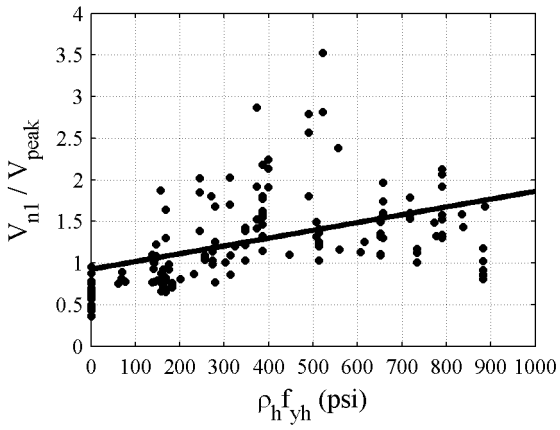


**Figure 4-2 Variation of $V_{n1}/V_{peak}$ with $\rho_h f_{yh}$**

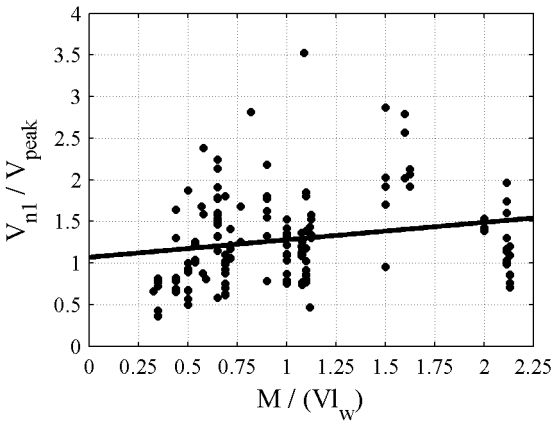


**Figure 4-3 Variation of $V_{n1}/V_{peak}$ with moment-to-shear ratio**

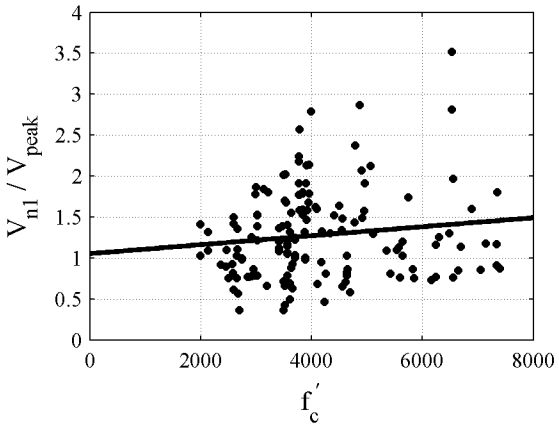


**Figure 4-4 Variation of $V_{n1}/V_{peak}$ with $f_c'$**

Figure 4-5 presents the variation of $V_{n1}/V_{peak}$ and $V_{n1*}/V_{peak}$ with horizontal web reinforcement ratio (along with corresponding linear fits), where $V_{n1*}$ is the computation of Equation Set I without the upper stress limit of $10\sqrt{f_c'}$ that is linked to the change of failure mode from diagonal tension to diagonal compression. The vertical dashed line in this figure (and in Figure 4-6, Figure 4-11, and Figure 4-12) represents the limiting value of $\rho_h f_{yh}$ in Section 21.9 of ACI 318-08 for Grade 60 reinforcement. Figure 4-6 presents the variation of normalized shear stress [shear force divided by the product of web area ($A_w$) and $\sqrt{f_c'}$] obtained using Equation Set I ($V_{n1}$) and measured peak shear strength ($V_{peak}$) with $\rho_h f_{yh}$. Figure 4-5 and Figure 4-6 indicate that the upper shear stress limit of $10\sqrt{f_c'}$ governs the peak shear strength of walls with $\rho_h f_{yh}$ larger than approximately 500 psi. As expected, the slope of the linear fit on $V_{n1*}/V_{peak}$ of Figure 4-5 is considerably steeper than the slope of the linear fit on $V_{n1}/V_{peak}$.

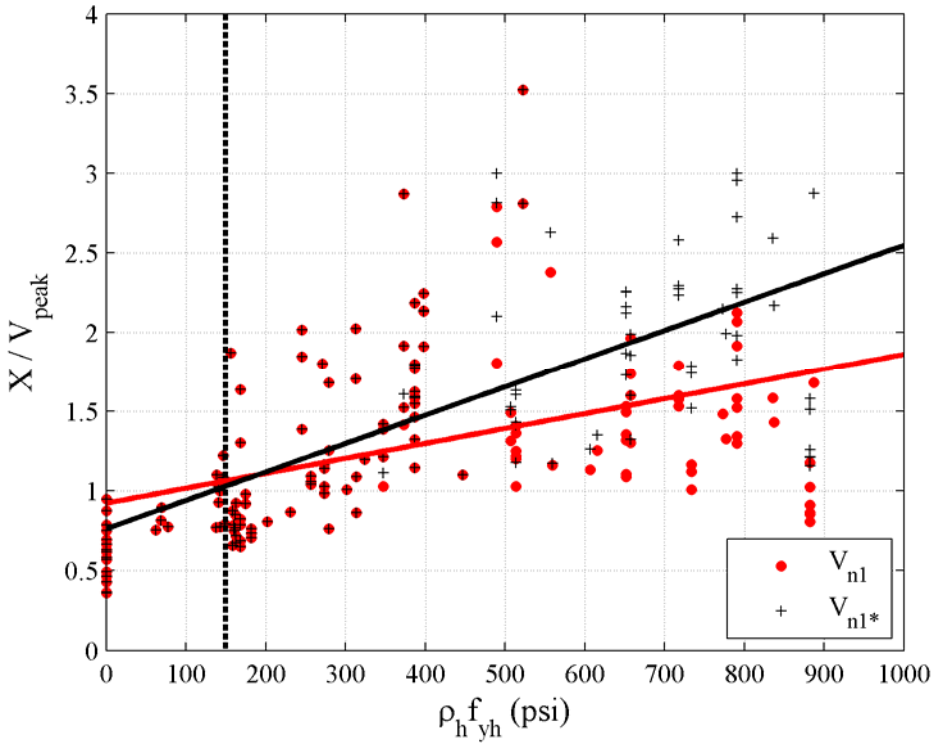


**Figure 4-5 Variation of $V_{n1}/V_{peak}$ and $V_{n1*}/V_{peak}$ with $\rho_h f_{yh}$**

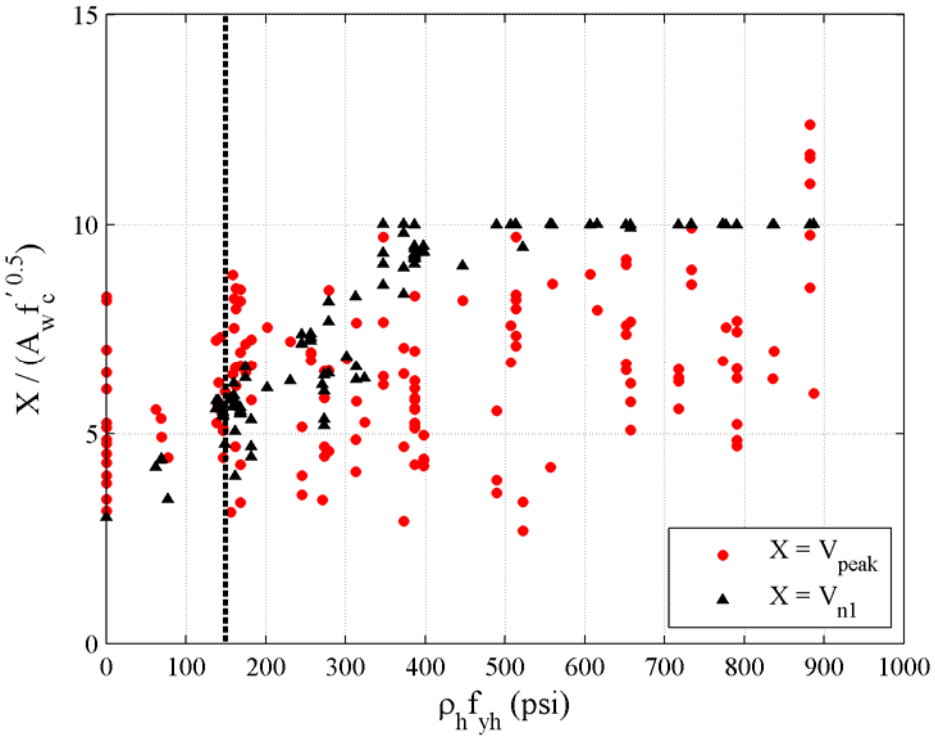


**Figure 4-6 Variation of normalized shear stress obtained using Equation Set I ($V_{n1}$) and measured peak shear strength ($V_{peak}$) with $\rho_h f_{yh}$**

The upper shear stress limit improves the overall performance of Equation Set I, especially by improving the accuracy of the predictions for more heavily reinforced walls. As seen in Figure 4-6, 52 of the 150 predictions of Equation Set I were governed by the upper shear stress limit whereas only 4 walls, all of which had horizontal and vertical web reinforcement ratios higher than 1%, reached an experimental normalized shear stresses ($V_{peak} / A_w$) greater than $10\sqrt{f_c'}$.

#### 4.3.1.2 ACI 318-08 Chapter 11 Equations (Equation Set II)

Equation Set II overpredicts the peak shear strength of 49% of the walls in the rectangular wall database giving mean and median values of $V_{n2} / V_{peak}$ ($V_{n2*} / V_{peak}$) of 1.06 (1.22) and 0.97 (1.17). The corresponding standard deviation and coefficient of variation are 0.41 (0.52) and 0.39 (0.43). The scatter in the predictions of Equation Set II (COV=0.39) are slightly smaller than that in the predictions of Equation Set I (COV=0.42). However, the scatter is large for an accurate predictive model.

Figure 4-7 through Figure 4-10 present the distribution of $V_{n2} / V_{peak}$ with the design variables used by Equation Set II, namely, horizontal reinforcement ratio, aspect ratio (represented using moment-to-shear ratio), concrete compressive strength, and normalized axial stress (axial force divided by the product of the wall area and concrete compressive strength), respectively. Figure 4-7 shows that, similar to those of Equation Set I, the predictions of Equation Set II become more unconservative with increasing horizontal web reinforcement ratio. The majority of the predictions of Equation Set II for $\rho_h f_{yh}$ less than 300 psi is conservative (less than) with respect to the measured peak shear strengths. Figure 4-8 through Figure 4-10 show that the variance associated with the predictions of Equation Set II is relatively constant over the ranges considered for aspect ratio, concrete compressive strength, and axial force (denoted in Figure 4-10 and in following figures by $P$ to unify the presentation), as indicated by the near-horizontal lines of linear fit. However, significant scatter is evident in the peak shear-strength predictions.

Figure 4-11 presents the variation of $V_{n1} / V_{peak}$ and $V_{n2} / V_{peak}$ with horizontal web reinforcement ratio together with the corresponding linear fits. As seen in Figure 4-11, the predictions of Equation Set I and II follow similar trends except that the latter is more conservative. This may be largely attributed to the effective shear area for Equation Set II ($d_1 t_w$) being smaller than that of Equation Set I ($A_w$). The average, minimum, maximum ratios of effective depth ($d_1$) to wall length ($l_w$) are 0.82, 0.80 and 0.95, respectively. The corresponding standard deviation is 0.04. Note that Section 11.9 of ACI 318-08 limits the minimum effective depth to $0.8 l_w$, which governs 103 of the 150 effective depth calculations performed using strain compatibility analysis.

Figure 4-12 presents the variation of normalized shear stress [shear force divided by the product of effective shear area ($d_1 t_w$) and $\sqrt{f_c'}$ ] obtained using Equation Set II ($V_{n2}$) and measured peak shear strength ($V_{peak}$) with $\rho_h f_{yh}$. As presented in Figure 4-12, the upper stress limit of Equation Set II governs the calculated strengths of walls with $\rho_h f_{yh}$ larger than 500 psi. Forty-nine of the 150 predictions of Equation Set II are governed by the upper shear stress limit, which makes the

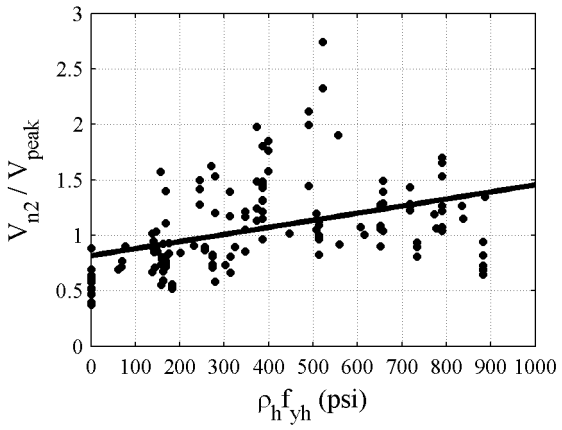


**Figure 4-7 Variation of $V_{n2}/V_{peak}$ with $\rho_h f_{yh}$**

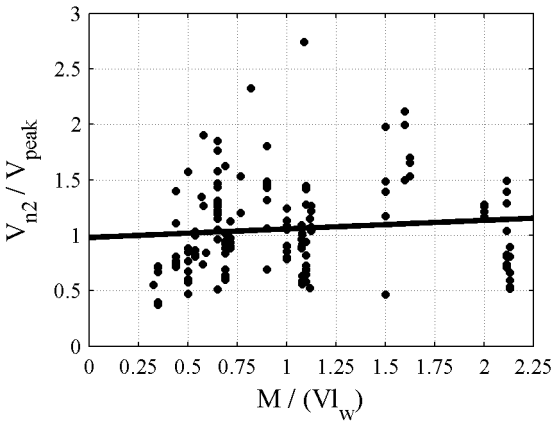


**Figure 4-8 Variation of $V_{n2}/V_{peak}$ with moment-to-shear ratio**

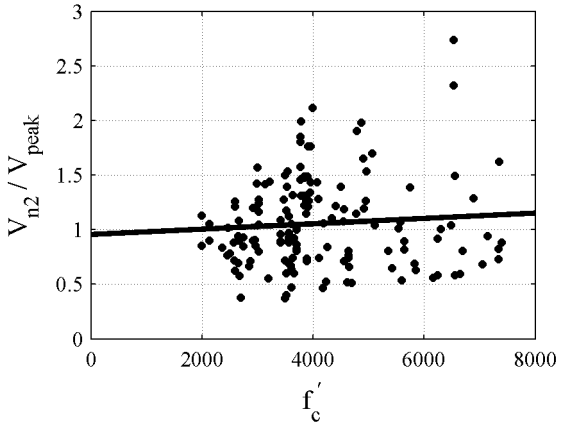


**Figure 4-9 Variation of $V_{n2}/V_{peak}$ with $f_c'$**

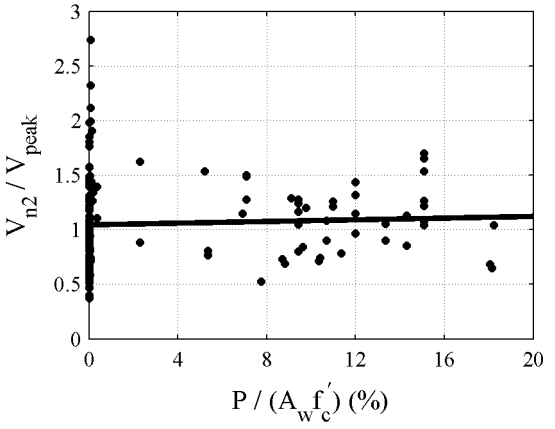


**Figure 4-10 Variation of $V_{n2}/V_{peak}$ with normalized axial stress**

predictions more conservative. The measured peak shear stress ($V_{peak}/d_1 t_w$) of 23 of the 150 specimens is higher than $10\sqrt{f_c'}$.

### 4.3.1.3 Barda et al. (1977) Equations (Equation Set III)

This equation set was derived by Barda et al. (1977) using data from tests of 8 squat reinforced concrete walls with flanges. The equation considers concrete compressive strength, aspect ratio, vertical reinforcement ratio, and axial force in the calculation of the peak shear strength. Horizontal reinforcement ratio is not a variable in the Barda peak shear-strength equation.

Equation Set III overpredicts the peak shear strength of 85% of the walls in the database with mean and median values of $V_{n3}/V_{peak}$ of 1.46 and 1.38, respectively. The corresponding standard deviation and coefficient of variation are 0.47 and 0.32. Note that Equation Set III uses an effective depth ($d_2$) to calculate the peak shear strength. For the rectangular walls considered

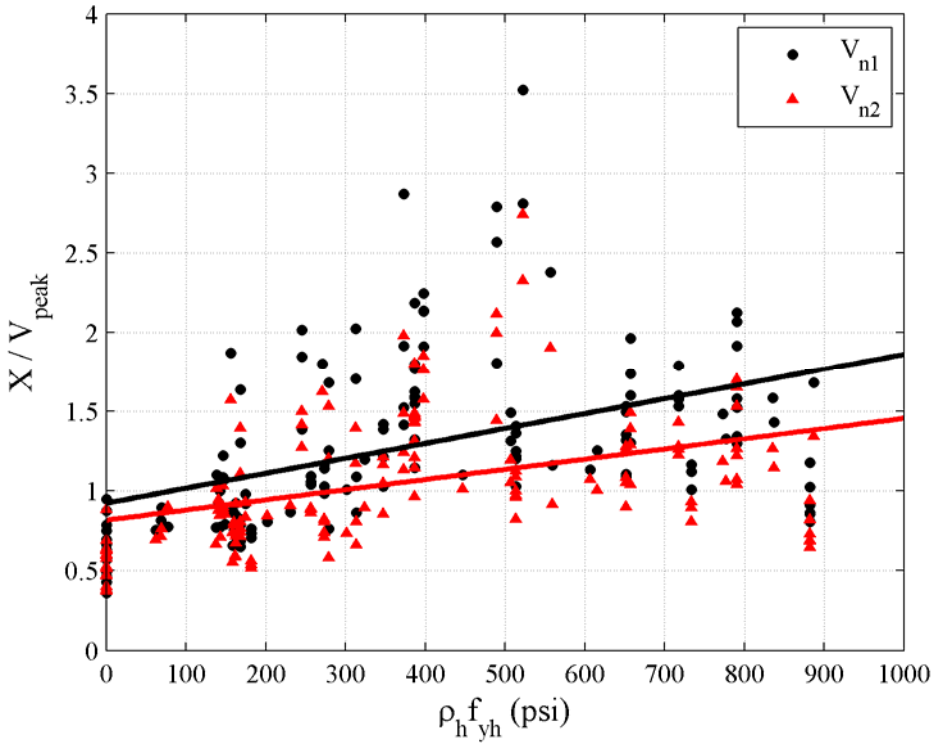


**Figure 4-11 Variation of $V_{n1}/V_{peak}$ and $V_{n2}/V_{peak}$ with $\rho_h f_{yh}$**

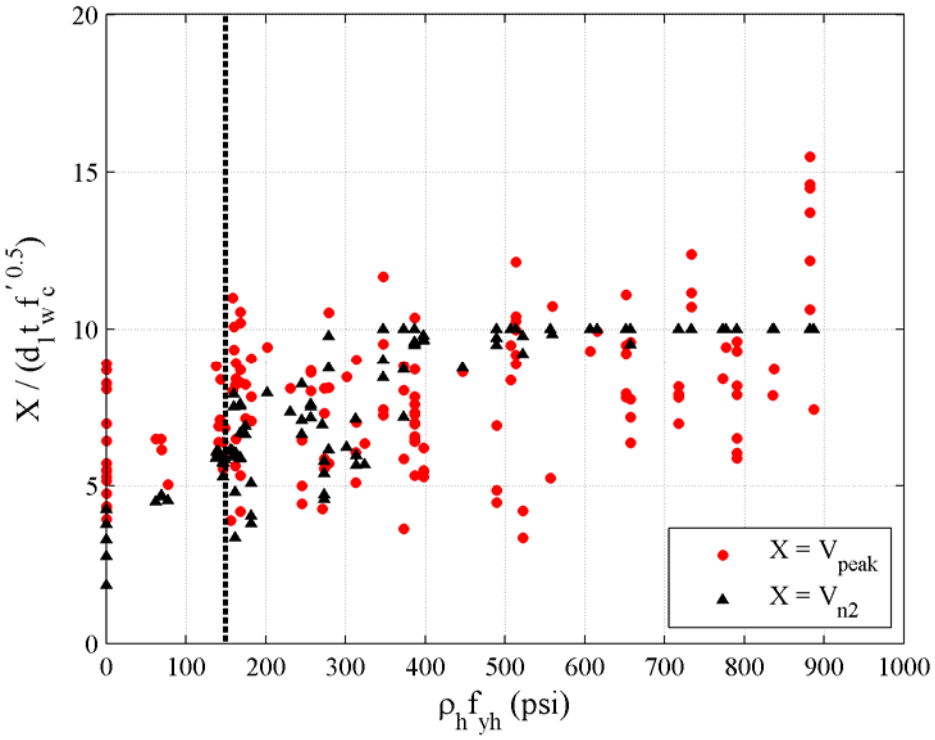


**Figure 4-12 Variation of normalized shear stress obtained using Equation Set II ($V_{n2}$) and measured peak shear strength ($V_{peak}$) with $\rho_h f_{yh}$**

here, the average, minimum, and maximum ratios of effective depth to wall length are 0.72, 0.54, and 0.95, respectively; the corresponding standard deviation is 0.11.

Figure 4-13 presents the variation of $V_{n3}/V_{peak}$ with wall vertical web reinforcement ratio. As shown by the linear fit in the figure, the overestimation of peak shear strength with Barda equation is greater for walls with heavy vertical web reinforcement ratio. The under estimations of Equation Set III are for a small number of walls, most of which do not comply with the minimum vertical reinforcement requirements of ACI 318-08 ($\rho_v f_{yv} \leq$ 150 psi for $f_{yv}$ = 60 ksi). Similar trends are seen in Figure 4-14 and Figure 4-15, which present the variation of $V_{n3}/V_{peak}$ with moment-to-shear ratio and concrete compressive strength, respectively. The Barda Equation becomes more unconservative for increasing values of both moment-to-shear ratio and concrete compressive strength. Equation Set III substantially overestimates the peak shear strength of rectangular walls with moment-to-shear ratios greater than 1.5 and $\rho_v f_{yv}$ greater than 200 psi. The equation captures the influence of axial stress on peak shear strength reasonably well as indicated by the near-horizontal line of linear fit in Figure 4-16.

Figure 4-17 presents the variation of normalized shear stress [shear force divided by the product of effective shear area ($d_2 t_w$) and $\sqrt{f_c'}$ ] computed using Equation Set III ($V_{n3}$) and the measured peak shear strength ($V_{peak}$), with $\rho_v f_{yv}$. The shear strength predictions of Equation Set III are not subject to an upper bound unlike the other four procedures investigated herein. As seen in Figure 4-17, the average shear stress calculated by Equation Set III (solid triangles) is higher than those computed using experimental data (solid circles). This observation is attributed to the type of specimens from which the Barda equation was derived, namely, walls with heavily reinforced flanges. Equation Set III should not be used for squat walls with rectangular cross-sections. An upper bound on the vertical web reinforcement ratio will improve the accuracy of the procedure by reducing the overestimation of peak shear strength for heavily reinforced walls.

#### 4.3.1.4 ASCE 43-05 Equations (Equation Set IV)

Equation Set IV is a variant on the Barda equation (Equation Set III). The major difference between the Equation Set III and Equation Set IV is the calculation of the contribution of reinforcement to the peak shear strength. The Barda equation uses vertical web reinforcement only to calculate shear carried by reinforcement whereas the ASCE 43-05 equation (Equation Set IV) uses both the horizontal and vertical web reinforcement ratios and calculates a combined reinforcement ratio as a function of wall aspect ratio. Equation Set IV overpredicts the peak shear strength of 87% of the walls in the database with mean and median values of $V_{n4}/V_{peak}$ of 1.52 and 1.46, respectively. The corresponding standard deviation and coefficient of variation are 0.48 and 0.31. The dispersion in the ratio of predicted to experimentally measured peak shear strength obtained using Equation Set IV is smaller (COV=0.31) than that of Equation Set III (COV=0.32).

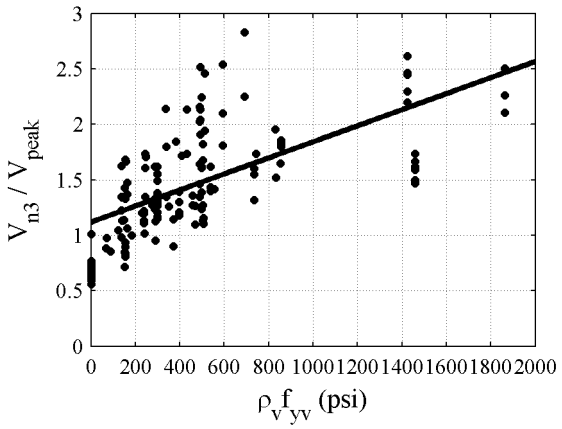


**Figure 4-13 Variation of $V_{n3}/V_{peak}$ with $\rho_v f_{yv}$**

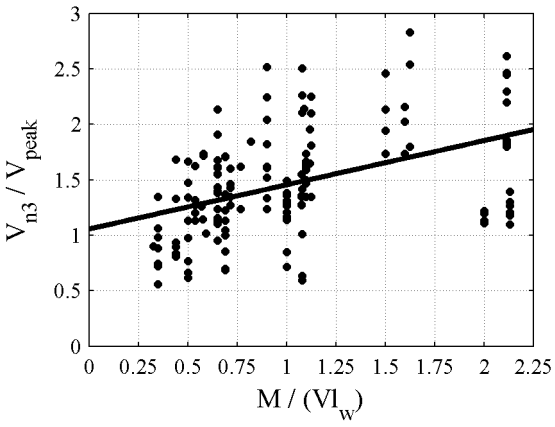


**Figure 4-14 Variation of $V_{n3}/V_{peak}$ with moment-to-shear ratio**

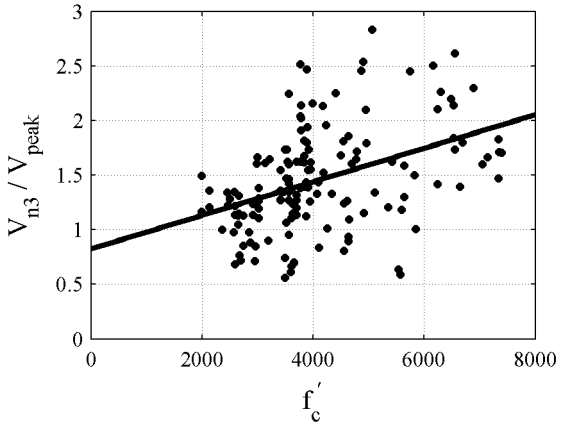


**Figure 4-15 Variation of $V_{n3}/V_{peak}$ with $f_c'$**

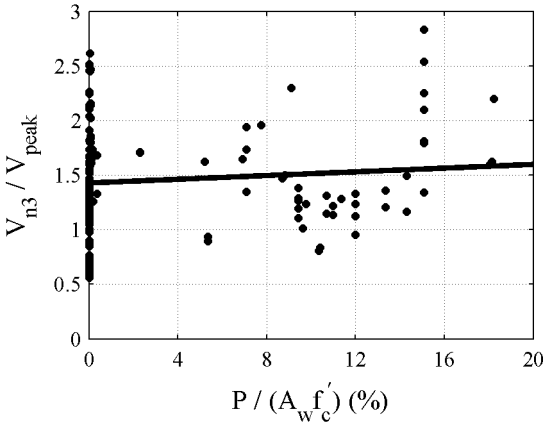


**Figure 4-16 Variation of $V_{n3}/V_{peak}$ with normalized axial stress**

Figure 4-18 through Figure 4-22 present the variation of $V_{n4}/V_{peak}$ with horizontal web reinforcement ratio, vertical web reinforcement ratio, aspect ratio (represented using moment-to-shear ratio), normalized axial stress (axial force divided by the product of wall area and $f_c'$), and $f_c'$, respectively. Of the five procedures considered, only the ASCE 43-05 procedure considers five design variables in calculation of peak shear strength. As indicated by the near-horizontal linear fit lines in Figure 4-18 through Figure 4-22, the variance associated with the predictions of Equation Set IV with respect to the considered variables is relatively constant except for horizontal web reinforcement ratio. The percentage overestimation of peak shear strength by Equation Set IV increases significantly with increasing horizontal reinforcement ratio.

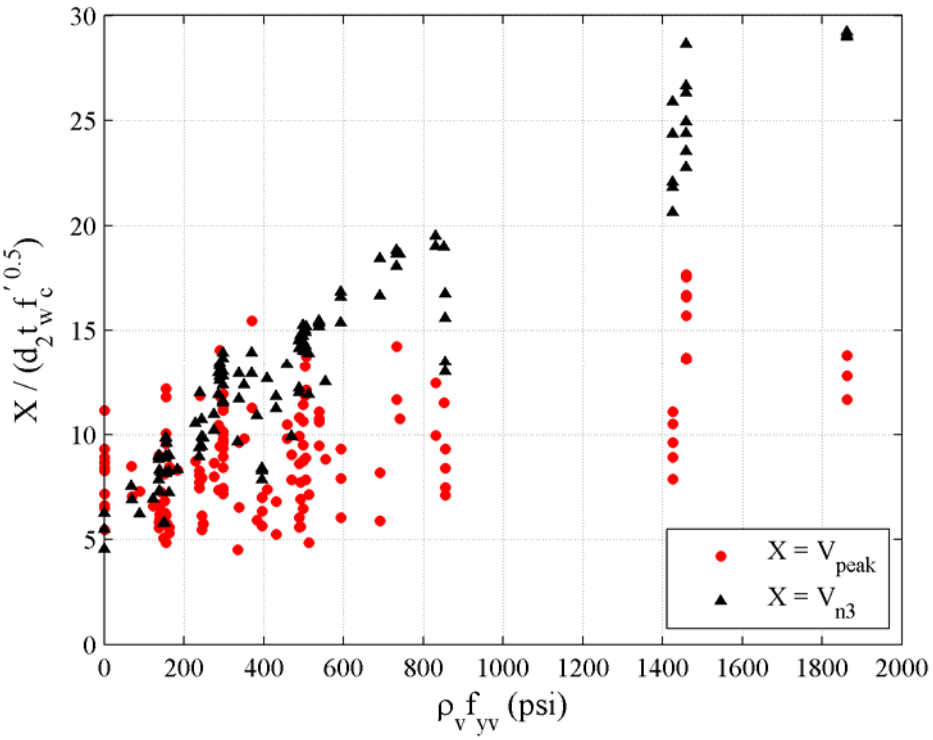


**Figure 4-17 Variation of normalized shear stress obtained using Equation Set III ($V_{n3}$) and measured peak shear strength ($V_{peak}$) with $\rho_v f_{yv}$**

Figure 4-23, which presents the variation of measured peak shear strength normalized by the product of $\sqrt{f_c'}$ and ($d_3 t_w$) with the combined reinforcement ratio ($\rho_{se} f_{y1}$), shows that the $20\sqrt{f_c'}$ upper bound on peak shear stress was not reached by any of the 150 walls in the database. The predictions of Equation Set IV are not governed by the upper stress limit and the utility of this upper stress limit is most questionable. As seen in Figure 4-23, Equation Set IV (solid triangles) is accurate for lightly reinforced walls only and is unconservative for higher combined reinforcement ratios. Equation Set IV should not be used to design rectangular walls.

Equation Set IV uses an effective depth ($d_3$) to calculate the peak shear strength. For the rectangular walls considered here, the average, minimum, and maximum ratios of effective depth to wall length are 0.74, 0.56, and 0.95, respectively. The standard deviation is 0.10.

### 4.3.1.5 Wood's Equation

Equation Set V is based in part on the shear friction analogy [e. g., Hofbeck et al. (1969)] and was developed by Wood (1990). Figure 4-24 and Figure 4-25 present the variation of $V_{n5}/V_{peak}$ with the ratio of the total area of vertical reinforcement to the wall area ($\rho_{vall}$) and concrete compressive strength, which are the two parameters considered in the Wood procedure. Unlike the other procedures considered herein, Wood's equation becomes more conservative as the reinforcement ratio increases, as seen in Figure 4-24. Of the five equation sets studied, Wood

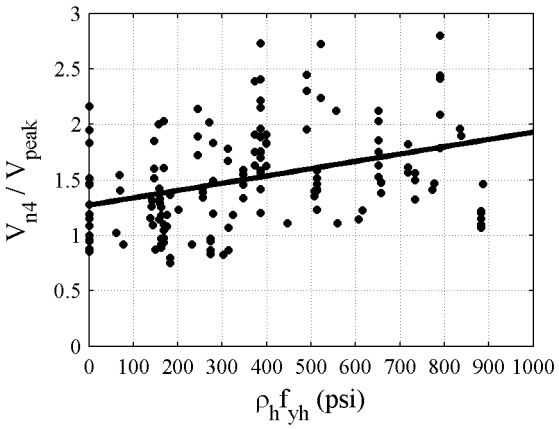


**Figure 4-18 Variation of $V_{n4}/V_{peak}$ with $\rho_h f_{yh}$**

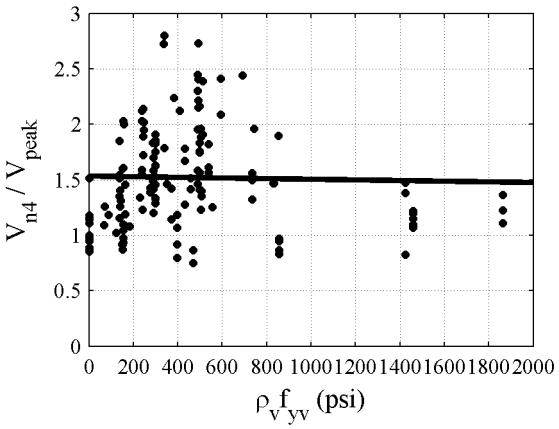


**Figure 4-19 Variation of $V_{n4}/V_{peak}$ with $\rho_v f_{yv}$**

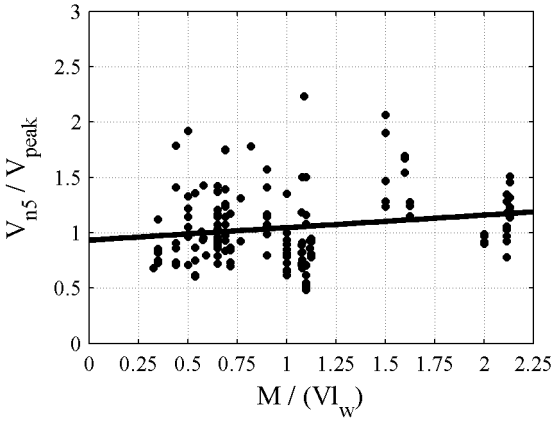


**Figure 4-20 Variation of $V_{n4}/V_{peak}$ with moment-to-shear ratio**

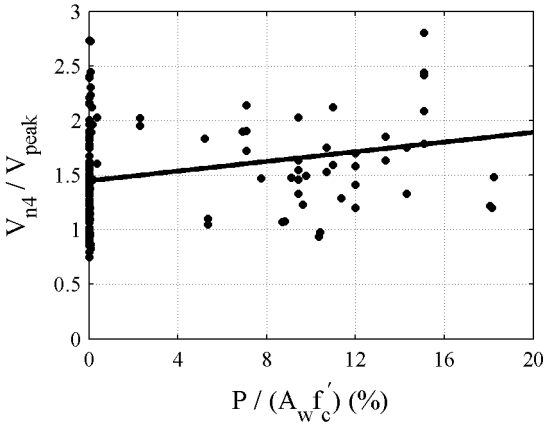


**Figure 4-21 Variation of $V_{n4}/V_{peak}$ with normalized axial stress**

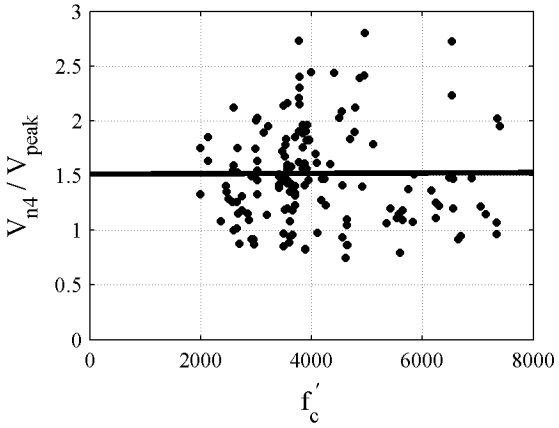


**Figure 4-22 Variation of $V_{n4}/V_{peak}$ with concrete $f_c'$**

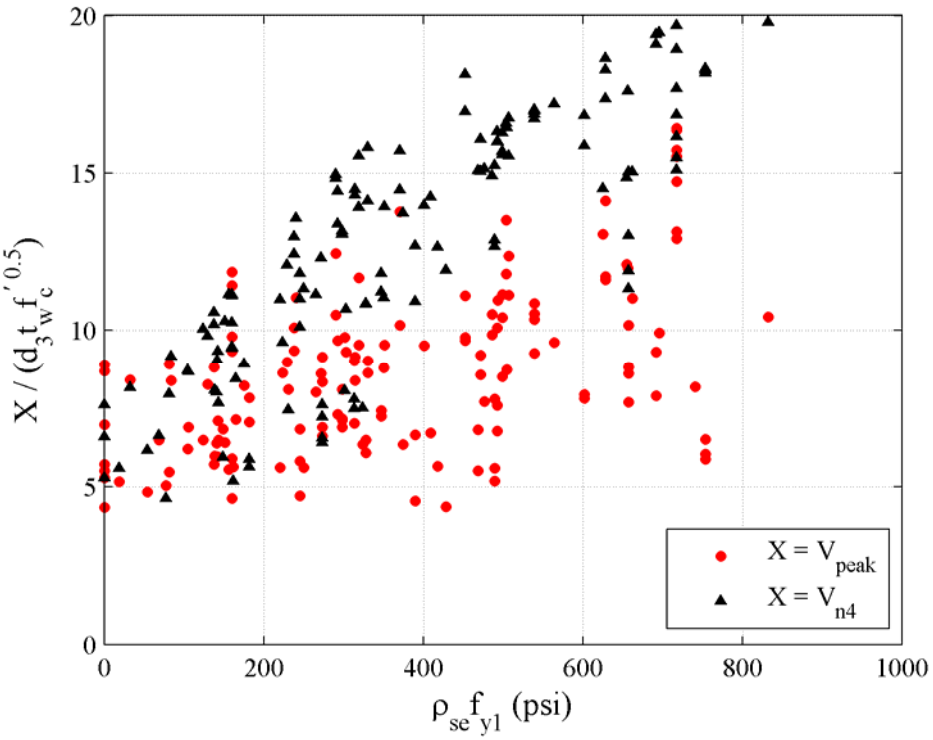


**Figure 4-23 Variation of normalized shear stress obtained using Equation Set IV ($V_{n4}$) and measured peak shear strength ($V_{peak}$) with $\rho_{se} f_{y1}$**

equation yields the most conservative estimates of peak shear strength (54% are conservative). The mean and median value of $V_{n5}/V_{peak}$ are 1.05 and 0.97, respectively. The corresponding standard deviation and coefficient of variation are 0.33 and 0.32. Eighty-nine percent of the values of $V_{n5}/V_{peak}$ are between 0.50 and 1.50.

Figure 4-26 presents the variation of normalized shear stress [shear force divided by the product of effective shear area ($A_w$) and $\sqrt{f_c'}$ ] obtained using Equation Set V ($V_{n5}$) and measured peak shear strength ($V_{peak}$) with the product of the reinforcement yield stress and the ratio of the total area of vertical wall reinforcement to the wall area. As indicated in Figure 4-26, only 10 of the 150 peak shear strength predictions were governed by the part of Equation Set V associated with the vertical reinforcement area (solid triangles with an ordinate greater than 6) and the remaining 140 predictions were associated with the lower bound limit on shear stress of $6\sqrt{f_c'}$ . None of the predictions was governed by the upper limit on shear stress. Of the five sets of predictive equations, Wood's equation provides the best median estimate of peak shear strength (0.97) and the second smallest coefficient of variation (0.32).

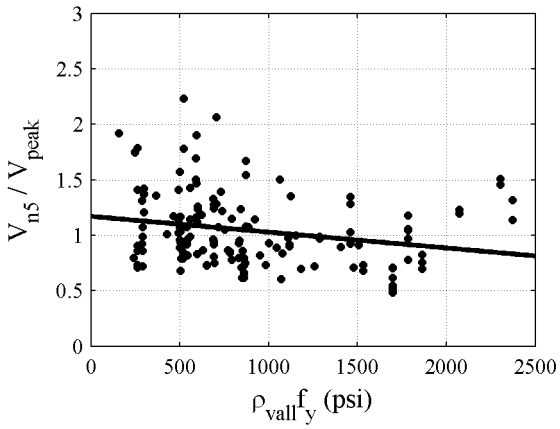


**Figure 4-24 Variation of $V_{n5}/V_{peak}$ with $\rho_{vall} f_{y2}$**

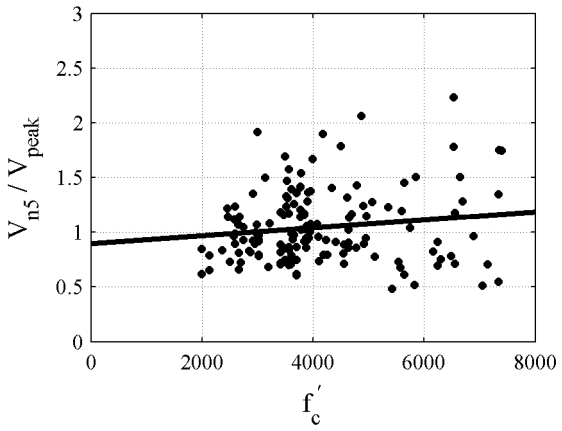


**Figure 4-25 Variation of $V_{n5}/V_{peak}$ with $f_c'$**

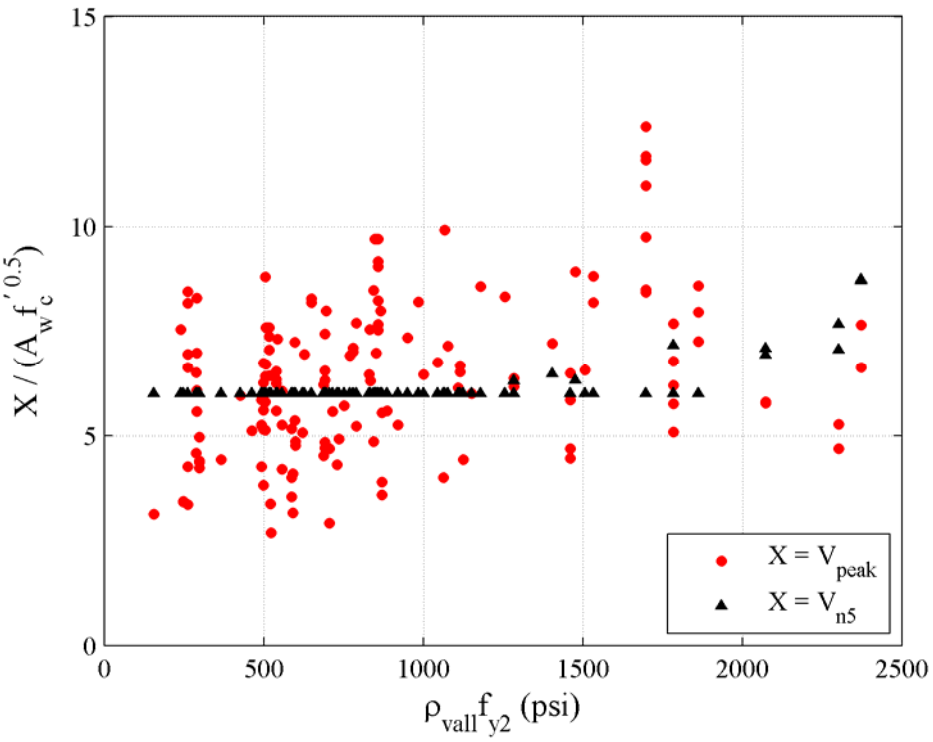


**Figure 4-26 Variation of normalized shear stress obtained using Equation Set V ($V_{n5}$) and measured peak shear strength ($V_{peak}$) with $\rho_{vall} f_{y2}$**

### 4.3.2 Group 2: Shear-Critical Squat Rectangular Walls

A shear-critical wall is defined as a wall with measured peak shear strength less than the shear force associated with the development of expected flexural strength (shear-flexural strength, $V_{flex}$) as determined using cross-section analysis. Ninety-one of the 150 squat walls were judged to be shear-critical.

Figure 4-27 presents the variation of $V_{peak}/V_{flex}$ with moment-to-shear ratio. The data points in Figure 4-27 that are less than 1.0 correspond to the shear-critical walls in this group. Figure 4-27 reveals, as expected, that walls with small moment-to-shear ratio are generally shear-critical and that walls with moment-to-shear ratios of 1.5 and greater are generally flexure-critical. However, some walls with lower aspect ratios developed their flexural strength.

Table 4-2 summarizes results for the shear-critical walls. Figure 4-28 presents box-and-whisker plots, similar to Figure 4-1, for the shear-critical walls. A comparison of results presented in Table 4-2 and Table 4-1 shows a reduction in the percentage of unconservative predictions for Equation Sets I, II, III, and IV for the Group 2 walls. Wood's equation ($V_{n5}$) best estimates the shear strength of shear-critical walls with a median value of $V_{n5}/V_{peak}$ equal to 0.99 and a relatively small coefficient of variation. The equations of Chapter 11 of ACI 318-08 provide the most conservative estimations as measured using median results.

The procedures of Barda and ASCE 43 are substantially unconservative for shear-critical walls. Overall, the results obtained using the Group 1 and Group 2 walls differ only modestly.

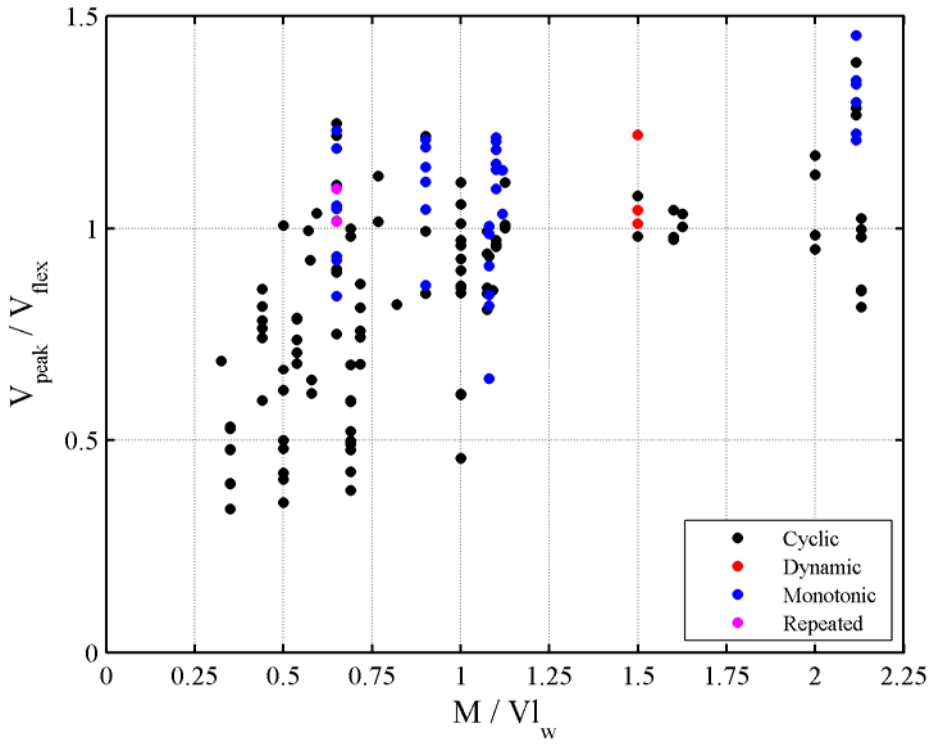


**Figure 4-27 Variation of the ratio of measured peak shear strength to the shear-flexural strength with moment-to-shear-ratio**

**Table 4-2 Statistics of the ratio of the shear strength predicted using Equation Sets 1 through 5 to measured peak shear strength of shear-critical walls (Group 2)**

| | Mean | Median | St. Dev. | COV | Min | Max | % Over-Predictions |
|---|---|---|---|---|---|---|---|
| $V_{n1}/V_{peak}$ | 1.16 | 1.04 | 0.57 | 0.49 | 0.36 | 3.52 | 56 |
| $V_{n1*}/V_{peak}$ | 1.25 | 1.09 | 0.66 | 0.52 | 0.36 | 3.52 | 56 |
| $V_{n2}/V_{peak}$ | 0.99 | 0.89 | 0.42 | 0.43 | 0.37 | 2.74 | 36 |
| $V_{n2*}/V_{peak}$ | 1.07 | 0.91 | 0.49 | 0.46 | 0.37 | 2.74 | 45 |
| $V_{n3}/V_{peak}$ | 1.31 | 1.27 | 0.45 | 0.34 | 0.56 | 2.52 | 76 |
| $V_{n4}/V_{peak}$ | 1.45 | 1.41 | 0.44 | 0.31 | 0.75 | 2.73 | 85 |
| $V_{n5}/V_{peak}$ | 1.06 | 0.99 | 0.35 | 0.33 | 0.61 | 2.23 | 48 |

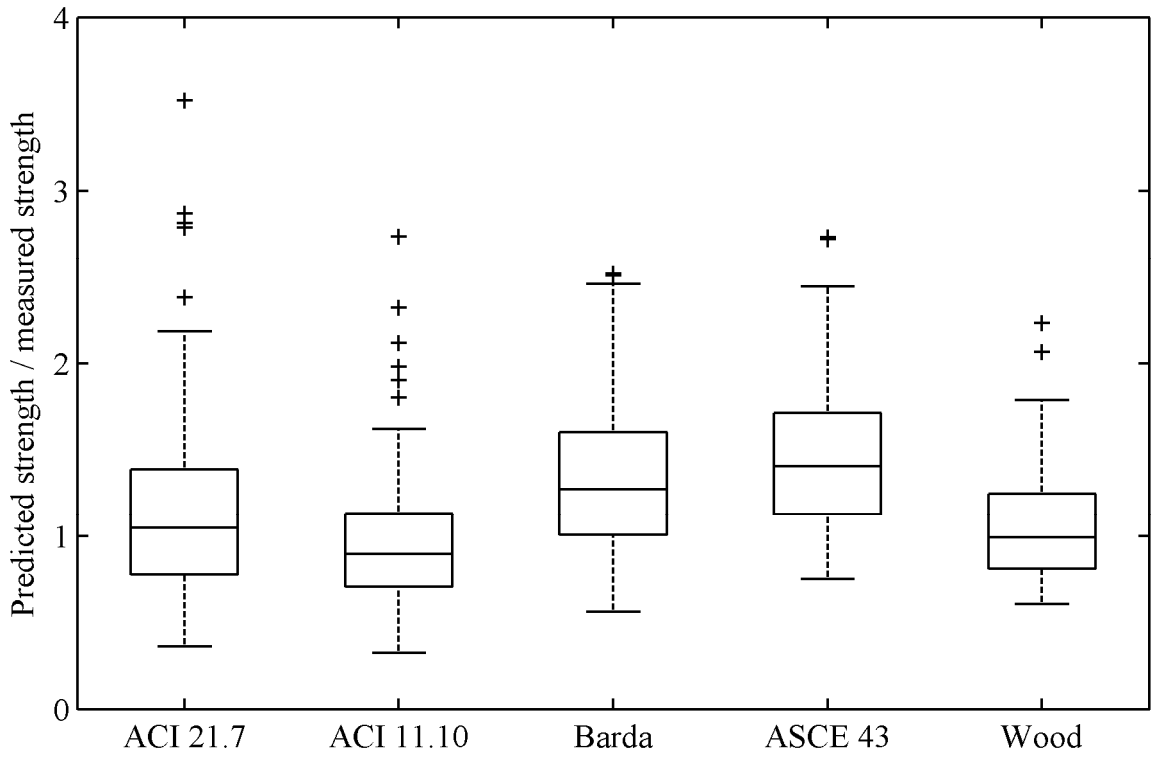


**Figure 4-28 Distribution of the ratio of the predicted shear strengths to measured peak shear strengths for shear-critical walls**

### 4.3.3 Group 3: ACI 318-Compliant, Shear-Critical Squat Rectangular Walls

Group 3 eliminates the walls that do not comply with the requirements of Section 21.9 of ACI 318-08, which limits the minimum horizontal and vertical web reinforcements to 0.0025 and requires that the vertical web reinforcement ratio be no less than the horizontal web

reinforcement ratio for walls with aspect ratios of less than 2.0, that spacing between the reinforcement in the wall web be no more than 18 in., and at least two curtains of web reinforcement be provided. As noted in Section 3, all walls in the rectangular wall database had a web reinforcement spacing less than 18 in. Figure 4-29 presents the variation of normalized measured peak shear strength with the moment-to-shear ratio as a function of the number of reinforcement curtains in the wall. As seen in the figure, the difference between the peak shear strengths measured for walls that include single or double reinforcement is modest. Therefore, the ACI 318 limit on the number of reinforcement curtains is not used to identify ACI 318-compliant walls. As a result, all walls in Group 2 that comply with a) the minimum web reinforcement requirements (0.0025) of Chapter 21.7 of ACI 318 (0.0025), and b) the requirement that the vertical web reinforcement ratio be no less than horizontal web reinforcement ratio, are included in Group 3.

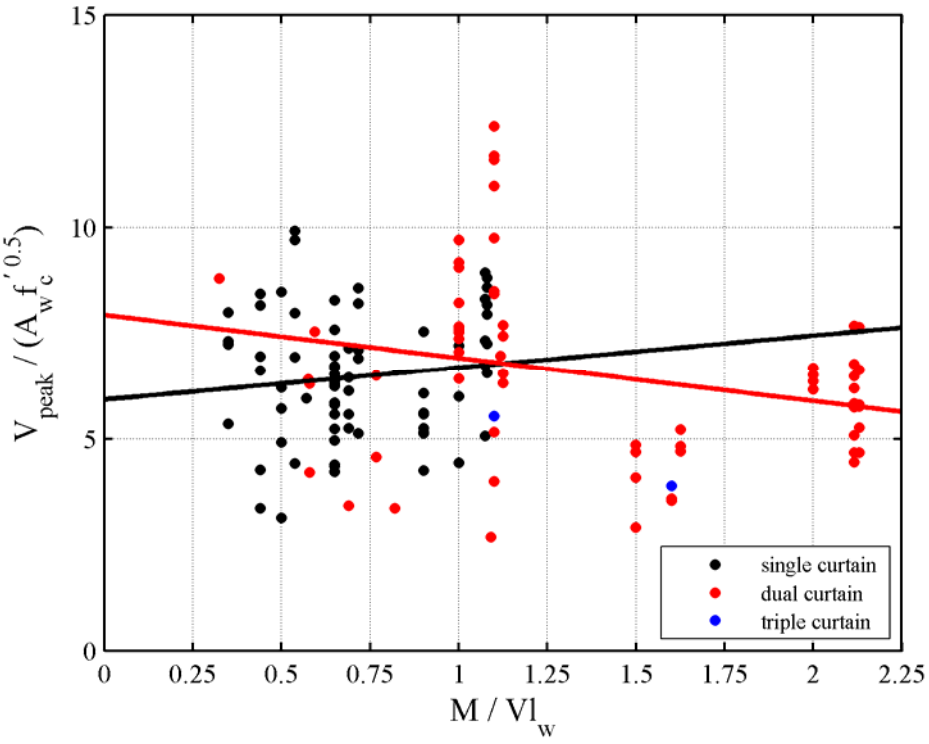


**Figure 4-29 Variation of normalized measured peak shear strength ($V_{peak}$) with moment-to-shear ratio as a function of the number of reinforcement curtains**

Forty-three of the 91 shear-critical walls in Group 2 are considered ACI 318-compliant. Table 4-3 summarizes results for Group 3 walls. A comparison of the results presented in Table 4-3 and Table 4-2 shows an improvement in the predictions of Equations Sets I, II, and III for the Group 3 walls in terms of coefficients of variation. Wood's equation once again provides the best estimates of the peak shear strength of ACI 318-compliant, shear-critical walls with a mean value of $V_{n5}/V_{peak}$ of 1.06 and a relatively small coefficient of variation. The procedure of Chapter 11 of ACI 318-08 provides again the most conservative estimates of peak shear strength as measured by median results.

**Table 4-3 Distribution of the ratio of the predicted shear strengths to measured peak shear strengths for ACI 318-compliant, shear-critical walls**

| | Mean | Median | St. Dev. | COV | Min | Max | % Over-Predictions |
|---|---|---|---|---|---|---|---|
| $V_{n1}/V_{peak}$ | 1.23 | 1.09 | 0.54 | 0.44 | 0.65 | 2.87 | 62.8 |
| $V_{n1*}/V_{peak}$ | 1.30 | 1.10 | 0.57 | 0.44 | 0.65 | 3.00 | 62.8 |
| $V_{n2}/V_{peak}$ | 1.02 | 0.89 | 0.39 | 0.38 | 0.52 | 2.12 | 39.5 |
| $V_{n2*}/V_{peak}$ | 1.08 | 0.97 | 0.40 | 0.37 | 0.52 | 2.12 | 48.8 |
| $V_{n3}/V_{peak}$ | 1.43 | 1.32 | 0.46 | 0.32 | 0.81 | 2.52 | 83.7 |
| $V_{n4}/V_{peak}$ | 1.49 | 1.37 | 0.48 | 0.32 | 0.75 | 2.73 | 86.0 |
| $V_{n5}/V_{peak}$ | 1.06 | 0.94 | 0.36 | 0.34 | 0.61 | 2.06 | 48.8 |

Although the accuracy of the equation sets differs slightly between Groups 1, 2 and 3, the trends are similar across groups. In all groups, the Barda and ASCE 43-05 equations yield substantially unconservative estimations (i.e., overpredict) of the peak shear strength. The equation in Chapter 11 of ACI 318-08 and the Wood equation yield the most conservative estimates of peak shear strength. For all groups, the trends associated with the predictions of Chapter 21 and Chapter 11 of ACI 318-08 are similar. The percentage of conservative predictions (i.e., underpredictions) of peak shear strength is consistently higher for the Chapter 11 equation, in the large part due to the smaller effective depth used by the Chapter 11 equation.

## 4.4 Walls with Barbells and Flanges

In this section, experimentally measured peak shear strengths of walls with boundary elements are compared with the predictions obtained using five equations identified in Section 4.2. Section 3 presents detailed information on the database that included 284 walls with boundary elements (barbells or flanges). During the preliminary data investigation, it was observed that walls tested using dynamic pulses, to mimic blast loading, had approximately a 25% higher peak shear strength on average than identical walls tested under quasi-static monotonic loading [Antebi et al. (1960)]. This outcome is expected since the compressive and tensile strengths of concrete and steel increase substantially at high-strain rates. Given that the focus of the study is the seismic behavior of squat walls, for which the strain-rate effects are not significant, the data from the blast tests (30 of the 284 walls) are not included in analysis described below. The accuracy of the five predictive equations is therefore evaluated using the experimentally measured peak strengths of the 254 squat walls remaining in the database: 161 barbell and 93 flanged walls. For the cyclically loaded walls, the peak strength is taken as the average of the peak shear strengths recorded in the opposite directions. The 254 walls with boundary elements are parsed into three groups: Group 1—all 254 squat walls, Group 2—shear-critical squat walls, Group 3—ACI 318-compliant, shear-critical squat walls.

Similar to evaluation of the rectangular walls, the area centroid of the wall vertical reinforcement in tension (and $d_2$ in Equation 4-7), the location of the resultant tensile force in the vertical reinforcement (to calculate $d_1$ in Equations 4-2, 4-3, 4-4 and 4-5, and $d_3$ in Equation 4-8) and the ultimate moment capacity (to identify shear-critical walls in Group 2) were computed using XTRACT [Imbsen and Associates, Inc. (2007)] for each wall in the database. The assumptions for modeling the concrete and reinforcement are those listed in Section 4.3. The reported values of geometry (wall cross-sectional layout, reinforcement size and layout), material ( $f_c'$, yield and fracture stresses for reinforcement) and loading properties (axial force) are used for the cross-section analysis.

### 4.4.1 Group 1: All 254 Walls with Boundary Elements

A statistical presentation of the ratio of the predicted to measured peak shear strength is presented in Table 4-4 for each of the five equation sets. The ratios of predicted to measured peak strength tagged with an asterisk (e.g., $V_{n1*}$) present statistics for the equation sets without the corresponding upper shear stress limits. Values in columns 2 (arithmetic mean) or 3 (median or 50$^{th}$ percentile) in Table 4-4 greater than 1.0 indicate that the corresponding strength equation is unconservative in a mean or median sense, respectively. Figure 4-30 presents the distributions of the ratios of the predicted peak strength to measured peak strength for the five procedures using box and whisker plots, which present the lower quartile ($Q_1$), median ($Q_2$), upper quartile ($Q_3$), and extreme values.

**Table 4-4 Statistics of the ratio of the shear strength predicted using Equation Sets 1 through 5 to measured peak shear strength of all 254 walls (Group 1)**

| | Mean | Median | St. Dev. | COV | Min | Max | % Over-Predictions |
|---|---|---|---|---|---|---|---|
| $V_{n1}/V_{peak}$ | 0.75 | 0.69 | 0.30 | 0.40 | 0.18 | 2.19 | 17 |
| $V_{n1*}/V_{peak}$ | 0.87 | 0.81 | 0.42 | 0.48 | 0.18 | 2.98 | 27 |
| $V_{n2}/V_{peak}$ | 0.64 | 0.59 | 0.23 | 0.36 | 0.21 | 1.75 | 7 |
| $V_{n2*}/V_{peak}$ | 0.78 | 0.75 | 0.31 | 0.40 | 0.21 | 2.43 | 19 |
| $V_{n3}/V_{peak}$ | 0.83 | 0.81 | 0.23 | 0.28 | 0.39 | 1.73 | 20 |
| $V_{n4}/V_{peak}$ | 0.94 | 0.91 | 0.26 | 0.28 | 0.47 | 2.16 | 39 |
| $V_{n4*}/V_{peak}$ | 0.94 | 0.91 | 0.26 | 0.28 | 0.47 | 2.16 | 40 |
| $V_{n5}/V_{peak}$ | 0.60 | 0.56 | 0.21 | 0.35 | 0.27 | 1.31 | 5 |

The mean and median values of the shear strength ratios presented in Table 4-4 and Figure 4-30 for Equation Sets I ($V_{n1}$) and II ($V_{n2}$) indicate that both equation sets are conservative for walls with boundary elements. As noted previously for rectangular walls, the assumption for the effective shear area of the wall is the principal reason why Equation Set II is more conservative

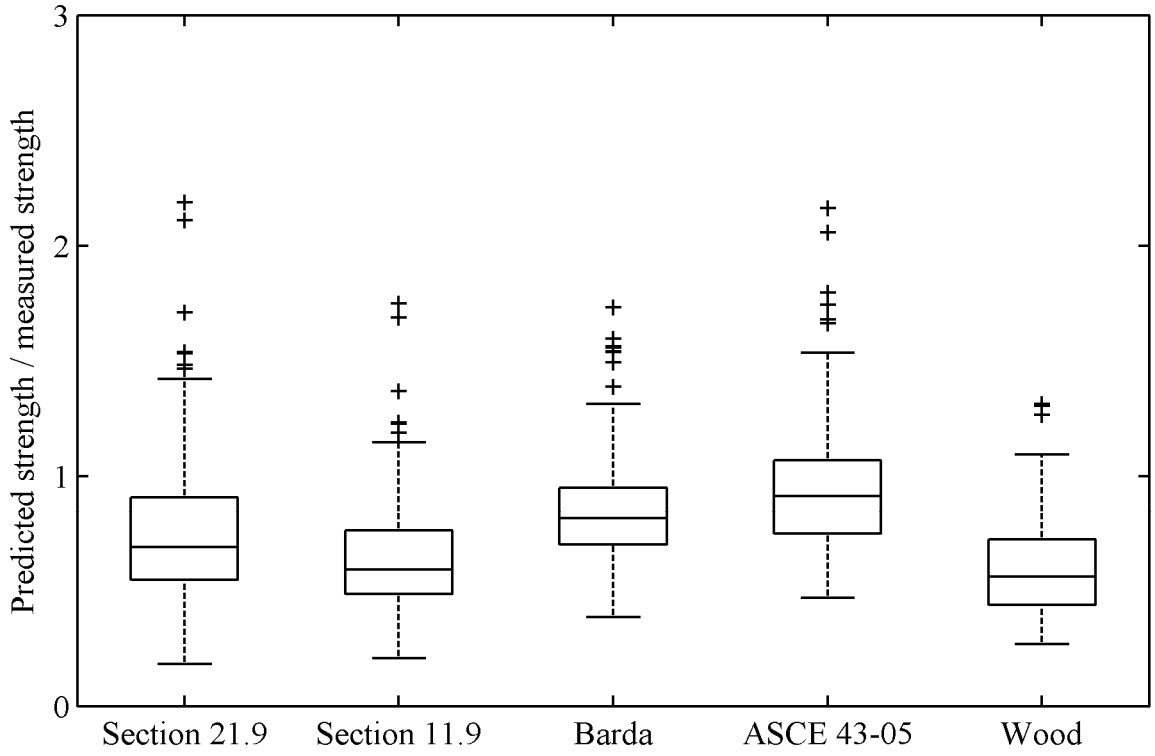


**Figure 4-30 Distribution of the ratio of the predicted shear strengths to measured peak shear strengths for all 254 walls (Group 1)**

than Equation Set I. The scatter, as measured by coefficient of variation, is smaller for Equation Set II. The Barda and ASCE 43-05 predictive equations, $V_{n3}$ and $V_{n4}$, respectively, yield the best predictions of peak strength in median sense and the smallest coefficients of variation. The ASCE 43-05 equation overestimates the peak shear strength of 39% of the walls the in the database: the highest percentage of the five procedures. Equation Set V ($V_{n5}$) is the most conservative of the five procedures.

#### 4.4.1.1 ACI 318-08 Chapter 21 Equation

Equation Set I overpredicts the peak shear strength of 17% of the walls in the database with mean and median values of $V_{n1}/V_{peak}$ of 0.75 and 0.69, respectively. The corresponding standard deviation and coefficient of variation are 0.30 and 0.40, respectively. The coefficient of variation associated with the predictions of Equation Set I is the greatest of the five procedures investigated.

Figure 4-31 through Figure 4-33 present the variation of $V_{n1}/V_{peak}$ with horizontal reinforcement ratio, moment-to-shear ratio, and $f_c'$, respectively. Figure 4-31 through Figure 4-33 indicate that the Chapter 21 procedure becomes less conservative with increasing horizontal reinforcement ratio and moment-to-shear ratio and becomes more conservative with increasing $f_c'$. The significant scatter observed in Figure 4-31 through Figure 4-33 indicates model deficiency. Note that the dominant failure mode was diagonal compression for walls in the barbell and flanged

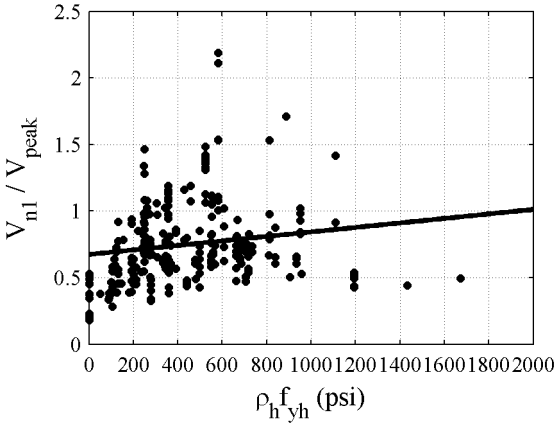


**Figure 4-31 Variation of $V_{n1}/V_{peak}$ with $\rho_h f_{yh}$**

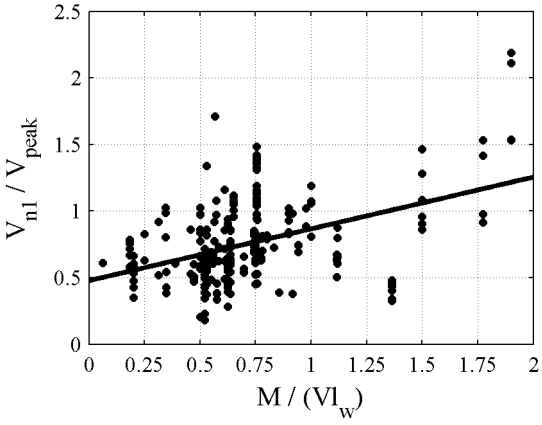


**Figure 4-32 Variation of $V_{n1}/V_{peak}$ with moment-to-shear ratio**

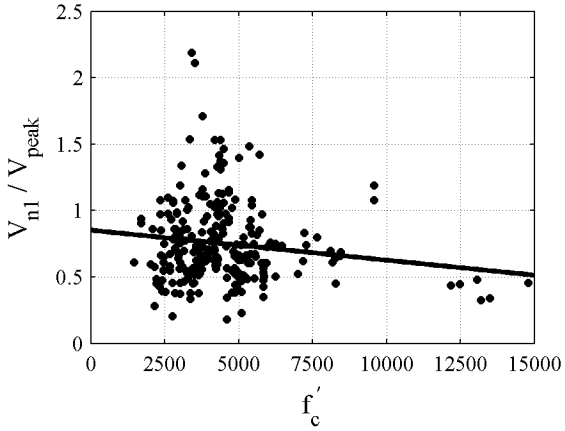


**Figure 4-33 Variation of $V_{n1}/V_{peak}$ with $f_c'$**

wall database. The confinement effect of the boundary elements on wall web may delay diagonal tension failure and limit the opening of cracks.

Figure 4-34 presents the variation of the $V_{n1}/V_{peak}$ and $V_{n1*}/V_{peak}$ with horizontal web reinforcement ratio along with the corresponding linear fits. Figure 4-35 presents the variation of normalized shear stress [shear force divided by the product of web area ($A_w$) and $\sqrt{f_c'}$ ] obtained using Equation Set I ($V_{n1}$) and measured peak shear strength ($V_{peak}$) with $\rho_h f_{yh}$. Figure 4-34 and Figure 4-35 indicate that the upper stress limit governs the peak shear strength predictions of Equation Set I with $\rho_h f_{yh}$ larger than approximately 400 psi. The upper shear stress limit increases the conservatism of Equation Set I but its utility is somewhat questionable since 165 of the 254 walls in the dataset had normalized measured shear stresses of greater than $10\sqrt{f_c'}$ psi.

As seen in Figure 4-35, Equation Set I underpredicts the measured peak shear strength ($V_{peak}$) for most values of $\rho_h f_{yh}$.

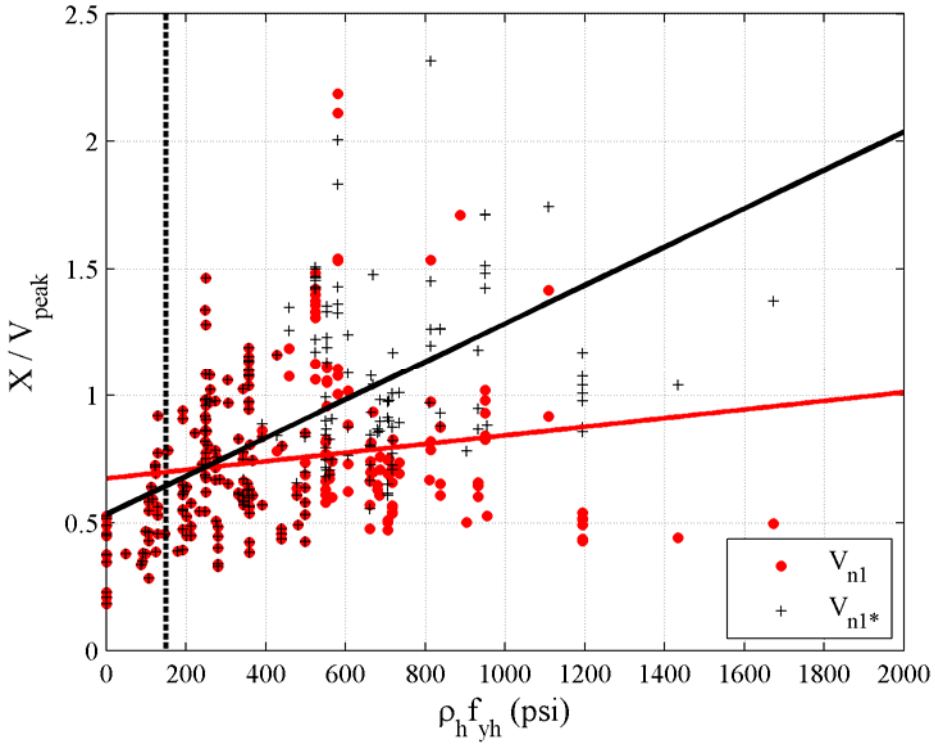


**Figure 4-34 Variation of $V_{n1}/V_{peak}$ and $V_{n1*}/V_{peak}$ ratios with $\rho_h f_{yh}$**

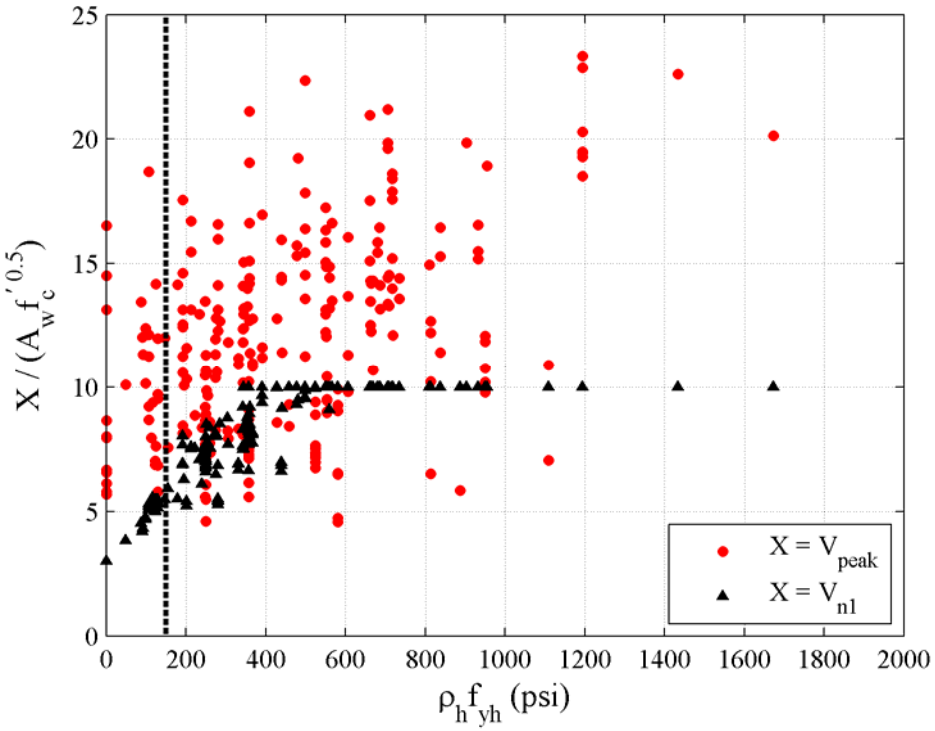


**Figure 4-35 Variation of normalized shear stress obtained using Equation Set I ($V_{n1}$) and measured peak shear strength ($V_{peak}$) with $\rho_h f_{yh}$**

### 4.4.1.2 ACI 318-08 Chapter 11 Equation

Equation Set II overpredicts the peak shear strength of 7% of the walls in the database. Equation Set II yields more conservative predictions of peak shear strength than Equation Set I mainly as a result of the use of a smaller effective web area. The mean and median values of $V_{n2}/V_{peak}$ are 0.64 and 0.59, respectively. The corresponding standard deviation and coefficient of variation are 0.23 and 0.36. The scatter in the predictions of Equation Set II (COV=0.36) are smaller than those of Equation Set I (COV=0.40).

Figure 4-36 through Figure 4-39 present the variation of $V_{n2}/V_{peak}$ with the design variables used by Equation Set II, namely, horizontal web reinforcement ratio, moment-to-shear ratio, $f_c'$, and axial stress, respectively. The lines of best fit are shown in the figures. Most of the predictions of the equation set corresponding to values of $\rho_h f_{yh}$ less than 200 psi are smaller than the corresponding measured peak shear strengths. As seen in Figure 4-37, the ratio of predicted to measured peak shear strength increases significantly with increasing moment-to-shear ratio, which indicates that the procedure cannot capture the influence of moment-to-shear ratio on peak shear strength. The predictions of the procedure with respect to horizontal web reinforcement ratio, $f_c'$ and axial force are somewhat better as indicated by the near zero-slope lines of linear fit. The scatter in the predictions of Equation Set II is significant although it is slightly smaller than that of Equation Set I.

Figure 4-40 presents the variation of normalized shear stress [shear force divided by the product of effective shear area ($d_1 t_w$) and $\sqrt{f_c'}$ ] obtained using Equation Set II ($V_{n2}$) and measured peak shear strength ($V_{peak}$) with $\rho_h f_{yh}$. Similar to Equation Set I, the upper stress limit governs the peak shear strength predictions of Equation Set II for $\rho_h f_{yh}$ larger than approximately 400 psi. The predictions of Equation Set II produce a lower bound estimate for the measured peak shear strength ($V_{peak}$) for a wide range of $\rho_h f_{yh}$.

### 4.4.1.3 Barda et al. (1977) Equation

Equation Set III overpredicts the peak shear strength of 20% of the walls in the dataset with mean and median values of $V_{n3}/V_{peak}$ of 0.83 (0.83 for flanged walls, 0.83 for barbell walls) and 0.81, respectively. The standard deviation and coefficient of variation are 0.24 (0.20 for flanged walls, 0.25 for barbell walls) and 0.28, respectively.

Figure 4-41 through Figure 4-44 present the variation of $V_{n3}/V_{peak}$ with the design variables used by Equation Set III, namely, vertical web reinforcement ratio, moment-to-shear ratio, $f_c'$, and axial force, respectively. As indicated by Figure 4-41 and Figure 4-42, the accuracy of Equation Set III varies significantly with respect to vertical web reinforcement ratio and moment-to-shear ratio. The predictions are generally unconservative for walls with aspect ratios of 1.5 and higher, and conservative for walls with $\rho_v f_{yv}$ of less than 200 psi. The predictions become more conservative with increasing $f_c'$ as seen in Figure 4-43. Equation Set III is conservative for all walls with $f_c'$ > 6000 psi. The Barda equation is generally unconservative (i.e., overpredicts

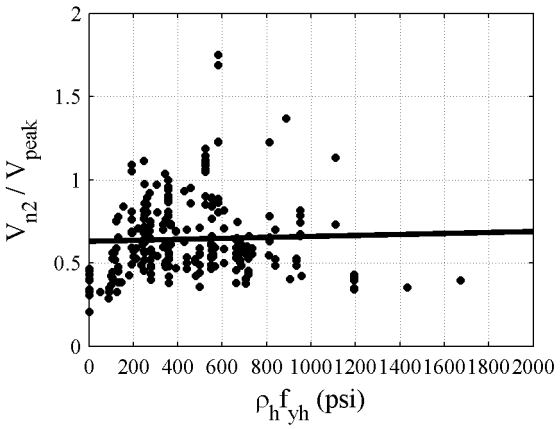


**Figure 4-36 Variation of $V_{n2}/V_{peak}$ with $\rho_h f_{yh}$**

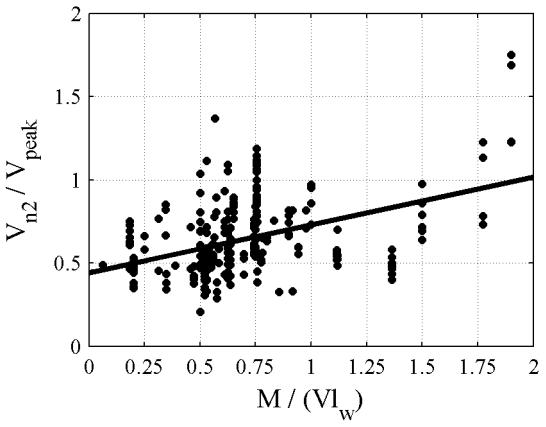


**Figure 4-37 Variation of $V_{n2}/V_{peak}$ with moment-to-shear ratio**

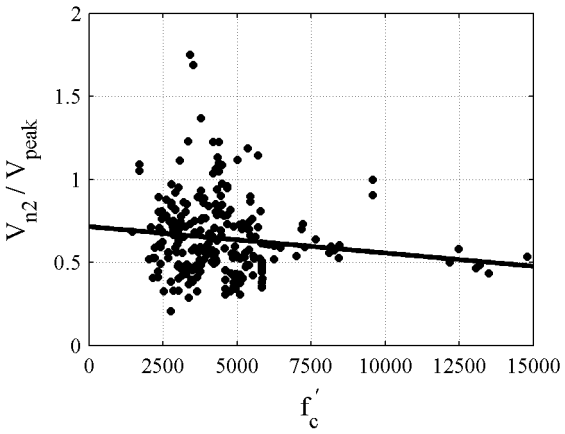


**Figure 4-38 Variation of $V_{n2}/V_{peak}$ with $f_c'$**

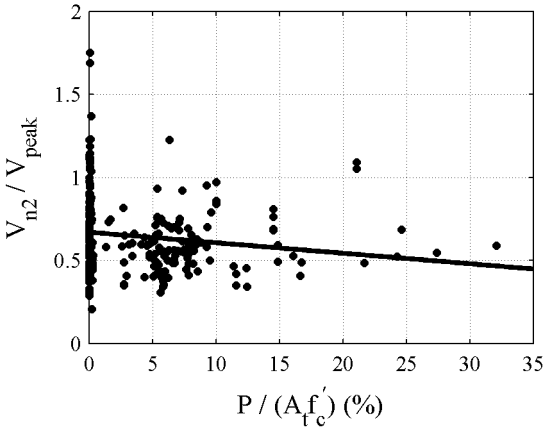


**Figure 4-39 Variation of $V_{n2}/V_{peak}$ with normalized axial stress**

peak shear strength) for walls with normalized axial stress in excess of 20% although the number of data points in this range is limited.

Figure 4-45 presents the variation of normalized shear stress [shear force divided by the product of effective shear area ($d_2 t_w$) and $\sqrt{f_c'}$ ] computed using Equation Set III ($V_{n3}$) and the measured peak shear strength ($V_{peak}$), with $\rho_v f_{yv}$. The predictions of Equation Set III are not limited by an upper bound shear stress unlike the other four procedures investigated herein. As seen in Figure 4-45, Equation Set III produces better estimates of the peak shear strength of heavily reinforced walls than the ACI 318-08 procedures. As seen in Figure 4-35 and Figure 4-40, the predictions of ACI 318-08 for heavily reinforced walls are governed by the upper shear stress limit of $10\sqrt{f_c'}$, which results in significant underestimation of the measured peak shear strength.

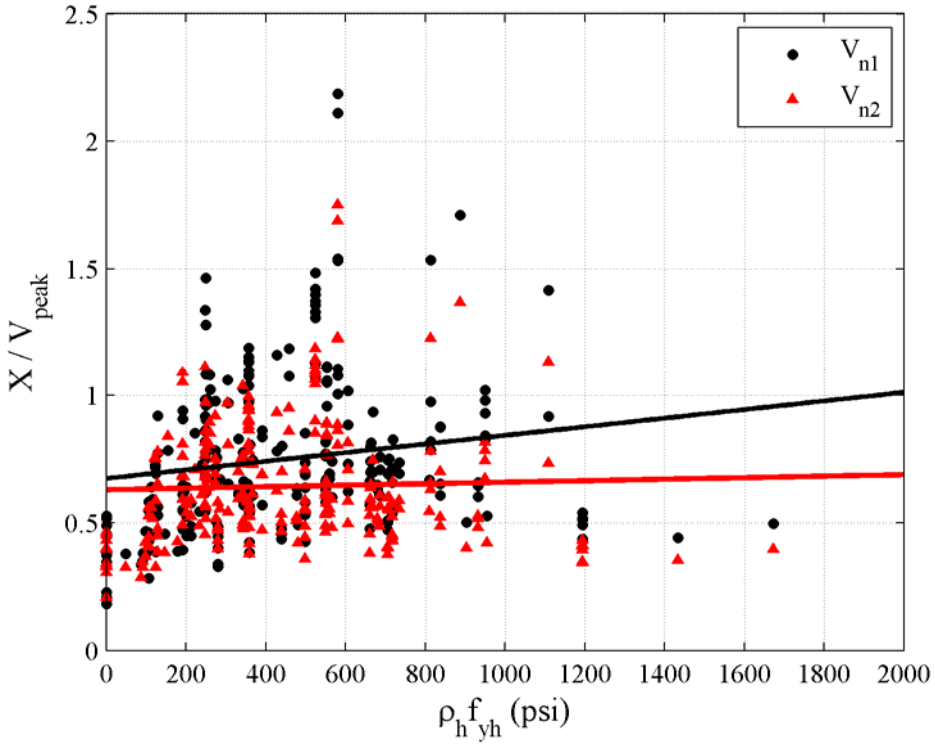


**Figure 4-40 Variation of normalized shear stress obtained using Equation Set II ($V_{n2}$) and measured peak shear strength ($V_{peak}$) with $\rho_h f_{yh}$**

### 4.4.1.4 ASCE 43-05 Equation

The ASCE 43-05 equation provides reasonable estimates of peak shear strength with mean and median values of predicted to measured peak shear strength of 0.94 and 0.91. The corresponding standard deviation and coefficient of variation are 0.26 and 0.28. Equation Set IV overpredicts the peak strength of 39% of the walls in the dataset: the highest percentage of the five equation sets studied.

Figure 4-46 through Figure 4-50 present the variation of $V_{n4}/V_{peak}$ with the design variables used by Equation Set IV, namely, horizontal web reinforcement ratio, vertical web reinforcement ratio, moment-to-shear ratio, concrete compressive strength, and normalized axial stress, respectively. The major difference between Equation Set III and IV is the calculation of the shear carried by the reinforcement. Equation Set III uses vertical web reinforcement ratio whereas Equation Set IV uses a combined reinforcement ratio ($\rho_{se}$) calculated using both horizontal and vertical web reinforcement ratios that varies as a function of wall aspect ratio. An upper limit of 1% is imposed on the combined reinforcement ratio of Equation Set IV. Accordingly, the ASCE 43-05 predictions become more conservative with increasing reinforcement ratios. The accuracy of the predictions are dependent on moment-to-shear ratio and $f_c'$ as seen in Figure 4-48 and Figure 4-50 but are independent of normalized axial stress. The ASCE 43-05 predictive equation produces the best estimates of peak shear strength in a median sense (0.91) with the smallest coefficient of variation (0.28) of the five procedures considered.

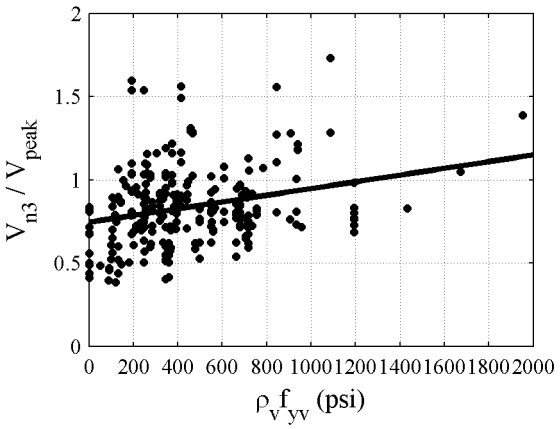


**Figure 4-41 Variation of $V_{n3}/V_{peak}$ with $\rho_v f_{yv}$**

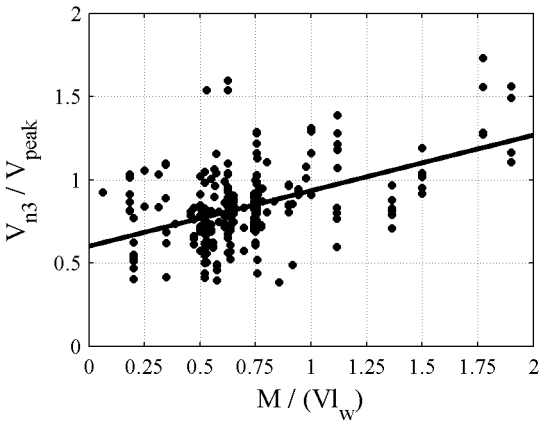


**Figure 4-42 Variation of $V_{n3}/V_{peak}$ with moment-to-shear ratio**

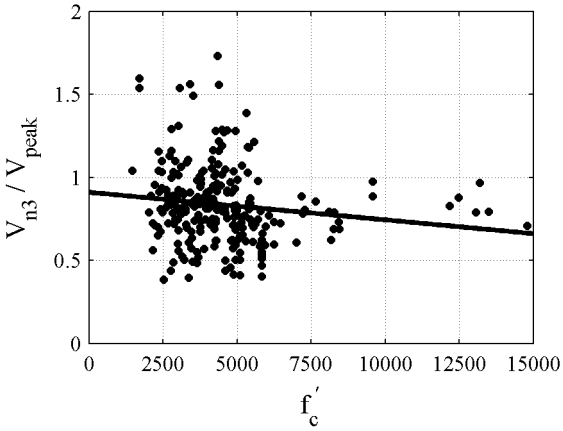


**Figure 4-43 Variation of $V_{n3}/V_{peak}$ with $f_c'$**

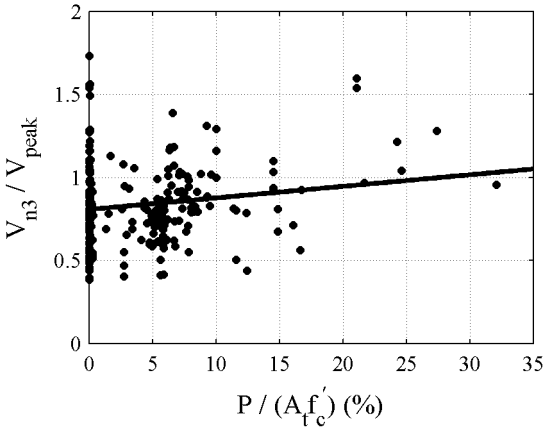


**Figure 4-44 Variation of $V_{n3}/V_{peak}$ with normalized axial stress**

Figure 4-51 presents the variation of normalized shear stress [shear force divided by the product of effective shear area ($d_3 t_w$) and $\sqrt{f_c'}$ ] computed using Equation Set IV and the measured peak shear strength ($V_{peak}$) with $\rho_{se} f_{y1}$. The upper shear stress limit of $20\sqrt{f_c'}$ psi controls the shear strength of only 14 of the 254 walls in the dataset and so its influence on the shear strength predictions of Equations Set IV is insignificant.

In addition, the normalized measured shear stresses for 62 walls exceeded the upper shear stress limit of $20\sqrt{f_c'}$ psi and the utility of this limit is questionable for walls with boundary elements, if effective web area is used as a basis for calculating shear strength.

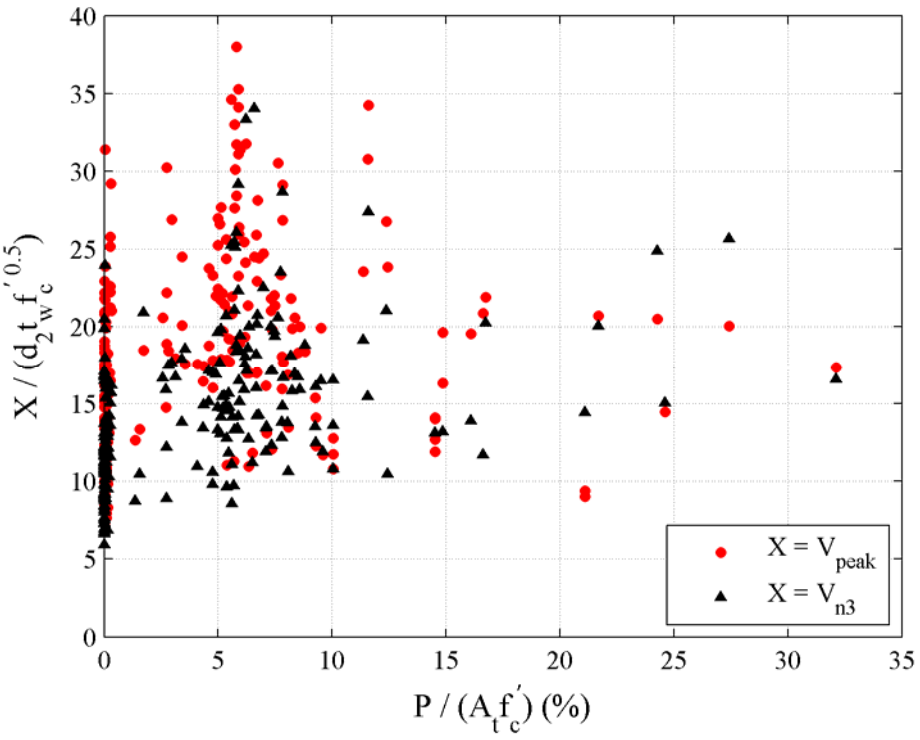


**Figure 4-45 Variation of normalized shear stress obtained using Equation Set III ($V_{n3}$) and measured peak shear strength ($V_{peak}$) with $\rho_v f_{yv}$**

### 4.4.1.5 Wood's Equation

Figure 4-52 and Figure 4-53 present the variation of $V_{n5}/V_{peak}$ with the product of the reinforcement yield stress and the ratio of the total area of vertical reinforcement (includes vertical web reinforcement and reinforcement in boundary elements) to the total wall area, and concrete compressive strength, respectively. Figure 4-52 shows that the ratio of predicted to measured peak shear strength for Equation Set V decreases with increasing vertical reinforcement. The mean and median values of $V_{n5}/V_{peak}$ are 0.60 and 0.56, respectively. The corresponding standard deviation and coefficient of variation are 0.21 and 0.35. Of the five equation sets studied, Wood's equation provides the most conservative estimates of peak shear strength. Figure 4-54 presents the variation of normalized shear stress [shear force divided by the product of the effective shear area ($A_w$) and $\sqrt{f_c'}$ ] obtained using Equation Set V ($V_{n5}$) and measured peak shear strength ($V_{peak}$) with the product of the reinforcement yield stress and the ratio of the total area of wall vertical reinforcement to the total wall area. Note that only 50 of the 254 predictions are governed by the part of Equation Set V associated with the area of vertical reinforcement and the remaining predictions are limited by either the lower (195 of 204) or upper bound (9 of 204) limits on shear stress of $6\sqrt{f_c'}$ and $10\sqrt{f_c'}$ psi, respectively.

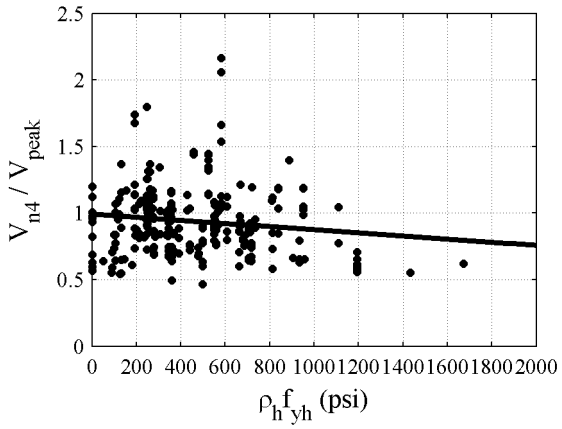


**Figure 4-46 Variation of $V_{n4}/V_{peak}$ with $\rho_h f_{yh}$**

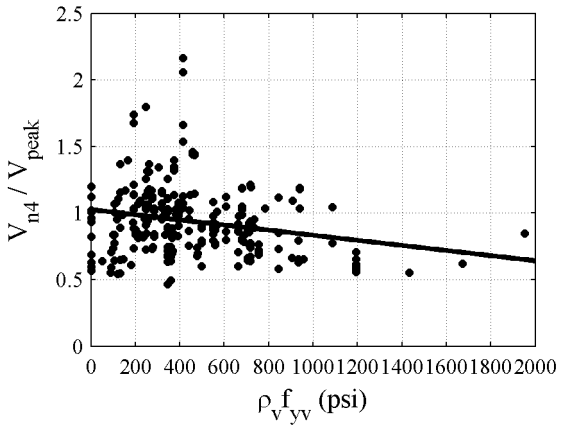


**Figure 4-47 Variation of $V_{n4}/V_{peak}$ with $\rho_v f_{yv}$**

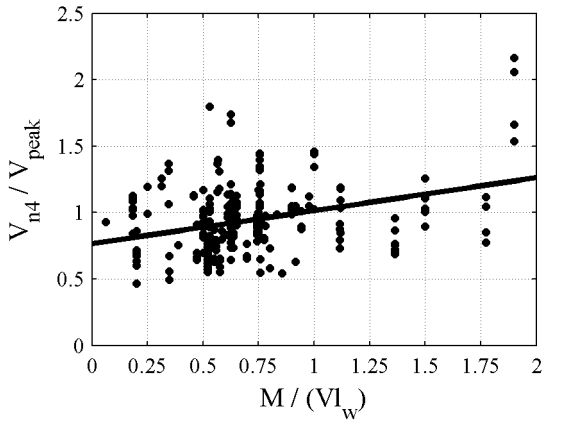


**Figure 4-48 Variation of $V_{n4}/V_{peak}$ with moment-to-shear ratio**

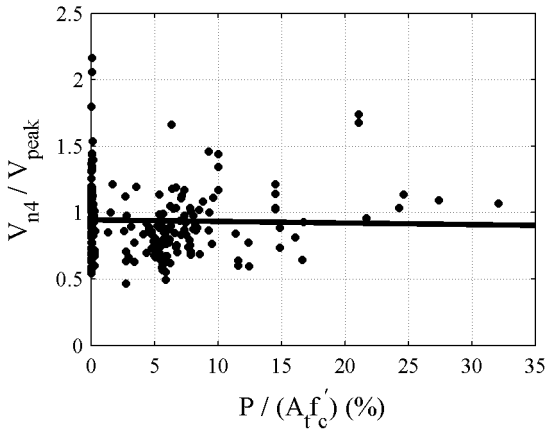


**Figure 4-49 Variation of $V_{n4}/V_{peak}$ with normalized axial stress**

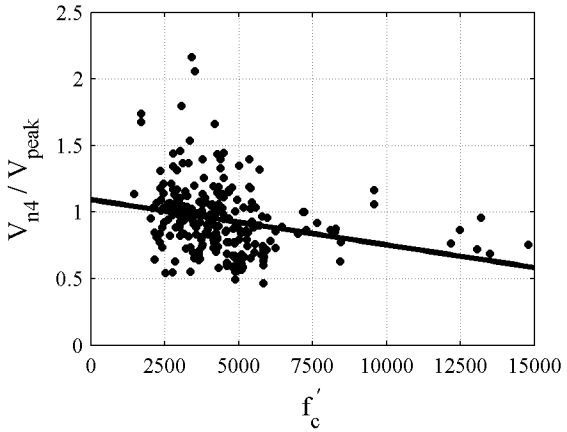


**Figure 4-50 Variation of $V_{n4}/V_{peak}$ with $f_c'$**

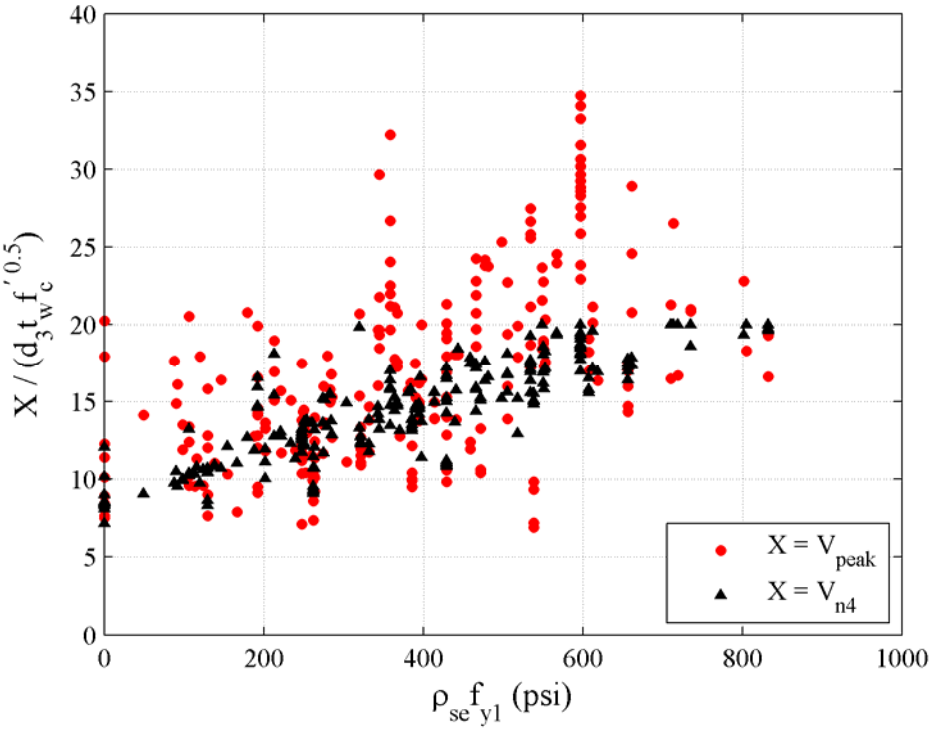


**Figure 4-51 Variation of normalized shear stress obtained using Equation Set IV ($V_{n4}$) and measured peak shear strength ($V_{peak}$) with $\rho_{se} f_{y1}$**

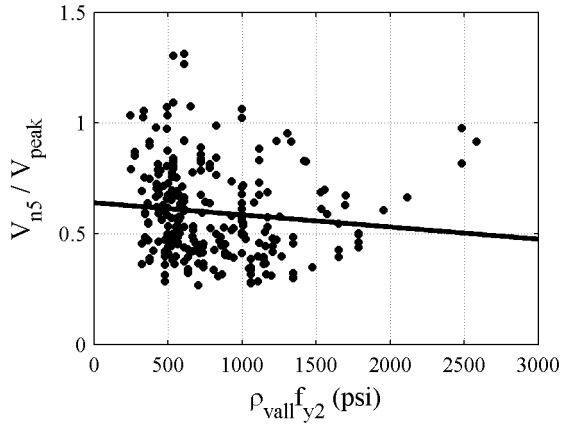


**Figure 4-52 Variation of $V_{n5}/V_{peak}$ with $\rho_{vall} f_{y2}$**

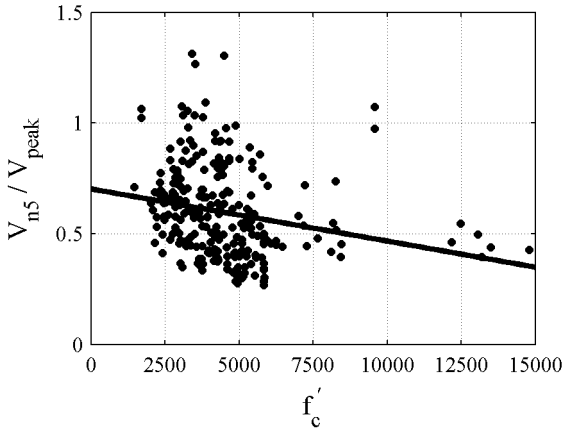


**Figure 4-53 Variation of $V_{n5}/V_{peak}$ with $f_c'$**

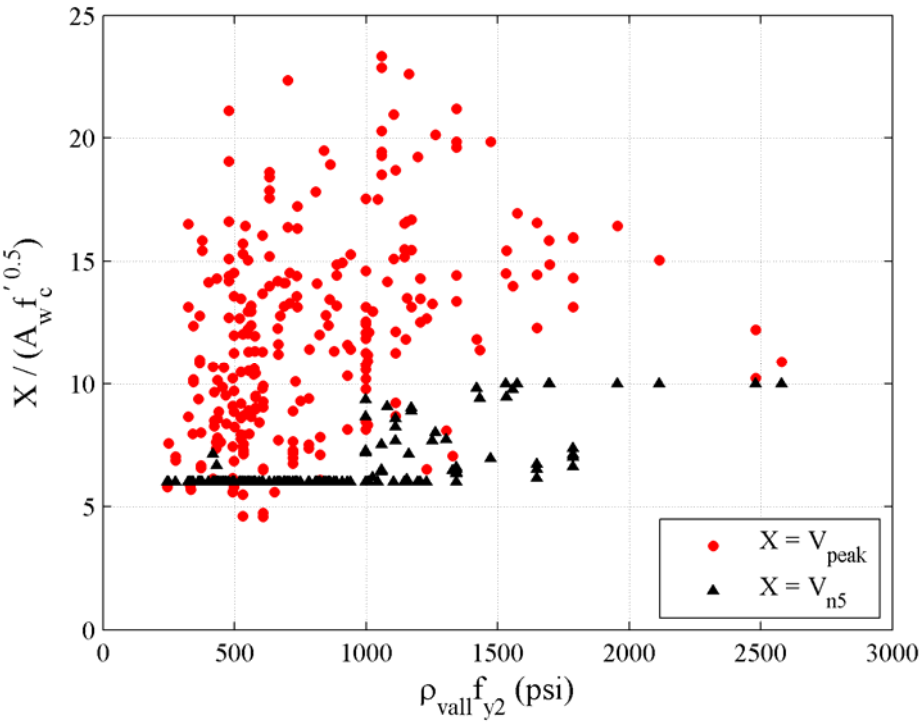


**Figure 4-54 Variation of normalized shear stress obtained using Equation Set V ($V_{n5}$) and measured peak shear strength ($V_{peak}$) with $\rho_{vall} f_{y2}$**

## 4.4.2 Group 2: Shear-Critical Walls with Boundary Elements

Two hundred and twenty-three of the 254 squat walls with boundary elements (88%) were judged to be shear-critical. (The percentage of shear-critical rectangular walls in the rectangular wall dataset was 61%.) Figure 4-55 presents the variation of $V_{peak}/V_{flex}$ with moment-to-shear ratio, as a function of loading type.

Table 4-5 summarizes results for the shear-critical walls. If the dataset is limited to these walls, a comparison of results presented in Table 4-5 and Table 4-4 shows a minor reduction in the percentage of unconservative predictions for all five equation sets. The ASCE 43-05 equation (Equation Set IV) estimates best the shear strength of shear-critical walls with a median value of $V_{n4}/V_{peak}$ of 0.89 and a relatively small coefficient of variation (0.26). The equation of Wood provides the most conservative estimations as measured by median results (97%). The ASCE 43-05 equation overestimates the peak shear strength of 35% of the 223 shear-critical walls, which is greatest of the five equation sets. The procedures of ACI 318-08 (Equation Set I and II) are generally conservative for shear-critical walls. Figure 4-56 presents box-and-whisker plots for the shear-critical walls.

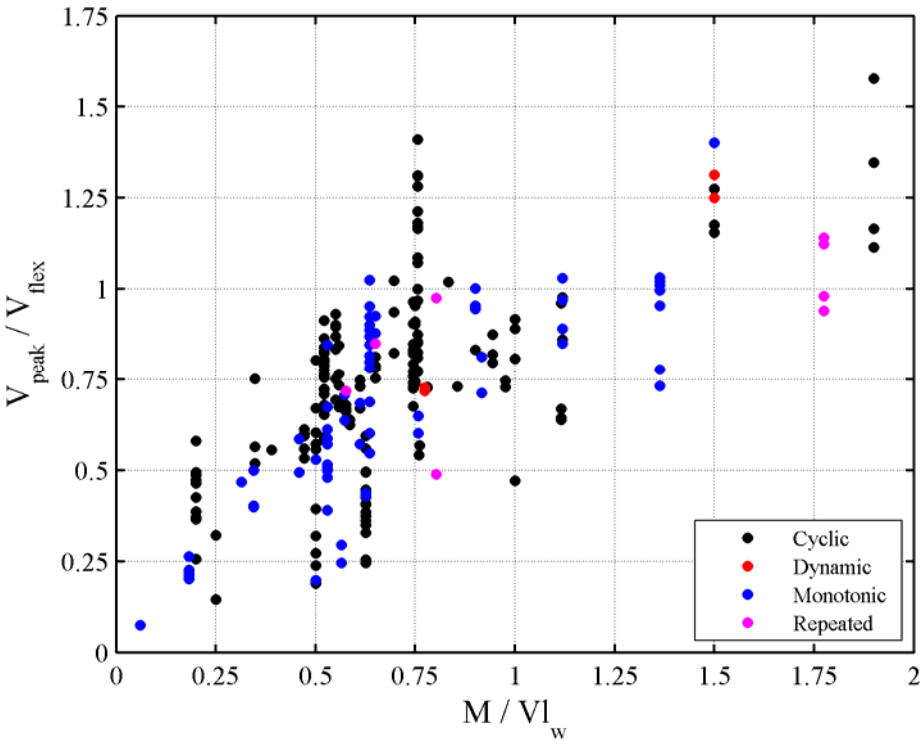


**Figure 4-55 Variation of the ratio of measured peak shear strength to the shear-flexural strength with moment-to-shear-ratio**

**Table 4-5 Statistics of the ratio of the shear strength predicted using Equation Sets 1 through 5 to measured peak shear strength of shear-critical walls (Group 2)**

| | **Mean** | **Median** | **St. Dev.** | **COV** | **Min** | **Max** | **% Over-Predictions** |
|---|---|---|---|---|---|---|---|
| $V_{n1}/V_{peak}$ | 0.70 | 0.66 | 0.25 | 0.35 | 0.18 | 1.71 | 12 |
| $V_{n1*}/V_{peak}$ | 0.82 | 0.78 | 0.35 | 0.42 | 0.18 | 2.98 | 23 |
| $V_{n2}/V_{peak}$ | 0.61 | 0.57 | 0.20 | 0.32 | 0.21 | 1.37 | 5 |
| $V_{n2*}/V_{peak}$ | 0.75 | 0.73 | 0.28 | 0.37 | 0.21 | 2.43 | 18 |
| $V_{n3}/V_{peak}$ | 0.81 | 0.80 | 0.22 | 0.27 | 0.39 | 1.60 | 18 |
| $V_{n4}/V_{peak}$ | 0.92 | 0.89 | 0.24 | 0.26 | 0.47 | 1.80 | 35 |
| $V_{n4*}/V_{peak}$ | 0.92 | 0.89 | 0.24 | 0.26 | 0.47 | 1.80 | 36 |
| $V_{n5}/V_{peak}$ | 0.57 | 0.53 | 0.18 | 0.33 | 0.27 | 1.07 | 3 |

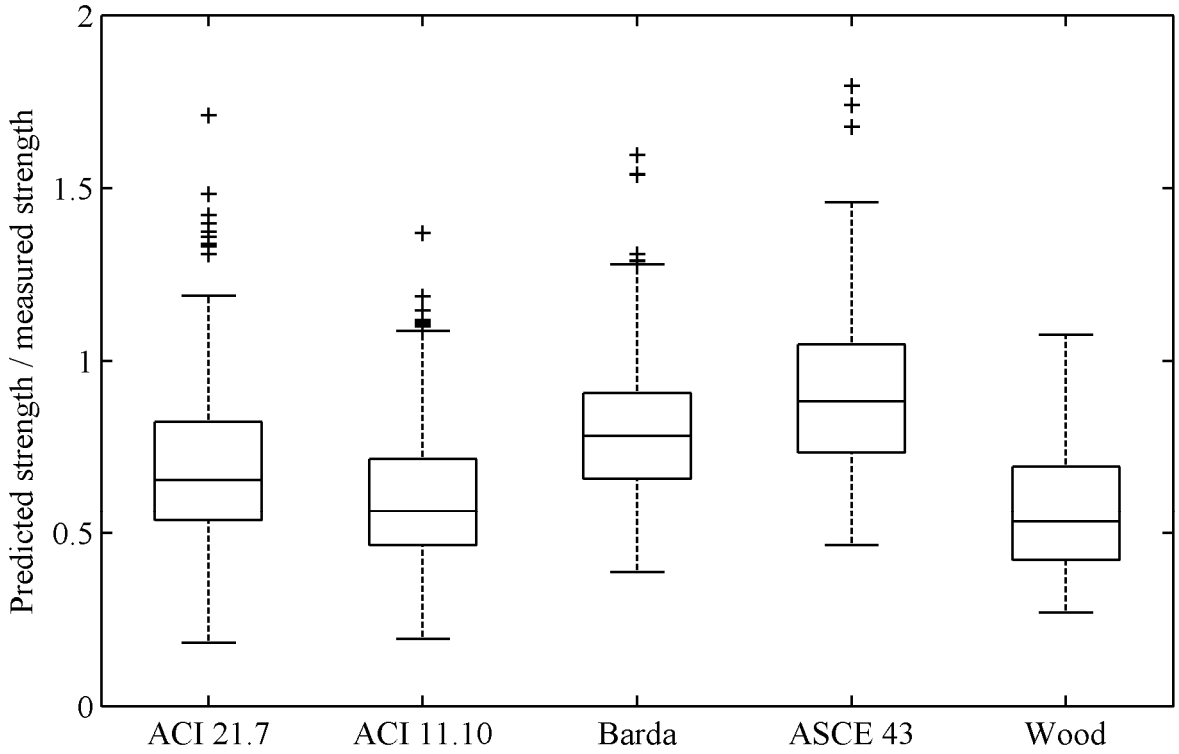


**Figure 4-56 Distribution of the ratio of the predicted shear strengths to measured peak shear strengths for shear-critical walls**

### 4.4.3 Group 3: ACI 318-Compliant, Shear-Critical Walls with Boundary Elements

Group 3 eliminates the walls that do not comply with the requirements of Section 21.9 of ACI 318-08. Figure 4-57 presents the variation of normalized measured peak shear strength with the moment-to-shear ratio as a function of the number of reinforcement curtains in the wall. As seen in the figure, the variations of experimental peak shear strength with moment-to-shear ratio are quite similar for walls with single and double reinforcement curtains. Therefore, the number of reinforcement curtains is not used to identify the ACI-compliant walls. As a result, all walls considered in this group, had horizontal and vertical web reinforcement ratios of at least 0.0025 and vertical web reinforcement ratio not less than horizontal web reinforcement ratio. One hundred and seventy-five of the 223 shear-critical walls in Group 2 are considered to be ACI 318-compliant. Table 4-6 summarizes results for Group 3 walls. A comparison of the results presented in Table 4-6 and Table 4-5 shows an improvement in the predictions of all equation sets in terms of the coefficients of variation. The ASCE 43-05 equation provides the best estimates of the peak shear strength of ACI 318-compliant, shear-critical walls with a mean value of $V_{n4}/V_{peak}$ of 0.91 and a relatively small coefficient of variation. The equations of Chapter 11 of ACI 318-05 and Wood again provide the most conservative estimates of peak shear strength as measured by median results. The ASCE 43-05 equation yields the highest percentage of overestimations of peak shear strength (33%) in Group 3, of the five procedures considered.

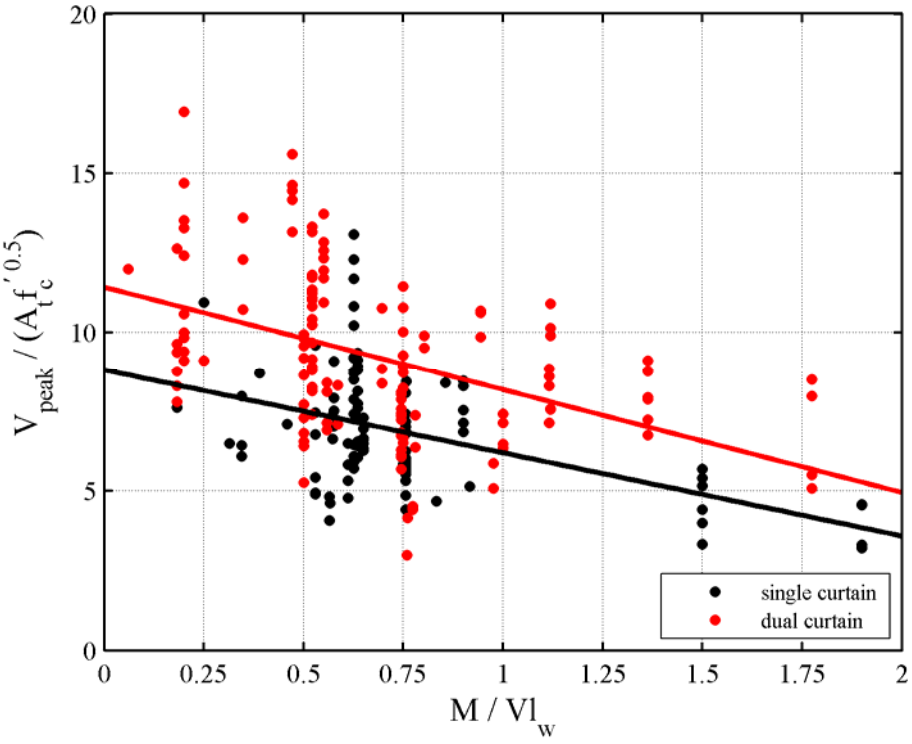


**Figure 4-57 Variation of normalized measured peak shear strength ($V_{peak}$) with moment-to-shear ratio as a function of the number of reinforcement curtains**

**Table 4-6 Distribution of the ratio of the predicted shear strengths to measured peak shear strengths for ACI 318-compliant, shear-critical walls**

| | **Mean** | **Median** | **St. Dev.** | **COV** | **Min** | **Max** | **% Over-Predictions** |
|---|---|---|---|---|---|---|---|
| $V_{n1}/V_{peak}$ | 0.68 | 0.66 | 0.18 | 0.26 | 0.28 | 1.34 | 4.6 |
| $V_{n1*}/V_{peak}$ | 0.79 | 0.78 | 0.25 | 0.31 | 0.28 | 1.74 | 16.0 |
| $V_{n2}/V_{peak}$ | 0.59 | 0.56 | 0.15 | 0.25 | 0.34 | 1.11 | 1.7 |
| $V_{n2*}/V_{peak}$ | 0.74 | 0.73 | 0.20 | 0.28 | 0.37 | 1.31 | 12.0 |
| $V_{n3}/V_{peak}$ | 0.82 | 0.79 | 0.21 | 0.26 | 0.42 | 1.60 | 19.4 |
| $V_{n4}/V_{peak}$ | 0.90 | 0.87 | 0.23 | 0.25 | 0.49 | 1.80 | 31.4 |
| $V_{n4*}/V_{peak}$ | 0.91 | 0.87 | 0.23 | 0.26 | 0.49 | 1.80 | 33.1 |
| $V_{n5}/V_{peak}$ | 0.53 | 0.49 | 0.17 | 0.32 | 0.28 | 1.07 | 2.3 |

The performances of the different equation sets vary only slightly for the Group 1, 2 and 3 walls. For all groups, the ASCE 43-05 equation provides the best estimates of the peak shear strength in a median sense. The equations of Chapter 11 of ACI 318-08 and the Wood equation give the most conservative estimates of the peak shear strength whereas the ASCE 43-05 equation give the most unconservative estimates of the peak shear strength. The trends associated with the predictions of Chapter 21 and Chapter 11 of ACI 318-08 are similar but the Chapter 11 equation consistently provides more conservative (lower) estimates. The performance of the Barda equation is superior to the ACI 318-08 and Wood equations but inferior to the ASCE 43-05 equation for predicting the peak shear strength of squat walls with boundary elements.

# 5 FINITE ELEMENT MODELING OF SQUAT REINFORCED CONCRETE WALLS

## 5.1 Introduction

Finite element studies of reinforced concrete started in late 1960s with the concurrent development of discrete- and smeared-crack approaches to represent the cracking behavior of concrete. Significant advances in finite element modeling of reinforced concrete have been made in the past 40 years. The number of studies using smeared models of cracks has significantly outnumbered those used discrete models of cracks. The two major advantages of smeared-crack modeling over discrete-crack modeling are simplicity and computational efficiency. Section 2.3.4 presents a literature review of crack modeling.

Another important component of finite element of reinforced concrete structures is the selection of material constitutive relationships. A number of constitutive models based on elasticity- and plasticity-based theories have been developed. Each theoretical approach includes a unique set of model parameters and may yield substantially different results. Modeling decisions and selection of material parameters are of significant importance in predicting the response of reinforced concrete structures using finite element analysis tools.

Squat reinforced concrete walls pose unique challenges in terms of finite element modeling because of their low ratios of moment to shearing force. The plane-section hypothesis is violated since shear deformations contribute substantially to the response of squat walls. High shear demands invoke relatively brittle failure mechanisms (i.e., diagonal tension, diagonal compression, and sliding shear) resulting in a more complex and less predictable response than in taller walls, which are flexure dominated. In many cases, damage to concrete in the form of widespread crushing and/or cracking govern the response of squat reinforced concrete walls and reinforcement yielding is generally modest in these components.

This section focuses on the analytical modeling of squat reinforced concrete walls using widely used commercial nonlinear finite element tools. The intention here is not to match experimental data by calibration but rather to assess the performances of the codes by making viable modeling assumptions and to identify key parameters and modeling techniques that significantly affect the predicted response. The impact of the key parameters on predicted response is investigated.

Two finite element codes, namely, ABAQUS [Hibbitt, Karlsson & Sorensen, Inc. (2004)] and VecTor2 [VecTor Analysis Group (2007)] are used to model the behavior of squat walls. ABAQUS is a general-purpose finite element code whereas VecTor2 is limited to reinforced concrete. Each code has a different approach in simulating the behavior of reinforced concrete. The concrete model in ABAQUS is a plasticity-damage type model based on the work of Lubliner et al. (1989) and Lee and Fenves (1998). VecTor2 accommodates two smeared-crack formulations for finite element analysis of reinforced concrete structures, namely, *Modified Compression Field Theory* (MCFT) [Vecchio and Collins (1986)] and *Disturbed Stress Field Model* (DSFM) [Vecchio (2000), Vecchio et al. (2001)]. MCFT is a rotating crack approach that models concrete as an orthotropic material and assumes that the orientations of the principal strain and stress are identical. DSFM does not enforce alignment of the principal strain and stress directions and is considered as a delayed rotating-crack model [Wong and Vecchio (2002)]. The

MCFT and DSFM were developed at the University of Toronto. The results of experiments on reinforced concrete panels had significant impact on the development of MCFT and DSFM formulations [Vecchio and Collins (1982), Bhide and Collins (1987)]. Detailed information on the two formulations is included in Appendix B.

The experimental responses of six squat walls are simulated using ABAQUS and VecTor2. Section 5.2 presents information on the experimental behavior of the walls that are selected for finite element modeling. Sections 5.3 and 5.4 present the behaviors predicted using ABAQUS and VecTor2, respectively. Section 5.5 presents a discussion on prediction of behavior of walls with boundary elements using VecTor2.

## 5.2 Selected Wall Experiments for Finite Element Modeling

Six squat walls from three different experimental programs are analyzed using the finite element method. The simulated structures are walls S4 and S9 tested by Maier and Thürlimann (1985), walls LSW1, LSW2, and LSW3 tested by Salonikios et al. (1999), and wall DP1 tested by Palermo and Vecchio (2002a). These walls are selected because their experimental behaviors were representative of different failure modes observed in squat reinforced concrete walls. More importantly, the experimental data for these walls are reported in substantial detail including discussions of the damage progression and wall failure modes.

Walls S4, S9, LSW1, LSW2, and LSW3 have rectangular cross-sections and wall DP1 has flanges. Walls S4 and S9 were tested under monotonic loading whereas the other four walls were tested using cycling loading protocols. Walls S4 and S9 tested by Maier and Thürlimann (1985) were identical except for horizontal web reinforcement ratio. Wall S9 included vertical web reinforcement but no horizontal web reinforcement, and failed due to a corner-to-corner crack (diagonal tension). Wall S4, which included approximately 1.0% horizontal web reinforcement, failed by concrete crushing in the compression toe. The failures of walls LSW1 and LSW2 tested by Salonikios et al. (1999) were due to sliding at the bottom of the wall web. Wall LSW3 tested by Salonikios et al. (1999) was identical to wall LSW2 except that wall LSW3 was tested with an imposed axial force of $0.07 A_w f_c'$. Application of axial force on wall LSW3 helped limiting the sliding displacements but the wall experienced significant crushing at the compression toes. Wall DP1 included a relatively heavy top slab and foundation and wide flanges. Wall DP1 also failed due to crushing but crushing was widespread at the mid-height of the wall web rather than being localized in the compression toes. The six walls selected for finite element modeling cover the wide range of failure modes observed in squat reinforced concrete walls. The following subsections summarize the experimental response of the six squat walls in more detail.

### 5.2.1 Walls S4 and S9 – Maier and Thürlimann (1985)

Walls SW4 and SW9 tested by Maier and Thürlimann (1985) had rectangular cross-sections and were tested under quasi-statically applied monotonic loading. The walls were 1.18 m long, 1.20 m high, and 0.10 m thick. The aspect ratio and the moment-to-shear ratio of the walls were 1.02 and 1.12, respectively. Wall S4 included uniformly distributed vertical and horizontal web reinforcement whereas wall S9 was reinforced with vertical web reinforcement only. The vertical web reinforcement in each wall and the horizontal web reinforcement in wall S4 consisted of two curtains of 8 mm diameter rebar spaced at 100 mm on center, corresponding to a rebar ratio of

approximately 1.0%. Axial and lateral loads were transferred to the walls through the beams constructed over the wall webs. Wall foundations were clamped to the laboratory strong floor. Table 5-1 presents construction and test data for walls S4 and S9.

**Table 5-1 Experimental parameters for walls S4 and S9 [Maier and Thürlimann (1985)]**

| | Concrete | | Reinforcement ( Φ 8) | | | $\rho_h$ (%) | $\rho_v$ (%) | $P$ (kN) |
|---|---|---|---|---|---|---|---|---|
| Wall ID | $f_c'$ (MPa) | $E_c$ (MPa) | $f_y$ (MPa) | $f_u$ (MPa) | $E_s$ (MPa) | | | |
| S4 | 32.9 | 31600 | 574 | 764 | 198000 | 1.01 | 1.02 | 262 |
| S9 | 29.2 | 28800 | 560 | 762 | 200000 | 0.0 | 1.02 | 260 |

Figure 5-1 presents the experimental cracking patterns for wall S4 at various displacement levels and the load-drift relationship for the wall. The response of the wall was dominated by flexural and shear cracking that was uniformly distributed over the wall web. The peak shear strength of the wall (392 kN) was attained at 0.95% drift. Wall failure was due to crushing in the compression toe of the web. First yielding in the vertical reinforcement was observed at a displacement of 5.4 mm (drift = 0.45%) at the extreme tension edge of the wall section. The recorded strains in the horizontal web reinforcement were less than the yield strain at all stages of the testing.

Figure 5-2 presents data for wall S9. As seen in Figure 5-2a, the response of wall S9 was initially dominated by flexural cracking. First yield in the vertical reinforcement was observed at a displacement of 6.2 mm (drift = 0.52%) at the extreme tension edge of the wall section. Shear cracks began to dominate the wall response as the displacement demand on the wall was increased. The peak shear strength of the wall (342 kN) was attained at 0.76% drift. At greater drift, the lateral strength degraded as the diagonal shear cracks widened, the stability of the compression toe was compromised by propagation of the diagonal cracks into this region (see Figure 5-2c).

## 5.2.2 Walls LSW1, LSW2, and LSW3 – Salonikios et al. (1999)

Salonikios et al. (1999) tested 11 squat reinforced concrete walls of rectangular cross-sections under quasi-static cyclic loading. Six walls had an aspect ratio of 1.5 and five walls had an aspect ratio of 1.0. Two walls with an aspect ratio of 1.5 and two walls with an aspect ratio of 1.0 included diagonal reinforcement. Herein, the three orthogonally reinforced walls with an aspect ratio of 1.0 (LSW1, LSW2, and LSW3) are modeled.

Walls LSW1, LSW2, and LSW3 were 1.20 m (47.2 in.) long, 1.20 m (47.2 in.) high, and 0.10 m (3.94 in.) thick. Twenty-four cm (9.45 in.) long boundary elements were formed at the wall ends using confinement reinforcement $\phi$4.4 rectangular hoops at 2.6 mm on center. The compressive strengths of the concrete used to construct walls LSW1, LSW2 and LSW3 were 22.2, 21.6, and 23.9 MPa, respectively. The reinforcement details of the walls are summarized in Table 5-2. In Table 5-2, $\rho_v$ is vertical web reinforcement ratio, $\rho_h$ is horizontal web reinforcement ratio, and $\rho_{be}$ is the flexural reinforcement ratio. As seen in the table, all walls included isotropic web reinforcement ( $\rho_v = \rho_h$ ). The walls were constructed using a combination of $\phi$4.2 and $\phi$8

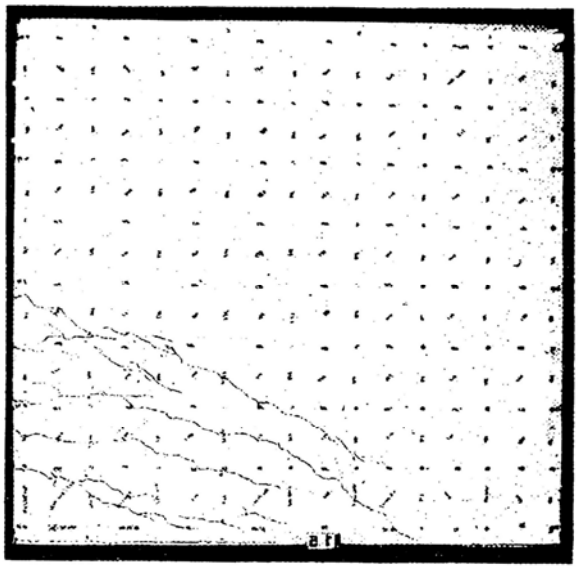

a) displacement = 3 mm (drift = 0.25%)

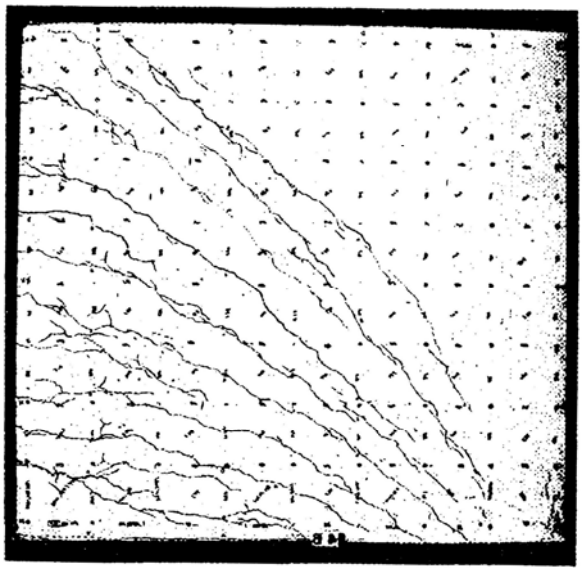

b) displacement = 9.4 mm (drift = 0.78%)

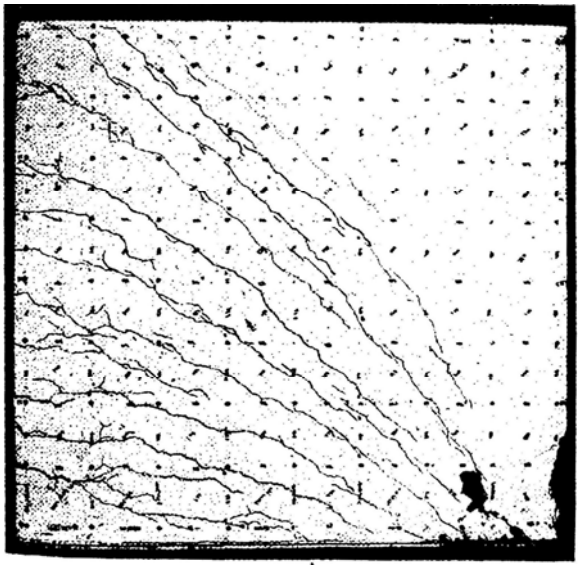

c) displacement = 18.5 mm (drift = 1.55%)

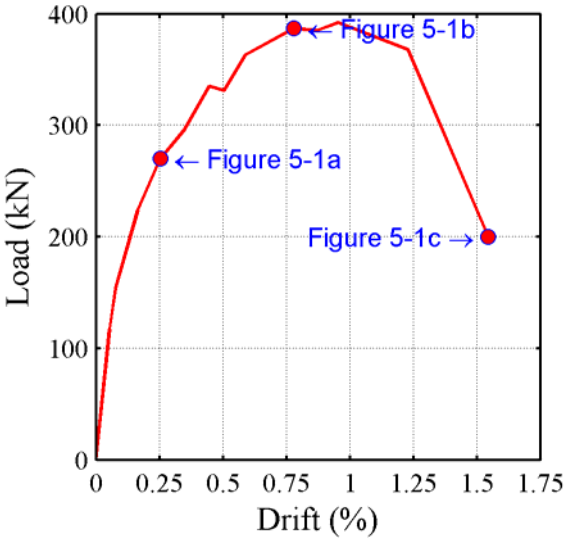


d) Load-drift relationship

**Figure 5-1 Cracking patterns for wall S4 at various displacement levels [Maier and Thürlimann (1985)] and the experimental load-drift relationship**

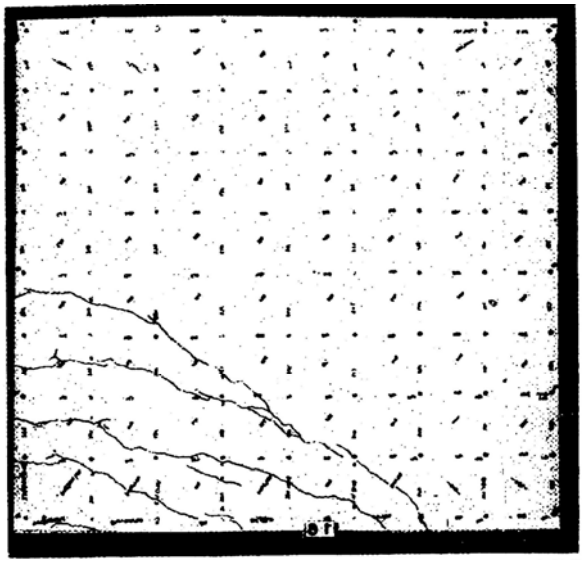

**a) displacement = 3 mm (drift = 0.25%)**

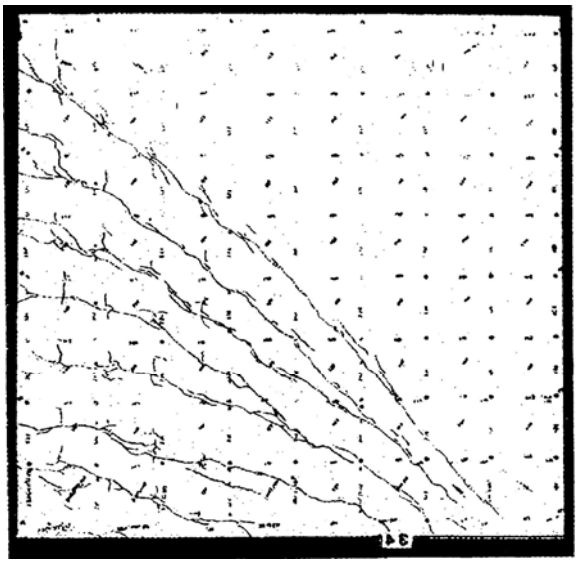

**b) displacement = 6.2 mm (drift = 0.52%)**

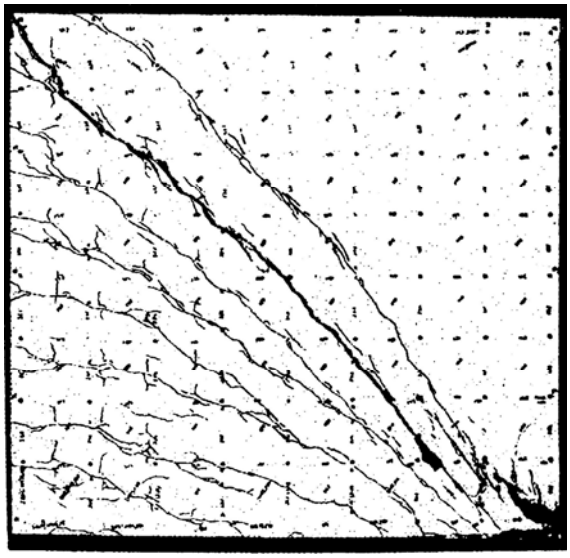

**c) displacement = 14.6 mm (drift = 1.22%)**

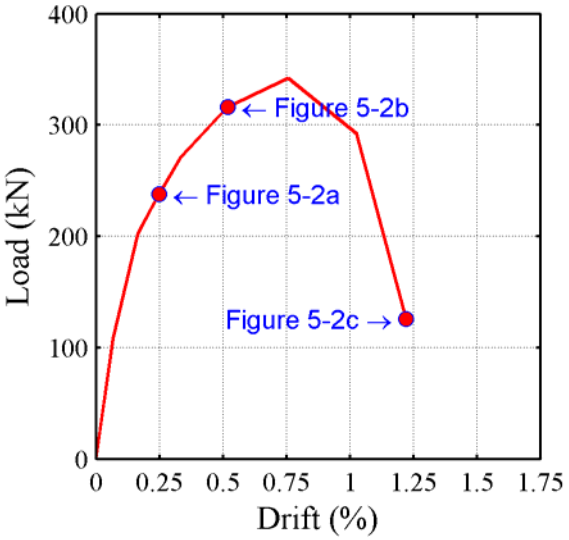


**d) Load-drift relationship**

**Figure 5-2 Cracking patterns for wall S9 at various displacement levels [Maier and Thürlimann (1985)] and the experimental load-drift relationship**

**Table 5-2 Reinforcement details for walls LSW1, LSW2, and LSW3**

| Wall ID | $\rho_{be}$ (%) | $\rho_v$ (%) | $\rho_h$ (%) |
|---|---|---|---|
| LSW1 | 1.70<br>[8 $\phi$ 8] | 0.565<br>[2# $\phi$ 4.2@100 mm] +<br>[1# $\phi$ 8@180 mm] | 0.565<br>[2# $\phi$ 4.2@100 mm] +<br>[1# $\phi$ 8@180 mm] |
| LSW2 | 1.30<br>[6 $\phi$ 8] | 0.277<br>[2# $\phi$ 4.2@100 mm] | 0.277<br>[2# $\phi$ 4.2@100 mm] |
| LSW3 | 1.30<br>[6 $\phi$ 8] | 0.277<br>[2# $\phi$ 4.2@100 mm] | 0.277<br>[2# $\phi$ 4.2@100 mm] |

reinforcement for which the measured yield stresses were 610 MPa (88.5 ksi) and 585 (84.8 ksi), respectively. Wall LSW1 included 0.57% web reinforcement and walls LSW2 and LSW3 included 0.28% web reinforcement. The ratio of the flexural reinforcement in the boundary elements ( $\rho_{be}$ ) was 1.70% for wall LSW1 and 1.30% for walls LSW2 and LSW3. Walls LSW1 and LSW2 were tested without axial forces whereas wall LSW3 was tested with an axial force of $0.07 A_w f_c'$. Walls LSW2 and LSW3 were identical except for a small difference in the compressive strength of the concrete. Axial and lateral loads were transferred to the walls through the beams constructed over the wall webs. All walls were fixed to the laboratory floor using prestressing bars.

Figure 5-3 and Figure 5-4 present the experimental load-displacement relationships for the specimens LSW1 and LSW2 (identical except for reinforcement ratios) and LSW2 and LSW3 (identical except for axial force), respectively. Pinched hysteretic behavior, which is a characteristic of squat wall response, can be seen clearly in the reported load-displacement relationships for all three walls. The hysteresis loop for wall LSW3 is less pinched than those of walls LSW1 and LSW2, which can be attributed to the compressive axial load applied to wall LSW3. The dissipated energy and the recorded peak shear strength for wall LSW3 are substantially higher than those of the other two walls. The peak shear strength of wall LSW1 is higher than that of wall LSW2 because wall LSW1 included twice the web reinforcement used in wall LSW2. Significant residual displacements, defined here as the zero-force displacement intercept are seen in all three walls in the latter stages of the test.

Figure 5-5 presents the conditions of walls LSW1, LSW2, and LSW3 at the end of testing. Near horizontal flexural cracks at the base were the first cracks to initiate during the testing of each wall. For walls LSW1 and LSW2, flexural cracks on each side of the wall web near the base joined forming a major crack spanning the wall length as a result of the cyclic loading. The concrete at the bases of the walls started to deteriorate and local concrete crushing was observed in these regions due to sliding. Walls LSW1 and LSW2 experienced rapid degradation of strength and stiffness following the attainment of peak shear strength as sliding between wall web and foundation became the dominant deformation mechanism. The sliding deformations experienced by wall LSW3 were smaller than that those in the other two walls due to the application of compressive axial load. Crushing in the compression toes of wall LSW3 was more widespread than those of walls LSW1 and LSW2, which can again be attributed to the higher

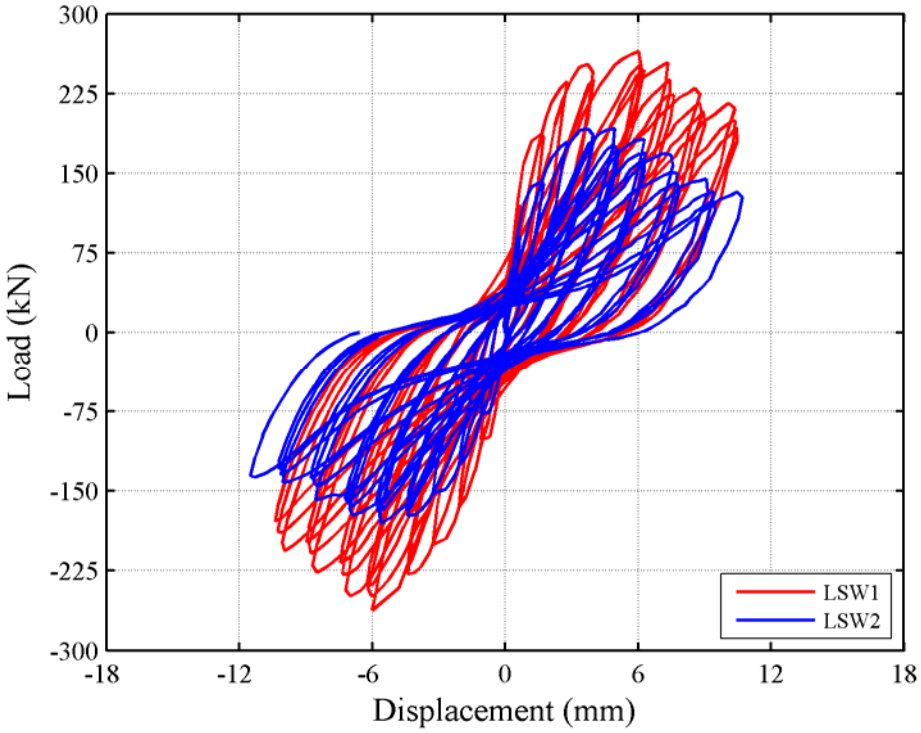


**Figure 5-3 Experimental load-displacement relationships for wall LSW1 and LSW2**

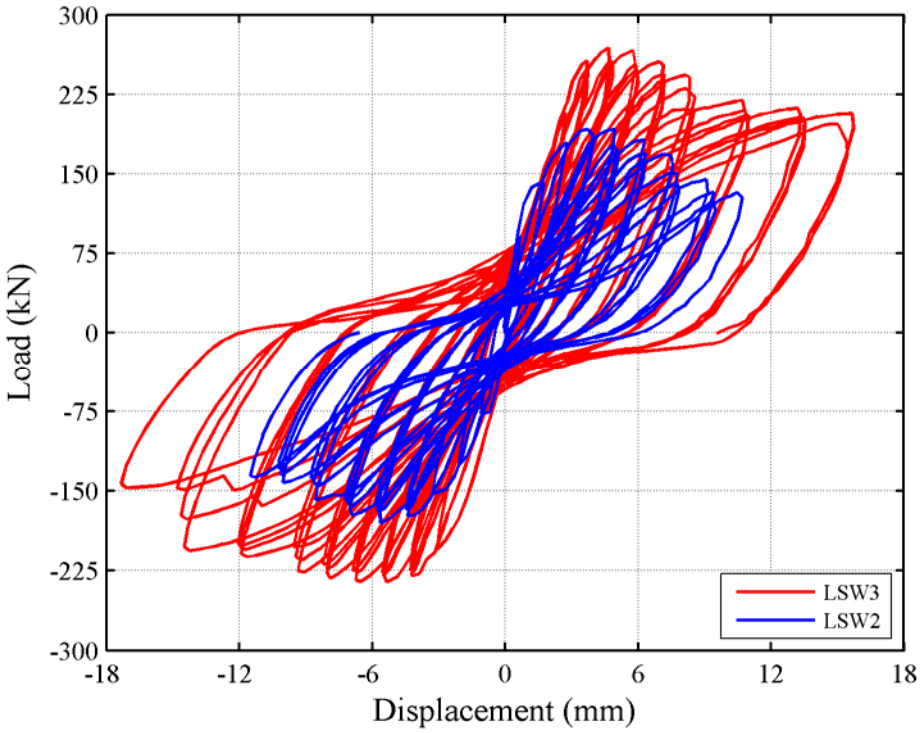


**Figure 5-4 Experimental load-displacement relationships for wall LSW2 and LSW3**

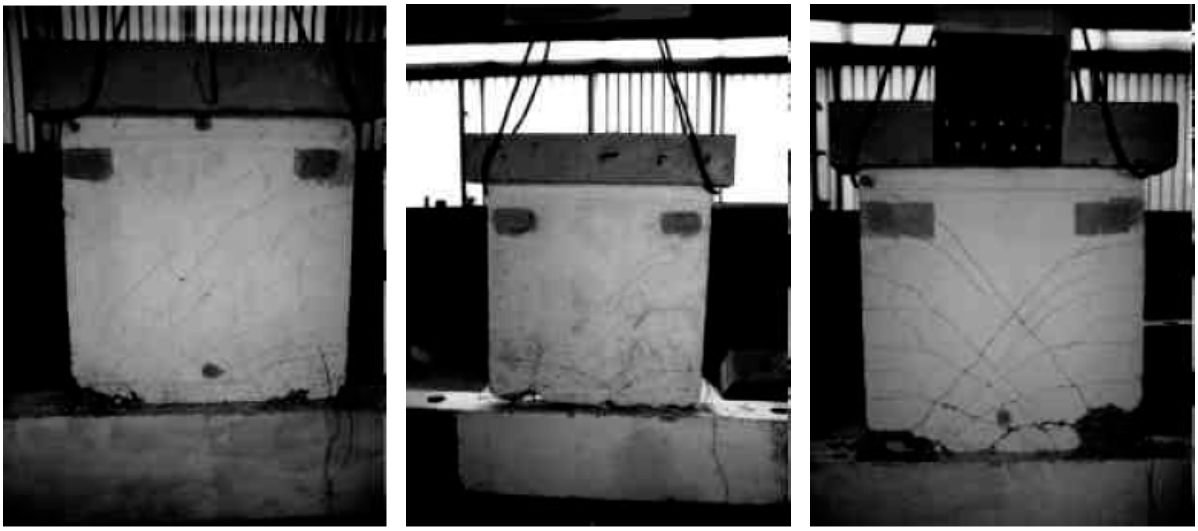

**a) LSW1** **b) LSW2** **c) LSW3**

**Figure 5-5 Conditions of walls LSW1, LSW2, and LSW3 tested by Salonikios et al. (1999) after the testing**

axial force demand on wall LSW3 that was effective in limiting the sliding deformations. Limiting the sliding displacements also increased the shear forces in the web, and as a result, shear cracking was more widespread in the web of wall LSW3 (see Figure 5-5). In all three walls, the shear cracks were generally inclined at approximately 45 degrees near the wall center. The inclination of the shear cracks significantly decreased towards web boundaries due to the heavily reinforced boundary elements.

### 5.2.3 Wall DP1 – Palermo and Vecchio (2002a)

Palermo and Vecchio (2002a) tested two flanged walls (DP1 and DP2) under quasi-static cyclic loading, which were similar in terms of geometry to the two NUPEC wall specimens that were tested using earthquake simulators [Kitada et al. (1997)]. Only wall DP1 is modeled herein because wall DP2 failed in an unorthodox manner due to sliding between wall web and the top slab. Palermo and Vecchio (2002a) noted that this failure could be a result of either relatively weaker concrete at the upper part of the wall web or a thinner web section near the top slab.

Wall DP1 was 3075 mm long, 2020 mm high, and 75 mm thick, and included flanges that were 95 mm thick and 3045 mm long. A top slab was (4415 mm x 4000 mm x 640 mm) constructed to transfer the applied lateral and axial forces to the wall web. The wall was constructed on a relatively large foundation (4415 mm x 4000 mm x 640 mm) which was clamped to the laboratory floor. The dimensions of wall DP1 are illustrated in Figure 5-6. Figure 5-7 presents a photograph of wall DP1 before testing.

Different concrete strengths were used for the top slab, foundation and the web/flanges of wall DP1. The compressive strength of the concrete used in the wall web and flanges was 21.7 MPa (3.15 ksi). Compressive strengths for the concrete used in the top slab and the foundation were 43.9 MPa (6.37 ksi) and 34.7 MPa (5.03 ksi), respectively. The corresponding moduli of

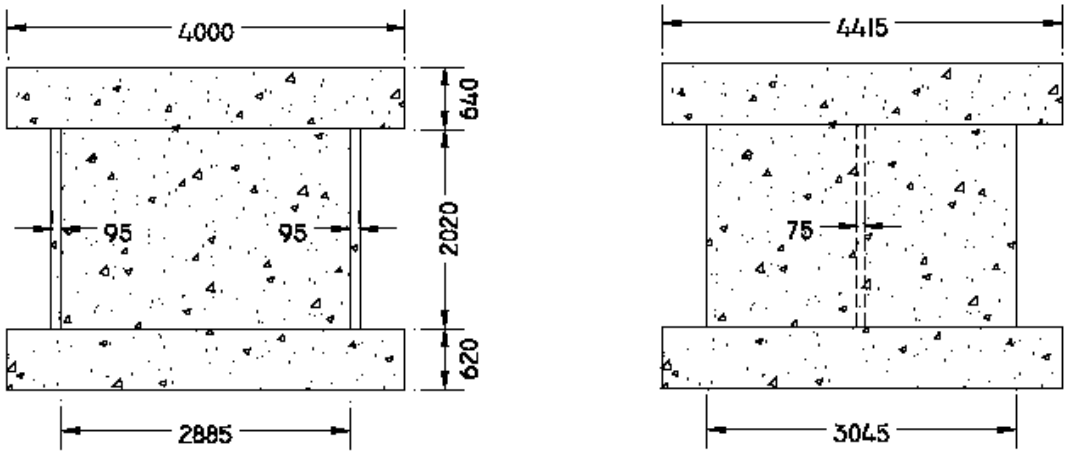


**a) Side view** **b) Front view**

**Figure 5-6 Dimensions (in mm) of wall DP1 [Palermo and Vecchio (2002a)]**

**Figure 5-7 Wall DP1 before testing [Palermo and Vecchio (2002a)]**

elasticity for web and flanges, top slab and foundation concrete were 25900 MPa, 43700 MPa, and 36900 MPa, respectively.

The horizontal web reinforcement consisted of two curtains of D6 rebar (nominal diameter = 7 mm) spaced at 140 mm and the vertical web reinforcement consisted of two curtains of D6 rebar spaced at 130 mm. The corresponding horizontal and vertical web reinforcement ratios were

0.737% and 0.794%, respectively. Flange vertical reinforcement consisted of two curtains of D6 bars spaced at 130 mm near the wall web and D6 bars spaced at 355 mm remote from the wall web. The flange horizontal reinforcement consisted of two curtains of D6 bars spaced at 140 mm. Figure 5-8 illustrates the details of the reinforcement in the web and flanges of wall DP1. The yield and the fracture stresses of the D6 rebar were 605 MPa (87.7 ksi) and 652 MPa (94.6 ksi), respectively. D30 rebar (nominal diameter = 29.9 mm) spaced at 350 mm in each direction was used in two layers (at the top and bottom) in the top slab and foundation. The reinforcement ratios for the top slab and foundation were 0.63% and 0.65 %, respectively. The yield and the fracture stresses of the D30 rebar were 550 MPa (79.8 ksi) and 696 MPa (100.9 ksi), respectively. The measured moduli of elasticity for D6 and D30 rebar were 190,250 MPa and 220,000 MPa, respectively. The wall foundation was clamped to the laboratory strong floor using forty 2 in. diameter bolts post-tensioned to 8000 psi.

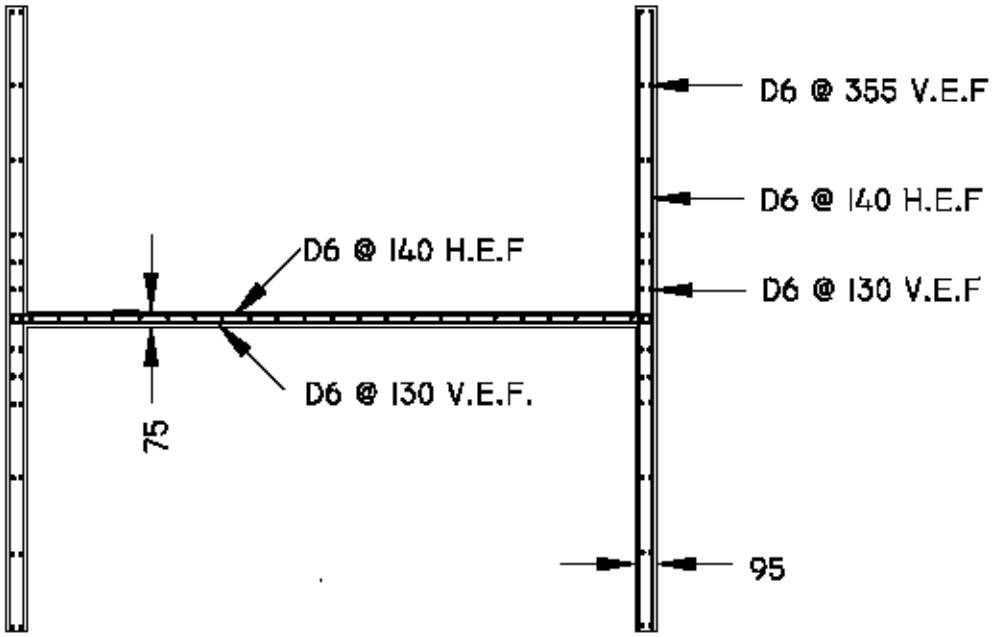


Note: V.E.F : Vertical, each face ; H.E.F : Horizontal, each face

**Figure 5-8 Top view of reinforcement in wall DP1 [Palermo and Vecchio (2002a)]**

Wall DP1 was tested using a quasi-static loading protocol. Lateral force was transferred to the wall through the top slab that was laterally displaced using two 1000 kN actuators. Displacement was incremented 1 mm at each load step and two cycles were imposed at each displacement level. An axial force of $0.054 A_t f_c'$ (940 kN) was applied to the wall. The experimental load-displacement relationship for wall DP1 is presented in Figure 5-9. Notable in the figure is the highly pinched hysteresis and rapid strength and stiffness degradation following the attainment of the peak shear strength.

The experimental peak shear strength of wall DP1 was 1298 kN at a lateral displacement of 11.1 mm (0.55% drift). Wall DP1 failed by crushing of the web concrete as seen in Figure 5-10. Following the attainment of peak shear, crushing was seen in the web of the wall and the shear strength of the wall began to degrade rapidly. As the displacement demand on the specimen

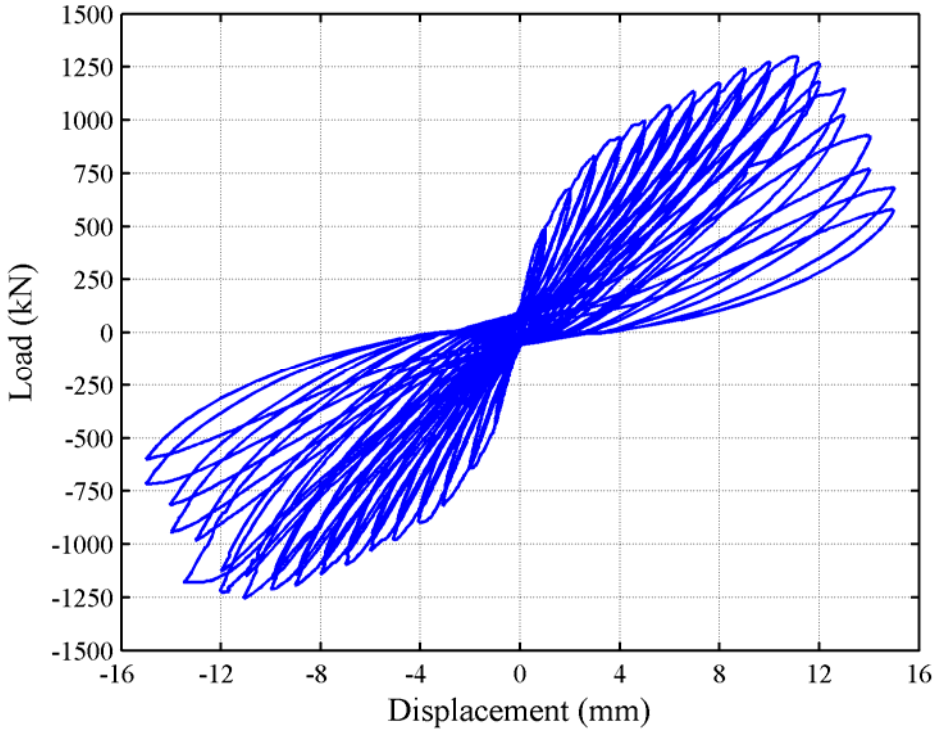


**Figure 5-9 Experimental load-displacement relationship for wall DP1 [Palermo and Vecchio (2002b)]**

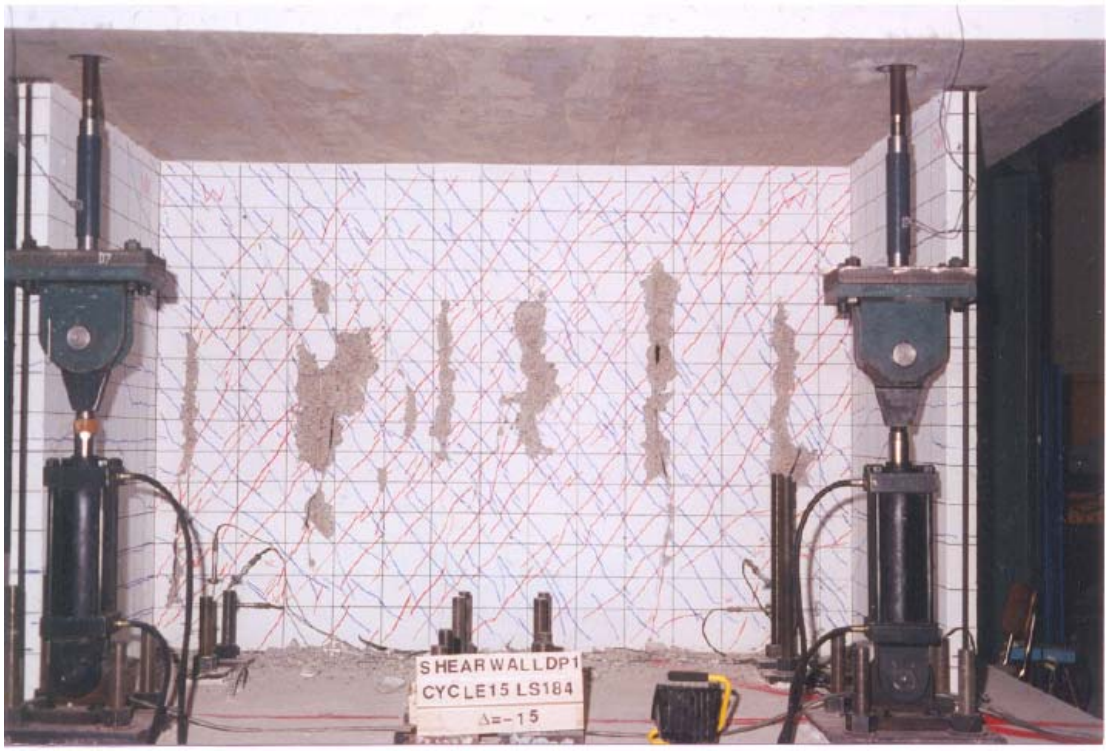


**Figure 5-10 Wall DP1 condition at failure (15 mm lateral displacement) [Palermo and Vecchio (2002a)]**

increased, crushing and strength degradation became more severe and the test was terminated at the completion of the displacement cycle to the lateral displacement of 15 mm.

Flexural cracking was observed in the flanges of the wall. No other major damage was observed in the wall flanges. Of the 40 strain gauges used on the web and flange reinforcement of wall DP1, only two on horizontal web reinforcement recorded strains in excess of yield. However, this observation should be evaluated with caution since the location of the gages may have significantly influenced the recordings (i.e., gages at cracks record much higher strains than those in uncracked concrete).

First yielding in horizontal web reinforcement was observed at a lateral displacement of 11.6 mm (0.57% drift) near the center of the wall web in the first displacement cycle to 13 mm. The maximum strain in vertical web reinforcement (0.0019) was recorded in tension during the first cycle to a lateral displacement of 14 mm (0.69% drift) at a gage at the base of the web near the flange in compression. The maximum strain (0.00218) in vertical flange reinforcement was recorded during the first cycle to a lateral displacement of 12 mm (0.59% drift) at a gage located slightly below the center of the flange near the flange web intersection. The yield strain for D6 reinforcement used in the web and flanges of the wall was 0.00318.

## 5.3 ABAQUS Models

### 5.3.1 General

The *Concrete Damaged Plasticity* (CDP) model in ABAQUS uses the concepts of isotropic damaged elasticity and hardening plasticity to represent the behavior of concrete. The model uses the yield function of Lubliner et al. (1989) with the modifications proposed by Lee and Fenves (1998) to account for the multiple damage states (compression and tension damage). The flow potential is defined using a Drucker-Prager function of the hyperbolic type. Detailed information on the constitutive model is presented in Appendix B.

Attempts to simulate cyclic loading using the CDP model in ABAQUS were unsuccessful due to the lack of convergence[1]. Therefore, monotonic force-displacement (pushover) curves for walls S4 and S9 tested by Maier and Thürlimann (1985) and wall DP1 tested by Palermo and Vecchio (2002a) are developed using the CDP model. Walls LSW1, LSW2 and LSW3 tested by Salonikios et al. (1999) are not modeled using CDP since these walls experienced significant sliding which is a phenomenon that is peculiar to cyclically loaded squat walls.

### 5.3.2 Modeling Parameters

For rate- and temperature-independent analyses, the CDP model in ABAQUS requires the definition of the following data associated with concrete behavior: a) uniaxial response in compression, b) uniaxial response in tension, c) ratio of initial equibiaxial compressive yield stress to initial uniaxial compressive yield stress ($\sigma_{b0}/\sigma_{c0}$), d) ratio of the second deviatoric stress invariant on the tensile meridian to that on the compressive meridian ($K_c$), and e) eccentricity and dilation parameters for the flow potential.

[1] The damage parameters are calibrated using the cyclic stress-strain relationships proposed by Mander et al. (1988).

The evolution of the yield surface in the CDP model is controlled by two hardening parameters that are internally calculated by the software using the user-defined uniaxial responses of concrete under compression and tension. The uniaxial compressive response of concrete is represented using the stress-strain curves reported by the researcher for concrete. For those cases where this data are not reported by the researcher, the numerical model of Popovics (1973) is used to represent the uniaxial compressive response, $f_c'$, of concrete. The *Popovics* model is represented by the following equations:

$$f_c = f_c' \frac{r\left(\varepsilon_c / \varepsilon_{co}\right)}{r - 1 + \left(\varepsilon_c / \varepsilon_{co}\right)^r} \tag{5-1}$$

$$r = \frac{E_c}{E_c - E_{sec}} \tag{5-2}$$

$$E_{sec} = \frac{f_c'}{\varepsilon_{co}} \tag{5-3}$$

where $f_c'$ is compressive strength, $\varepsilon_{c0}$ is the strain corresponding to $f_c'$, and $E_c$ is the modulus of elasticity of concrete. In the absence of experimental data, $E_c$ is calculated using

$$E_c = 5000\sqrt{f_c'} \quad \text{(MPa)} \tag{5-4}$$

and $\varepsilon_{c0}$ is assumed as 0.002. Figure 5-11 presents stress-strain relationships obtained using the *Popovics* model for different values of $f_c'$.

In reinforced concrete, the intact concrete between the cracks can carry tensile stresses due to the bond between the rebar and surrounding concrete. This effect is known as *tension-stiffening* and needs to be considered in modeling the behavior of reinforced concrete structures. When the interaction between concrete and reinforcement is not explicitly modeled, a common approach has been to introduce an empirical tension-stiffening model to simulate the tensile stress carried by the concrete between cracks. The CDP model in ABAQUS requires modeling the behavior of concrete in tension using either a post-cracking stress-strain relationship or a fracture-energy-cracking model. The former is used here. The tension-stiffening model proposed by Vecchio and Collins (1986) is adopted for all finite element analyses conducted using ABAQUS.

In this model, the stress-strain relationship for concrete in tension is linear up to the onset of cracking. Following the initiation of cracking, the tension-stiffening relationship presented in Equation 5-5 is used to represent the behavior of reinforced concrete under tension. Equation 5-5 is based on the results of experiments of reinforced concrete panels at University of Toronto.

$$f_t = \frac{f_t'}{1 + \sqrt{c_t \varepsilon_t}} \tag{5-5}$$

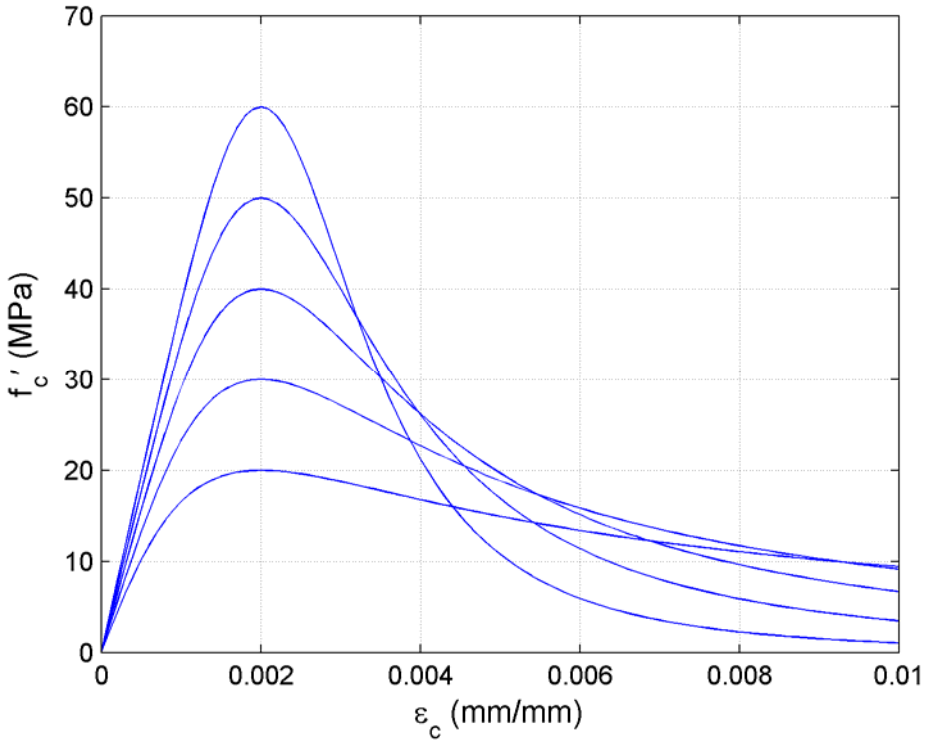


**Figure 5-11 Uniaxial compressive stress – strain relationships obtained using Popovics model for unconfined concrete**

where $\varepsilon_t$ is tensile strain and the constant $c_t$ determines the rate at which the tensile stress, $f_t$, diminishes and was determined experimentally to be 200 by Vecchio and Collins (1982). The tensile strength of concrete, $f_t'$, is calculated using Equation 5-6 in the Vecchio-Collins *tension-stiffening* model.

$$f_t' = 4\sqrt{f_c'} \text{ (psi)} \quad \left[ = 0.33\sqrt{f_c'} \text{ (MPa)} \right] \tag{5-6}$$

In addition to the hardening variables calculated internally by the software using the user-defined compressive and tensile responses, two other parameters are required to define the yield function for the CDP model. These parameters are the ratio of initial equibiaxial compressive yield stress to initial uniaxial compressive yield stress ($\sigma_{b0}/\sigma_{c0}$) and the ratio of the second deviatoric stress invariant on the tensile meridian to that on the compressive meridian ($K_c$). Lubliner et al. (1989) states that $\sigma_{b0}/\sigma_{c0}$ ranges between 1.10 and 1.16 and $K_c$ typically ranges between 0.64 and 0.80 for concrete. The software defaults for $\sigma_{b0}/\sigma_{c0}$ and $K_c$ parameters, 1.16 and 0.67, respectively, are used for the analyses.

The CDP model uses a non-associated flow rule, where the yield function and the plastic potential function are not identical, that is, the plastic strain increment vector is not normal to the yield surface. In the CDP model, the plastic potential function is a hyperbolic type Drucker-Prager function for which a detailed discussion is provided in Appendix B. Three parameters are required to define the function, namely, uniaxial tensile stress ($\sigma_{t0}$), dilation angle ($\psi$) and

eccentricity ( $\varepsilon$ ). The uniaxial tensile stress is adopted directly from the user-defined stress-strain response under tension. The dilation angle is the slope of the plastic potential function measured in the $\overline{p} - \overline{q}$ [2] plane at higher confining pressures (see Figure B-1). The dilation angle is a critical parameter in the CDP formulation because it determines the direction of the plastic flow via the incremental plastic strain vector. Experimental evaluation of this parameter requires monitoring of the incremental plastic strains in concrete for various triaxial stress states. This data was not provided for any of the wall experiments modeled in this study. Therefore, the effect of dilation angle on the predicted response is investigated using a parametric study.

Eccentricity is the parameter that defines the rate at which the hyperbolic potential function approaches the asymptote. The plastic potential function becomes a straight line (linear type Drucker-Prager function) for $e$ = 0. However, the use of the linear form of the function is not desirable from computational standpoint because of the discontinuity of the function at $\overline{p}$ axis intersection (see Figure B-1). The software default (0.1) is used for the analyses herein because it enables a near constant value of the dilation angle over a wide range of confinement stresses.

### 5.3.3 Finite Element Models of Walls S4 and S9

Detailed information on the geometry, material properties and experimental response of walls S4 and S9 tested by Maier and Thürlimann (1985) is presented in Section 5.2.1. In this section, corresponding finite element analysis results obtained using ABAQUS are presented. Figure 5-12a presents the finite element model constructed using ABAQUS/CAE (pre- and post-processor for ABAQUS) that is used to simulate walls S4 and S9. Walls S4 and S9 were tested under monotonic lateral loading that was applied quasi-statically. The lateral load was transferred to the web of the wall through the top beam using two hydraulic jacks. As illustrated by the horizontal arrows in Figure 5-12a, nodal displacement boundary conditions applied at the mid-height of the top beam are used to simulate the lateral load on the walls. Axial load is simulated by defining an equivalent pressure at the top surface of the top beam (vertical arrows in Figure 5-12a). The orange symbols below the wall foundation in Figure 5-12a represent the fixed boundary conditions imposed on the model. Figure 5-12b illustrates the reinforcement model constructed in ABAQUS/CAE for wall S4. As seen in the figure, the reinforcement is modeled explicitly. The same reinforcement model, but without the horizontal web reinforcement, is used for wall S9.

Finite element results for walls S4 and S9 are obtained using two different meshes, namely, mesh-1 and mesh-2, for each wall. The meshes are illustrated in Figure 5-12c and Figure 5-12d, respectively. In mesh-1, the web of the wall consists of 144 brick elements (12 x 12 x 1). The primary objective for constructing mesh-1 was to include reinforcement (modeled discretely) within each solid element to maintain uniform distribution of reinforcement into the solid elements that represent concrete. Therefore, the number of elements to be used along the height and the length of the wall web were determined based on the spacing of the reinforcement in the corresponding directions. Only one brick element is used through the thickness of the web; as a result two rebars are embedded in each brick element. Mesh-2 is an h-refinement extension of mesh-1 for the web region of the wall. In mesh-2, the web of the wall consisted of 1152 (24 x 24 x 2) brick elements. The top beam and foundation meshes remain elastic throughout the loading

[2] Variable $\overline{p}$ is hydrostatic pressure and variable $\overline{q}$ is Mises equivalent effective stress.

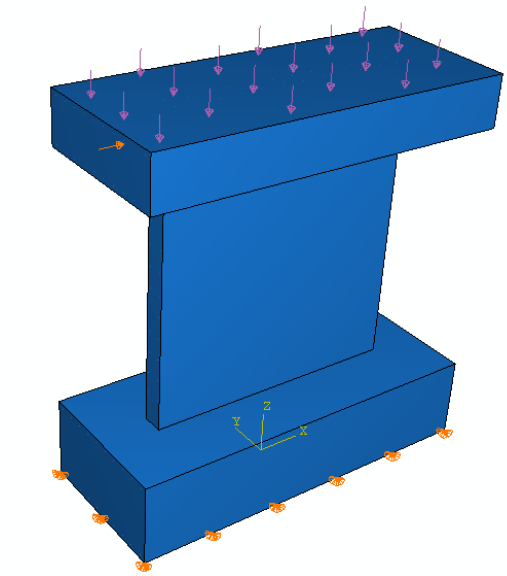

**a) ABAQUS model for walls S4 and S9**

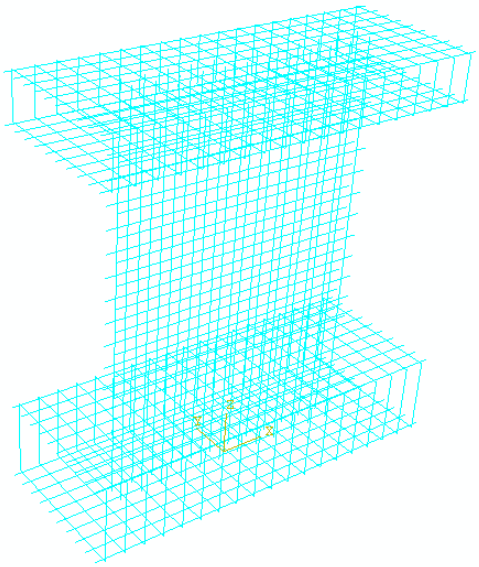

**b) Reinforcement scheme (wall S4)**

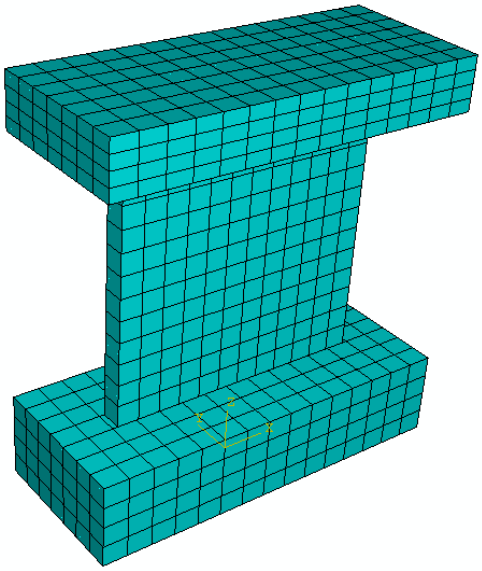

**c) Mesh-1**

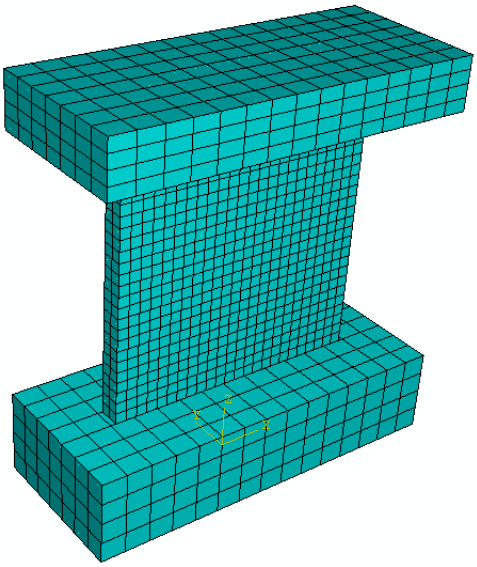

**d) Mesh-2**

**Figure 5-12 ABAQUS models used to simulate the response of walls S4 and S9**

history therefore a mesh refinement is unnecessary for these regions. The top beam and the foundation consist of 420 elements (15 x 7 x 4) in both meshes. The reinforcement in the walls is redistributed to include reinforcement in each solid element in mesh-2 but the total area of the reinforcement is unchanged from that in the test specimen. Further refinement of the mesh would have resulted in four elements through the thickness of the wall web and a redistribution of the reinforcement into even smaller elements, both of which were deemed inappropriate. The brick elements that represent concrete are 8-node linear, fully integrated, hexagonal elements (*C3D8*).

The wall reinforcement is modeled discretely using the reported reinforcement scheme and meshed using 2-noded linear truss elements (*T3D2*). Full bond between concrete and reinforcement is assumed using the *embedded elements* constraint in ABAQUS. This technique constrains the translational degrees of freedom of the nodes of the embedded elements with respect to the response of the host elements (hexagonal elements herein). The top beam-wall web and foundation-wall web interfaces are modeled using a *tie constraint*, which constraints the displacement of the translational degrees of freedoms on the tied surfaces to be equal.

For walls S4 and S9, reported values of $f_c'$ along with Popovics concrete model are used to simulate the compressive behavior of concrete. The parameters that are associated with tensile behavior of concrete are adopted from the empirical model introduced in Section 5.3.2. Poisson's ratio for concrete was set equal to 0.18 [Mindess et al. (2003)]. The two parameters associated with the yield function, $\sigma_{b0}/\sigma_{c0}$ and $K_c$, are assumed to be 1.16 and 0.67: the defaults set by the software and within the ranges provided by Lubliner et al. (1989). The eccentricity ($\varepsilon$) parameter associated with the flow potential is assumed to be 0.1, which is the default value set by the software. The effect of the second parameter associated with flow potential, dilation angle ($\psi$), on the finite element results is investigated parametrically. The wall reinforcement, which consisted of 8-mm diameter rebars, is modeled as an elasto-plastic material with isotropic hardening. The reported values of modulus of elasticity, yield stress, ultimate stress, failure strain, and strain at the onset of strain hardening are used to define the reinforcement behavior. Poisson's ratio for steel was set equal to 0.30.

Figure 5-13 presents the load-displacement relationships obtained as a function of dilation angle for wall S4 and mesh-1. The calculated response is significantly affected by variation of $\psi$. A softening regime could only be observed for the response calculated using $\psi$ = 55.

Wall ductility is overestimated in all cases and the rate of strength degradation following the attainment of the peak shear strength could not be predicted accurately. Experimental peak shear strength is best predicted using $\psi$ = 45 but the overall response is best predicted using $\psi$ = 55. The load-displacement relationship obtained using $\psi$ = 55 can be improved by imposing a failure strain on the compressive response of concrete modeled using the Popovics model.

Figure 5-14 and Figure 5-15 present the deformed shapes under 10x magnification and the variation of maximum principal strains over the wall web for $\psi$ = 55 and $\psi$ = 15, respectively, at a lateral displacement of 18.5 mm (1.55% drift). It is clear that the deformed shape obtained for $\psi$ = 55 is a significantly better representation of the experimental behavior at 1.55% drift, which is presented in Figure 5-1c. For the response predicted using $\psi$ = 55, the maximum principal strains peak at the toe of the wall web that is subjected to tension as seen in Figure 5-14. On the other hand, a horizontal failure plane near the base of the wall web is observed for the response predicted using $\psi$ = 15 that is the reason for significant underestimation of the measured peak shear strength.

Figure 5-16 presents the load-displacement relationships obtained as a function of dilation angle for wall S9 and mesh-1. The effect of $\psi$ on the predicted response is more significant than for wall S4. This is expected because wall S9 does not include horizontal web reinforcement and the demand on the concrete formulation is relatively higher in terms of predicting the experimental response. Therefore, the predicted response for wall S9 is more sensitive to $\psi$, which is related

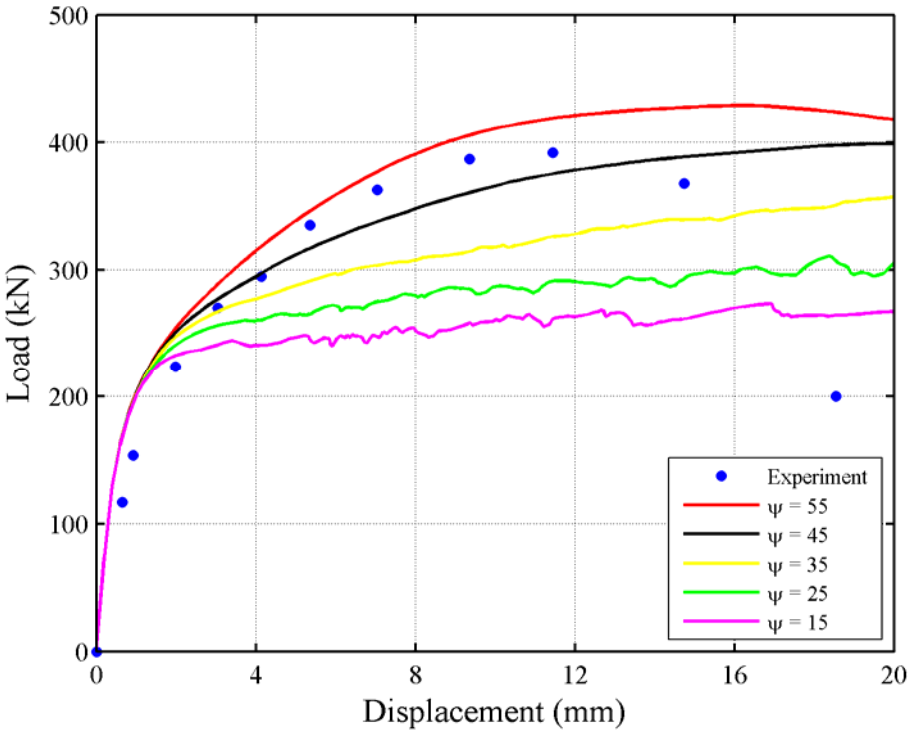


**Figure 5-13 Variation in predicted response as a function of dilation angle for wall S4 and mesh-1**

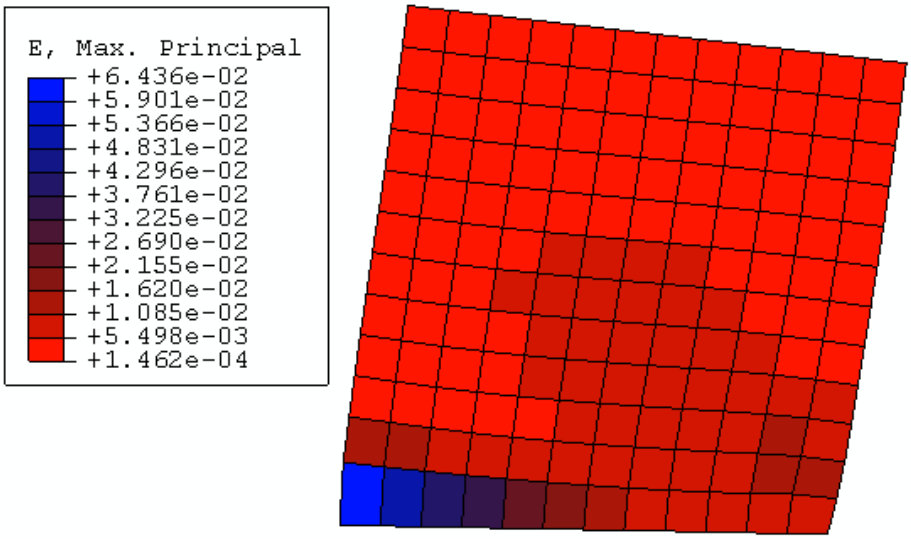


**Figure 5-14 Deformed shape and variation of maximum principal strains over the wall web for wall S4 and $\psi$ = 55**

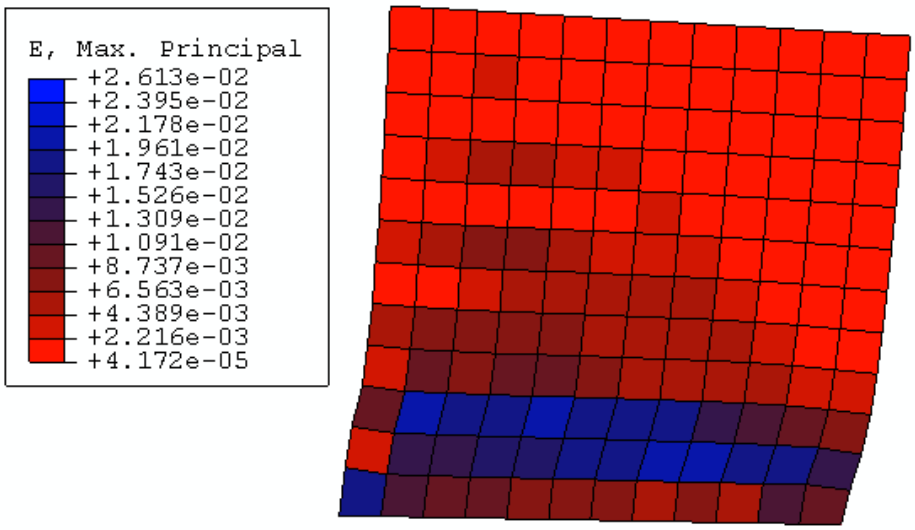


**Figure 5-15 Deformed shape and variation of maximum principal strains over the wall web for wall S4 and $\psi$ = 15**

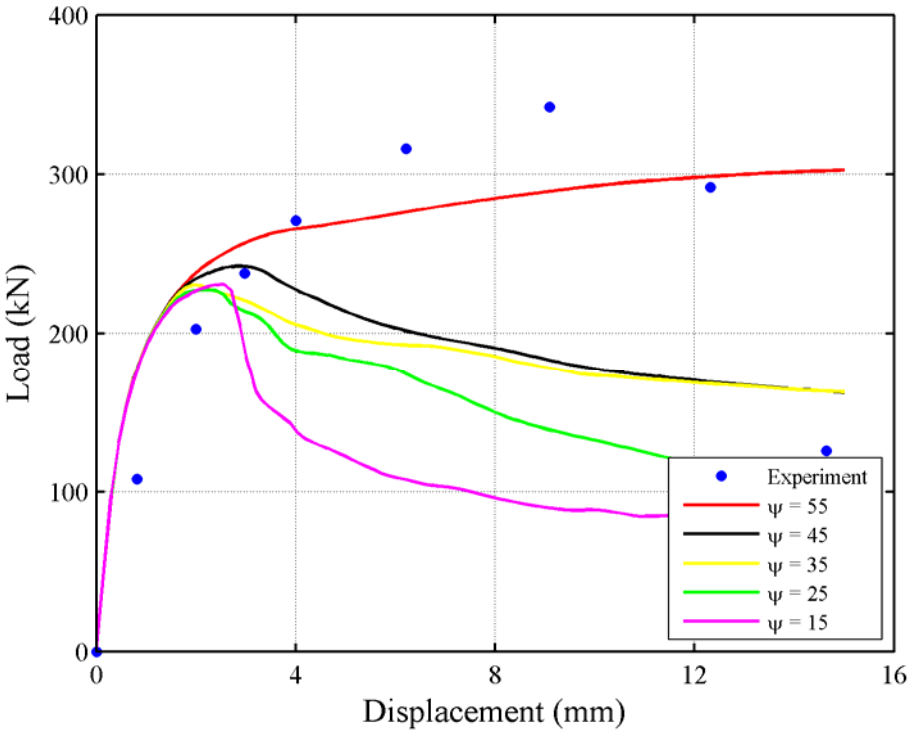


**Figure 5-16 Variation of predicted response as a function of dilation angle for wall S9 and mesh-1**

to modeling the response of concrete. The measured peak shear strength is underestimated for all values of $\psi$ with the best prediction obtained using $\psi$ = 55. The cracking patterns associated with the experimental response of wall S9 are presented in Figure 5-2. As seen in that figure, the failure of the wall was triggered by a wide corner-to-corner crack, which accounted for the

majority of the damage as the displacement demand on the wall was increased. Figure 5-17 presents the deformed shapes under 10x magnification and the variation of maximum principal strains over the wall web for $\psi$ = 55 at a lateral displacement of 14.6 mm (1.22% drift). As seen in the figure, the maximum principal strains peak near the center of the wall web and at the toe of the wall web that is subjected to tension due to flexural loading, which is in agreement with the observed experimental response.

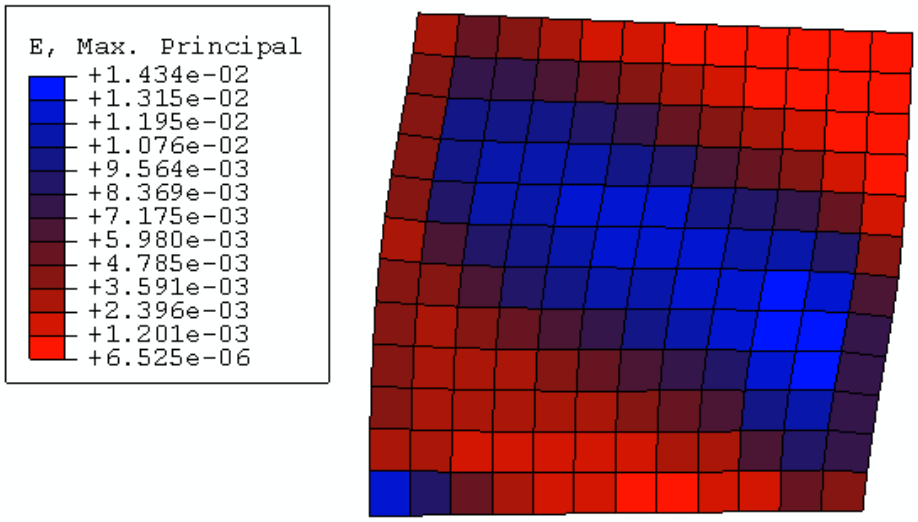


**Figure 5-17 Deformed shape and variation of maximum principal strains over the wall web for wall S9 and $\psi$ = 55**

Figure 5-18 and Figure 5-19 present the load-displacement relationships for walls S4 and S9, respectively, obtained using mesh-1 and mesh-2. The effect of mesh refinement on the calculated response is insignificant for wall S4, which includes heavy web reinforcement in horizontal and vertical directions. The effect of mesh refinement is more pronounced for wall S9, which has no horizontal web reinforcement. The coarser mesh (mesh-1) better reproduces the measured load-displacement response than the finer mesh (mesh-2).

### 5.3.4 Finite Element Model of Wall DP1

Detailed information on the geometry, material properties and experimental response of wall DP1 [Palermo and Vecchio (2002a)] is presented in Section 5.2.3. Figure 5-20a presents the wall geometry for wall DP1 constructed using ABAQUS/CAE. Wall DP1 was tested using a displacement controlled loading protocol that was applied quasi-statically. Lateral load was transferred to the wall through the top slab using two hydraulic jacks. As illustrated by the horizontal arrows in Figure 5-20a, lateral load is modeled at the mid-height of the top slab using nodal displacement boundary conditions. The axial load on the wall is simulated by defining an equivalent pressure at the upper surface of the top slab (vertical arrows in Figure 5-20a). The orange symbols below the wall foundation represent the fixed boundary conditions imposed on the model. The specimen was clamped to the laboratory strong floor using post-tensioned bolts designed to prevent rocking of the wall. Figure 5-20b illustrates the reinforcement model constructed in ABAQUS/CAE for wall DP1. As seen in the figure, the reinforcement was

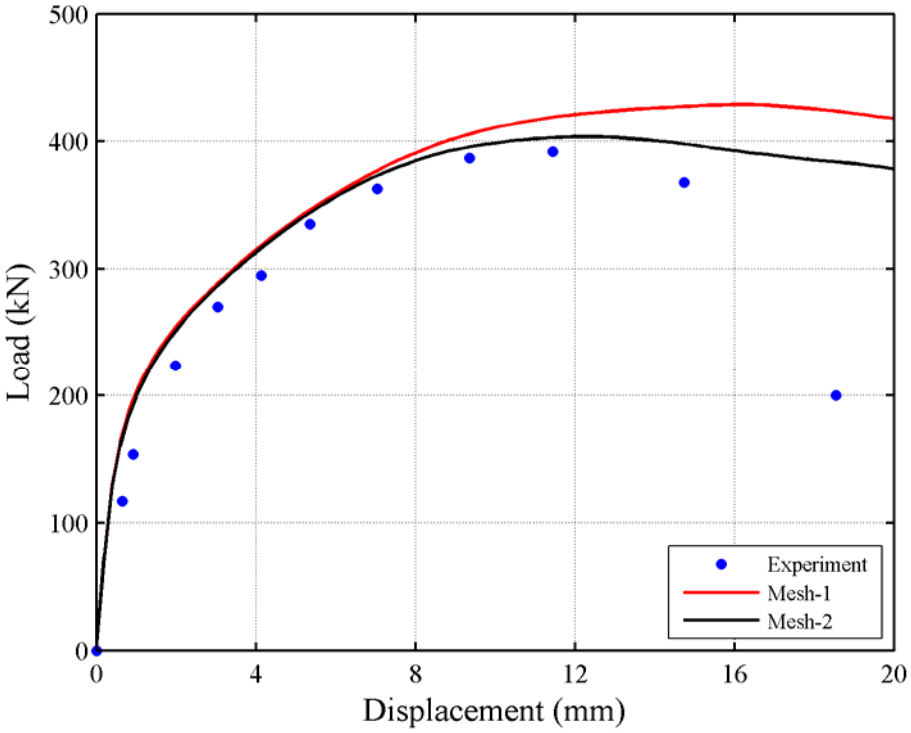


**Figure 5-18 Load-displacement relationships for wall S4 obtained using mesh-1 and mesh-2 with $\psi$ = 55**

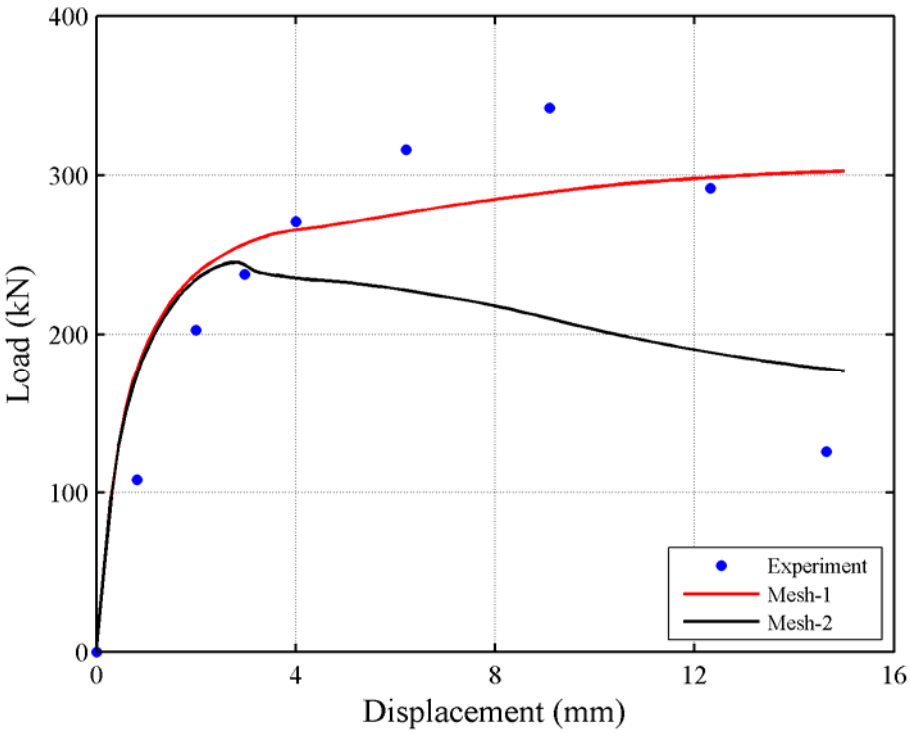


**Figure 5-19 Load-displacement relationships for wall S9 obtained using mesh-1 and mesh-2 with $\psi$ = 55**

represented discretely in the analyses.

For wall DP1, the uniaxial stress-strain relationship in compression was reported by Palermo and Vecchio (2002a) so was used in the analysis. The parameters that are associated with tensile behavior of concrete are adopted from the empirical model introduced in Section 5.3.2. Palermo and Vecchio (2002a) did not report uniaxial tensile strength of concrete ( $f_t'$ ) therefore, Equation 5-6 is used to calculate this parameter. Poisson's ratio for concrete was set equal to 0.18.

The two parameters associated with the yield function, $\sigma_{b0}/\sigma_{c0}$ and $K_c$, are assumed to be 1.16 and 0.67. The assumed values are the defaults set by the software and within the range provided by Lubliner et al. (1989). The eccentricity ($\varepsilon$) parameter associated with the flow potential is assumed to be 0.1, for the reason given previously. The effect of the dilation angle, on the finite element results is investigated parametrically.

The wall reinforcement, which consisted of D6 and D30 rebars, is modeled as an elasto-plastic material with isotropic hardening. The experimental uniaxial stress-strain relationships reported by Palermo and Vecchio (2002a) are used to define the material parameters for reinforcement (i. e., modulus of elasticity, yield stress, variation of post-yield stress with equivalent plastic strains). Poisson's ratio for steel was set equal to 0.30.

Wall DP1 is analyzed using two different meshes, mesh-1 and mesh-2, which are illustrated in Figure 5-20c and Figure 5-20d, respectively. In mesh-1, the web of the wall consisted of 345 brick elements (15 x 23) and each flange consisted of 300 brick elements (15 x 20). The primary objective of mesh-1 is to include reinforcement (modeled discretely) within each solid element to maintain a uniform distribution of reinforcement in the solid elements that represent concrete. Therefore, the number of elements to be used along the height and the length of the wall web and flanges were determined based on the reinforcement spacings. Only one element was used through the thickness of the web and flanges therefore two rebars were embedded in each solid element. In mesh-2, the web of the wall consisted of 1380 brick elements (30 x 46) and each flange consisted of 1200 brick elements (30 x 40). The top slab and the foundation consisted of 1600 elements (20 x 20 x 4) in mesh-1 and mesh-2. The top slab and foundation meshes were not refined since these components remain mostly elastic in the analyses. The reinforcement in the web and flanges of the wall is redistributed into each solid element in mesh-2; the total areas of the reinforcement are those of the test specimens.

The brick elements that simulate concrete behavior in ABAQUS finite element analyses are 8-node linear, fully integrated, hexagonal elements (*C3D8*). The wall reinforcement is modeled discretely using the reported reinforcement scheme and meshed using 2-node linear truss elements (*T3D2*). Full bond between concrete and reinforcement is assumed. This behavior is modeled using the *embedded elements* constraint in ABAQUS. The top beam-wall web and foundation-wall web interfaces are modeled using a *tie constraint*, which constraints the displacement of the translational degrees of freedoms on the tied surfaces to be equal.

Figure 5-21 presents lateral load-displacement relationships for wall DP1 obtained using values of the dilation angle ranging between 15 and 55. In the figure, the curve that represents the "experiment" is a backbone curve obtained from the reported cyclic lateral load-displacement relationship for wall DP1 (see Figure 5-9). Figure 5-21 shows that the analytical response of wall DP1 computed using ABAQUS varies significantly with the dilation angle parameter in the inelastic range. It can be observed in Figure 5-21 that experimentally measured elastic wall

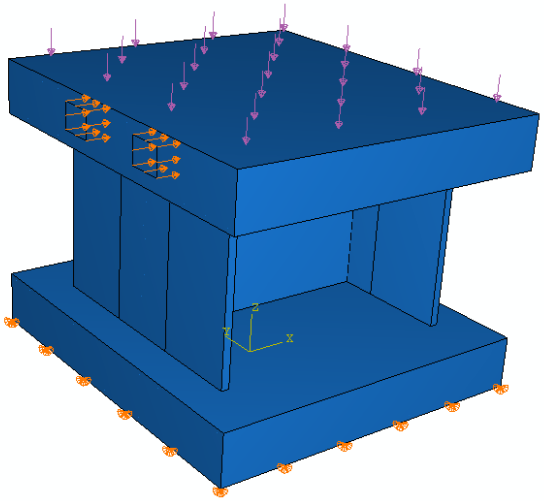

**a) ABAQUS model for wall DP1**

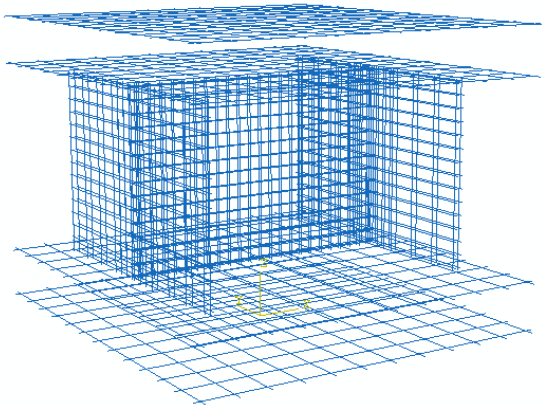

**b) Reinforcement scheme for wall DP1**

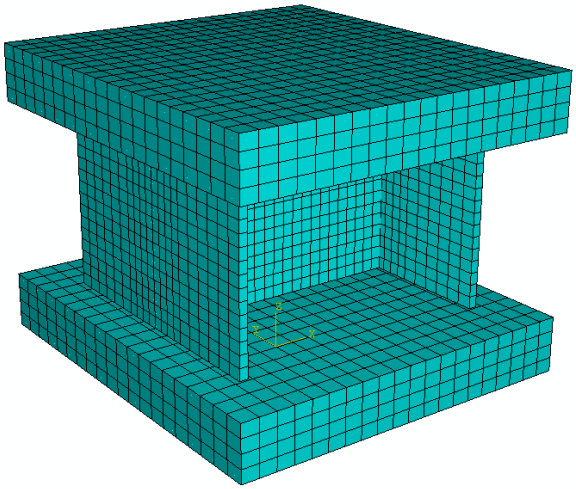

**c) Mesh-1**

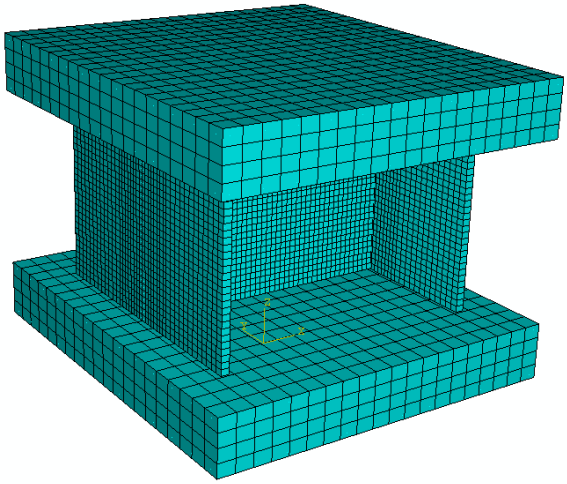

**d) Mesh-2**

**Figure 5-20 ABAQUS models used to simulate the response of wall DP1**

stiffness and the analytically calculated value are in good agreement, which indicates that the boundary conditions and loads are successfully simulated in the finite element model. The backbone load-displacement from the experimental data is best captured by the model with a dilation angle of 55 degrees and the predicted response becomes less accurate as dilation angle is reduced. The analysis conducted with a dilation angle of 55 degrees is used for further comparisons with the experimental response.

Table 5-3 lists various experimentally measured and predicted responses for wall DP1. Response parameters RP1 through RP4 are associated with the global response of wall DP1. Comparison of the calculated and experimental values for RP1 through RP4 shows that the finite element model accurately simulates the global experimental response of wall DP1. Parameters RP5

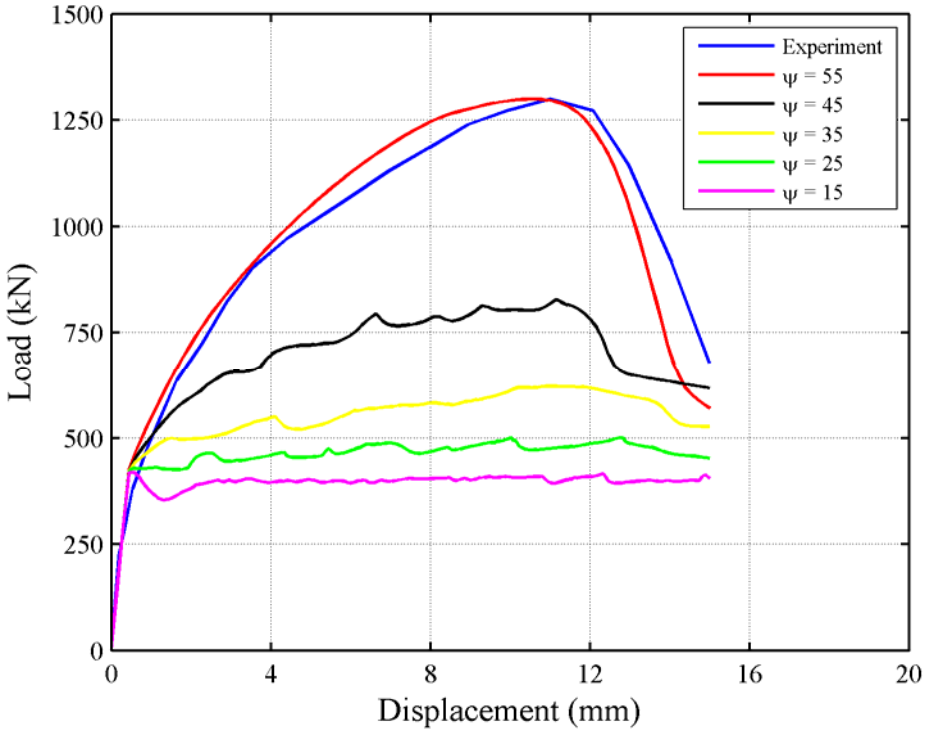


**Figure 5-21 Predicted load-displacement relationships for DP1 as a function of $\psi$**

**Table 5-3 Comparison of predicted and experimental response parameters for wall DP1 and $\psi$ = 55**

| ID | Response parameter | Experiment (Exp) | Finite element analysis (FEA) | $\frac{\text{FEA}}{\text{Exp}}$ |
|---|---|---|---|---|
| RP1 | Peak shear strength | 1300 kN | 1299 kN | 1.00 |
| RP2 | Displacement at peak shear strength | 11.0 mm | 10.6 mm | 0.97 |
| RP3 | Displacement at shear strength equal to 80% of the peak (pre-peak region) | 5.5 mm | 4.9 mm | 0.89 |
| RP4 | Displacement at shear strength equal to 80% of the peak (post-peak region) | 13.5 mm | 13.0 mm | 0.97 |
| RP5 | Displacement at initiation of yielding in horizontal web reinforcement | 11.6 mm | 11.1 mm | 0.96 |
| RP6 | Maximum strain recorded in vertical web reinforcement | 0.00190 @ 14 mm | 0.00228 @ 15 mm | 1.20 |
| RP7 | Maximum strain recorded in vertical flange reinforcement | 0.00218 @ 12 mm | 0.00293 @ 15 mm | 1.34 |

through RP7 in Table 5-3 are associated with reinforcement response. As indicated in Section 5.2.3, only the horizontal web reinforcement experienced inelastic strains. The vertical web and flange reinforcement remained elastic throughout the experiment at the locations of the gages. Response data for RP5 through RP7 reveal that the experimental response of reinforcement was captured reasonably using the ABAQUS model. Similar to that observed in the experiment, yielding was observed only in the horizontal web reinforcement in the finite element model.

Figure 5-22 presents the predicted load-displacement relationships for wall DP1 obtained using mesh-1 and mesh-2. The response computed using mesh-2 is more flexible than that using mesh-1 although the differences are minor. The peak shear strengths obtained using mesh-1 and mesh-2 are similar.

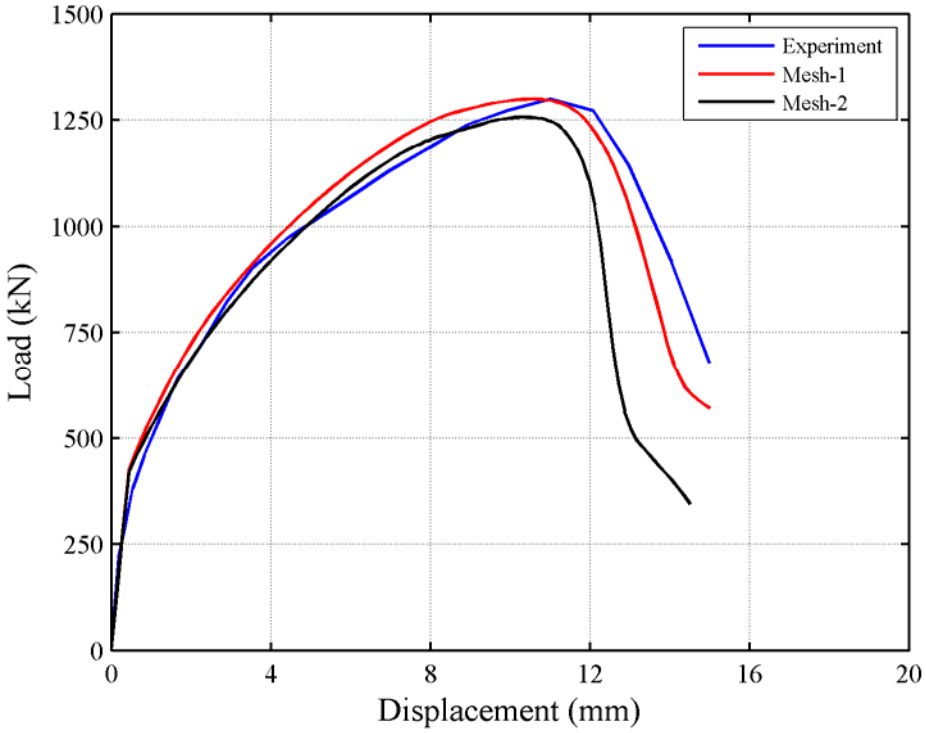


**Figure 5-22 Predicted load-displacement relationships for wall DP1 with mesh-1 and mesh-2**

# 5.4 VecTor2 Models

## 5.4.1 General

VecTor2 uses *Modified Compression Field Theory* (MCFT) [Vecchio and Collins (1986)] and *Disturbed Stress Field Model* (DSFM) [Vecchio (2000)] to simulate behavior of reinforced concrete. The major difference between the two models is that DSFM incorporates slip deformation in crack surfaces within its formulation, and as a result, the alignment of the directions of principal stresses and strains is no longer enforced. Explicit calculation of the crack slip deformations in DSFM eliminates the necessity of a crack shear check used with MCFT formulation. Vecchio et al. (2001) concludes that DSFM performs better than MCFT under

certain circumstances (i.e., for panels and beams without transverse reinforcement, for heavily reinforced panels subjected to biaxial compression) but also notes that the difference between the predictions of the two algorithms is generally minor.

Herein, finite element analyses on reinforced concrete squat walls are conducted using both algorithms. The calculation of slip deformations within the DSFM algorithm is undertaken using the model proposed by Lai (2001). Appendix B provides detailed information on the MCFT and DSFM formulations.

## 5.4.2 Modeling Assumptions

VecTor2 includes a list of constitutive models to represent the behavior of reinforcement and concrete. This section presents a discussion of the constitutive models selected for the analyses. Unless mentioned otherwise, the selected model is a default in the software.

VecTor2 does not accommodate a user-supplied curve to represent the compressive response of concrete but rather includes various formulations for compressive response. The software allows use of different concrete models to model the pre- and post-peak ranges of compressive behavior of concrete. In this study, the same concrete model is used to represent the pre- and post-peak response of concrete in compression (choosing *base curve* option in the software). Two widely used concrete models are used to simulate the compressive response, namely, *Popovics (NSC)* model [Popovics (1973)] and the *Smith-Young* model [Smith and Young (1956)]. The software defaults to represent the pre- and post-peak compressive response are the *Hognestad parabola* and the *Modified Park-Kent* model [Park et al. (1982)], respectively. The *Vecchio 1992-A model* [Vecchio and Collins (1993)] is used to simulate the *compression-softening* behavior of concrete. This model accounts for reduction in both the uniaxial compressive strength of concrete and the corresponding strain to compute the softened response of concrete as a function of the transverse tensile strains. *Tension-stiffening* effects, which represent the tensile stresses in concrete between the cracks that exist due to the interaction of concrete and reinforcement, are simulated using the *Modified Bentz model* [Vecchio (2000)]. Another model associated with tensile behavior of concrete is called *tension-softening* that represents the behavior of plain concrete following initiation of cracking. In VecTor2, this behavior is simulated as a linear descending branch using fracture energy ($G_f$). In VecTor2, the tensile post-cracking stress of an element is determined using the larger of the stresses provided from the *tension-stiffening* and *tension-softening* models for a given strain. The *Kupfer-Richart* model [Vecchio (1992)] is used to simulate the strength enhancement in concrete in compression due to confinement. The *Variable-Kupfer* model [Vecchio (1992)] is used to represent the dilatational characteristics of concrete. The rate of lateral expansion in concrete increases as a result of micro-cracking as compressive strains increase and the model increases the Poisson's ratio as a nonlinear function of compressive strain to simulate such behavior. Even though the MCFT and DSFM algorithms in VecTor2 are formulated assuming plane stress, the software is capable of incorporating confinement effects under triaxial stress conditions through modeling of out-of-plane reinforcement. The cracking stress for concrete is calculated using the *Mohr-Coulomb stress* model using an angle of friction of 37 degrees [Wong and Vecchio (2002)]. The use of the MCFT algorithm requires a crack shear check to ensure that local shear stresses at a crack do not exceed a maximum that is specified using a sliding shear failure. The model proposed by Vecchio and Collins (1986), which is based on the work of Walraven (1981), is used to calculate the maximum permissible

shear stress at a crack. Another constraint related to crack formation is a check on concrete crack width. The compressive stresses in concrete are reduced when the calculated crack widths exceed the specified limit. Herein, the limit is set equal to 20% of the aggregate size (i.e., 2 mm for 10 mm aggregate). The model proposed by Palermo and Vecchio (2002a), a non-default hysteresis model in VecTor2, is used to represent the hysteretic behavior of concrete. This is the only hysteresis model in the software that includes degradation of strength and stiffness in the reloading curves. The model proposed by Seckin (1981) is used to represent the hysteretic behavior of reinforcement. The model can simulate the strain hardening and Bauschinger effects, which are important characteristics associated with the behavior of steel reinforcement. The default (and only) model to simulate reinforcement buckling in VecTor2 is the *Asatsu* model. The utilization of the reinforcement buckling model requires discrete modeling of reinforcement and use of bond elements to define interaction between concrete and reinforcement [Wong and Vecchio (2002)]. Reinforcement buckling behavior is not considered in the analyses herein because 1) significant computational effort is required for cyclic analyses since it requires discrete modeling of reinforcement and modeling of bond elements between concrete and reinforcement, and 2) a validation study is not available regarding the implementation of the model into VecTor2 (to the author's knowledge). Dowel resistance of reinforcement is modeled using the *Tassios* model [Wong and Vecchio (2002)]. This is the default (and only) model provided for dowel resistance. This model requires calculation of slip deformations using the DSFM algorithm therefore it is not associated with MCFT analyses. The dowel model is not included in the analyses to allow a direct comparison between the results obtained using the MCFT and DSFM formulations.

Smeared reinforcement elements are used in all VecTor2 analyses. Such modeling is preferred to discrete models of reinforcement because smeared models require smaller computational effort. Further, squat reinforced concrete walls generally include uniformly distributed reinforcement in both orthogonal directions and it is convenient to model such rebar as smeared. The displacement compatibility between reinforcement and concrete requires the assumption of perfect bond. The elements used in the analyses are four-node rectangular plane stress elements with linear strain fields.

### 5.4.3 VecTor2 Modeling of Walls S4 and S9

Four different finite element meshes (mesh-10x10, mesh-15x15, mesh-20x20, and mesh-25x25) are constructed for walls S4 and S9 to identify the sensitivity of the analysis results to element size. The mesh names indicate the number of mesh seeds used along the length and height of the wall web. A consistent approach is followed for the construction of meshes in the VecTor2 analyses. The number of elements to be used for the smallest dimension of the wall web ($d_{\min}$), the smaller of the wall height and wall length is selected first. The number of elements to be used in the orthogonal direction is then established by maintaining the element aspect ratio around 1.0. Herein, element aspect ratio is defined as the ratio of the larger dimension of an element to its smaller dimension. For walls S4 and S9, the web geometry is approximately square (1.18 m high, 1.20 m long), therefore using the same number of elements along the height and length of the web provides an element aspect ratio of around 1.0. The meshes for the topbeam and the foundation are determined following the mesh seeds of the wall web and limiting the maximum aspect ratio for an element to 1.5. Figure 5-23 illustrates the mesh-10x10 and mesh-20x20 for walls S4 and S9. Application of the translational boundary conditions and experimental lateral

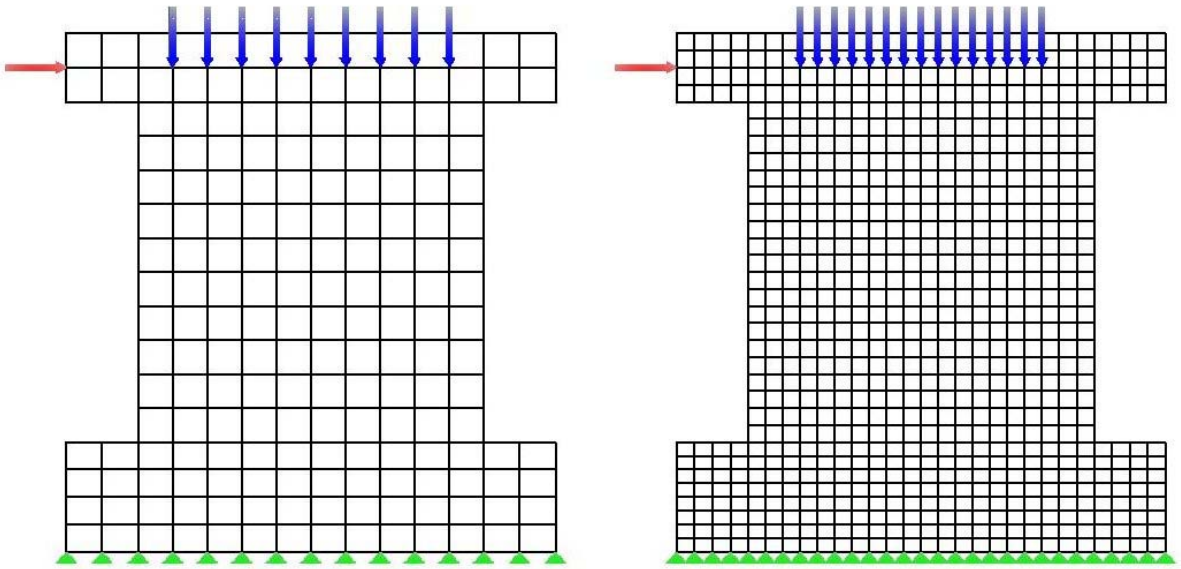

**a) Mesh-10x10** **b) Mesh-20x20**

**Figure 5-23 Example meshes used to model walls S4 and S9**

and axial forces on the finite element meshes are also shown. Note that mesh-20x20 is an h-refinement over mesh-10x10.

Figure 5-24 through Figure 5-27 present the load-displacement relationships obtained for wall S9 using mesh-10x10, mesh-15x15, mesh-20x20, and mesh-25x25, respectively. Each figure includes four load-displacement relationships generated using one of the two formulations, MCFT and DSFM, and one of the two models to represent the compressive behavior of concrete, Smith-Young and Popovics (NSC). A comparison of the finite element analysis results presented in Figure 5-24 through Figure 5-27 for wall S9 reveals that,

- The difference between the responses obtained using MCFT and DSFM formulations for the same concrete model is minor for all four meshes. The peak shear strengths are achieved at lower displacements for the DSFM formulation.
- The responses obtained using the Smith-Young and Popovics concrete models for the same formulation differ significantly, especially in the post-peak range. For all four meshes, the load-displacement relationships obtained using the Smith-Young model experience a sudden loss of shear strength at a displacement less than the experimentally measured displacement at peak shear strength. Therefore, post-peak shear strength is underestimated for all four meshes by the Smith-Young model. The most accurate prediction involving the Smith-Young model is obtained with mesh-10x10 and the MCFT formulation (see Figure 5-24). On the other hand, the load-displacement relationships obtained using the Popovics model exhibit a gradual loss of lateral strength following peak strength, which matches better the experimental data than the Smith-Young model.

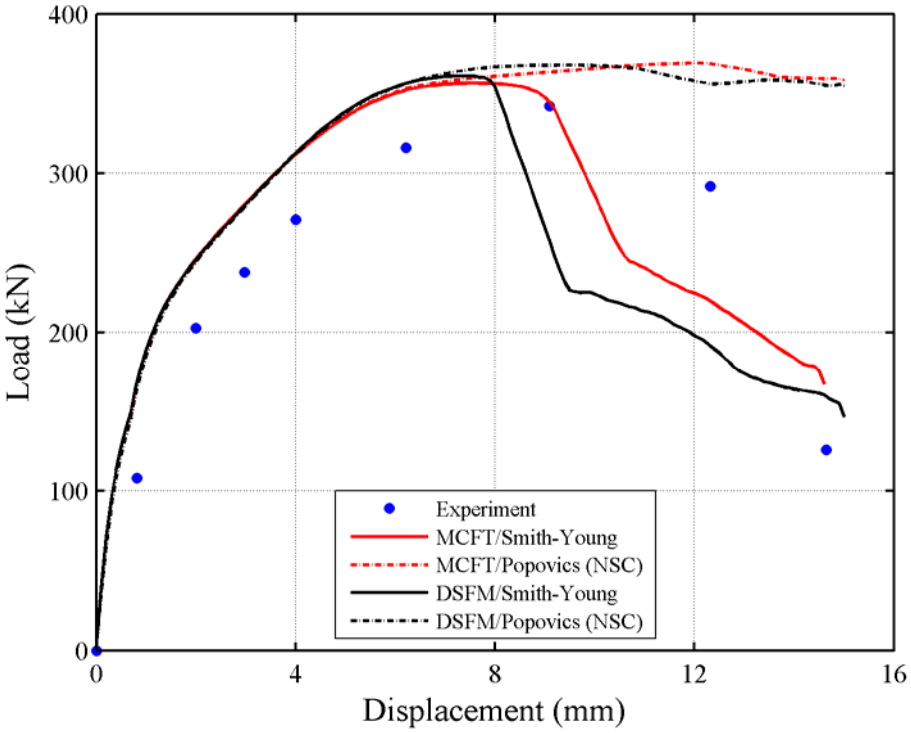


**Figure 5-24 Predicted load-displacement relationships for wall S9 obtained using mesh-10x10**

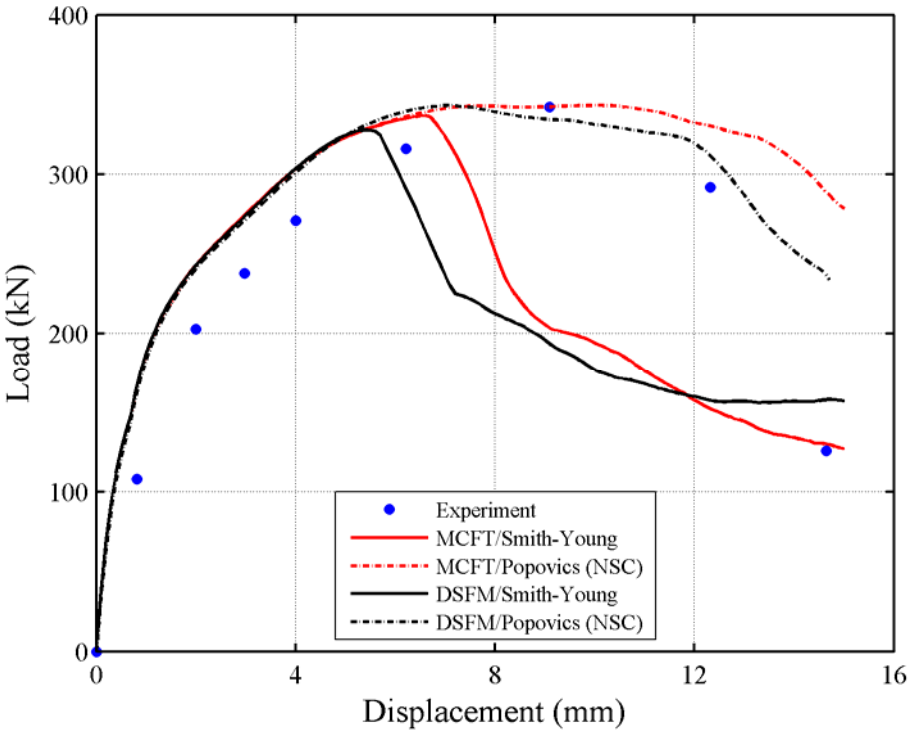


**Figure 5-25 Predicted load-displacement relationships for wall S9 obtained using mesh-15x15**

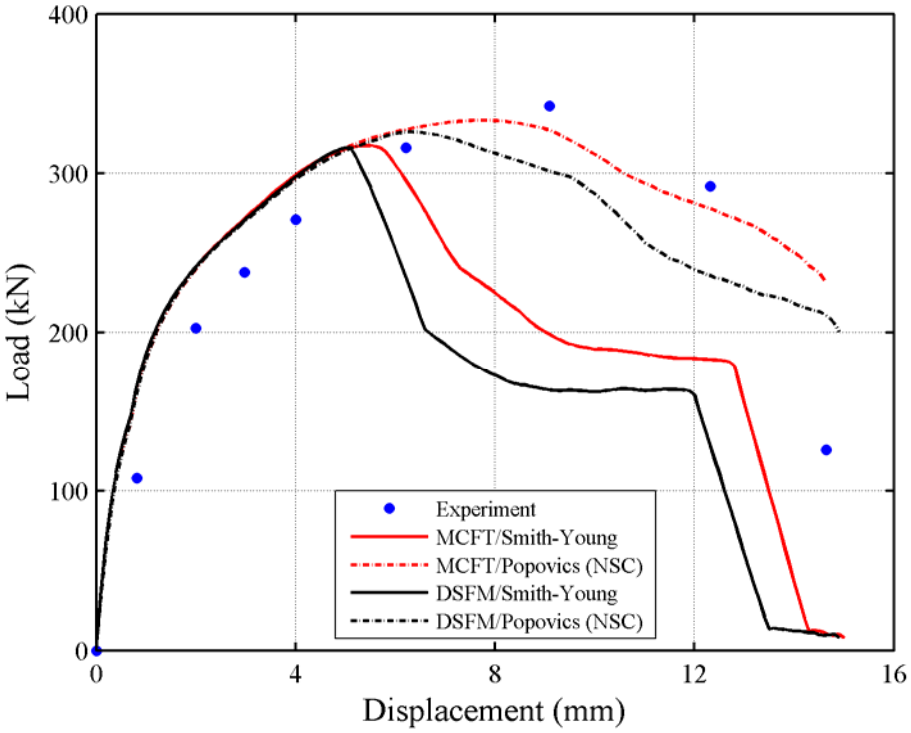


**Figure 5-26 Predicted load-displacement relationships for wall S9 obtained using mesh-20x20**

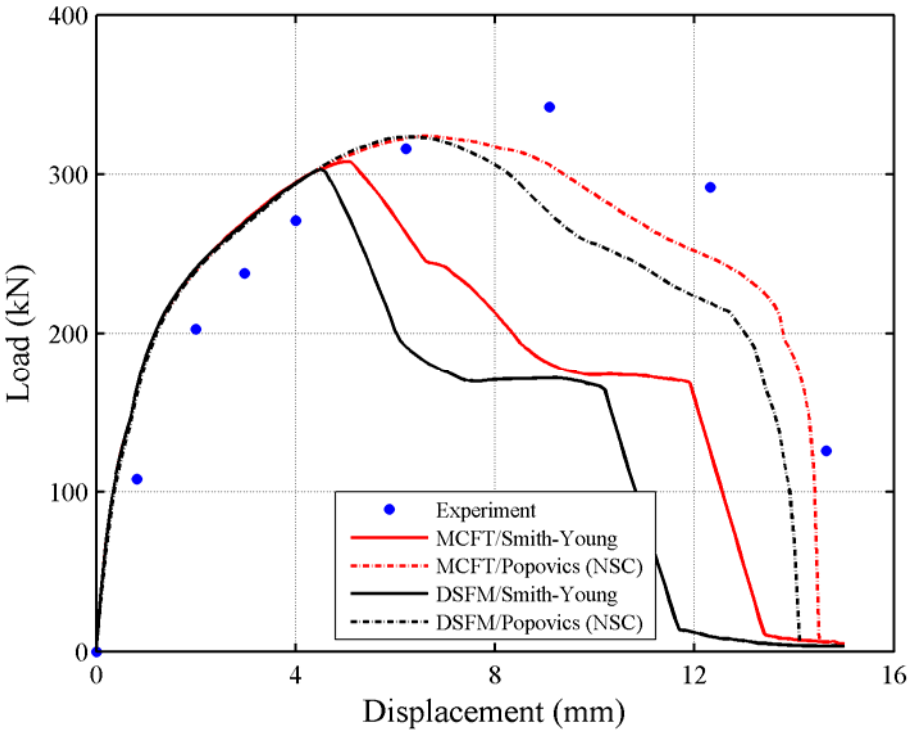


**Figure 5-27 Predicted load-displacement relationships for wall S9 obtained using mesh-25x25**

- The experimental peak shear strength is consistently overpredicted using mesh-10x10. The best predictions of the experimental results are obtained using mesh-15x15 with the DSFM formulation and mesh-20x20 with the MCFT formulation as seen in Figure 5-28, which presents load-displacement relationships obtained using Popovics concrete for the four mesh types considered. The response calculated using mesh-25x25 underestimates the measured displacement at peak shear strength.

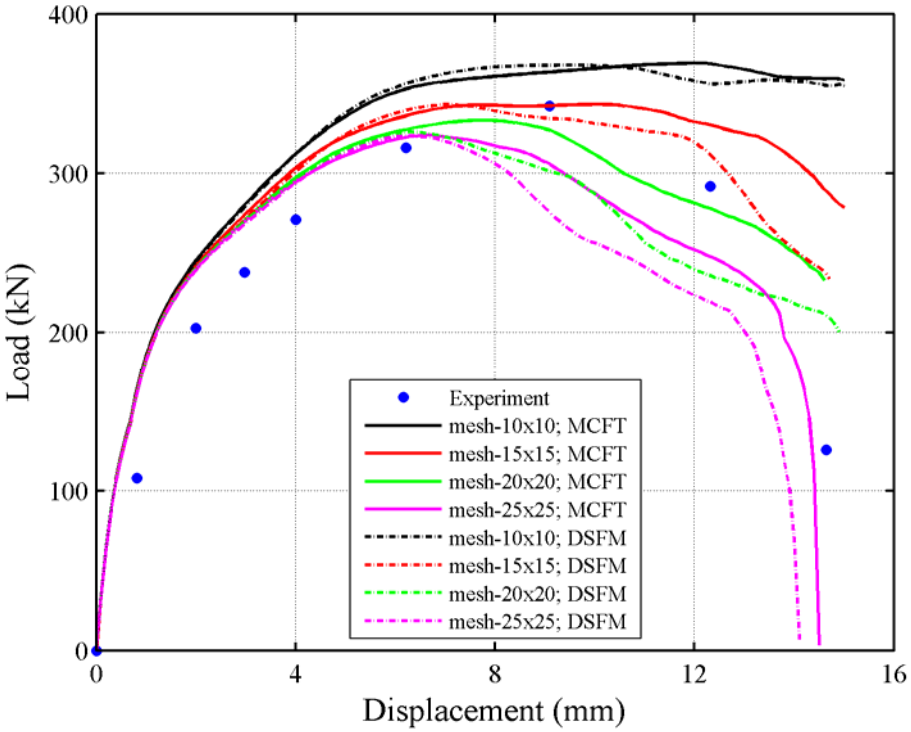


**Figure 5-28 Predicted load-displacement relationships for wall S9 obtained using the Popovics concrete model**

- The experimentally measured elastic stiffness is overestimated by the VecTor2 finite element models. However, as noted in Section 2.3.1, measurements of elastic stiffness can be affected significantly by a number of factors, including instrumentation resolution and shrinkage cracking, all of which would have to be eliminated to enable a comparison of results from experimentation and numerical simulation.

Figure 5-29 presents the cracking pattern for wall S9 at the end of the testing and Figure 5-30 presents the corresponding cracking pattern obtained VecTor2. The cracking patterns are in reasonable agreement. Wall S9 started to lose its lateral resistance as the diagonal corner-to-corner cracks propagated into the compressive toe of the wall as seen in Figure 5-29. A similar failure mode is captured using VecTor2. Vertical cracks and significant deformations near the compression toe are marked using a red rectangular box in Figure 5-30.

Table 5-4 presents experimentally measured and analytically predicted (mesh-20x20, Popovics concrete, MCFT) values for various response parameters. Of the response parameters considered here, the largest difference between the measured and calculated value is observed for the displacement at first yielding of vertical reinforcement. The reinforcement strains were not

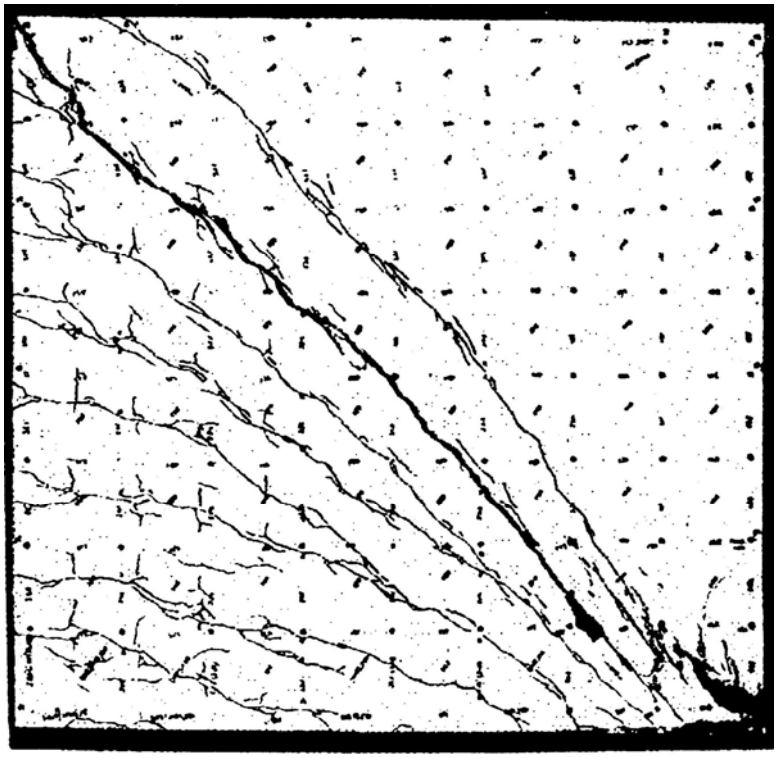

**Figure 5-29 Cracking pattern for wall S9 at the end of the testing (14.7 mm displacement, 1.22% drift)**

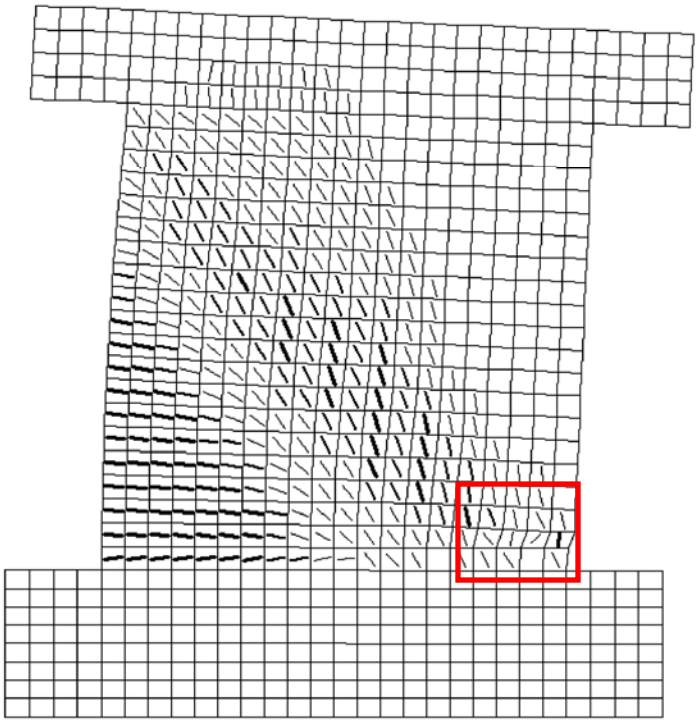

**Figure 5-30 Cracking pattern predicted for wall S9 (Mesh-20x20, MCFT, Popovics concrete, 5x magnification) at 1.22% drift**

**Table 5-4 Experimentally measured and analytically predicted (mesh-20x20, MCFT, Popovics) response parameters for wall S9**

| ID | Response parameter | Experiment (Exp) | Finite element analysis (FEA) | $\frac{\text{FEA}}{\text{Exp}}$ |
|---|---|---|---|---|
| RP1 | Peak shear strength | 342 kN | 334 kN | 0.98 |
| RP2 | Displacement at shear strength equal to 80% of the peak (pre-peak region) | 4.1 mm | 2.9 mm | 0.69 |
| RP3 | Displacement at peak shear strength | 9.1 mm | 7.8 mm | 0.86 |
| RP4 | Displacement at shear strength equal to 80% of the peak (post-peak region) | 12.6 mm | 13.2 mm | 1.05 |
| RP5 | Displacement at initiation of yielding in vertical reinforcement | ≤ 6.2 mm | 4.0 mm | 0.65 |
| RP6 | Horizontal expansion at the mid-height the wall at peak shear strength | 1.6 mm | 1.9 mm | 1.19 |

reported at each load step in the experiment. Therefore, the experimental value used for the lateral displacement at first yielding of vertical reinforcement should be interpreted as less than or equal to 6.2 mm.

The finite element analysis results presented in this section for wall S9 indicate that mesh structure and selected concrete model plays a significant role in predicting the response of squat reinforced concrete walls using VecTor2. Another factor that affects the calculated response using VecTor2 is the choice of formulation type (MCFT or DSFM). Interestingly, for wall S9, the DSFM formulation better simulates the experimental response for mesh-15x15 but the MCFT formulation better simulates the experimental response for mesh-20x20. Considering the responses calculated for all four meshes, it is not clear which formulation is best for the analysis of squat reinforced concrete walls. Nevertheless, it is concluded that use of a mesh that includes between 15 to 20 elements along the short dimension of a squat wall ($d_{\min}$) is appropriate for modeling of these structures using VecTor2. The results obtained using the Popovics model in general matched the experimental results better than those obtained using the Smith-Young model; the differences in the predictions of the two concrete models in the post-peak shear range is significant. Accordingly, only the Popovics model is used for further VecTor2 analysis.

Figure 5-31 presents the load-displacement relationships for wall S4 obtained using the Popovics concrete model with MCFT and DSFM formulations, and for different meshes. As seen in the figure, the experimental response is best simulated using mesh-15x15 and DSFM formulation. That said, the difference between the predictions using the MCFT and DSFM formulations is minor. The experimental peak shear and the post-capping stiffness[3] are overestimated using mesh-10x10 and underestimated using mesh-20x20 and mesh-25x25. However, the data of Figure 5-31 show that the peak shear strengths predicted using mesh-15x15, mesh-20x20 and mesh-25x25 are very close.

[3] Post-capping stiffness is stiffness of the wall following the attainment of the peak shear strength.

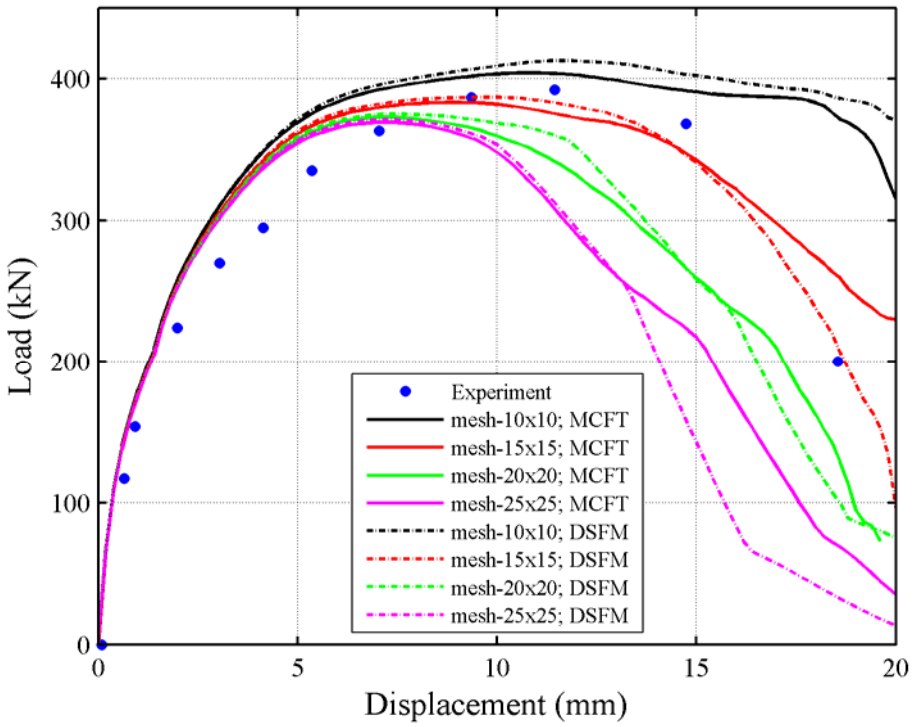


**Figure 5-31 Load-displacement relationships for wall S4 obtained using the Popovics concrete model**

Figure 5-32 presents the cracking pattern for wall S4 at the end of the testing and Figure 5-33 presents the corresponding cracking pattern predicted using VecTor2. In the experiment, the loss of lateral strength was due to concrete crushing in the compression toe of the wall as seen in Figure 5-32. The damage in the compression toe is simulated well using VecTor2 as shown in Figure 5-33. The predicted and the reported cracking patterns agree reasonably except that the predicted flexural cracks are more concentrated (wider) near the base of the wall web. The reported cracking pattern also includes several near-horizontal flexural cracks near the wall base but the widths of the cracks appear similar.

Table 5-5 presents experimentally measured and analytically predicted (mesh-15x15, Popovics concrete, DSFM) values for various response parameters. For the response parameters considered, the largest difference is between RP2 and RP5 but the overall agreement between the experimental and predicted response is reasonable. Note that strains in the reinforcement were not reported at each load step and the experimental value used for the displacement at first yielding of vertical reinforcement should be interpreted as less than or equal to 5.4 mm.

The finite element analysis results presented for wall S4 support a similar conclusion drawn from the finite element analysis of wall S9, namely, the choice of mesh can play a significant role in predicting the response of squat reinforced concrete walls using VecTor2. The results obtained using mesh-15x15 are in good agreement with the experimental data for walls S4 and S9, both of which have an aspect ratio of approximately 1.0. Although the effect of the formulation type (MCFT vs. DSFM) on the predicted response is less significant, finite element results are reported for each formulation type.

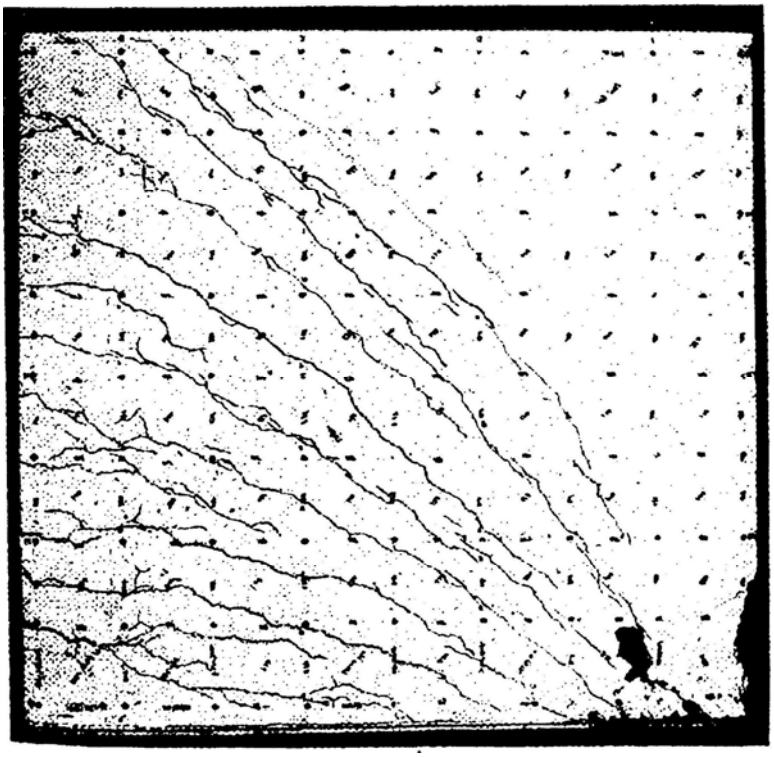

**Figure 5-32 Cracking pattern for wall S4 at the end of the testing (18.5 mm displacement, 1.55% drift)**

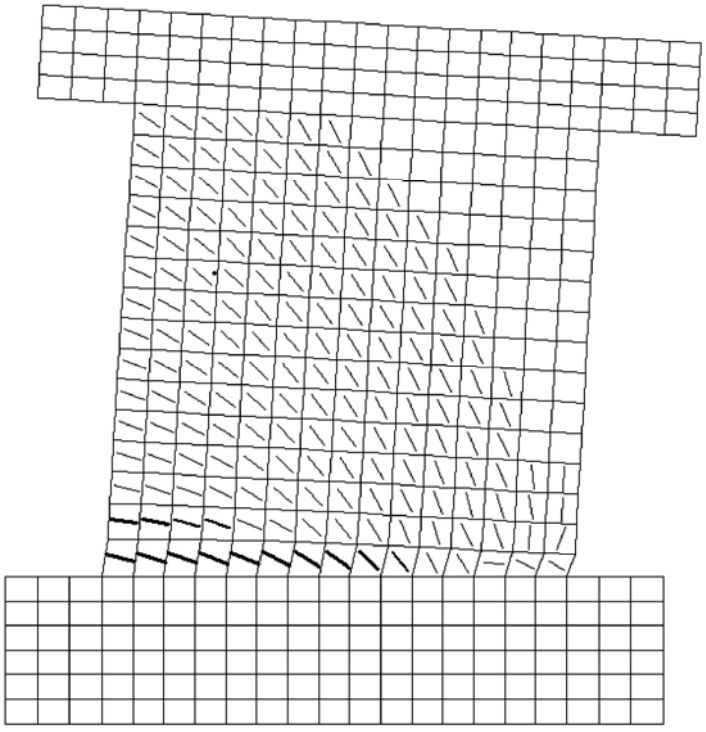

**Figure 5-33 Cracking pattern predicted for wall S4 (Mesh-15x15, DSFM, Popovics concrete, 5x magnification) at 1.55% drift**

**Table 5-5 Experimentally measured and analytically predicted (mesh-15x15, DSFM, Popovics-NSC) response parameters for wall S4**

| ID | Response parameter | Experiment (Exp) | Finite element analysis (FEA) | $\frac{\text{FEA}}{\text{Exp}}$ |
|---|---|---|---|---|
| RP1 | Peak shear strength | 392 kN | 388 kN | 0.99 |
| RP2 | Displacement at shear strength equal to 80% of the peak (pre-peak region) | 4.7 mm | 3.1 mm | 0.66 |
| RP3 | Displacement at peak shear strength | 11.4 mm | 9.2 mm | 0.80 |
| RP4 | Displacement at shear strength equal to 80% of the peak (post-peak region) | 16.0 mm | 16.1 mm | 1.01 |
| RP5 | Displacement at initiation of yielding in vertical reinforcement | ≤ 5.4 mm | 3.6 mm | 0.67 |
| RP6 | Horizontal expansion at the mid-height the wall at peak shear strength | 0.7 mm | 0.6 mm | 0.86 |

## 5.4.4 VecTor2 Model for Walls LSW1, LSW2, and LSW3

Figure 5-34 presents the finite element mesh used to analyze wall LSW1, LSW2, and LSW3 in VecTor2. The lateral load is applied near the center of the top beam on two nodes as illustrated by the red arrows in Figure 5-34. The axial force on wall LSW3 is distributed to 10 nodes at the mid-height of the top beam as shown using blue arrows in Figure 5-34. Translational restraints are imposed on the bottom nodes of the wall foundation to simulate the fixed boundary condition. For walls LSW1, LSW2 and LSW3, square elements of 80 mm by 80 mm are used to mesh the wall web. This element size corresponds to 1/15 of the smallest wall dimension $(d_{\min})$. The walls have an aspect ratio of 1.0 and therefore $d_{\min} = h_w = l_w$. A total of 225 elements are used to mesh the wall web; 145 elements are used in the foundation mesh and 76 elements are used in the top beam mesh. The first three elements from each side of the wall web (colored gray in Figure 5-34) are used to model the boundary elements of the web that are reinforced using stirrups. Two analyses, one using the MCFT formulation and the other using the DSFM formulation, are performed for each wall; the Popovics concrete model is used for all analyses.

Figure 5-35 and Figure 5-36 present the load-displacement relationships for wall LSW1 obtained using the MCFT and DSFM algorithms, respectively. The response obtained using each formulation adequately simulates the experimental results.

The major difference between the predictions of the MCFT and DSFM formulations is the simulation of the pinched region of the experimental load-displacement relationship. As seen in Figure 5-35, the experimentally measured pinching is overestimated using the MCFT formulation whereas the DSFM formulation better simulates the pinched region. The rate of degradation in strength following the cycle to peak shear strength is underpredicted by both formulations.

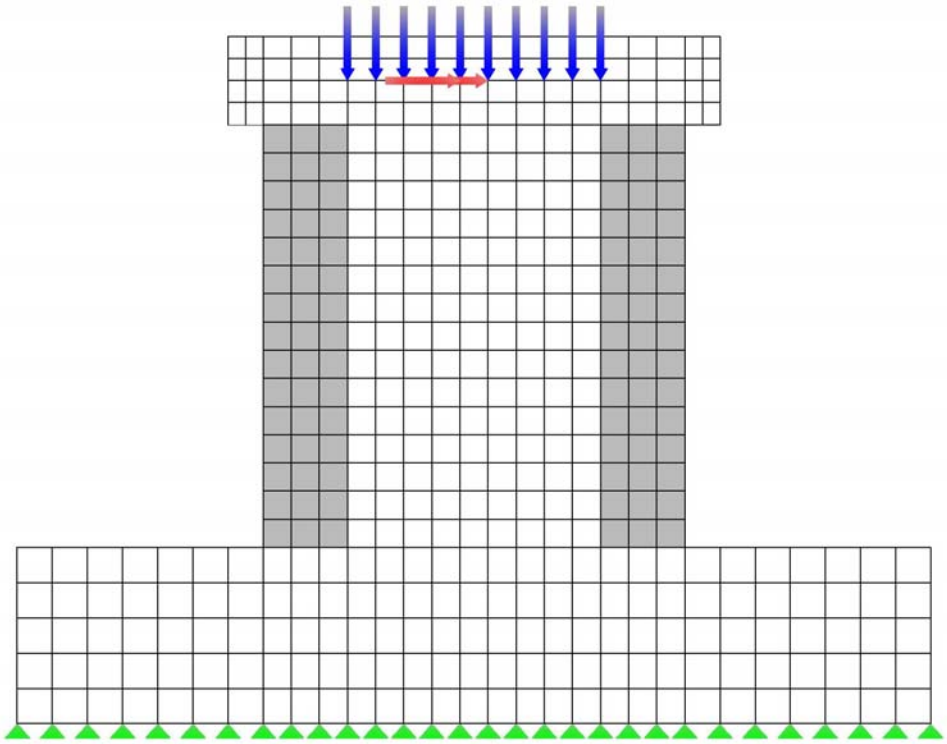

**Figure 5-34 Finite element mesh used for VecTor2 finite element analysis of walls LSW1, LSW2, and LSW3 (walls LSW1 and LSW2 were tested without axial loading)**

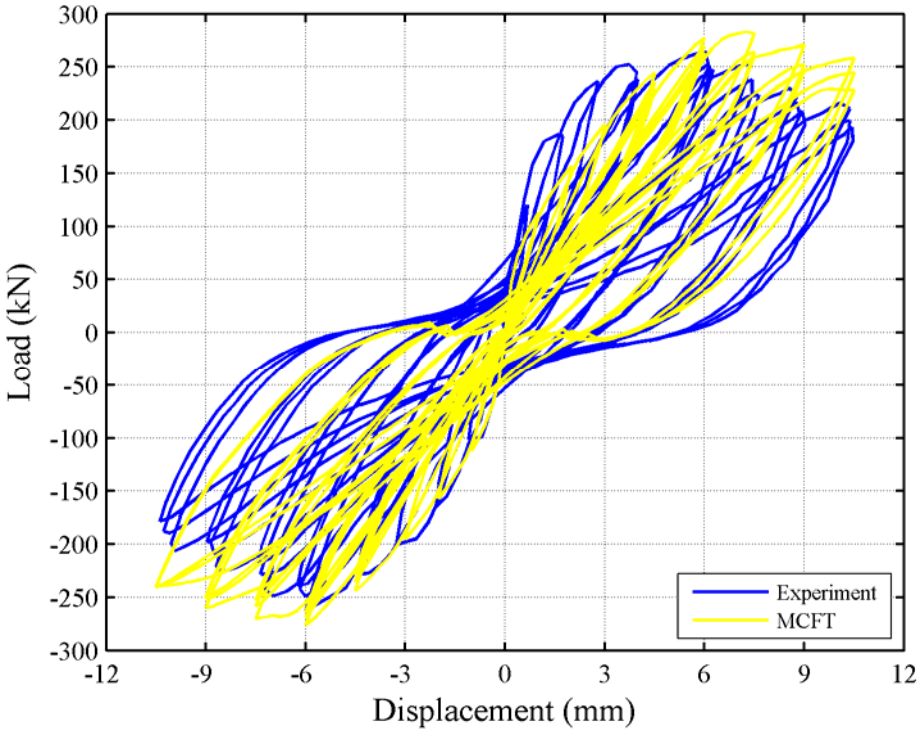


**Figure 5-35 Predicted load-displacement relationship for wall LSW1 obtained using MCFT formulation**

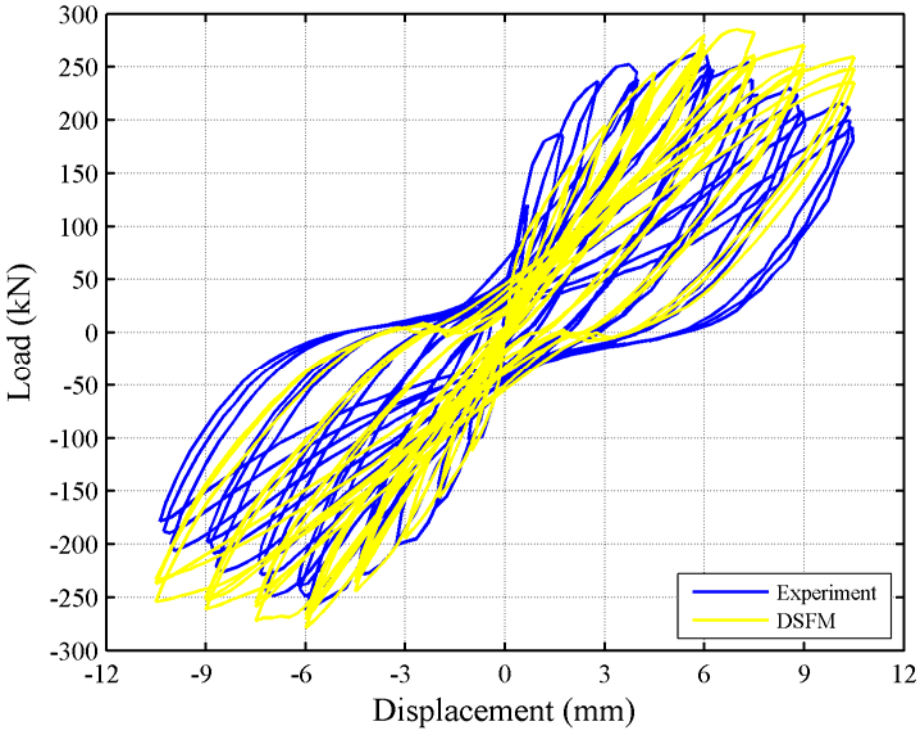


**Figure 5-36 Predicted load-displacement relationship for wall LSW1 obtained using DSFM formulation**

Table 5-6 presents measured and VecTor2-computed values for selected response parameters associated with wall LSW1. As seen in Table 5-6, the experimental peak shear strength is overestimated by 7% and 8% using the MCFT and DSFM formulations, respectively. Each formulation overestimates slightly the displacement at peak shear strength. The load-displacement relationships predicted by VecTor2 in Figure 5-35 and Figure 5-36 reproduce well the rate of strength degradation (as measured by the slope of the backbone curve) at displacements greater than that at the peak shear strength but do not match the experimental results, in part because the peak shear strength is overestimated. The total dissipated energy in the positive and negative loading directions[4] is underestimated by each formulation. Figure 5-37 presents the variation of cumulative dissipated energy computed using experimental data and VecTor2 with number of displacement excursions for wall LSW1. As seen in the figure, the energy dissipation computed using VecTor2 is less than that computed using the experimental data in the early excursions (1~10), which correspond to the displacement cycles at or before the attainment of peak shear strength. In the remaining displacement cycles, the dissipated energies are close as revealed by similar slopes of the curves in Figure 5-37. Although the dissipated energy estimations of MCFT and DSFM are very close in excursions 1 to 10, the DSFM estimation of the dissipated energy is more accurate than the MCFT estimation in an overall sense.

[4] The total dissipated energy in the positive and negative loading directions is calculated by adding the areas under each displacement cycle of the corresponding loading directions. The digital load-displacement relationships provided by the experimenter are used for the calculations. The calculations are performed using MATLAB [The MathWorks, Inc. (2006)].

**Table 5-6 Experimentally measured and analytically predicted response parameters associated with wall LSW1**

| ID | Response parameter | Exp | MCFT | MCFT / Exp | DSFM | DSFM / Exp |
|---|---|---|---|---|---|---|
| RP1 | Peak shear strength | 265 kN | 283 kN | 1.07 | 285 kN | 1.08 |
| RP2 | Displacement at peak shear strength | 6.0 mm | 7.3 mm | 1.21 | 7.0 mm | 1.16 |
| RP3 | Total dissipated energy in the positive loading direction | 9488 kN-mm | 6902 kN-mm | 0.73 | 7327 kN-mm | 0.77 |
| RP4 | Total dissipated energy in the negative loading direction | 8792 kN-mm | 6978 kN-mm | 0.79 | 7476 kN-mm | 0.85 |

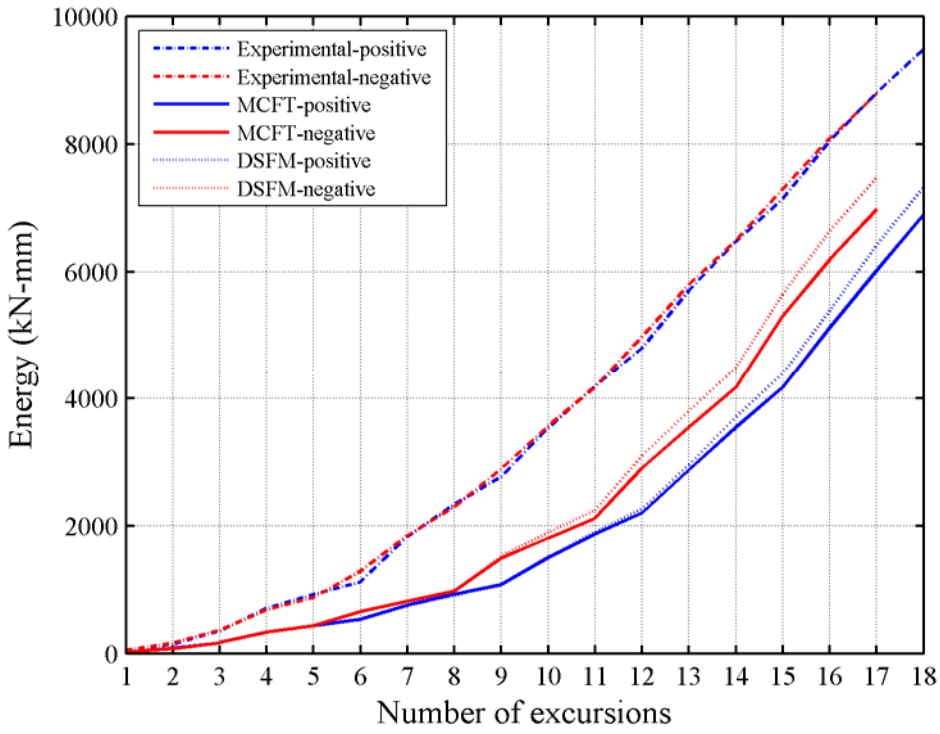


**Figure 5-37 Experimental and analytical cumulative dissipated energy variation with number of excursions for wall LSW1**

To identify the impact of mesh refinement on the analytical predictions of cyclic response, wall LSW1 was re-analyzed using an h-refined mesh and the DSFM algorithm. The initial mesh (mesh-1) included 225 elements in the wall web; the refined mesh (mesh-2) includes 900 elements. The load-displacement relationships are presented in Figure 5-38. The calculated responses for mesh-1 and mesh-2 are very similar up to the point of peak shear strength. Thereafter, the predicted response using mesh-2 exhibits a sudden loss of shear strength at a displacement of 8 mm whereas the response predicted using mesh-1 does not and is in better agreement with the experimental data (see Figure 5-36). The effect of mesh refinement under

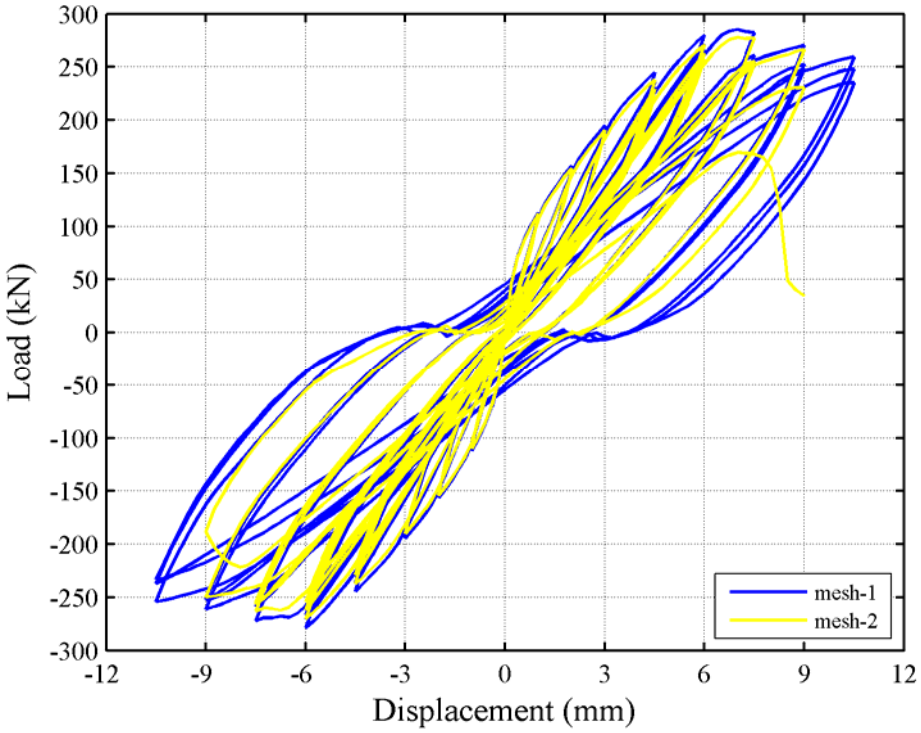


**Figure 5-38 Analytical load-displacement relationship for wall LSW1 obtained using the mesh-1 and mesh-2 (DSFM formulation)**

cyclic loading conditions is similar to that observed under monotonic loading (see Section 5.4.3), namely, a) pre-peak and peak shear strength responses are only affected modestly by mesh size, and b) the effect of element size is more pronounced in the post-peak shear strength (or post-capping stiffness) region of the response.

Figure 5-39 and Figure 5-40 present the load-displacement relationships for wall LSW2 obtained using the MCFT and DSFM formulations, respectively. Table 5-7 presents values that characterize the response of LSW2. Both formulations predict the experimental peak shear strength and the displacement at peak shear strength to within 6%. Similar to that observed for wall LSW1, the DSFM formulation better captures the pinching in the experimental load-displacement relationship. Each formulation underpredicts the total dissipated energy in both the positive and negative loading directions. Nevertheless, the total dissipated energy calculated using the DSFM formulation is higher than that calculated using MCFT formulation. Figure 5-41 presents the variation of cumulative dissipated energy computed using experimental data and VecTor2 with number of displacement excursions for wall LSW2. Similar to that observed for wall LSW1, the VecTor2 predictions underestimate those computed using the experimental data in the early excursions (1 to 9) in both negative and positive directions. Excursions 1 to 9 are displacement cycles up to and including those corresponding to peak shear strength. In the following excursions (10 to 19), the dissipated energy is simulated well by the analytical models.

Figure 5-42 and Figure 5-43 present the load-displacement relationships for wall LSW3 obtained using the MCFT and DSFM algorithms, respectively. Table 5-8 presents values for the response parameters for LSW2. Note that wall LSW3 is identical to wall LSW2 except that an axial force of $0.07\,A_w\,f_c'$ was applied to wall LSW3. For wall LSW3, the experimental peak shear strength

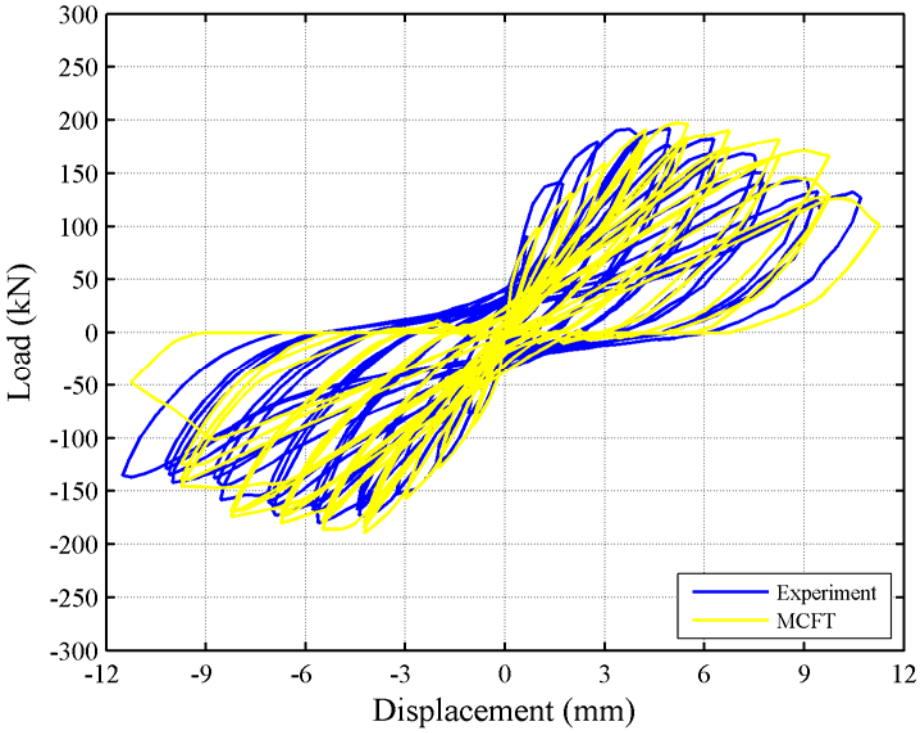


**Figure 5-39 Analytical load-displacement relationship for wall LSW2 obtained using the MCFT formulation**

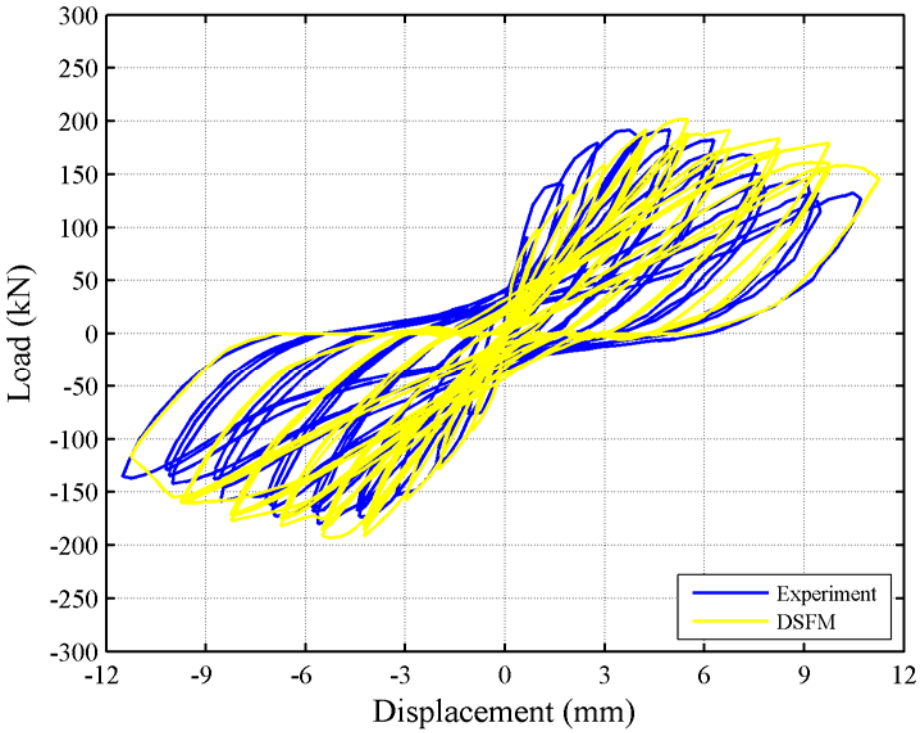


**Figure 5-40 Analytical load-displacement relationship for wall LSW2 obtained using the DSFM formulation**

**Table 5-7 Experimentally measured and analytically obtained response parameters associated with wall LSW2**

| ID | Response parameter | Exp | MCFT | MCFT / Exp | DSFM | DSFM / Exp |
|---|---|---|---|---|---|---|
| RP1 | Peak shear strength | 192 kN | 197 kN | 1.03 | 202 kN | 1.05 |
| RP2 | Displacement at peak shear strength | 4.9 mm | 5.3 mm | 1.06 | 5.3 mm | 1.06 |
| RP3 | Total dissipated energy in the positive loading direction | 7129 kN-mm | 5780 kN-mm | 0.81 | 6133 kN-mm | 0.86 |
| RP4 | Total dissipated energy in the negative loading direction | 7033 kN-mm | 5798 kN-mm | 0.82 | 6433 kN-mm | 0.91 |

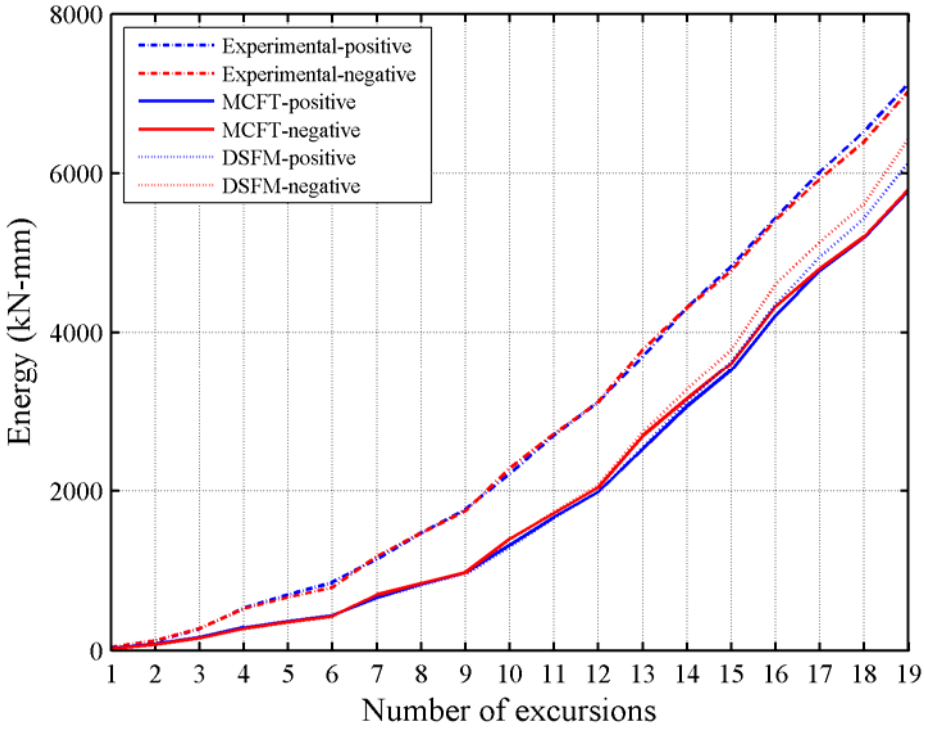


**Figure 5-41 Experimental and analytical cumulative dissipated energy variation with number of excursions for wall LSW2**

was measured at a lateral displacement of 4.7 mm in the positive loading direction; thereafter the lateral strength degraded. The analytical predictions did not capture this response and the lateral strength continued to increase up to a lateral displacement of 13.5 mm using each formulation. The backbone load-displacement response of walls LSW1 and LSW2 are predicted more accurately than the response of LSW3, which was tested with an imposed axial force. The difference between the predicted and experimental response for LSW3 could be attributed to either the VecTor2 formulations and/or experimental control associated with the application of axial loading.

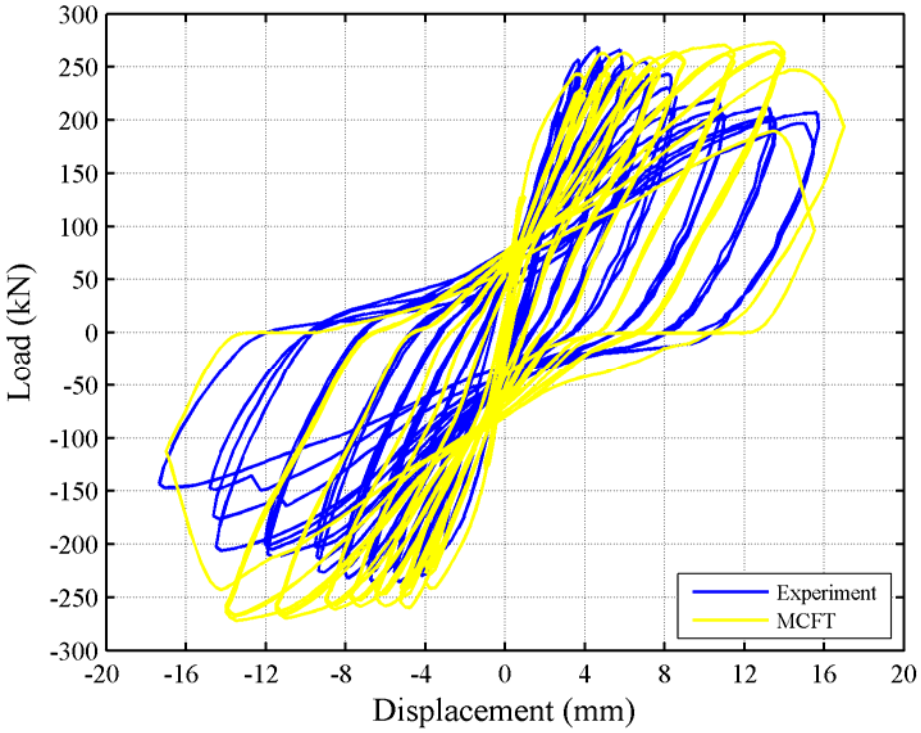


**Figure 5-42 Analytical load-displacement relationship for wall LSW3 obtained using the MCFT formulation**

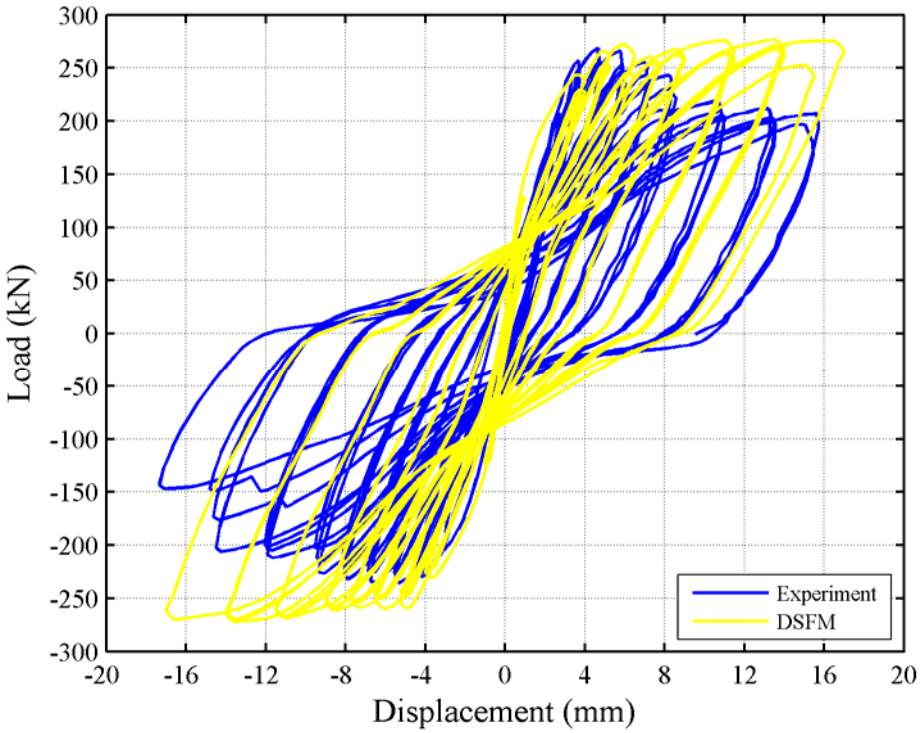


**Figure 5-43 Analytical load-displacement relationship for wall LSW3 obtained using the DSFM formulation**

**Table 5-8 Experimentally measured and analytically obtained response parameters associated with wall LSW3**

| ID | Response parameter | Exp | MCFT | MCFT / Exp | DSFM | DSFM / Exp |
|---|---|---|---|---|---|---|
| RP1 | Peak shear strength | 269 kN | 273 kN | 1.01 | 277 kN | 1.03 |
| RP2 | Displacement at peak shear strength | 4.7 mm | 13.5 mm | 2.89 | 13.5 mm | 2.89 |
| RP3 | Total dissipated energy in the positive loading direction | 22453 kN-mm | 20464 kN-mm | 0.91 | 20905 kN-mm | 0.93 |
| RP4 | Total dissipated energy in the negative loading direction | 17936 kN-mm | 19241 kN-mm | 1.07 | 19180 kN-mm | 1.07 |

Figure 5-44 presents the variation of cumulative dissipated energy computed using experimental data and VecTor2 with number of displacement excursions for wall LSW3. The energy dissipated in the experiment was captured reasonably by both formulations. Note that the dissipated energies calculated using the DSFM and MCFT formulations are almost identical for wall LSW3. This was not the case for walls LSW1 and LSW2 since the dissipated energy calculated using the DSFM formulation is considerably higher than that calculated using the MCFT formulation.

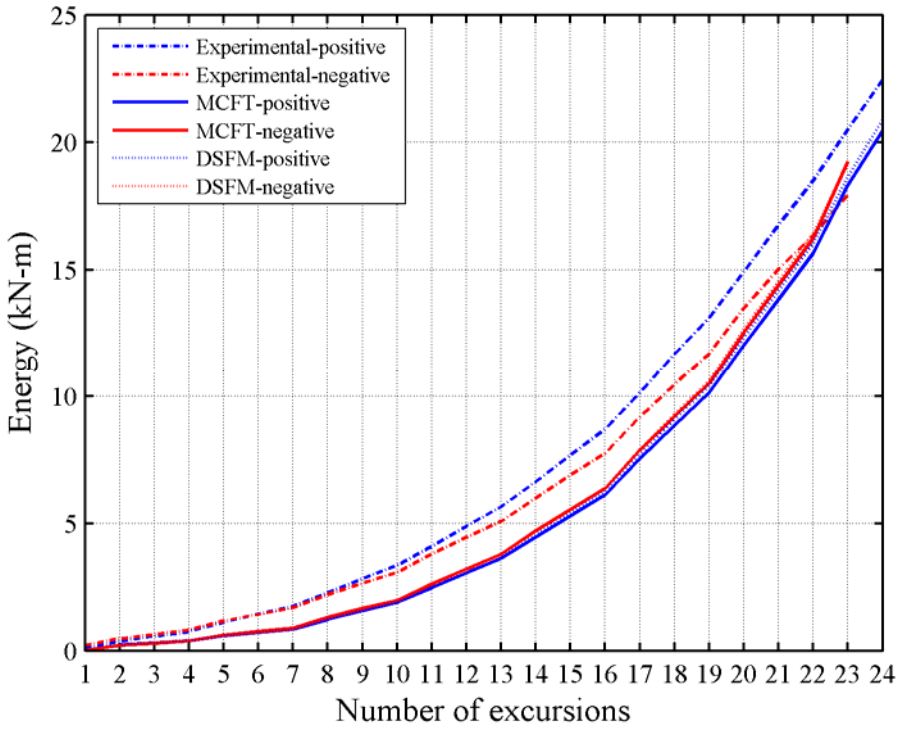


**Figure 5-44 Experimental and analytical cumulative dissipated energy variation with number of excursions for wall LSW3**

The load-displacement relationship of wall LSW3 exhibited significantly less pinching than those of walls LSW2 and LSW3 due to axial force being applied during the testing. Both formulations capture reasonably the pinched region in the experimental load-displacement relationship.

As seen in Table 5-6 through Table 5-8 and Figure 5-35 through Figure 5-44, the global experimental responses of walls LSW1, LSW2, and LSW3 are reasonably captured using VecTor2. The peak shear strengths of the specimens are generally overpredicted but the percentage overprediction is small: less than 10%.The DSFM formulation generally provided a slightly higher peak shear strength than the MCFT formulation. The experimentally measured displacements at peak shear strength are reasonably captured by each formulation for walls LSW1 and LSW2. The corresponding values for wall LSW3, which was tested with an axial force, are significantly overpredicted by each formulation. The total energy dissipated in each experiment is generally underpredicted by each formulation with the DSFM formulation providing closer agreement.

Figure 5-45 through Figure 5-47 present the analytically obtained (using DSFM) deformation fields and cracking patterns at final displacement cycles for walls LSW1, LSW2 and LSW3, respectively. As seen in Figure 5-5, the widest crack in each of walls LSW1 and LSW2 was observed near the bottom of the wall web. These cracks were horizontal and continuous along the length of the wall indicating a sliding shear failure. The damage in the wall web was modest in both walls and was limited to cracks that were inclined near the center of the wall web and approximately horizontal at the ends of the wall web. The deformed shapes and cracking patterns obtained using VecTor2 for walls LSW1 and LSW2 predict the widest cracks near the bottom of the wall web and that most of the lateral displacement was due to deformations that take place in this region. The simulated web cracks were inclined near the center and approximately horizontal at the ends of the wall web. The deformations in walls LSW1 and LSW2 are simulated with reasonable success by VecTor2.

As seen in Figure 5-5, wall LSW3 failed in a different manner than walls LSW1 and LSW2, in part because they were not subjected to imposed axial load during the testing. For wall LSW3, the contribution of sliding deformation to the overall deformation at the end of the test was modest in comparison to those of LSW1 and LSW3. Wall LSW3 exhibited significant crushing in the bottom corners of the wall web (see Figure 5-5) due to increased compressive demands associated with the application of axial force. As seen in Figure 5-47, which presents the analytically predicted deformed shape for wall LSW3, sliding deformations do not dominate the deformed shape of wall LSW3. Also seen in this figure are significant deformations and vertical splitting cracks that take place in the compression toe of the wall.

### 5.4.5 VecTor2 Model for Wall DP1

The major challenge in modeling wall DP1 using VecTor2 is simulating the behavior of the wide flanges. VecTor2 uses a two dimensional formulation with plane stress elements. The wall flanges cannot be meshed in the out-of-plane direction and the effects of mechanisms such as shear lag on the wall response cannot be captured explicitly. The effective flange width (efw) analogy is used herein to simulate the behavior of wall DP1. Finite element analyses are undertaken for effective flange widths of 100%, 75%, 50%, 25%, and 0% of the original flange width.

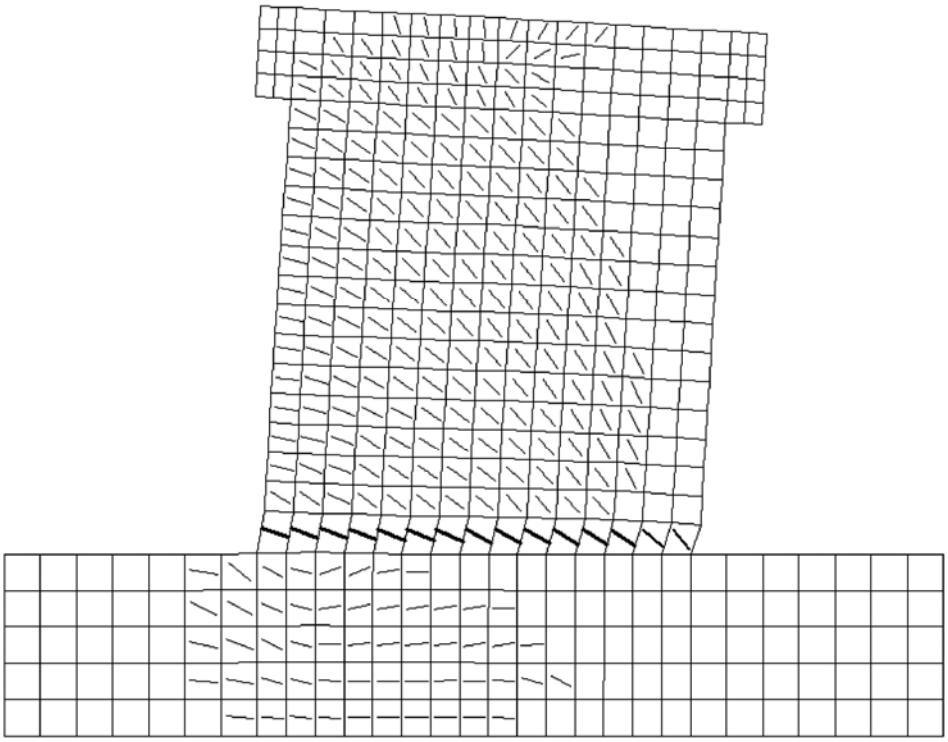

**Figure 5-45 Deformed shape (magnified by 10) and cracking pattern for wall LSW1 at 10.5 mm lateral displacement obtained using the DSFM formulation**

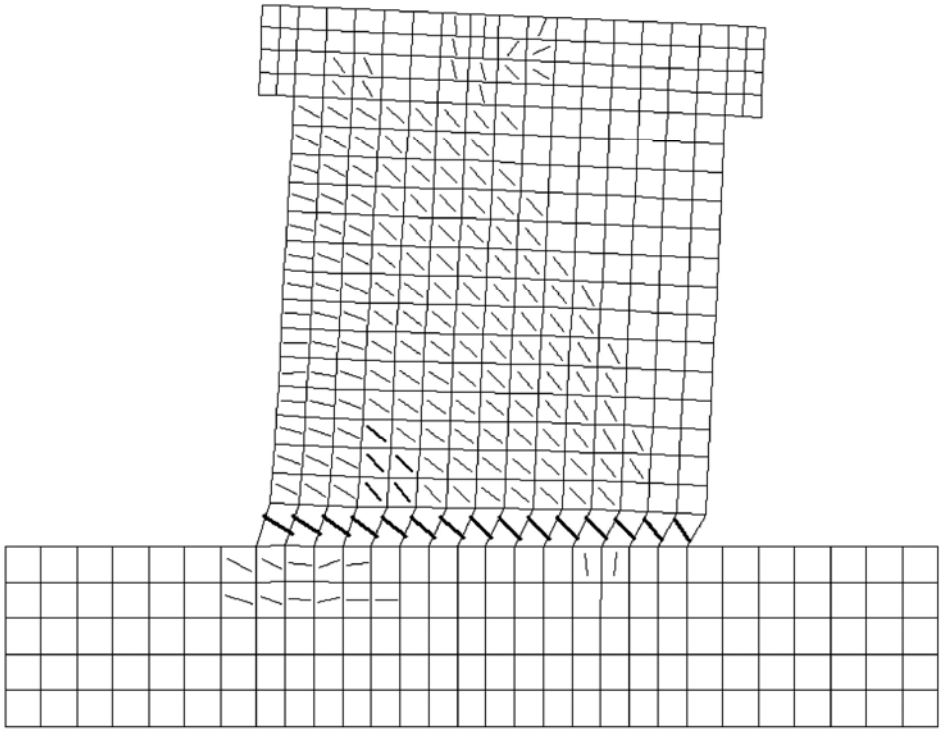

**Figure 5-46 Deformed shape (magnified by 10) and cracking pattern for wall LSW2 at 11.25 mm lateral displacement obtained using the DSFM formulation**

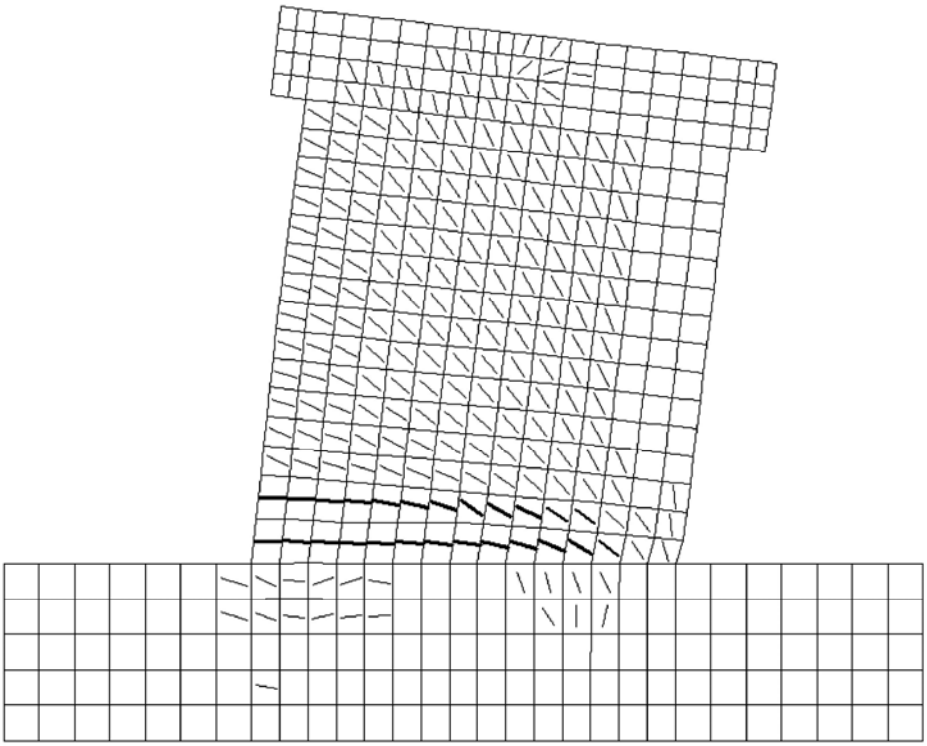

**Figure 5-47 Deformed shape (magnified by 10) and cracking pattern for wall LSW3 at 17 mm lateral displacement obtained using the DSFM formulation**

Figure 5-48 presents the wall geometry and finite element mesh used to model wall DP1. The web of the wall consists of 320 elements as a result of using 16 mesh seeds in the vertical direction and 20 mesh seeds in the horizontal direction. The flanges are modeled at each end of the wall web using 16 elements per flange. Effective flange widths are used to determine the thickness of these elements. The solid squares in Figure 5-48 represent the translational restraints used to simulate fixed boundary condition. The experimental axial force is simulated by imposing vertical nodal loads (15 x 80 kN = 1200 kN) on the top beam of the finite element model. The lateral load is simulated by imposing a horizontal displacement boundary condition at center of the top beam.

The modeling decisions presented in Section 5.4.2 are adopted for the analysis of wall DP1. Analyses are performed using the MCFT formulation only since the difference in the predicted responses obtained using the MCFT and DSFM formulations were small in prior predictions. A uniaxial compressive stress-strain curve for concrete was reported for wall DP1 and compared with the concrete models used for VecTor2 analyses. (Such data was unavailable for the walls evaluated previously.) Figure 5-49 compares the reported compressive stress – strain curve with those calculated using the Popovics and Smith-Young models. The figure shows that the experimental stress-strain curve has the smallest post-capping stiffness of all three curves. The Smith-Young model matches the experimental curve better than the Popovics model. For this reason, the Smith-Young concrete model is also used for the finite element analysis of wall DP1.

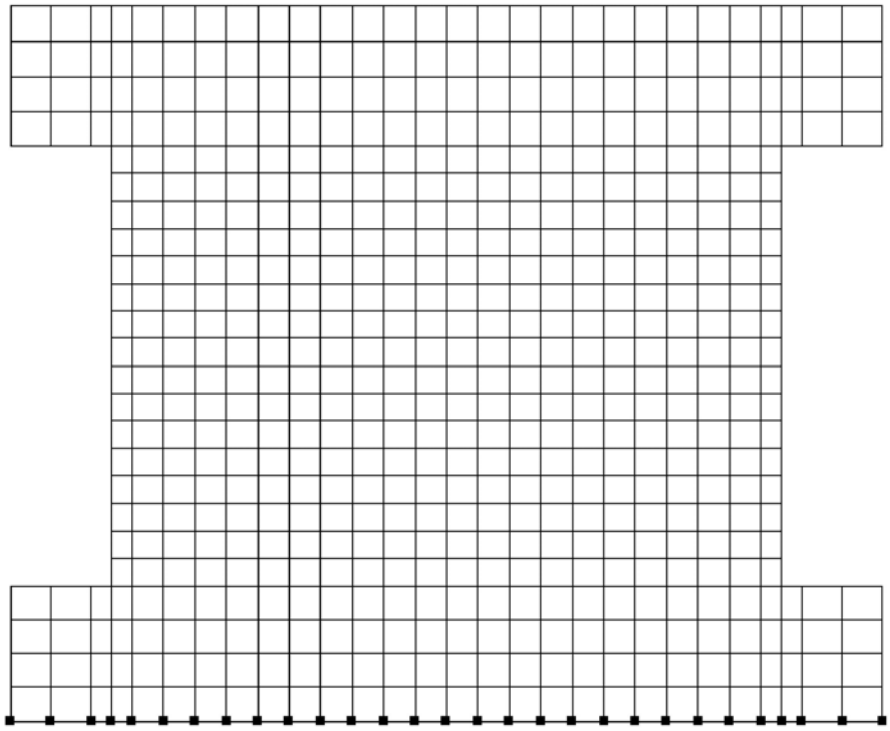

**Figure 5-48 VecTor2 mesh for wall DP1**

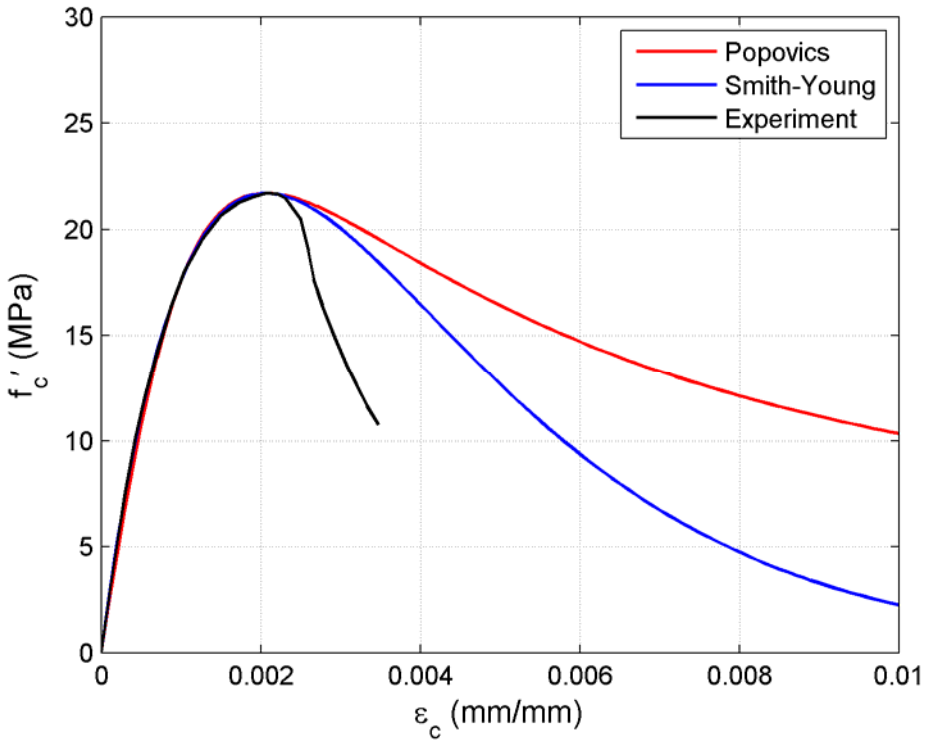


**Figure 5-49 Comparison of experimental and analytical compressive strain-stress curves for wall DP1**

Figure 5-50 presents the predicted load-displacement relationships for wall DP1 obtained using various effective flange widths and the Smith-Young concrete model. The figure shows that peak shear strength of the wall is significantly affected by variation of the effective flange width. Elastic stiffness and peak shear strength are significantly underestimated when the effective flange width is 0%, which is equivalent to a rectangular wall with no flanges[5]. The elastic stiffness is estimated best by an effective flange width of 100% but effective flange widths of 25% and 50% give the best estimates for peak shear strength. Figure 5-51 presents the predicted load-displacement relationships for wall DP1 obtained using various effective flange widths and the Popovics concrete model. The peak shear strengths predicted using Popovics model are higher than those predicted using the Smith-Young model for equal effective flange widths. For the Popovics model, 25% effective flange width provides the best estimate for the peak shear strength. The elastic stiffness and the peak shear strength are significantly underestimated for an effective flange width of 0%.

Vecchio (1998) investigated the response of NUPEC wall [Kitada et al. (1997)] using a two-dimensional implementation of the MCFT formulation. Note that the geometry of the NUPEC wall and wall DP1 are similar. Vecchio (1998) concluded that the best estimates of the peak shear strength were obtained when assuming effective flange widths between 67% and 100% of the original flange width. This results provided herein do not agree with this conclusion.

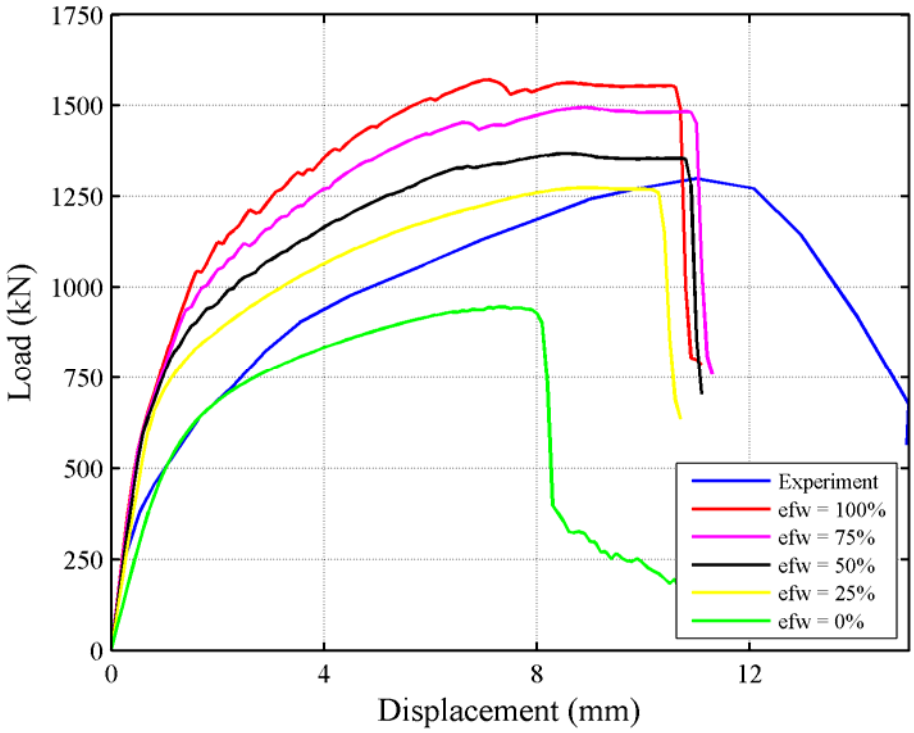


**Figure 5-50 Predicted load-displacement relationships for wall DP1 obtained using Smith-Young concrete and various effective flange widths (efw)**

[5] Note that the widely used peak shear strength procedures evaluated in Chapter 4 do not account for the effect of boundary elements to calculate peak shear strength.

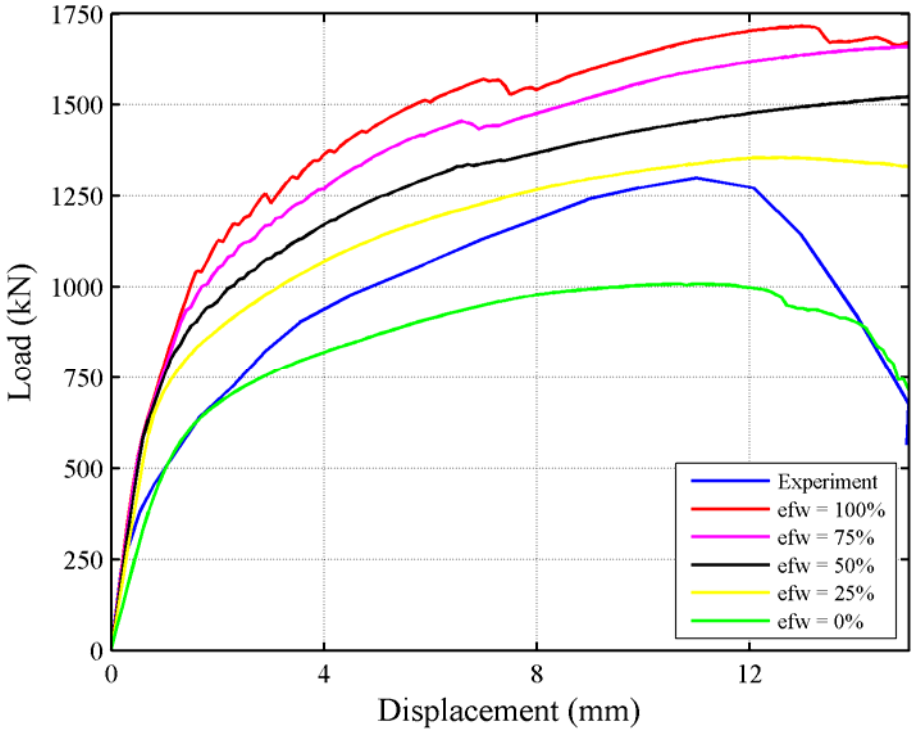


**Figure 5-51 Predicted load-displacement relationships for wall DP1 obtained using Popovics (NSC) concrete and various effective flange widths (efw)**

The following conclusions can be drawn from the finite element analyses of DP1 using VecTor2,

- The predicted response obtained using the Popovics and Smith-Young models are significantly different. The optimum effective flange widths obtained by the two concrete models vary.
- The elastic stiffness of the wall is estimated best assuming fully effective flanges (100%).
- An effective flange width of 25 to 50% provides the best estimate of peak shear strength.

Considering these observations, the computation of the response of squat walls with wide flanges using VecTor2 should be made with care.

## 5.5 Finite Element Modeling of Walls with Boundary Elements Using VecTor2

The analyses presented in Section 5.4 showed that VecTor2 can predict successfully the response of squat rectangular walls but identified some issues regarding the use of 2-D formulations to predict the response of a wall with wide flanges. Wall DP1 modeled in Section 5.4.5 included wide flanges (flange width = 1.5 × wall height) and the peak shear strength of the wall was overestimated using VecTor2. A large number of barbell and flanged walls are modeled in this section using VecTor2 to further address the issue of boundary element effectiveness in squat wall response. Sections 5.5.1 and 5.5.2 present the VecTor2 analysis results for flanged and barbell walls, respectively.

The modeling assumptions listed in Section 5.4.2, the Popovics concrete model and the MCFT formulation are used for the VecTor2 analyses of Sections 5.5.1 and 5.5.2. Mesh details for the modeled walls are presented in the corresponding sections.

### 5.5.1 VecTor2 Analyses for Squat Walls with Flanges

A brief summary of the fifteen squat flanged walls modeled using VecTor2 is presented in Table 5-9. In Table 5-9 (and Table 5-11), $b_f$ is the boundary element width, $h_f$ is the boundary element thickness, $t_w$ is the web thickness, $l_w$ is the wall length, $h_w$ is the wall height, $N$ is the axial force on the wall calculated using both the externally applied force and force due to self-weight of the top beam, $A$ is the total wall area, $\rho_h$ is the horizontal web reinforcement ratio, $\rho_v$ is the vertical web reinforcement ratio, and $\rho_{be}$ is the boundary element reinforcement ratio.

The geometry of the NUPEC wall [Kitada et al. (1997)] is very similar to wall DP1 tested by Palermo and Vecchio (2002a), and the analysis results for this wall can be compared directly to those obtained in Section 5.4.5 for wall DP1. Note the mesh adopted for wall DP1 is used to analyze the NUPEC wall. All six Seki et al. (1995) walls in the database are modeled because they include relatively wide flanges and the program varies two crucial parameters that are known to effect the squat wall response, namely, aspect ratio and axial load. Of the twenty-two Sato et al. (1989) walls in the squat wall database, the four with the highest $b_f / h_w$ ratio are modeled using VecTor2. The selected experiments are relatively large-scale simulations. More information on these walls can be found in the squat wall database presented in Appendix A.

As seen in Table 5-9, the all Maier walls (S1, S2, S3, and S6) have identical geometry and the same mesh structure is used for all. A total of 400 elements is used to mesh the wall web and flanges by using the same number of elements (20) along the height and length of the walls, since the aspect ratio of Maier walls is approximately 1.0. With this mesh structure, the first two rows of elements on each side of the walls represent the wall flanges as shaded yellow in Table 5-9. This mesh structure predicts the peak shear strength of rectangular Maier walls (S4 and S9) with reasonable accuracy (see Section 5.4.3). Since the predicted peak shear strength is not significantly affected by mesh size, only one relatively fine mesh is used for predictions.

The aspect ratios of the Sato and Seki walls modeled herein are less than 1.0. For these walls, twenty elements are used along the height of the walls and the number of elements used along the wall length is determined by using approximately square elements.

Table 5-10 presents the experimental ($V_{peak}$) and predicted ($V_{peak\_FE}$) peak shear strengths for the squat flanged walls modeled using VecTor2. The data of Table 5-10 shows that the experimental peak shear strength of squat flanged walls can be predicted with reasonable accuracy using VecTor2 even for walls with flanges as wide as the wall height. This is an important conclusion because it reveals that flanges significantly contribute to peak shear strength of squat walls. If flange effectiveness in contributing the peak shear was questionable, significant overestimations of the peak shear strength would be expected using VecTor2, which employs a 2-D finite element algorithm. The most significant overestimations of the experimental peak shear strength are observed for walls with very wide flanges, namely, walls U-1 and DP-1. The flange widths for these walls are approximately equal to 1.5 times the wall height. As noted in Section 5.4.5,

**Table 5-9 Squat flanged walls modeled using VecTor2**

| Program ID | Wall ID | $b_f$ (mm) | $h_f$ (mm) | $t_w$ (in) | $l_w$ (in) | $b_f/h_w$ | $h_w/l_w$ | $P/A_t f_c'$ (%) | $\rho_h$ (%) | $\rho_v$ (%) | $\rho_{be}$ (%) | $f_c'$ (MPa) |
|---|---|---|---|---|---|---|---|---|---|---|---|---|
| Maier | S1 | 400 | 100 | 100 | 1180 | 0.33 | 1.02 | 6.7 | 1.01 | 1.13 | 1.13 | 36.9 |
| | S2 | 400 | 100 | 100 | 1180 | 0.33 | 1.02 | 24.3 | 1.01 | 1.13 | 1.13 | 38.4 |
| | S3 | 400 | 100 | 100 | 1180 | 0.33 | 1.02 | 6.6 | 1.01 | 2.54 | 2.55 | 36.7 |
| | S6 | 400 | 100 | 100 | 1180 | 0.33 | 1.02 | 6.7 | 0.57 | 1.13 | 1.13 | 35.6 |
| NUPEC | U-1 | 2980 | 100 | 75 | 3100 | 1.48 | 0.65 | 5.1 | 1.20 | 1.20 | 0.47[1] | 28.6 |
| Seki | RA-00P | 1500 | 75 | 75 | 3075 | 1.06 | 0.46 | 1.5 | 1.20 | 1.20 | 1.20 | 31.6 |
| | RA-15P | 1500 | 75 | 75 | 3075 | 1.06 | 0.46 | 5.0 | 1.20 | 1.20 | 1.20 | 29.5 |
| | RB-00P | 1500 | 75 | 75 | 3075 | 0.74 | 0.66 | 1.6 | 1.20 | 1.20 | 1.20 | 28.9 |
| | RB-15P | 1500 | 75 | 75 | 3075 | 0.74 | 0.66 | 5.1 | 1.20 | 1.20 | 1.20 | 28.9 |
| | RC-00P | 1500 | 75 | 75 | 3075 | 0.57 | 0.85 | 1.5 | 1.20 | 1.20 | 1.20 | 30.1 |
| | RC-15P | 1500 | 75 | 75 | 3075 | 0.57 | 0.85 | 5.0 | 1.20 | 1.20 | 1.20 | 29.2 |
| Sato | 24M6-30 | 1000 | 150 | 150 | 2150 | 1.0 | 0.47 | 5.1 | 0.80 | 0.80 | 0.80 | 40.1 |
| | 24M6-40 | 1000 | 150 | 150 | 2150 | 1.0 | 0.47 | 5.0 | 0.60 | 0.60 | 0.60 | 41.0 |
| | 36M6-30 | 1000 | 150 | 150 | 2150 | 1.0 | 0.47 | 6.1 | 1.16 | 1.16 | 1.16 | 33.4 |
| | 36M6-40 | 1000 | 150 | 150 | 2150 | 1.0 | 0.47 | 5.9 | 0.90 | 0.90 | 0.90 | 34.6 |

1. Vertical reinforcement in the flanges was not uniformly distributed. The provided value is the total reinforcement area divided by the flange area.

the response of such walls requires further investigation and more experimental data is needed to assess their performance.

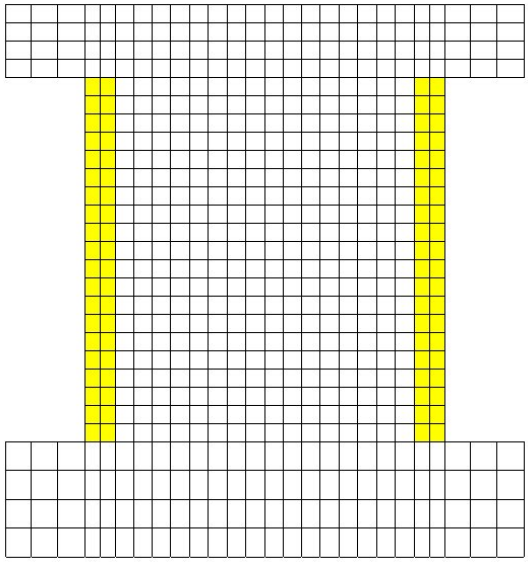

**Figure 5-52 VecTor2 mesh for walls S1, S2, S3 and S6 tested by Maier and Thürlimann (1985)**

**Table 5-10 Comparison of experimental ($V_{peak}$) peak shear strengths to those predicted using VecTor2 ($V_{peak\_FE}$) for squat flanged walls**

| Program ID | Wall ID | $b_f / h_w$ | $V_{peak}$ (kN) | $V_{peak\_FE}$ (kN) | $\frac{V_{peak\_FE}}{V_{peak}}$ |
|---|---|---|---|---|---|
| Maier | S1 | 0.33 | 680 | 688 | 1.01 |
| | S2 | 0.33 | 928 | 994 | 1.07 |
| | S3 | 0.33 | 977 | 995 | 1.02 |
| | S6 | 0.33 | 667 | 618 | 0.93 |
| Palermo | DP1 | 1.51 | 1298 | 1572 | 1.21 |
| NUPEC | U-1 | 1.48 | 1638 | 1855 | 1.13 |
| Seki | RA-00P | 1.06 | 1474 | 1579 | 1.07 |
| | RA-15P | 1.06 | 1672 | 1737 | 1.04 |
| | RB-00P | 0.74 | 1265 | 1337 | 1.06 |
| | RB-15P | 0.74 | 1465 | 1499 | 1.02 |
| | RC-00P | 0.57 | 1032 | 1056 | 1.02 |
| | RC-15P | 0.57 | 1170 | 1228 | 1.05 |
| Sato | 24M6-30 | 1.0 | 2100 | 2129 | 1.01 |
| | 24M6-40 | 1.0 | 2190 | 2179 | 0.99 |
| | 36M6-30 | 1.0 | 2250 | 2391 | 1.06 |
| | 36M6-40 | 1.0 | 2370 | 2460 | 1.04 |

## 5.5.2 VecTor2 Analyses for Squat Walls with Barbells

A brief summary of the twenty-three barbell walls modeled using VecTor2 is presented in Table 5-11. The selected walls constitute a large experimental program on squat barbell walls and were documented in AIJ (1985a), AIJ (1986c), and AIJ (1985b). The variables considered in the experimental program were aspect ratio (via wall height), boundary element vertical reinforcement ratio, web reinforcement ratios, axial force, and $f_c'$. These walls are selected for modeling because they include relatively large barbells with a ratio of the total barbell area to total wall area of 0.57. All 22 walls had the same wall cross-section. Of the 22 walls modeled, 16 had an aspect ratio of 0.46, three had an aspect ratio of 0.28, and three had an aspect ratio of 0.63.

**Table 5-11 Squat barbell walls modeled using VecTor2**

| Program ID | Wall ID | $b_f$ (mm) | $h_f$ (mm) | $t_w$ (mm) | $l_w$ (mm) | $\frac{h_w}{l_w}$ | $\frac{P}{A_t f_c'}$ (%) | $\rho_h$ (%) | $\rho_v$ (%) | $\rho_{be}$ (%) | $f_c'$ (MPa) |
|---|---|---|---|---|---|---|---|---|---|---|---|
| Chiba | 1 | 300 | 300 | 80 | 2300 | 0.46 | 5.8 | 1.20 | 1.20 | 1.04 | 34.0 |
| | 3 | 300 | 300 | 80 | 2300 | 0.46 | 5.0 | 0.80 | 0.80 | 1.04 | 39.7 |
| | 4 | 300 | 300 | 80 | 2300 | 0.46 | 5.9 | 1.60 | 1.60 | 1.44 | 33.6 |
| | 5 | 300 | 300 | 80 | 2300 | 0.46 | 5.7 | 2.00 | 2.00 | 1.76 | 34.6 |
| | 6 | 300 | 300 | 80 | 2300 | 0.46 | 12.4 | 1.20 | 1.20 | 1.04 | 31.8 |
| | 7 | 300 | 300 | 80 | 2300 | 0.28 | 6.0 | 1.20 | 1.20 | 1.04 | 33.0 |
| | 8 | 300 | 300 | 80 | 2300 | 0.63 | 5.9 | 1.20 | 1.20 | 1.04 | 33.4 |
| Yagishita | 2 | 300 | 300 | 80 | 2300 | 0.46 | 6.8 | 0.60 | 0.60 | 1.04 | 29.1 |
| | 3 | 300 | 300 | 80 | 2300 | 0.46 | 6.7 | 0.80 | 0.80 | 1.04 | 29.6 |
| | 6 | 300 | 300 | 80 | 2300 | 0.46 | 0.1 | 1.20 | 1.20 | 1.04 | 28.7 |
| Fukuzawa | 1 | 300 | 300 | 80 | 2300 | 0.46 | 5.6 | 0.00 | 0.00 | 1.04 | 35.2 |
| | 2 | 300 | 300 | 80 | 2300 | 0.46 | 5.6 | 0.30 | 0.30 | 1.04 | 35.2 |
| | 3 | 300 | 300 | 80 | 2300 | 0.46 | 5.9 | 2.40 | 2.40 | 1.76 | 33.6 |
| | 4 | 300 | 300 | 80 | 2300 | 0.46 | 6.2 | 2.80 | 2.80 | 1.76 | 31.7 |
| | 5 | 300 | 300 | 80 | 2300 | 0.46 | 0.0 | 0.00 | 0.00 | 1.04 | 31.7 |
| | 6 | 300 | 300 | 80 | 2300 | 0.46 | 12.4 | 0.00 | 0.00 | 1.04 | 31.7 |
| | 7 | 300 | 300 | 80 | 2300 | 0.46 | 0.0 | 0.60 | 0.60 | 1.04 | 35.2 |
| | 8 | 300 | 300 | 80 | 2300 | 0.46 | 11.6 | 0.60 | 0.60 | 1.04 | 34.0 |
| | 9 | 300 | 300 | 80 | 2300 | 0.28 | 5.9 | 0.60 | 0.60 | 1.04 | 33.6 |
| | 10 | 300 | 300 | 80 | 2300 | 0.63 | 5.9 | 0.60 | 0.60 | 1.04 | 33.5 |
| | 11 | 300 | 300 | 80 | 2300 | 0.28 | 5.8 | 2.00 | 2.00 | 1.76 | 34.0 |
| | 12 | 300 | 300 | 80 | 2300 | 0.63 | 5.8 | 2.00 | 2.00 | 1.76 | 34.3 |

Figure 5-53 presents the mesh for Table 5-11 walls with an aspect ratio of 0.46. Four rows of elements on each side of the mesh represent the barbells as shown in yellow in Figure 5-53. The

element aspect ratio is approximately square throughout the mesh of the wall web and barbells. Table 5-12 presents the experimental and predicted peak shear strengths for the squat barbell walls modeled using VecTor2. As seen in Table 5-12, VecTor2 can predict the peak shear strength of squat barbell walls with reasonable accuracy. This is an important result because the total barbell area forms 57% of the total wall area, and if the effectiveness of the barbells on wall response was questionable, significant overestimations of the experimental peak shear strength would be expected. It can be concluded that the barbells are fully effective in resisting the lateral forces. Note that the failure mode for all barbell walls listed in Table 5-11 was diagonal compression. VecTor2 accurately predicted the failure mode for all walls.

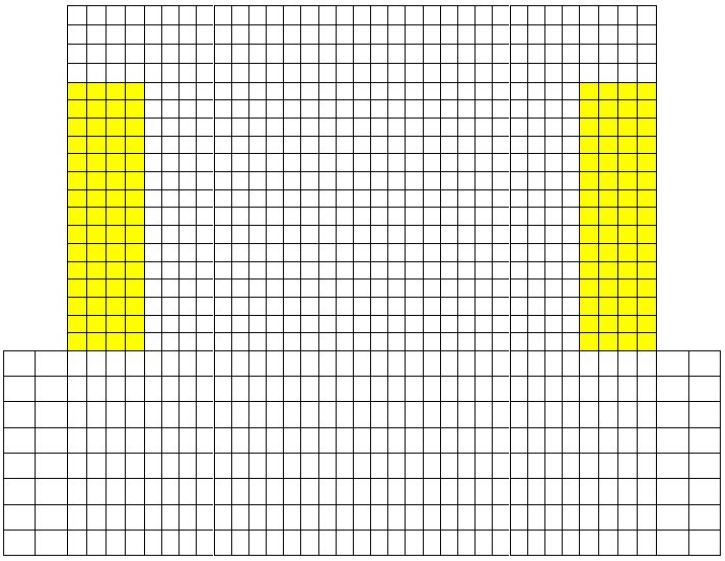

**Figure 5-53 VecTor2 mesh for squat barbell walls with an aspect ratio of 0.46**

**Table 5-12 Comparison of experimental ($V_{peak}$) peak shear strengths to those predicted using VecTor2 ($V_{peak\_FE}$) for squat barbell walls**

| Program ID | Wall ID | $V_{peak}$ (kN) | $V_{peak\_FE}$ (kN) | $\frac{V_{peak\_FE}}{V_{peak}}$ |
|---|---|---|---|---|
| Chiba | 1 | 1658 | 1496 | 0.90 |
| | 3 | 1475 | 1506 | 1.02 |
| | 4 | 1677 | 1663 | 0.99 |
| | 5 | 1823 | 1819 | 1.00 |
| | 6 | 1515 | 1603 | 1.06 |
| | 7 | 1617 | 1812 | 1.12 |
| | 8 | 1343 | 1260 | 0.94 |
| Yagishita | 2 | 1246 | 1298 | 1.04 |
| | 3 | 1307 | 1345 | 1.03 |
| | 6 | 1146 | 1177 | 1.03 |
| Fukuzawa | 1 | 1192 | 1041 | 0.87 |
| | 2 | 1283 | 1278 | 1.00 |
| | 3 | 2003 | 1834 | 0.92 |
| | 4 | 1732 | 1823 | 1.05 |
| | 5 | 744 | 635 | 0.85 |
| | 6 | 1421 | 1139 | 0.80 |
| | 7 | 1151 | 975 | 0.85 |
| | 8 | 1698 | 1602 | 0.94 |
| | 9 | 1871 | 1709 | 0.91 |
| | 10 | 1275 | 1123 | 0.88 |
| | 11 | 2081 | 2150 | 1.03 |
| | 12 | 1656 | 1584 | 0.96 |

# 6 EMPIRICAL EQUATIONS FOR PEAK SHEAR STRENGTH

## 6.1 Introduction

The peak shear-strength equations used in the United States were presented in Sections 1 and 2. Section 4 identified the utility of five peak shear-strength equations using the squat wall database introduced in Section 3. The results presented in Section 4 showed that these equations are inaccurate in the sense that a) the utility of the equations vary significantly with respect to wall geometry (rectangular, flanged and barbell), and b) the coefficients of variation associated with the distributions of the ratio of predicted to experimental peak shear strength are generally large. An ideal equation would provide a mean ratio of predicted to measured peak shear strengths of 1.0 and a small dispersion as measured by a coefficient of variation. In this section, equations to predict the peak shear strength of squat reinforced concrete walls are developed empirically using the squat wall database. Section 6.2 presents an evaluation of the effect of various design variables on peak shear strength using the experimental data presented in Appendix A. Section 6.3 performs a similar investigation to that of Section 6.2 but using the finite element analysis code VecTor2 [VecTor Analysis Group (2007)], which was shown in Section 5 to satisfactorily predict the behavior of squat walls. Section 6.4 presents the empirically developed peak shear-strength models using the data of Appendix A.

During the preliminary data evaluation phase, it was observed that the walls tested under large amplitude dynamic pulses (blast loading) had 25% higher peak shear strength on average than identical walls tested under pseudo-static monotonic loading [Antebi et al. (1960)]. This result is expected since the compressive and tensile strengths of concrete increase substantially at high-strain rates. Given that the focus of the study is the seismic behavior of squat walls, for which the strain-rate effects are insignificant, the data from the blast tests (30 of the 434 selected walls) are not included in the dataset used for developing peak shear-strength models.

The second step in the process of developing empirical peak shear strength models for squat walls is to limit the wall dataset to those for which the failure mode is predominantly shear (shear-critical walls). Two strategies can be employed to identify the shear-critical walls: 1) identification through visual observation of the reported damage photos, and 2) comparing the experimental peak shear strength with the shearing force ($V_{flex}$) associated with the development of wall flexural strength as determined by cross-section analysis. The disadvantages of using the first approach are two-fold: 1) damage photos were not reported for all walls in the database, and 2) a decision based on visual observation is subjective. Accordingly, the second approach is used herein. Paulay et al. (1982) showed that cross-section analysis can satisfactorily predict the flexural strength of squat walls. Cross-section analysis was performed for all 404 walls as a part of the analyses presented in Section 4. Therefore, the values of $V_{flex}$ used herein to identify shear-critical walls are those of Section 4. The assumptions associated with the cross-section analyses are listed in Section 4 and are not repeated. It should be noted that the plane-section hypothesis, which is one of the underlying assumptions of cross-section analysis, is not valid for squat walls since the contributions of shear deformation to total deformation is generally large.

Figure 6-1 presents the variation of $V_{peak}/V_{flex}$ with moment-to-shear ratio for all 404 squat walls. The walls with $V_{peak}/V_{flex}$ less than 1.0 are assumed to be shear-critical.

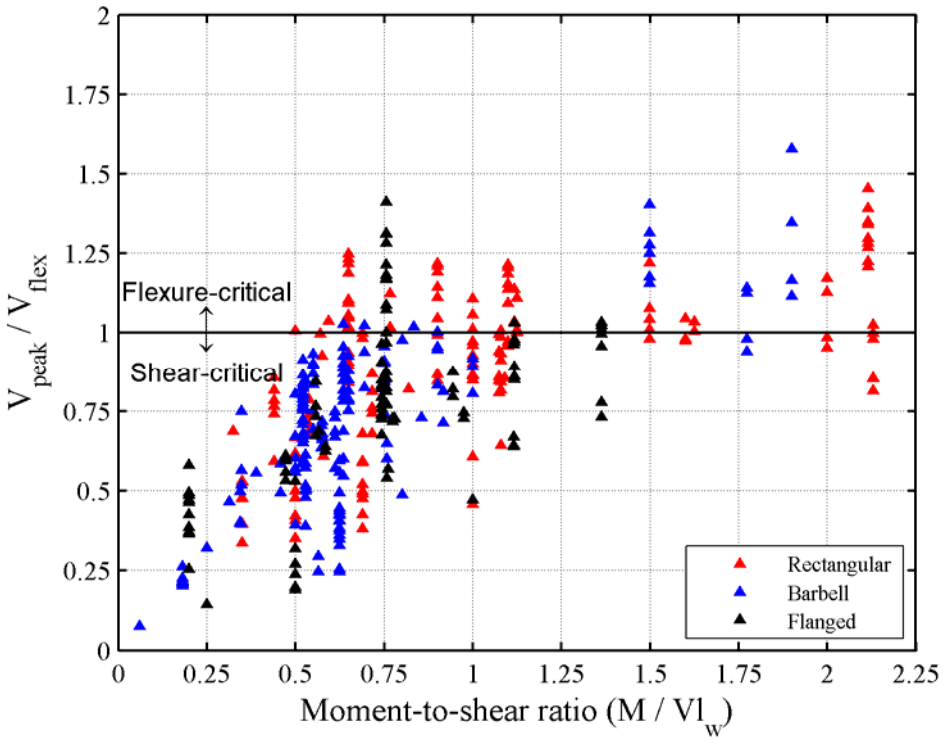


**Figure 6-1 Variation of $V_{peak}/V_{flex}$ with moment-to-shear ratio for squat walls**

Figure 6-1 shows that the likelihood of flexure-critical response increases with an increase in the ratio of moment to shear. In general, walls with a ratio of moment to shear of less than 1.0 are shear-critical whereas those with moment-to-shear ratios of higher than 1.0 are flexure-critical. Further, rectangular walls are more likely to develop their flexural strength than walls with boundary elements. To summarize, 59 of the 150 squat walls with rectangular cross-sections, 15 of the 93 squat walls with flanges and 16 of the 161 squat walls with barbells are judged to be flexure-critical walls.

## 6.2 Effect of Design Variables on Peak Shear Strength – Evaluation of Experimental Data

To study the effect of variation in the design variables on the peak shear strength of a squat wall, the database of Appendix A is mined to identify shear-critical companion walls (same test series and loading type) that were identical except for one design variable. The aim of these tests was to investigate the effect of a single design variable[1] on wall behavior by performing one-factor at-a-

[1] In some cases, $f_c'$ differed for the companion walls in addition to the single factor varied. These companion walls are not completely excluded from the analyses presented in this section but a rule is followed to evaluate these walls. In a group of companion walls, if the ratio of the largest to smallest $f_c'$ is greater than 1.2, the group is excluded from the analysis.

time experiments. The database of Appendix A include companion walls for design variables aspect ratio, axial load, horizontal web reinforcement ratio, vertical web reinforcement ratio, $f_c'$, and boundary element vertical reinforcement ratio.

Equations currently used to predict the peak shear strength of squat walls (see Sections 1 and 2) include design variables such as aspect ratio, axial load, horizontal and vertical web reinforcement ratio, and $f_c'$, but generally ignore the effects of wall cross-section type and boundary element reinforcement.

### 6.2.1 Aspect Ratio

Many have observed that walls with smaller aspect ratios generate higher peak shear strengths than taller walls with similar material properties. Therefore, aspect ratio is generally used as a design variable to estimate peak shear strength. The effect of aspect ratio on peak shear strength is generally introduced within the concrete contribution term as in Chapter 11 and 21 of ACI 318-08 [ACI (2008)], the Barda procedure [Barda et al. (1977)] and ASCE 43-05 [ASCE (2005)]. However, the forms of these terms differ significantly and there is no unified approach to incorporate the effect of wall aspect ratio on peak shear strength.

Table 6-1 presents data on the groups of companion shear-critical walls that focused on the effect of aspect ratio on squat wall behavior. Figure 6-2 shows the variation in peak shear strength [normalized by wall web area ($A_w$)] with aspect ratio ($h_w / l_w$) for the companion walls of

Table 6-1. In Figure 6-2 (and in Figures 6-3 through 6-7), the lines corresponding to groups of companion walls with more than two walls per group are determined using linear regression. The data presented in Figure 6-2 indicates that the peak shear strength of squat walls increase with decreasing aspect ratio. The near-parallel trend lines in Figure 6-2 indicate that the effect of wall aspect ratio on peak shear strength is somewhat similar for the three wall geometries considered.

### 6.2.2 Horizontal Web Reinforcement Ratio

Horizontal web reinforcement ratio is another key parameter used in the peak shear equations. However, the effect of horizontal web reinforcement ratio on peak shear strength is still unclear. Barda (1972), Maier and Thürlimann (1985) and Lefas et al. (1990) conclude that the effect of horizontal web reinforcement ratio on peak shear strength is negligible in comparison with that of the vertical web reinforcement ratio. However, the Lefas et al. (1990) walls failed predominantly in flexure and some of the Maier and Thürlimann (1985) walls exhibited mixed failure modes (i.e., flexure-diagonal tension). The two companion walls (B3-2 and B4-3) of Barda (1972) tested to observe the effect of horizontal web reinforcement ratio on wall behavior had significantly different $f_c'$ (2760 psi vs. 3920 psi) and a direct comparison of the strength of the two walls is not possible. Cardenas et al. (1980) conclude that both horizontal and vertical web reinforcement contribute to peak shear strength. Cardenas et al. (1980) tested two groups of companion walls (first group: walls SW-8 and SW-9, second group: walls SW-11 and SW-12) to investigate the effect of horizontal web reinforcement ratio on wall behavior. However, walls SW-9 had $V_{peak} / V_{flex}$ of greater than 1.0 and walls SW-11 and SW-12 failed prematurely due to insufficient anchorage so the Cardenas et al. (1980) walls are also excluded from the discussion.

**Table 6-1 Information on the test programs focused on the influence of aspect ratio on wall behavior**

| Cross-Section | Group | Researcher | Wall ID | $h_w / l_w$ | $f_c'$ (psi) | $V_{peak} / A_w$ (psi) |
|---|---|---|---|---|---|---|
| Rectangular | 1 | Wiradinata | Wall-2 | 0.25 | 3191 | 493 |
| | | | Wall-1 | 0.50 | 3626 | 417 |
| | 2 | Sheu | SW11 | 0.50 | 3776 | 342 |
| | | | SW17 | 0.75 | 3769 | 267 |
| Barbell | 1 | Chiba | 7 | 0.28 | 4793 | 1275 |
| | | | 1 | 0.46 | 4935 | 1307 |
| | | | 8 | 0.63 | 4850 | 1059 |
| | 2 | Fukuzawa | 11 | 0.28 | 4935 | 1640 |
| | | Chiba | 5 | 0.46 | 5021 | 1437 |
| | | Hatori | 3 | 0.46 | 5149 | 1399 |
| | | Fukuzawa | 12 | 0.63 | 4978 | 1306 |
| | 3 | Fukuzawa | 9 | 0.28 | 4878 | 1475 |
| | | Chiba | 2 | 0.46 | 4281 | 929 |
| | | Yagishita | 2 | 0.46 | 4224 | 982 |
| Flanged | 1 | Barda | B7-5 | 0.21 | 3730 | 854 |
| | | | B3-2 | 0.46 | 3920 | 830 |
| | | | B8-5 | 0.96 | 3400 | 664 |
| | 2 | Saito | W12-1 | 0.35 | 5106 | 1515 |
| | | | W12-6 | 0.83 | 4807 | 1001 |
| | 3 | Saito | W15-1 | 0.35 | 3598 | 997 |
| | | | W15-2 | 0.83 | 3755 | 827 |
| | 4 | Saito | W12-4 | 0.35 | 5191 | 1414 |
| | | | W12-7 | 0.83 | 4921 | 939 |
| | 5 | Seki | RA-00P | 0.46 | 4580 | 926 |
| | | | RB-00P | 0.66 | 4196 | 795 |
| | | | RC-00P | 0.85 | 4366 | 649 |
| | 6 | Seki | RA-15P | 0.46 | 4281 | 1051 |
| | | | RB-15P | 0.66 | 4196 | 921 |
| | | | RC-15P | 0.85 | 4238 | 736 |

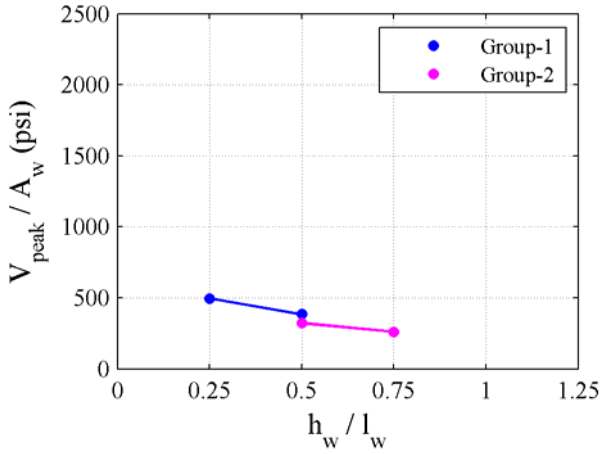


**a) Rectangular walls**

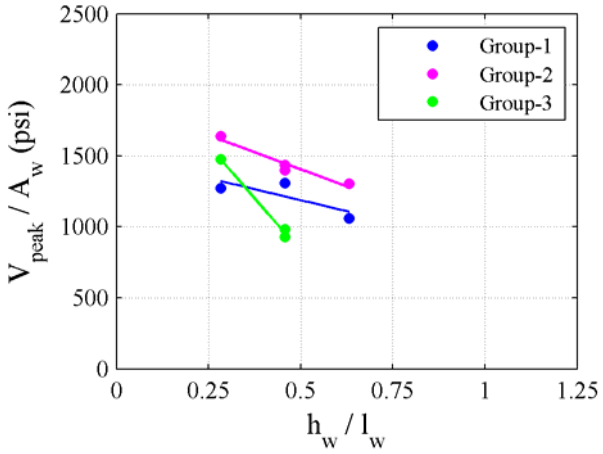


**b) Barbell walls**

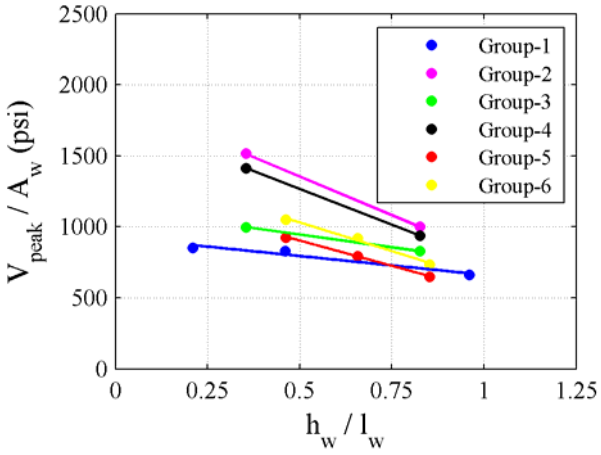


**c) Flanged walls**

**Figure 6-2 Variation of peak shear strength with aspect ratio**

Table 6-2 presents data on the groups of shear-critical companion walls that focused on the effect of horizontal web reinforcement ratio on squat wall behavior. All presented data are for rectangular walls and no data was identified for the walls with flanged or barbell cross-sections presented in Appendix A. Figure 6-3 shows the variation in peak shear strength with the horizontal web reinforcement ratio ($\rho_h$). The effect of horizontal web reinforcement ratio on peak shear strength was significant for lightly reinforced walls, which did not comply with the minimum reinforcement requirements of ACI 318-08 [ACI (2008)]. In contrast, the effect was almost negligible for walls with horizontal web reinforcement ratios of higher than 0.25%. More experimental work is needed to identify the effect of horizontal web reinforcement ratio on squat wall behavior.

**Table 6-2 Information on the test programs focused on the influence of horizontal web reinforcement ratio on wall behavior**

| Cross-Section | Group | Researcher | Wall ID | $\rho_h$(%) | $f_c'$ (psi) | $V_{peak} / A_w$ (psi) |
|---|---|---|---|---|---|---|
| Rectangular | 1 | Hidalgo | 1 | 0.13 | 2915 | 212 |
| | | | 2 | 0.25 | 2959 | 322 |
| | 2 | Hidalgo | 6 | 0.13 | 2654 | 333 |
| | | | 8 | 0.25 | 2364 | 342 |
| | 3 | Hidalgo | 11 | 0.13 | 2451 | 245 |
| | | | 13 | 0.26 | 2741 | 301 |
| | 4 | Hidalgo | 14 | 0.13 | 2582 | 272 |
| | | | 16 | 0.25 | 2843 | 382 |
| | 5 | Hirosawa | 73 | 0.26 | 3015 | 387 |
| | | | 74 | 0.57 | 3015 | 434 |
| | 6 | Hirosawa | 75 | 1.08 | 2133 | 429 |
| | | | 76 | 1.08 | 2660 | 486 |

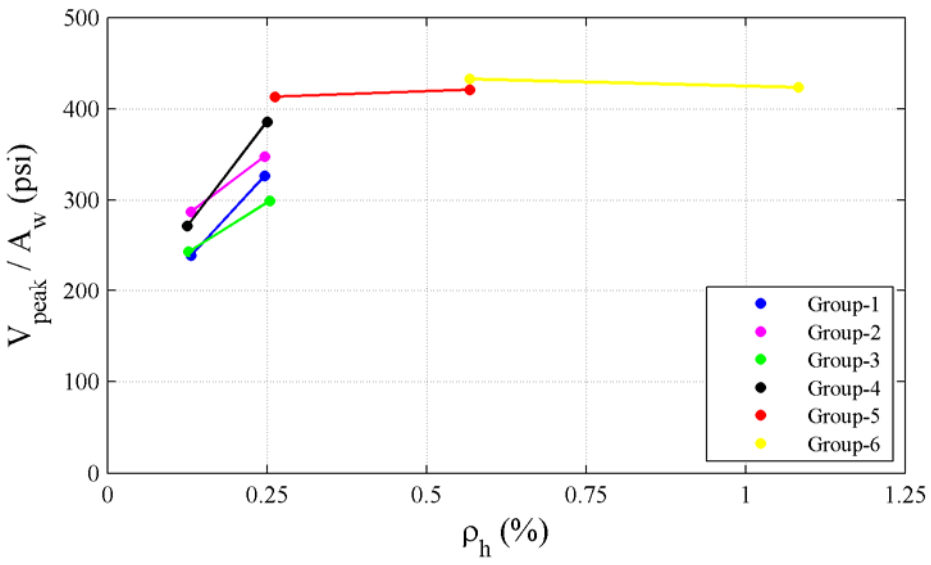


**Figure 6-3 Variation of peak shear strength with horizontal web reinforcement ratio**

## 6.2.3 Vertical Web Reinforcement Ratio

Vertical web reinforcement ratio is not considered in the ACI 318-08 [ACI (2008)] equations to predict peak shear strength but is a key component of the Barda et al. (1977), ASCE 43-05 [ASCE (2005)] and Wood (1990) equations. Table 6-3 presents data on the groups of shear-critical companion walls that focused on the effect of vertical web reinforcement ratio on squat wall behavior. Figure 6-4 shows the variation in peak shear strength with the vertical web

**Table 6-3 Information on the test programs focused on the influence of vertical web reinforcement ratio on wall behavior**

| Cross-Section | Group | Researcher | Wall ID | $\rho_v$(%) | $f_c'$ (psi) | $V_{peak} / A_w$ (psi) |
|---|---|---|---|---|---|---|
| Rectangular | 1 | Hidalgo | 7 | 0.13 | 2741 | 341 |
| | | | 8 | 0.26 | 2364 | 342 |
| | 2 | Hidalgo | 12 | 0.13 | 2567 | 315 |
| | | | 13 | 0.26 | 2741 | 301 |
| | 3 | Hidalgo | 15 | 0.13 | 2872 | 389 |
| | | | 16 | 0.25 | 2843 | 382 |
| | 4 | Hidalgo | 21 | 0.00 | 3655 | 288 |
| | | | 24 | 0.25 | 3611 | 261 |
| | 5 | Hidalgo | 25 | 0.00 | 3611 | 408 |
| | | | 28 | 0.25 | 3510 | 296 |
| | 6 | Hidalgo | 29 | 0.00 | 3495 | 428 |
| | | | 32 | 0.25 | 3510 | 445 |
| Flanged | 1 | Barda | B3-2 | 0.50 | 3920 | 830 |
| | | | B5-4 | 0.00 | 4190 | 524 |

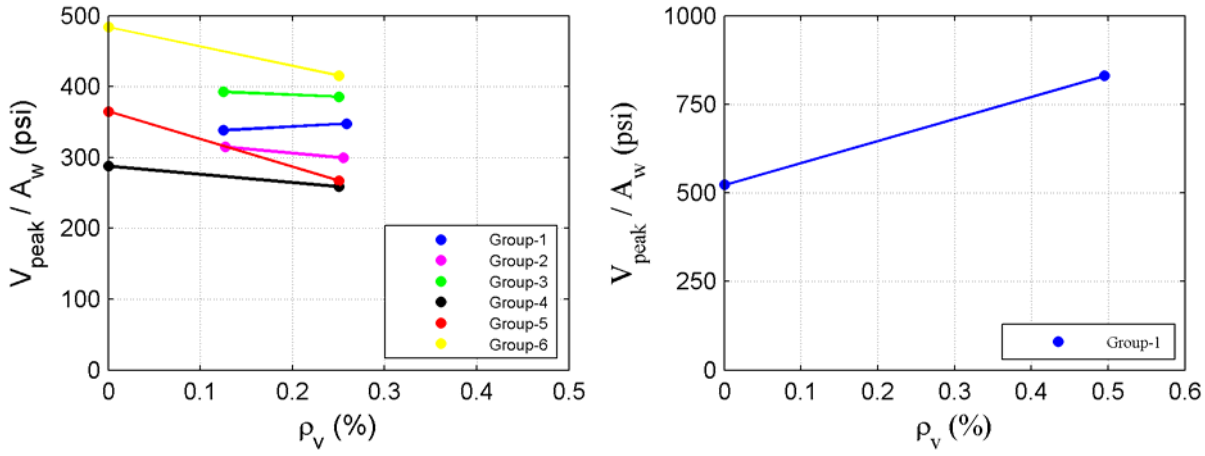


**a) Rectangular walls** **b) Flanged walls**

**Figure 6-4 Variation of peak shear strength with vertical web reinforcement ratio**

reinforcement ratio ( $\rho_v$ ). The rectangular wall dataset is limited to the lightly reinforced Hidalgo et al. (2002) walls ( $\rho_v \leq 0.26$ ). Figure 6-4a shows that vertical web reinforcement ratio was not a factor in the peak shear strength of Hidalgo walls. However, all of the Hidalgo walls included significant amount of vertical reinforcement at the wall ends and the total area of vertical web reinforcement was modest in comparison to the total area of vertical reinforcement in the wall

section. Figure 6-4b shows that the peak shear strength of squat flanged walls are significantly affected by variation in the vertical web reinforcement ratio. As for horizontal reinforcement ratio, more experimental work is needed to identify the effect of vertical web reinforcement ratio on squat wall behavior.

### 6.2.4 Compressive Axial Force

Axial force is not considered in the Chapter 21 equation of ACI 318-08 [ACI (2008)] and the Wood (1990) equation but is included in the Chapter 11 equation of ACI 318-08 [ACI (2008)] through the concrete contribution term ($V_c$). In contrast, the equations of Barda et al. (1977) and ASCE 43-05 [ASCE (2005)] account for the effect of axial force on peak shear strength through a separate term. Note that none of the walls in Appendix A was tested using axial tensile forces. Table 6-4 presents data on the groups of shear-critical companion walls that focused on the effect of axial force on squat wall behavior. Figure 6-5 shows the variation in peak shear strength with the axial force [normalized by total wall area ($A_t$)]. For all cross section types, the experimental data shows consistently that the peak shear strength of squat walls increases with increasing axial force, and so, axial force should be considered as a variable in peak shear strength calculations.

### 6.2.5 Concrete Compressive Strength

A concrete contribution term, as a function of $\sqrt{f_c'}$, is included ACI 318-08 [ACI (2008)], Barda et al. (1977) and ASCE 43-05 [ASCE (2005)] peak shear strength procedures. Wood (1990) procedure does not use $f_c'$ in any form to predict the peak shear strength of squat walls. Table 6-5 presents data on the groups of shear-critical companion walls that focused on the effect of $f_c'$ on squat wall behavior. Figure 6-6 shows the variation in peak shear strength with $f_c'$. As seen in Figure 6-6, the effect of $f_c'$ on peak shear strength varies across the different groups of companion walls. For some of the companion wall groups for rectangular and barbell walls, peak shear strength increases with increasing $f_c'$. The data for flanged walls indicates that the effect of $f_c'$ on peak shear strength is insignificant.

### 6.2.6 Vertical Boundary Element Reinforcement Ratio

Vertical boundary element reinforcement ratio is not considered in the ACI 318-08 [ACI (2008)], Barda et al. (1977) and ASCE 43-05 [ASCE (2005)] peak shear strength calculations. The Wood (1990) equation, which is based on shear-friction, considers all vertical reinforcement in the horizontal cross-section of a wall to calculate its peak shear strength. Table 6-6 presents data on the groups of shear-critical companion walls that focused on the effect of vertical boundary-element reinforcement ratio on squat wall behavior.

Figure 6-7 shows the variation in peak shear strength with the vertical boundary-element reinforcement ratio ($\rho_{be}$). As seen in the figure, the peak shear strength of squat walls increased consistently with increasing boundary element reinforcement ratio for all five companion wall groups considered. No companion data are available for walls with flanged cross-sections.

**Table 6-4 Information on the test programs focused on the influence of axial stress on wall behavior**

| Cross-Section | Group | Researcher | Wall ID | $P / A_t$ [1] (psi) | $f_c'$ (psi) | $V_{peak} / A_w$ (psi) |
|---|---|---|---|---|---|---|
| Rectangular | 1 | Massone | wp110-5 | 16.2 | 4340 | 281 |
| | | | wp1105-7 | 248.2 | 4640 | 491 |
| | | | wp1105-8 | 247.7 | 4630 | 454 |
| | | | wp111-9 | 426.2 | 4100 | 556 |
| | | | wp111-10 | 471.2 | 4550 | 546 |
| Barbell | 1 | Shiga | WB-6 | 1.4 | 2148 | 610 |
| | | | WB-7 | 357.0 | 2219 | 787 |
| | | | WB-8 | 712.6 | 2219 | 729 |
| | 2 | Shiga | WB-4 | 1.4 | 2333 | 587 |
| | | | WB-9 | 357.0 | 2461 | 622 |
| | 3 | XiangDong | FSW-6 | 112.1 | 7216 | 707 |
| | | | FSW-5 | 334.4 | 8172 | 987 |
| | | | FSW-4 | 667.9 | 7181 | 947 |
| | 4 | XiangDong | FSW-13 | 112.1 | 8254 | 739 |
| | | | FSW-8 | 334.4 | 7004 | 864 |
| | | | FSW-12 | 667.9 | 8277 | 1056 |
| | 5 | Yagishita | 6 | 2.2 | 4167 | 904 |
| | | Chiba | 1 | 286.7 | 4935 | 1307 |
| | | | 6 | 571.2 | 4608 | 1194 |
| | 6 | Fukuzawa | 5 | 2.2 | 4594 | 587 |
| | | | 1 | 286.7 | 5106 | 940 |
| | | | 6 | 571.2 | 4594 | 1120 |
| | 7 | Fukuzawa | 7 | 2.2 | 5106 | 908 |
| | | | 8 | 571.2 | 4935 | 1339 |
| | 8 | Hatori | 1 | 2.2 | 4893 | 1350 |
| | | Chiba | 5 | 286.7 | 5021 | 1437 |
| | | Hatori | 2 | 571.2 | 4921 | 1604 |
| Flanged | 1 | Palermo | DP1 | 220.1 | 2727 | 567 |
| | | | DP2 | 46.8 | 3147 | 816 |
| | 2 | Saito | W12-4 | 154.6 | 5191 | 1414 |
| | | | W12-1 | 296.8 | 5106 | 1515 |

1. The weight of top beam (or slab) is included in the axial load calculations.

**Table 6-4 Information on the test programs focused on the influence of axial stress on wall behavior (cont'd)**

| Cross-Section | Group | Researcher | Wall ID | $P / A_t$ (psi) | $f_c'$ (psi) | $V_{peak} / A_w$ (psi) |
|---|---|---|---|---|---|---|
| Flanged (cont'd) | 3 | Saito | W12-7 | 154.6 | 4921 | 939 |
| | | | W12-6 | 296.8 | 4807 | 1001 |
| | 4 | Seki | RA-00P | 51.4 | 4580 | 926 |
| | | | RA-15P | 197.9 | 4281 | 1051 |
| | 5 | Seki | RB-00P | 51.4 | 4196 | 795 |
| | | | RB-15P | 197.9 | 4196 | 921 |
| | 6 | Seki | RC-00P | 51.4 | 4366 | 649 |
| | | | RC-15P | 197.9 | 4238 | 736 |

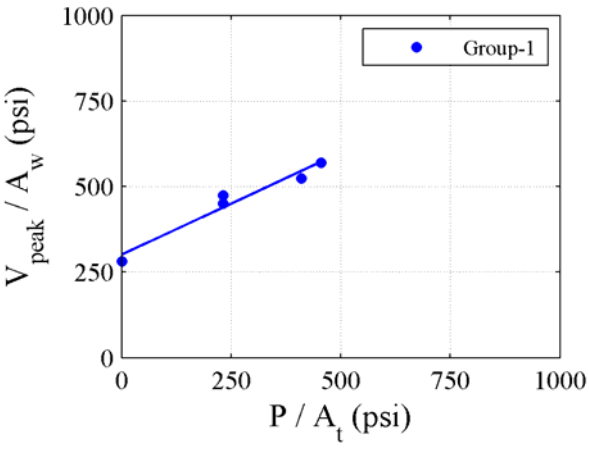


**a) Rectangular walls**

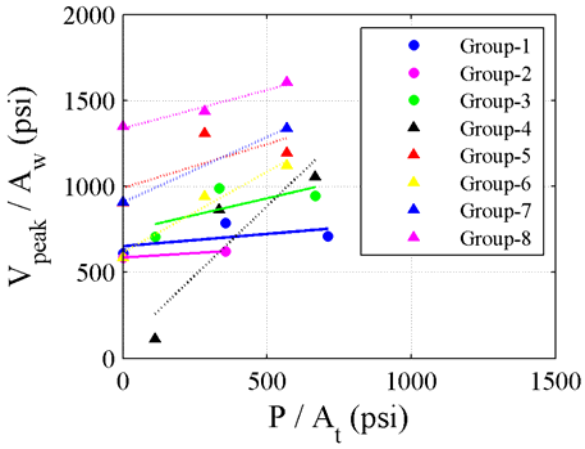


**b) Barbell walls**

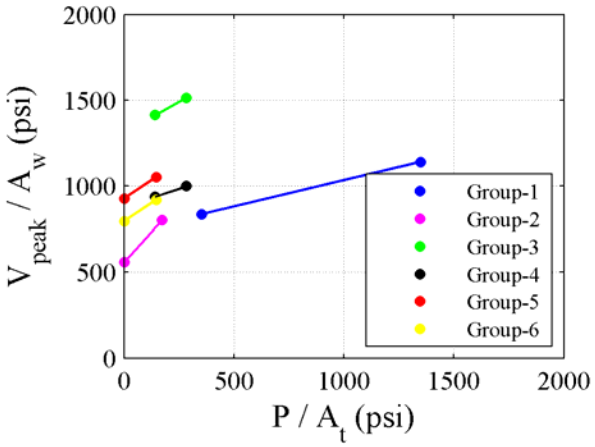


**c) Flanged walls**

**Figure 6-5 Variation of peak shear strength with axial compressive stress**

**Table 6-5 Information on the test programs focused on the influence of $f_c'$ on wall behavior**

| Cross-Section | Group | Researcher | Wall ID | $f_c'$ (psi) | $V_{peak} / A_w$ (psi) |
|---|---|---|---|---|---|
| Rectangular | 1 | Hidalgo | 21 | 3655 | 288 |
| | | Hidalgo | 22 | 2596 | 261 |
| | 2 | Hidalgo | 25 | 3611 | 408 |
| | | Hidalgo | 26 | 2669 | 275 |
| | 3 | Hidalgo | 29 | 3495 | 428 |
| | | Hidalgo | 30 | 2698 | 317 |
| | 4 | Hirosawa | 72 | 2503 | 431 |
| | | Hirosawa | 73 | 3015 | 387 |
| | 5 | Hirosawa | 74 | 3015 | 434 |
| | | Hirosawa | 75 | 1991 | 431 |
| Barbell | 1 | Antebi | 13 | 2669 | 655 |
| | | | 25 | 5973 | 648 |
| | | | 32 | 3880 | 704 |
| | | | 35 | 3700 | 641 |
| | | | 37 | 4100 | 570 |
| | 2 | Benjamin | M-2 | 2750 | 629 |
| | | | M-3 | 3680 | 589 |
| | 3 | Chiba | 5 | 5021 | 1437 |
| | | Hatori | 6 | 3655 | 1176 |
| | 4 | Chiba | 1 | 4935 | 1307 |
| | | Hatori | 5 | 3755 | 1096 |
| | 5 | Taga | No1 | 3940 | 905 |
| | | | No2 | 5561 | 1109 |
| | | | No3 | 8463 | 1215 |
| | 6 | Taga | No5 | 3726 | 946 |
| | | | No6 | 5391 | 1215 |
| | | | No7 | 8434 | 1395 |
| Flanged | 1 | Mo | LN6-2 | 4380 | 482 |
| | | | LM6-2 | 5366 | 494 |
| | 2 | Mo | LN6-3 | 4380 | 506 |
| | | | LM6-3 | 5004 | 506 |
| | 4 | Saito | W12-1 | 5106 | 1515 |
| | | | W12-5 | 5860 | 1521 |

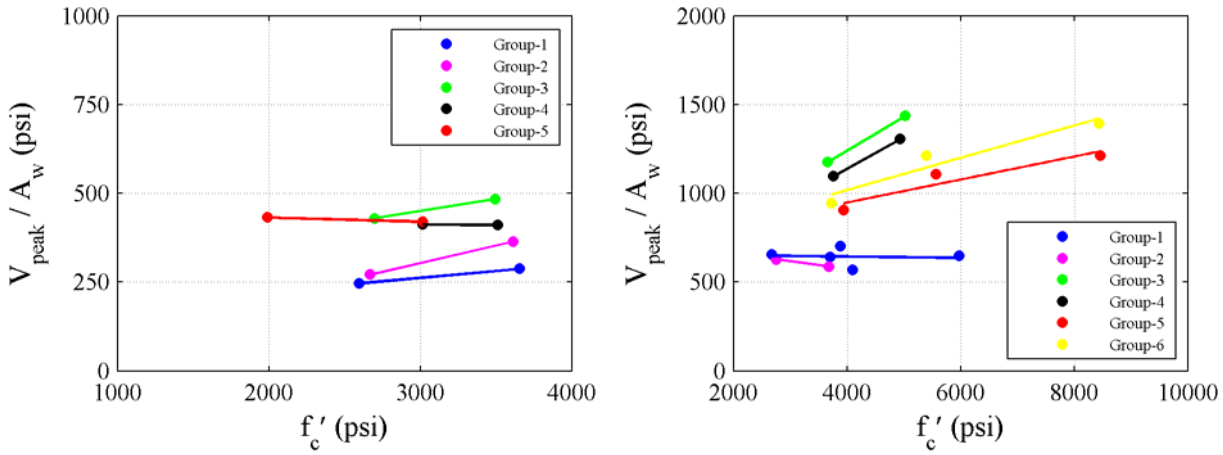


**a) Rectangular walls** **b) Barbell walls**

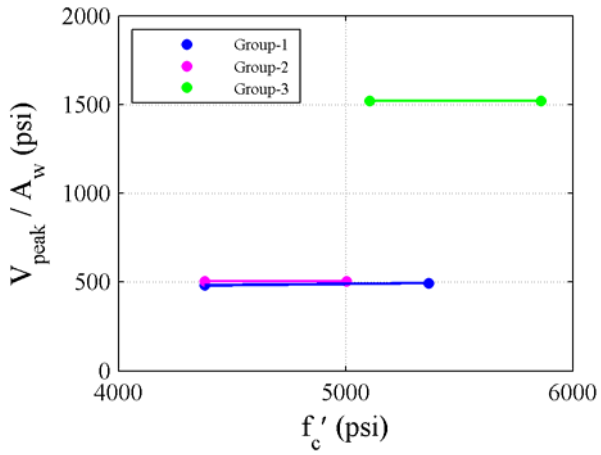


**c) Flanged walls**

**Figure 6-6 Variation of peak shear strength with $f_c'$**

# 6.3 Effect of Design Variables on Peak Shear Strength through Numerical Simulation

## 6.3.1 Introduction

The analysis results of Section 5 led to the conclusion that VecTor2 can predict reasonably the experimental response of squat reinforced concrete walls. The peak shear strength predictions of the MCFT and DSFM formulations included in VecTor2 were generally within 10% of the experimentally measured values for all three wall geometries (rectangular, barbell and flanged).

In this section, a numerical experiment is designed and implemented using VecTor2 to provide more insight into the contribution of the various design variables to the peak shear strength of squat walls. Given that a reliable numerical modeling tool is available, the obvious advantage of numerical analysis over physical experimentation is the cost of the experiment. In addition, more

**Table 6-6 Information on the test programs focused on the influence of vertical boundary element reinforcement ratio on wall behavior**

| Cross-Section | Group | Researcher | Wall ID | $\rho_{be}$ (%) | $f'_c$ (psi) | $V_{peak} / A_w$ (psi) |
|---|---|---|---|---|---|---|
| Rectangular | 1 | Yoshizaki | 171 | 3.92 | 3556 | 474 |
| | | | 173 | 5.92 | 3556 | 524 |
| | 2 | Yoshizaki | 176 | 2.94 | 3698 | 486 |
| | | | 178 | 4.44 | 3698 | 578 |
| Barbell | 1 | Antebi | 6 | 2.10 | 3160 | 570 |
| | | | 10 | 4.71 | 3360 | 718 |
| | 2 | Antebi | 35 | 2.10 | 3700 | 641 |
| | | | 41 | 4.71 | 3310 | 746 |
| | 3 | Kabeyasawa | K3 | 2.14 | 2788 | 491 |
| | | | K4 | 1.43 | 3015 | 462 |

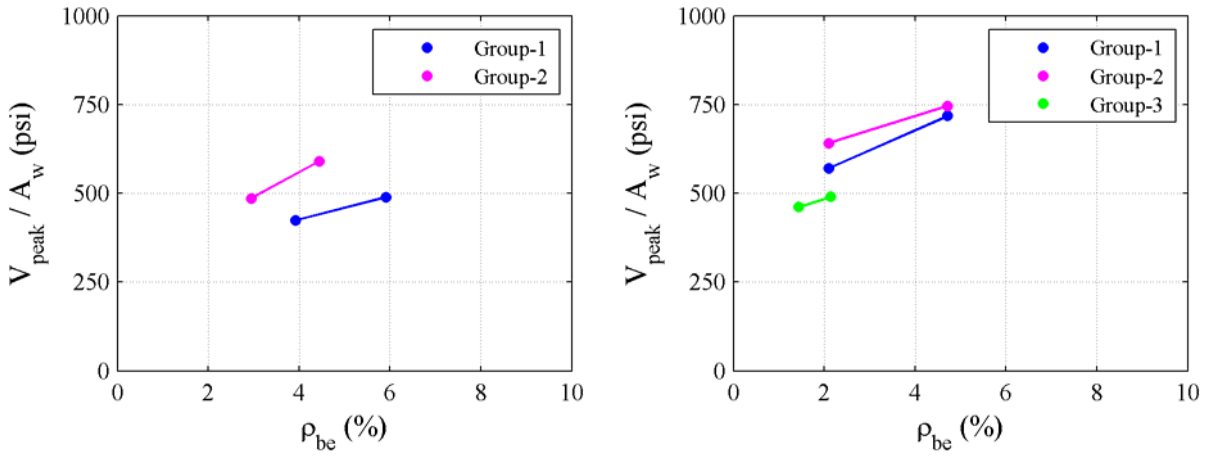


**a) Rectangular walls** **b) Barbell walls**

**Figure 6-7 Variation of peak shear strength with vertical boundary element reinforcement ratio**

scenarios can be studied in a much shorter timeframe. The drawback of using computational experimentation is that the quality of the results is limited by the ability of the numerical model to predict the response variable. Nevertheless, the intention here is not to create a statistical robust predictive model for peak shear strength using VecTor2, but rather, to assess the effects of various design parameters (factors) to wall peak shear strength (response variable).

## 6.3.2 Factorial Design

*Factorial experimentation* is used to design the numerical experiments conducted herein. This technique allows the experimenter to determine formally the relative effect of each design factor on the response variable and the presence of interaction between these factors. Efficiency (fewer number of experiments required) and identification of the interaction between the factors are the major advantages of the *factorial experimentation* over the classical *one-factor-at-a-time* experimentation. The subject of *factorial experimentation* is not discussed in detail herein since information on the subject is widely available in many texts on design of experiments [i.e., Box et al. (1978) and Montgomery (2005)].

The first step in factorial design of experiments is to determine the factors that potentially affect the response variable of interest. Once the design factors are determined, the subsequent steps in the factorial design are to select the number of levels for the design factors, factorial design type (i.e., full, one-half, one-quarter), and run the experiments for all possible combinations of the factor levels. Herein, the response variable is peak shear strength. All six design variables evaluated in Section 6.2 are selected as factors for the factorial design. These factors are wall aspect ratio (AR), horizontal web reinforcement ratio (HR), vertical web reinforcement ratio (VR), compressive strength of concrete (fc), axial force (AF), and vertical boundary-element reinforcement ratio (BER).

A two-level factorial design is judged appropriate since the number of design factors is not small. Selection of a two-level factorial design is associated with the assumption that the response is approximately linear over the range of the factor levels chosen. A two-level full factorial design with 6 factors requires 64 runs, or more generally, a two-level full factorial design that includes k factors requires $2^k$ runs for the experiment. Assuming that high-order interactions are negligible, information on the main effects and low-order interactions can be obtained by running only a fraction of a full experiment. One-half fraction of a two-level full factorial design with 6 factors, which is referred as $2^{6-1}$ design, requires 32 analyses and reduces the overall experimental burden by half. In addition, no main effects or two-factor interaction is aliased with any other main effect or two-factor interaction [Box et al. (1978)]. Therefore, this particular design maintains a good balance between economy and accuracy.

The factor levels selected for the numerical experiment conducted herein are presented in Table 6-7. The effects of the six factors on the peak shear strength of squat walls are investigated separately for rectangular and barbell walls. The factor levels presented in Table 6-7 are used to design both experiments, therefore the only difference between the runs of the two computational experiments is the cross-section shape as illustrated in Figure 6-8.

**Table 6-7 Factor levels**

| **Level** | **Factor** | | | | | |
|---|---|---|---|---|---|---|
| | AR | HR (%) | VR (%) | fc (MPa) | AF (kN) | BER |
| Low (-1) | 0.35 | 0.25 | 0.25 | 20 | 200 | 4 Φ 12 |
| High (1) | 0.70 | 0.75 | 0.75 | 40 | 400 | 8 Φ 12 |

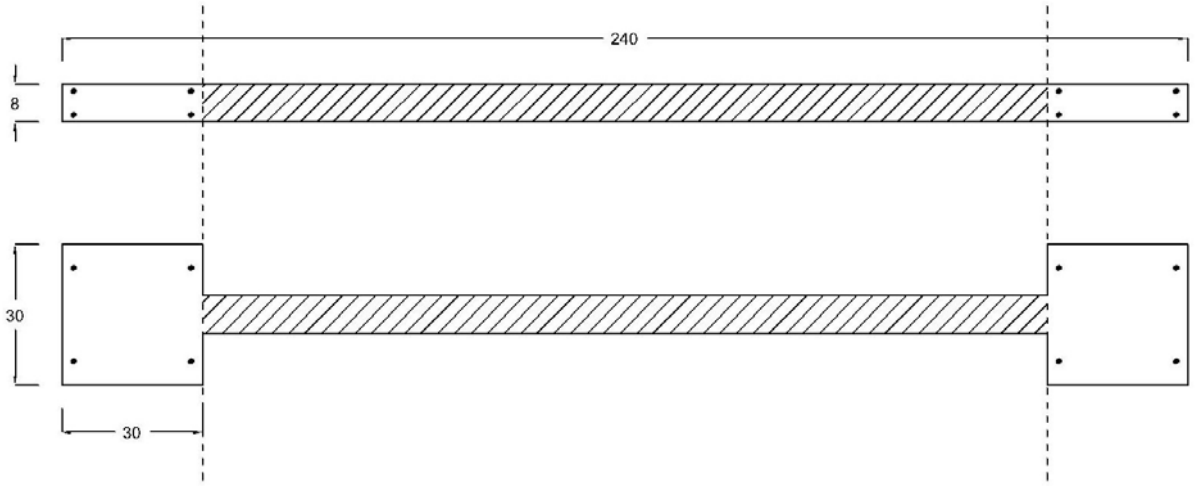


**Figure 6-8 Cross-section geometries used for computational experiments (measurements in cm)**

A numerical experiment using a flanged wall cross-section is not designed because the flange thicknesses are much smaller than the depth of the boundary elements in rectangular or barbell walls. Therefore, a numerical experiment design including flanged walls would result in unrealistic reinforcement schemes in the boundary elements of the rectangular and barbell walls since the objective is to place reinforcement at the same locations in each cross-section to allow direct comparison of results.

The barbell cross-section geometry selected for the numerical experimentation is similar to the wall geometry adopted in the tests associated with squat walls in nuclear-structures summarized by the Architectural Institute of Japan [AIJ (1985a, b), AIJ (1986b, c)]. Relatively small aspect ratios are selected for the walls (0.35 for the low-level and 0.70 for the high-level) to ensure failure in shear. The selected axial forces represent a variation of normalized axial forces between 2.6% (fc = 40 MPa, AF = 200 kN) and 10.4% (fc = 20 MPa, AF = 400 kN) of the product of total wall area and $f_c'$ for rectangular wall cross-section: reasonable limiting values for squat walls. The boundary element reinforcement is selected such that it comprises approximately the 50% of the total vertical reinforcement in the rectangular wall cross-section for the corresponding low-level design (VR = 0.25%, BER = 4 Φ 12). The low-level values for HR and VR are set to the minimum values required by ACI 318-08. Table 6-8 presents the design matrix that includes all combination of the factor levels. In Table 6-8, $V_{peak\_R}$ and $V_{peak\_B}$ are the predicted peak shear strengths for the rectangular and barbell wall analyses, respectively.

## 6.3.3 Numerical Model

Two finite element models are constructed to run the numerical experiments. The first model is for analysis of walls with an aspect ratio of 0.35 and the second model is for analysis of walls with an aspect ratio of 0.70. The common properties of the two finite element models are:

- The topbeam and foundation are 3.0 m long, 0.4 m high, and 0.8 m thick,

**Table 6-8 Design matrix for the experiment and the computed response variables**

| Run | Factor Levels | | | | | | $V_{peak\_R}$ (kN) | $V_{peak\_B}$ (kN) | $\frac{V_{peak\_B}}{V_{peak\_R}}$ |
|---|---|---|---|---|---|---|---|---|---|
| | AR | HR | VR | fc | AF | BER | | | |
| 1 | -1 | -1 | 1 | 1 | 1 | 1 | 1231.8 | 1535.3 | 1.25 |
| 2 | -1 | 1 | 1 | -1 | -1 | -1 | 743.0 | 951.6 | 1.28 |
| 3 | -1 | 1 | -1 | -1 | 1 | -1 | 737.5 | 893.0 | 1.21 |
| 4 | -1 | 1 | -1 | -1 | -1 | 1 | 777.9 | 971.3 | 1.25 |
| 5 | -1 | -1 | -1 | -1 | 1 | 1 | 771.8 | 1027.4 | 1.33 |
| 6 | 1 | -1 | 1 | 1 | -1 | 1 | 747.8 | 874.0 | 1.17 |
| 7 | 1 | 1 | 1 | -1 | -1 | 1 | 649.3 | 785.2 | 1.21 |
| 8 | -1 | 1 | -1 | 1 | -1 | -1 | 740.9 | 842.0 | 1.14 |
| 9 | 1 | 1 | -1 | 1 | 1 | -1 | 547.5 | 610.9 | 1.12 |
| 10 | -1 | 1 | -1 | 1 | 1 | 1 | 1148.3 | 1334.3 | 1.16 |
| 11 | 1 | -1 | -1 | 1 | -1 | -1 | 438.8 | 487.9 | 1.11 |
| 12 | -1 | -1 | 1 | -1 | -1 | 1 | 804.3 | 1082.8 | 1.35 |
| 13 | 1 | -1 | -1 | -1 | -1 | 1 | 475.7 | 631.7 | 1.33 |
| 14 | 1 | 1 | -1 | 1 | -1 | 1 | 640.2 | 719.4 | 1.12 |
| 15 | -1 | -1 | 1 | 1 | -1 | -1 | 938.4 | 1106.8 | 1.18 |
| 16 | 1 | 1 | -1 | -1 | 1 | 1 | 644.6 | 758.0 | 1.18 |
| 17 | -1 | -1 | 1 | -1 | 1 | -1 | 783.7 | 1015.6 | 1.30 |
| 18 | 1 | 1 | 1 | 1 | -1 | -1 | 596.6 | 663.6 | 1.11 |
| 19 | 1 | -1 | -1 | -1 | 1 | -1 | 480.8 | 563.9 | 1.17 |
| 20 | 1 | -1 | -1 | 1 | 1 | 1 | 673.4 | 806.5 | 1.20 |
| 21 | 1 | 1 | 1 | 1 | 1 | 1 | 861.8 | 1001.4 | 1.16 |
| 22 | -1 | 1 | 1 | -1 | 1 | 1 | 882.1 | 1162.7 | 1.32 |
| 23 | -1 | -1 | -1 | 1 | 1 | -1 | 852.8 | 1021.7 | 1.20 |
| 24 | -1 | 1 | 1 | 1 | 1 | -1 | 1086.2 | 1310.0 | 1.21 |
| 25 | 1 | 1 | -1 | -1 | -1 | -1 | 409.2 | 460.6 | 1.13 |
| 26 | -1 | -1 | -1 | -1 | -1 | -1 | 605.7 | 721.9 | 1.19 |
| 27 | 1 | -1 | 1 | 1 | 1 | -1 | 678.3 | 776.7 | 1.15 |
| 28 | 1 | -1 | 1 | -1 | 1 | 1 | 626.7 | 810.6 | 1.29 |
| 29 | -1 | 1 | 1 | 1 | -1 | 1 | 1169.1 | 1442.0 | 1.23 |
| 30 | 1 | -1 | 1 | -1 | -1 | -1 | 500.9 | 606.8 | 1.21 |
| 31 | -1 | -1 | -1 | 1 | -1 | 1 | 935.6 | 1147.5 | 1.23 |
| 32 | 1 | 1 | 1 | -1 | 1 | -1 | 594 | 704.6 | 1.19 |

- The reinforcement ratio in the horizontal and vertical directions of the top beam and foundation are each 1.0%,
- The lateral load is applied at the mid-height of the left end of the top beam,
- The axial load is applied as equivalent concentrated forces along the mid-height of the top beam,
- The wall length is 2.4 m,
- The bottom nodes of the foundation are fixed against translation in the $X$ and $Y$ directions, and
- The element geometry for the FE meshes is 50 mm × 56 mm (width × height).

Figure 6-9 presents the meshes used in the experiments. The yellow shaded elements in the figure identify the boundary elements.

All of the analyses were executed using the Popovics concrete model and the MCFT algorithm. All other modeling assumptions are those made in Section 5.4. The calculated peak shear strengths for each experiment are presented in Table 6-8. Note that the coded design variables (-1 for low level and 1 for high level) are used to analyze the factorial design. The other alternative is to use the uncoded design variables that are the design variables in original (engineering) units. However, the magnitudes of the model coefficients are directly comparable when coded design variables are used since the coded variables are dimensionless and are estimated with the same precision (standard error). Therefore, coded variables are very effective for determining the relative effects of the factors on the response variable [Montgomery (2005)].

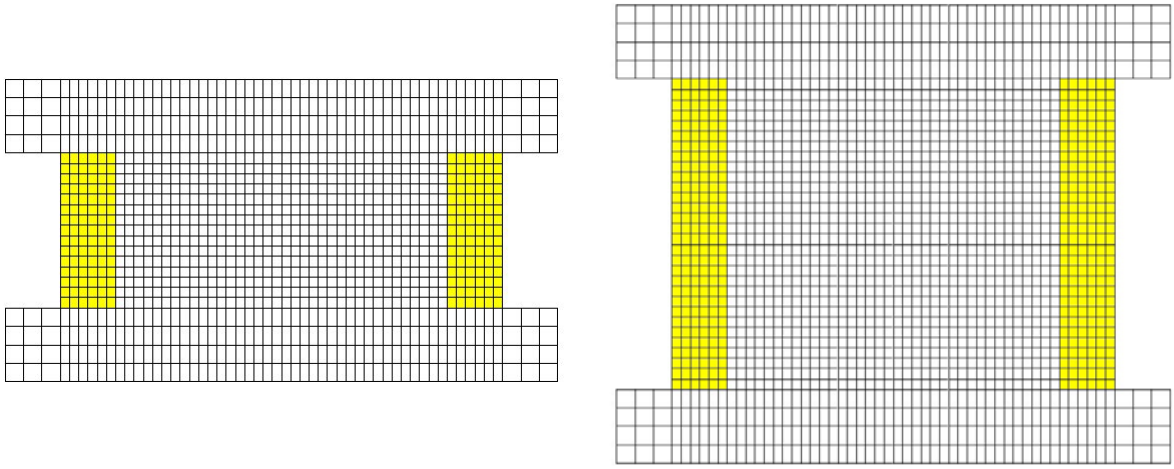

**a) wall aspect ratio = 0.35** **b) wall aspect ratio = 0.70**

**Figure 6-9 Finite element models constructed for the numerical analyses**

### 6.3.4 Analysis Results

The factorial experimentations are analyzed using the commercial statistics software Minitab [Minitab Inc. (2007)]. The calculated factor effects together with the corresponding sums of squares are presented in Table 6-9 and Table 6-10 for the experiments conducted using rectangular and barbell cross-sections, respectively. In these tables, the column labeled "Percent contribution" presents the ratio of the sums of squares calculated for the effects to the total sum of squares. This parameter implicates the relative importance of each factor for the model used to predict the response variable.

As seen in Table 6-9, five main effects influence the peak shear strength of rectangular walls: aspect ratio (AR), axial force (AF), vertical web reinforcement ratio (VR), boundary element reinforcement ratio (BER), and concrete compressive strength (fc). Following these five main effects in influence order are two interactions effects, namely, AR*fc and fc*BER. The effect of the horizontal web reinforcement ratio (HR) on peak shear strength is smaller than these interaction terms. The effect of horizontal web reinforcement ratio (HR) on the peak shear strength is insignificant when compared with the other main factors. Figure 6-10 and Figure 6-11 present the main effects and interaction plots for the factors of the experiment. In Figure 6-11, parallel or near-parallel red and black lines in the interaction plots indicate a lack of interaction between the corresponding two factors. The effects of the interaction terms on peak shear strength are generally insignificant for rectangular walls. The peak shear strength of rectangular walls can be computed with reasonable accuracy using only the main factors. The effect of horizontal web reinforcement ratio and the effects of the interaction terms on peak shear strength are modest. Note that the model that includes the five main factors only yields an *adjusted* $R^2$ statistic of 91%, which is considerably high.

Similar to that observed for rectangular walls, the most influential factors on the peak shear strength of barbell walls are aspect ratio (AR), axial force (AF), vertical web reinforcement ratio (VR), boundary element reinforcement ratio (BER), and concrete compressive strength (fc) as seen in Table 6-10. The effect of horizontal web reinforcement ratio (HR) on peak shear is relatively modest by comparison with the other main factors.

Figure 6-12 and Figure 6-13 present the main effects and interaction plots for the factors of the experiment. In Figure 6-12, parallel or near-parallel red and black lines in a panel indicate a lack of interaction between the corresponding two factors. It can be concluded that the peak shear strength of barbell walls can be represented with reasonable accuracy using only the main factors. The effects of horizontal web reinforcement ratio and the interaction terms on peak shear strength are modest. A linear model for the experiment that includes the five main factors only yields an *adjusted* $R^2$ statistic of 94%, which is slightly higher than the comparable statistic calculated for rectangular walls (91%). The increase in accuracy may be partially attributed to the effect of horizontal web reinforcement ratio on peak shear strength that is smaller for barbell walls. A comparison of "percent contribution" data presented in Table 6-9 and Table 6-10 show that the effects of aspect ratio (AR), vertical web reinforcement ratio (VR), and axial force (AF) on peak shear strength are comparable for walls with rectangular and barbell cross-sections. The effect of $f_c'$ (fc) is higher for rectangular walls and the effect of vertical boundary-element reinforcement ratio (BER) is higher for barbell walls.

**Table 6-9 Calculated factor effects and the sums of squares for rectangular wall experiments**

| | Model term | Effect estimate | Sum of squares | Percent contribution |
|---|---|---|---|---|
| **Main Effects** | AR | -290.2 | 673728 | 48.63 |
| | HR | 42.6 | 14518 | 1.05 |
| | VR | 125.8 | 126605 | 9.14 |
| | fc | 175 | 245000 | 17.68 |
| | AF | 89.2 | 63653 | 4.59 |
| | BER | 144.1 | 166118 | 11.99 |
| **Interactions** | AR*HR | -2.5 | 50 | 0.00 |
| | AR*VR | -7.7 | 474 | 0.03 |
| | AR*fc | -74.6 | 44521 | 3.21 |
| | AR*AF | -8.2 | 538 | 0.04 |
| | AR*BER | -10 | 800 | 0.06 |
| | HR*VR | -8.8 | 620 | 0.04 |
| | HR*fc | -5.9 | 278 | 0.02 |
| | HR*AF | 7.7 | 474 | 0.03 |
| | HR*BER | 20.7 | 3428 | 0.25 |
| | VR*fc | 40.7 | 13252 | 0.96 |
| | VR*AF | -14.8 | 1752 | 0.13 |
| | VR*BER | -12.7 | 1290 | 0.09 |
| | fc*AF | 19.8 | 3136 | 0.23 |
| | fc*BER | 46.9 | 17597 | 1.27 |
| | AF*BER | -9.2 | 677 | 0.05 |
| | AR*HR*VR | 5.7 | 260 | 0.02 |
| | AR*HR*fc | -7.3 | 426 | 0.03 |
| | AR*HR*AF | -0.7 | 4 | 0.00 |
| | AR*HR*BER | 7.3 | 426 | 0.03 |
| | AR*VR*fc | -12.7 | 1290 | 0.09 |
| | AR*VR*AF | 0.3 | 1 | 0.00 |
| | AR*VR*BER | 7.4 | 438 | 0.03 |
| | AR*fc*AF | -16.5 | 2178 | 0.16 |
| | AR*fc*BER | -15.6 | 1947 | 0.14 |
| | AR*AF*BER | 1.5 | 18 | 0.00 |
| | | Total | 1385500 | 100 |

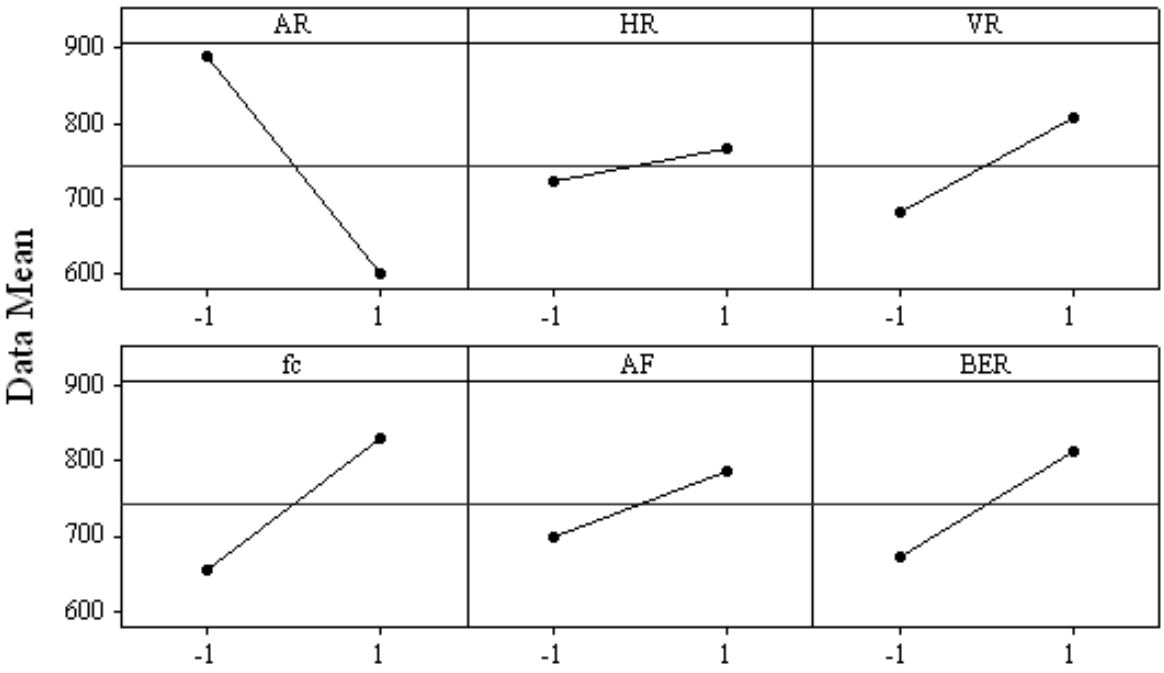


**Figure 6-10 Average response plots for the main effects of the numerical experiment conducted using a rectangular cross-section**

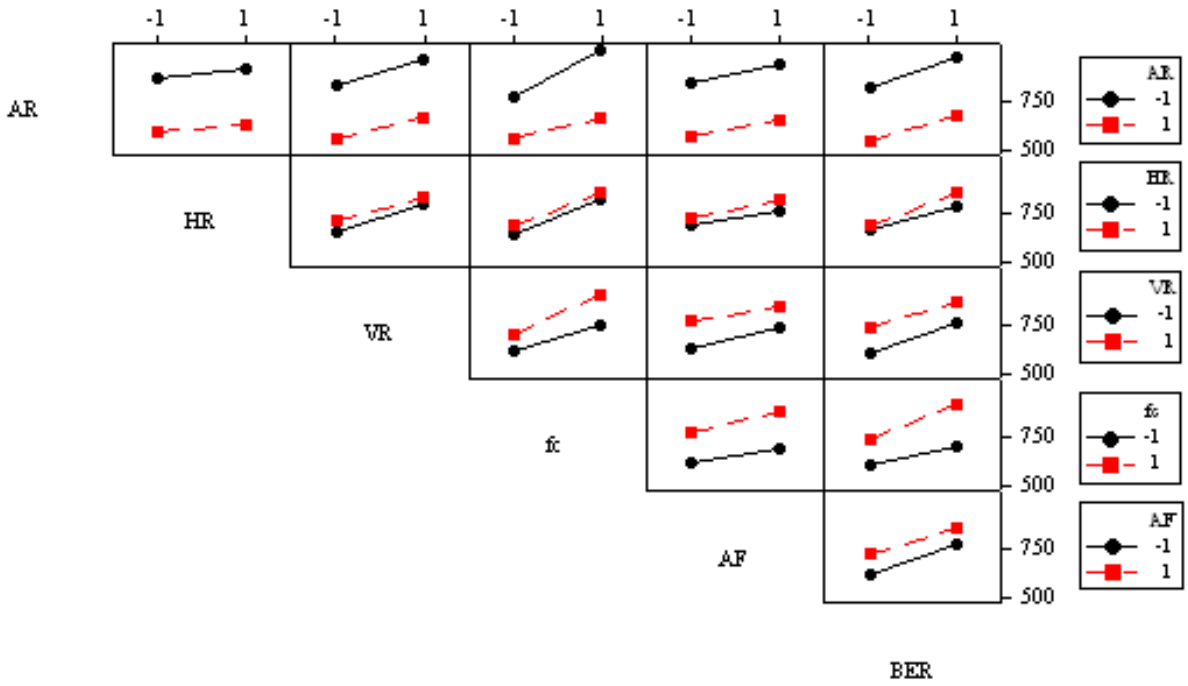


**Figure 6-11 Two-factor interactions matrix for the numerical experiment conducted using a rectangular cross-section**

**Table 6-10 Calculated factor effects and the sums of squares for barbell wall experiments**

| | Model term | Effect estimate | Sum of squares | Percent contribution |
|---|---|---|---|---|
| **Main Effects** | AR | -394 | 1241888 | 54.75 |
| | HR | 24.6 | 4841 | 0.21 |
| | VR | 177 | 250632 | 11.05 |
| | fc | 158.3 | 200471 | 8.84 |
| | AF | 114.8 | 105432 | 4.65 |
| | BER | 209.5 | 351122 | 15.48 |
| **Interactions** | AR*HR | -6.4 | 328 | 0.01 |
| | AR*VR | -29 | 6728 | 0.30 |
| | AR*fc | -80.9 | 52358 | 2.31 |
| | AR*AF | -14.4 | 1659 | 0.07 |
| | AR*BER | -20.6 | 3395 | 0.15 |
| | HR*VR | 2 | 32 | 0.00 |
| | HR*fc | -3.7 | 110 | 0.00 |
| | HR*AF | 2.6 | 54 | 0.00 |
| | HR*BER | 7.7 | 474 | 0.02 |
| | VR*fc | 40.5 | 13122 | 0.58 |
| | VR*AF | -14.3 | 1636 | 0.07 |
| | VR*BER | -14.7 | 1729 | 0.08 |
| | fc*AF | 24.4 | 4763 | 0.21 |
| | fc*BER | 45.6 | 16635 | 0.73 |
| | AF*BER | -17.1 | 2339 | 0.10 |
| | AR*HR*VR | 1.5 | 18 | 0.00 |
| | AR*HR*fc | -2 | 32 | 0.00 |
| | AR*HR*AF | 8.5 | 578 | 0.03 |
| | AR*HR*BER | 9.4 | 707 | 0.03 |
| | AR*VR*fc | -15.7 | 1972 | 0.09 |
| | AR*VR*AF | 4.8 | 184 | 0.01 |
| | AR*VR*BER | 5.6 | 251 | 0.01 |
| | AR*fc*AF | -12.1 | 1171 | 0.05 |
| | AR*fc*BER | -19 | 2888 | 0.13 |
| | AR*AF*BER | 8.2 | 538 | 0.02 |
| | | Total | 2268087 | 100 |

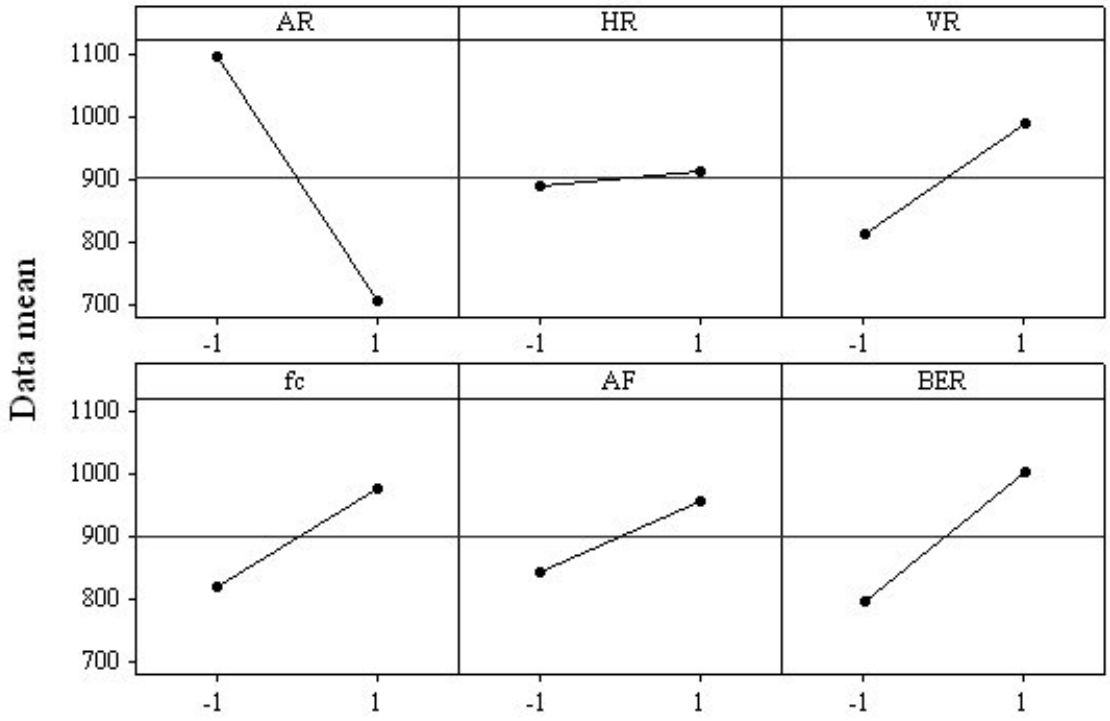


**Figure 6-12 Average response plots for the main effects of the numerical experiment conducted using a barbell cross-section**

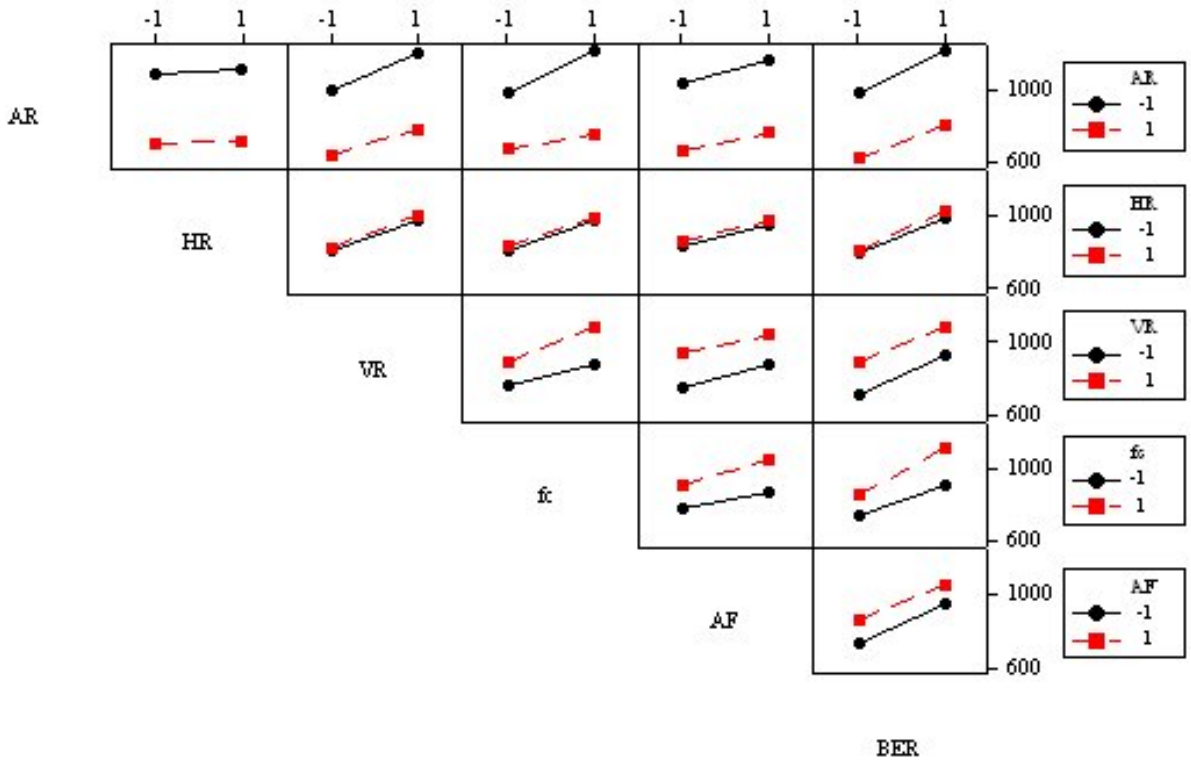


**Figure 6-13 Interactions for the numerical experiment conducted using a barbell cross-section**

A comparison of the calculated peak shear strengths presented in Table 6-8 for rectangular and barbell walls shows that the addition of barbells increased the peak shear strength between 11% and 35% across the experiments. The average strength increase was approximately 20%.

## 6.4 Proposed Peak Shear Strength Equations

### 6.4.1 Methodology

Herein, new models to predict the peak shear strength of squat reinforced concrete walls are obtained using nonlinear regression. The wall data summarized in Section 3 is used for this purpose. The values for the unknown coefficients of the models are calculated using the *fmincon*[2] nonlinear solver in MATLAB [The MathWorks, Inc. (2006)]. *Fmincon* can find the minimum of a scalar function of several variables starting at an initial estimate and allows definition of constraints. Herein, the constraint is that the mean of the predicted to experimental peak shear strengths is set equal to 1.0. No upper or lower values are set for the model unknowns. The unknowns are calculated by minimizing the coefficient of variation associated with the ratios of predicted to experimental peak shear strength as shown in Equations 6-1 and 6-2.

$$r(i) = \frac{V_m(i)}{V_{peak}(i)} \tag{6-1}$$

$$\begin{aligned} constraint \rightarrow \quad & mean\left[r(i)\right] = \frac{\sum_{i=1}^{n} r(i)}{n} = 1 \\ minimize \rightarrow \quad & \sqrt{\frac{1}{n-1}\sum_{i=1}^{n}\left[r(i) - mean\left[r(i)\right]\right]^2} \end{aligned} \tag{6-2}$$

where, $V_{peak}$[3] is the experimental peak shear strength, $V_m$ is the predicted peak shear strength, $r(i)$ is the ratio of the predicted to experimental peak shear strength for $i^{th}$ wall in the dataset, and $n$ is the number of data points used for the model.

### 6.4.2 Selected Model Form

The major challenge in creating a new model for the peak shear strength is to determine the model parameters and their functional relationship. As seen in Section 4, several models with substantially different functional forms are used for the peak shear calculation and all of the models investigated to date provide less-than-satisfactory estimates of the peak shear resistance. Experimental data and numerical analysis results show that a robust model to predict the peak shear strength of squat reinforced concrete walls should consider the following design variables:

[2] The function uses Sequential Quadratic Programming (SQP) to find the minimum of a constrained nonlinear function with multiple variables.

[3] For cyclically or dynamically loaded specimens, the peak shear is taken as the average of the first and third quadrant values.

1) aspect ratio, 2) vertical web reinforcement ratio, 3) axial force, 4) boundary element reinforcement ratio, 5) concrete compressive strength, and 6) wall cross-section shape. The data presented in Sections 6.2 and 6.3 shows that the effect of horizontal web reinforcement ratio on peak shear strength is modest for squat walls. However, horizontal web reinforcement ratio will also be included in the models for completeness.

To determine the general form of the regression mode, a simple free body diagram that is based on the occurrence of inclined (shear) cracks in a squat reinforced concrete wall is presented in Figure 6-14. The forces along a crack that crosses through the upper corner of the wall web are used to form the free body diagram. This assumption is based on the experimental cracking patterns observed in squat walls and independent of the failure mode because shear inclined cracking at achievement of peak shear strength is a common characteristic for diagonal tension, diagonal compression and sliding shear failures.

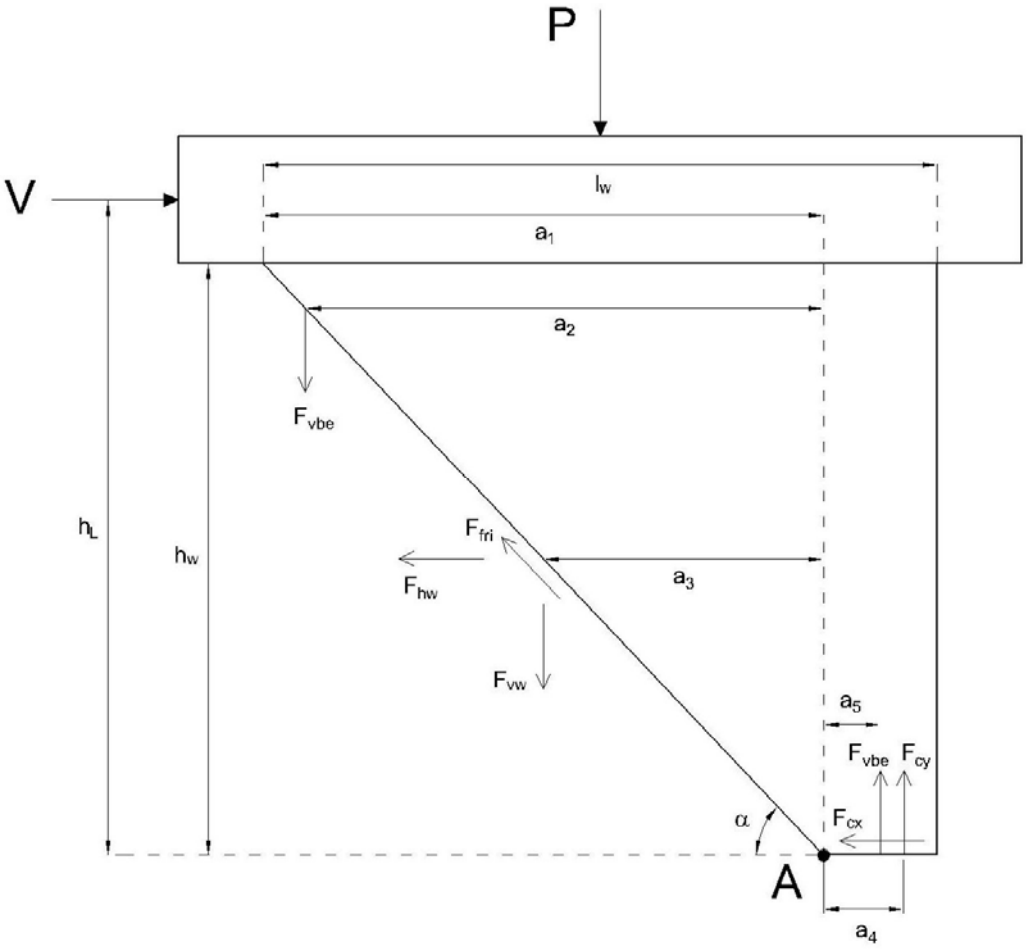


**Figure 6-14 Free body diagram of a reinforced concrete squat wall following the occurrence of a inclined crack**

In Figure 6-14, $V$ is the lateral force; $P$ is the axial force; $F_{vbe}$[4] is the force carried by the vertical boundary element reinforcement; $F_{vw}$ is the total force carried by the vertical web reinforcement; $F_{hw}$ is the total force carried by the horizontal web reinforcement; $F_{fri}$ is the friction force associated with aggregate interlock between the two surfaces of the cracks; $F_{cx}$ and $F_{cy}$ are the components of the compression strut force; $h_w$ is the wall height; $l_w$ is the wall length; $h_L$ is the moment-to-shear ratio; $\alpha$ is the angle of inclination for the crack, and $a_1$ through $a_5$ are the horizontal distances used to identify the moment arms for the vertical forces. Equations 6-3 through 6-5 present the relationship between the external and internal forces illustrated in Figure 6-14.

$$\Sigma M_A = Vh_L - P(a_1 - l_w/2) - F_{vbe}a_2 - F_{vbe}a_5 - F_{vw}(a_1/2) - F_{hw}(a_1 tan\alpha/2) - F_{cy}a_4 = 0 \quad (6\text{-}3)$$

$$V = \frac{P(a_1 - l_w/2) + F_{vbe}(a_2 + a_5) + F_{vw}(a_1/2) + F_{hw}(a_1 tan\alpha/2) + F_c a_4}{h_L} \quad (6\text{-}4)$$

$$V = F_{cx} + F_{hw} + F_{fri}\cos\alpha \quad (6\text{-}5)$$

Equations 6-4 and 6-5 provide two relationships for shear strength calculation of a squat wall. Note that, complex behavior of concrete under biaxial stresses, concrete–reinforcement interaction, and existence of stiff boundary conditions complicate the calculation of the components (i.e., $\alpha$, $a_1$ through $a_5$, rebar strains, friction terms) of Equations 6-4 and 6-5 and the overall squat wall problem is challenging even for advanced finite element analysis studies [Palermo and Vecchio (2007)]. Herein, simplified models using the data of Appendix A are created.

Equation 6-4 includes all design variables that were shown to affect the peak shear strength of squat walls and therefore its form is more desirable than that of Equation 6-5. There is substantial uncertainty in calculation of the terms associated with friction forces ($F_{fri}$) and shear carried in the compressive zone ($F_{cx}$) in Equation 6-5. Note that these two forces are also related to axial force demands and the amount of vertical reinforcement. The final form of the peak shear model determined using the free body diagram of Figure 6-14 is presented in Equation 6-6 ($V_m$). The equation calculates the peak shear strength using boundary element reinforcement, vertical web reinforcement, horizontal web reinforcement, axial force, moment-to-shear ratio, and concrete contribution.

[4] Assumed equal in at the tension and compression boundary elements for brevity. In fact, the reinforcement in the compression zone may be less likely to yield than the tensile reinforcement. However, the experimental data Palermo and Vecchio (2002) shows that near-yield strains are also observed for boundary element vertical reinforcement in compression.

$$V_m = \frac{\beta_1 \left( f_c' \right)^{\beta_2} A_{eff} + \beta_3 F_{vw} + \beta_4 F_{hw} + \beta_5 F_{vbe} + \beta_6 P}{\left( h_w / l_w \right)^{\beta_7}} \tag{6-6}$$

In Equation 6-6, wall aspect ratio ($h_w / l_w$) is used rather than $h_L$, which is equivalent to wall moment-to-shear ratio. The terms associated with reinforcement and axial force are defined using linear functions. The forces associated with wall reinforcement, $F_{vw}$, $F_{vh}$, and $F_{vbe}$, are calculated using the total reinforcement area and yield stresses. In squat reinforced concrete walls, the strains in reinforcement are close to the yield strain at the displacement corresponding to peak shear strength. Therefore, it is reasonable to ignore strain hardening in the reinforcement when calculating the forces $F_{vw}$, $F_{vh}$, and $F_{vbe}$. The terms addressing the concrete contribution and wall aspect ratio are defined using more general functional forms to improve the model accuracy.

### 6.4.3 Data Reduction

As seen in Appendix A, different experimental setups were used for testing of squat walls. The most realistic simulation of a prototype wall structure can be performed using a *cantilever* experimental setup, which is the most widely used form of testing structural walls. In the cantilever experimental setup, a continuous fixed support condition is achieved by anchoring the foundation to the laboratory floor. The wall web is constructed over the wall foundation. The lateral and axial forces are transferred to the wall web using a relatively rigid concrete or steel member constructed above the wall web that simulates a slab or a beam in a prototype structure. Another experimental setup used to test reinforced concrete walls was similar to a three-point test of a beam. In this setup, walls were placed horizontally on two simple supports and were tested using a vertical point load at the mid-span. Specific information on the experimental setup of each wall in the database is presented in Appendix A. Herein, the datasets to obtain peak shear strength models are limited to walls that were tested using the cantilever experimental setup to minimize the variation of data with respect to boundary conditions.

Two rectangular walls, SW-11 and SW-12, tested by Cardenas et al. (1980) were reported to have failed prematurely due insufficient anchorage length for the vertical reinforcement at the top of the wall web. These walls are excluded from the analyses performed in the following sections.

The following sub-sections present the equations obtained for rectangular, and barbell and flanged walls, respectively.

### 6.4.4 Rectangular Walls

Two models based on Equation 6-6 are created using the rectangular wall dataset. The first model ($V_{m1a}$) sets $\beta_2$ equal to 0.5. The concrete contribution term in widely used peak shear strength equations is generally a function of $\sqrt{f_c'}$, which is related to the tensile strength of concrete. In the second model ($V_{m1b}$), an alternative concrete contribution term that is function of $f_c'$ is considered by setting $\beta_2$ equal to 1.0. The concrete contribution term in models $V_{m1a}$ and

$V_{m1b}$ is normalized using wall area ($A_{eff} = A_w$). Two other peak shear models based on the procedures of Chapter 21.9 of ACI 318-08 (Equation 6-7) and ASCE 43-05 (Equation 6-8) are optimized similarly and the performance of the four models is compared with the currently used procedures.

$$V_{m2} = \left(\beta_1 \sqrt{f_c'} + \beta_2 \rho_h f_{yh}\right) A_w \tag{6-7}$$

$$V_{m3} = \left(\beta_1 \sqrt{f_c'} - \beta_2 \sqrt{f_c'} \frac{h_w}{l_w} + \beta_3 \rho_{se} f_y + \beta_4 \frac{P}{A_w}\right) d_3 t_w \tag{6-8}$$

The calculated coefficients for the four models are presented in Table 6-11. Table 6-12 presents the statistics for the ratio of the predicted to experimental peak shear strength using the five procedures investigated in Section 4 and four models created herein.

As seen in Table 6-12, model $V_{m1a}$ provides the best estimates of the peak shear with a median ratio of predicted to experimentally measured shear strength of 0.99 and a coefficient of variation of 0.135, which is the smallest among the procedures investigated. The error (or residual) sum of squares statistics associated with each model presented in the last column of Table 6-12 also reveal that model $V_{m1a}$ yields the smallest error in calculating the peak shear strength. The difference in the performances of the two models based on Equation 6-6 ($V_{m1a}$ and $V_{m1b}$) is modest.

The optimized ACI 318-08 ($V_{m2}$) and ASCE 43-05 ($V_{m3}$) procedures perform better than the codified versions ($V_{n1}$ and $V_{n4}$, respectively) but are poorer than those of models $V_{m1a}$ and $V_{m1b}$. This observation suggests that the functional forms of ACI 318-08 and ASCE 43-05 are not successful in accounting for the factors that affect the peak shear strength of squat rectangular reinforced concrete walls. Another interesting observation is that $\beta_4$ for models $V_{m1a}$, $V_{m1b}$, and $\beta_2$ for model $V_{m2}$, both of which are related to the contribution of horizontal web reinforcement ratio to peak shear strength, are very small. This observation agrees with the outcome of the computational experiments performed using VecTor2 for rectangular walls (Section 6.3).

Figure 6-15 through Figure 6-20 present the variation of the ratio of the calculated to experimental shear strengths for models $V_{m1a}$ and $V_{n1}$ (ACI 318-08, Chapter 21.9) with the design parameters aspect ratio, horizontal web reinforcement ratio, vertical web reinforcement ratio, vertical boundary element reinforcement ratio, normalized axial force, and $f_c'$. In a well-specified model, the data points in Figure 6-15 through Figure 6-20 should be scattered without a trend in a shallow band around the value of 1.0 for the ratio of calculated to experimental peak shear strength. The figures indicate that model $V_{m1a}$ captures the peak shear strength accurately for all design variables over their corresponding ranges. The majority of the ratios associated with model $V_{m1a}$ are between 0.75 and 1.25 whereas the ratios for model $V_{n1}$ are widely scattered and range between 0.36 and 3.52. In Figure 6-15 through Figure 6-20, the data points corresponding to model $V_{n1}$ indicate signs of model under-specification and/or heterogeneous variance.

**Table 6-11 Coefficients calculated for the four models defined using Equations 6-6 through 6-8**

| Model ID | $\beta_1$ | $\beta_2$ | $\beta_3$ | $\beta_4$ | $\beta_5$ | $\beta_6$ | $\beta_7$ |
|---|---|---|---|---|---|---|---|
| $V_{m1a}$ | 1.29 | 0.50 | 0.26 | 0.04 | 0.20 | 0.39 | 0.58 |
| $V_{m1b}$ | 0.014 | 1.00 | 0.28 | 0.05 | 0.22 | 0.40 | 0.64 |
| $V_{m2}$ | 5.72 | 0.00 | | | | | |
| $V_{m3}$ | 6.79 | 0.91 | 0.20 | 0.64 | | | |

**Table 6-12 Statistics for the ratio of predicted to experimental peak shear strength obtained using five procedures investigated in Section 4 and the four additional models introduced in this section**

| | Mean | Median | St. Dev. | COV | Min | Max | % Over-Predictions | SSE[1] |
|---|---|---|---|---|---|---|---|---|
| $V_{n1}/V_{peak}$ | 1.09 | 0.82 | 0.660 | 0.607 | 0.362 | 3.522 | 34.5 | 176876 |
| $V_{n2}/V_{peak}$ | 0.96 | 0.79 | 0.515 | 0.536 | 0.371 | 2.740 | 29.3 | 112721 |
| $V_{n3}/V_{peak}$ | 1.26 | 1.16 | 0.488 | 0.389 | 0.561 | 2.517 | 65.5 | 132814 |
| $V_{n4}/V_{peak}$ | 1.38 | 1.26 | 0.475 | 0.345 | 0.751 | 2.731 | 77.6 | 116640 |
| $V_{n5}/V_{peak}$ | 1.07 | 0.99 | 0.327 | 0.306 | 0.619 | 2.233 | 50.0 | 45361 |
| $V_{m1a}/V_{peak}$ | 1.00 | 0.99 | 0.135 | 0.135 | 0.746 | 1.359 | 44.6 | 9837 |
| $V_{m1b}/V_{peak}$ | 1.00 | 0.99 | 0.138 | 0.138 | 0.741 | 1.347 | 44.6 | 10384 |
| $V_{m2}/V_{peak}$ | 1.00 | 0.94 | 0.303 | 0.303 | 0.587 | 2.119 | 41.4 | 48888 |
| $V_{m3}/V_{peak}$ | 1.00 | 0.97 | 0.213 | 0.213 | 0.574 | 1.601 | 44.8 | 20412 |

1. Error sum of squares.

Figure 6-21 presents the variation of experimental peak shear and peak shear calculated using model $V_{m1a}$ (normalized with total wall area and $\sqrt{f_c'}$) with aspect ratio. Figure 6-21 shows that normalized experimental peak shear strengths for the walls in the dataset are below the shear stress of $10\sqrt{f_c'}$, which is used as an upper limit in ACI 318-08 on peak shear strength.

As seen in Figure 6-21, the normalized peak shear strengths calculated using model $V_{m1a}$ do not exceed the shear stress limit of $10\sqrt{f_c'}$. The need for an upper shear stress limit is therefore inconclusive at this time since the procedure does not yield unconservative estimations of the peak shear strength for walls that developed relatively high shear stresses. The equation $V_{m1a}$ is

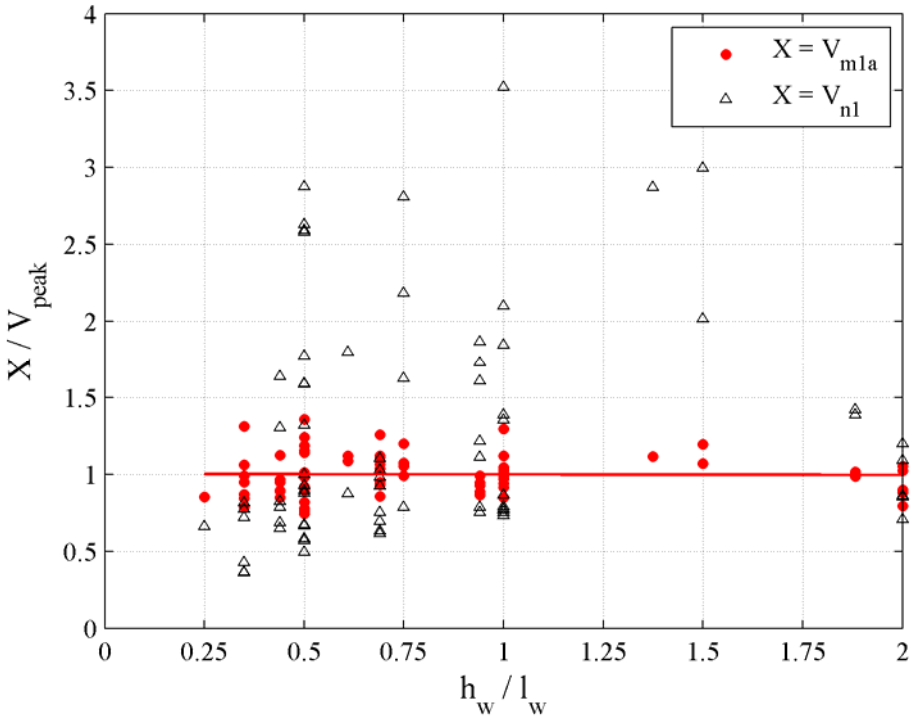


**Figure 6-15 Variation of the ratio of predicted shear strength to experimental peak shear strength with aspect ratio for $V_{n1}$ and $V_{m1a}$**

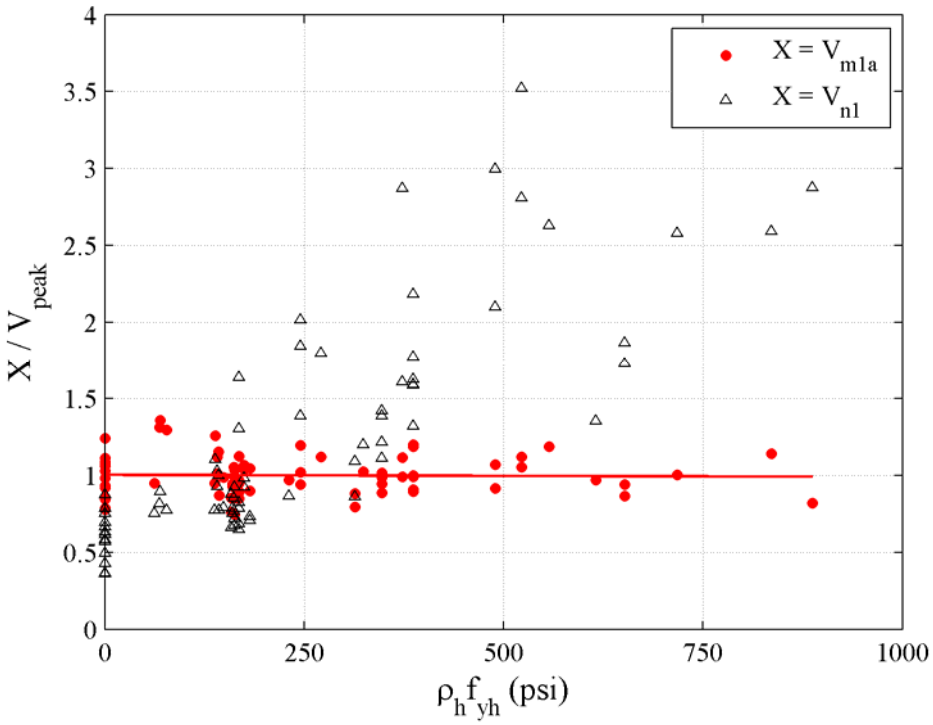


**Figure 6-16 Variation of the ratio of predicted shear strength to experimental peak shear strength with $\rho_h f_{yh}$ for $V_{n1}$ and $V_{m1a}$**

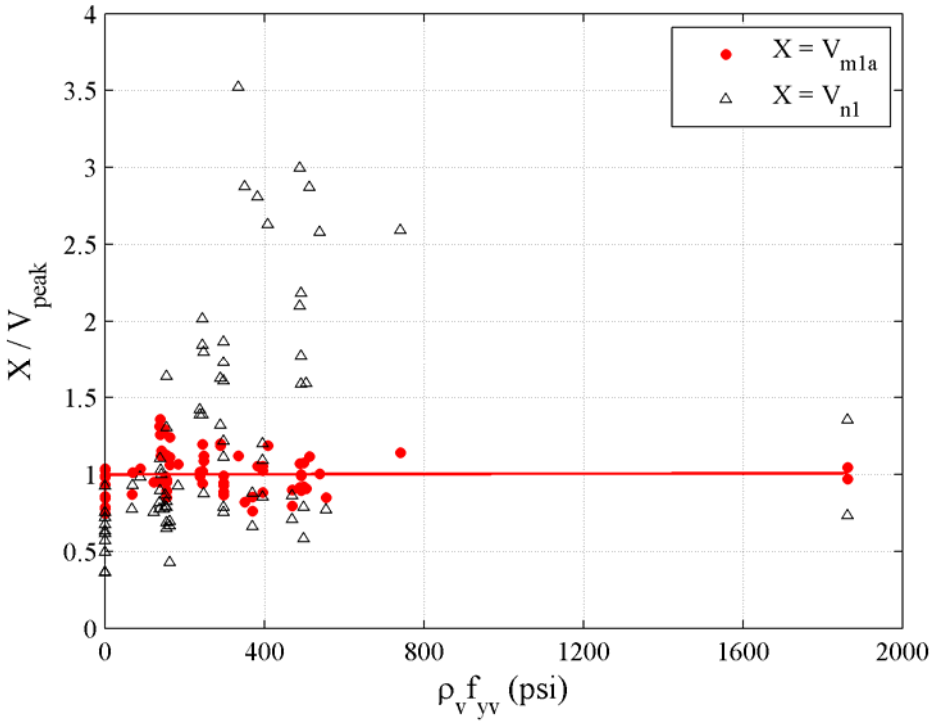


**Figure 6-17 Variation of the ratio of predicted shear strength to experimental peak shear strength with $\rho_v f_{yv}$ for $V_{n1}$ and $V_{m1a}$**

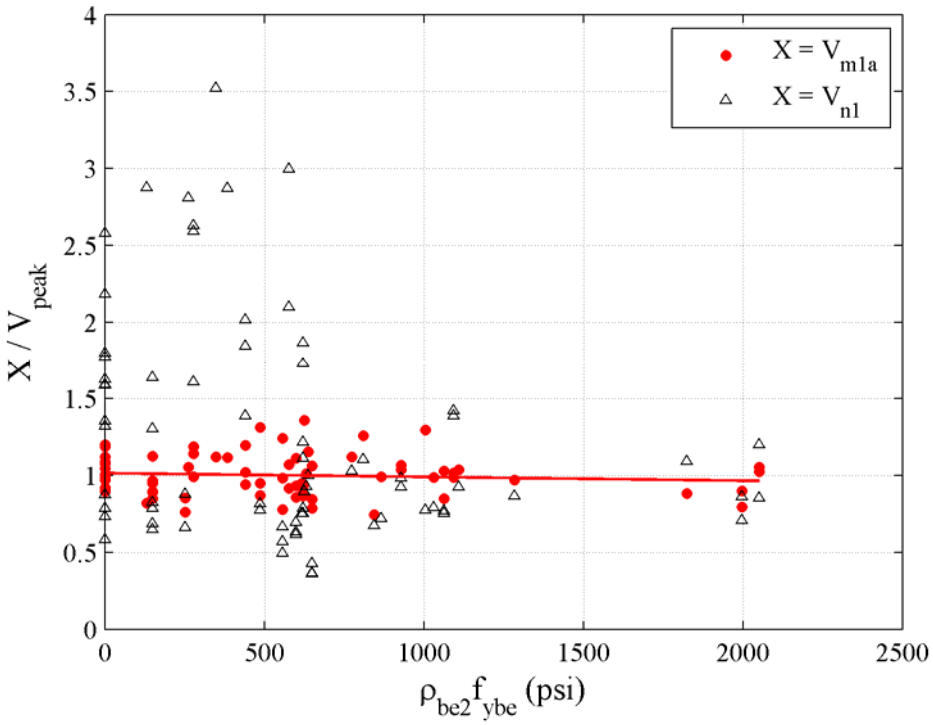


**Figure 6-18 Variation of the ratio of predicted shear strength to experimental peak shear strength with $\rho_{be2} f_{ybe}$ for $V_{n1}$ and $V_{m1a}$**

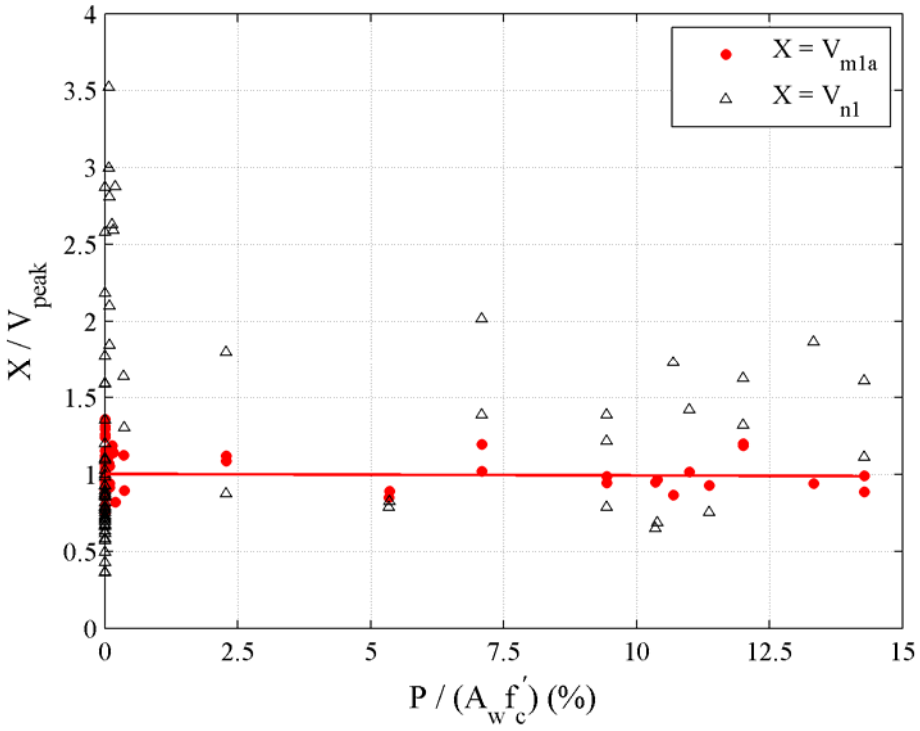


**Figure 6-19 Variation of the ratio of predicted shear strength to experimental peak shear strength with normalized axial force for $V_{n1}$ and $V_{m1a}$**

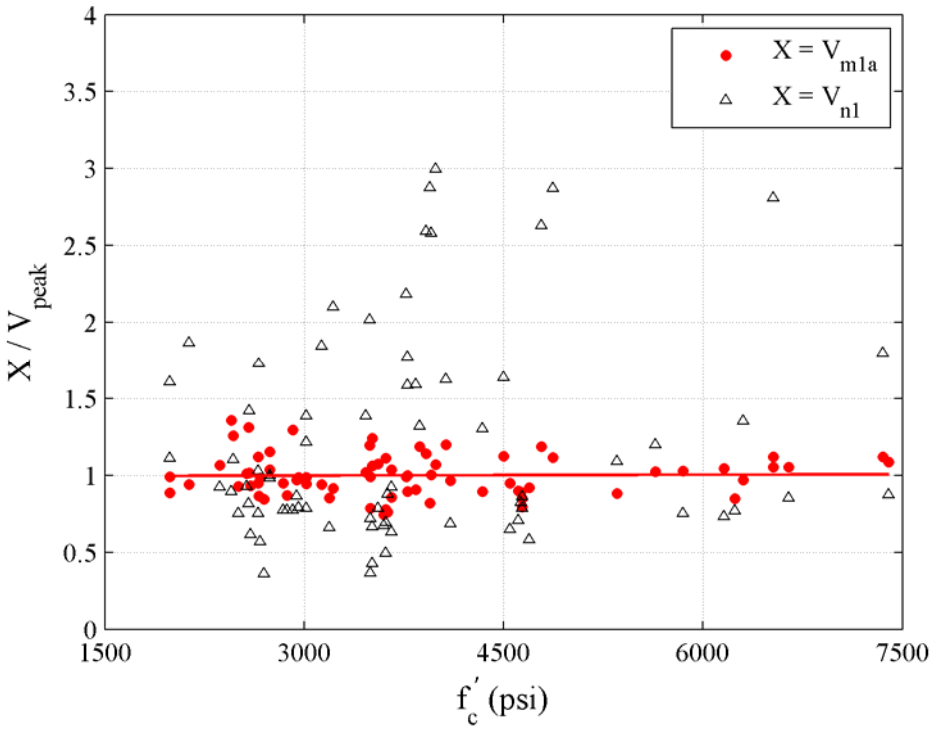


**Figure 6-20 Variation of the ratio of predicted shear strength to experimental peak shear strength with $f_c'$ for $V_{n1}$ and $V_{m1a}$**

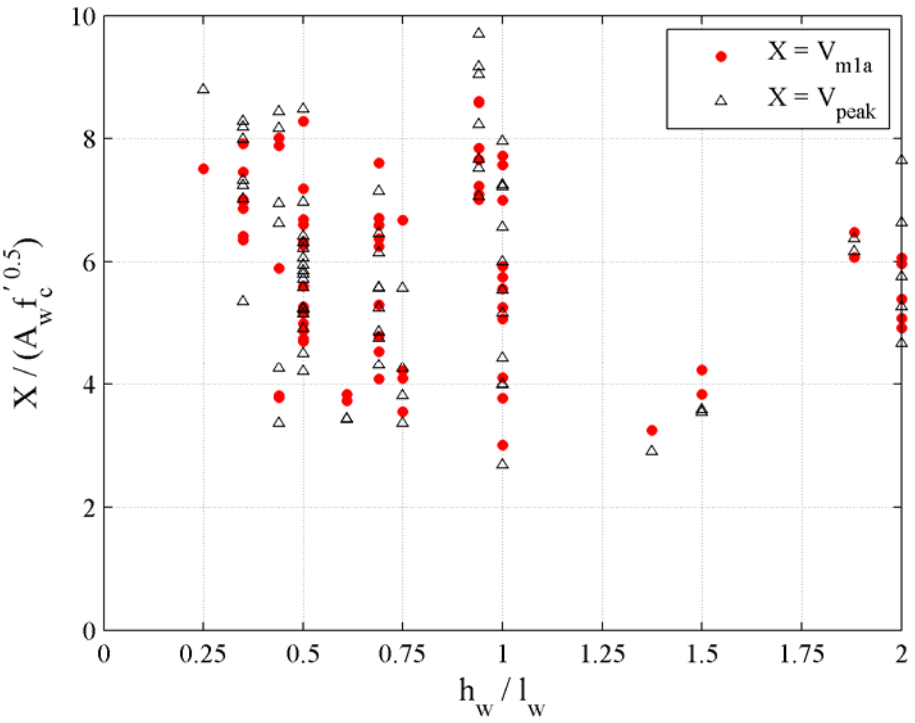


**Figure 6-21 Variation of the ratio of predicted ($V_{m1a}$) and experimental shear strengths (normalized using total wall area and $\sqrt{f_c'}$) with moment-to-shear ratio**

valid for the range of data it was created from, namely, between 0.25 and 2.0 for aspect ratio; 0 and 835 psi for $\rho_h f_{yh}$; 0 and 1862 psi for $\rho_v f_{yv}$; 0 and 2051 psi for $\rho_{be2} f_{ybe}$; 0 and 14.3% for $P / A_w f_c'$; and 1991 and 6643 psi for $f_c'$. Model $V_{m1a}$ predicts the experimental peak shear strength accurately for heavily reinforced walls and for walls that were subjected to relatively high axial forces, namely, $P / A_w f_c' > 0.10$.

## 6.4.5 Barbell and Flanged Walls

The finite element analysis results presented in Section 5 show that the peak shear strength of squat barbell walls can be predicted reasonably well using VecTor2. Therefore, it is assumed that barbells are fully effective in resisting shear in squat walls. In contrast, flanges are less stiff in the loading direction than barbells and an assumption of effective flange width is needed to calculate their peak shear strength. As shown in Section 5, peak shear strength was overestimated using VecTor2 for some walls with wide flanges. Herein, the peak shear model introduced in Equation 6-6 is optimized using different effective flange widths. The barbell and flanged wall datasets are merged since both cross-section types result in a similar history of damage in squat walls (i.e., shear cracking, concrete spalling and crushing, and diagonal compression failure). The barbell and flanged walls in the database failed mostly under diagonal compression, which may be attributed to the effect of the boundary elements that restrain the widening of the web cracks. Once the cracking in the web area is limited, the demand on the compression concrete struts increase and lateral load is transferred mostly through the compression struts until a

diagonal compression failure occurs. The analyses presented in this section are also performed using walls that were tested using a cantilever test fixture.

The calculation of the unknown coefficients for the peak shear model of Equation 6-6 for walls with boundary elements requires an assumption of effective flange width ($b_{eff}$) for the flanged walls. Herein, the model coefficients are obtained for four different effective flange widths. The first case assumes that flanges are fully effective in resisting peak shear ($b_{eff} = b_f$). For the other three cases, the effective flange width are assumed equal to fractions of wall height[5], namely, $h_w$, $h_w/2$, and $h_w/4$. In addition, the model coefficients are calculated by assuming a concrete contribution term as a function of either $\sqrt{f_c'}$ or $f_c'$ for each effective flange width case. Therefore, the performances of eight models presented in Table 6-13 are investigated to predict the peak shear strength of squat walls with boundary elements. In addition, two other peak shear models based on the procedures of Chapter 21.9 of ACI 318-08 (Equation 6-7) and ASCE 43-05 (Equation 6-8) are optimized similarly and the performance of the ten models is compared with the currently used procedures. The coefficients calculated using the barbell and flanged walls dataset for the ten models based on Equations 6-6 through 6-8 are presented in Table 6-14. Table 6-15 presents the statistics for the ratio of the predicted to experimental peak shear strength using the five procedures investigated in Section 4 and ten models created herein for squat walls with boundary elements. Table 6-16 presents similar statistics for the eight models created based on Equation 6-6 but the statistics are presented separately for barbell and flanged walls to investigate the performance of each model for each cross-section type. The data presented in Table 6-14 through Table 6-16 for models $V_{m1a}$ through $V_{m1h}$ is obtained by setting an upper limit of 0.15 on $P/A_t f_c'$ because a preliminary analysis showed that these models overestimated the peak shear strength of walls with $P/A_t f_c'$ of greater than 0.15.

As seen in Table 6-15, model $V_{m1e}$, which uses an effective flange width of $h_w/2$ and a concrete contribution term as a linear function of $f_c'$, provides the best estimates of the peak shear strength with a median ratio of predicted to experimental peak shear strength of 0.99 and a coefficient of variation of 0.11, which is the smallest among the models investigated. The model also yields the smallest error (or residual) sum of squares statistics among the ten models considered. Note that the best model for the rectangular wall dataset was obtained for the model that uses a concrete contribution term based on $\sqrt{f_c'}$, which is not the case for walls with boundary elements. The model that uses an effective flange width of $h_w/2$ and a concrete contribution term with $\sqrt{f_c'}$ ($V_{m1f}$) yields a coefficient of variation of 0.134, which is much higher than that observed for model $V_{m1e}$ (COV = 0.11). Figure 6-22 shows the variation of ratio of predicted to experimental peak shear strength with $f_c'$ for models $V_{m1e}$ and $V_{m1f}$. The use of a concrete contribution term based on $\sqrt{f_c'}$ underestimates the peak shear strength of walls with

[5]A similar approach is used in ACI 318-08 to calculate the effective flange widths for flexure and axial load design. In ACI 318-08, unless a more detailed analysis is performed, the effective flange widths are required to be extended from the face of the web to the smaller of one-half the distance to an adjacent wall web and 25% of the total wall height.

**Table 6-13 Effective flange width and concrete contribution term specifications for the eight models used to predict the peak shear strength of squat walls with boundary elements**

| Model ID | $b_{eff}$ | $\beta_2$ |
|---|---|---|
| $V_{m1a}$ | $b_f$ | 1.0 |
| $V_{m1b}$ | $b_f$ | 0.5 |
| $V_{m1c}$ | $h_w$ | 1.0 |
| $V_{m1d}$ | $h_w$ | 0.5 |
| $V_{m1e}$ | $h_w / 2$ | 1.0 |
| $V_{m1f}$ | $h_w / 2$ | 0.5 |
| $V_{m1g}$ | $h_w / 4$ | 1.0 |
| $V_{m1h}$ | $h_w / 4$ | 0.5 |

**Table 6-14 Coefficients calculated for the eleven models defined using Equations 6-6 through 6-8**

| Model ID | $\beta_1$ | $\beta_2$ | $\beta_3$ | $\beta_4$ | $\beta_5$ | $\beta_6$ | $\beta_7$ |
|---|---|---|---|---|---|---|---|
| $V_{m1a}$ | 0.04 | 1.0 | 0.30 | 0.12 | 0.12 | 0.37 | 0.51 |
| $V_{m1b}$ | 2.08 | 0.5 | 0.29 | 0.18 | 0.11 | 0.39 | 0.57 |
| $V_{m1c}$ | 0.04 | 1.0 | 0.34 | 0.05 | 0.13 | 0.35 | 0.49 |
| $V_{m1d}$ | 2.49 | 0.5 | 0.33 | 0.09 | 0.11 | 0.36 | 0.53 |
| $V_{m1e}$ | 0.04 | 1.0 | 0.43 | -0.09 | 0.14 | 0.34 | 0.48 |
| $V_{m1f}$ | 2.91 | 0.5 | 0.43 | -0.06 | 0.11 | 0.35 | 0.51 |
| $V_{m1g}$ | 0.05 | 1.0 | 0.52 | -0.12 | 0.13 | 0.32 | 0.48 |
| $V_{m1h}$ | 3.21 | 0.5 | 0.52 | -0.09 | 0.09 | 0.33 | 0.51 |
| $V_{m2}$ | 10.70 | 0.22 | | | | | |
| $V_{m3}$ | 17.42 | 14.77 | 0.93 | 0.56 | | | |

higher concrete strength. Model $V_{m1e}$ successfully predicts peak shear strength across a wide range of concrete compressive strength. As seen in Table 6-15, the optimized ACI 318-08 ($V_{m2}$) and ASCE 43-05 ($V_{m3}$) procedures perform better than the codified versions ($V_{n1}$ and $V_{n4}$, respectively) but are poorer than that of model $V_{m1e}$.

**Table 6-15 Statistics for the ratio of predicted to experimental peak shear strength obtained using five procedures investigated in Section 4, eight models based on Equation 6-6, and two models based on Equations 6-7 and 6-8**

| | Mean | Median | St. Dev. | COV | Min | Max | % Over-Predictions | SSE |
|---|---|---|---|---|---|---|---|---|
| $V_{n1}/V_{peak}$ | 0.86 | 0.82 | 0.370 | 0.429 | 0.182 | 2.984 | 28.8 | 3971144 |
| $V_{n2}/V_{peak}$ | 0.79 | 0.76 | 0.283 | 0.359 | 0.207 | 2.432 | 21.6 | 4953880 |
| $V_{n3}/V_{peak}$ | 0.80 | 0.79 | 0.195 | 0.243 | 0.404 | 1.389 | 13.1 | 3980676 |
| $V_{n4}/V_{peak}$ | 0.89 | 0.86 | 0.223 | 0.251 | 0.467 | 1.462 | 30.1 | 2736754 |
| $V_{n5}/V_{peak}$ | 0.52 | 0.48 | 0.165 | 0.317 | 0.269 | 1.026 | 0.7 | 9638110 |
| $V_{m1a}/V_{peak}$ | 1.00 | 0.98 | 0.151 | 0.151 | 0.725 | 1.688 | 46.4 | 548395 |
| $V_{m1b}/V_{peak}$ | 1.00 | 1.00 | 0.173 | 0.173 | 0.702 | 1.860 | 48.4 | 649504 |
| $V_{m1c}/V_{peak}$ | 1.00 | 0.99 | 0.130 | 0.130 | 0.723 | 1.445 | 47.7 | 482817 |
| $V_{m1d}/V_{peak}$ | 1.00 | 1.00 | 0.151 | 0.151 | 0.704 | 1.625 | 49.0 | 575108 |
| $V_{m1e}/V_{peak}$ | 1.00 | 0.99 | 0.110 | 0.110 | 0.705 | 1.264 | 44.4 | 432125 |
| $V_{m1f}/V_{peak}$ | 1.00 | 0.99 | 0.134 | 0.134 | 0.680 | 1.383 | 43.8 | 545335 |
| $V_{m1g}/V_{peak}$ | 1.00 | 0.99 | 0.129 | 0.129 | 0.672 | 1.344 | 45.8 | 597209 |
| $V_{m1h}/V_{peak}$ | 1.00 | 0.98 | 0.151 | 0.151 | 0.649 | 1.428 | 43.1 | 742765 |
| $V_{m2}/V_{peak}$ | 1.00 | 0.92 | 0.307 | 0.307 | 0.544 | 2.379 | 35.3 | 1906717 |
| $V_{m3}/V_{peak}$ | 1.00 | 0.95 | 0.216 | 0.216 | 0.581 | 1.600 | 39.9 | 886590 |

Another interesting observation is that $\beta_4$ for model $V_{m1e}$, which is related to the contribution of horizontal web reinforcement ratio to peak shear strength, is less than zero. A relatively small value for $\beta_4$ may be expected as seen in the peak shear model created for rectangular walls and the numerical experimentation presented in Section 6.3. However, a negative value may be a result of either experimental variability and/or multicollinearity[6] between the vertical and horizontal web reinforcement ratios since most walls were constructed using similar reinforcement ratios in the horizontal and vertical directions. Therefore, the term associated with the contribution of horizontal web reinforcement to peak shear strength is eliminated and the remaining coefficients are recalculated in the next section that presents simplified versions of the peak shear strength models suitable for implementation in codes and standards.

The statistics presented in Table 6-16 show that assumption of fully effective flanges on average results in an overestimation of the experimental peak shear strengths for flanged walls and

[6] Intercorrelation between the predictor variables.

**Table 6-16 Statistics for the ratio of predicted to experimental peak shear strength obtained using the eight models based on Equation 6-6**

| | Cross-Section | Mean | Median | St. Dev. | COV | Min | Max | % Over-Predictions |
|---|---|---|---|---|---|---|---|---|
| $V_{m1a}/V_{peak}$ | Barbell | 0.95 | 0.94 | 0.105 | 0.111 | 0.728 | 1.191 | 27.8 |
| | Flanged | 1.05 | 1.05 | 0.172 | 0.163 | 0.725 | 1.688 | 66.2 |
| $V_{m1b}/V_{peak}$ | Barbell | 0.96 | 0.95 | 0.142 | 0.148 | 0.702 | 1.284 | 35.4 |
| | Flanged | 1.04 | 1.03 | 0.193 | 0.185 | 0.712 | 1.860 | 62.2 |
| $V_{m1c}/V_{peak}$ | Barbell | 0.95 | 0.94 | 0.102 | 0.106 | 0.738 | 1.183 | 27.8 |
| | Flanged | 1.05 | 1.05 | 0.139 | 0.132 | 0.723 | 1.445 | 68.9 |
| $V_{m1d}/V_{peak}$ | Barbell | 0.97 | 0.95 | 0.136 | 0.141 | 0.713 | 1.268 | 34.2 |
| | Flanged | 1.04 | 1.04 | 0.157 | 0.152 | 0.704 | 1.625 | 64.9 |
| $V_{m1e}/V_{peak}$ | Barbell | 0.99 | 0.98 | 0.106 | 0.106 | 0.780 | 1.261 | 40.5 |
| | Flanged | 1.01 | 1.00 | 0.115 | 0.114 | 0.705 | 1.264 | 48.6 |
| $V_{m1f}/V_{peak}$ | Barbell | 1.00 | 0.98 | 0.141 | 0.141 | 0.750 | 1.342 | 43.0 |
| | Flanged | 1.00 | 0.99 | 0.126 | 0.126 | 0.680 | 1.383 | 44.6 |
| $V_{m1g}/V_{peak}$ | Barbell | 1.05 | 1.04 | 0.109 | 0.104 | 0.819 | 1.344 | 63.3 |
| | Flanged | 0.95 | 0.95 | 0.130 | 0.137 | 0.672 | 1.246 | 27.0 |
| $V_{m1h}/V_{peak}$ | Barbell | 1.05 | 1.04 | 0.145 | 0.138 | 0.790 | 1.428 | 57.0 |
| | Flanged | 0.95 | 0.95 | 0.138 | 0.146 | 0.649 | 1.339 | 28.4 |

underestimation of those with barbells (see rows 1 through 4 in Table 6-16). In contrast, an assumption of an effective flange width of $h_w/4$ results on average in an underestimation of the experimental peak shear strengths for flanged walls and overestimation of those of barbells (see rows 13 through 16 in Table 6-16). The assumption of an effective flange width of $h_w/2$ for flanged walls results on average in an accurate prediction of the experimental peak shear strength.

Figure 6-23 through Figure 6-28 present the variation of the ratio of calculated to experimental shear strengths for model $V_{m1e}$ with aspect ratio, $f_c'$, normalized axial force, horizontal web reinforcement ratio, vertical web reinforcement ratio, and vertical boundary element reinforcement ratio, respectively. As seen in the figures, the data points are generally scattered in a shallow band around 1.0 for both cross-section types. The majority of the ratios associated with model $V_{m1e}$ are between 0.75 and 1.25. The observed trends in the figures are generally weak indicating that the model can successfully simulate the peak shear strength of squat walls with

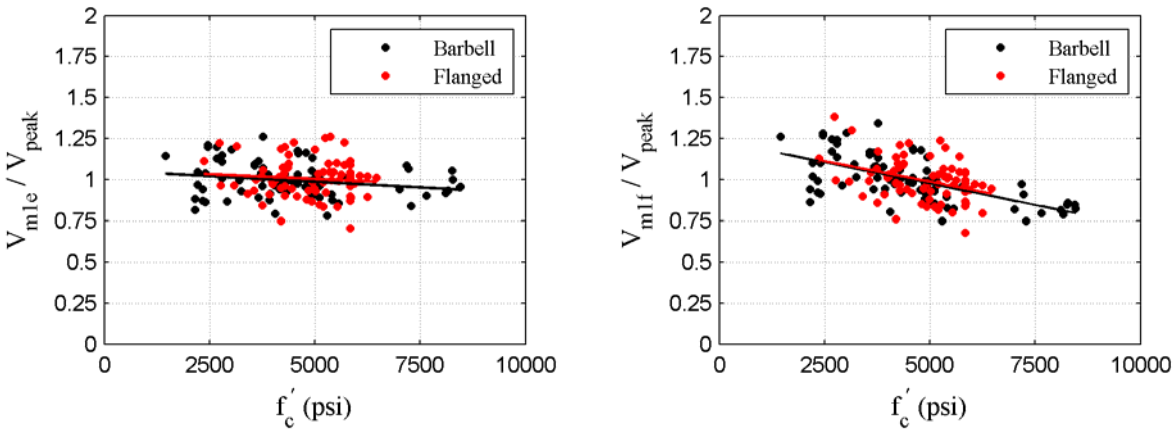


**a) Model $V_{m1e}$** **b) Model $V_{m1f}$**

**Figure 6-22 Variation of ratio of predicted shear strength to experimental peak shear strength with $f_c'$ for $V_{m1e}$ and $V_{m1f}$ procedures**

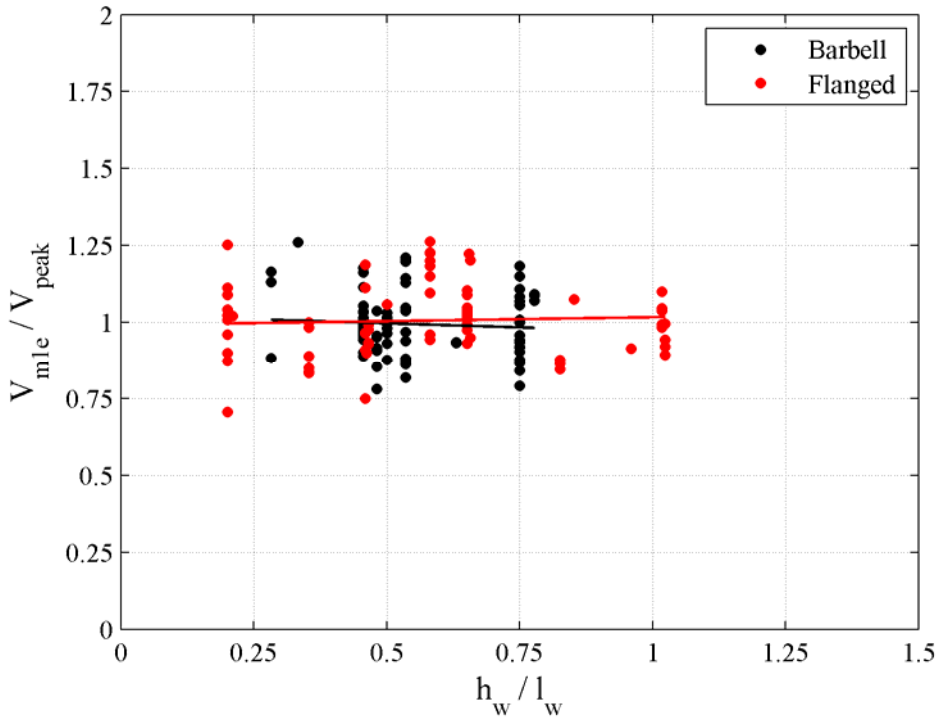


**Figure 6-23 Variation of the ratio of predicted shear strength to experimental peak shear strength with aspect ratio for model $V_{m1e}$**

boundary elements within the ranges of the design variables considered. Figure 6-29 and Figure 6-30 present the variation of the ratio of predicted to experimental shear strength with $A_{be} / A_t$ and $b_f / h_w$, respectively, where $A_{be} / A_t$ is the ratio of the total boundary element area to total

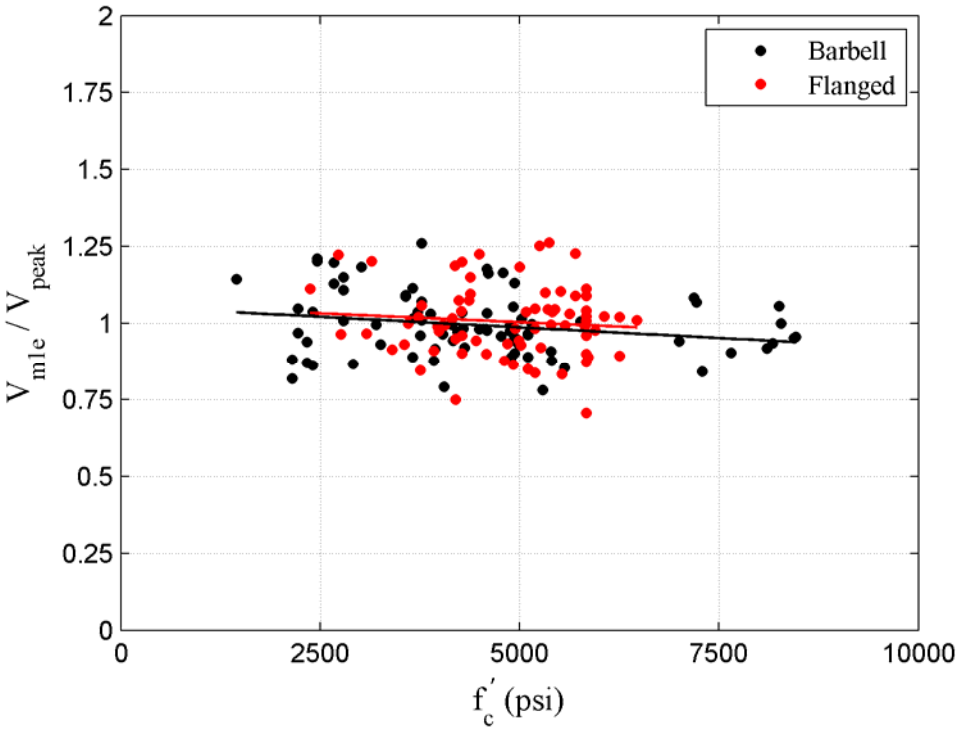


**Figure 6-24 Variation of the ratio of predicted shear strength to experimental peak shear strength with $f_c'$ for model $V_{m1e}$**

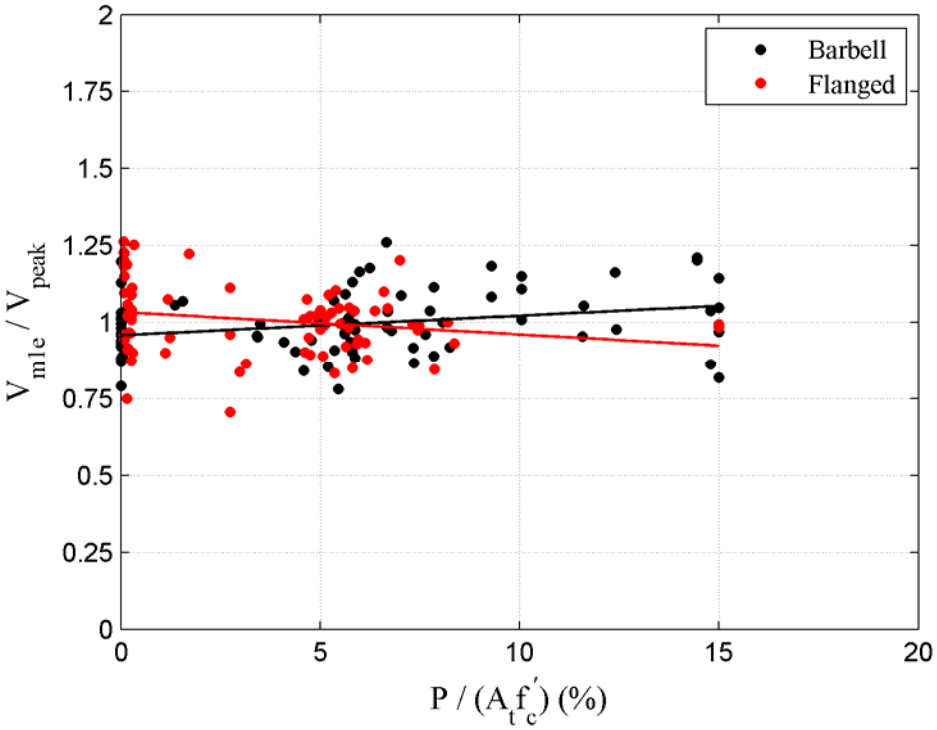


**Figure 6-25 Variation of the ratio of predicted shear strength to experimental peak shear strength with normalized axial force for model $V_{m1e}$**

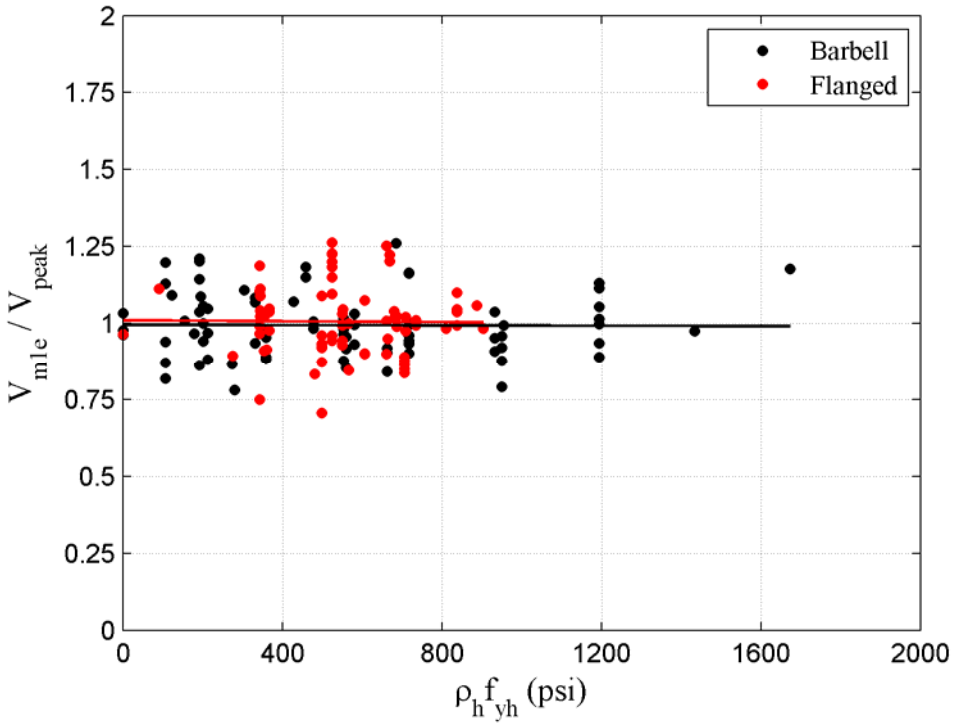


**Figure 6-26 Variation of the ratio of predicted shear strength to experimental peak shear strength with $\rho_h f_{yh}$ for model $V_{m1e}$**

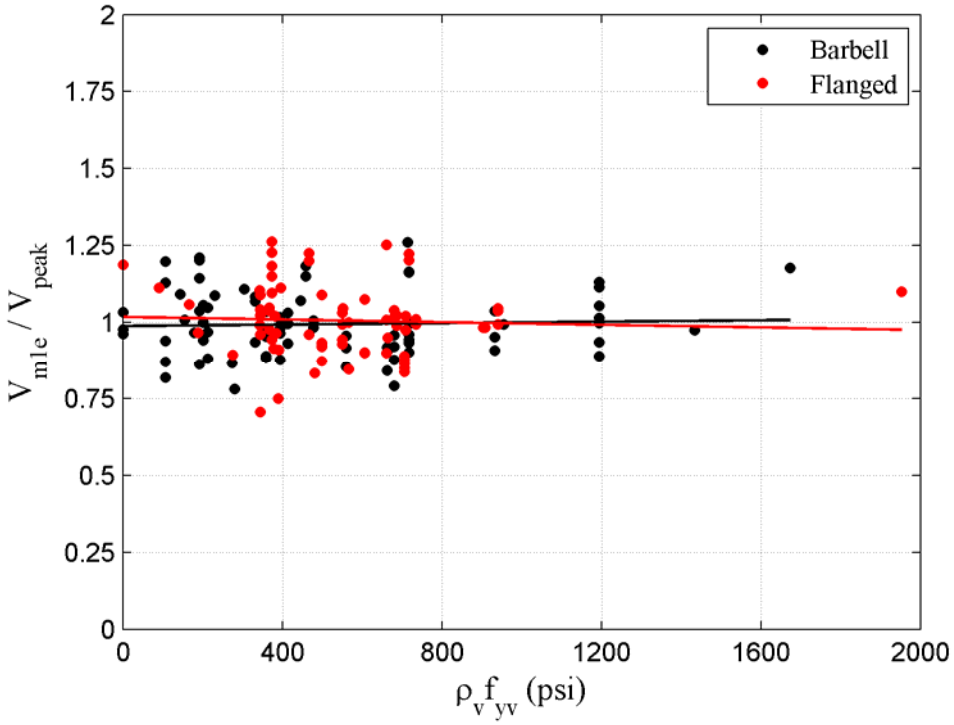


**Figure 6-27 Variation of the ratio of predicted shear strength to experimental peak shear strength with $\rho_v f_{yv}$ for model $V_{m1e}$**

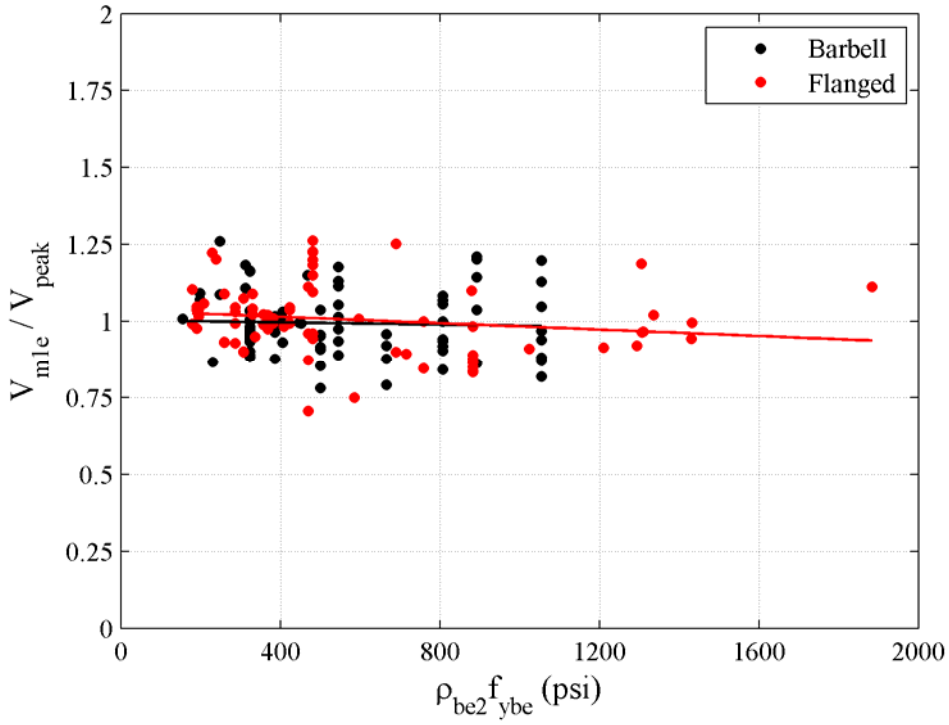


**Figure 6-28 Variation of the ratio of predicted shear strength to experimental peak shear strength with $\rho_{be2} f_{ybe}$ for model $V_{m1e}$**

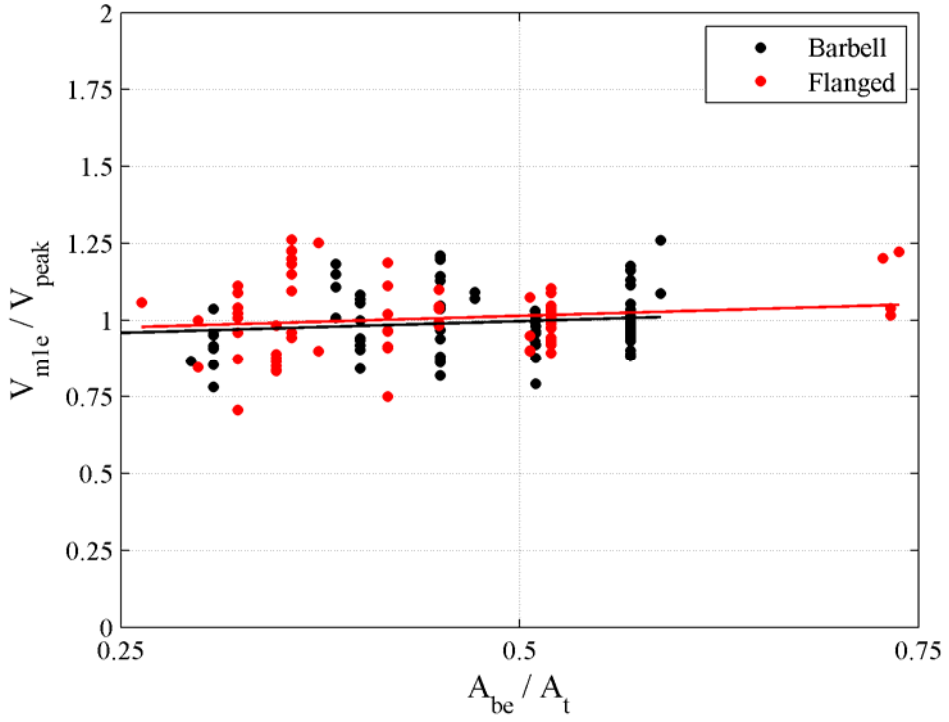


**Figure 6-29 Variation of the ratio of predicted shear strength to experimental peak shear strength with $A_{be} / A_t$ for model $V_{m1e}$**

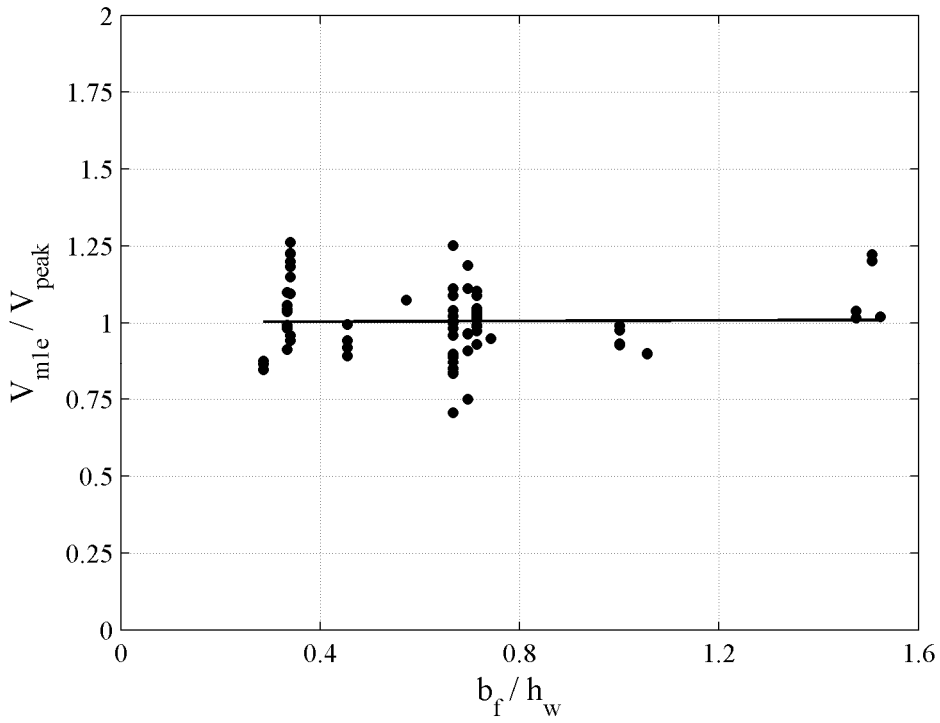


**Figure 6-30 Variation of the ratio of predicted shear strength to experimental peak shear strength with $b_f / h_w$ for model $V_{m1e}$ and flanged walls**

wall area[7]. The weak trends seen in Figure 6-29 indicate that the model can successfully account for the effect of the area of barbells or flanges on peak shear strength. The data of Figure 6-30, which is relevant only to squat flanged walls, indicate that the assumption of an effective flange width of $h_w / 2$ is reasonable. As seen in the figure, the ratios of predicted to experimental peak shear strengths do not exhibit a trend with respect to the ratio of flange width to wall height.

Figure 6-31 presents the variation of experimental peak shear and peak shear calculated using model $V_{m1e}$ (normalized with total wall area and $\sqrt{f_c'}$) with aspect ratio. As seen in the figure and for similar to rectangular walls, the need for an upper shear stress limit on model $V_{m1e}$ is unclear at this time since the procedure did not yield unconservative estimations of the peak shear strength for walls that developed relatively high shear stresses. Equation $V_{m1e}$ is valid for the range of data it was created from, namely, between 0.20 and 1.02 for aspect ratio; 0 and 1672 psi for $\rho_h f_{yh}$; 0 and 1953 psi for $\rho_v f_{yv}$; and 155 and 1884 psi for $\rho_{be2} f_{ybe}$. The model $V_{m1e}$ yielded accurate predictions of the experimental peak shear strength for heavily reinforced walls.

## 6.5 Empirical Equations for Peak Shear Strength

The empirical equations of Section 6.4 provide substantially better estimations of the peak shear strength of squat reinforced concrete walls than the procedures in codes, standards, and the literature. In this section, the optimized peak shear-strength equations of Section 6.4 are

[7] Total wall area is calculated using an effective flange width of one-half the wall height for walls with flanges.

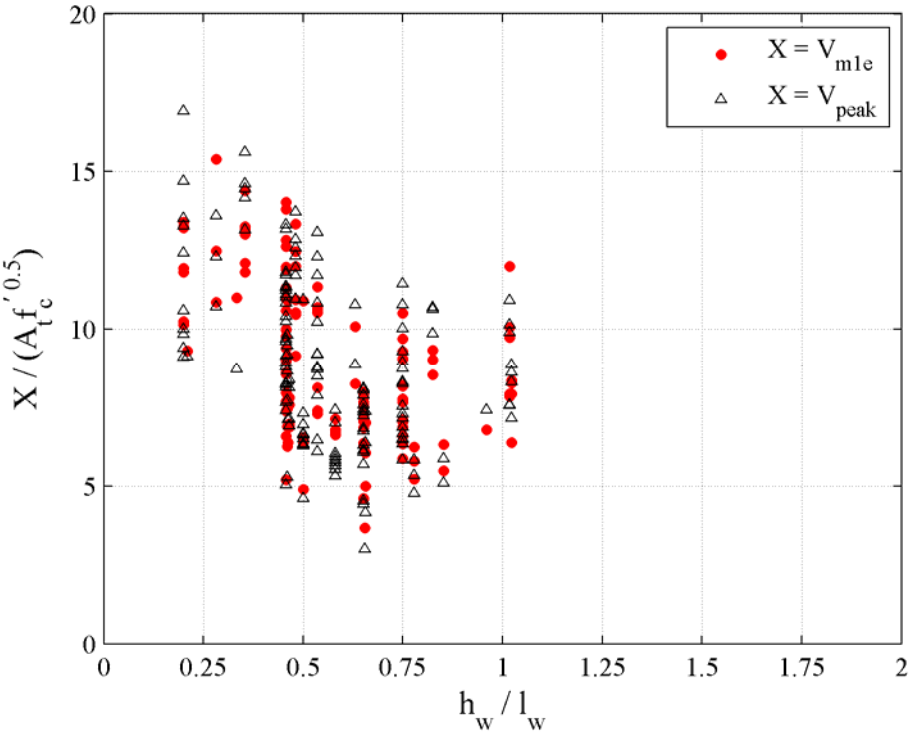


**Figure 6-31 Variation of the ratio of predicted ($V_{m1e}$) and experimental shear strengths (normalized using total wall area and $\sqrt{f_c'}$) with moment-to-shear ratio**

simplified with a little sacrifice in performance into a form suitable for application in a design office. In Section 6.4, it was shown that model $V_{m1a}$ performed best for rectangular walls and model $V_{m1e}$ performed best for walls with barbells or flanges and so these models are used as the basis for the code-oriented design equations. To simplify these equations, two additional changes are made to model $V_{m1a}$ for rectangular walls and model $V_{m1e}$ for walls with boundary elements:

1. The numerical analyses performed using VecTor2 in Section 6.3 and the evaluation of available data (see Section 6.4) show that the effect of horizontal web reinforcement ratio on peak shear strength is modest in comparison with the effects of other variables. Accordingly, a term associated with horizontal web reinforcement ratio is not included in the equations for walls with either rectangular cross-sections or with boundary elements.
2. The coefficient $\beta_7$, which is associated with aspect ratio in Equation 6-6 [i.e., $(h_w / l_w)^{\beta_7}$] is 0.58 for model $V_{m1a}$ for rectangular walls and 0.48 for model $V_{m1e}$ for walls with boundary elements was. This coefficient is set equal to 0.5 below.

The proposed peak shear strength equation for shear-critical rectangular walls with an aspect ratio of 1.0 or less ($V_{rec}$) is presented in Equation 6-9:

$$V_{rec} = \frac{1.5\sqrt{f_c'}A_w + 0.25F_{vw} + 0.20F_{vbe} + 0.40P}{\sqrt{h_w / l_w}} \quad (6\text{-}9)$$

where $A_w$ is the wall area, $f_c'$ is the compressive strength of concrete, $F_{vw}$ is the force attributed to vertical web reinforcement (calculated as the product of area of vertical web reinforcement with reinforcement yield stress), $F_{be}$ is the force attributed to boundary element reinforcement (calculated as the product of total area of vertical boundary element reinforcement at each end of the wall and the reinforcement yield stress), $P$ is the axial force, $h_w$ is the wall height, and $l_w$ is the wall length.

The performance of models $V_{m1a}$ and $V_{rec}$ is compared in Table 6-17; the coefficients of variation for the two models are similar.

**Table 6-17 Statistics for the ratio of predicted to experimental peak shear strengths obtained using models $V_{m1a}$ and $V_{rec}$**

| | Mean | Median | St. Dev. | COV | Min | Max |
|---|---|---|---|---|---|---|
| $V_{m1a} / V_{peak}$ | 1.00 | 0.99 | 0.135 | 0.135 | 0.746 | 1.359 |
| $V_{rec} / V_{peak}$ | 0.98 | 0.95 | 0.135 | 0.138 | 0.720 | 1.319 |

Consider now Figure 6-21. The experimentally measured peak shear strength is always less than $10\sqrt{f_c'}A_w$ for rectangular walls and so an upper shear stress limit of $10\sqrt{f_c'}A_w$ is imposed on Equation 6-9.

The proposed peak shear strength equation for symmetric shear-critical walls with boundary elements and an aspect ratio of 1.0 or less ($V_{BE}$) is presented in Equation 6-10.

$$V_{BE} = \frac{\left(0.04 f_c'\right) A_t + 0.40 F_{vw} + 0.15 F_{vbe} + 0.35 P}{\sqrt{h_w / l_w}} \tag{6-10}$$

where $A_t$ is the total wall area for barbell walls and the effective area for flanged walls (equal to the sum of the area of the web plus twice the effective flange area, calculated as the product of effective flange width, equal to one-half the wall height minus the web thickness, and the flange thickness). Equation 6-10 can be applied to all barbell walls and flanged walls for which $A_t / A_w \geq 1.25$. For design of flanged walls with $1.0 \leq A_t / A_w \leq 1.25$, the peak shear strength should be taken as the smaller of the values calculated using Equation 6-9 and 6-10. Equation 6-10 is a simplification of model $V_{m1e}$, but the loss of performance is only modest (see Table 6-18).

Figure 6-31 shows that the experimentally measured peak shear strength of walls with barbells and flanges is generally less than $15\sqrt{f_c'}A_t$. Accordingly, $15\sqrt{f_c'}A_t$ is an appropriate upper limit on Equation 6-10 until additional data are available to support an alternative limit.

The experimental data used to develop the peak shear-strength equations for squat walls was based on tests of walls loaded in the plane of the web. For walls with flanges or orthogonal walls sharing common boundary elements, where the flanges or boundary elements are subjected to

**Table 6-18 Statistics for the ratio of predicted to experimental peak shear strengths obtained using models $V_{m1e}$ and $V_{BE}$**

| | Mean | Median | St. Dev. | COV | Min | Max |
|---|---|---|---|---|---|---|
| $V_{m1e} / V_{peak}$ | 1.00 | 0.99 | 0.110 | 0.110 | 0.705 | 1.264 |
| $V_{BE} / V_{peak}$ | 1.02 | 1.02 | 0.114 | 0.112 | 0.721 | 1.292 |

loading perpendicular to the web, the equations must be used with care because orthogonal loading will generally degrade the integrity of the boundary elements and may effectively reduce the cross-section to a rectangular shape. Large-scale test data are needed. In the interim, Equation 6-10 should only be used for walls with flanges if loading in the plane of the flanges does not result in damage. Otherwise, Equation 6-9 should be used.

# 7 MACRO HYSTERETIC MODELING OF SQUAT REINFORCED CONCRETE WALLS

## 7.1 Introduction

Section 5 of this report introduced finite element models of squat reinforced concrete walls and presented strategies and made recommendations for modeling such walls under monotonic and cyclic (earthquake-type) loading. Detailed finite element models of such walls are appropriate for research but are not appropriate for either design or performance-based assessment of buildings and infrastructure that include squat walls. For design and/or performance assessment, macro-level hysteretic models of building components are generally needed, where the macro models reproduce cyclic force-displacement relationships at the story level.

A robust (empirical) macro model for a squat or shear-critical squat wall should be able to reproduce monotonic and cyclic response with reasonable accuracy. Unfortunately, empirical macro models generally include a large number of parameters, most of which have to be determined by calibration of experimental data. Although physics-based models are preferable to empirical models, a physics-based representation of squat wall response is unavailable at this time and large-scale testing of squat wall specimens will be required to provide the required knowledge and technical basis.

Macro models of reinforced concrete walls have been proposed by many researchers, including Kabeyasawa et al. (1982), Vulcano and Bertero (1987), Sozen and Moehle (1993), and Orakcal et al. (2006) among others. Many of these models include combinations of nonlinear springs to accommodate flexural, shear, and sliding responses. Degradation in shear resistance with repeated cycling has been the major challenge facing the modelers. The simplest macro model is the piece-wise linear representation of the shearing force-horizontal displacement relationships (also known as a backbone or skeleton curve). ASCE 41-06 [ASCE (2007)] includes the backbone shearing force-horizontal displacement relationship for the cyclic response of squat walls presented in Figure 1-8, where the control points are for yielding (point B) and peak shear (point C). Wallace (2007) recommended changes to this cyclic loading backbone relationship as presented in Figure 2-1, where an additional control point was added to represent cracking (point F). The success of these backbone curves in modeling wall behavior is directly related to accurate prediction of their control points. A more detailed review of macro models used for reinforced concrete walls is presented in Sections 1 and 2.

Herein, the objective is to simulate the load (shearing force)-(horizontal) displacement response of a limited number of squat walls using a hysteretic macro model. Significant effort has been expended developing hysteretic models, with key contributions from Bouc (1967), Takeda et al. (1970), Wen (1976), Sivaselvan and Reinhorn (2000), and Ibarra et al. (2005). The hysteretic model proposed by Ibarra et al. (2005) is used in this study. This model includes energy-controlled strength and stiffness degradation under cyclic loading and can simulate successfully the response of steel [Lignos (2008)] and reinforced concrete components under cyclic loading. Values of model parameters (i.e., control points associated with the backbone curve and hysteretic energy capacities for deterioration modes) are obtained for squat walls by calibration of a small set of test data mined from the database of Section 3 and Appendix A.

Ibarra et al. (2005) modified three traditional hysteretic models, namely, *bilinear*, *peak-oriented*, and *pinching* to incorporate four cyclic deterioration modes: *basic strength*, *post-capping strength*, *unloading stiffness*, and *accelerated stiffness*. An energy-based approach is used to implement these deterioration modes. The (simple) bilinear model is based on bilinear hysteretic rules with kinematic hardening. The peak-oriented model uses the hysteretic rules proposed by Clough and Johnston (1966) as later modified by Mahin and Bertero (1976). The pinching model is similar to the peak-oriented model except that the reloading curve includes two segments to simulate pinched hysteretic behavior that is a characteristic of squat walls. For this reason, the pinching model is selected for the analyses performed in this section. This model is referred to as the *Ibarra-Krawinkler pinching* (IKP) model hereafter and is introduced in the following section.

## 7.2 Ibarra-Krawinkler Pinching (IKP) Model

### 7.2.1 Backbone Curve

The three Ibarra et al. (2005) hysteretic models are defined using one backbone force-displacement curve, which is presented in Figure 7-1. This backbone curve is piece-wise linear and includes three control points, which correspond to changes in wall stiffness with increasing displacement or drift. The first control point is associated with yielding, the second corresponds to peak strength, and the third point is associated with residual strength.

In Figure 7-1, $K_e$ is the elastic stiffness, $F_y$ is the yield strength, $F_c$ is the peak strength, $F_r$ ($\lambda F_y$) is the residual strength, $K_s$ ($\alpha_s K_e$) is the post-yielding stiffness, $K_c$ ($\alpha_c K_e$) is the (negative) post-capping stiffness, $\delta_y$ is the displacement at yield, $\delta_c$ is the displacement at peak strength, and $\delta_r$ is the displacement beyond which lateral strength is assumed equal to the residual strength ($F_r$).

The backbone curve for the IKP model aims to simulate the load-displacement response of a component subjected to monotonically increasing displacement. Some of the parameters can be predicted analytically (e.g., elastic stiffness, peak shear strength) but others require calibration using experimental data (e.g., yield strength).

### 7.2.2 Model Rules – No Cyclic Deterioration

Figure 7-2 presents a load-displacement relationship constructed following the IKP model. In this figure (and in Figure 7-3 through Figure 7-6), the dashed lines represent the backbone curve. As shown in Figure 7-2, the load-displacement relationship follows the backbone curve up to the displacement at which the component is unloaded (point A). In the absence of deterioration, the unloading stiffness is equal to the elastic stiffness ($K_e$). The reloading part of the load-displacement relationship consists of two segments with stiffnesses $K_{rel\_a}$ and $K_{rel\_b}$. Reloading (represented by stiffness $K_{rel\_a}$) is directed initially towards a control point that is a function of the maximum force (e.g., $F_{1+}$ in Figure 7-2) and the maximum residual displacement (e.g., $\delta_{r1+}$ in Figure 7-2) in the same quadrant of the previous cycle. As seen in Figure 7-2, the control point associated with the pinching region (point E) is established using the displacement coordinate

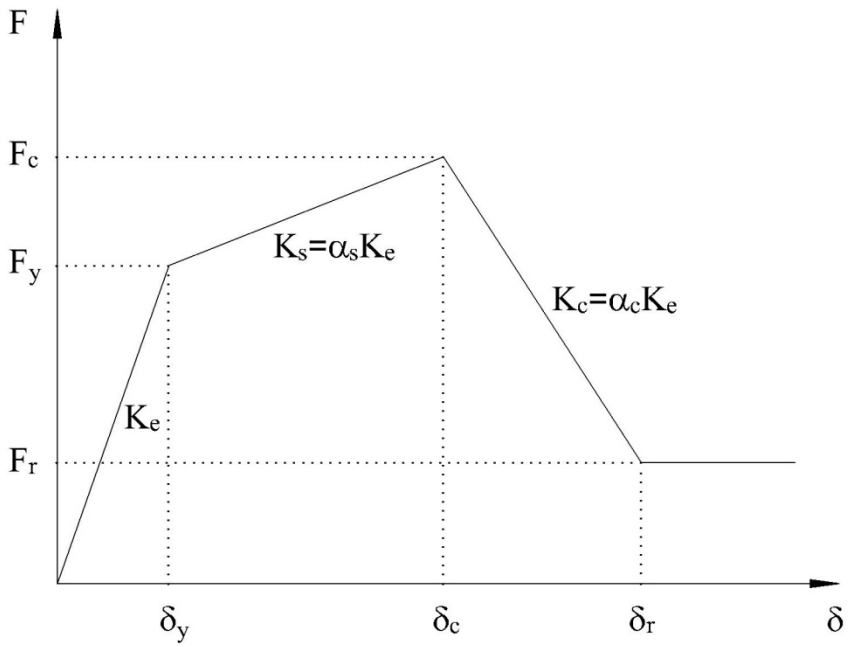


**Figure 7-1 Backbone curve for the Ibarra et al. (2005) hysteretic models**

$(1-\kappa_D)\delta_{r1+}$ and force coordinate of $\kappa_F F_{1+}$ for the second displacement cycle. The coefficients $\kappa_D$ and $\kappa_F$ are empirical parameters that must be determined using experimental data. The second part of the reloading (represented by stiffness $K_{rel\_b}$) targets the maximum displacement achieved in the same quadrant in the previous cycle (e.g., $\delta_{t1+}$ in Figure 7-2).

The only exception to these rules for the non-deteriorating IKP model is for the initial loading in the negative direction that starts at point B in Figure 7-2. In this case, since there is no prior history to determine the location of the control point, the reloading stiffness $K_{rel\_a}$ is calculated using a fraction of the yield strength and the yield displacement $(-\delta_y, -\kappa_F F_y)$ and the corresponding control point (point C) is taken as zero-displacement intercept. The second part of the loading, defined by stiffness $K_{rel\_b}$, is directed to the control point associated with yielding in the third quadrant (point D).

## 7.2.3 Cyclic Deterioration Rules

Four cyclic deterioration modes, namely, *basic strength*, *post-capping strength*, *unloading stiffness*, and *accelerated stiffness*, are implemented in the IKP model. These deterioration modes are implemented if the specimen displacement exceeds the yield displacement. All four deterioration modes are implemented using a parameter that is a function of energy dissipated under cyclic loading using the rules proposed by Rahnama and Krawinkler (1993). The deterioration parameter in excursion *i* ($\beta_i$) is calculated as:

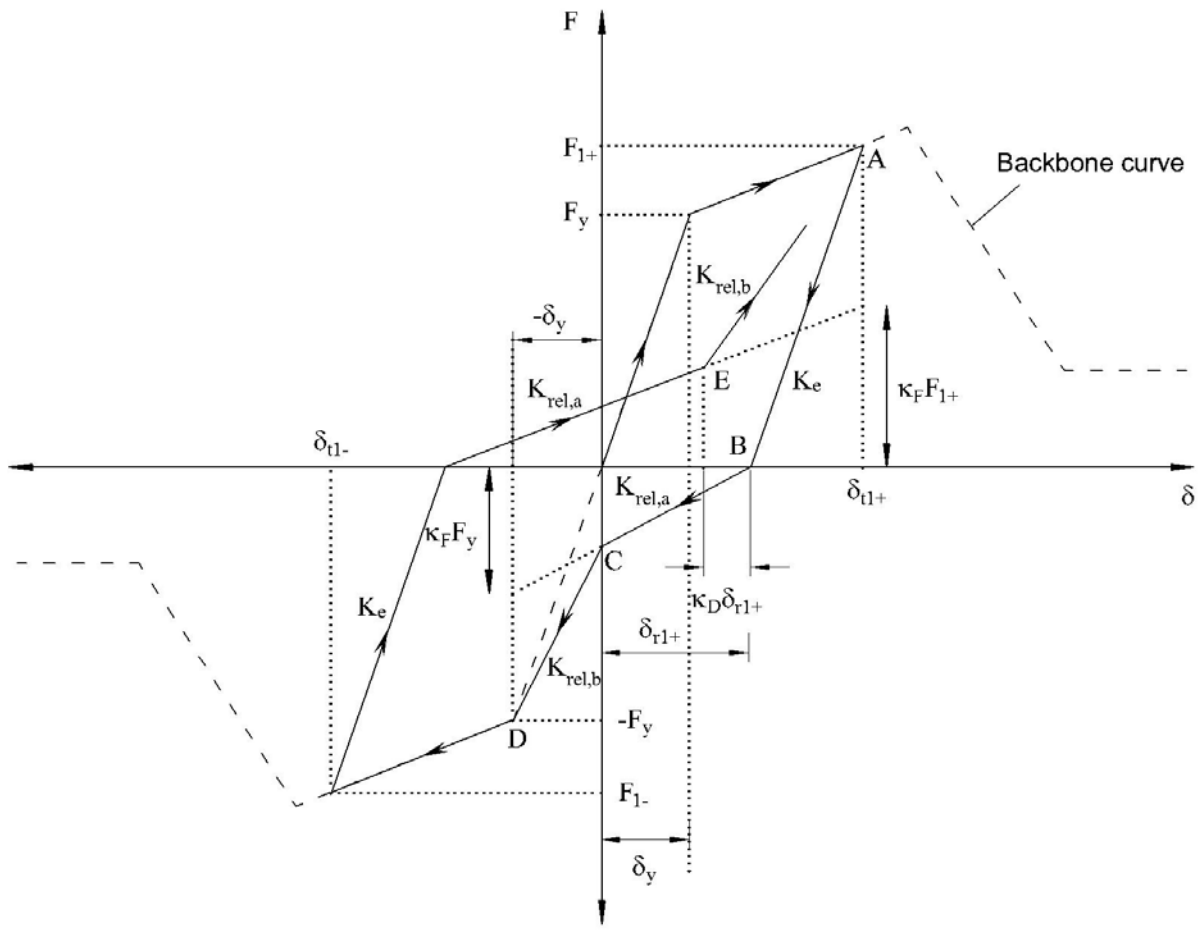


**Figure 7-2 Basic rules for the pinching hysteretic model**

$$\beta_i = \left[ E_i / \left( E_t - \sum_{j=1}^{i} E_j \right) \right]^c \tag{7-1}$$

where $E_i$ is the hysteretic energy dissipated in excursion $i$, $\Sigma E_j$ is the sum of the hysteretic energy dissipated in all previous excursions, $E_t$ is the inherent hysteretic energy dissipation capacity that is equal to $\gamma F_y \delta_y$, and $c$ determines the rate of deterioration. Note that the rate of deterioration can differ for each deterioration mode by assuming different hysteretic energy capacities and/or rates of deterioration ($c$). The deterioration parameter is re-calculated each time the force changes sign and the parameters for the corresponding deterioration modes are updated accordingly. The deterioration parameter is calculated twice in each displacement cycle, once for loading in the positive direction and once for loading in the negative direction.

The parameter $\beta_i$ takes values within the interval $0 < \beta_i \leq 1$. The condition that $\beta_i$ takes values outside this interval, as defined by Equation 7-2, identifies collapse.

$$\gamma F_y \delta_y - \sum_{j=1}^{i} E_j < E_i \tag{7-2}$$

According to Rahnama and Krawinkler (1993), a reasonable range for coefficient $c$ in Equation 7-1 is between 1.0 and 2.0. For cyclic loading at a constant displacement amplitude, a value of $c$ equal to 1.0 refers to a constant rate of deterioration and $c$ equal to 2.0 refers to an increasing rate of deterioration with number of cycles. Each deterioration mode is described below.

### 7.2.3.1 Basic Strength Deterioration

Basic strength deterioration corresponds to reduction in yield strength ($F_y$ in the backbone curve) and post-yielding stiffness ($K_s$ in the backbone curve) with cyclic loading. Equation 7-3 presents the mathematical representation of this deterioration mode.

$$F_{y,k}^{+/-} = \left(1 - \beta_{s,i}\right) F_{y,k-1}^{+/-} \quad ; \quad K_{s,k}^{+/-} = \left(1 - \beta_{s,i}\right) K_{s,k-1}^{+/-} \tag{7-3}$$

where $k$ is the number of the displacement cycle and all other terms have been described previously. The deterioration parameter $\beta_s$ is calculated at points A and B in this example, or more generally, as the force changes arithmetic sign, which identifies reloading in the opposite direction. The yield strength and the post-yielding stiffness in the direction of the loading are updated using the deterioration parameter calculated using Equation 7-3. Figure 7-3 illustrates the effect of the basic strength deterioration mode on hysteretic response.

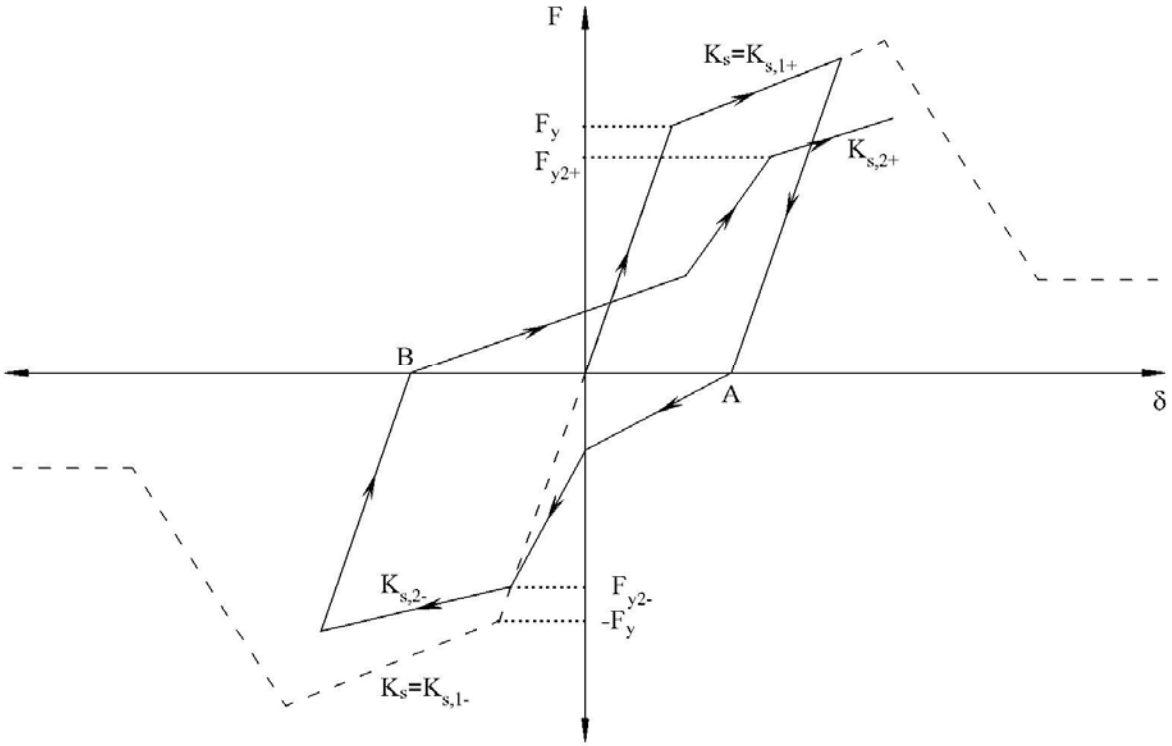


**Figure 7-3 Basic strength deterioration mode**

In Figure 7-3, the yield strength and the post-yield stiffness in the first quadrant of the first displacement cycle are $F_y$ and $K_s$, respectively. In the second displacement cycle, the corresponding values are reduced to $F_{y2+}$ and $K_{s,2+}$.

### 7.2.3.2 Post-Capping Strength Deterioration

Post-capping[1] strength deterioration corresponds to translation of the post-capping branch towards the origin as shown in Figure 7-4; points A and B illustrate the translation in the first quadrant. The post-capping stiffness ($K_c$) is kept constant as the post-capping branch is translated. For the first and third quadrants of displacement cycle *k*, the post-capping strength deterioration can be represented as:

$$F_{ref,k}^{+/-} = \left(1 - \beta_{c,i}\right) F_{ref,k-1}^{+/-} \tag{7-4}$$

where $F_{ref,k}$ is the reference force for displacement cycle *k*. The reference force diminishes with repeated cyclic loading using parameter $\beta_c$ calculated using Equation 7-4.

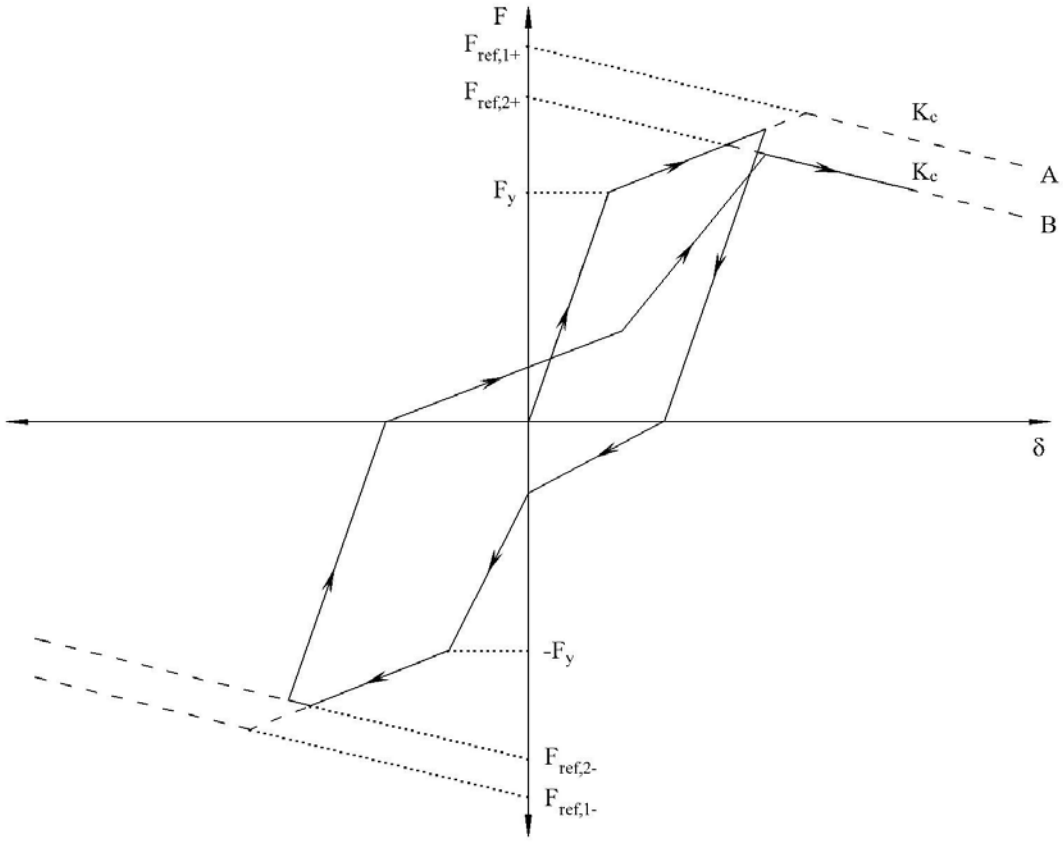


**Figure 7-4 Post-capping strength deterioration mode**

[1] Capping point is defined by the displacement coordinate $\delta_c$ and the force coordinate $F_c$ (see Figure 7-1).

### 7.2.3.3 Unloading Stiffness Deterioration

In this mode, the unloading stiffness diminishes or deteriorates with repeated cyclic loading using Equation 7-5.

$$K_{u,i} = \left(1 - \beta_{k,i}\right) K_{u,i-1} \tag{7-5}$$

where *i* is the excursion number. In the other three deterioration modes, the rate of deterioration is determined using the data recorded in the same quadrant of the previous displacement cycle. However, for the unloading stiffness deterioration mode, the unloading stiffness is updated using the unloading stiffness recorded previously in the opposite direction.

Figure 7-5 illustrates the effect of the unloading stiffness deterioration mode on the hysteretic response. For example, in Figure 7-5, the unloading stiffness $K_{u,1}$ is obtained using the elastic stiffness $K_e$ and Equation 7-5 and the unloading stiffness $K_{u,2}$ is calculated using $K_{u,1}$ and Equation 7-5.

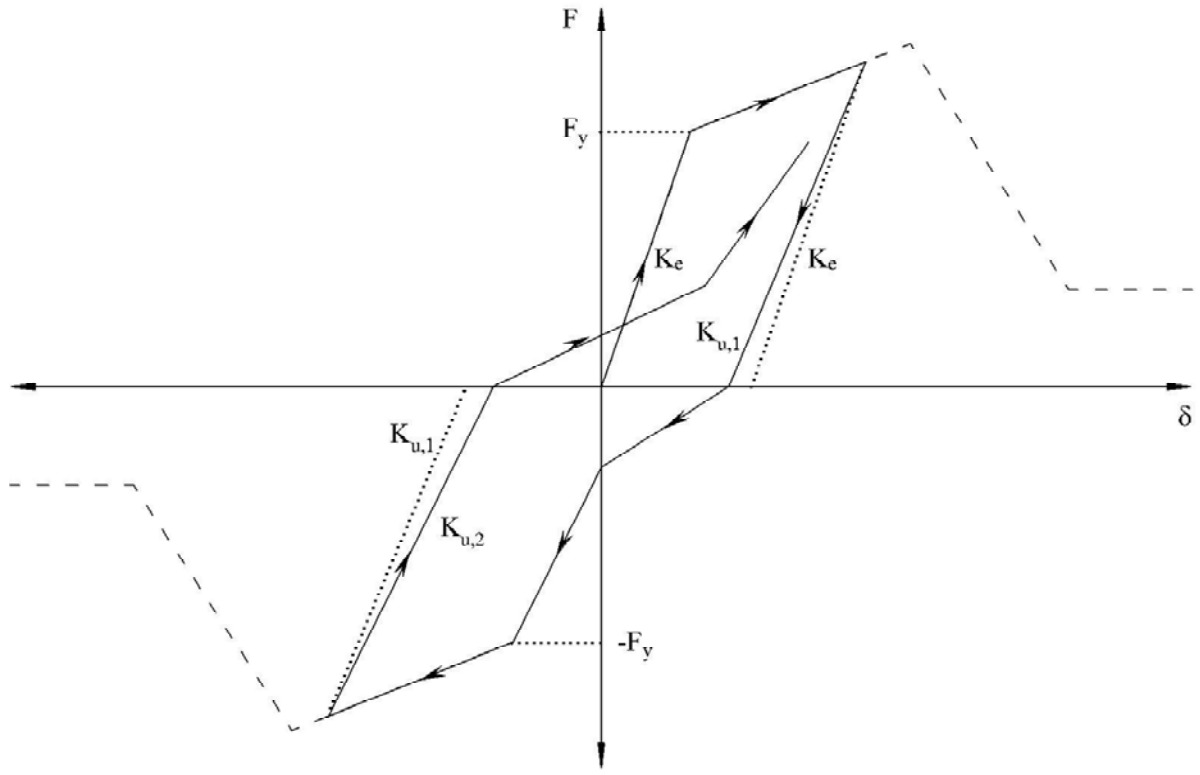


**Figure 7-5 Unloading stiffness deterioration mode**

### 7.2.3.4 Accelerated Stiffness Deterioration

The accelerated stiffness deterioration mode is associated with increasing the absolute value of the target displacement to diminish or deteriorate the reloading stiffness. Figure 7-6 illustrates the effect of the accelerated stiffness deterioration mode on the hysteretic response. As mentioned previously, the target displacement during the reloading phase is equal to the

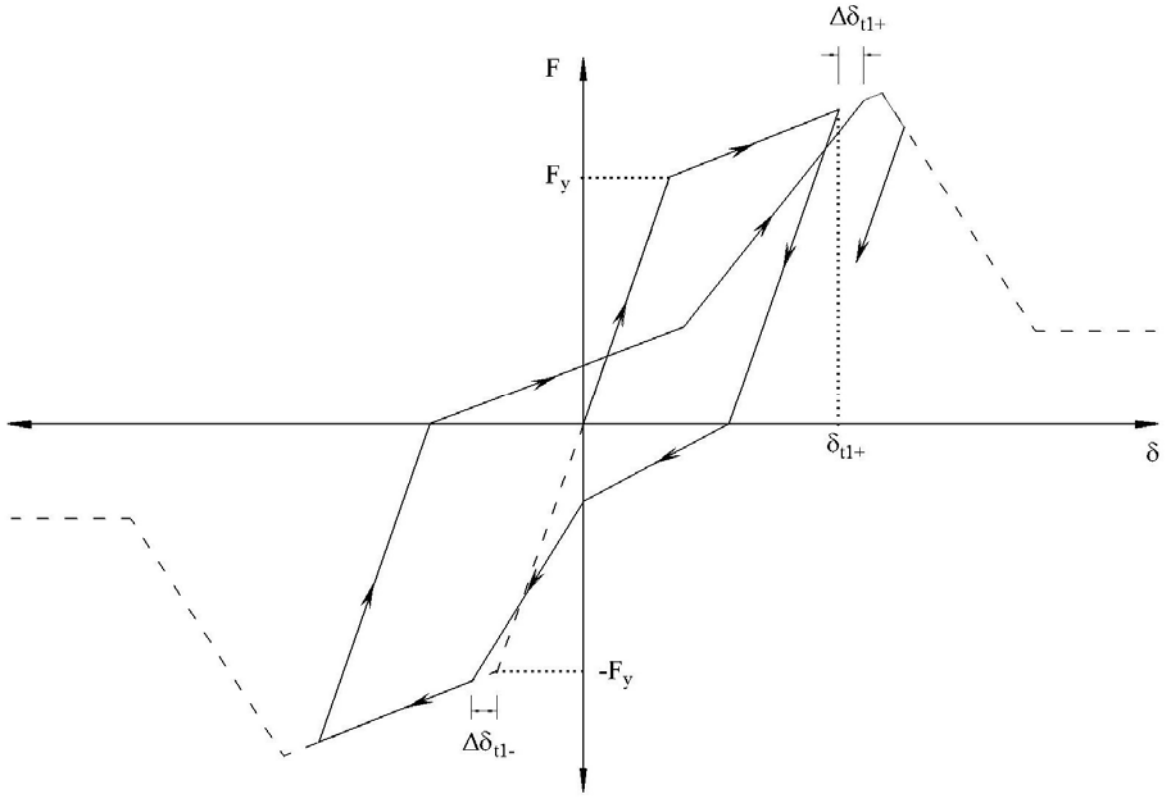


**Figure 7-6 Accelerated stiffness deterioration mode**

maximum displacement achieved in the same quadrant of the previous displacement cycle ($\delta_{t,k-1}$). In the accelerated stiffness deterioration mode, the target displacement that determines the reloading stiffness ($K_{rel,b}$) is updated using Equation 7-6.

$$\delta_{t,k}^{+/-} = \left(1+\beta_{a,i}\right)\delta_{t,k-1}^{+/-} \tag{7-6}$$

# 7.3 Calibration of Model Parameters Using Experimental Data

## 7.3.1 Introduction

Every structural component possesses different hysteretic behavior characteristics. The key hysteretic characteristics of squat walls include pinching, relatively poor energy dissipation capacity, and rapid loss of stiffness with repeated cyclic loading. The objective herein is to identify values of the parameters for the IKP model that enable realistic simulation of the response of squat reinforced concrete walls that represent a relatively small design space. Experimental load-displacement data in a digital format are required for this purpose.

The digital load (shearing force)-(horizontal) displacement relationships provided by Salonikios et al. (1999) for six walls and Palermo and Vecchio (2002b) for one wall are used to generate the macro hysteretic models. Table 7-1 presents the design space associated with these seven specimens. The utility of the macro models is described using figures that compare measured and predicted hysteretic response.

**Table 7-1 Design space**

| Researcher | Wall ID | Cross-Section | $h_w / l_w$ | $P / A_t f_c'$ (%) | $\rho_h$ (%) | $\rho_v$ (%) | $\rho_{be}$ (%) | $f_c'$ (psi) |
|---|---|---|---|---|---|---|---|---|
| Salonikios | LSW1 | Rectangular | 1.0 | 0.0 | 0.57 | 0.57 | 1.70 | 3219 |
| Salonikios | LSW2 | Rectangular | 1.0 | 0.0 | 0.28 | 0.28 | 1.30 | 3132 |
| Salonikios | LSW3 | Rectangular | 1.0 | 7.0 | 0.28 | 0.28 | 1.30 | 3466 |
| Salonikios | MSW1 | Rectangular | 1.5 | 0.0 | 0.57 | 0.57 | 1.70 | 3785 |
| Salonikios | MSW3 | Rectangular | 1.5 | 7.0 | 0.28 | 0.28 | 1.30 | 3495 |
| Salonikios | MSW6 | Rectangular | 1.5 | 0.0 | 0.57 | 0.57 | 1.70 | 3988 |
| Palermo | DP1 | Flanged | 0.66 | 5.4 | 0.76 | 0.82 | 0.37 | 3147 |

The availability of data limits the scope of the analysis presented here. The utility of the models, size of the design space and the accuracy of the proposed model parameters (and their dependence on squat wall design variables such as aspect ratio, rebar ratio, and concrete strength) could be improved by analysis of additional data generated by either robust finite element analysis or physical simulation.

## 7.3.2 Modeling Assumptions

To implement the IKP model as intended by Ibarra et al. (2005), two walls of identical construction and materials have to be tested using: 1) monotonic loading to failure to identify the backbone curve, and 2) cyclic loading to identify the model parameters for the fourdeterioration modes. Although the database of Section 3 includes 434 squat walls, such test data are unavailable for any wall, which required the use of an alternate procedure.

Digital load-displacement data is available for the seven cyclically loaded walls identified above. The experimental backbone curves for these walls are obtained from the cyclic load-displacement relationships. The basic strength and post-capping strength deterioration modes are set aside because these deterioration modes are related to degradation of the backbone curve under cyclic loading as presented in Sections 7.2.3.1 and 7.2.3.2. Figure 7-7 illustrates the backbone curve identified for wall LSW1 tested by Salonikios et al. (1999).

As presented in Figure 7-1, the Ibarra-Krawinkler backbone curve is piece-wise linear with three line segments corresponding to the stages of elastic, post-yielding, and post-capping response. Therefore, the experimentally obtained backbone curves have to be represented in this form. The elastic wall stiffness ($K_e$), peak strength ($F_c$), and the displacement at peak strength ($\delta_c$) can be obtained directly from the experimental backbone curve. However, the control point associated with yielding (i.e., [$\delta_y$, $F_y$]) and the post-capping stiffness ($K_c$) must be estimated. The post-yielding stiffness ($K_s$) is calculated once the yielding control point is established. The optimization routine *fmincon* in MATLAB [The Mathworks, Inc. (2006)] is used to identify the yield strength ($F_y$), the corresponding displacement ($\delta_y$), and the post-capping stiffness ($K_c$). The optimized backbone curve is shown in Figure 7-8. The optimization is performed assuming: a) the elastic stiffness ($K_e$) for the calculated backbone curve is equal to that obtained

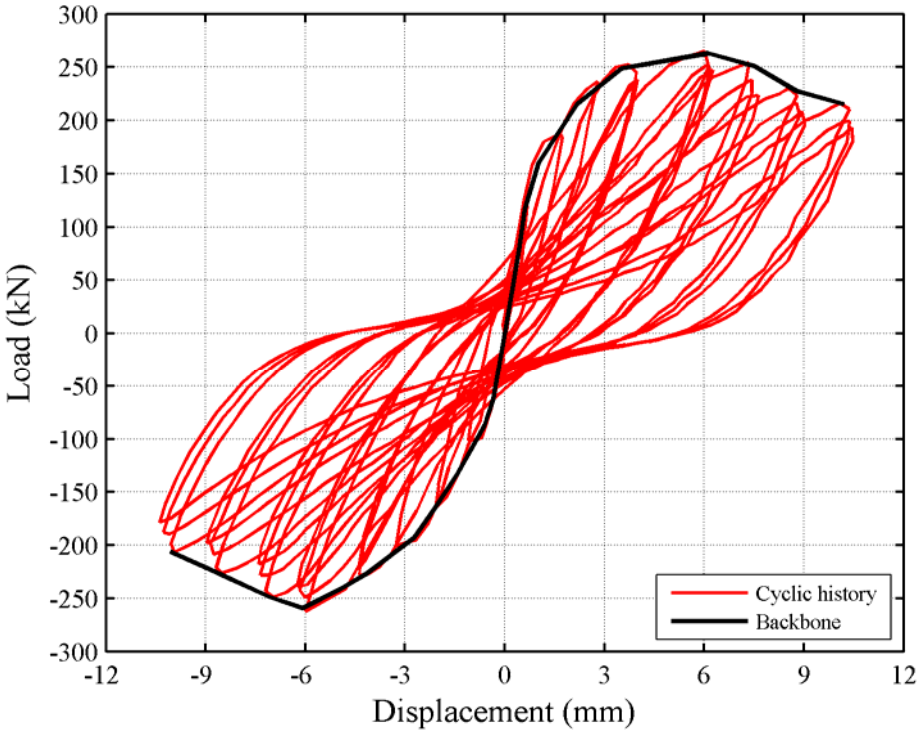


**Figure 7-7 Cyclic load-displacement relationship and the corresponding backbone curve for wall LSW1 tested by Salonikios et al. (1999)**

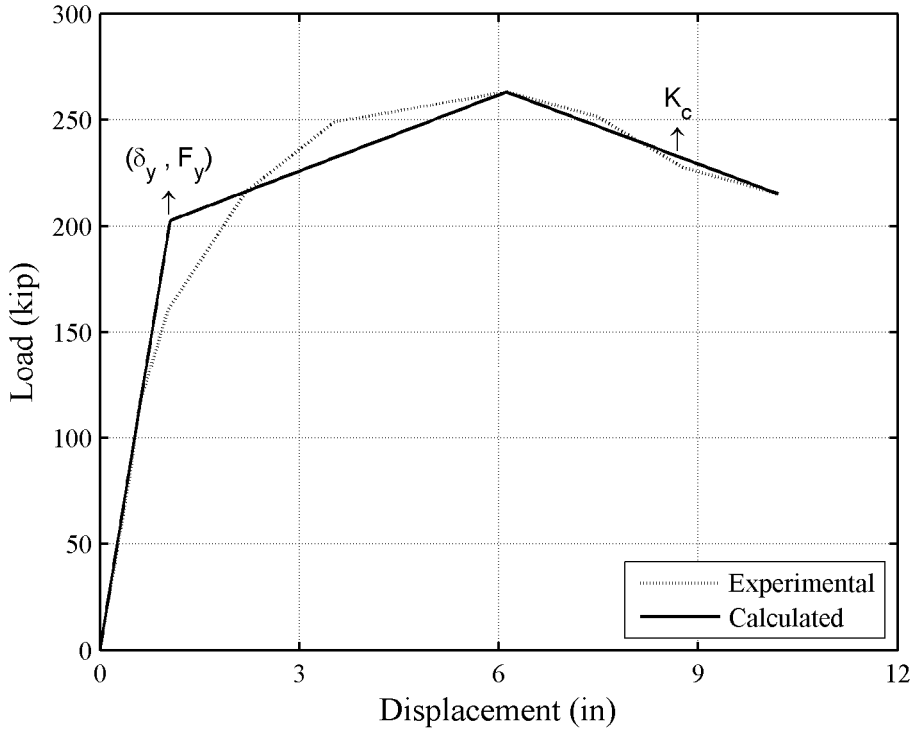


**Figure 7-8 Experimental and calculated backbone relationships for wall LSW1 tested by Salonikios et al. (1999)**

experimentally, b) the peak strength ($F_c$) and the corresponding displacement ($\delta_c$) for the calculated backbone curve are equal to those obtained experimentally, and c) the areas under the calculated backbone curve and the experimentally obtained backbone curve are equal. A residual strength for the backbone curve (see $F_r$ in Figure 7-1) could not be identified using the experimental data because the tests were terminated before the wall shear strength dropped significantly. Accordingly, residual strength for the backbone curve is not considered here.

Table 7-2 presents the analytical backbone curve parameters obtained using the first quadrant data of the experimental load-displacement relationships for the seven test specimens.

The IKP pinching model is formulated in MATLAB [The MathWorks, Inc. (2006)]. The computed[2] values for the hysteretic model parameters are listed in Table 7-3.

**Table 7-2 Calculated backbone parameters**

| Researcher | Wall ID | $K_e$ (kN/mm) | $F_y$ (kN) | $\delta_y$ (mm) | $F_c$ (kN) | $\delta_c$ (mm) | $\frac{F_y}{F_c}$ | $\alpha_s$ (%) | $\alpha_c$ (%) |
|---|---|---|---|---|---|---|---|---|---|
| Salonikios | LSW1 | 192 | 203 | 1.1 | 263 | 6.1 | 0.77 | 6.2 | -6.1 |
| Salonikios | LSW2 | 148 | 156 | 1.1 | 193 | 5.0 | 0.81 | 6.3 | -7.1 |
| Salonikios | LSW3 | 90.4 | 228 | 2.5 | 268 | 4.7 | 0.85 | 20.2 | -7.5 |
| Salonikios | MSW1 | 42.4 | 153 | 3.6 | 197 | 11.9 | 0.78 | 12.6 | -7.4 |
| Salonikios | MSW3 | 47.6 | 147 | 3.1 | 176 | 9.9 | 0.83 | 9.0 | -5.5 |
| Salonikios | MSW6 | 29[1] | 127 | 4.4 | 202 | 16.1 | 0.63 | 22.2 | -17.0 |
| Palermo | DP1 | 288 | 1069 | 3.7 | 1300 | 11.0 | 0.82 | 10.9 | -37.7 |

1. Wall included a cold-joint between the wall web and the foundation; its elastic stiffness is much lower than those of comparable specimens (MSW1 and MSW3).

**Table 7-3 Calculated pinching and deterioration parameters**

| Researcher | Wall ID | $\kappa_F$ | $\kappa_D$ | $\gamma_k$ | $\gamma_a$ | $c_k$ | $c_a$ |
|---|---|---|---|---|---|---|---|
| Salonikios | LSW1 | 0.30 | 0.40 | 150 | 150 | 1 | 1 |
| Salonikios | LSW2 | 0.30 | 0.45 | 165 | 165 | 1 | 1 |
| Salonikios | LSW3 | 0.70 | 0.70 | 130 | 100 | 1 | 1 |
| Salonikios | MSW1 | 0.50 | 0.40 | 170 | 170 | 1 | 1 |
| Salonikios | MSW3 | 0.60 | 0.40 | 175 | 175 | 1 | 1 |
| Salonikios | MSW6 | 0.50 | 0.50 | 225 | 125 | 1 | 1 |
| Palermo | DP1 | 0.20 | 0.50 | 35 | 30 | 1 | 1 |

For all seven walls, the best results are obtained using $c_k$ and $c_a$ equal to 1.0, which corresponds to a constant rate of deterioration over the loading history. A greater value (e.g., 2) for $c_k$ and $c_a$

[2] A standard least squares fit is used to minimize the difference between the hysteretic dissipated energy in the experiment and the analytical prediction.

for a constant amplitude displacement history corresponds to slow degradation in early cycles and fast degradation in latter cycles of loading. Identical values of $\gamma_k$ and $\gamma_a$ could be used to simulate the response of walls LSW1, LSW2, LSW3, MSW1, and MSW3, whereas a greater value $\gamma_k$ produces better results for MSW6 and DP1.

The coefficients $\gamma_k$ and $\gamma_a$, normalized by $F_y\delta_y$, characterize the hysteretic energy capacity of a wall. As seen in Table 7-3, the walls with larger aspect ratios (MSW1, MSW3, MSW6) have relatively higher energy dissipation capacity. This result is expected because such walls can dissipate significant energy through flexural yielding. The coefficient $\kappa_F$, which determines the control point associated with pinching, is smaller for walls with highly pinched hysteretic behavior (e.g., wall DP1). More experimental work is needed to better characterize the parameters of the IKP model for squat reinforced concrete walls.

The utility of the hysteretic models defined using the data of Table 7-3 is investigated in Figure 7-9 by plotting experimentally measured and predicted load-displacement relationships, where the predicted responses are computed using the corresponding experimental displacement histories. As seen in the figure, the IKP model can simulate reasonably the hysteretic response of squat walls. However, the addition of another control point [similar to that of Wallace (2007), see Figure 2-1] to the backbone curve of the IKP model would improve significantly the accuracy of the predictions, especially for walls similar to DP1 (see Figure 7-9g1). A bilinear approximation to the pre-peak shearing force-lateral displacement relationship for the experimental backbone curve is likely insufficient. A tri-linear relationship that characterizes the elastic, post-cracking, and post-yielding stages of wall response prior peak shearing strength would improve the quality of the simulation.

Another difference between the experimental and IKP-predicted load-displacement relationships is the continuity of response. The IKP predictions are piece-wise linear whereas the experimental results are continuous.

The hysteretic response of a small class of squat walls can be predicted with the IKP model, a robust backbone curve and the appropriate model parameters of Table 7-3. Care must be exercised in the development of the backbone curve and the choice of model parameters. The peak shear strength of the squat wall should be computed using either Equation 6-9 or 6-10.

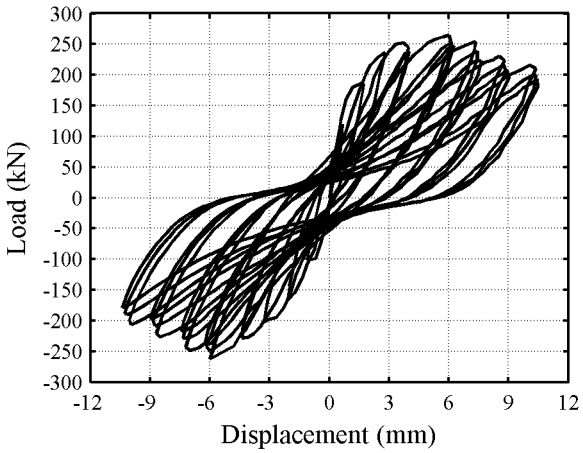


**a1) Wall LSW1 – Experimental**

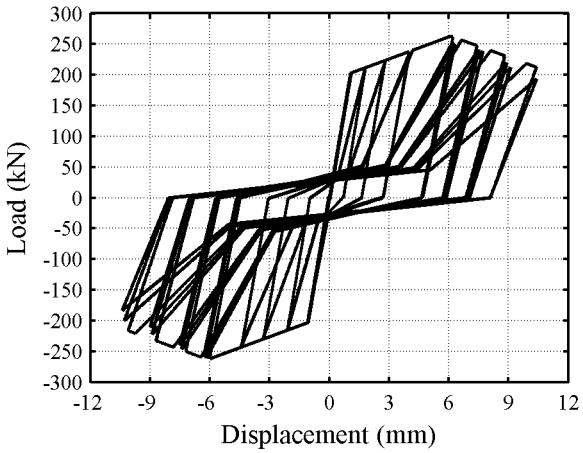


**a2) Wall LSW1 – IKP model**

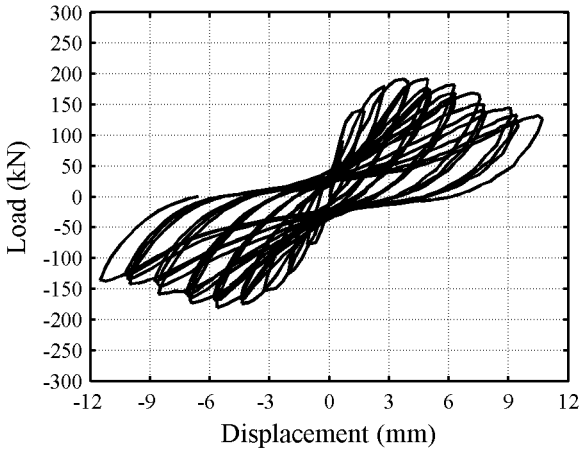


**b1) Wall LSW2 – Experimental**

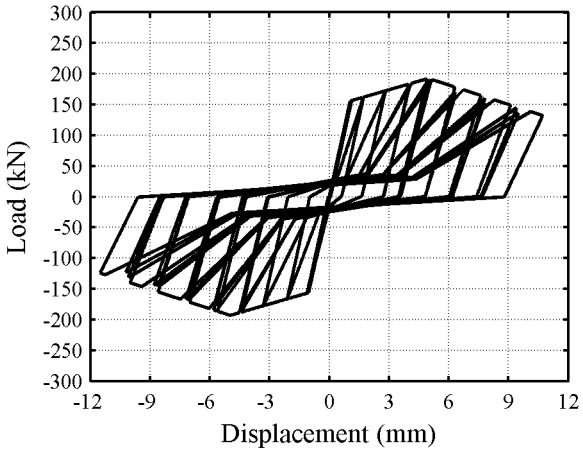


**b2) Wall LSW2 – IKP model**

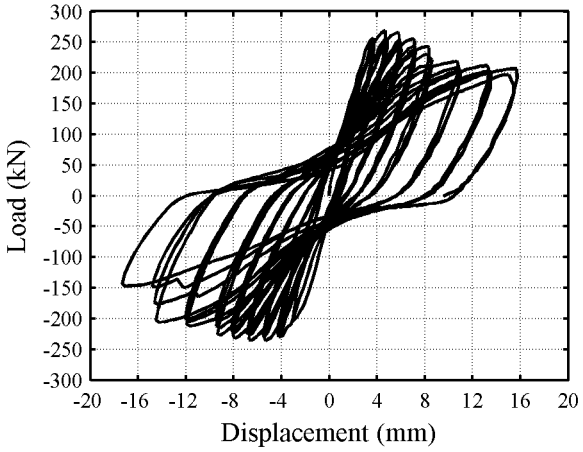


**c1) Wall LSW3 – Experimental**

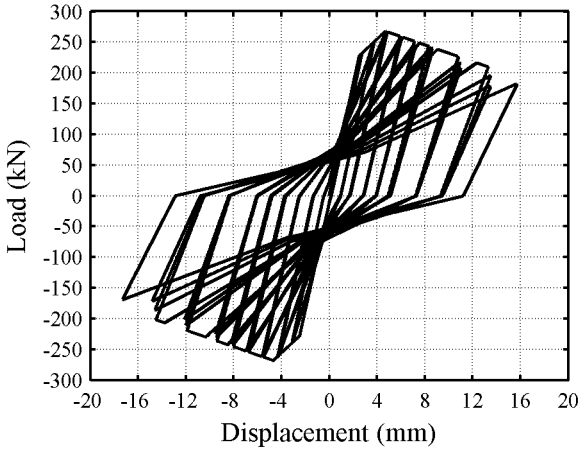


**c2) Wall LSW3 – IKP model**

**Figure 7-9 Experimental [Salonikios et al. (1999), Palermo and Vecchio (2002b)] and predicted load-displacement relationships**

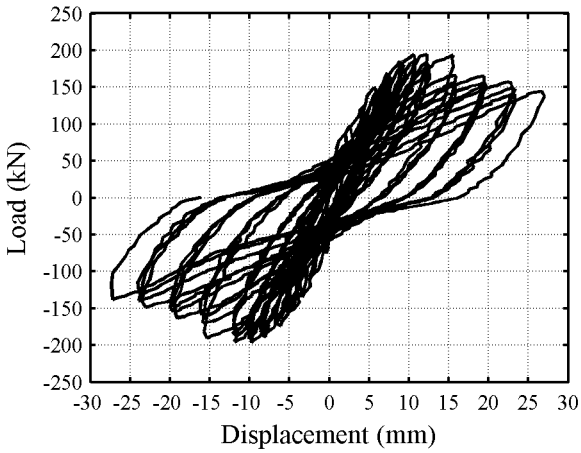


**d1) Wall MSW1 – Experimental**

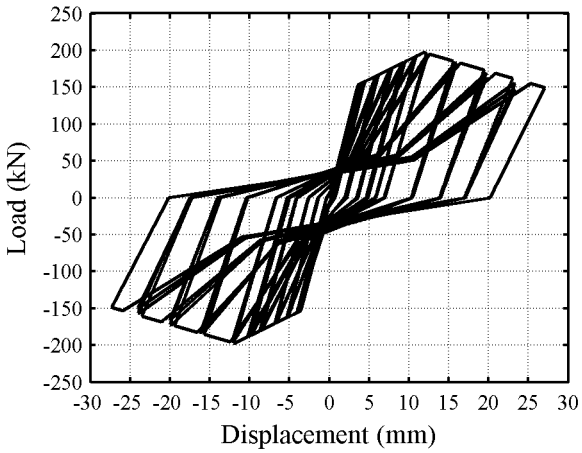


**d2) Wall MSW1 – IKP model**

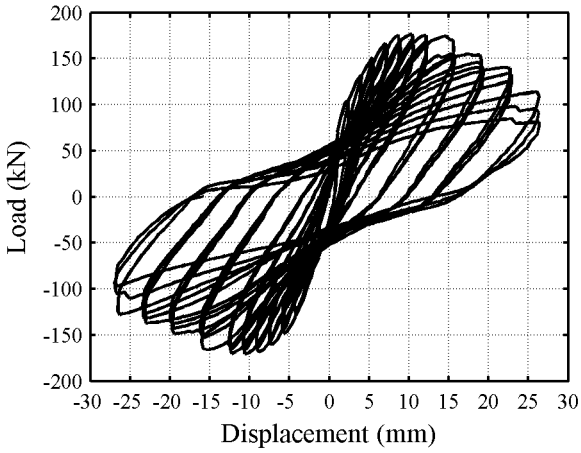


**e1) Wall MSW3 – Experimental**

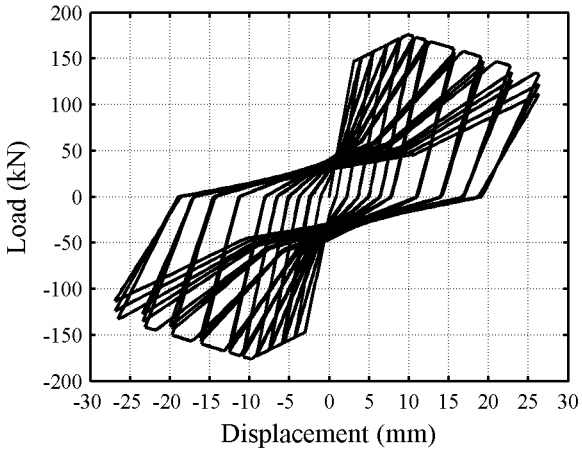


**e2) Wall MSW3 – IKP model**

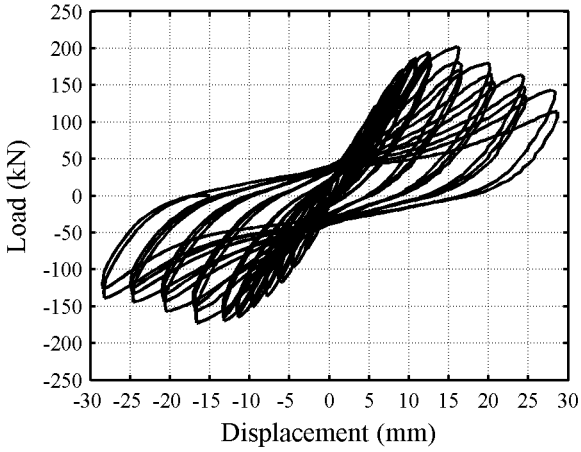


**f1) Wall MSW6 – Experimental**

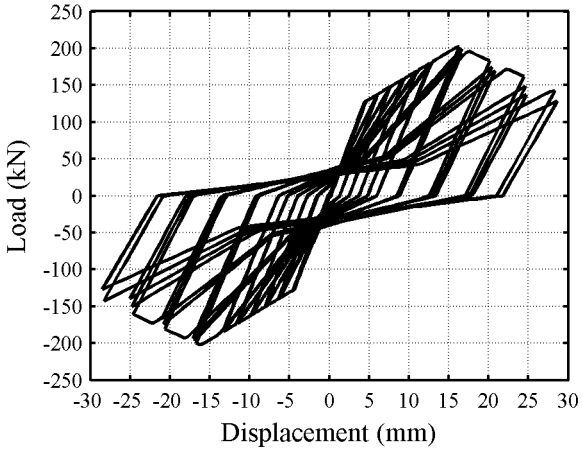


**f2) Wall MSW6 – IKP model**

**Figure 7-9 Experimental [Salonikios et al. (1999), Palermo and Vecchio (2002b)] and predicted load-displacement relationships (cont'd)**

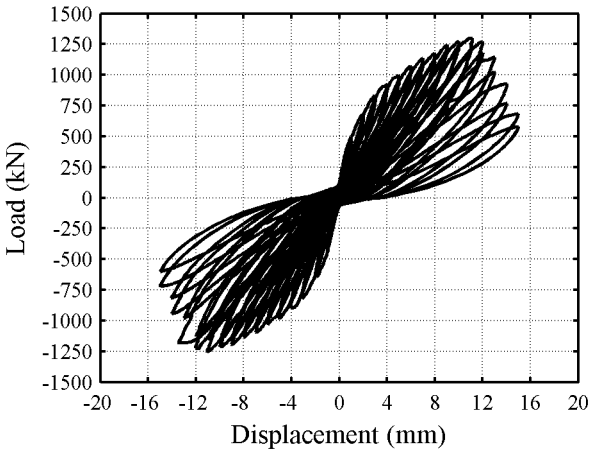


**g1) Wall DP1 – Experimental**

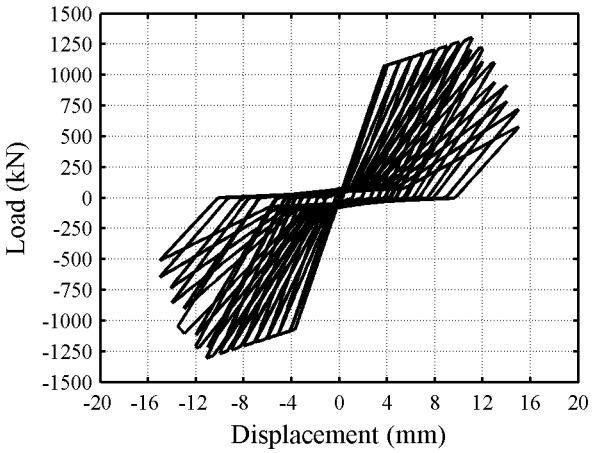


**g2) Wall DP1 – IKP model**

**Figure 7-9 Experimental [Salonikios et al. (1999), Palermo and Vecchio (2002b)] and predicted load-displacement relationships (cont'd)**

# 8 DAMAGE STATES AND FRAGILITY CURVES FOR SQUAT REINFORCED CONCRETE WALLS

## 8.1 Introduction

A general framework for seismic performance assessment and loss computations is provided in the 50% draft of the ATC-58 *Guidelines for Seismic Performance Assessment of Buildings* [ATC (2008)]. A key component of the framework is fragility functions for components and elements of seismic framing systems. Fragility functions relate the probability of exceeding one or more damage thresholds (described using damage states and repair measures) to a demand parameter such as story drift or component plastic deformation. This section summarizes the development of fragility curves for squat reinforced concrete walls.

Damage states are characterized typically using descriptors such as concrete crack width, extent of concrete crushing, sliding shear displacement, and reinforcement yielding and buckling. However, to compute dollars losses and estimates of building downtime, damage states must be characterized by measures (or scopes) of repair and such descriptions are presented herein, and Appendices C, D and E.

Information is used from experiments on squat walls reported in the literature to generate damage data as a function of an efficient demand parameter. Alternate probability distributions are used to present the damage data. Goodness-of-fit tests are performed to evaluate the utility of these distributions.

## 8.2 Summary of Experimental Data

As presented in Section 3, a significant number of squat reinforced concrete walls have been tested in the past 60 years. Most of the experimental programs focused on the maximum strength and initial (elastic) stiffness of such walls. The progression of damage with increasing lateral displacement (drift) was of secondary interest. Information that is key to the development of damage states and fragility curves such as maximum crack width, reinforcement yielding and buckling, extent of concrete crushing, and photographs illustrating the condition of specimens at various stages of the experiments was not always reported. Accordingly, only a fraction of the experimental data presented in Section 3 could be used to develop fragility functions.

The properties of the test specimens used to develop fragility functions are summarized in Table 8-1 through Table 8-6. Specimens are grouped with respect to wall geometry: rectangular, barbell and flanged. In these tables, $P$ is axial force; $A_t$ is total wall area; $f_c'$ is concrete compressive strength; $h_w$ is wall height; $l_w$ is wall length; $t_w$ is web thickness; $b_f$ and $h_f$ are width and depth of the boundary element, respectively; $M/V$ is moment-to-shear ratio at the base of the wall; $\rho_{be}$ is boundary element reinforcement ratio, $\rho_v$ is vertical web reinforcement ratio, and $\rho_h$ is the horizontal web reinforcement ratio. The column labeled *scale* in Table 8-2, Table 8-4, and Table 8-6 identifies the size of the test specimen with respect to typical building construction by presenting the ratio of web panel thickness to 8 inches. The acronym MoR in these tables denotes Method of Repair, which is defined in Section 8.4 of this section.

**Table 8-1 Summary of rectangular wall data used to create fragility functions**

| No | Reference | Wall ID | Loading | $P / A_t f_c'$ (%) | Number of damage data per MoR | | | |
|---|---|---|---|---|---|---|---|---|
| | | | | | 1 | 2 | 3 | 4 |
| 1 | Pilakoutas (1991) | SW4 | Cyclic | 0.0 | 1 | 1 | 1 | 1 |
| 2 | | SW5 | Cyclic | 0.0 | 1 | 1 | 0 | 1 |
| 3 | | SW6 | Cyclic | 0.0 | 1 | 1 | 1 | 1 |
| 4 | | SW7 | Cyclic | 0.0 | 1 | 1 | 0 | 1 |
| 5 | | SW8 | Cyclic | 0.0 | 1 | 1 | 1 | 1 |
| 6 | | SW9 | Cyclic | 0.0 | 1 | 1 | 1 | 1 |
| 7 | Greifenhagen et al. (2005) | M1 | Cyclic | 2.2 | 2 | 1 | 1 | 2 |
| 8 | | M2 | Cyclic | 2.2 | 0 | 1 | 3 | 1 |
| 9 | | M3 | Cyclic | 9.5 | 2 | 1 | 3 | 1 |
| 10 | | M4 | Monotonic | 5.0 | 2 | 1 | 3 | 1 |
| 11 | Lefas et al. (1990) | SW11 | Monotonic | 0.0 | 0 | 0 | 0 | 1 |
| 12 | | SW12 | Monotonic | 8.7 | 0 | 0 | 0 | 1 |
| 13 | | SW13 | Monotonic | 18.1 | 2 | 1 | 1 | 0 |
| 14 | | SW14 | Monotonic | 0.0 | 2 | 1 | 1 | 0 |
| 15 | | SW15 | Monotonic | 8.8 | 2 | 1 | 1 | 0 |
| 16 | | SW16 | Monotonic | 18.0 | 2 | 1 | 1 | 0 |
| 17 | | SW17 | Monotonic | 0.0 | 2 | 1 | 1 | 0 |
| 18 | | SW21 | Monotonic | 0.0 | 2 | 1 | 1 | 0 |
| 19 | | SW22 | Monotonic | 9.1 | 2 | 1 | 1 | 0 |
| 20 | | SW23 | Monotonic | 18.2 | 2 | 1 | 1 | 0 |
| 21 | | SW24 | Monotonic | 0.0 | 2 | 1 | 1 | 0 |
| 22 | | SW26 | Monotonic | 0.0 | 2 | 1 | 1 | 0 |
| 23 | Maier and Thürlimann (1985) | S4 | Monotonic | 6.7 | 2 | 1 | 1 | 0 |
| 24 | | S9 | Cyclic | 7.5 | 2 | 1 | 1 | 0 |
| 25 | Wiradinata (1985) | Wall-1 | Cyclic | 0.0 | 1 | 3 | 1 | 0 |
| 26 | | Wall-2 | Cyclic | 0.0 | 1 | 3 | 0 | 1 |
| 27 | Pilette (1987) | Wall-4 | Cyclic | 0.0 | 1 | 3 | 2 | 1 |
| 28 | | Wall-5 | Cyclic | 0.0 | 1 | 3 | 0 | 1 |
| 29 | Mohammadi-Doostdar (1994) | Wall-7 | Cyclic | 0.0 | 2 | 2 | 0 | 1 |
| 30 | | Wall-8 | Cyclic | 0.0 | 1 | 2 | 1 | 1 |

**Table 8-1 Summary of rectangular wall data used to create fragility functions (cont'd)**

| No | Reference | Wall ID | Loading | $P / A_t f_c'$ (%) | Number of damage data per MoR | | | |
|---|---|---|---|---|---|---|---|---|
| | | | | | 1 | 2 | 3 | 4 |
| 31 | Salonikios et al. (1999) | MSW1 | Cyclic | 0.0 | 0 | 0 | 0 | 1 |
| 32 | | MSW3 | Cyclic | 7.0 | 0 | 0 | 0 | 1 |
| 33 | | MSW6 | Cyclic | 0.0 | 0 | 0 | 0 | 1 |
| 34 | | LSW3 | Cyclic | 7.0 | 0 | 0 | 0 | 1 |
| 35 | Synge (1980) | Wall-1 | Cyclic | 0.0 | 1 | 3 | 2 | 1 |
| 36 | Massone (2006) | wp111-9 | Cyclic | 10.0 | 1 | 3 | 0 | 1 |
| 37 | | wp111-10 | Cyclic | 10.0 | 1 | 3 | 0 | 1 |
| 38 | | wp1105-8 | Cyclic | 5.0 | 1 | 3 | 0 | 1 |
| 39 | | wp1105-7 | Cyclic | 5.0 | 1 | 3 | 0 | 1 |
| 40 | | wp110-5 | Cyclic | 0.0 | 0 | 3 | 0 | 1 |
| 41 | | wp110-6 | Monotonic | 0.0 | 0 | 3 | 0 | 1 |
| 42 | Xie and Xiao (2000) | W-1A | Cyclic | 9.4 | 2 | 0 | 1 | 1 |
| 43 | Hidalgo et al. (2002) | 23 | Cyclic | 0.0 | 2 | 1 | 0 | 1 |
| 44 | | 27 | Cyclic | 0.0 | 3 | 1 | 0 | 1 |
| 45 | Lopes and Elnashai (1991) | SW11 | Cyclic | 0.0 | 2 | 2 | 1 | 1 |
| 46 | | SW12 | Cyclic | 0.0 | 1 | 1 | 1 | 1 |
| 47 | | SW13 | Cyclic | 0.0 | 3 | 2 | 0 | 1 |
| 48 | | SW14 | Cyclic | 0.0 | 1 | 1 | 0 | 2 |
| 49 | | SW15 | Cyclic | 0.0 | 1 | 1 | 1 | 2 |
| 50 | | SW16 | Cyclic | 0.0 | 0 | 0 | 0 | 1 |
| 51 | | SW17 | Monotonic | 0.0 | 0 | 0 | 0 | 1 |

**Table 8-2 Geometric and material properties of the rectangular wall data**

| No | $h_w / l_w$ | $M / Vl_w$ | $h_w$ (in) | $l_w$ (in) | $t_w$ (in) | Scale | $b_f$ (in) | $h_f$ (in) | $\rho_{be}$ (%) | $\rho_v$ (%) | $\rho_h$ (%) | $f_c'$ (psi) |
|---|---|---|---|---|---|---|---|---|---|---|---|---|
| 1 | 2.00 | 2.13 | 47.2 | 23.6 | 2.36 | 0.30 | 2.4 | 4.3 | 6.9 | 0.50 | 0.39 | 5352 |
| 2 | 2.00 | 2.13 | 47.2 | 23.6 | 2.36 | 0.30 | 2.4 | 2.4 | 12.7 | 0.59 | 0.31 | 4612 |
| 3 | 2.00 | 2.13 | 47.2 | 23.6 | 2.36 | 0.30 | 2.4 | 4.3 | 6.9 | 0.50 | 0.31 | 5599 |
| 4 | 2.00 | 2.13 | 47.2 | 23.6 | 2.36 | 0.30 | 2.4 | 2.4 | 12.7 | 0.59 | 0.39 | 4641 |
| 5 | 2.00 | 2.13 | 47.2 | 23.6 | 2.36 | 0.30 | 2.4 | 4.3 | 7.1 | 0.50 | 0.28 | 6643 |
| 6 | 2.00 | 2.13 | 47.2 | 23.6 | 2.36 | 0.30 | 2.4 | 4.3 | 7.1 | 0.50 | 0.56 | 5642 |
| 7 | 0.61 | 0.69 | 24.0 | 39.4 | 3.94 | 0.49 | 0.0 | 0.0 | 0.0 | 0.34 | 0.37 | 7352 |
| 8 | 0.61 | 0.69 | 24.0 | 39.4 | 3.94 | 0.49 | 0.0 | 0.0 | 0.0 | 0.34 | 0.00 | 7395 |
| 9 | 0.68 | 0.77 | 24.0 | 35.4 | 3.15 | 0.39 | 0.0 | 0.0 | 0.0 | 0.39 | 0.26 | 2915 |
| 10 | 0.68 | 0.77 | 24.0 | 35.4 | 3.15 | 0.39 | 0.0 | 0.0 | 0.0 | 0.39 | 0.26 | 3538 |
| 11 | 1.00 | 1.10 | 29.5 | 29.5 | 2.76 | 0.34 | 3.9 | 5.1 | 8.5 | 2.14 | 1.17 | 7140 |
| 12 | 1.00 | 1.10 | 29.5 | 29.5 | 2.76 | 0.34 | 3.9 | 5.5 | 6.5 | 2.14 | 1.17 | 7332 |
| 13 | 1.00 | 1.10 | 29.5 | 29.5 | 2.76 | 0.34 | 2.8 | 5.5 | 3.1 | 2.14 | 1.17 | 5423 |
| 14 | 1.00 | 1.10 | 29.5 | 29.5 | 2.76 | 0.34 | 2.8 | 5.5 | 3.1 | 2.14 | 1.17 | 5642 |
| 15 | 1.00 | 1.10 | 29.5 | 29.5 | 2.76 | 0.34 | 2.8 | 5.5 | 3.1 | 2.14 | 1.17 | 5819 |
| 16 | 1.00 | 1.10 | 29.5 | 29.5 | 2.76 | 0.34 | 2.8 | 5.5 | 3.1 | 2.14 | 1.17 | 7052 |
| 17 | 1.00 | 1.10 | 29.5 | 29.5 | 2.76 | 0.34 | 2.8 | 5.5 | 3.1 | 2.14 | 0.37 | 6553 |
| 18 | 2.00 | 2.12 | 51.2 | 25.6 | 2.56 | 0.32 | 2.8 | 5.5 | 3.1 | 2.09 | 0.87 | 5745 |
| 19 | 2.00 | 2.12 | 51.2 | 25.6 | 2.56 | 0.32 | 2.8 | 5.5 | 3.1 | 2.09 | 0.87 | 6891 |
| 20 | 2.00 | 2.12 | 51.2 | 25.6 | 2.56 | 0.32 | 2.6 | 5.5 | 3.3 | 2.09 | 0.87 | 6480 |
| 21 | 2.00 | 2.12 | 51.2 | 25.6 | 2.56 | 0.32 | 2.6 | 5.5 | 3.3 | 2.09 | 0.87 | 6553 |
| 22 | 2.00 | 2.12 | 51.2 | 25.6 | 2.56 | 0.32 | 2.6 | 5.5 | 3.3 | 2.09 | 0.40 | 3881 |
| 23 | 1.02 | 1.12 | 47.2 | 46.5 | 3.94 | 0.49 | 2.6 | 5.5 | 3.3 | 1.02 | 1.01 | 4772 |
| 24 | 1.02 | 1.12 | 47.2 | 46.5 | 3.94 | 0.49 | 2.6 | 5.5 | 3.3 | 1.02 | 0.00 | 4235 |
| 25 | 0.50 | 0.58 | 39.4 | 78.7 | 3.94 | 0.49 | 0.0 | 0.0 | 0.0 | 0.59 | 0.26 | 3626 |
| 26 | 0.25 | 0.33 | 19.7 | 78.7 | 3.94 | 0.49 | 0.0 | 0.0 | 0.0 | 0.59 | 0.26 | 3191 |
| 27 | 0.50 | 0.58 | 39.4 | 78.7 | 3.94 | 0.49 | 3.9 | 12.6 | 1.3 | 0.59 | 0.80 | 4786 |
| 28 | 0.50 | 0.58 | 39.4 | 78.7 | 3.94 | 0.49 | 3.9 | 12.6 | 1.3 | 1.07 | 1.20 | 3916 |
| 29 | 0.75 | 0.82 | 59.1 | 78.7 | 3.94 | 0.49 | 3.9 | 12.6 | 1.3 | 0.59 | 0.80 | 6527 |
| 30 | 1.00 | 1.09 | 59.1 | 59.1 | 3.94 | 0.49 | 3.9 | 9.8 | 1.6 | 0.51 | 0.80 | 6527 |
| 31 | 1.50 | 1.60 | 70.9 | 47.2 | 3.94 | 0.49 | 3.9 | 9.4 | 1.7 | 0.57 | 0.57 | 3785 |
| 32 | 1.50 | 1.60 | 70.9 | 47.2 | 3.94 | 0.49 | 3.9 | 9.4 | 1.3 | 0.28 | 0.28 | 3495 |

**Table 8-2 Geometric and material properties of the rectangular wall data (cont'd)**

| No | $h_w / l_w$ | $M / Vl_w$ | $h_w$ (in) | $l_w$ (in) | $t_w$ (in) | Scale | $b_f$ (in) | $h_f$ (in) | $\rho_{be}$ (%) | $\rho_v$ (%) | $\rho_h$ (%) | $f_c'$ (psi) |
|---|---|---|---|---|---|---|---|---|---|---|---|---|
| 33 | 1.50 | 1.60 | 70.9 | 47.2 | 3.94 | 0.49 | 3.9 | 9.4 | 1.7 | 0.57 | 0.57 | 3988 |
| 34 | 1.00 | 1.10 | 47.2 | 47.2 | 3.94 | 0.49 | 3.9 | 9.4 | 1.3 | 0.57 | 0.57 | 3219 |
| 35 | 0.50 | 0.57 | 59.1 | 118.1 | 3.94 | 0.49 | 3.9 | 9.4 | 1.9 | 0.81 | 1.61 | 3945 |
| 36 | 0.89 | 0.44 | 48.0 | 54.0 | 6.00 | 0.75 | 6.0 | 7.5 | 0.9 | 0.25 | 0.27 | 4100 |
| 37 | 0.89 | 0.44 | 48.0 | 54.0 | 6.00 | 0.75 | 6.0 | 7.5 | 0.9 | 0.25 | 0.27 | 4550 |
| 38 | 0.89 | 0.44 | 48.0 | 54.0 | 6.00 | 0.75 | 6.0 | 7.5 | 0.9 | 0.25 | 0.27 | 4630 |
| 39 | 0.89 | 0.44 | 48.0 | 54.0 | 6.00 | 0.75 | 6.0 | 7.5 | 0.9 | 0.25 | 0.27 | 4640 |
| 40 | 0.89 | 0.44 | 48.0 | 54.0 | 6.00 | 0.75 | 6.0 | 7.5 | 0.9 | 0.25 | 0.27 | 4340 |
| 41 | 0.89 | 0.44 | 48.0 | 54.0 | 6.00 | 0.75 | 6.0 | 7.5 | 0.9 | 0.25 | 0.27 | 4500 |
| 42 | 0.50 | 0.59 | 48.0 | 96.0 | 6.00 | 0.75 | 0.0 | 0.0 | 0.0 | 0.37 | 0.31 | 4250 |
| 43 | 1.38 | 0.69 | 70.9 | 51.2 | 3.94 | 0.49 | 1.8 | 3.1 | 5.9 | 0.00 | 0.25 | 3655 |
| 44 | 1.00 | 0.50 | 55.1 | 55.1 | 3.94 | 0.49 | 1.8 | 3.1 | 5.9 | 0.00 | 0.25 | 3597 |
| 45 | 1.90 | 1.10 | 33.7 | 17.7 | 1.77 | 0.22 | 1.8 | 3.1 | 5.9 | 0.39 | 0.92 | 6230 |
| 46 | 1.90 | 1.10 | 33.7 | 17.7 | 1.77 | 0.22 | 1.8 | 3.1 | 5.9 | 0.39 | 0.92 | 6421 |
| 47 | 1.90 | 1.10 | 33.7 | 17.7 | 1.77 | 0.22 | 1.8 | 3.1 | 5.9 | 0.39 | 0.92 | 7537 |
| 48 | 1.90 | 1.10 | 33.7 | 17.7 | 1.77 | 0.22 | 1.8 | 3.1 | 5.9 | 0.39 | 0.92 | 6289 |
| 49 | 1.90 | 1.10 | 33.7 | 17.7 | 1.77 | 0.22 | 1.8 | 3.1 | 5.9 | 0.39 | 0.51 | 6436 |
| 50 | 1.90 | 1.10 | 33.7 | 17.7 | 1.77 | 0.22 | 3.9 | 9.4 | 1.7 | 0.00 | 0.62 | 5995 |
| 51 | 1.90 | 1.10 | 33.7 | 17.7 | 1.77 | 0.22 | 3.9 | 9.4 | 1.3 | 0.00 | 0.80 | 6083 |
| | | | | | | | | | | | | |
| Min | 0.25 | 0.33 | 19.7 | 17.7 | 1.77 | 0.22 | 0.0 | 0.0 | 0.0 | 0.00 | 0.00 | 2915 |
| Max | 2.00 | 2.13 | 70.9 | 118.1 | 6.00 | 0.75 | 6.0 | 14.2 | 12.7 | 2.14 | 1.61 | 7537 |
| Mean | 1.27 | 1.15 | 43.3 | 41.7 | 3.41 | 0.43 | 2.9 | 5.6 | 3.3 | 0.83 | 0.61 | 5249 |

**Table 8-3 Summary of barbell wall data used to create fragility functions**

| No | Reference | Wall ID | Loading | $P / A_t f_c'$ (%) | Number of damage data per MoR | | | |
|---|---|---|---|---|---|---|---|---|
| | | | | | 1 | 2 | 3 | 4 |
| 1 | AIJ (1985a) | CW-0.6-1.2-20 | Cyclic | 5.8 | 1 | 1 | 0 | 1 |
| 2 | | CW-0.6-0.6-20 | Cyclic | 6.6 | 1 | 1 | 0 | 1 |
| 3 | | CW-0.6-0.8-20 | Cyclic | 4.9 | 1 | 1 | 0 | 1 |
| 4 | | CW-0.6-1.6-20 | Cyclic | 5.8 | 1 | 0 | 0 | 1 |
| 5 | | CW-0.6-2.0-20 | Cyclic | 5.7 | 1 | 0 | 0 | 1 |
| 6 | | CW-0.6-1.2-40 | Cyclic | 12.3 | 1 | 0 | 0 | 1 |
| 7 | | CW-0.4-1.2-20 | Cyclic | 5.9 | 1 | 0 | 0 | 1 |
| 8 | | CW-0.8-1.2-20 | Cyclic | 5.9 | 1 | 0 | 0 | 1 |
| 9 | AIJ (1986c) | CW-0.6-0.6-20a | Cyclic | 6.7 | 2 | 2 | 1 | 1 |
| 10 | | CW-0.6-0.8-20a | Cyclic | 6.6 | 2 | 3 | 1 | 1 |
| 11 | | CW-0.6-1.2-0 | Cyclic | 0.0 | 2 | 3 | 1 | 1 |
| 12 | AIJ (1985b) | CW-0.6-0-20 | Cyclic | 5.6 | 2 | 1 | 1 | 1 |
| 13 | | CW-0.6-0.3-20 | Cyclic | 5.6 | 2 | 3 | 1 | 1 |
| 14 | | CW-0.6-2.4-20 | Cyclic | 5.8 | 2 | 2 | 1 | 1 |
| 15 | | CW-0.6-2.8-20 | Cyclic | 6.2 | 2 | 1 | 1 | 1 |
| 16 | | CW-0.6-0-0 | Cyclic | 0.0 | 2 | 1 | 1 | 1 |
| 17 | | CW-0.6-0-40 | Cyclic | 12.4 | 2 | 1 | 1 | 1 |
| 18 | | CW-0.6-0.6-0 | Cyclic | 0.0 | 2 | 3 | 1 | 1 |
| 19 | | CW-0.6-0.6-40 | Cyclic | 11.5 | 2 | 3 | 1 | 1 |
| 20 | | CW-0.4-0.6-20 | Cyclic | 5.8 | 2 | 3 | 1 | 1 |
| 21 | | CW-0.8-0.6-20 | Cyclic | 5.8 | 2 | 3 | 1 | 1 |
| 22 | | CW-0.4-2.0-20 | Cyclic | 5.8 | 2 | 1 | 1 | 1 |
| 23 | | CW-0.8-2.0-20 | Cyclic | 5.7 | 2 | 3 | 1 | 1 |
| 24 | AIJ (1986b) | CW-0.6-2-0 | Cyclic | 0.0 | 1 | 0 | 0 | 1 |
| 25 | | CW-0.6-2-40 | Cyclic | 11.6 | 1 | 0 | 0 | 1 |
| 26 | | CW-0.6-2-20B | Cyclic | 5.5 | 1 | 0 | 0 | 1 |
| 27 | | CW-0.6-0.6-20L | Cyclic | 7.8 | 1 | 0 | 0 | 1 |
| 28 | | CW-0.6-1.2-20L | Cyclic | 7.6 | 1 | 0 | 0 | 1 |
| 29 | | CW-0.6-2-20L | Cyclic | 7.8 | 1 | 0 | 0 | 1 |
| 30 | AIJ (1986a) | No1 | Cyclic | 7.2 | 0 | 0 | 0 | 1 |
| 31 | | No2 | Cyclic | 5.1 | 0 | 0 | 0 | 1 |
| 32 | | No3 | Cyclic | 3.4 | 0 | 0 | 0 | 1 |

**Table 8-4 Geometric and material properties of the barbell wall data**

| No | $h_w / l_w$ | $M / Vl_w$ | $h_w$ (in) | $l_w$ (in) | $t_w$ (in) | Scale | $b_f$ (in) | $h_f$ (in) | $\rho_{be}$ (%) | $\rho_v$ (%) | $\rho_h$ (%) | $f_c'$ (psi) |
|---|---|---|---|---|---|---|---|---|---|---|---|---|
| 1 | 0.46 | 0.52 | 41.3 | 90.6 | 3.15 | 0.39 | 11.8 | 11.8 | 1.0 | 1.20 | 1.20 | 4935 |
| 2 | 0.46 | 0.52 | 41.3 | 90.6 | 3.15 | 0.39 | 11.8 | 11.8 | 1.0 | 0.60 | 0.60 | 4281 |
| 3 | 0.46 | 0.52 | 41.3 | 90.6 | 3.15 | 0.39 | 11.8 | 11.8 | 1.0 | 0.80 | 0.80 | 5760 |
| 4 | 0.46 | 0.52 | 41.3 | 90.6 | 3.15 | 0.39 | 11.8 | 11.8 | 1.4 | 1.60 | 1.60 | 4878 |
| 5 | 0.46 | 0.52 | 41.3 | 90.6 | 3.15 | 0.39 | 11.8 | 11.8 | 1.8 | 2.00 | 2.00 | 5021 |
| 6 | 0.46 | 0.52 | 41.3 | 90.6 | 3.15 | 0.39 | 11.8 | 11.8 | 1.0 | 1.20 | 1.20 | 4608 |
| 7 | 0.28 | 0.35 | 25.6 | 90.6 | 3.15 | 0.39 | 11.8 | 11.8 | 1.0 | 1.20 | 1.20 | 4793 |
| 8 | 0.63 | 0.70 | 57.1 | 90.6 | 3.15 | 0.39 | 11.8 | 11.8 | 1.0 | 1.20 | 1.20 | 4850 |
| 9 | 0.46 | 0.52 | 41.3 | 90.6 | 3.15 | 0.39 | 11.8 | 11.8 | 1.0 | 0.60 | 0.60 | 4224 |
| 10 | 0.46 | 0.52 | 41.3 | 90.6 | 3.15 | 0.39 | 11.8 | 11.8 | 1.0 | 0.80 | 0.80 | 4295 |
| 11 | 0.46 | 0.52 | 41.3 | 90.6 | 3.15 | 0.39 | 11.8 | 11.8 | 1.0 | 1.20 | 1.20 | 4167 |
| 12 | 0.46 | 0.52 | 41.3 | 90.6 | 3.15 | 0.39 | 11.8 | 11.8 | 1.0 | 0.00 | 0.00 | 5106 |
| 13 | 0.46 | 0.52 | 41.3 | 90.6 | 3.15 | 0.39 | 11.8 | 11.8 | 1.0 | 0.30 | 0.30 | 5106 |
| 14 | 0.46 | 0.52 | 41.3 | 90.6 | 3.15 | 0.39 | 11.8 | 11.8 | 1.8 | 2.40 | 2.40 | 4878 |
| 15 | 0.46 | 0.52 | 41.3 | 90.6 | 3.15 | 0.39 | 11.8 | 11.8 | 1.8 | 2.80 | 2.80 | 4594 |
| 16 | 0.46 | 0.52 | 41.3 | 90.6 | 3.15 | 0.39 | 11.8 | 11.8 | 1.0 | 0.00 | 0.00 | 4594 |
| 17 | 0.46 | 0.52 | 41.3 | 90.6 | 3.15 | 0.39 | 11.8 | 11.8 | 1.0 | 0.00 | 0.00 | 4594 |
| 18 | 0.46 | 0.52 | 41.3 | 90.6 | 3.15 | 0.39 | 11.8 | 11.8 | 1.0 | 0.60 | 0.60 | 5106 |
| 19 | 0.46 | 0.52 | 41.3 | 90.6 | 3.15 | 0.39 | 11.8 | 11.8 | 1.0 | 0.60 | 0.60 | 4935 |
| 20 | 0.28 | 0.35 | 25.6 | 90.6 | 3.15 | 0.39 | 11.8 | 11.8 | 1.0 | 0.60 | 0.60 | 4878 |
| 21 | 0.63 | 0.70 | 57.1 | 90.6 | 3.15 | 0.39 | 11.8 | 11.8 | 1.0 | 0.60 | 0.60 | 4864 |
| 22 | 0.28 | 0.35 | 25.6 | 90.6 | 3.15 | 0.39 | 11.8 | 11.8 | 1.8 | 2.00 | 2.00 | 4935 |
| 23 | 0.63 | 0.70 | 57.1 | 90.6 | 3.15 | 0.39 | 11.8 | 11.8 | 1.8 | 2.00 | 2.00 | 4978 |
| 24 | 0.46 | 0.52 | 41.3 | 90.6 | 3.15 | 0.39 | 11.8 | 11.8 | 1.8 | 2.00 | 2.00 | 4893 |
| 25 | 0.46 | 0.52 | 41.3 | 90.6 | 3.15 | 0.39 | 11.8 | 11.8 | 1.8 | 2.00 | 2.00 | 4921 |
| 26 | 0.46 | 0.52 | 41.3 | 90.6 | 3.15 | 0.39 | 11.8 | 11.8 | 1.0 | 2.00 | 2.00 | 5149 |
| 27 | 0.46 | 0.52 | 41.3 | 90.6 | 3.15 | 0.39 | 11.8 | 11.8 | 1.0 | 0.60 | 0.60 | 3655 |
| 28 | 0.46 | 0.52 | 41.3 | 90.6 | 3.15 | 0.39 | 11.8 | 11.8 | 1.0 | 1.20 | 1.20 | 3755 |
| 29 | 0.46 | 0.52 | 41.3 | 90.6 | 3.15 | 0.39 | 11.8 | 11.8 | 1.8 | 2.00 | 2.00 | 3655 |
| 30 | 0.48 | 0.55 | 41.3 | 85.8 | 3.15 | 0.39 | 7.1 | 7.1 | 2.9 | 1.20 | 1.20 | 3940 |
| 31 | 0.48 | 0.55 | 41.3 | 85.8 | 3.15 | 0.39 | 7.1 | 7.1 | 2.9 | 1.20 | 1.20 | 5561 |
| 32 | 0.48 | 0.55 | 41.3 | 85.8 | 3.15 | 0.39 | 7.1 | 7.1 | 2.9 | 1.20 | 1.20 | 8463 |
| | | | | | | | | | | | | |
| Min | 0.28 | 0.35 | 25.6 | 85.8 | 3.15 | 0.39 | 7.1 | 7.1 | 1.0 | 0.00 | 0.00 | 3655 |
| Max | 0.63 | 0.70 | 57.1 | 90.6 | 3.15 | 0.39 | 11.8 | 11.8 | 2.9 | 2.80 | 2.80 | 8463 |
| Mean | 0.46 | 0.52 | 41.3 | 90.1 | 3.15 | 0.39 | 11.4 | 11.4 | 1.4 | 1.18 | 1.18 | 4824 |

**Table 8-5 Summary of flanged wall data used to create fragility functions**

| No | Reference | Wall ID | Loading | $P / A_t f_c'$ (%) | Number of damage data per MoR | | | |
|---|---|---|---|---|---|---|---|---|
| | | | | | 1 | 2 | 3 | 4 |
| 1 | Barda (1972) | B1-1 | Monotonic | 0.0 | 4 | 2 | 1 | 0 |
| 2 | | B2-1 | Monotonic | 0.0 | 4 | 2 | 1 | 1 |
| 3 | | B3-2 | Cyclic | 0.0 | 4 | 1 | 1 | 1 |
| 4 | | B4-3 | Cyclic | 0.0 | 4 | 2 | 1 | 1 |
| 5 | | B5-4 | Cyclic | 0.0 | 2 | 2 | 1 | 0 |
| 6 | | B6-4 | Cyclic | 0.0 | 4 | 3 | 1 | 1 |
| 7 | | B7-5 | Cyclic | 0.0 | 3 | 3 | 1 | 1 |
| 8 | | B8-5 | Cyclic | 0.0 | 3 | 3 | 1 | 1 |
| 9 | Maier and Thürlimann (1985) | S1 | Monotonic | 6.6 | 1 | 3 | 1 | 1 |
| 10 | | S2 | Monotonic | 24.2 | 2 | 1 | 1 | 1 |
| 11 | | S3 | Monotonic | 6.5 | 1 | 3 | 0 | 1 |
| 12 | | S5 | Cyclic | 6.3 | 1 | 4 | 1 | 1 |
| 13 | | S6 | Monotonic | 6.6 | 1 | 4 | 1 | 1 |
| 14 | | S7 | Cyclic | 27.3 | 2 | 1 | 0 | 1 |
| 15 | Synge (1980) | Wall-3 | Cyclic | 0.0 | 1 | 2 | 2 | 1 |
| 16 | Kitada et al. (1997) | U-1 | ES | 3.9 | 0 | 0 | 0 | 1 |
| 17 | Palermo and Vecchio (2002a) | DP1 | Cyclic | 5.4 | 3 | 3 | 1 | 1 |
| 18 | | DP2 | Cyclic | 0.0 | 3 | 2 | 1 | 1 |
| 19 | Saito et al. (1989) | W12-1 | Cyclic | 5.6 | 1 | 1 | 0 | 1 |
| 20 | Sato et al. (1989) | 24M 8-30 | Cyclic | 5.3 | 0 | 1 | 1 | 0 |
| 21 | | 24M 8-40 | Cyclic | 5.6 | 0 | 1 | 1 | 0 |
| 22 | | 24M 8-50 | Cyclic | 5.7 | 0 | 1 | 1 | 0 |
| 23 | | 36M 8-30 | Cyclic | 5.1 | 2 | 2 | 1 | 1 |
| 24 | | 36M 8-40 | Cyclic | 5.2 | 0 | 1 | 1 | 0 |
| 25 | | 36M 8-50 | Cyclic | 5.3 | 2 | 2 | 1 | 1 |
| 26 | | 48M 8-30 | Cyclic | 7.3 | 0 | 1 | 1 | 0 |
| 27 | | 48M 8-40 | Cyclic | 7.3 | 0 | 1 | 1 | 0 |
| 28 | | 48M 8-50 | Cyclic | 7.1 | 0 | 1 | 1 | 0 |

**Table 8-6 Geometric and material properties of the flanged wall data**

| No | $h_w / l_w$ | $M / Vl_w$ | $h_w$ (in) | $l_w$ (in) | $t_w$ (in) | Scale | $b_f$ (in) | $h_f$ (in) | $\rho_{be}$ (%) | $\rho_v$ (%) | $\rho_h$ (%) | $f_c'$ (psi) |
|---|---|---|---|---|---|---|---|---|---|---|---|---|
| 1 | 0.46 | 0.50 | 34.5 | 75.0 | 4.00 | 0.50 | 24.0 | 4.0 | 1.8 | 0.50 | 0.48 | 4200 |
| 2 | 0.46 | 0.50 | 34.5 | 75.0 | 4.00 | 0.50 | 24.0 | 4.0 | 6.4 | 0.50 | 0.48 | 2370 |
| 3 | 0.46 | 0.50 | 34.5 | 75.0 | 4.00 | 0.50 | 24.0 | 4.0 | 4.1 | 0.50 | 0.48 | 3920 |
| 4 | 0.46 | 0.50 | 34.5 | 75.0 | 4.00 | 0.50 | 24.0 | 4.0 | 4.1 | 0.50 | 0.00 | 2760 |
| 5 | 0.46 | 0.50 | 34.5 | 75.0 | 4.00 | 0.50 | 24.0 | 4.0 | 4.1 | 0.00 | 0.48 | 4190 |
| 6 | 0.46 | 0.50 | 34.5 | 75.0 | 4.00 | 0.50 | 24.0 | 4.0 | 4.1 | 0.26 | 0.48 | 3080 |
| 7 | 0.21 | 0.25 | 15.8 | 75.0 | 4.00 | 0.50 | 24.0 | 4.0 | 4.1 | 0.50 | 0.49 | 3730 |
| 8 | 0.96 | 1.00 | 72.0 | 75.0 | 4.00 | 0.50 | 24.0 | 4.0 | 4.1 | 0.50 | 0.50 | 3400 |
| 9 | 1.02 | 1.12 | 47.2 | 46.5 | 3.94 | 0.49 | 15.7 | 3.9 | 1.1 | 1.13 | 1.01 | 5352 |
| 10 | 1.02 | 1.12 | 47.2 | 46.5 | 3.94 | 0.49 | 15.7 | 3.9 | 1.1 | 1.13 | 1.01 | 5568 |
| 11 | 1.02 | 1.12 | 47.2 | 46.5 | 3.94 | 0.49 | 15.7 | 3.9 | 2.5 | 2.54 | 1.01 | 5323 |
| 12 | 1.02 | 1.12 | 47.2 | 46.5 | 3.94 | 0.49 | 15.7 | 3.9 | 1.1 | 1.13 | 1.01 | 5410 |
| 13 | 1.02 | 1.12 | 47.2 | 46.5 | 3.94 | 0.49 | 15.7 | 3.9 | 1.1 | 1.13 | 0.57 | 5163 |
| 14 | 1.02 | 1.12 | 47.2 | 46.5 | 3.94 | 0.49 | 15.7 | 3.9 | 1.1 | 1.13 | 1.01 | 4946 |
| 15 | 0.50 | 0.57 | 59.1 | 118.1 | 3.94 | 0.49 | 19.7 | 3.9 | 1.8 | 0.37 | 1.61 | 3771 |
| 16 | 0.65 | 0.77 | 79.5 | 122.0 | 2.95 | 0.37 | 117.3 | 3.9 | 0.5 | 1.20 | 1.20 | 4153 |
| 17 | 0.66 | 0.76 | 79.5 | 121.1 | 2.95 | 0.37 | 119.9 | 3.7 | 0.4 | 0.82 | 0.76 | 3147 |
| 18 | 0.65 | 0.76 | 79.5 | 121.5 | 2.95 | 0.37 | 119.9 | 3.9 | 0.4 | 0.82 | 0.76 | 2727 |
| 19 | 0.35 | 0.47 | 29.5 | 83.5 | 4.72 | 0.59 | 19.7 | 4.7 | 4.8 | 1.32 | 1.32 | 5106 |
| 20 | 0.65 | 0.74 | 55.1 | 84.6 | 5.91 | 0.74 | 39.4 | 5.9 | 0.8 | 0.80 | 0.80 | 5512 |
| 21 | 0.65 | 0.74 | 55.1 | 84.6 | 5.91 | 0.74 | 39.4 | 5.9 | 0.6 | 0.60 | 0.60 | 5192 |
| 22 | 0.65 | 0.74 | 55.1 | 84.6 | 5.91 | 0.74 | 39.4 | 5.9 | 0.5 | 0.48 | 0.48 | 5076 |
| 23 | 0.65 | 0.74 | 55.1 | 84.6 | 5.91 | 0.74 | 39.4 | 5.9 | 1.2 | 1.16 | 1.16 | 5700 |
| 24 | 0.65 | 0.74 | 55.1 | 84.6 | 5.91 | 0.74 | 39.4 | 5.9 | 0.9 | 0.90 | 0.90 | 5628 |
| 25 | 0.65 | 0.74 | 55.1 | 84.6 | 5.91 | 0.74 | 39.4 | 5.9 | 0.7 | 0.72 | 0.72 | 5439 |
| 26 | 0.65 | 0.74 | 55.1 | 84.6 | 5.91 | 0.74 | 39.4 | 5.9 | 1.6 | 1.60 | 1.60 | 3974 |
| 27 | 0.65 | 0.74 | 55.1 | 84.6 | 5.91 | 0.74 | 39.4 | 5.9 | 1.2 | 1.16 | 1.16 | 3989 |
| 28 | 0.65 | 0.74 | 55.1 | 84.6 | 5.91 | 0.74 | 39.4 | 5.9 | 1.0 | 0.96 | 0.96 | 4061 |
| | | | | | | | | | | | | |
| Min | 0.21 | 0.25 | 15.8 | 46.5 | 2.95 | 0.37 | 15.7 | 3.7 | 0.4 | 0.00 | 0.00 | 2370 |
| Max | 1.02 | 1.12 | 79.5 | 122.0 | 5.91 | 0.74 | 119.9 | 5.9 | 6.4 | 2.54 | 1.61 | 5700 |
| Mean | 0.67 | 0.75 | 50.1 | 78.8 | 4.51 | 0.56 | 37.0 | 4.6 | 2.0 | 0.87 | 0.82 | 4389 |

Experimental data from 111 squat walls that met the above criteria provided the damage data presented below. Twenty-eight walls had flanges, 32 walls had barbells, and 51 walls had rectangular cross-sections. The web thickness ranged between 1.77 in. and 6 in. The aspect ratios $(h_w / l_w)$ ranged between 0.21 and 2.0; moment-to-shear ratios $(M / Vl_w)$ ranged between 0.25 and 2.13. The maximum aspect ratio in the barbell and flanged wall datasets are 0.63 and 1.02, respectively. Sixty-five walls were tested with applied axial load ranging between $0.022 A_t f_c'$ and $0.273 A_t f_c'$, where $A_t$ is total wall area and $f_c'$ is concrete compressive strength. Concrete compressive strength, based on standard cylindrical tests, varied between 2370 and 8463 psi. Eight walls did not have vertical web reinforcement, 6 walls did not have horizontal web reinforcement and 3 walls did not have any web reinforcement. Eleven of the 111 test specimens did not comply with the minimum reinforcement requirements ( $\rho_h = \rho_v = 0.25\%$) of ACI 318-08 [ACI (2008)] for *Special Structural Walls and Concrete Beams* (Chapter 21.9). The maximum observed horizontal and vertical reinforcement ratios were 2.80%. Eighty-nine of the 111 test specimens were tested using cyclic loading, 21 were tested using monotonic loading and 1 was tested using an earthquake simulator. The scales in the dataset ranged between 0.22 and 0.75.

## 8.3 Demand Parameter Selection

The experimental data described in Section 8.2 was mined to prepare fragility curves. The fragility curves are presented as a function of racking drift, which is the best single story-level demand parameter for most structural elements. Importantly, drift is the demand parameter most reported in the literature.

Two other demand parameters were considered for this study but were set aside. Dissipated hysteretic energy [Park and Ang (1985)] has been used to assess damage to concrete components. However, the literature rarely includes hysteretic loops that are amenable to digitization and calculation of dissipated energy and so this demand parameter cannot be computed with high confidence. Pagni and Lowes (2006) and Brown and Lowes (2007) proposed a variant on dissipated hysteretic energy for assessment of reinforced concrete beam-column joints, namely, a demand parameter whose functional form included maximum story drift and number of load (or displacement) cycles as variables. Unfortunately, many sources did not report the relationship between damage and number of loading cycles and so the Lowes demand parameter was not pursued.

## 8.4 Damage States and Methods of Repair

Damage states (DS) define threshold levels of damage sustained by structural components under earthquake loading. A family of damage states, which are listed in Table 8-7, was assembled following analysis of test data and review of the literature. Damage states are characterized generally by direct indicators of damage such as initiation of cracking, maximum concrete crack width, extent of concrete crushing, sliding shear displacement, and reinforcement yielding, buckling, and fracture. Each of these damage states is linked with one of four methods of repair in the table.

**Table 8-7 Damage states and corresponding methods of repairs**

| ID | Damage States | Method of Repair (MoR) |
|---|---|---|
| DS1.1 | Initiation of cracking | Cosmetic repair (MoR-1) |
| DS1.2 | Initiation of flexural cracking | |
| DS1.3 | Initiation of shear cracking | |
| DS1.4 | Maximum measured crack widths less than 0.02 in. (0.5 mm) | |
| DS2.1 | Initiation of yielding in horizontal web reinforcement | Epoxy injection (MoR-2) |
| DS2.2 | Initiation of yielding in vertical web reinforcement | |
| DS2.3 | Initiation of yielding in vertical boundary element reinforcement | |
| DS2.4a | Maximum measured shear crack widths larger than 0.02 in (0.5 mm) but less than 0.12 in. (3 mm) | |
| DS2.5a | Maximum measured flexural crack widths larger than 0.02 in (0.5 mm) but less than 0.12 in. (3 mm) | |
| DS2.4b | Maximum measured shear crack widths larger than 0.04 in (1.0 mm) but less than 0.12 in. (3 mm) | |
| DS2.5b | Maximum measured flexural crack widths larger than 0.04 in (1.0 mm) but less than 0.12 in. (3 mm) | |
| DS3.1 | Concrete crushing at the compression toes / initiation of crushing in the wall web | Partial wall replacement (MoR-3) |
| DS3.2 | Vertical cracking in the toe regions of the web | |
| DS3.3 | Buckling of boundary element vertical reinforcement | |
| DS3.4 | Flexural crack widths exceeding 0.12 in. (3 mm) | |
| DS4.1 | Initiation of sliding | Wall replacement (MoR-4) |
| DS4.2 | Wide diagonal cracks | |
| DS4.3 | Widespread crushing of concrete | |
| DS4.4 | Reinforcement fracture | |
| DS4.5 | Shear crack widths exceeding 0.12 in (3 mm) | |

Documents that provide guidelines for repair of reinforced concrete walls (e.g., FEMA 306 [ATC (1998b)] and FEMA 308 [ATC (1998a)]), repair of concrete (e.g., ACI 546R-04 [ACI (2004)]), observations from experimental programs, previous research on retrofit of squat walls and expert opinion [Hooper (2008)] were used to identify the most appropriate damage states and their corresponding methods of repair. The following subsections present information on each Method of Repair (MoR) and the corresponding damage states. The number of damage data obtained for each wall and method of repair is presented in Table 8-1, Table 8-3, and Table 8-5, for rectangular, barbell and flanged walls, respectively. Appendix C presents all of the damage data analyzed in the body of the report.

## 8.4.1 MoR-1, Cosmetic Repair

Damage states DS1.1 through DS1.4 of Table 8-7 are associated with cosmetic repair. These damage states represent the initiation of cracking in concrete and propagation of these cracks under earthquake loading. For cosmetic repair, crack widths are small (less than 0.02 in. as defined in DS1.4) and structural repair to restore strength and stiffness is unnecessary. Repair of the surface finishes may be required to restore the aesthetic appearance, maintain fire resistance and prevent water infiltration into the wall [ATC (1998a)].

Cosmetic repair has no impact on structural performance. Method of Repair MoR-1 is similar to Cosmetic Repair 1 (CR1) of FEMA 308. Examples of damage states 1.2 and 1.3, each of which is linked to MoR-1, are presented in Figure 8-1 and Figure 8-2.

## 8.4.2 MoR-2, Epoxy Injection

### 8.4.2.1 Introduction

Damage states DS2.1, DS2.2, DS2.3, DS2.4a, DS2.5a, DS2.4b, and DS2.5b of Table 8-7 are associated with epoxy-injection repair. Epoxy injection is widely used to restore the stiffness and strength of cracked concrete components. Crack width (DS2.4a, DS2.5a, DS2.4b, and DS2.5b) and reinforcement yielding (DS2.1, DS2.2, and DS2.3) are considered two indicators of the need for epoxy injection repair.

Method of Repair MoR-2 is similar to Structural Repair 1 of FEMA 308. Examples of damage states DS2.1, DS2.3, and DS2.4a, each of which is linked to MoR-2, are presented in Figure 8-3, Figure 8-4 and Figure 8-5, respectively.

There is no consensus in the design professional community on the minimum residual crack width for epoxy injection. Herein, two options are presented, MoR-2a and MoR-2b.

### 8.4.2.2 MoR-2a

Lowes and Li (2008) note that residual crack widths in excess of 0.01 to 0.02 in. require epoxy injection to restore component strength and stiffness. However, residual crack widths are not reported in the literature and could therefore not be used to identify the need for injection grouting. Rather, maximum crack width, which is presented in the literature, is used as a surrogate for residual crack width: if the reported maximum crack width under loading exceeds 0.02 in (0.5 mm), (assumed equivalent to DS2.4a and DS2.5a in Table 8-7) epoxy injection is

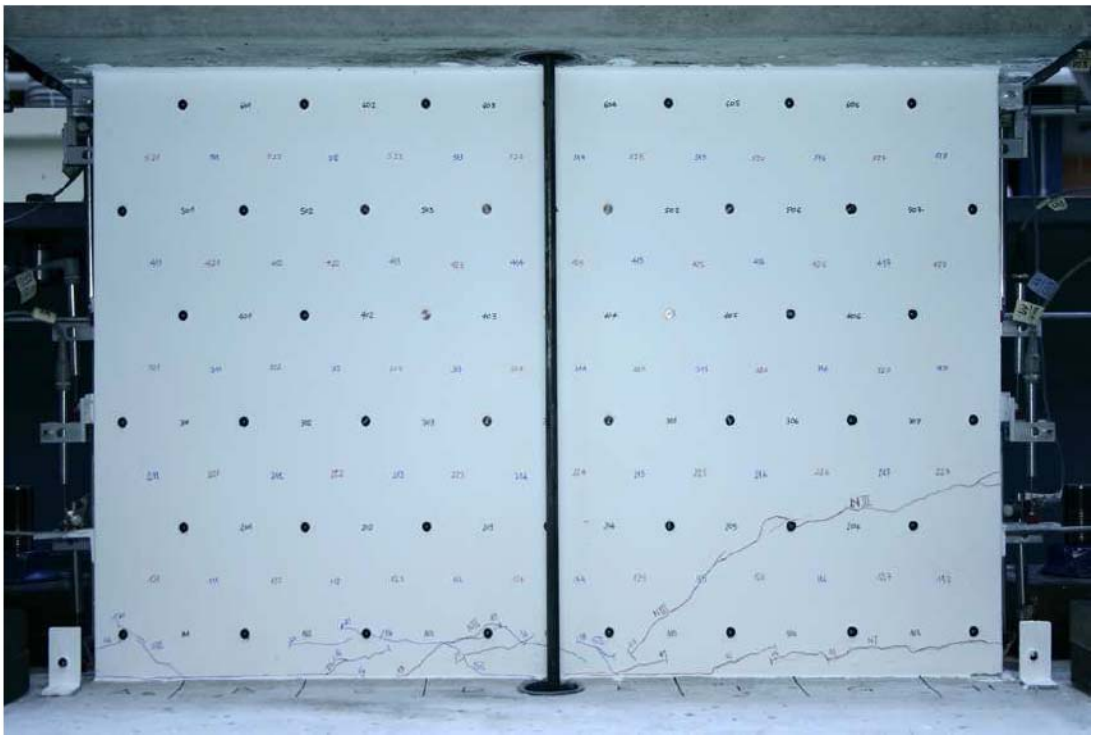

**Figure 8-1 Initial flexural cracks on wall M4 tested by Greifenhagen et al. (2005)**

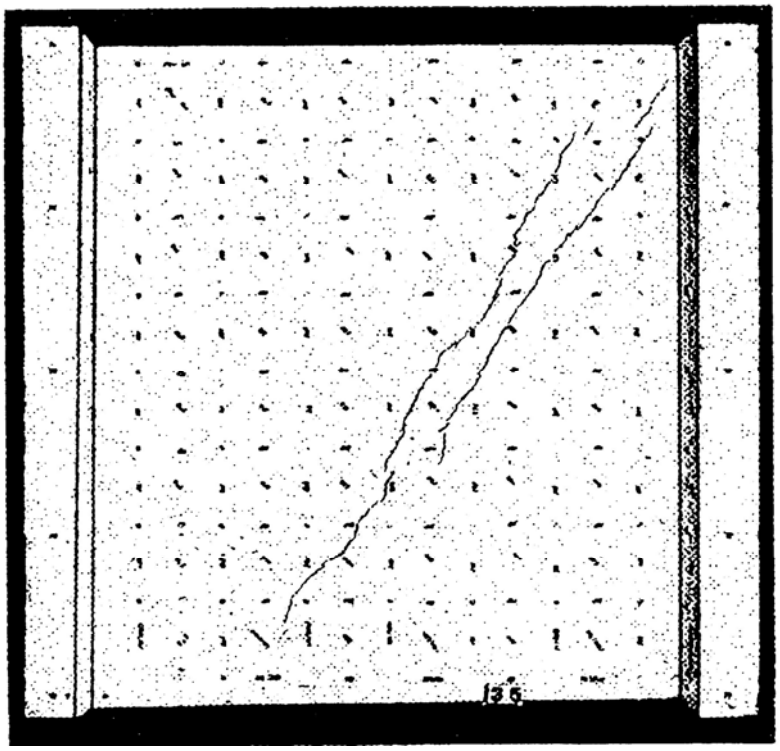

**Figure 8-2 Initial shear cracks on wall S2 tested by Maier and Thürlimann (1985)**

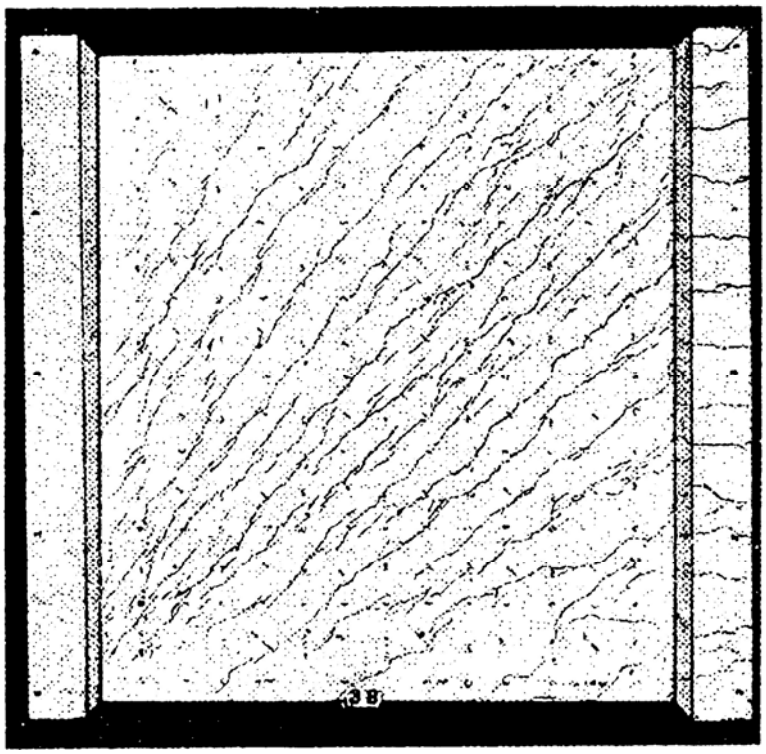

**Figure 8-3 Cracking pattern for wall S3 tested by Maier and Thürlimann (1985) at first yielding of horizontal web reinforcement**

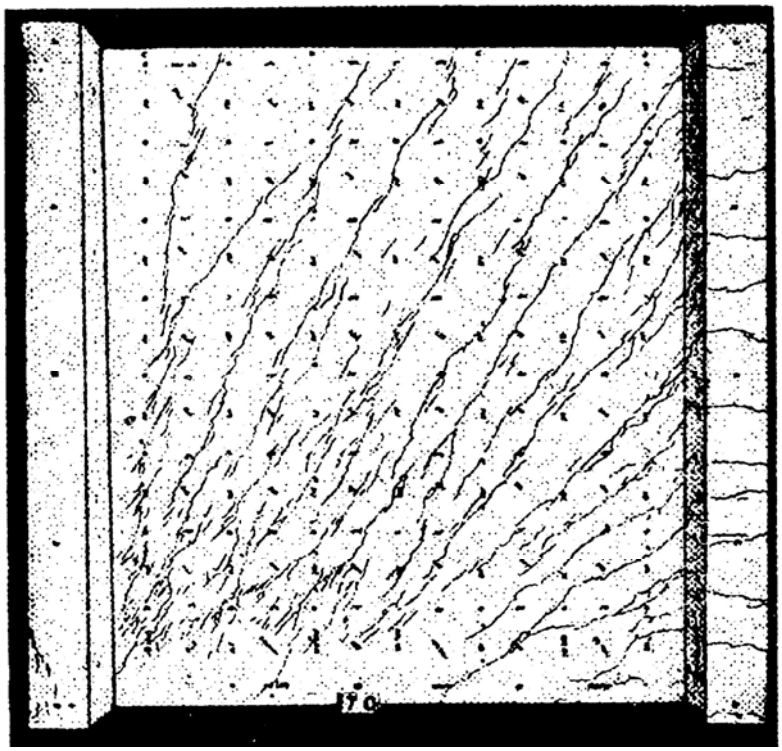

**Figure 8-4 Cracking pattern for wall S2 tested by Maier and Thürlimann (1985) at first yielding of flange vertical reinforcement**

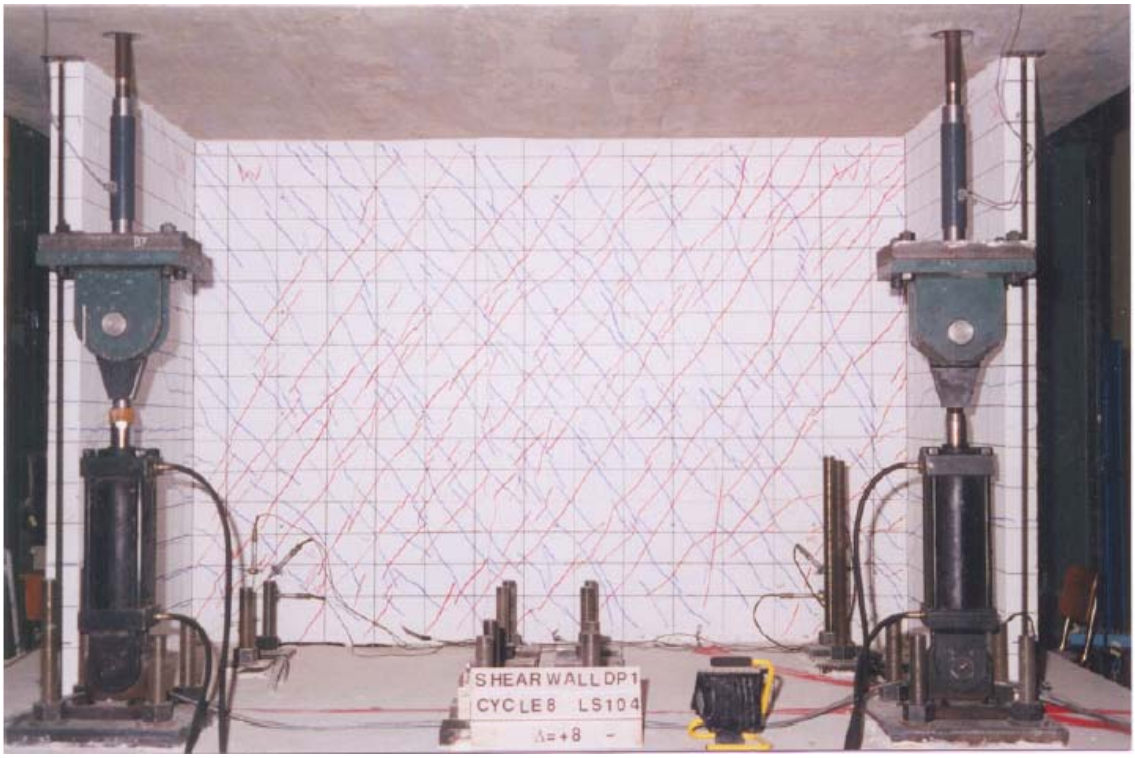


**Figure 8-5 Cracking pattern for wall DP1 tested by Palermo and Vecchio (2002a) at a maximum shear crack width of 0.5 mm**

required. Reinforcement yielding (DS2.1, DS2.2, and DS2.3) was used as another indicator for epoxy injection, on the basis that reinforcement yielding will result in residual cracks of substantial width. This relationship is studied in Section 8.6.

#### 8.4.2.3 MoR-2b

Method of Repair MoR-2b involves injection grouting of cracks for which the maximum crack width under loading exceeds 0.04 in (1.0 mm), that is DS2.4b and DS2.5b in Table 8-7.

### 8.4.3 MoR-3, Partial Wall Replacement

Damage states DS3.1 through DS3.4 of Table 8-7 are associated with removal and replacement of damaged concrete. Localized crushing at boundary elements and in the wall web will require replacement of damaged concrete. Vertical splitting cracks in boundary elements (DS3.2) and buckling of boundary element vertical reinforcement (DS3.3) are also linked to this MoR. Photographs of test specimens and observations made by the cited authors were used to identify data for damage states DS3.1, DS3.2, and DS3.3. Damage state DS3.4 assumes that a wall with flexural crack widths greater than 0.12 in. (3 mm) cannot be repaired to its pre-earthquake condition using epoxy injection and that damaged concrete and rebar must be replaced. Examples of damage states DS3.1 and DS3.4 are presented in Figure 8-6 and Figure 8-7, respectively.

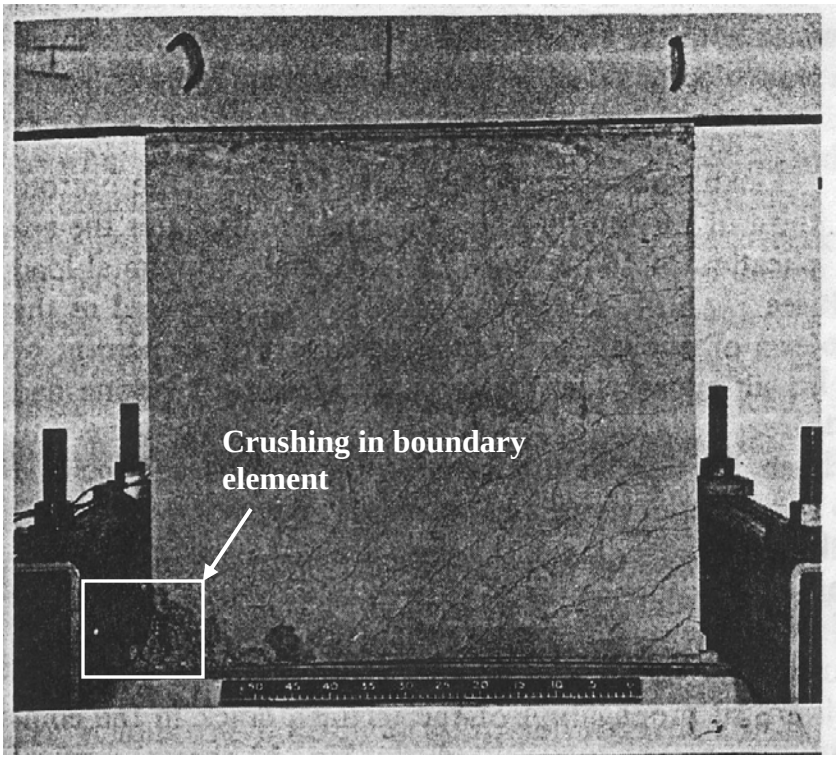


**Figure 8-6 Cracking pattern for wall SW11 tested by Lefas et al. (1990) at compression zone failure**

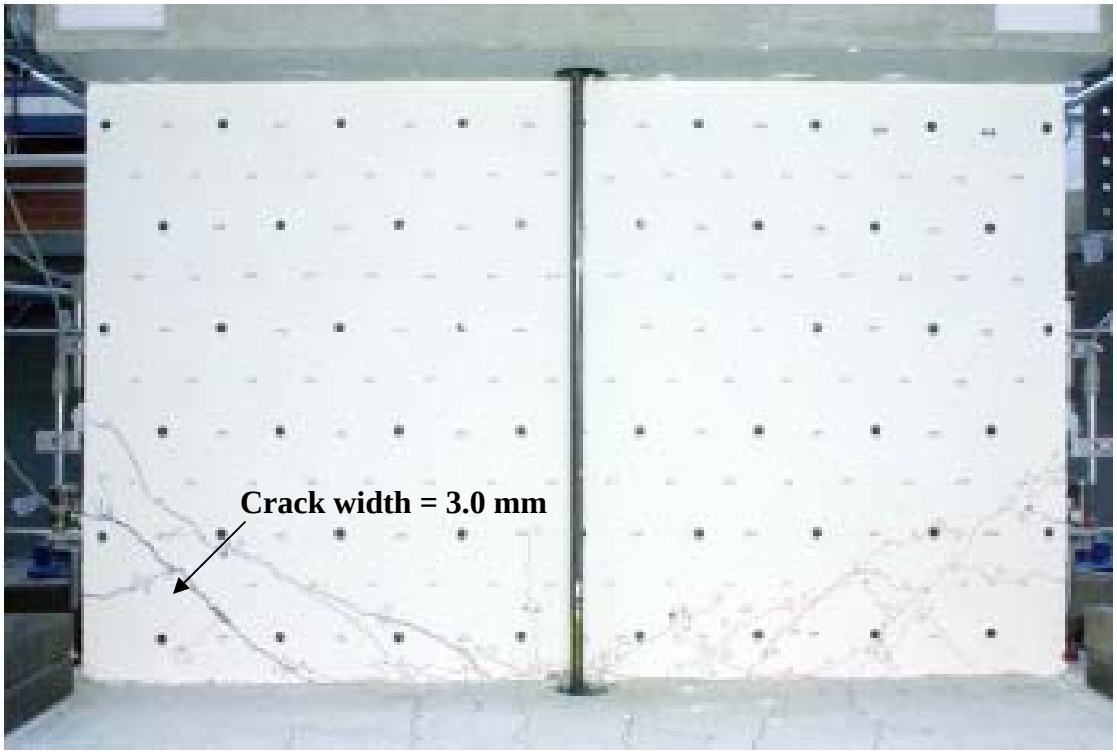


**Figure 8-7 Cracking pattern for wall M2 tested by Greifenhagen et al. (2005) at a maximum flexural crack width of 3.0 mm**

### 8.4.4 MoR-4, Wall Replacement

Damage states DS4.1 through DS4.5 of Table 8-7 are associated with complete replacement of the wall panel.

Sliding at the interface between the wall web and the foundation (DS4.1) will require wall panel replacement, especially if the residual displacement is significant. Squat walls with low vertical reinforcement ratio and low axial load are susceptible to sliding shear. A sample cracking pattern for damage state DS4.1 is presented in Figure 8-8. Substantial corner-to-corner diagonal cracks (DS 4.2) which are indicators of diagonal tension (DT) or flexure-diagonal tension (F-DT) failures [see Section 1.2], trigger a rapid loss of strength and stiffness. Such walls cannot be repaired using epoxy injection because the crack widths are too great and partial wall replacement is not feasible because of the orientation and length of the cracks. Squat walls with light horizontal reinforcement are susceptible to this type of damage. Figure 8-9 presents a cracking pattern for damage state DS4.2.

Walls with heavy reinforcement and/or high axial loads usually fail in diagonal compression (crushing of compression struts) as shown in Figure 8-10. The damage is so widespread that partial wall replacement is not feasible and the entire wall panel must be replaced (DS4.3). Reinforcement fracture (DS4.4) is rarely seen in tests of squat walls. Reinforcement fractured in only 3 of the 111 walls. Damage state DS4.4 is linked to wall replacement because reinforcement fracture followed other significant damage in all three cases. Figure 8-11 shows the cracking pattern in a wall at the fracture of boundary element vertical reinforcement. Widespread damage at the interface between the wall web and foundation is evident in the figure. Damage State DS4.5 assumes that wall panels with maximum shear crack widths larger than 0.12 in (3 mm) must be replaced. FEMA 306 [ATC (1998b)] notes that when the width of shear cracks in a wall exceed 1/8 in. (3.2 mm), the damage is considered *heavy* and restoration of the pre-earthquake strength and stiffness requires replacement of the wall. This damage state is similar to damage state DS4.2 in the sense that it is also closely related to diagonal tension (DT) and flexure-diagonal tension (F-DT) failures observed in squat walls.

The available images of damage together with the author's descriptions of damage were used wherever possible to identify the drift associated with wall replacement. A major challenge was the identification of drift corresponding to sliding shear failure (DS4.1). The author-reported drifts for sliding shear failures exhibited significant variance, for example, in some cases the authors reported the drifts at initiation of sliding whereas in others the author-reported drifts corresponding to significant sliding displacements. Two supplemental criteria are therefore used herein to aid in the identification of drift for DS4.1: 1) residual drift exceeding 0.5% ($SC_1$), and 2) drift associated with wall strength less than 50% of the peak strength ($SC_2$). Each criterion is described in more detail below. For a wall reported to have failed by sliding shear, the drift is calculated using $SC_1$. If a drift cannot be computed using $SC_1$, $SC_2$ is used. If a drift cannot be computed using $SC_2$, no data is reported for DS4.1.

*Supplemental Criterion* $SC_1$: If a cyclic force-displacement relationship was available, the peak transient drift associated with a residual drift angle of 0.5% was estimated. The residual drift angle of 0.5% was associated with a zero-force displacement intercept of 1% story drift angle. Given that the coda portion of earthquake ground motions will generally serve to partially re-center displaced components, elements and building frames, we assumed that a residual drift

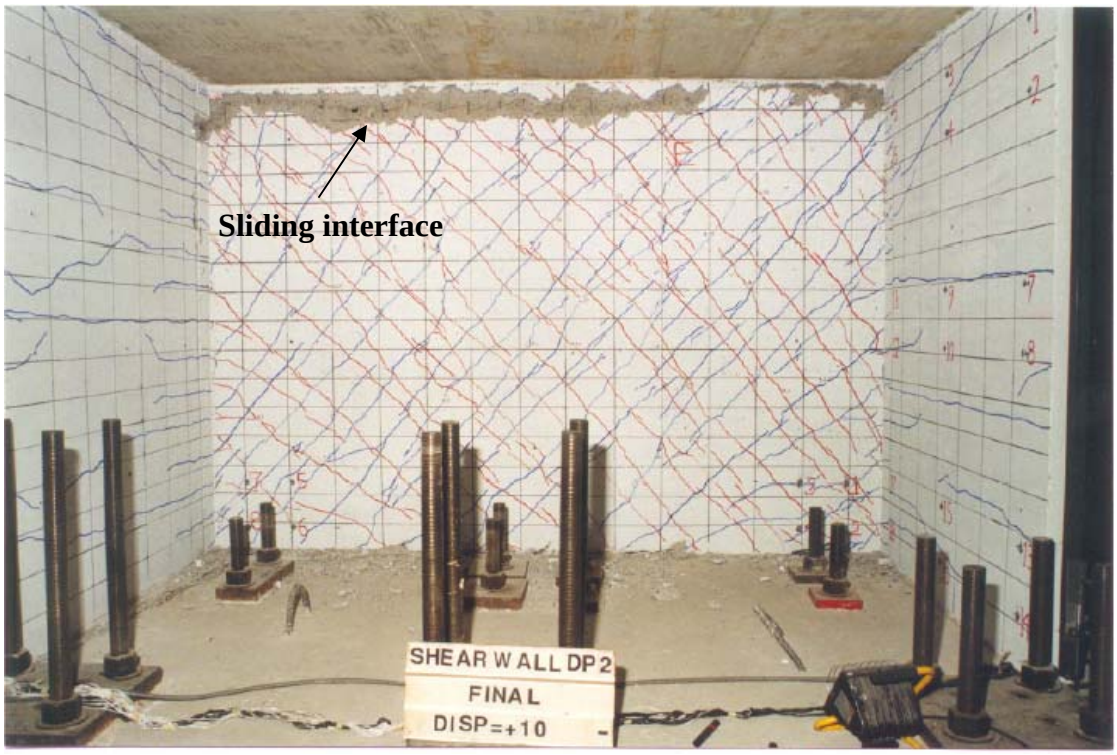


**Figure 8-8 Cracking pattern for wall DP2 tested by Palermo and Vecchio (2002a) at a sliding failure between the wall web and top slab**

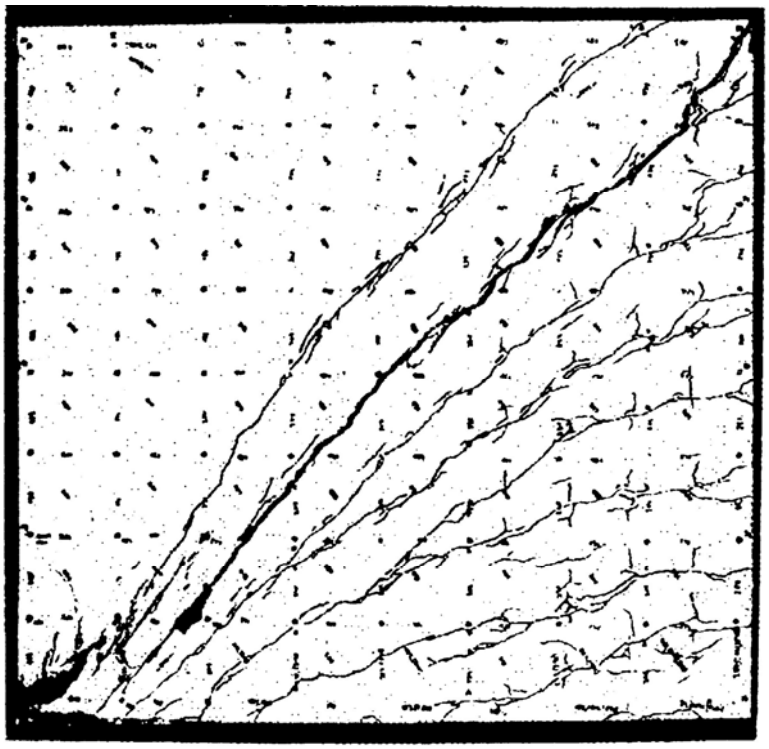

**Figure 8-9 Cracking pattern for wall S9 tested by Maier and Thürlimann (1985) at diagonal tension failure**

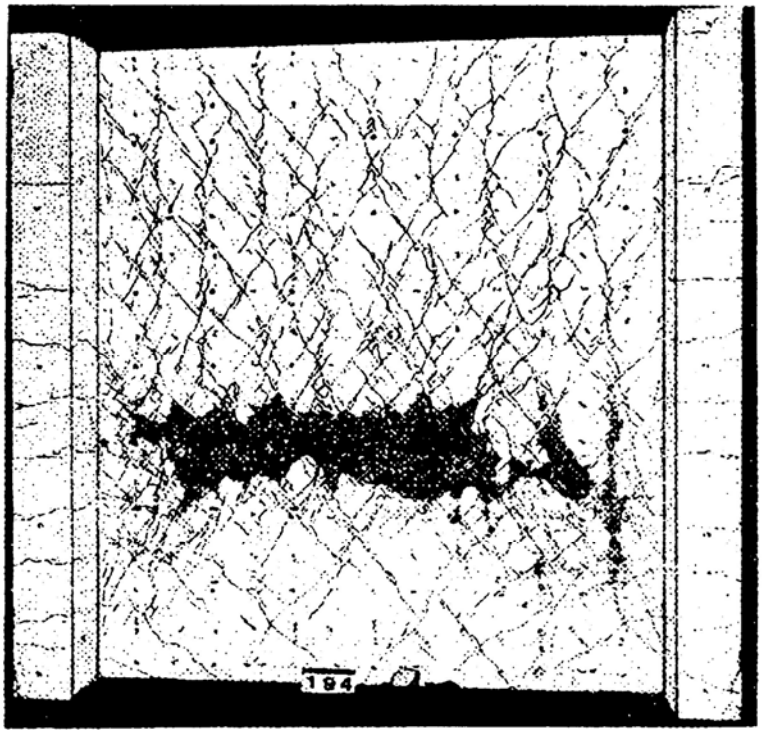


**Figure 8-10 Cracking pattern for wall S7 tested by Maier and Thürlimann (1985) at crushing of diagonal compression struts**

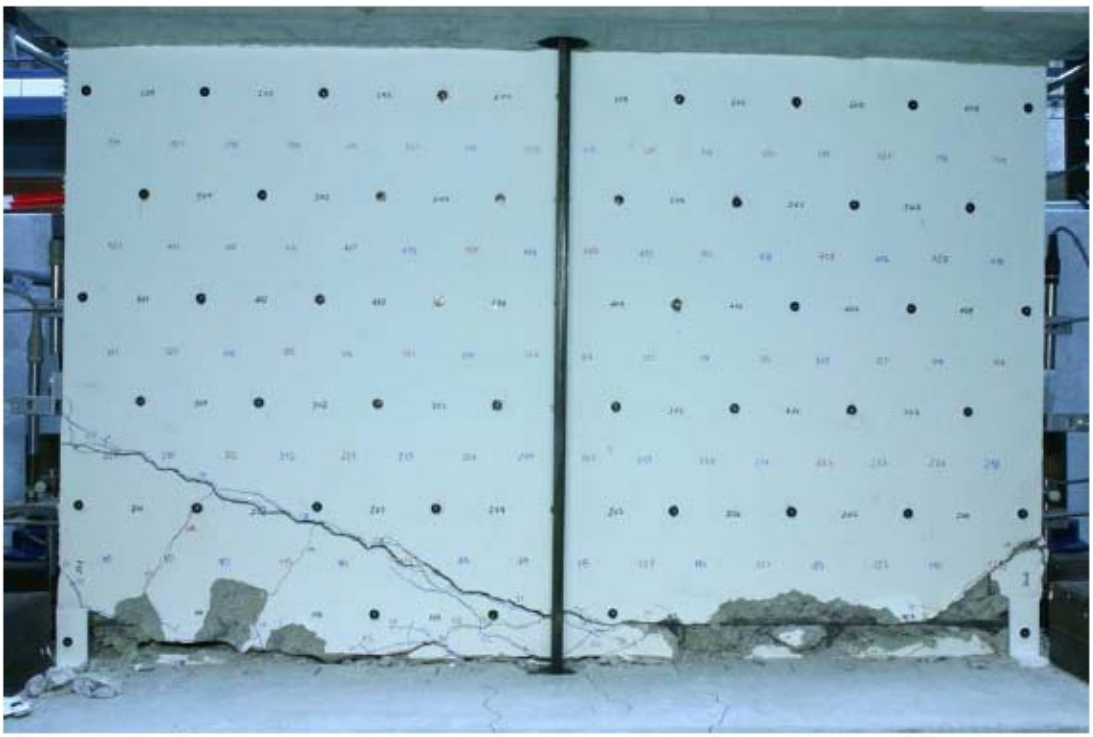

**Figure 8-11 Cracking pattern for wall M1 tested by Greifenhagen et al. (2005) at reinforcement fracture**

angle of 1% from a displacement-controlled cyclic test would be reduced to 0.5% in an earthquake. Only first cycle curves at each displacement level were considered for computation of the drifts at which the drifts at zero-load exceed 1.0%.To illustrate this computation, consider Figure 8-12 that presents the load-displacement data for wall M1 reported in Greifenhagen et al. (2005). In the figure, the peak transient drifts in the first (1.47%) and third quadrants (2.70%) for which the residual drifts exceed 1.0% are identified using red circles. The smaller of the two drifts is assumed to mark the onset of sliding shear failure and used for further analysis.

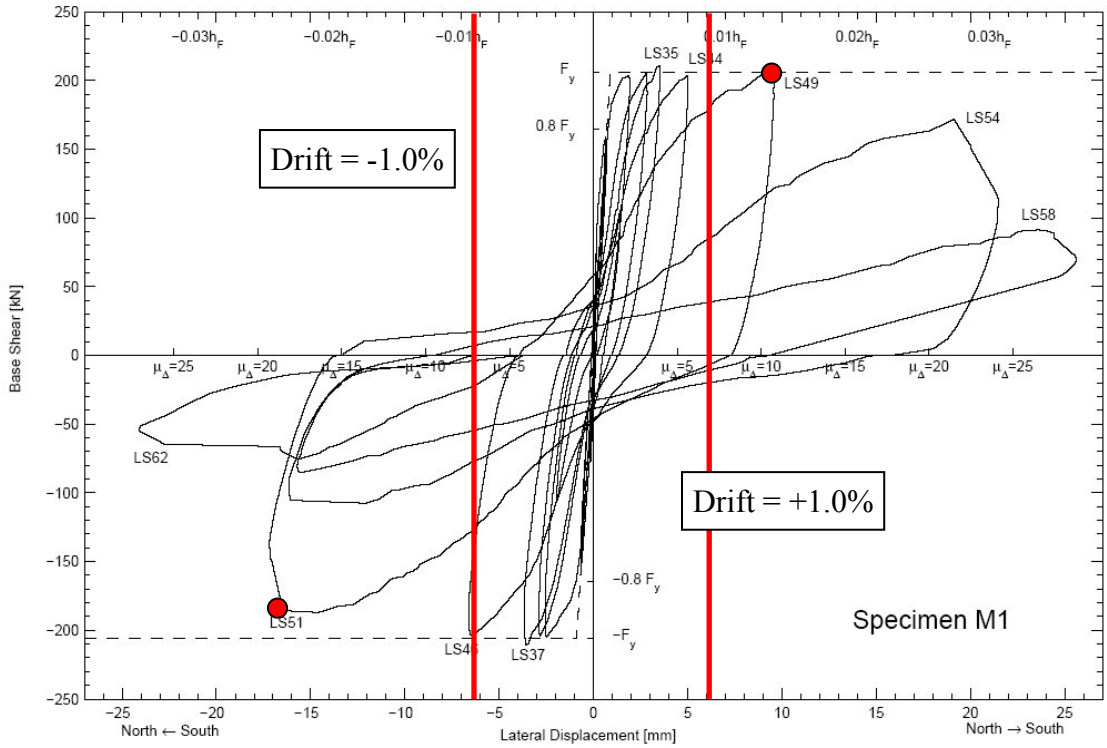


**Figure 8-12 Residual drift computation on the force-drift relationship for M1 tested by Greifenhagen et al. (2005)**

*Supplemental Criterion* $SC_2$: A backbone load-displacement relationship for the first and third quadrants is prepared using the first cycle shear strengths at each displacement increment. The peak resistance of the wall is computed as the maximum force in the first and third quadrants. The story drifts in the first and third quadrants at which the resistance dropped below 50% of the peak resistance are calculated and the smaller of the two story drifts is chosen for further analysis. The computation is illustrated in Figure 8-13 in which backbone force-displacement curves are presented in the first and third quadrants. The peak shear strengths of the wall (in the first quadrant in this case) and the drifts at a post-capping shear strength equal to 50% of the peak resistance in the first quadrant and third quadrants, equal to 3.84% and -3.47%, respectively, are identified in the figure.

The supplemental criteria are used primarily to identify transient drifts associated with sliding shear failures but are also used if a failure by either diagonal tension or compression is reported but the drift at failure is not, the drift associated with $SC_2$ is reported.

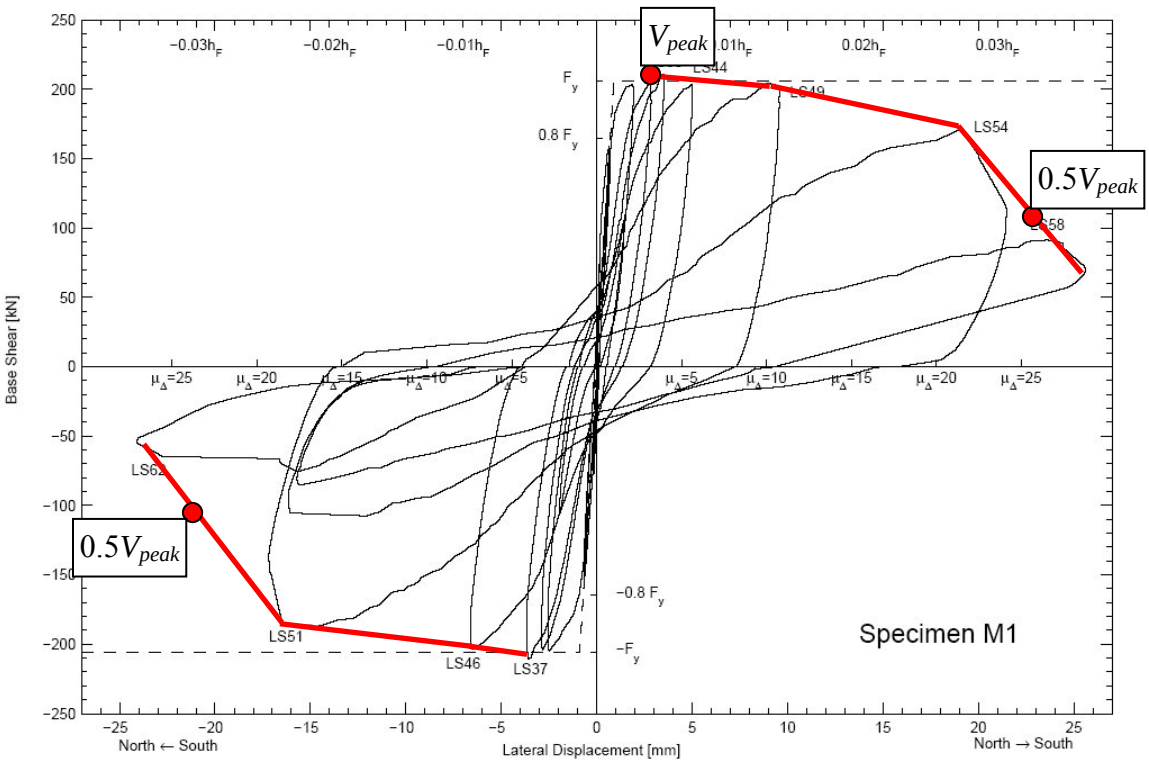


**Figure 8-13 Determination of drifts at which the force-peak shear strength drops to 50% of the peak for M1 tested by Greifenhagen et al. (2005)**

# 8.5 Fragility Analysis

## 8.5.1 Introduction

Herein, fragility functions are developed to characterize the probability that a specific MoR will be required as a function of racking (shear) drift. The data that links drift to damage states, and thus repair, is presented using continuous probability distributions. The method of maximum likelihood is used to fit the data. Four continuous probability distributions are considered, namely: lognormal, gamma, Weibull, and beta. Empirical cumulative distribution functions are presented below together with the fitted distributions.

## 8.5.2 Characterization of Damage Data

Careful mining of damage data is essential because data for more than one damage state was identified for a given method of repair in many of the walls.

Two methods were considered to capture data for the purpose of developing fragility curves:

> **Method 1**: Data for all damage states is used, resulting in multiple data points per specimen for a given MoR.
>
> **Method 2**: Each MoR is represented by a single data point that corresponds to the damage state with the smallest drift value for a given specimen.

Figure 8-14 illustrates the application of the two methods. In this figure, MoR-N is any method of repair, and DSN.1 through DSN.5 are the available damage data for MoR-N.

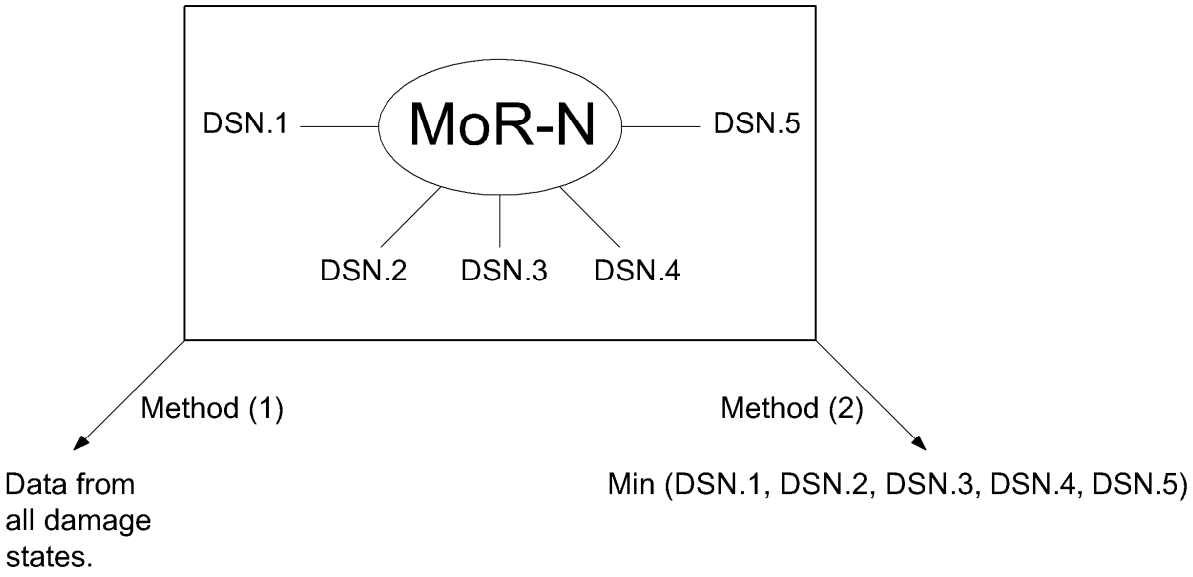


**Figure 8-14 Schematic representation of data characterization**

Using all available demand parameter-damage state pairs to create fragility curves will yield the greatest number of data points for each MoR (a maximum of 5 pairs per Figure 8-14). However, in most cases, the use of Method 1 will result in a higher mean value for a fragility function than that of Method 2 (one value per Figure 8-14). Fragility curves were developed using both methods to investigate the impact of the choice of data representation. Means and standard deviations for the drift data obtained using the two methods are presented in

Table 8-8 for each MoR; data are presented for both MoR-2a and MoR-2b. As seen in the table, the means calculated using Method 1 are higher than those calculated using Method 2. Variability, as measured by coefficient of variation, is higher for Method 1 except for MoR-3. The impact of the choice of method is more significant for MoR-1 and MoR-2a because, in many cases, two or more values of drift could be associated with these methods of repair for a given wall. In most instances, a single drift could be identified for each wall for MoR-2b, MoR-3, and MoR-4.

## 8.5.3 Probability Distributions

Four probability distributions that are widely used for engineering applications, namely, lognormal, gamma, Weibull, and beta, were used to fit the compiled damage data. All four distributions require positive values of the random variable (demand parameter). Figure 8-15 presents sample probability density functions for the four distributions. The following subsections present summary information on these probability distributions. The variable $x$ is used to represent the random variable (= story drift).

**Table 8-8 Statistical summary of the drifts (all cross-sections) obtained using two methods for data mining for each MoR**

| MoR | Method 1 | | | Method 2 | | |
|---|---|---|---|---|---|---|
| | Mean | Standard deviation | Coeff. of Variation | Mean | Standard deviation | Coeff. of Variation |
| 1 | 0.12 | 0.14 | 1.20 | 0.07 | 0.09 | 1.20 |
| 2a | 0.50 | 0.28 | 0.55 | 0.42 | 0.18 | 0.44 |
| 2b | 0.62 | 0.22 | 0.36 | 0.62 | 0.23 | 0.37 |
| 3 | 0.84 | 0.39 | 0.46 | 0.83 | 0.41 | 0.50 |
| 4 | 1.23 | 0.51 | 0.42 | 1.19 | 0.47 | 0.39 |

### 8.5.3.1 Lognormal Distribution

The lognormal distribution is a one-sided probability distribution of a random variable whose logarithm is normally distributed. This distribution is widely used for fragility studies because the demand parameter (drift or acceleration) must be positive and its relationship with the normal or Gaussian distribution. Equation 8-1 presents the probability density function (pdf) for the lognormal distribution.

$$f_X(x) = \begin{cases} \dfrac{1}{x\sigma_{\ln x}\sqrt{2\pi}} \exp\left[ -\dfrac{\left(\ln(x) - \mu_{\ln x}\right)^2}{2\sigma_{\ln x}^2} \right] & \text{for } x \geq 0 \\ 0, \quad \text{elsewhere} \end{cases} \tag{8-1}$$

In Equation 8-1, $\mu_{\ln x}$ and $\sigma_{\ln x}$ are the mean and standard deviation of the natural logs of the demand parameter. The standard deviation of the natural log of the data, $\sigma_{\ln x}$, is termed dispersion in the ATC-58 project [ATC (2008)] and is denoted as $\beta$. The median ($\theta$), mean ($\mu$) and standard deviation ($\sigma$) for a lognormally distributed demand parameter ($x$) are presented in Equations 8-2 through 8-4.

$$\theta = \exp(\mu_{\ln x}) \tag{8-2}$$

$$\mu = \theta \exp\left( \frac{\sigma_{\ln x}^2}{2} \right) \tag{8-3}$$

$$\sigma = \mu \sqrt{\exp\left(\sigma_{\ln x}^2\right) - 1} \tag{8-4}$$

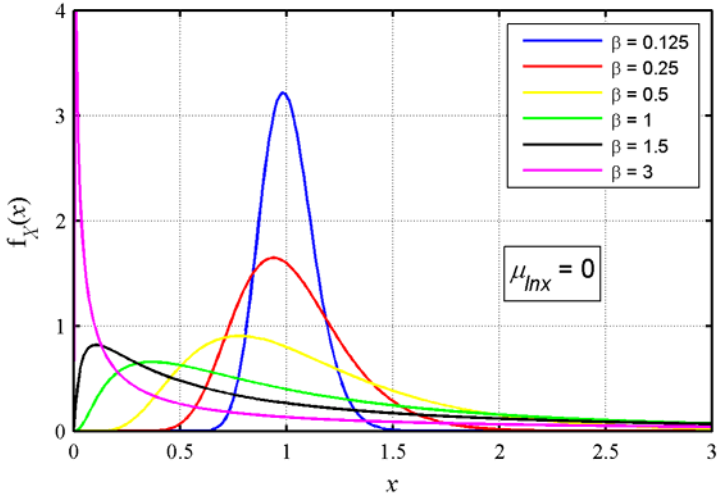


**a) lognormal distribution**

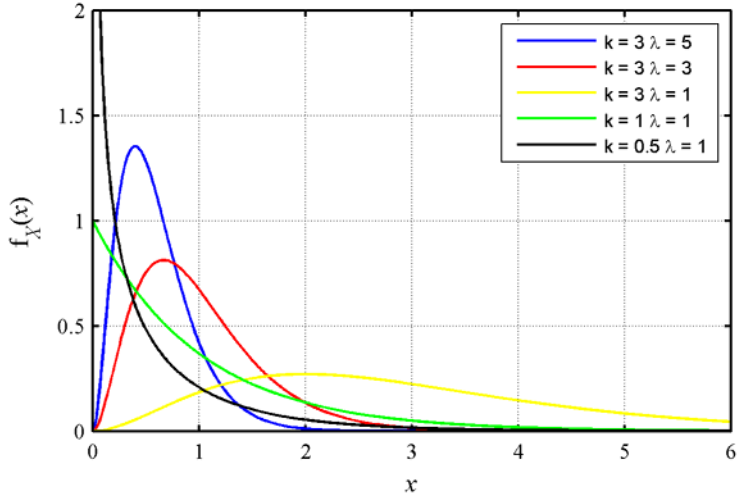


**b) gamma distribution**

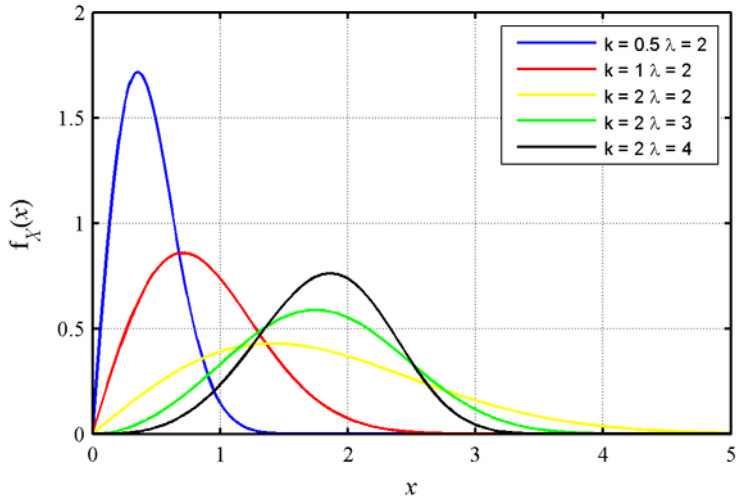


**c) Weibull distribution**

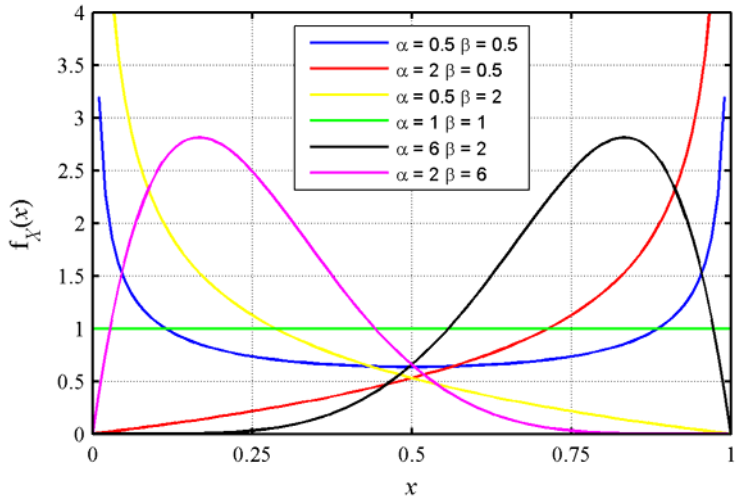


**d) beta distribution**

**Figure 8-15 Families of probability density functions for the four distributions utilized herein**

### 8.5.3.2 Gamma Distribution

Similar to the lognormal distribution, the gamma distribution is also one-sided. Equation 8-5 presents the probability density function for the gamma distribution. The gamma distribution uses two parameters, $k$ and $\lambda$. The parameter $k$ defines the shape of the distribution and $\lambda$ is a scale parameter. The probability density function for the gamma distribution is unimodal with its peak at $x = 0$ for $k \le 1$, and at $x = (k-1)/\lambda$ for $k > 1$ [Soong (2004)].

$$f_X(x) = \begin{cases} \dfrac{\lambda^k}{\Gamma(k)} x^{k-1} e^{-\lambda x} & \text{for } x \ge 0 \\ 0, \quad \text{elsewhere} \end{cases} \tag{8-5}$$

where $\Gamma(k)$ is the gamma function:

$$\Gamma(k) = \int_0^\infty u^{k-1} e^{-u} du \tag{8-6}$$

If $k$ is a positive integer, the gamma function takes the form:

$$\Gamma(k) = (k-1)! \tag{8-7}$$

where ! denotes factorial. The mean ($\mu$) and standard deviation ($\sigma$) for a gamma-distributed variable are:

$$\mu = \frac{k}{\lambda} \quad \text{and} \quad \sigma = \frac{\sqrt{k}}{\lambda} \tag{8-8}$$

### 8.5.3.3 Weibull Distribution

The Weibull distribution is an extreme value distribution of type III [Soong (2004)]. Equation 8-9 presents the probability density function for the Weibull distribution. Similar to the gamma distribution, $k$ defines the shape of the distribution and $\lambda$ is a scale parameter.

$$f_X(x) = \frac{k}{\lambda}\left(\frac{x}{\lambda}\right)^{k-1} \exp\left[-\left(\frac{x}{\lambda}\right)^k\right] \quad k, \lambda > 0 \quad x \ge 0 \tag{8-9}$$

The mean ($\mu$) and the standard deviation ($\sigma$) for a Weibull-distributed variable are:

$$\mu = \lambda\Gamma\left(1+\frac{1}{k}\right) \quad \text{and} \quad \sigma = \lambda\sqrt{\Gamma\left(1+\frac{2}{k}\right) - \Gamma^2\left(1+\frac{1}{k}\right)} \tag{8-10}$$

Brown (2008) notes that the Weibull distribution is appropriate for developing fragility functions because it provides accurate results with small data sets and represents a broad range of distribution shapes, which enables easier fitting.

#### 8.5.3.4 Beta Distribution

The beta distribution is a versatile distribution defined on the interval [0, 1]. The probability density function for the beta distribution is:

$$f_X(x) = \begin{cases} \dfrac{1}{B(\alpha,\beta)} x^{\alpha-1}(1-x)^{\beta-1} & \text{for } 0 \le x \le 1 \\ 0, \quad \text{elsewhere} \end{cases} \tag{8-11}$$

where *B* is the beta function as calculated using Equation 8-12.

$$B(\alpha,\beta) = \frac{\Gamma(\alpha)\Gamma(\beta)}{\Gamma(\alpha+\beta)} \tag{8-12}$$

The parameters $\alpha$ and $\beta$ are both shape parameters that take on positive values only. When $\alpha, \beta > 1$, the density function is unimodal with the peak at $(\alpha-1)/(\alpha+\beta-2)$. The density function becomes U-shaped when $\alpha, \beta < 1$; J-shaped when $\alpha \ge 1$, $\beta < 1$; reverse J-shaped when $\alpha < 1$, $\beta \ge 1$; and uniform when $\alpha = \beta = 1$ [Soong (2004)]. The mean ($\mu$) and standard deviation ($\sigma$) of a beta-distributed variable are:

$$\mu = \frac{\alpha}{\alpha+\beta} \quad \text{and} \quad \sigma = \frac{1}{\alpha+\beta}\sqrt{\frac{\alpha\beta}{\alpha+\beta+1}} \tag{8-13}$$

Since the beta distribution is defined on the interval [0, 1], experimental data must be transformed to the interval [0, 1] before fitting the distribution.

### 8.5.4 Method of Maximum Likelihood

The method of maximum likelihood is the most widely used rule for finding point estimations of distribution parameters for sample data and is used below to estimate the parameters for the aforementioned distributions. This method makes use of the sample likelihood function that is presented below for completeness.

First, let $f(x;\theta)$ be the probability density function of the population where $\theta$ is(are) the parameter(s) of the distribution $X$. The joint density function of a sample $X_1, X_2, \ldots, X_n$ has the form:

$$f_{X_1,X_2,\ldots,X_n}(x_1,x_2,\ldots,x_n|\theta) = f_{X_1}(x_1) f_{X_2}(x_2) \cdots f_{X_n}(x_n) = \Pi f_X(x_i|\theta) \tag{8-14}$$

where $\Pi$ denotes product.

The *likelihood function* $L(\theta)$ of a set of $n$ sample values is

$$L(\theta|x_1, x_2, ...x_n) = \prod_{i=1}^{n} f_X(x_i|\theta) \tag{8-15}$$

which gives the *relative likelihood* of having observed this particular sample ($X_1 = x_1$, $X_2 = x_2$,…, $X_n = x_n$) as a function of $\theta$ [Benjamin and Cornell (1970)].

The *maximum likelihood estimate* (MLE) of $\theta$ is the value that maximizes the *likelihood function* $L(\theta)$. Per Benjamin and Cornell, maximum likelihood estimators possess the following desirable properties

- *Asymptotical unbiasedness*: means are asymptotically ($n \to \infty$) equal to the true parameter value(s), $\theta$
- *Efficiency*: minimum expected squared error among all possible unbiased estimators,
- *Consistency*: be close to the true parameter values as the sample size increases with increasingly high probability, and
- *Sufficiency*: make maximum use of the information contained in the data.

## 8.5.5 Goodness-of-Fit Testing

To quantify the utility of the distributions, goodness-of-fit tests were performed on each fit. The Kolmogorov-Smirnov test (denoted hereafter as the K-S test) is a general test that is applicable to any distribution. The Lilliefors test is a special case of Kolmogorov-Smirnov test that can assess normality only.

### 8.5.5.1 Kolmogorov-Smirnov test (K-S test)

Given a set of sample values $x_1$, $x_2$, …, $x_n$ observed from a population $X$, the test parameter for the K-S test ($D$) is calculated as:

$$D = \max_{i=1}^{n} \left\{ \left| F_X(x_i) - S_X(x_i) \right| \right\} \tag{8-16}$$

In Equation 8-16, $F_X(x_i)$ and $S_X(x_i)$ are the theoretical and empirical CDFs, respectively, calculated at the $i^{th}$ observation. Thus, the test parameter ($D$) of the K-S test corresponds to the maximum of the absolute values of $n$ (sample size) differences between the empirical CDF and the hypothesized CDF evaluated for the observed samples. The distribution of $D$ is independent of the hypothesized distribution and is a function of $n$ only [Benjamin and Cornell (1970)].

The null hypothesis, $H_0$, for the K-S test is that the population $X$ comes from the hypothesized probability distribution. At a specified significance level ($\alpha$), if $D$ is less than or equal to $D_{crit}$, the null hypothesis is accepted.

$$P(D \le D_{crit}) = 1 - \alpha \tag{8-17}$$

Values for $D_{crit}$ have been tabulated [e.g., Soong (2004)] as a function of the sample size ($n$) and significance level ($\alpha$).

The advantage of the K-S test is that it is applicable to all sample sizes and uses data in unaltered form (does not require arbitrary grouping of the sample data) unlike the chi-square goodness-of-fit test. However, the K-S test is valid strictly for continuous distributions and values for $D_{crit}$ are based on a completely specified hypothesized distribution (parameters known). This is not the case herein since the distribution parameters are unknown and must be estimated from the data. Using the K-S test with estimated distribution parameters may result in an unconservative acceptance of the null hypothesis [Benjamin and Cornell (1970)]. Herein, the K-S test is used to evaluate the quality of the fit of the distributions relative to one another.

#### 8.5.5.2 Lilliefors test

The Lilliefors test evaluates the normality of a given data. Herein, the test is used to assess the acceptability of the lognormal distribution by testing the logarithm of the available data. This test is a variant of the K-S test to account for computation of the distribution parameters from the sample data [Lilliefors (1967)]. The test statistic for the Lilliefors test is calculated in a similar manner to that for the K-S test; the difference is in the calculation of $D_{crit}$. The Lilliefors test accounts for the unknown sample mean and variance and uses Monte Carlo simulation to determine approximate values of $D_{crit}$. The Lilliefors test is valid for small sample sizes but is also appropriate when the distribution parameters are unknown [Lilliefors (1967)], which is the case in this study.

### 8.5.6 Parameters That Effect the Earthquake Performance of Squat Walls

A detailed discussion of the failure modes for squat reinforced concrete walls was presented in Section 1. Based on that discussion, wall geometry, aspect ratio, horizontal web reinforcement ratio, vertical web reinforcement ratio, and axial load are identified as the five key parameters that affect the earthquake response of squat reinforced concrete walls. Walls with boundary elements are more susceptible to diagonal compression failure than rectangular walls. As aspect ratio increases, the likelihood of developing wall flexural strength increases and the likelihood of shear failure decreases. Flexural and shear failures exhibit different damage patterns. Horizontal reinforcement is effective in resisting diagonal tension failure, and shear crack width is affected by horizontal web reinforcement ratio. Vertical web reinforcement is effective in resisting the opening of diagonal cracks and helps to anchor compression struts that transfer lateral forces to the wall foundation. Higher axial force delays diagonal tension cracking but can trigger diagonal compression failure. The effect of these five parameters on the damage data is investigated below.

Table 8-9 and Table 8-10 present a statistical summary of drifts for each MoR obtained using Methods 1 and 2, respectively, with respect to wall geometry. Results are presented to two decimal digits. In these tables, means ($\bar{x}$), standard deviations ($sd$), and coefficient of variation ($cv$) are calculated as follows

**Table 8-9 Statistical summary of drifts for each MoR and Method 1**

| MoR | Wall geometry | | | | | | | | |
|---|---|---|---|---|---|---|---|---|---|
| | Rectangular | | | Barbell | | | Flanged | | |
| | $\overline{x}$ | *sd* | *cv* | $\overline{x}$ | *sd* | *cv* | $\overline{x}$ | *sd* | *cv* |
| 1 | 0.17 | 0.16 | 0.95 | 0.04 | 0.02 | 0.57 | 0.13 | 0.16 | 1.24 |
| 2a | 0.47 | 0.19 | 0.40 | 0.43 | 0.20 | 0.46 | 0.59 | 0.38 | 0.64 |
| 2b | 0.58 | 0.20 | 0.34 | N/A[1] | N/A | N/A | 0.75 | 0.27 | 0.37 |
| 3 | 1.07 | 0.29 | 0.27 | 0.35 | 0.16 | 0.46 | 0.80 | 0.33 | 0.42 |
| 4 | 1.39 | 0.51 | 0.36 | 0.88 | 0.14 | 0.16 | 1.45 | 0.63 | 0.43 |

1. There is one data point for MoR-2b and barbell walls.

**Table 8-10 Statistical summary of drifts for each MoR and Method 2**

| MoR | Wall geometry | | | | | | | | |
|---|---|---|---|---|---|---|---|---|---|
| | Rectangular | | | Barbell | | | Flanged | | |
| | $\overline{x}$ | *sd* | *cv* | $\overline{x}$ | *sd* | *cv* | $\overline{x}$ | *sd* | *cv* |
| 1 | 0.11 | 0.11 | 1.06 | 0.03 | 0.01 | 0.33 | 0.06 | 0.05 | 0.86 |
| 2a | 0.43 | 0.15 | 0.36 | 0.38 | 0.19 | 0.50 | 0.42 | 0.22 | 0.53 |
| 2b | 0.58 | 0.20 | 0.34 | N/A[1] | N/A | N/A | 0.77 | 0.30 | 0.39 |
| 3 | 1.10 | 0.31 | 0.29 | 0.35 | 0.16 | 0.46 | 0.80 | 0.34 | 0.43 |
| 4 | 1.32 | 0.42 | 0.32 | 0.88 | 0.14 | 0.16 | 1.45 | 0.63 | 0.43 |

1. There is one data point for MoR-2b and barbell walls.

$$\overline{x} = \frac{1}{n}\sum_{i=1}^{n} x_i \quad , \quad sd = \left[\frac{1}{n-1}\sum_{i=1}^{n}\left(x_i - \overline{x}\right)^2\right]^{1/2} \quad , \quad cv = sd / \overline{x} \tag{8-18}$$

where n is the number of samples of $x_i$. The drift values obtained for walls with barbell cross sections are generally much lower than those for walls with rectangular and flanged cross sections. Note that the mean drifts for MoR-3 are smaller than MoR-2 for walls with barbell cross sections, which is attributed to the dataset used to generate damage data for barbell walls that includes many walls with low-aspect ratios and high vertical and horizontal web reinforcement ratios (see Table 8-3 and Table 8-4). Given the results of Table 8-10 and the ranges of data presented in Table 8-1 through Table 8-6, families of fragility functions are presented for each wall geometry.

Figure 8-16 presents the variation of drift with aspect ratio for MoR-1, MoR-2a, MoR-3, and MoR-4. All available damage data are included in the figure (also in Figure 8-17, Figure 8-18, and Figure 8-19). For barbell and flanged walls, no trends are evident for any of the MoRs considered. For walls with rectangular cross-sections, there is a weak trend of increasing drift

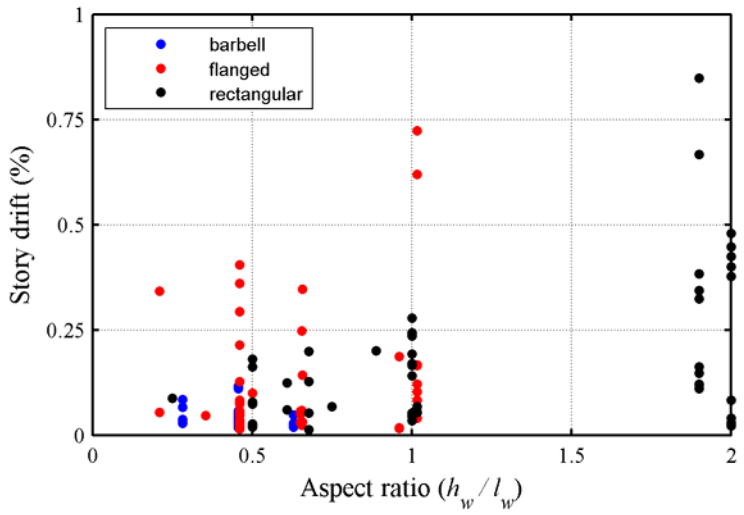


**a) MoR-1**

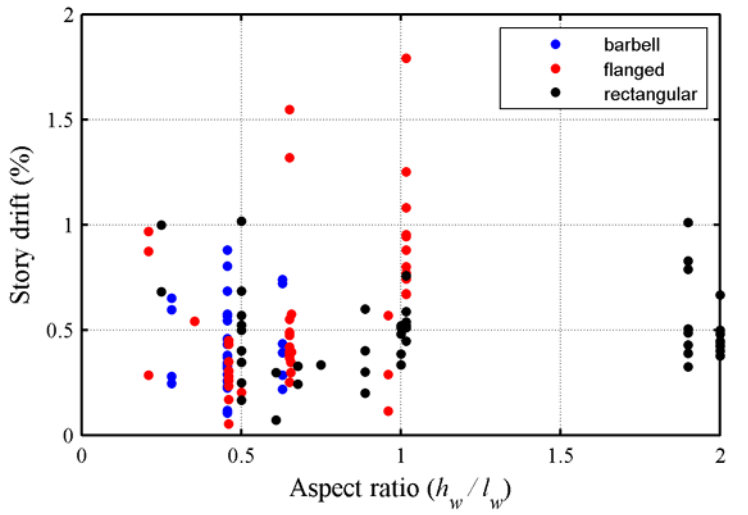


**b) MoR-2a**

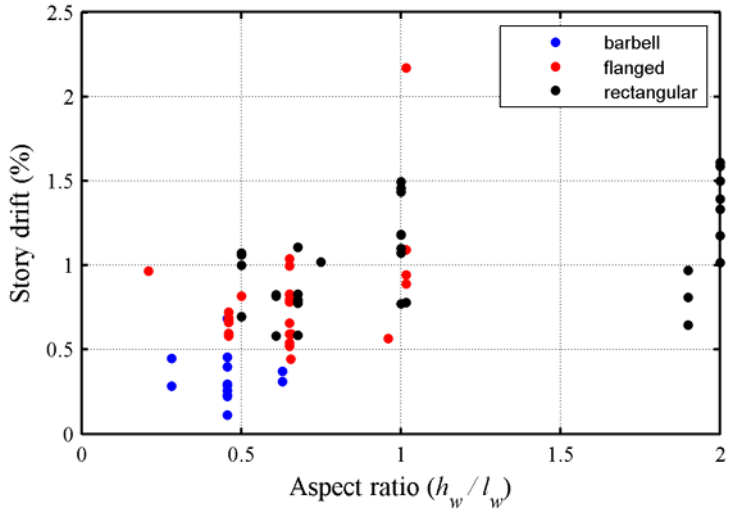


**c) MoR-3**

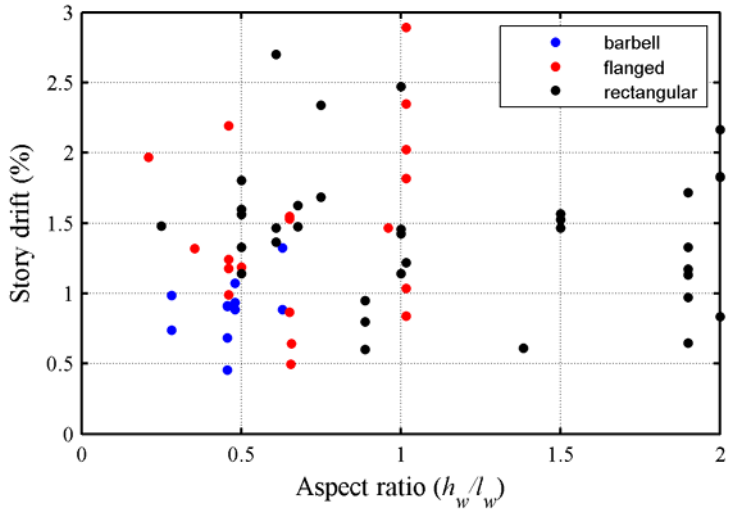


**d) MoR-4**

**Figure 8-16 Variation of drift with aspect ratio for different methods of repair**

with increasing aspect ratio for MoR-1. However, scatter is significant and the size of the rectangular wall dataset for MoR-1 for aspect ratios of between 1.0 and 2.0 is small, with most of the data clustered around 2.0. In summary, the available data do not reveal any strong correlation between aspect ratio and damage for any wall geometry.

Figure 8-17 presents the variation of drift with horizontal web reinforcement ratio for each method of repair. No relationship between drift and horizontal web reinforcement ratio can be identified for any method of repair for either rectangular or flanged walls. The limiting drifts for MoR-1, MoR-3, and MoR-4 for barbell walls are independent of horizontal web reinforcement ratio. A weak trend of increasing drift with increasing horizontal web reinforcement ratio is seen for MoR-2a but the scatter is quite large and sample size is modest.

Figure 8-18 presents the variation of drift with vertical web reinforcement ratio for each method of repair. No visible trends between drift and vertical web reinforcement ratio are evident for any method of repair for rectangular and flanged walls. For the barbell walls, the limiting drifts for MoR-1, MoR-3 and MoR-4 are independent of vertical web reinforcement ratio. For MoR-2a, a trend of increasing drift with increasing vertical web reinforcement ratio is evident. Note that all barbell walls considered herein had equal percentages of horizontal and vertical web reinforcement and that the trends observed with drift and vertical web reinforcement ratio for barbell walls for all methods of repair are similar to those observed with drift and horizontal web reinforcement ratio.

Figure 8-19 presents the variation of drift with normalized axial load for each method of repair. No significant trends between drift and normalized axial load are evident for any method of repair for any cross-section type. However, the number of data for normalized axial loads of higher than 10% is very small as seen in Figure 8-19.

In summary, the available data do not support the use of aspect ratio, horizontal and vertical web reinforcement ratio, and axial load as variables in the presentation of fragility curves. Although horizontal and vertical web reinforcement ratios have an impact on the limiting drifts for MoR-2a, the dispersion is substantial. Only wall geometry substantially influences the relationships. The barbell wall dataset yielded significantly different damage characteristics than walls with flanged and rectangular walls as presented in Table 8-9 and Table 8-10. Although the damage data for rectangular and flanged walls are comparable, the ranges on the two datasets are significantly different.

### 8.5.7 Fragility Functions

Fragility functions that define the probability that a certain method of repair will be required conditional on story drift developed in this section. The damage states, which are associated with specific methods of repairs (see Section 8.4), are used as the basis for collecting the damage data. The data characterization methods discussed in Section 8.5.2 are used to group the available damage data.

This section utilizes the distributions summarized in Section 8.5.3 to fit the damage data using the method of maximum likelihood (see Section 8.5.4). Fragility functions are generated for each type of wall geometry.

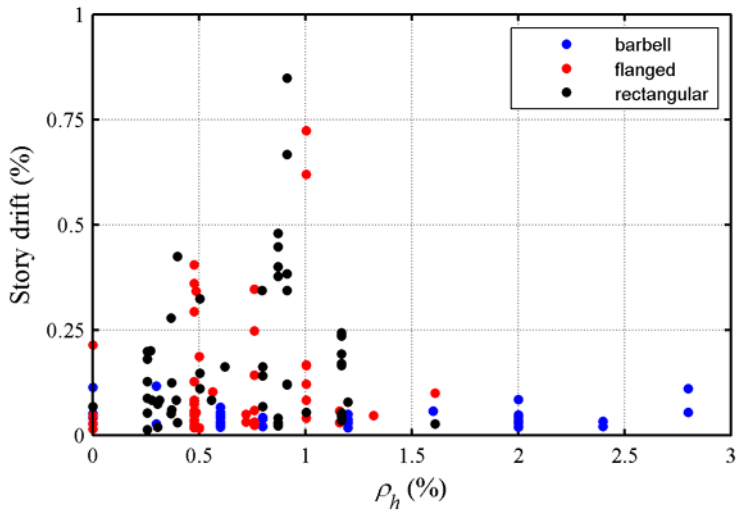


**a) MoR-1**

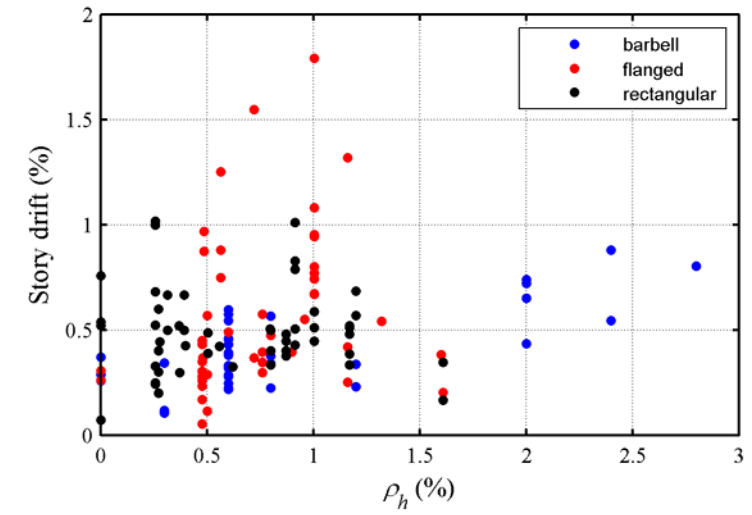


**b) MoR-2a**

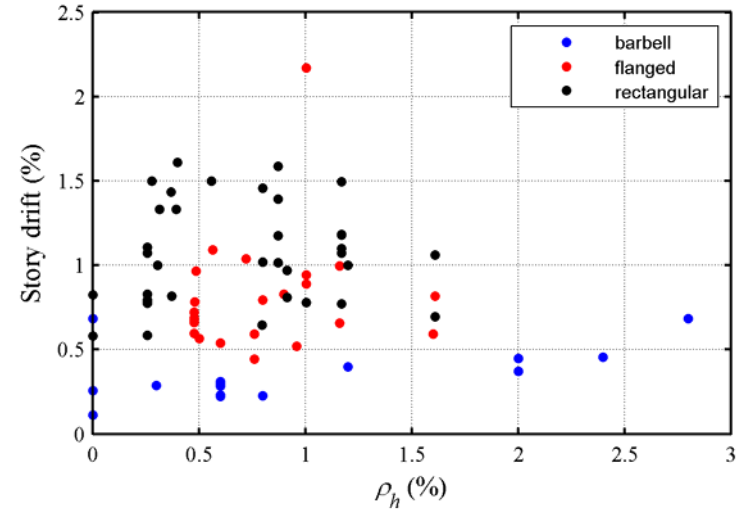


**c) MoR-3**

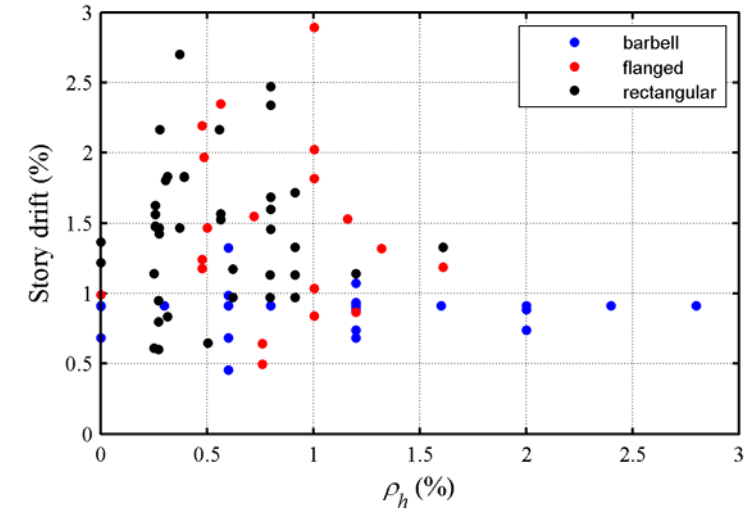


**d) MoR-4**

**Figure 8-17 Variation of drift with horizontal web reinforcement ratio for different methods of repair**

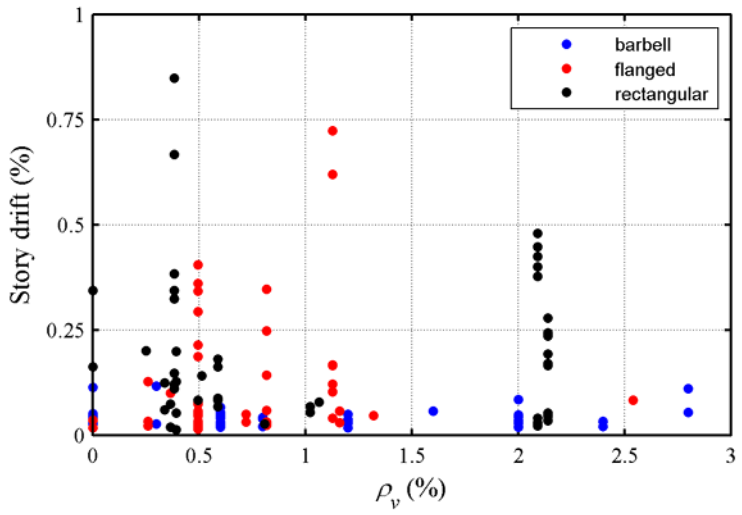


**a) MoR-1**

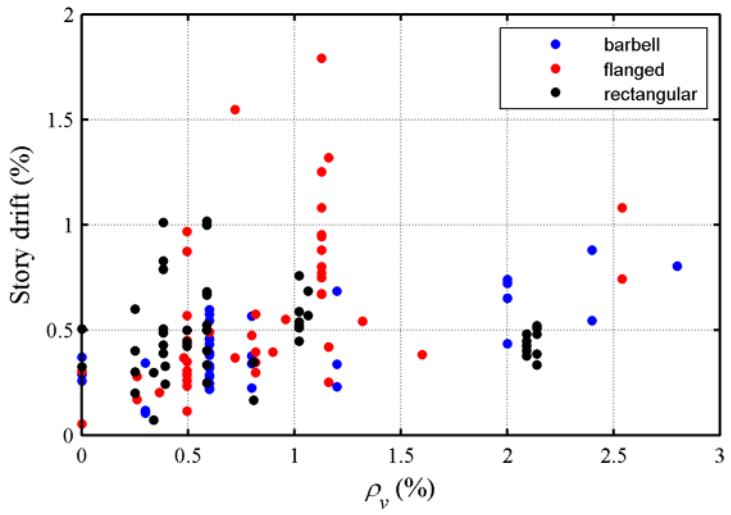


**b) MoR-2a**

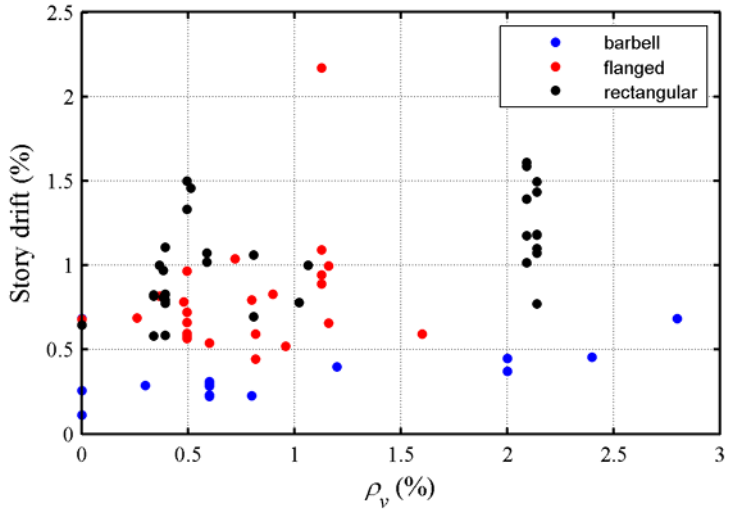


**c) MoR-3**

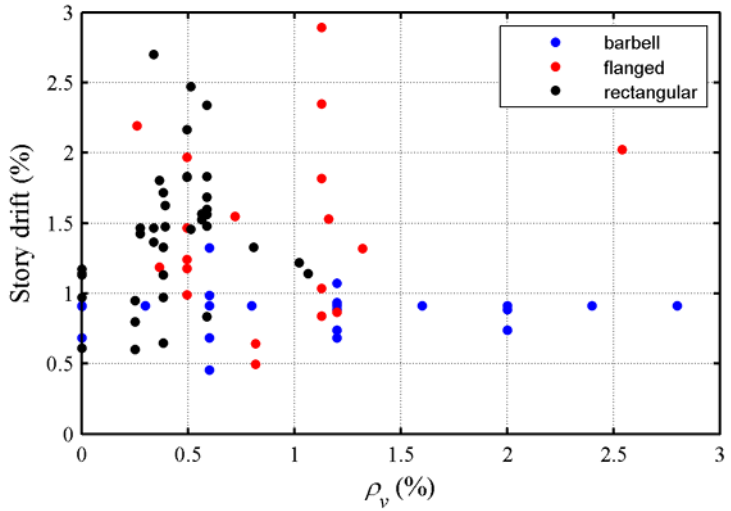


**d) MoR-4**

**Figure 8-18 Variation of drift with vertical web reinforcement ratio for different methods of repair**

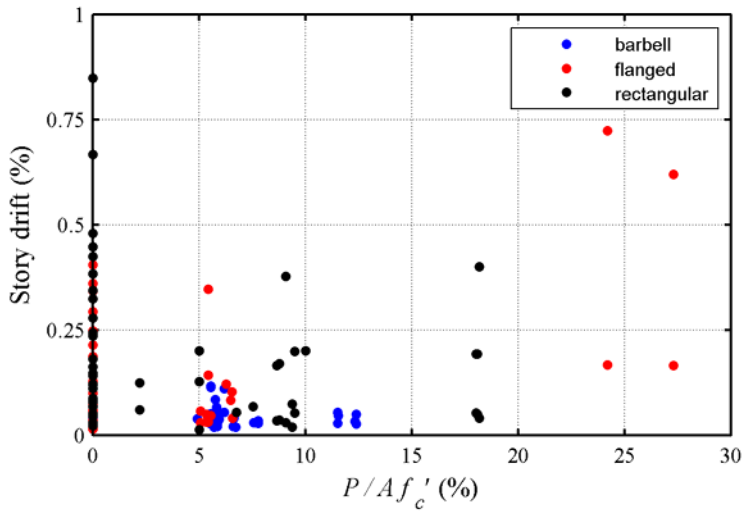


**a) MoR-1**

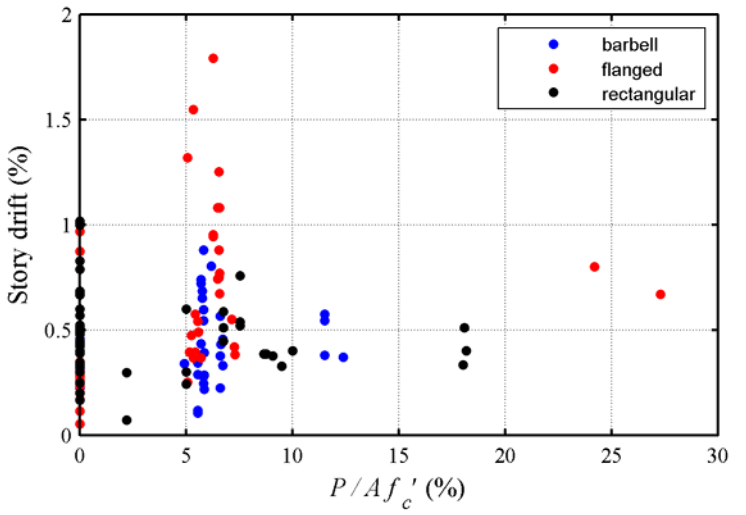


**b) MoR-2a**

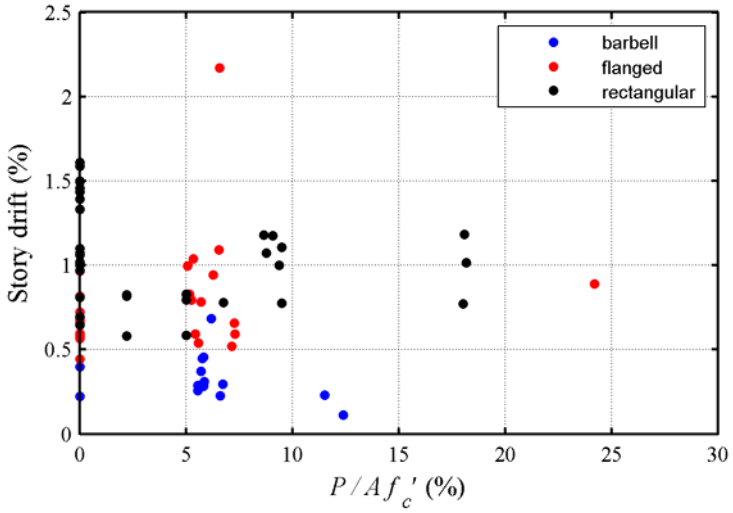


**c) MoR-3**

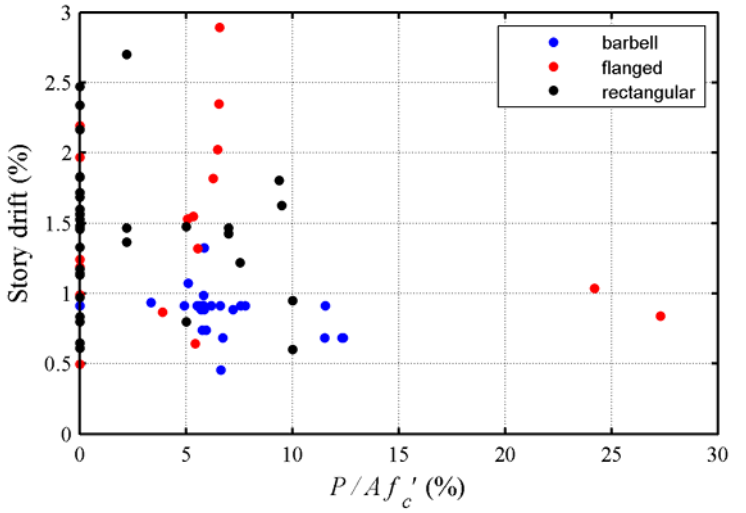


**d) MoR-4**

**Figure 8-19 Variation of drift with normalized axial load for different methods of repair**

### 8.5.7.1 Fragility Functions Developed Using Method 1

Method 1 utilizes all available damage data for each method of repair. The distribution parameters (as defined in Section 8.5.3) estimated using the *method of maximum likelihood* are presented in Table 8-11 for rectangular, barbell and flanged walls. Results for the K-S (all distributions) and Lilliefors (lognormal distribution only) goodness-of-fit tests are presented in Table 8-12 and Table 8-13. The goodness-of-fit tests of Table 8-12 and Table 8-13 were conducted at the 5% significance level.

**Table 8-11 Distribution parameters computed using Method 1**

| Wall Geometry | MoR | Distribution Parameters | | | | | | | |
|---|---|---|---|---|---|---|---|---|---|
| | | lognormal | | gamma | | Weibull | | beta | |
| | | $\theta$ | $\beta$ | $k$ | $\lambda$ | $k$ | $\lambda$ | $\alpha$ | $\beta$ |
| Rectangular | 1 | 0.11 | 0.92 | 1.40 | 8.37 | 0.18 | 1.16 | 1.20 | 5.54 |
| | 2a | 0.43 | 0.43 | 6.06 | 12.98 | 0.53 | 2.61 | 2.63 | 3.38 |
| | 2b | 0.54 | 0.36 | 8.49 | 14.76 | 0.64 | 3.26 | 2.16 | 2.79 |
| | 3 | 1.03 | 0.28 | 13.43 | 12.59 | 1.18 | 4.09 | 1.39 | 1.58 |
| | 4 | 1.30 | 0.37 | 7.69 | 5.52 | 1.56 | 3.00 | 1.70 | 2.95 |
| Barbell | 1 | 0.04 | 0.47 | 4.27 | 101.72 | 0.05 | 1.92 | 0.87 | 2.47 |
| | 2a | 0.38 | 0.50 | 4.61 | 10.76 | 0.48 | 2.37 | 2.26 | 3.20 |
| | 3 | 0.32 | 0.45 | 5.29 | 15.05 | 0.40 | 2.37 | 1.97 | 2.17 |
| | 4 | 0.87 | 0.17 | 25.20 | 28.82 | 0.94 | 6.24 | 3.95 | 4.20 |
| Flanged | 1 | 0.07 | 1.03 | 1.02 | 8.08 | 0.12 | 0.94 | 0.68 | 3.85 |
| | 2a | 0.48 | 0.68 | 2.54 | 4.32 | 0.66 | 1.66 | 2.15 | 4.94 |
| | 2b | 0.71 | 0.34 | 8.78 | 11.69 | 0.84 | 3.28 | 0.36 | 0.40 |
| | 3 | 0.75 | 0.32 | 8.79 | 11.00 | 0.90 | 2.42 | 0.69 | 2.66 |
| | 4 | 1.32 | 0.44 | 5.54 | 3.82 | 1.64 | 2.56 | 1.01 | 1.52 |

The data presented in Table 8-12 include the K-S test parameter ($D$), decision on the null hypothesis that the data comes from the hypothesized probability distribution (A = Accept, R = Reject), $p$ value of the test and the critical test parameter ($D_{crit}$). As noted previously, if $D \le D_{crit}$, the null hypothesis ($H_0$) is accepted. The null hypothesis for the K-S test is rejected in 1 of the 14 cases (3 wall geometries x 5 MoR except for MoR-2b and barbell walls) for the gamma, Weibull and lognormal distributions (barbell walls, MoR4), and rejected two times for the beta distribution (rectangular walls, MoR-2; barbell walls, MoR-4). The $D$ statistic for the K-S test represents the maximum absolute difference between the empirical CDF and the theoretical CDF. Therefore, it is a measure of the deviation between the reported data and the hypothesized CDF. In Table 8-12, the yellow shaded cells represented the smallest $D$ for the K-S test conducted on the corresponding wall geometry and method of repair. For 6 of the 14 cases investigated, the lognormal distribution yields the smallest values of $D$. In another three instances, the value of $D$ for the lognormal distribution is only marginally (<10%) larger than

**Table 8-12 K-S test results for each distribution obtained using Method 1**

| Wall geometry | MoR | K-S Test Results | | | | | | | | | | | |
|---|---|---|---|---|---|---|---|---|---|---|---|---|---|
| | | $D_{crit}$ | lognormal | | | gamma | | | Weibull | | | beta | | |
| | | | $p$ | $H_0$ | $D$ | $p$ | $H_0$ | $D$ | $p$ | $H_0$ | $D$ | $p$ | $H_0$ | $D$ |
| **Rectangular** | **1** | 0.166 | 0.911 | A | 0.068 | 0.492 | A | 0.102 | 0.498 | A | 0.101 | 0.237 | A | 0.126 |
| | **2a** | 0.161 | 0.327 | A | 0.113 | 0.508 | A | 0.097 | 0.193 | A | 0.128 | 0.038 | R | 0.167 |
| | **2b** | 0.294 | 0.288 | A | 0.213 | 0.399 | A | 0.194 | 0.720 | A | 0.150 | 0.491 | A | 0.180 |
| | **3** | 0.215 | 0.627 | A | 0.119 | 0.556 | A | 0.126 | 0.535 | A | 0.128 | 0.656 | A | 0.116 |
| | **4** | 0.203 | 0.678 | A | 0.108 | 0.892 | A | 0.086 | 0.921 | A | 0.082 | 0.815 | A | 0.095 |
| **Barbell** | **1** | 0.201 | 0.770 | A | 0.098 | 0.558 | A | 0.117 | 0.273 | A | 0.147 | 0.348 | A | 0.138 |
| | **2a** | 0.221 | 0.903 | A | 0.093 | 0.946 | A | 0.086 | 0.81 | A | 0.104 | 0.632 | A | 0.122 |
| | **3** | 0.338 | 0.885 | A | 0.145 | 0.857 | A | 0.151 | 0.725 | A | 0.172 | 0.132 | A | 0.290 |
| | **4** | 0.234 | 0.002 | R | 0.327 | 0.002 | R | 0.327 | 0.005 | R | 0.297 | 0.005 | R | 0.298 |
| **Flanged** | **1** | 0.194 | 0.410 | A | 0.127 | 0.078 | A | 0.182 | 0.175 | A | 0.158 | 0.111 | A | 0.172 |
| | **2a** | 0.183 | 0.853 | A | 0.082 | 0.661 | A | 0.098 | 0.573 | A | 0.106 | 0.124 | A | 0.159 |
| | **2b** | 0.483 | 0.714 | A | 0.249 | 0.737 | A | 0.244 | 0.792 | A | 0.232 | 0.971 | A | 0.174 |
| | **3** | 0.264 | 0.936 | A | 0.104 | 0.730 | A | 0.134 | 0.273 | A | 0.194 | 0.241 | A | 0.200 |
| | **4** | 0.301 | 0.999 | A | 0.081 | 1.000 | A | 0.078 | 0.976 | A | 0.106 | 0.983 | A | 0.103 |

**Table 8-13 Lilliefors results for the lognormal distribution computed using Method 1**

| Wall Geometry | MoR | Lilliefors Test Results | | | |
|---|---|---|---|---|---|
| | | $D_{crit}$ | $p$ | $H_0$ | $D$ |
| **Rectangular** | **1** | 0.110 | 0.500 | A | 0.067 |
| | **2a** | 0.107 | 0.028 | R | 0.113 |
| | **2b** | 0.192 | 0.020 | R | 0.210 |
| | **3** | 0.142 | 0.214 | A | 0.116 |
| | **4** | 0.134 | 0.247 | A | 0.106 |
| **Barbell** | **1** | 0.132 | 0.381 | A | 0.096 |
| | **2a** | 0.146 | 0.500 | A | 0.090 |
| | **3** | 0.219 | 0.438 | A | 0.153 |
| | **4** | 0.154 | 0.001 | R | 0.326 |
| **Flanged** | **1** | 0.128 | 0.058 | A | 0.126 |
| | **2a** | 0.121 | 0.500 | A | 0.080 |
| | **2b** | 0.304 | 0.322 | A | 0.230 |
| | **3** | 0.173 | 0.500 | A | 0.107 |
| | **4** | 0.197 | 0.500 | A | 0.084 |

the smallest value of $D$. The lognormal distribution is therefore judged to be the best of the distributions considered here. Table 8-13 presents the Lilliefors goodness-of-fit test results on the lognormal distribution. The Lilliefors test yields smaller values of $D_{crit}$ than for the K-S test for a given sample size and significance level (see Section 8.5.5). As seen in Table 8-13, the lognormal distribution fails the Lilliefors goodness-of-fit test for MoR-2a and MoR-2b for the rectangular walls and for MoR-4 for the barbell walls. Note that no outlier analysis was undertaken before processing the data.

The functions developed using lognormal distribution for each wall geometry and method of repair type can be compared using the medians ($\theta$) and logarithmic standard deviations ($\beta$) presented in the gray shaded columns of Table 8-11. The standard deviations for MoR-1 are generally high, which is attributed to the use of Method 1 that includes all available damage data. The standard deviations for other methods of repair are generally reasonable. ATC-58 [ATC (2008)] qualifies the fragility functions that pass the Lilliefors goodness-of-fit test and yield logarithmic standard deviations ($\beta$) of less than 0.6 as *high quality*. One interesting observation is that for barbell walls, MoR-3 precedes MoR-2a, that is, the median drift associated for MoR-3 is less than that of MoR-2a. This anomaly is attributed to the characteristics of the barbell wall data used herein, namely, low-aspect ratio and heavy web reinforcement in most cases. Figure 8-20, Figure 8-21, and Figure 8-22 present the empirical and theoretical fragility functions for rectangular, barbell and flanged walls, respectively.

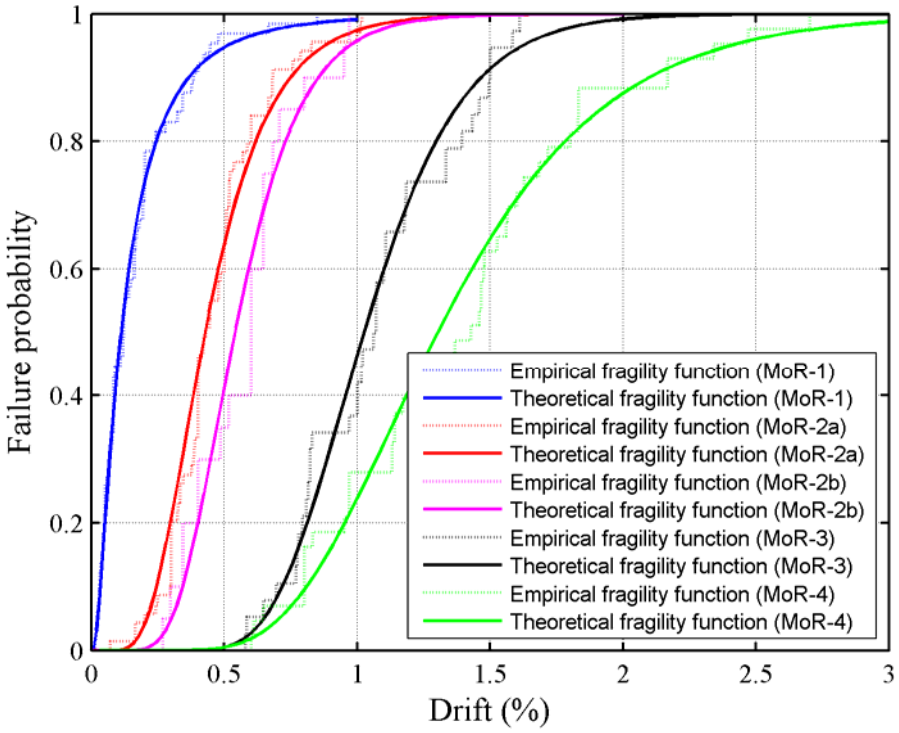


**Figure 8-20 Method 1 fragility functions for rectangular walls**

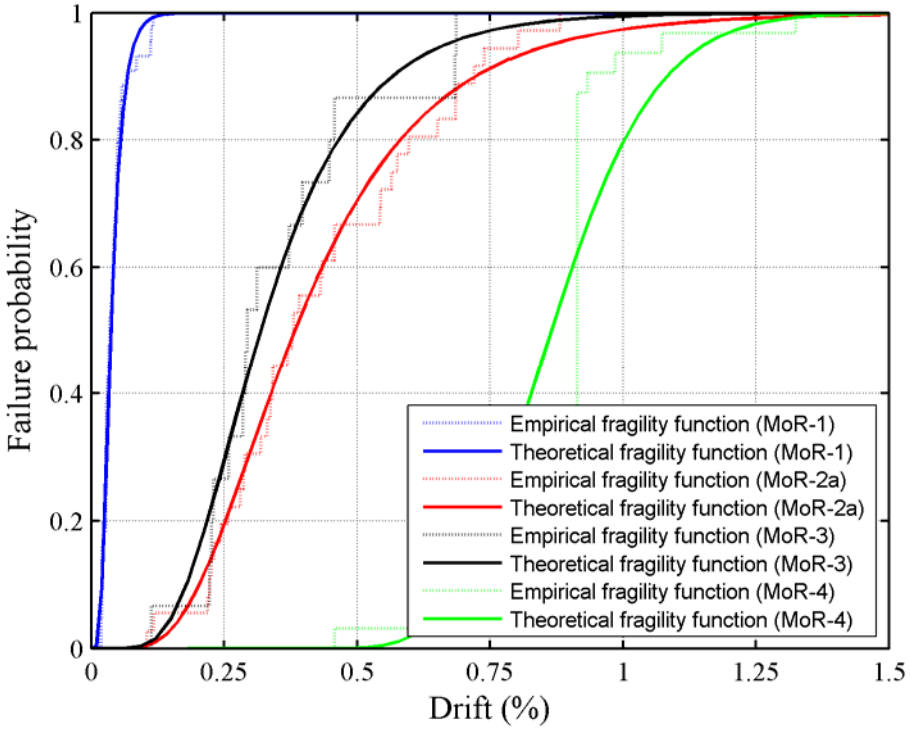


**Figure 8-21 Method 1 fragility functions for barbell walls**

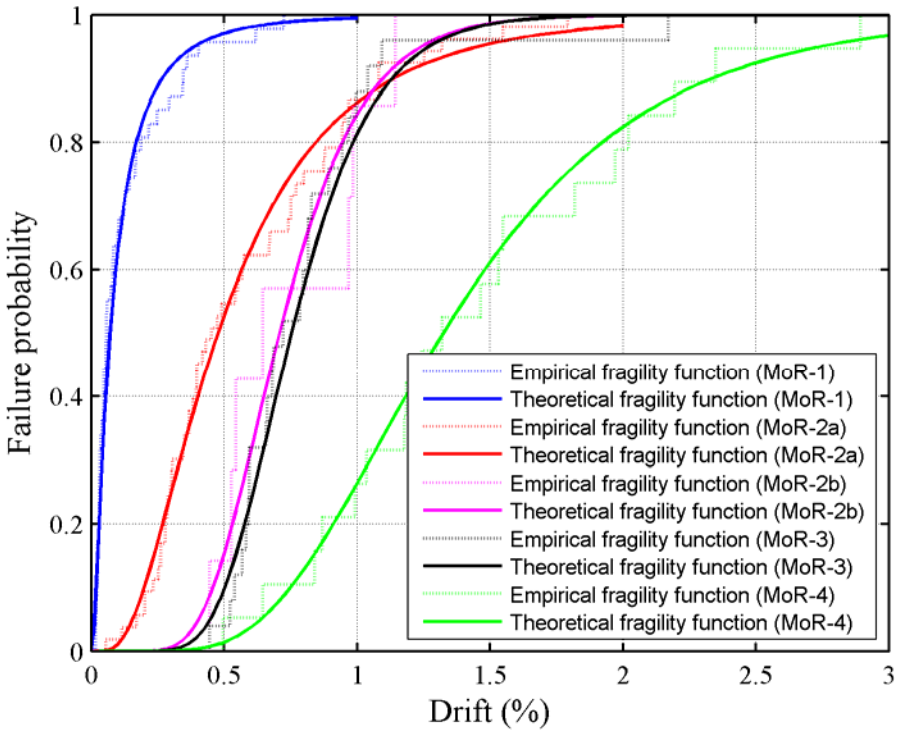


**Figure 8-22 Method 1 fragility functions for flanged walls**

### 8.5.7.2 Fragility Functions Developed Using Method 2

Method 2 utilizes the damage data with the smallest demand parameter (drift) for each method of repair of each specimen. The distribution parameters are presented in Table 8-14 for rectangular, barbell and flanged walls. Results for the K-S (all distributions) and Lilliefors (lognormal distribution only) goodness-of-fit tests are presented in Table 8-15 and

Table 8-16 at the 5% significance level. As seen in Table 8-15, the null hypothesis for the K-S test is rejected once (rectangular walls, MoR-4) for each distribution type for Method 2.

In Table 8-15, the yellow shaded cells identify the smallest values of $D$ for the K-S test for each wall geometry and method of repair. For 5 of the 14 cases investigated, the lognormal distribution yields the smallest $D$. Accordingly, the lognormal distribution is used to develop fragility curves for squat reinforced concrete walls.

Table 8-16 presents the Lilliefors goodness-of-fit test results. The lognormal distribution fails the goodness-of-fit test for MoR-2a, MoR-2b and MoR-4 for rectangular walls and MoR-4 for barbell walls.

The logarithmic standard deviations corresponding to MoR-1 are generally high but less than those observed for Method 1. The logarithmic standard deviations for MoR-2a, MoR-2b, MoR-3 and MoR-4 are less than 0.60 except for the flanged walls and MoR-2a ($\beta$ = 0.62). Similar to that observed for Method 1, MoR-3 precedes MoR-2a for barbell walls and MOR-2a. Figure 8-23, Figure 8-24, and Figure 8-25 present the empirical and theoretical fragility functions developed using data characterization Method 2.

**Table 8-14 Distribution parameters computed using Method 2**

| Wall Geometry | MoR | Distribution Parameters | | | | | | | |
|---|---|---|---|---|---|---|---|---|---|
| | | lognormal | | gamma | | Weibull | | beta | |
| | | $\theta$ | $\beta$ | $k$ | $\lambda$ | $k$ | $\lambda$ | $\alpha$ | $\beta$ |
| Rectangular | 1 | 0.07 | 0.81 | 1.58 | 15.04 | 0.11 | 1.18 | 2.13 | 15.34 |
| | 2a | 0.40 | 0.42 | 6.81 | 15.88 | 0.48 | 3.01 | 5.78 | 6.34 |
| | 2b | 0.54 | 0.36 | 8.49 | 14.76 | 0.64 | 3.26 | 2.16 | 2.79 |
| | 3 | 1.05 | 0.30 | 11.79 | 10.75 | 1.21 | 4.03 | 1.27 | 1.32 |
| | 4 | 1.25 | 0.35 | 9.10 | 6.90 | 1.47 | 3.55 | 2.15 | 2.96 |
| Barbell | 1 | 0.03 | 0.31 | 10.11 | 316.82 | 0.04 | 3.19 | 1.32 | 2.48 |
| | 2 | 0.33 | 0.49 | 4.48 | 11.93 | 0.43 | 2.21 | 0.90 | 1.42 |
| | 3 | 0.32 | 0.45 | 5.29 | 15.05 | 0.40 | 2.37 | 1.97 | 2.17 |
| | 4 | 0.87 | 0.17 | 35.22 | 40.12 | 0.94 | 6.24 | 3.95 | 4.20 |
| Flanged | 1 | 0.04 | 0.79 | 1.71 | 29.17 | 0.06 | 1.29 | 0.65 | 1.48 |
| | 2a | 0.36 | 0.62 | 3.27 | 7.71 | 0.48 | 2.03 | 3.81 | 5.45 |
| | 2b | 0.72 | 0.37 | 7.79 | 10.14 | 0.86 | 3.22 | 0.33 | 0.35 |
| | 3 | 0.75 | 0.32 | 8.45 | 10.58 | 0.90 | 2.39 | 0.65 | 2.51 |
| | 4 | 1.32 | 0.44 | 5.54 | 3.82 | 1.64 | 2.56 | 1.01 | 1.52 |

**Table 8-15 K-S test results for each distribution computed using Method 2**

| Wall geometry | MoR | K-S Test Results | | | | | | | | | | | |
|---|---|---|---|---|---|---|---|---|---|---|---|---|---|
| | | $D_{crit}$ | lognormal | | | gamma | | | Weibull | | | beta | | |
| | | | $p$ | $H_0$ | $D$ | $p$ | $H_0$ | $D$ | $p$ | $H_0$ | $D$ | $p$ | $H_0$ | $D$ |
| Rectangular | 1 | 0.205 | 0.902 | A | 0.086 | 0.304 | A | 0.147 | 0.365 | A | 0.139 | 0.234 | A | 0.156 |
| | 2a | 0.203 | 0.266 | A | 0.150 | 0.526 | A | 0.121 | 0.369 | A | 0.137 | 0.555 | A | 0.119 |
| | 2b | 0.294 | 0.288 | A | 0.213 | 0.399 | A | 0.194 | 0.720 | A | 0.150 | 0.491 | A | 0.180 |
| | 3 | 0.242 | 0.752 | A | 0.120 | 0.766 | A | 0.119 | 0.781 | A | 0.117 | 0.852 | A | 0.108 |
| | 4 | 0.215 | 0.318 | A | 0.152 | 0.440 | A | 0.138 | 0.717 | A | 0.111 | 0.088 | A | 0.198 |
| Barbell | 1 | 0.246 | 0.662 | A | 0.132 | 0.529 | A | 0.146 | 0.398 | A | 0.162 | 0.607 | A | 0.138 |
| | 2a | 0.309 | 0.869 | A | 0.136 | 0.893 | A | 0.131 | 0.785 | A | 0.149 | 0.386 | A | 0.206 |
| | 3 | 0.338 | 0.885 | A | 0.145 | 0.857 | A | 0.151 | 0.725 | A | 0.172 | 0.132 | A | 0.290 |
| | 4 | 0.234 | 0.002 | R | 0.327 | 0.002 | R | 0.317 | 0.005 | R | 0.297 | 0.005 | R | 0.298 |
| Flanged | 1 | 0.301 | 0.568 | A | 0.174 | 0.357 | A | 0.206 | 0.419 | A | 0.196 | 0.290 | A | 0.218 |
| | 2a | 0.254 | 0.881 | A | 0.110 | 0.993 | A | 0.081 | 0.945 | A | 0.099 | 0.299 | A | 0.182 |
| | 2b | 0.519 | 0.609 | A | 0.291 | 0.637 | A | 0.285 | 0.584 | A | 0.297 | 0.980 | A | 0.180 |
| | 3 | 0.269 | 0.910 | A | 0.111 | 0.835 | A | 0.123 | 0.282 | A | 0.196 | 0.226 | A | 0.207 |
| | 4 | 0.301 | 0.999 | A | 0.081 | 1.000 | A | 0.078 | 0.976 | A | 0.106 | 0.983 | A | 0.103 |

**Table 8-16 Lilliefors results for the lognormal distribution computed using Method 2**

| Wall Geometry | MoR | Lilliefors Test Results | | | |
|---|---|---|---|---|---|
| | | $D_{crit}$ | $p$ | $H_0$ | $D$ |
| **Rectangular** | 1 | 0.135 | 0.500 | A | 0.087 |
| | 2a | 0.134 | 0.015 | R | 0.151 |
| | 2b | 0.192 | 0.020 | R | 0.210 |
| | 3 | 0.159 | 0.364 | A | 0.116 |
| | 4 | 0.142 | 0.029 | R | 0.150 |
| **Barbell** | 1 | 0.161 | 0.194 | A | 0.134 |
| | 2a | 0.201 | 0.417 | A | 0.143 |
| | 3 | 0.219 | 0.438 | A | 0.153 |
| | 4 | 0.154 | 0.001 | R | 0.326 |
| **Flanged** | 1 | 0.197 | 0.148 | A | 0.171 |
| | 2a | 0.167 | 0.500 | A | 0.110 |
| | 2b | 0.324 | 0.194 | A | 0.270 |
| | 3 | 0.176 | 0.500 | A | 0.109 |
| | 4 | 0.197 | 0.500 | A | 0.084 |

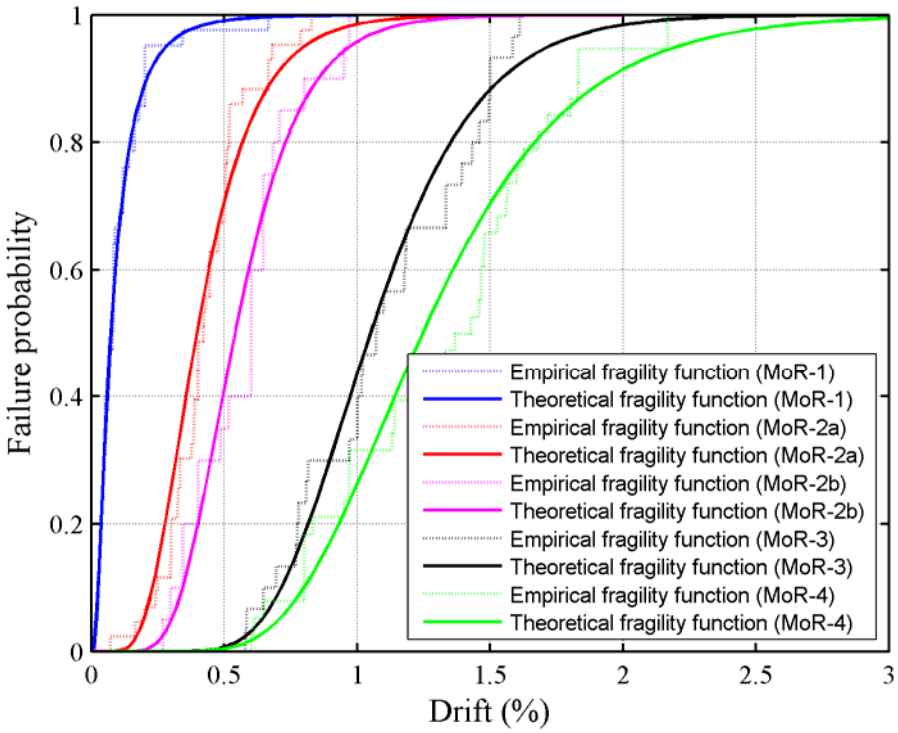


**Figure 8-23 Method 2 fragility functions for rectangular walls**

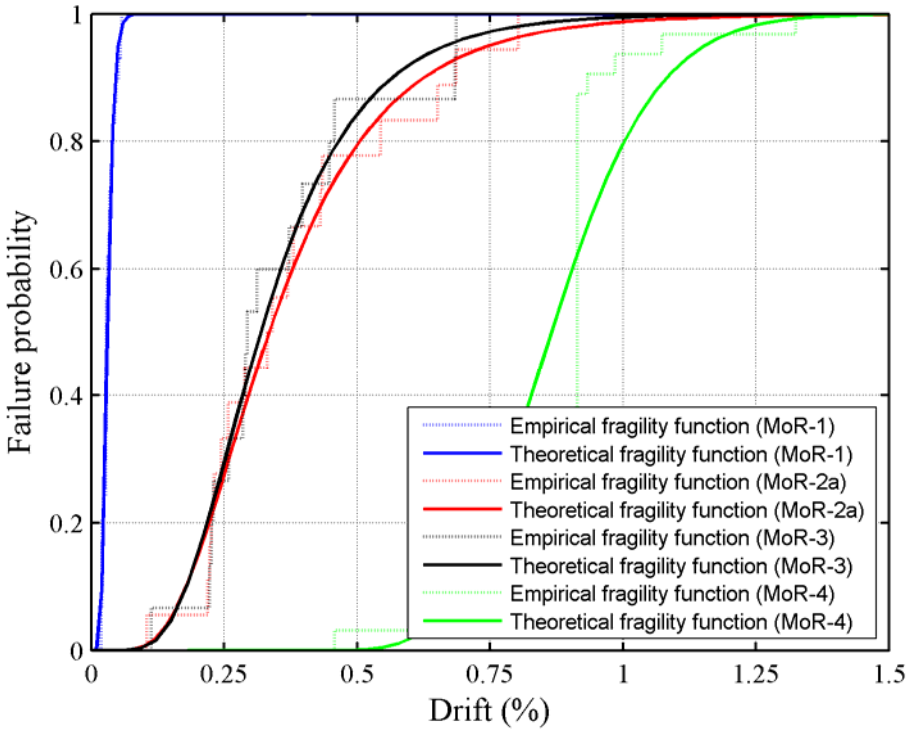


**Figure 8-24 Method 2 fragility functions for barbell walls**

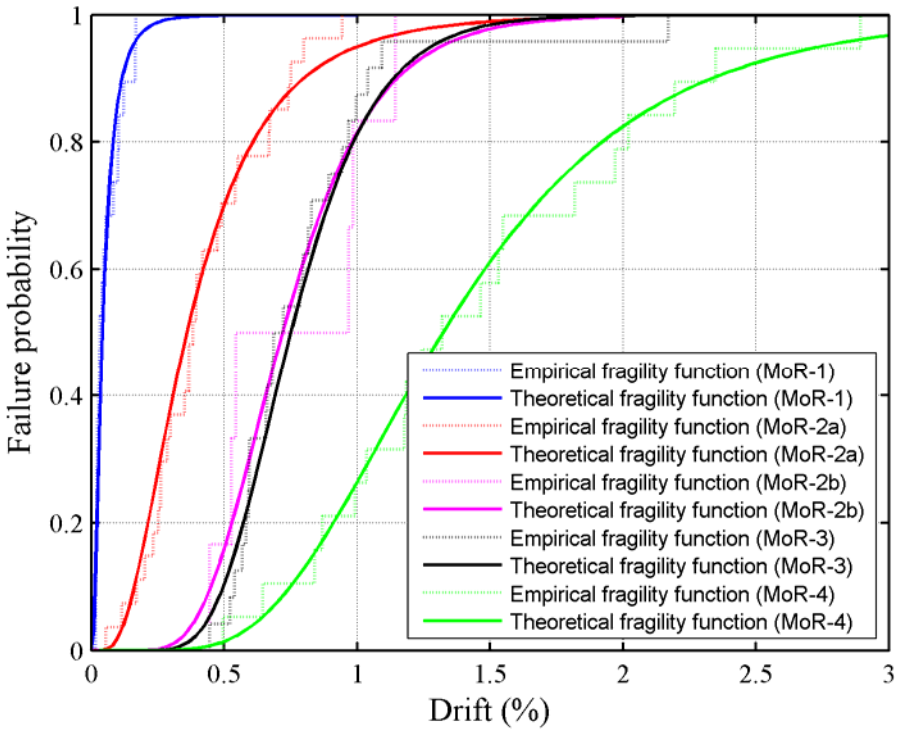


**Figure 8-25 Method 2 fragility functions for flanged walls**

## 8.6 Fragility Function Recommendations

### 8.6.1 Probability Distribution

The fragility data presented in Section 8.5.7 reveal that the lognormal distribution is the best of the four distributions considered for representing fragility functions for squat reinforced concrete walls for both Method 1 and Method 2.

### 8.6.2 Data Characterization

The fragility curves obtained using the lognormal distribution differ only modestly for Method 1 and Method 2 (see the gray shaded cells in Table 8-11 and Table 8-14). The dispersions for Method 1 are generally greater than those for Method 2 for the four methods of repair. Accordingly, fragility functions are developed using Method 2.

Table 8-17, which is based principally on Table 8-14, lists the values of median and dispersion obtained using the lognormal distribution and Method 2 for the three wall geometries and four methods of repair. Two significant figures are used to report median ($\theta$) drift. Two decimal digits are used for dispersion ($\beta$).

### 8.6.3 Evaluation of Damage States

#### 8.6.3.1 Damages States Associated with Reinforcement Yielding for MoR-2a

MoR-2a uses reinforcement yielding data (DS2.1, DS2.2, and DS2.3) together with DS2.4a and DS2.5a that are associated with crack widths of 0.5+ mm. This assumption is evaluated herein by fitting lognormal distribution using Method 2 to a) reinforcement yielding data (DS2.1, DS2.2 and DS2.3), and crack width data (DS2.4a and DS2.5a). Table 8-18 presents the parameters of the distribution. The parameters for barbell walls and DS2.4a and DS2.5a cannot be obtained due to a lack of data. For rectangular and flanged walls, the medians calculated using yielding data (DS2.1, DS2.2, and DS2.3) and crack width data (DS2.4a and DS2.5a) are in close agreement.

The data of Table 8-18 support the use of reinforcement yielding data and crack width data for MoR-2a.

#### 8.6.3.2 Damage States Associated with Supplemental Criteria for MoR-4

Two supplemental criteria are suggested for MoR-4 to aid in identification of damage for cases where the reported data is insufficient to make an assessment. The first, $SC_1$, serves to identify drift at sliding shear failure. The second, $SC_2$, is intended to the identify threshold drift for wall replacement for walls that fail under diagonal tension or compression, for cases where the drift at failure is unclear. The drifts identified using the supplemental criteria are presented in Appendix C.

Table 8-19 presents the distribution parameters for MoR-4 calculated with and without $SC_1$ and $SC_2$. As seen in the table, the use of the supplemental criteria does not significantly alter the distribution parameters. Criterion $SC_1$ identifies 13 data points for rectangular walls, 5 data

**Table 8-17 Lognormal distribution parameters calculated using Method 2**

| Wall geometry | MoR | $\theta$ | $\beta$ |
|---|---|---|---|
| **Rectangular** | **1** | 0.07 | 0.81 |
| | **2a** | 0.40 | 0.42 |
| | **2b** | 0.54 | 0.36 |
| | **3** | 1.05 | 0.30 |
| | **4** | 1.25 | 0.35 |
| **Barbell**[1] | **1** | 0.03 | 0.31 |
| | **2a** | 0.33 | 0.49 |
| | **3** | 0.32 | 0.45 |
| | **4** | 0.87 | 0.17 |
| **Flanged** | **1** | 0.04 | 0.79 |
| | **2a** | 0.36 | 0.62 |
| | **2b** | 0.72 | 0.37 |
| | **3** | 0.75 | 0.32 |
| | **4** | 1.32 | 0.44 |

1. Data not presented for MoR-2b; see footnote in Table 8-10.

**Table 8-18 Lognormal distribution parameters calculated using Method 2 for MoR-2a damage states**

| Wall geometry | Damage states | $\theta$ | $\beta$ |
|---|---|---|---|
| **Rectangular** | DS2.1, DS2.2, DS2.3 | 0.41 | 0.31 |
| | DS2.4a, DS2.5a | 0.42 | 0.54 |
| | DS2.1, DS2.2, DS2.3, DS2.4a, DS2.5a | 0.40 | 0.42 |
| **Barbell** | DS2.1, DS2.2, DS2.3 | 0.31 | 0.49 |
| | DS2.4a, DS2.5a | N/A[1] | N/A |
| | DS2.1, DS2.2, DS2.3, DS2.4a, DS2.5a | 0.33 | 0.49 |
| **Flanged** | DS2.1, DS2.2, DS2.3 | 0.41 | 0.51 |
| | DS2.4a, DS2.5a | 0.40 | 0.84 |
| | DS2.1, DS2.2, DS2.3, DS2.4a, DS2.5a | 0.36 | 0.62 |

1. Fitting is not possible since there are only 3 data points associated with these damage states.

points for flanged walls and 0 data points for barbell walls. Criterion $SC_2$ identifies 6 data points for flanged walls, 2 data points for barbell walls and 0 data points for rectangular walls.

The data of Table 8-19 shows that the use of the two supplemental criteria does not substantially modify the values of the distribution parameters. Accordingly, the recommended medians and dispersions presented below make use of supplemental criteria.

**Table 8-19 Effect of $SC_1$ and $SC_2$ on the MoR-4 lognormal distribution parameters for Method 2**

| Wall geometry | $SC_1$ | $SC_2$ | $\theta$ | $\beta$ |
|---|---|---|---|---|
| **Rectangular** | Considered | Considered | 1.25 | 0.35 |
| | Considered | Not considered | 1.25 | 0.35 |
| | Not considered | Not considered | 1.15 | 0.40 |
| **Barbell** | Considered | Considered | 0.87 | 0.17 |
| | Considered | Not considered | 0.86 | 0.18 |
| | Not considered | Not considered | 0.86 | 0.18 |
| **Flanged** | Considered | Considered | 1.32 | 0.44 |
| | Considered | Not considered | 1.31 | 0.51 |
| | Not considered | Not considered | 1.27 | 0.61 |

## 8.6.4 ACI 318-08 Compliance

Eleven of the 111 test specimens (6 rectangular, 2 flanged and 3 barbell) used to develop fragility functions do not comply with the minimum reinforcement requirements ($\rho_h = \rho_v = 0.25\%$) of ACI 318-08 [ACI (2008)] for *Special Structural Walls and Concrete Beams* (Chapter 21.9). This section presents fragility functions for walls that comply with the minimum reinforcement requirements of ACI 318-08 [ACI (2008)]. The lognormal distribution and Method 2 are used to develop the fragility functions. Results are presented in Table 8-20.

A comparison of the distribution parameters presented in Table 8-17 and Table 8-20 reveal that limiting the minimum web reinforcement ratios per ACI 318-08 [ACI (2008)] does not significantly affect the distribution parameters. The most significant effect is observed for MoR-2a for flanged walls for which the median drift increased from 0.36% to 0.39% and logarithmic standard deviation decreased from 0.62 to 0.51.

Given that most squat walls will likely comply with the ACI 318-08 [ACI (2008)] requirements for minimum rebar ratio, the medians and dispersions recommended in Section 8.6.5 are based on the data of Table 8-20.

**Table 8-20 Lognormal distribution parameters and the corresponding Lilliefors test results for squat walls that comply with the minimum reinforcement requirements of ACI 318-08 [ACI (2008)]**

| Wall geometry | MoR | Lognormal | | Lilliefors Test Results | | | |
|---|---|---|---|---|---|---|---|
| | | $\theta$ | $\beta$ | $D_{crit}$ | $p$ | $H_0$ | $D$ |
| Rectangular | **1** | 0.07 | 0.79 | 0.140 | 0.500 | A | 0.082 |
| | **2a** | 0.41 | 0.34 | 0.140 | 0.182 | A | 0.118 |
| | **2b** | 0.55 | 0.34 | 0.207 | 0.143 | A | 0.181 |
| | **3** | 1.09 | 0.27 | 0.164 | 0.338 | A | 0.122 |
| | **4** | 1.30 | 0.35 | 0.154 | 0.002 | R | 0.202 |
| Barbell | **1** | 0.03 | 0.31 | 0.170 | 0.379 | A | 0.123 |
| | **2a** | 0.34 | 0.53 | 0.219 | 0.500 | A | 0.140 |
| | **3** | 0.33 | 0.33 | 0.242 | 0.500 | A | 0.159 |
| | **4** | 0.87 | 0.18 | 0.161 | 0.001 | R | 0.327 |
| Flanged | **1** | 0.05 | 0.76 | 0.207 | 0.190 | A | 0.173 |
| | **2a** | 0.39 | 0.51 | 0.173 | 0.500 | A | 0.089 |
| | **2b** | 0.72 | 0.37 | 0.324 | 0.194 | A | 0.270 |
| | **3** | 0.76 | 0.33 | 0.184 | 0.500 | A | 0.100 |
| | **4** | 1.34 | 0.45 | 0.201 | 0.500 | A | 0.110 |

## 8.6.5 Recommendations

### 8.6.5.1 Rectangular Walls

Table 8-21 presents the recommended medians and dispersions for rectangular walls. On the basis of input from the ATC-58 project team, MoR-2 is represented by MoR-2b, namely, cracks widths in excess of 1.0 mm. The methods of repair in column 1 of the table are mapped to damage states per the ATC-58 notation in column 2.

**Table 8-21 Distribution parameters for rectangular walls**

| MoR | Damage State | $\theta$ | $\beta$ |
|---|---|---|---|
| **1** | DS0 | 0.07 | 0.79 |
| **2** | DS1 | 0.55 | 0.34 |
| **3** | DS2 | 1.09 | 0.27 |
| **4** | DS3 | 1.30 | 0.35 |

### 8.6.5.2 Barbell Walls

Table 8-22 presents the recommended medians and dispersions for barbell walls. Since the median drifts for MoR-2a and MoR-3 are virtually identical, MoR-2 is set aside for barbell walls. The methods of repair in column 1 of the table are mapped to damage states per the ATC-58 notation in column 2.

**Table 8-22 Distribution parameters for barbell walls**

| MoR | Damage State | $\theta$ | $\beta$ |
|---|---|---|---|
| **1** | DS0 | 0.03 | 0.31 |
| **3** | DS2 | 0.33 | 0.33 |
| **4** | DS3 | 0.87 | 0.18 |

### 8.6.5.3 Flanged Walls

Table 8-23 presents the recommended medians and dispersions for flanged walls. For the reason given in Section 8.6.5.1, MoR-2 is represented by MoR-2b. However, given that the median drifts for MoR-2 (=0.72) is virtually identical to that for MoR-3 (=0.76), MoR-2 is set aside for flanged walls. The methods of repair in column 1 of the table are mapped to damage states per the ATC-58 notation in column 2.

**Table 8-23 Distribution parameters for flanged walls**

| MoR | Damage State | $\theta$ | $\beta$ |
|---|---|---|---|
| **1** | DS0 | 0.05 | 0.76 |
| **3** | DS2 | 0.76 | 0.33 |
| **4** | DS3 | 1.34 | 0.45 |

## 8.7 Scopes of Repair

To establish consequence functions and costs of repair, a list of repair activities must be assigned to each method of repair. Such lists are presented in Appendix E for methods of repair MoR-1 through MoR-4.

# 9 SUMMARY AND CONCLUSIONS

## 9.1 Summary

Squat walls, defined herein as walls with ratios of height to length of less than or equal to two, are important structural components that are widely used in commercial buildings and safety-related nuclear structures. Accurate assessment of their seismic performance is crucial because they are designed to provide most of the lateral strength and stiffness to a structure.

The failure of squat reinforced concrete walls is generally by shear-related mechanisms, which result in brittle response. Current design provisions in codes and standards for reinforced concrete walls focus on slender (flexural) walls that can be designed and detailed to respond in a ductile manner. Much less attention is paid to squat, shear-critical walls although they are more common than slender flexure-critical walls. Shear-critical walls are the focus of this report.

The objectives of the report are six-fold, namely, 1) to assemble a squat wall database that includes data from all tests reported in the literature from 1950s, 2) to evaluate the utility of equations used in North America to predict the peak shear strength of squat walls, 3) to simulate the response of squat reinforced concrete walls using finite element analysis, 4) to simulate the response of squat reinforced concrete walls using a macro-level hysteretic deterioration model, 5) to develop predictive equations that provide unbiased estimates of peak shear strength with a small coefficient of variation, and 6) to develop fragility functions for squat walls suitable for use in seismic performance assessment.

A comprehensive literature review is conducted to inventory available experimental and analytical data on squat walls. A database that includes information from tests of 434 squat reinforced concrete walls is assembled. This database plays a key role in achieving all of the objectives listed above.

Peak shear strength is the key variable for force-based design and performance assessment of squat reinforced concrete walls. The utility of five widely used peak shear strength calculation procedures for squat walls, namely, Chapter 11 and 21 equations of ACI 318-08 [ACI (2008)], Barda et al. (1977) equation, ASCE 43-05 [ASCE (2005)] equation, and Wood (1990) equation, are evaluated using information from the database. The finite element codes ABAQUS [Hibbitt, Karlsson & Sorensen (2004)] and VecTor2 [VecTor Analysis Group (2007)], which employ different approaches to modeling reinforced concrete, are used for the finite element simulations of squat walls to a) determine those modeling parameters (or decisions) that are critical in predicting the response of squat walls, b) identify the formulation that best simulates the response of squat walls, and c) expand the parameter space for squat walls to enable development of new predictive equations.

New predictive equations for the peak shear strength of squat walls are proposed using reported experimental data and results from the finite element simulations. The parameters that most affect peak shear strength are identified using experimental data and finite element simulations.

A cyclic deterioration model is used to simulate the hysteretic response of squat walls. Load-displacement relationships from the database are used to identify the appropriate deterioration model parameters.

Performance-based seismic assessment and design makes use of fragility functions, damage states, and repair descriptions to identify economic loss, downtime or business interruption, and casualties. Such information is unavailable for squat reinforced concrete walls. Performance-oriented information and data are mined from the database and the literature to establish appropriate damage states, methods of repair, and fragility functions for squat walls, suitable for assessment of buildings and infrastructure.

## 9.2 Conclusions

The key conclusions of this study are listed below:

1. The scatter in the values of peak shear strength predicted by the five equations evaluated in this study is substantial. The utility of these equations is affected significantly by wall geometry (i.e., rectangular, barbell-shaped, flanged). The best predictions of peak shear strength (i.e., median ratio of predicted to measured peak shear strength close to 1.0 and a small coefficient of variation) are obtained using the equation of Wood (1990) for walls with rectangular cross-sections and the equations of ASCE 43-05 for walls with boundary elements.
2. Finite element predictions of squat wall response obtained using ABAQUS are affected significantly by the dilation angle ($\psi$) that controls the volumetric component of the plastic strain increment. For squat walls, the best simulations of the experimental results (i.e., load-displacement relationships and failure modes) are obtained for $\psi \simeq 55^{\circ}$. However, the optimal value for the dilation angle is likely different for alternate walls and $\psi \simeq 55^{\circ}$ must be used with care.
3. Both the MCFT and DSFM formulations implemented in VecTor2 provide more accurate predictions of squat wall response than the ABAQUS formulation. The difference in the predictions obtained by the DSFM and MCFT formulations is generally modest. The only notable difference between the responses calculated by the two formulations is in the pinched regions of the cyclic load-displacement relationships, for which the DSFM simulations better match the experimental data. The VecTor2 finite element analyses use two concrete models, namely, Popovics [Popovics (1973)] and Smith-Young [Smith and Young (1956)]. The predicted responses are similar up to the displacement at peak shear strength but the Popovics model is better for simulating the experimental response at displacements greater than that corresponding to peak shear strength.
4. The predictions of peak shear strength and the pre-peak shear strength shearing force-lateral displacement response are affected modestly by the granularity of the finite element mesh adopted for the ABAQUS and VecTor2 analyses. The impact of mesh refinement on the post-peak force-displacement relationship (i.e., post-capping stiffness) is more significant. For VecTor2, the use of 15 to 20 elements along the height of a wall with near-square element geometry should result in reasonable simulations of response for the entire loading history.
5. The experimental data and finite element analyses conducted using VecTor2 indicate that wall aspect ratio, vertical web reinforcement ratio, axial force, concrete compressive strength, wall geometry, and vertical boundary element reinforcement affect the peak

shear strength of squat walls. The effect of horizontal web reinforcement ratio on peak shear strength is modest.

6. New predictive equations for peak shear strength of squat walls are developed using nonlinear optimization tools. The proposed equations provide average ratios of predicted to measured peak shear strength close to 1.0 with a coefficient of variation as low as 0.10. These equations perform significantly better than the equations currently used for predicting the peak shear strength of squat walls.
7. The Ibarra et al. (2005) pinching model can simulate the cyclic load-displacement behavior of squat reinforced concrete walls if an appropriate backbone curve and model parameters are used. The performance of the model could be improved by a) updating the backbone curve to include a control point to represent the initiation cracking, b) providing a functional form for each of the control points in the backbone curve, and c) providing a functional form for each of the model parameters, which will require much additional testing and subsequent processing of digital data.
8. Fragility curves, damage states, and method of repair have been developed for squat walls in buildings and infrastructure. Four methods of repair, namely, cosmetic repair, epoxy injection, partial wall replacement, and wall replacement, are appropriate for performance-based evaluation of squat reinforced concrete walls. Each method of repair is associated with a damage state and experimental data are used to develop fragility functions for each method of repair using different probability distributions. The best fit on the fragility data is generally obtained using the lognormal distribution.

## 9.3 Future Research

A list of future research topics relevant to squat reinforced concrete walls follows based on the gaps in knowledge identified in, but not addressed by this report:

1. More experimental data are needed to assess the affect of horizontal web reinforcement ratio on squat wall behavior.
2. Digital load-displacement relationships from squat wall tests are essential to optimize the parameters for hysteretic deterioration models. The parameters evaluated in this study should be reassessed as new data becomes available.
3. Boundary elements can significantly affect the response of squat reinforced concrete walls. Barbells can be considered to be fully effective in resisting lateral loads. However, finite element analysis results and statistical evaluation of available data show that the peak shear strength of squat walls with wide flanges can be simulated best using an effective flange width. However, the volume of test data for squat walls with wide flanges is modest and further experimental data is needed to establish robust rules for the effectiveness of flanges in resisting shear.
4. The flow potential function in ABAQUS, more specifically, the form of the dilation angle parameter can be improved. Currently, the predictions are affected significantly by the choice of dilation angle. More test data on the triaxial behavior of concrete is needed to accurately define this parameter. The parameters of the experimental program should

include concrete compressive strength and degree of confinement. The direction of plastic strain increments must be monitored.

# 10 REFERENCES


ABAQUS Standard, Version 6.5.1, 2004, Hibbitt, Karlsson & Sorensen, Inc., Pawtucket, RI.

ACI Committee 349, 2001, "Code Requirements for Nuclear Safety Related Concrete Structures (ACI 349-01) and Commentary (ACI 349R-01)," American Concrete Institute, Farmington Hills, MI, 134 pp.

ACI Committee 546, 2004, "Concrete Repair Guide (ACI 546R-04)," American Concrete Institute, Farmington Hills, MI, 53 pp.

ACI Committee 349, 2006, "Code Requirements for Nuclear Safety Related Concrete Structures (ACI 349-06) and Commentary (ACI 349R-06)," American Concrete Institute, Farmington Hills, MI, 153 pp.

ACI Committee 318, 2008, "Building Code Requirements for Structural Concrete and Commentary (ACI 318-08)," American Concrete Institute, Farmington Hills, MI, 467 pp.

ADINA Version 6.1.4, 1995, ADINA R&D, Inc., Watertown, MA.

AIJ, 1985a, "Load-Deflection Characteristics of Nuclear Reactor Building Structures: Parts 8-9-10," *Summaries of Technical Papers, Structural Division*, Vol. 58, Architectural Institute of Japan, Japan. (in Japanese)

AIJ, 1985b, "Load-Deflection Characteristics of Nuclear Reactor Building Structures: Parts 37-38-39-40," *Summaries of Technical Papers of Annual Meeting, B, Structures I*, Architectural Institute of Japan, Japan. (in Japanese)

AIJ, 1986a, "Load-Deflection Characteristics of Nuclear Reactor Building Structures: Parts 62-63," *Summaries of Technical Papers of Annual Meeting, B, Structures I*, Architectural Institute of Japan, Japan. (in Japanese)

AIJ, 1986b, "Load-Deflection Characteristics of Nuclear Reactor Building Structures: Parts 59-60-61," *Summaries of Technical Papers of Annual Meeting, B, Structures I*, Architectural Institute of Japan, Japan. (in Japanese)

AIJ, 1986c, "Load-Deflection Characteristics of Nuclear Reactor Building Structures: Parts 21-22," *Summaries of Technical Papers, Structural Division*, Vol. 59, Architectural Institute of Japan, Japan. (in Japanese)

Alexander, C. M., Heidebrecht, A. C., and Tso, W. K., 1973, "Cyclic Load Tests on Shear Wall Panels," *Proceedings*, Fifth World Conference on Earthquake Engineering, Rome, Italy, pp. 1116-1119.

Antebi, J., Utku, S., and Hansen, R. J., 1960, "The Response of Shear Walls to Dynamic Loads," Department of Civil and Sanitary Engineering, Massachusetts Institute of Technology, Cambridge, MA.

ASCE, 1982, *State-of-the-Art Report on Finite Element Analysis of Reinforced Concrete*, American Society of Civil Engineers, New York, NY, 545 pp.

ASCE, 1986, *Finite Element Analysis of Reinforced Concrete Structures*, American Society of Civil Engineers, New York, NY.

ASCE, 1993, *Finite Element Analysis of Reinforced Concrete Structures II*, American Society of Civil Engineers, New York, NY, 717 pp.

ASCE, 1994, *Stiffness of Low-Rise Reinforced Concrete Shear Walls*, American Society of Civil Engineers, The Society, NY, 196 pp.

American Society of Civil Engineers, 2005, "Seismic Design Criteria for Structures, Systems, and Components in Nuclear Facilities (ASCE/SEI 43-05)," ASCE, Reston, VA, 96 pp.

American Society of Civil Engineers, 2007, "Seismic Rehabilitation of Existing Buildings (ASCE/SEI 41-06)," ASCE, Reston, VA, 411 pp.

Asfura, A. P., and Bruin, W. M., 1997, "Dynamic Behavior of a Shear Wall: Comparison between Tests and Analyses," *Proceedings*, Fourteenth International Conference on Structural Mechanics in Reactor Technology, HKW/7, Lyon, France, pp. 377-384.

ATC, 1998a, "Repair of Earthquake Damaged Concrete and Masonry Wall Buildings (FEMA 308)," Federal Emergency Management Agency, Washington, DC, 66 pp.

ATC, 1998b, "Evaluation of Earthquake Damaged Concrete and Masonry Buildings - Basic Procedures Manual (FEMA 306)," Federal Emergency Management Agency, Washington, DC, 250 pp.

ATC, 2008, "Guidelines for Seismic Performance Assessment of Buildings (ATC-58)," Applied Technology Council, <http://www.atcouncil.org/atc-58.shtml>.

Barda, F., 1972, "Shear Strength of Low-Rise Walls with Boundary Elements," PhD Dissertation, Lehigh University, Bethlehem, PA.

Barda, F., Hanson, J. M., and Corley, W. G., 1977, "Shear Strength of Low-Rise Walls with Boundary Elements," *Reinforced Concrete Structures in Seismic Zones*, SP 53-8, American Concrete Institute, Farmington Hills, MI, pp. 149-202.

Benjamin, J. R., and Williams, H. A., 1953, "Investigation of Shear Walls, Part 3 – Experimental and Mathematical Studies of Reinforced Concrete Walled Bents under Static Shear Loading," *Report* No. 1, Department of Civil Engineering, Stanford University, Stanford, CA.

Benjamin, J. R., and Williams, H. A., 1954, "Investigation of Shear Walls, Part 6 – Continued Experimental and Mathematical Studies of Reinforced Concrete Walled Bents under Static Shear Loading," *Report* No. 4, Department of Civil Engineering, Stanford University, Stanford, CA.

Benjamin, J. R., and Williams, H. A., 1956, "Investigation of Shear Walls, Part 12 – Studies of Reinforced Concrete Shear Wall Assemblies," *Report* No. 10, Department of Civil Engineering, Stanford University, Stanford.

Benjamin, J. R., and Cornell, C. A., 1970, *Probability, Statistics, and Decision for Civil Engineers*, McGraw-Hill, New York, 684 pp.

Bennett, J. G., Dove, R. C., Dunwoody, W. E., Endebrock, E. G., Farrar, C. R., and Goldman, P., 1987a, "Simulated Seismic Tests on 1/42- and 1/14-Scale Category I, Auxiliary Buildings," *Report* No. NUREG/CR-4987, Nuclear Regulatory Commission, Washington, D.C.

Bennett, J. G., Dove, R. C., Dunwoody, W. E., Farrar, C. R., and Goldman, P., 1987b, "The Seismic Category I Structures Program: Results for FY 1985," *Report* No. NUREG/CR-4998, Nuclear Regulatory Commission, Washington, D.C.

Bennett, J. G., Dove, R. C., Dunwoody, W. E., Farrar, C. R., and Goldman, P., 1988, "The Seismic Category I Structures Program: Results for FY 1986," *Report* No. NUREG/CR-5182, Nuclear Regulatory Commission, Washington, D.C.

Bentz, E. C., 2005, "Explaining the Riddle of Tension Stiffening Models for Shear Panel Model Experiments," *Journal of Structural Engineering*, ASCE, Vol. 131, No. 9, pp. 1422-1425.

Bhide, S. B., and Collins, M. P., 1987, "Reinforced Concrete Elements in Shear and Tension," *Report* No. 87-02, Department of Civil Engineering, University of Toronto, Toronto, ON, Canada.

Bolong, Z. W., Mingshun, W., and Kunlian, Z., 1980, "A Study of Hysteretic Curve of Reinforced Concrete Members under Cyclic Loading," *Proceedings*, Seventh World Conference on Earthquake Engineering, Istanbul, Turkey, pp. 509-516.

Bouc, R., 1967, "Forced Vibration of Mechanical Systems with Hysteresis," *Proceedings*, Fourth Conference on Nonlinear Oscillation.

Bouchon, M., Orbovic, N., and Foure, N., 2004, "Tests on Reinforced Concrete Low-Rise Shear Walls under Static Cyclic Loading," *Proceedings*, Thirteenth World Conference on Earthquake Engineering, No. 257, Vancouver, BC, Canada.

Box, G. E., Hunter, W. G., and Hunter, J. S., 1978, *Statistics for Experimenters*, John Wiley & Sons, Inc., 653 pp.

Brown, P. C., and Lowes, L. N., 2007, "Fragility Functions for Modern Reinforced-Concrete Beam-Column Joints," *Earthquake Spectra*, Vol. 23, No. 2, May, pp. 263-289.

Brown, P. C., 2008, "Probabilistic Earthquake Damage Prediction for Reinforced Concrete Building Components," MS Thesis, Department of Civil and Environmental Engineering, University of Washington, Seattle, WA, 173 pp.

Cardenas, A. E., Hanson, J. M., Corley, W. G., and Hognestad, E., 1973, "Design Provisions for Shear Walls," *ACI Journal*, Vol. 70-23, March, pp. 221-230.

Cardenas, A. E., Russell, H. G., and Corley, W. G., 1980, "Strength of Low Rise Structural Walls," *Reinforced Concrete Structures Subjected to Wind and Earthquake Forces*, SP 63-10, American Concrete Institute, Farmington Hills, MI, pp. 221-241.

Cervenka, V., 1970, "Inelastic Finite Element Analysis of Reinforced Concrete Panels under In-Plane Loads," PhD Dissertation, Department of Civil Engineering, University of Colorado, Boulder, CO.

Cheng, F. Y., 1992, "Coupling Bending and Shear Hysteretic Models of Low-Rise R. C. walls," *Concrete Shear in Earthquake*, University of Houston, Houston, TX, pp. 276-288.

Cheng, F. Y., Lou, K. Y., and Yang, J. S., 1994, "Analytical and Experimental Studies of RC Structures with Low-Rise Shear Walls," *Proceedings*, Fifth U.S. National Conference on Earthquake Engineering, Chicago, IL, pp. 45-54.

Cheng, F. Y., and Yang, J. S., 1996, "Hysteresis Rules and Design Parameter Assessment of RC Low-Rise Shear Walls and Buildings with Openings," Department of Civil Engineering, University of Missouri-Rolla, Rolla, MO.

Clough, R. W., and Johnston, S. B., 1966, "Effect of Stiffness Degradation on Earthquake Ductility Requirements," *Proceedings*, Japan Earthquake Engineering Symposium, Tokyo, Japan.

Collins, M. P., and Mitchell, D., 1987, *Prestressed Concrete Basics*, Canadian Prestressed Concrete Institute, Ottawa, ON, Canada.

Colotti, V., and Vulcano, A., 1987, "Behavior of Reinforced Concrete Structural Walls Subjected to Severe Loadings," *Proceedings*, Italian Association of Reinforced and Prestressed Concrete Conference, Stresa, Italy, pp. 87-102.

Dove, R. C., Bennett, J. G., Farrar, C. R., and Anderson, C. A., 1987, "Seismic Category I Structures Program Final Report, FY 1983-1984," *Report* No. NUREG/CR-4924, Nuclear Regulatory Commission, Washington, D.C.

Endebrock, E. G., Dove, R. C., and Dunwoody, W. E., 1985, "Analysis and Tests on Small-Scale Shear Walls, FY-82 final report," *Report* No. NUREG/CR-4274, Nuclear Regulatory Commission, Washington, D.C.

Farrar, C. R., Bennett, J. G., Dunwoody, W. E., and Baker, W. E., 1989, "Static Load cycle Testing of a Low-Aspect-Ratio Six-inch Wall, TRG-Type Structure, TRG-4-6 (1.0, 0.25)," *Report* No. NUREG/CR-5222, Nuclear Regulatory Commission, Washington, D.C.

Farrar, C. R., Bennett, J. G., Baker, W. E., and Dunwoody, W. E., 1990a, "Static Load Cycle Testing of a Very Low-Aspect-Ratio Six-inch Wall, TRG-Type Structure, TRG-6-6 (0.27, 0.50)," *Report* No. NUREG/CR-5533, Nuclear Regulatory Commission, Washington, D.C.

Farrar, C. R., Bennett, J. G., Dunwoody, W. E., and Baker, W. E., 1990b, "Static Load Cycle Testing of a Low-Aspect-Ratio Four-inch Wall, TRG-Type Structure, TRG-5-4 (1.0, 0.56)," *Report* No. NUREG/CR-5487, Nuclear Regulatory Commission, Washington, D.C.

Farrar, C. R., Baker, W. E., and Dove, R. C., 1991, "Static and Simulated Seismic Testing of the TRG-7 through TRG-16 Shear Wall Structures," *Report* No. NUREG/CR-5660, Nuclear Regulatory Commission, Washington, DC.

Farrar, C. R., and Baker, W. E., 1993, "Stiffness of Low-Aspect-Ratio Reinforced Concrete Shear Walls," *Report* No. NUREG/CR-5755, Nuclear Regulatory Commission, Washington, DC.

Farvashany, F. E., Foster, S. J., and Rangan, B. V., 2008, "Strength and Deformation of High-Strength Concrete Shearwalls," *ACI Structural Journal*, Vol. 105, No. 1, Jan.-Feb., pp. 21-29.

FEM-I [Computer software], 1990, Ewing, Kariotis, Englekirk & Hart, Rancho Palos Verdes, CA.

Fukuzawa, R., Chiba, O., Hatori, T., Yagishita, K., and Watabe, M., 1988, "Study on Load-Deflection Characteristics of Heavily Reinforced Concrete Shear Walls," *Proceedings*, Ninth World Conference on Earthquake Engineering, Tokyo-Kyoto, Japan, pp. 4/517-4/522.

Galletly, G. D., 1952, "Behavior of Reinforced Concrete Walls under Static Load," Department of Civil and Sanitary Engineering, Massachusetts Institute of Technology, Cambridge, MA.

Greifenhagen, C., Papas, D., and Lestuzzi, P., 2005, "Static-Cyclic Tests on Reinforced Concrete Shear Walls with Low Reinforcement Ratios," *Report* No. N4, School of Architecture, Civil and Environmental Engineering, Ecole Polytechnique Federale De Lausanne, Lausanne, Switzerland, 113 pp.

Gulec, C. K., 2005, "Ultimate Shear Strength of Squat Rectangular Reinforced Concrete Walls," MS Thesis, Department of Civil, Structural and Environmental Engineering, State University of New York at Buffalo, Buffalo, NY, 222 pp.

Gulec, C. K., Whittaker, A. S., and Stojadinovic, B., 2007, "Shear Strength of Squat Reinforced Concrete Walls with Flanges and Barbells," *Proceedings*, Nineteenth International Conference on Structural Mechanics in Reactor Technology, K08/5, Toronto, ON, Canada.

Gulec, C. K., Whittaker, A. S., and Stojadinovic, B., 2008, "Shear Strength of Squat Rectangular Reinforced Concrete Walls," *ACI Structural Journal*, Vol. 105, No. 4, Jul.-Aug., pp. 488-497.

Gulec, C. K., Whittaker, A. S., and Stojadinovic, B., 2009, "Shear Strength of Squat Reinforced Concrete Walls with Boundary Flanges or Barbells," *ACI Structural Journal*, Vol. 106, No. 3, May-June, pp. 368-377.

Hernandez, O. B., 1980, "Diseno de muros de concreto con falla por cortante," PhD Dissertation, Instituto de Ingenieria, Universidad Nacional Autonoma de Mexico, Mexico City, Mexico, 165 pp. (in Spanish)

Hidalgo, P. A., Jordan, R., and Ledezma, C. A., 1998, "Experimental Study of Reinforced Concrete Walls under Shear Failure," *Proceedings*, Sixth U.S. National Conference on Earthquake Engineering, Seattle, WA.

Hidalgo, P. A., Jordan, R. M., and Martinez, M. P., 2001, "An Analytical Model to Predict the Inelastic Seismic Behavior of Shear Wall, Reinforced Concrete Structures," *Engineering Structures*, Vol. 24, pp. 85-98.

Hidalgo, P. A., Ledezma, C. A., and Jordan, R. M., 2002, "Seismic Behavior of Squat Reinforced Concrete Shear Walls," *Earthquake Spectra*, EERI, Vol. 18, No. 2, pp. 287-308.

Hirosawa, M., 1975, "Past Experimental Results on Reinforced Concrete Shear Walls and Analysis on Them," *Kenchiku Kenkyu Shiryo*, No. 6, Building Research Institute, Ministry of Construction, Tokyo, Japan, 277 pp. (in Japanese)

Hofbeck, J. F., Ibrahim, I. O., and Mattock, A. H., 1969, "Shear Transfer in Reinforced Concrete," *ACI Journal*, Vol. 66, No. 2, February, pp. 119-128.

Hooper, J., 2008, *Personal Communication*.

Huang, C. C., and Sheu, M. S., 1988, "Experimental and Theoretical Study on Aseismic Behaviors of Low-Rise RC Shear Walls," *Proceedings*, Ninth World Conference on Earthquake Engineering, Tokyo-Kyoto, Japan, pp. 6/35-6/40.

Huang, C. C., and Sheu, M. S., 1994, "Experimental and Theoretical Studies of R.C. Shear Walls under Varying Axial and Lateral Loads," *Proceedings*, Fifth U.S. National Conference on Earthquake Engineering, Chicago, IL, pp. 15-24.

Hwang, S. J., Fang, W. H., Lee, H. J., and Yu, H. W., 2001, "Analytical Model for Predicting Shear Strength of Squat Walls," *Journal of Structural Engineering*, ASCE, Vol. 127, No. 1, pp. 43-50.

Ibarra, L. F., Medina, R. A., and Krawinkler, H., 2005, "Hysteretic Models that Incorporate Strength and Stiffness Deterioration," *Earthquake Engineering and Structural Dynamics*, Vol. 34, pp. 1489-1511.

IDARC2D Version 4.0, 1996, Reinhorn, A. M., Valles-Mattox, R., and Kunnath, S., Buffalo, NY.

Ile, N., Reynouard, J. M., and Merabet, O., 1998, "Dynamic Nonlinear 2-D and 3-D Analyses of RC Shear Wall under Seismic Loading," *Proceedings*, Eleventh European Conference on Earthquake Engineering, Rotterdam, Netherlands.

Imran, I., 1994, "Applications of Non-Associated Plasticity in Modelling the Mechanical Response of Concrete," PhD Dissertation, Department of Civil Engineering, University of Toronto, Toronto, ON, Canada, 208 pp.

Kabeyasawa, H., Shiora, H., Otani, S., and Aoyama, H., 1982, "Analysis of the Full-Scale Seven-Story Reinforced Concrete Test Structure: Test PSD3," *Proceedings*, Third Joint Technical Coordinating Committee, U.S.-Japan Cooperative Earthquake Research Program, Building Research Institute, Tsukaba, Japan.

Kabeyasawa, T., and Somaki, T., 1985, "Reinforcement Details for Reinforced Concrete Shear Walls with Thick Panel," *Transactions of the Japan Concrete Institute*, Vol. 7, pp. 369-372. (in Japanese)

Kitada, Y., Akino, K., Terada, K., Aoyama, H., and Miller, A., 1997, "Report on Seismic Shear Wall International Standard Problem Organized by OECD/NEA/CSNI," *Proceedings*, Fourteenth International Conference on Structural Mechanics in Reactor Technology, HKW/1, Lyon, France.

Kuang, J. S., and Ho, Y. B., 2008, "Seismic Behavior and Ductility of Squat Reinforced Concrete Shear Walls with Nonseismic Detailing," *ACI Structural Journal*, Vol. 105, No. 2, Mar.-Apr., pp. 225-231.

Kwak, H. G., and Kim, D. Y., 2001, "Nonlinear Analysis of RC Shear Walls Considering Tension-Stiffening Effect," *Computers and Structures*, Vol. 79, pp. 499-517.

Kwak, H. G., and Kim, D. Y., 2004, "Material Nonlinear Analysis of RC Shear Walls Subject to Cyclic Loadings," *Engineering Structures*, Vol. 26, pp. 1423-1436.

Lai, D., 2001, "Crack Shear-Slip in Reinforced Concrete Elements," MS Thesis, Department of Civil Engineering, University of Toronto, Toronto, ON, Canada, 154 pp.

Lee, J., and Fenves, G. L., 1998, "Plastic-Damage Model for Cyclic Loading of Reinforced Concrete Structures," *Journal of Engineering Mechanics*, ASCE, Vol. 124, No. 8, pp. 892-900.

Lefas, I. D., and Kotsovos, M. D., 1990, "Strength and Deformation Characteristics of Reinforced Concrete Walls under Load Reversals," *ACI Structural Journal*, Vol. 87, No. 6, Nov.-Dec., pp. 716-726.

Lefas, I. D., Kotsovos, M. D., and Ambraseys, N. N., 1990, "Behavior of Reinforced Concrete Structural Walls: Strength, Deformation Characteristics, and Failure Mechanism," *ACI Structural Journal*, Vol. 87, No. 1, Jan.-Feb., pp. 23-31.

Lignos, D., 2008, "Sidesway Collapse of Deteriorating Structural Systems under Seismic Excitations," PhD Dissertation, Civil and Environmental Engineering, Stanford University, Stanford, CA.

Lilliefors, H. W., 1967, "On the K-S Test for Normality with Mean and Variance Unknown," *Journal of American Statistical Association*, Vol. 62, June, pp. 399-402.

Lopes, M. S., and Elnashai, A. S., 1991, "Seismic Behaviour of RC Walls with Low Shear Ratio," *Report* No. 91-9, ESEE Research Report, Civil Engineering Department, Imperial College, London, UK, 439 pp.

Lowes, L. N., and Li, J., 2008, "Fragility Curves for Reinforced Concrete Special and Intermediate Moment Frames," Report to ATC-58.

Lubliner, J., Oliver, J., Oller, S., and Onate, E., 1989, "A Plastic-Damage Model for Concrete," *International Journal of Solids and Structures*, Vol. 25, No. 3, pp. 299-326.

Mahin, S. A., and Bertero, V. V., 1976, "Nonlinear Seismic Response of a Coupled Wall System," *ASCE Journal of the Structural Division*, Vol. 102, pp. 1759-1780.

Maier, J., and Thürlimann, B., 1985, "Bruchversuche an Stahlbetonscheiben," Institut für Baustatik und Konstruktion, Eidgenössische Technische Hochschule (ETH) Zürich, Zürich, Switzerland, 130 pp. (in German)

Massone, L. M., and Wallace, J. W., 2004, "Load-Deformation Responses of Slender Reinforced Concrete Walls," *ACI Structural Journal*, Vol. 101, No. 1, Jan.-Feb., pp. 103-113.

Massone, L. M., 2006, "RC Wall Shear-Flexure Interaction: Analytical and Experimental Responses," PhD Dissertation, Department of Civil and Environmental Engineering, University of California, Los Angeles, CA, 398 pp.

MATLAB Version 7.3.0, 2006, The MathWorks, Inc., Natick, MA.

Mattock, A. H., 1976, "Shear Transfer Under Monotonic Loading, Across an Interface Between Concretes Cast at Different Times, Final Report, Part 1," *Report* No. SM 76-3, Department of Civil Engineering, University at Washington, Seattle, WA.

Mattock, A. H., 1977, "Shear Transfer Under Cyclically Reversing Loading Across an Interface Between Concretes Cast at Different Times, Final Report, Part 2," *Report* No. SM 77-1, Department of Civil Engineering, University at Washington, Seattle, WA.

Menegotto, M., and Pinto, E., 1973, "Method of Analysis for Cyclically Loaded Reinforced Concrete Plane Frames Including Changes in Geometry and Non-Elastic Behavior of Elements Under Combined Normal Force and Bending," *Proceedings*, IABSE Symposium, Lisbon, Portugal.

Mindess, S., Young, J. F., and Darwin, D., 2003, *Concrete*, Prentice Hall, Englewood Cliffs, NJ, 644 pp.

Minitab 15, 2007, Minitab Inc.

Mo, Y. L., and Chan, J., 1996, "Behavior of Reinforced-Concrete Framed Shear Walls," *Nuclear Engineering and Design*, Vol. 166, No. 1, pp. 55-68.

Mohammadi-Doostdar, H., 1994, "Behavior and Design of Earthquake Resistant Low-Rise Shear Walls," Department of Civil Engineering, University of Ottawa, Ottawa, ON, Canada, 234 pp.

Montgomery, D. C., 2005, *Design and Analysis of Experiments (6th edition)*, John Wiley & Sons, Inc., 643 pp.

Naze, P. A., and Sidaner, J. F., 2001, "Presentation and Interpretation of SAFE Tests: Reinforced Concrete Walls Subjected to Shearing," *Proceedings*, Sixteenth International Conference on Structural Mechanics in Reactor Technology, H04/01, Washington, DC.

Ngo, D., and Scordelis, A. C., 1967, "Finite Element Analyses of Reinforced Concrete Beams," *American Concrete Institute Journal*, Vol. 64, No. 3, March.

Nilson, A. H., 1968, "Nonlinear Analysis of Reinforced Concrete by the Finite Element Method," *American Concrete Institute Journal*, Vol. 65, No. 9, September.

OECD/NEA/CSNI, 1996, "Seismic Shear Wall ISP NUPEC's Seismic Ultimate Dynamic Response Test, Comparison Report," *Report* No. OCDE/GD(96)188, Committee on the Safety of Nuclear Installations OECD Nuclear Energy Agency, Issy-Les-Moulineaux, France, 412 pp.

Ogata, K., and Kabeyasawa, T., 1984, "Experimental Study on the Hysteretic Behavior of Reinforced Concrete Shear Walls under the Loading of Different Moment-to-Shear Ratios," *Transactions of the Japan Concrete Institute*, Vol. 6, pp. 717-724.

Orakcal, K., Massone, L. M., and Wallace, J. W., 2006, "Analytical Modeling of Reinforced Concrete Walls for Predicting Flexural and Coupled-Shear-Flexural Responses," *Report* No. PEER 2006/07, Pacific Earthquake Engineering Research Center, University of California, Los Angeles, CA.

Orbovic, N., Abrishami, H. H., Dikic, D., Lee, N., and Elgohary, M., 2007, "The Capacity of Reinforced Concrete Squat Shear Walls under Seismic Loading for the Design of the ACR-1000$^{TM}$ NPP," *Proceedings*, Nineteenth International Conference on Structural Mechanics in Reactor Technology, K10/2, K10/2, Toronto, ON, Canada.

Pagni, C. A., and Lowes, L. N., 2006, "Fragility Functions for Older Reinforced Concrete Beam Column Joints," *Earthquake Spectra*, EERI, Vol. 22, No. 1, pp. 215-238.

Palermo, D., and Vecchio, F. J., 2002a, "Behavior and Analysis of Reinforced Concrete Walls Subjected to Reversed Cyclic Loading," *Report* No. 2002-01, Department of Civil Engineering, University of Toronto, Toronto, ON, Canada, 351 pp.

Palermo, D., and Vecchio, F. J., 2002b, "Behavior of Three-Dimensional Reinforced Concrete Shear Walls," *ACI Structural Journal*, Vol. 99, No. 1, Jan.-Feb., pp. 81-89.

Palermo, D., and Vecchio, F. J., 2007, "Simulation of Cyclically Loaded Concrete Structures Based on the Finite-Element Method," *Journal of Structural Engineering*, ASCE, Vol. 133, No. 5, pp. 728-738.

Pang, X. D., and Hsu, T. T. C., 1995, "Behavior of Reinforced Concrete Membrane Elements in Shear," *ACI Structural Journal*, Vol. 92, No. 6, Nov.-Dec., pp. 665-679.

Park, R., Priestley, M. J. N., and Gill, W. D., 1982, "Ductility of Square-Confined Concrete Columns," *Journal of the Structural Division*, ASCE, Vol. 108, No. 4, pp. 929-950.

Park, Y. J., and Ang, A. H. S., 1985, "Mechanistic Seismic Damage Model for Reinforced-Concrete," *Journal of Structural Engineering*, ASCE, Vol. 111, No. 4, pp. 722-739.

Paulay, T., Priestley, M. J. N., and Synge, A. J., 1982, "Ductility in Earthquake Resisting Squat Shearwalls," *ACI Journal*, Vol. 79, No. 4, Jul.-Aug., pp. 257-269.

Paulay, T., and Priestley, M. J. N., 1992, *Seismic Design of Reinforced Concrete and Masonry Buildings*, John Wiley & Sons.

Pilakoutas, K., 1991, "Earthquake Resistant Design of Reinforced Concrete Walls," *Report* No. 91-4, ESEE Research Report, Civil Engineering Department, Imperial College, London, UK, 360 pp.

Pilakoutas, K., and Elnashai, A. S., 1995, "Cyclic Behavior of Reinforced Concrete Cantilever Walls, Part I: Experimental Results," *ACI Structural Journal*, Vol. 92, No. 3, May-June, pp. 271-281.

Pilette, F. C., 1987, "Behavior of Earthquake Resistant Squat Shear Walls," MS Thesis, Department of Civil Engineering, University of Ottawa, Ottawa, ON, Canada, 177 pp.

Popovics, S., 1973, "A Numerical Approach to the Complete Stress-Strain Curve of Concrete," *Cement and Concrete Research*, Vol. 3, No. 5, pp. 583-599.

Rahnama, M., and Krawinkler, H., 1993, "Effects of Soft Soil and Hysteresis Model on Seismic Demands," *Report* No. 108, The John A. Blume Earthquake Engineering Center, Department of Civil Engineering, Stanford University, Stanford, CA.

Rashid, Y. R., 1968, "Ultimate Strength Analysis of Prestressed Concrete Pressure Vessels," *Nuclear Engineering and Design*, Vol. 7.

Rothe, D., 1992, "Untersuchungen zum Nichtlinearen Verhalten von Stahlbeton Wandschieben unter Erdbebenbeanspruchung," PhD Dissertation, Fachbereich Konstruktiver Ingenieurbau, der Technischen Hochschule Darmstadt, Darmstadt, Germany, 161 pp. (in German)

Saito, H., Kikuchi, R., Kanechika, M., and Okamoto, K., 1989, "Experimental Study on the Effect of Concrete Strength on Shear Wall Behavior," *Proceedings*, Tenth International Conference on Structural Mechanics in Reactor Technology, H08/05, Anaheim, CA.

Salonikios, T. N., Kappos, A. J., Tegos, I. A., and Penelis, G. G., 1999, "Cyclic Load Behavior of Low-Slenderness Reinforced Concrete Walls: Design Basis and Test Results," *ACI Structural Journal*, Vol. 96, No. 4, Jul.-Aug., pp. 649-660.

Sato, S., Ogata, Y., Yoshizaki, S., Kanata, K., Yamaguchi, T., Nakayama, T., Inada, Y., and Kadoriku, J., 1989, "Behavior of Shear Wall Using Various Yield Strength of Rebar, Part 1: An Experimental Study," *Proceedings*, Tenth International Conference on Structural Mechanics in Reactor Technology, H09/01, Anaheim, CA.

Seckin, M., 1981, "Hysteretic Behavior of Cast-in-Place Exterior Beam-Column-Slab Subassemblies," PhD Dissertation, Department of Civil Engineering, University of Toronto, Toronto, ON, Canada, 266 pp.

Seki, M., Kobayashi, J., Shibata, A., Kubo, T., Taira, T., and Akino, K., 1995, "Restoring Force Verification Test on RC Shear Wall," *Proceedings*, Thirteenth International Conference on Structural Mechanics in Reactor Technology, H06, Porto Alegre, Brazil.

Sheu, M. S., 2007, *Personal Communication*.

Shiga, T., Shibata, A., and Takahashi, J., 1973, "Experimental Study on Dynamic Properties of Reinforced Concrete Shear Walls," *Proceedings*, Fifth World Conference on Earthquake Engineering, Vol. 1, Rome, Italy, pp. 1157-1166.

Shiga, T., Shibata, A., and Takahashi, J., 1975, "Hysteretic Behavior of Reinforced Concrete Shear Walls," *Proceedings*, Review Meeting of the US-Japan Co-operative Research Program in Earthquake Engineering, Honolulu, HI, pp. 107-117.

Sittipunt, C., and Wood, S. L., 1993, "Finite Element Analysis of Reinforced Concrete Shear Walls," *Report* No. UILU-ENG-93-2015, Department of Civil Engineering, University of Illinois - Urbana Champaign, Urbana, IL, 384 pp.

Sivaselvan, M. V., and Reinhorn, A. M., 2000, "Hysteretic Models for Deteriorating Inelastic Structures," *Journal of Engineering Mechanics*, ASCE, Vol. 126, pp. 633-640.

Smith, G. M., and Young, L. E., 1956, "Ultimate Flexural Analysis Based on Stress-Strain Curves of Cylinders," *Journal of the American Concrete Institute*, Vol. 28, No. 6, December, pp. 597-609.

Smith, S. S., William, K. J., Gerstle, K. H., and Sture, S., 1989, "Concrete over the Top, or: Is There Life after Peak?," *ACI Materials Journal*, Vol. 86, No. 5, Sep.-Oct., pp. 491-497.

Soong, T. T., 2004, *Fundamentals of Probability and Statistics for Engineers*, John Wiley & Sons, Chichester, England, 391 pp.

Sozen, A. M., and Moehle, J. P., 1993, "Stiffness of Reinforced Concrete Walls Resisting In-plane Shear," *Report* No. EPRI TR-102731, Electrical Power Research Institute, Paolo Alto, CA.

Synge, A. J., 1980, "Ductility of Squat Shear Walls," *Report* No. 80-8, Department of Civil Engineering, University of Canterbury, Christchurch, New Zealand, 142 pp.

Takeda, T., Sozen, A. M., and Nielson, N. N., 1970, "Reinforced Concrete Response to Simulated Earthquakes," *Journal of the Structural Division*, ASCE, Vol. 96, pp. 2557-2573.

Vecchio, F. J., and Collins, M. P., 1982, "Response of Reinforced Concrete to In-Plane Shear and Normal Stresses," *Report* No. 82-03, Department of Civil Engineering, University of Toronto, Toronto, ON, Canada.

Vecchio, F. J., and Collins, M. P., 1986, "The Modified Compression-Field Theory for Reinforced Concrete Elements Subjected to Shear," *ACI Journal*, Vol. 83, No. 2, Mar.-Apr., pp. 219-231.

Vecchio, F. J., 1992, "Finite Element Modeling of Concrete Expansion and Confinement," *Journal of Structural Engineering*, ASCE, Vol. 118, No. 9, pp. 2390-2406.

Vecchio, F. J., and Collins, M. P., 1993, "Compression Response of Cracked Reinforced Concrete," *Journal of Structural Engineering*, ASCE, Vol. 119, No. 12, pp. 3590-3610.

Vecchio, F. J., 1998, "Lessons from the Analysis of a 3-D Concrete Shear Wall," *Structural Engineering and Mechanics*, Vol. 6, No. 4, pp. 439-455.

Vecchio, F. J., 2000, "Disturbed Stress Field Model for Reinforced Concrete: Formulation," *Journal of Structural Engineering*, ASCE, Vol. 126, No. 9, pp. 1070-1077.

Vecchio, F. J., Lai, D., Shim, W., and Ng, J., 2001, "Disturbed Stress Field Model for Reinforced Concrete: Validation," *Journal of Structural Engineering*, ASCE, Vol. 127, No. 4, pp. 350-358.

VecTor2, 2007, VecTor Analysis Group, University of Toronto, Toronto, ON, Canada.

Vulcano, A., and Bertero, V. V., 1987, "Analytical Models for Predicting the Lateral Response of RC Shear Walls: Evaluation of Their Reliability," *Report* No. UCB/EERC - 87/19, Earthquake Engineering Research Center, University of California, Berkeley, CA, 92 pp.

Vulcano, A., Bertero, V. V., and Colotti, V., 1988, "Analytical Modeling of RC Structural Walls," *Proceedings*, Ninth World Conference on Earthquake Engineering, Tokyo-Kyoto, Japan, pp. 41-46.

Wallace, J. W., 2007, "Modeling Issues for Tall Reinforced Concrete Core Wall Buildings," *Structural Design of Tall and Special Buildings*, Vol. 16, No. 5, pp. 615-632.

Walraven, J. C., 1981, "Fundamental Analysis of Aggregate Interlock," *Journal of the Structural Division*, ASCE, Vol. 107, No. 11, pp. 2245-2270.

Wasiewicz, Z. F., 1988, "Sliding Shear in Low-Rise Walls under Lateral Load Reversals," MS Thesis, Department of Civil Engineering, University of Ottawa, Ottawa, ON, Canada, 127 pp.

Wen, Y. K., 1976, "Method for Random Vibration of Hysteretic Systems," *Journal of the Engineering Mechanics Division*, ASCE, Vol. 112, pp. 249-263.

Wiradinata, S., 1985, "Behavior of Squat Walls Subjected to Load Reversals," MS Thesis, Department of Civil Engineering, University of Toronto, Toronto, ON, Canada, 171 pp.

Wong, P. S., and Vecchio, F. J., 2002, *VecTor2 and Formworks User's Manual*, 213 pp.

Wood, S. L., 1990, "Shear Strength of Low-Rise Reinforced Concrete Walls," *ACI Structural Journal*, Vol. 87, No. 1, Jan.-Feb., pp. 99-107.

XiangDong, G., 1999, "Framed Shear Walls under Cyclic Loading," PhD Dissertation, Department of Civil and Environmental Engineering, University of Houston, Houston, TX, 285 pp.

Xie, L., and Xiao, Y., 2000, "Study on Retrofit of Existing Squat Concrete Shear Walls," *Report* No. USC-SERP 2000-5, Department of Civil Engineering, University of Southern California, Los Angeles, CA, 111 pp.

XTRACT v.3.0.8, 2007, Imbsen and Associates, Inc., Fresno, CA.

Zhang, L. X. B., and Hsu, T. T. C., 1998, "Behavior and Analysis of 100 MPa Concrete Membrane Elements," *Journal of Structural Engineering*, ASCE, Vol. 124, No. 1, pp. 24-34.

## MCEER Technical Reports

MCEER publishes technical reports on a variety of subjects written by authors funded through MCEER. These reports are available from both MCEER Publications and the National Technical Information Service (NTIS). Requests for reports should be directed to MCEER Publications, MCEER, University at Buffalo, State University of New York, Red Jacket Quadrangle, Buffalo, New York 14261. Reports can also be requested through NTIS, 5285 Port Royal Road, Springfield, Virginia 22161. NTIS accession numbers are shown in parenthesis, if available.

NCEER-87-0001 "First-Year Program in Research, Education and Technology Transfer," 3/5/87, (PB88-134275, A04, MF-A01).

NCEER-87-0002 "Experimental Evaluation of Instantaneous Optimal Algorithms for Structural Control," by R.C. Lin, T.T. Soong and A.M. Reinhorn, 4/20/87, (PB88-134341, A04, MF-A01).

NCEER-87-0003 "Experimentation Using the Earthquake Simulation Facilities at University at Buffalo," by A.M. Reinhorn and R.L. Ketter, to be published.

NCEER-87-0004 "The System Characteristics and Performance of a Shaking Table," by J.S. Hwang, K.C. Chang and G.C. Lee, 6/1/87, (PB88-134259, A03, MF-A01). This report is available only through NTIS (see address given above).

NCEER-87-0005 "A Finite Element Formulation for Nonlinear Viscoplastic Material Using a Q Model," by O. Gyebi and G. Dasgupta, 11/2/87, (PB88-213764, A08, MF-A01).

NCEER-87-0006 "Symbolic Manipulation Program (SMP) - Algebraic Codes for Two and Three Dimensional Finite Element Formulations," by X. Lee and G. Dasgupta, 11/9/87, (PB88-218522, A05, MF-A01).

NCEER-87-0007 "Instantaneous Optimal Control Laws for Tall Buildings Under Seismic Excitations," by J.N. Yang, A. Akbarpour and P. Ghaemmaghami, 6/10/87, (PB88-134333, A06, MF-A01). This report is only available through NTIS (see address given above).

NCEER-87-0008 "IDARC: Inelastic Damage Analysis of Reinforced Concrete Frame - Shear-Wall Structures," by Y.J. Park, A.M. Reinhorn and S.K. Kunnath, 7/20/87, (PB88-134325, A09, MF-A01). This report is only available through NTIS (see address given above).

NCEER-87-0009 "Liquefaction Potential for New York State: A Preliminary Report on Sites in Manhattan and Buffalo," by M. Budhu, V. Vijayakumar, R.F. Giese and L. Baumgras, 8/31/87, (PB88-163704, A03, MF-A01). This report is available only through NTIS (see address given above).

NCEER-87-0010 "Vertical and Torsional Vibration of Foundations in Inhomogeneous Media," by A.S. Veletsos and K.W. Dotson, 6/1/87, (PB88-134291, A03, MF-A01). This report is only available through NTIS (see address given above).

NCEER-87-0011 "Seismic Probabilistic Risk Assessment and Seismic Margins Studies for Nuclear Power Plants," by Howard H.M. Hwang, 6/15/87, (PB88-134267, A03, MF-A01). This report is only available through NTIS (see address given above).

NCEER-87-0012 "Parametric Studies of Frequency Response of Secondary Systems Under Ground-Acceleration Excitations," by Y. Yong and Y.K. Lin, 6/10/87, (PB88-134309, A03, MF-A01). This report is only available through NTIS (see address given above).

NCEER-87-0013 "Frequency Response of Secondary Systems Under Seismic Excitation," by J.A. HoLung, J. Cai and Y.K. Lin, 7/31/87, (PB88-134317, A05, MF-A01). This report is only available through NTIS (see address given above).

NCEER-87-0014 "Modelling Earthquake Ground Motions in Seismically Active Regions Using Parametric Time Series Methods," by G.W. Ellis and A.S. Cakmak, 8/25/87, (PB88-134283, A08, MF-A01). This report is only available through NTIS (see address given above).

NCEER-87-0015 "Detection and Assessment of Seismic Structural Damage," by E. DiPasquale and A.S. Cakmak, 8/25/87, (PB88-163712, A05, MF-A01). This report is only available through NTIS (see address given above).

NCEER-87-0016 "Pipeline Experiment at Parkfield, California," by J. Isenberg and E. Richardson, 9/15/87, (PB88-163720, A03, MF-A01). This report is available only through NTIS (see address given above).

NCEER-87-0017 "Digital Simulation of Seismic Ground Motion," by M. Shinozuka, G. Deodatis and T. Harada, 8/31/87, (PB88-155197, A04, MF-A01). This report is available only through NTIS (see address given above).

NCEER-87-0018 "Practical Considerations for Structural Control: System Uncertainty, System Time Delay and Truncation of Small Control Forces," J.N. Yang and A. Akbarpour, 8/10/87, (PB88-163738, A08, MF-A01). This report is only available through NTIS (see address given above).

NCEER-87-0019 "Modal Analysis of Nonclassically Damped Structural Systems Using Canonical Transformation," by J.N. Yang, S. Sarkani and F.X. Long, 9/27/87, (PB88-187851, A04, MF-A01).

NCEER-87-0020 "A Nonstationary Solution in Random Vibration Theory," by J.R. Red-Horse and P.D. Spanos, 11/3/87, (PB88-163746, A03, MF-A01).

NCEER-87-0021 "Horizontal Impedances for Radially Inhomogeneous Viscoelastic Soil Layers," by A.S. Veletsos and K.W. Dotson, 10/15/87, (PB88-150859, A04, MF-A01).

NCEER-87-0022 "Seismic Damage Assessment of Reinforced Concrete Members," by Y.S. Chung, C. Meyer and M. Shinozuka, 10/9/87, (PB88-150867, A05, MF-A01). This report is available only through NTIS (see address given above).

NCEER-87-0023 "Active Structural Control in Civil Engineering," by T.T. Soong, 11/11/87, (PB88-187778, A03, MF-A01).

NCEER-87-0024 "Vertical and Torsional Impedances for Radially Inhomogeneous Viscoelastic Soil Layers," by K.W. Dotson and A.S. Veletsos, 12/87, (PB88-187786, A03, MF-A01).

NCEER-87-0025 "Proceedings from the Symposium on Seismic Hazards, Ground Motions, Soil-Liquefaction and Engineering Practice in Eastern North America," October 20-22, 1987, edited by K.H. Jacob, 12/87, (PB88-188115, A23, MF-A01). This report is available only through NTIS (see address given above).

NCEER-87-0026 "Report on the Whittier-Narrows, California, Earthquake of October 1, 1987," by J. Pantelic and A. Reinhorn, 11/87, (PB88-187752, A03, MF-A01). This report is available only through NTIS (see address given above).

NCEER-87-0027 "Design of a Modular Program for Transient Nonlinear Analysis of Large 3-D Building Structures," by S. Srivastav and J.F. Abel, 12/30/87, (PB88-187950, A05, MF-A01). This report is only available through NTIS (see address given above).

NCEER-87-0028 "Second-Year Program in Research, Education and Technology Transfer," 3/8/88, (PB88-219480, A04, MF-A01).

NCEER-88-0001 "Workshop on Seismic Computer Analysis and Design of Buildings With Interactive Graphics," by W. McGuire, J.F. Abel and C.H. Conley, 1/18/88, (PB88-187760, A03, MF-A01). This report is only available through NTIS (see address given above).

NCEER-88-0002 "Optimal Control of Nonlinear Flexible Structures," by J.N. Yang, F.X. Long and D. Wong, 1/22/88, (PB88-213772, A06, MF-A01).

NCEER-88-0003 "Substructuring Techniques in the Time Domain for Primary-Secondary Structural Systems," by G.D. Manolis and G. Juhn, 2/10/88, (PB88-213780, A04, MF-A01).

NCEER-88-0004 "Iterative Seismic Analysis of Primary-Secondary Systems," by A. Singhal, L.D. Lutes and P.D. Spanos, 2/23/88, (PB88-213798, A04, MF-A01).

NCEER-88-0005 "Stochastic Finite Element Expansion for Random Media," by P.D. Spanos and R. Ghanem, 3/14/88, (PB88-213806, A03, MF-A01).

NCEER-88-0006 "Combining Structural Optimization and Structural Control," by F.Y. Cheng and C.P. Pantelides, 1/10/88, (PB88-213814, A05, MF-A01).

NCEER-88-0007 "Seismic Performance Assessment of Code-Designed Structures," by H.H-M. Hwang, J-W. Jaw and H-J. Shau, 3/20/88, (PB88-219423, A04, MF-A01). This report is only available through NTIS (see address given above).

NCEER-88-0008 "Reliability Analysis of Code-Designed Structures Under Natural Hazards," by H.H-M. Hwang, H. Ushiba and M. Shinozuka, 2/29/88, (PB88-229471, A07, MF-A01). This report is only available through NTIS (see address given above).

NCEER-88-0009 "Seismic Fragility Analysis of Shear Wall Structures," by J-W Jaw and H.H-M. Hwang, 4/30/88, (PB89-102867, A04, MF-A01).

NCEER-88-0010 "Base Isolation of a Multi-Story Building Under a Harmonic Ground Motion - A Comparison of Performances of Various Systems," by F-G Fan, G. Ahmadi and I.G. Tadjbakhsh, 5/18/88, (PB89-122238, A06, MF-A01). This report is only available through NTIS (see address given above).

NCEER-88-0011 "Seismic Floor Response Spectra for a Combined System by Green's Functions," by F.M. Lavelle, L.A. Bergman and P.D. Spanos, 5/1/88, (PB89-102875, A03, MF-A01).

NCEER-88-0012 "A New Solution Technique for Randomly Excited Hysteretic Structures," by G.Q. Cai and Y.K. Lin, 5/16/88, (PB89-102883, A03, MF-A01).

NCEER-88-0013 "A Study of Radiation Damping and Soil-Structure Interaction Effects in the Centrifuge," by K. Weissman, supervised by J.H. Prevost, 5/24/88, (PB89-144703, A06, MF-A01).

NCEER-88-0014 "Parameter Identification and Implementation of a Kinematic Plasticity Model for Frictional Soils," by J.H. Prevost and D.V. Griffiths, to be published.

NCEER-88-0015 "Two- and Three- Dimensional Dynamic Finite Element Analyses of the Long Valley Dam," by D.V. Griffiths and J.H. Prevost, 6/17/88, (PB89-144711, A04, MF-A01).

NCEER-88-0016 "Damage Assessment of Reinforced Concrete Structures in Eastern United States," by A.M. Reinhorn, M.J. Seidel, S.K. Kunnath and Y.J. Park, 6/15/88, (PB89-122220, A04, MF-A01). This report is only available through NTIS (see address given above).

NCEER-88-0017 "Dynamic Compliance of Vertically Loaded Strip Foundations in Multilayered Viscoelastic Soils," by S. Ahmad and A.S.M. Israil, 6/17/88, (PB89-102891, A04, MF-A01).

NCEER-88-0018 "An Experimental Study of Seismic Structural Response With Added Viscoelastic Dampers," by R.C. Lin, Z. Liang, T.T. Soong and R.H. Zhang, 6/30/88, (PB89-122212, A05, MF-A01). This report is available only through NTIS (see address given above).

NCEER-88-0019 "Experimental Investigation of Primary - Secondary System Interaction," by G.D. Manolis, G. Juhn and A.M. Reinhorn, 5/27/88, (PB89-122204, A04, MF-A01).

NCEER-88-0020 "A Response Spectrum Approach For Analysis of Nonclassically Damped Structures," by J.N. Yang, S. Sarkani and F.X. Long, 4/22/88, (PB89-102909, A04, MF-A01).

NCEER-88-0021 "Seismic Interaction of Structures and Soils: Stochastic Approach," by A.S. Veletsos and A.M. Prasad, 7/21/88, (PB89-122196, A04, MF-A01). This report is only available through NTIS (see address given above).

NCEER-88-0022 "Identification of the Serviceability Limit State and Detection of Seismic Structural Damage," by E. DiPasquale and A.S. Cakmak, 6/15/88, (PB89-122188, A05, MF-A01). This report is available only through NTIS (see address given above).

NCEER-88-0023 "Multi-Hazard Risk Analysis: Case of a Simple Offshore Structure," by B.K. Bhartia and E.H. Vanmarcke, 7/21/88, (PB89-145213, A05, MF-A01).

NCEER-88-0024 "Automated Seismic Design of Reinforced Concrete Buildings," by Y.S. Chung, C. Meyer and M. Shinozuka, 7/5/88, (PB89-122170, A06, MF-A01). This report is available only through NTIS (see address given above).

NCEER-88-0025 "Experimental Study of Active Control of MDOF Structures Under Seismic Excitations," by L.L. Chung, R.C. Lin, T.T. Soong and A.M. Reinhorn, 7/10/88, (PB89-122600, A04, MF-A01).

NCEER-88-0026 "Earthquake Simulation Tests of a Low-Rise Metal Structure," by J.S. Hwang, K.C. Chang, G.C. Lee and R.L. Ketter, 8/1/88, (PB89-102917, A04, MF-A01).

NCEER-88-0027 "Systems Study of Urban Response and Reconstruction Due to Catastrophic Earthquakes," by F. Kozin and H.K. Zhou, 9/22/88, (PB90-162348, A04, MF-A01).

NCEER-88-0028 "Seismic Fragility Analysis of Plane Frame Structures," by H.H-M. Hwang and Y.K. Low, 7/31/88, (PB89-131445, A06, MF-A01).

NCEER-88-0029 "Response Analysis of Stochastic Structures," by A. Kardara, C. Bucher and M. Shinozuka, 9/22/88, (PB89-174429, A04, MF-A01).

NCEER-88-0030 "Nonnormal Accelerations Due to Yielding in a Primary Structure," by D.C.K. Chen and L.D. Lutes, 9/19/88, (PB89-131437, A04, MF-A01).

NCEER-88-0031 "Design Approaches for Soil-Structure Interaction," by A.S. Veletsos, A.M. Prasad and Y. Tang, 12/30/88, (PB89-174437, A03, MF-A01). This report is available only through NTIS (see address given above).

NCEER-88-0032 "A Re-evaluation of Design Spectra for Seismic Damage Control," by C.J. Turkstra and A.G. Tallin, 11/7/88, (PB89-145221, A05, MF-A01).

NCEER-88-0033 "The Behavior and Design of Noncontact Lap Splices Subjected to Repeated Inelastic Tensile Loading," by V.E. Sagan, P. Gergely and R.N. White, 12/8/88, (PB89-163737, A08, MF-A01).

NCEER-88-0034 "Seismic Response of Pile Foundations," by S.M. Mamoon, P.K. Banerjee and S. Ahmad, 11/1/88, (PB89-145239, A04, MF-A01).

NCEER-88-0035 "Modeling of R/C Building Structures With Flexible Floor Diaphragms (IDARC2)," by A.M. Reinhorn, S.K. Kunnath and N. Panahshahi, 9/7/88, (PB89-207153, A07, MF-A01).

NCEER-88-0036 "Solution of the Dam-Reservoir Interaction Problem Using a Combination of FEM, BEM with Particular Integrals, Modal Analysis, and Substructuring," by C-S. Tsai, G.C. Lee and R.L. Ketter, 12/31/88, (PB89-207146, A04, MF-A01).

NCEER-88-0037 "Optimal Placement of Actuators for Structural Control," by F.Y. Cheng and C.P. Pantelides, 8/15/88, (PB89-162846, A05, MF-A01).

NCEER-88-0038 "Teflon Bearings in Aseismic Base Isolation: Experimental Studies and Mathematical Modeling," by A. Mokha, M.C. Constantinou and A.M. Reinhorn, 12/5/88, (PB89-218457, A10, MF-A01). This report is available only through NTIS (see address given above).

NCEER-88-0039 "Seismic Behavior of Flat Slab High-Rise Buildings in the New York City Area," by P. Weidlinger and M. Ettouney, 10/15/88, (PB90-145681, A04, MF-A01).

NCEER-88-0040 "Evaluation of the Earthquake Resistance of Existing Buildings in New York City," by P. Weidlinger and M. Ettouney, 10/15/88, to be published.

NCEER-88-0041 "Small-Scale Modeling Techniques for Reinforced Concrete Structures Subjected to Seismic Loads," by W. Kim, A. El-Attar and R.N. White, 11/22/88, (PB89-189625, A05, MF-A01).

NCEER-88-0042 "Modeling Strong Ground Motion from Multiple Event Earthquakes," by G.W. Ellis and A.S. Cakmak, 10/15/88, (PB89-174445, A03, MF-A01).

NCEER-88-0043 "Nonstationary Models of Seismic Ground Acceleration," by M. Grigoriu, S.E. Ruiz and E. Rosenblueth, 7/15/88, (PB89-189617, A04, MF-A01).

NCEER-88-0044 "SARCF User's Guide: Seismic Analysis of Reinforced Concrete Frames," by Y.S. Chung, C. Meyer and M. Shinozuka, 11/9/88, (PB89-174452, A08, MF-A01).

NCEER-88-0045 "First Expert Panel Meeting on Disaster Research and Planning," edited by J. Pantelic and J. Stoyle, 9/15/88, (PB89-174460, A05, MF-A01).

NCEER-88-0046 "Preliminary Studies of the Effect of Degrading Infill Walls on the Nonlinear Seismic Response of Steel Frames," by C.Z. Chrysostomou, P. Gergely and J.F. Abel, 12/19/88, (PB89-208383, A05, MF-A01).

NCEER-88-0047 "Reinforced Concrete Frame Component Testing Facility - Design, Construction, Instrumentation and Operation," by S.P. Pessiki, C. Conley, T. Bond, P. Gergely and R.N. White, 12/16/88, (PB89-174478, A04, MF-A01).

NCEER-89-0001 "Effects of Protective Cushion and Soil Compliancy on the Response of Equipment Within a Seismically Excited Building," by J.A. HoLung, 2/16/89, (PB89-207179, A04, MF-A01).

NCEER-89-0002 "Statistical Evaluation of Response Modification Factors for Reinforced Concrete Structures," by H.H-M. Hwang and J-W. Jaw, 2/17/89, (PB89-207187, A05, MF-A01).

NCEER-89-0003 "Hysteretic Columns Under Random Excitation," by G-Q. Cai and Y.K. Lin, 1/9/89, (PB89-196513, A03, MF-A01).

NCEER-89-0004 "Experimental Study of `Elephant Foot Bulge' Instability of Thin-Walled Metal Tanks," by Z-H. Jia and R.L. Ketter, 2/22/89, (PB89-207195, A03, MF-A01).

NCEER-89-0005 "Experiment on Performance of Buried Pipelines Across San Andreas Fault," by J. Isenberg, E. Richardson and T.D. O'Rourke, 3/10/89, (PB89-218440, A04, MF-A01). This report is available only through NTIS (see address given above).

NCEER-89-0006 "A Knowledge-Based Approach to Structural Design of Earthquake-Resistant Buildings," by M. Subramani, P. Gergely, C.H. Conley, J.F. Abel and A.H. Zaghw, 1/15/89, (PB89-218465, A06, MF-A01).

NCEER-89-0007 "Liquefaction Hazards and Their Effects on Buried Pipelines," by T.D. O'Rourke and P.A. Lane, 2/1/89, (PB89-218481, A09, MF-A01).

NCEER-89-0008 "Fundamentals of System Identification in Structural Dynamics," by H. Imai, C-B. Yun, O. Maruyama and M. Shinozuka, 1/26/89, (PB89-207211, A04, MF-A01).

NCEER-89-0009 "Effects of the 1985 Michoacan Earthquake on Water Systems and Other Buried Lifelines in Mexico," by A.G. Ayala and M.J. O'Rourke, 3/8/89, (PB89-207229, A06, MF-A01).

NCEER-89-R010 "NCEER Bibliography of Earthquake Education Materials," by K.E.K. Ross, Second Revision, 9/1/89, (PB90-125352, A05, MF-A01). This report is replaced by NCEER-92-0018.

NCEER-89-0011 "Inelastic Three-Dimensional Response Analysis of Reinforced Concrete Building Structures (IDARC-3D), Part I - Modeling," by S.K. Kunnath and A.M. Reinhorn, 4/17/89, (PB90-114612, A07, MF-A01). This report is available only through NTIS (see address given above).

NCEER-89-0012 "Recommended Modifications to ATC-14," by C.D. Poland and J.O. Malley, 4/12/89, (PB90-108648, A15, MF-A01).

NCEER-89-0013 "Repair and Strengthening of Beam-to-Column Connections Subjected to Earthquake Loading," by M. Corazao and A.J. Durrani, 2/28/89, (PB90-109885, A06, MF-A01).

NCEER-89-0014 "Program EXKAL2 for Identification of Structural Dynamic Systems," by O. Maruyama, C-B. Yun, M. Hoshiya and M. Shinozuka, 5/19/89, (PB90-109877, A09, MF-A01).

NCEER-89-0015 "Response of Frames With Bolted Semi-Rigid Connections, Part I - Experimental Study and Analytical Predictions," by P.J. DiCorso, A.M. Reinhorn, J.R. Dickerson, J.B. Radziminski and W.L. Harper, 6/1/89, to be published.

NCEER-89-0016 "ARMA Monte Carlo Simulation in Probabilistic Structural Analysis," by P.D. Spanos and M.P. Mignolet, 7/10/89, (PB90-109893, A03, MF-A01).

NCEER-89-P017 "Preliminary Proceedings from the Conference on Disaster Preparedness - The Place of Earthquake Education in Our Schools," Edited by K.E.K. Ross, 6/23/89, (PB90-108606, A03, MF-A01).

NCEER-89-0017 "Proceedings from the Conference on Disaster Preparedness - The Place of Earthquake Education in Our Schools," Edited by K.E.K. Ross, 12/31/89, (PB90-207895, A012, MF-A02). This report is available only through NTIS (see address given above).

NCEER-89-0018 "Multidimensional Models of Hysteretic Material Behavior for Vibration Analysis of Shape Memory Energy Absorbing Devices, by E.J. Graesser and F.A. Cozzarelli, 6/7/89, (PB90-164146, A04, MF-A01).

NCEER-89-0019 "Nonlinear Dynamic Analysis of Three-Dimensional Base Isolated Structures (3D-BASIS)," by S. Nagarajaiah, A.M. Reinhorn and M.C. Constantinou, 8/3/89, (PB90-161936, A06, MF-A01). This report has been replaced by NCEER-93-0011.

NCEER-89-0020 "Structural Control Considering Time-Rate of Control Forces and Control Rate Constraints," by F.Y. Cheng and C.P. Pantelides, 8/3/89, (PB90-120445, A04, MF-A01).

NCEER-89-0021 "Subsurface Conditions of Memphis and Shelby County," by K.W. Ng, T-S. Chang and H-H.M. Hwang, 7/26/89, (PB90-120437, A03, MF-A01).

NCEER-89-0022 "Seismic Wave Propagation Effects on Straight Jointed Buried Pipelines," by K. Elhmadi and M.J. O'Rourke, 8/24/89, (PB90-162322, A10, MF-A02).

NCEER-89-0023 "Workshop on Serviceability Analysis of Water Delivery Systems," edited by M. Grigoriu, 3/6/89, (PB90-127424, A03, MF-A01).

NCEER-89-0024 "Shaking Table Study of a 1/5 Scale Steel Frame Composed of Tapered Members," by K.C. Chang, J.S. Hwang and G.C. Lee, 9/18/89, (PB90-160169, A04, MF-A01).

NCEER-89-0025 "DYNA1D: A Computer Program for Nonlinear Seismic Site Response Analysis - Technical Documentation," by Jean H. Prevost, 9/14/89, (PB90-161944, A07, MF-A01). This report is available only through NTIS (see address given above).

NCEER-89-0026 "1:4 Scale Model Studies of Active Tendon Systems and Active Mass Dampers for Aseismic Protection," by A.M. Reinhorn, T.T. Soong, R.C. Lin, Y.P. Yang, Y. Fukao, H. Abe and M. Nakai, 9/15/89, (PB90-173246, A10, MF-A02). This report is available only through NTIS (see address given above).

NCEER-89-0027 "Scattering of Waves by Inclusions in a Nonhomogeneous Elastic Half Space Solved by Boundary Element Methods," by P.K. Hadley, A. Askar and A.S. Cakmak, 6/15/89, (PB90-145699, A07, MF-A01).

NCEER-89-0028 "Statistical Evaluation of Deflection Amplification Factors for Reinforced Concrete Structures," by H.H.M. Hwang, J-W. Jaw and A.L. Ch'ng, 8/31/89, (PB90-164633, A05, MF-A01).

NCEER-89-0029 "Bedrock Accelerations in Memphis Area Due to Large New Madrid Earthquakes," by H.H.M. Hwang, C.H.S. Chen and G. Yu, 11/7/89, (PB90-162330, A04, MF-A01).

NCEER-89-0030 "Seismic Behavior and Response Sensitivity of Secondary Structural Systems," by Y.Q. Chen and T.T. Soong, 10/23/89, (PB90-164658, A08, MF-A01).

NCEER-89-0031 "Random Vibration and Reliability Analysis of Primary-Secondary Structural Systems," by Y. Ibrahim, M. Grigoriu and T.T. Soong, 11/10/89, (PB90-161951, A04, MF-A01).

NCEER-89-0032 "Proceedings from the Second U.S. - Japan Workshop on Liquefaction, Large Ground Deformation and Their Effects on Lifelines, September 26-29, 1989," Edited by T.D. O'Rourke and M. Hamada, 12/1/89, (PB90-209388, A22, MF-A03).

NCEER-89-0033 "Deterministic Model for Seismic Damage Evaluation of Reinforced Concrete Structures," by J.M. Bracci, A.M. Reinhorn, J.B. Mander and S.K. Kunnath, 9/27/89, (PB91-108803, A06, MF-A01).

NCEER-89-0034 "On the Relation Between Local and Global Damage Indices," by E. DiPasquale and A.S. Cakmak, 8/15/89, (PB90-173865, A05, MF-A01).

NCEER-89-0035 "Cyclic Undrained Behavior of Nonplastic and Low Plasticity Silts," by A.J. Walker and H.E. Stewart, 7/26/89, (PB90-183518, A10, MF-A01).

NCEER-89-0036 "Liquefaction Potential of Surficial Deposits in the City of Buffalo, New York," by M. Budhu, R. Giese and L. Baumgrass, 1/17/89, (PB90-208455, A04, MF-A01).

NCEER-89-0037 "A Deterministic Assessment of Effects of Ground Motion Incoherence," by A.S. Veletsos and Y. Tang, 7/15/89, (PB90-164294, A03, MF-A01).

NCEER-89-0038 "Workshop on Ground Motion Parameters for Seismic Hazard Mapping," July 17-18, 1989, edited by R.V. Whitman, 12/1/89, (PB90-173923, A04, MF-A01).

NCEER-89-0039 "Seismic Effects on Elevated Transit Lines of the New York City Transit Authority," by C.J. Costantino, C.A. Miller and E. Heymsfield, 12/26/89, (PB90-207887, A06, MF-A01).

NCEER-89-0040 "Centrifugal Modeling of Dynamic Soil-Structure Interaction," by K. Weissman, Supervised by J.H. Prevost, 5/10/89, (PB90-207879, A07, MF-A01).

NCEER-89-0041 "Linearized Identification of Buildings With Cores for Seismic Vulnerability Assessment," by I-K. Ho and A.E. Aktan, 11/1/89, (PB90-251943, A07, MF-A01).

NCEER-90-0001 "Geotechnical and Lifeline Aspects of the October 17, 1989 Loma Prieta Earthquake in San Francisco," by T.D. O'Rourke, H.E. Stewart, F.T. Blackburn and T.S. Dickerman, 1/90, (PB90-208596, A05, MF-A01).

NCEER-90-0002 "Nonnormal Secondary Response Due to Yielding in a Primary Structure," by D.C.K. Chen and L.D. Lutes, 2/28/90, (PB90-251976, A07, MF-A01).

NCEER-90-0003 "Earthquake Education Materials for Grades K-12," by K.E.K. Ross, 4/16/90, (PB91-251984, A05, MF-A05). This report has been replaced by NCEER-92-0018.

NCEER-90-0004 "Catalog of Strong Motion Stations in Eastern North America," by R.W. Busby, 4/3/90, (PB90-251984, A05, MF-A01).

NCEER-90-0005 "NCEER Strong-Motion Data Base: A User Manual for the GeoBase Release (Version 1.0 for the Sun3)," by P. Friberg and K. Jacob, 3/31/90 (PB90-258062, A04, MF-A01).

NCEER-90-0006 "Seismic Hazard Along a Crude Oil Pipeline in the Event of an 1811-1812 Type New Madrid Earthquake," by H.H.M. Hwang and C-H.S. Chen, 4/16/90, (PB90-258054, A04, MF-A01).

NCEER-90-0007 "Site-Specific Response Spectra for Memphis Sheahan Pumping Station," by H.H.M. Hwang and C.S. Lee, 5/15/90, (PB91-108811, A05, MF-A01).

NCEER-90-0008 "Pilot Study on Seismic Vulnerability of Crude Oil Transmission Systems," by T. Ariman, R. Dobry, M. Grigoriu, F. Kozin, M. O'Rourke, T. O'Rourke and M. Shinozuka, 5/25/90, (PB91-108837, A06, MF-A01).

NCEER-90-0009 "A Program to Generate Site Dependent Time Histories: EQGEN," by G.W. Ellis, M. Srinivasan and A.S. Cakmak, 1/30/90, (PB91-108829, A04, MF-A01).

NCEER-90-0010 "Active Isolation for Seismic Protection of Operating Rooms," by M.E. Talbott, Supervised by M. Shinozuka, 6/8/9, (PB91-110205, A05, MF-A01).

NCEER-90-0011 "Program LINEARID for Identification of Linear Structural Dynamic Systems," by C-B. Yun and M. Shinozuka, 6/25/90, (PB91-110312, A08, MF-A01).

NCEER-90-0012 "Two-Dimensional Two-Phase Elasto-Plastic Seismic Response of Earth Dams," by A.N. Yiagos, Supervised by J.H. Prevost, 6/20/90, (PB91-110197, A13, MF-A02).

NCEER-90-0013 "Secondary Systems in Base-Isolated Structures: Experimental Investigation, Stochastic Response and Stochastic Sensitivity," by G.D. Manolis, G. Juhn, M.C. Constantinou and A.M. Reinhorn, 7/1/90, (PB91-110320, A08, MF-A01).

NCEER-90-0014 "Seismic Behavior of Lightly-Reinforced Concrete Column and Beam-Column Joint Details," by S.P. Pessiki, C.H. Conley, P. Gergely and R.N. White, 8/22/90, (PB91-108795, A11, MF-A02).

NCEER-90-0015 "Two Hybrid Control Systems for Building Structures Under Strong Earthquakes," by J.N. Yang and A. Danielians, 6/29/90, (PB91-125393, A04, MF-A01).

NCEER-90-0016 "Instantaneous Optimal Control with Acceleration and Velocity Feedback," by J.N. Yang and Z. Li, 6/29/90, (PB91-125401, A03, MF-A01).

NCEER-90-0017 "Reconnaissance Report on the Northern Iran Earthquake of June 21, 1990," by M. Mehrain, 10/4/90, (PB91-125377, A03, MF-A01).

NCEER-90-0018 "Evaluation of Liquefaction Potential in Memphis and Shelby County," by T.S. Chang, P.S. Tang, C.S. Lee and H. Hwang, 8/10/90, (PB91-125427, A09, MF-A01).

NCEER-90-0019 "Experimental and Analytical Study of a Combined Sliding Disc Bearing and Helical Steel Spring Isolation System," by M.C. Constantinou, A.S. Mokha and A.M. Reinhorn, 10/4/90, (PB91-125385, A06, MF-A01). This report is available only through NTIS (see address given above).

NCEER-90-0020 "Experimental Study and Analytical Prediction of Earthquake Response of a Sliding Isolation System with a Spherical Surface," by A.S. Mokha, M.C. Constantinou and A.M. Reinhorn, 10/11/90, (PB91-125419, A05, MF-A01).

NCEER-90-0021 "Dynamic Interaction Factors for Floating Pile Groups," by G. Gazetas, K. Fan, A. Kaynia and E. Kausel, 9/10/90, (PB91-170381, A05, MF-A01).

NCEER-90-0022 "Evaluation of Seismic Damage Indices for Reinforced Concrete Structures," by S. Rodriguez-Gomez and A.S. Cakmak, 9/30/90, PB91-171322, A06, MF-A01).

NCEER-90-0023 "Study of Site Response at a Selected Memphis Site," by H. Desai, S. Ahmad, E.S. Gazetas and M.R. Oh, 10/11/90, (PB91-196857, A03, MF-A01).

NCEER-90-0024 "A User's Guide to Strongmo: Version 1.0 of NCEER's Strong-Motion Data Access Tool for PCs and Terminals," by P.A. Friberg and C.A.T. Susch, 11/15/90, (PB91-171272, A03, MF-A01).

NCEER-90-0025 "A Three-Dimensional Analytical Study of Spatial Variability of Seismic Ground Motions," by L-L. Hong and A.H.-S. Ang, 10/30/90, (PB91-170399, A09, MF-A01).

NCEER-90-0026 "MUMOID User's Guide - A Program for the Identification of Modal Parameters," by S. Rodriguez-Gomez and E. DiPasquale, 9/30/90, (PB91-171298, A04, MF-A01).

NCEER-90-0027 "SARCF-II User's Guide - Seismic Analysis of Reinforced Concrete Frames," by S. Rodriguez-Gomez, Y.S. Chung and C. Meyer, 9/30/90, (PB91-171280, A05, MF-A01).

NCEER-90-0028 "Viscous Dampers: Testing, Modeling and Application in Vibration and Seismic Isolation," by N. Makris and M.C. Constantinou, 12/20/90 (PB91-190561, A06, MF-A01).

NCEER-90-0029 "Soil Effects on Earthquake Ground Motions in the Memphis Area," by H. Hwang, C.S. Lee, K.W. Ng and T.S. Chang, 8/2/90, (PB91-190751, A05, MF-A01).

NCEER-91-0001 "Proceedings from the Third Japan-U.S. Workshop on Earthquake Resistant Design of Lifeline Facilities and Countermeasures for Soil Liquefaction, December 17-19, 1990," edited by T.D. O'Rourke and M. Hamada, 2/1/91, (PB91-179259, A99, MF-A04).

NCEER-91-0002 "Physical Space Solutions of Non-Proportionally Damped Systems," by M. Tong, Z. Liang and G.C. Lee, 1/15/91, (PB91-179242, A04, MF-A01).

NCEER-91-0003 "Seismic Response of Single Piles and Pile Groups," by K. Fan and G. Gazetas, 1/10/91, (PB92-174994, A04, MF-A01).

NCEER-91-0004 "Damping of Structures: Part 1 - Theory of Complex Damping," by Z. Liang and G. Lee, 10/10/91, (PB92-197235, A12, MF-A03).

NCEER-91-0005 "3D-BASIS - Nonlinear Dynamic Analysis of Three Dimensional Base Isolated Structures: Part II," by S. Nagarajaiah, A.M. Reinhorn and M.C. Constantinou, 2/28/91, (PB91-190553, A07, MF-A01). This report has been replaced by NCEER-93-0011.

NCEER-91-0006 "A Multidimensional Hysteretic Model for Plasticity Deforming Metals in Energy Absorbing Devices," by E.J. Graesser and F.A. Cozzarelli, 4/9/91, (PB92-108364, A04, MF-A01).

NCEER-91-0007 "A Framework for Customizable Knowledge-Based Expert Systems with an Application to a KBES for Evaluating the Seismic Resistance of Existing Buildings," by E.G. Ibarra-Anaya and S.J. Fenves, 4/9/91, (PB91-210930, A08, MF-A01).

NCEER-91-0008 "Nonlinear Analysis of Steel Frames with Semi-Rigid Connections Using the Capacity Spectrum Method," by G.G. Deierlein, S-H. Hsieh, Y-J. Shen and J.F. Abel, 7/2/91, (PB92-113828, A05, MF-A01).

NCEER-91-0009 "Earthquake Education Materials for Grades K-12," by K.E.K. Ross, 4/30/91, (PB91-212142, A06, MF-A01). This report has been replaced by NCEER-92-0018.

NCEER-91-0010 "Phase Wave Velocities and Displacement Phase Differences in a Harmonically Oscillating Pile," by N. Makris and G. Gazetas, 7/8/91, (PB92-108356, A04, MF-A01).

NCEER-91-0011 "Dynamic Characteristics of a Full-Size Five-Story Steel Structure and a 2/5 Scale Model," by K.C. Chang, G.C. Yao, G.C. Lee, D.S. Hao and Y.C. Yeh," 7/2/91, (PB93-116648, A06, MF-A02).

NCEER-91-0012 "Seismic Response of a 2/5 Scale Steel Structure with Added Viscoelastic Dampers," by K.C. Chang, T.T. Soong, S-T. Oh and M.L. Lai, 5/17/91, (PB92-110816, A05, MF-A01).

NCEER-91-0013 "Earthquake Response of Retaining Walls; Full-Scale Testing and Computational Modeling," by S. Alampalli and A-W.M. Elgamal, 6/20/91, to be published.

NCEER-91-0014 "3D-BASIS-M: Nonlinear Dynamic Analysis of Multiple Building Base Isolated Structures," by P.C. Tsopelas, S. Nagarajaiah, M.C. Constantinou and A.M. Reinhorn, 5/28/91, (PB92-113885, A09, MF-A02).

NCEER-91-0015 "Evaluation of SEAOC Design Requirements for Sliding Isolated Structures," by D. Theodossiou and M.C. Constantinou, 6/10/91, (PB92-114602, A11, MF-A03).

NCEER-91-0016 "Closed-Loop Modal Testing of a 27-Story Reinforced Concrete Flat Plate-Core Building," by H.R. Somaprasad, T. Toksoy, H. Yoshiyuki and A.E. Aktan, 7/15/91, (PB92-129980, A07, MF-A02).

NCEER-91-0017 "Shake Table Test of a 1/6 Scale Two-Story Lightly Reinforced Concrete Building," by A.G. El-Attar, R.N. White and P. Gergely, 2/28/91, (PB92-222447, A06, MF-A02).

NCEER-91-0018 "Shake Table Test of a 1/8 Scale Three-Story Lightly Reinforced Concrete Building," by A.G. El-Attar, R.N. White and P. Gergely, 2/28/91, (PB93-116630, A08, MF-A02).

NCEER-91-0019 "Transfer Functions for Rigid Rectangular Foundations," by A.S. Veletsos, A.M. Prasad and W.H. Wu, 7/31/91, to be published.

NCEER-91-0020 "Hybrid Control of Seismic-Excited Nonlinear and Inelastic Structural Systems," by J.N. Yang, Z. Li and A. Danielians, 8/1/91, (PB92-143171, A06, MF-A02).

NCEER-91-0021 "The NCEER-91 Earthquake Catalog: Improved Intensity-Based Magnitudes and Recurrence Relations for U.S. Earthquakes East of New Madrid," by L. Seeber and J.G. Armbruster, 8/28/91, (PB92-176742, A06, MF-A02).

NCEER-91-0022 "Proceedings from the Implementation of Earthquake Planning and Education in Schools: The Need for Change - The Roles of the Changemakers," by K.E.K. Ross and F. Winslow, 7/23/91, (PB92-129998, A12, MF-A03).

NCEER-91-0023 "A Study of Reliability-Based Criteria for Seismic Design of Reinforced Concrete Frame Buildings," by H.H.M. Hwang and H-M. Hsu, 8/10/91, (PB92-140235, A09, MF-A02).

NCEER-91-0024 "Experimental Verification of a Number of Structural System Identification Algorithms," by R.G. Ghanem, H. Gavin and M. Shinozuka, 9/18/91, (PB92-176577, A18, MF-A04).

NCEER-91-0025 "Probabilistic Evaluation of Liquefaction Potential," by H.H.M. Hwang and C.S. Lee," 11/25/91, (PB92-143429, A05, MF-A01).

NCEER-91-0026 "Instantaneous Optimal Control for Linear, Nonlinear and Hysteretic Structures - Stable Controllers," by J.N. Yang and Z. Li, 11/15/91, (PB92-163807, A04, MF-A01).

NCEER-91-0027 "Experimental and Theoretical Study of a Sliding Isolation System for Bridges," by M.C. Constantinou, A. Kartoum, A.M. Reinhorn and P. Bradford, 11/15/91, (PB92-176973, A10, MF-A03).

NCEER-92-0001 "Case Studies of Liquefaction and Lifeline Performance During Past Earthquakes, Volume 1: Japanese Case Studies," Edited by M. Hamada and T. O'Rourke, 2/17/92, (PB92-197243, A18, MF-A04).

NCEER-92-0002 "Case Studies of Liquefaction and Lifeline Performance During Past Earthquakes, Volume 2: United States Case Studies," Edited by T. O'Rourke and M. Hamada, 2/17/92, (PB92-197250, A20, MF-A04).

NCEER-92-0003 "Issues in Earthquake Education," Edited by K. Ross, 2/3/92, (PB92-222389, A07, MF-A02).

NCEER-92-0004 "Proceedings from the First U.S. - Japan Workshop on Earthquake Protective Systems for Bridges," Edited by I.G. Buckle, 2/4/92, (PB94-142239, A99, MF-A06).

NCEER-92-0005 "Seismic Ground Motion from a Haskell-Type Source in a Multiple-Layered Half-Space," A.P. Theoharis, G. Deodatis and M. Shinozuka, 1/2/92, to be published.

NCEER-92-0006 "Proceedings from the Site Effects Workshop," Edited by R. Whitman, 2/29/92, (PB92-197201, A04, MF-A01).

NCEER-92-0007 "Engineering Evaluation of Permanent Ground Deformations Due to Seismically-Induced Liquefaction," by M.H. Baziar, R. Dobry and A-W.M. Elgamal, 3/24/92, (PB92-222421, A13, MF-A03).

NCEER-92-0008 "A Procedure for the Seismic Evaluation of Buildings in the Central and Eastern United States," by C.D. Poland and J.O. Malley, 4/2/92, (PB92-222439, A20, MF-A04).

NCEER-92-0009 "Experimental and Analytical Study of a Hybrid Isolation System Using Friction Controllable Sliding Bearings," by M.Q. Feng, S. Fujii and M. Shinozuka, 5/15/92, (PB93-150282, A06, MF-A02).

NCEER-92-0010 "Seismic Resistance of Slab-Column Connections in Existing Non-Ductile Flat-Plate Buildings," by A.J. Durrani and Y. Du, 5/18/92, (PB93-116812, A06, MF-A02).

NCEER-92-0011 "The Hysteretic and Dynamic Behavior of Brick Masonry Walls Upgraded by Ferrocement Coatings Under Cyclic Loading and Strong Simulated Ground Motion," by H. Lee and S.P. Prawel, 5/11/92, to be published.

NCEER-92-0012 "Study of Wire Rope Systems for Seismic Protection of Equipment in Buildings," by G.F. Demetriades, M.C. Constantinou and A.M. Reinhorn, 5/20/92, (PB93-116655, A08, MF-A02).

NCEER-92-0013 "Shape Memory Structural Dampers: Material Properties, Design and Seismic Testing," by P.R. Witting and F.A. Cozzarelli, 5/26/92, (PB93-116663, A05, MF-A01).

NCEER-92-0014 "Longitudinal Permanent Ground Deformation Effects on Buried Continuous Pipelines," by M.J. O'Rourke, and C. Nordberg, 6/15/92, (PB93-116671, A08, MF-A02).

NCEER-92-0015 "A Simulation Method for Stationary Gaussian Random Functions Based on the Sampling Theorem," by M. Grigoriu and S. Balopoulou, 6/11/92, (PB93-127496, A05, MF-A01).

NCEER-92-0016 "Gravity-Load-Designed Reinforced Concrete Buildings: Seismic Evaluation of Existing Construction and Detailing Strategies for Improved Seismic Resistance," by G.W. Hoffmann, S.K. Kunnath, A.M. Reinhorn and J.B. Mander, 7/15/92, (PB94-142007, A08, MF-A02).

NCEER-92-0017 "Observations on Water System and Pipeline Performance in the Limón Area of Costa Rica Due to the April 22, 1991 Earthquake," by M. O'Rourke and D. Ballantyne, 6/30/92, (PB93-126811, A06, MF-A02).

NCEER-92-0018 "Fourth Edition of Earthquake Education Materials for Grades K-12," Edited by K.E.K. Ross, 8/10/92, (PB93-114023, A07, MF-A02).

NCEER-92-0019 "Proceedings from the Fourth Japan-U.S. Workshop on Earthquake Resistant Design of Lifeline Facilities and Countermeasures for Soil Liquefaction," Edited by M. Hamada and T.D. O'Rourke, 8/12/92, (PB93-163939, A99, MF-E11).

NCEER-92-0020 "Active Bracing System: A Full Scale Implementation of Active Control," by A.M. Reinhorn, T.T. Soong, R.C. Lin, M.A. Riley, Y.P. Wang, S. Aizawa and M. Higashino, 8/14/92, (PB93-127512, A06, MF-A02).

NCEER-92-0021 "Empirical Analysis of Horizontal Ground Displacement Generated by Liquefaction-Induced Lateral Spreads," by S.F. Bartlett and T.L. Youd, 8/17/92, (PB93-188241, A06, MF-A02).

NCEER-92-0022 "IDARC Version 3.0: Inelastic Damage Analysis of Reinforced Concrete Structures," by S.K. Kunnath, A.M. Reinhorn and R.F. Lobo, 8/31/92, (PB93-227502, A07, MF-A02).

NCEER-92-0023 "A Semi-Empirical Analysis of Strong-Motion Peaks in Terms of Seismic Source, Propagation Path and Local Site Conditions, by M. Kamiyama, M.J. O'Rourke and R. Flores-Berrones, 9/9/92, (PB93-150266, A08, MF-A02).

NCEER-92-0024 "Seismic Behavior of Reinforced Concrete Frame Structures with Nonductile Details, Part I: Summary of Experimental Findings of Full Scale Beam-Column Joint Tests," by A. Beres, R.N. White and P. Gergely, 9/30/92, (PB93-227783, A05, MF-A01).

NCEER-92-0025 "Experimental Results of Repaired and Retrofitted Beam-Column Joint Tests in Lightly Reinforced Concrete Frame Buildings," by A. Beres, S. El-Borgi, R.N. White and P. Gergely, 10/29/92, (PB93-227791, A05, MF-A01).

NCEER-92-0026 "A Generalization of Optimal Control Theory: Linear and Nonlinear Structures," by J.N. Yang, Z. Li and S. Vongchavalitkul, 11/2/92, (PB93-188621, A05, MF-A01).

NCEER-92-0027 "Seismic Resistance of Reinforced Concrete Frame Structures Designed Only for Gravity Loads: Part I - Design and Properties of a One-Third Scale Model Structure," by J.M. Bracci, A.M. Reinhorn and J.B. Mander, 12/1/92, (PB94-104502, A08, MF-A02).

NCEER-92-0028 "Seismic Resistance of Reinforced Concrete Frame Structures Designed Only for Gravity Loads: Part II - Experimental Performance of Subassemblages," by L.E. Aycardi, J.B. Mander and A.M. Reinhorn, 12/1/92, (PB94-104510, A08, MF-A02).

NCEER-92-0029 "Seismic Resistance of Reinforced Concrete Frame Structures Designed Only for Gravity Loads: Part III - Experimental Performance and Analytical Study of a Structural Model," by J.M. Bracci, A.M. Reinhorn and J.B. Mander, 12/1/92, (PB93-227528, A09, MF-A01).

NCEER-92-0030 "Evaluation of Seismic Retrofit of Reinforced Concrete Frame Structures: Part I - Experimental Performance of Retrofitted Subassemblages," by D. Choudhuri, J.B. Mander and A.M. Reinhorn, 12/8/92, (PB93-198307, A07, MF-A02).

NCEER-92-0031 "Evaluation of Seismic Retrofit of Reinforced Concrete Frame Structures: Part II - Experimental Performance and Analytical Study of a Retrofitted Structural Model," by J.M. Bracci, A.M. Reinhorn and J.B. Mander, 12/8/92, (PB93-198315, A09, MF-A03).

NCEER-92-0032 "Experimental and Analytical Investigation of Seismic Response of Structures with Supplemental Fluid Viscous Dampers," by M.C. Constantinou and M.D. Symans, 12/21/92, (PB93-191435, A10, MF-A03). This report is available only through NTIS (see address given above).

NCEER-92-0033 "Reconnaissance Report on the Cairo, Egypt Earthquake of October 12, 1992," by M. Khater, 12/23/92, (PB93-188621, A03, MF-A01).

NCEER-92-0034 "Low-Level Dynamic Characteristics of Four Tall Flat-Plate Buildings in New York City," by H. Gavin, S. Yuan, J. Grossman, E. Pekelis and K. Jacob, 12/28/92, (PB93-188217, A07, MF-A02).

NCEER-93-0001 "An Experimental Study on the Seismic Performance of Brick-Infilled Steel Frames With and Without Retrofit," by J.B. Mander, B. Nair, K. Wojtkowski and J. Ma, 1/29/93, (PB93-227510, A07, MF-A02).

NCEER-93-0002 "Social Accounting for Disaster Preparedness and Recovery Planning," by S. Cole, E. Pantoja and V. Razak, 2/22/93, (PB94-142114, A12, MF-A03).

NCEER-93-0003 "Assessment of 1991 NEHRP Provisions for Nonstructural Components and Recommended Revisions," by T.T. Soong, G. Chen, Z. Wu, R-H. Zhang and M. Grigoriu, 3/1/93, (PB93-188639, A06, MF-A02).

NCEER-93-0004 "Evaluation of Static and Response Spectrum Analysis Procedures of SEAOC/UBC for Seismic Isolated Structures," by C.W. Winters and M.C. Constantinou, 3/23/93, (PB93-198299, A10, MF-A03).

NCEER-93-0005 "Earthquakes in the Northeast - Are We Ignoring the Hazard? A Workshop on Earthquake Science and Safety for Educators," edited by K.E.K. Ross, 4/2/93, (PB94-103066, A09, MF-A02).

NCEER-93-0006 "Inelastic Response of Reinforced Concrete Structures with Viscoelastic Braces," by R.F. Lobo, J.M. Bracci, K.L. Shen, A.M. Reinhorn and T.T. Soong, 4/5/93, (PB93-227486, A05, MF-A02).

NCEER-93-0007 "Seismic Testing of Installation Methods for Computers and Data Processing Equipment," by K. Kosar, T.T. Soong, K.L. Shen, J.A. HoLung and Y.K. Lin, 4/12/93, (PB93-198299, A07, MF-A02).

NCEER-93-0008 "Retrofit of Reinforced Concrete Frames Using Added Dampers," by A. Reinhorn, M. Constantinou and C. Li, to be published.

NCEER-93-0009 "Seismic Behavior and Design Guidelines for Steel Frame Structures with Added Viscoelastic Dampers," by K.C. Chang, M.L. Lai, T.T. Soong, D.S. Hao and Y.C. Yeh, 5/1/93, (PB94-141959, A07, MF-A02).

NCEER-93-0010 "Seismic Performance of Shear-Critical Reinforced Concrete Bridge Piers," by J.B. Mander, S.M. Waheed, M.T.A. Chaudhary and S.S. Chen, 5/12/93, (PB93-227494, A08, MF-A02).

NCEER-93-0011 "3D-BASIS-TABS: Computer Program for Nonlinear Dynamic Analysis of Three Dimensional Base Isolated Structures," by S. Nagarajaiah, C. Li, A.M. Reinhorn and M.C. Constantinou, 8/2/93, (PB94-141819, A09, MF-A02).

NCEER-93-0012 "Effects of Hydrocarbon Spills from an Oil Pipeline Break on Ground Water," by O.J. Helweg and H.H.M. Hwang, 8/3/93, (PB94-141942, A06, MF-A02).

NCEER-93-0013 "Simplified Procedures for Seismic Design of Nonstructural Components and Assessment of Current Code Provisions," by M.P. Singh, L.E. Suarez, E.E. Matheu and G.O. Maldonado, 8/4/93, (PB94-141827, A09, MF-A02).

NCEER-93-0014 "An Energy Approach to Seismic Analysis and Design of Secondary Systems," by G. Chen and T.T. Soong, 8/6/93, (PB94-142767, A11, MF-A03).

NCEER-93-0015 "Proceedings from School Sites: Becoming Prepared for Earthquakes - Commemorating the Third Anniversary of the Loma Prieta Earthquake," Edited by F.E. Winslow and K.E.K. Ross, 8/16/93, (PB94-154275, A16, MF-A02).

NCEER-93-0016 "Reconnaissance Report of Damage to Historic Monuments in Cairo, Egypt Following the October 12, 1992 Dahshur Earthquake," by D. Sykora, D. Look, G. Croci, E. Karaesmen and E. Karaesmen, 8/19/93, (PB94-142221, A08, MF-A02).

NCEER-93-0017 "The Island of Guam Earthquake of August 8, 1993," by S.W. Swan and S.K. Harris, 9/30/93, (PB94-141843, A04, MF-A01).

NCEER-93-0018 "Engineering Aspects of the October 12, 1992 Egyptian Earthquake," by A.W. Elgamal, M. Amer, K. Adalier and A. Abul-Fadl, 10/7/93, (PB94-141983, A05, MF-A01).

NCEER-93-0019 "Development of an Earthquake Motion Simulator and its Application in Dynamic Centrifuge Testing," by I. Krstelj, Supervised by J.H. Prevost, 10/23/93, (PB94-181773, A-10, MF-A03).

NCEER-93-0020 "NCEER-Taisei Corporation Research Program on Sliding Seismic Isolation Systems for Bridges: Experimental and Analytical Study of a Friction Pendulum System (FPS)," by M.C. Constantinou, P. Tsopelas, Y-S. Kim and S. Okamoto, 11/1/93, (PB94-142775, A08, MF-A02).

NCEER-93-0021 "Finite Element Modeling of Elastomeric Seismic Isolation Bearings," by L.J. Billings, Supervised by R. Shepherd, 11/8/93, to be published.

NCEER-93-0022 "Seismic Vulnerability of Equipment in Critical Facilities: Life-Safety and Operational Consequences," by K. Porter, G.S. Johnson, M.M. Zadeh, C. Scawthorn and S. Eder, 11/24/93, (PB94-181765, A16, MF-A03).

NCEER-93-0023 "Hokkaido Nansei-oki, Japan Earthquake of July 12, 1993, by P.I. Yanev and C.R. Scawthorn, 12/23/93, (PB94-181500, A07, MF-A01).

NCEER-94-0001 "An Evaluation of Seismic Serviceability of Water Supply Networks with Application to the San Francisco Auxiliary Water Supply System," by I. Markov, Supervised by M. Grigoriu and T. O'Rourke, 1/21/94, (PB94-204013, A07, MF-A02).

NCEER-94-0002 "NCEER-Taisei Corporation Research Program on Sliding Seismic Isolation Systems for Bridges: Experimental and Analytical Study of Systems Consisting of Sliding Bearings, Rubber Restoring Force Devices and Fluid Dampers," Volumes I and II, by P. Tsopelas, S. Okamoto, M.C. Constantinou, D. Ozaki and S. Fujii, 2/4/94, (PB94-181740, A09, MF-A02 and PB94-181757, A12, MF-A03).

NCEER-94-0003 "A Markov Model for Local and Global Damage Indices in Seismic Analysis," by S. Rahman and M. Grigoriu, 2/18/94, (PB94-206000, A12, MF-A03).

NCEER-94-0004 "Proceedings from the NCEER Workshop on Seismic Response of Masonry Infills," edited by D.P. Abrams, 3/1/94, (PB94-180783, A07, MF-A02).

NCEER-94-0005 "The Northridge, California Earthquake of January 17, 1994: General Reconnaissance Report," edited by J.D. Goltz, 3/11/94, (PB94-193943, A10, MF-A03).

NCEER-94-0006 "Seismic Energy Based Fatigue Damage Analysis of Bridge Columns: Part I - Evaluation of Seismic Capacity," by G.A. Chang and J.B. Mander, 3/14/94, (PB94-219185, A11, MF-A03).

NCEER-94-0007 "Seismic Isolation of Multi-Story Frame Structures Using Spherical Sliding Isolation Systems," by T.M. Al-Hussaini, V.A. Zayas and M.C. Constantinou, 3/17/94, (PB94-193745, A09, MF-A02).

NCEER-94-0008 "The Northridge, California Earthquake of January 17, 1994: Performance of Highway Bridges," edited by I.G. Buckle, 3/24/94, (PB94-193851, A06, MF-A02).

NCEER-94-0009 "Proceedings of the Third U.S.-Japan Workshop on Earthquake Protective Systems for Bridges," edited by I.G. Buckle and I. Friedland, 3/31/94, (PB94-195815, A99, MF-A06).

NCEER-94-0010 "3D-BASIS-ME: Computer Program for Nonlinear Dynamic Analysis of Seismically Isolated Single and Multiple Structures and Liquid Storage Tanks," by P.C. Tsopelas, M.C. Constantinou and A.M. Reinhorn, 4/12/94, (PB94-204922, A09, MF-A02).

NCEER-94-0011 "The Northridge, California Earthquake of January 17, 1994: Performance of Gas Transmission Pipelines," by T.D. O'Rourke and M.C. Palmer, 5/16/94, (PB94-204989, A05, MF-A01).

NCEER-94-0012 "Feasibility Study of Replacement Procedures and Earthquake Performance Related to Gas Transmission Pipelines," by T.D. O'Rourke and M.C. Palmer, 5/25/94, (PB94-206638, A09, MF-A02).

NCEER-94-0013 "Seismic Energy Based Fatigue Damage Analysis of Bridge Columns: Part II - Evaluation of Seismic Demand," by G.A. Chang and J.B. Mander, 6/1/94, (PB95-18106, A08, MF-A02).

NCEER-94-0014 "NCEER-Taisei Corporation Research Program on Sliding Seismic Isolation Systems for Bridges: Experimental and Analytical Study of a System Consisting of Sliding Bearings and Fluid Restoring Force/Damping Devices," by P. Tsopelas and M.C. Constantinou, 6/13/94, (PB94-219144, A10, MF-A03).

NCEER-94-0015 "Generation of Hazard-Consistent Fragility Curves for Seismic Loss Estimation Studies," by H. Hwang and J-R. Huo, 6/14/94, (PB95-181996, A09, MF-A02).

NCEER-94-0016 "Seismic Study of Building Frames with Added Energy-Absorbing Devices," by W.S. Pong, C.S. Tsai and G.C. Lee, 6/20/94, (PB94-219136, A10, A03).

NCEER-94-0017 "Sliding Mode Control for Seismic-Excited Linear and Nonlinear Civil Engineering Structures," by J. Yang, J. Wu, A. Agrawal and Z. Li, 6/21/94, (PB95-138483, A06, MF-A02).

NCEER-94-0018 "3D-BASIS-TABS Version 2.0: Computer Program for Nonlinear Dynamic Analysis of Three Dimensional Base Isolated Structures," by A.M. Reinhorn, S. Nagarajaiah, M.C. Constantinou, P. Tsopelas and R. Li, 6/22/94, (PB95-182176, A08, MF-A02).

NCEER-94-0019 "Proceedings of the International Workshop on Civil Infrastructure Systems: Application of Intelligent Systems and Advanced Materials on Bridge Systems," Edited by G.C. Lee and K.C. Chang, 7/18/94, (PB95-252474, A20, MF-A04).

NCEER-94-0020 "Study of Seismic Isolation Systems for Computer Floors," by V. Lambrou and M.C. Constantinou, 7/19/94, (PB95-138533, A10, MF-A03).

NCEER-94-0021 "Proceedings of the U.S.-Italian Workshop on Guidelines for Seismic Evaluation and Rehabilitation of Unreinforced Masonry Buildings," Edited by D.P. Abrams and G.M. Calvi, 7/20/94, (PB95-138749, A13, MF-A03).

NCEER-94-0022 "NCEER-Taisei Corporation Research Program on Sliding Seismic Isolation Systems for Bridges: Experimental and Analytical Study of a System Consisting of Lubricated PTFE Sliding Bearings and Mild Steel Dampers," by P. Tsopelas and M.C. Constantinou, 7/22/94, (PB95-182184, A08, MF-A02).

NCEER-94-0023 “Development of Reliability-Based Design Criteria for Buildings Under Seismic Load,” by Y.K. Wen, H. Hwang and M. Shinozuka, 8/1/94, (PB95-211934, A08, MF-A02).

NCEER-94-0024 “Experimental Verification of Acceleration Feedback Control Strategies for an Active Tendon System,” by S.J. Dyke, B.F. Spencer, Jr., P. Quast, M.K. Sain, D.C. Kaspari, Jr. and T.T. Soong, 8/29/94, (PB95-212320, A05, MF-A01).

NCEER-94-0025 “Seismic Retrofitting Manual for Highway Bridges,” Edited by I.G. Buckle and I.F. Friedland, published by the Federal Highway Administration (PB95-212676, A15, MF-A03).

NCEER-94-0026 “Proceedings from the Fifth U.S.-Japan Workshop on Earthquake Resistant Design of Lifeline Facilities and Countermeasures Against Soil Liquefaction,” Edited by T.D. O’Rourke and M. Hamada, 11/7/94, (PB95-220802, A99, MF-E08).

NCEER-95-0001 "Experimental and Analytical Investigation of Seismic Retrofit of Structures with Supplemental Damping: Part 1 - Fluid Viscous Damping Devices," by A.M. Reinhorn, C. Li and M.C. Constantinou, 1/3/95, (PB95-266599, A09, MF-A02).

NCEER-95-0002 "Experimental and Analytical Study of Low-Cycle Fatigue Behavior of Semi-Rigid Top-And-Seat Angle Connections," by G. Pekcan, J.B. Mander and S.S. Chen, 1/5/95, (PB95-220042, A07, MF-A02).

NCEER-95-0003 "NCEER-ATC Joint Study on Fragility of Buildings," by T. Anagnos, C. Rojahn and A.S. Kiremidjian, 1/20/95, (PB95-220026, A06, MF-A02).

NCEER-95-0004 "Nonlinear Control Algorithms for Peak Response Reduction," by Z. Wu, T.T. Soong, V. Gattulli and R.C. Lin, 2/16/95, (PB95-220349, A05, MF-A01).

NCEER-95-0005 "Pipeline Replacement Feasibility Study: A Methodology for Minimizing Seismic and Corrosion Risks to Underground Natural Gas Pipelines," by R.T. Eguchi, H.A. Seligson and D.G. Honegger, 3/2/95, (PB95-252326, A06, MF-A02).

NCEER-95-0006 "Evaluation of Seismic Performance of an 11-Story Frame Building During the 1994 Northridge Earthquake," by F. Naeim, R. DiSulio, K. Benuska, A. Reinhorn and C. Li, to be published.

NCEER-95-0007 "Prioritization of Bridges for Seismic Retrofitting," by N. Basöz and A.S. Kiremidjian, 4/24/95, (PB95-252300, A08, MF-A02).

NCEER-95-0008 "Method for Developing Motion Damage Relationships for Reinforced Concrete Frames," by A. Singhal and A.S. Kiremidjian, 5/11/95, (PB95-266607, A06, MF-A02).

NCEER-95-0009 "Experimental and Analytical Investigation of Seismic Retrofit of Structures with Supplemental Damping: Part II - Friction Devices," by C. Li and A.M. Reinhorn, 7/6/95, (PB96-128087, A11, MF-A03).

NCEER-95-0010 "Experimental Performance and Analytical Study of a Non-Ductile Reinforced Concrete Frame Structure Retrofitted with Elastomeric Spring Dampers," by G. Pekcan, J.B. Mander and S.S. Chen, 7/14/95, (PB96-137161, A08, MF-A02).

NCEER-95-0011 "Development and Experimental Study of Semi-Active Fluid Damping Devices for Seismic Protection of Structures," by M.D. Symans and M.C. Constantinou, 8/3/95, (PB96-136940, A23, MF-A04).

NCEER-95-0012 "Real-Time Structural Parameter Modification (RSPM): Development of Innervated Structures," by Z. Liang, M. Tong and G.C. Lee, 4/11/95, (PB96-137153, A06, MF-A01).

NCEER-95-0013 "Experimental and Analytical Investigation of Seismic Retrofit of Structures with Supplemental Damping: Part III - Viscous Damping Walls," by A.M. Reinhorn and C. Li, 10/1/95, (PB96-176409, A11, MF-A03).

NCEER-95-0014 "Seismic Fragility Analysis of Equipment and Structures in a Memphis Electric Substation," by J-R. Huo and H.H.M. Hwang, 8/10/95, (PB96-128087, A09, MF-A02).

NCEER-95-0015 "The Hanshin-Awaji Earthquake of January 17, 1995: Performance of Lifelines," Edited by M. Shinozuka, 11/3/95, (PB96-176383, A15, MF-A03).

NCEER-95-0016 "Highway Culvert Performance During Earthquakes," by T.L. Youd and C.J. Beckman, available as NCEER-96-0015.

NCEER-95-0017 "The Hanshin-Awaji Earthquake of January 17, 1995: Performance of Highway Bridges," Edited by I.G. Buckle, 12/1/95, to be published.

NCEER-95-0018 "Modeling of Masonry Infill Panels for Structural Analysis," by A.M. Reinhorn, A. Madan, R.E. Valles, Y. Reichmann and J.B. Mander, 12/8/95, (PB97-110886, MF-A01, A06).

NCEER-95-0019 "Optimal Polynomial Control for Linear and Nonlinear Structures," by A.K. Agrawal and J.N. Yang, 12/11/95, (PB96-168737, A07, MF-A02).

NCEER-95-0020 "Retrofit of Non-Ductile Reinforced Concrete Frames Using Friction Dampers," by R.S. Rao, P. Gergely and R.N. White, 12/22/95, (PB97-133508, A10, MF-A02).

NCEER-95-0021 "Parametric Results for Seismic Response of Pile-Supported Bridge Bents," by G. Mylonakis, A. Nikolaou and G. Gazetas, 12/22/95, (PB97-100242, A12, MF-A03).

NCEER-95-0022 "Kinematic Bending Moments in Seismically Stressed Piles," by A. Nikolaou, G. Mylonakis and G. Gazetas, 12/23/95, (PB97-113914, MF-A03, A13).

NCEER-96-0001 "Dynamic Response of Unreinforced Masonry Buildings with Flexible Diaphragms," by A.C. Costley and D.P. Abrams," 10/10/96, (PB97-133573, MF-A03, A15).

NCEER-96-0002 "State of the Art Review: Foundations and Retaining Structures," by I. Po Lam, to be published.

NCEER-96-0003 "Ductility of Rectangular Reinforced Concrete Bridge Columns with Moderate Confinement," by N. Wehbe, M. Saiidi, D. Sanders and B. Douglas, 11/7/96, (PB97-133557, A06, MF-A02).

NCEER-96-0004 "Proceedings of the Long-Span Bridge Seismic Research Workshop," edited by I.G. Buckle and I.M. Friedland, to be published.

NCEER-96-0005 "Establish Representative Pier Types for Comprehensive Study: Eastern United States," by J. Kulicki and Z. Prucz, 5/28/96, (PB98-119217, A07, MF-A02).

NCEER-96-0006 "Establish Representative Pier Types for Comprehensive Study: Western United States," by R. Imbsen, R.A. Schamber and T.A. Osterkamp, 5/28/96, (PB98-118607, A07, MF-A02).

NCEER-96-0007 "Nonlinear Control Techniques for Dynamical Systems with Uncertain Parameters," by R.G. Ghanem and M.I. Bujakov, 5/27/96, (PB97-100259, A17, MF-A03).

NCEER-96-0008 "Seismic Evaluation of a 30-Year Old Non-Ductile Highway Bridge Pier and Its Retrofit," by J.B. Mander, B. Mahmoodzadegan, S. Bhadra and S.S. Chen, 5/31/96, (PB97-110902, MF-A03, A10).

NCEER-96-0009 "Seismic Performance of a Model Reinforced Concrete Bridge Pier Before and After Retrofit," by J.B. Mander, J.H. Kim and C.A. Ligozio, 5/31/96, (PB97-110910, MF-A02, A10).

NCEER-96-0010 "IDARC2D Version 4.0: A Computer Program for the Inelastic Damage Analysis of Buildings," by R.E. Valles, A.M. Reinhorn, S.K. Kunnath, C. Li and A. Madan, 6/3/96, (PB97-100234, A17, MF-A03).

NCEER-96-0011 "Estimation of the Economic Impact of Multiple Lifeline Disruption: Memphis Light, Gas and Water Division Case Study," by S.E. Chang, H.A. Seligson and R.T. Eguchi, 8/16/96, (PB97-133490, A11, MF-A03).

NCEER-96-0012 "Proceedings from the Sixth Japan-U.S. Workshop on Earthquake Resistant Design of Lifeline Facilities and Countermeasures Against Soil Liquefaction, Edited by M. Hamada and T. O'Rourke, 9/11/96, (PB97-133581, A99, MF-A06).

NCEER-96-0013 "Chemical Hazards, Mitigation and Preparedness in Areas of High Seismic Risk: A Methodology for Estimating the Risk of Post-Earthquake Hazardous Materials Release," by H.A. Seligson, R.T. Eguchi, K.J. Tierney and K. Richmond, 11/7/96, (PB97-133565, MF-A02, A08).

NCEER-96-0014 "Response of Steel Bridge Bearings to Reversed Cyclic Loading," by J.B. Mander, D-K. Kim, S.S. Chen and G.J. Premus, 11/13/96, (PB97-140735, A12, MF-A03).

NCEER-96-0015 "Highway Culvert Performance During Past Earthquakes," by T.L. Youd and C.J. Beckman, 11/25/96, (PB97-133532, A06, MF-A01).

NCEER-97-0001 "Evaluation, Prevention and Mitigation of Pounding Effects in Building Structures," by R.E. Valles and A.M. Reinhorn, 2/20/97, (PB97-159552, A14, MF-A03).

NCEER-97-0002 "Seismic Design Criteria for Bridges and Other Highway Structures," by C. Rojahn, R. Mayes, D.G. Anderson, J. Clark, J.H. Hom, R.V. Nutt and M.J. O'Rourke, 4/30/97, (PB97-194658, A06, MF-A03).

NCEER-97-0003 “Proceedings of the U.S.-Italian Workshop on Seismic Evaluation and Retrofit,” Edited by D.P. Abrams and G.M. Calvi, 3/19/97, (PB97-194666, A13, MF-A03).

NCEER-97-0004 "Investigation of Seismic Response of Buildings with Linear and Nonlinear Fluid Viscous Dampers," by A.A. Seleemah and M.C. Constantinou, 5/21/97, (PB98-109002, A15, MF-A03).

NCEER-97-0005 "Proceedings of the Workshop on Earthquake Engineering Frontiers in Transportation Facilities," edited by G.C. Lee and I.M. Friedland, 8/29/97, (PB98-128911, A25, MR-A04).

NCEER-97-0006 "Cumulative Seismic Damage of Reinforced Concrete Bridge Piers," by S.K. Kunnath, A. El-Bahy, A. Taylor and W. Stone, 9/2/97, (PB98-108814, A11, MF-A03).

NCEER-97-0007 "Structural Details to Accommodate Seismic Movements of Highway Bridges and Retaining Walls," by R.A. Imbsen, R.A. Schamber, E. Thorkildsen, A. Kartoum, B.T. Martin, T.N. Rosser and J.M. Kulicki, 9/3/97, (PB98-108996, A09, MF-A02).

NCEER-97-0008 "A Method for Earthquake Motion-Damage Relationships with Application to Reinforced Concrete Frames," by A. Singhal and A.S. Kiremidjian, 9/10/97, (PB98-108988, A13, MF-A03).

NCEER-97-0009 "Seismic Analysis and Design of Bridge Abutments Considering Sliding and Rotation," by K. Fishman and R. Richards, Jr., 9/15/97, (PB98-108897, A06, MF-A02).

NCEER-97-0010 "Proceedings of the FHWA/NCEER Workshop on the National Representation of Seismic Ground Motion for New and Existing Highway Facilities," edited by I.M. Friedland, M.S. Power and R.L. Mayes, 9/22/97, (PB98-128903, A21, MF-A04).

NCEER-97-0011 "Seismic Analysis for Design or Retrofit of Gravity Bridge Abutments," by K.L. Fishman, R. Richards, Jr. and R.C. Divito, 10/2/97, (PB98-128937, A08, MF-A02).

NCEER-97-0012 "Evaluation of Simplified Methods of Analysis for Yielding Structures," by P. Tsopelas, M.C. Constantinou, C.A. Kircher and A.S. Whittaker, 10/31/97, (PB98-128929, A10, MF-A03).

NCEER-97-0013 "Seismic Design of Bridge Columns Based on Control and Repairability of Damage," by C-T. Cheng and J.B. Mander, 12/8/97, (PB98-144249, A11, MF-A03).

NCEER-97-0014 "Seismic Resistance of Bridge Piers Based on Damage Avoidance Design," by J.B. Mander and C-T. Cheng, 12/10/97, (PB98-144223, A09, MF-A02).

NCEER-97-0015 “Seismic Response of Nominally Symmetric Systems with Strength Uncertainty,” by S. Balopoulou and M. Grigoriu, 12/23/97, (PB98-153422, A11, MF-A03).

NCEER-97-0016 “Evaluation of Seismic Retrofit Methods for Reinforced Concrete Bridge Columns,” by T.J. Wipf, F.W. Klaiber and F.M. Russo, 12/28/97, (PB98-144215, A12, MF-A03).

NCEER-97-0017 “Seismic Fragility of Existing Conventional Reinforced Concrete Highway Bridges,” by C.L. Mullen and A.S. Cakmak, 12/30/97, (PB98-153406, A08, MF-A02).

NCEER-97-0018 “Loss Asssessment of Memphis Buildings,” edited by D.P. Abrams and M. Shinozuka, 12/31/97, (PB98-144231, A13, MF-A03).

NCEER-97-0019 “Seismic Evaluation of Frames with Infill Walls Using Quasi-static Experiments,” by K.M. Mosalam, R.N. White and P. Gergely, 12/31/97, (PB98-153455, A07, MF-A02).

NCEER-97-0020 “Seismic Evaluation of Frames with Infill Walls Using Pseudo-dynamic Experiments,” by K.M. Mosalam, R.N. White and P. Gergely, 12/31/97, (PB98-153430, A07, MF-A02).

NCEER-97-0021 “Computational Strategies for Frames with Infill Walls: Discrete and Smeared Crack Analyses and Seismic Fragility,” by K.M. Mosalam, R.N. White and P. Gergely, 12/31/97, (PB98-153414, A10, MF-A02).

NCEER-97-0022 "Proceedings of the NCEER Workshop on Evaluation of Liquefaction Resistance of Soils," edited by T.L. Youd and I.M. Idriss, 12/31/97, (PB98-155617, A15, MF-A03).

MCEER-98-0001 "Extraction of Nonlinear Hysteretic Properties of Seismically Isolated Bridges from Quick-Release Field Tests," by Q. Chen, B.M. Douglas, E.M. Maragakis and I.G. Buckle, 5/26/98, (PB99-118838, A06, MF-A01).

MCEER-98-0002 "Methodologies for Evaluating the Importance of Highway Bridges," by A. Thomas, S. Eshenaur and J. Kulicki, 5/29/98, (PB99-118846, A10, MF-A02).

MCEER-98-0003 "Capacity Design of Bridge Piers and the Analysis of Overstrength," by J.B. Mander, A. Dutta and P. Goel, 6/1/98, (PB99-118853, A09, MF-A02).

MCEER-98-0004 "Evaluation of Bridge Damage Data from the Loma Prieta and Northridge, California Earthquakes," by N. Basoz and A. Kiremidjian, 6/2/98, (PB99-118861, A15, MF-A03).

MCEER-98-0005 "Screening Guide for Rapid Assessment of Liquefaction Hazard at Highway Bridge Sites," by T. L. Youd, 6/16/98, (PB99-118879, A06, not available on microfiche).

MCEER-98-0006 "Structural Steel and Steel/Concrete Interface Details for Bridges," by P. Ritchie, N. Kauhl and J. Kulicki, 7/13/98, (PB99-118945, A06, MF-A01).

MCEER-98-0007 "Capacity Design and Fatigue Analysis of Confined Concrete Columns," by A. Dutta and J.B. Mander, 7/14/98, (PB99-118960, A14, MF-A03).

MCEER-98-0008 "Proceedings of the Workshop on Performance Criteria for Telecommunication Services Under Earthquake Conditions," edited by A.J. Schiff, 7/15/98, (PB99-118952, A08, MF-A02).

MCEER-98-0009 "Fatigue Analysis of Unconfined Concrete Columns," by J.B. Mander, A. Dutta and J.H. Kim, 9/12/98, (PB99-123655, A10, MF-A02).

MCEER-98-0010 "Centrifuge Modeling of Cyclic Lateral Response of Pile-Cap Systems and Seat-Type Abutments in Dry Sands," by A.D. Gadre and R. Dobry, 10/2/98, (PB99-123606, A13, MF-A03).

MCEER-98-0011 "IDARC-BRIDGE: A Computational Platform for Seismic Damage Assessment of Bridge Structures," by A.M. Reinhorn, V. Simeonov, G. Mylonakis and Y. Reichman, 10/2/98, (PB99-162919, A15, MF-A03).

MCEER-98-0012 "Experimental Investigation of the Dynamic Response of Two Bridges Before and After Retrofitting with Elastomeric Bearings," by D.A. Wendichansky, S.S. Chen and J.B. Mander, 10/2/98, (PB99-162927, A15, MF-A03).

MCEER-98-0013 "Design Procedures for Hinge Restrainers and Hinge Sear Width for Multiple-Frame Bridges," by R. Des Roches and G.L. Fenves, 11/3/98, (PB99-140477, A13, MF-A03).

MCEER-98-0014 "Response Modification Factors for Seismically Isolated Bridges," by M.C. Constantinou and J.K. Quarshie, 11/3/98, (PB99-140485, A14, MF-A03).

MCEER-98-0015 "Proceedings of the U.S.-Italy Workshop on Seismic Protective Systems for Bridges," edited by I.M. Friedland and M.C. Constantinou, 11/3/98, (PB2000-101711, A22, MF-A04).

MCEER-98-0016 "Appropriate Seismic Reliability for Critical Equipment Systems: Recommendations Based on Regional Analysis of Financial and Life Loss," by K. Porter, C. Scawthorn, C. Taylor and N. Blais, 11/10/98, (PB99-157265, A08, MF-A02).

MCEER-98-0017 "Proceedings of the U.S. Japan Joint Seminar on Civil Infrastructure Systems Research," edited by M. Shinozuka and A. Rose, 11/12/98, (PB99-156713, A16, MF-A03).

MCEER-98-0018 "Modeling of Pile Footings and Drilled Shafts for Seismic Design," by I. PoLam, M. Kapuskar and D. Chaudhuri, 12/21/98, (PB99-157257, A09, MF-A02).

MCEER-99-0001 "Seismic Evaluation of a Masonry Infilled Reinforced Concrete Frame by Pseudodynamic Testing," by S.G. Buonopane and R.N. White, 2/16/99, (PB99-162851, A09, MF-A02).

MCEER-99-0002 "Response History Analysis of Structures with Seismic Isolation and Energy Dissipation Systems: Verification Examples for Program SAP2000," by J. Scheller and M.C. Constantinou, 2/22/99, (PB99-162869, A08, MF-A02).

MCEER-99-0003 "Experimental Study on the Seismic Design and Retrofit of Bridge Columns Including Axial Load Effects," by A. Dutta, T. Kokorina and J.B. Mander, 2/22/99, (PB99-162877, A09, MF-A02).

MCEER-99-0004 "Experimental Study of Bridge Elastomeric and Other Isolation and Energy Dissipation Systems with Emphasis on Uplift Prevention and High Velocity Near-source Seismic Excitation," by A. Kasalanati and M. C. Constantinou, 2/26/99, (PB99-162885, A12, MF-A03).

MCEER-99-0005 "Truss Modeling of Reinforced Concrete Shear-flexure Behavior," by J.H. Kim and J.B. Mander, 3/8/99, (PB99-163693, A12, MF-A03).

MCEER-99-0006 "Experimental Investigation and Computational Modeling of Seismic Response of a 1:4 Scale Model Steel Structure with a Load Balancing Supplemental Damping System," by G. Pekcan, J.B. Mander and S.S. Chen, 4/2/99, (PB99-162893, A11, MF-A03).

MCEER-99-0007 "Effect of Vertical Ground Motions on the Structural Response of Highway Bridges," by M.R. Button, C.J. Cronin and R.L. Mayes, 4/10/99, (PB2000-101411, A10, MF-A03).

MCEER-99-0008 "Seismic Reliability Assessment of Critical Facilities: A Handbook, Supporting Documentation, and Model Code Provisions," by G.S. Johnson, R.E. Sheppard, M.D. Quilici, S.J. Eder and C.R. Scawthorn, 4/12/99, (PB2000-101701, A18, MF-A04).

MCEER-99-0009 "Impact Assessment of Selected MCEER Highway Project Research on the Seismic Design of Highway Structures," by C. Rojahn, R. Mayes, D.G. Anderson, J.H. Clark, D'Appolonia Engineering, S. Gloyd and R.V. Nutt, 4/14/99, (PB99-162901, A10, MF-A02).

MCEER-99-0010 "Site Factors and Site Categories in Seismic Codes," by R. Dobry, R. Ramos and M.S. Power, 7/19/99, (PB2000-101705, A08, MF-A02).

MCEER-99-0011 "Restrainer Design Procedures for Multi-Span Simply-Supported Bridges," by M.J. Randall, M. Saiidi, E. Maragakis and T. Isakovic, 7/20/99, (PB2000-101702, A10, MF-A02).

MCEER-99-0012 "Property Modification Factors for Seismic Isolation Bearings," by M.C. Constantinou, P. Tsopelas, A. Kasalanati and E. Wolff, 7/20/99, (PB2000-103387, A11, MF-A03).

MCEER-99-0013 "Critical Seismic Issues for Existing Steel Bridges," by P. Ritchie, N. Kauhl and J. Kulicki, 7/20/99, (PB2000-101697, A09, MF-A02).

MCEER-99-0014 "Nonstructural Damage Database," by A. Kao, T.T. Soong and A. Vender, 7/24/99, (PB2000-101407, A06, MF-A01).

MCEER-99-0015 "Guide to Remedial Measures for Liquefaction Mitigation at Existing Highway Bridge Sites," by H.G. Cooke and J. K. Mitchell, 7/26/99, (PB2000-101703, A11, MF-A03).

MCEER-99-0016 "Proceedings of the MCEER Workshop on Ground Motion Methodologies for the Eastern United States," edited by N. Abrahamson and A. Becker, 8/11/99, (PB2000-103385, A07, MF-A02).

MCEER-99-0017 "Quindío, Colombia Earthquake of January 25, 1999: Reconnaissance Report," by A.P. Asfura and P.J. Flores, 10/4/99, (PB2000-106893, A06, MF-A01).

MCEER-99-0018 "Hysteretic Models for Cyclic Behavior of Deteriorating Inelastic Structures," by M.V. Sivaselvan and A.M. Reinhorn, 11/5/99, (PB2000-103386, A08, MF-A02).

MCEER-99-0019 "Proceedings of the 7th U.S.- Japan Workshop on Earthquake Resistant Design of Lifeline Facilities and Countermeasures Against Soil Liquefaction," edited by T.D. O'Rourke, J.P. Bardet and M. Hamada, 11/19/99, (PB2000-103354, A99, MF-A06).

MCEER-99-0020 "Development of Measurement Capability for Micro-Vibration Evaluations with Application to Chip Fabrication Facilities," by G.C. Lee, Z. Liang, J.W. Song, J.D. Shen and W.C. Liu, 12/1/99, (PB2000-105993, A08, MF-A02).

MCEER-99-0021 "Design and Retrofit Methodology for Building Structures with Supplemental Energy Dissipating Systems," by G. Pekcan, J.B. Mander and S.S. Chen, 12/31/99, (PB2000-105994, A11, MF-A03).

MCEER-00-0001 "The Marmara, Turkey Earthquake of August 17, 1999: Reconnaissance Report," edited by C. Scawthorn; with major contributions by M. Bruneau, R. Eguchi, T. Holzer, G. Johnson, J. Mander, J. Mitchell, W. Mitchell, A. Papageorgiou, C. Scaethorn, and G. Webb, 3/23/00, (PB2000-106200, A11, MF-A03).

MCEER-00-0002 "Proceedings of the MCEER Workshop for Seismic Hazard Mitigation of Health Care Facilities," edited by G.C. Lee, M. Ettouney, M. Grigoriu, J. Hauer and J. Nigg, 3/29/00, (PB2000-106892, A08, MF-A02).

MCEER-00-0003 "The Chi-Chi, Taiwan Earthquake of September 21, 1999: Reconnaissance Report," edited by G.C. Lee and C.H. Loh, with major contributions by G.C. Lee, M. Bruneau, I.G. Buckle, S.E. Chang, P.J. Flores, T.D. O'Rourke, M. Shinozuka, T.T. Soong, C-H. Loh, K-C. Chang, Z-J. Chen, J-S. Hwang, M-L. Lin, G-Y. Liu, K-C. Tsai, G.C. Yao and C-L. Yen, 4/30/00, (PB2001-100980, A10, MF-A02).

MCEER-00-0004 "Seismic Retrofit of End-Sway Frames of Steel Deck-Truss Bridges with a Supplemental Tendon System: Experimental and Analytical Investigation," by G. Pekcan, J.B. Mander and S.S. Chen, 7/1/00, (PB2001-100982, A10, MF-A02).

MCEER-00-0005 "Sliding Fragility of Unrestrained Equipment in Critical Facilities," by W.H. Chong and T.T. Soong, 7/5/00, (PB2001-100983, A08, MF-A02).

MCEER-00-0006 "Seismic Response of Reinforced Concrete Bridge Pier Walls in the Weak Direction," by N. Abo-Shadi, M. Saiidi and D. Sanders, 7/17/00, (PB2001-100981, A17, MF-A03).

MCEER-00-0007 "Low-Cycle Fatigue Behavior of Longitudinal Reinforcement in Reinforced Concrete Bridge Columns," by J. Brown and S.K. Kunnath, 7/23/00, (PB2001-104392, A08, MF-A02).

MCEER-00-0008 "Soil Structure Interaction of Bridges for Seismic Analysis," I. PoLam and H. Law, 9/25/00, (PB2001-105397, A08, MF-A02).

MCEER-00-0009 "Proceedings of the First MCEER Workshop on Mitigation of Earthquake Disaster by Advanced Technologies (MEDAT-1), edited by M. Shinozuka, D.J. Inman and T.D. O'Rourke, 11/10/00, (PB2001-105399, A14, MF-A03).

MCEER-00-0010 "Development and Evaluation of Simplified Procedures for Analysis and Design of Buildings with Passive Energy Dissipation Systems, Revision 01," by O.M. Ramirez, M.C. Constantinou, C.A. Kircher, A.S. Whittaker, M.W. Johnson, J.D. Gomez and C. Chrysostomou, 11/16/01, (PB2001-105523, A23, MF-A04).

MCEER-00-0011 "Dynamic Soil-Foundation-Structure Interaction Analyses of Large Caissons," by C-Y. Chang, C-M. Mok, Z-L. Wang, R. Settgast, F. Waggoner, M.A. Ketchum, H.M. Gonnermann and C-C. Chin, 12/30/00, (PB2001-104373, A07, MF-A02).

MCEER-00-0012 "Experimental Evaluation of Seismic Performance of Bridge Restrainers," by A.G. Vlassis, E.M. Maragakis and M. Saiid Saiidi, 12/30/00, (PB2001-104354, A09, MF-A02).

MCEER-00-0013 "Effect of Spatial Variation of Ground Motion on Highway Structures," by M. Shinozuka, V. Saxena and G. Deodatis, 12/31/00, (PB2001-108755, A13, MF-A03).

MCEER-00-0014 "A Risk-Based Methodology for Assessing the Seismic Performance of Highway Systems," by S.D. Werner, C.E. Taylor, J.E. Moore, II, J.S. Walton and S. Cho, 12/31/00, (PB2001-108756, A14, MF-A03).

MCEER-01-0001 "Experimental Investigation of P-Delta Effects to Collapse During Earthquakes," by D. Vian and M. Bruneau, 6/25/01, (PB2002-100534, A17, MF-A03).

MCEER-01-0002 "Proceedings of the Second MCEER Workshop on Mitigation of Earthquake Disaster by Advanced Technologies (MEDAT-2)," edited by M. Bruneau and D.J. Inman, 7/23/01, (PB2002-100434, A16, MF-A03).

MCEER-01-0003 "Sensitivity Analysis of Dynamic Systems Subjected to Seismic Loads," by C. Roth and M. Grigoriu, 9/18/01, (PB2003-100884, A12, MF-A03).

MCEER-01-0004 "Overcoming Obstacles to Implementing Earthquake Hazard Mitigation Policies: Stage 1 Report," by D.J. Alesch and W.J. Petak, 12/17/01, (PB2002-107949, A07, MF-A02).

MCEER-01-0005 "Updating Real-Time Earthquake Loss Estimates: Methods, Problems and Insights," by C.E. Taylor, S.E. Chang and R.T. Eguchi, 12/17/01, (PB2002-107948, A05, MF-A01).

MCEER-01-0006 "Experimental Investigation and Retrofit of Steel Pile Foundations and Pile Bents Under Cyclic Lateral Loadings," by A. Shama, J. Mander, B. Blabac and S. Chen, 12/31/01, (PB2002-107950, A13, MF-A03).

MCEER-02-0001 "Assessment of Performance of Bolu Viaduct in the 1999 Duzce Earthquake in Turkey" by P.C. Roussis, M.C. Constantinou, M. Erdik, E. Durukal and M. Dicleli, 5/8/02, (PB2003-100883, A08, MF-A02).

MCEER-02-0002 "Seismic Behavior of Rail Counterweight Systems of Elevators in Buildings," by M.P. Singh, Rildova and L.E. Suarez, 5/27/02. (PB2003-100882, A11, MF-A03).

MCEER-02-0003 "Development of Analysis and Design Procedures for Spread Footings," by G. Mylonakis, G. Gazetas, S. Nikolaou and A. Chauncey, 10/02/02, (PB2004-101636, A13, MF-A03, CD-A13).

MCEER-02-0004 "Bare-Earth Algorithms for Use with SAR and LIDAR Digital Elevation Models," by C.K. Huyck, R.T. Eguchi and B. Houshmand, 10/16/02, (PB2004-101637, A07, CD-A07).

MCEER-02-0005 "Review of Energy Dissipation of Compression Members in Concentrically Braced Frames," by K.Lee and M. Bruneau, 10/18/02, (PB2004-101638, A10, CD-A10).

MCEER-03-0001 "Experimental Investigation of Light-Gauge Steel Plate Shear Walls for the Seismic Retrofit of Buildings" by J. Berman and M. Bruneau, 5/2/03, (PB2004-101622, A10, MF-A03, CD-A10).

MCEER-03-0002 "Statistical Analysis of Fragility Curves," by M. Shinozuka, M.Q. Feng, H. Kim, T. Uzawa and T. Ueda, 6/16/03, (PB2004-101849, A09, CD-A09).

MCEER-03-0003 "Proceedings of the Eighth U.S.-Japan Workshop on Earthquake Resistant Design f Lifeline Facilities and Countermeasures Against Liquefaction," edited by M. Hamada, J.P. Bardet and T.D. O'Rourke, 6/30/03, (PB2004-104386, A99, CD-A99).

MCEER-03-0004 "Proceedings of the PRC-US Workshop on Seismic Analysis and Design of Special Bridges," edited by L.C. Fan and G.C. Lee, 7/15/03, (PB2004-104387, A14, CD-A14).

MCEER-03-0005 "Urban Disaster Recovery: A Framework and Simulation Model," by S.B. Miles and S.E. Chang, 7/25/03, (PB2004-104388, A07, CD-A07).

MCEER-03-0006 "Behavior of Underground Piping Joints Due to Static and Dynamic Loading," by R.D. Meis, M. Maragakis and R. Siddharthan, 11/17/03, (PB2005-102194, A13, MF-A03, CD-A00).

MCEER-04-0001 "Experimental Study of Seismic Isolation Systems with Emphasis on Secondary System Response and Verification of Accuracy of Dynamic Response History Analysis Methods," by E. Wolff and M. Constantinou, 1/16/04 (PB2005-102195, A99, MF-E08, CD-A00).

MCEER-04-0002 "Tension, Compression and Cyclic Testing of Engineered Cementitious Composite Materials," by K. Kesner and S.L. Billington, 3/1/04, (PB2005-102196, A08, CD-A08).

MCEER-04-0003 "Cyclic Testing of Braces Laterally Restrained by Steel Studs to Enhance Performance During Earthquakes," by O.C. Celik, J.W. Berman and M. Bruneau, 3/16/04, (PB2005-102197, A13, MF-A03, CD-A00).

MCEER-04-0004 "Methodologies for Post Earthquake Building Damage Detection Using SAR and Optical Remote Sensing: Application to the August 17, 1999 Marmara, Turkey Earthquake," by C.K. Huyck, B.J. Adams, S. Cho, R.T. Eguchi, B. Mansouri and B. Houshmand, 6/15/04, (PB2005-104888, A10, CD-A00).

MCEER-04-0005 "Nonlinear Structural Analysis Towards Collapse Simulation: A Dynamical Systems Approach," by M.V. Sivaselvan and A.M. Reinhorn, 6/16/04, (PB2005-104889, A11, MF-A03, CD-A00).

MCEER-04-0006 "Proceedings of the Second PRC-US Workshop on Seismic Analysis and Design of Special Bridges," edited by G.C. Lee and L.C. Fan, 6/25/04, (PB2005-104890, A16, CD-A00).

MCEER-04-0007 "Seismic Vulnerability Evaluation of Axially Loaded Steel Built-up Laced Members," by K. Lee and M. Bruneau, 6/30/04, (PB2005-104891, A16, CD-A00).

MCEER-04-0008 "Evaluation of Accuracy of Simplified Methods of Analysis and Design of Buildings with Damping Systems for Near-Fault and for Soft-Soil Seismic Motions," by E.A. Pavlou and M.C. Constantinou, 8/16/04, (PB2005-104892, A08, MF-A02, CD-A00).

MCEER-04-0009 "Assessment of Geotechnical Issues in Acute Care Facilities in California," by M. Lew, T.D. O'Rourke, R. Dobry and M. Koch, 9/15/04, (PB2005-104893, A08, CD-A00).

MCEER-04-0010 "Scissor-Jack-Damper Energy Dissipation System," by A.N. Sigaher-Boyle and M.C. Constantinou, 12/1/04 (PB2005-108221).

MCEER-04-0011 "Seismic Retrofit of Bridge Steel Truss Piers Using a Controlled Rocking Approach," by M. Pollino and M. Bruneau, 12/20/04 (PB2006-105795).

MCEER-05-0001 "Experimental and Analytical Studies of Structures Seismically Isolated with an Uplift-Restraint Isolation System," by P.C. Roussis and M.C. Constantinou, 1/10/05 (PB2005-108222).

MCEER-05-0002 "A Versatile Experimentation Model for Study of Structures Near Collapse Applied to Seismic Evaluation of Irregular Structures," by D. Kusumastuti, A.M. Reinhorn and A. Rutenberg, 3/31/05 (PB2006-101523).

MCEER-05-0003 "Proceedings of the Third PRC-US Workshop on Seismic Analysis and Design of Special Bridges," edited by L.C. Fan and G.C. Lee, 4/20/05, (PB2006-105796).

MCEER-05-0004 "Approaches for the Seismic Retrofit of Braced Steel Bridge Piers and Proof-of-Concept Testing of an Eccentrically Braced Frame with Tubular Link," by J.W. Berman and M. Bruneau, 4/21/05 (PB2006-101524).

MCEER-05-0005 "Simulation of Strong Ground Motions for Seismic Fragility Evaluation of Nonstructural Components in Hospitals," by A. Wanitkorkul and A. Filiatrault, 5/26/05 (PB2006-500027).

MCEER-05-0006 "Seismic Safety in California Hospitals: Assessing an Attempt to Accelerate the Replacement or Seismic Retrofit of Older Hospital Facilities," by D.J. Alesch, L.A. Arendt and W.J. Petak, 6/6/05 (PB2006-105794).

MCEER-05-0007 "Development of Seismic Strengthening and Retrofit Strategies for Critical Facilities Using Engineered Cementitious Composite Materials," by K. Kesner and S.L. Billington, 8/29/05 (PB2006-111701).

MCEER-05-0008 "Experimental and Analytical Studies of Base Isolation Systems for Seismic Protection of Power Transformers," by N. Murota, M.Q. Feng and G-Y. Liu, 9/30/05 (PB2006-111702).

MCEER-05-0009 "3D-BASIS-ME-MB: Computer Program for Nonlinear Dynamic Analysis of Seismically Isolated Structures," by P.C. Tsopelas, P.C. Roussis, M.C. Constantinou, R. Buchanan and A.M. Reinhorn, 10/3/05 (PB2006-111703).

MCEER-05-0010 "Steel Plate Shear Walls for Seismic Design and Retrofit of Building Structures," by D. Vian and M. Bruneau, 12/15/05 (PB2006-111704).

MCEER-05-0011 "The Performance-Based Design Paradigm," by M.J. Astrella and A. Whittaker, 12/15/05 (PB2006-111705).

MCEER-06-0001 "Seismic Fragility of Suspended Ceiling Systems," H. Badillo-Almaraz, A.S. Whittaker, A.M. Reinhorn and G.P. Cimellaro, 2/4/06 (PB2006-111706).

MCEER-06-0002 "Multi-Dimensional Fragility of Structures," by G.P. Cimellaro, A.M. Reinhorn and M. Bruneau, 3/1/06 (PB2007-106974, A09, MF-A02, CD A00).

MCEER-06-0003 "Built-Up Shear Links as Energy Dissipators for Seismic Protection of Bridges," by P. Dusicka, A.M. Itani and I.G. Buckle, 3/15/06 (PB2006-111708).

MCEER-06-0004 "Analytical Investigation of the Structural Fuse Concept," by R.E. Vargas and M. Bruneau, 3/16/06 (PB2006-111709).

MCEER-06-0005 "Experimental Investigation of the Structural Fuse Concept," by R.E. Vargas and M. Bruneau, 3/17/06 (PB2006-111710).

MCEER-06-0006 "Further Development of Tubular Eccentrically Braced Frame Links for the Seismic Retrofit of Braced Steel Truss Bridge Piers," by J.W. Berman and M. Bruneau, 3/27/06 (PB2007-105147).

MCEER-06-0007 "REDARS Validation Report," by S. Cho, C.K. Huyck, S. Ghosh and R.T. Eguchi, 8/8/06 (PB2007-106983).

MCEER-06-0008 "Review of Current NDE Technologies for Post-Earthquake Assessment of Retrofitted Bridge Columns," by J.W. Song, Z. Liang and G.C. Lee, 8/21/06 (PB2007-106984).

MCEER-06-0009 "Liquefaction Remediation in Silty Soils Using Dynamic Compaction and Stone Columns," by S. Thevanayagam, G.R. Martin, R. Nashed, T. Shenthan, T. Kanagalingam and N. Ecemis, 8/28/06 (PB2007-106985).

MCEER-06-0010 "Conceptual Design and Experimental Investigation of Polymer Matrix Composite Infill Panels for Seismic Retrofitting," by W. Jung, M. Chiewanichakorn and A.J. Aref, 9/21/06 (PB2007-106986).

MCEER-06-0011 "A Study of the Coupled Horizontal-Vertical Behavior of Elastomeric and Lead-Rubber Seismic Isolation Bearings," by G.P. Warn and A.S. Whittaker, 9/22/06 (PB2007-108679).

MCEER-06-0012 "Proceedings of the Fourth PRC-US Workshop on Seismic Analysis and Design of Special Bridges: Advancing Bridge Technologies in Research, Design, Construction and Preservation," Edited by L.C. Fan, G.C. Lee and L. Ziang, 10/12/06 (PB2007-109042).

MCEER-06-0013 "Cyclic Response and Low Cycle Fatigue Characteristics of Plate Steels," by P. Dusicka, A.M. Itani and I.G. Buckle, 11/1/06 06 (PB2007-106987).

MCEER-06-0014 "Proceedings of the Second US-Taiwan Bridge Engineering Workshop," edited by W.P. Yen, J. Shen, J-Y. Chen and M. Wang, 11/15/06 (PB2008-500041).

MCEER-06-0015 "User Manual and Technical Documentation for the REDARS$^{TM}$ Import Wizard," by S. Cho, S. Ghosh, C.K. Huyck and S.D. Werner, 11/30/06 (PB2007-114766).

MCEER-06-0016 "Hazard Mitigation Strategy and Monitoring Technologies for Urban and Infrastructure Public Buildings: Proceedings of the China-US Workshops," edited by X.Y. Zhou, A.L. Zhang, G.C. Lee and M. Tong, 12/12/06 (PB2008-500018).

MCEER-07-0001 "Static and Kinetic Coefficients of Friction for Rigid Blocks," by C. Kafali, S. Fathali, M. Grigoriu and A.S. Whittaker, 3/20/07 (PB2007-114767).

MCEER-07-0002 "Hazard Mitigation Investment Decision Making: Organizational Response to Legislative Mandate," by L.A. Arendt, D.J. Alesch and W.J. Petak, 4/9/07 (PB2007-114768).

MCEER-07-0003 "Seismic Behavior of Bidirectional-Resistant Ductile End Diaphragms with Unbonded Braces in Straight or Skewed Steel Bridges," by O. Celik and M. Bruneau, 4/11/07 (PB2008-105141).

MCEER-07-0004 "Modeling Pile Behavior in Large Pile Groups Under Lateral Loading," by A.M. Dodds and G.R. Martin, 4/16/07(PB2008-105142).

MCEER-07-0005 "Experimental Investigation of Blast Performance of Seismically Resistant Concrete-Filled Steel Tube Bridge Piers," by S. Fujikura, M. Bruneau and D. Lopez-Garcia, 4/20/07 (PB2008-105143).

MCEER-07-0006 "Seismic Analysis of Conventional and Isolated Liquefied Natural Gas Tanks Using Mechanical Analogs," by I.P. Christovasilis and A.S. Whittaker, 5/1/07.

MCEER-07-0007 "Experimental Seismic Performance Evaluation of Isolation/Restraint Systems for Mechanical Equipment – Part 1: Heavy Equipment Study," by S. Fathali and A. Filiatrault, 6/6/07 (PB2008-105144).

MCEER-07-0008 "Seismic Vulnerability of Timber Bridges and Timber Substructures," by A.A. Sharma, J.B. Mander, I.M. Friedland and D.R. Allicock, 6/7/07 (PB2008-105145).

MCEER-07-0009 "Experimental and Analytical Study of the XY-Friction Pendulum (XY-FP) Bearing for Bridge Applications," by C.C. Marin-Artieda, A.S. Whittaker and M.C. Constantinou, 6/7/07 (PB2008-105191).

MCEER-07-0010 "Proceedings of the PRC-US Earthquake Engineering Forum for Young Researchers," Edited by G.C. Lee and X.Z. Qi, 6/8/07 (PB2008-500058).

MCEER-07-0011 "Design Recommendations for Perforated Steel Plate Shear Walls," by R. Purba and M. Bruneau, 6/18/07, (PB2008-105192).

MCEER-07-0012 "Performance of Seismic Isolation Hardware Under Service and Seismic Loading," by M.C. Constantinou, A.S. Whittaker, Y. Kalpakidis, D.M. Fenz and G.P. Warn, 8/27/07, (PB2008-105193).

MCEER-07-0013 "Experimental Evaluation of the Seismic Performance of Hospital Piping Subassemblies," by E.R. Goodwin, E. Maragakis and A.M. Itani, 9/4/07, (PB2008-105194).

MCEER-07-0014 "A Simulation Model of Urban Disaster Recovery and Resilience: Implementation for the 1994 Northridge Earthquake," by S. Miles and S.E. Chang, 9/7/07, (PB2008-106426).

MCEER-07-0015 "Statistical and Mechanistic Fragility Analysis of Concrete Bridges," by M. Shinozuka, S. Banerjee and S-H. Kim, 9/10/07, (PB2008-106427).

MCEER-07-0016 "Three-Dimensional Modeling of Inelastic Buckling in Frame Structures," by M. Schachter and AM. Reinhorn, 9/13/07, (PB2008-108125).

MCEER-07-0017 "Modeling of Seismic Wave Scattering on Pile Groups and Caissons," by I. Po Lam, H. Law and C.T. Yang, 9/17/07 (PB2008-108150).

MCEER-07-0018 "Bridge Foundations: Modeling Large Pile Groups and Caissons for Seismic Design," by I. Po Lam, H. Law and G.R. Martin (Coordinating Author), 12/1/07 (PB2008-111190).

MCEER-07-0019 "Principles and Performance of Roller Seismic Isolation Bearings for Highway Bridges," by G.C. Lee, Y.C. Ou, Z. Liang, T.C. Niu and J. Song, 12/10/07 (PB2009-110466).

MCEER-07-0020 "Centrifuge Modeling of Permeability and Pinning Reinforcement Effects on Pile Response to Lateral Spreading," by L.L Gonzalez-Lagos, T. Abdoun and R. Dobry, 12/10/07 (PB2008-111191).

MCEER-07-0021 "Damage to the Highway System from the Pisco, Perú Earthquake of August 15, 2007," by J.S. O'Connor, L. Mesa and M. Nykamp, 12/10/07, (PB2008-108126).

MCEER-07-0022 "Experimental Seismic Performance Evaluation of Isolation/Restraint Systems for Mechanical Equipment – Part 2: Light Equipment Study," by S. Fathali and A. Filiatrault, 12/13/07 (PB2008-111192).

MCEER-07-0023 "Fragility Considerations in Highway Bridge Design," by M. Shinozuka, S. Banerjee and S.H. Kim, 12/14/07 (PB2008-111193).

MCEER-07-0024 "Performance Estimates for Seismically Isolated Bridges," by G.P. Warn and A.S. Whittaker, 12/30/07 (PB2008-112230).

MCEER-08-0001 "Seismic Performance of Steel Girder Bridge Superstructures with Conventional Cross Frames," by L.P. Carden, A.M. Itani and I.G. Buckle, 1/7/08, (PB2008-112231).

MCEER-08-0002 "Seismic Performance of Steel Girder Bridge Superstructures with Ductile End Cross Frames with Seismic Isolators," by L.P. Carden, A.M. Itani and I.G. Buckle, 1/7/08 (PB2008-112232).

MCEER-08-0003 "Analytical and Experimental Investigation of a Controlled Rocking Approach for Seismic Protection of Bridge Steel Truss Piers," by M. Pollino and M. Bruneau, 1/21/08 (PB2008-112233).

MCEER-08-0004 "Linking Lifeline Infrastructure Performance and Community Disaster Resilience: Models and Multi-Stakeholder Processes," by S.E. Chang, C. Pasion, K. Tatebe and R. Ahmad, 3/3/08 (PB2008-112234).

MCEER-08-0005 "Modal Analysis of Generally Damped Linear Structures Subjected to Seismic Excitations," by J. Song, Y-L. Chu, Z. Liang and G.C. Lee, 3/4/08 (PB2009-102311).

MCEER-08-0006 "System Performance Under Multi-Hazard Environments," by C. Kafali and M. Grigoriu, 3/4/08 (PB2008-112235).

MCEER-08-0007 "Mechanical Behavior of Multi-Spherical Sliding Bearings," by D.M. Fenz and M.C. Constantinou, 3/6/08 (PB2008-112236).

MCEER-08-0008 "Post-Earthquake Restoration of the Los Angeles Water Supply System," by T.H.P. Tabucchi and R.A. Davidson, 3/7/08 (PB2008-112237).

MCEER-08-0009 "Fragility Analysis of Water Supply Systems," by A. Jacobson and M. Grigoriu, 3/10/08 (PB2009-105545).

MCEER-08-0010 "Experimental Investigation of Full-Scale Two-Story Steel Plate Shear Walls with Reduced Beam Section Connections," by B. Qu, M. Bruneau, C-H. Lin and K-C. Tsai, 3/17/08 (PB2009-106368).

MCEER-08-0011 "Seismic Evaluation and Rehabilitation of Critical Components of Electrical Power Systems," S. Ersoy, B. Feizi, A. Ashrafi and M. Ala Saadeghvaziri, 3/17/08 (PB2009-105546).

MCEER-08-0012 "Seismic Behavior and Design of Boundary Frame Members of Steel Plate Shear Walls," by B. Qu and M. Bruneau, 4/26/08 . (PB2009-106744).

MCEER-08-0013 "Development and Appraisal of a Numerical Cyclic Loading Protocol for Quantifying Building System Performance," by A. Filiatrault, A. Wanitkorkul and M. Constantinou, 4/27/08 (PB2009-107906).

MCEER-08-0014 "Structural and Nonstructural Earthquake Design: The Challenge of Integrating Specialty Areas in Designing Complex, Critical Facilities," by W.J. Petak and D.J. Alesch, 4/30/08 (PB2009-107907).

MCEER-08-0015 "Seismic Performance Evaluation of Water Systems," by Y. Wang and T.D. O'Rourke, 5/5/08 (PB2009-107908).

MCEER-08-0016 "Seismic Response Modeling of Water Supply Systems," by P. Shi and T.D. O'Rourke, 5/5/08 (PB2009-107910).

MCEER-08-0017 "Numerical and Experimental Studies of Self-Centering Post-Tensioned Steel Frames," by D. Wang and A. Filiatrault, 5/12/08 (PB2009-110479).

MCEER-08-0018 "Development, Implementation and Verification of Dynamic Analysis Models for Multi-Spherical Sliding Bearings," by D.M. Fenz and M.C. Constantinou, 8/15/08 (PB2009-107911).

MCEER-08-0019 "Performance Assessment of Conventional and Base Isolated Nuclear Power Plants for Earthquake Blast Loadings," by Y.N. Huang, A.S. Whittaker and N. Luco, 10/28/08 (PB2009-107912).

MCEER-08-0020 "Remote Sensing for Resilient Multi-Hazard Disaster Response – Volume I: Introduction to Damage Assessment Methodologies," by B.J. Adams and R.T. Eguchi, 11/17/08.

MCEER-08-0021 "Remote Sensing for Resilient Multi-Hazard Disaster Response – Volume II: Counting the Number of Collapsed Buildings Using an Object-Oriented Analysis: Case Study of the 2003 Bam Earthquake," by L. Gusella, C.K. Huyck and B.J. Adams, 11/17/08.

MCEER-08-0022 "Remote Sensing for Resilient Multi-Hazard Disaster Response – Volume III: Multi-Sensor Image Fusion Techniques for Robust Neighborhood-Scale Urban Damage Assessment," by B.J. Adams and A. McMillan, 11/17/08.

MCEER-08-0023 "Remote Sensing for Resilient Multi-Hazard Disaster Response – Volume IV: A Study of Multi-Temporal and Multi-Resolution SAR Imagery for Post-Katrina Flood Monitoring in New Orleans," by A. McMillan, J.G. Morley, B.J. Adams and S. Chesworth, 11/17/08.

MCEER-08-0024 "Remote Sensing for Resilient Multi-Hazard Disaster Response – Volume V: Integration of Remote Sensing Imagery and VIEWS$^{TM}$ Field Data for Post-Hurricane Charley Building Damage Assessment," by J.A. Womble, K. Mehta and B.J. Adams, 11/17/08.

MCEER-08-0025 "Building Inventory Compilation for Disaster Management: Application of Remote Sensing and Statistical Modeling," by P. Sarabandi, A.S. Kiremidjian, R.T. Eguchi and B. J. Adams, 11/20/08 (PB2009-110484).

MCEER-08-0026 "New Experimental Capabilities and Loading Protocols for Seismic Qualification and Fragility Assessment of Nonstructural Systems," by R. Retamales, G. Mosqueda, A. Filiatrault and A. Reinhorn, 11/24/08 (PB2009-110485).

MCEER-08-0027 "Effects of Heating and Load History on the Behavior of Lead-Rubber Bearings," by I.V. Kalpakidis and M.C. Constantinou, 12/1/08.

MCEER-08-0028 "Experimental and Analytical Investigation of Blast Performance of Seismically Resistant Bridge Piers," by S.Fujikura and M. Bruneau, 12/8/08.

MCEER-08-0029 "Evolutionary Methodology for Aseismic Decision Support," by Y. Hu and G. Dargush, 12/15/08.

MCEER-08-0030 "Development of a Steel Plate Shear Wall Bridge Pier System Conceived from a Multi-Hazard Perspective," by D. Keller and M. Bruneau, 12/19/08.

MCEER-09-0001 "Modal Analysis of Arbitrarily Damped Three-Dimensional Linear Structures Subjected to Seismic Excitations," by Y.L. Chu, J. Song and G.C. Lee, 1/31/09.

MCEER-09-0002 "Air-Blast Effects on Structural Shapes," by G. Ballantyne, A.S. Whittaker, A.J. Aref and G.F. Dargush, 2/2/09.

MCEER-09-0003 "Water Supply Performance During Earthquakes and Extreme Events," by A.L. Bonneau and T.D. O'Rourke, 2/16/09.

MCEER-09-0004 "Generalized Linear (Mixed) Models of Post-Earthquake Ignitions," by R.A. Davidson, 7/20/09.

MCEER-09-0005 "Seismic Testing of a Full-Scale Two-Story Light-Frame Wood Building: NEESWood Benchmark Test," by I.P. Christovasilis, A. Filiatrault and A. Wanitkorkul, 7/22/09.

MCEER-09-0006 "IDARC2D Version 7.0: A Program for the Inelastic Damage Analysis of Structures," by A.M. Reinhorn, H. Roh, M. Sivaselvan, S.K. Kunnath, R.E. Valles, A. Madan, C. Li, R. Lobo and Y.J. Park, 7/28/09.

MCEER-09-0007 "Enhancements to Hospital Resiliency: Improving Emergency Planning for and Response to Hurricanes," by D.B. Hess and L.A. Arendt, 7/30/09.

MCEER-09-0008 "Assessment of Base-Isolated Nuclear Structures for Design and Beyond-Design Basis Earthquake Shaking," by Y.N. Huang, A.S. Whittaker, R.P. Kennedy and R.L. Mayes, 8/20/09.

MCEER-09-0009 “Quantification of Disaster Resilience of Health Care Facilities,” by G.P. Cimellaro, C. Fumo, A.M Reinhorn and M. Bruneau, 9/14/09.

MCEER-09-0010 “Performance-Based Assessment and Design of Squat Reinforced Concrete Shear Walls,” by C.K. Gulec and A.S. Whittaker, 9/15/09.

# Appendix A – Squat Wall Database

Table A-1 through Table A-4 present information on the rectangular walls; Table A-5 through Table A-8 present information on walls with barbells and flanges. In Table A-1 through Table A-8, $t_w$ is the thickness of the wall, $h_w$ is the height of the wall, $l_w$ is the length of the wall, $M/Vl_w$ is the moment-to-shear ratio, $h_{be}$ is the length of the boundary element, $\rho_{be}$ is the vertical boundary element reinforcement ratio calculated by dividing the area of the reinforcement in the boundary element to the area of the boundary element, $\rho_v$ is the vertical web reinforcement ratio, $\rho_{vall}$ is the ratio area of the all vertical reinforcement to the wall area, $\rho_h$ is the horizontal web reinforcement ratio, Noc-HR and Noc-VR are the number of reinforcement curtains for horizontal and vertical web reinforcement, $s_h$ and $s_v$ are the spacing of the horizontal and vertical web reinforcement, $f_c'$ is the peak compressive stress of concrete, $f_{ybe}$ and $f_{ube}$ are the yield and ultimate strengths of the vertical boundary element reinforcement, $f_{yv}$ and $f_{uv}$ are the yield and ultimate strengths of the vertical web reinforcement, $f_{yh}$ and $f_{uh}$ are the yield and ultimate strengths of the horizontal web reinforcement, $P$ is the axial force at the wall, $A_w$ is the wall area for walls with rectangular cross sections, $A_t$ is the total wall area for barbell and flanged walls, $V_{flex}$ is the shear corresponding to flexural strength of the wall, and $V_{peak}$ is the experimentally measured peak shear strength of the wall.

**Table A-1 Geometric properties of the walls with rectangular cross-sections**

| No. | Researcher | Specimen ID | $t_w$ (in) | $h_w$ (in) | $l_w$ (in) | $h_w / l_w$ | $M / Vl_w$ | $l_w / t_w$ | $h_{be}$ (in) |
|---|---|---|---|---|---|---|---|---|---|
| 1 | Alexander | 1 | 4.00 | 54.0 | 108.0 | 0.50 | 0.50 | 27.0 | none |
| 2 | Cardenas | SW-7 | 3.00 | 75.0 | 75.0 | 1.00 | 1.08 | 25.0 | 7.50 |
| 3 | Cardenas | SW-8 | 3.00 | 75.0 | 75.0 | 1.00 | 1.08 | 25.0 | none |
| 4 | Cardenas | SW-9 | 3.00 | 75.0 | 75.0 | 1.00 | 1.08 | 25.0 | none |
| 5 | Cardenas | SW-10 | 3.00 | 75.0 | 75.0 | 1.00 | 1.08 | 25.0 | 7.50 |
| 6 | Cardenas | SW-11 | 3.00 | 75.0 | 75.0 | 1.00 | 1.08 | 25.0 | 7.50 |
| 7 | Cardenas | SW-12 | 3.00 | 75.0 | 75.0 | 1.00 | 1.08 | 25.0 | 7.50 |
| 8 | Cardenas | SW-13 | 3.00 | 75.0 | 75.0 | 1.00 | 1.08 | 25.0 | none |
| 9 | Pilakoutas | SW4 | 2.36 | 47.2 | 23.6 | 2.00 | 2.13 | 10.0 | 4.33 |
| 10 | Pilakoutas | SW5 | 2.36 | 47.2 | 23.6 | 2.00 | 2.13 | 10.0 | 2.36 |
| 11 | Pilakoutas | SW6 | 2.36 | 47.2 | 23.6 | 2.00 | 2.13 | 10.0 | 4.33 |
| 12 | Pilakoutas | SW7 | 2.36 | 47.2 | 23.6 | 2.00 | 2.13 | 10.0 | 2.36 |
| 13 | Pilakoutas | SW8 | 2.36 | 47.2 | 23.6 | 2.00 | 2.13 | 10.0 | 4.33 |
| 14 | Pilakoutas | SW9 | 2.36 | 47.2 | 23.6 | 2.00 | 2.13 | 10.0 | 4.33 |
| 15 | Greifenhagen | M1 | 3.94 | 24.0 | 39.4 | 0.61 | 0.69 | 10.0 | none |
| 16 | Greifenhagen | M2 | 3.94 | 24.0 | 39.4 | 0.61 | 0.69 | 10.0 | none |
| 17 | Greifenhagen | M3 | 3.15 | 24.0 | 35.4 | 0.68 | 0.69 | 11.3 | none |
| 18 | Greifenhagen | M4 | 3.15 | 24.0 | 35.4 | 0.68 | 0.69 | 11.3 | none |
| 19 | Hidalgo | 1 | 4.72 | 78.7 | 39.4 | 2.00 | 1.00 | 8.3 | 3.94 |
| 20 | Hidalgo | 2 | 4.72 | 78.7 | 39.4 | 2.00 | 1.00 | 8.3 | 3.94 |
| 21 | Hidalgo | 4 | 4.72 | 78.7 | 39.4 | 2.00 | 1.00 | 8.3 | 3.94 |
| 22 | Hidalgo | 6 | 4.72 | 70.9 | 51.2 | 1.38 | 0.69 | 10.8 | 5.12 |
| 23 | Hidalgo | 7 | 4.72 | 70.9 | 51.2 | 1.38 | 0.69 | 10.8 | 5.12 |
| 24 | Hidalgo | 8 | 4.72 | 70.9 | 51.2 | 1.38 | 0.69 | 10.8 | 5.12 |
| 25 | Hidalgo | 9 | 3.94 | 70.9 | 51.2 | 1.38 | 0.69 | 13.0 | 5.12 |
| 26 | Hidalgo | 10 | 3.15 | 70.9 | 51.2 | 1.38 | 0.69 | 16.3 | 5.12 |
| 27 | Hidalgo | 11 | 3.94 | 55.1 | 55.1 | 1.00 | 0.50 | 14.0 | 5.51 |
| 28 | Hidalgo | 12 | 3.94 | 55.1 | 55.1 | 1.00 | 0.50 | 14.0 | 5.51 |
| 29 | Hidalgo | 13 | 3.94 | 55.1 | 55.1 | 1.00 | 0.50 | 14.0 | 5.51 |
| 30 | Hidalgo | 14 | 3.15 | 47.2 | 66.9 | 0.71 | 0.35 | 21.3 | 6.69 |
| 31 | Hidalgo | 15 | 3.15 | 47.2 | 66.9 | 0.71 | 0.35 | 21.3 | 6.69 |
| 32 | Hidalgo | 16 | 3.15 | 47.2 | 66.9 | 0.71 | 0.35 | 21.3 | 6.69 |
| 33 | Hidalgo | 21 | 3.94 | 70.9 | 51.2 | 1.38 | 0.69 | 13.0 | 5.12 |

**Table A-1 Geometric properties of the walls with rectangular cross-sections (cont'd)**

| No. | Researcher | Specimen ID | $t_w$ (in) | $h_w$ (in) | $l_w$ (in) | $h_w / l_w$ | $M / Vl_w$ | $l_w / t_w$ | $h_{be}$ (in) |
|---|---|---|---|---|---|---|---|---|---|
| 34 | Hidalgo | 22 | 3.94 | 70.9 | 51.2 | 1.38 | 0.69 | 13.0 | 5.12 |
| 35 | Hidalgo | 23 | 3.94 | 70.9 | 51.2 | 1.38 | 0.69 | 13.0 | 5.12 |
| 36 | Hidalgo | 24 | 3.94 | 70.9 | 51.2 | 1.38 | 0.69 | 13.0 | 5.12 |
| 37 | Hidalgo | 25 | 3.94 | 55.1 | 55.1 | 1.00 | 0.50 | 14.0 | 5.51 |
| 38 | Hidalgo | 26 | 3.94 | 55.1 | 55.1 | 1.00 | 0.50 | 14.0 | 5.51 |
| 39 | Hidalgo | 27 | 3.94 | 55.1 | 55.1 | 1.00 | 0.50 | 14.0 | 5.51 |
| 40 | Hidalgo | 28 | 3.94 | 55.1 | 55.1 | 1.00 | 0.50 | 14.0 | 5.51 |
| 41 | Hidalgo | 29 | 3.15 | 41.3 | 59.1 | 0.70 | 0.35 | 18.8 | 5.91 |
| 42 | Hidalgo | 30 | 3.15 | 41.3 | 59.1 | 0.70 | 0.35 | 18.8 | 5.91 |
| 43 | Hidalgo | 31 | 3.15 | 41.3 | 59.1 | 0.70 | 0.35 | 18.8 | 5.91 |
| 44 | Hidalgo | 32 | 3.15 | 41.3 | 59.1 | 0.70 | 0.35 | 18.8 | 5.91 |
| 45 | Hirosawa | 72 | 6.30 | 63.0 | 66.9 | 0.94 | 1.00 | 10.6 | 6.69 |
| 46 | Hirosawa | 73 | 6.30 | 63.0 | 66.9 | 0.94 | 1.00 | 10.6 | 6.69 |
| 47 | Hirosawa | 74 | 6.30 | 63.0 | 66.9 | 0.94 | 1.00 | 10.6 | 6.69 |
| 48 | Hirosawa | 75 | 6.30 | 63.0 | 66.9 | 0.94 | 1.00 | 10.6 | 6.69 |
| 49 | Hirosawa | 76 | 6.30 | 63.0 | 66.9 | 0.94 | 1.00 | 10.6 | 6.69 |
| 50 | Hirosawa | 77 | 6.30 | 63.0 | 66.9 | 0.94 | 1.00 | 10.6 | 6.69 |
| 51 | Hirosawa | 78 | 6.30 | 63.0 | 66.9 | 0.94 | 1.00 | 10.6 | 6.69 |
| 52 | Hirosawa | 79 | 6.30 | 63.0 | 66.9 | 0.94 | 1.00 | 10.6 | 6.69 |
| 53 | Hirosawa | 80 | 6.30 | 63.0 | 66.9 | 0.94 | 1.00 | 10.6 | 6.69 |
| 54 | Hirosawa | 81 | 6.30 | 63.0 | 66.9 | 0.94 | 1.00 | 10.6 | 6.69 |
| 55 | Hirosawa | 82 | 6.30 | 63.0 | 33.5 | 1.88 | 2.00 | 5.3 | 3.35 |
| 56 | Hirosawa | 83 | 6.30 | 63.0 | 33.5 | 1.88 | 2.00 | 5.3 | 3.35 |
| 57 | Hirosawa | 84 | 6.30 | 63.0 | 33.5 | 1.88 | 2.00 | 5.3 | 3.35 |
| 58 | Hirosawa | 85 | 6.30 | 63.0 | 33.5 | 1.88 | 2.00 | 5.3 | 3.35 |
| 59 | Lefas | SW11 | 2.76 | 29.5 | 29.5 | 1.00 | 1.10 | 10.7 | 5.51 |
| 60 | Lefas | SW12 | 2.76 | 29.5 | 29.5 | 1.00 | 1.10 | 10.7 | 5.51 |
| 61 | Lefas | SW13 | 2.76 | 29.5 | 29.5 | 1.00 | 1.10 | 10.7 | 5.51 |
| 62 | Lefas | SW14 | 2.76 | 29.5 | 29.5 | 1.00 | 1.10 | 10.7 | 5.51 |
| 63 | Lefas | SW15 | 2.76 | 29.5 | 29.5 | 1.00 | 1.10 | 10.7 | 5.51 |
| 64 | Lefas | SW16 | 2.76 | 29.5 | 29.5 | 1.00 | 1.10 | 10.7 | 5.51 |
| 65 | Lefas | SW17 | 2.76 | 29.5 | 29.5 | 1.00 | 1.10 | 10.7 | 5.51 |
| 66 | Lefas | SW21 | 2.56 | 51.2 | 25.6 | 2.00 | 2.12 | 10.0 | 5.51 |

**Table A-1 Geometric properties of the walls with rectangular cross-sections (cont'd)**

| No. | Researcher | Specimen ID | $t_w$ (in) | $h_w$ (in) | $l_w$ (in) | $h_w / l_w$ | $M / Vl_w$ | $l_w / t_w$ | $h_{be}$ (in) |
|---|---|---|---|---|---|---|---|---|---|
| 67 | Lefas | SW22 | 2.56 | 51.2 | 25.6 | 2.00 | 2.12 | 10.0 | 5.51 |
| 68 | Lefas | SW23 | 2.56 | 51.2 | 25.6 | 2.00 | 2.12 | 10.0 | 5.51 |
| 69 | Lefas | SW24 | 2.56 | 51.2 | 25.6 | 2.00 | 2.12 | 10.0 | 5.51 |
| 70 | Lefas | SW26 | 2.56 | 51.2 | 25.6 | 2.00 | 2.12 | 10.0 | 5.51 |
| 71 | Lefas | SW30 | 2.56 | 51.2 | 25.6 | 2.00 | 2.12 | 10.0 | 5.51 |
| 72 | Lefas | SW31 | 2.56 | 51.2 | 25.6 | 2.00 | 2.12 | 10.0 | 5.51 |
| 73 | Lefas | SW32 | 2.56 | 51.2 | 25.6 | 2.00 | 2.12 | 10.0 | 5.51 |
| 74 | Lefas | SW33 | 2.56 | 51.2 | 25.6 | 2.00 | 2.12 | 10.0 | 5.51 |
| 75 | Maier | S4 | 3.94 | 47.2 | 46.5 | 1.02 | 1.12 | 11.8 | none |
| 76 | Maier | S9 | 3.94 | 47.2 | 46.5 | 1.02 | 1.12 | 11.8 | none |
| 77 | Rothe | T01 | 3.15 | 43.3 | 31.5 | 1.38 | 1.50 | 10.0 | 5.91 |
| 78 | Rothe | T04 | 3.15 | 43.3 | 31.5 | 1.38 | 1.50 | 10.0 | 5.91 |
| 79 | Rothe | T05 | 3.15 | 43.3 | 31.5 | 1.38 | 1.50 | 10.0 | 5.91 |
| 80 | Rothe | T10 | 3.15 | 43.3 | 31.5 | 1.38 | 1.50 | 10.0 | 5.91 |
| 81 | Rothe | T11 | 3.15 | 43.3 | 31.5 | 1.38 | 1.50 | 10.0 | 5.91 |
| 82 | Wiradinata | Wall-1 | 3.94 | 39.4 | 78.7 | 0.50 | 0.58 | 20.0 | 12.60 |
| 83 | Wiradinata | Wall-2 | 3.94 | 19.7 | 78.7 | 0.25 | 0.33 | 20.0 | 12.60 |
| 84 | Pilette | Wall-4 | 3.94 | 39.4 | 78.7 | 0.50 | 0.58 | 20.0 | 12.60 |
| 85 | Pilette | Wall-5 | 3.94 | 39.4 | 78.7 | 0.50 | 0.58 | 20.0 | 9.84 |
| 86 | M.-Doostdar | Wall-7 | 3.94 | 59.1 | 78.7 | 0.75 | 0.82 | 20.0 | 12.60 |
| 87 | M.-Doostdar | Wall-8 | 3.94 | 59.1 | 59.1 | 1.00 | 1.09 | 15.0 | 14.17 |
| 88 | Salonikios | MSW1 | 3.94 | 70.9 | 47.2 | 1.50 | 1.60 | 12.0 | 9.45 |
| 89 | Salonikios | MSW3 | 3.94 | 70.9 | 47.2 | 1.50 | 1.60 | 12.0 | 9.45 |
| 90 | Salonikios | MSW6 | 3.94 | 70.9 | 47.2 | 1.50 | 1.60 | 12.0 | 9.45 |
| 91 | Salonikios | LSW1 | 3.94 | 47.2 | 47.2 | 1.00 | 1.10 | 12.0 | 9.45 |
| 92 | Salonikios | LSW2 | 3.94 | 47.2 | 47.2 | 1.00 | 1.10 | 12.0 | 9.45 |
| 93 | Salonikios | LSW3 | 3.94 | 47.2 | 47.2 | 1.00 | 1.10 | 12.0 | 9.45 |
| 94 | Sheu | SWN-1B | 3.94 | 19.7 | 39.4 | 0.50 | 0.65 | 10.0 | none |
| 95 | Sheu | SWN-5B | 3.94 | 29.5 | 39.4 | 0.75 | 0.90 | 10.0 | none |
| 96 | Sheu | SWN-1D | 3.94 | 19.7 | 39.4 | 0.50 | 0.65 | 10.0 | none |
| 97 | Sheu | SWN-5D | 3.94 | 29.5 | 39.4 | 0.75 | 0.90 | 10.0 | none |
| 98 | Sheu | SW-0E | 3.94 | 19.7 | 39.4 | 0.50 | 0.65 | 10.0 | none |
| 99 | Sheu | SW-1E | 3.94 | 19.7 | 39.4 | 0.50 | 0.65 | 10.0 | none |

**Table A-1 Geometric properties of the walls with rectangular cross-sections (cont'd)**

| No. | Researcher | Specimen ID | $t_w$ (in) | $h_w$ (in) | $l_w$ (in) | $h_w / l_w$ | $M / Vl_w$ | $l_w / t_w$ | $h_{be}$ (in) |
|---|---|---|---|---|---|---|---|---|---|
| 100 | Sheu | SW-9E | 3.94 | 29.5 | 39.4 | 0.75 | 0.90 | 10.0 | none |
| 101 | Sheu | SW-1 | 3.94 | 19.7 | 39.4 | 0.50 | 0.65 | 10.0 | none |
| 102 | Sheu | SW-1A | 3.94 | 19.7 | 39.4 | 0.50 | 0.65 | 10.0 | none |
| 103 | Sheu | SW-2 | 3.94 | 19.7 | 39.4 | 0.50 | 0.65 | 10.0 | none |
| 104 | Sheu | SW-3 | 3.94 | 19.7 | 39.4 | 0.50 | 0.65 | 10.0 | none |
| 105 | Sheu | SW-4 | 3.94 | 19.7 | 39.4 | 0.50 | 0.65 | 10.0 | none |
| 106 | Sheu | SW-4A | 3.94 | 19.7 | 39.4 | 0.50 | 0.65 | 10.0 | none |
| 107 | Sheu | SW-5 | 3.94 | 19.7 | 39.4 | 0.50 | 0.65 | 10.0 | none |
| 108 | Sheu | SW-6 | 3.94 | 19.7 | 39.4 | 0.50 | 0.65 | 10.0 | none |
| 109 | Sheu | SW9 | 3.94 | 19.7 | 39.4 | 0.50 | 0.65 | 10.0 | none |
| 110 | Sheu | SW10 | 3.94 | 19.7 | 39.4 | 0.50 | 0.65 | 10.0 | none |
| 111 | Sheu | SW11 | 3.94 | 19.7 | 39.4 | 0.50 | 0.65 | 10.0 | none |
| 112 | Sheu | SW12 | 3.94 | 19.7 | 39.4 | 0.50 | 0.65 | 10.0 | none |
| 113 | Sheu | SW13 | 3.94 | 19.7 | 39.4 | 0.50 | 0.65 | 10.0 | none |
| 114 | Sheu | SW14 | 3.94 | 19.7 | 39.4 | 0.50 | 0.65 | 10.0 | none |
| 115 | Sheu | SW15 | 3.94 | 29.5 | 39.4 | 0.75 | 0.90 | 10.0 | none |
| 116 | Sheu | SW16 | 3.94 | 29.5 | 39.4 | 0.75 | 0.90 | 10.0 | none |
| 117 | Sheu | SW17 | 3.94 | 29.5 | 39.4 | 0.75 | 0.90 | 10.0 | none |
| 118 | Sheu | SW18 | 3.94 | 29.5 | 39.4 | 0.75 | 0.90 | 10.0 | none |
| 119 | Sheu | SW19 | 3.94 | 29.5 | 39.4 | 0.75 | 0.90 | 10.0 | none |
| 120 | Sheu | SW20 | 3.94 | 29.5 | 39.4 | 0.75 | 0.90 | 10.0 | none |
| 121 | Synge | Wall-1 | 3.94 | 59.1 | 118.1 | 0.50 | 0.57 | 30.0 | 9.45 |
| 122 | Xie | W-1A | 6.00 | 48.0 | 96.0 | 0.50 | 0.59 | 16.0 | none |
| 123 | Yoshizaki | 165 | 2.36 | 31.5 | 31.5 | 1.00 | 1.08 | 13.3 | 3.15 |
| 124 | Yoshizaki | 166 | 2.36 | 31.5 | 31.5 | 1.00 | 1.08 | 13.3 | 3.15 |
| 125 | Yoshizaki | 167 | 2.36 | 31.5 | 31.5 | 1.00 | 1.08 | 13.3 | 3.15 |
| 126 | Yoshizaki | 168 | 2.36 | 31.5 | 31.5 | 1.00 | 1.08 | 13.3 | 3.15 |
| 127 | Yoshizaki | 169 | 2.36 | 31.5 | 31.5 | 1.00 | 1.08 | 13.3 | 3.15 |
| 128 | Yoshizaki | 170 | 2.36 | 31.5 | 47.2 | 0.67 | 0.72 | 20.0 | 4.72 |
| 129 | Yoshizaki | 171 | 2.36 | 31.5 | 47.2 | 0.67 | 0.72 | 20.0 | 4.72 |
| 130 | Yoshizaki | 172 | 2.36 | 31.5 | 47.2 | 0.67 | 0.72 | 20.0 | 4.72 |
| 131 | Yoshizaki | 173 | 2.36 | 31.5 | 47.2 | 0.67 | 0.72 | 20.0 | 4.72 |
| 132 | Yoshizaki | 174 | 2.36 | 31.5 | 47.2 | 0.67 | 0.72 | 20.0 | 4.72 |

**Table A-1 Geometric properties of the walls with rectangular cross-sections (cont'd)**

| No. | Researcher | Specimen ID | $t_w$ (in) | $h_w$ (in) | $l_w$ (in) | $h_w / l_w$ | $M / Vl_w$ | $l_w / t_w$ | $h_{be}$ (in) |
|---|---|---|---|---|---|---|---|---|---|
| 133 | Yoshizaki | 175 | 2.36 | 31.5 | 63.0 | 0.50 | 0.54 | 26.7 | 6.30 |
| 134 | Yoshizaki | 176 | 2.36 | 31.5 | 63.0 | 0.50 | 0.54 | 26.7 | 6.30 |
| 135 | Yoshizaki | 177 | 2.36 | 31.5 | 63.0 | 0.50 | 0.54 | 26.7 | 6.30 |
| 136 | Yoshizaki | 178 | 2.36 | 31.5 | 63.0 | 0.50 | 0.54 | 26.7 | 6.30 |
| 137 | Yoshizaki | 179 | 2.36 | 31.5 | 63.0 | 0.50 | 0.54 | 26.7 | 6.30 |
| 138 | Massone | wp111-9 | 6.00 | 48.0 | 54.0 | 0.89 | 0.44 | 9.0 | 7.50 |
| 139 | Massone | wp111-10 | 6.00 | 48.0 | 54.0 | 0.89 | 0.44 | 9.0 | 7.50 |
| 140 | Massone | wp1105-8 | 6.00 | 48.0 | 54.0 | 0.89 | 0.44 | 9.0 | 7.50 |
| 141 | Massone | wp1105-7 | 6.00 | 48.0 | 54.0 | 0.89 | 0.44 | 9.0 | 7.50 |
| 142 | Massone | wp110-5 | 6.00 | 48.0 | 54.0 | 0.89 | 0.44 | 9.0 | 7.50 |
| 143 | Massone | wp110-6 | 6.00 | 48.0 | 54.0 | 0.89 | 0.44 | 9.0 | 7.50 |
| 144 | Kuang | U1.0 | 3.94 | 47.2 | 47.2 | 1.00 | 1.13 | 12.0 | none |
| 145 | Kuang | U1.5 | 3.94 | 70.9 | 47.2 | 1.50 | 1.63 | 12.0 | none |
| 146 | Kuang | C1.0 | 3.94 | 47.2 | 47.2 | 1.00 | 1.13 | 12.0 | 9.84 |
| 147 | Kuang | C1.5 | 3.94 | 70.9 | 47.2 | 1.50 | 1.63 | 12.0 | 9.84 |
| 148 | Kuang | U1.0-BC | 3.94 | 47.2 | 47.2 | 1.00 | 1.13 | 12.0 | 11.81 |
| 149 | Kuang | U1.5-BC | 3.94 | 70.9 | 47.2 | 1.50 | 1.63 | 12.0 | 11.81 |
| 150 | Kuang | U1.0-BC2 | 3.94 | 47.2 | 47.2 | 1.00 | 1.13 | 12.0 | 11.81 |

**Table A-2 Reinforcement information for the walls with rectangular cross-sections**

| No. | Researcher | Specimen ID | $\rho_{be}$ (%) | $\rho_v$ (%) | $\rho_{vall}$ (%) | $\rho_h$ (%) | NoC-HR | NoC-VR | $s_h$ (in) | $s_v$ (in) |
|---|---|---|---|---|---|---|---|---|---|---|
| 1 | Alexander | 1 | 0.00 | 0.30 | 0.30 | 0.30 | 1 | 1 | 4.5 | 4.5 |
| 2 | Cardenas | SW-7 | 8.19 | 0.85 | 2.32 | 0.27 | 1 | 1 | 5.0 | 10.0 |
| 3 | Cardenas | SW-8 | 0.00 | 2.87 | 2.87 | 0.27 | 1 | 1 | 5.0 | 3.5 |
| 4 | Cardenas | SW-9 | 0.00 | 2.87 | 2.87 | 0.93 | 1 | 1 | 3.8 | 3.5 |
| 5 | Cardenas | SW-10 | 8.19 | 0.00 | 1.64 | 0.00 | none | none | none | none |
| 6 | Cardenas | SW-11 | 11.79 | 0.00 | 2.36 | 0.69 | 1 | none | 5.0 | none |
| 7 | Cardenas | SW-12 | 11.79 | 0.00 | 2.36 | 0.93 | 1 | none | 3.8 | none |
| 8 | Cardenas | SW-13 | 0.00 | 2.87 | 2.87 | 0.93 | 1 | 1 | 3.8 | 3.5 |
| 9 | Pilakoutas | SW4 | 6.86 | 0.50 | 2.83 | 0.39 | 2 | 2 | 9.4 | 5.5 |
| 10 | Pilakoutas | SW5 | 12.75 | 0.59 | 3.02 | 0.31 | 2 | 2 | 4.7 | 4.7 |
| 11 | Pilakoutas | SW6 | 6.86 | 0.50 | 2.83 | 0.31 | 2 | 2 | 4.7 | 5.5 |
| 12 | Pilakoutas | SW7 | 12.75 | 0.59 | 3.02 | 0.39 | 2 | 2 | 9.4 | 4.7 |
| 13 | Pilakoutas | SW8 | 7.14 | 0.50 | 2.93 | 0.28 | 2 | 2 | 3.9 | 5.5 |
| 14 | Pilakoutas | SW9 | 7.14 | 0.50 | 2.93 | 0.56 | 2 | 2 | 2.8 | 5.5 |
| 15 | Greifenhagen | M1 | 0.00 | 0.34 | 0.34 | 0.37 | 2 | 2 | 7.9 | 7.5 |
| 16 | Greifenhagen | M2 | 0.00 | 0.34 | 0.34 | 0.00 | none | 2 | none | 7.5 |
| 17 | Greifenhagen | M3 | 0.00 | 0.39 | 0.39 | 0.26 | 2 | 2 | 4.8 | 8.6 |
| 18 | Greifenhagen | M4 | 0.00 | 0.39 | 0.39 | 0.26 | 2 | 2 | 4.8 | 8.6 |
| 19 | Hidalgo | 1 | 8.50 | 0.25 | 1.90 | 0.13 | 1 | 1 | NR | NR |
| 20 | Hidalgo | 2 | 8.50 | 0.25 | 1.90 | 0.25 | 1 | 1 | NR | NR |
| 21 | Hidalgo | 4 | 10.58 | 0.25 | 2.32 | 0.38 | 1 | 1 | NR | NR |
| 22 | Hidalgo | 6 | 6.54 | 0.26 | 1.51 | 0.13 | 1 | 1 | NR | NR |
| 23 | Hidalgo | 7 | 6.54 | 0.13 | 1.41 | 0.25 | 1 | 1 | NR | NR |
| 24 | Hidalgo | 8 | 6.54 | 0.26 | 1.51 | 0.25 | 1 | 1 | NR | NR |
| 25 | Hidalgo | 9 | 7.00 | 0.26 | 1.60 | 0.26 | 1 | 1 | NR | NR |
| 26 | Hidalgo | 10 | 7.31 | 0.25 | 1.66 | 0.25 | 1 | 1 | NR | NR |
| 27 | Hidalgo | 11 | 5.71 | 0.26 | 1.35 | 0.13 | 1 | 1 | NR | NR |
| 28 | Hidalgo | 12 | 5.71 | 0.13 | 1.24 | 0.26 | 1 | 1 | NR | NR |
| 29 | Hidalgo | 13 | 5.71 | 0.26 | 1.35 | 0.26 | 1 | 1 | NR | NR |
| 30 | Hidalgo | 14 | 4.41 | 0.25 | 1.08 | 0.13 | 1 | 1 | NR | NR |
| 31 | Hidalgo | 15 | 4.41 | 0.13 | 0.98 | 0.26 | 1 | 1 | NR | NR |
| 32 | Hidalgo | 16 | 4.41 | 0.25 | 1.08 | 0.25 | 1 | 1 | NR | NR |
| 33 | Hidalgo | 21 | 4.62 | 0.00 | 0.92 | 0.00 | none | none | none | none |

**Table A-2 Reinforcement information for the walls with rectangular cross-sections (cont'd)**

| No. | Researcher | Specimen ID | $\rho_{be}$ (%) | $\rho_v$ (%) | $\rho_{vall}$ (%) | $\rho_h$ (%) | NoC-HR | NoC-VR | $s_h$ (in) | $s_v$ (in) |
|---|---|---|---|---|---|---|---|---|---|---|
| 34 | Hidalgo | 22 | 4.62 | 0.00 | 0.92 | 0.00 | none | none | none | none |
| 35 | Hidalgo | 23 | 8.54 | 0.00 | 1.71 | 0.25 | 1 | none | NR | N/A |
| 36 | Hidalgo | 24 | 4.62 | 0.25 | 1.12 | 0.00 | none | 1 | none | NR |
| 37 | Hidalgo | 25 | 4.29 | 0.00 | 0.86 | 0.00 | none | none | none | none |
| 38 | Hidalgo | 26 | 4.29 | 0.00 | 0.86 | 0.00 | none | none | none | none |
| 39 | Hidalgo | 27 | 6.50 | 0.00 | 1.30 | 0.25 | 1 | none | NR | none |
| 40 | Hidalgo | 28 | 4.29 | 0.25 | 1.06 | 0.00 | none | 1 | none | NR |
| 41 | Hidalgo | 29 | 5.00 | 0.00 | 1.00 | 0.00 | none | none | none | none |
| 42 | Hidalgo | 30 | 5.00 | 0.00 | 1.00 | 0.00 | none | none | none | none |
| 43 | Hidalgo | 31 | 6.67 | 0.00 | 1.33 | 0.25 | 1 | none | NR | none |
| 44 | Hidalgo | 32 | 5.00 | 0.25 | 1.20 | 0.00 | none | 1 | none | NR |
| 45 | Hirosawa | 72 | 5.68 | 0.51 | 1.54 | 0.26 | 2 | 2 | 5.2 | 5.2 |
| 46 | Hirosawa | 73 | 5.68 | 0.51 | 1.54 | 0.26 | 2 | 2 | 5.2 | 5.2 |
| 47 | Hirosawa | 74 | 5.68 | 0.51 | 1.54 | 0.57 | 2 | 2 | 2.6 | 5.2 |
| 48 | Hirosawa | 75 | 5.68 | 0.51 | 1.54 | 0.57 | 2 | 2 | 2.6 | 5.2 |
| 49 | Hirosawa | 76 | 5.68 | 0.51 | 1.54 | 1.08 | 2 | 2 | 1.3 | 5.2 |
| 50 | Hirosawa | 77 | 5.68 | 0.51 | 1.54 | 1.08 | 2 | 2 | 1.3 | 5.2 |
| 51 | Hirosawa | 78 | 2.51 | 0.51 | 0.91 | 0.61 | 2 | 2 | 2.6 | 5.2 |
| 52 | Hirosawa | 79 | 2.51 | 0.51 | 0.91 | 0.61 | 2 | 2 | 2.6 | 5.2 |
| 53 | Hirosawa | 80 | 2.51 | 0.51 | 0.91 | 1.08 | 2 | 2 | 1.3 | 5.2 |
| 54 | Hirosawa | 81 | 2.51 | 0.51 | 0.91 | 1.08 | 2 | 2 | 1.3 | 5.2 |
| 55 | Hirosawa | 82 | 9.91 | 0.40 | 2.31 | 0.57 | 2 | 2 | 2.6 | 5.2 |
| 56 | Hirosawa | 83 | 9.91 | 0.40 | 2.31 | 0.57 | 2 | 2 | 2.6 | 5.2 |
| 57 | Hirosawa | 84 | 8.44 | 0.40 | 2.01 | 1.08 | 2 | 2 | 1.3 | 5.2 |
| 58 | Hirosawa | 85 | 8.44 | 0.40 | 2.01 | 1.08 | 2 | 2 | 1.3 | 5.2 |
| 59 | Lefas | SW11 | 3.08 | 2.14 | 2.49 | 1.17 | 2 | 2 | 3.1 | 2.4 |
| 60 | Lefas | SW12 | 3.08 | 2.14 | 2.49 | 1.17 | 2 | 2 | 3.1 | 2.4 |
| 61 | Lefas | SW13 | 3.08 | 2.14 | 2.49 | 1.17 | 2 | 2 | 3.1 | 2.4 |
| 62 | Lefas | SW14 | 3.08 | 2.14 | 2.49 | 1.17 | 2 | 2 | 3.1 | 2.4 |
| 63 | Lefas | SW15 | 3.08 | 2.14 | 2.49 | 1.17 | 2 | 2 | 3.1 | 2.4 |
| 64 | Lefas | SW16 | 3.08 | 2.14 | 2.49 | 1.17 | 2 | 2 | 3.1 | 2.4 |
| 65 | Lefas | SW17 | 3.08 | 2.14 | 2.49 | 0.37 | 2 | 2 | 9.4 | 2.4 |

**Table A-2 Reinforcement information for the walls with rectangular cross-sections (cont'd)**

| No. | Researcher | Specimen ID | $\rho_{be}$ (%) | $\rho_v$ (%) | $\rho_{vall}$ (%) | $\rho_h$ (%) | NoC-HR | NoC-VR | $s_h$ (in) | $s_v$ (in) |
|---|---|---|---|---|---|---|---|---|---|---|
| 66 | Lefas | SW21 | 3.32 | 2.09 | 2.62 | 0.87 | 2 | 2 | 4.5 | 2.4 |
| 67 | Lefas | SW22 | 3.32 | 2.09 | 2.62 | 0.87 | 2 | 2 | 4.5 | 2.4 |
| 68 | Lefas | SW23 | 3.32 | 2.09 | 2.62 | 0.87 | 2 | 2 | 4.5 | 2.4 |
| 69 | Lefas | SW24 | 3.32 | 2.09 | 2.62 | 0.87 | 2 | 2 | 4.5 | 2.4 |
| 70 | Lefas | SW26 | 3.32 | 2.09 | 2.62 | 0.40 | 2 | 2 | 4.5 | 2.4 |
| 71 | Lefas | SW30 | 3.32 | 1.26 | 2.14 | 0.36 | 2 | 2 | 4.5 | 2.4 |
| 72 | Lefas | SW31 | 3.32 | 1.26 | 2.14 | 0.36 | 2 | 2 | 4.5 | 2.4 |
| 73 | Lefas | SW32 | 3.32 | 1.26 | 2.14 | 0.36 | 2 | 2 | 4.5 | 2.4 |
| 74 | Lefas | SW33 | 3.32 | 1.26 | 2.14 | 0.36 | 2 | 2 | 9.1 | 2.4 |
| 75 | Maier | S4 | 0.00 | 1.02 | 1.02 | 1.01 | 2 | 2 | 3.9 | 3.9 |
| 76 | Maier | S9 | 0.00 | 1.02 | 1.02 | 0.00 | none | 2 | none | 3.9 |
| 77 | Rothe | T01 | 1.41 | 0.71 | 0.97 | 0.51 | 2 | 2 | 6.2 | 4.7 |
| 78 | Rothe | T04 | 1.41 | 0.71 | 0.97 | 0.00 | none | 2 | none | 4.7 |
| 79 | Rothe | T05 | 2.51 | 0.71 | 1.38 | 0.51 | 2 | 2 | 6.2 | 4.7 |
| 80 | Rothe | T10 | 1.41 | 0.71 | 0.97 | 0.51 | 2 | 2 | 6.2 | 4.7 |
| 81 | Rothe | T11 | 1.41 | 0.71 | 0.97 | 0.51 | 2 | 2 | 6.2 | 4.7 |
| 82 | Wiradinata | Wall-1 | 1.25 | 0.59 | 0.80 | 0.26 | 2 | 2 | 11.8 | 11.2 |
| 83 | Wiradinata | Wall-2 | 1.25 | 0.59 | 0.80 | 0.26 | 2 | 2 | 11.8 | 11.2 |
| 84 | Pilette | Wall-4 | 1.25 | 0.59 | 0.80 | 0.80 | 2 | 2 | 9.8 | 11.2 |
| 85 | Pilette | Wall-5 | 1.60 | 1.07 | 1.20 | 1.20 | 2 | 2 | 6.9 | 6.9 |
| 86 | M.-Doostdar | Wall-7 | 1.25 | 0.59 | 0.80 | 0.80 | 2 | 2 | 9.8 | 11.2 |
| 87 | M.-Doostdar | Wall-8 | 1.11 | 0.51 | 0.80 | 0.80 | 2 | 2 | 9.8 | 11.2 |
| 88 | Salonikios | MSW1 | 1.70 | 0.57 | 1.02 | 0.57 | 3 | 3 | 3.9 | 3.9 |
| 89 | Salonikios | MSW3 | 1.30 | 0.28 | 0.69 | 0.28 | 2 | 2 | 3.9 | 3.9 |
| 90 | Salonikios | MSW6 | 1.70 | 0.57 | 1.02 | 0.57 | 2 | 2 | 3.9 | 3.9 |
| 91 | Salonikios | LSW1 | 1.70 | 0.57 | 1.02 | 0.57 | 3 | 3 | 3.9 | 3.9 |
| 92 | Salonikios | LSW2 | 1.30 | 0.28 | 0.69 | 0.28 | 2 | 2 | 3.9 | 3.9 |
| 93 | Salonikios | LSW3 | 1.30 | 0.28 | 0.69 | 0.28 | 2 | 2 | 3.9 | 3.9 |
| 94 | Sheu | SWN-1B | 0.00 | 0.43 | 0.43 | 0.57 | 1 | 1 | 5.9 | 7.1 |
| 95 | Sheu | SWN-5B | 0.00 | 0.43 | 0.43 | 0.57 | 1 | 1 | 5.1 | 7.1 |
| 96 | Sheu | SWN-1D | 0.00 | 0.43 | 0.43 | 0.57 | 1 | 1 | 5.9 | 7.1 |
| 97 | Sheu | SWN-5D | 0.00 | 0.43 | 0.43 | 0.57 | 1 | 1 | 5.1 | 7.1 |

**Table A-2 Reinforcement information for the walls with rectangular cross-sections (cont'd)**

| No. | Researcher | Specimen ID | $\rho_{be}$ (%) | $\rho_v$ (%) | $\rho_{vall}$ (%) | $\rho_h$ (%) | NoC-HR | NoC-VR | $s_h$ (in) | $s_v$ (in) |
|---|---|---|---|---|---|---|---|---|---|---|
| 98 | Sheu | SW-0E | 0.00 | 0.71 | 0.71 | 0.71 | 1 | 1 | 3.9 | 4.1 |
| 99 | Sheu | SW-1E | 0.00 | 0.71 | 0.71 | 0.71 | 1 | 1 | 3.9 | 4.1 |
| 100 | Sheu | SW-9E | 0.00 | 1.27 | 1.27 | 1.18 | 1 | 1 | 4.3 | 4.1 |
| 101 | Sheu | SW-1 | 0.00 | 0.43 | 0.43 | 0.57 | 1 | 1 | 5.9 | 7.1 |
| 102 | Sheu | SW-1A | 0.00 | 0.43 | 0.43 | 0.57 | 1 | 1 | 5.9 | 7.1 |
| 103 | Sheu | SW-2 | 0.00 | 0.43 | 0.43 | 0.57 | 1 | 1 | 5.9 | 7.1 |
| 104 | Sheu | SW-3 | 0.00 | 0.43 | 0.43 | 0.57 | 1 | 1 | 5.9 | 7.1 |
| 105 | Sheu | SW-4 | 0.00 | 0.77 | 0.77 | 1.03 | 1 | 1 | 5.9 | 7.1 |
| 106 | Sheu | SW-4A | 0.00 | 0.77 | 0.77 | 1.03 | 1 | 1 | 5.9 | 7.1 |
| 107 | Sheu | SW-5 | 0.00 | 0.77 | 0.77 | 1.03 | 1 | 1 | 5.9 | 7.1 |
| 108 | Sheu | SW-6 | 0.00 | 0.77 | 0.77 | 1.03 | 1 | 1 | 5.9 | 7.1 |
| 109 | Sheu | SW9 | 0.00 | 0.79 | 0.79 | 0.57 | 1 | 1 | 5.3 | 8.9 |
| 110 | Sheu | SW10 | 0.00 | 0.76 | 0.76 | 0.57 | 1 | 1 | 5.3 | 7.1 |
| 111 | Sheu | SW11 | 0.00 | 0.79 | 0.79 | 0.57 | 1 | 1 | 5.3 | 8.9 |
| 112 | Sheu | SW12 | 0.00 | 0.78 | 0.78 | 0.57 | 1 | 1 | 5.3 | 8.9 |
| 113 | Sheu | SW13 | 0.00 | 0.76 | 0.76 | 0.00 | none | 1 | none | 7.1 |
| 114 | Sheu | SW14 | 0.00 | 0.76 | 0.76 | 1.14 | 1 | 1 | 2.3 | 7.1 |
| 115 | Sheu | SW15 | 0.00 | 0.79 | 0.79 | 0.57 | 1 | 1 | 5.1 | 8.9 |
| 116 | Sheu | SW16 | 0.00 | 0.76 | 0.76 | 0.57 | 1 | 1 | 5.1 | 7.1 |
| 117 | Sheu | SW17 | 0.00 | 0.79 | 0.79 | 0.57 | 1 | 1 | 5.1 | 8.9 |
| 118 | Sheu | SW18 | 0.00 | 0.78 | 0.78 | 0.57 | 1 | 1 | 5.1 | 8.9 |
| 119 | Sheu | SW19 | 0.00 | 0.76 | 0.76 | 0.00 | none | 1 | none | 7.1 |
| 120 | Sheu | SW20 | 0.00 | 0.76 | 0.76 | 0.57 | 1 | 1 | 5.1 | 7.1 |
| 121 | Synge | Wall-1 | 1.89 | 0.81 | 0.98 | 1.61 | 1 | 1 | 4.7 | 5.5 |
| 122 | Xie | W-1A | 0.00 | 0.37 | 0.37 | 0.31 | 2 | 2 | 13.5 | 13.5 |
| 123 | Yoshizaki | 165 | 5.29 | 0.22 | 1.23 | 0.23 | 1 | 1 | 9.4 | 9.4 |
| 124 | Yoshizaki | 166 | 5.88 | 0.73 | 1.76 | 0.82 | 1 | 1 | 2.4 | 2.4 |
| 125 | Yoshizaki | 167 | 8.29 | 0.44 | 2.01 | 0.41 | 1 | 1 | 4.7 | 4.7 |
| 126 | Yoshizaki | 168 | 8.88 | 0.73 | 2.36 | 0.82 | 1 | 1 | 2.4 | 2.4 |
| 127 | Yoshizaki | 169 | 8.88 | 1.17 | 2.71 | 1.17 | 1 | 1 | 1.6 | 1.6 |
| 128 | Yoshizaki | 170 | 3.53 | 0.24 | 0.90 | 0.23 | 1 | 1 | 9.4 | 9.4 |
| 129 | Yoshizaki | 171 | 3.92 | 0.78 | 1.41 | 0.82 | 1 | 1 | 2.4 | 2.4 |

**Table A-2 Reinforcement information for the walls with rectangular cross-sections (cont'd)**

| No. | Researcher | Specimen ID | $\rho_{be}$ (%) | $\rho_v$ (%) | $\rho_{vall}$ (%) | $\rho_h$ (%) | NoC-HR | NoC-VR | $s_h$ (in) | $s_v$ (in) |
|---|---|---|---|---|---|---|---|---|---|---|
| 130 | Yoshizaki | 172 | 5.53 | 0.44 | 1.46 | 0.41 | 1 | 1 | 4.7 | 4.7 |
| 131 | Yoshizaki | 173 | 5.92 | 0.78 | 1.81 | 0.82 | 1 | 1 | 2.4 | 2.4 |
| 132 | Yoshizaki | 174 | 5.92 | 1.17 | 2.12 | 1.17 | 1 | 1 | 1.6 | 1.6 |
| 133 | Yoshizaki | 175 | 2.65 | 0.22 | 0.70 | 0.23 | 1 | 1 | 9.4 | 9.4 |
| 134 | Yoshizaki | 176 | 2.94 | 0.80 | 1.23 | 0.82 | 1 | 1 | 2.4 | 2.4 |
| 135 | Yoshizaki | 177 | 4.44 | 0.37 | 1.18 | 0.41 | 1 | 1 | 4.7 | 4.7 |
| 136 | Yoshizaki | 178 | 4.44 | 0.80 | 1.53 | 0.82 | 1 | 1 | 2.4 | 2.4 |
| 137 | Yoshizaki | 179 | 4.73 | 1.17 | 1.88 | 1.17 | 1 | 1 | 1.6 | 1.6 |
| 138 | Massone | wp111-9 | 0.87 | 0.25 | 0.42 | 0.27 | 1 | 1 | 12.0 | 13.0 |
| 139 | Massone | wp111-10 | 0.87 | 0.25 | 0.42 | 0.27 | 1 | 1 | 12.0 | 13.0 |
| 140 | Massone | wp1105-8 | 0.87 | 0.25 | 0.42 | 0.27 | 1 | 1 | 12.0 | 13.0 |
| 141 | Massone | wp1105-7 | 0.87 | 0.25 | 0.42 | 0.27 | 1 | 1 | 12.0 | 13.0 |
| 142 | Massone | wp110-5 | 0.87 | 0.25 | 0.42 | 0.27 | 1 | 1 | 12.0 | 13.0 |
| 143 | Massone | wp110-6 | 0.87 | 0.25 | 0.42 | 0.27 | 1 | 1 | 12.0 | 13.0 |
| 144 | Kuang | U1.0 | 0.00 | 0.92 | 0.92 | 1.05 | 2 | 2 | 5.9 | 7.1 |
| 145 | Kuang | U1.5 | 0.00 | 0.92 | 0.92 | 1.05 | 2 | 2 | 5.9 | 7.1 |
| 146 | Kuang | C1.0 | 1.89 | 0.45 | 1.05 | 1.05 | 2 | 2 | 5.9 | 11.8 |
| 147 | Kuang | C1.5 | 1.89 | 0.45 | 1.05 | 1.05 | 2 | 2 | 5.9 | 11.8 |
| 148 | Kuang | U1.0-BC | 1.05 | 0.79 | 0.92 | 1.05 | 2 | 2 | 5.9 | 7.1 |
| 149 | Kuang | U1.5-BC | 1.05 | 0.79 | 0.92 | 1.05 | 2 | 2 | 5.9 | 7.1 |
| 150 | Kuang | U1.0-BC2 | 1.05 | 0.79 | 0.92 | 1.05 | 2 | 2 | 5.9 | 7.1 |

**Table A-3 Material properties of the walls with rectangular cross-sections**

| No. | Researcher | Specimen ID | $f_c'$ (psi) | $f_{ybe}$ (ksi) | $f_{ube}$ (ksi) | $f_{yv}$ (ksi) | $f_{uv}$ (ksi) | $f_{yh}$ (ksi) | $f_{uh}$ (ksi) |
|---|---|---|---|---|---|---|---|---|---|
| 1 | Alexander | 1 | 3000 | N/A | NR | 52.0 | NR | 52.0 | NR |
| 2 | Cardenas | SW-7 | 6240 | 65.0 | NR | 65.0 | NR | 60.0 | NR |
| 3 | Cardenas | SW-8 | 6160 | N/A | NR | 65.0 | NR | 67.5 | NR |
| 4 | Cardenas | SW-9 | 6240 | N/A | NR | 65.0 | NR | 60.0 | NR |
| 5 | Cardenas | SW-10 | 5850 | 65.0 | NR | N/A | NR | N/A | NR |
| 6 | Cardenas | SW-11 | 5540 | 65.0 | NR | N/A | NR | 65.0 | NR |
| 7 | Cardenas | SW-12 | 5570 | 65.0 | NR | N/A | NR | 65.0 | NR |
| 8 | Cardenas | SW-13 | 6300 | N/A | NR | 65.0 | NR | 66.0 | NR |
| 9 | Pilakoutas | SW4 | 5352 | 72.5 | 94.3 | 79.8 | 84.8 | 79.8 | 84.8 |
| 10 | Pilakoutas | SW5 | 4612 | 78.3 | 85.6 | 79.8 | 84.8 | 58.0 | 65.3 |
| 11 | Pilakoutas | SW6 | 5599 | 72.5 | 94.3 | 79.8 | 84.8 | 58.0 | 65.3 |
| 12 | Pilakoutas | SW7 | 4641 | 78.3 | 85.6 | 79.8 | 84.8 | 79.8 | 84.8 |
| 13 | Pilakoutas | SW8 | 6643 | 78.3 | 94.3 | 79.8 | 84.8 | 58.0 | 65.3 |
| 14 | Pilakoutas | SW9 | 5642 | 78.3 | 94.3 | 79.8 | 84.8 | 58.0 | 65.3 |
| 15 | Greifenhagen | M1 | 7352 | N/A | N/A | 73.1 | 92.0 | 73.1 | 92.0 |
| 16 | Greifenhagen | M2 | 7395 | N/A | N/A | 73.1 | 92.0 | N/A | N/A |
| 17 | Greifenhagen | M3 | 2915 | N/A | N/A | 73.1 | 92.0 | 108.1 | 116.0 |
| 18 | Greifenhagen | M4 | 3538 | N/A | N/A | 73.1 | 92.0 | 108.1 | 116.0 |
| 19 | Hidalgo | 1 | 2915 | 59.2 | NR | 59.2 | NR | 59.2 | NR |
| 20 | Hidalgo | 2 | 2959 | 60.6 | NR | 60.6 | NR | 60.6 | NR |
| 21 | Hidalgo | 4 | 2944 | 60.6 | NR | 60.6 | NR | 60.6 | NR |
| 22 | Hidalgo | 6 | 2654 | 47.3 | NR | 47.3 | NR | 47.3 | NR |
| 23 | Hidalgo | 7 | 2741 | 71.1 | NR | 71.1 | NR | 71.1 | NR |
| 24 | Hidalgo | 8 | 2364 | 71.1 | NR | 71.1 | NR | 71.1 | NR |
| 25 | Hidalgo | 9 | 2654 | 55.3 | NR | 55.3 | NR | 55.3 | NR |
| 26 | Hidalgo | 10 | 2466 | 55.4 | NR | 55.4 | NR | 55.4 | NR |
| 27 | Hidalgo | 11 | 2451 | 54.7 | NR | 54.7 | NR | 54.7 | NR |
| 28 | Hidalgo | 12 | 2567 | 55.3 | NR | 55.3 | NR | 55.3 | NR |
| 29 | Hidalgo | 13 | 2741 | 55.8 | NR | 55.8 | NR | 55.8 | NR |
| 30 | Hidalgo | 14 | 2582 | 55.3 | NR | 55.3 | NR | 55.3 | NR |
| 31 | Hidalgo | 15 | 2872 | 55.3 | NR | 55.3 | NR | 55.3 | NR |
| 32 | Hidalgo | 16 | 2843 | 55.3 | NR | 55.3 | NR | 55.3 | NR |
| 33 | Hidalgo | 21 | 3655 | 65.0 | NR | N/A | NR | N/A | NR |

**Table A-3 Material properties of the walls with rectangular cross-sections (cont'd)**

| No. | Researcher | Specimen ID | $f'_c$ (psi) | $f_{ybe}$ (ksi) | $f_{ube}$ (ksi) | $f_{yv}$ (ksi) | $f_{uv}$ (ksi) | $f_{yh}$ (ksi) | $f_{uh}$ (ksi) |
|---|---|---|---|---|---|---|---|---|---|
| 34 | Hidalgo | 22 | 2596 | 65.0 | NR | N/A | NR | N/A | NR |
| 35 | Hidalgo | 23 | 3655 | 65.0 | NR | N/A | NR | 65.0 | NR |
| 36 | Hidalgo | 24 | 3611 | 65.0 | NR | 65.0 | NR | N/A | NR |
| 37 | Hidalgo | 25 | 3611 | 65.0 | NR | N/A | NR | N/A | NR |
| 38 | Hidalgo | 26 | 2669 | 65.0 | NR | N/A | NR | N/A | NR |
| 39 | Hidalgo | 27 | 3597 | 65.0 | NR | N/A | NR | 65.0 | NR |
| 40 | Hidalgo | 28 | 3510 | 65.0 | NR | 65.0 | NR | N/A | NR |
| 41 | Hidalgo | 29 | 3495 | 65.0 | NR | N/A | NR | N/A | NR |
| 42 | Hidalgo | 30 | 2698 | 65.0 | NR | N/A | NR | N/A | NR |
| 43 | Hidalgo | 31 | 3495 | 65.0 | NR | N/A | NR | 65.0 | NR |
| 44 | Hidalgo | 32 | 3510 | 65.0 | NR | 65.0 | NR | N/A | NR |
| 45 | Hirosawa | 72 | 2503 | 54.6 | NR | 59.0 | NR | 60.8 | NR |
| 46 | Hirosawa | 73 | 3015 | 54.6 | NR | 59.0 | NR | 60.8 | NR |
| 47 | Hirosawa | 74 | 3015 | 54.6 | NR | 59.0 | NR | 61.1 | NR |
| 48 | Hirosawa | 75 | 1991 | 54.6 | NR | 59.0 | NR | 61.1 | NR |
| 49 | Hirosawa | 76 | 2133 | 54.6 | NR | 59.0 | NR | 60.2 | NR |
| 50 | Hirosawa | 77 | 2660 | 54.6 | NR | 59.0 | NR | 60.2 | NR |
| 51 | Hirosawa | 78 | 3015 | 55.4 | NR | 59.0 | NR | 61.0 | NR |
| 52 | Hirosawa | 79 | 1991 | 55.4 | NR | 59.0 | NR | 61.0 | NR |
| 53 | Hirosawa | 80 | 2133 | 55.4 | NR | 59.0 | NR | 60.2 | NR |
| 54 | Hirosawa | 81 | 2660 | 55.4 | NR | 59.0 | NR | 60.2 | NR |
| 55 | Hirosawa | 82 | 3015 | 55.2 | NR | 59.0 | NR | 61.1 | NR |
| 56 | Hirosawa | 83 | 2589 | 55.2 | NR | 59.0 | NR | 61.1 | NR |
| 57 | Hirosawa | 84 | 2589 | 54.8 | NR | 59.0 | NR | 60.2 | NR |
| 58 | Hirosawa | 85 | 3015 | 54.8 | NR | 59.0 | NR | 60.2 | NR |
| 59 | Lefas | SW11 | 7140 | 68.2 | 81.9 | 68.2 | 81.9 | 75.4 | 88.5 |
| 60 | Lefas | SW12 | 7332 | 68.2 | 81.9 | 68.2 | 81.9 | 75.4 | 88.5 |
| 61 | Lefas | SW13 | 5423 | 68.2 | 81.9 | 68.2 | 81.9 | 75.4 | 88.5 |
| 62 | Lefas | SW14 | 5642 | 68.2 | 81.9 | 68.2 | 81.9 | 75.4 | 88.5 |
| 63 | Lefas | SW15 | 5819 | 68.2 | 81.9 | 68.2 | 81.9 | 75.4 | 88.5 |
| 64 | Lefas | SW16 | 7052 | 68.2 | 81.9 | 68.2 | 81.9 | 75.4 | 88.5 |
| 65 | Lefas | SW17 | 6553 | 68.2 | 81.9 | 68.2 | 81.9 | 75.4 | 88.5 |
| 66 | Lefas | SW21 | 5745 | 68.2 | 81.9 | 68.2 | 81.9 | 75.4 | 88.5 |

**Table A-3 Material properties of the walls with rectangular cross-sections (cont'd)**

| No. | Researcher | Specimen ID | $f_c'$ (psi) | $f_{ybe}$ (ksi) | $f_{ube}$ (ksi) | $f_{yv}$ (ksi) | $f_{uv}$ (ksi) | $f_{yh}$ (ksi) | $f_{uh}$ (ksi) |
|---|---|---|---|---|---|---|---|---|---|
| 67 | Lefas | SW22 | 6891 | 68.2 | 81.9 | 68.2 | 81.9 | 75.4 | 88.5 |
| 68 | Lefas | SW23 | 6480 | 68.2 | 81.9 | 68.2 | 81.9 | 75.4 | 88.5 |
| 69 | Lefas | SW24 | 6553 | 68.2 | 81.9 | 68.2 | 81.9 | 75.4 | 88.5 |
| 70 | Lefas | SW26 | 3881 | 68.2 | 81.9 | 68.2 | 81.9 | 75.4 | 88.5 |
| 71 | Lefas | SW30 | 3881 | 68.2 | 81.9 | 68.2 | 81.9 | 75.4 | 88.5 |
| 72 | Lefas | SW31 | 4630 | 68.2 | 81.9 | 68.2 | 81.9 | 75.4 | 88.5 |
| 73 | Lefas | SW32 | 7332 | 68.2 | 81.9 | 68.2 | 81.9 | 75.4 | 88.5 |
| 74 | Lefas | SW33 | 6685 | 68.2 | 81.9 | 68.2 | 81.9 | 75.4 | 88.5 |
| 75 | Maier | S4 | 4772 | N/A | N/A | 83.3 | 110.8 | 83.3 | 110.8 |
| 76 | Maier | S9 | 4235 | N/A | N/A | 81.2 | 110.5 | N/A | N/A |
| 77 | Rothe | T01 | 3526 | 60.9 | 72.5 | 60.9 | 72.5 | 60.9 | 72.5 |
| 78 | Rothe | T04 | 4177 | 60.9 | 72.5 | 60.9 | 72.5 | N/A | 72.5 |
| 79 | Rothe | T05 | 3510 | 60.9 | 72.5 | 60.9 | 72.5 | 60.9 | 72.5 |
| 80 | Rothe | T10 | 4869 | 72.5 | 79.8 | 72.5 | 79.8 | 72.5 | 79.8 |
| 81 | Rothe | T11 | 3896 | 72.5 | 79.8 | 72.5 | 79.8 | 72.5 | 79.8 |
| 82 | Wiradinata | Wall-1 | 3626 | 63.1 | 94.3 | 63.1 | 94.3 | 61.6 | 79.8 |
| 83 | Wiradinata | Wall-2 | 3191 | 63.1 | 94.3 | 63.1 | 94.3 | 61.6 | 79.8 |
| 84 | Pilette | Wall-4 | 4786 | 69.6 | 111.7 | 69.6 | 111.7 | 69.6 | 111.7 |
| 85 | Pilette | Wall-5 | 3916 | 69.6 | 111.7 | 69.6 | 111.7 | 69.6 | 111.7 |
| 86 | M.-Doostdar | Wall-7 | 6527 | 65.3 | 94.3 | 65.3 | 94.3 | 65.3 | 94.3 |
| 87 | M.-Doostdar | Wall-8 | 6527 | 65.3 | 94.3 | 65.3 | 94.3 | 65.3 | 94.3 |
| 88 | Salonikios | MSW1 | 3785 | 84.8 | NR | 86.7 | NR | 86.7 | NR |
| 89 | Salonikios | MSW3 | 3495 | 84.8 | NR | 88.5 | NR | 88.5 | NR |
| 90 | Salonikios | MSW6 | 3988 | 84.8 | NR | 86.7 | NR | 86.7 | NR |
| 91 | Salonikios | LSW1 | 3219 | 84.8 | NR | 86.7 | NR | 86.7 | NR |
| 92 | Salonikios | LSW2 | 3132 | 84.8 | NR | 88.5 | NR | 88.5 | NR |
| 93 | Salonikios | LSW3 | 3466 | 84.8 | NR | 88.5 | NR | 88.5 | NR |
| 94 | Sheu | SWN-1B | 3556 | N/A | N/A | 67.8 | 104.7 | 67.8 | 104.7 |
| 95 | Sheu | SWN-5B | 3627 | N/A | N/A | 67.8 | 104.7 | 67.8 | 104.7 |
| 96 | Sheu | SWN-1D | 3869 | N/A | N/A | 67.8 | 104.7 | 67.8 | 104.7 |
| 97 | Sheu | SWN-5D | 4068 | N/A | N/A | 67.8 | 104.7 | 67.8 | 104.7 |
| 98 | Sheu | SW-0E | 3613 | N/A | N/A | 71.2 | 109.9 | 71.2 | 109.9 |
| 99 | Sheu | SW-1E | 4907 | N/A | N/A | 71.2 | 109.9 | 71.2 | 109.9 |

**Table A-3 Material properties of the walls with rectangular cross-sections (cont'd)**

| No. | Researcher | Specimen ID | $f'_c$ (psi) | $f_{ybe}$ (ksi) | $f_{ube}$ (ksi) | $f_{yv}$ (ksi) | $f_{uv}$ (ksi) | $f_{yh}$ (ksi) | $f_{uh}$ (ksi) |
|---|---|---|---|---|---|---|---|---|---|
| 100 | Sheu | SW-9E | 4182 | N/A | N/A | 65.7 | 102.4 | 65.7 | 102.4 |
| 101 | Sheu | SW-1 | 3769 | N/A | N/A | 70.1 | 110.9 | 70.1 | 110.9 |
| 102 | Sheu | SW-1A | 3911 | N/A | N/A | 70.1 | 110.9 | 70.1 | 110.9 |
| 103 | Sheu | SW-2 | 3769 | N/A | N/A | 70.1 | 110.9 | 70.1 | 110.9 |
| 104 | Sheu | SW-3 | 3954 | N/A | N/A | 70.1 | 110.9 | 70.1 | 110.9 |
| 105 | Sheu | SW-4 | 3840 | N/A | N/A | 69.7 | 113.4 | 69.7 | 113.4 |
| 106 | Sheu | SW-4A | 3869 | N/A | N/A | 69.7 | 113.4 | 69.7 | 113.4 |
| 107 | Sheu | SW-5 | 3954 | N/A | N/A | 69.7 | 113.4 | 69.7 | 113.4 |
| 108 | Sheu | SW-6 | 4096 | N/A | N/A | 69.7 | 113.4 | 69.7 | 113.4 |
| 109 | Sheu | SW9 | 3776 | N/A | N/A | 62.6 | 105.6 | 67.8 | 104.7 |
| 110 | Sheu | SW10 | 3911 | N/A | N/A | 65.7 | 102.4 | 67.8 | 104.7 |
| 111 | Sheu | SW11 | 3776 | N/A | N/A | 62.6 | 105.6 | 67.8 | 104.7 |
| 112 | Sheu | SW12 | 3840 | N/A | N/A | 65.0 | 96.6 | 67.8 | 104.7 |
| 113 | Sheu | SW13 | 4694 | N/A | N/A | 65.7 | 102.4 | N/A | N/A |
| 114 | Sheu | SW14 | 4551 | N/A | N/A | 65.7 | 102.4 | 67.8 | 104.7 |
| 115 | Sheu | SW15 | 3769 | N/A | N/A | 62.6 | 105.6 | 67.8 | 104.7 |
| 116 | Sheu | SW16 | 3840 | N/A | N/A | 65.7 | 102.4 | 67.8 | 104.7 |
| 117 | Sheu | SW17 | 3769 | N/A | N/A | 62.6 | 105.6 | 67.8 | 104.7 |
| 118 | Sheu | SW18 | 3840 | N/A | N/A | 65.0 | 96.6 | 67.8 | 104.7 |
| 119 | Sheu | SW19 | 3556 | N/A | N/A | 65.7 | 102.4 | N/A | N/A |
| 120 | Sheu | SW20 | 2987 | N/A | N/A | 65.7 | 102.4 | 67.8 | 104.7 |
| 121 | Synge | Wall-1 | 3945 | 43.5 | 66.7 | 43.5 | 66.7 | 55.1 | 55.1 |
| 122 | Xie | W-1A | 4250 | N/A | N/A | 65.8 | 106.2 | 65.8 | 106.2 |
| 123 | Yoshizaki | 165 | 3414 | 48.3 | NR | 62.9 | NR | 62.9 | NR |
| 124 | Yoshizaki | 166 | 3414 | 49.7 | NR | 62.9 | NR | 62.9 | NR |
| 125 | Yoshizaki | 167 | 3414 | 49.7 | NR | 62.9 | NR | 62.9 | NR |
| 126 | Yoshizaki | 168 | 3414 | 50.1 | NR | 62.9 | NR | 62.9 | NR |
| 127 | Yoshizaki | 169 | 3414 | 50.1 | NR | 62.9 | NR | 62.9 | NR |
| 128 | Yoshizaki | 170 | 3556 | 48.3 | NR | 62.9 | NR | 62.9 | NR |
| 129 | Yoshizaki | 171 | 3556 | 49.7 | NR | 62.9 | NR | 62.9 | NR |
| 130 | Yoshizaki | 172 | 3556 | 49.7 | NR | 62.9 | NR | 62.9 | NR |
| 131 | Yoshizaki | 173 | 3556 | 50.1 | NR | 62.9 | NR | 62.9 | NR |
| 132 | Yoshizaki | 174 | 3556 | 50.1 | NR | 62.9 | NR | 62.9 | NR |

**Table A-3 Material properties of the walls with rectangular cross-sections (cont'd)**

| No. | Researcher | Specimen ID | $f_c'$ (psi) | $f_{ybe}$ (ksi) | $f_{ube}$ (ksi) | $f_{yv}$ (ksi) | $f_{uv}$ (ksi) | $f_{yh}$ (ksi) | $f_{uh}$ (ksi) |
|---|---|---|---|---|---|---|---|---|---|
| 133 | Yoshizaki | 175 | 3698 | 48.3 | NR | 62.9 | NR | 62.9 | NR |
| 134 | Yoshizaki | 176 | 3698 | 49.7 | NR | 62.9 | NR | 62.9 | NR |
| 135 | Yoshizaki | 177 | 3698 | 50.1 | NR | 62.9 | NR | 62.9 | NR |
| 136 | Yoshizaki | 178 | 3698 | 50.1 | NR | 62.9 | NR | 62.9 | NR |
| 137 | Yoshizaki | 179 | 3698 | 50.9 | NR | 62.9 | NR | 62.9 | NR |
| 138 | Massone | wp111-9 | 4100 | 61.5 | 91.5 | 61.5 | 91.5 | 61.5 | 91.5 |
| 139 | Massone | wp111-10 | 4550 | 61.5 | 91.5 | 61.5 | 91.5 | 61.5 | 91.5 |
| 140 | Massone | wp1105-8 | 4630 | 61.5 | 91.5 | 61.5 | 91.5 | 61.5 | 91.5 |
| 141 | Massone | wp1105-7 | 4640 | 61.5 | 91.5 | 61.5 | 91.5 | 61.5 | 91.5 |
| 142 | Massone | wp110-5 | 4340 | 61.5 | 91.5 | 61.5 | 91.5 | 61.5 | 91.5 |
| 143 | Massone | wp110-6 | 4500 | 61.5 | 91.5 | 61.5 | 91.5 | 61.5 | 91.5 |
| 144 | Kuang | U1.0 | 4409 | N/A | NR | 75.4 | NR | 75.4 | NR |
| 145 | Kuang | U1.5 | 5062 | N/A | NR | 75.4 | NR | 75.4 | NR |
| 146 | Kuang | C1.0 | 5105 | 75.4 | NR | 75.4 | NR | 75.4 | NR |
| 147 | Kuang | C1.5 | 4960 | 75.4 | NR | 75.4 | NR | 75.4 | NR |
| 148 | Kuang | U1.0-BC | 4540 | 75.4 | NR | 75.4 | NR | 75.4 | NR |
| 149 | Kuang | U1.5-BC | 4902 | 75.4 | NR | 75.4 | NR | 75.4 | NR |
| 150 | Kuang | U1.0-BC2 | 4946 | 75.4 | NR | 75.4 | NR | 75.4 | NR |

**Table A-4 Loading and performance information for the walls with rectangular cross-sections**

| No. | Researcher | Specimen ID | Loading Type | $P/(A_t f_c')$ (%) | $V_{flex}$ (kips) | $V_{peak}$ (kips) | Governing failure |
|---|---|---|---|---|---|---|---|
| 1 | Alexander | 1 | Cyclic | 0.0 | 73.5 | 74.0 | flexure |
| 2 | Cardenas | SW-7 | Monotonic | 0.0 | 142.7 | 116.7 | shear |
| 3 | Cardenas | SW-8 | Monotonic | 0.0 | 151.9 | 128.1 | shear |
| 4 | Cardenas | SW-9 | Monotonic | 0.0 | 151.9 | 152.7 | flexure |
| 5 | Cardenas | SW-10 | Monotonic | 0.0 | 106.6 | 68.7 | shear |
| 6 | Cardenas | SW-11 | Monotonic | 0.0 | 150.4 | 137.0 | shear |
| 7 | Cardenas | SW-12 | Monotonic | 0.0 | 150.0 | 148.0 | shear |
| 8 | Cardenas | SW-13 | Cyclic | 0.0 | 152.1 | 142.1 | shear |
| 9 | Pilakoutas | SW4 | Cyclic | 0.0 | 23.6 | 23.5 | shear |
| 10 | Pilakoutas | SW5 | Cyclic | 0.0 | 29.5 | 25.1 | shear |
| 11 | Pilakoutas | SW6 | Cyclic | 0.0 | 23.7 | 24.2 | flexure |
| 12 | Pilakoutas | SW7 | Cyclic | 0.0 | 29.7 | 29.1 | shear |
| 13 | Pilakoutas | SW8 | Cyclic | 0.0 | 26.1 | 21.3 | shear |
| 14 | Pilakoutas | SW9 | Cyclic | 0.0 | 25.8 | 22.1 | shear |
| 15 | Greifenhagen | M1 | Cyclic | 2.2 | 46.3 | 45.5 | shear |
| 16 | Greifenhagen | M2 | Cyclic | 2.2 | 45.8 | 45.7 | shear |
| 17 | Greifenhagen | M3 | Cyclic | 9.5 | 38.8 | 39.2 | flexure |
| 18 | Greifenhagen | M4 | Cyclic | 5.0 | 33.2 | 30.3 | shear |
| 19 | Hidalgo | 1 | Cyclic | 0.0 | 97.3 | 44.5 | shear |
| 20 | Hidalgo | 2 | Cyclic | 0.0 | 100.0 | 60.7 | shear |
| 21 | Hidalgo | 4 | Cyclic | 0.0 | 119.8 | 72.8 | shear |
| 22 | Hidalgo | 6 | Cyclic | 0.0 | 117.1 | 69.5 | shear |
| 23 | Hidalgo | 7 | Cyclic | 0.0 | 164.3 | 81.8 | shear |
| 24 | Hidalgo | 8 | Cyclic | 0.0 | 171.6 | 84.1 | shear |
| 25 | Hidalgo | 9 | Cyclic | 0.0 | 152.3 | 58.0 | shear |
| 26 | Hidalgo | 10 | Cyclic | 0.0 | 98.9 | 42.0 | shear |
| 27 | Hidalgo | 11 | Cyclic | 0.0 | 150.0 | 52.8 | shear |
| 28 | Hidalgo | 12 | Cyclic | 0.0 | 142.7 | 68.3 | shear |
| 29 | Hidalgo | 13 | Cyclic | 0.0 | 154.0 | 65.0 | shear |
| 30 | Hidalgo | 14 | Cyclic | 0.0 | 170.2 | 57.3 | shear |
| 31 | Hidalgo | 15 | Cyclic | 0.0 | 157.1 | 82.7 | shear |
| 32 | Hidalgo | 16 | Cyclic | 0.0 | 170.8 | 81.4 | shear |

**Table A-4 Loading and performance information for the walls with rectangular cross-sections (cont'd)**

| No. | Researcher | Specimen ID | Loading Type | $P/(A_t f_c')$ (%) | $V_{flex}$ (kips) | $V_{peak}$ (kips) | Governing failure |
|---|---|---|---|---|---|---|---|
| 33 | Hidalgo | 21 | Cyclic | 0.0 | 85.4 | 58.0 | shear |
| 34 | Hidalgo | 22 | Cyclic | 0.0 | 84.6 | 49.9 | shear |
| 35 | Hidalgo | 23 | Cyclic | 0.0 | 157.0 | 74.9 | shear |
| 36 | Hidalgo | 24 | Cyclic | 0.0 | 100.3 | 52.2 | shear |
| 37 | Hidalgo | 25 | Cyclic | 0.0 | 118.7 | 79.1 | shear |
| 38 | Hidalgo | 26 | Cyclic | 0.0 | 117.9 | 58.9 | shear |
| 39 | Hidalgo | 27 | Cyclic | 0.0 | 178.7 | 110.4 | shear |
| 40 | Hidalgo | 28 | Cyclic | 0.0 | 142.4 | 58.0 | shear |
| 41 | Hidalgo | 29 | Cyclic | 0.0 | 169.7 | 90.0 | shear |
| 42 | Hidalgo | 30 | Cyclic | 0.0 | 167.3 | 80.0 | shear |
| 43 | Hidalgo | 31 | Cyclic | 0.0 | 220.9 | 87.9 | shear |
| 44 | Hidalgo | 32 | Cyclic | 0.0 | 195.2 | 77.3 | shear |
| 45 | Hirosawa | 72 | Cyclic | 11.4 | 201.7 | 173.6 | shear |
| 46 | Hirosawa | 73 | Cyclic | 9.4 | 205.3 | 174.2 | shear |
| 47 | Hirosawa | 74 | Cyclic | 9.4 | 205.3 | 177.5 | shear |
| 48 | Hirosawa | 75 | Cyclic | 14.3 | 196.6 | 182.5 | shear |
| 49 | Hirosawa | 76 | Cyclic | 13.3 | 198.1 | 178.6 | shear |
| 50 | Hirosawa | 77 | Cyclic | 10.7 | 202.6 | 196.8 | shear |
| 51 | Hirosawa | 78 | Cyclic | 9.4 | 147.3 | 148.8 | flexure |
| 52 | Hirosawa | 79 | Cyclic | 14.3 | 138.5 | 132.9 | shear |
| 53 | Hirosawa | 80 | Cyclic | 13.3 | 139.9 | 147.7 | flexure |
| 54 | Hirosawa | 81 | Cyclic | 10.7 | 144.9 | 160.4 | flexure |
| 55 | Hirosawa | 82 | Cyclic | 9.4 | 72.6 | 71.4 | shear |
| 56 | Hirosawa | 83 | Cyclic | 11.0 | 71.9 | 68.4 | shear |
| 57 | Hirosawa | 84 | Cyclic | 11.0 | 63.6 | 71.7 | flexure |
| 58 | Hirosawa | 85 | Cyclic | 9.4 | 64.4 | 75.5 | flexure |
| 59 | Lefas | SW11 | Monotonic | 0.0 | 51.4 | 58.5 | flexure |
| 60 | Lefas | SW12 | Monotonic | 8.7 | 64.5 | 76.4 | flexure |
| 61 | Lefas | SW13 | Monotonic | 18.1 | 64.4 | 74.2 | flexure |
| 62 | Lefas | SW14 | Monotonic | 0.0 | 49.4 | 59.6 | flexure |
| 63 | Lefas | SW15 | Monotonic | 8.8 | 59.2 | 71.9 | flexure |
| 64 | Lefas | SW16 | Monotonic | 18.0 | 73.0 | 79.8 | flexure |

**Table A-4 Loading and performance information for the walls with rectangular cross-sections (cont'd)**

| No. | Researcher | Specimen ID | Loading Type | $P/(A_t f_c')$ (%) | $V_{flex}$ (kips) | $V_{peak}$ (kips) | Governing failure |
|---|---|---|---|---|---|---|---|
| 65 | Lefas | SW17 | Monotonic | 0.0 | 50.8 | 55.5 | flexure |
| 66 | Lefas | SW21 | Monotonic | 0.0 | 22.0 | 28.6 | flexure |
| 67 | Lefas | SW22 | Monotonic | 9.1 | 27.6 | 33.7 | flexure |
| 68 | Lefas | SW23 | Monotonic | 18.2 | 30.2 | 40.5 | flexure |
| 69 | Lefas | SW24 | Monotonic | 0.0 | 22.3 | 27.0 | flexure |
| 70 | Lefas | SW26 | Monotonic | 0.0 | 20.5 | 27.7 | flexure |
| 71 | Lefas | SW30 | Monotonic | 0.0 | 18.2 | 26.5 | flexure |
| 72 | Lefas | SW31 | Cyclic | 0.0 | 18.7 | 26.0 | flexure |
| 73 | Lefas | SW32 | Cyclic | 0.0 | 19.7 | 25.0 | flexure |
| 74 | Lefas | SW33 | Cyclic | 0.0 | 19.5 | 25.1 | flexure |
| 75 | Maier | S4 | Monotonic | 7.7 | 77.5 | 88.1 | flexure |
| 76 | Maier | S9 | Monotonic | 8.6 | 74.4 | 76.9 | flexure |
| 77 | Rothe | T01 | Dynamic | 0.0 | 19.7 | 24.1 | flexure |
| 78 | Rothe | T04 | Dynamic | 0.0 | 20.0 | 20.2 | flexure |
| 79 | Rothe | T05 | Dynamic | 0.0 | 27.4 | 28.6 | flexure |
| 80 | Rothe | T10 | Cyclic | 0.0 | 20.5 | 20.1 | shear |
| 81 | Rothe | T11 | Cyclic | 7.1 | 26.9 | 29.0 | flexure |
| 82 | Saatcioglu | Wall-1 | Cyclic | 0.0 | 129.4 | 119.7 | shear |
| 83 | Saatcioglu | Wall-2 | Cyclic | 0.0 | 223.6 | 154.0 | shear |
| 84 | Saatcioglu | Wall-4 | Cyclic | 0.0 | 148.0 | 90.1 | shear |
| 85 | Saatcioglu | Wall-5 | Cyclic | 0.0 | 190.7 | 122.4 | shear |
| 86 | Saatcioglu | Wall-7 | Cyclic | 0.0 | 102.8 | 84.3 | shear |
| 87 | Saatcioglu | Wall-8 | Cyclic | 0.0 | 59.0 | 50.5 | shear |
| 88 | Salonikios | MSW1 | Cyclic | 0.0 | 42.7 | 44.5 | flexure |
| 89 | Salonikios | MSW3 | Cyclic | 7.0 | 40.0 | 39.0 | shear |
| 90 | Salonikios | MSW6 | Cyclic | 0.0 | 43.0 | 42.1 | shear |
| 91 | Salonikios | LSW1 | Cyclic | 0.0 | 60.7 | 58.5 | shear |
| 92 | Salonikios | LSW2 | Cyclic | 0.0 | 43.5 | 41.6 | shear |
| 93 | Salonikios | LSW3 | Cyclic | 7.0 | 58.2 | 56.5 | shear |
| 94 | Sheu | SWN-1B | Monotonic | 12.0 | 70.0 | 76.6 | flexure |
| 95 | Sheu | SWN-5B | Monotonic | 12.0 | 51.1 | 56.7 | flexure |
| 96 | Sheu | SWN-1D | Cyclic | 12.0 | 74.3 | 67.2 | shear |

**Table A-4 Loading and performance information for the walls with rectangular cross-sections (cont'd)**

| No. | Researcher | Specimen ID | Loading Type | $P/(A_t f_c')$ (%) | $V_{flex}$ (kips) | $V_{peak}$ (kips) | Governing failure |
|---|---|---|---|---|---|---|---|
| 97 | Sheu | SWN-5D | Cyclic | 12.0 | 55.5 | 55.1 | shear |
| 98 | Sheu | SW-0E | Cyclic | 0.0 | 56.7 | 70.8 | flexure |
| 99 | Sheu | SW-1E | Cyclic | 0.0 | 59.7 | 72.8 | flexure |
| 100 | Sheu | SW-9E | Cyclic | 0.0 | 62.1 | 75.6 | flexure |
| 101 | Sheu | SW-1 | Monotonic | 0.0 | 38.4 | 47.2 | flexure |
| 102 | Sheu | SW-1A | Repeated | 0.0 | 38.9 | 42.5 | flexure |
| 103 | Sheu | SW-2 | Cyclic | 0.0 | 38.4 | 40.2 | flexure |
| 104 | Sheu | SW-3 | Cyclic | 0.0 | 38.6 | 42.5 | flexure |
| 105 | Sheu | SW-4 | Monotonic | 0.0 | 60.0 | 62.7 | flexure |
| 106 | Sheu | SW-4A | Repeated | 0.0 | 60.2 | 61.1 | flexure |
| 107 | Sheu | SW-5 | Cyclic | 0.0 | 60.7 | 54.4 | shear |
| 108 | Sheu | SW-6 | Cyclic | 0.0 | 60.9 | 62.0 | flexure |
| 109 | Sheu | SW9 | Monotonic | 0.0 | 66.3 | 55.8 | shear |
| 110 | Sheu | SW10 | Monotonic | 0.0 | 57.6 | 60.7 | flexure |
| 111 | Sheu | SW11 | Cyclic | 0.0 | 66.3 | 49.8 | shear |
| 112 | Sheu | SW12 | Monotonic | 0.0 | 59.7 | 55.8 | shear |
| 113 | Sheu | SW13 | Monotonic | 0.0 | 59.2 | 54.7 | shear |
| 114 | Sheu | SW14 | Monotonic | 0.0 | 59.3 | 70.4 | flexure |
| 115 | Sheu | SW15 | Monotonic | 0.0 | 47.9 | 50.0 | flexure |
| 116 | Sheu | SW16 | Monotonic | 0.0 | 41.7 | 49.6 | flexure |
| 117 | Sheu | SW17 | Cyclic | 0.0 | 47.9 | 40.5 | shear |
| 118 | Sheu | SW18 | Monotonic | 0.0 | 43.1 | 49.3 | flexure |
| 119 | Sheu | SW19 | Monotonic | 0.0 | 40.7 | 35.2 | shear |
| 120 | Sheu | SW20 | Monotonic | 0.0 | 39.3 | 47.5 | flexure |
| 121 | Synge | Wall-1 | Cyclic | 0.0 | 174.7 | 173.8 | shear |
| 122 | Xie | W-1A | Cyclic | 9.4 | 273.5 | 283.4 | flexure |
| 123 | Yoshizaki | 165 | Cyclic | 0.0 | 23.5 | 22.1 | shear |
| 124 | Yoshizaki | 166 | Cyclic | 0.0 | 32.1 | 31.9 | shear |
| 125 | Yoshizaki | 167 | Cyclic | 0.0 | 36.2 | 29.3 | shear |
| 126 | Yoshizaki | 168 | Cyclic | 0.0 | 42.1 | 36.2 | shear |
| 127 | Yoshizaki | 169 | Cyclic | 0.0 | 45.8 | 38.8 | shear |
| 128 | Yoshizaki | 170 | Cyclic | 0.0 | 39.2 | 34.1 | shear |

**Table A-4 Loading and performance information for the walls with rectangular cross-sections (cont'd)**

| No. | Researcher | Specimen ID | Loading Type | $P/(A_t f_c')$ (%) | $V_{flex}$ (kips) | $V_{peak}$ (kips) | Governing failure |
|---|---|---|---|---|---|---|---|
| 129 | Yoshizaki | 171 | Cyclic | 0.0 | 58.2 | 47.3 | shear |
| 130 | Yoshizaki | 172 | Cyclic | 0.0 | 60.5 | 46.0 | shear |
| 131 | Yoshizaki | 173 | Cyclic | 0.0 | 73.5 | 54.6 | shear |
| 132 | Yoshizaki | 174 | Cyclic | 0.0 | 83.8 | 57.0 | shear |
| 133 | Yoshizaki | 175 | Cyclic | 0.0 | 54.2 | 40.0 | shear |
| 134 | Yoshizaki | 176 | Cyclic | 0.0 | 91.9 | 72.3 | shear |
| 135 | Yoshizaki | 177 | Cyclic | 0.0 | 88.8 | 62.8 | shear |
| 136 | Yoshizaki | 178 | Cyclic | 0.0 | 111.3 | 87.8 | shear |
| 137 | Yoshizaki | 179 | Cyclic | 0.0 | 131.5 | 89.7 | shear |
| 138 | Wallace | wp111-9 | Cyclic | 10.0 | 221.3 | 169.5 | shear |
| 139 | Wallace | wp111-10 | Cyclic | 10.0 | 235.5 | 184.5 | shear |
| 140 | Wallace | wp1105-8 | Cyclic | 5.0 | 178.9 | 146.0 | shear |
| 141 | Wallace | wp1105-7 | Cyclic | 5.0 | 179.0 | 153.5 | shear |
| 142 | Wallace | wp110-5 | Cyclic | 0.0 | 122.6 | 91.0 | shear |
| 143 | Wallace | wp110-6 | Cyclic | 0.0 | 123.2 | 73.0 | shear |

**Table A-5 Geometric properties of the walls with barbell and flanged cross-sections**

| No. | Researcher | Specimen ID | $t_w$ (in) | $h_w$ (in) | $l_w$ (in) | $h_w / l_w$ | $M / Vl_w$ | $l_w / t_w$ | $h_{be}$ (in) |
|---|---|---|---|---|---|---|---|---|---|
| 1 | Antebi | 4 | 2.00 | 36.6 | 71.0 | 0.52 | 0.64 | 7.50 | 5.00 |
| 2 | Antebi | 5 | 2.00 | 36.6 | 71.0 | 0.52 | 0.64 | 7.50 | 5.00 |
| 3 | Antebi | 6 | 2.00 | 36.6 | 71.0 | 0.52 | 0.64 | 7.50 | 5.00 |
| 4 | Antebi | 7 | 2.00 | 36.6 | 71.0 | 0.52 | 0.64 | 7.50 | 5.00 |
| 5 | Antebi | 8 | 2.00 | 36.6 | 71.0 | 0.52 | 0.64 | 7.50 | 5.00 |
| 6 | Antebi | 9 | 2.00 | 36.6 | 71.0 | 0.52 | 0.64 | 7.50 | 5.00 |
| 7 | Antebi | 10 | 2.00 | 36.6 | 71.0 | 0.52 | 0.64 | 7.50 | 5.00 |
| 8 | Antebi | 11 | 2.00 | 36.6 | 71.0 | 0.52 | 0.64 | 7.50 | 5.00 |
| 9 | Antebi | 12 | 2.00 | 36.6 | 71.0 | 0.52 | 0.64 | 7.50 | 5.00 |
| 10 | Antebi | 13 | 2.00 | 36.6 | 71.0 | 0.52 | 0.64 | 7.50 | 5.00 |
| 11 | Antebi | 14 | 2.00 | 36.6 | 71.0 | 0.52 | 0.64 | 7.50 | 5.00 |
| 12 | Antebi | 15 | 2.00 | 36.6 | 71.0 | 0.52 | 0.64 | 7.50 | 5.00 |
| 13 | Antebi | 16 | 2.00 | 36.6 | 71.0 | 0.52 | 0.64 | 7.50 | 5.00 |
| 14 | Antebi | 17 | 2.00 | 36.6 | 71.0 | 0.52 | 0.64 | 7.50 | 5.00 |
| 15 | Antebi | 18 | 2.00 | 36.6 | 71.0 | 0.52 | 0.64 | 7.50 | 5.00 |
| 16 | Antebi | 19 | 2.00 | 36.6 | 71.0 | 0.52 | 0.64 | 7.50 | 5.00 |
| 17 | Antebi | 20 | 2.00 | 36.6 | 71.0 | 0.52 | 0.64 | 7.50 | 5.00 |
| 18 | Antebi | 25 | 2.00 | 36.6 | 71.0 | 0.52 | 0.64 | 7.50 | 5.00 |
| 19 | Antebi | 31 | 2.00 | 36.6 | 71.0 | 0.52 | 0.64 | 7.50 | 5.00 |
| 20 | Antebi | 32 | 2.00 | 36.6 | 71.0 | 0.52 | 0.64 | 7.50 | 5.00 |
| 21 | Antebi | 33 | 2.00 | 36.6 | 71.0 | 0.52 | 0.64 | 7.50 | 5.00 |
| 22 | Antebi | 34 | 2.00 | 36.6 | 71.0 | 0.52 | 0.64 | 7.50 | 5.00 |
| 23 | Antebi | 35 | 2.00 | 36.6 | 71.0 | 0.52 | 0.64 | 7.50 | 5.00 |
| 24 | Antebi | 36 | 2.00 | 36.6 | 71.0 | 0.52 | 0.64 | 7.50 | 5.00 |
| 25 | Antebi | 37 | 2.00 | 36.6 | 71.0 | 0.52 | 0.64 | 7.50 | 5.00 |
| 26 | Antebi | 38 | 2.00 | 36.6 | 71.0 | 0.52 | 0.64 | 7.50 | 5.00 |
| 27 | Antebi | 40 | 2.00 | 36.6 | 71.0 | 0.52 | 0.64 | 7.50 | 5.00 |
| 28 | Antebi | 41 | 2.00 | 36.6 | 71.0 | 0.52 | 0.64 | 7.50 | 5.00 |
| 29 | Antebi | 43 | 2.00 | 36.6 | 71.0 | 0.52 | 0.64 | 7.50 | 5.00 |
| 30 | Antebi | 44 | 2.00 | 36.6 | 71.0 | 0.52 | 0.64 | 7.50 | 5.00 |
| 31 | Antebi | 45 | 3.00 | 36.6 | 71.0 | 0.52 | 0.64 | 7.50 | 5.00 |
| 32 | Antebi | 46 | 3.00 | 36.6 | 71.0 | 0.52 | 0.64 | 7.50 | 5.00 |
| 33 | Antebi | 47 | 3.00 | 36.6 | 71.0 | 0.52 | 0.64 | 7.50 | 5.00 |

**Table A-5 Geometric properties of the walls with barbell and flanged cross-sections (cont'd)**

| No. | Researcher | Specimen ID | $t_w$ (in) | $h_w$ (in) | $l_w$ (in) | $h_w / l_w$ | $M / Vl_w$ | $l_w / t_w$ | $h_{be}$ (in) |
|---|---|---|---|---|---|---|---|---|---|
| 34 | Antebi | 48 | 3.00 | 36.6 | 71.0 | 0.52 | 0.64 | 7.50 | 5.00 |
| 35 | Antebi | 49 | 3.00 | 36.6 | 71.0 | 0.52 | 0.64 | 7.50 | 5.00 |
| 36 | Antebi | 50 | 3.00 | 36.6 | 71.0 | 0.52 | 0.64 | 7.50 | 5.00 |
| 37 | Antebi | 51 | 3.00 | 36.6 | 71.0 | 0.52 | 0.64 | 7.50 | 5.00 |
| 38 | Antebi | 52 | 3.00 | 36.6 | 71.0 | 0.52 | 0.64 | 7.50 | 5.00 |
| 39 | Antebi | 53 | 3.00 | 36.6 | 71.0 | 0.52 | 0.64 | 7.50 | 5.00 |
| 40 | Antebi | 54 | 3.00 | 36.6 | 71.0 | 0.52 | 0.64 | 7.50 | 5.00 |
| 41 | Antebi | 55 | 2.00 | 36.6 | 131.0 | 0.28 | 0.34 | 7.50 | 5.00 |
| 42 | Antebi | 56 | 2.00 | 36.6 | 131.0 | 0.28 | 0.34 | 7.50 | 5.00 |
| 43 | Antebi | 57 | 2.00 | 36.6 | 131.0 | 0.28 | 0.34 | 7.50 | 5.00 |
| 44 | Antebi | 58 | 2.00 | 36.6 | 131.0 | 0.28 | 0.34 | 7.50 | 5.00 |
| 45 | Antebi | 59 | 2.00 | 36.6 | 131.0 | 0.28 | 0.34 | 7.50 | 5.00 |
| 46 | Antebi | 60 | 2.00 | 36.6 | 131.0 | 0.28 | 0.34 | 7.50 | 5.00 |
| 47 | Aoyagi | 148 | 3.15 | 47.2 | 107.1 | 0.44 | 0.50 | 12.60 | 12.60 |
| 48 | Aoyagi | 149 | 3.15 | 47.2 | 107.1 | 0.44 | 0.50 | 12.60 | 12.60 |
| 49 | Aoyagi | 150 | 6.30 | 47.2 | 107.1 | 0.44 | 0.50 | 12.60 | 12.60 |
| 50 | Aoyagi | 151 | 3.15 | 47.2 | 107.1 | 0.44 | 0.50 | 12.60 | 12.60 |
| 51 | Aoyagi | 152 | 6.30 | 47.2 | 107.1 | 0.44 | 0.50 | 12.60 | 12.60 |
| 52 | Barda | B1-1 | 4.00 | 34.5 | 75.0 | 0.46 | 0.50 | 24.00 | 4.00 |
| 53 | Barda | B2-1 | 4.00 | 34.5 | 75.0 | 0.46 | 0.50 | 24.00 | 4.00 |
| 54 | Barda | B3-2 | 4.00 | 34.5 | 75.0 | 0.46 | 0.50 | 24.00 | 4.00 |
| 55 | Barda | B4-3 | 4.00 | 34.5 | 75.0 | 0.46 | 0.50 | 24.00 | 4.00 |
| 56 | Barda | B5-4 | 4.00 | 34.5 | 75.0 | 0.46 | 0.50 | 24.00 | 4.00 |
| 57 | Barda | B6-4 | 4.00 | 34.5 | 75.0 | 0.46 | 0.50 | 24.00 | 4.00 |
| 58 | Barda | B7-5 | 4.00 | 15.8 | 75.0 | 0.21 | 0.25 | 24.00 | 4.00 |
| 59 | Barda | B8-5 | 4.00 | 72.0 | 75.0 | 0.96 | 1.00 | 24.00 | 4.00 |
| 60 | Benjamin | 4BI-1 | 2.00 | 20.0 | 24.0 | 0.83 | 0.92 | 5.00 | 4.00 |
| 61 | Benjamin | 4BI-2 | 2.00 | 20.0 | 36.0 | 0.56 | 0.61 | 5.00 | 4.00 |
| 62 | Benjamin | 4BI-3 | 2.00 | 20.0 | 48.0 | 0.42 | 0.46 | 5.00 | 4.00 |
| 63 | Benjamin | 4BI-4 | 2.00 | 20.0 | 70.0 | 0.29 | 0.31 | 5.00 | 4.00 |
| 64 | Benjamin | 4BII-1 | 2.00 | 20.0 | 24.0 | 0.83 | 0.92 | 5.00 | 4.00 |
| 65 | Benjamin | 4BII-2 | 2.00 | 20.0 | 36.0 | 0.56 | 0.61 | 5.00 | 4.00 |

**Table A-5 Geometric properties of the walls with barbell and flanged cross-sections (cont'd)**

| No. | Researcher | Specimen ID | $t_w$ (in) | $h_w$ (in) | $l_w$ (in) | $h_w / l_w$ | $M / Vl_w$ | $l_w / t_w$ | $h_{be}$ (in) |
|---|---|---|---|---|---|---|---|---|---|
| 66 | Benjamin | 4BII-3 | 2.00 | 20.0 | 48.0 | 0.42 | 0.46 | 5.00 | 4.00 |
| 67 | Benjamin | 4BII-4 | 2.00 | 20.0 | 70.0 | 0.29 | 0.31 | 5.00 | 4.00 |
| 68 | Benjamin | 3BI-1 | 2.00 | 33.5 | 68.0 | 0.49 | 0.53 | 3.75 | 5.00 |
| 69 | Benjamin | 1BII-2 | 2.00 | 33.5 | 68.0 | 0.49 | 0.53 | 7.50 | 5.00 |
| 70 | Benjamin | 1BII-2a | 2.00 | 33.5 | 68.0 | 0.49 | 0.53 | 7.50 | 5.00 |
| 71 | Benjamin | 1BII-2b | 2.00 | 33.5 | 68.0 | 0.49 | 0.53 | 7.50 | 5.00 |
| 72 | Benjamin | 3BI-3 | 2.00 | 33.5 | 68.0 | 0.49 | 0.53 | 12.00 | 5.00 |
| 73 | Benjamin | 1bI-2 | 2.00 | 33.5 | 68.0 | 0.49 | 0.53 | 7.50 | 5.00 |
| 74 | Benjamin | 1bI-2a | 2.00 | 33.5 | 68.0 | 0.49 | 0.53 | 7.50 | 5.00 |
| 75 | Benjamin | 1bI-3 | 3.00 | 50.3 | 102.0 | 0.49 | 0.53 | 11.25 | 7.50 |
| 76 | Benjamin | 1bII-3 | 3.00 | 50.3 | 102.0 | 0.49 | 0.53 | 11.25 | 7.50 |
| 77 | Benjamin | R-1 | 2.00 | 33.5 | 68.0 | 0.49 | 0.53 | 7.50 | 5.00 |
| 78 | Benjamin | M-1 | 2.00 | 34.0 | 62.0 | 0.55 | 0.56 | 7.50 | 4.75 |
| 79 | Benjamin | M-2 | 2.00 | 70.0 | 62.0 | 1.13 | 0.76 | 7.50 | 4.75 |
| 80 | Benjamin | M-3 | 2.00 | 70.0 | 62.0 | 1.13 | 0.76 | 7.50 | 4.75 |
| 81 | Benjamin | M-4 | 2.00 | 34.0 | 62.0 | 0.55 | 0.56 | 7.50 | 4.75 |
| 82 | Benjamin | SD-1A | 2.00 | 25.0 | 48.0 | 0.52 | 0.57 | 4.00 | 4.00 |
| 83 | Benjamin | SD-1B | 2.00 | 25.0 | 48.0 | 0.52 | 0.57 | 4.00 | 4.00 |
| 84 | Benjamin | SD-1C | 2.00 | 25.0 | 48.0 | 0.52 | 0.57 | 4.00 | 4.00 |
| 85 | Kabeyasawa | K1 | 3.15 | 59.1 | 78.7 | 0.75 | 0.75 | 7.87 | 7.87 |
| 86 | Kabeyasawa | K2 | 3.15 | 59.1 | 78.7 | 0.75 | 1.00 | 7.87 | 7.87 |
| 87 | Kabeyasawa | K3 | 3.15 | 59.1 | 78.7 | 0.75 | 1.00 | 7.87 | 7.87 |
| 88 | Kabeyasawa | K4 | 3.15 | 59.1 | 78.7 | 0.75 | 1.00 | 7.87 | 7.87 |
| 89 | Kabeyasawa | K7 | 4.72 | 59.1 | 78.7 | 0.75 | 0.50 | 7.87 | 7.87 |
| 90 | Maier | S1 | 3.94 | 47.2 | 46.5 | 1.02 | 1.12 | 15.75 | 3.94 |
| 91 | Maier | S2 | 3.94 | 47.2 | 46.5 | 1.02 | 1.12 | 15.75 | 3.94 |
| 92 | Maier | S3 | 3.94 | 47.2 | 46.5 | 1.02 | 1.12 | 15.75 | 3.94 |
| 93 | Maier | S5 | 3.94 | 47.2 | 46.5 | 1.02 | 1.12 | 15.75 | 3.94 |
| 94 | Maier | S6 | 3.94 | 47.2 | 46.5 | 1.02 | 1.12 | 15.75 | 3.94 |
| 95 | Maier | S7 | 3.94 | 47.2 | 46.5 | 1.02 | 1.12 | 15.75 | 3.94 |
| 96 | Rothe | T02 | 1.97 | 43.3 | 31.5 | 1.38 | 1.50 | 3.94 | 5.91 |
| 97 | Rothe | T03 | 1.97 | 43.3 | 31.5 | 1.38 | 1.50 | 3.94 | 5.91 |

**Table A-5 Geometric properties of the walls with barbell and flanged cross-sections (cont'd)**

| No. | Researcher | Specimen ID | $t_w$ (in) | $h_w$ (in) | $l_w$ (in) | $h_w / l_w$ | $M / Vl_w$ | $l_w / t_w$ | $h_{be}$ (in) |
|---|---|---|---|---|---|---|---|---|---|
| 98 | Rothe | T06 | 1.97 | 43.3 | 31.5 | 1.38 | 1.50 | 3.94 | 5.91 |
| 99 | Rothe | T07 | 1.97 | 43.3 | 31.5 | 1.38 | 1.50 | 3.94 | 5.91 |
| 100 | Rothe | T08 | 1.97 | 43.3 | 31.5 | 1.38 | 1.50 | 3.94 | 5.91 |
| 101 | Rothe | T09 | 1.97 | 43.3 | 31.5 | 1.38 | 1.50 | 3.94 | 5.91 |
| 102 | Ryo | 29 | 3.07 | 47.2 | 90.6 | 0.52 | 0.58 | 9.84 | 9.84 |
| 103 | Ryo | 30 | 2.95 | 47.2 | 90.6 | 0.52 | 0.58 | 9.84 | 9.84 |
| 104 | Ryo | 31 | 3.15 | 47.2 | 61.0 | 0.77 | 0.85 | 9.84 | 9.84 |
| 105 | SAFE | T03 | 6.30 | 47.2 | 118.1 | 0.40 | 0.20 | 31.50 | 6.30 |
| 106 | SAFE | T04 | 6.30 | 47.2 | 118.1 | 0.40 | 0.20 | 31.50 | 6.30 |
| 107 | SAFE | T05 | 7.87 | 47.2 | 118.1 | 0.40 | 0.20 | 31.50 | 6.30 |
| 108 | SAFE | T06 | 7.87 | 47.2 | 118.1 | 0.40 | 0.20 | 31.50 | 6.30 |
| 109 | SAFE | T07 | 7.87 | 47.2 | 118.1 | 0.40 | 0.20 | 31.50 | 6.30 |
| 110 | SAFE | T08 | 7.87 | 47.2 | 118.1 | 0.40 | 0.20 | 31.50 | 6.30 |
| 111 | SAFE | T09 | 7.87 | 47.2 | 118.1 | 0.40 | 0.20 | 31.50 | 6.30 |
| 112 | SAFE | T10 | 7.87 | 47.2 | 118.1 | 0.40 | 0.20 | 31.50 | 6.30 |
| 113 | SAFE | T11 | 7.87 | 47.2 | 118.1 | 0.40 | 0.20 | 31.50 | 6.30 |
| 114 | SAFE | T12 | 7.87 | 47.2 | 118.1 | 0.40 | 0.20 | 31.50 | 6.30 |
| 115 | Shiga | WB-1 | 1.97 | 23.6 | 44.1 | 0.54 | 0.63 | 5.91 | 4.72 |
| 116 | Shiga | WB-2 | 1.97 | 23.6 | 44.1 | 0.54 | 0.63 | 5.91 | 4.72 |
| 117 | Shiga | WB-3 | 1.97 | 23.6 | 44.1 | 0.54 | 0.63 | 5.91 | 4.72 |
| 118 | Shiga | WB-4 | 1.97 | 23.6 | 44.1 | 0.54 | 0.63 | 5.91 | 4.72 |
| 119 | Shiga | WB-5 | 1.97 | 23.6 | 44.1 | 0.54 | 0.63 | 5.91 | 4.72 |
| 120 | Shiga | WB-6 | 1.97 | 23.6 | 44.1 | 0.54 | 0.63 | 5.91 | 4.72 |
| 121 | Shiga | WB-7 | 1.97 | 23.6 | 44.1 | 0.54 | 0.63 | 5.91 | 4.72 |
| 122 | Shiga | WB-8 | 1.97 | 23.6 | 44.1 | 0.54 | 0.63 | 5.91 | 4.72 |
| 123 | Shiga | WB-9 | 1.97 | 23.6 | 44.1 | 0.54 | 0.63 | 5.91 | 4.72 |
| 124 | Shiga | WB-10 | 1.97 | 23.6 | 44.1 | 0.54 | 0.63 | 5.91 | 4.72 |
| 125 | Shiga | WB-11 | 1.97 | 23.6 | 44.1 | 0.54 | 0.63 | 5.91 | 4.72 |
| 126 | Shiga | WB-12 | 1.97 | 23.6 | 44.1 | 0.54 | 0.63 | 5.91 | 4.72 |
| 127 | Shiga | WB-13 | 1.97 | 23.6 | 44.1 | 0.54 | 0.63 | 5.91 | 4.72 |
| 128 | Shiga | WB-14 | 1.97 | 23.6 | 44.1 | 0.54 | 0.63 | 5.91 | 4.72 |
| 129 | Shiga | WB-15 | 1.97 | 23.6 | 44.1 | 0.54 | 0.63 | 5.91 | 4.72 |

**Table A-5 Geometric properties of the walls with barbell and flanged cross-sections (cont'd)**

| No. | Researcher | Specimen ID | $t_w$ (in) | $h_w$ (in) | $l_w$ (in) | $h_w / l_w$ | $M / Vl_w$ | $l_w / t_w$ | $h_{be}$ (in) |
|---|---|---|---|---|---|---|---|---|---|
| 130 | Shiga | WB-16 | 1.97 | 23.6 | 44.1 | 0.54 | 0.63 | 5.91 | 4.72 |
| 131 | Shiga | WB-17 | 1.97 | 23.6 | 44.1 | 0.54 | 0.63 | 5.91 | 4.72 |
| 132 | Sugano | 70 | 2.91 | 47.2 | 90.6 | 0.52 | 0.58 | 9.84 | 9.84 |
| 133 | Sugano | 71 | 3.27 | 47.2 | 90.6 | 0.52 | 0.58 | 9.84 | 9.84 |
| 134 | Sugano | 140 | 4.72 | 56.7 | 155.9 | 0.36 | 0.18 | 14.17 | 14.17 |
| 135 | Sugano | 141 | 4.72 | 56.7 | 155.9 | 0.36 | 0.06 | 14.17 | 14.17 |
| 136 | Sugano | 142 | 4.72 | 56.7 | 155.9 | 0.36 | 0.18 | 14.17 | 14.17 |
| 137 | Sugano | 143 | 4.72 | 56.7 | 155.9 | 0.36 | 0.18 | 14.17 | 14.17 |
| 138 | Sugano | 144 | 4.72 | 56.7 | 155.9 | 0.36 | 0.18 | 14.17 | 14.17 |
| 139 | Sugano | 145 | 4.72 | 56.7 | 155.9 | 0.36 | 0.18 | 14.17 | 14.17 |
| 140 | Sugano | 146 | 4.72 | 56.7 | 155.9 | 0.36 | 0.18 | 14.17 | 14.17 |
| 141 | Sugano | 147 | 4.72 | 56.7 | 155.9 | 0.36 | 0.18 | 14.17 | 14.17 |
| 142 | Synge | Wall-3 | 3.94 | 59.1 | 118.1 | 0.50 | 0.57 | 19.69 | 3.94 |
| 143 | Tsuboi | 130 | 2.64 | 32.0 | 20.0 | 1.60 | 1.77 | 4.21 | 4.72 |
| 144 | Tsuboi | 131 | 2.64 | 32.0 | 20.0 | 1.60 | 1.77 | 4.21 | 4.72 |
| 145 | Tsuboi | 132 | 2.64 | 32.0 | 20.0 | 1.60 | 1.77 | 4.21 | 4.72 |
| 146 | Tsuboi | 133 | 2.64 | 32.0 | 20.0 | 1.60 | 1.77 | 4.21 | 4.72 |
| 147 | Tsuboi | 134 | 2.64 | 32.0 | 20.0 | 1.60 | 0.80 | 4.21 | 4.72 |
| 148 | Tsuboi | 135 | 2.64 | 32.0 | 20.0 | 1.60 | 0.80 | 4.21 | 4.72 |
| 149 | Mo | HN4-1 | 2.76 | 19.7 | 33.9 | 0.58 | 0.76 | 6.69 | 3.15 |
| 150 | Mo | HN4-2 | 2.76 | 19.7 | 33.9 | 0.58 | 0.76 | 6.69 | 3.15 |
| 151 | Mo | HN4-3 | 2.76 | 19.7 | 33.9 | 0.58 | 0.76 | 6.69 | 3.15 |
| 152 | Mo | HN6-1 | 2.76 | 19.7 | 33.9 | 0.58 | 0.76 | 6.69 | 3.15 |
| 153 | Mo | HN6-2 | 2.76 | 19.7 | 33.9 | 0.58 | 0.76 | 6.69 | 3.15 |
| 154 | Mo | HN6-3 | 2.76 | 19.7 | 33.9 | 0.58 | 0.76 | 6.69 | 3.15 |
| 155 | Mo | HM4-1 | 2.76 | 19.7 | 33.9 | 0.58 | 0.76 | 6.69 | 3.15 |
| 156 | Mo | HM4-2 | 2.76 | 19.7 | 33.9 | 0.58 | 0.76 | 6.69 | 3.15 |
| 157 | Mo | HM4-3 | 2.76 | 19.7 | 33.9 | 0.58 | 0.76 | 6.69 | 3.15 |
| 158 | Mo | LN4-1 | 2.76 | 19.7 | 33.9 | 0.58 | 0.76 | 6.69 | 3.15 |
| 159 | Mo | LN4-2 | 2.76 | 19.7 | 33.9 | 0.58 | 0.76 | 6.69 | 3.15 |
| 160 | Mo | LN4-3 | 2.76 | 19.7 | 33.9 | 0.58 | 0.76 | 6.69 | 3.15 |
| 161 | Mo | LN6-1 | 2.76 | 19.7 | 33.9 | 0.58 | 0.76 | 6.69 | 3.15 |

**Table A-5 Geometric properties of the walls with barbell and flanged cross-sections (cont'd)**

| No. | Researcher | Specimen ID | $t_w$ (in) | $h_w$ (in) | $l_w$ (in) | $h_w / l_w$ | $M / Vl_w$ | $l_w / t_w$ | $h_{be}$ (in) |
|---|---|---|---|---|---|---|---|---|---|
| 162 | Mo | LN6-2 | 2.76 | 19.7 | 33.9 | 0.58 | 0.76 | 6.69 | 3.15 |
| 163 | Mo | LN6-3 | 2.76 | 19.7 | 33.9 | 0.58 | 0.76 | 6.69 | 3.15 |
| 164 | Mo | LM6-1 | 2.76 | 19.7 | 33.9 | 0.58 | 0.76 | 6.69 | 3.15 |
| 165 | Mo | LM6-2 | 2.76 | 19.7 | 33.9 | 0.58 | 0.76 | 6.69 | 3.15 |
| 166 | Mo | LM6-3 | 2.76 | 19.7 | 33.9 | 0.58 | 0.76 | 6.69 | 3.15 |
| 167 | Mo | LM4-2 | 2.76 | 19.7 | 33.9 | 0.58 | 0.76 | 6.69 | 3.15 |
| 168 | Mo | LM4-3 | 2.76 | 19.7 | 33.9 | 0.58 | 0.76 | 6.69 | 3.15 |
| 169 | Bouchon | No.3 | 3.94 | 29.5 | 59.1 | 0.50 | 0.25 | 7.09 | 3.94 |
| 170 | Endo | 1 | 3.15 | 68.9 | 88.6 | 0.78 | 0.61 | 9.84 | 9.84 |
| 171 | Endo | 2 | 3.15 | 68.9 | 88.6 | 0.78 | 0.61 | 9.84 | 9.84 |
| 172 | Endo | 3 | 3.15 | 68.9 | 88.6 | 0.78 | 0.83 | 9.84 | 9.84 |
| 173 | Endo | 4 | 1.97 | 68.9 | 88.6 | 0.78 | 0.61 | 9.84 | 9.84 |
| 174 | Endo | 5 | 1.97 | 29.5 | 88.6 | 0.33 | 0.39 | 9.84 | 9.84 |
| 175 | NUPEC | U-1 | 2.95 | 79.5 | 122.0 | 0.65 | 0.77 | 117.32 | 3.94 |
| 176 | NUPEC | U-2 | 2.95 | 79.5 | 122.0 | 0.65 | 0.77 | 117.32 | 3.94 |
| 177 | Vecchio | DP1 | 2.95 | 79.5 | 121.1 | 0.66 | 0.76 | 119.88 | 3.74 |
| 178 | Vecchio | DP2 | 2.95 | 79.5 | 121.5 | 0.65 | 0.76 | 119.88 | 3.94 |
| 179 | XiangDong | FSW-4 | 3.00 | 36.0 | 48.0 | 0.75 | 0.75 | 6.00 | 6.00 |
| 180 | XiangDong | FSW-5 | 3.00 | 36.0 | 48.0 | 0.75 | 0.75 | 6.00 | 6.00 |
| 181 | XiangDong | FSW-6 | 3.00 | 36.0 | 48.0 | 0.75 | 0.75 | 6.00 | 6.00 |
| 182 | XiangDong | FSW-7 | 3.00 | 36.0 | 48.0 | 0.75 | 0.75 | 6.00 | 6.00 |
| 183 | XiangDong | FSW-8 | 3.00 | 36.0 | 48.0 | 0.75 | 0.75 | 6.00 | 6.00 |
| 184 | XiangDong | FSW-9 | 3.00 | 36.0 | 48.0 | 0.75 | 0.75 | 6.00 | 6.00 |
| 185 | XiangDong | FSW-10 | 3.00 | 36.0 | 48.0 | 0.75 | 0.75 | 6.00 | 6.00 |
| 186 | XiangDong | FSW-12 | 3.00 | 36.0 | 48.0 | 0.75 | 0.75 | 6.00 | 6.00 |
| 187 | XiangDong | FSW-13 | 3.00 | 36.0 | 48.0 | 0.75 | 0.75 | 6.00 | 6.00 |
| 188 | Sheu | SWB-1A | 2.76 | 19.7 | 39.4 | 0.50 | 0.65 | 6.69 | 5.91 |
| 189 | Sheu | SWB-2A | 2.76 | 19.7 | 39.4 | 0.50 | 0.65 | 6.69 | 5.91 |
| 190 | Sheu | SWB-3A | 2.76 | 19.7 | 39.4 | 0.50 | 0.65 | 6.69 | 5.91 |
| 191 | Sheu | SWB-4A | 2.76 | 19.7 | 39.4 | 0.50 | 0.65 | 6.69 | 5.91 |
| 192 | Sheu | SWB-5A | 2.76 | 19.7 | 39.4 | 0.50 | 0.65 | 6.69 | 5.91 |
| 193 | Sheu | SWB-1B | 2.76 | 29.5 | 39.4 | 0.75 | 0.90 | 6.69 | 5.91 |

**Table A-5 Geometric properties of the walls with barbell and flanged cross-sections (cont'd)**

| No. | Researcher | Specimen ID | $t_w$ (in) | $h_w$ (in) | $l_w$ (in) | $h_w / l_w$ | $M / Vl_w$ | $l_w / t_w$ | $h_{be}$ (in) |
|---|---|---|---|---|---|---|---|---|---|
| 194 | Sheu | SWB-2B | 2.76 | 29.5 | 39.4 | 0.75 | 0.90 | 6.69 | 5.91 |
| 195 | Sheu | SWB-3B | 2.76 | 29.5 | 39.4 | 0.75 | 0.90 | 6.69 | 5.91 |
| 196 | Sheu | SWB-4B | 2.76 | 29.5 | 39.4 | 0.75 | 0.90 | 6.69 | 5.91 |
| 197 | Sheu | SWB-5B | 2.76 | 29.5 | 39.4 | 0.75 | 0.90 | 6.69 | 5.91 |
| 198 | Sheu | SWB-6A | 2.76 | 19.7 | 39.4 | 0.50 | 0.65 | 6.69 | 5.91 |
| 199 | Sheu | SWB-8A | 2.76 | 19.7 | 39.4 | 0.50 | 0.65 | 6.69 | 5.91 |
| 200 | Sheu | SWB-17A | 2.76 | 19.7 | 39.4 | 0.50 | 0.65 | 6.69 | 5.91 |
| 201 | Sheu | SWB-1C | 2.76 | 49.2 | 39.4 | 1.25 | 1.90 | 6.69 | 5.91 |
| 202 | Sheu | SWB-2C | 2.76 | 49.2 | 39.4 | 1.25 | 1.90 | 6.69 | 5.91 |
| 203 | Sheu | SWB-3C | 2.76 | 49.2 | 39.4 | 1.25 | 1.90 | 6.69 | 5.91 |
| 204 | Sheu | SWB-1D | 2.76 | 49.2 | 39.4 | 1.25 | 1.90 | 6.69 | 5.91 |
| 205 | Saito | W12-1 | 4.72 | 29.5 | 83.5 | 0.35 | 0.47 | 19.69 | 4.72 |
| 206 | Saito | W12-2 | 4.72 | 29.5 | 83.5 | 0.35 | 0.47 | 19.69 | 4.72 |
| 207 | Saito | W12-3 | 4.72 | 29.5 | 83.5 | 0.35 | 0.47 | 19.69 | 4.72 |
| 208 | Saito | W12-4 | 4.72 | 29.5 | 83.5 | 0.35 | 0.47 | 19.69 | 4.72 |
| 209 | Saito | W12-5 | 4.72 | 29.5 | 83.5 | 0.35 | 0.47 | 19.69 | 4.72 |
| 210 | Saito | W12-6 | 4.72 | 68.9 | 83.5 | 0.83 | 0.94 | 19.69 | 4.72 |
| 211 | Saito | W12-7 | 4.72 | 68.9 | 83.5 | 0.83 | 0.94 | 19.69 | 4.72 |
| 212 | Saito | W15-1 | 5.91 | 29.5 | 83.5 | 0.35 | 0.47 | 19.69 | 4.72 |
| 213 | Saito | W15-2 | 5.91 | 68.9 | 83.5 | 0.83 | 0.94 | 19.69 | 4.72 |
| 214 | Seki | RA-00P | 2.95 | 55.9 | 121.1 | 0.46 | 0.59 | 59.06 | 2.95 |
| 215 | Seki | RA-15P | 2.95 | 55.9 | 121.1 | 0.46 | 0.59 | 59.06 | 2.95 |
| 216 | Seki | RB-00P | 2.95 | 79.5 | 121.1 | 0.66 | 0.78 | 59.06 | 2.95 |
| 217 | Seki | RB-15P | 2.95 | 79.5 | 121.1 | 0.66 | 0.78 | 59.06 | 2.95 |
| 218 | Seki | RC-00P | 2.95 | 103.1 | 121.1 | 0.85 | 0.98 | 59.06 | 2.95 |
| 219 | Seki | RC-15P | 2.95 | 103.1 | 121.1 | 0.85 | 0.98 | 59.06 | 2.95 |
| 220 | Sato | 18M 12-40 | 5.91 | 86.6 | 84.6 | 1.02 | 1.12 | 39.37 | 5.91 |
| 221 | Sato | 24M 8-30 | 5.91 | 55.1 | 84.6 | 0.65 | 0.74 | 39.37 | 5.91 |
| 222 | Sato | 24M 8-40 | 5.91 | 55.1 | 84.6 | 0.65 | 0.74 | 39.37 | 5.91 |
| 223 | Sato | 24M 8-50 | 5.91 | 55.1 | 84.6 | 0.65 | 0.74 | 39.37 | 5.91 |
| 224 | Sato | 24M 6-30 | 5.91 | 39.4 | 84.6 | 0.47 | 0.56 | 39.37 | 5.91 |
| 225 | Sato | 24M 6-40 | 5.91 | 39.4 | 84.6 | 0.47 | 0.56 | 39.37 | 5.91 |

**Table A-5 Geometric properties of the walls with barbell and flanged cross-sections (cont'd)**

| No. | Researcher | Specimen ID | $t_w$ (in) | $h_w$ (in) | $l_w$ (in) | $h_w / l_w$ | $M / Vl_w$ | $l_w / t_w$ | $h_{be}$ (in) |
|---|---|---|---|---|---|---|---|---|---|
| 226 | Sato | 36M 12-30 | 5.91 | 86.6 | 84.6 | 1.02 | 1.12 | 39.37 | 5.91 |
| 227 | Sato | 36M 12-40 | 5.91 | 86.6 | 84.6 | 1.02 | 1.12 | 39.37 | 5.91 |
| 228 | Sato | 36M 12-50 | 5.91 | 86.6 | 84.6 | 1.02 | 1.12 | 39.37 | 5.91 |
| 229 | Sato | 36L 8-30 | 5.91 | 55.1 | 84.6 | 0.65 | 0.74 | 39.37 | 5.91 |
| 230 | Sato | 36L 8-40 | 5.91 | 55.1 | 84.6 | 0.65 | 0.74 | 39.37 | 5.91 |
| 231 | Sato | 36M 8-30 | 5.91 | 55.1 | 84.6 | 0.65 | 0.74 | 39.37 | 5.91 |
| 232 | Sato | 36M 8-40 | 5.91 | 55.1 | 84.6 | 0.65 | 0.74 | 39.37 | 5.91 |
| 233 | Sato | 36M 8-50 | 5.91 | 55.1 | 84.6 | 0.65 | 0.74 | 39.37 | 5.91 |
| 234 | Sato | 36M 6-30 | 5.91 | 39.4 | 84.6 | 0.47 | 0.56 | 39.37 | 5.91 |
| 235 | Sato | 36M 6-40 | 5.91 | 39.4 | 84.6 | 0.47 | 0.56 | 39.37 | 5.91 |
| 236 | Sato | 48M 8-30 | 5.91 | 55.1 | 84.6 | 0.65 | 0.74 | 39.37 | 5.91 |
| 237 | Sato | 48M 8-40 | 5.91 | 55.1 | 84.6 | 0.65 | 0.74 | 39.37 | 5.91 |
| 238 | Sato | 48M 8-50 | 5.91 | 55.1 | 84.6 | 0.65 | 0.74 | 39.37 | 5.91 |
| 239 | Sato | 48H 8-30 | 5.91 | 55.1 | 84.6 | 0.65 | 0.74 | 39.37 | 5.91 |
| 240 | Sato | 48H 8-40 | 5.91 | 55.1 | 84.6 | 0.65 | 0.74 | 39.37 | 5.91 |
| 241 | Sato | 48H 8-50 | 5.91 | 55.1 | 84.6 | 0.65 | 0.74 | 39.37 | 5.91 |
| 242 | Chiba | CW-0.6-1.2-20 | 3.15 | 41.3 | 90.6 | 0.46 | 0.52 | 11.81 | 11.81 |
| 243 | Chiba | CW-0.6-0.6-20 | 3.15 | 41.3 | 90.6 | 0.46 | 0.52 | 11.81 | 11.81 |
| 244 | Chiba | CW-0.6-0.8-20 | 3.15 | 41.3 | 90.6 | 0.46 | 0.52 | 11.81 | 11.81 |
| 245 | Chiba | CW-0.6-1.6-20 | 3.15 | 41.3 | 90.6 | 0.46 | 0.52 | 11.81 | 11.81 |
| 246 | Chiba | CW-0.6-2.0-20 | 3.15 | 41.3 | 90.6 | 0.46 | 0.52 | 11.81 | 11.81 |
| 247 | Chiba | CW-0.6-1.2-40 | 3.15 | 41.3 | 90.6 | 0.46 | 0.52 | 11.81 | 11.81 |
| 248 | Chiba | CW-0.4-1.2-20 | 3.15 | 25.6 | 90.6 | 0.28 | 0.35 | 11.81 | 11.81 |
| 249 | Chiba | CW-0.8-1.2-20 | 3.15 | 57.1 | 90.6 | 0.63 | 0.70 | 11.81 | 11.81 |
| 250 | Yagishita | CW-0.6-0.6-20a | 3.15 | 41.3 | 90.6 | 0.46 | 0.52 | 11.81 | 11.81 |
| 251 | Yagishita | CW-0.6-0.8-20a | 3.15 | 41.3 | 90.6 | 0.46 | 0.52 | 11.81 | 11.81 |
| 252 | Yagishita | CW-0.6-1.2-0 | 3.15 | 41.3 | 90.6 | 0.46 | 0.52 | 11.81 | 11.81 |
| 253 | Fukuzawa | CW-0.6-0-20 | 3.15 | 41.3 | 90.6 | 0.46 | 0.52 | 11.81 | 11.81 |
| 254 | Fukuzawa | CW-0.6-0.3-20 | 3.15 | 41.3 | 90.6 | 0.46 | 0.52 | 11.81 | 11.81 |
| 255 | Fukuzawa | CW-0.6-2.4-20 | 3.15 | 41.3 | 90.6 | 0.46 | 0.52 | 11.81 | 11.81 |
| 256 | Fukuzawa | CW-0.6-2.8-20 | 3.15 | 41.3 | 90.6 | 0.46 | 0.52 | 11.81 | 11.81 |
| 257 | Fukuzawa | CW-0.6-0-0 | 3.15 | 41.3 | 90.6 | 0.46 | 0.52 | 11.81 | 11.81 |

**Table A-5 Geometric properties of the walls with barbell and flanged cross-sections (cont'd)**

| No. | Researcher | Specimen ID | $t_w$ (in) | $h_w$ (in) | $l_w$ (in) | $h_w / l_w$ | $M / Vl_w$ | $l_w / t_w$ | $h_{be}$ (in) |
|---|---|---|---|---|---|---|---|---|---|
| 258 | Fukuzawa | CW-0.6-0-40 | 3.15 | 41.3 | 90.6 | 0.46 | 0.52 | 11.81 | 11.81 |
| 259 | Fukuzawa | CW-0.6-0.6-0 | 3.15 | 41.3 | 90.6 | 0.46 | 0.52 | 11.81 | 11.81 |
| 260 | Fukuzawa | CW-0.6-0.6-40 | 3.15 | 41.3 | 90.6 | 0.46 | 0.52 | 11.81 | 11.81 |
| 261 | Fukuzawa | CW-0.4-0.6-20 | 3.15 | 25.6 | 90.6 | 0.28 | 0.35 | 11.81 | 11.81 |
| 262 | Fukuzawa | CW-0.8-0.6-20 | 3.15 | 57.1 | 90.6 | 0.63 | 0.70 | 11.81 | 11.81 |
| 263 | Fukuzawa | CW-0.4-2.0-20 | 3.15 | 25.6 | 90.6 | 0.28 | 0.35 | 11.81 | 11.81 |
| 264 | Fukuzawa | CW-0.8-2.0-20 | 3.15 | 57.1 | 90.6 | 0.63 | 0.70 | 11.81 | 11.81 |
| 265 | Hatori | CW-0.6-2-0 | 3.15 | 41.3 | 90.6 | 0.46 | 0.52 | 11.81 | 11.81 |
| 266 | Hatori | CW-0.6-2-40 | 3.15 | 41.3 | 90.6 | 0.46 | 0.52 | 11.81 | 11.81 |
| 267 | Hatori | CW-0.6-2-20B | 3.15 | 41.3 | 90.6 | 0.46 | 0.52 | 11.81 | 11.81 |
| 268 | Hatori | CW-0.6-0.6-20L | 3.15 | 41.3 | 90.6 | 0.46 | 0.52 | 11.81 | 11.81 |
| 269 | Hatori | CW-0.6-1.2-20L | 3.15 | 41.3 | 90.6 | 0.46 | 0.52 | 11.81 | 11.81 |
| 270 | Hatori | CW-0.6-2-20L | 3.15 | 41.3 | 90.6 | 0.46 | 0.52 | 11.81 | 11.81 |
| 271 | Taga | No1 | 3.15 | 41.3 | 85.8 | 0.48 | 0.55 | 7.09 | 7.09 |
| 272 | Taga | No2 | 3.15 | 41.3 | 85.8 | 0.48 | 0.55 | 7.09 | 7.09 |
| 273 | Taga | No3 | 3.15 | 41.3 | 85.8 | 0.48 | 0.55 | 7.09 | 7.09 |
| 274 | Taga | No4 | 3.15 | 41.3 | 85.8 | 0.48 | 0.55 | 7.09 | 7.09 |
| 275 | Taga | No5 | 3.15 | 41.3 | 85.8 | 0.48 | 0.55 | 7.09 | 7.09 |
| 276 | Taga | No6 | 3.15 | 41.3 | 85.8 | 0.48 | 0.55 | 7.09 | 7.09 |
| 277 | Taga | No7 | 3.15 | 41.3 | 85.8 | 0.48 | 0.55 | 7.09 | 7.09 |
| 278 | Farvashany | HSCW1 | 2.95 | 43.3 | 34.6 | 1.25 | 1.36 | 11.7 | 3.54 |
| 279 | Farvashany | HSCW2 | 2.95 | 43.3 | 34.6 | 1.25 | 1.36 | 11.7 | 3.54 |
| 280 | Farvashany | HSCW3 | 2.95 | 43.3 | 34.6 | 1.25 | 1.36 | 11.7 | 3.54 |
| 281 | Farvashany | HSCW4 | 2.95 | 43.3 | 34.6 | 1.25 | 1.36 | 11.7 | 3.54 |
| 282 | Farvashany | HSCW5 | 2.95 | 43.3 | 34.6 | 1.25 | 1.36 | 11.7 | 3.54 |
| 283 | Farvashany | HSCW6 | 2.95 | 43.3 | 34.6 | 1.25 | 1.36 | 11.7 | 3.54 |
| 284 | Farvashany | HSCW7 | 2.95 | 43.3 | 34.6 | 1.25 | 1.36 | 11.7 | 3.54 |

**Table A-6 Reinforcement information for walls with barbell and flanged cross-sections**

| No. | Researcher | $\rho_{be}$ (%) | $\rho_v$ (%) | $\rho_{vall}$ (%) | $\rho_h$ (%) | NoC-HR | NoC-VR | $s_h$ (in) | $s_v$ (in) |
|---|---|---|---|---|---|---|---|---|---|
| 1 | Antebi | 2.10 | 0.25 | 0.95 | 0.25 | 1 | 1 | 11.0 | 12.2 |
| 2 | Antebi | 2.10 | 0.25 | 0.95 | 0.25 | 1 | 1 | 11.0 | 12.2 |
| 3 | Antebi | 2.10 | 0.25 | 0.95 | 0.25 | 1 | 1 | 11.0 | 12.2 |
| 4 | Antebi | 4.71 | 0.25 | 1.95 | 0.25 | 1 | 1 | 11.0 | 12.2 |
| 5 | Antebi | 4.71 | 0.25 | 1.95 | 0.25 | 1 | 1 | 11.0 | 12.2 |
| 6 | Antebi | 4.71 | 0.25 | 1.95 | 0.25 | 1 | 1 | 11.0 | 12.2 |
| 7 | Antebi | 4.71 | 0.25 | 1.95 | 0.25 | 1 | 1 | 11.0 | 12.2 |
| 8 | Antebi | 2.10 | 0.25 | 0.95 | 0.25 | 1 | 1 | 11.0 | 12.2 |
| 9 | Antebi | 2.10 | 0.25 | 0.95 | 0.25 | 1 | 1 | 11.0 | 12.2 |
| 10 | Antebi | 2.10 | 0.50 | 1.11 | 0.50 | 1 | 1 | 11.0 | 12.2 |
| 11 | Antebi | 2.10 | 0.50 | 1.11 | 0.50 | 1 | 1 | 11.0 | 12.2 |
| 12 | Antebi | 2.10 | 0.50 | 1.11 | 0.50 | 1 | 1 | 11.0 | 12.2 |
| 13 | Antebi | 2.10 | 0.50 | 1.11 | 0.50 | 1 | 1 | 11.0 | 12.2 |
| 14 | Antebi | 2.10 | 0.50 | 1.11 | 0.50 | 1 | 1 | 11.0 | 12.2 |
| 15 | Antebi | 2.10 | 0.50 | 1.11 | 0.50 | 1 | 1 | 11.0 | 12.2 |
| 16 | Antebi | 2.10 | 1.00 | 1.42 | 1.00 | 1 | 1 | 6.0 | 6.1 |
| 17 | Antebi | 2.10 | 1.00 | 1.42 | 1.00 | 1 | 1 | 6.0 | 6.1 |
| 18 | Antebi | 2.10 | 0.50 | 1.11 | 0.50 | 1 | 1 | 11.0 | 12.2 |
| 19 | Antebi | 2.10 | 0.50 | 1.11 | 0.50 | 1 | 1 | 11.0 | 12.2 |
| 20 | Antebi | 2.10 | 0.50 | 1.11 | 0.50 | 1 | 1 | 11.0 | 12.2 |
| 21 | Antebi | 2.10 | 0.50 | 1.11 | 0.50 | 1 | 1 | 11.0 | 12.2 |
| 22 | Antebi | 2.10 | 0.50 | 1.11 | 0.50 | 1 | 1 | 11.0 | 12.2 |
| 23 | Antebi | 2.10 | 0.50 | 1.11 | 0.50 | 1 | 1 | 11.0 | 12.2 |
| 24 | Antebi | 2.10 | 0.50 | 1.11 | 0.50 | 1 | 1 | 11.0 | 12.2 |
| 25 | Antebi | 2.10 | 0.50 | 1.11 | 0.50 | 1 | 1 | 11.0 | 12.2 |
| 26 | Antebi | 4.71 | 0.50 | 2.10 | 0.50 | 1 | 1 | 11.0 | 12.2 |
| 27 | Antebi | 4.71 | 0.50 | 2.10 | 0.50 | 1 | 1 | 11.0 | 12.2 |
| 28 | Antebi | 4.71 | 0.50 | 2.10 | 0.50 | 1 | 1 | 11.0 | 12.2 |
| 29 | Antebi | 4.71 | 0.50 | 2.10 | 0.50 | 1 | 1 | 11.0 | 12.2 |
| 30 | Antebi | 4.71 | 0.50 | 2.10 | 0.50 | 1 | 1 | 11.0 | 12.2 |
| 31 | Antebi | 2.10 | 0.25 | 0.79 | 0.25 | 1 | 1 | 11.0 | 15.3 |
| 32 | Antebi | 2.10 | 0.25 | 0.79 | 0.25 | 1 | 1 | 11.0 | 15.3 |
| 33 | Antebi | 2.10 | 0.25 | 0.79 | 0.25 | 1 | 1 | 11.0 | 15.3 |

**Table A-6 Reinforcement information for walls with barbell and flanged cross-sections (cont'd)**

| No. | Researcher | $\rho_{be}$ (%) | $\rho_v$ (%) | $\rho_{vall}$ (%) | $\rho_h$ (%) | NoC-HR | NoC-VR | $s_h$ (in) | $s_v$ (in) |
|---|---|---|---|---|---|---|---|---|---|
| 34 | Antebi | 2.10 | 0.25 | 0.79 | 0.25 | 1 | 1 | 11.0 | 15.3 |
| 35 | Antebi | 2.10 | 0.25 | 0.79 | 0.25 | 1 | 1 | 11.0 | 15.3 |
| 36 | Antebi | 2.10 | 0.50 | 0.96 | 0.50 | 1 | 1 | 7.2 | 7.6 |
| 37 | Antebi | 2.10 | 0.50 | 0.96 | 0.50 | 1 | 1 | 7.2 | 7.6 |
| 38 | Antebi | 2.10 | 0.50 | 0.96 | 0.50 | 1 | 1 | 7.2 | 7.6 |
| 39 | Antebi | 2.10 | 0.50 | 0.96 | 0.50 | 1 | 1 | 7.2 | 7.6 |
| 40 | Antebi | 2.10 | 0.50 | 0.96 | 0.50 | 1 | 1 | 7.2 | 7.6 |
| 41 | Antebi | 2.10 | 0.50 | 0.88 | 0.50 | 1 | 1 | 11.0 | 10.9 |
| 42 | Antebi | 2.10 | 0.50 | 0.88 | 0.50 | 1 | 1 | 11.0 | 10.9 |
| 43 | Antebi | 2.10 | 0.50 | 0.88 | 0.50 | 1 | 1 | 11.0 | 10.9 |
| 44 | Antebi | 2.10 | 0.50 | 0.88 | 0.50 | 1 | 1 | 11.0 | 10.9 |
| 45 | Antebi | 2.10 | 0.50 | 0.88 | 0.50 | 1 | 1 | 11.0 | 10.9 |
| 46 | Antebi | 2.10 | 0.50 | 0.88 | 0.50 | 1 | 1 | 11.0 | 10.9 |
| 47 | Aoyagi | 1.74 | 0.71 | 1.28 | 0.76 | 2 | 2 | 4.9 | 4.9 |
| 48 | Aoyagi | 1.74 | 0.71 | 1.28 | 0.76 | 2 | 2 | 4.9 | 4.9 |
| 49 | Aoyagi | 1.74 | 0.58 | 1.02 | 0.62 | 2 | 2 | 2.5 | 2.5 |
| 50 | Aoyagi | 6.48 | 0.71 | 3.89 | 0.76 | 2 | 2 | 4.9 | 4.9 |
| 51 | Aoyagi | 6.48 | 0.58 | 2.83 | 0.62 | 2 | 2 | 2.5 | 2.5 |
| 52 | Barda | 1.84 | 0.50 | 1.06 | 0.48 | 2 | 2 | 4.3 | 11.2 |
| 53 | Barda | 6.39 | 0.50 | 2.96 | 0.48 | 2 | 2 | 4.3 | 11.2 |
| 54 | Barda | 4.09 | 0.50 | 2.00 | 0.48 | 2 | 2 | 4.3 | 11.2 |
| 55 | Barda | 4.09 | 0.50 | 2.00 | 0.00 | none | 2 | none | 11.2 |
| 56 | Barda | 4.09 | 0.00 | 1.71 | 0.48 | 2 | none | 4.3 | none |
| 57 | Barda | 4.09 | 0.26 | 1.86 | 0.48 | 2 | 2 | 4.3 | 8.4 |
| 58 | Barda | 4.09 | 0.50 | 2.00 | 0.49 | 2 | 2 | 5.3 | 11.2 |
| 59 | Barda | 4.09 | 0.50 | 2.00 | 0.50 | 2 | 2 | 4.5 | 11.2 |
| 60 | Benjamin | 2.21 | 0.00 | 1.23 | 0.00 | none | none | none | none |
| 61 | Benjamin | 2.21 | 0.00 | 0.92 | 0.00 | none | none | none | none |
| 62 | Benjamin | 2.21 | 0.00 | 0.74 | 0.00 | none | none | none | none |
| 63 | Benjamin | 2.21 | 0.00 | 0.54 | 0.00 | none | none | none | none |
| 64 | Benjamin | 2.21 | 0.50 | 1.45 | 0.50 | 1 | 1 | 1.0 | 1.0 |
| 65 | Benjamin | 2.21 | 0.50 | 1.21 | 0.50 | 1 | 1 | 1.0 | 1.0 |

**Table A-6 Reinforcement information for walls with barbell and flanged cross-sections (cont'd)**

| No. | Researcher | $\rho_{be}$ (%) | $\rho_v$ (%) | $\rho_{vall}$ (%) | $\rho_h$ (%) | NoC-HR | NoC-VR | $s_h$ (in) | $s_v$ (in) |
|---|---|---|---|---|---|---|---|---|---|
| 66 | Benjamin | 2.21 | 0.50 | 1.07 | 0.50 | 1 | 1 | 1.0 | 1.0 |
| 67 | Benjamin | 2.21 | 0.50 | 0.92 | 0.50 | 1 | 1 | 1.0 | 1.0 |
| 68 | Benjamin | 4.19 | 0.50 | 1.40 | 0.50 | 1 | 1 | 1.0 | 1.0 |
| 69 | Benjamin | 2.10 | 0.25 | 0.97 | 0.25 | 1 | 1 | 2.0 | 2.0 |
| 70 | Benjamin | 2.10 | 0.50 | 1.13 | 0.50 | 1 | 1 | 1.0 | 1.0 |
| 71 | Benjamin | 2.10 | 0.50 | 1.13 | 0.50 | 1 | 1 | 1.0 | 1.0 |
| 72 | Benjamin | 1.31 | 0.50 | 0.91 | 0.50 | 1 | 1 | 1.0 | 1.0 |
| 73 | Benjamin | 2.10 | 0.00 | 0.82 | 0.00 | none | none | none | none |
| 74 | Benjamin | 2.10 | 0.00 | 0.82 | 0.00 | none | none | none | none |
| 75 | Benjamin | 2.10 | 0.00 | 0.82 | 0.00 | none | none | none | none |
| 76 | Benjamin | 2.10 | 0.50 | 1.13 | 0.50 | NR | NR | NR | NR |
| 77 | Benjamin | 2.10 | 0.25 | 0.97 | 0.25 | 1 | 1 | 9.8 | 9.8 |
| 78 | Benjamin | 2.21 | 0.25 | 1.04 | 0.25 | 1 | 1 | 9.8 | 9.8 |
| 79 | Benjamin | 2.21 | 0.25 | 1.04 | 0.25 | 1 | 1 | 9.8 | 9.8 |
| 80 | Benjamin | 2.21 | 0.25 | 1.04 | 0.25 | 1 | 1 | 9.8 | 9.8 |
| 81 | Benjamin | 2.21 | 0.25 | 1.04 | 0.25 | 1 | 1 | 9.8 | 9.8 |
| 82 | Benjamin | 2.76 | 0.50 | 1.15 | 0.50 | 1 | 1 | 5.0 | 5.0 |
| 83 | Benjamin | 2.76 | 0.50 | 1.15 | 0.50 | 1 | 1 | 5.0 | 5.0 |
| 84 | Benjamin | 2.76 | 0.50 | 1.15 | 0.50 | 1 | 1 | 5.0 | 5.0 |
| 85 | Kabeyasawa | 0.71 | 0.27 | 0.44 | 0.27 | 1 | 1 | 5.9 | 5.9 |
| 86 | Kabeyasawa | 1.43 | 0.53 | 0.88 | 0.53 | 2 | 2 | 5.9 | 5.9 |
| 87 | Kabeyasawa | 2.14 | 0.80 | 1.32 | 0.80 | 2 | 2 | 3.9 | 3.9 |
| 88 | Kabeyasawa | 1.43 | 0.80 | 1.04 | 0.80 | 2 | 2 | 3.9 | 3.9 |
| 89 | Kabeyasawa | 1.43 | 0.53 | 0.79 | 0.53 | 2 | 2 | 3.9 | 3.9 |
| 90 | Maier | 1.13 | 1.13 | 1.13 | 1.01 | 2 | 2 | 3.9 | 3.9 |
| 91 | Maier | 1.13 | 1.13 | 1.13 | 1.01 | 2 | 2 | 3.9 | 3.9 |
| 92 | Maier | 2.55 | 2.54 | 2.54 | 1.01 | 2 | 2 | 3.9 | 3.9 |
| 93 | Maier | 1.13 | 1.13 | 1.13 | 1.01 | 2 | 2 | 3.9 | 3.9 |
| 94 | Maier | 1.13 | 1.13 | 1.13 | 0.57 | 2 | 2 | 3.9 | 3.9 |
| 95 | Maier | 1.13 | 1.13 | 1.13 | 1.01 | 2 | 2 | 3.9 | 3.9 |
| 96 | Rothe | 1.13 | 0.57 | 0.87 | 0.41 | 1 | 1 | 6.2 | 4.9 |
| 97 | Rothe | 2.01 | 0.57 | 1.35 | 0.41 | 1 | 1 | 6.2 | 4.9 |

**Table A-6 Reinforcement information for walls with barbell and flanged cross-sections (cont'd)**

| No. | Researcher | $\rho_{be}$ (%) | $\rho_v$ (%) | $\rho_{vall}$ (%) | $\rho_h$ (%) | NoC-HR | NoC-VR | $s_h$ (in) | $s_v$ (in) |
|---|---|---|---|---|---|---|---|---|---|
| 98 | Rothe | 2.01 | 0.57 | 1.35 | 0.41 | 1 | 1 | 6.2 | 4.9 |
| 99 | Rothe | 1.13 | 0.57 | 0.87 | 0.41 | 1 | 1 | 6.2 | 4.9 |
| 100 | Rothe | 2.01 | 0.57 | 1.35 | 0.41 | 1 | 1 | 6.2 | 4.9 |
| 101 | Rothe | 1.13 | 0.57 | 0.87 | 0.41 | 1 | 1 | 6.2 | 4.9 |
| 102 | Ryo | 2.55 | 0.18 | 1.30 | 0.18 | 1 | 1 | 7.9 | 7.9 |
| 103 | Ryo | 2.55 | 0.19 | 1.32 | 0.19 | 1 | 1 | 7.9 | 7.9 |
| 104 | Ryo | 2.55 | 0.17 | 1.59 | 0.18 | 1 | 1 | 7.9 | 7.9 |
| 105 | SAFE | 2.41 | 0.80 | 1.40 | 0.80 | 2 | 2 | 4.9 | 4.9 |
| 106 | SAFE | 2.41 | 0.80 | 1.40 | 0.80 | 2 | 2 | 4.9 | 4.9 |
| 107 | SAFE | 2.41 | 0.80 | 1.32 | 0.80 | 2 | 2 | 4.9 | 4.9 |
| 108 | SAFE | 1.77 | 0.40 | 0.84 | 0.60 | 2 | 2 | 4.9 | 4.9 |
| 109 | SAFE | 1.77 | 0.40 | 0.84 | 0.60 | 2 | 2 | 4.9 | 4.9 |
| 110 | SAFE | 1.23 | 0.40 | 0.67 | 0.40 | 2 | 2 | 4.9 | 4.9 |
| 111 | SAFE | 1.23 | 0.40 | 0.67 | 0.40 | 2 | 2 | 4.9 | 4.9 |
| 112 | SAFE | 1.77 | 0.60 | 0.98 | 0.60 | 2 | 2 | 4.9 | 4.9 |
| 113 | SAFE | 1.23 | 0.40 | 0.67 | 0.40 | 2 | 2 | 4.9 | 4.9 |
| 114 | SAFE | 1.77 | 0.11 | 0.65 | 0.11 | 2 | 2 | 9.8 | 9.8 |
| 115 | Shiga | 4.22 | 0.25 | 2.04 | 0.25 | 1 | 1 | 2.4 | 2.4 |
| 116 | Shiga | 4.22 | 0.25 | 2.04 | 0.25 | 1 | 1 | 2.4 | 2.4 |
| 117 | Shiga | 4.22 | 0.25 | 2.04 | 0.25 | 1 | 1 | 2.4 | 2.4 |
| 118 | Shiga | 4.22 | 0.25 | 2.04 | 0.25 | 1 | 1 | 2.4 | 2.4 |
| 119 | Shiga | 4.22 | 0.25 | 2.04 | 0.25 | 1 | 1 | 2.4 | 2.4 |
| 120 | Shiga | 4.22 | 0.50 | 2.18 | 0.50 | 1 | 1 | 1.2 | 1.2 |
| 121 | Shiga | 4.22 | 0.50 | 2.18 | 0.50 | 1 | 1 | 1.2 | 1.2 |
| 122 | Shiga | 4.22 | 0.50 | 2.18 | 0.50 | 1 | 1 | 1.2 | 1.2 |
| 123 | Shiga | 4.22 | 0.25 | 2.04 | 0.25 | 1 | 1 | 2.4 | 2.4 |
| 124 | Shiga | 4.22 | 0.25 | 2.04 | 0.25 | 1 | 1 | 2.4 | 2.4 |
| 125 | Shiga | 4.22 | 0.25 | 2.04 | 0.25 | 1 | 1 | 2.4 | 2.4 |
| 126 | Shiga | 4.22 | 0.25 | 2.04 | 0.25 | 1 | 1 | 2.4 | 2.4 |
| 127 | Shiga | 4.22 | 0.25 | 2.04 | 0.25 | 1 | 1 | 2.4 | 2.4 |
| 128 | Shiga | 4.22 | 0.25 | 2.04 | 0.25 | 1 | 1 | 2.4 | 2.4 |
| 129 | Shiga | 4.22 | 0.25 | 2.04 | 0.25 | 1 | 1 | 2.4 | 2.4 |

**Table A-6 Reinforcement information for walls with barbell and flanged cross-sections (cont'd)**

| No. | Researcher | $\rho_{be}$ (%) | $\rho_v$ (%) | $\rho_{vall}$ (%) | $\rho_h$ (%) | NoC-HR | NoC-VR | $s_h$ (in) | $s_v$ (in) |
|---|---|---|---|---|---|---|---|---|---|
| 130 | Shiga | 4.22 | 0.25 | 2.04 | 0.25 | 1 | 1 | 2.4 | 2.4 |
| 131 | Shiga | 4.22 | 0.25 | 2.04 | 0.25 | 1 | 1 | 2.4 | 2.4 |
| 132 | Sugano | 2.54 | 0.18 | 1.33 | 0.18 | 1 | 1 | 7.9 | 7.9 |
| 133 | Sugano | 2.54 | 0.07 | 1.20 | 0.07 | 1 | 1 | 7.9 | 7.9 |
| 134 | Sugano | 1.77 | 0.66 | 1.11 | 0.66 | 2 | 2 | 5.9 | 5.9 |
| 135 | Sugano | 1.77 | 0.66 | 1.11 | 0.66 | 2 | 2 | 5.9 | 5.9 |
| 136 | Sugano | 1.77 | 0.66 | 1.11 | 0.66 | 2 | 2 | 5.9 | 5.9 |
| 137 | Sugano | 1.77 | 0.33 | 0.91 | 0.33 | 1 | 1 | 5.9 | 5.9 |
| 138 | Sugano | 1.77 | 0.33 | 0.91 | 0.33 | 2 | 2 | 5.9 | 5.9 |
| 139 | Sugano | 1.77 | 0.69 | 1.12 | 0.66 | 2 | 2 | 5.9 | 5.9 |
| 140 | Sugano | 1.77 | 0.69 | 1.12 | 0.66 | 2 | 2 | 5.9 | 5.9 |
| 141 | Sugano | 1.77 | 0.77 | 1.17 | 0.74 | 2 | 2 | 5.9 | 5.9 |
| 142 | Synge | 1.81 | 0.37 | 0.75 | 1.61 | 1 | 1 | 4.7 | 7.9 |
| 143 | Tsuboi | 3.96 | 1.97 | 3.14 | 1.89 | 2 | 2 | 0.8 | 0.8 |
| 144 | Tsuboi | 8.27 | 1.97 | 5.68 | 1.89 | 2 | 2 | 0.8 | 0.8 |
| 145 | Tsuboi | 3.96 | 2.53 | 3.37 | 2.58 | 2 | 2 | 0.8 | 0.8 |
| 146 | Tsuboi | 8.27 | 2.53 | 5.91 | 2.58 | 2 | 2 | 0.8 | 0.8 |
| 147 | Tsuboi | 3.96 | 1.97 | 3.14 | 1.89 | 2 | 2 | 0.8 | 0.8 |
| 148 | Tsuboi | 8.27 | 1.97 | 5.68 | 1.89 | 2 | 2 | 0.8 | 0.8 |
| 149 | Mo | 2.10 | 0.73 | 1.22 | 0.82 | 1 | 1 | 4.3 | 4.6 |
| 150 | Mo | 2.10 | 0.73 | 1.22 | 0.82 | 1 | 1 | 4.3 | 4.6 |
| 151 | Mo | 2.10 | 0.73 | 1.22 | 0.82 | 1 | 1 | 4.3 | 4.6 |
| 152 | Mo | 2.10 | 0.73 | 1.22 | 0.82 | 1 | 1 | 4.3 | 4.6 |
| 153 | Mo | 2.10 | 0.73 | 1.22 | 0.82 | 1 | 1 | 4.3 | 4.6 |
| 154 | Mo | 2.10 | 0.73 | 1.22 | 0.82 | 1 | 1 | 4.3 | 4.6 |
| 155 | Mo | 2.10 | 0.73 | 1.22 | 0.82 | 1 | 1 | 4.3 | 4.6 |
| 156 | Mo | 2.10 | 0.73 | 1.22 | 0.82 | 1 | 1 | 4.3 | 4.6 |
| 157 | Mo | 2.10 | 0.73 | 1.22 | 0.82 | 1 | 1 | 4.3 | 4.6 |
| 158 | Mo | 2.10 | 0.58 | 1.12 | 0.82 | 1 | 1 | 4.3 | 5.5 |
| 159 | Mo | 2.10 | 0.58 | 1.12 | 0.82 | 1 | 1 | 4.3 | 5.5 |
| 160 | Mo | 2.10 | 0.58 | 1.12 | 0.82 | 1 | 1 | 4.3 | 5.5 |
| 161 | Mo | 2.10 | 0.58 | 1.12 | 0.82 | 1 | 1 | 4.3 | 5.5 |

**Table A-6 Reinforcement information for walls with barbell and flanged cross-sections (cont'd)**

| No. | Researcher | $\rho_{be}$ (%) | $\rho_v$ (%) | $\rho_{vall}$ (%) | $\rho_h$ (%) | NoC-HR | NoC-VR | $s_h$ (in) | $s_v$ (in) |
|---|---|---|---|---|---|---|---|---|---|
| 162 | Mo | 2.10 | 0.58 | 1.12 | 0.82 | 1 | 1 | 4.3 | 5.5 |
| 163 | Mo | 2.10 | 0.58 | 1.12 | 0.82 | 1 | 1 | 4.3 | 5.5 |
| 164 | Mo | 2.10 | 0.58 | 1.12 | 0.82 | 1 | 1 | 4.3 | 5.5 |
| 165 | Mo | 2.10 | 0.58 | 1.12 | 0.82 | 1 | 1 | 4.3 | 5.5 |
| 166 | Mo | 2.10 | 0.58 | 1.12 | 0.82 | 1 | 1 | 4.3 | 5.5 |
| 167 | Mo | 2.10 | 0.58 | 1.12 | 0.82 | 1 | 1 | 4.3 | 5.5 |
| 168 | Mo | 2.10 | 0.58 | 1.12 | 0.82 | 1 | 1 | 4.3 | 5.5 |
| 169 | Bouchon | 2.51 | 0.80 | 1.17 | 0.80 | 1 | 1 | 3.9 | 3.9 |
| 170 | Endo | 0.81 | 0.49 | 0.64 | 0.47 | 1 | 1 | 2.0 | 2.0 |
| 171 | Endo | 0.81 | 0.16 | 0.47 | 0.14 | 1 | 1 | 5.9 | 5.9 |
| 172 | Endo | 0.81 | 0.16 | 0.47 | 0.14 | 1 | 1 | 5.9 | 5.9 |
| 173 | Endo | 0.81 | 0.26 | 0.58 | 0.22 | 1 | 1 | 5.9 | 5.9 |
| 174 | Endo | 0.81 | 0.79 | 0.80 | 0.76 | 1 | 1 | 2.0 | 2.0 |
| 175 | NUPEC | 0.47 | 1.20 | 0.66 | 1.20 | 2 | 2 | 2.8 | 2.8 |
| 176 | NUPEC | 0.47 | 1.20 | 0.66 | 1.20 | 2 | 2 | 2.8 | 2.8 |
| 177 | Vecchio | 0.37 | 0.82 | 0.49 | 0.76 | 2 | 2 | 5.5 | 5.1 |
| 178 | Vecchio | 0.35 | 0.82 | 0.48 | 0.76 | 2 | 2 | 5.5 | 5.1 |
| 179 | XiangDong | 3.27 | 0.55 | 1.64 | 0.55 | 2 | 2 | 6.0 | 6.0 |
| 180 | XiangDong | 3.27 | 0.55 | 1.64 | 0.55 | 2 | 2 | 6.0 | 6.0 |
| 181 | XiangDong | 3.27 | 0.55 | 1.64 | 0.55 | 2 | 2 | 6.0 | 6.0 |
| 182 | XiangDong | 3.27 | 1.09 | 1.96 | 1.09 | 2 | 2 | 3.0 | 3.0 |
| 183 | XiangDong | 3.27 | 0.23 | 1.45 | 0.23 | 2 | 2 | 6.0 | 6.0 |
| 184 | XiangDong | 3.27 | 1.09 | 1.96 | 1.09 | 2 | 2 | 3.0 | 3.0 |
| 185 | XiangDong | 3.27 | 1.09 | 1.96 | 1.09 | 2 | 2 | 3.0 | 3.0 |
| 186 | XiangDong | 3.27 | 0.23 | 1.45 | 0.23 | 2 | 2 | 6.0 | 6.0 |
| 187 | XiangDong | 3.27 | 0.23 | 1.45 | 0.23 | 2 | 2 | 6.0 | 6.0 |
| 188 | Sheu | 1.12 | 0.58 | 0.86 | 0.82 | 1 | 1 | 4.9 | 5.5 |
| 189 | Sheu | 1.12 | 0.58 | 0.86 | 0.82 | 1 | 1 | 4.9 | 5.5 |
| 190 | Sheu | 1.12 | 0.58 | 0.86 | 0.82 | 1 | 1 | 4.9 | 5.5 |
| 191 | Sheu | 1.12 | 0.58 | 0.86 | 0.82 | 1 | 1 | 4.9 | 5.5 |
| 192 | Sheu | 1.12 | 0.58 | 0.86 | 0.82 | 1 | 1 | 4.9 | 5.5 |
| 193 | Sheu | 1.99 | 1.04 | 1.52 | 1.45 | 1 | 1 | 4.9 | 5.5 |

**Table A-6 Reinforcement information for walls with barbell and flanged cross-sections (cont'd)**

| No. | Researcher | $\rho_{be}$ (%) | $\rho_v$ (%) | $\rho_{vall}$ (%) | $\rho_h$ (%) | NoC-HR | NoC-VR | $s_h$ (in) | $s_v$ (in) |
|---|---|---|---|---|---|---|---|---|---|
| 194 | Sheu | 1.99 | 1.04 | 1.52 | 1.45 | 1 | 1 | 4.9 | 5.5 |
| 195 | Sheu | 1.99 | 1.04 | 1.52 | 1.45 | 1 | 1 | 4.9 | 5.5 |
| 196 | Sheu | 1.99 | 1.04 | 1.52 | 1.45 | 1 | 1 | 4.9 | 5.5 |
| 197 | Sheu | 1.99 | 1.04 | 1.52 | 1.45 | 1 | 1 | 4.9 | 5.5 |
| 198 | Sheu | 1.12 | 0.58 | 0.86 | 0.82 | 1 | 1 | 4.9 | 5.5 |
| 199 | Sheu | 1.12 | 0.58 | 0.86 | 0.82 | 1 | 1 | 4.9 | 5.5 |
| 200 | Sheu | 1.12 | 0.58 | 0.86 | 0.82 | 1 | 1 | 4.9 | 5.5 |
| 201 | Sheu | 1.12 | 0.58 | 0.86 | 0.82 | 1 | 1 | 4.9 | 5.5 |
| 202 | Sheu | 1.12 | 0.58 | 0.86 | 0.82 | 1 | 1 | 4.9 | 5.5 |
| 203 | Sheu | 1.12 | 0.58 | 0.86 | 0.82 | 1 | 1 | 4.9 | 5.5 |
| 204 | Sheu | 1.12 | 0.58 | 0.86 | 0.82 | 1 | 1 | 4.9 | 5.5 |
| 205 | Saito | 4.75 | 1.32 | 2.51 | 1.32 | 2 | 2 | 3.5 | 3.5 |
| 206 | Saito | 4.75 | 0.90 | 2.24 | 0.90 | 2 | 2 | 5.1 | 5.1 |
| 207 | Saito | 4.75 | 1.69 | 2.75 | 1.69 | 2 | 2 | 2.8 | 2.8 |
| 208 | Saito | 4.75 | 1.32 | 2.51 | 1.32 | 2 | 2 | 3.5 | 3.5 |
| 209 | Saito | 4.75 | 1.32 | 2.51 | 1.32 | 2 | 2 | 3.5 | 3.5 |
| 210 | Saito | 4.75 | 1.32 | 2.51 | 1.32 | 2 | 2 | 3.5 | 3.5 |
| 211 | Saito | 4.75 | 1.32 | 2.51 | 1.32 | 2 | 2 | 3.5 | 3.5 |
| 212 | Saito | 4.75 | 1.06 | 2.16 | 1.06 | 2 | 2 | 3.5 | 3.5 |
| 213 | Saito | 4.75 | 1.06 | 2.16 | 1.06 | 2 | 2 | 3.5 | 3.5 |
| 214 | Seki | 1.20 | 1.20 | 1.20 | 1.20 | 2 | 2 | 2.8 | 2.8 |
| 215 | Seki | 1.20 | 1.20 | 1.20 | 1.20 | 2 | 2 | 2.8 | 2.8 |
| 216 | Seki | 1.20 | 1.20 | 1.20 | 1.20 | 2 | 2 | 2.8 | 2.8 |
| 217 | Seki | 1.20 | 1.20 | 1.20 | 1.20 | 2 | 2 | 2.8 | 2.8 |
| 218 | Seki | 1.20 | 1.20 | 1.20 | 1.20 | 2 | 2 | 2.8 | 2.8 |
| 219 | Seki | 1.20 | 1.20 | 1.20 | 1.20 | 2 | 2 | 2.8 | 2.8 |
| 220 | Sato | 2.25 | 0.45 | 1.39 | 0.45 | 2 | 2 | 7.9 | 7.9 |
| 221 | Sato | 0.80 | 0.80 | 0.80 | 0.80 | 2 | 2 | 4.6 | 4.6 |
| 222 | Sato | 0.60 | 0.60 | 0.60 | 0.60 | 2 | 2 | 6.1 | 6.1 |
| 223 | Sato | 0.48 | 0.48 | 0.48 | 0.48 | 2 | 2 | 7.9 | 7.9 |
| 224 | Sato | 0.80 | 0.80 | 0.80 | 0.80 | 2 | 2 | 4.9 | 4.9 |
| 225 | Sato | 0.60 | 0.60 | 0.60 | 0.60 | 2 | 2 | 6.6 | 6.6 |

**Table A-6 Reinforcement information for walls with barbell and flanged cross-sections (cont'd)**

| No. | Researcher | $\rho_{be}$ (%) | $\rho_v$ (%) | $\rho_{vall}$ (%) | $\rho_h$ (%) | NoC-HR | NoC-VR | $s_h$ (in) | $s_v$ (in) |
|---|---|---|---|---|---|---|---|---|---|
| 226 | Sato | 5.80 | 1.16 | 3.57 | 1.16 | 2 | 2 | 3.2 | 3.2 |
| 227 | Sato | 4.50 | 0.90 | 2.77 | 0.90 | 2 | 2 | 4.1 | 4.1 |
| 228 | Sato | 3.60 | 0.72 | 2.22 | 0.72 | 2 | 2 | 5.1 | 5.1 |
| 229 | Sato | 1.16 | 1.16 | 1.16 | 1.16 | 2 | 2 | 3.2 | 3.2 |
| 230 | Sato | 0.90 | 0.90 | 0.90 | 0.90 | 2 | 2 | 4.3 | 4.3 |
| 231 | Sato | 1.16 | 1.16 | 1.16 | 1.16 | 2 | 2 | 3.2 | 3.2 |
| 232 | Sato | 0.90 | 0.90 | 0.90 | 0.90 | 2 | 2 | 4.3 | 4.3 |
| 233 | Sato | 0.72 | 0.72 | 0.72 | 0.72 | 2 | 2 | 5.0 | 5.0 |
| 234 | Sato | 1.16 | 1.16 | 1.16 | 1.16 | 2 | 2 | 3.2 | 3.2 |
| 235 | Sato | 0.90 | 0.90 | 0.90 | 0.90 | 2 | 2 | 4.4 | 4.4 |
| 236 | Sato | 1.60 | 1.60 | 1.60 | 1.60 | 2 | 2 | 2.3 | 2.3 |
| 237 | Sato | 1.16 | 1.16 | 1.16 | 1.16 | 2 | 2 | 3.2 | 3.2 |
| 238 | Sato | 0.96 | 0.96 | 0.96 | 0.96 | 2 | 2 | 3.9 | 3.9 |
| 239 | Sato | 1.60 | 1.60 | 1.60 | 1.60 | 2 | 2 | 2.3 | 2.3 |
| 240 | Sato | 1.16 | 1.16 | 1.16 | 1.16 | 2 | 2 | 3.2 | 3.2 |
| 241 | Sato | 0.96 | 0.96 | 0.96 | 0.96 | 2 | 2 | 3.9 | 3.9 |
| 242 | Chiba | 1.04 | 1.20 | 1.11 | 1.20 | 2 | 2 | 2.6 | 2.6 |
| 243 | Chiba | 1.04 | 0.60 | 0.85 | 0.60 | 2 | 2 | 5.2 | 5.2 |
| 244 | Chiba | 1.04 | 0.80 | 0.94 | 0.80 | 2 | 2 | 3.9 | 3.9 |
| 245 | Chiba | 1.44 | 1.60 | 1.51 | 1.60 | 2 | 2 | 2.0 | 2.0 |
| 246 | Chiba | 1.76 | 2.00 | 1.86 | 2.00 | 2 | 2 | 1.6 | 1.6 |
| 247 | Chiba | 1.04 | 1.20 | 1.11 | 1.20 | 2 | 2 | 2.6 | 2.6 |
| 248 | Chiba | 1.04 | 1.20 | 1.11 | 1.20 | 2 | 2 | 2.6 | 2.6 |
| 249 | Chiba | 1.04 | 1.20 | 1.11 | 1.20 | 2 | 2 | 2.6 | 2.6 |
| 250 | Yagishita | 1.04 | 0.60 | 0.85 | 0.60 | 2 | 2 | 5.2 | 5.2 |
| 251 | Yagishita | 1.04 | 0.80 | 0.94 | 0.80 | 2 | 2 | 3.9 | 3.9 |
| 252 | Yagishita | 1.04 | 1.20 | 1.11 | 1.20 | 2 | 2 | 2.6 | 2.6 |
| 253 | Fukuzawa | 1.04 | 0.00 | 0.59 | 0.00 | none | none | none | none |
| 254 | Fukuzawa | 1.04 | 0.30 | 0.72 | 0.30 | 2 | 2 | 10.5 | 10.5 |
| 255 | Fukuzawa | 1.76 | 2.40 | 2.04 | 2.40 | 2 | 2 | 1.3 | 1.3 |
| 256 | Fukuzawa | 1.76 | 2.80 | 2.21 | 2.80 | 2 | 2 | 1.1 | 1.1 |
| 257 | Fukuzawa | 1.04 | 0.00 | 0.59 | 0.00 | none | none | none | none |

**Table A-6 Reinforcement information for walls with barbell and flanged cross-sections (cont'd)**

| No. | Researcher | $\rho_{be}$ (%) | $\rho_v$ (%) | $\rho_{vall}$ (%) | $\rho_h$ (%) | NoC-HR | NoC-VR | $s_h$ (in) | $s_v$ (in) |
|---|---|---|---|---|---|---|---|---|---|
| 258 | Fukuzawa | 1.04 | 0.00 | 0.59 | 0.00 | none | none | none | none |
| 259 | Fukuzawa | 1.04 | 0.60 | 0.85 | 0.60 | 2 | 2 | 5.2 | 5.2 |
| 260 | Fukuzawa | 1.04 | 0.60 | 0.85 | 0.60 | 2 | 2 | 5.2 | 5.2 |
| 261 | Fukuzawa | 1.04 | 0.60 | 0.85 | 0.60 | 2 | 2 | 5.2 | 5.2 |
| 262 | Fukuzawa | 1.04 | 0.60 | 0.85 | 0.60 | 2 | 2 | 5.2 | 5.2 |
| 263 | Fukuzawa | 1.76 | 2.00 | 1.86 | 2.00 | 2 | 2 | 1.6 | 1.6 |
| 264 | Fukuzawa | 1.76 | 2.00 | 1.86 | 2.00 | 2 | 2 | 1.6 | 1.6 |
| 265 | Hatori | 1.76 | 2.00 | 1.86 | 2.00 | 2 | 2 | 1.6 | 1.6 |
| 266 | Hatori | 1.76 | 2.00 | 1.86 | 2.00 | 2 | 2 | 1.6 | 1.6 |
| 267 | Hatori | 1.04 | 2.00 | 1.45 | 2.00 | 2 | 2 | 1.6 | 1.6 |
| 268 | Hatori | 1.04 | 0.60 | 0.85 | 0.60 | 2 | 2 | 5.2 | 5.2 |
| 269 | Hatori | 1.04 | 1.20 | 1.11 | 1.20 | 2 | 2 | 2.6 | 2.6 |
| 270 | Hatori | 1.76 | 2.00 | 1.86 | 2.00 | 2 | 2 | 1.6 | 1.6 |
| 271 | Taga | 2.89 | 1.20 | 1.72 | 1.20 | 2 | 2 | 2.6 | 2.6 |
| 272 | Taga | 2.89 | 1.20 | 1.72 | 1.20 | 2 | 2 | 2.6 | 2.6 |
| 273 | Taga | 2.89 | 1.20 | 1.72 | 1.20 | 2 | 2 | 2.6 | 2.6 |
| 274 | Taga | 2.89 | 0.60 | 1.30 | 0.60 | 2 | 2 | 5.2 | 5.2 |
| 275 | Taga | 2.89 | 2.00 | 2.27 | 2.00 | 2 | 2 | 1.6 | 1.6 |
| 276 | Taga | 2.89 | 2.00 | 2.27 | 2.00 | 2 | 2 | 1.6 | 1.6 |
| 277 | Taga | 2.89 | 2.00 | 2.27 | 2.00 | 2 | 2 | 1.6 | 1.6 |
| 278 | Farvashany | 4.02 | 1.29 | 2.83 | 0.48 | 2 | 2 | 6.3 | 2.4 |
| 279 | Farvashany | 4.02 | 1.29 | 2.83 | 0.48 | 2 | 2 | 6.3 | 2.4 |
| 280 | Farvashany | 4.02 | 0.75 | 2.59 | 0.48 | 2 | 2 | 6.3 | 3.9 |
| 281 | Farvashany | 4.02 | 0.75 | 2.59 | 0.48 | 2 | 2 | 6.3 | 3.9 |
| 282 | Farvashany | 4.02 | 1.29 | 2.83 | 0.75 | 2 | 2 | 3.9 | 2.4 |
| 283 | Farvashany | 4.02 | 1.29 | 2.83 | 0.75 | 2 | 2 | 3.9 | 2.4 |
| 284 | Farvashany | 4.02 | 0.75 | 2.59 | 0.75 | 2 | 2 | 3.9 | 3.9 |

**Table A-7 Material properties of the walls with barbell and flanged cross-sections**

| No. | Researcher | $f_c'$ (psi) | $f_{ybe}$ (ksi) | $f_{ube}$ (ksi) | $f_{yv}$ (ksi) | $f_{uv}$ (ksi) | $f_{yh}$ (ksi) | $f_{uh}$ (ksi) |
|---|---|---|---|---|---|---|---|---|
| 1 | Antebi | 2890 | 47.0 | 83.9 | 39.3 | 52.0 | 39.3 | 52.0 |
| 2 | Antebi | 3180 | 47.0 | 83.9 | 39.3 | 52.0 | 39.3 | 52.0 |
| 3 | Antebi | 3160 | 47.0 | 83.9 | 39.3 | 52.0 | 39.3 | 52.0 |
| 4 | Antebi | 3780 | 44.3 | 67.8 | 39.3 | 52.0 | 39.3 | 52.0 |
| 5 | Antebi | 3660 | 44.3 | 67.8 | 39.3 | 52.0 | 39.3 | 52.0 |
| 6 | Antebi | 3480 | 44.3 | 67.8 | 39.3 | 52.0 | 39.3 | 52.0 |
| 7 | Antebi | 3360 | 44.3 | 67.8 | 39.3 | 52.0 | 39.3 | 52.0 |
| 8 | Antebi | 5126 | 47.0 | 83.9 | 39.3 | 52.0 | 39.3 | 52.0 |
| 9 | Antebi | 4565 | 47.0 | 83.9 | 39.3 | 52.0 | 39.3 | 52.0 |
| 10 | Antebi | 2669 | 43.0 | 69.6 | 57.0 | 90.5 | 57.0 | 90.5 |
| 11 | Antebi | 3081 | 43.3 | 69.4 | 60.0 | 92.7 | 60.0 | 92.7 |
| 12 | Antebi | 2904 | 43.3 | 69.5 | 60.0 | 92.3 | 60.0 | 92.3 |
| 13 | Antebi | 2170 | 43.1 | 68.7 | 58.8 | 92.6 | 58.8 | 92.6 |
| 14 | Antebi | 2288 | 43.4 | 71.2 | 58.1 | 92.7 | 58.1 | 92.7 |
| 15 | Antebi | 3037 | 42.8 | 70.4 | 59.9 | 93.2 | 59.9 | 93.2 |
| 16 | Antebi | 2939 | 43.4 | 71.8 | 48.3 | 73.6 | 48.3 | 73.6 |
| 17 | Antebi | 2904 | 42.1 | 67.7 | 59.4 | 93.6 | 59.4 | 93.6 |
| 18 | Antebi | 5973 | 40.0 | 69.5 | 48.0 | 74.5 | 48.0 | 74.5 |
| 19 | Antebi | 3880 | 49.5 | 76.5 | 49.5 | 74.8 | 49.5 | 74.8 |
| 20 | Antebi | 3880 | 50.0 | 76.4 | 50.0 | 76.4 | 50.0 | 76.4 |
| 21 | Antebi | 3520 | 49.5 | 73.8 | 49.5 | 77.3 | 49.5 | 77.3 |
| 22 | Antebi | 3380 | 49.5 | 74.9 | 49.5 | 76.4 | 49.5 | 76.4 |
| 23 | Antebi | 3700 | 50.0 | 78.8 | 50.0 | 77.3 | 50.0 | 77.3 |
| 24 | Antebi | 3570 | 49.5 | 73.5 | 49.5 | 78.2 | 49.5 | 78.2 |
| 25 | Antebi | 4100 | 50.0 | 79.3 | 50.0 | 78.9 | 50.0 | 78.9 |
| 26 | Antebi | 3510 | 45.9 | 74.1 | 48.4 | 72.1 | 48.4 | 72.1 |
| 27 | Antebi | 4925 | 45.9 | 74.1 | 46.9 | 72.1 | 46.9 | 72.1 |
| 28 | Antebi | 3310 | 49.0 | 74.1 | 46.9 | 72.1 | 46.9 | 72.1 |
| 29 | Antebi | 5000 | 45.9 | 74.1 | 46.9 | 72.1 | 46.9 | 72.1 |
| 30 | Antebi | 4575 | 45.9 | 74.1 | 46.9 | 72.1 | 46.9 | 72.1 |
| 31 | Antebi | 2950 | 42.9 | 74.1 | 45.4 | 72.1 | 45.4 | 72.1 |
| 32 | Antebi | 1720 | 45.4 | 74.1 | 42.9 | 72.1 | 42.9 | 72.1 |

**Table A-7 Material properties of the walls with barbell and flanged cross-sections (cont'd)**

| No. | Researcher | $f_c'$ (psi) | $f_{ybe}$ (ksi) | $f_{ube}$ (ksi) | $f_{yv}$ (ksi) | $f_{uv}$ (ksi) | $f_{yh}$ (ksi) | $f_{uh}$ (ksi) |
|---|---|---|---|---|---|---|---|---|
| 33 | Antebi | 2600 | 45.5 | 74.1 | 42.6 | 72.1 | 42.6 | 72.1 |
| 34 | Antebi | 2720 | 48.2 | 74.1 | 48.8 | 72.1 | 48.8 | 72.1 |
| 35 | Antebi | 2030 | 45.9 | 74.1 | 46.3 | 72.1 | 46.3 | 72.1 |
| 36 | Antebi | 2380 | 46.3 | 74.1 | 44.4 | 72.1 | 44.4 | 72.1 |
| 37 | Antebi | 2470 | 46.2 | 74.1 | 49.8 | 72.1 | 49.8 | 72.1 |
| 38 | Antebi | 2640 | 45.8 | 74.1 | 50.5 | 72.1 | 50.5 | 72.1 |
| 39 | Antebi | 2989 | 46.0 | 74.1 | 49.5 | 72.1 | 49.5 | 72.1 |
| 40 | Antebi | 2089 | 45.3 | 74.1 | 50.2 | 72.1 | 50.2 | 72.1 |
| 41 | Antebi | 3305 | 46.5 | 74.1 | 52.3 | 72.1 | 52.3 | 72.1 |
| 42 | Antebi | 3329 | 45.9 | 74.1 | 53.8 | 72.1 | 53.8 | 72.1 |
| 43 | Antebi | 3023 | 45.9 | 74.1 | 50.6 | 72.1 | 50.6 | 72.1 |
| 44 | Antebi | 2901 | 48.7 | 74.1 | 50.5 | 72.1 | 50.5 | 72.1 |
| 45 | Antebi | 2723 | 45.5 | 74.1 | 50.4 | 72.1 | 50.4 | 72.1 |
| 46 | Antebi | 2844 | 46.2 | 74.1 | 50.8 | 72.1 | 50.8 | 72.1 |
| 47 | Aoyagi | 2859 | 52.6 | NR | 51.2 | NR | 51.2 | NR |
| 48 | Aoyagi | 3755 | 52.6 | NR | 51.2 | NR | 51.2 | NR |
| 49 | Aoyagi | 4267 | 52.6 | NR | 49.2 | NR | 49.2 | NR |
| 50 | Aoyagi | 3456 | 39.5 | NR | 51.2 | NR | 51.2 | NR |
| 51 | Aoyagi | 4239 | 39.5 | NR | 49.2 | NR | 49.2 | NR |
| 52 | Barda | 4200 | 76.2 | 118.7 | 78.8 | 123.1 | 71.9 | 98.6 |
| 53 | Barda | 2370 | 70.6 | 119.0 | 80.0 | 126.5 | 72.4 | 97.0 |
| 54 | Barda | 3920 | 60.0 | 96.7 | 79.0 | 123.3 | 74.4 | 97.5 |
| 55 | Barda | 2760 | 76.5 | 117.2 | 77.6 | 119.6 | N/A | N/A |
| 56 | Barda | 4190 | 76.4 | 117.0 | N/A | N/A | 71.8 | 98.3 |
| 57 | Barda | 3080 | 76.7 | 116.3 | 72.0 | 94.8 | 72.0 | 94.8 |
| 58 | Barda | 3730 | 78.2 | 115.1 | 77.0 | 120.4 | 72.7 | 96.0 |
| 59 | Barda | 3400 | 70.9 | 112.8 | 76.5 | 109.5 | 71.9 | 97.9 |
| 60 | Benjamin | 2850 | 45.3 | 76.0 | N/A | N/A | N/A | N/A |
| 61 | Benjamin | 3290 | 45.3 | 76.0 | N/A | N/A | N/A | N/A |
| 62 | Benjamin | 3260 | 45.3 | 76.0 | N/A | N/A | N/A | N/A |
| 63 | Benjamin | 3500 | 45.3 | 76.0 | N/A | N/A | N/A | N/A |
| 64 | Benjamin | 2920 | 45.3 | 76.0 | 49.5 | 55.3 | 49.5 | 55.3 |

**Table A-7 Material properties of the walls with barbell and flanged cross-sections (cont'd)**

| No. | Researcher | $f_c'$ (psi) | $f_{ybe}$ (ksi) | $f_{ube}$ (ksi) | $f_{yv}$ (ksi) | $f_{uv}$ (ksi) | $f_{yh}$ (ksi) | $f_{uh}$ (ksi) |
|---|---|---|---|---|---|---|---|---|
| 65 | Benjamin | 3120 | 45.3 | 76.0 | 49.5 | 55.3 | 49.5 | 55.3 |
| 66 | Benjamin | 2830 | 45.3 | 76.0 | 49.5 | 55.3 | 49.5 | 55.3 |
| 67 | Benjamin | 3830 | 45.3 | 76.0 | 49.5 | 55.3 | 49.5 | 55.3 |
| 68 | Benjamin | 3060 | 45.3 | 76.0 | 49.5 | 55.3 | 49.5 | 55.3 |
| 69 | Benjamin | 2920 | 45.3 | 76.0 | 49.5 | 55.3 | 49.5 | 55.3 |
| 70 | Benjamin | 3220 | 45.3 | 76.0 | 49.5 | 55.3 | 49.5 | 55.3 |
| 71 | Benjamin | 3470 | 45.3 | 76.0 | 49.5 | 55.3 | 49.5 | 55.3 |
| 72 | Benjamin | 3250 | 45.3 | 76.0 | 49.5 | 55.3 | 49.5 | 55.3 |
| 73 | Benjamin | 3020 | 45.3 | 76.0 | N/A | N/A | N/A | N/A |
| 74 | Benjamin | 3024 | 45.3 | 76.0 | N/A | N/A | N/A | N/A |
| 75 | Benjamin | 3450 | 45.3 | 76.0 | N/A | N/A | N/A | N/A |
| 76 | Benjamin | 3000 | 45.3 | 76.0 | 49.5 | 55.3 | 49.5 | 55.3 |
| 77 | Benjamin | 3000 | 47.0 | 74.0 | 52.0 | 83.0 | 52.0 | 83.0 |
| 78 | Benjamin | 3200 | 47.0 | 74.0 | 52.0 | 83.0 | 52.0 | 83.0 |
| 79 | Benjamin | 2750 | 47.0 | 74.0 | 52.0 | 83.0 | 52.0 | 83.0 |
| 80 | Benjamin | 3680 | 47.0 | 74.0 | 52.0 | 83.0 | 52.0 | 83.0 |
| 81 | Benjamin | 3100 | 47.0 | 74.0 | 52.0 | 83.0 | 52.0 | 83.0 |
| 82 | Benjamin | 2340 | 43.0 | 69.0 | 52.0 | 83.0 | 52.0 | 83.0 |
| 83 | Benjamin | 2340 | 43.0 | 69.0 | 52.0 | 83.0 | 52.0 | 83.0 |
| 84 | Benjamin | 2340 | 43.0 | 69.0 | 52.0 | 83.0 | 52.0 | 83.0 |
| 85 | Kabeyasawa | 2788 | 56.8 | 80.7 | 57.3 | 76.3 | 57.3 | 76.3 |
| 86 | Kabeyasawa | 2788 | 56.8 | 80.7 | 57.3 | 76.3 | 57.3 | 76.3 |
| 87 | Kabeyasawa | 2788 | 56.8 | 80.7 | 57.3 | 76.3 | 57.3 | 76.3 |
| 88 | Kabeyasawa | 3015 | 56.8 | 80.7 | 57.3 | 76.3 | 57.3 | 76.3 |
| 89 | Kabeyasawa | 2913 | 54.8 | 79.0 | 51.7 | 73.2 | 51.7 | 73.2 |
| 90 | Maier | 5352 | 83.3 | 110.8 | 83.3 | 110.8 | 83.3 | 110.8 |
| 91 | Maier | 5568 | 83.3 | 110.8 | 83.3 | 110.8 | 83.3 | 110.8 |
| 92 | Maier | 5323 | 76.9 | 107.2 | 76.9 | 107.2 | 83.3 | 110.8 |
| 93 | Maier | 5410 | 83.3 | 110.8 | 83.3 | 110.8 | 83.3 | 110.8 |
| 94 | Maier | 5163 | 69.5 | 110.8 | 69.5 | 110.8 | 77.9 | 108.2 |
| 95 | Maier | 4946 | 80.5 | 113.4 | 80.5 | 113.4 | 80.5 | 113.4 |
| 96 | Rothe | 4496 | 60.9 | 72.5 | 60.9 | 72.5 | 60.9 | 72.5 |

**Table A-7 Material properties of the walls with barbell and flanged cross-sections (cont'd)**

| No. | Researcher | $f_c'$ (psi) | $f_{ybe}$ (ksi) | $f_{ube}$ (ksi) | $f_{yv}$ (ksi) | $f_{uv}$ (ksi) | $f_{yh}$ (ksi) | $f_{uh}$ (ksi) |
|---|---|---|---|---|---|---|---|---|
| 97 | Rothe | 4308 | 60.9 | 72.5 | 60.9 | 72.5 | 60.9 | 72.5 |
| 98 | Rothe | 4881 | 60.9 | 72.5 | 60.9 | 72.5 | 60.9 | 72.5 |
| 99 | Rothe | 4483 | 60.9 | 72.5 | 60.9 | 72.5 | 60.9 | 72.5 |
| 100 | Rothe | 4444 | 60.9 | 72.5 | 60.9 | 72.5 | 60.9 | 72.5 |
| 101 | Rothe | 3858 | 60.9 | 72.5 | 60.9 | 72.5 | 60.9 | 72.5 |
| 102 | Ryo | 3371 | 67.8 | N/A | 48.6 | N/A | 48.6 | N/A |
| 103 | Ryo | 4779 | 67.8 | N/A | 48.6 | N/A | 48.6 | N/A |
| 104 | Ryo | 2518 | 67.8 | N/A | 70.4 | N/A | 70.4 | N/A |
| 105 | SAFE | 5246 | 76.7 | 89.7 | 82.7 | 94.4 | 82.7 | 94.4 |
| 106 | SAFE | 5834 | 76.7 | 89.7 | 82.7 | 94.4 | 82.7 | 94.4 |
| 107 | SAFE | 5834 | 76.7 | 89.7 | 82.7 | 94.4 | 82.7 | 94.4 |
| 108 | SAFE | 5834 | 82.2 | 94.5 | 86.2 | 97.5 | 83.1 | 94.4 |
| 109 | SAFE | 5834 | 82.2 | 94.5 | 86.2 | 97.5 | 83.1 | 94.4 |
| 110 | SAFE | 5834 | 83.1 | 94.4 | 86.2 | 97.5 | 86.2 | 97.5 |
| 111 | SAFE | 5834 | 83.1 | 94.4 | 86.2 | 97.5 | 86.2 | 97.5 |
| 112 | SAFE | 5834 | 82.2 | 94.5 | 83.1 | 94.4 | 83.1 | 94.4 |
| 113 | SAFE | 5834 | 83.1 | 94.4 | 86.2 | 97.5 | 86.2 | 97.5 |
| 114 | SAFE | 5834 | 82.2 | 94.5 | 82.5 | 96.3 | 82.5 | 96.3 |
| 115 | Shiga | 2674 | 55.5 | 79.6 | 42.7 | 58.3 | 42.7 | 58.3 |
| 116 | Shiga | 2674 | 55.5 | 79.6 | 42.7 | 58.3 | 42.7 | 58.3 |
| 117 | Shiga | 2333 | 55.5 | 79.6 | 42.7 | 58.3 | 42.7 | 58.3 |
| 118 | Shiga | 2333 | 55.5 | 79.6 | 42.7 | 58.3 | 42.7 | 58.3 |
| 119 | Shiga | 2148 | 55.5 | 79.6 | 42.7 | 58.3 | 42.7 | 58.3 |
| 120 | Shiga | 2148 | 55.5 | 79.6 | 42.7 | 58.3 | 42.7 | 58.3 |
| 121 | Shiga | 2219 | 55.5 | 79.6 | 42.7 | 58.3 | 42.7 | 58.3 |
| 122 | Shiga | 2219 | 55.5 | 79.6 | 42.7 | 58.3 | 42.7 | 58.3 |
| 123 | Shiga | 2461 | 46.9 | 74.0 | 76.8 | 82.5 | 76.8 | 82.5 |
| 124 | Shiga | 2461 | 46.9 | 74.0 | 76.8 | 82.5 | 76.8 | 82.5 |
| 125 | Shiga | 2404 | 46.9 | 74.0 | 76.8 | 82.5 | 76.8 | 82.5 |
| 126 | Shiga | 2404 | 46.9 | 74.0 | 76.8 | 82.5 | 76.8 | 82.5 |
| 127 | Shiga | 2461 | 46.9 | 74.0 | 76.8 | 82.5 | 76.8 | 82.5 |
| 128 | Shiga | 2461 | 46.9 | 74.0 | 76.8 | 82.5 | 76.8 | 82.5 |

**Table A-7 Material properties of the walls with barbell and flanged cross-sections (cont'd)**

| No. | Researcher | $f'_c$ (psi) | $f_{ybe}$ (ksi) | $f_{ube}$ (ksi) | $f_{yv}$ (ksi) | $f_{uv}$ (ksi) | $f_{yh}$ (ksi) | $f_{uh}$ (ksi) |
|---|---|---|---|---|---|---|---|---|
| 129 | Shiga | 1693 | 46.9 | 74.0 | 76.8 | 82.5 | 76.8 | 82.5 |
| 130 | Shiga | 1693 | 46.9 | 74.0 | 76.8 | 82.5 | 76.8 | 82.5 |
| 131 | Shiga | 1451 | 46.9 | 74.0 | 76.8 | 82.5 | 76.8 | 82.5 |
| 132 | Sugano | 3499 | 60.7 | NR | 79.6 | NR | 79.6 | NR |
| 133 | Sugano | 3655 | 60.7 | NR | 66.8 | NR | 66.8 | NR |
| 134 | Sugano | 2987 | 57.6 | NR | 82.9 | NR | 82.9 | NR |
| 135 | Sugano | 3015 | 57.6 | NR | 82.9 | NR | 82.9 | NR |
| 136 | Sugano | 3086 | 57.6 | NR | 82.9 | NR | 82.9 | NR |
| 137 | Sugano | 2845 | 57.6 | NR | 82.9 | NR | 82.9 | NR |
| 138 | Sugano | 3015 | 57.6 | NR | 82.9 | NR | 82.9 | NR |
| 139 | Sugano | 2973 | 57.6 | NR | 41.2 | NR | 41.2 | NR |
| 140 | Sugano | 2845 | 57.6 | NR | 41.2 | NR | 41.2 | NR |
| 141 | Sugano | 3029 | 57.6 | NR | 57.6 | NR | 57.6 | NR |
| 142 | Synge | 3771 | 43.5 | 66.7 | 45.7 | 63.8 | 55.1 | 83.5 |
| 143 | Tsuboi | 4381 | 37.8 | NR | 43.0 | NR | 43.0 | NR |
| 144 | Tsuboi | 4551 | 43.8 | NR | 43.0 | NR | 43.0 | NR |
| 145 | Tsuboi | 4338 | 37.8 | NR | 43.0 | NR | 43.0 | NR |
| 146 | Tsuboi | 4665 | 43.8 | NR | 43.0 | NR | 43.0 | NR |
| 147 | Tsuboi | 4310 | 37.8 | NR | 43.0 | NR | 43.0 | NR |
| 148 | Tsuboi | 4153 | 43.8 | NR | 43.0 | NR | 43.0 | NR |
| 149 | Mo | 4670 | 43.8 | NR | 43.8 | NR | 43.8 | NR |
| 150 | Mo | 4670 | 43.8 | NR | 43.8 | NR | 43.8 | NR |
| 151 | Mo | 4656 | 43.8 | NR | 43.8 | NR | 43.8 | NR |
| 152 | Mo | 4279 | 64.3 | NR | 64.3 | NR | 64.3 | NR |
| 153 | Mo | 4279 | 64.3 | NR | 64.3 | NR | 64.3 | NR |
| 154 | Mo | 4496 | 64.3 | NR | 64.3 | NR | 64.3 | NR |
| 155 | Mo | 5439 | 43.8 | NR | 43.8 | NR | 43.8 | NR |
| 156 | Mo | 5439 | 43.8 | NR | 43.8 | NR | 43.8 | NR |
| 157 | Mo | 5787 | 43.8 | NR | 43.8 | NR | 43.8 | NR |
| 158 | Mo | 2611 | 43.8 | NR | 43.8 | NR | 43.8 | NR |
| 159 | Mo | 2611 | 43.8 | NR | 43.8 | NR | 43.8 | NR |
| 160 | Mo | 4308 | 43.8 | NR | 43.8 | NR | 43.8 | NR |

**Table A-7 Material properties of the walls with barbell and flanged cross-sections (cont'd)**

| No. | Researcher | $f_c'$ (psi) | $f_{ybe}$ (ksi) | $f_{ube}$ (ksi) | $f_{yv}$ (ksi) | $f_{uv}$ (ksi) | $f_{yh}$ (ksi) | $f_{uh}$ (ksi) |
|---|---|---|---|---|---|---|---|---|
| 161 | Mo | 4453 | 64.3 | NR | 64.3 | NR | 64.3 | NR |
| 162 | Mo | 4380 | 64.3 | NR | 64.3 | NR | 64.3 | NR |
| 163 | Mo | 4380 | 64.3 | NR | 64.3 | NR | 64.3 | NR |
| 164 | Mo | 5700 | 64.3 | NR | 64.3 | NR | 64.3 | NR |
| 165 | Mo | 5366 | 64.3 | NR | 64.3 | NR | 64.3 | NR |
| 166 | Mo | 5004 | 64.3 | NR | 64.3 | NR | 64.3 | NR |
| 167 | Mo | 9573 | 43.8 | NR | 43.8 | NR | 43.8 | NR |
| 168 | Mo | 9573 | 43.8 | NR | 43.8 | NR | 43.8 | NR |
| 169 | Bouchon | 4148 | 81.9 | 86.3 | 89.9 | 95.0 | 89.9 | 95.0 |
| 170 | Endo | 3769 | 52.1 | NR | 90.5 | NR | 90.5 | NR |
| 171 | Endo | 3570 | 52.1 | NR | 90.5 | NR | 90.5 | NR |
| 172 | Endo | 3769 | 52.1 | NR | 90.5 | NR | 90.5 | NR |
| 173 | Endo | 3570 | 52.1 | NR | 90.5 | NR | 90.5 | NR |
| 174 | Endo | 3769 | 52.1 | NR | 90.5 | NR | 90.5 | NR |
| 175 | NUPEC | 4153 | 56.7 | 71.8 | 56.7 | 71.8 | 56.7 | 71.8 |
| 176 | NUPEC | 4267 | 56.7 | 71.8 | 56.7 | 71.8 | 56.7 | 71.8 |
| 177 | Vecchio | 3147 | 87.7 | 94.6 | 87.7 | 94.6 | 87.7 | 94.6 |
| 178 | Vecchio | 2727 | 87.7 | 94.6 | 87.7 | 94.6 | 87.7 | 94.6 |
| 179 | XiangDong | 7181 | 61.6 | 78.3 | 60.8 | 81.6 | 60.8 | 81.6 |
| 180 | XiangDong | 8172 | 61.6 | 78.3 | 60.8 | 81.6 | 60.8 | 81.6 |
| 181 | XiangDong | 7216 | 61.6 | 78.3 | 60.8 | 81.6 | 60.8 | 81.6 |
| 182 | XiangDong | 7652 | 61.6 | 78.3 | 60.8 | 81.6 | 60.8 | 81.6 |
| 183 | XiangDong | 7004 | 61.6 | 78.3 | 87.0 | 94.3 | 87.0 | 94.3 |
| 184 | XiangDong | 7287 | 61.6 | 78.3 | 60.8 | 81.6 | 60.8 | 81.6 |
| 185 | XiangDong | 8100 | 61.6 | 78.3 | 60.8 | 81.6 | 60.8 | 81.6 |
| 186 | XiangDong | 8277 | 61.6 | 78.3 | 87.0 | 94.3 | 87.0 | 94.3 |
| 187 | XiangDong | 8254 | 61.6 | 78.3 | 87.0 | 94.3 | 87.0 | 94.3 |
| 188 | Sheu | 3926 | 67.8 | 104.7 | 67.8 | 104.7 | 67.8 | 104.7 |
| 189 | Sheu | 4039 | 67.8 | 104.7 | 67.8 | 104.7 | 67.8 | 104.7 |
| 190 | Sheu | 3670 | 67.8 | 104.7 | 67.8 | 104.7 | 67.8 | 104.7 |
| 191 | Sheu | 3769 | 67.8 | 104.7 | 67.8 | 104.7 | 67.8 | 104.7 |
| 192 | Sheu | 4494 | 67.8 | 104.7 | 67.8 | 104.7 | 67.8 | 104.7 |

**Table A-7 Material properties of the walls with barbell and flanged cross-sections (cont'd)**

| No. | Researcher | $f_c'$ (psi) | $f_{ybe}$ (ksi) | $f_{ube}$ (ksi) | $f_{yv}$ (ksi) | $f_{uv}$ (ksi) | $f_{yh}$ (ksi) | $f_{uh}$ (ksi) |
|---|---|---|---|---|---|---|---|---|
| 193 | Sheu | 4480 | 65.7 | 102.4 | 65.7 | 102.4 | 65.7 | 102.4 |
| 194 | Sheu | 4765 | 65.7 | 102.4 | 65.7 | 102.4 | 65.7 | 102.4 |
| 195 | Sheu | 4054 | 65.7 | 102.4 | 65.7 | 102.4 | 65.7 | 102.4 |
| 196 | Sheu | 4310 | 65.7 | 102.4 | 65.7 | 102.4 | 65.7 | 102.4 |
| 197 | Sheu | 5405 | 65.7 | 102.4 | 65.7 | 102.4 | 65.7 | 102.4 |
| 198 | Sheu | 3883 | 71.2 | 103.6 | 71.2 | 103.6 | 71.2 | 103.6 |
| 199 | Sheu | 3200 | 71.2 | 103.6 | 71.2 | 103.6 | 71.2 | 103.6 |
| 200 | Sheu | 3257 | 71.2 | 103.6 | 71.2 | 103.6 | 71.2 | 103.6 |
| 201 | Sheu | 3342 | 71.2 | 103.6 | 71.2 | 103.6 | 71.2 | 103.6 |
| 202 | Sheu | 3527 | 71.2 | 103.6 | 71.2 | 103.6 | 71.2 | 103.6 |
| 203 | Sheu | 3414 | 71.2 | 103.6 | 71.2 | 103.6 | 71.2 | 103.6 |
| 204 | Sheu | 4196 | 71.2 | 103.6 | 71.2 | 103.6 | 71.2 | 103.6 |
| 205 | Saito | 5106 | 53.5 | 76.2 | 53.5 | 76.2 | 53.5 | 76.2 |
| 206 | Saito | 5533 | 53.5 | 76.2 | 53.5 | 76.2 | 53.5 | 76.2 |
| 207 | Saito | 5191 | 53.5 | 76.2 | 53.5 | 76.2 | 53.5 | 76.2 |
| 208 | Saito | 5191 | 53.5 | 76.2 | 53.5 | 76.2 | 53.5 | 76.2 |
| 209 | Saito | 5860 | 53.5 | 76.2 | 53.5 | 76.2 | 53.5 | 76.2 |
| 210 | Saito | 4807 | 53.5 | 76.2 | 53.5 | 76.2 | 53.5 | 76.2 |
| 211 | Saito | 4921 | 53.5 | 76.2 | 53.5 | 76.2 | 53.5 | 76.2 |
| 212 | Saito | 3598 | 53.5 | 76.2 | 53.5 | 76.2 | 53.5 | 76.2 |
| 213 | Saito | 3755 | 53.5 | 76.2 | 53.5 | 76.2 | 53.5 | 76.2 |
| 214 | Seki | 4580 | 50.6 | 78.7 | 50.6 | 78.7 | 50.6 | 78.7 |
| 215 | Seki | 4281 | 50.6 | 78.7 | 50.6 | 78.7 | 50.6 | 78.7 |
| 216 | Seki | 4196 | 55.3 | 78.7 | 55.3 | 78.7 | 55.3 | 78.7 |
| 217 | Seki | 4196 | 55.3 | 78.7 | 55.3 | 78.7 | 55.3 | 78.7 |
| 218 | Seki | 4366 | 50.6 | 78.7 | 50.6 | 78.7 | 50.6 | 78.7 |
| 219 | Seki | 4238 | 50.6 | 78.7 | 50.6 | 78.7 | 50.6 | 78.7 |
| 220 | Sato | 6251 | 61.2 | 81.2 | 61.2 | 81.2 | 61.2 | 81.2 |
| 221 | Sato | 5512 | 42.9 | 69.6 | 42.9 | 69.6 | 42.9 | 69.6 |
| 222 | Sato | 5192 | 61.2 | 81.2 | 61.2 | 81.2 | 61.2 | 81.2 |
| 223 | Sato | 5076 | 76.6 | 89.9 | 76.6 | 89.9 | 76.6 | 89.9 |
| 224 | Sato | 5816 | 42.9 | 69.6 | 42.9 | 69.6 | 42.9 | 69.6 |

**Table A-7 Material properties of the walls with barbell and flanged cross-sections (cont'd)**

| No. | Researcher | $f_c'$ (psi) | $f_{ybe}$ (ksi) | $f_{ube}$ (ksi) | $f_{yv}$ (ksi) | $f_{uv}$ (ksi) | $f_{yh}$ (ksi) | $f_{uh}$ (ksi) |
|---|---|---|---|---|---|---|---|---|
| 225 | Sato | 5947 | 61.2 | 81.2 | 61.2 | 81.2 | 61.2 | 81.2 |
| 226 | Sato | 5265 | 42.9 | 69.6 | 42.9 | 69.6 | 42.9 | 69.6 |
| 227 | Sato | 4989 | 61.2 | 81.2 | 61.2 | 81.2 | 61.2 | 81.2 |
| 228 | Sato | 5395 | 76.6 | 89.9 | 76.6 | 89.9 | 76.6 | 89.9 |
| 229 | Sato | 3553 | 42.9 | 69.6 | 42.9 | 69.6 | 42.9 | 69.6 |
| 230 | Sato | 4032 | 61.2 | 81.2 | 61.2 | 81.2 | 61.2 | 81.2 |
| 231 | Sato | 5700 | 42.9 | 69.6 | 42.9 | 69.6 | 42.9 | 69.6 |
| 232 | Sato | 5628 | 61.2 | 81.2 | 61.2 | 81.2 | 61.2 | 81.2 |
| 233 | Sato | 5439 | 76.6 | 89.9 | 76.6 | 89.9 | 76.6 | 89.9 |
| 234 | Sato | 4844 | 42.9 | 69.6 | 42.9 | 69.6 | 42.9 | 69.6 |
| 235 | Sato | 5018 | 61.2 | 81.2 | 61.2 | 81.2 | 61.2 | 81.2 |
| 236 | Sato | 3974 | 42.9 | 69.6 | 42.9 | 69.6 | 42.9 | 69.6 |
| 237 | Sato | 3989 | 61.2 | 81.2 | 61.2 | 81.2 | 61.2 | 81.2 |
| 238 | Sato | 4061 | 76.6 | 89.9 | 76.6 | 89.9 | 76.6 | 89.9 |
| 239 | Sato | 6063 | 42.9 | 69.6 | 42.9 | 69.6 | 42.9 | 69.6 |
| 240 | Sato | 6251 | 61.2 | 81.2 | 61.2 | 81.2 | 61.2 | 81.2 |
| 241 | Sato | 6469 | 76.6 | 89.9 | 76.6 | 89.9 | 76.6 | 89.9 |
| 242 | Chiba | 4935 | 54.9 | 83.4 | 59.7 | 77.8 | 59.7 | 77.8 |
| 243 | Chiba | 4281 | 54.9 | 83.4 | 59.7 | 77.8 | 59.7 | 77.8 |
| 244 | Chiba | 5760 | 54.9 | 83.4 | 59.7 | 77.8 | 59.7 | 77.8 |
| 245 | Chiba | 4878 | 55.0 | 82.7 | 59.7 | 77.8 | 59.7 | 77.8 |
| 246 | Chiba | 5021 | 54.3 | 83.8 | 59.7 | 77.8 | 59.7 | 77.8 |
| 247 | Chiba | 4608 | 54.9 | 83.4 | 59.7 | 77.8 | 59.7 | 77.8 |
| 248 | Chiba | 4793 | 54.9 | 83.4 | 59.7 | 77.8 | 59.7 | 77.8 |
| 249 | Chiba | 4850 | 54.9 | 83.4 | 59.7 | 77.8 | 59.7 | 77.8 |
| 250 | Yagishita | 4224 | 54.9 | 83.4 | 59.7 | 77.8 | 59.7 | 77.8 |
| 251 | Yagishita | 4295 | 54.9 | 83.4 | 59.7 | 77.8 | 59.7 | 77.8 |
| 252 | Yagishita | 4167 | 54.9 | 83.4 | 59.7 | 77.8 | 59.7 | 77.8 |
| 253 | Fukuzawa | 5106 | 54.9 | 83.4 | N/A | N/A | N/A | N/A |
| 254 | Fukuzawa | 5106 | 54.9 | 83.4 | 59.7 | 77.8 | 59.7 | 77.8 |
| 255 | Fukuzawa | 4878 | 54.3 | 83.8 | 59.7 | 77.8 | 59.7 | 77.8 |
| 256 | Fukuzawa | 4594 | 54.3 | 83.8 | 59.7 | 77.8 | 59.7 | 77.8 |

**Table A-7 Material properties of the walls with barbell and flanged cross-sections (cont'd)**

| No. | Researcher | $f_c'$ (psi) | $f_{ybe}$ (ksi) | $f_{ube}$ (ksi) | $f_{yv}$ (ksi) | $f_{uv}$ (ksi) | $f_{yh}$ (ksi) | $f_{uh}$ (ksi) |
|---|---|---|---|---|---|---|---|---|
| 257 | Fukuzawa | 4594 | 54.9 | 83.4 | N/A | N/A | N/A | N/A |
| 258 | Fukuzawa | 4594 | 54.9 | 83.4 | N/A | N/A | N/A | N/A |
| 259 | Fukuzawa | 5106 | 54.9 | 83.4 | 59.7 | 77.8 | 59.7 | 77.8 |
| 260 | Fukuzawa | 4935 | 54.9 | 83.4 | 59.7 | 77.8 | 59.7 | 77.8 |
| 261 | Fukuzawa | 4878 | 54.9 | 83.4 | 59.7 | 77.8 | 59.7 | 77.8 |
| 262 | Fukuzawa | 4864 | 54.9 | 83.4 | 59.7 | 77.8 | 59.7 | 77.8 |
| 263 | Fukuzawa | 4935 | 54.3 | 83.8 | 59.7 | 77.8 | 59.7 | 77.8 |
| 264 | Fukuzawa | 4978 | 54.3 | 83.8 | 59.7 | 77.8 | 59.7 | 77.8 |
| 265 | Hatori | 4893 | 54.3 | 83.8 | 59.7 | 77.8 | 59.7 | 77.8 |
| 266 | Hatori | 4921 | 54.3 | 83.8 | 59.7 | 77.8 | 59.7 | 77.8 |
| 267 | Hatori | 5149 | 54.9 | 83.4 | 59.7 | 77.8 | 59.7 | 77.8 |
| 268 | Hatori | 3655 | 54.9 | 83.4 | 59.7 | 77.8 | 59.7 | 77.8 |
| 269 | Hatori | 3755 | 54.9 | 83.4 | 59.7 | 77.8 | 59.7 | 77.8 |
| 270 | Hatori | 3655 | 54.3 | 83.8 | 59.7 | 77.8 | 59.7 | 77.8 |
| 271 | Taga | 3940 | 56.2 | 77.0 | 46.6 | 75.8 | 46.6 | 75.8 |
| 272 | Taga | 5561 | 56.2 | 77.0 | 46.6 | 75.8 | 46.6 | 75.8 |
| 273 | Taga | 8463 | 56.2 | 77.0 | 46.6 | 75.8 | 46.6 | 75.8 |
| 274 | Taga | 5291 | 56.2 | 77.0 | 46.6 | 75.8 | 46.6 | 75.8 |
| 275 | Taga | 3726 | 56.2 | 77.0 | 46.6 | 75.8 | 46.6 | 75.8 |
| 276 | Taga | 5391 | 56.2 | 77.0 | 46.6 | 75.8 | 46.6 | 75.8 |
| 277 | Taga | 8434 | 56.2 | 77.0 | 46.6 | 75.8 | 46.6 | 75.8 |
| 278 | Farvashany | 15084 | 64.4 | 77.6 | 58.3 | 79.8 | 79.8 | 58.3 |
| 279 | Farvashany | 13489 | 64.4 | 77.6 | 58.3 | 79.8 | 79.8 | 58.3 |
| 280 | Farvashany | 12473 | 64.4 | 77.6 | 58.3 | 79.8 | 79.8 | 58.3 |
| 281 | Farvashany | 13199 | 64.4 | 77.6 | 58.3 | 79.8 | 79.8 | 58.3 |
| 282 | Farvashany | 12183 | 64.4 | 77.6 | 58.3 | 79.8 | 79.8 | 58.3 |
| 283 | Farvashany | 13054 | 64.4 | 77.6 | 58.3 | 79.8 | 79.8 | 58.3 |
| 284 | Farvashany | 14794 | 64.4 | 77.6 | 58.3 | 79.8 | 79.8 | 58.3 |

**Table A-8 Loading and performance information of the walls with barbell and flanged cross-sections**

| No. | Researcher | Loading Type | $P/(A_t f_c')$ (%) | $V_{flex}$ (kips) | $V_{peak}$ (kips) | Governing failure |
|---|---|---|---|---|---|---|
| 1 | Antebi | Blast | 0.0 | 100.7 | 95.0 | shear |
| 2 | Antebi | Blast | 0.0 | 101.7 | 85.0 | shear |
| 3 | Antebi | Monotonic | 0.0 | 101.5 | 81.0 | shear |
| 4 | Antebi | Blast | 0.0 | 171.4 | 114.8 | shear |
| 5 | Antebi | Blast | 0.0 | 171.0 | 108.7 | shear |
| 6 | Antebi | Blast | 0.0 | 170.1 | 120.2 | shear |
| 7 | Antebi | Monotonic | 0.0 | 169.5 | 102.0 | shear |
| 8 | Antebi | Blast | 0.0 | 107.3 | 143.0 | flexure |
| 9 | Antebi | Blast | 0.0 | 106.3 | 117.5 | flexure |
| 10 | Antebi | Monotonic | 0.0 | 104.9 | 93.0 | shear |
| 11 | Antebi | Blast | 0.0 | 107.3 | 110.0 | flexure |
| 12 | Antebi | Blast | 0.0 | 107.1 | 125.0 | flexure |
| 13 | Antebi | Blast | 0.0 | 100.5 | 110.0 | flexure |
| 14 | Antebi | Blast | 0.0 | 102.7 | 116.8 | flexure |
| 15 | Antebi | Blast | 0.0 | 108.0 | 130.0 | flexure |
| 16 | Antebi | Blast | 0.0 | 118.1 | 186.6 | flexure |
| 17 | Antebi | Blast | 0.0 | 123.8 | 170.0 | flexure |
| 18 | Antebi | Monotonic | 0.0 | 112.7 | 92.0 | shear |
| 19 | Antebi | Blast | 0.0 | 114.6 | 130.0 | flexure |
| 20 | Antebi | Monotonic | 0.0 | 115.0 | 100.0 | shear |
| 21 | Antebi | Blast | 0.0 | 111.3 | 107.0 | shear |
| 22 | Antebi | Blast | 0.0 | 111.0 | 116.0 | flexure |
| 23 | Antebi | Monotonic | 0.0 | 116.4 | 91.0 | shear |
| 24 | Antebi | Blast | 0.0 | 111.8 | 102.0 | shear |
| 25 | Antebi | Monotonic | 0.0 | 117.8 | 81.0 | shear |
| 26 | Antebi | Blast | 0.0 | 193.2 | 144.0 | shear |
| 27 | Antebi | Blast | 0.0 | 201.7 | 152.0 | shear |
| 28 | Antebi | Monotonic | 0.0 | 193.9 | 106.0 | shear |
| 29 | Antebi | Blast | 0.0 | 202.1 | 126.0 | shear |
| 30 | Antebi | Blast | 0.0 | 199.3 | 133.0 | shear |
| 31 | Antebi | Monotonic | 0.0 | 99.5 | 92.0 | shear |
| 32 | Antebi | Blast | 0.0 | 92.0 | 87.0 | shear |

**Table A-8 Loading and performance information of the walls with barbell and flanged cross-sections (cont'd)**

| No. | Researcher | Loading Type | $P/(A_t f_c')$ (%) | $V_{flex}$ (kips) | $V_{peak}$ (kips) | Governing failure |
|---|---|---|---|---|---|---|
| 33 | Antebi | Blast | 0.0 | 98.3 | 110.0 | flexure |
| 34 | Antebi | Blast | 0.0 | 100.5 | 110.0 | flexure |
| 35 | Antebi | Monotonic | 0.0 | 94.5 | 90.0 | shear |
| 36 | Antebi | Monotonic | 0.0 | 108.7 | 92.0 | shear |
| 37 | Antebi | Monotonic | 0.0 | 110.2 | 113.0 | flexure |
| 38 | Antebi | Blast | 0.0 | 111.6 | 112.0 | flexure |
| 39 | Antebi | Blast | 0.0 | 114.0 | 117.0 | flexure |
| 40 | Antebi | Monotonic | 0.0 | 106.5 | 96.1 | shear |
| 41 | Antebi | Monotonic | 0.0 | 278.6 | 111.0 | shear |
| 42 | Antebi | Blast | 0.0 | 280.8 | 178.0 | shear |
| 43 | Antebi | Blast | 0.0 | 274.6 | 176.0 | shear |
| 44 | Antebi | Monotonic | 0.0 | 273.7 | 110.0 | shear |
| 45 | Antebi | Blast | 0.0 | 267.3 | 152.0 | shear |
| 46 | Antebi | Monotonic | 0.0 | 270.4 | 135.0 | shear |
| 47 | Aoyagi | Cyclic | 0.0 | 375.4 | 209.4 | shear |
| 48 | Aoyagi | Cyclic | 0.0 | 383.4 | 231.5 | shear |
| 49 | Aoyagi | Cyclic | 0.0 | 434.2 | 349.4 | shear |
| 50 | Aoyagi | Cyclic | 0.0 | 855.2 | 336.2 | shear |
| 51 | Aoyagi | Cyclic | 0.0 | 908.2 | 519.2 | shear |
| 52 | Barda | Monotonic | 0.0 | 516.8 | 273.9 | shear |
| 53 | Barda | Monotonic | 0.0 | 1110.4 | 220.0 | shear |
| 54 | Barda | Cyclic | 0.0 | 779.2 | 249.1 | shear |
| 55 | Barda | Cyclic | 0.0 | 842.7 | 228.7 | shear |
| 56 | Barda | Cyclic | 0.0 | 826.9 | 157.1 | shear |
| 57 | Barda | Cyclic | 0.0 | 825.9 | 197.0 | shear |
| 58 | Barda | Cyclic | 0.0 | 1771.2 | 256.2 | shear |
| 59 | Barda | Cyclic | 0.0 | 422.1 | 199.1 | shear |
| 60 | Benjamin | Monotonic | 0.0 | 25.1 | 20.4 | shear |
| 61 | Benjamin | Monotonic | 0.0 | 44.2 | 25.3 | shear |
| 62 | Benjamin | Monotonic | 0.0 | 63.2 | 31.2 | shear |
| 63 | Benjamin | Monotonic | 0.0 | 102.7 | 48.0 | shear |
| 64 | Benjamin | Monotonic | 0.0 | 28.0 | 20.0 | shear |

**Table A-8 Loading and performance information of the walls with barbell and flanged cross-sections (cont'd)**

| No. | Researcher | Loading Type | $P/(A_t f_c')$ (%) | $V_{flex}$ (kips) | $V_{peak}$ (kips) | Governing failure |
|---|---|---|---|---|---|---|
| 65 | Benjamin | Monotonic | 0.0 | 50.8 | 34.8 | shear |
| 66 | Benjamin | Monotonic | 0.0 | 77.3 | 45.3 | shear |
| 67 | Benjamin | Monotonic | 0.0 | 141.3 | 66.0 | shear |
| 68 | Benjamin | Monotonic | 0.0 | 107.5 | 42.0 | shear |
| 69 | Benjamin | Monotonic | 0.0 | 110.7 | 56.0 | shear |
| 70 | Benjamin | Monotonic | 0.0 | 122.9 | 104.0 | shear |
| 71 | Benjamin | Monotonic | 0.0 | 124.5 | 84.0 | shear |
| 72 | Benjamin | Monotonic | 0.0 | 131.9 | 66.0 | shear |
| 73 | Benjamin | Monotonic | 0.0 | 101.9 | 49.0 | shear |
| 74 | Benjamin | Monotonic | 0.0 | 102.1 | 60.0 | shear |
| 75 | Benjamin | Monotonic | 0.0 | 232.6 | 120.0 | shear |
| 76 | Benjamin | Monotonic | 0.0 | 269.1 | 154.0 | shear |
| 77 | Benjamin | Monotonic | 0.0 | 115.9 | 71.0 | shear |
| 78 | Benjamin | Monotonic | 0.0 | 162.1 | 48.0 | shear |
| 79 | Benjamin | Monotonic | 0.0 | 120.0 | 78.0 | shear |
| 80 | Benjamin | Monotonic | 0.0 | 121.3 | 73.0 | shear |
| 81 | Benjamin | Monotonic | 0.0 | 162.5 | 40.0 | shear |
| 82 | Benjamin | Monotonic | 0.0 | 56.6 | 40.0 | shear |
| 83 | Benjamin | Monotonic | 0.0 | 56.6 | 40.0 | shear |
| 84 | Benjamin | Monotonic | 0.0 | 56.6 | 36.0 | shear |
| 85 | Kabeyasawa | Cyclic | 9.8 | 109.3 | 99.2 | shear |
| 86 | Kabeyasawa | Cyclic | 9.8 | 117.8 | 108.0 | shear |
| 87 | Kabeyasawa | Cyclic | 9.8 | 150.7 | 121.7 | shear |
| 88 | Kabeyasawa | Cyclic | 9.1 | 128.7 | 114.6 | shear |
| 89 | Kabeyasawa | Cyclic | 7.2 | 247.3 | 166.0 | shear |
| 90 | Maier | Monotonic | 6.6 | 157.5 | 152.9 | shear |
| 91 | Maier | Monotonic | 24.2 | 234.0 | 208.6 | shear |
| 92 | Maier | Monotonic | 6.5 | 258.2 | 219.6 | shear |
| 93 | Maier | Cyclic | 6.3 | 157.0 | 153.4 | shear |
| 94 | Maier | Monotonic | 6.6 | 145.6 | 149.9 | flexure |
| 95 | Maier | Cyclic | 27.3 | 223.2 | 192.2 | shear |
| 96 | Rothe | ES | 0.0 | 15.3 | 19.1 | flexure |

**Table A-8 Loading and performance information of the walls with barbell and flanged cross-sections (cont'd)**

| No. | Researcher | Loading Type | $P/(A_t f_c')$ (%) | $V_{flex}$ (kips) | $V_{peak}$ (kips) | Governing failure |
|---|---|---|---|---|---|---|
| 97 | Rothe | ES | 0.0 | 22.0 | 28.9 | flexure |
| 98 | Rothe | Cyclic | 0.0 | 22.4 | 26.3 | flexure |
| 99 | Rothe | Cyclic | 9.6 | 24.2 | 30.9 | flexure |
| 100 | Rothe | Cyclic | 6.5 | 28.0 | 32.4 | flexure |
| 101 | Rothe | Monotonic | 0.0 | 15.1 | 21.1 | flexure |
| 102 | Ryo | Repeated | 0.0 | 302.7 | 217.2 | shear |
| 103 | Ryo | Cyclic | 0.0 | 308.4 | 209.4 | shear |
| 104 | Ryo | Cyclic | 0.0 | 187.3 | 136.7 | shear |
| 105 | SAFE | Cyclic | 0.0 | 3183.5 | 813.8 | shear |
| 106 | SAFE | Cyclic | 0.0 | 3205.5 | 1191.5 | shear |
| 107 | SAFE | Cyclic | 0.0 | 3399.8 | 1245.4 | shear |
| 108 | SAFE | Cyclic | 2.5 | 2731.8 | 1164.5 | shear |
| 109 | SAFE | Cyclic | 2.5 | 2731.8 | 1587.2 | shear |
| 110 | SAFE | Cyclic | 0.0 | 1898.2 | 881.3 | shear |
| 111 | SAFE | Cyclic | 0.0 | 1898.3 | 937.5 | shear |
| 112 | SAFE | Cyclic | 0.0 | 2681.8 | 1267.9 | shear |
| 113 | SAFE | Cyclic | 0.0 | 1898.3 | 921.7 | shear |
| 114 | SAFE | Cyclic | 2.5 | 2211.5 | 854.3 | shear |
| 115 | Shiga | Cyclic | 0.0 | 118.5 | 39.0 | shear |
| 116 | Shiga | Cyclic | 0.0 | 118.5 | 41.4 | shear |
| 117 | Shiga | Cyclic | 0.0 | 116.3 | 47.2 | shear |
| 118 | Shiga | Monotonic | 0.0 | 116.3 | 50.9 | shear |
| 119 | Shiga | Cyclic | 16.6 | 134.4 | 75.2 | shear |
| 120 | Shiga | Cyclic | 0.0 | 118.4 | 52.9 | shear |
| 121 | Shiga | Cyclic | 16.0 | 138.0 | 68.3 | shear |
| 122 | Shiga | Cyclic | 32.1 | 154.9 | 63.3 | shear |
| 123 | Shiga | Monotonic | 14.5 | 126.1 | 54.0 | shear |
| 124 | Shiga | Cyclic | 14.5 | 126.1 | 53.6 | shear |
| 125 | Shiga | Cyclic | 14.8 | 125.7 | 62.2 | shear |
| 126 | Shiga | Cyclic | 14.8 | 125.7 | 74.7 | shear |
| 127 | Shiga | Cyclic | 14.5 | 126.1 | 48.5 | shear |
| 128 | Shiga | Cyclic | 14.5 | 126.1 | 45.6 | shear |

**Table A-8 Loading and performance information of the walls with barbell and flanged cross-sections (cont'd)**

| No. | Researcher | Loading Type | $P/(A_t f_c')$ (%) | $V_{flex}$ (kips) | $V_{peak}$ (kips) | Governing failure |
|---|---|---|---|---|---|---|
| 129 | Shiga | Cyclic | 21.0 | 118.2 | 29.1 | shear |
| 130 | Shiga | Cyclic | 21.0 | 118.2 | 30.2 | shear |
| 131 | Shiga | Cyclic | 24.5 | 115.8 | 43.4 | shear |
| 132 | Sugano | Cyclic | 0.0 | 283.5 | 187.4 | shear |
| 133 | Sugano | Cyclic | 0.0 | 270.3 | 180.8 | shear |
| 134 | Sugano | Monotonic | 8.8 | 2500.1 | 529.1 | shear |
| 135 | Sugano | Monotonic | 16.7 | 8777.9 | 661.4 | shear |
| 136 | Sugano | Monotonic | 11.4 | 2679.1 | 705.5 | shear |
| 137 | Sugano | Monotonic | 7.1 | 2013.4 | 407.9 | shear |
| 138 | Sugano | Monotonic | 7.1 | 2058.5 | 429.9 | shear |
| 139 | Sugano | Monotonic | 8.0 | 2118.8 | 480.6 | shear |
| 140 | Sugano | Monotonic | 7.8 | 2074.4 | 445.3 | shear |
| 141 | Sugano | Monotonic | 8.5 | 2368.7 | 518.1 | shear |
| 142 | Synge | Cyclic | 0.0 | 242.3 | 166.9 | shear |
| 143 | Tsuboi | Repeated | 0.0 | 20.2 | 22.7 | flexure |
| 144 | Tsuboi | Repeated | 0.0 | 38.7 | 36.4 | shear |
| 145 | Tsuboi | Repeated | 0.0 | 21.4 | 24.5 | flexure |
| 146 | Tsuboi | Repeated | 0.0 | 40.0 | 39.2 | shear |
| 147 | Tsuboi | Repeated | 0.0 | 44.9 | 43.9 | shear |
| 148 | Tsuboi | Repeated | 0.0 | 84.7 | 41.4 | shear |
| 149 | Mo | Cyclic | 0.0 | 42.4 | 46.1 | flexure |
| 150 | Mo | Cyclic | 0.0 | 42.4 | 55.5 | flexure |
| 151 | Mo | Cyclic | 0.0 | 42.3 | 45.4 | flexure |
| 152 | Mo | Cyclic | 0.0 | 59.2 | 57.3 | shear |
| 153 | Mo | Cyclic | 0.0 | 59.2 | 45.9 | shear |
| 154 | Mo | Cyclic | 0.0 | 59.8 | 46.1 | shear |
| 155 | Mo | Cyclic | 0.0 | 42.8 | 50.1 | flexure |
| 156 | Mo | Cyclic | 0.0 | 42.8 | 51.9 | flexure |
| 157 | Mo | Cyclic | 0.0 | 42.9 | 56.2 | flexure |
| 158 | Mo | Cyclic | 0.0 | 37.2 | 43.4 | flexure |
| 159 | Mo | Cyclic | 0.0 | 37.2 | 48.8 | flexure |
| 160 | Mo | Cyclic | 0.0 | 38.6 | 45.6 | flexure |

**Table A-8 Loading and performance information of the walls with barbell and flanged cross-sections (cont'd)**

| No. | Researcher | Loading Type | $P/(A_t f_c')$ (%) | $V_{flex}$ (kips) | $V_{peak}$ (kips) | Governing failure |
|---|---|---|---|---|---|---|
| 161 | Mo | Cyclic | 0.0 | 55.3 | 55.3 | shear |
| 162 | Mo | Cyclic | 0.0 | 55.4 | 45.0 | shear |
| 163 | Mo | Cyclic | 0.0 | 55.4 | 47.2 | shear |
| 164 | Mo | Cyclic | 0.0 | 56.3 | 49.2 | shear |
| 165 | Mo | Cyclic | 0.0 | 55.8 | 46.1 | shear |
| 166 | Mo | Cyclic | 0.0 | 55.2 | 47.2 | shear |
| 167 | Mo | Cyclic | 0.0 | 39.8 | 56.2 | flexure |
| 168 | Mo | Cyclic | 0.0 | 39.8 | 51.0 | flexure |
| 169 | Bouchon | Cyclic | 3.5 | 564.4 | 181.3 | shear |
| 170 | Endo | Cyclic | 5.3 | 201.5 | 147.0 | shear |
| 171 | Endo | Cyclic | 5.6 | 156.7 | 117.3 | shear |
| 172 | Endo | Cyclic | 5.3 | 115.7 | 117.9 | flexure |
| 173 | Endo | Cyclic | 7.0 | 156.6 | 104.9 | shear |
| 174 | Endo | Cyclic | 6.7 | 316.4 | 176.1 | shear |
| 175 | NUPEC | ES | 3.9 | 506.3 | 367.8 | shear |
| 176 | NUPEC | ES | 3.8 | 506.4 | 363.8 | shear |
| 177 | Vecchio | Cyclic | 5.4 | 505.1 | 287.0 | shear |
| 178 | Vecchio | Cyclic | 0.0 | 370.1 | 200.4 | shear |
| 179 | XiangDong | Cyclic | 9.3 | 184.5 | 136.3 | shear |
| 180 | XiangDong | Cyclic | 4.1 | 157.3 | 142.2 | shear |
| 181 | XiangDong | Cyclic | 1.5 | 136.7 | 101.8 | shear |
| 182 | XiangDong | Cyclic | 4.4 | 174.3 | 157.8 | shear |
| 183 | XiangDong | Cyclic | 4.8 | 147.7 | 124.4 | shear |
| 184 | XiangDong | Cyclic | 4.6 | 173.5 | 165.6 | shear |
| 185 | XiangDong | Cyclic | 8.2 | 203.7 | 185.3 | shear |
| 186 | XiangDong | Cyclic | 8.1 | 179.0 | 152.0 | shear |
| 187 | XiangDong | Cyclic | 1.3 | 129.8 | 106.5 | shear |
| 188 | Sheu | Monotonic | 0.0 | 76.7 | 71.0 | shear |
| 189 | Sheu | Repeated | 0.0 | 77.1 | 65.5 | shear |
| 190 | Sheu | Cyclic | 0.0 | 75.3 | 58.9 | shear |
| 191 | Sheu | Cyclic | 0.0 | 76.1 | 60.1 | shear |
| 192 | Sheu | Monotonic | 0.0 | 78.3 | 68.8 | shear |

**Table A-8 Loading and performance information of the walls with barbell and flanged cross-sections (cont'd)**

| No. | Researcher | Loading Type | $P/(A_t f_c')$ (%) | $V_{flex}$ (kips) | $V_{peak}$ (kips) | Governing failure |
|---|---|---|---|---|---|---|
| 193 | Sheu | Monotonic | 0.0 | 87.7 | 87.8 | flexure |
| 194 | Sheu | Cyclic | 0.0 | 88.1 | 73.4 | shear |
| 195 | Sheu | Monotonic | 0.0 | 85.9 | 81.9 | shear |
| 196 | Sheu | Cyclic | 0.0 | 87.2 | 72.7 | shear |
| 197 | Sheu | Monotonic | 0.0 | 90.8 | 85.8 | shear |
| 198 | Sheu | Cyclic | 0.0 | 78.3 | 61.2 | shear |
| 199 | Sheu | Cyclic | 0.0 | 75.7 | 57.0 | shear |
| 200 | Sheu | Cyclic | 0.0 | 75.7 | 61.6 | shear |
| 201 | Sheu | Cyclic | 0.0 | 25.9 | 40.8 | flexure |
| 202 | Sheu | Cyclic | 0.0 | 26.2 | 30.6 | flexure |
| 203 | Sheu | Cyclic | 0.0 | 26.1 | 29.0 | flexure |
| 204 | Sheu | Cyclic | 6.3 | 34.1 | 46.0 | flexure |
| 205 | Saito | Cyclic | 5.6 | 975.9 | 597.4 | shear |
| 206 | Saito | Cyclic | 5.1 | 944.9 | 564.4 | shear |
| 207 | Saito | Cyclic | 5.5 | 1009.9 | 564.4 | shear |
| 208 | Saito | Cyclic | 2.7 | 937.3 | 557.8 | shear |
| 209 | Saito | Cyclic | 4.9 | 1000.5 | 599.7 | shear |
| 210 | Saito | Cyclic | 5.9 | 481.3 | 394.6 | shear |
| 211 | Saito | Cyclic | 2.9 | 464.4 | 370.4 | shear |
| 212 | Saito | Cyclic | 7.9 | 923.3 | 491.6 | shear |
| 213 | Saito | Cyclic | 7.6 | 465.7 | 407.9 | shear |
| 214 | Seki | Cyclic | 0.0 | 518.0 | 331.1 | shear |
| 215 | Seki | Cyclic | 3.4 | 601.0 | 375.7 | shear |
| 216 | Seki | Cyclic | 0.0 | 390.4 | 284.2 | shear |
| 217 | Seki | Cyclic | 3.5 | 453.2 | 329.1 | shear |
| 218 | Seki | Cyclic | 0.0 | 310.5 | 231.9 | shear |
| 219 | Seki | Cyclic | 3.5 | 361.0 | 263.0 | shear |
| 220 | Sato | Cyclic | 4.6 | 526.4 | 505.8 | shear |
| 221 | Sato | Cyclic | 5.3 | 459.6 | 377.7 | shear |
| 222 | Sato | Cyclic | 5.6 | 432.1 | 391.2 | shear |
| 223 | Sato | Cyclic | 5.7 | 405.8 | 391.2 | shear |
| 224 | Sato | Cyclic | 5.0 | 616.6 | 472.1 | shear |

**Table A-8 Loading and performance information of the walls with barbell and flanged cross-sections (cont'd)**

| No. | Researcher | Loading Type | $P/(A_t f_c')$ (%) | $V_{flex}$ (kips) | $V_{peak}$ (kips) | Governing failure |
|---|---|---|---|---|---|---|
| 225 | Sato | Cyclic | 4.9 | 582.3 | 492.3 | shear |
| 226 | Sato | Cyclic | 5.5 | 876.0 | 559.8 | shear |
| 227 | Sato | Cyclic | 5.8 | 870.2 | 559.8 | shear |
| 228 | Sato | Cyclic | 5.4 | 816.2 | 546.3 | shear |
| 229 | Sato | Cyclic | 8.2 | 533.7 | 404.7 | shear |
| 230 | Sato | Cyclic | 7.2 | 532.1 | 411.4 | shear |
| 231 | Sato | Cyclic | 5.1 | 575.3 | 424.9 | shear |
| 232 | Sato | Cyclic | 5.2 | 552.3 | 458.6 | shear |
| 233 | Sato | Cyclic | 5.3 | 534.8 | 445.1 | shear |
| 234 | Sato | Cyclic | 6.0 | 749.9 | 505.8 | shear |
| 235 | Sato | Cyclic | 5.8 | 726.4 | 532.8 | shear |
| 236 | Sato | Cyclic | 7.3 | 659.1 | 445.1 | shear |
| 237 | Sato | Cyclic | 7.3 | 629.1 | 458.6 | shear |
| 238 | Sato | Cyclic | 7.1 | 619.1 | 458.6 | shear |
| 239 | Sato | Cyclic | 4.8 | 706.4 | 512.6 | shear |
| 240 | Sato | Cyclic | 4.6 | 662.8 | 526.1 | shear |
| 241 | Sato | Cyclic | 4.5 | 643.3 | 546.3 | shear |
| 242 | Chiba | Cyclic | 5.8 | 431.4 | 372.8 | shear |
| 243 | Chiba | Cyclic | 6.6 | 366.8 | 265.0 | shear |
| 244 | Chiba | Cyclic | 4.9 | 400.3 | 331.6 | shear |
| 245 | Chiba | Cyclic | 5.8 | 521.1 | 377.0 | shear |
| 246 | Chiba | Cyclic | 5.7 | 602.8 | 409.8 | shear |
| 247 | Chiba | Cyclic | 12.3 | 522.0 | 340.6 | shear |
| 248 | Chiba | Cyclic | 5.9 | 643.3 | 363.5 | shear |
| 249 | Chiba | Cyclic | 5.9 | 322.3 | 302.0 | shear |
| 250 | Yagishita | Cyclic | 6.7 | 365.8 | 280.2 | shear |
| 251 | Yagishita | Cyclic | 6.6 | 384.6 | 293.9 | shear |
| 252 | Yagishita | Cyclic | 0.0 | 326.4 | 257.7 | shear |
| 253 | Fukuzawa | Cyclic | 5.6 | 319.4 | 268.1 | shear |
| 254 | Fukuzawa | Cyclic | 5.6 | 350.3 | 288.4 | shear |
| 255 | Fukuzawa | Cyclic | 5.8 | 635.0 | 450.4 | shear |
| 256 | Fukuzawa | Cyclic | 6.2 | 659.3 | 389.3 | shear |

**Table A-8 Loading and performance information of the walls with barbell and flanged cross-sections (cont'd)**

| No. | Researcher | Loading Type | $P/(A_t f_c')$ (%) | $V_{flex}$ (kips) | $V_{peak}$ (kips) | Governing failure |
|---|---|---|---|---|---|---|
| 257 | Fukuzawa | Cyclic | 0.0 | 219.5 | 167.3 | shear |
| 258 | Fukuzawa | Cyclic | 12.4 | 411.5 | 319.4 | shear |
| 259 | Fukuzawa | Cyclic | 0.0 | 283.4 | 258.8 | shear |
| 260 | Fukuzawa | Cyclic | 11.5 | 473.3 | 381.8 | shear |
| 261 | Fukuzawa | Cyclic | 5.8 | 560.1 | 420.6 | shear |
| 262 | Fukuzawa | Cyclic | 5.8 | 280.4 | 286.6 | flexure |
| 263 | Fukuzawa | Cyclic | 5.8 | 901.1 | 467.8 | shear |
| 264 | Fukuzawa | Cyclic | 5.7 | 451.5 | 372.4 | shear |
| 265 | Hatori | Cyclic | 0.0 | 509.7 | 384.9 | shear |
| 266 | Hatori | Cyclic | 11.6 | 690.2 | 457.5 | shear |
| 267 | Hatori | Cyclic | 5.5 | 505.7 | 399.0 | shear |
| 268 | Hatori | Cyclic | 7.8 | 358.1 | 286.8 | shear |
| 269 | Hatori | Cyclic | 7.6 | 413.6 | 312.6 | shear |
| 270 | Hatori | Cyclic | 7.8 | 573.8 | 335.3 | shear |
| 271 | Taga | Cyclic | 7.2 | 325.5 | 244.7 | shear |
| 272 | Taga | Cyclic | 5.1 | 344.8 | 299.8 | shear |
| 273 | Taga | Cyclic | 3.4 | 364.1 | 328.5 | shear |
| 274 | Taga | Cyclic | 5.4 | 298.5 | 277.8 | shear |
| 275 | Taga | Cyclic | 7.6 | 368.7 | 255.7 | shear |
| 276 | Taga | Cyclic | 5.3 | 393.5 | 328.5 | shear |
| 277 | Taga | Cyclic | 3.4 | 421.0 | 377.0 | shear |
| 278 | Farvashany | Cyclic | 4.3 | N/A | 190.0 | N/A |
| 279 | Farvashany | Cyclic | 8.5 | N/A | 140.5 | N/A |
| 280 | Farvashany | Cyclic | 9.2 | N/A | 194.7 | N/A |
| 281 | Farvashany | Cyclic | 21.6 | N/A | 180.1 | N/A |
| 282 | Farvashany | Cyclic | 9.5 | N/A | 167.5 | N/A |
| 283 | Farvashany | Cyclic | 5.1 | N/A | 179.8 | N/A |
| 284 | Farvashany | Cyclic | 7.8 | N/A | 190.0 | N/A |

# Appendix B – Nonlinear Finite Element Constitutive Models for Reinforced Concrete

## B.1 Concrete Damaged Plasticity Model in ABAQUS

In damage-plasticity models, damage is implemented by reducing the elastic stiffness of the material as a function of the accumulated plastic strain. Summary information on the key aspects (yield condition and flow rule) of the Concrete Damaged Plasticity (CDP) model in ABAQUS is presented in the following sub-sections. The scope of the presentation is limited to rate- and temperature-independent formulation. See Lubliner et al. (1989), Lee and Fenves (1998), and Hibbitt, Karlsson & Sorensen, Inc. (2004) for more detailed information on the model.

### B.1.1 Yield Condition

The CDP model in ABAQUS uses the yield function developed by Lubliner et al. (1989) with the modifications proposed by Lee and Fenves (1998):

$$F(\bar{\sigma},\tilde{\varepsilon}^{pl}) = \frac{1}{1-\alpha}\left(\bar{q} - 3\alpha\bar{p} + \beta(\tilde{\varepsilon}^{pl})\left\langle\hat{\bar{\sigma}}_{\max}\right\rangle - \gamma\left\langle-\hat{\bar{\sigma}}_{\max}\right\rangle\right) - \bar{\sigma}_c(\tilde{\varepsilon}^{pl}) \le 0 \qquad \text{(B-1)}$$

where $\bar{p}$ is the hydrostatic pressure, $\bar{q}$ is the Mises equivalent stress, $\bar{S}$ is the deviatoric part of the stress tensor, and $\hat{\bar{\sigma}}_{\max}$ is the algebraically maximum principal stress. The coefficient $\alpha$ is a dimensionless constant that is a function of the initial equibiaxial and uniaxial compressive yield stresses, $\sigma_{b0}$ and $\sigma_{c0}$, respectively:

$$\alpha = \frac{\sigma_{b0} - \sigma_{c0}}{2\sigma_{b0} - \sigma_{c0}} \qquad \text{(B-2)}$$

Lubliner et al. (1989) states that the typical experimental values for the ratio $\sigma_{b0}/\sigma_{c0}$ for concrete range between 1.10 and 1.16. The function $\beta(\tilde{\varepsilon}^{pl})$ is defined as:

$$\beta(\tilde{\varepsilon}^{pl}) = \frac{\bar{\sigma}_c(\tilde{\varepsilon}_c^{pl})}{\bar{\sigma}_t(\tilde{\varepsilon}_t^{pl})}(1-\alpha) - (1+\alpha) \qquad \text{(B-3)}$$

where $\bar{\sigma}_c$ and $\bar{\sigma}_t$ are the tensile and compressive cohesion stresses, respectively. The parameter $\gamma$ in Equation B-1 is only effective under triaxial compression ($\hat{\bar{\sigma}}_{\max} < 0$) and defined as:

$$\gamma = \frac{3(1-K_c)}{2K_c - 1} \qquad \text{(B-4)}$$

where $K_c$ is the ratio of second invariant of the deviatoric stress tensor on the tensile meridian to the second invariant of the deviatoric stress tensor on the compression meridian. According to Lubliner et al. (1989), typical values for $K_c$ range between 0.64 and 0.80 for concrete. In biaxial compression ($\hat{\bar{\sigma}}_{\max} = 0$), Equation B-1 reduces to the well-known Drucker-Prager yield condition.

## B.1.2 Flow Rule

The flow rule defines the orientation of the plastic strain. The increment of plastic strain is defined in Equation B-5:

$$\dot{\varepsilon}^{pl} = \dot{\lambda} \frac{\partial G(\bar{\sigma})}{\partial \bar{\sigma}} \tag{B-5}$$

The flow rule used in the CDP model is non-associative, therefore the function used to define the yield surface, $F$, is not used to define the flow potential ($G$). The flow potential $G$ of the CDP model is a hyperbolic type Drucker-Prager function:

$$G = \sqrt{(\varepsilon \sigma_{t0} \tan\psi)^2 + \bar{q}^2} - \bar{p} \tan\psi \tag{B-6}$$

where $\psi$ is the dilation angle, $\sigma_{t0}$ is the uniaxial tensile stress at failure, and $\varepsilon$ is a parameter referred as eccentricity, which defines the rate at which the function approaches to the asymptote. The dilation angle ($\psi$) is defined as slope of the plastic potential function measured in the $\bar{p} - \bar{q}$ plane at higher confining pressures. Figure B-1 presents the flow potential defined in Equation B-6 in the $\bar{p} - \bar{q}$ plane. Note that the plastic potential function becomes a straight line (linear type Drucker-Prager function) for $\varepsilon$ = 0. Smaller values of the eccentricity enable a modestly varying dilation angle over a wide range of confining pressures.

As shown in Section 5, the dilation angle is crucial to modeling the response of squat reinforced concrete walls. This is an expected result because the response of squat reinforced concrete walls is mostly by the characteristics of concrete. In squat walls, reinforcement yielding is generally modest and crushing is widespread. In contrast, the behavior of flexure dominated-structures is dominated generally by reinforcement yielding and the effect of characteristics of concrete on the response is more modest.

Imran (1994) tested 130 concrete cylinder specimens subjected to triaxial loading. Using the results of these tests and of those obtained by Smith et al. (1989), Imran (1994) developed a constitutive model based on non-associated plasticity to simulate the behavior of concrete. Four variables were considered in the experiments, namely, water-to-cement ratio ($w/c$), confinement stress, moisture content, and load path. Imran (1994) used a linear Drucker-Prager type function that is presented in Equation B-7 to represent the flow potential. The form of this function is similar to the potential function used in the ABAQUS formulation. In Equation B-7, the $a$ controls concrete dilatancy.

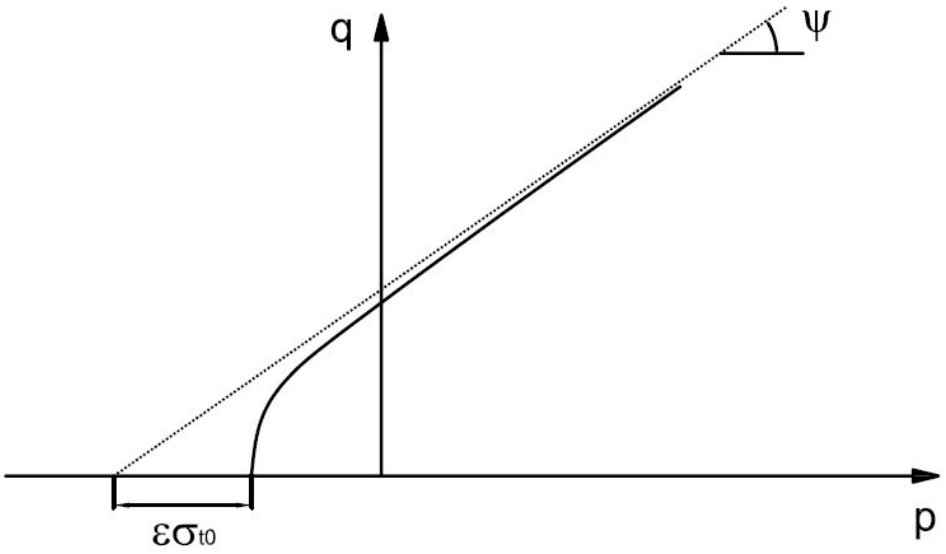


**Figure B-1 Illustration of the potential function in the $\bar{p}-\bar{q}$ plane**

$$G = \sqrt{2J_2} + a\frac{I_1}{\sqrt{3}} \tag{B-7}$$

Imran (1994) concluded that $a$ is a function of the confining stress and the amount of accumulated plastic strain and does not take on a unique value. Imran (1994) calibrated $a$ as a function of confining stress and accumulated plastic strain for three $w/c$ ratios (0.40, 0.55, and 0.75).

## B.2 VecTor2

VecTor2 [VecTor Analysis Group (2007)] is a nonlinear finite element analysis code used to model the behavior of reinforced concrete subjected to in-plane normal and shear stresses. The software includes two smeared-crack formulations, namely, *Modified Compression Field Theory* (MCFT) [Vecchio and Collins (1986)] and *Disturbed Stress Field Model* (DSFM) [Vecchio (2000)].

MCFT is a rotating crack approach that assumes that the orientations of the principal strains and principal concrete stresses are identical. DSFM does not enforce alignment of the principal strain and stress directions and considered as a delayed rotating-crack model [Wong and Vecchio (2002)]. The DSFM formulation was developed by modifying the MCFT formulation. Vecchio et al. (2001) concludes that DSFM performs better than MCFT under certain circumstances (i.e., for panels and beams without transverse reinforcement, for heavily reinforced panels subjected to biaxial compression). VecTor2 includes a plane-stress implementation of the MCFT and DSFM formulations.

The two formulations employed by VecTor2 treat the cracked concrete as a solid continuum with cracks smeared over the element. The cracked concrete is represented as an orthotropic material with empirically modeled response in compression and tension. The equilibrium and compatibility relationships of MCFT and DSFM for concrete and reinforcement are developed

using average stresses and strains over a membrane element that includes an orthogonal reinforcement layout. The constitutive relationships for cracked concrete were originally developed based on the tests of reinforced concrete panels at the University of Toronto in early 1980s [Vecchio and Collins (1982)]. The original constitutive relationships have been modified over the years as new experimental data became available. The MCFT and DSFM formulations are based on the smeared-crack approach that may not be appropriate for modeling lightly reinforced concrete elements for which the overall response is generally dominated by a single/localized crack. The main aspects of the MCFT and DSFM formulations are briefly introduced in the following sub-sections.

## B.2.1 Compatibility Equations

### B.2.1.1 MCFT

Average strains in a cracked element as illustrated in Figure B-2 are used to define the compatibility relationships for the MCFT. Assuming that the bond between the concrete and reinforcement is perfect, the average strains in the membrane element ($\varepsilon_x$, $\varepsilon_y$) are equal to the average strains in concrete ($\varepsilon_{cx}$, $\varepsilon_{cy}$) and reinforcement ($\varepsilon_{sx}$, $\varepsilon_{sy}$):

$$\begin{aligned} \varepsilon_x &= \varepsilon_{cx} = \varepsilon_{sx} \\ \varepsilon_y &= \varepsilon_{cy} = \varepsilon_{sy} \end{aligned} \tag{B-8}$$

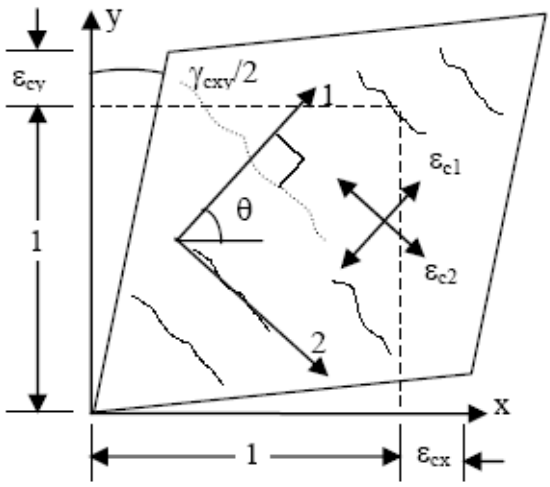


**Figure B-2 Average strains in a cracked element [Wong and Vecchio (2002)]**

The average concrete principal tensile ($\varepsilon_{c1}$) and compressive strain ($\varepsilon_{c2}$), and the orientation of the average principle tensile strain and stress axes with respect to the $x$ axis ($\theta_e$ and $\theta_\sigma$, respectively) can be calculated as shown in Equations B-9 and B-10 using $\varepsilon_x$, $\varepsilon_y$, and $\gamma_{xy}$.

$$\varepsilon_{c1}, \varepsilon_{c2} = \frac{1}{2}\left(\varepsilon_x + \varepsilon_y\right) \pm \frac{1}{2}\sqrt{\left(\varepsilon_x - \varepsilon_y\right)^2 + \gamma_{xy}^2} \tag{B-9}$$

$$\theta = \theta_e = \theta_\sigma = \frac{1}{2}\tan^{-1}\left(\frac{\gamma_{xy}}{\varepsilon_x - \varepsilon_y}\right) \tag{B-10}$$

### B.2.1.2 DSFM

The DSFM assumes that the total strains in an element consist of the strains in the concrete continuum ( $\varepsilon_{cx}, \varepsilon_{cy}, \gamma_{cxy}$ – net concrete strains) and components of the crack slip shear strain ( $\gamma_s$ ) as shown in Equation B-11.

$$\begin{aligned} \varepsilon_x &= \varepsilon_{cx} + \varepsilon_x^s \\ \varepsilon_y &= \varepsilon_{cy} + \varepsilon_y^s \\ \gamma_{xy} &= \gamma_{cxy} + \gamma_{xy}^s \end{aligned} \tag{B-11}$$

The crack slip shear strain $\gamma_s$ can be calculated by using crack slip ( $\delta_s$ ) and average crack spacing ( s ), which are illustrated in Figure B-3.

$$\gamma_s = \frac{\delta_s}{s} \tag{B-12}$$

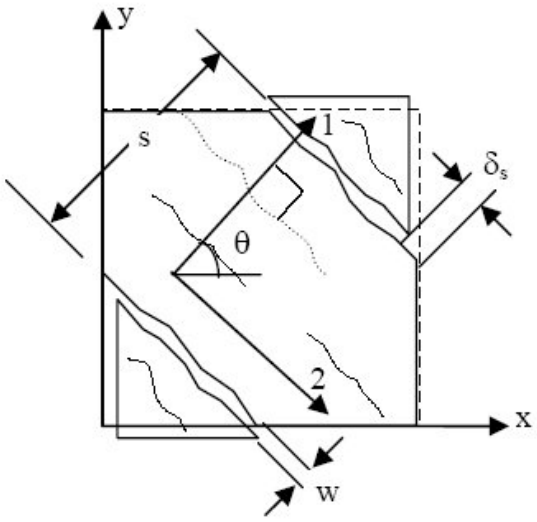


**Figure B-3 Illustration of crack slip on a membrane element [Wong and Vecchio (2002)]**

The components ($\varepsilon_x^s$, $\varepsilon_y^s$, $\gamma_{xy}^s$) of crack slip shear strain ($\gamma_s$) can be calculated using Mohr's circle:

$$\begin{aligned}\varepsilon_x^s &= -\frac{1}{2}\gamma_s \sin(2\theta)\\ \varepsilon_y^s &= \frac{1}{2}\gamma_s \sin(2\theta)\\ \gamma_{xy}^s &= \gamma_s \cos(2\theta)\end{aligned} \tag{B-13}$$

The principal net concrete strains, $\varepsilon_{c1}$ and $\varepsilon_{c2}$, can be calculated using transformation equations:

$$\varepsilon_{c1}, \varepsilon_{c2} = \frac{1}{2}\left(\varepsilon_{cx} + \varepsilon_{cy}\right) \pm \frac{1}{2}\sqrt{\left(\varepsilon_{cx} - \varepsilon_{cy}\right)^2 + \gamma_{cxy}^2} \tag{B-14}$$

The orientation of the principal net concrete strains ($\theta$) and stresses ($\theta_\sigma$) can be calculated as:

$$\theta = \theta_\sigma = \frac{1}{2}\tan^{-1}\left(\frac{\gamma_{cxy}}{\varepsilon_{cx} - \varepsilon_{cy}}\right) \tag{B-15}$$

The orientation of the principal total strains ($\theta_\varepsilon$) can be calculated as:

$$\theta_\varepsilon = \frac{1}{2}\tan^{-1}\left(\frac{\gamma_{xy}}{\varepsilon_x - \varepsilon_y}\right) \tag{B-16}$$

The difference between the orientation of the principal total strains and principal net concrete strains is equal to the rotation lag ($\Delta\theta$).

$$\Delta\theta = \theta_\varepsilon - \theta \tag{B-17}$$

Assumption of perfect bond requires the reinforcement strains ($\varepsilon_{sx}$ and $\varepsilon_{sy}$) be equal to the total strains in the corresponding directions ($\varepsilon_x$ and $\varepsilon_y$).

## Shear-slip relationships

The crack slip shear strain ($\gamma_s$) in the DSFM formulation is assumed as the larger of two slip shear strains ($\gamma_s^a$ and $\gamma_s^b$) calculated using two different approaches.

The first procedure is based on the work of Walraven (1981) that determines the crack slip ($\delta_s^a$) as a function of the applied shear stress.

$$\gamma_s^a = \frac{\delta_s^a}{s} = \frac{v_{ci}}{\left[1.8w^{-0.8} + \left(0.234w^{-0.707} - 0.20\right) f_{cc}\right] s} \tag{B-18}$$

where $f_{cc}$ is the concrete cube strength, $v_{ci}$ is the local shear at the crack, and $w$ is the average crack width. Vecchio (2000) concludes that there are two anomalies associated with using Equation B-18 to predict slip shear strain: 1) the equation predicts a slip shear strain of zero when the element is unreinforced, $\rho_x = \rho_y = 0$ (see Equation B-27), and 2) the equation does not account for the initial crack slip that occurs before the crack surfaces engage. The second relationship for the slip shear strain ($\gamma_s^b$) is used to address the cases where Equation B-18 fails.

The calculation of $\gamma_s^b$ was based on the observation that a constant rotation lag ($\theta^l$) existed between the directions of the principal total strains ($\theta_\varepsilon$) and concrete stresses ($\theta_\sigma$) [Vecchio (2000)]. The experimental data indicated that the lag was initiated after first cracking and was in the order of 5 to 10 degrees before reinforcement yielding.

To calculate $\gamma_s^b$, first, the post-cracking rotation of the principal total strain axis ($\Delta\theta_\varepsilon$) is calculated using Equation B-19, where $\theta_{ic}$ is the orientation of the principal stress and strain fields at first cracking:

$$\Delta\theta_\varepsilon = \theta_\varepsilon - \theta_{ic} \tag{B-19}$$

The post-cracking rotation of the principal stress field ($\Delta\theta_\sigma$) is then related to $\Delta\theta_\varepsilon$ using Equation B-20.

$$\Delta\theta_\sigma = \begin{cases} \Delta\theta_\varepsilon & for\ \left|\Delta\theta_\varepsilon\right| \le \theta^l \\ \left(\Delta\theta_\varepsilon - \theta^l\right) & for\ \left|\Delta\theta_\varepsilon\right| > \theta^l \end{cases} \tag{B-20}$$

The inclination of the principal stress field ($\theta_\sigma$) is then calculated using Equation B-21 and $\gamma_s^b$ is calculated using Equation B-22.

$$\theta_\sigma = \theta_{ic} + \Delta\theta_\sigma \tag{B-21}$$

$$\gamma_s^b = \gamma_{xy}\cos 2\theta_\sigma + \left(\varepsilon_y - \varepsilon_x\right)\sin 2\theta_\sigma \tag{B-22}$$

## B.2.2 Equilibrium Equations

### B.2.2.1 MCFT

Figure B-4 shows free-body diagram of a reinforced concrete element considered in the MCFT formulation. Assuming that the normal and shear stresses are uniformly distributed, the equilibrium relationships for the average become:

$$\begin{aligned} \sigma_x &= f_{cx} + \rho_{sx} f_{sx} \\ \sigma_y &= f_{cy} + \rho_{sy} f_{sy} \\ \tau_{xy} &= v_{cxy} \end{aligned} \tag{B-23}$$

In Equation B-23, $\rho_{sx}$ and $\rho_{sy}$ are the reinforcement ratios in the $x$ and $y$ directions; $\sigma_x$, $\sigma_y$ and $\tau_{xy}$ are the applied stresses; $f_{cx}$ and $f_{cy}$ are the average stresses in the concrete; and $f_{sx}$ and $f_{sy}$ are the average stresses in the reinforcement. The average concrete stresses ( $f_{cx}$ and $f_{cy}$) can be represented in terms of the average principal concrete tensile stress ( $f_{c1}$) using Mohr's circle:

$$\begin{aligned} f_{cx} &= f_{c1} - v_{cxy} \cot\left(90 - \theta_\sigma\right) \\ f_{cy} &= f_{c1} - v_{cxy} \tan\left(90 - \theta_\sigma\right) \end{aligned} \tag{B-24}$$

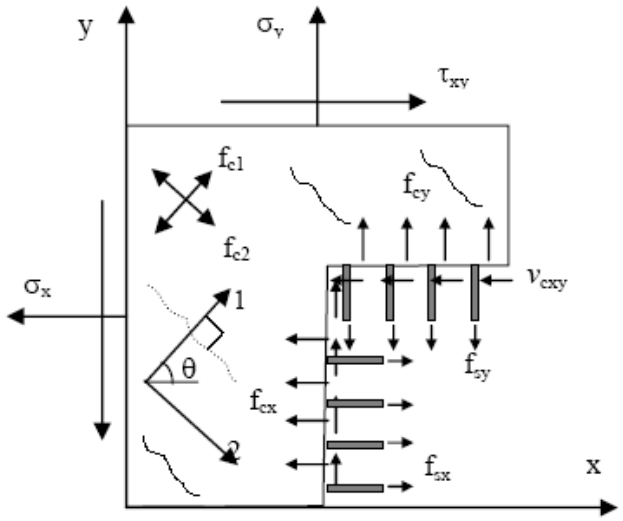


**Figure B-4 Free body diagram of the reinforced concrete element [Wong and Vecchio (2002)]**

The MCFT formulation was developed using average stresses and strains in a concrete element. However, the formulation also considers local failures at a crack that are associated with reinforcement yielding and/or sliding shear. The MCFT limits the local shear stress at a crack to prevent a sliding shear failure and limits the average concrete tensile stress at a crack to prevent failures associated local yielding of reinforcement. Figure B-5 illustrates the average and local stresses at a crack, where $f_{scrx}$ and $f_{scry}$ are the local reinforcement stresses at the crack, and $\theta_{nx}$ and $\theta_{ny}$ are the angles between the direction of average principal tensile stress and the reinforcement in the $x$ and $y$ directions.

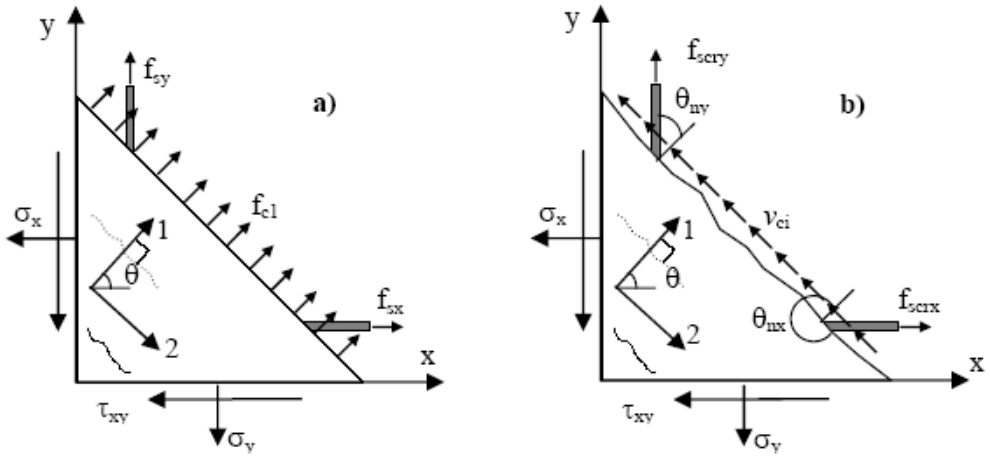


**Figure B-5 MCFT consideration of average and local stresses at a crack: a) average stresses, b) local stresses [Wong and Vecchio (2002)]**

Equation B-25 is derived using equilibrium of the average stresses illustrated in Figure B-5a with the local stresses illustrated in Figure B-5b in the direction of the average principal tensile strain (1).

$$f_{c1} = \rho_x \left( f_{scrx} - f_{sx} \right) \cos^2 \theta_{nx} + \rho_y \left( f_{scry} - f_{sy} \right) \cos^2 \theta_{ny} \tag{B-25}$$

If the local reinforcement stresses in Equation B-25 are replaced by the yield stresses for the reinforcement in $x$ and $y$ directions, $f_{sxyield}$ and $f_{syyield}$, an upper limit for the average principal tensile stress is obtained.

$$f_{c1} \le \rho_x \left( f_{sxyield} - f_{sx} \right) \cos^2 \theta_{nx} + \rho_y \left( f_{syyield} - f_{sy} \right) \cos^2 \theta_{ny} \tag{B-26}$$

Note that, the crack surface in Figure B-5a is a principal plane and shear stresses do not exist on this plane. However, the MCFT assumes that shear stresses may exist on this plane when considered locally because of the reinforcement crossing the crack at a skewed angle as shown in Figure B-5b. Equation B-27 is obtained using equilibrium of the average stresses illustrated in Figure B-5a with the local stresses illustrated in Figure B-5b in the direction of the average principal compressive strain (axis 2).

$$v_{ci} = \rho_x \left( f_{scrx} - f_{sx} \right) \cos \theta_{nx} \sin \theta_{nx} + \rho_y \left( f_{scry} - f_{sy} \right) \cos \theta_{ny} \sin \theta_{ny} \tag{B-27}$$

The MCFT limits the shear stress on a crack based on the research of Walraven (1981) on aggregate interlock mechanisms, which is presented Equation B-28. The upper shear stress limit presented in Equation B-28 increases with increasing aggregate size ($a$) and decreases with increasing crack width ($w$).

$$v_{ci} \le \frac{\sqrt{f'_c}}{0.31 + \frac{24w}{(a+26)}} \quad \text{(in mm, MPa)} \tag{B-28}$$

The average crack width ($w$) is calculated using Equations B-29 and B-30 where $\varepsilon_{c1}$ is the principle concrete tensile strain, $s_\theta$ is the average crack spacing perpendicular to the direction of the crack, and $s_{mx}$ and $s_{my}$ are the crack spacing characteristics associated with reinforcement in the $x$ and $y$ directions, respectively.

$$w = \varepsilon_{c1} s_\theta \tag{B-29}$$

$$s_\theta = \frac{1}{\frac{\cos\theta}{s_{mx}} + \frac{\sin\theta}{s_{my}}} \tag{B-30}$$

### B.2.2.2 DSFM

The equilibrium equations for the MCFT formulation are also valid for the DSFM formulation with one exception. The DSFM formulation explicitly includes slip deformations and therefore does not require the crack-shear check of the MCFT formulation, which is presented in Equation B-28.

## B.2.3 Constitutive relationships

The original constitutive models for cracked concrete are developed using the results of 30 experiments on reinforced concrete panels, which were subjected to various in-plane strain states [Vecchio and Collins (1982)]. The results of these experiments showed that compressive stress-strain relationship for cracked concrete is a function of the coexisting principal tensile strains ($\varepsilon_{c1}$), which is also known as compression-softening. Accordingly, the behavior of cracked concrete in compression is represented by modifying a uniaxial compressive stress-strain relationship with a softening parameter ($\beta_d$). Equation B-31 presents a principal compressive stress – strain ($f_{c2} - \varepsilon_{c2}$) relationship for cracked concrete using the Hognestad parabola for the uniaxial compressive response of concrete. The softening parameter in Equation B-31 is presented explicitly in Equation B-32 and is that proposed by Vecchio and Collins (1986).

$$f_{c2} = \beta_d f'_c \left[ 2\left(\varepsilon_{c2}/\varepsilon_0\right) - \left(\varepsilon_{c2}/\varepsilon_0\right)^2 \right] \tag{B-31}$$

$$\beta_d = \frac{1}{0.8 - 0.34\left(\varepsilon_{c1}/\varepsilon_0\right)} \le 1 \tag{B-32}$$

VecTor2 includes various models to represent the uniaxial compressive response of concrete [i.e., Smith and Young (1956), Popovics (1973), Park et al. (1982), Mander et al. (1988)]. In

addition to the softening model presented in Equation B-32, the softening models included in VecTor2 are those of Vecchio and Collins (1982, 1993). The original compression-softening models have been modified over the time as new experimental data has become available.

The behavior of concrete in tension is assumed linear elastic before initiation of cracking. Therefore, for a given uniaxial tensile stress ( $f_t'$ ) and modulus of elasticity ( $E_c$ ), the strain at cracking ( $\varepsilon_{cr}$ ) can be calculated using

$$\varepsilon_{cr} = f_t' / E_c \tag{B-33}$$

The default relationship to calculate $f_t'$ in VecTor2 is that of Equation B-34, but a user-specified value can also be used.

$$f_t' = 0.33\sqrt{f_c'} \quad \text{(in MPa)} \quad \text{or} \quad f_t' = 4\sqrt{f_c'} \quad \text{(in psi)} \tag{B-34}$$

Following the formation of a crack, the average principal tensile stress-strain relationship (tension-stiffening curve) was empirically defined using the following relationship [Vecchio and Collins (1982)]:

$$f_{c1} = \frac{f_t'}{1+\sqrt{c_t \varepsilon_{c1}}} \quad ; \quad c_t = 200 \tag{B-35}$$

The $c_t$ variable in Equation B-35 determines the rate at which the tensile stress diminishes. Tension-stiffening, which refers to development of tensile stress in concrete between cracks, is a result of bond between the reinforcement and the concrete.

Other tension-stiffening models included in VecTor2 are similar in formulation to that of Equation B-35. Based on the results of experiments on shell structures, Collins and Mitchell (1987) concluded that a value of $c_t = 500$ was more appropriate for large-scale elements. Bentz (2005) proposed the following empirical relationship to estimate $c_t$:

$$c_t = 3.6 \frac{A_c}{\Sigma \pi d_b} \tag{B-36}$$

where $A_c$ is the area of concrete section and $\Sigma \pi d_b$ is sum of the circumference of the bars in the concrete section. The tension-stiffening model proposed by Bentz (2005) is function of $A_c / \Sigma \pi d_b$, which is related to bond. Equation B-36 assumes that the tensile stresses in concrete after cracking will be higher for members that are detailed with reinforcement that is densely spaced using small diameters bars than for members detailed with an equivalent area of reinforcement but with larger diameter bars at a larger spacing.

A bilinear stress-strain relationship without strain-hardening was originally used in the MCFT formulation to represent steel reinforcement, but VecTor2 includes a trilinear curve as shown in Figure B-6 to include strain-hardening, where $f_y$ and $f_u$ are the yield and ultimate stress, $\varepsilon_y$ and

$\varepsilon_u$ are the corresponding strains, $\varepsilon_{sh}$ is the strain at the onset of strain hardening, and $E_s$ and $E_{sh}$ are the modulus of elasticity and modulus for strain hardening, respectively.

Note that the constitutive relationships presented for concrete and steel are generally valid for both formulations. In some cases, some minor modifications may be required for the DSFM formulation [Vecchio (2000)].

## B.2.4 Supplemental Models in VecTor2

The MCFT and DSFM formulations form the basis of reinforced concrete analysis using VecTor2. However, the code includes other models that are needed to simulate the response of reinforced concrete structures but not addressed within the core of the MCFT and DSFM formulations. Examples of these models are tension-softening, consideration of confinement effects, bond-slip mechanisms, hysteretic response of concrete and reinforcement, and reinforcement buckling and dowel resistance mechanisms. Detailed discussion on these models are presented in Wong and Vecchio (2002).

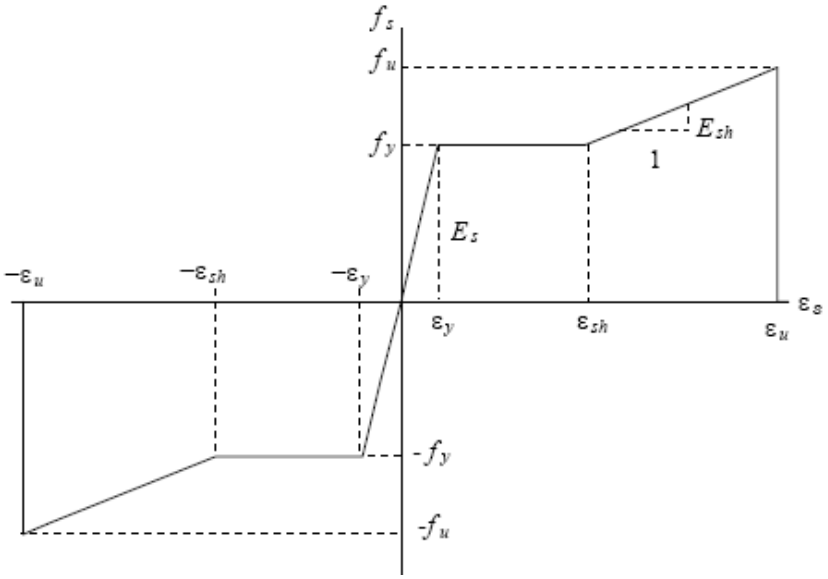


**Figure B-6 Reinforcement stress-strain relationship [Wong and Vecchio (2002)]**

# Appendix C – Damage Data for Reinforced Concrete Squat Walls

Sections C.1 through C.3 of this appendix present damage data for squat walls with rectangular, barbell and flanged cross-sections, respectively. The damage data is presented in tabular form. Reported load-displacement/drift relationships and images of damage are presented. The reported load-displacement relationships include a drift value (presented in a rectangular box) to help the reader identify the relationship between displacement and drift for that wall. The damage states for the two supplemental criteria (see Section 8.4.4) are denoted as $SC_1$ and $SC_2$, respectively, and the method of repair for $SC_1$ and $SC_2$ is denoted as $4^*$ throughout the appendix.

## C.1 Walls with Rectangular Cross-Sections

### C.1.1 Lefas et al. (1990) Walls

Lefas et al. (1990) tested 13 walls; seven (SW11 through SW17) were categorized as Type I and six (SW21 through SW26) were categorized as Type II walls. The major difference between the Type I and Type II walls was aspect ratio. Type I walls had an aspect ratio of 1.0 and Type II walls had an aspect ratio of 2.0. One wall (SW25) tested by Lefas is excluded from the analysis presented herein because Lefas noted that the wall failed prematurely due to experimental error.

All Lefas walls failed in the compression toe. The author states that the lateral strength for the specimens started to degrade as the integrity of concrete in the compression toe was compromised [Lefas et al. (1990), page 30]. Therefore, drifts at peak shear strength are used herein to identify Damage State 3.1. The typical wall condition at the end of tests for Lefas Type I and Type II walls are presented in Figure C-1 and Figure C-2, respectively. The damaged region requiring partial wall replacement in these figures is marked using a dashed rectangular box. Figure C-1 and Figure C-2 reveal that the damage in the Lefas walls at the end of the tests do not trigger wall replacement. In addition, Lefas and Kotsovos (1990) successfully repaired some of the tested walls using partial wall replacement (in the compression toe) and epoxy injection. Therefore, no data for MoR-4 was sought for Lefas walls. The two supplemental criteria are not applicable here since the walls were tested under monotonic loading and the load-displacement relationships were reported up to peak shear strength only.

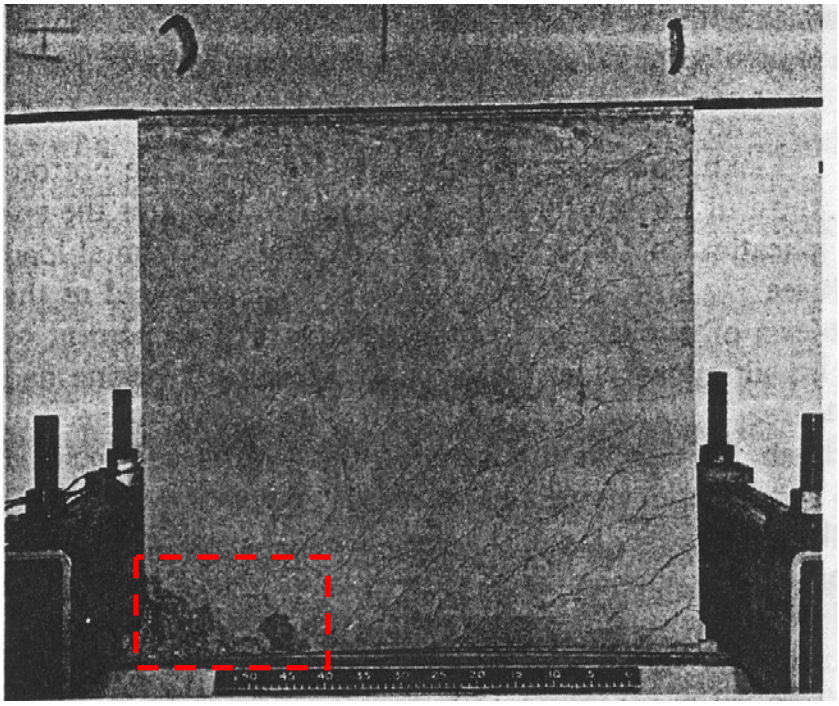

**Figure C-1 Typical condition of Lefas Type I walls at the end of a test [Lefas et al. (1990)]**

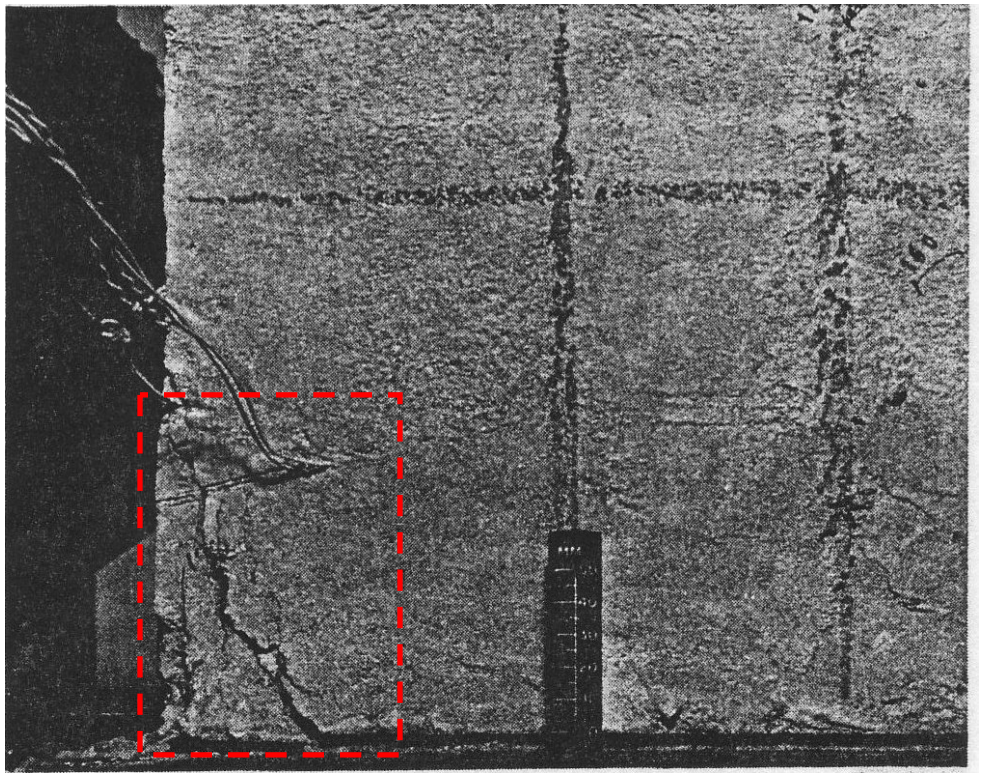

**Figure C-2 Typical condition of Lefas Type II walls at the end of a test [Lefas et al. (1990)]**

**Table C-1 Evaluation of damage data for walls SW11 through SW17 tested by Lefas**

| Wall ID | MoR | Damage State (DS) | Drift (%) | Comments |
|---|---|---|---|---|
| SW11 | 1 | 1.2 | 0.05 | The drifts for these damage states are provided by the researcher. |
| | | 1.3 | 0.24 | |
| | 2a | 2.3 | 0.48 | |
| | 3 | 3.1 | 1.10 | |
| SW12 | 1 | 1.2 | 0.03 | The drifts for these damage states are provided by the researcher. |
| | | 1.3 | 0.17 | |
| | 2a | 2.3 | 0.39 | |
| | 3 | 3.1 | 1.18 | |
| SW13 | 1 | 1.2 | 0.05 | The drifts for these damage states are provided by the researcher. |
| | | 1.3 | 0.19 | |
| | 2a | 2.3 | 0.51 | |
| | 3 | 3.1 | 1.18 | |
| SW14 | 1 | 1.2 | 0.05 | The drifts for these damage states are provided by the researcher. |
| | | 1.3 | 0.24 | |
| | 2a | 2.3 | 0.52 | |
| | 3 | 3.1 | 1.49 | |
| SW15 | 1 | 1.2 | 0.04 | The drifts for these damage states are provided by the researcher. |
| | | 1.3 | 0.17 | |
| | 2a | 2.3 | 0.39 | |
| | 3 | 3.1 | 1.07 | |
| SW16 | 1 | 1.2 | 0.05 | The drifts for these damage states are provided by the researcher. |
| | | 1.3 | 0.19 | |
| | 2a | 2.3 | 0.33 | |
| | 3 | 3.1 | 0.77 | |
| SW17 | 1 | 1.2 | 0.05 | The drifts for these damage states are provided by the researcher. |
| | | 1.3 | 0.28 | |
| | 2a | 2.3 | 0.52 | |
| | 3 | 3.1 | 1.43 | |

**Table C-2 Evaluation of damage data for walls SW21, SW22, SW23, SW24 and SW26 tested by Lefas**

| Wall ID | MoR | Damage State (DS) | Drift (%) | Comments |
|---|---|---|---|---|
| SW21 | 1 | 1.2 | 0.02 | The drifts for these damage states are provided by the researcher. |
| | | 1.3 | 0.45 | |
| | 2a | 2.3 | 0.45 | |
| | 3 | 3.1 | 1.59 | |
| SW22 | 1 | 1.2 | 0.03 | The drifts for these damage states are provided by the researcher. |
| | | 1.3 | 0.38 | |
| | 2a | 2.3 | 0.38 | |
| | 3 | 3.1 | 1.18 | |
| SW23 | 1 | 1.2 | 0.04 | The drifts for these damage states are provided by the researcher. |
| | | 1.3 | 0.40 | |
| | 2a | 2.3 | 0.40 | |
| | 3 | 3.1 | 1.01 | |
| SW24 | 1 | 1.2 | 0.02 | The drifts for these damage states are provided by the researcher. |
| | | 1.3 | 0.48 | |
| | 2a | 2.3 | 0.48 | |
| | 3 | 3.1 | 1.39 | |
| SW26 | 1 | 1.2 | 0.03 | The drifts for these damage states are provided by the researcher. |
| | | 1.3 | 0.42 | |
| | 2a | 2.3 | 0.42 | |
| | 3 | 3.1 | 1.61 | |

## C.1.2 Maier and Thürlimann (1985) Walls

### C.1.2.1 Wall S4

**Table C-3 Evaluation of damage data for wall S4 tested by Maier**

| Wall ID | MoR | Damage State (DS) | Drift (%) | Comments |
|---|---|---|---|---|
| S4 | 1 | 1.2 | 0.05 | The drifts for these damage states are provided by the researcher. |
| | 2a | 2.2 | 0.59 | |
| | | 2.3 | 0.45 | |
| | | 2.5a | 0.51 | |
| | 2b | 2.5b | 0.76 | |
| | 3 | 3.1 | 0.78 | The image reported at this drift (Figure C-8) shows damage that can be repaired by partial wall replacement (MoR-3). The damaged region requiring partial wall replacement is identified using a dashed box in Figure C-8. |
| | 4 | N/A | N/A | The damage observed at the end of the test does not require wall replacement (see Figure C-9). |

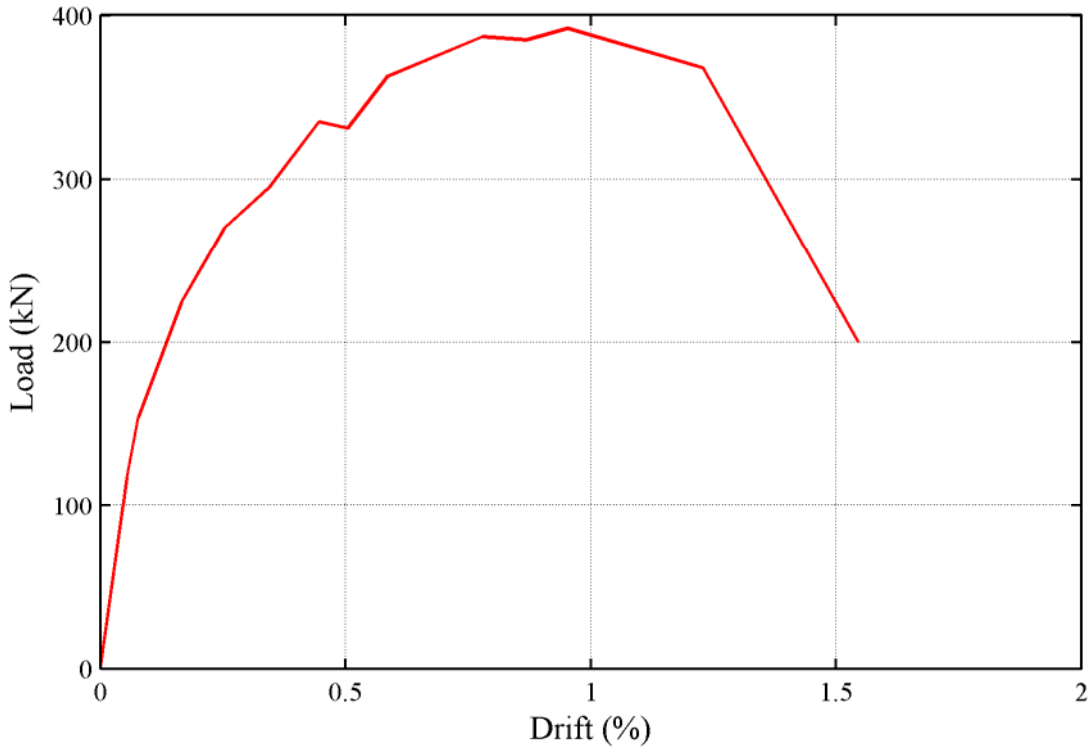


**Figure C-3 Load-drift relationship for wall S4**

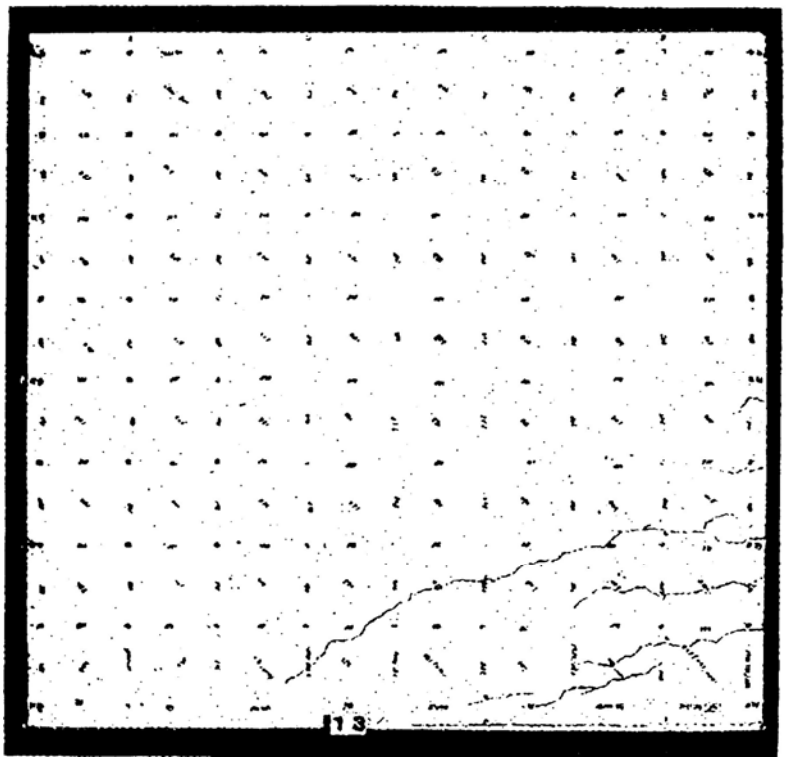


**Figure C-4 Condition of wall S4 at 0.17% drift [Maier and Thürlimann (1985)]**

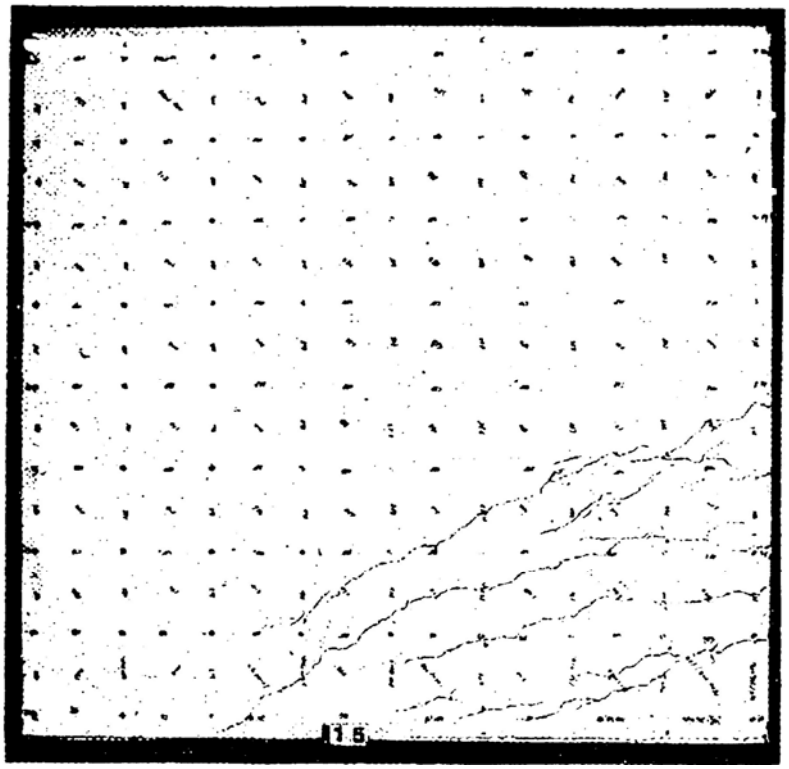


**Figure C-5 Condition of wall S4 at 0.25% drift [Maier and Thürlimann (1985)]**

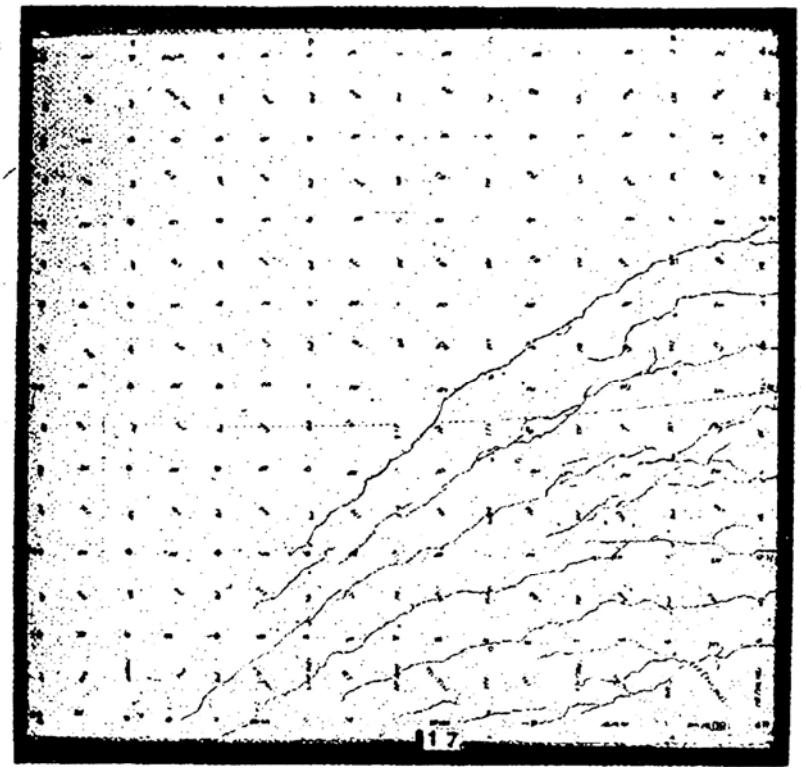


**Figure C-6 Condition of wall S4 at 0.35% drift [Maier and Thürlimann (1985)]**

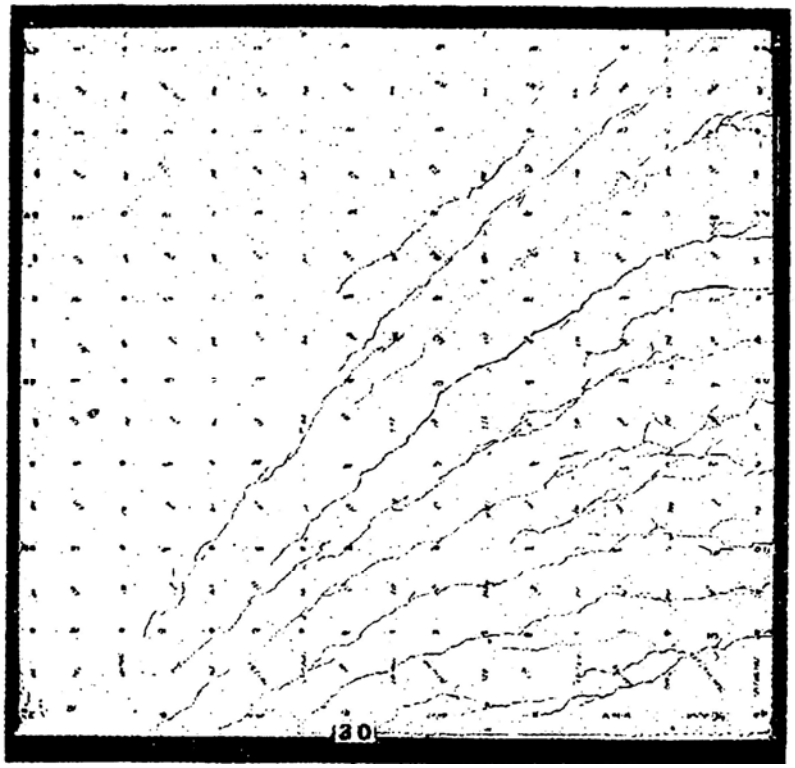


**Figure C-7 Condition of wall S4 at 0.50% drift [Maier and Thürlimann (1985)]**

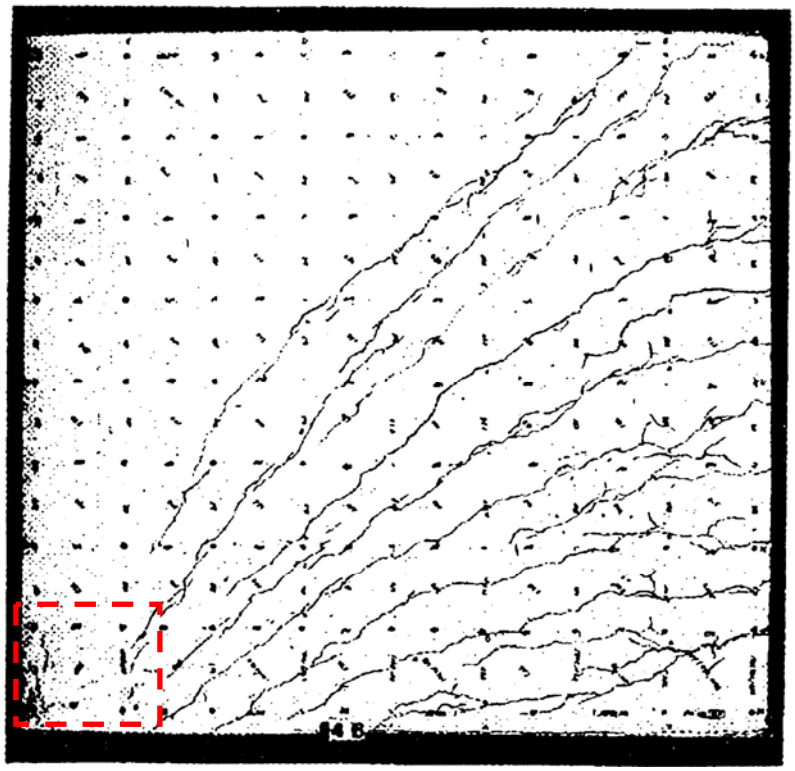

**Figure C-8 Condition of wall S4 at 0.78% drift [Maier and Thürlimann (1985)]**

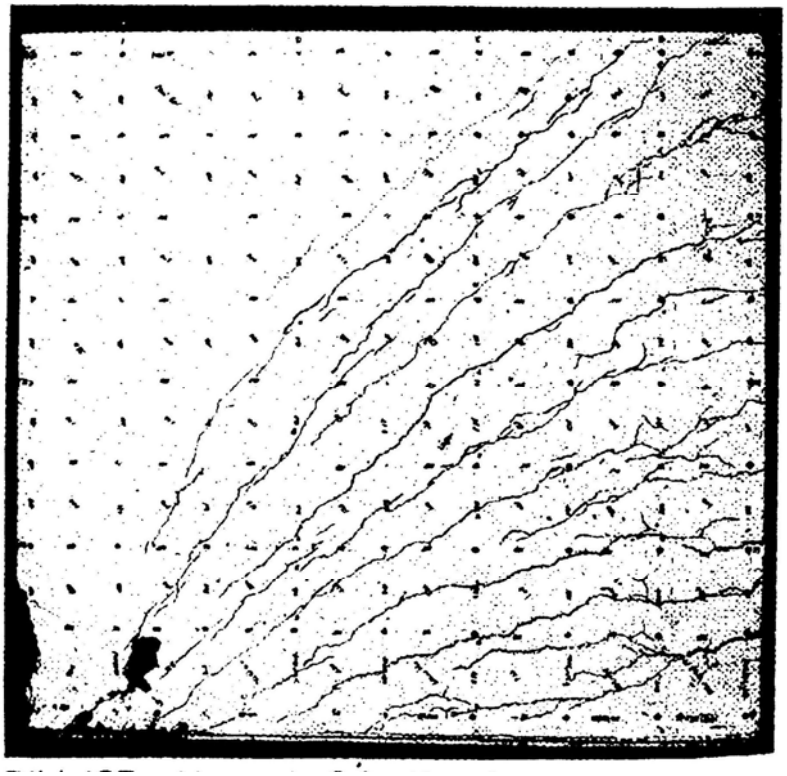

**Figure C-9 Condition of wall S4 at 1.55% drift [Maier and Thürlimann (1985)]**

### C.1.2.2 Wall S9

**Table C-4 Evaluation of damage data for wall S9 tested by Maier**

| Wall ID | MoR | Damage State (DS) | Drift (%) | Comments |
|---|---|---|---|---|
| S9 | 1 | 1.2 | 0.07 | The drifts for these damage states are provided by the researcher. |
| | 2a | 2.2 | 0.76 | |
| | | 2.3 | 0.52 | |
| | | 2.5a | 0.54 | |
| | 4 | 4.2 | 1.22 | The image reported at this drift (Figure C-13) shows a wide diagonal crack that is associated with a diagonal tension failure. |

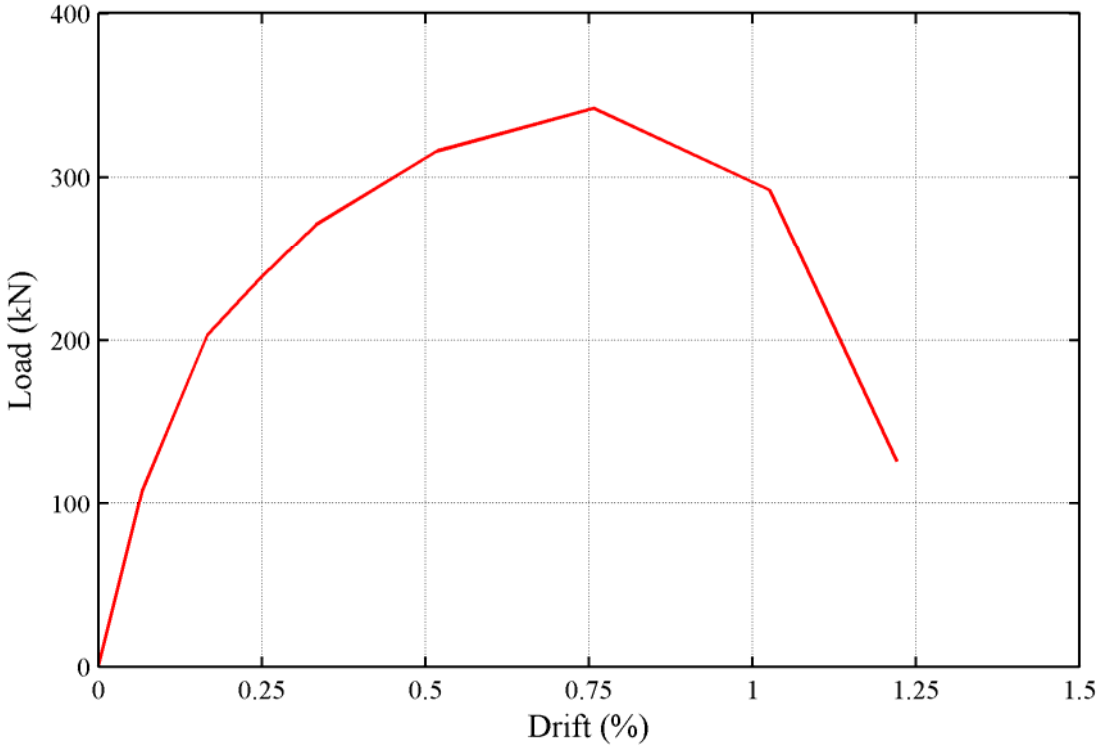


**Figure C-10 Load-drift relationship for wall S9**

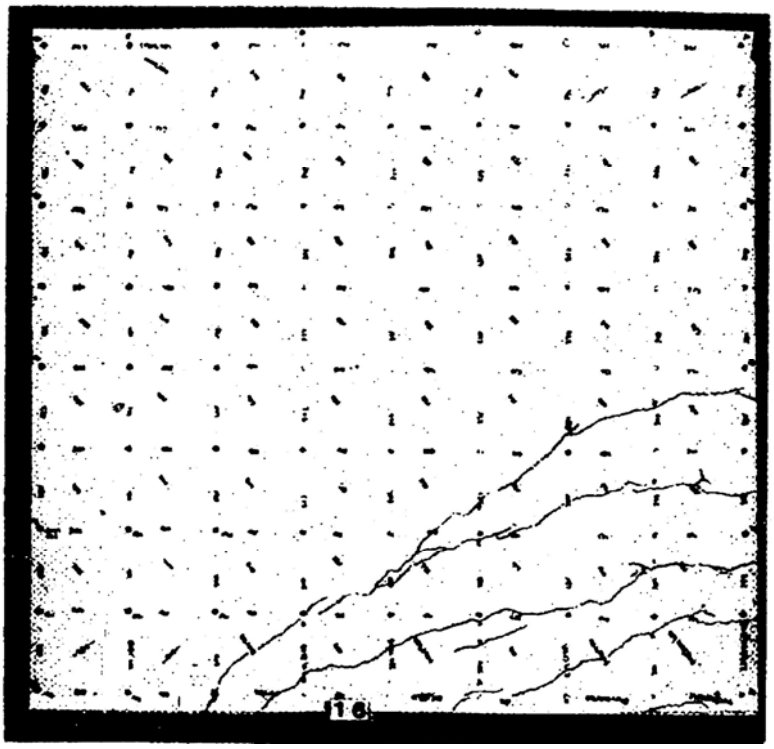


**Figure C-11 Condition of wall S9 at 0.25% drift [Maier and Thürlimann (1985)]**

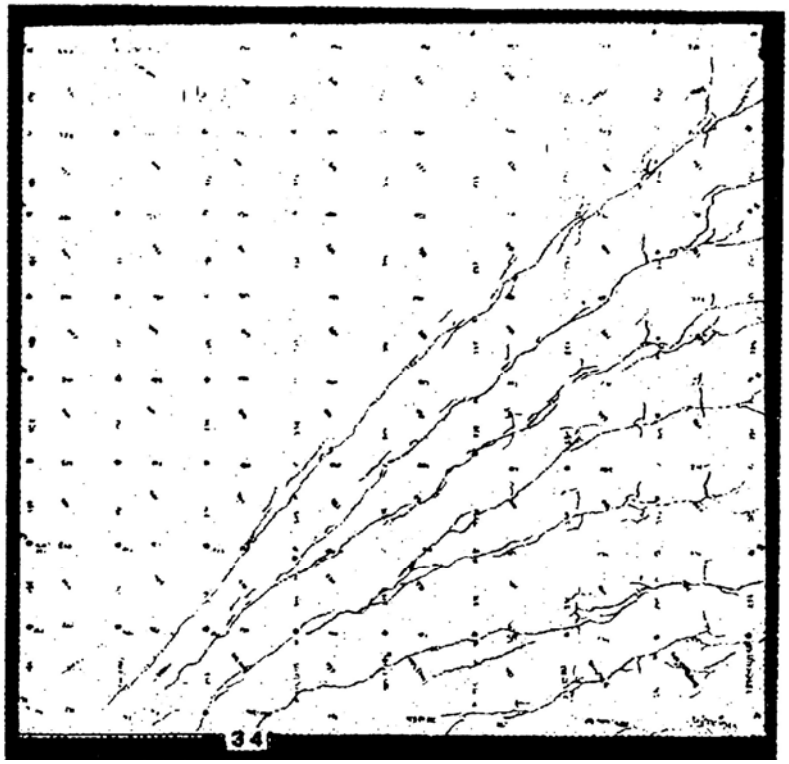


**Figure C-12 Condition of wall S9 at 0.52% drift [Maier and Thürlimann (1985)]**

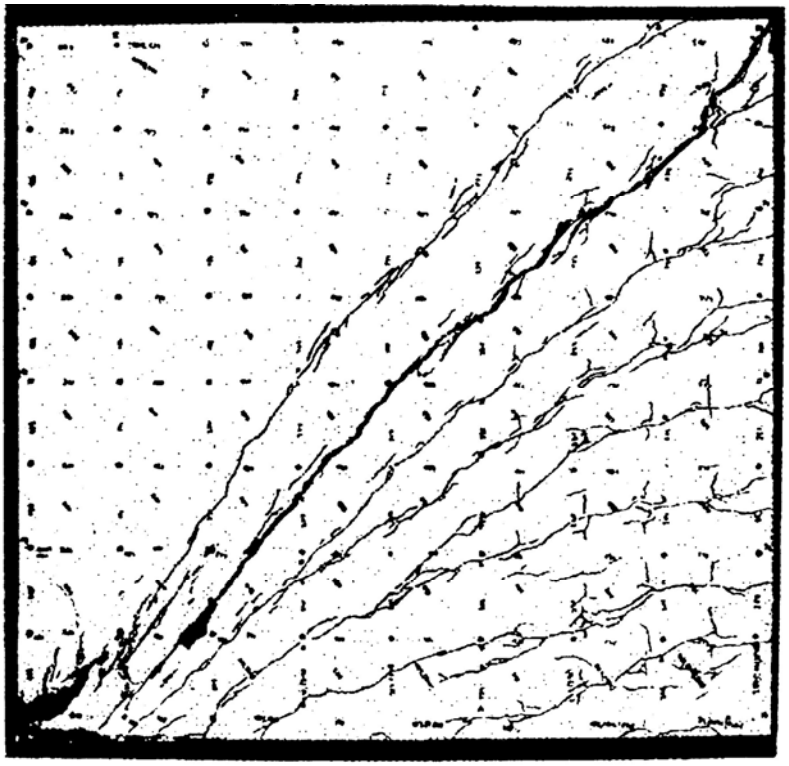

**Figure C-13 Condition of wall S9 at 1.22% drift [Maier and Thürlimann (1985)]**

## C.1.3 Synge (1980) Wall

### C.1.3.1 Wall 1

**Table C-5 Evaluation of damage data for wall 1 tested by Synge**

| Wall ID | MoR | Damage State (DS) | Drift (%) | Comments |
|---|---|---|---|---|
| Wall 1 | 1 | 1.1 | 0.03 | The drifts for these damage states are provided by the researcher. |
| | 2a | 2.2 | 0.17 | |
| | | 2.3 | 0.17 | |
| | | 2.5a | 0.34 | |
| | 2b | 2.5b | 0.34 | |
| | 3 | 3.1 | 0.69 | The image reported at this drift (Figure C-16) shows damage that can be repaired by partial wall replacement (MoR-3). The damaged region requiring partial wall replacement is identified using a dashed box in Figure C-16. |
| | | 3.4 | 1.06 | The drift for this damage state is provided by the researcher. |
| | 4 | 4.1 | 1.33 | The researcher reported that the wall failed by sliding shear and so the supplemental criteria are invoked to obtain a drift associated with this damage state. |
| | 4* | $SC_1$ | 1.33 | The data point is obtained from the 3rd quadrant of the load-displacement relationship (see Figure C-14). The same transient drift in the 1st quadrant yields a residual drift of slightly less than 1.0%. |
| | | $SC_2$ | 1.29 | The data point is obtained from the 3rd quadrant of the load-displacement relationship (see Figure C-14). A data point cannot be established in the 1st quadrant. |

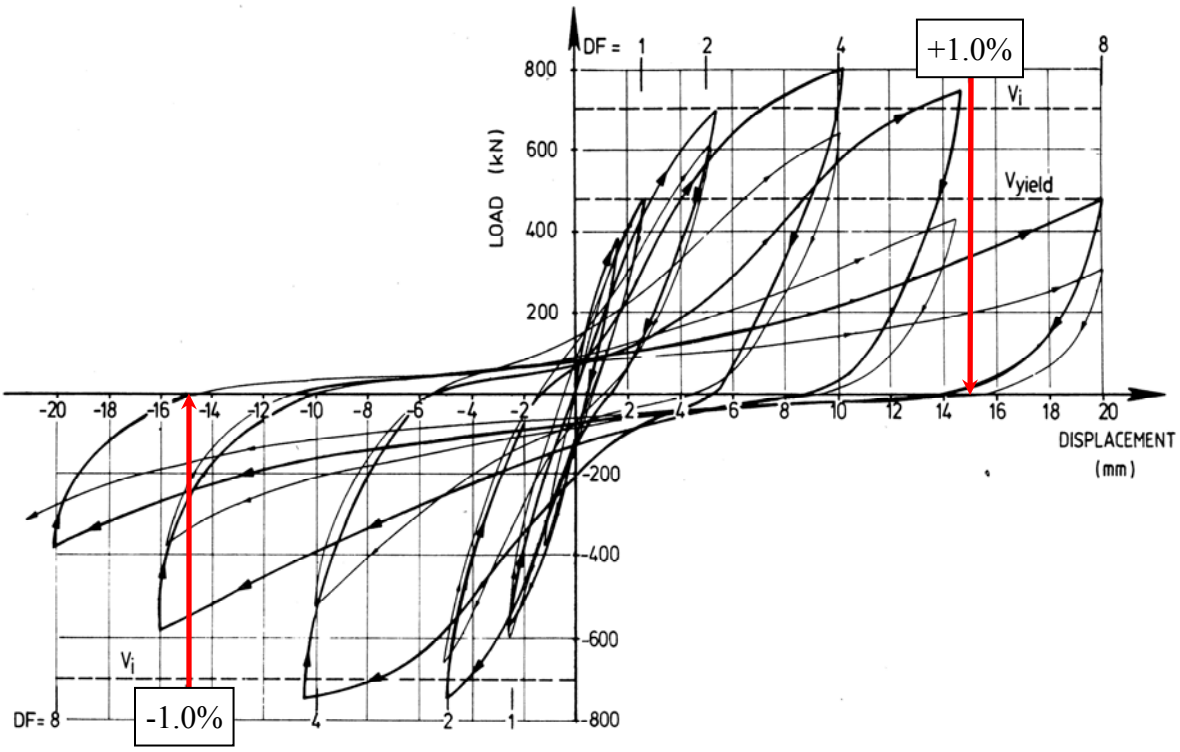


**Figure C-14 Load-displacement relationship for wall 1 [Synge (1980)]**

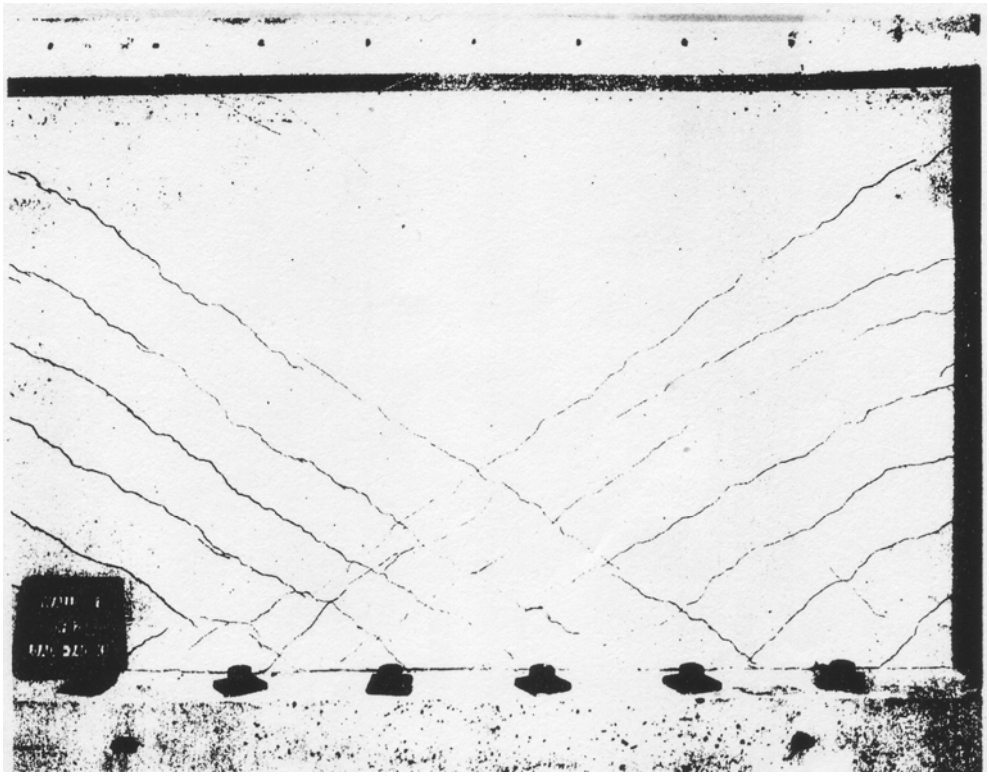

**Figure C-15 Condition of wall 1 at 0.34% drift [Synge (1980)]**

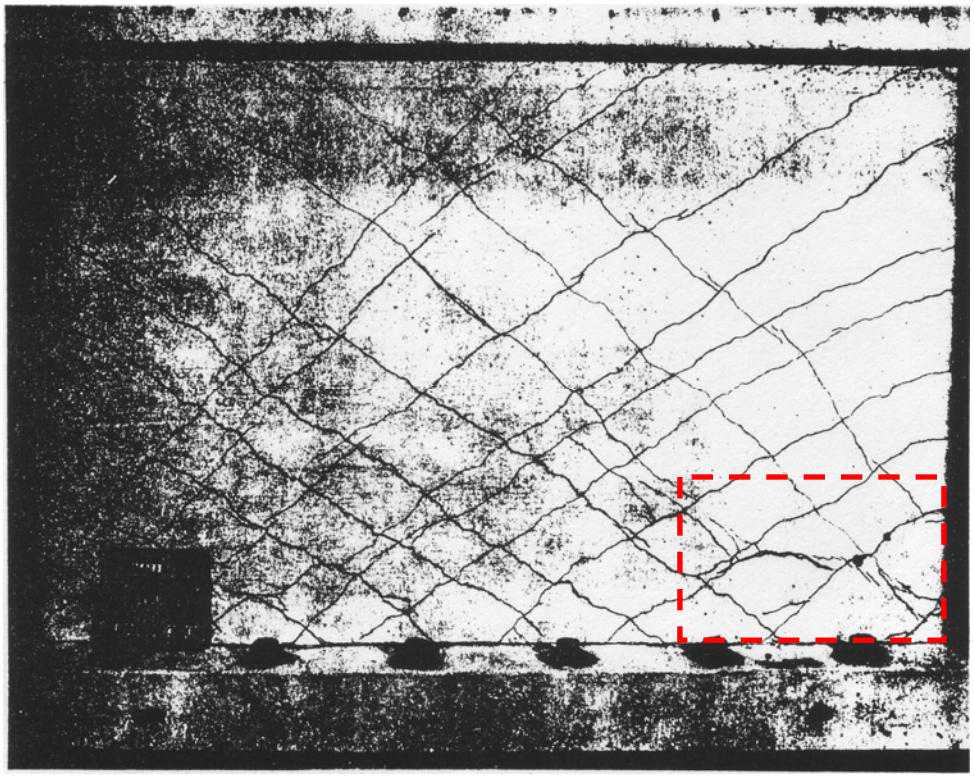

**Figure C-16 Condition of wall 1 at 0.69% drift [Synge (1980)]**

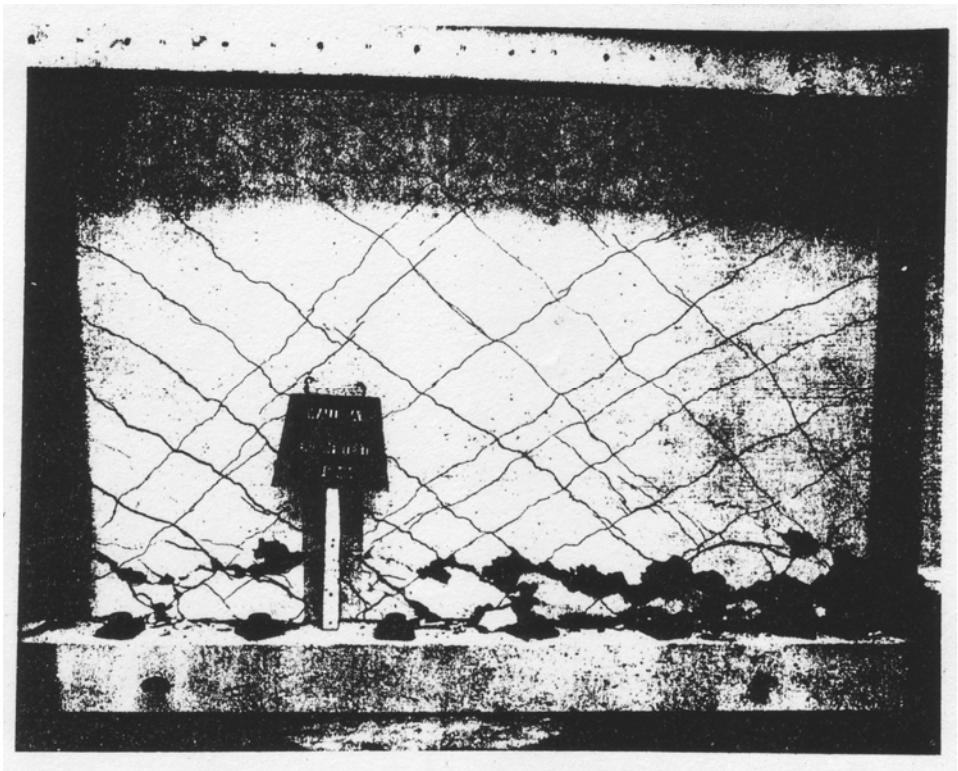

**Figure C-17 Condition of wall 1 at 1.33% drift [Synge (1980)]**

## C.1.4 Pilakoutas (1991) Walls

### C.1.4.1 Wall SW4

**Table C-6 Evaluation of damage data for wall SW4 tested by Pilakoutas**

| Wall ID | MoR | Damage State (DS) | Drift (%) | Comments |
|---|---|---|---|---|
| SW4 | 1 | 1.2 | 0.08 | The drifts for these damage states are reported by the researcher. |
| | 2a | 2.3 | 0.50 | |
| | 3 | 3.1 | 1.33 | The image reported at this drift (Figure C-22) shows damage that can be repaired by partial wall replacement (MoR-3). The damaged region requiring partial wall replacement is identified using dashed boxes in Figure C-22. |
| | 4 | 4.3 | 1.83 | The images reported at this drift (Figure C-23 and Figure C-24) show widespread crushing. |

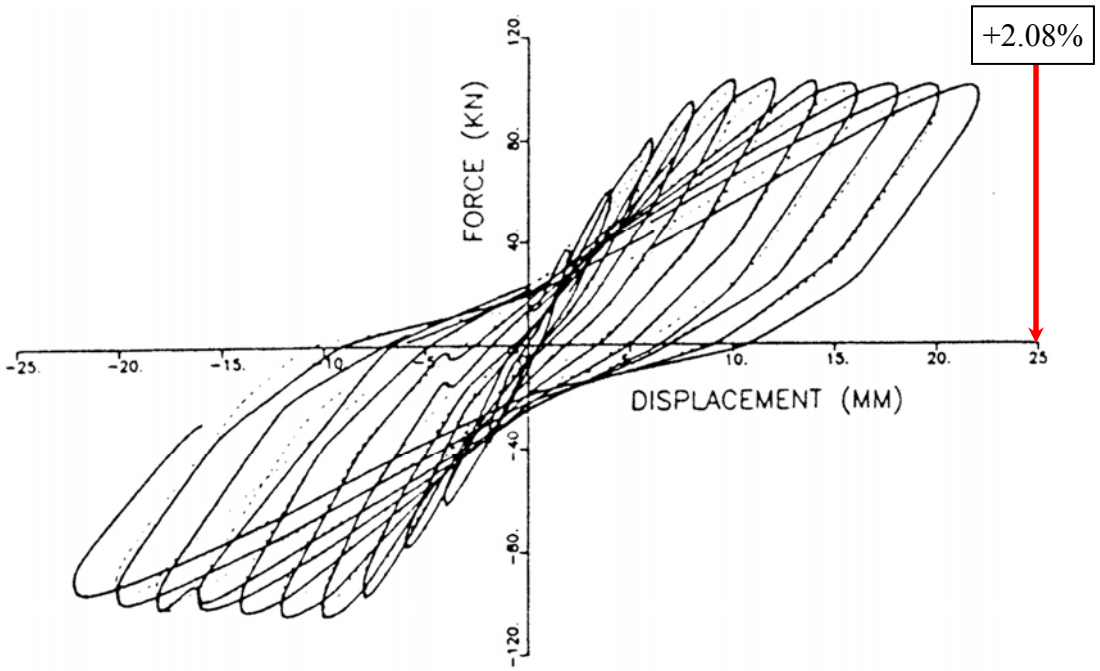


**Figure C-18 Load-displacement relationship for wall SW4 [Pilakoutas (1991)]**

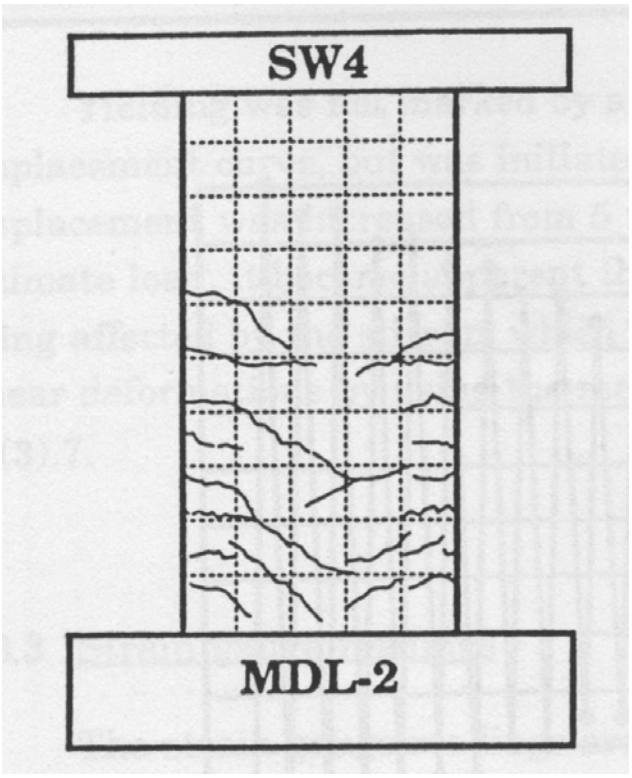


**Figure C-19 Condition of SW4 at 0.17% drift [Pilakoutas (1991)]**

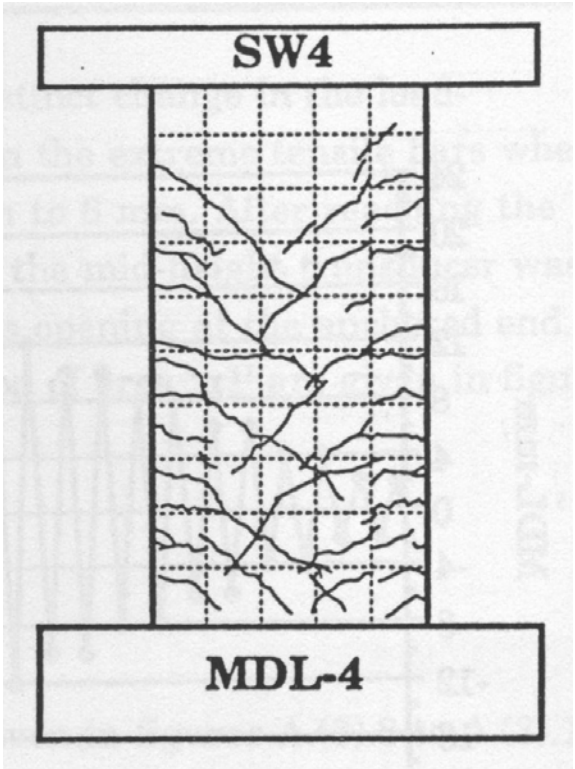


**Figure C-20 Condition of SW4 at 0.33% drift [Pilakoutas (1991)]**

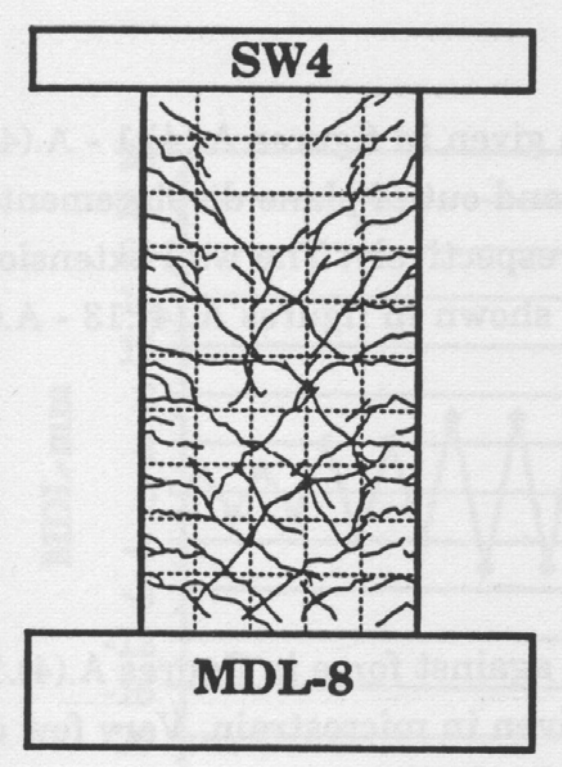


**Figure C-21 Condition of SW4 at 0.67% drift [Pilakoutas (1991)]**

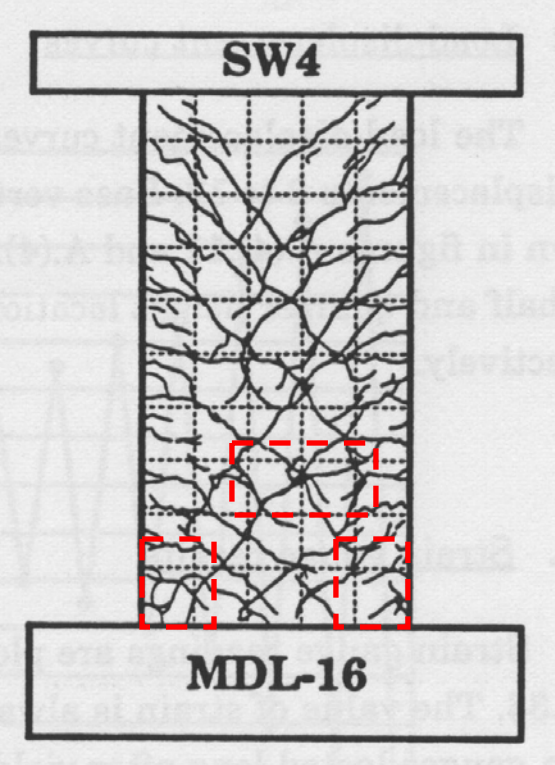


**Figure C-22 Condition of SW4 at 1.33% drift [Pilakoutas (1991)]**

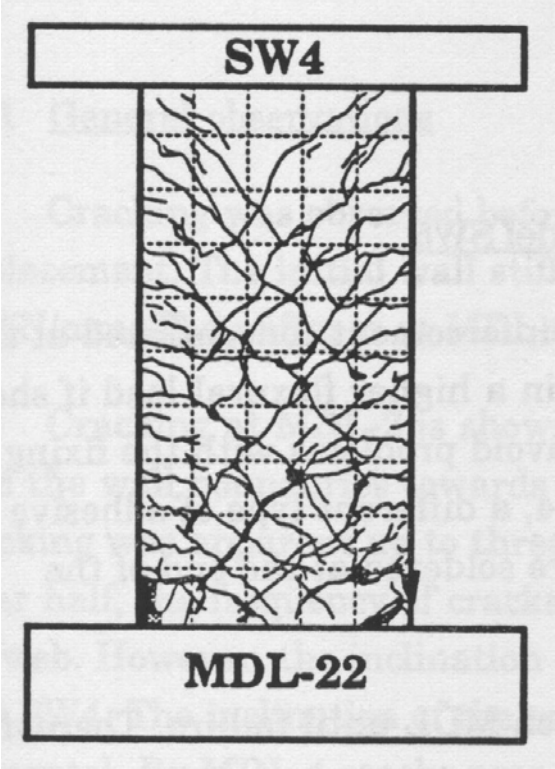


**Figure C-23 Condition of SW4 at 1.83% drift [Pilakoutas (1991)]**

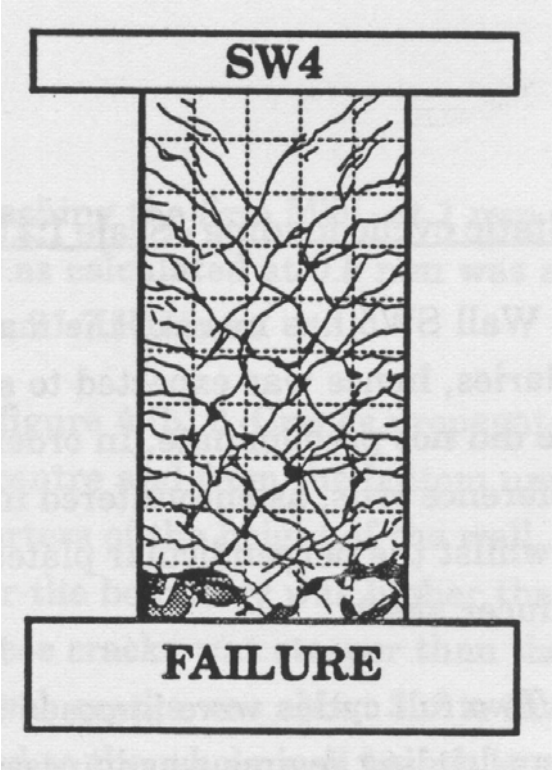


**Figure C-24 Condition of SW4 at 1.83% drift (additional cycles at the same drift level) [Pilakoutas (1991)]**

### C.1.4.2 Wall SW5

**Table C-7 Evaluation of damage data for wall SW5 tested by Pilakoutas**

| Wall ID | MoR | Damage State (DS) | Drift (%) | Comments |
|---|---|---|---|---|
| SW5 | 1 | 1.2 | 0.08 | The drift for this damage state is reported by the researcher. |
| | 2a | 2.1 | 0.67 | The researcher reported a drift of 0.83% for this damage state. However, this value is judged to be too high for MoR-2a based on the cracking pattern presented in Figure C-28 in which the formation of major diagonal cracks that led to failure of the wall can be observed. Therefore, a drift value of 0.67% is used for this damage state in lieu of 0.83% that is reported by the researcher. |
| | 4 | 4.2 | 0.83 | Based on the researcher's description of damage at this drift: "On attempting to achieve MDL-10 in the reverse direction, abrupt failure occurred at a load of about 110 kN. At this stage two of the main web cracks opened up significantly." [Pilakoutas (1991), page 106]. The image presented at this drift (Figure C-29) also supports this observation. |

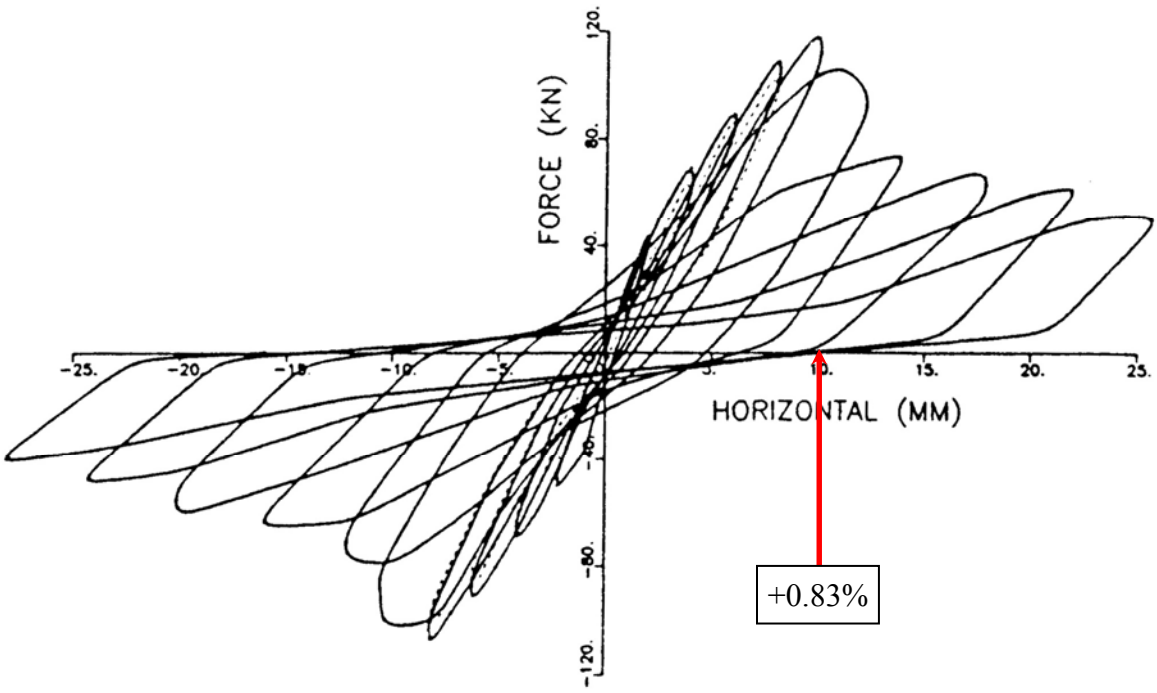


**Figure C-25 The load-displacement relationship for wall SW5 [Pilakoutas (1991)]**

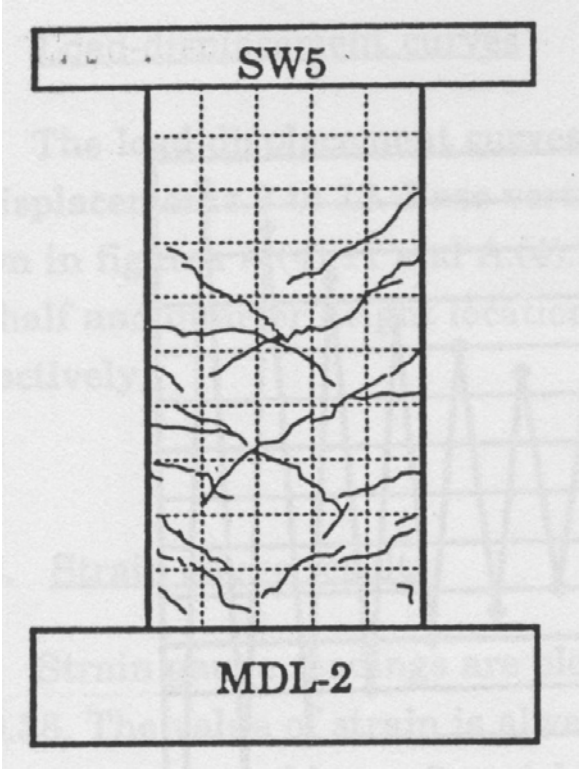


**Figure C-26 Condition of SW5 at 0.17% drift [Pilakoutas (1991)]**

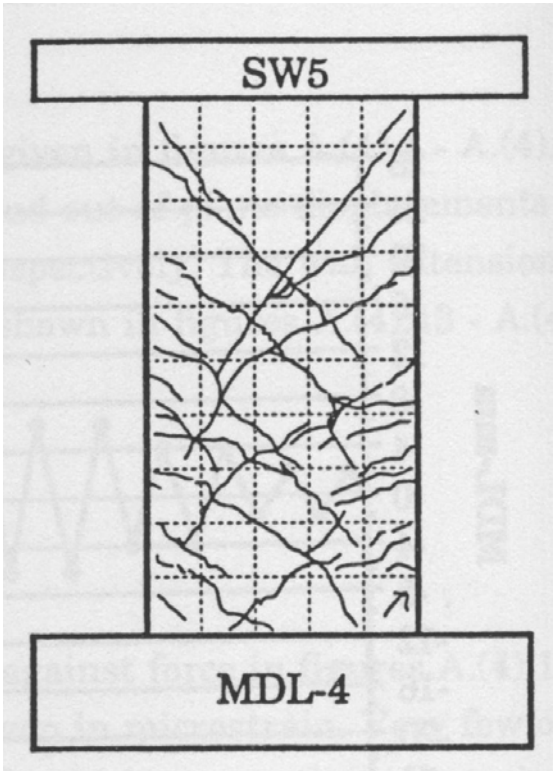


**Figure C-27 Condition of SW5 at 0.33% drift [Pilakoutas (1991)]**

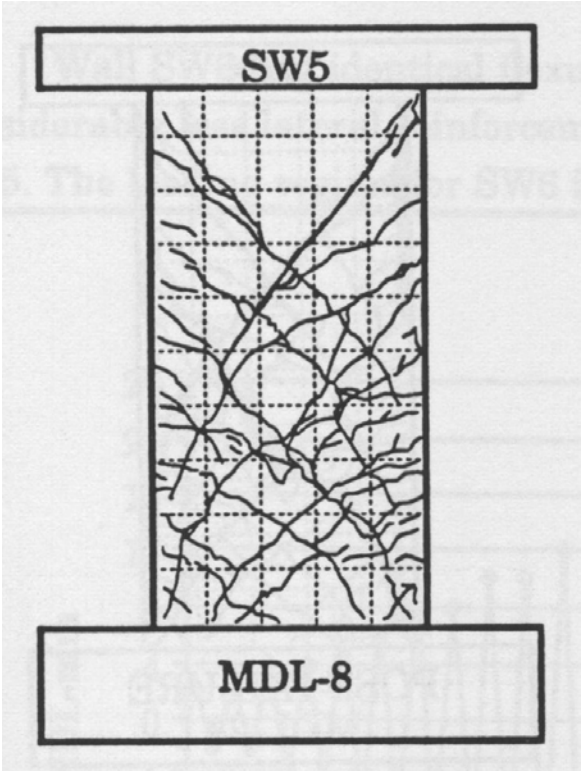


**Figure C-28 Condition of SW5 at 0.67% drift [Pilakoutas (1991)]**

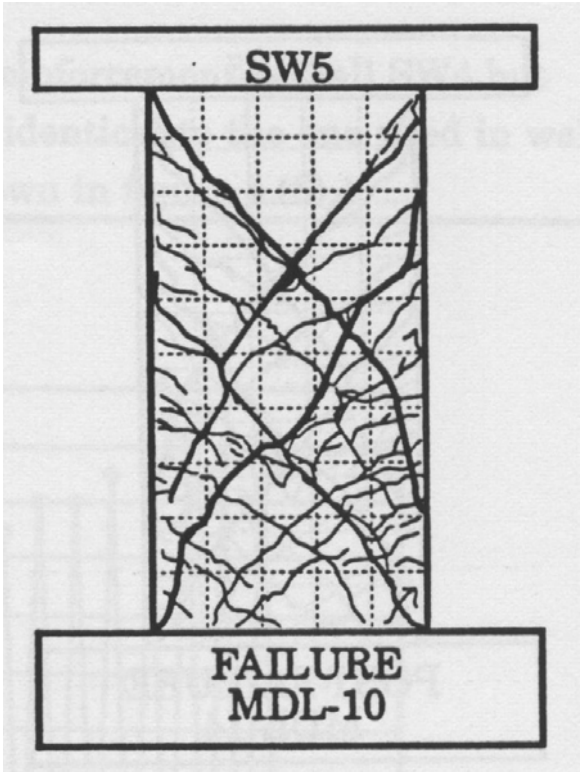


**Figure C-29 Condition of SW5 at 0.83% drift [Pilakoutas (1991)]**

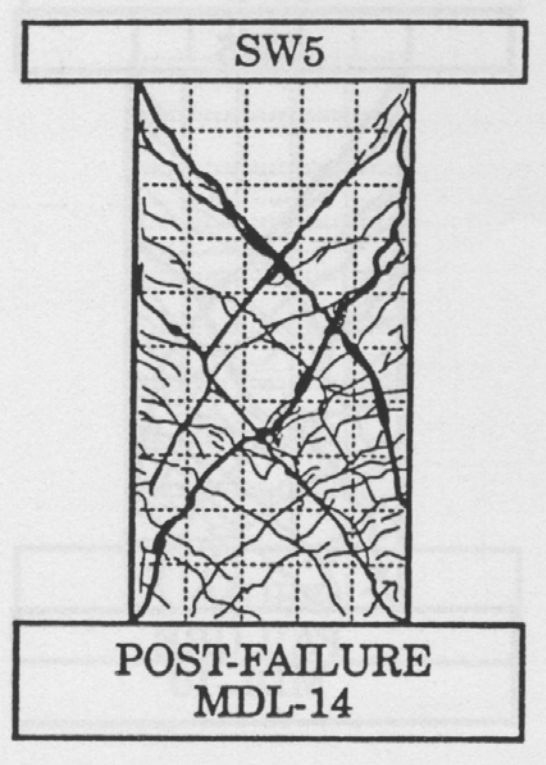


**Figure C-30 Condition of SW5 at 1.17% drift [Pilakoutas (1991)]**

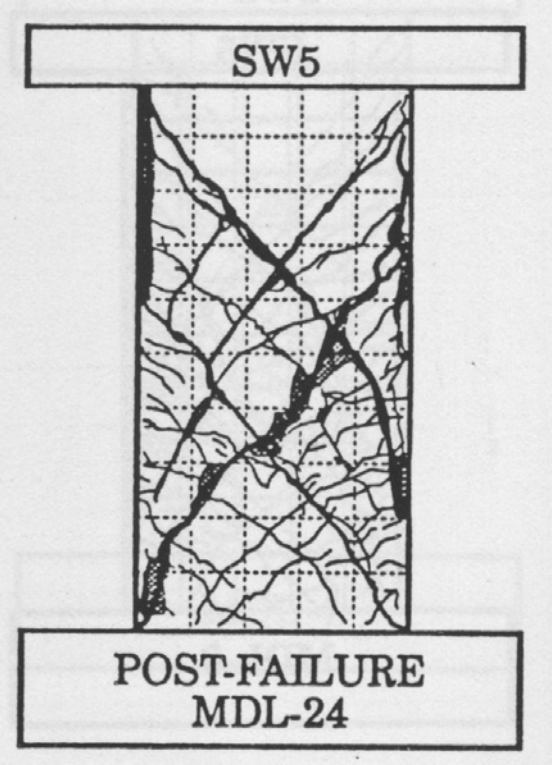


**Figure C-31 Condition of SW5 at 1.71% drift [Pilakoutas (1991)]**

### C.1.4.3 Wall SW6

**Table C-8 Evaluation of damage data for wall SW6 tested by Pilakoutas**

| Wall ID | MoR | Damage State (DS) | Drift (%) | Comments |
|---|---|---|---|---|
| SW6 | 1 | 1.2 | 0.08 | The drifts for these damage states are reported by the researcher. |
| | 2a | 2.3 | 0.50 | |
| | 3 | 3.1 | 1.33 | The image reported at this drift (Figure C-36) shows damage that can be repaired by partial wall replacement (MoR-3). Although not clear in the figure, the web compression toes were also damaged at this drift as reported by the researcher [Pilakoutas (1991), page 110]. The damaged region requiring wall replacement is identified using dashed boxes in Figure C-36. |
| | 4 | 4.3 | 1.83 | The image reported at this drift (Figure C-38) shows widespread crushing. |

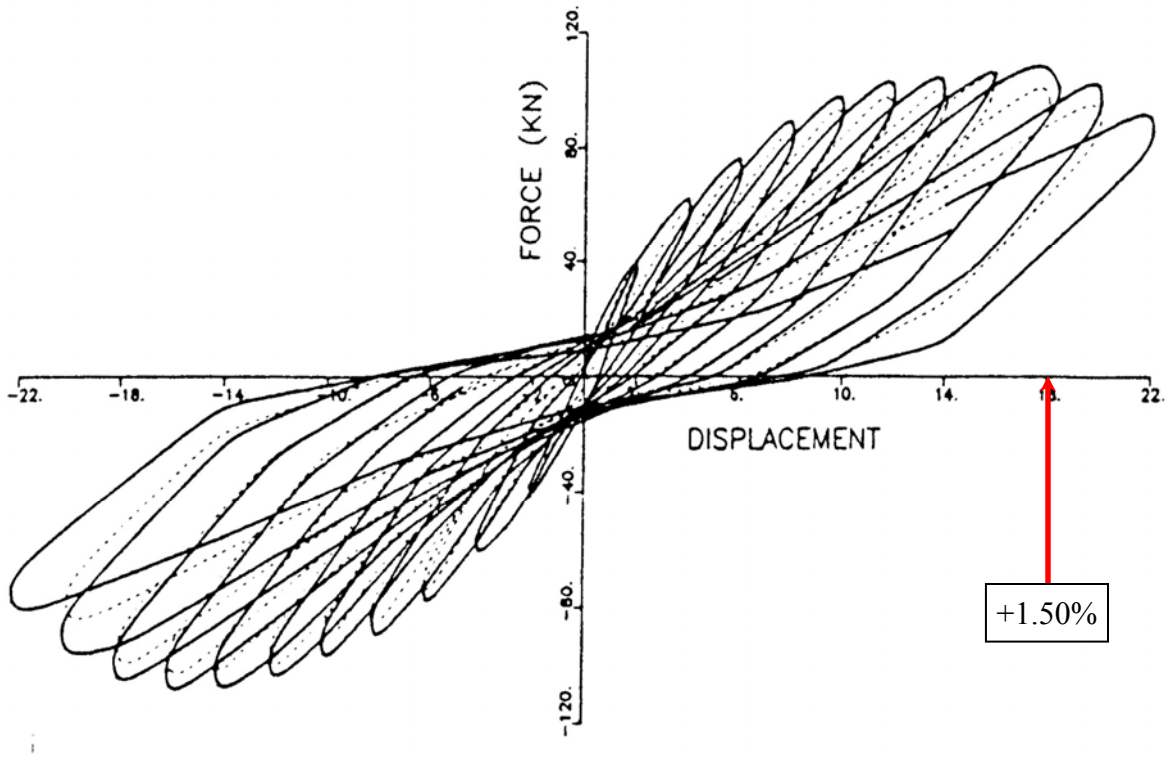


**Figure C-32 Load-displacement relationship for wall SW6 [Pilakoutas (1991)]**

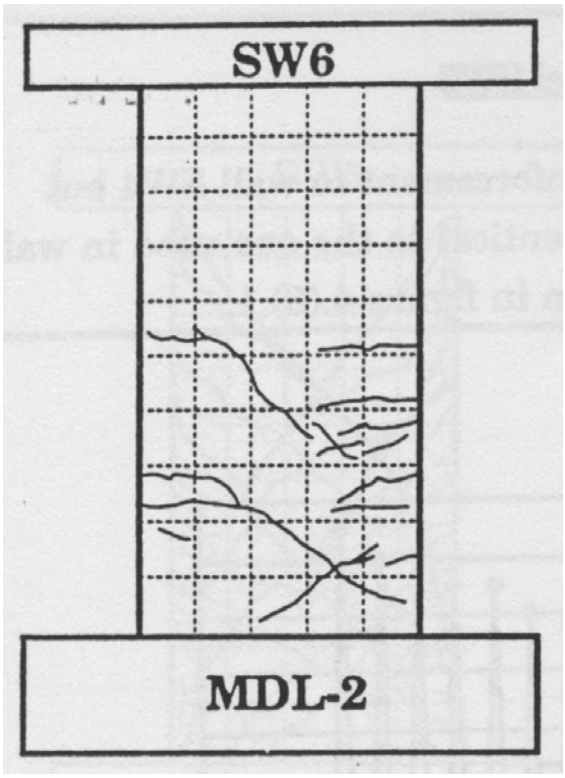


**Figure C-33 Condition of wall SW6 at 0.17% drift [Pilakoutas (1991)]**

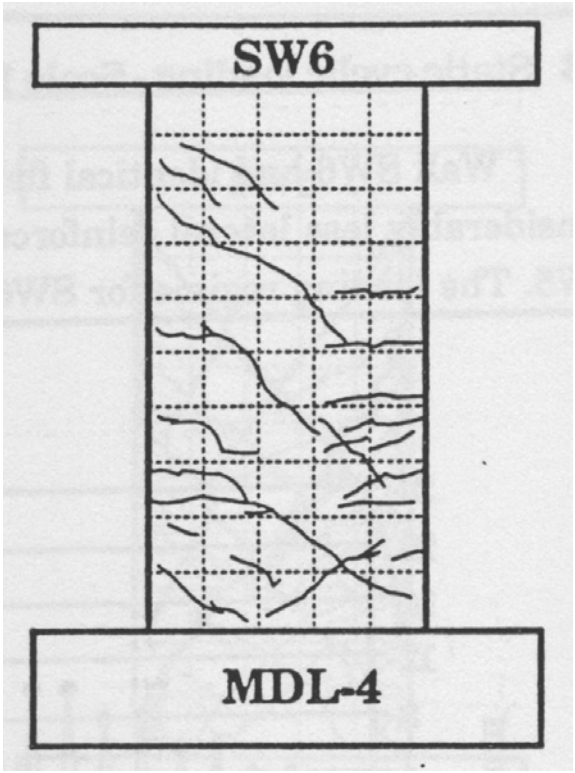


**Figure C-34 Condition of wall SW6 at 0.33% drift [Pilakoutas (1991)]**

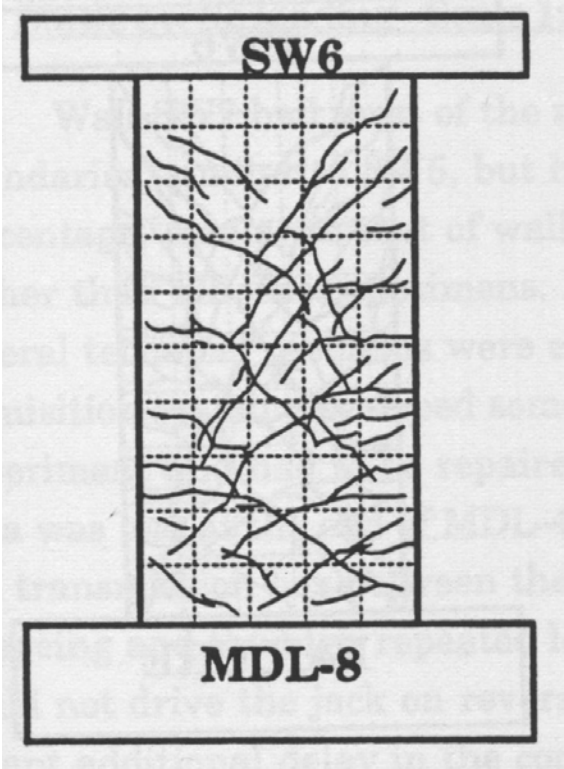


**Figure C-35 Condition of wall SW6 at 0.67% drift [Pilakoutas (1991)]**

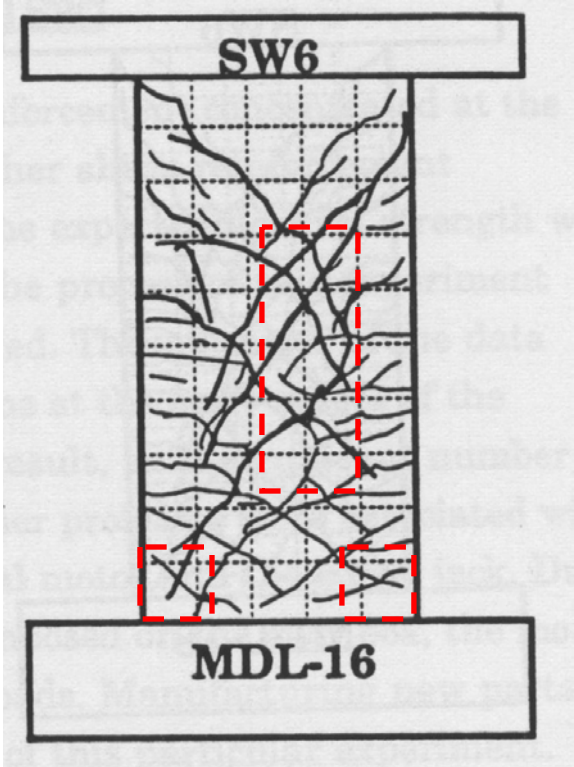


**Figure C-36 Condition of wall SW6 at 1.33% drift [Pilakoutas (1991)]**

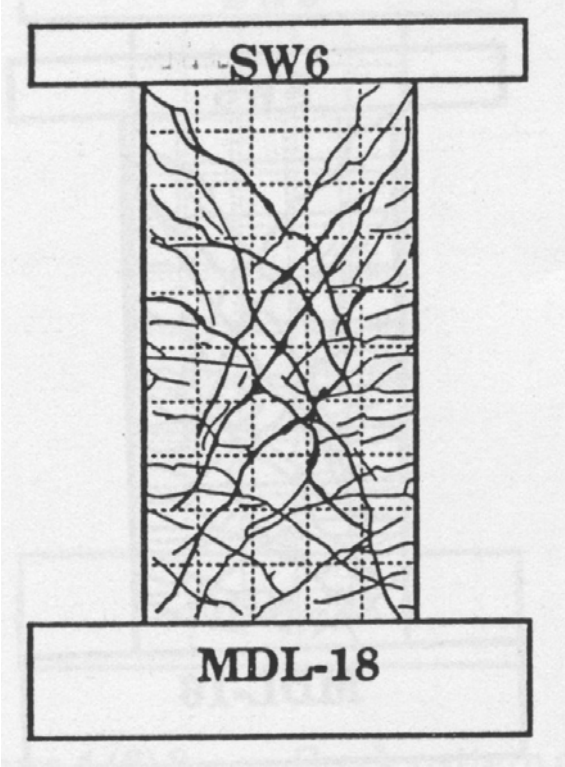


**Figure C-37 Condition of wall SW6 at 1.50% drift [Pilakoutas (1991)]**

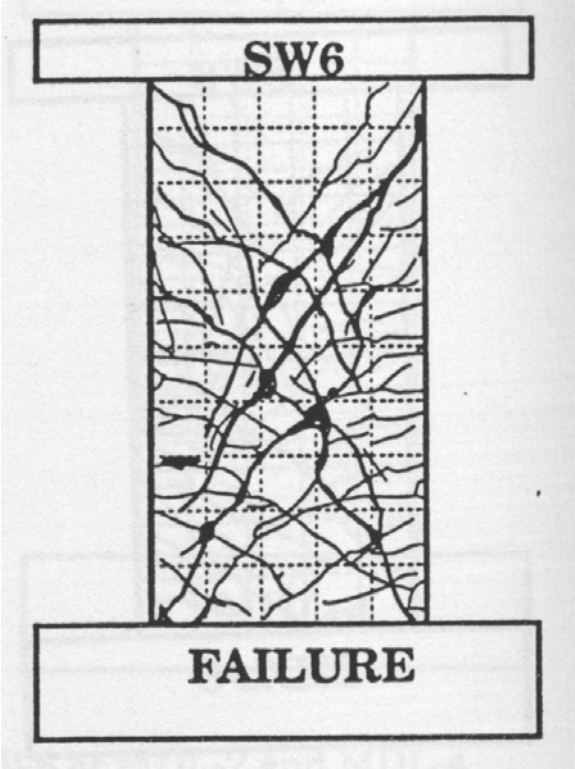


**Figure C-38 Condition of wall SW6 at 1.83% drift [Pilakoutas (1991)]**

### C.1.4.4 Wall SW7

**Table C-9 Evaluation of damage data for wall SW7 tested by Pilakoutas**

| Wall ID | MoR | Damage State (DS) | Drift (%) | Comments |
|---|---|---|---|---|
| SW7 | 1 | 1.2 | 0.08 | The drifts for these damage states are provided by the researcher. The drift associated with MoR-4 is specified as 1.83% based on a horizontal rebar fracture (DS4.4). The image reported at this drift (Figure C-44) supports this conclusion. |
| | 2a | 2.3 | 0.67 | |
| | 4 | 4.4 | 1.83 | |

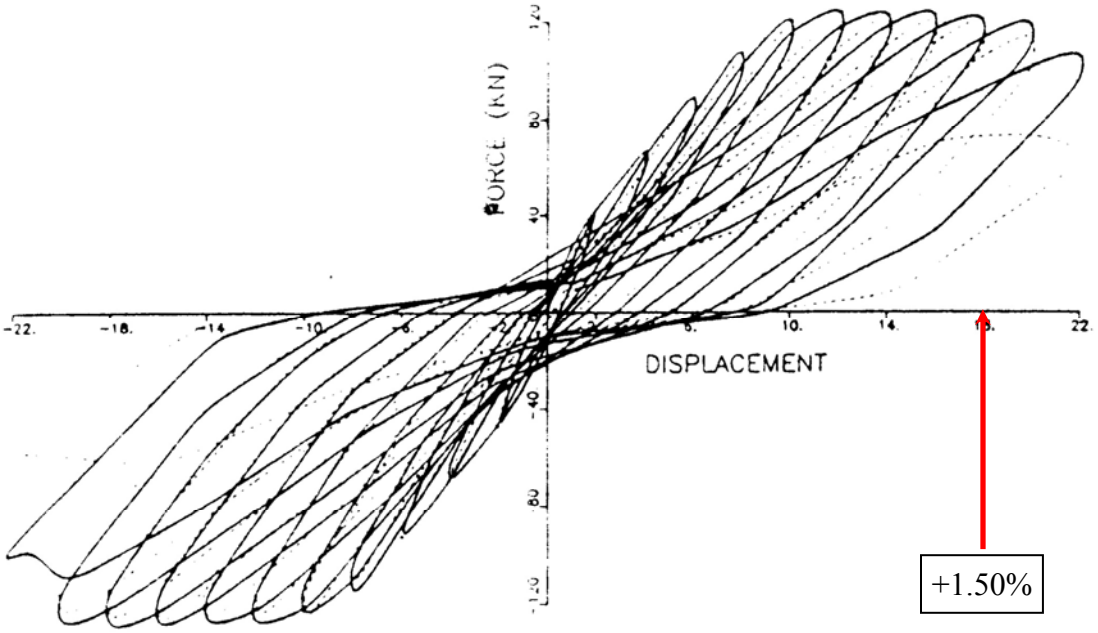


**Figure C-39 The load-displacement relationship for wall SW7 [Pilakoutas (1991)]**

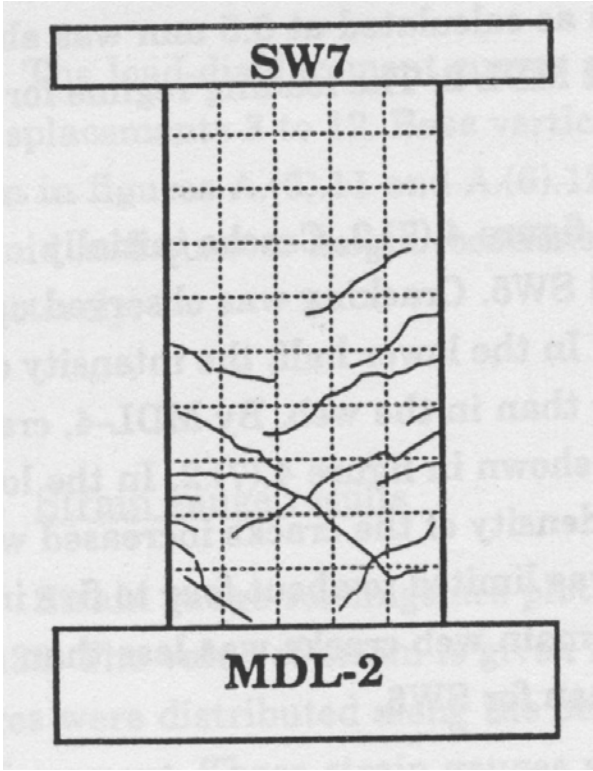


**Figure C-40 Condition of wall SW7 at 0.17% drift [Pilakoutas (1991)]**

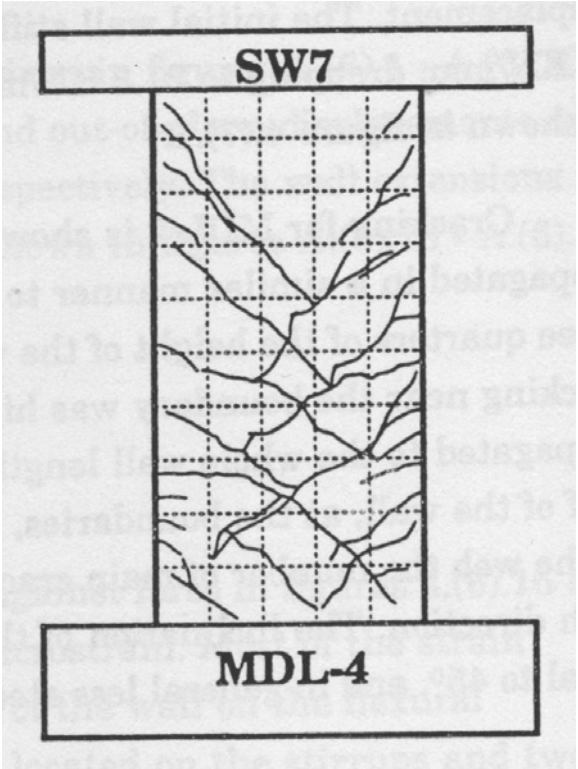


**Figure C-41 Condition of wall SW7 at 0.33% drift [Pilakoutas (1991)]**

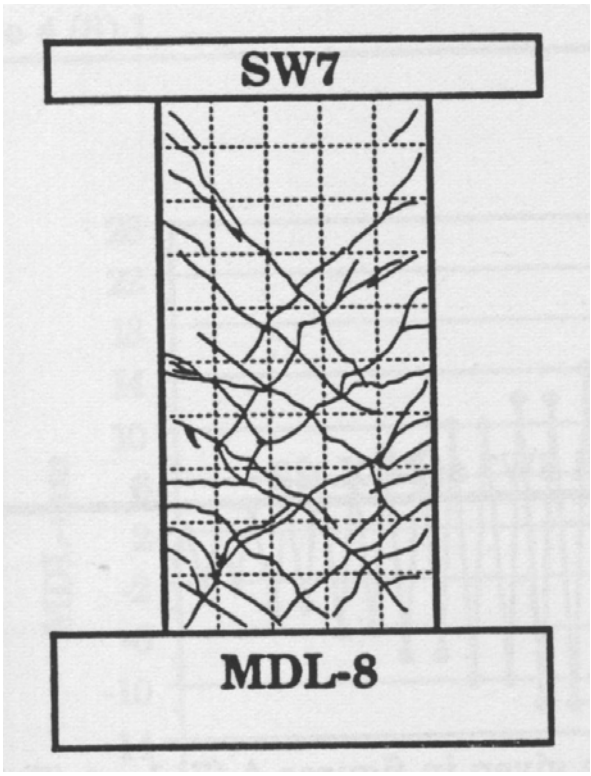


**Figure C-42 Condition of wall SW7 at 0.67% drift [Pilakoutas (1991)]**

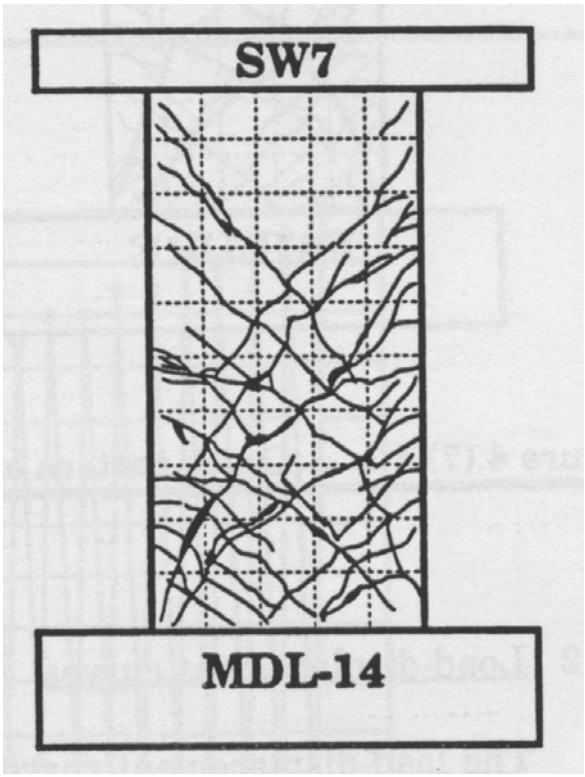


**Figure C-43 Condition of wall SW7 at 1.17% drift [Pilakoutas (1991)]**

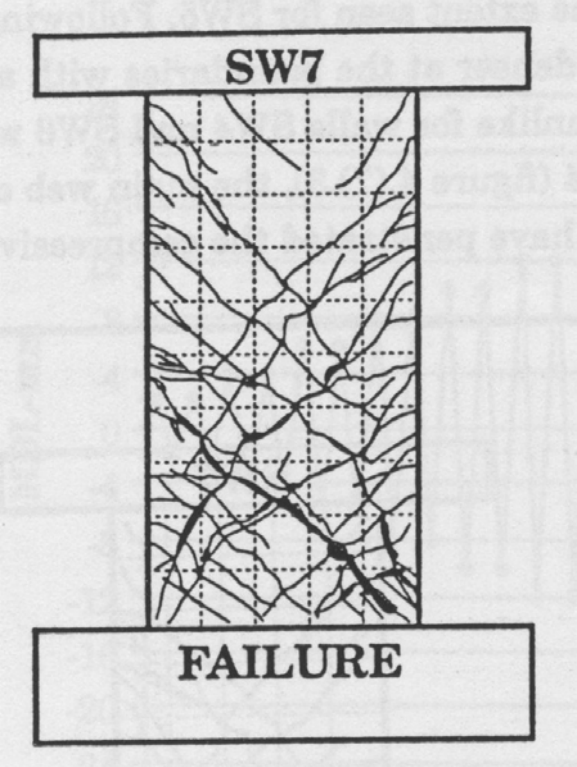


**Figure C-44 Condition of wall SW7 at 1.83% drift [Pilakoutas (1991)]**

### C.1.4.5 Wall SW8

**Table C-10 Evaluation of damage data for wall SW8 tested by Pilakoutas**

| Wall ID | MoR | Damage State (DS) | Drift (%) | Comments |
|---|---|---|---|---|
| SW8 | 1 | 1.2 | 0.08 | The drifts for these damage states are reported by the researcher. |
| | 2a | 2.3 | 0.44 | |
| | 3 | 3.1 | 1.50 | Based on the researcher's description of damage at this drift: "Spalling of the concrete on the inside of the boundary elements indicated the degradation of concrete at that location. At this stage, vertical cracks which appeared by MDL-14 at the bottom end main reinforcement were also visible." [Pilakoutas (1991), page 118]. The damaged region requiring partial wall replacement is identified using dashed boxes in Figure C-50. |
| | 4 | 4.3 | 2.17 | The image reported at this drift (Figure C-51) shows widespread crushing. |

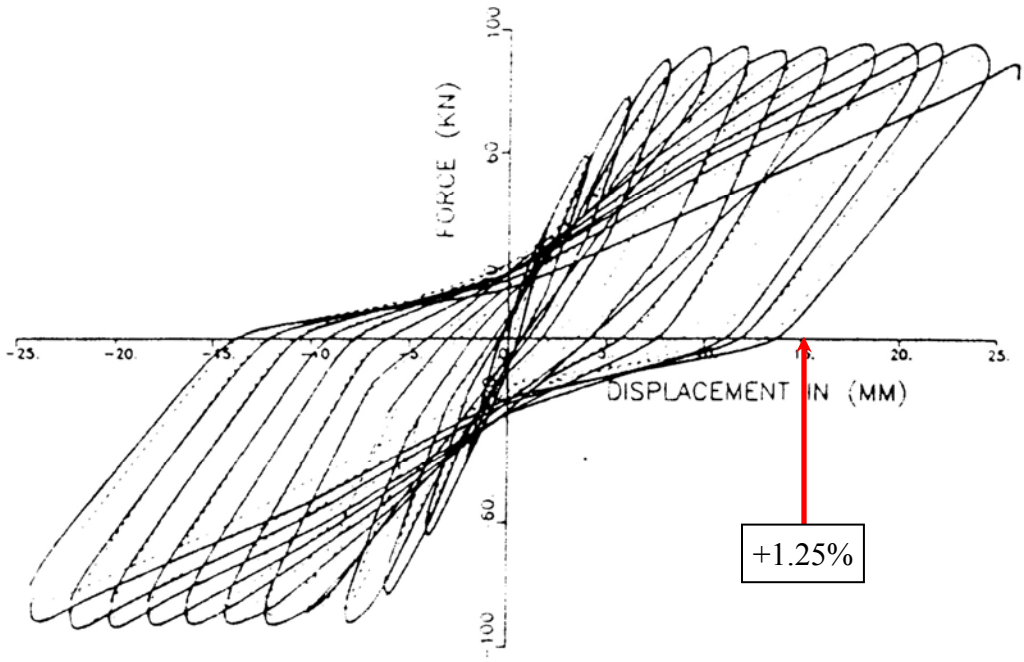


**Figure C-45 Load-displacement relationship for wall SW8 [Pilakoutas (1991)]**

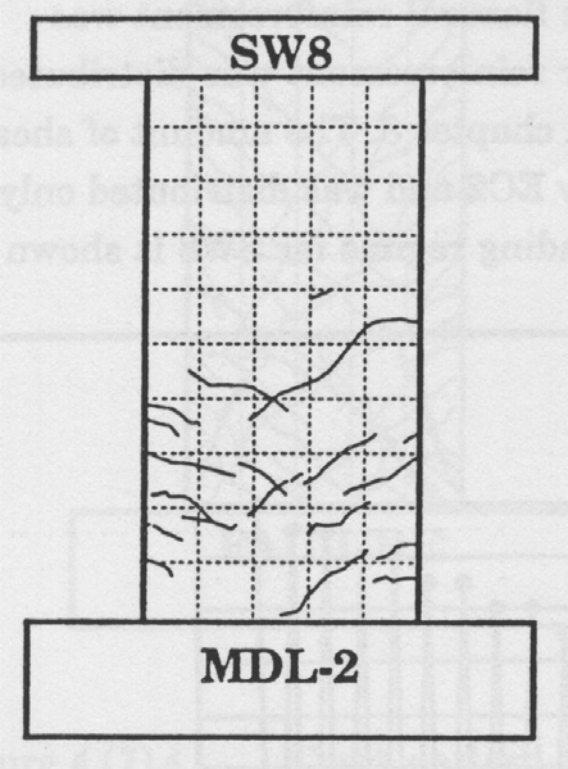


**Figure C-46 Condition of wall SW8 at 0.17% drift [Pilakoutas (1991)]**

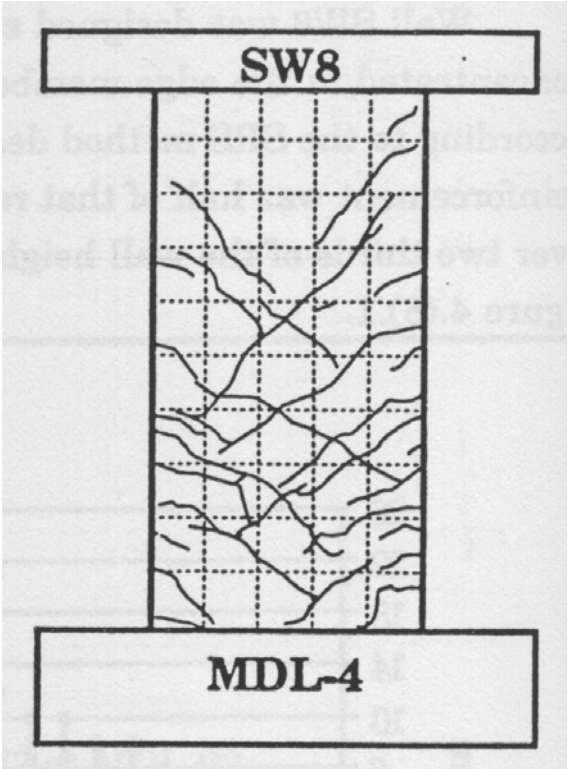


**Figure C-47 Condition of wall SW8 at 0.33% drift [Pilakoutas (1991)]**

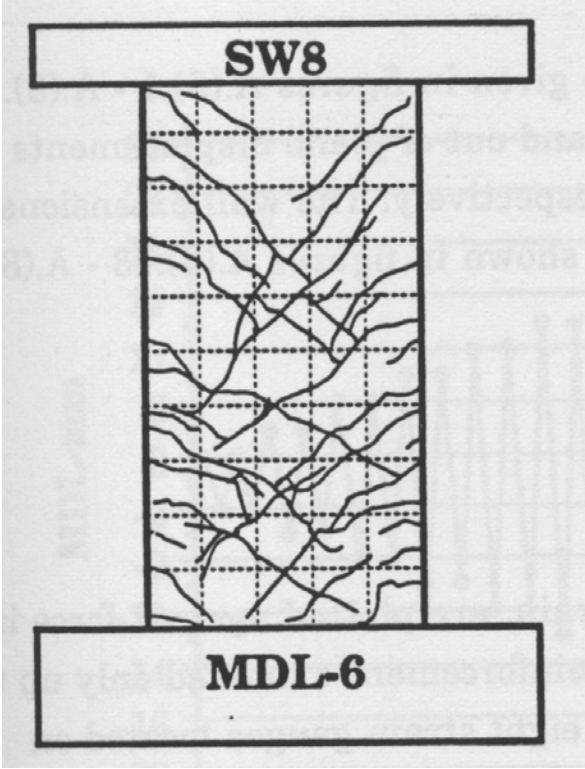


**Figure C-48 Condition of wall SW8 at 0.50% drift [Pilakoutas (1991)]**

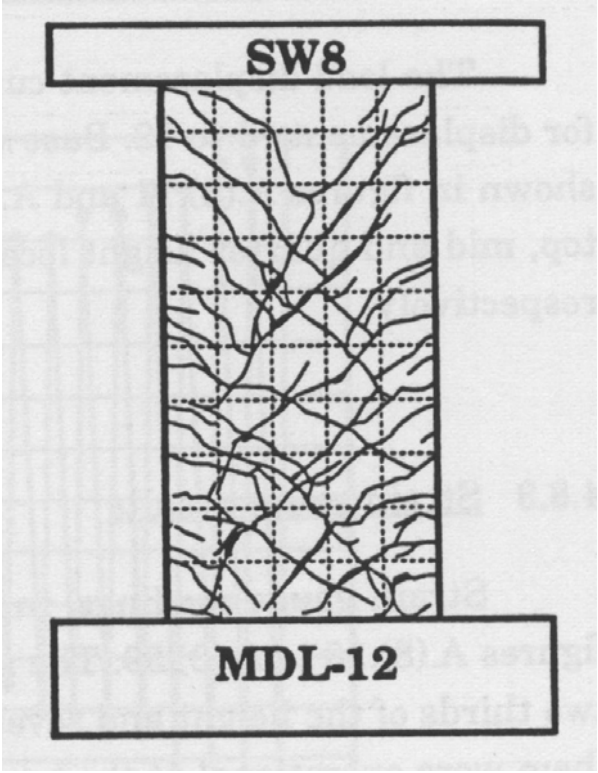


**Figure C-49 Condition of wall SW8 at 1.00% drift [Pilakoutas (1991)]**

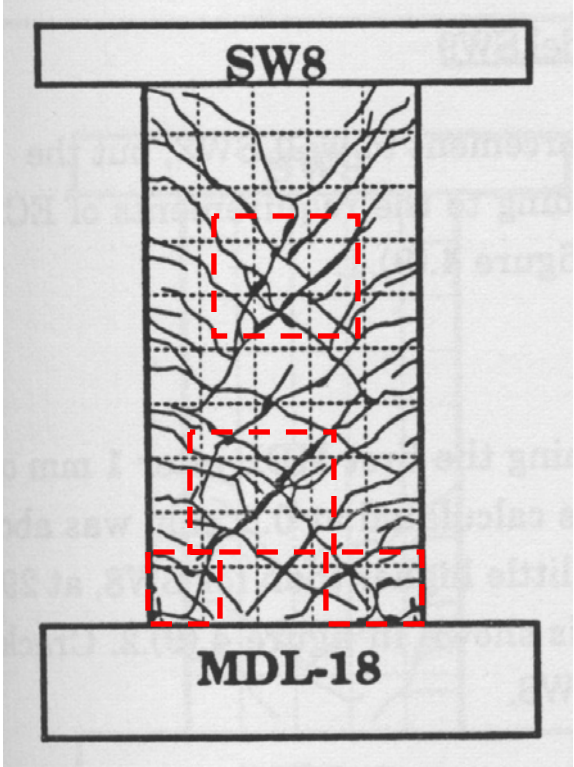


**Figure C-50 Condition of wall SW8 at 1.50% drift [Pilakoutas (1991)]**

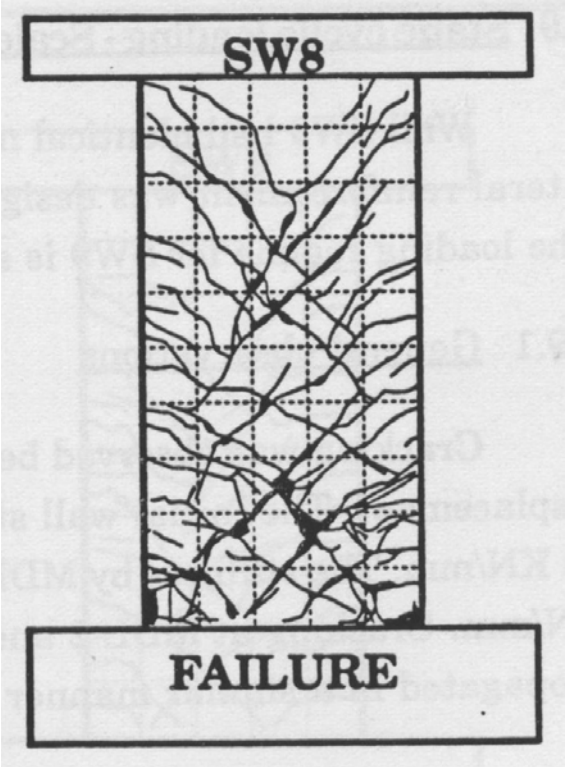


**Figure C-51 Condition of wall SW8 at 2.17% drift [Pilakoutas (1991)]**

### C.1.4.6 Wall SW9

**Table C-11 Evaluation of damage data for wall SW9 tested by Pilakoutas**

| Wall ID | MoR | Damage State (DS) | Drift (%) | Comments |
|---|---|---|---|---|
| SW9 | 1 | 1.2 | 0.08 | The drifts for these damage states are provided by the researcher. |
| | 2a | 2.3 | 0.42 | |
| | 3 | 3.1 | 1.50 | Based on the researcher's description of damage at this drift: "Spalling of concrete in the web at the intersections of main cracks was only confined to the lower quarter of the wall." [Pilakoutas (1991), page 122]. The damaged region requiring partial wall replacement is identified using dashed boxes in Figure C-57. |
| | 4 | 4.3 | 2.17 | The image reported at this drift (Figure C-58) shows widespread crushing. |

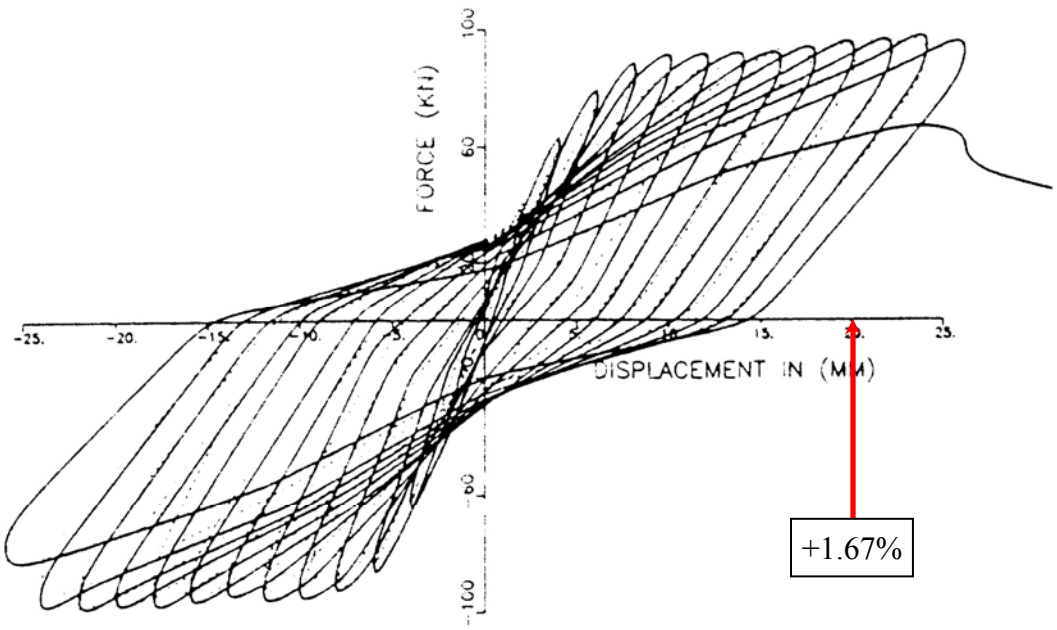


**Figure C-52 Load-displacement relationship for wall SW9 [Pilakoutas (1991)]**

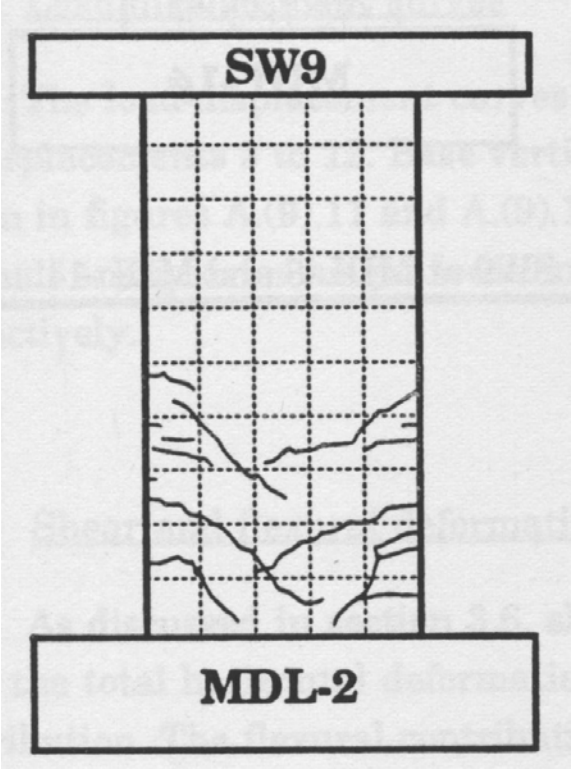


**Figure C-53 Condition of wall SW9 at 0.17% drift [Pilakoutas (1991)]**

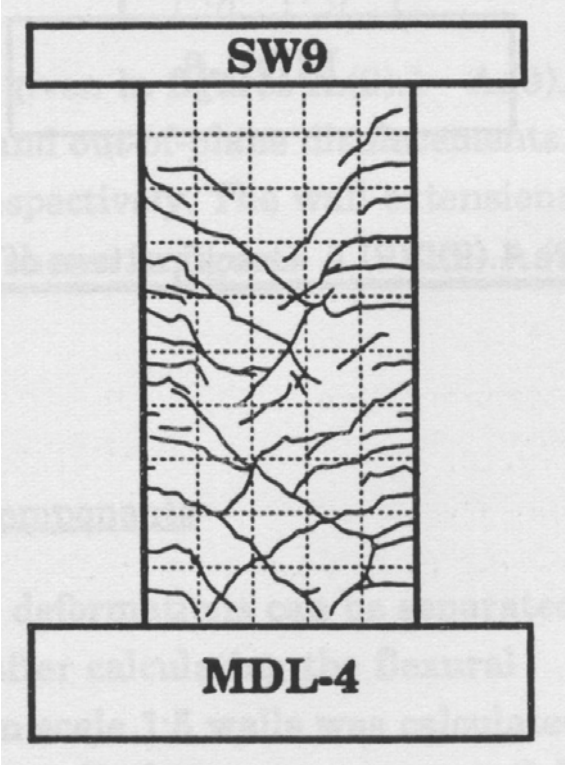


**Figure C-54 Condition of wall SW9 at 0.33% drift [Pilakoutas (1991)]**

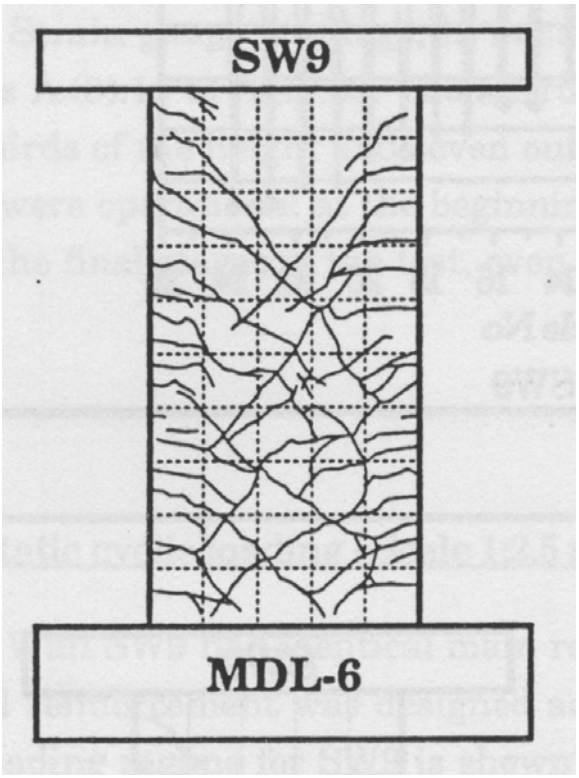


**Figure C-55 Condition of wall SW9 at 0.50% drift [Pilakoutas (1991)]**

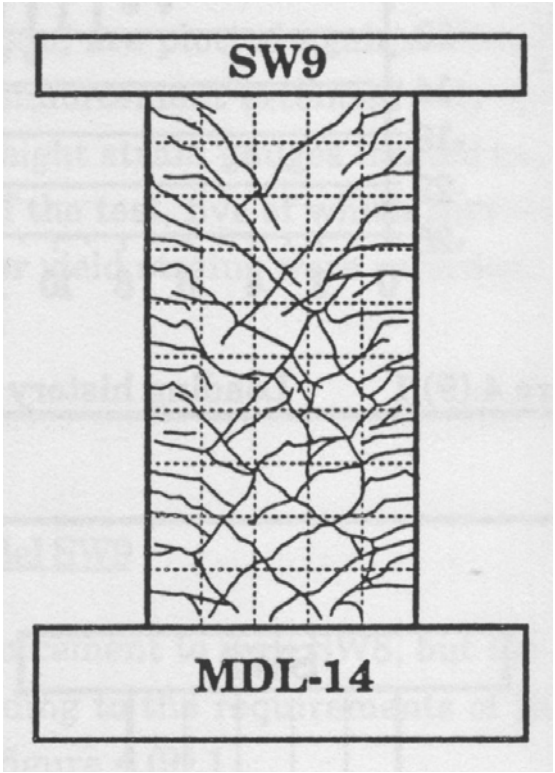


**Figure C-56 Condition of wall SW9 at 1.17% drift [Pilakoutas (1991)]**

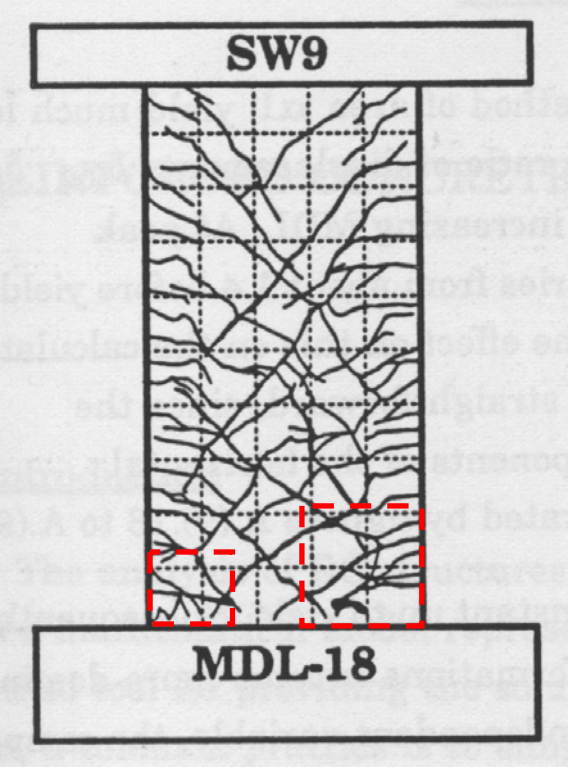


**Figure C-57 Condition of wall SW9 at 1.50% drift [Pilakoutas (1991)]**

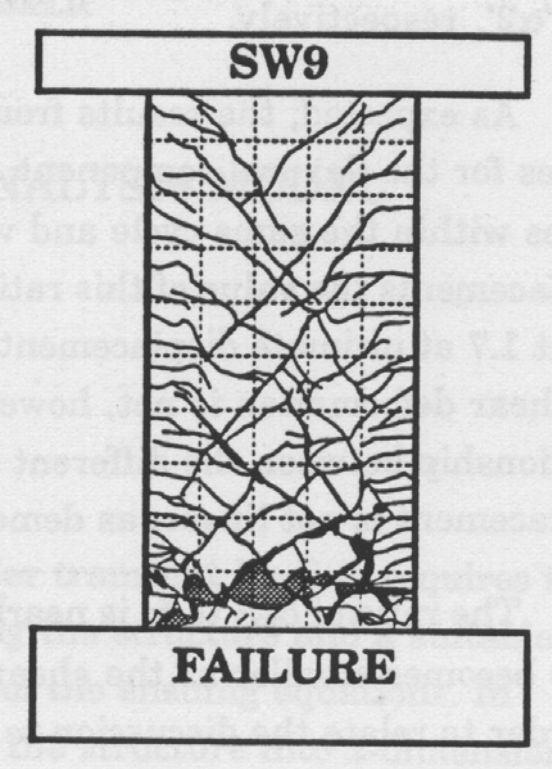


**Figure C-58 Condition of wall SW9 at 2.17% drift [Pilakoutas (1991)]**

## C.1.5 Massone (2006) Walls

### C.1.5.1 Wall WP111-9

**Table C-12 Evaluation of damage data for wall WP111-9 tested by Massone**

| Wall ID | MoR | Damage State (DS) | Drift (%) | Comments |
|---|---|---|---|---|
| WP111-9 | 1 | 1.3 | 0.20 | The drifts for these damage states are provided by the researcher. |
| | 2a | 2.1 | 0.40 | |
| | | 2.3 | 0.40 | |
| | | 2.4a | 0.40 | |
| | 2b | 2.4b | 0.40 | |
| | 4 | 4.2 | 0.60 | Based on the researcher's description of damage at this drift: "In Test 5, the diagonal crack from corner to corner widened, sliding along the crack was observed, and lateral strength degraded to near zero (for positive loading)." [Massone (2006), page 171]. |

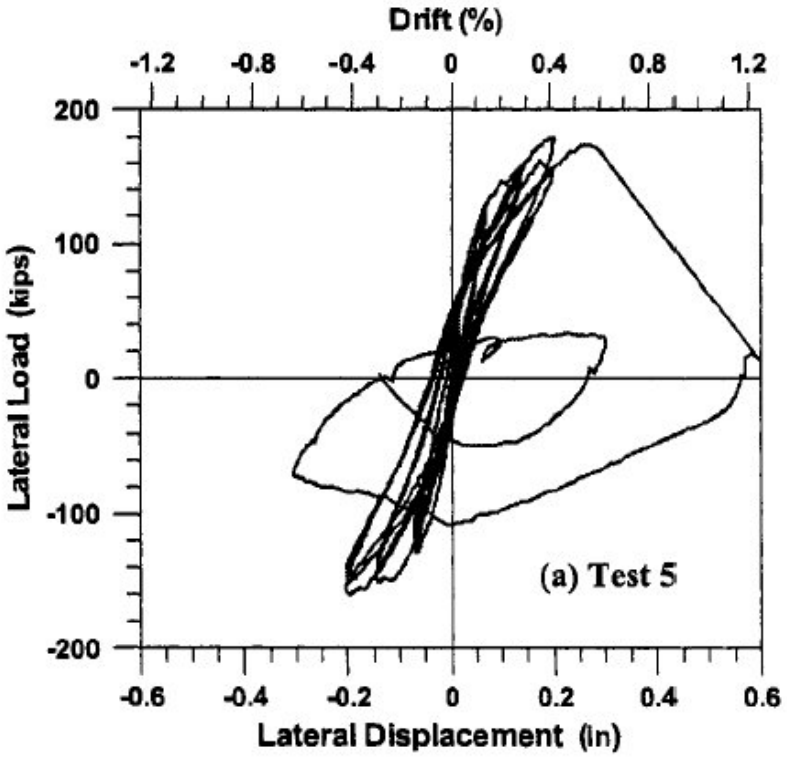


**Figure C-59 Load-displacement relationship for wall WP111-9 [Massone (2006)]**

### C.1.5.1.1 Wall WP111-10

**Table C-13 Evaluation of damage data for wall WP111-10 tested by Massone**

| Wall ID | MoR | Damage State (DS) | Drift (%) | Comments |
|---|---|---|---|---|
| WP111-10 | 1 | 1.3 | 0.20 | The drifts for these damage states are provided by the researcher. |
| | 2a | 2.1 | 0.40 | |
| | | 2.3 | 0.40 | |
| | | 2.4a | 0.40 | |
| | 2b | 2.4b | 0.40 | |
| | 4 | 4.2 | 0.95 | The reported load-drift relationship (Figure C-60) indicates a sudden loss of shear strength at this drift. |

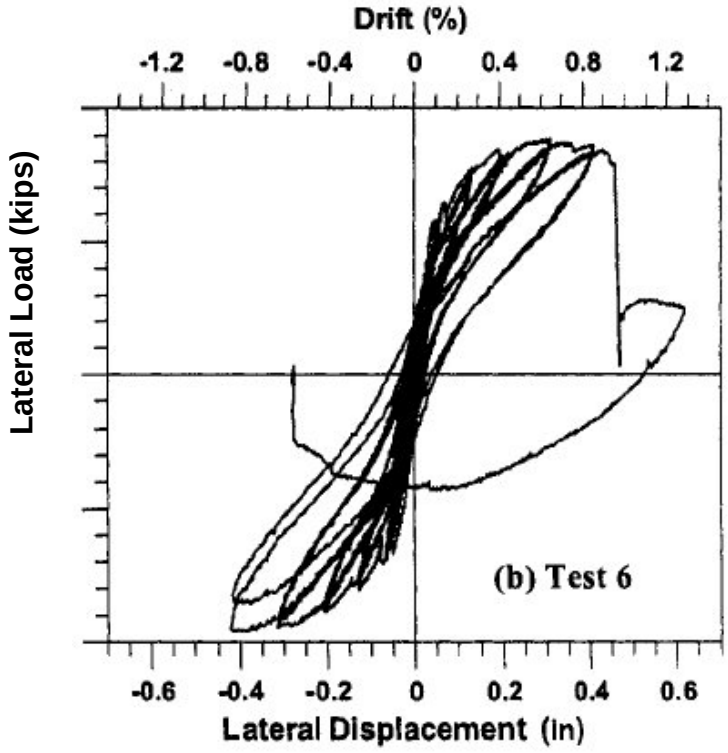


**Figure C-60 Load-displacement relationship for wall WP111-10 [Massone (2006)]**

### C.1.5.2 Wall WP1105-8

**Table C-14 Evaluation of damage data for wall WP1105-8 tested by Massone**

| Wall ID | MoR | Damage State (DS) | Drift (%) | Comments |
|---|---|---|---|---|
| WP1105-8 | 1 | 1.3 | 0.20 | The drifts for these damage states are provided by the researcher. |
| | 2a | 2.1 | 0.30 | |
| | | 2.3 | 0.30 | |
| | | 2.4a | 0.30 | |
| | 2b | 2.4b | 0.60 | |
| | 4 | 4.2 | 0.80 | Based on the researcher's description of damage at this drift: "…lateral strength degradation is observed for the first positive cycle due to a combination of concrete crushing at the mid-height at the center of the wall and widening of primary diagonal cracks." [Massone (2006), page 178]. In addition, the reported load-drift relationship (Figure C-61) indicates a sudden loss of shear strength at this drift. |

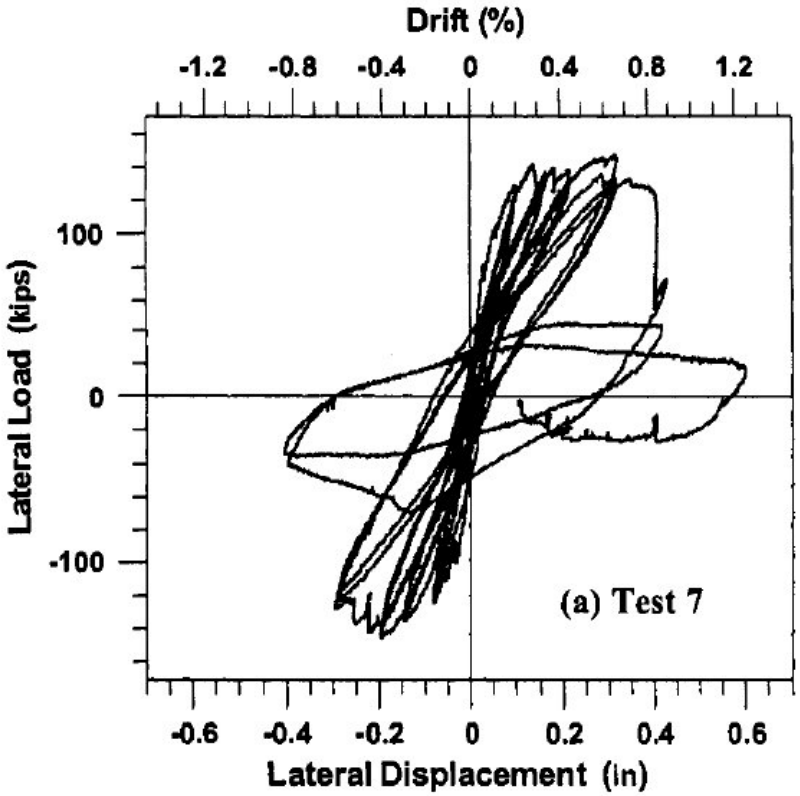


**Figure C-61 Load-displacement relationship for wall WP1105-8 [Massone (2006)]**

### C.1.5.2.1 Wall WP1105-7

**Table C-15 Evaluation of damage data for wall WP1105-7 tested by Massone**

| Wall ID | MoR | Damage State (DS) | Drift (%) | Comments |
|---|---|---|---|---|
| WP1105-7 | 1 | 1.3 | 0.20 | The drifts for these damage states are provided by the researcher. |
| | 2a | 2.1 | 0.60 | |
| | | 2.3 | 0.30 | |
| | | 2.4a | 0.30 | |
| | 2b | 2.4b | 0.60 | |
| | 4 | 4.2 | 0.80 | Based on the researcher's description of damage at this drift: "…primary crack widened, sliding was observed along the diagonal crack plane, reducing the lateral strength for negative loading to zero." [Massone (2006), page 178]. In addition, the reported load-drift relationship (Figure C-62) indicates a sudden loss of shear strength at this drift. |

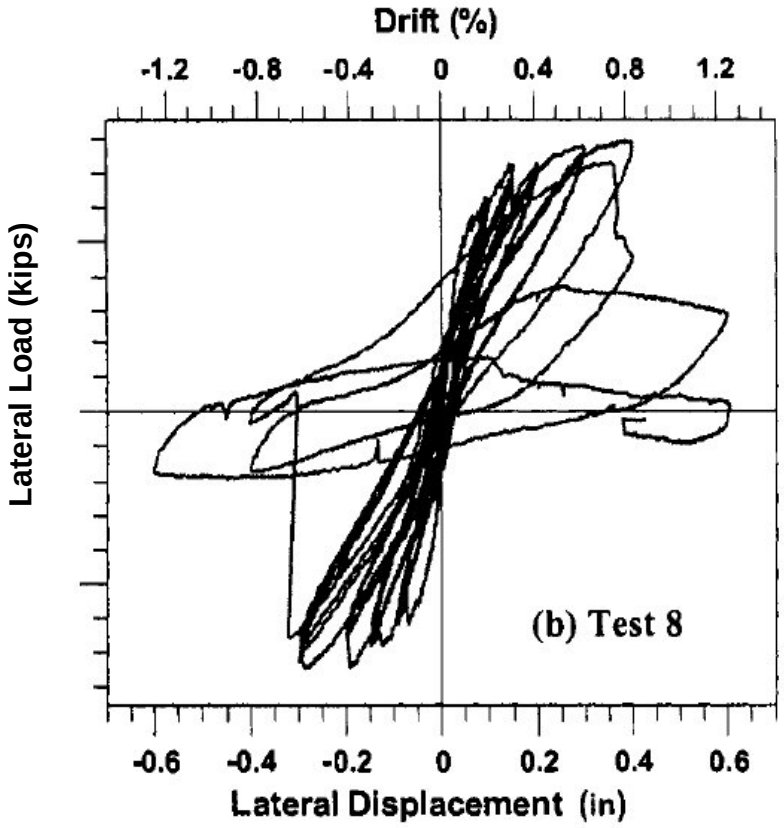


**Figure C-62 Load-displacement relationship for wall WP1105-7 [Massone (2006)]**

### C.1.5.2.2 Wall WP110-5

**Table C-16 Evaluation of damage data for wall WP110-5 tested by Massone**

| Wall ID | MoR | Damage State (DS) | Drift (%) | Comments |
|---|---|---|---|---|
| WP110-5 | 2a | 2.1 | 0.40 | The drifts for these damage states are provided by the researcher. |
| | | 2.3 | 0.20 | |
| | | 2.4a | 0.40 | |
| | 2b | 2.4b | 0.60 | |
| | 4 | 4.5 | 0.80 | |

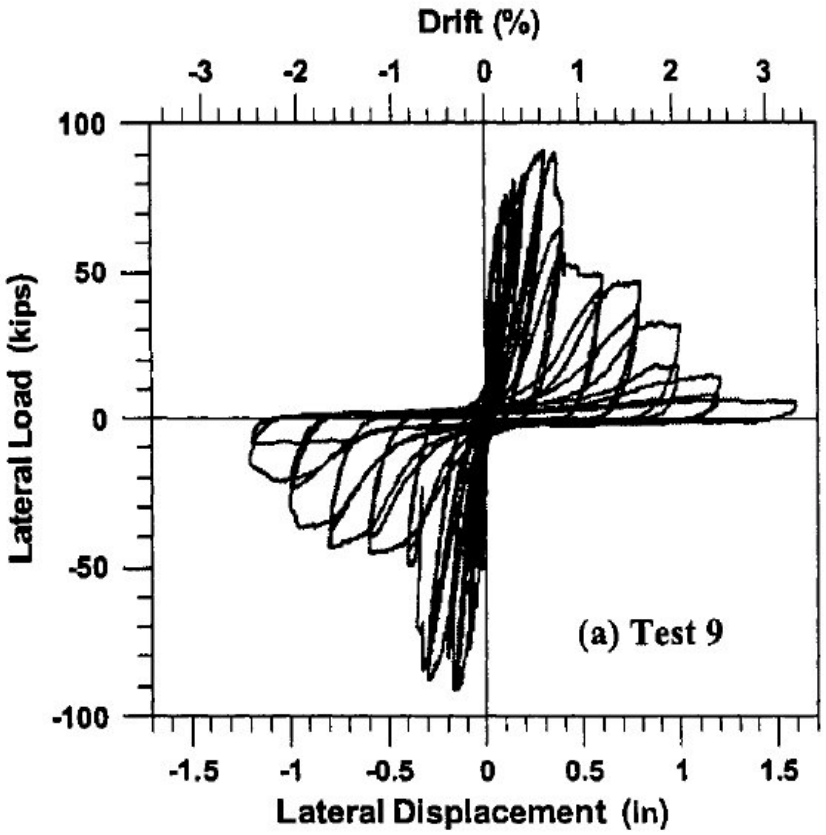


**Figure C-63 Load-displacement relationship for wall WP110-5 [Massone (2006)]**

### C.1.5.3 Wall WP110-6

**Table C-17 Evaluation of damage data for wall WP110-6 tested by Massone**

| Wall ID | MoR | Damage State (DS) | Drift (%) | Comments |
|---|---|---|---|---|
| WP110-6 | 2a | 2.1 | 0.30 | The drifts for these damage states are provided by the researcher. |
| | | 2.3 | 0.30 | |
| | | 2.4a | 0.40 | |
| | 2b | 2.4b | 0.60 | |
| | 4 | 4.5 | 0.80 | |

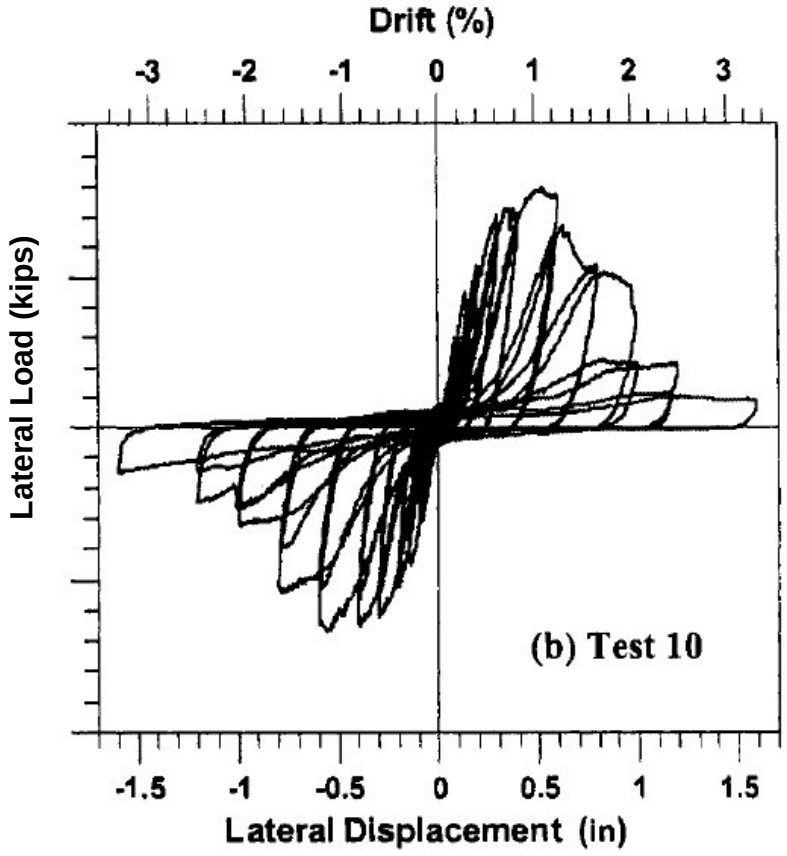


**Figure C-64 Load-displacement relationship for wall WP110-6 [Massone (2006)]**

## C.1.6 Greifenhagen et al. (2005) Walls

### C.1.6.1 Wall M1

**Table C-18 Evaluation of damage data for wall M1 tested by Greifenhagen**

| Wall ID | MoR | Damage State (DS) | Drift (%) | Comments |
|---|---|---|---|---|
| M1 | 1 | 1.2 | 0.06 | The drifts for these damage states are provided by the researcher. The researcher reported that the wall failed by sliding shear and the so supplemental criteria are invoked to obtain a drift associated with DS4.1. |
| | | 1.4 | 0.12 | |
| | 2a | 2.5a | 0.30 | |
| | 2b | 2.5b | 0.30 | |
| | 3 | 3.4 | 0.82 | |
| | 4 | 4.1 | 1.47 | |
| | | 4.4 | 2.70 | |
| | 4* | $SC_1$ | 1.47 | The smaller of the two drifts is obtained from the 1st quadrant of the load-displacement relationship (see Figure C-65, red circle). |
| | | $SC_2$ | 3.47 | The smaller of the two drifts is obtained from the 3rd quadrant of the load-displacement relationship (see Figure C-65). |

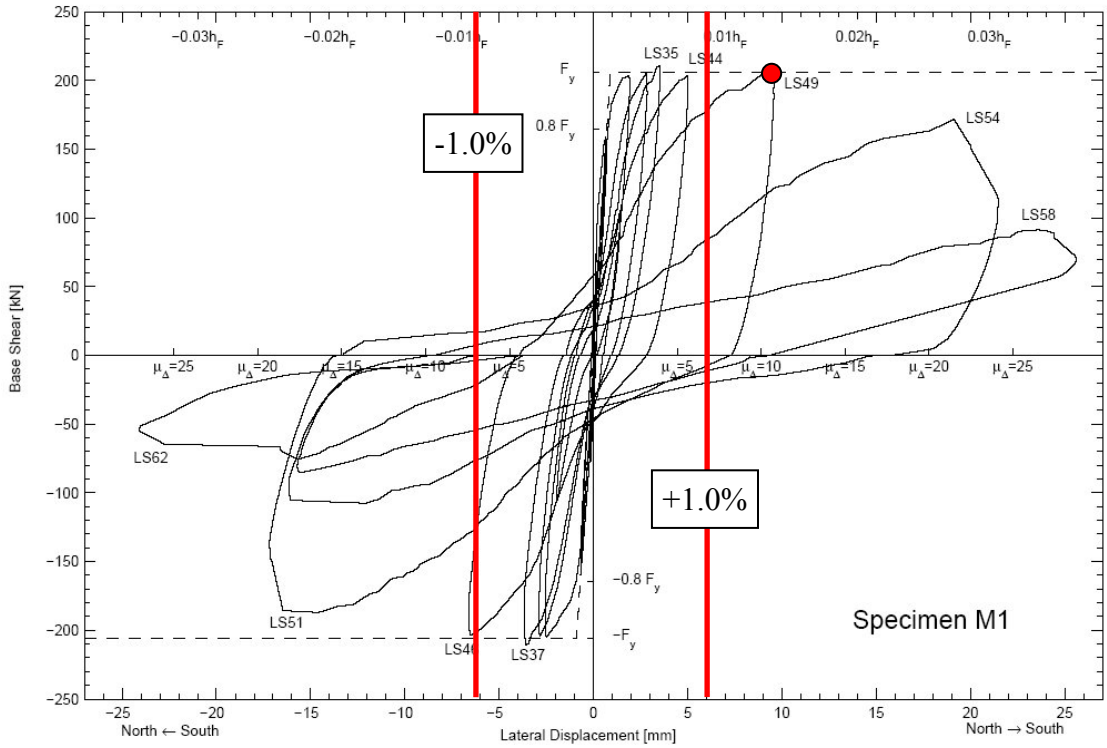


**Figure C-65 Load-displacement relationship for wall M1 [Greifenhagen et al. (2005)]**

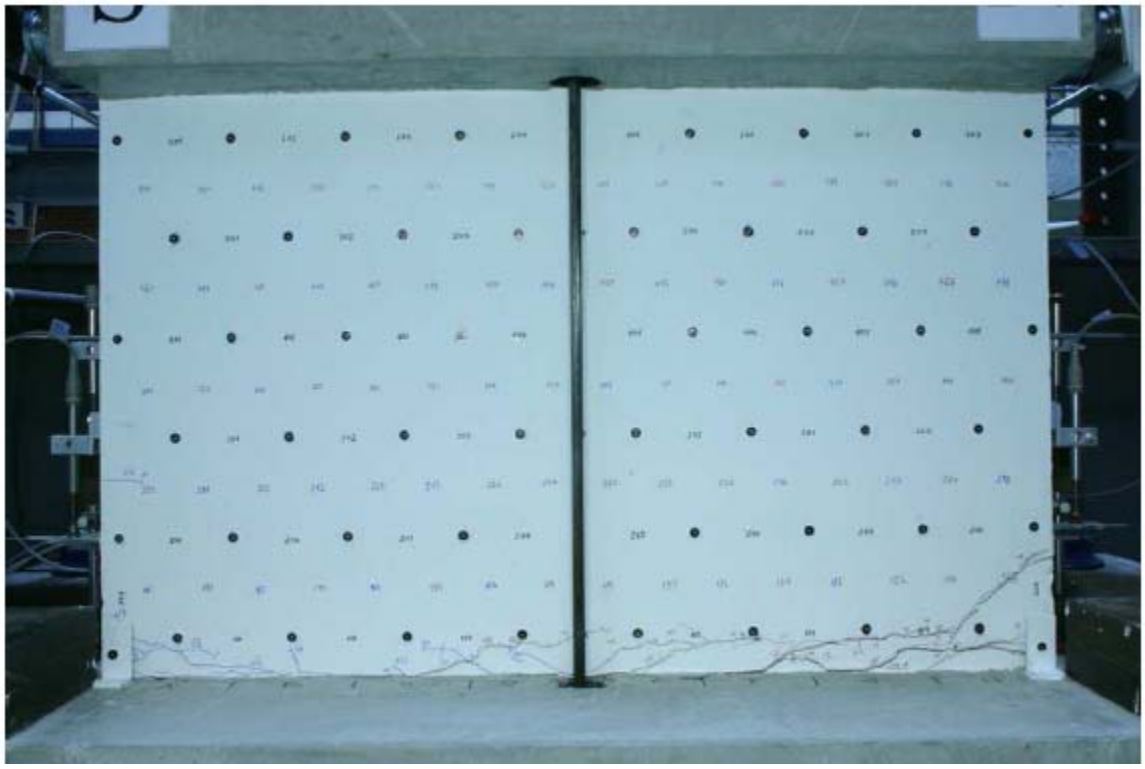

**Figure C-66 Condition of wall M1 at 0.57% drift [Greifenhagen et al. (2005)]**

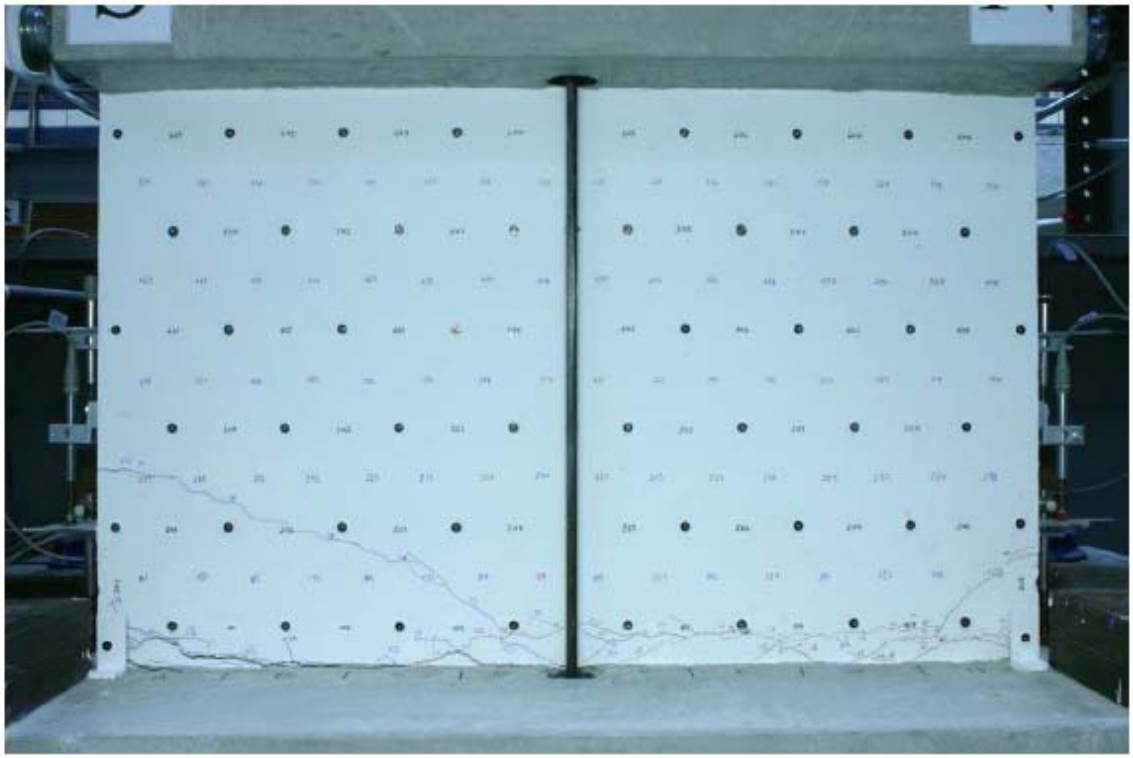

**Figure C-67 Condition of wall M1 at -0.58% drift [Greifenhagen et al. (2005)]**

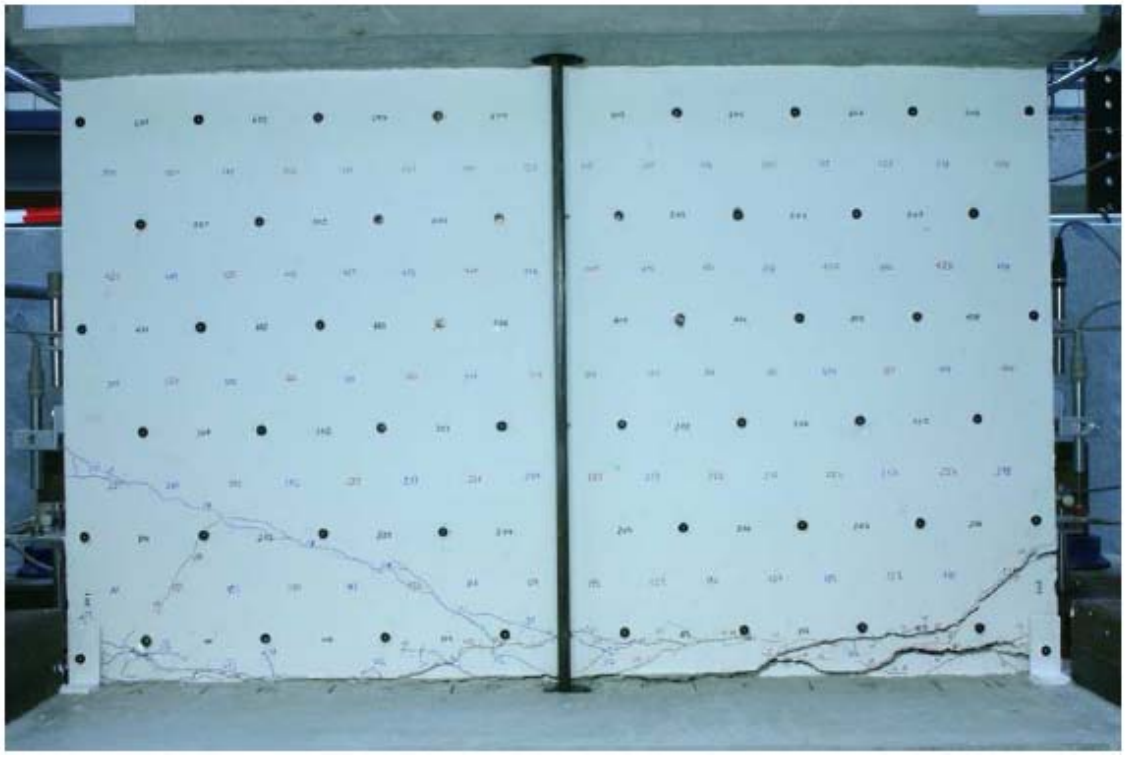

**Figure C-68 Condition of wall M1 at 1.47% drift [Greifenhagen et al. (2005)]**

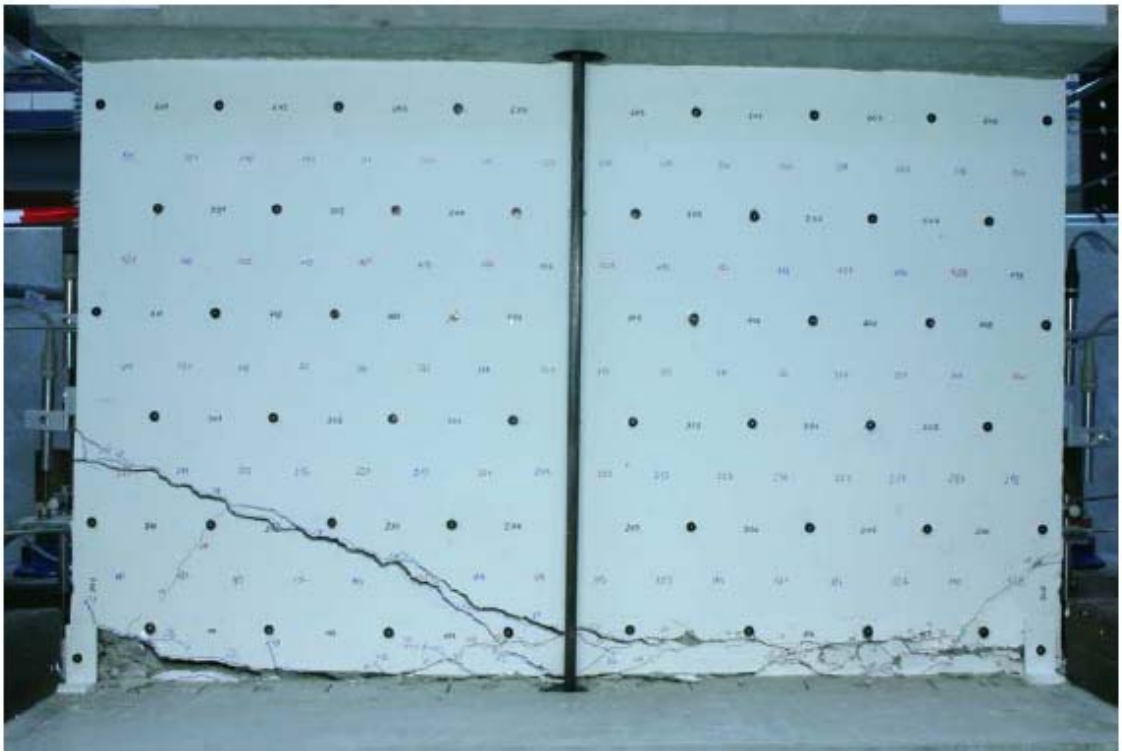

**Figure C-69 Condition of wall M1 at -2.70% drift [Greifenhagen et al. (2005)]**

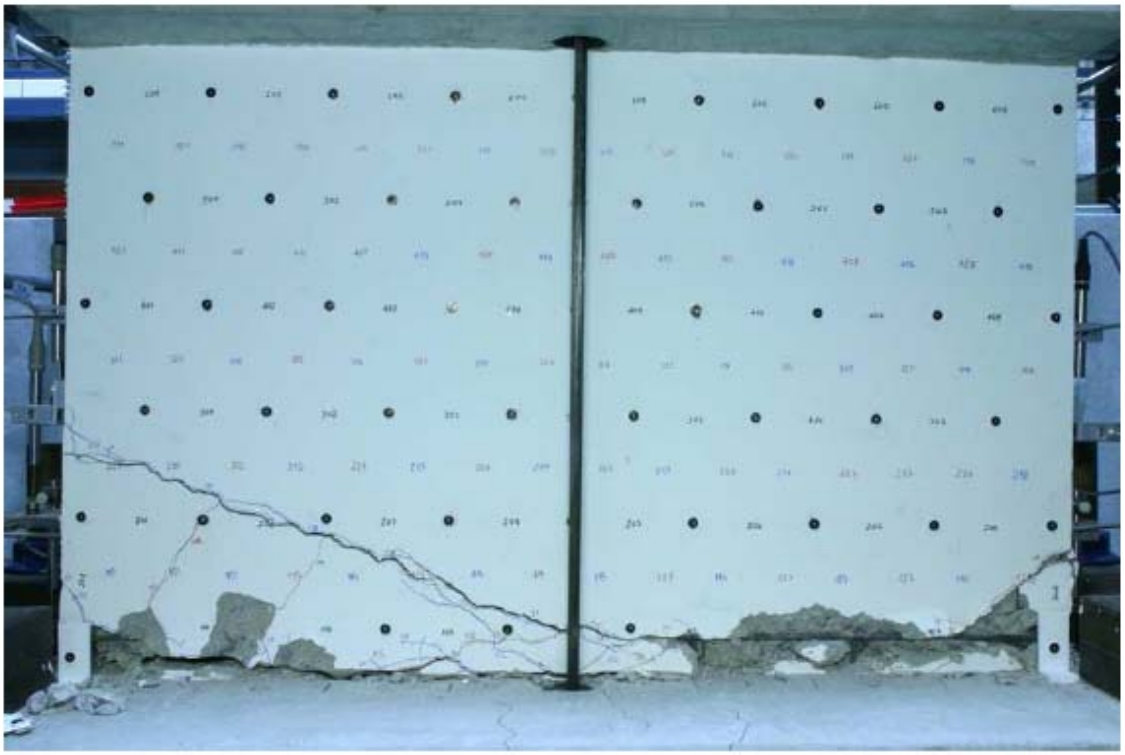

**Figure C-70 Condition of wall M1 at -2.70% drift (2nd cycle) [Greifenhagen et al. (2005)]**

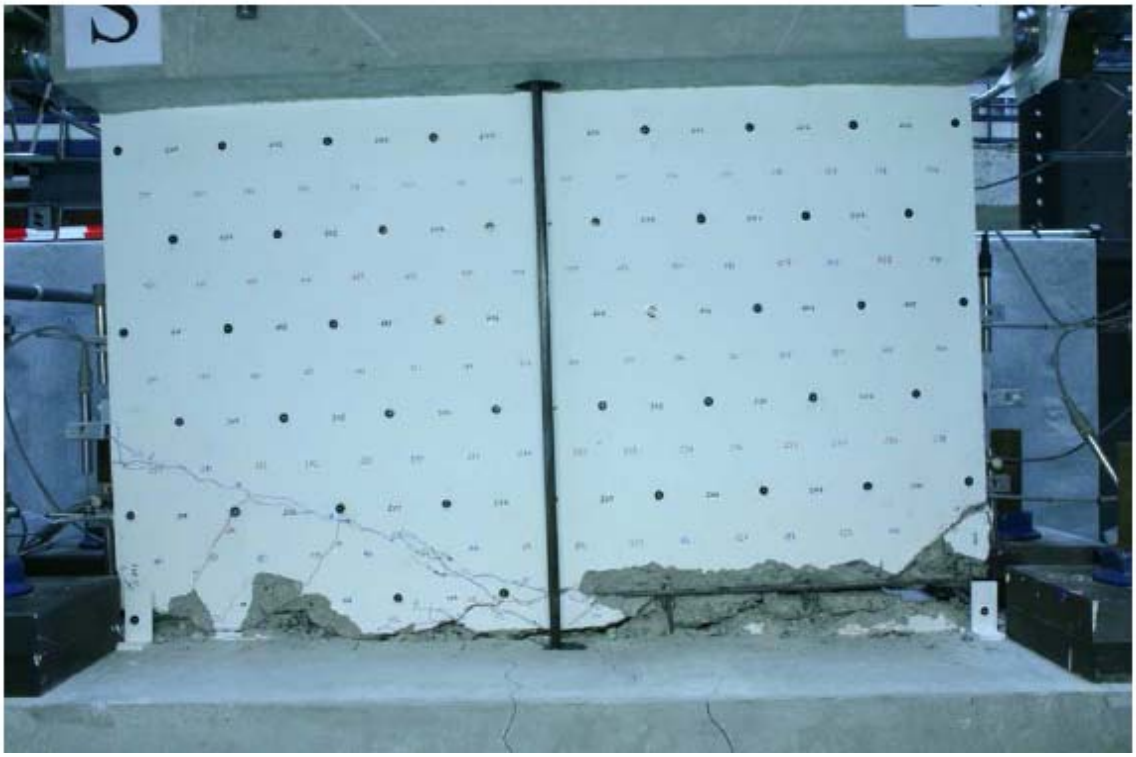

**Figure C-71 Condition of wall M1 at 4.19% drift [Greifenhagen et al. (2005)]**

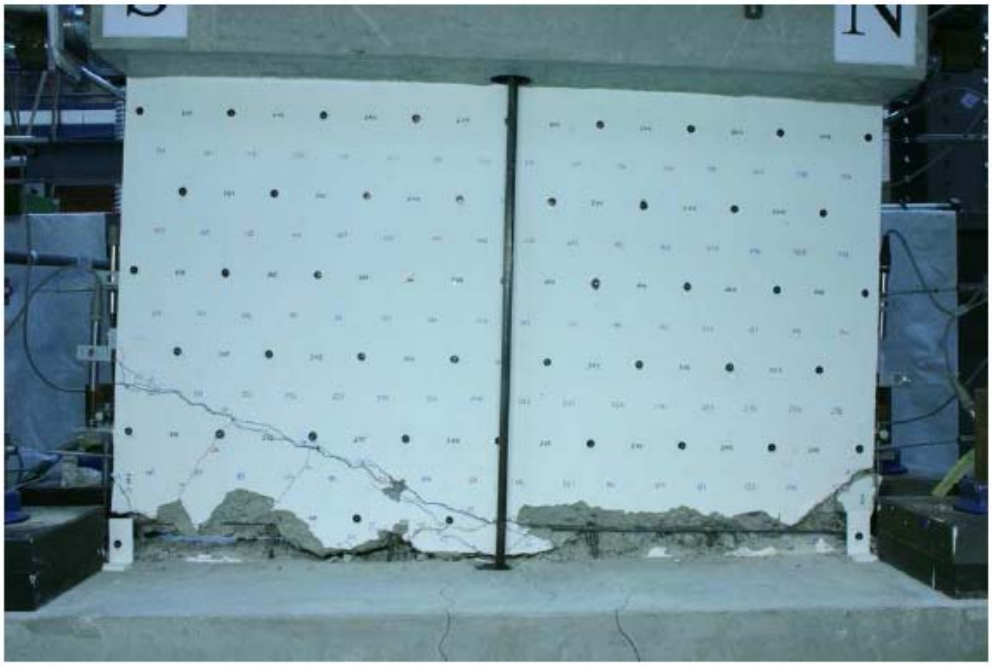

**Figure C-72 Condition of wall M1 at -3.95% drift [Greifenhagen et al. (2005)]**

### C.1.6.2 Wall M2

**Table C-19 Evaluation of damage data for wall M2 tested by Greifenhagen**

| Wall ID | MoR | Damage State (DS) | Drift (%) | Comments |
|---|---|---|---|---|
| M2 | 2a | 2.5a | 0.07 | The drifts for these damage states are provided by the researcher. Drifts for DS3.1 and 3.3 are based on the researcher's description of damage at the corresponding drifts: "…the concrete cover spalled on the front face in zone H due to buckling of vertical rebars." [Greifenhagen et al. (2005), page 42]. |
| | 2b | 2.5b | 0.27 | |
| | 3 | 3.1 | 0.82 | |
| | | 3.3 | 0.82 | |
| | | 3.4 | 0.58 | |
| | 4 | 4.1 | 1.37 | The researcher reported that the wall failed by sliding shear and so the supplemental criteria are invoked to obtain a drift associated with this damage state. |
| | 4* | $SC_1$ | 1.37 | The smaller of the two drifts is obtained from the 1st quadrant of the load-displacement relationship (see Figure C-73, red circle). The corresponding residual drift is slightly less than 1.0%. |
| | | $SC_2$ | N/A | The post-peak resistance computed using the first cycle backbone curve did not drop to $0.5V_{peak}$ (see Figure C-73). |

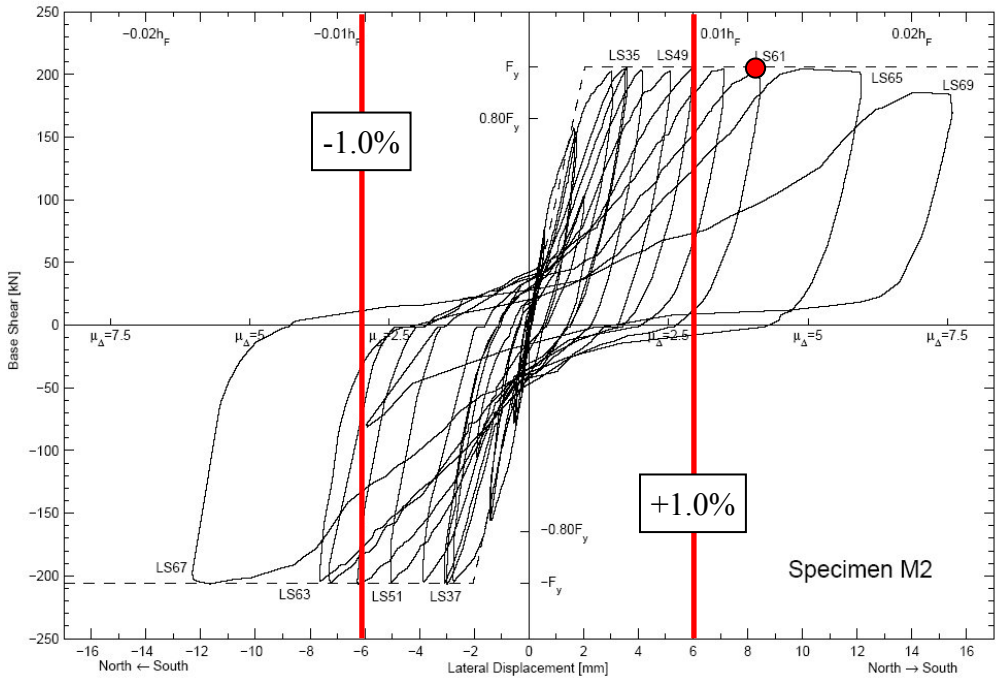


**Figure C-73 Load-displacement relationship for wall M2 [Greifenhagen et al. (2005)]**

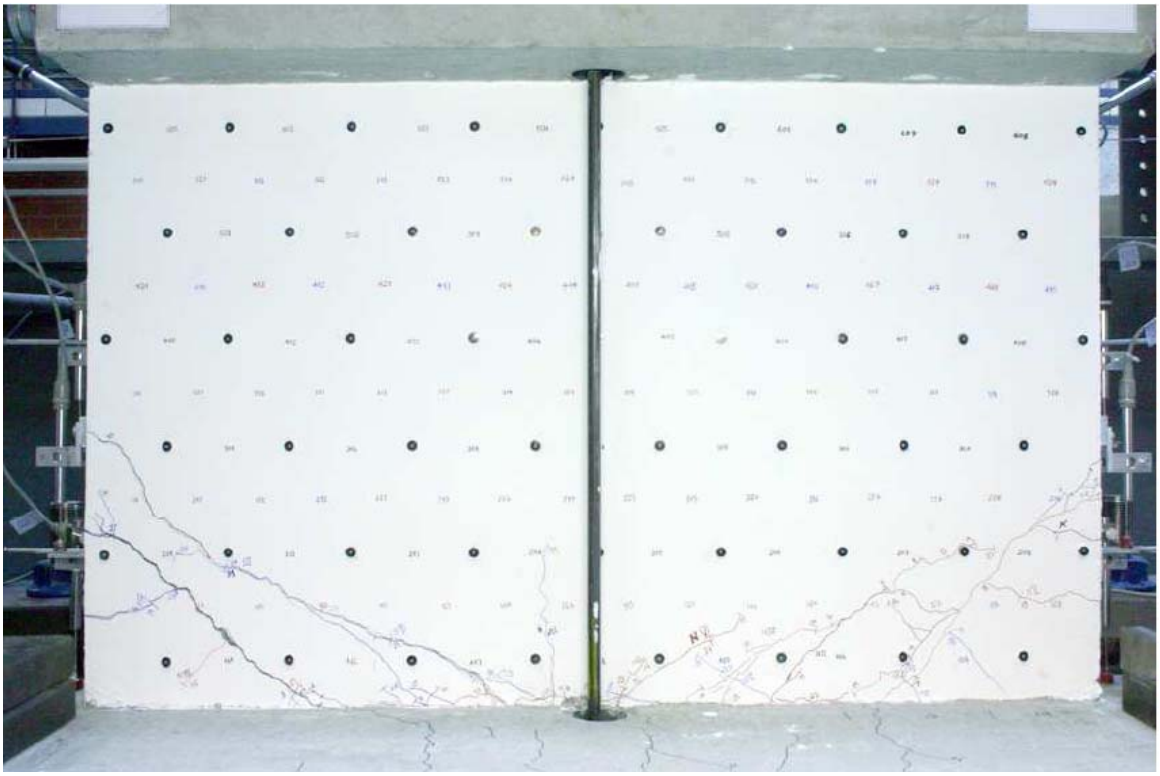

**Figure C-74 Condition of wall M2 at -0.49% drift [Greifenhagen et al. (2005)]**

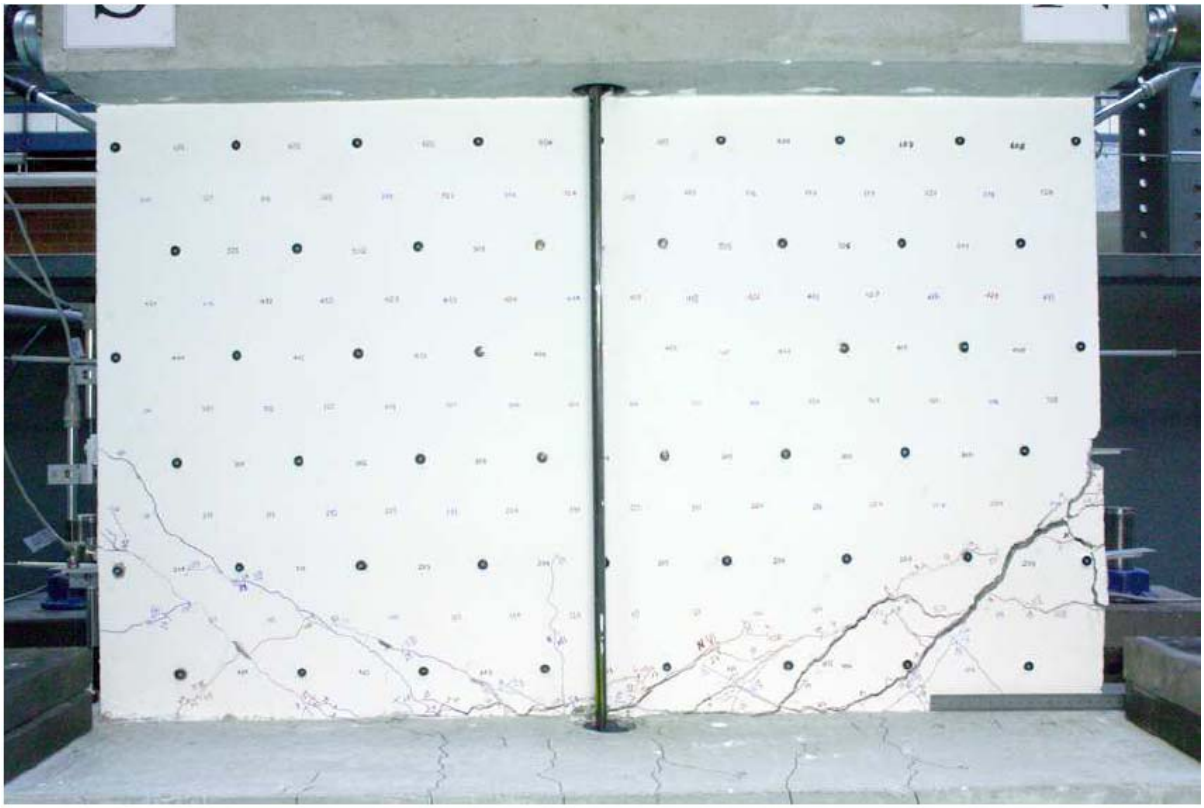

**Figure C-75 Condition of wall M2 at 0.97% drift [Greifenhagen et al. (2005)]**

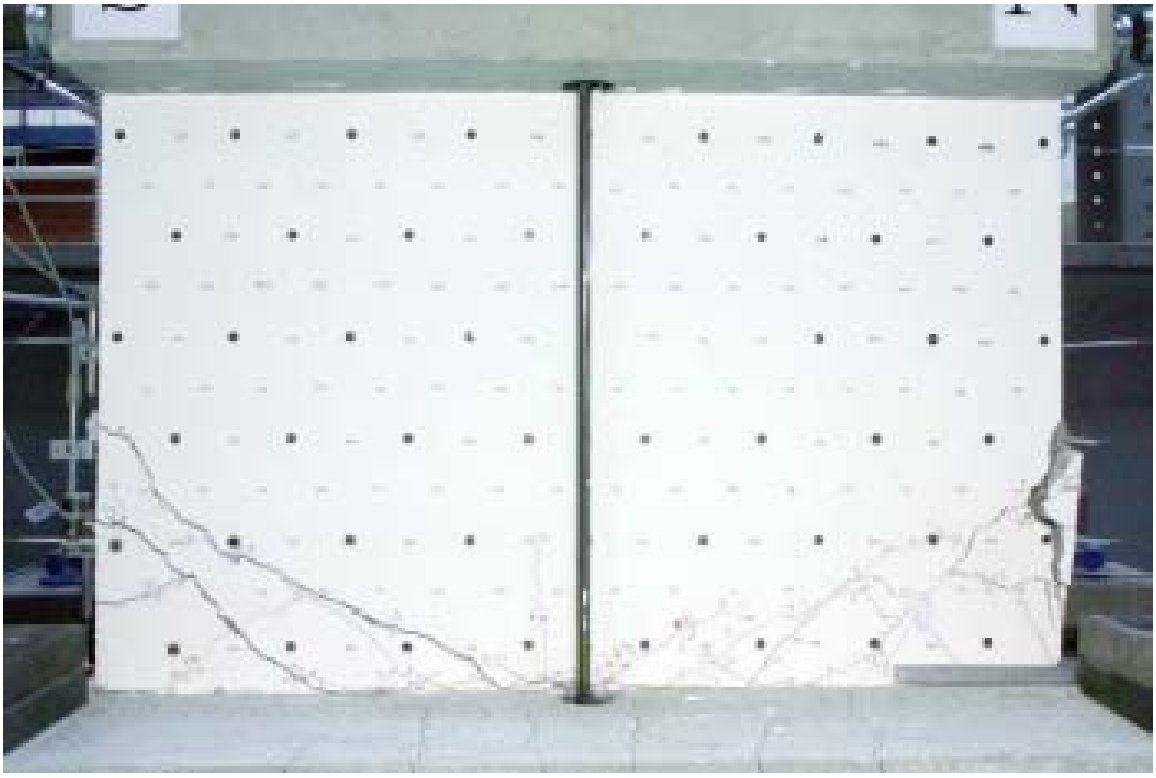

**Figure C-76 Condition of wall M2 at -1.02% drift [Greifenhagen et al. (2005)]**

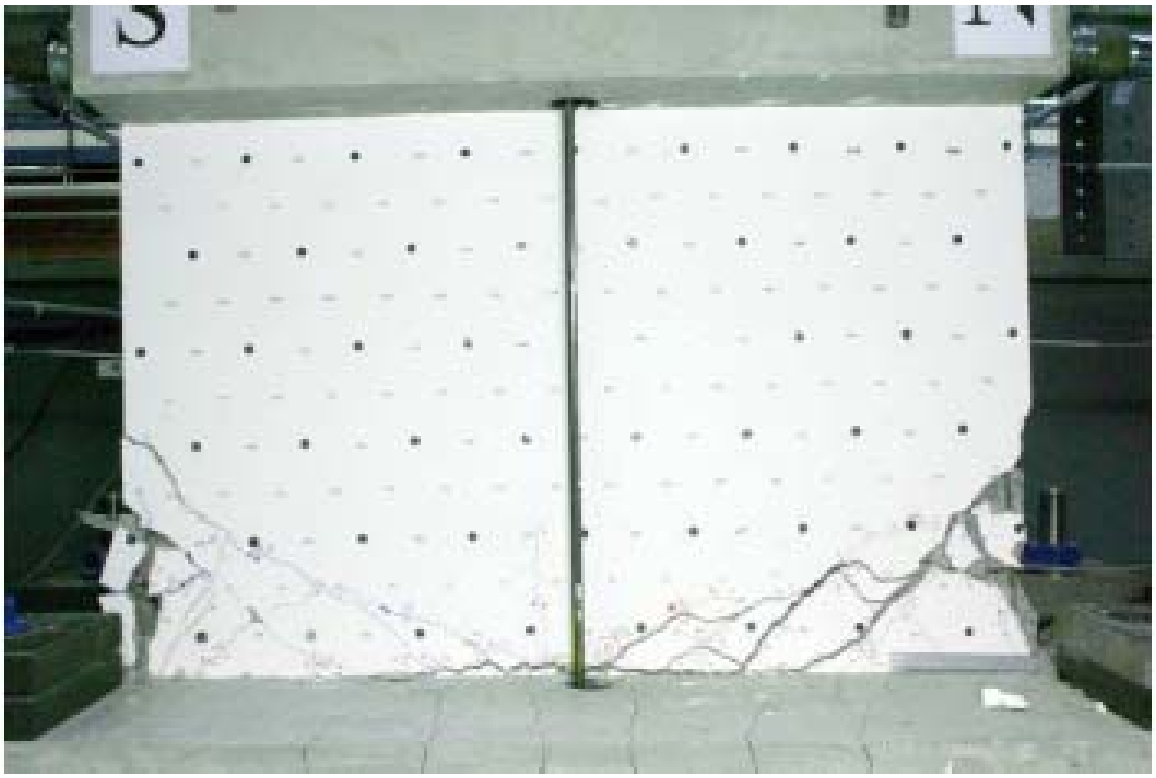

**Figure C-77 Condition of wall M2 at 1.98% drift [Greifenhagen et al. (2005)]**

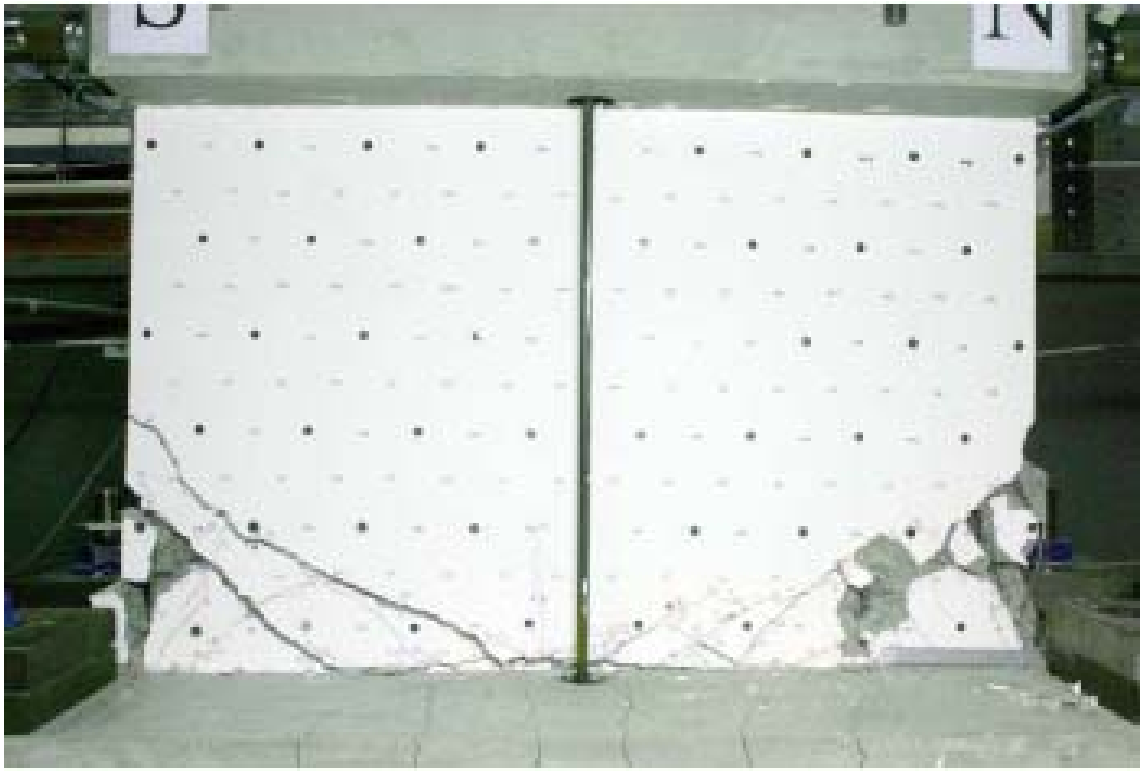

**Figure C-78 Condition of wall M2 at -2.00% drift [Greifenhagen et al. (2005)]**

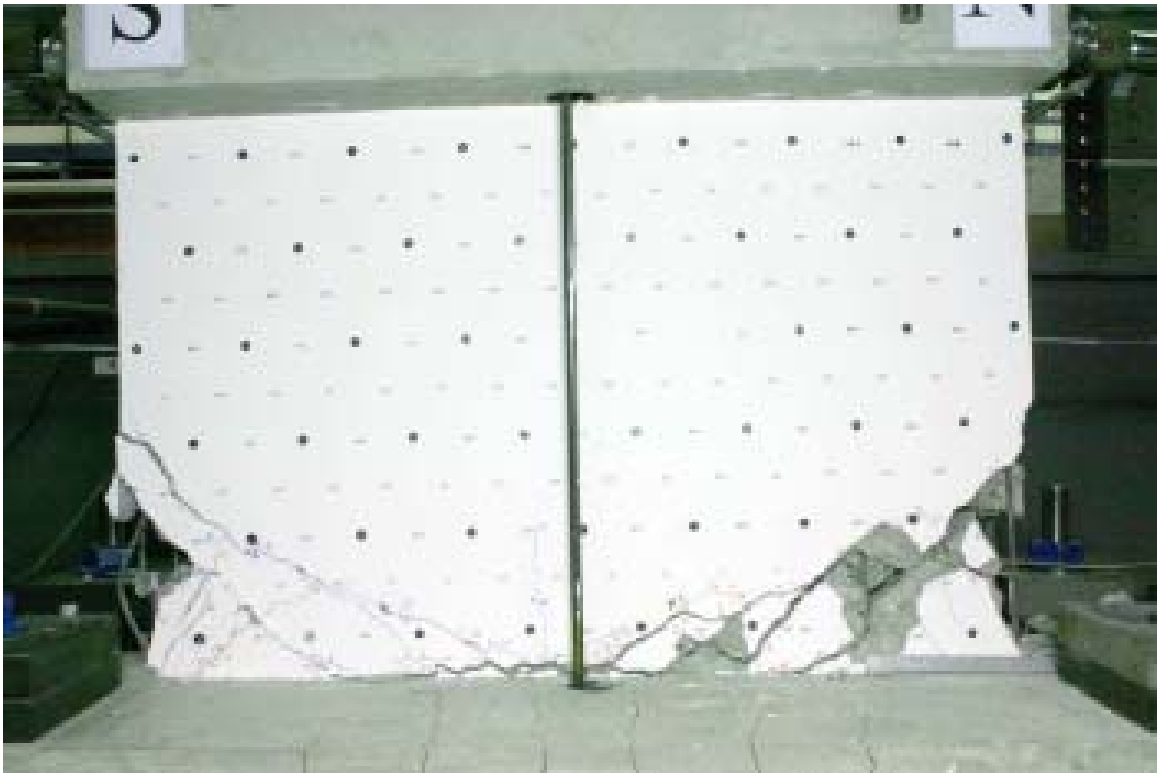

**Figure C-79 Condition of wall M2 at 2.52% drift [Greifenhagen et al. (2005)]**

### C.1.6.3 Wall M3

**Table C-20 Evaluation of damage data for wall M3 tested by Greifenhagen**

| Wall ID | MoR | Damage State (DS) | Drift (%) | Comments |
|---|---|---|---|---|
| M3 | 1 | 1.2 | 0.05 | The drifts for these damage states are provided by the researcher. Drifts for DS3.1 and 3.3 are based on the researcher's description of damage at the corresponding drifts: "…the concrete cover disintegrated due to the buckling of the outermost rebars in zone H." [Greifenhagen et al. (2005), page 53]. The damaged region associated with DS3.4 is identified using a dashed box in Figure C-83. The damaged regions associated with DS3.1 and DS3.3 are identified using dashed boxes in Figure C-84. |
| | | 1.4 | 0.20 | |
| | 2a | 2.5a | 0.33 | |
| | 2b | 2.5b | 0.52 | |
| | 3 | 3.1 | 1.11 | |
| | | 3.3 | 1.11 | |
| | | 3.4 | 0.78 | |
| | 4 | 4.2 | 1.63 | The researcher associated wall failure with diagonal crack formation at this drift level [Greifenhagen et al. (2005), page 53]. |

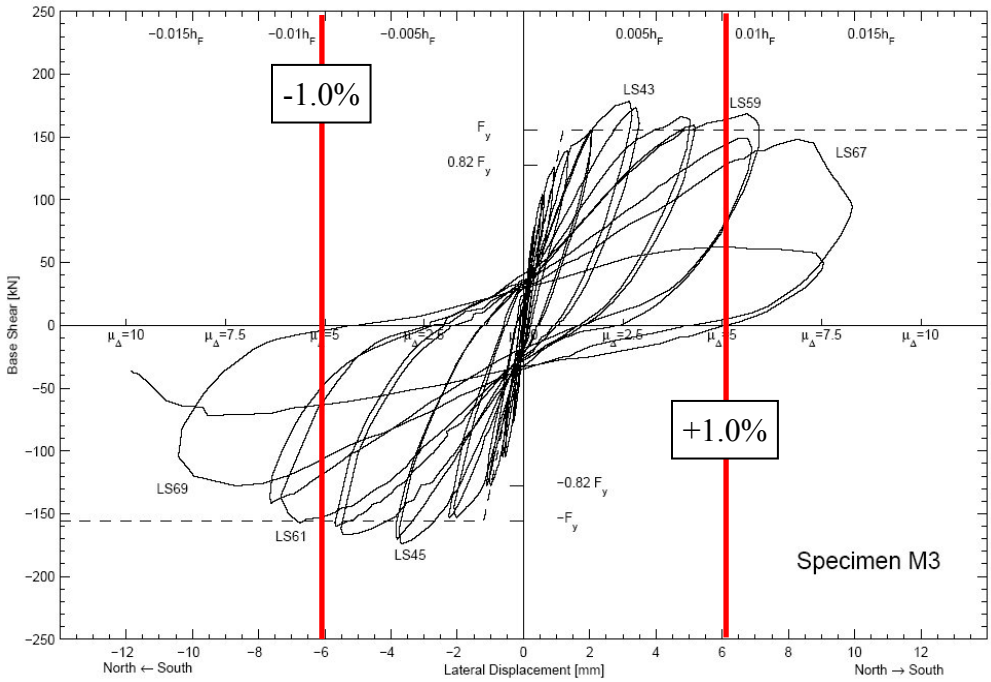


**Figure C-80 Load-displacement relationship for wall M3 [Greifenhagen et al. (2005)]**

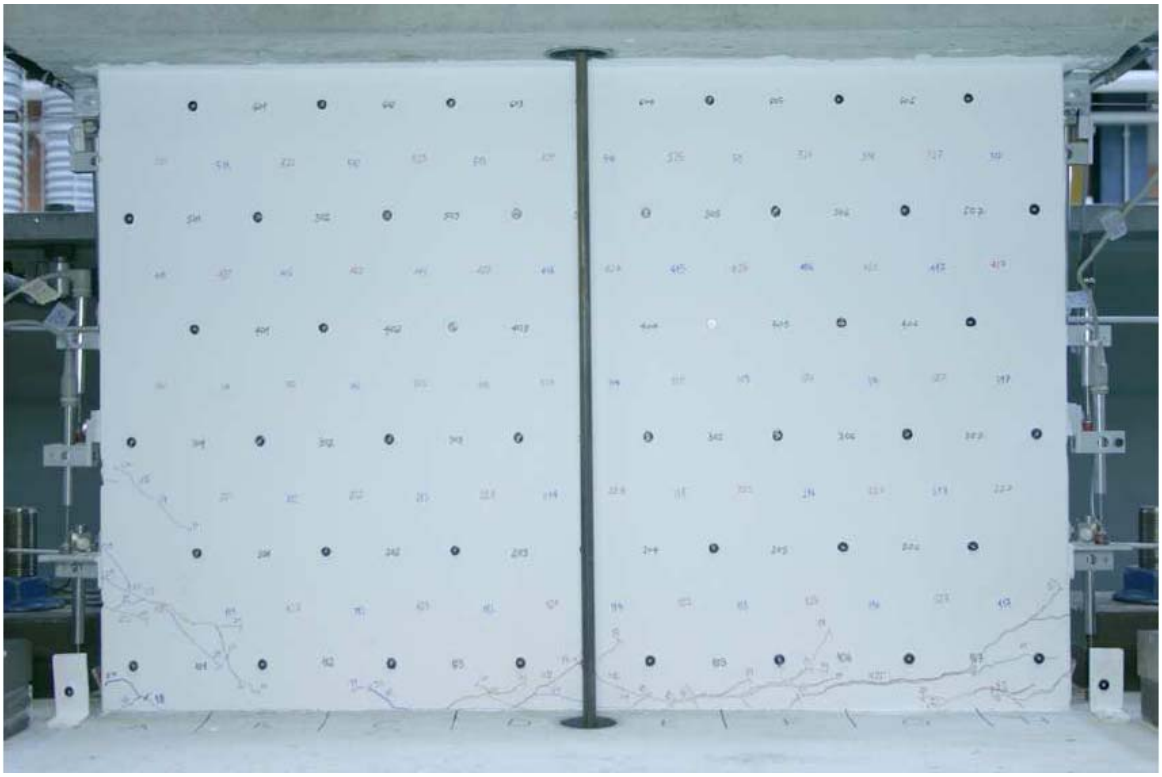

**Figure C-81 Condition of wall M3 at 0.33% drift [Greifenhagen et al. (2005)]**

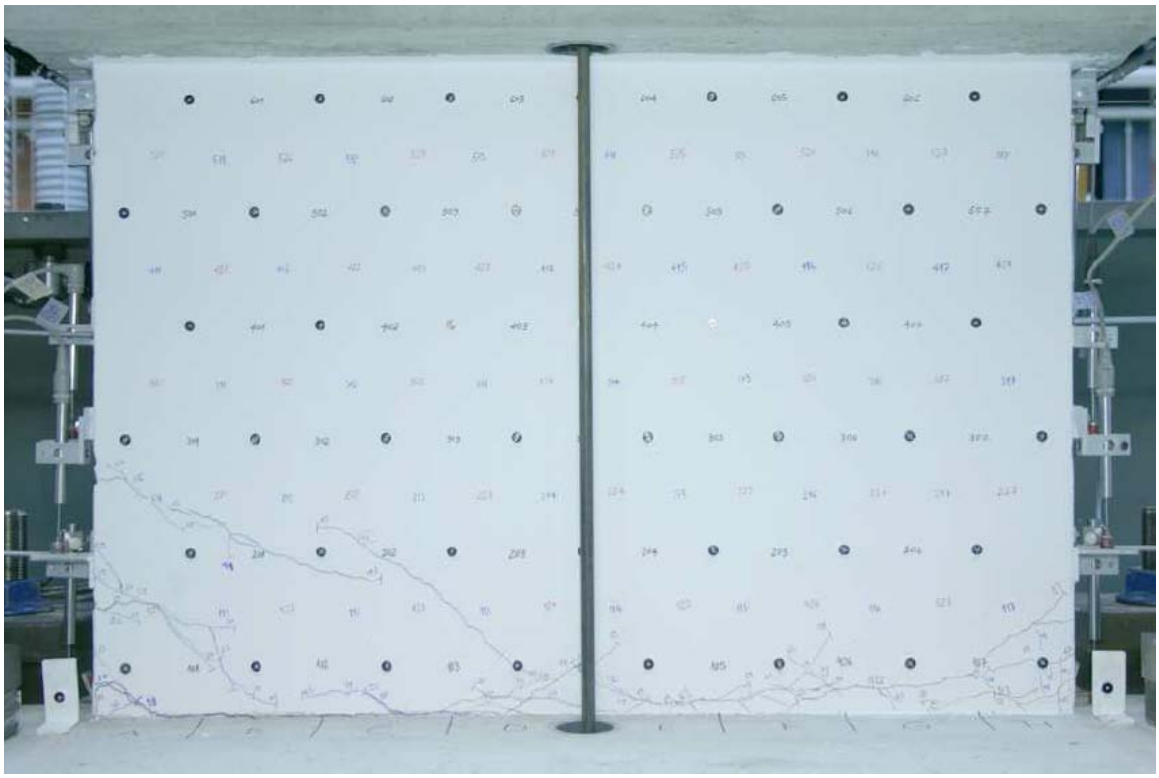

**Figure C-82 Condition of wall M3 at -0.61% drift (2nd cycle) [Greifenhagen et al. (2005)]**

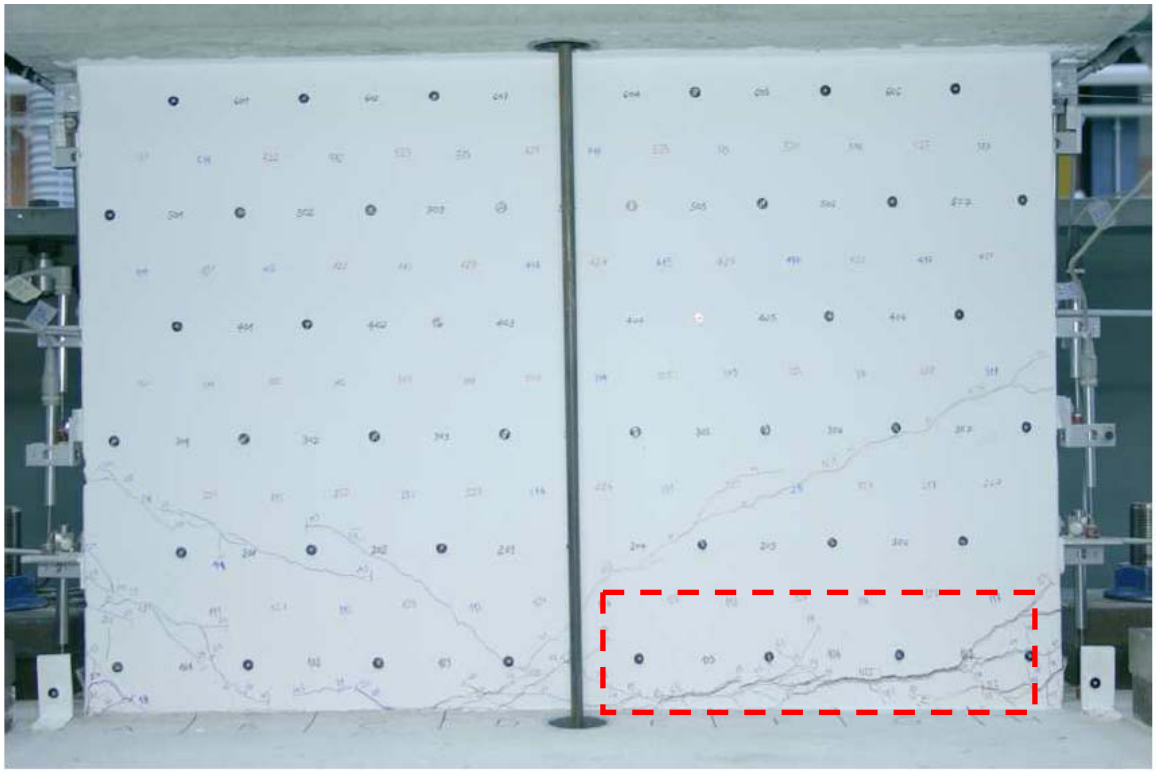

**Figure C-83 Condition of wall M3 at 0.78% drift [Greifenhagen et al. (2005)]**

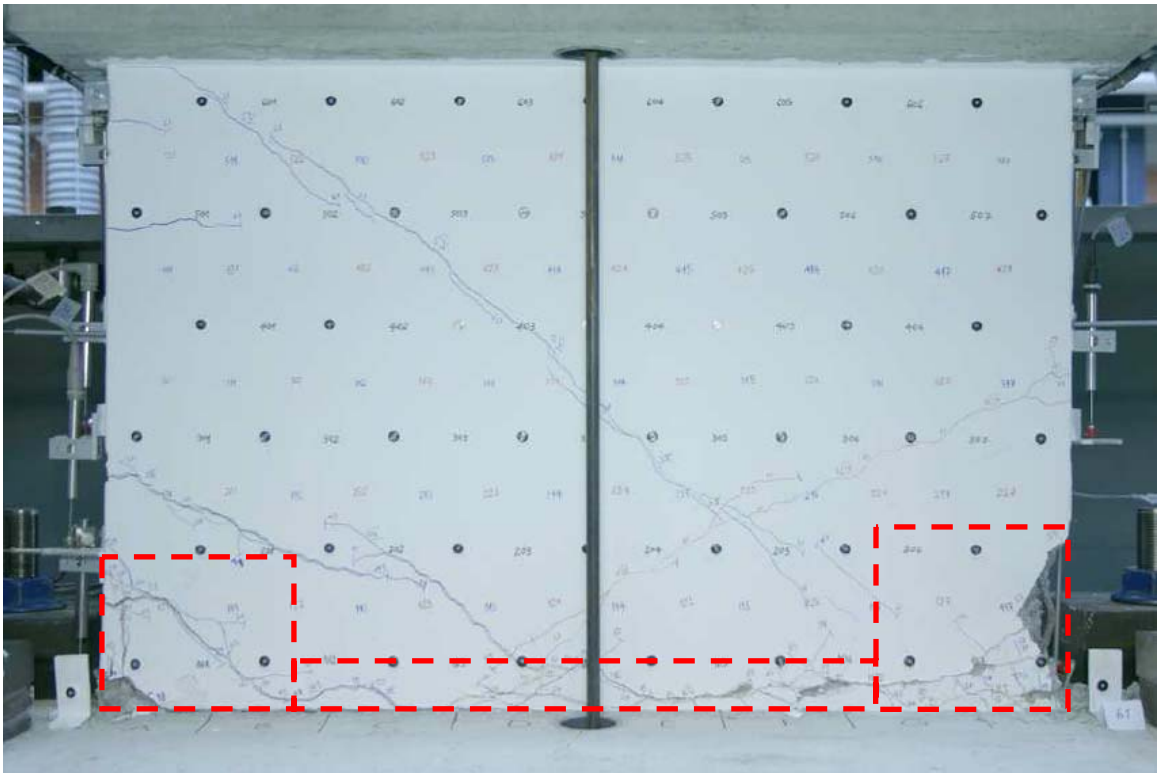

**Figure C-84 Condition of wall M3 at -1.11% drift [Greifenhagen et al. (2005)]**

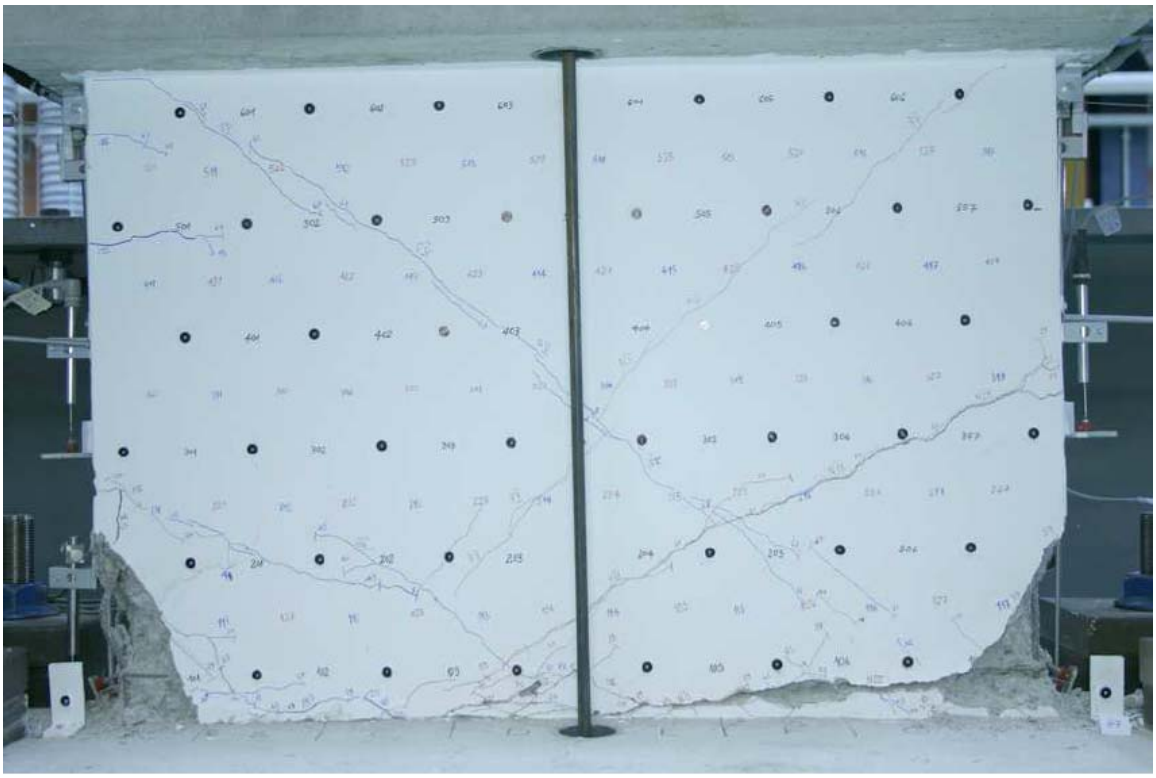

**Figure C-85 Condition of wall M3 at 1.63% drift [Greifenhagen et al. (2005)]**

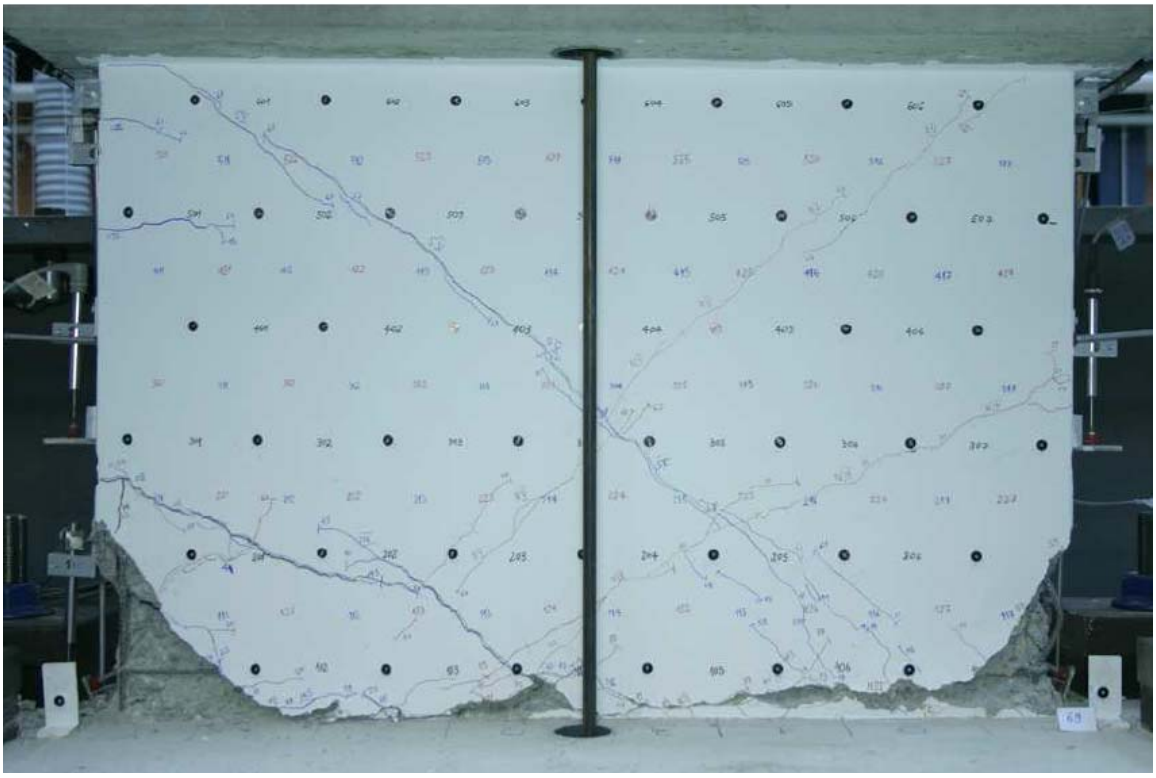

**Figure C-86 Condition of wall M3 at -1.94% drift [Greifenhagen et al. (2005)]**

### C.1.6.4 Wall M4

**Table C-21 Evaluation of damage data for wall M4 tested by Greifenhagen**

| Wall ID | MoR | Damage State (DS) | Drift (%) | Comments |
|---|---|---|---|---|
| M4 | 1 | 1.2 | 0.01 | The drifts for these damage states are provided by the researcher. The drift associated with DS3.1 is based on the researcher's description of damage at this drift: "Small inclined and vertical cracks of length about 20 to 30 mm formed in bottom part of zone H when it was subjected to compression in LS 57. Furthermore, the cover concrete started to spall in this part of the specimen." [Greifenhagen et al. (2005), page 63]. |
| | | 1.4 | 0.13 | |
| | 2a | 2.5a | 0.24 | |
| | 2b | 2.5b | 0.34 | |
| | 3 | 3.1 | 0.58 | |
| | | 3.3 | 0.83 | |
| | | 3.4 | 0.79 | |
| | 4 | 4.1 | 1.48 | The researcher reported that the wall failed by sliding shear and so the supplemental criteria are invoked to obtain a drift associated with this damage state. |
| | 4* | $SC_1$ | 1.48 | The smaller of the two drifts is obtained from the 1st quadrant of the load-drift relationship (see Figure C-87, red circle). |
| | | $SC_2$ | 2.03 | The data point is obtained from the 3rd quadrant of the load-displacement relationship (see Figure C-87). A data point cannot be established in the 1st quadrant. |

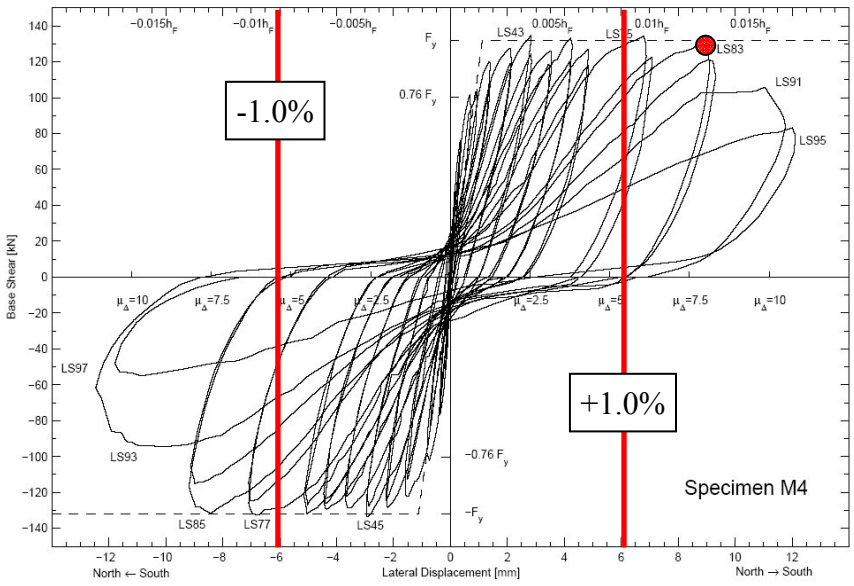


**Figure C-87 The load-displacement relationship for wall M4 [Greifenhagen et al. (2005)]**

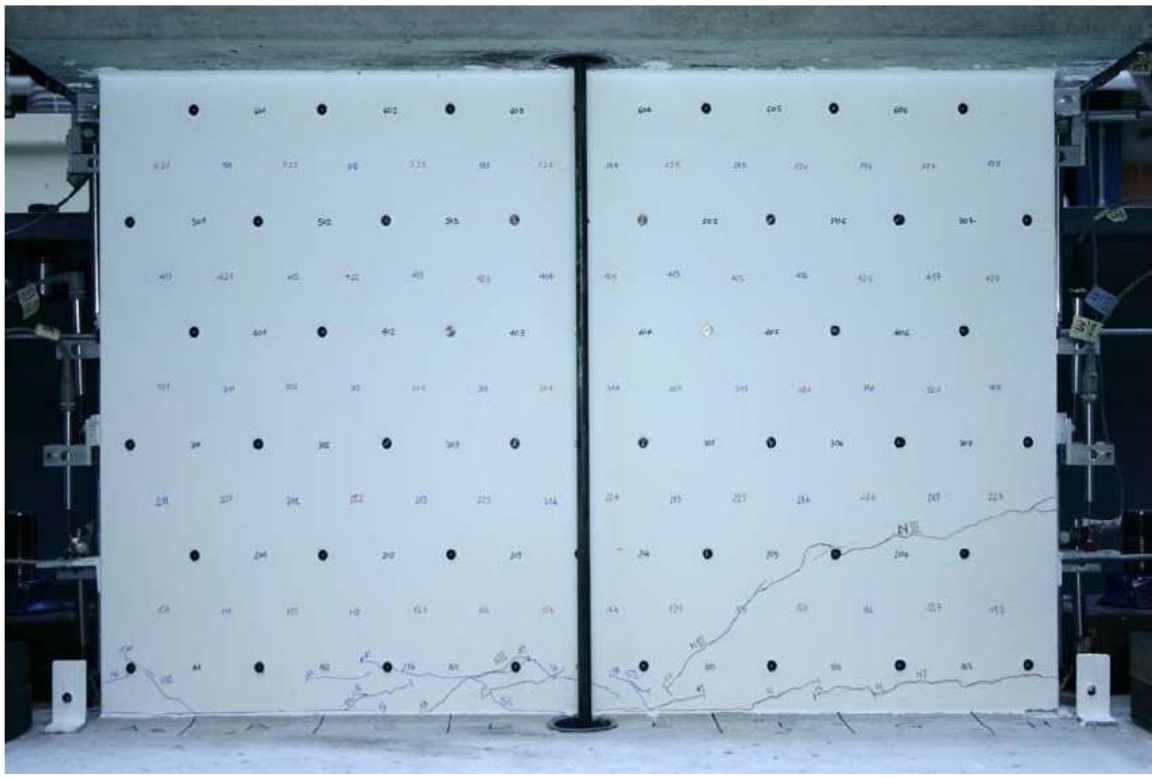

**Figure C-88 Condition of wall M4 at 0.20% drift [Greifenhagen et al. (2005)]**

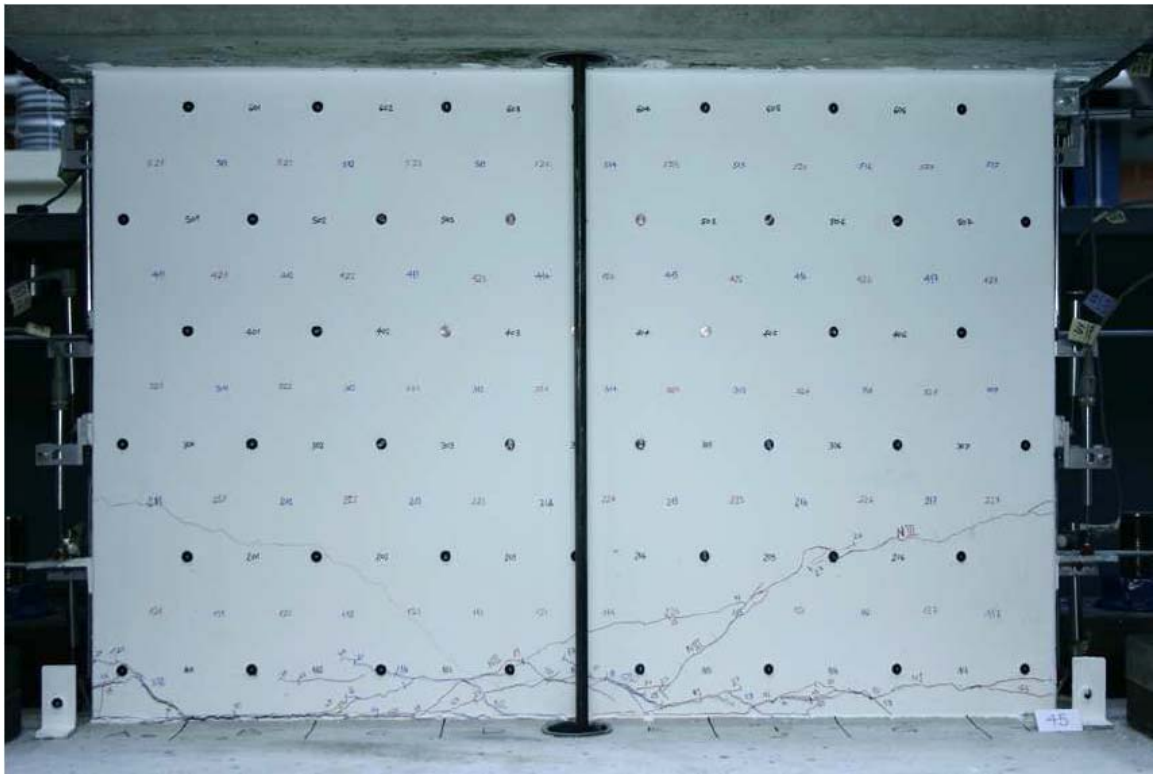

**Figure C-89 Condition of wall M4 at -0.48% drift [Greifenhagen et al. (2005)]**

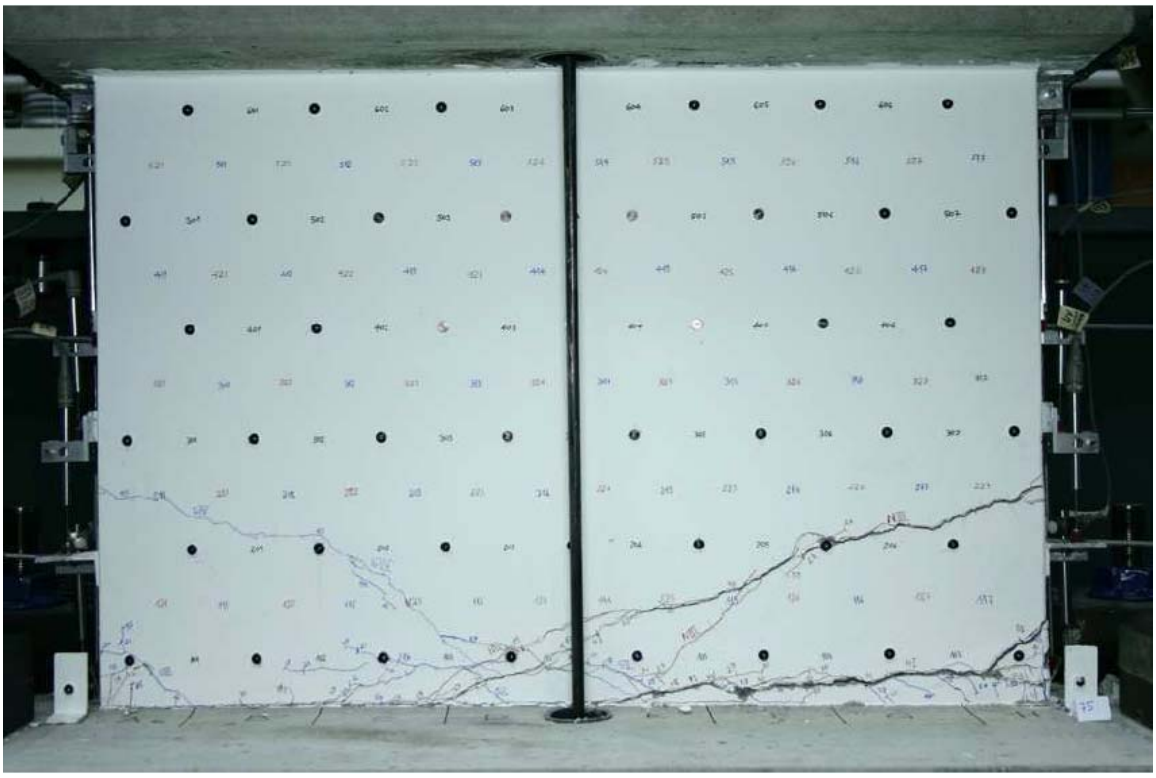

**Figure C-90 Condition of wall M4 at 1.12% drift [Greifenhagen et al. (2005)]**

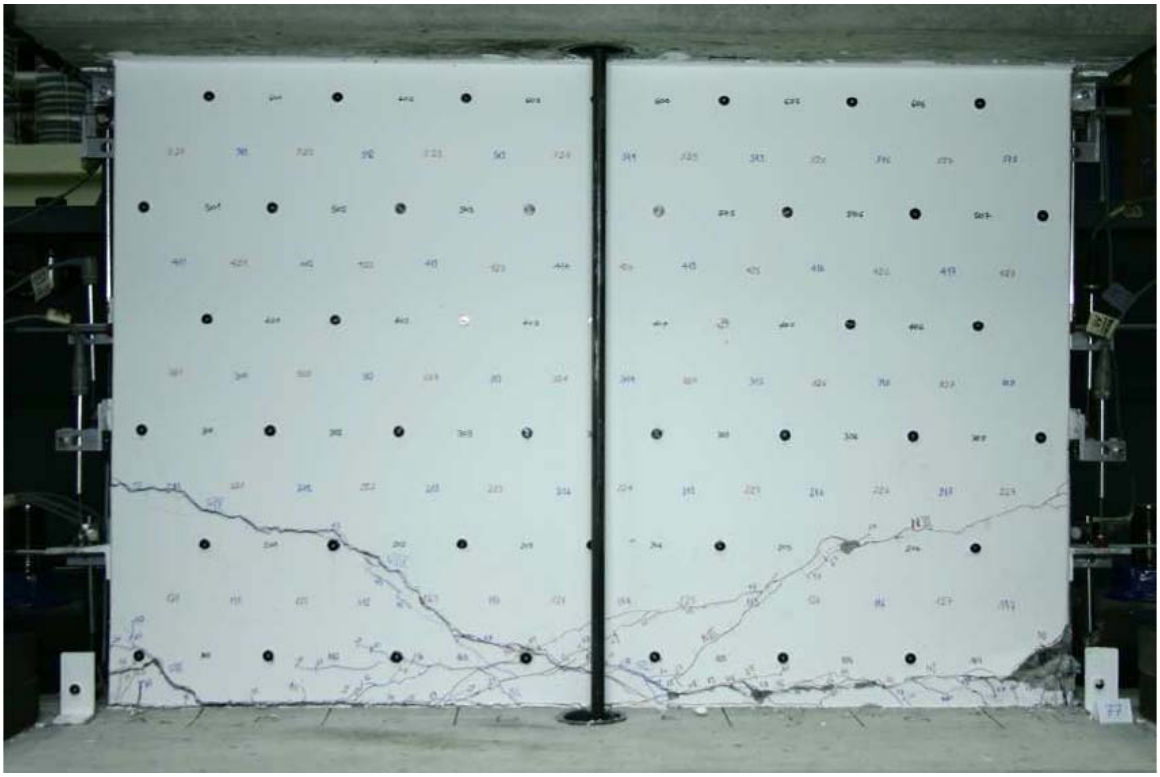

**Figure C-91 Condition of wall M4 at -1.11% drift [Greifenhagen et al. (2005)]**

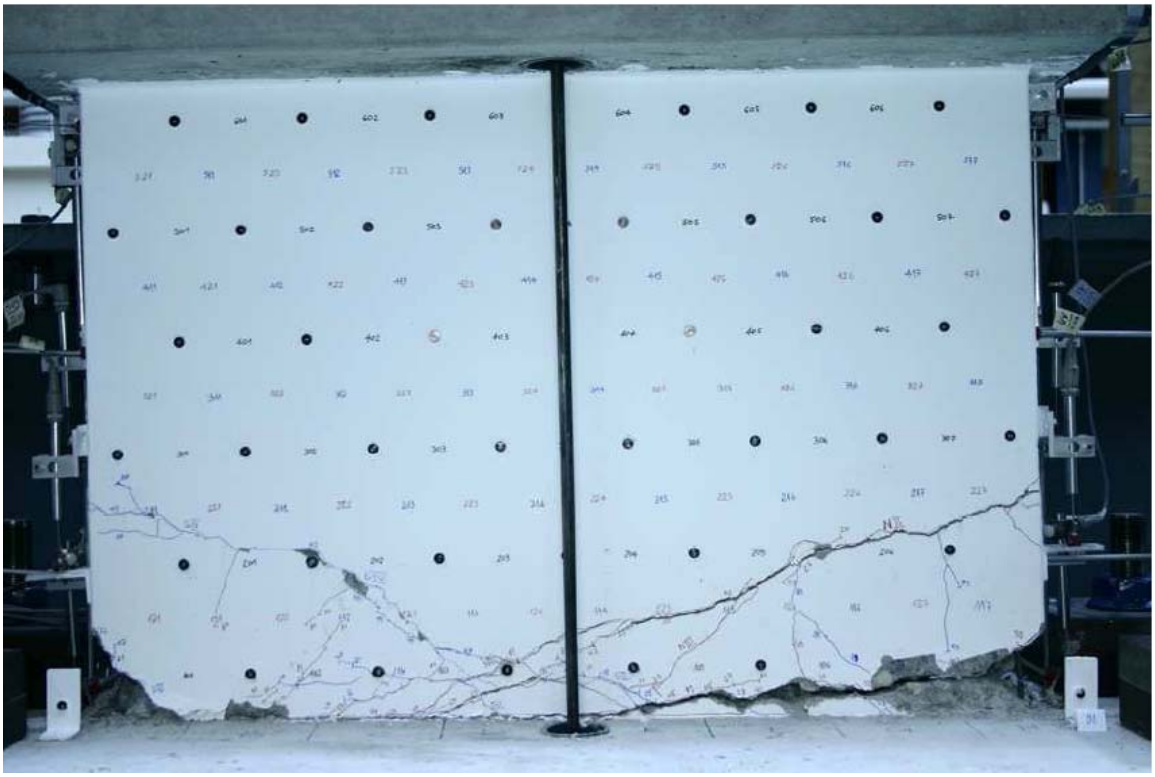

**Figure C-92 Condition of wall M4 at 1.81% drift [Greifenhagen et al. (2005)]**

**Figure C-93 Condition of wall M4 at -2.05% drift [Greifenhagen et al. (2005)]**

**Figure C-94 Condition of wall M4 at 1.97% drift [Greifenhagen et al. (2005)]**

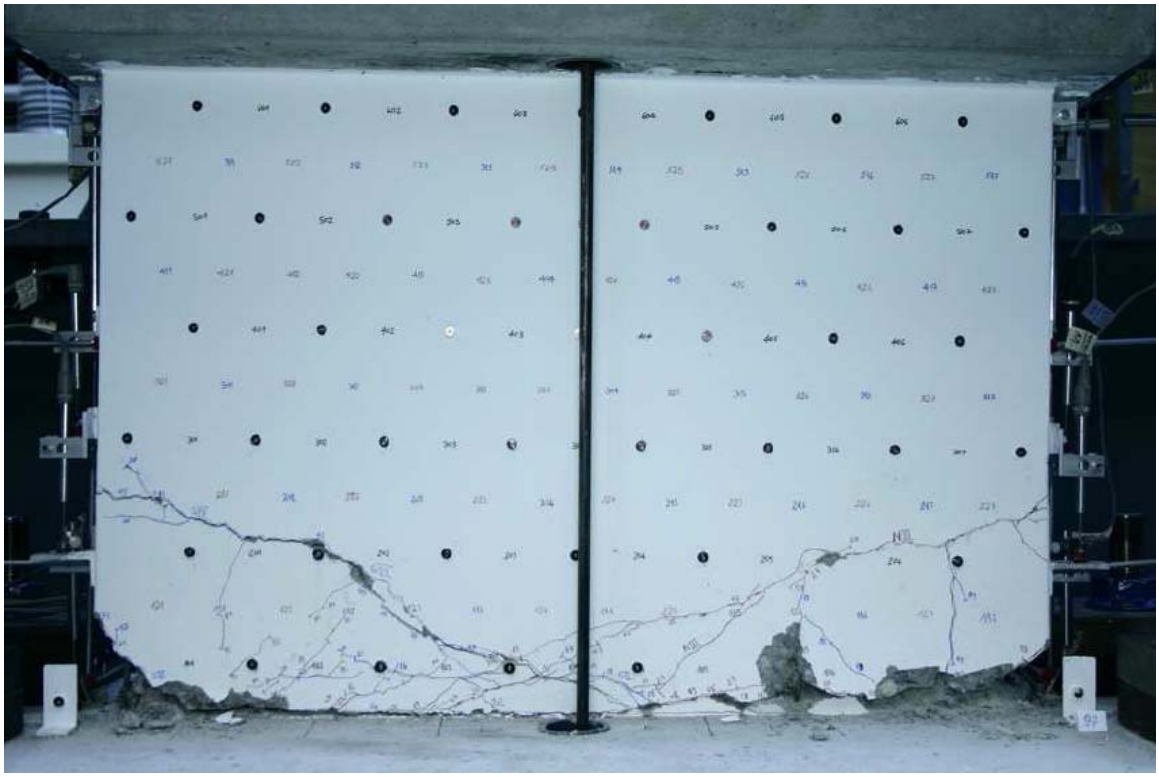

**Figure C-95 Condition of wall M4 at -2.05% drift (2nd cycle) [Greifenhagen et al. (2005)]**

## C.1.7 Lopes and Elnashai (1991) Walls

### C.1.7.1 Wall SW11

**Table C-22 Evaluation of damage data for wall SW11 tested by Lopes**

| Wall ID | MoR | Damage State (DS) | Drift (%) | Comments |
|---|---|---|---|---|
| SW11 | 1 | 1.3 | 0.12 | The drifts for these damage states are provided by the researcher. |
| | | 1.4 | 0.38 | |
| | 2a | 2.4a | 0.79 | |
| | 2b | 2.4b | 0.95 | |
| | 4 | 4.5 | 1.33 | The reported width of the major diagonal crack was 1.50 mm and 2.90 mm at 1.05% and 1.31% drift, respectively. No other crack data were reported at drifts greater than 1.31%. Therefore, a drift associated with DS4.5 (shear crack width = 3.0 mm) is calculated using extrapolation. |

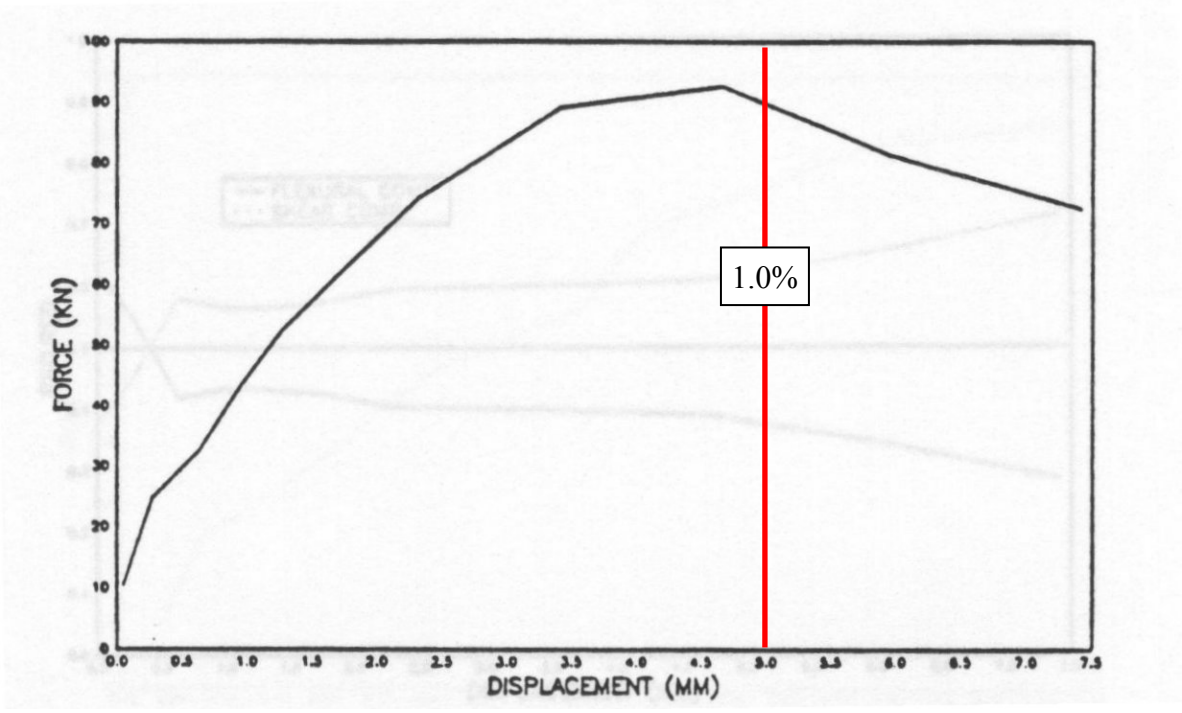


**Figure C-96 Load-displacement relationship for wall SW11 [Lopes and Elnashai (1991)]**

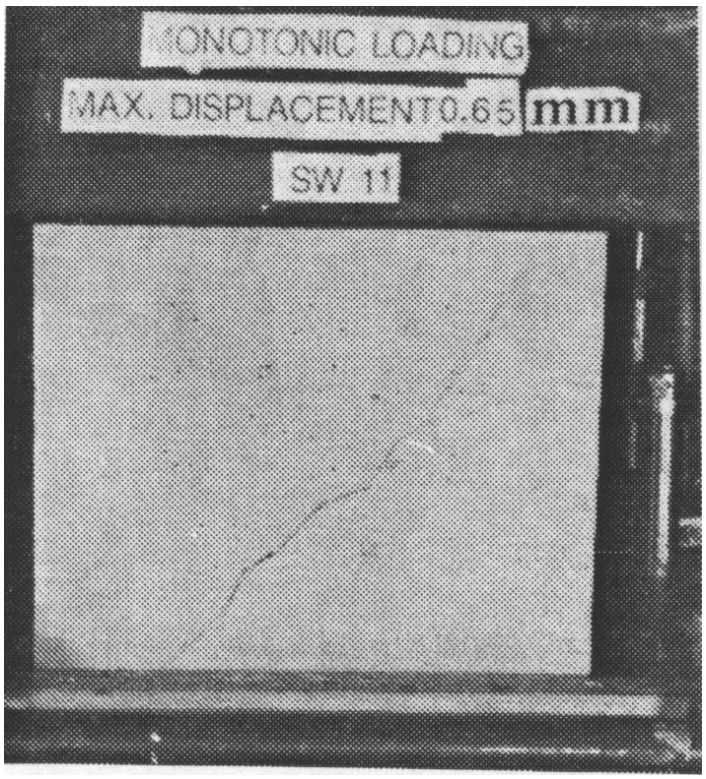


**Figure C-97 Condition of wall SW11 at 0.13% drift [Lopes and Elnashai (1991)]**

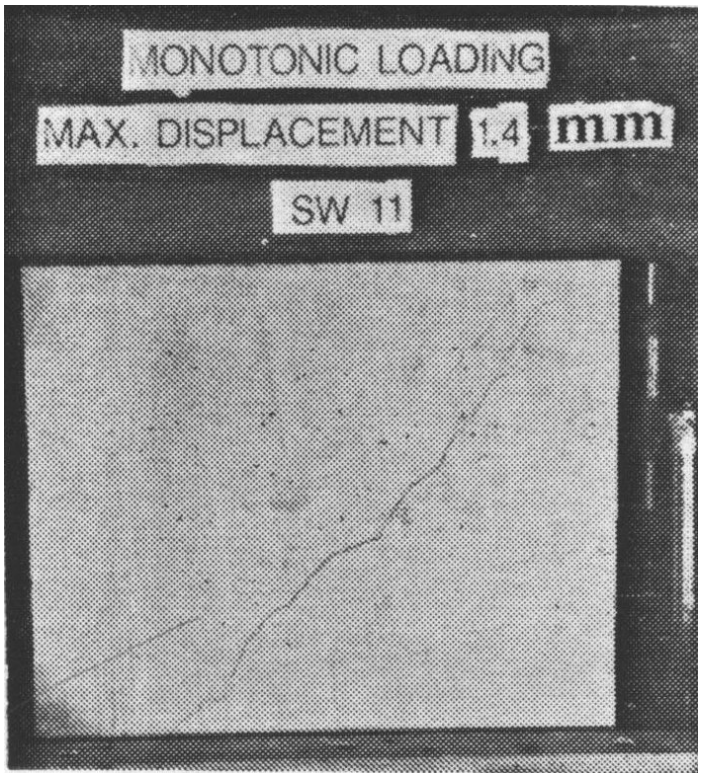


**Figure C-98 Condition of wall SW11 at 0.28% drift [Lopes and Elnashai (1991)]**

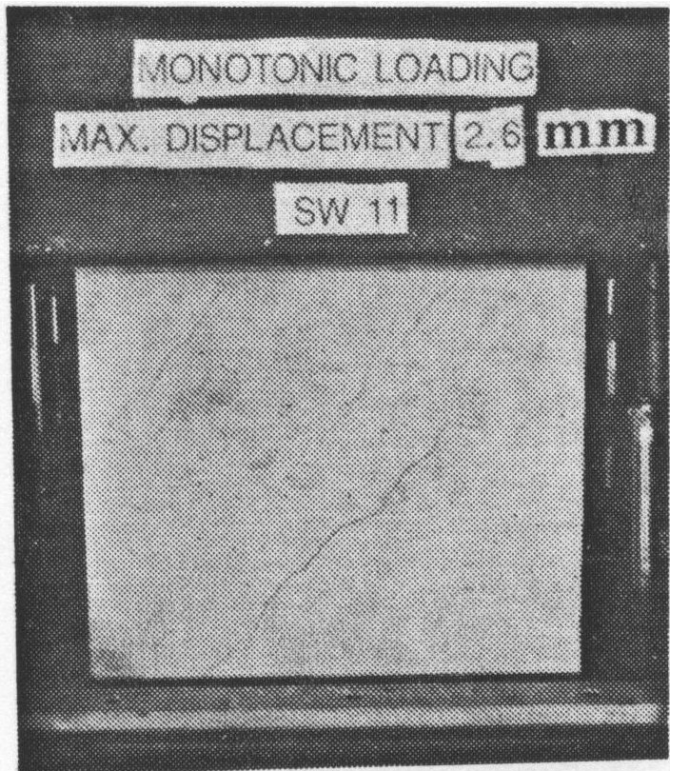


**Figure C-99 Condition of wall SW11 at 0.53% drift [Lopes and Elnashai (1991)]**

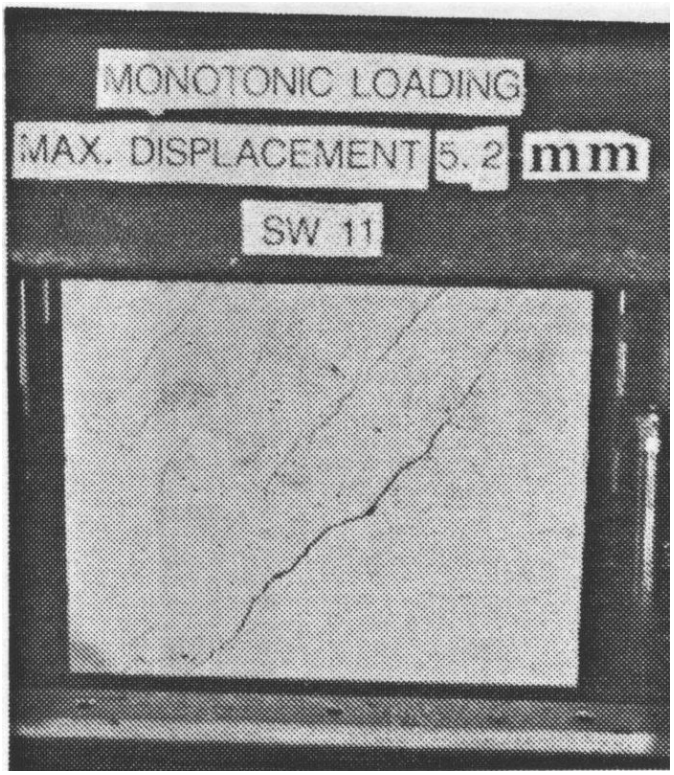


**Figure C-100 Condition of wall SW11 at 1.05% drift [Lopes and Elnashai (1991)]**

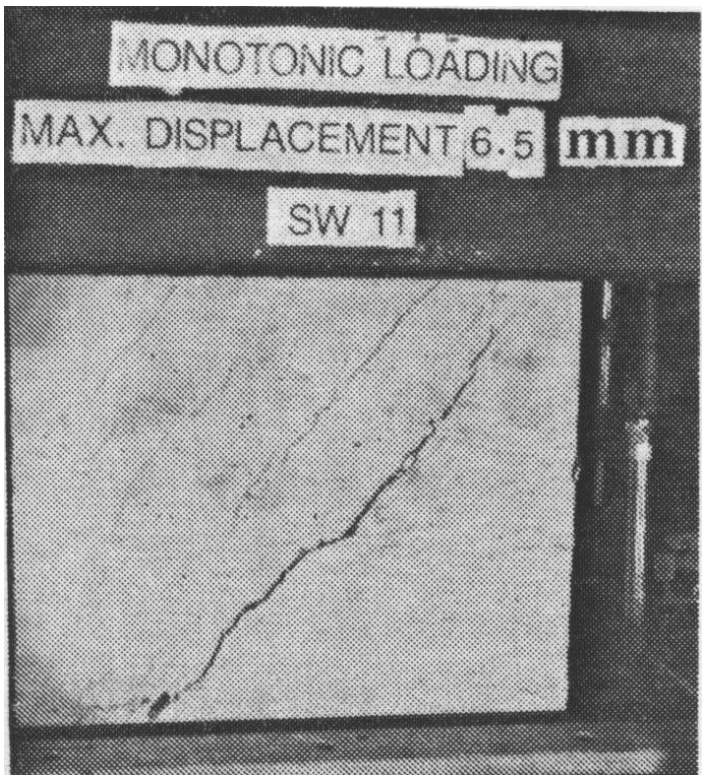


**Figure C-101 Condition of wall SW11 at 1.31% drift [Lopes and Elnashai (1991)]**

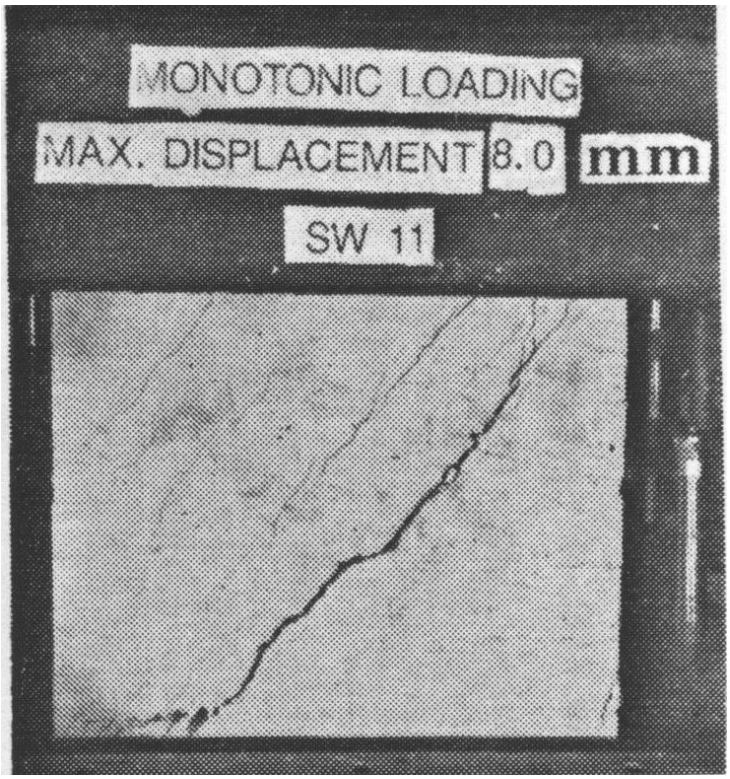


**Figure C-102 Condition of wall SW11 at 1.62% drift [Lopes and Elnashai (1991)]**

### C.1.7.2 Wall SW12

**Table C-23 Evaluation of damage data for wall SW12 tested by Lopes**

| Wall ID | MoR | Damage State (DS) | Drift (%) | Comments |
|---|---|---|---|---|
| SW12 | 1 | 1.2 | 0.12 | The drifts for these damage states are provided by the researcher. |
| | | 1.3 | 0.12 | |
| | | 1.4 | 0.34 | |
| | 2a | 2.4a | 0.51 | |
| | 2b | 2.4b | 0.65 | |
| | 4 | 4.5 | 0.97 | |

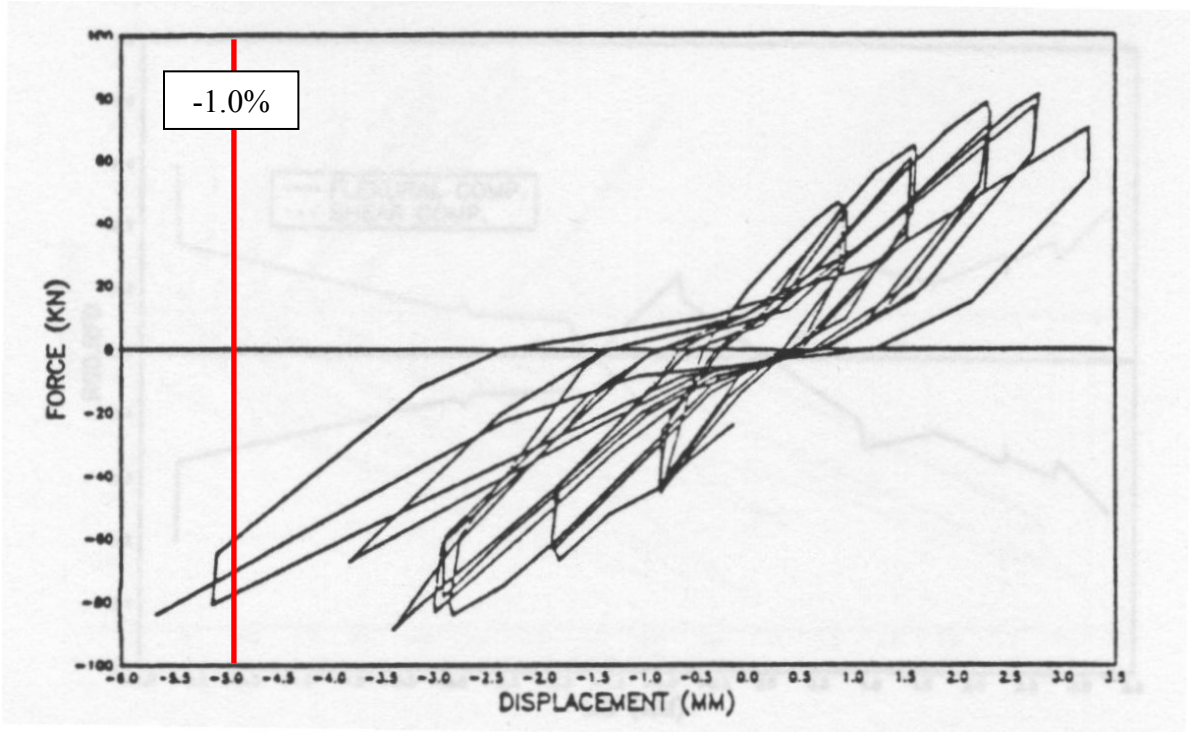


**Figure C-103 Load-displacement relationship for wall SW12 [Lopes and Elnashai (1991)]**

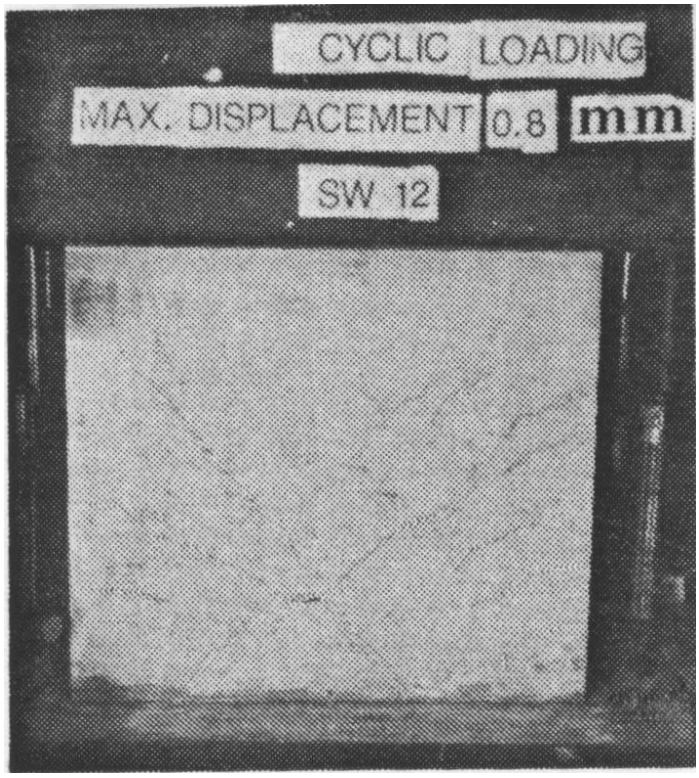


**Figure C-104 Condition of wall SW12 at 0.16% drift [Lopes and Elnashai (1991)]**

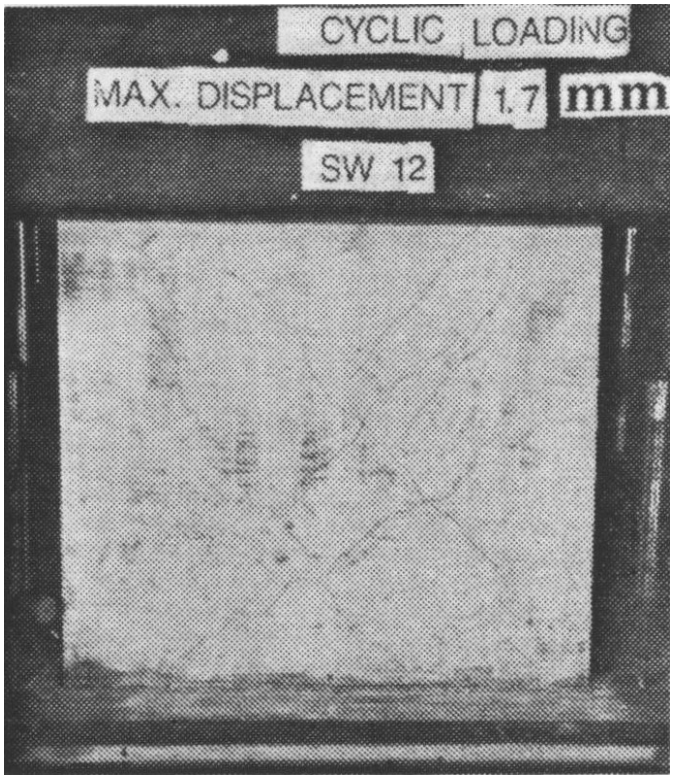


**Figure C-105 Condition of wall SW12 at 0.34% drift [Lopes and Elnashai (1991)]**

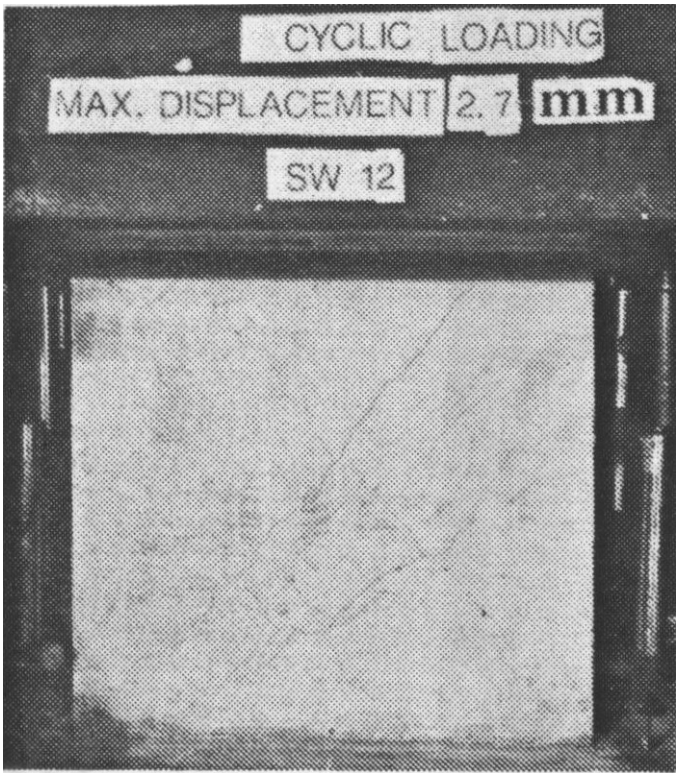


**Figure C-106 Condition of wall SW12 at 0.55% drift [Lopes and Elnashai (1991)]**

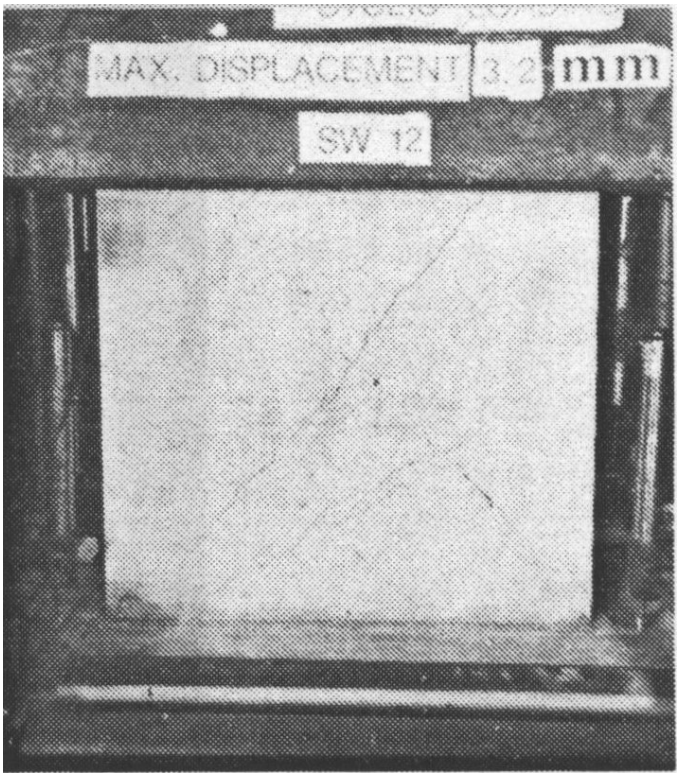


**Figure C-107 Condition of wall SW12 at 0.65% drift [Lopes and Elnashai (1991)]**

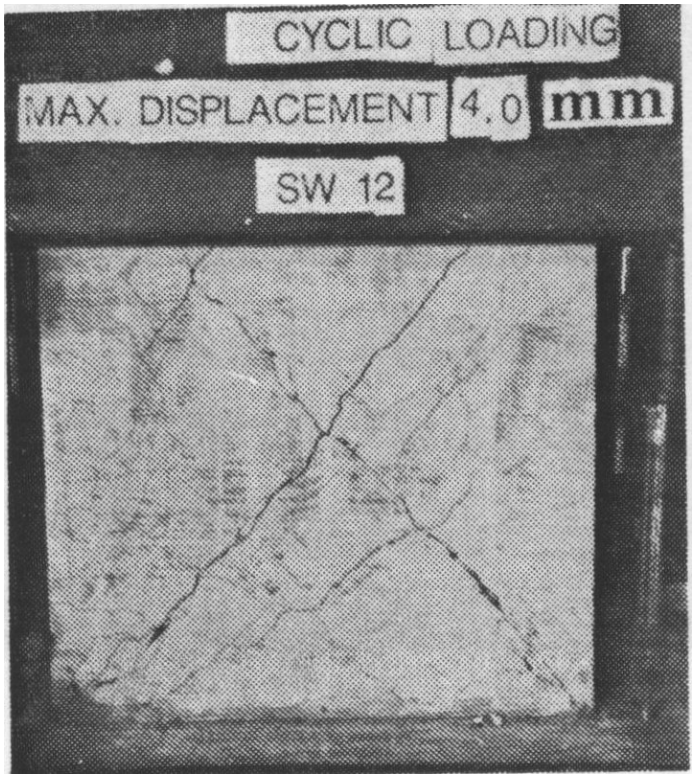


**Figure C-108 Condition of wall SW12 at 0.81% drift [Lopes and Elnashai (1991)]**

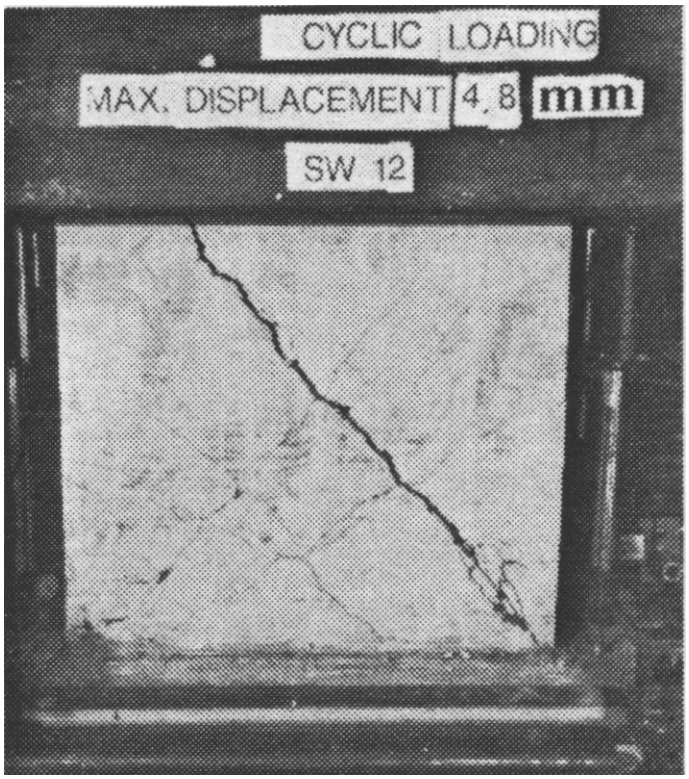


**Figure C-109 Condition of wall SW12 at 0.97% drift [Lopes and Elnashai (1991)]**

### C.1.7.3 Wall SW13

**Table C-24 Evaluation of damage data for wall SW13 tested by Lopes**

| Wall ID | MoR | Damage State (DS) | Drift (%) | Comments |
|---|---|---|---|---|
| SW13 | 1 | 1.3 | 0.12 | The drifts for these damage states are provided by the researcher. |
| | | 1.4 | 0.85 | |
| | 2a | 2.3 | 0.43 | |
| | | 2.4a | 1.01 | |
| | 3 | 3.1 | 0.97 | The image reported at this drift (Figure C-115) shows damage that can be repaired by partial wall replacement (MoR-3). The damaged region requiring partial wall replacement is identified using dashed boxes in Figure C-115. |
| | 4 | 4.3 | 1.72 | The image reported at this drift (Figure C-118) shows widespread crushing. |

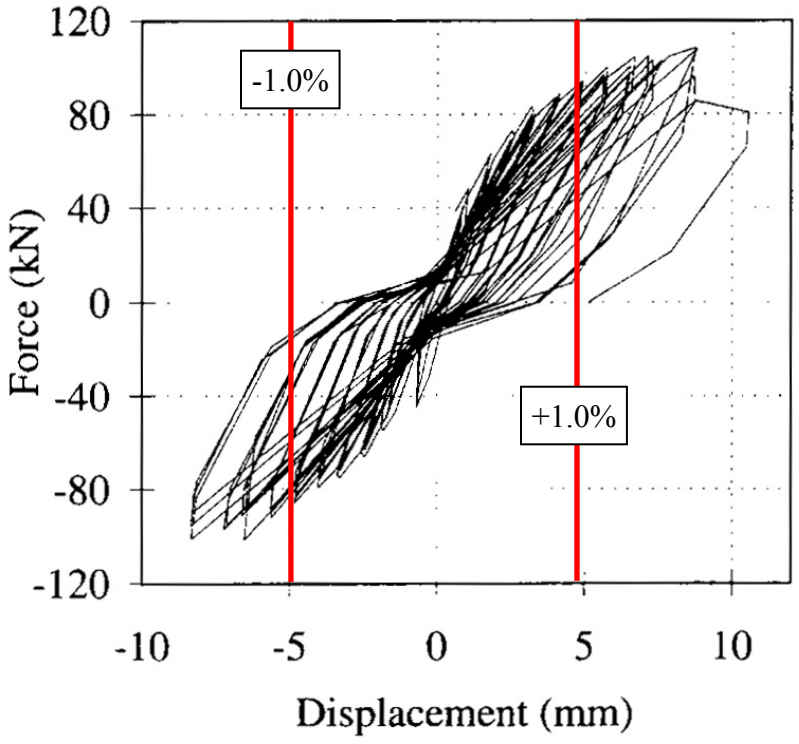


**Figure C-110 Load-displacement relationship for wall SW13 [Lopes and Elnashai (1991)]**

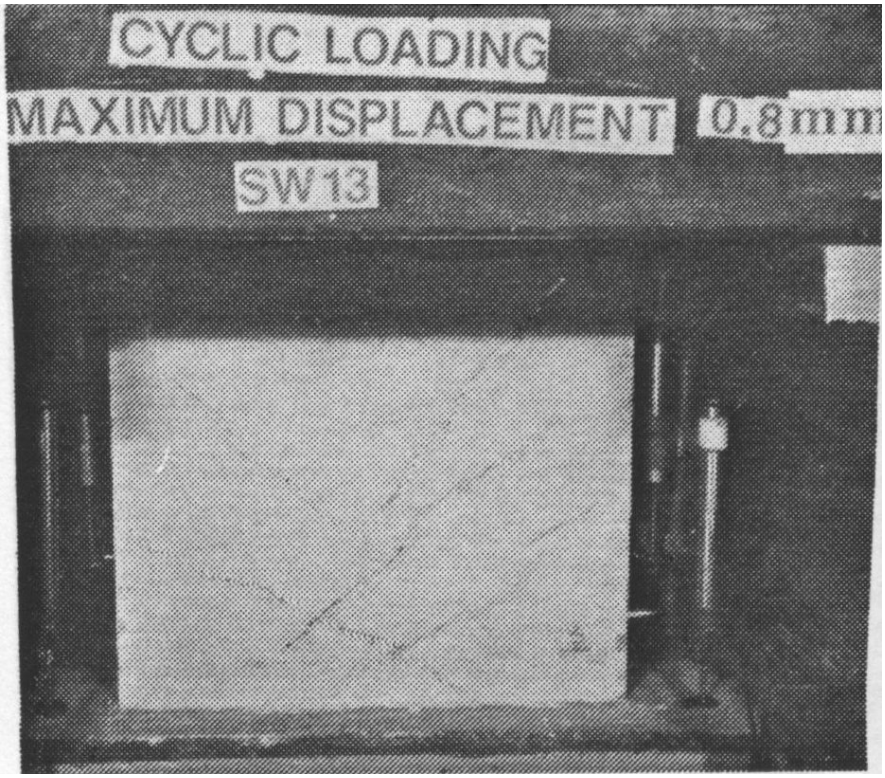


**Figure C-111 Condition of wall SW13 at 0.16% drift [Lopes and Elnashai (1991)]**

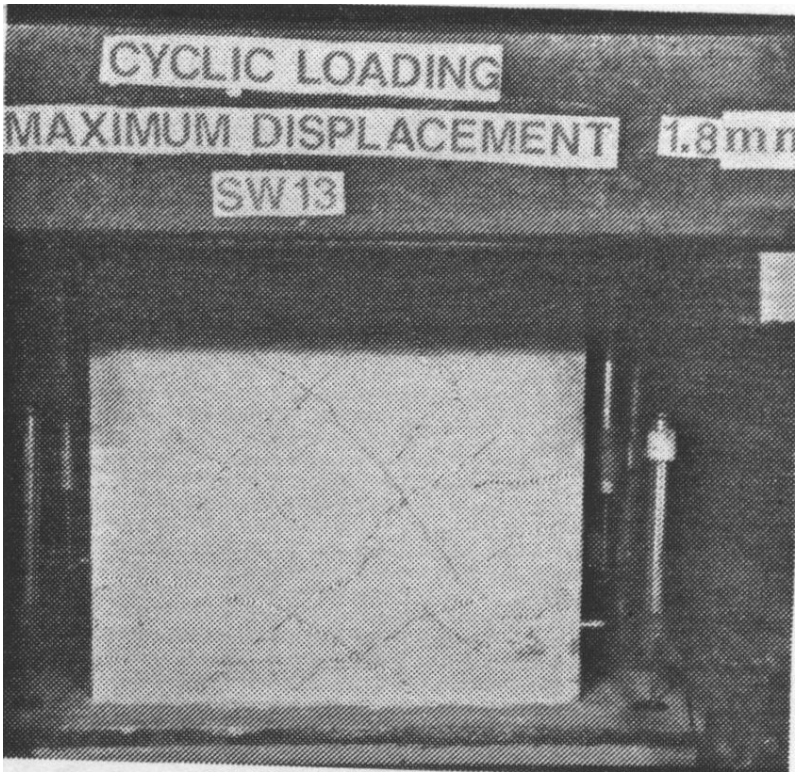


**Figure C-112 Condition of wall SW13 at 0.36% drift [Lopes and Elnashai (1991)]**

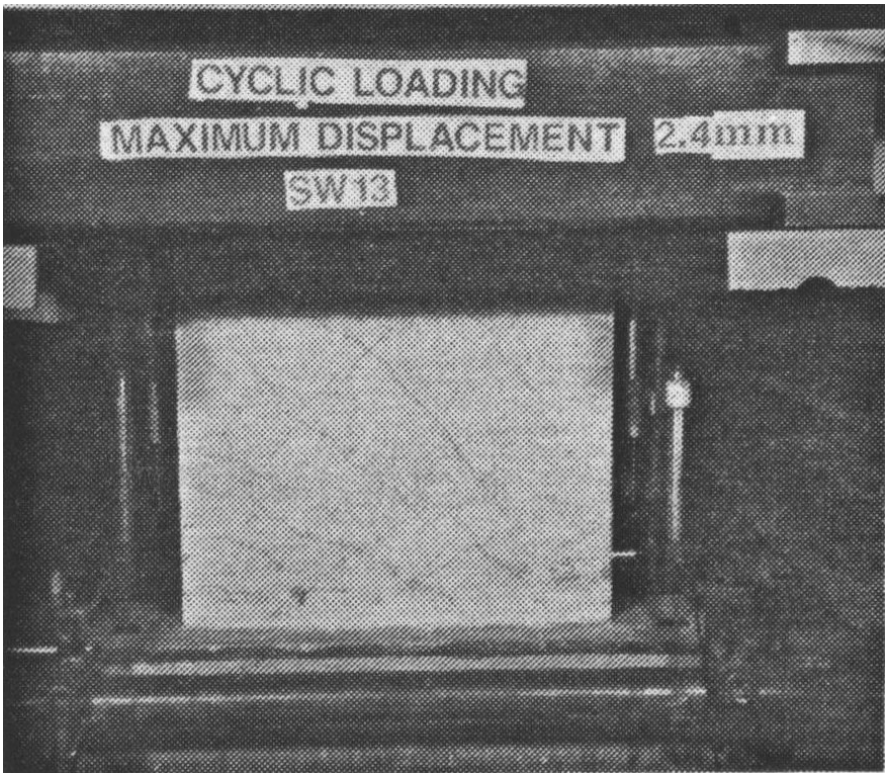


**Figure C-113 Condition of wall SW13 at 0.48% drift [Lopes and Elnashai (1991)]**

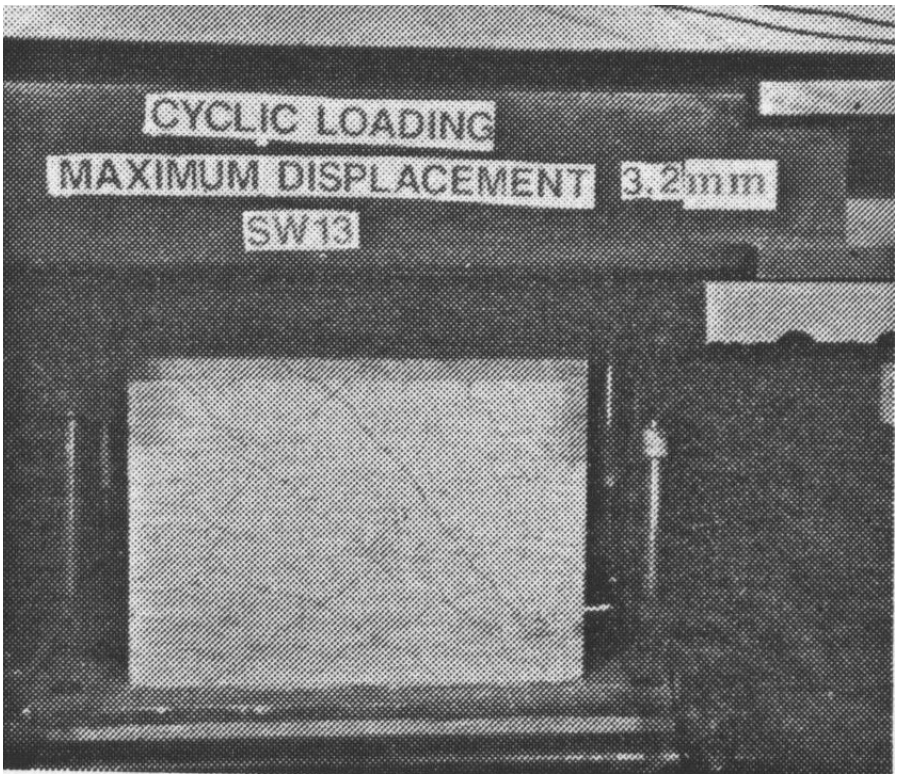


**Figure C-114 Condition of wall SW13 at 0.65% drift [Lopes and Elnashai (1991)]**

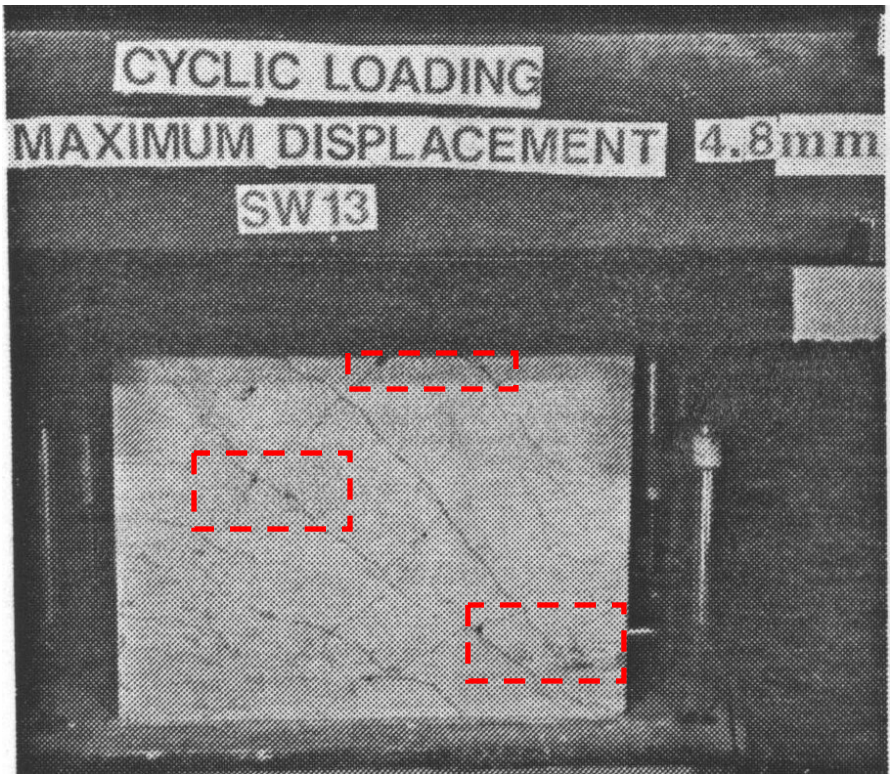


**Figure C-115 Condition of wall SW13 at 0.97% drift [Lopes and Elnashai (1991)]**

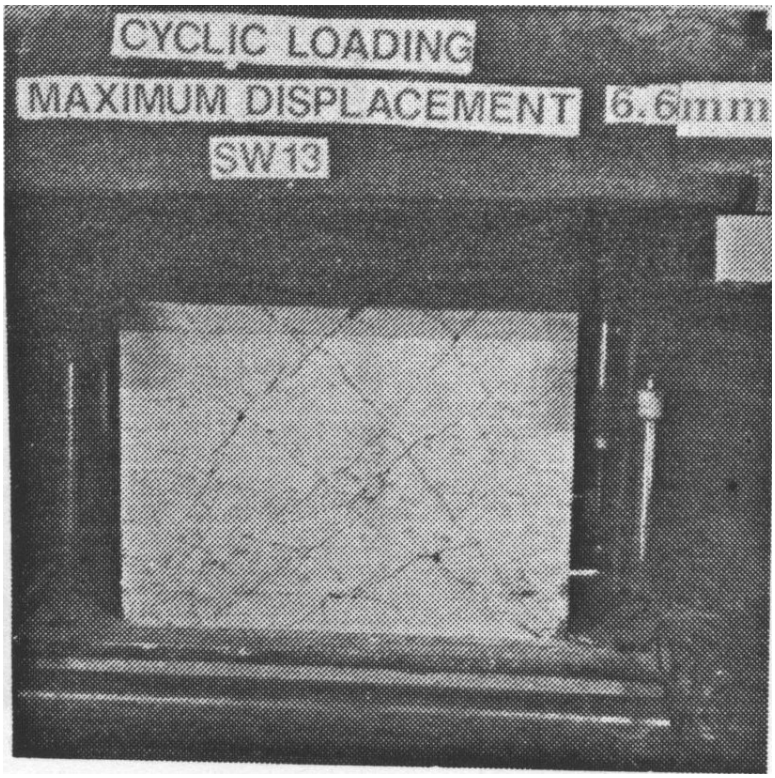


**Figure C-116 Condition of wall SW13 at 1.33% drift [Lopes and Elnashai (1991)]**

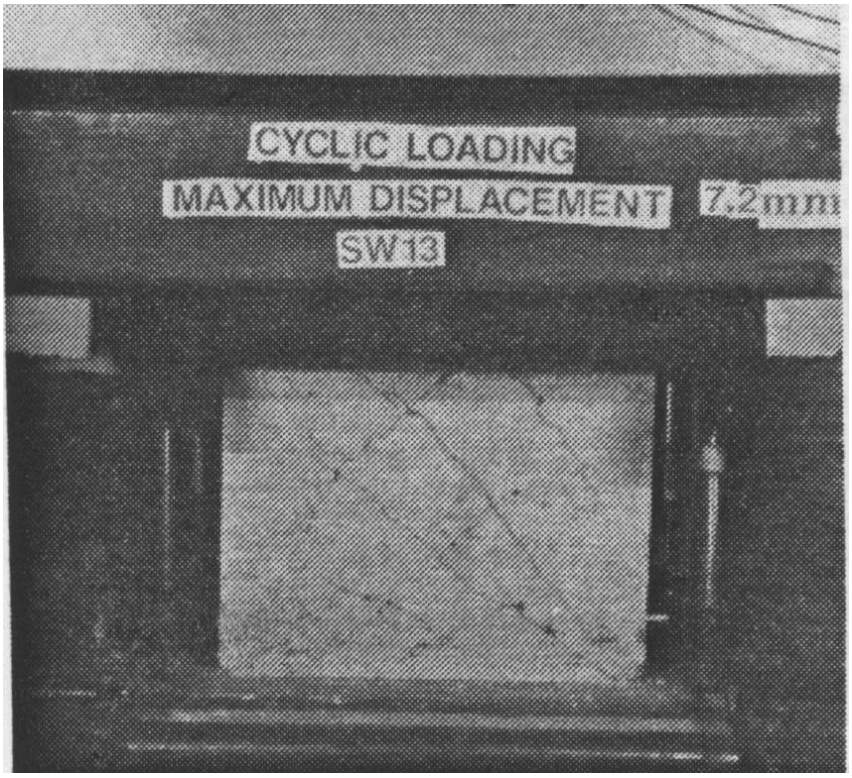


**Figure C-117 Condition of wall SW13 at 1.45% drift [Lopes and Elnashai (1991)]**

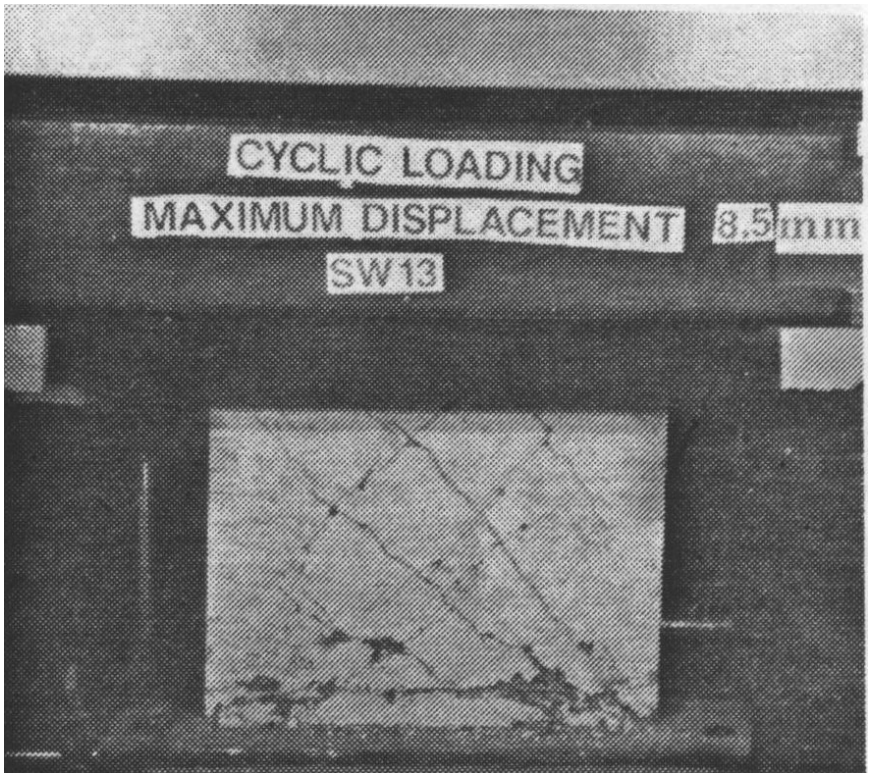


**Figure C-118 Condition of wall SW13 at 1.72% drift [Lopes and Elnashai (1991)]**

### C.1.7.4 Wall SW14

**Table C-25 Evaluation of damage data for wall SW14 tested by Lopes**

| Wall ID | MoR | Damage State (DS) | Drift (%) | Comments |
|---|---|---|---|---|
| SW14 | 1 | 1.4 | 0.67 | The drifts for these damage states are provided by the researcher. |
| | 2a | 2.4a | 0.83 | |
| | 2b | 2.4b | 0.97 | |
| | 3 | 3.1 | 0.81 | The image reported at this drift (Figure C-123) shows damage that can be repaired by partial wall replacement (MoR-3). The damaged region requiring partial wall replacement is identified using dashed boxes in Figure C-123. |
| | 4 | 4.3 | 1.13 | The image reported at this drift (Figure C-125) shows widespread crushing. |

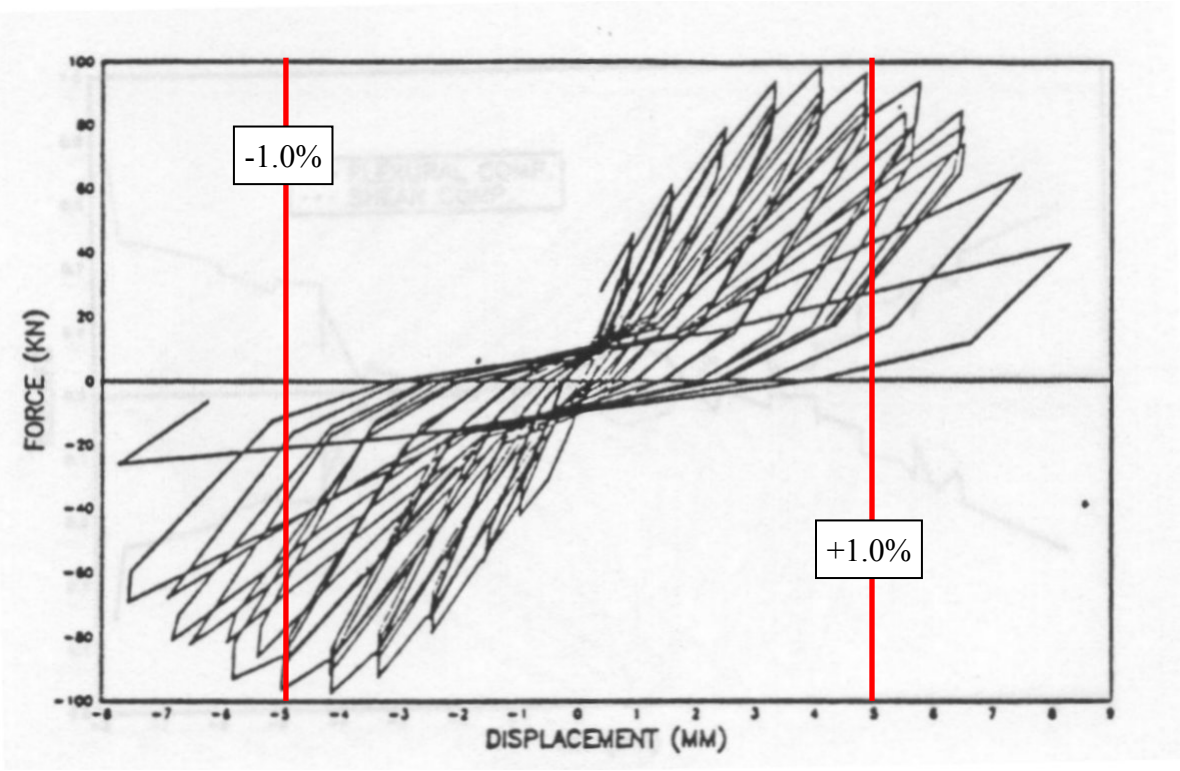


**Figure C-119 Load-displacement relationship for wall SW14 [Lopes and Elnashai (1991)]**

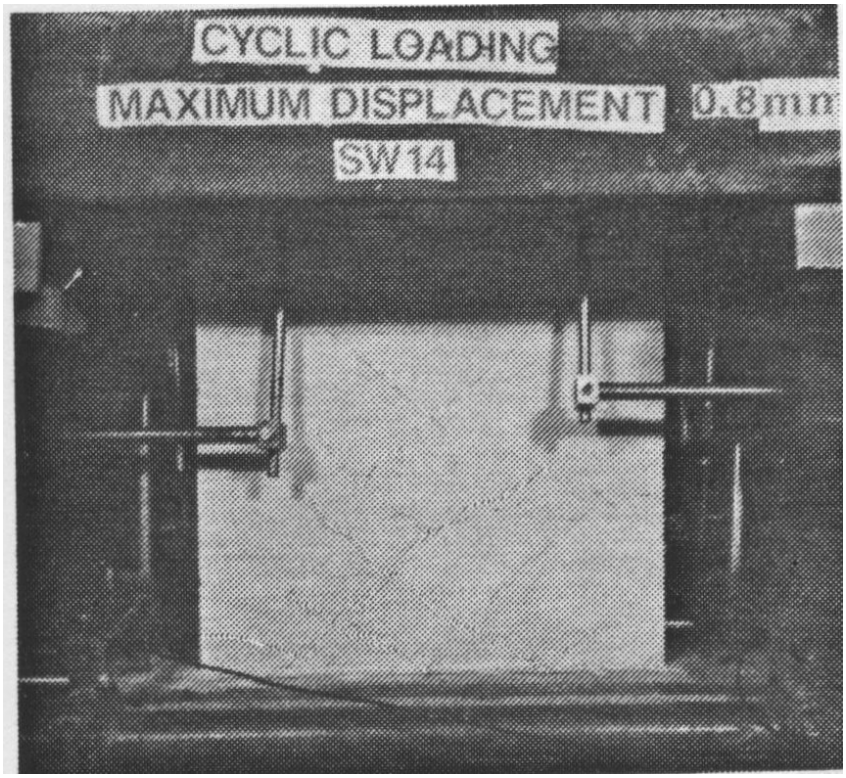


**Figure C-120 Condition of wall SW14 at 0.16% drift [Lopes and Elnashai (1991)]**

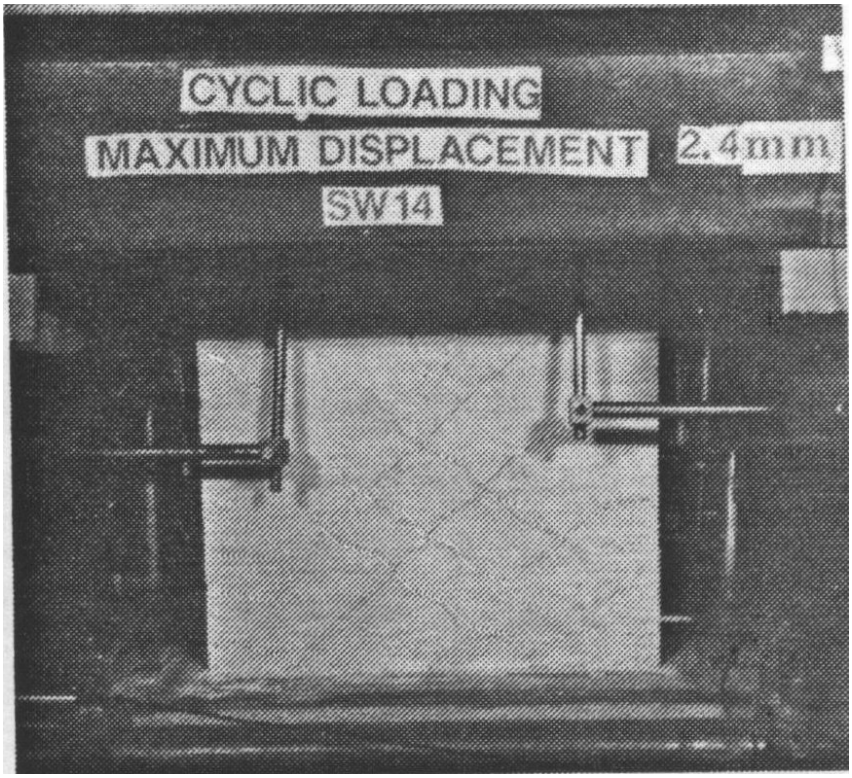


**Figure C-121 Condition of wall SW14 at 0.48% drift [Lopes and Elnashai (1991)]**

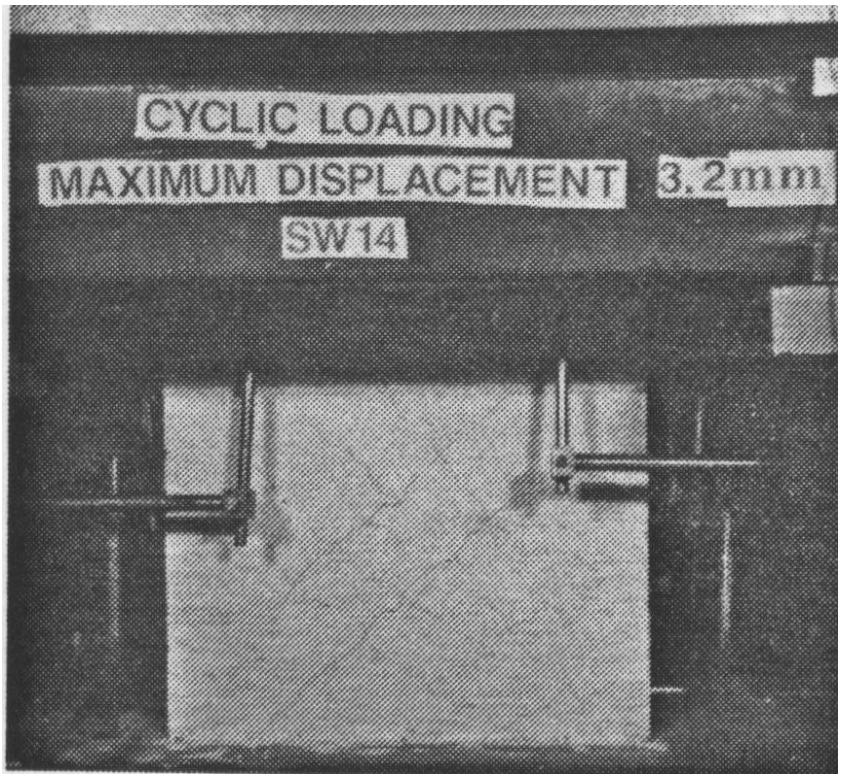


**Figure C-122 Condition of wall SW14 at 0.65% drift [Lopes and Elnashai (1991)]**

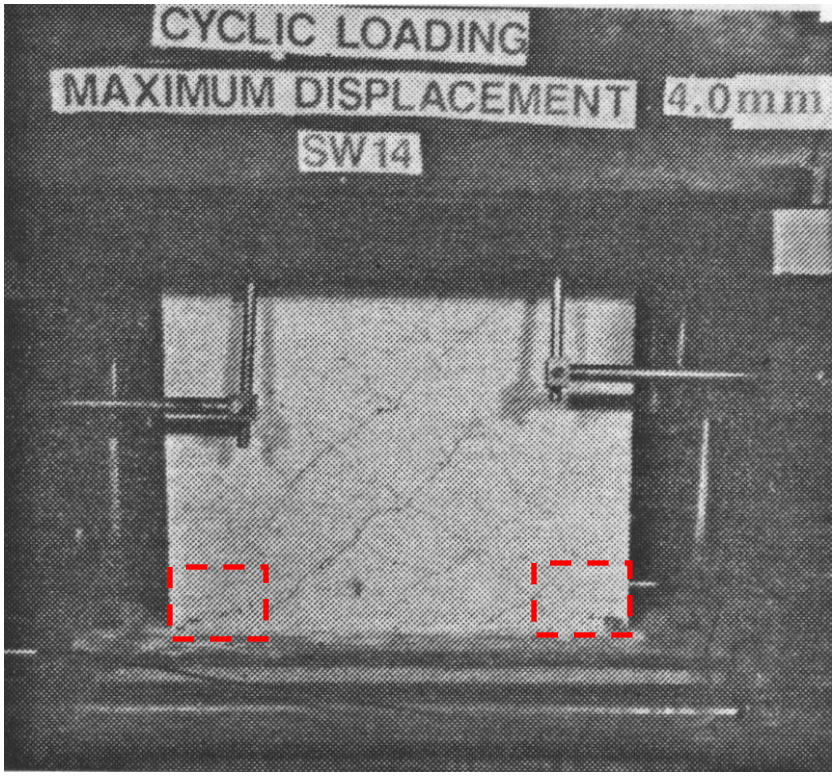


**Figure C-123 Condition of wall SW14 at 0.81% drift [Lopes and Elnashai (1991)]**

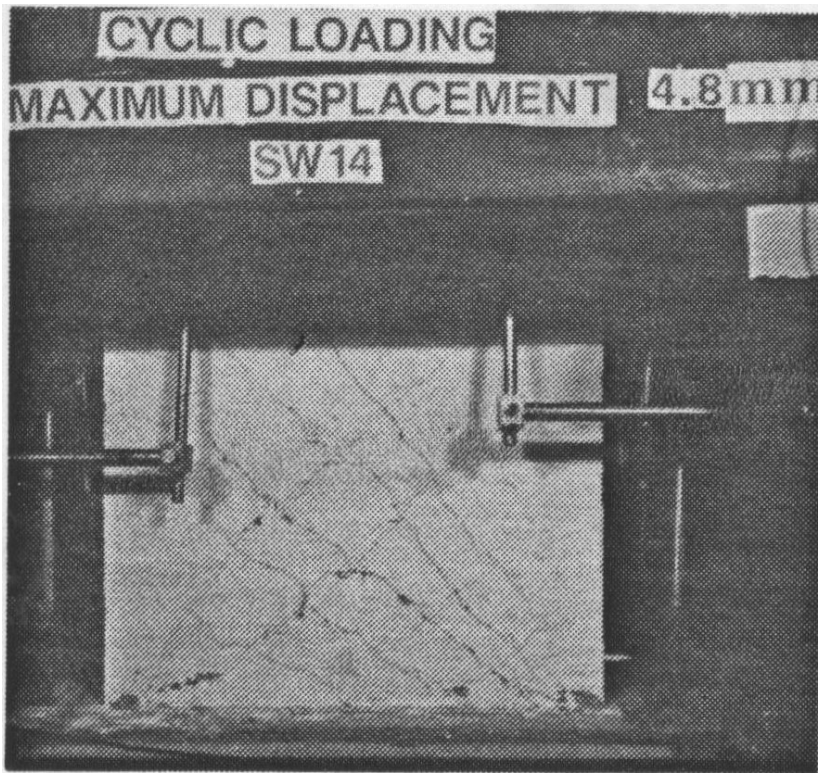


**Figure C-124 Condition of wall SW14 at 0.97% drift [Lopes and Elnashai (1991)]**

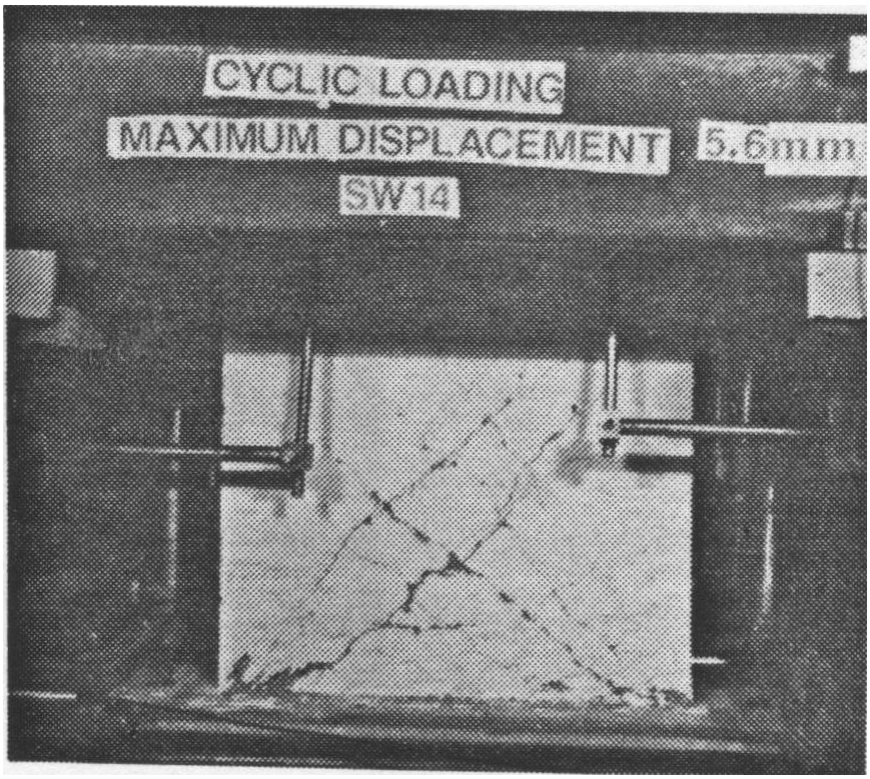


**Figure C-125 Condition of wall SW14 at 1.13% drift [Lopes and Elnashai (1991)]**

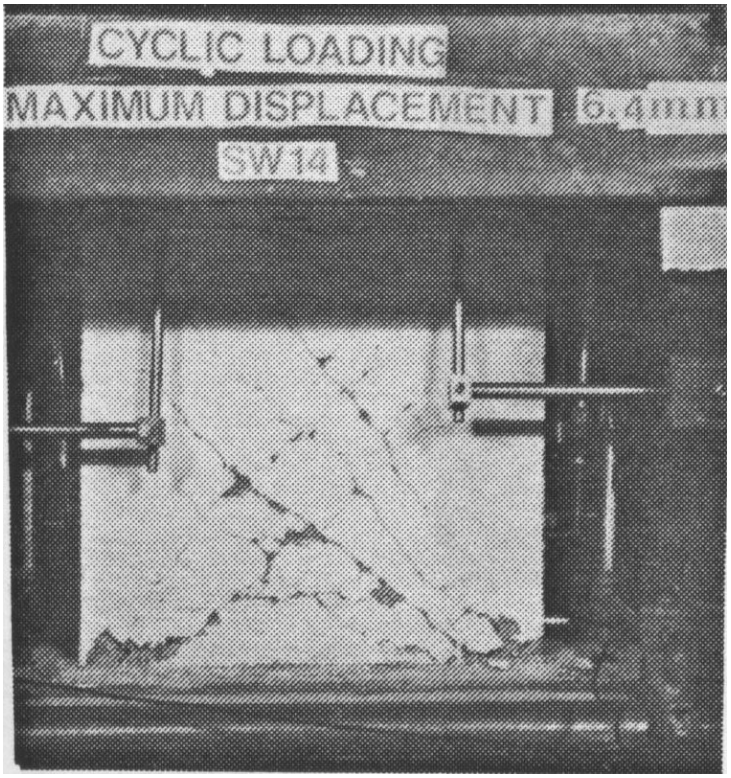


**Figure C-126 Condition of wall SW14 at 1.29% drift [Lopes and Elnashai (1991)]**

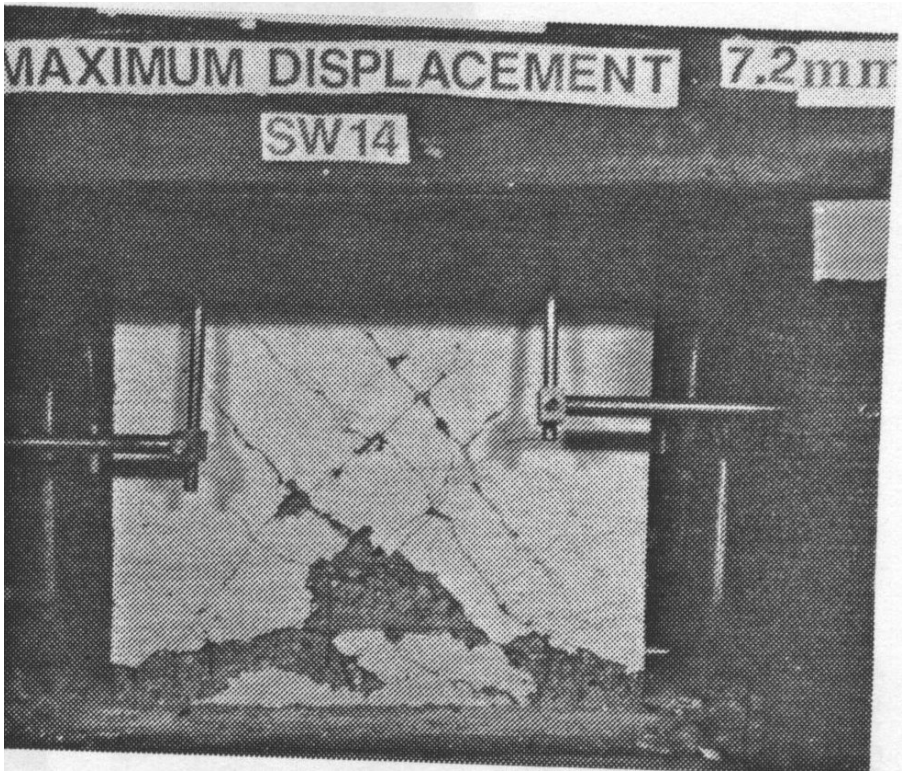


**Figure C-127 Condition of wall SW14 at 1.45% drift [Lopes and Elnashai (1991)]**

### C.1.7.5 Wall SW15

**Table C-26 Evaluation of damage data for wall SW15 tested by Lopes**

| Wall ID | MoR | Damage State (DS) | Drift (%) | Comments |
|---|---|---|---|---|
| SW15 | 1 | 1.2 | 0.11 | The drifts for these damage states are provided by the researcher. |
| | | 1.3 | 0.15 | |
| | | 1.4 | 0.32 | |
| | 2a | 2.3 | 0.39 | |
| | | 2.4a | 0.48 | |
| | 2b | 2.4b | 0.48 | |
| | 4 | 4.2 | 0.65 | Based on the researcher's description of damage at this drift: "Upon reloading in the opposite direction, a loud noise was heard and sudden and considerable loss of load carrying capacity was registered." [Lopes and Elnashai (1991), page 178]. |

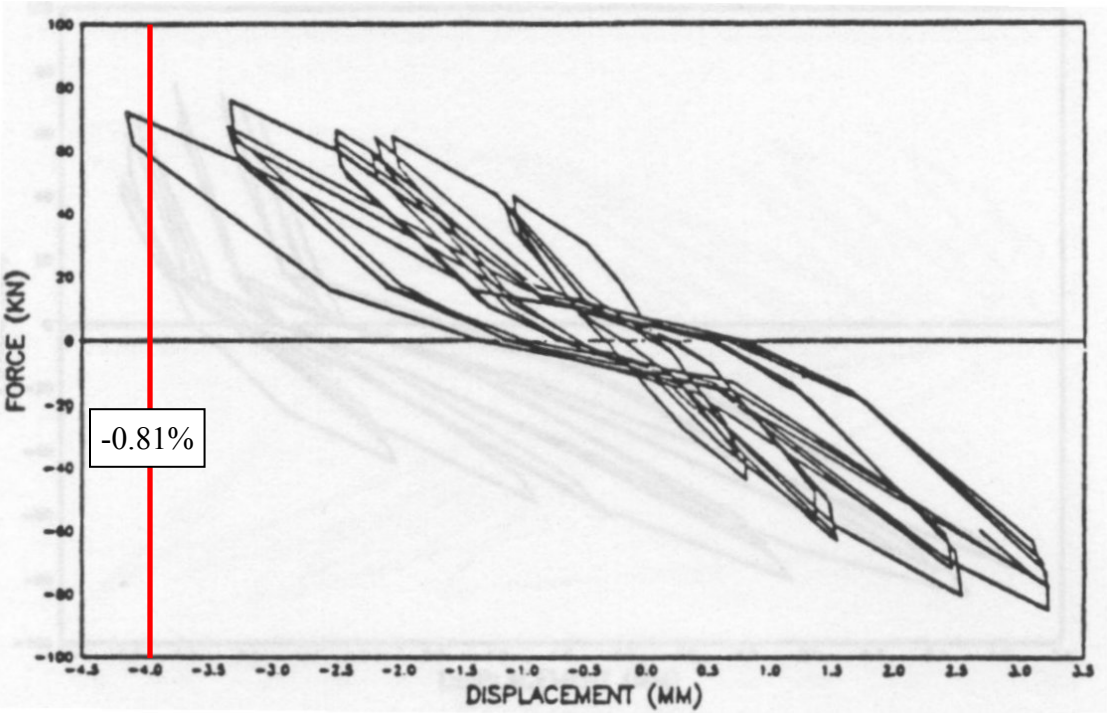


**Figure C-128 Load-displacement relationship for wall SW15 [Lopes and Elnashai (1991)]**

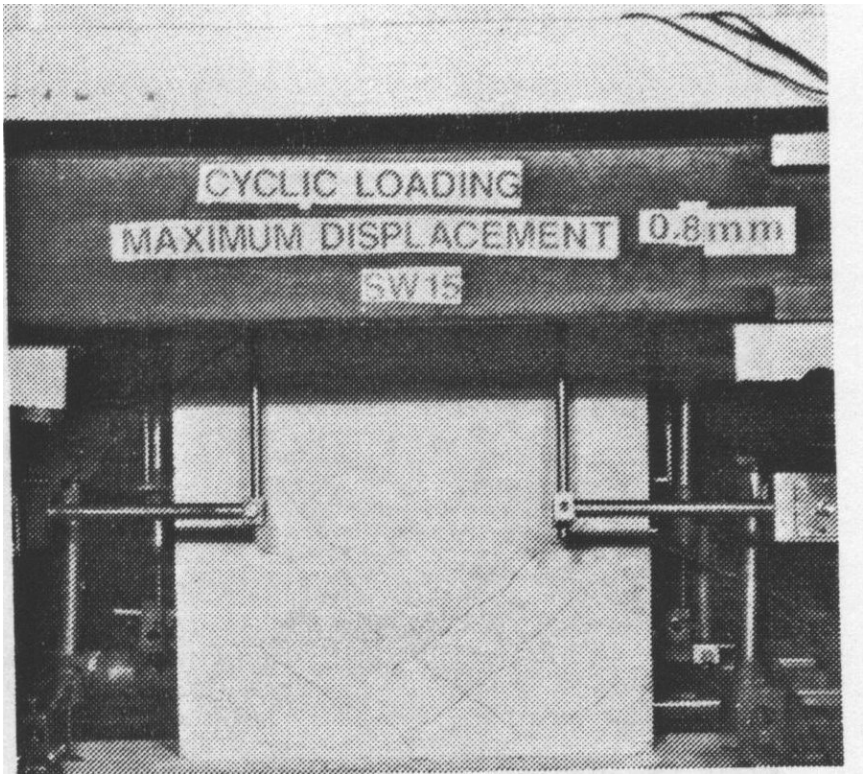


**Figure C-129 Condition of wall SW15 at 0.16% drift [Lopes and Elnashai (1991)]**

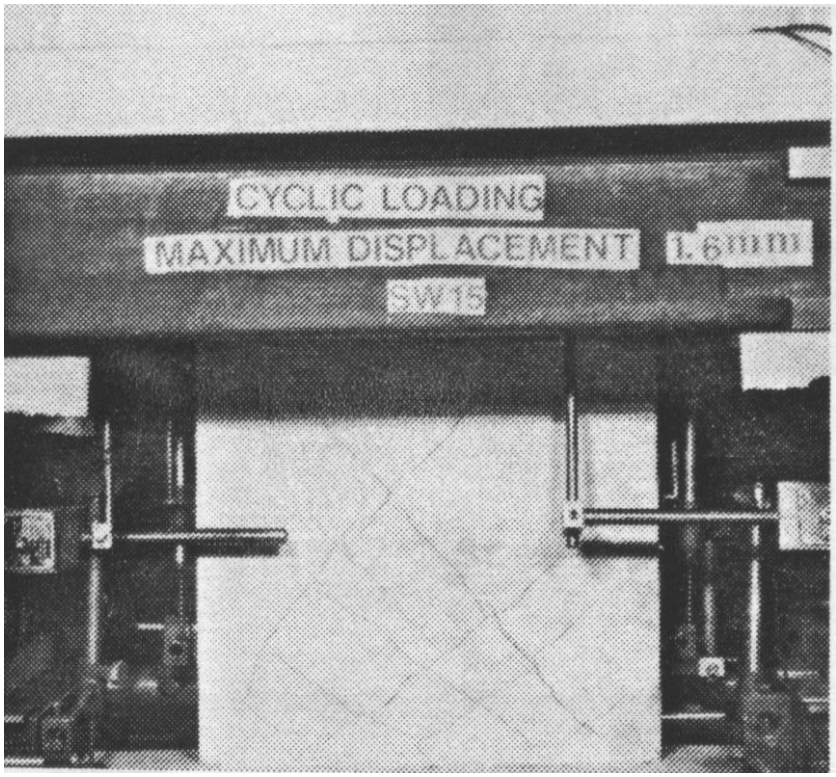


**Figure C-130 Condition of wall SW15 at 0.32% drift [Lopes and Elnashai (1991)]**

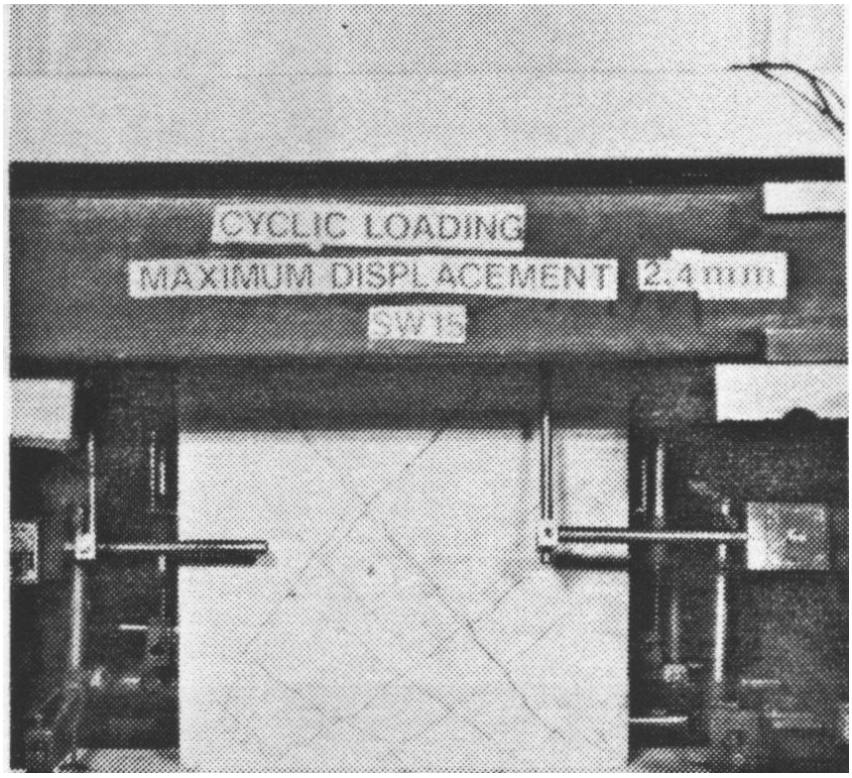


**Figure C-131 Condition of wall SW15 at 0.48% drift [Lopes and Elnashai (1991)]**

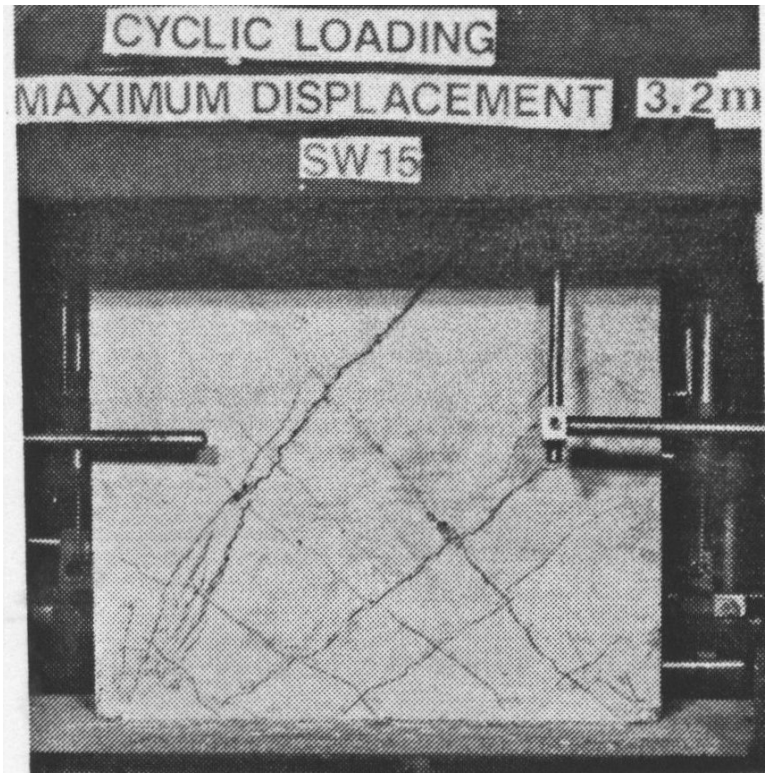


**Figure C-132 Condition of wall SW15 at 0.65% drift [Lopes and Elnashai (1991)]**

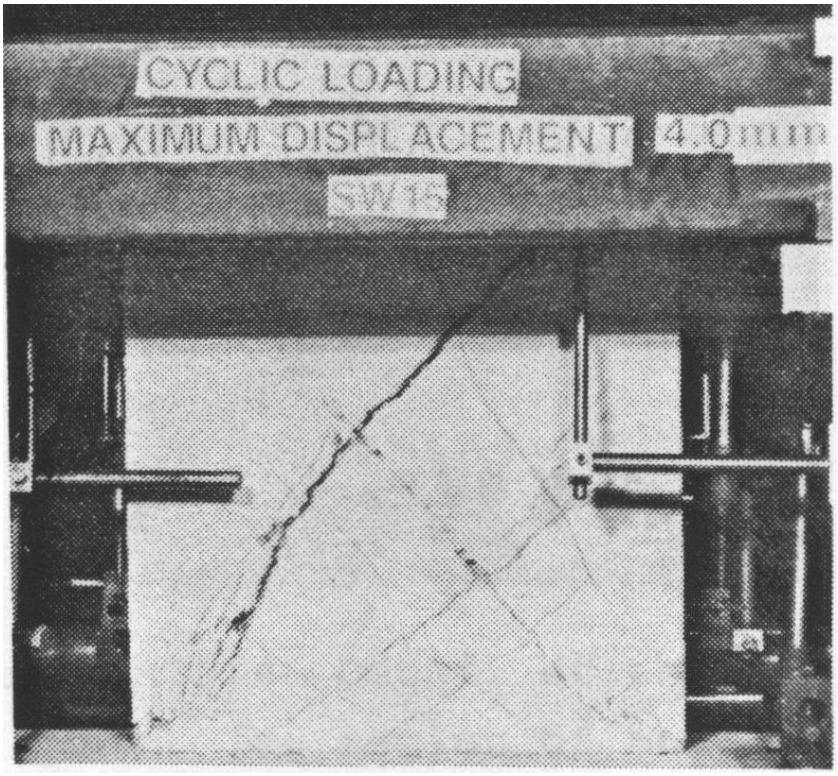


**Figure C-133 Condition of wall SW15 at 0.81% drift [Lopes and Elnashai (1991)]**

### C.1.7.6 Wall SW16

**Table C-27 Evaluation of damage data for wall SW16 tested by Lopes**

| Wall ID | MoR | Damage State (DS) | Drift (%) | Comments |
|---|---|---|---|---|
| SW16 | 1 | 1.4 | 0.16 | The drifts for these damage states are provided by the researcher. |
| | 2a | 2.4a | 0.32 | |
| | 2b | 2.4b | 0.65 | |
| | 4 | 4.3 | 1.17 | The image reported at this drift (Figure C-140) shows widespread crushing. |
| | | 4.5 | 0.97 | The drift for this damage state is reported by the researcher. |

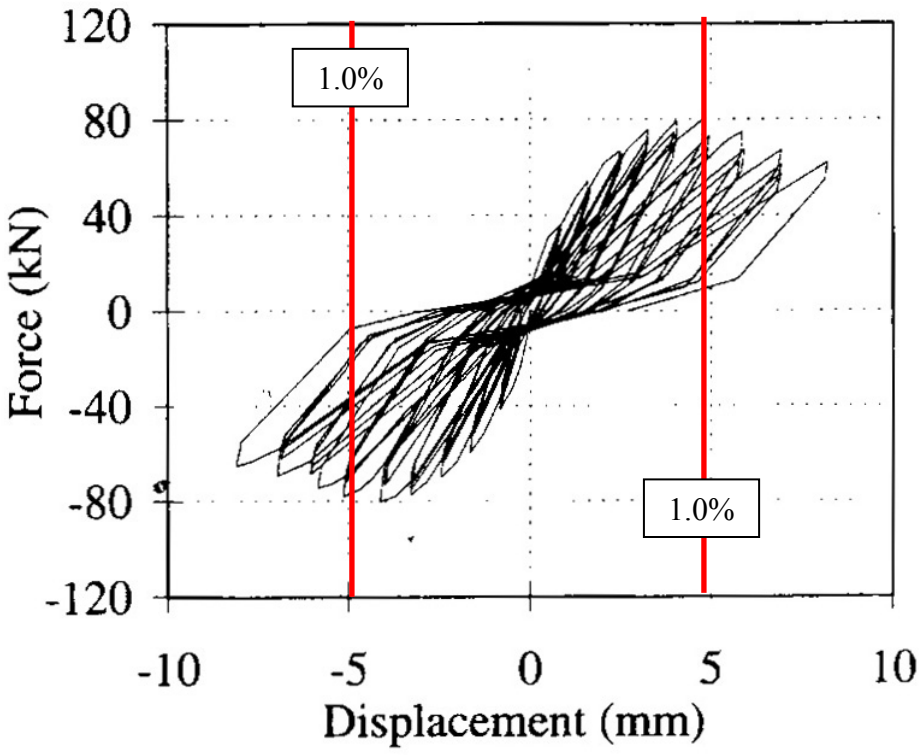


**Figure C-134 Load-displacement relationship for wall SW16 [Lopes and Elnashai (1991)]**

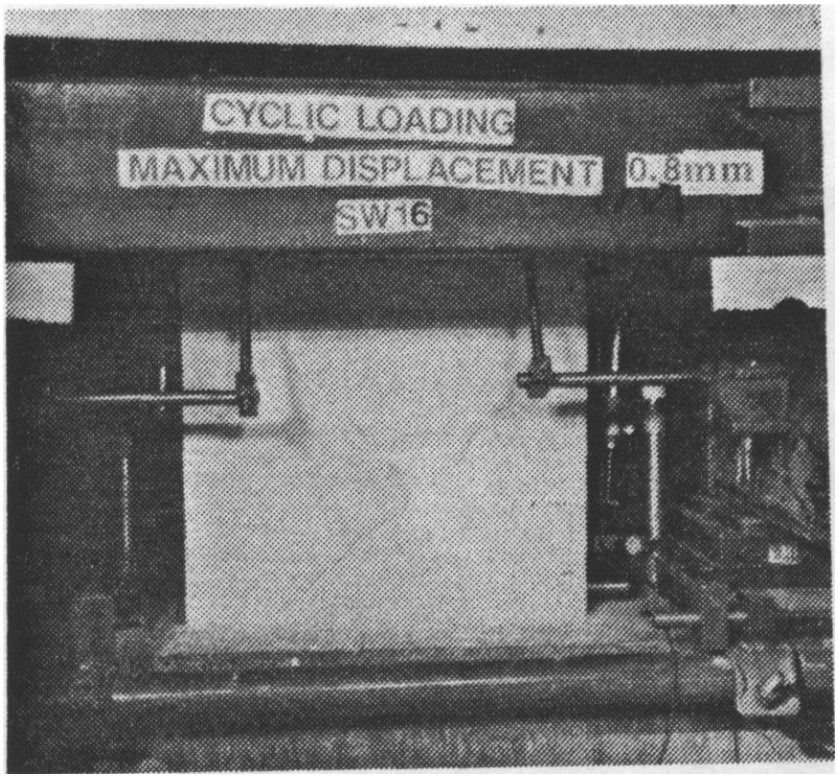


**Figure C-135 Condition of wall SW16 at 0.16% drift [Lopes and Elnashai (1991)]**

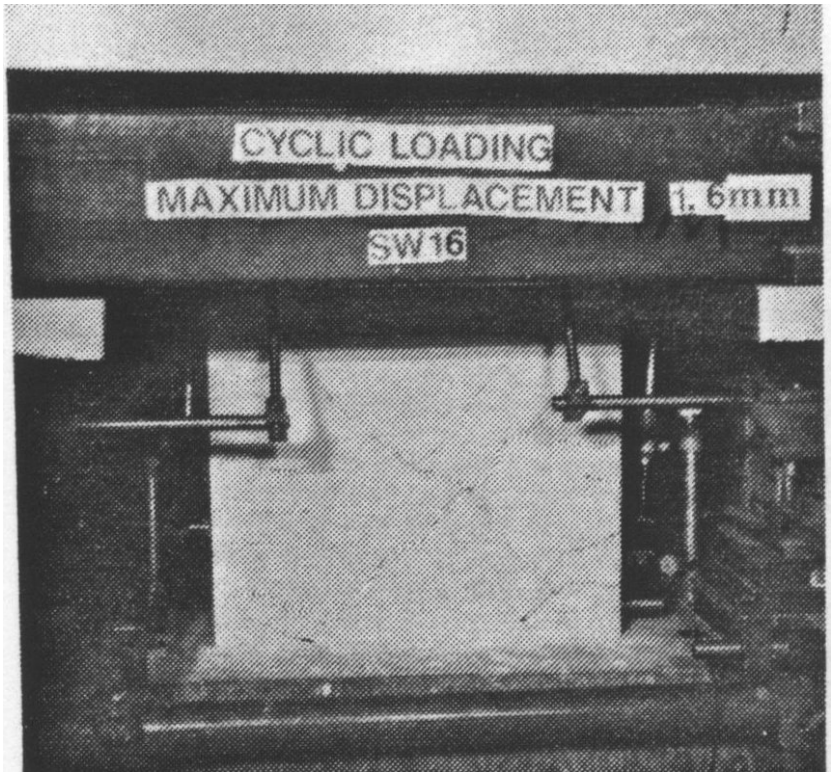


**Figure C-136 Condition of wall SW16 at 0.32% drift [Lopes and Elnashai (1991)]**

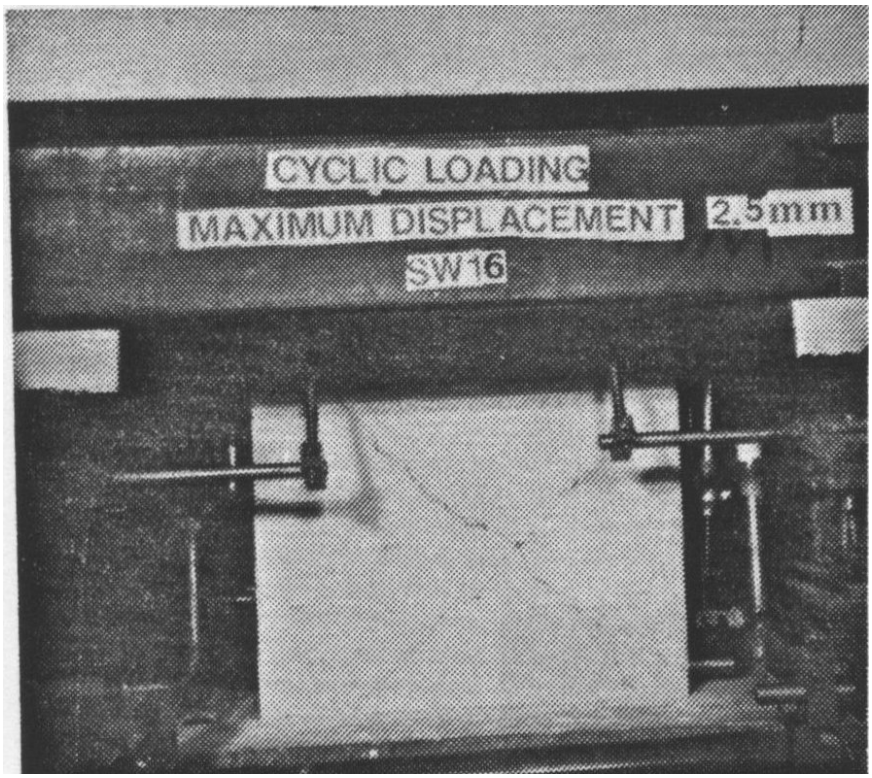


**Figure C-137 Condition of wall SW16 at 0.51% drift [Lopes and Elnashai (1991)]**

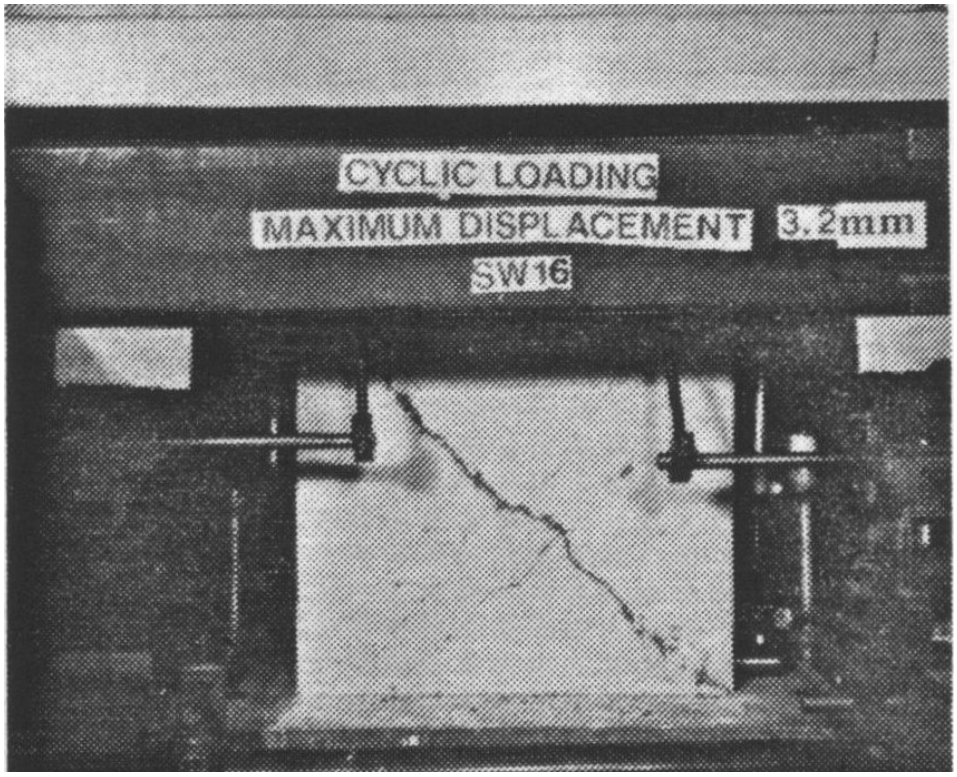


**Figure C-138 Condition of wall SW16 at 0.65% drift [Lopes and Elnashai (1991)]**


**Figure C-139 Condition of wall SW16 at 0.81% drift [Lopes and Elnashai (1991)]**

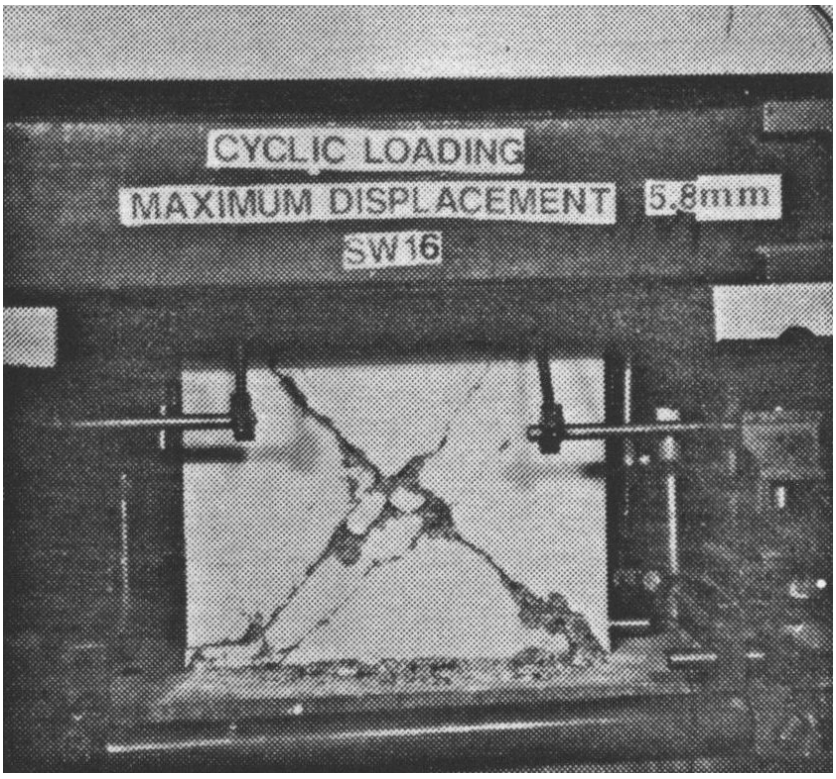


**Figure C-140 Condition of wall SW16 at 1.17% drift [Lopes and Elnashai (1991)]**

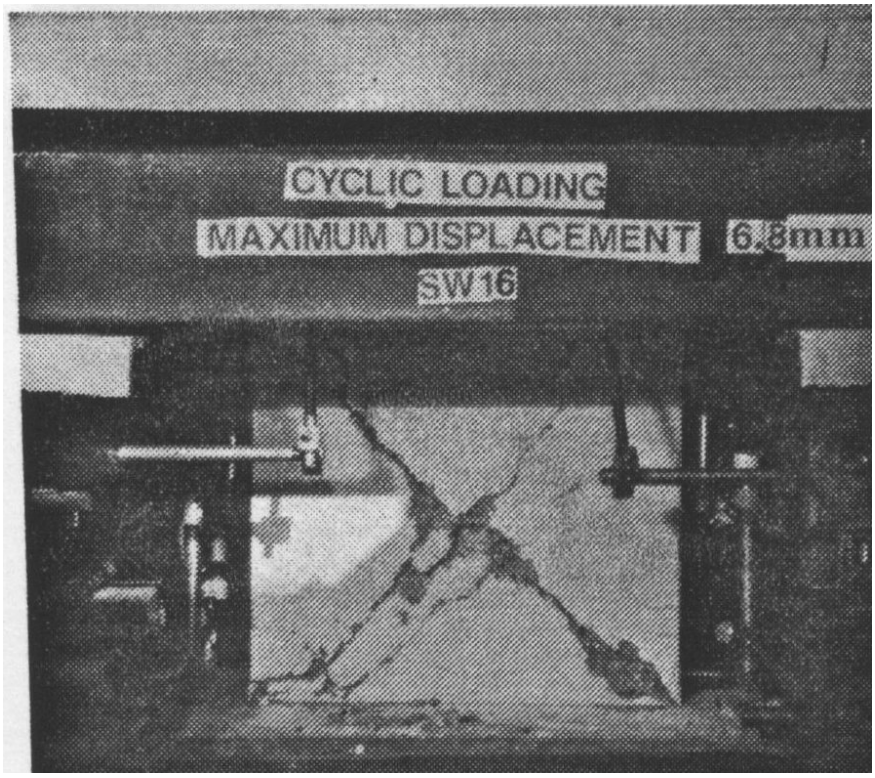


**Figure C-141 Condition of wall SW16 at 1.37% drift [Lopes and Elnashai (1991)]**

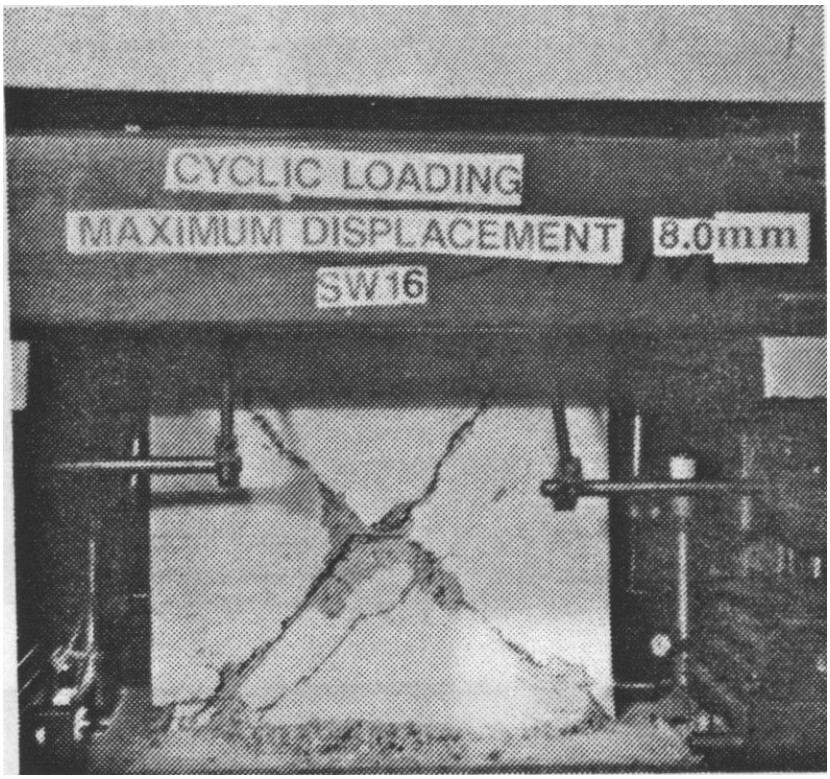


**Figure C-142 Condition of wall SW16 at 1.62% drift [Lopes and Elnashai (1991)]**

### C.1.7.7 Wall SW17

**Table C-28 Evaluation of damage data for wall SW17 tested by Lopes**

| Wall ID | MoR | Damage State (DS) | Drift (%) | Comments |
|---|---|---|---|---|
| SW17 | 1 | 1.4 | 0.34 | The drifts for these damage states are provided by the researcher. |
| | 2a | 2.4a | 0.51 | |
| | 2b | 2.4b | 0.65 | |
| | 3 | 3.1 | 0.65 | The image reported at this drift (Figure C-146) shows damage that can be repaired by partial wall replacement (MoR-3). The damaged region requiring partial wall replacement is identified using a dashed box in Figure C-146. |
| | 4 | 4.3 | 1.13 | The image reported at this drift (Figure C-149) shows widespread crushing. |
| | | 4.5 | 0.97 | The drift for this damage state is reported by the researcher. |

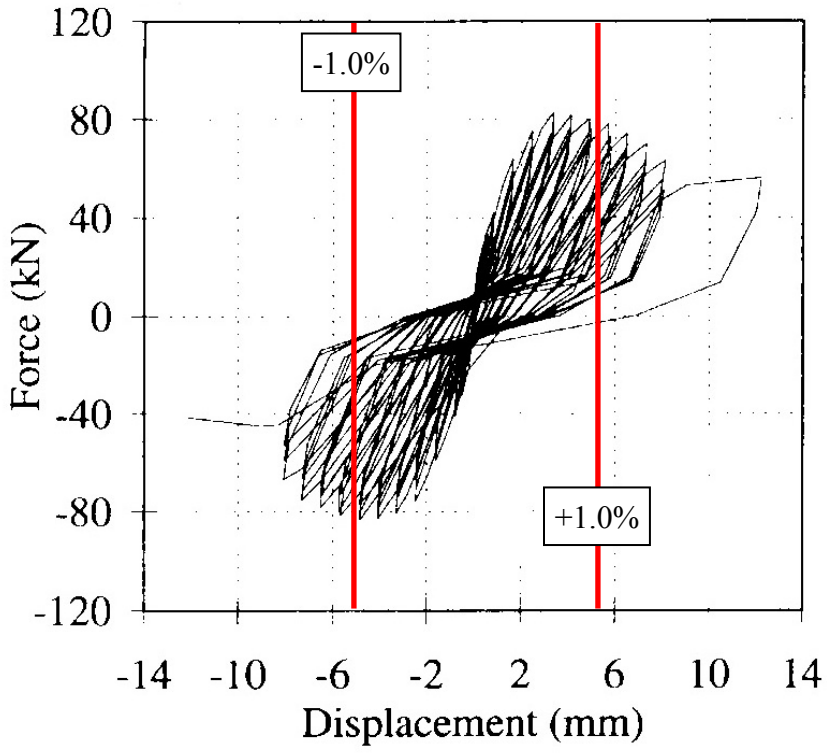


**Figure C-143 Load-displacement relationship for wall SW17 [Lopes and Elnashai (1991)]**

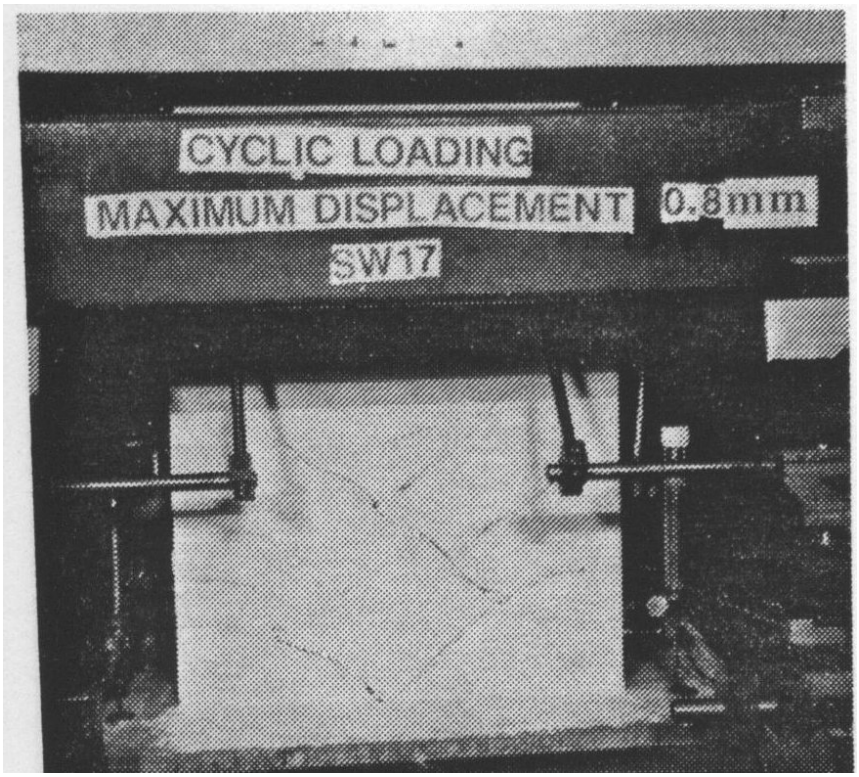


**Figure C-144 Condition of wall SW17 at 0.16% drift [Lopes and Elnashai (1991)]**

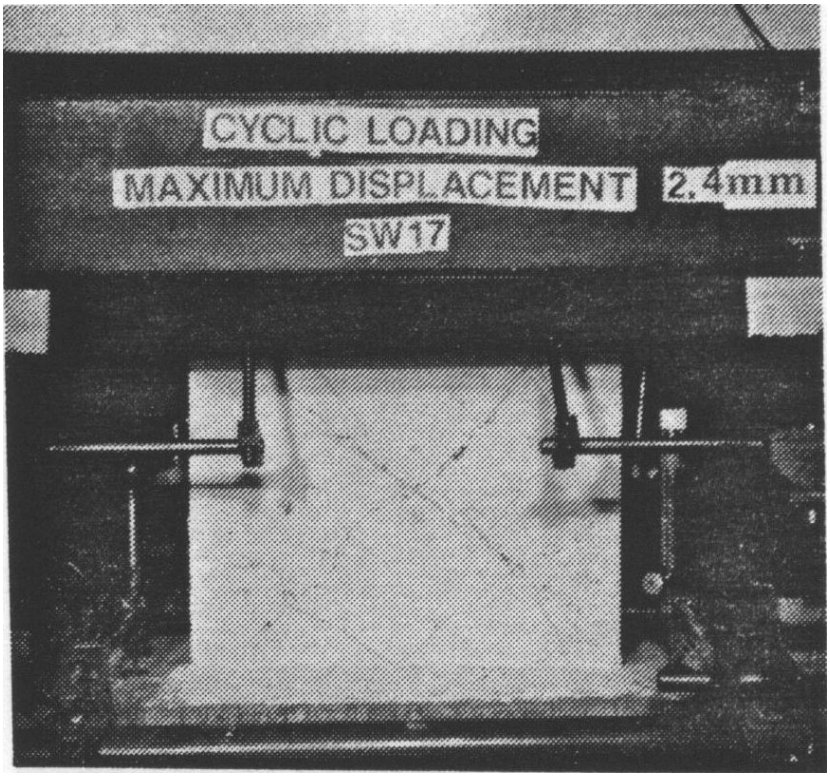


**Figure C-145 Condition of wall SW17 at 0.48% drift [Lopes and Elnashai (1991)]**

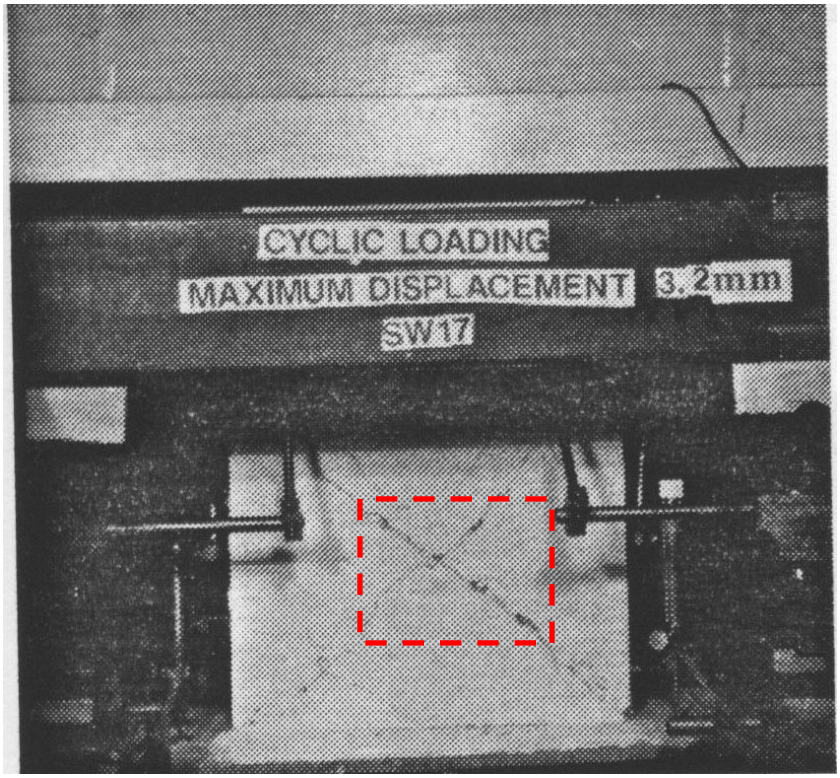


**Figure C-146 Condition of wall SW17 at 0.65% drift [Lopes and Elnashai (1991)]**


**Figure C-147 Condition of wall SW17 at 0.81% drift [Lopes and Elnashai (1991)]**

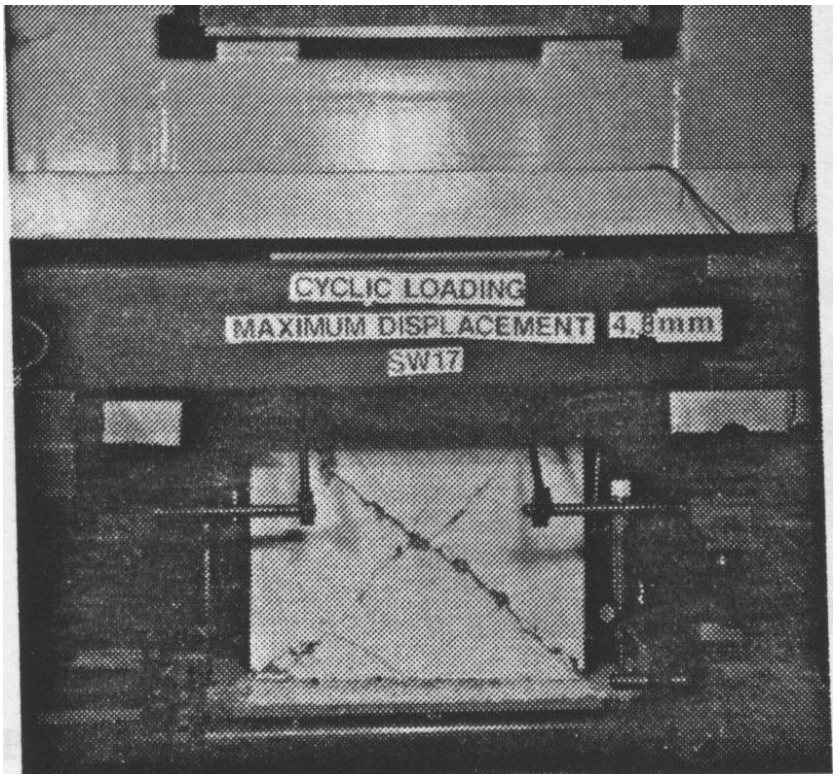


**Figure C-148 Condition of wall SW17 at 0.97% drift [Lopes and Elnashai (1991)]**

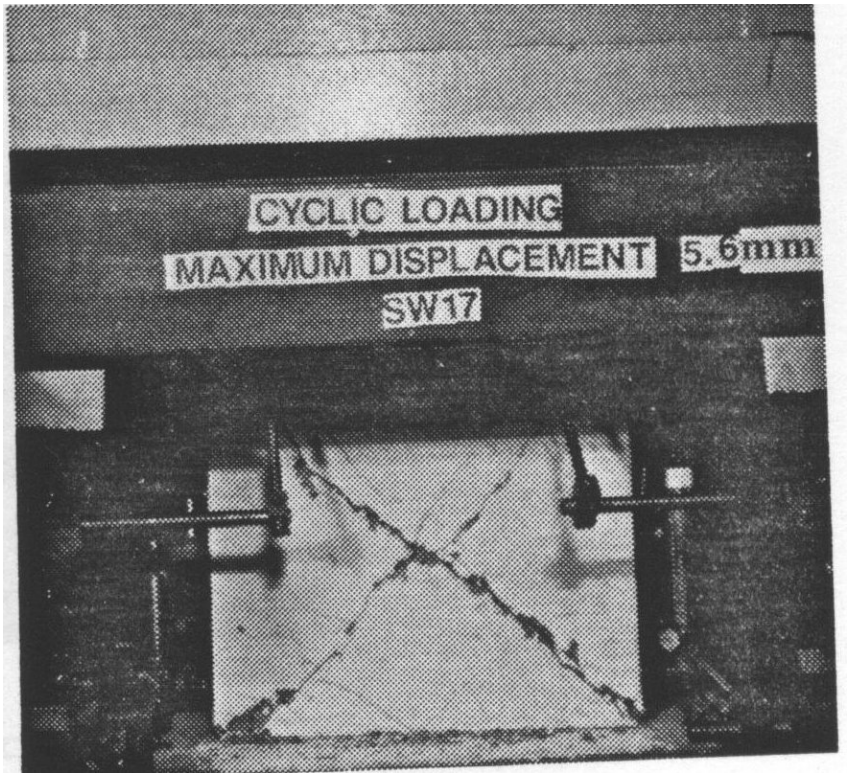


**Figure C-149 Condition of wall SW17 at 1.13% drift [Lopes and Elnashai (1991)]**

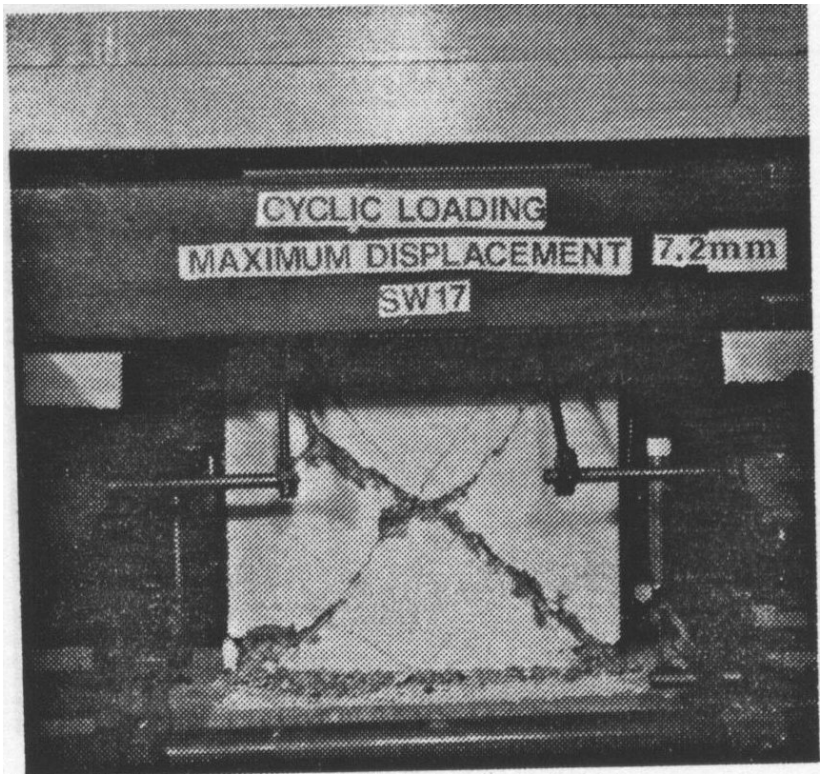


**Figure C-150 Condition of wall SW17 at 1.45% drift [Lopes and Elnashai (1991)]**

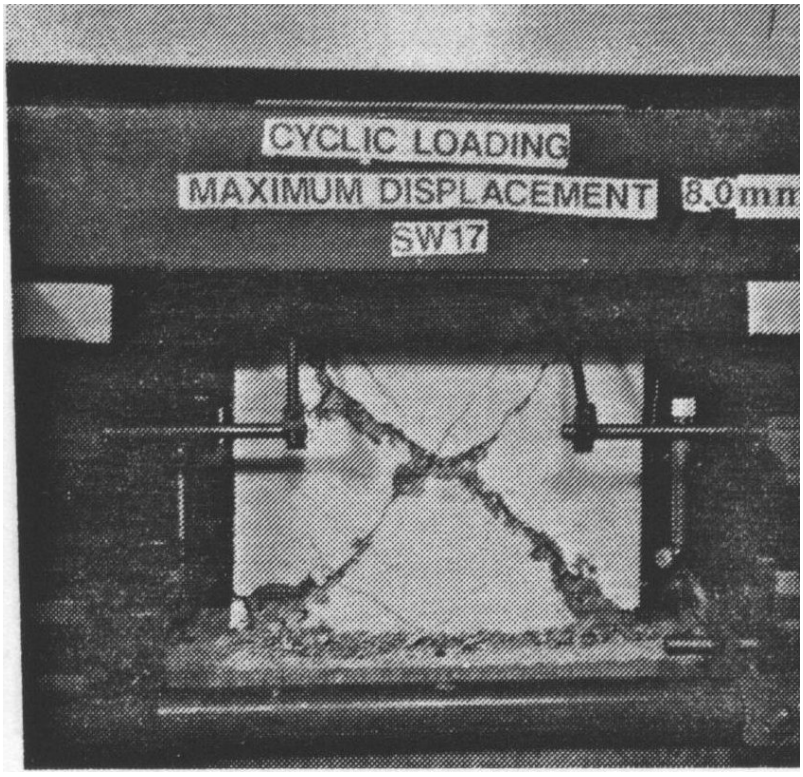


**Figure C-151 Condition of wall SW17 at 1.62% drift [Lopes and Elnashai (1991)]**

## C.1.8 Wiradinata (1985) Walls

### C.1.8.1 Wall 1

**Table C-29 Evaluation of damage data for wall 1 tested by Wiradinata**

| Wall ID | MoR | Damage State (DS) | Drift (%) | Comments |
|---|---|---|---|---|
| Wall 1 | 1 | 1.3 | 0.18 | The drifts for these damage states are provided by the researcher. |
| | 2a | 2.1 | 0.52 | |
| | | 2.2 | 0.25 | |
| | | 2.3 | 1.02 | |
| | 3 | 3.1 | 1.07 | The image reported at this drift (Figure C-155) shows damage that can be repaired by partial wall replacement (MoR-3). The damaged region requiring partial wall replacement is identified using dashed boxes in Figure C-155. |
| | | 3.4 | 1.07 | The drifts for these damage states are provided by the researcher. |
| | 4 | 4.5 | 1.56 | |

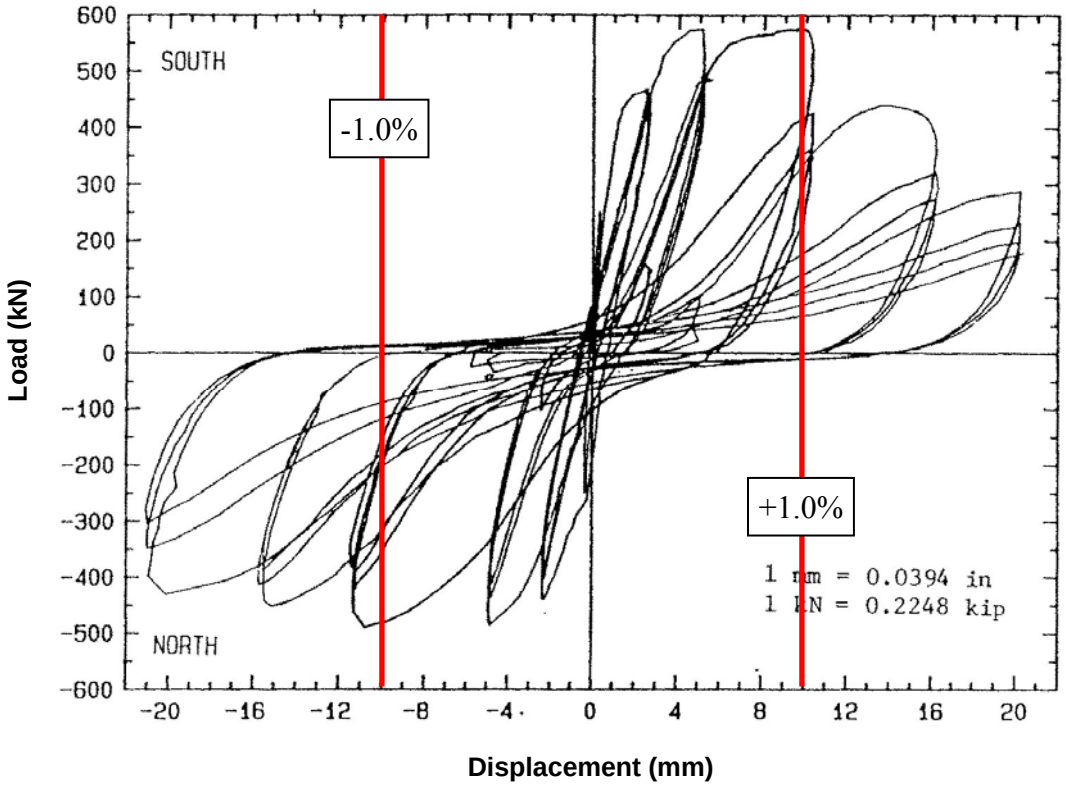


**Figure C-152 Load-displacement relationship for wall 1 [Wiradinata (1985)]**

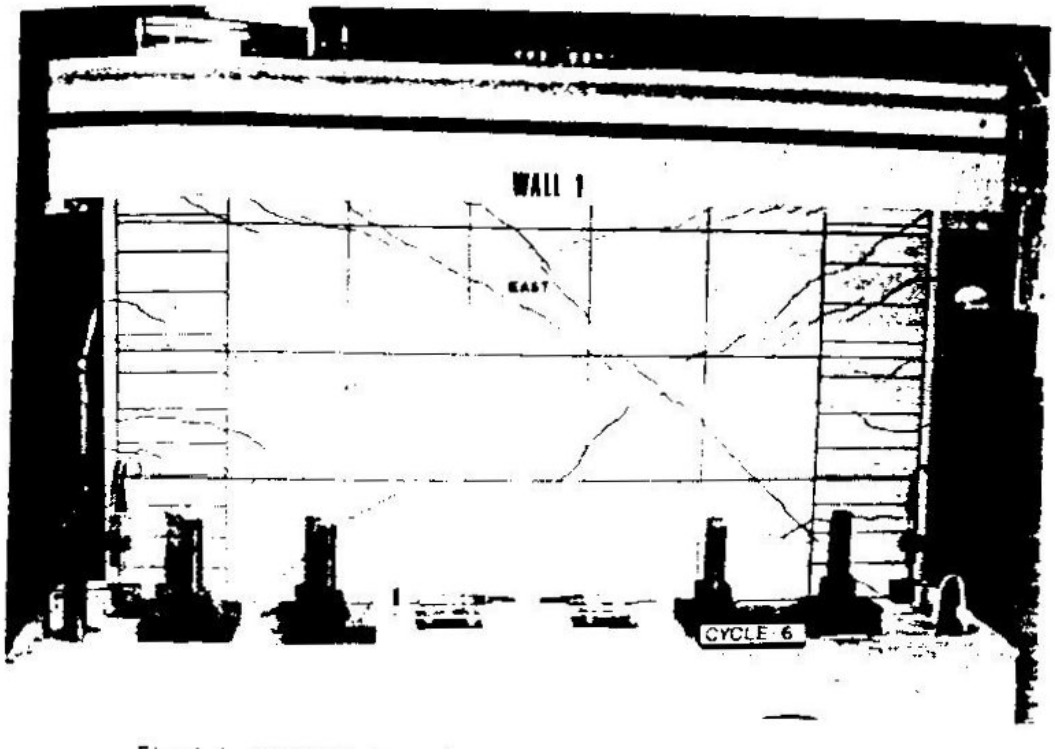


**Figure C-153 Condition of wall 1 at 0.25% drift [Wiradinata (1985)]**

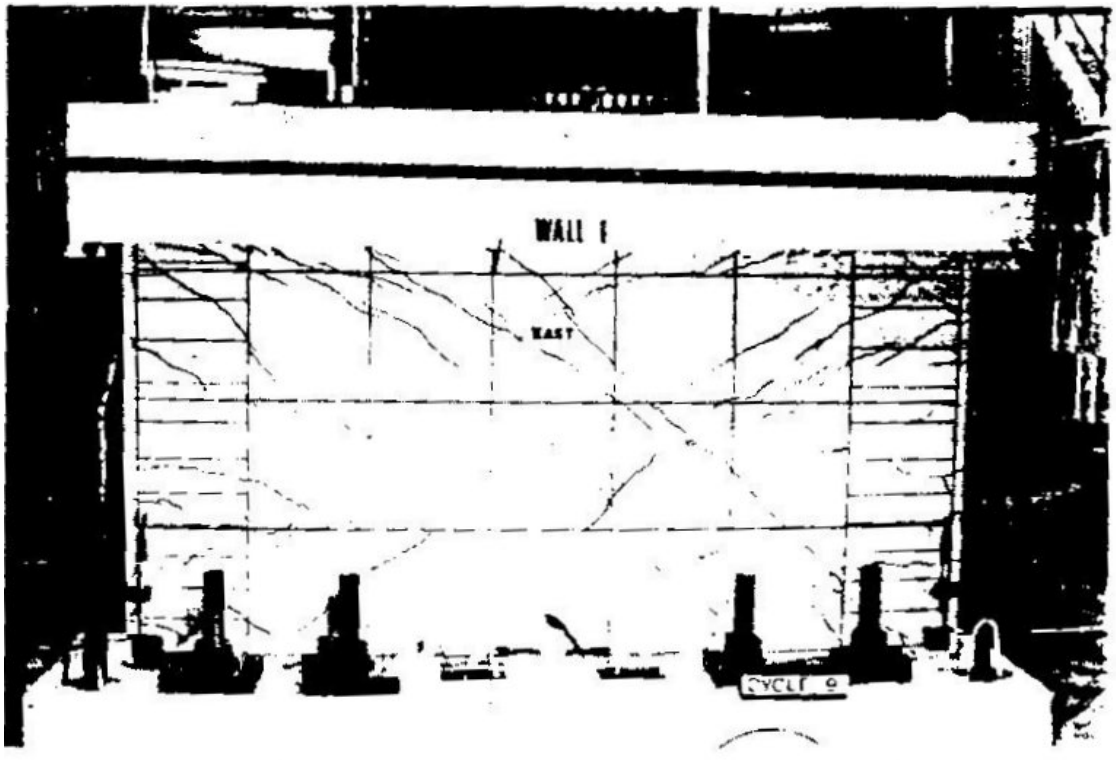


**Figure C-154 Condition of wall 1 at 0.52% drift [Wiradinata (1985)]**

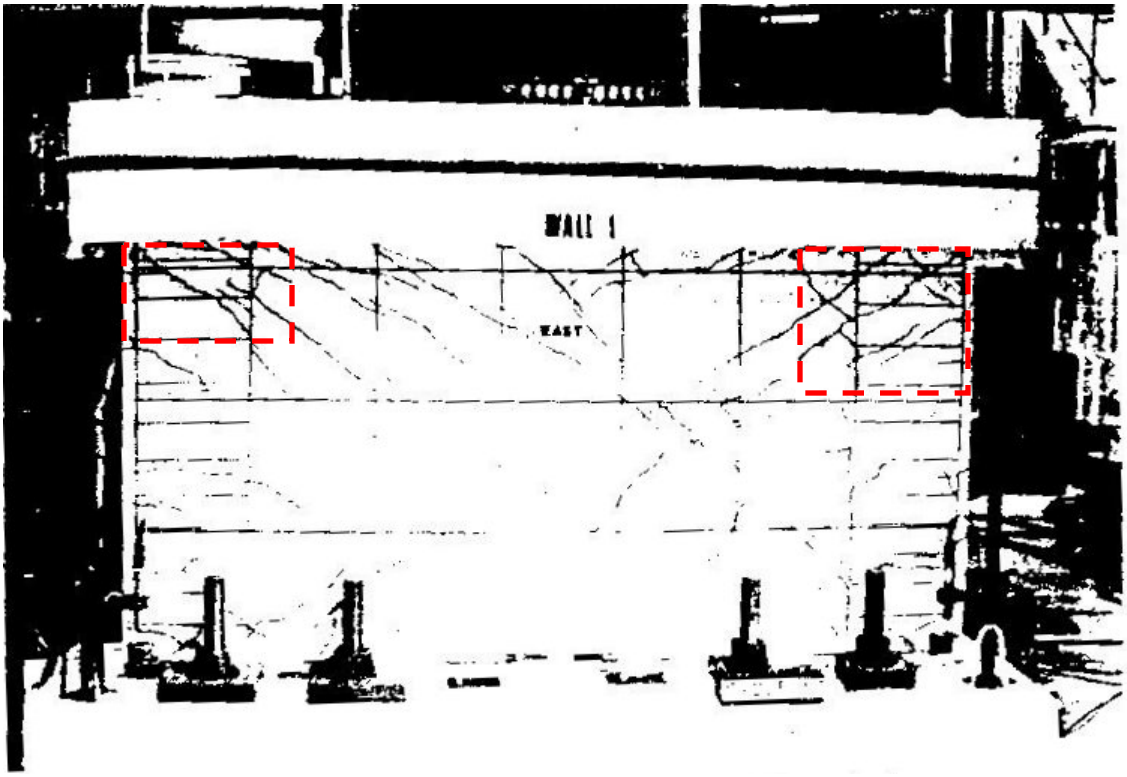


**Figure C-155 Condition of wall 1 at 1.07% drift [Wiradinata (1985)]**

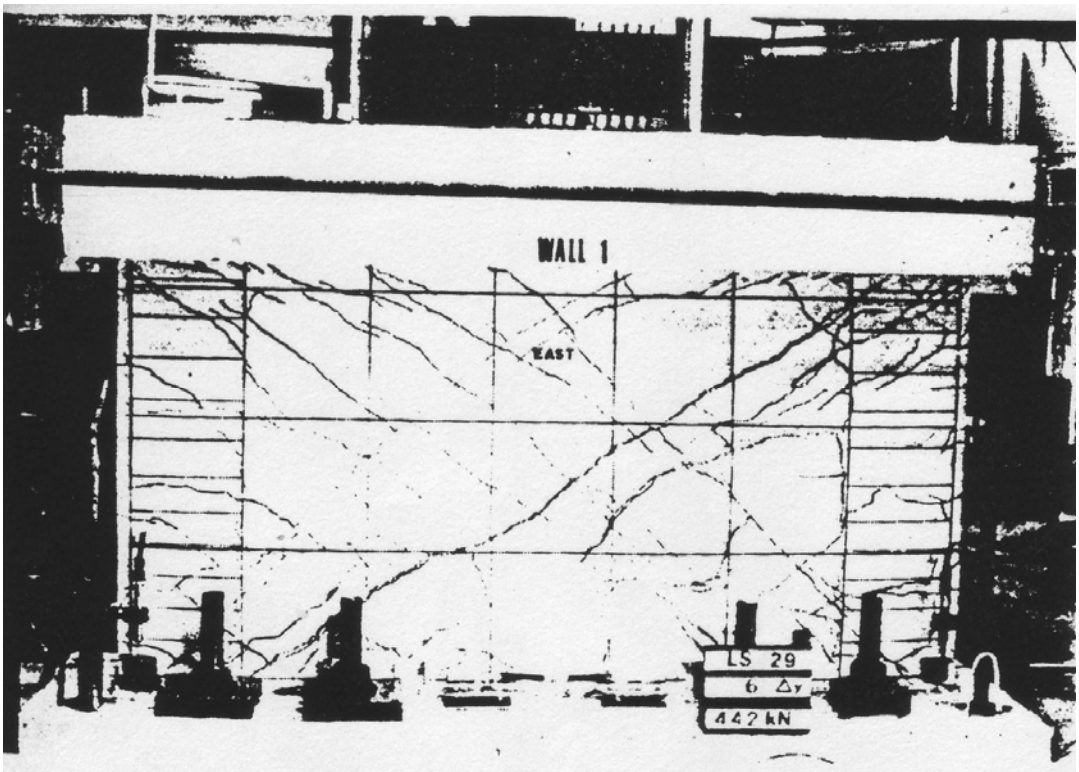


**Figure C-156 Condition of wall 1 at 1.56% drift [Wiradinata (1985)]**

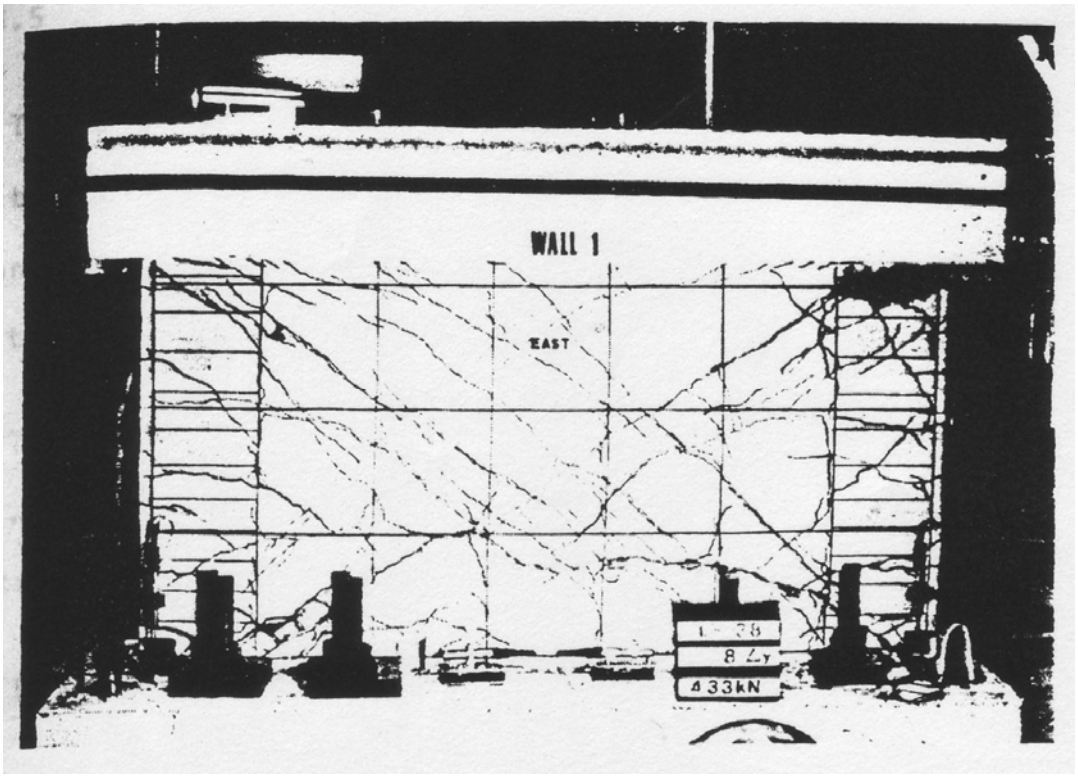


**Figure C-157 Condition of wall 1 at 2.00% drift [Wiradinata (1985)]**

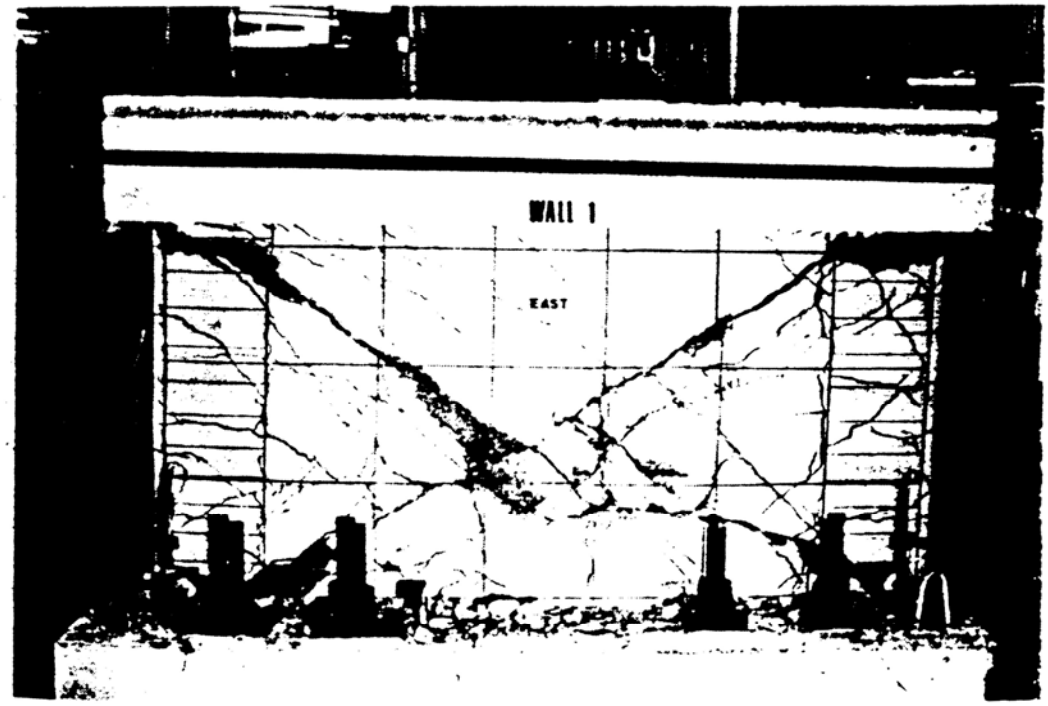


**Figure C-158 Condition of wall 1 at 2.00% drift (after the 3rd cycle at this drift level) [Wiradinata (1985)]**

### C.1.8.2 Wall 2

**Table C-30 Evaluation of damage data for wall 2 tested by Wiradinata**

| Wall ID | MoR | Damage State (DS) | Drift (%) | Comments |
|---|---|---|---|---|
| Wall 2 | 1 | 1.3 | 0.09 | The drifts for these damage states are provided by the researcher. |
| | 2a | 2.1 | 1.00 | |
| | | 2.2 | 0.68 | |
| | | 2.3 | 0.68 | |
| | 4 | 4.1 | 1.48 | The researcher reported that the wall failed by sliding shear and so the supplemental criteria are invoked to obtain a drift associated with this damage state. |
| | 4* | $SC_1$ | 1.48 | The smaller of the two drifts is obtained from the 1st quadrant of the load-displacement relationship (see Figure C-159). Note that, first exceedance of 1.0% residual drift limit corresponds to a peak transient drift of 2.24% with a residual drift of 1.77%. Therefore, linear interpolation is done to get the peak transient drift corresponding to a residual drift of 1.0%. |
| | | $SC_2$ | N/A | The post-peak resistance computed using the first cycle backbone curve did not drop to $0.5V_{peak}$ (see Figure C-159). |

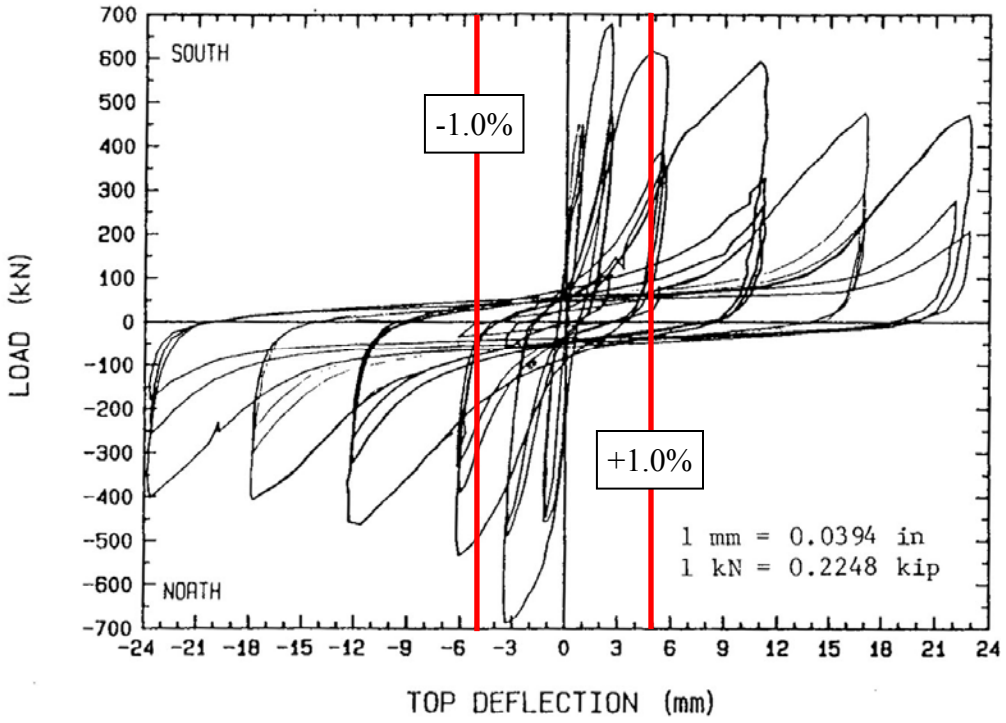


**Figure C-159 Load-displacement relationship for wall 2 [Wiradinata (1985)]**

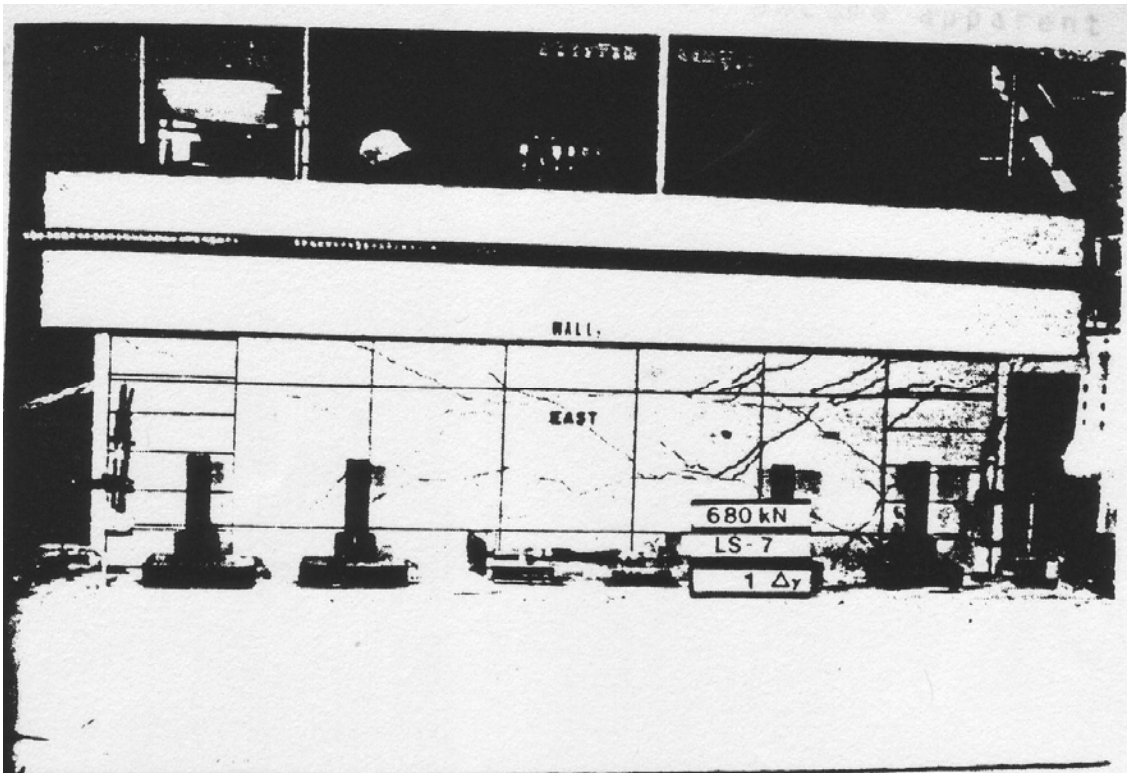


**Figure C-160 Condition of wall 2 at 0.53% drift [Wiradinata (1985)]**

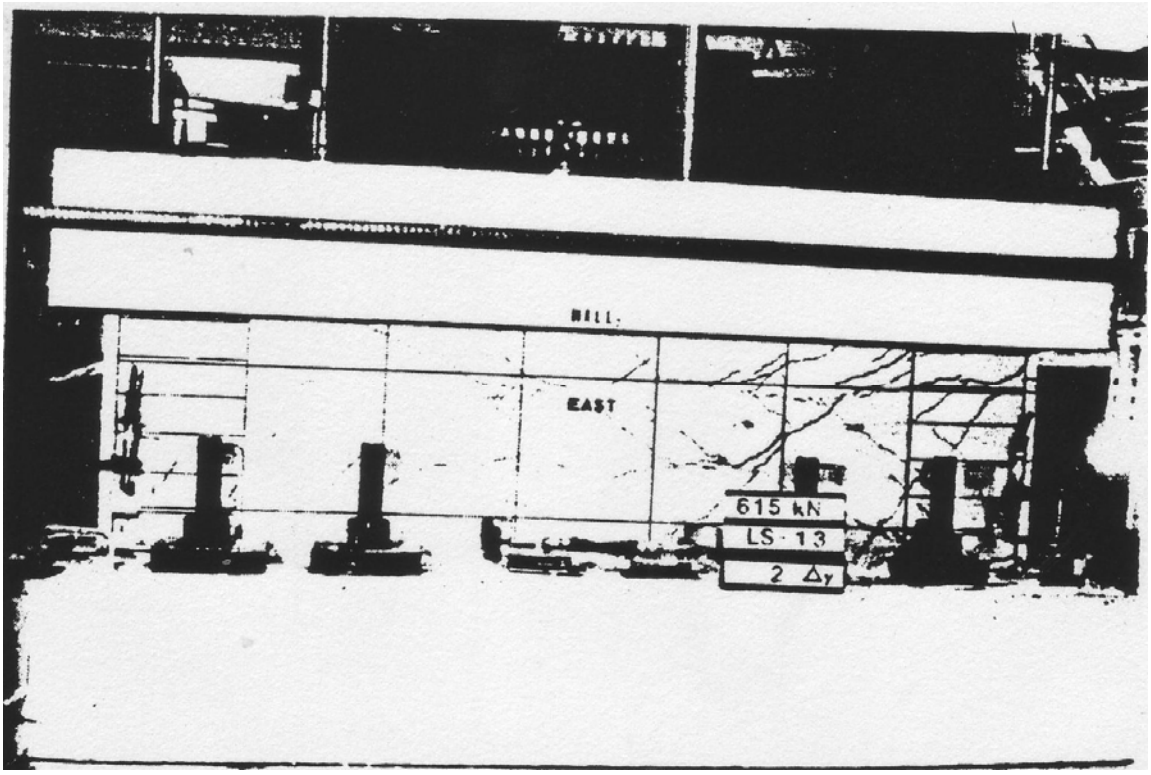


**Figure C-161 Condition of wall 2 at 1.0% drift [Wiradinata (1985)]**

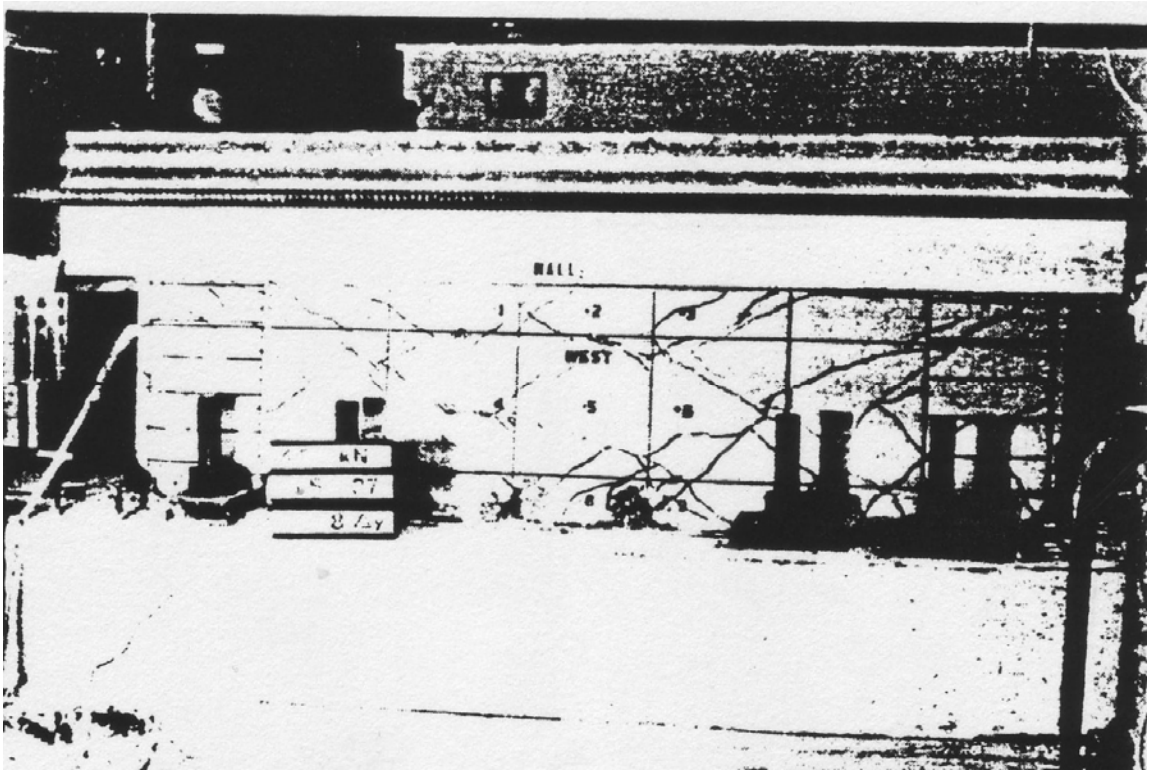


**Figure C-162 Condition of wall 2 at 4.58% drift [Wiradinata (1985)]**

### C.1.8.3 Pilette (1987) Walls

### C.1.8.4 Wall 4

**Table C-31 Evaluation of damage data for wall 4 tested by Pilette**

| Wall ID | MoR | Damage State (DS) | Drift (%) | Comments |
|---|---|---|---|---|
| Wall 4 | 1 | 1.2 | 0.16 | The drifts for these damage states are provided by the researcher. |
| | | 1.3 | 0.16 | |
| | 2a | 2.3 | 0.50 | |
| | | 2.5a | 0.40 | |
| | 2b | 2.5b | 0.80 | |
| | 4 | 4.1 | 1.60 | The researcher reported that the wall failed by sliding shear and so the supplemental criteria are invoked to obtain a drift associated with this damage state. |
| | 4* | $SC_1$ | 1.60 | The same drift is obtained from both quadrants (see Figure C-163, red circles). |
| | | $SC_2$ | N/A | The post-peak resistance computed using the first cycle backbone curve did not drop to $0.5V_{peak}$ (see Figure C-163). |

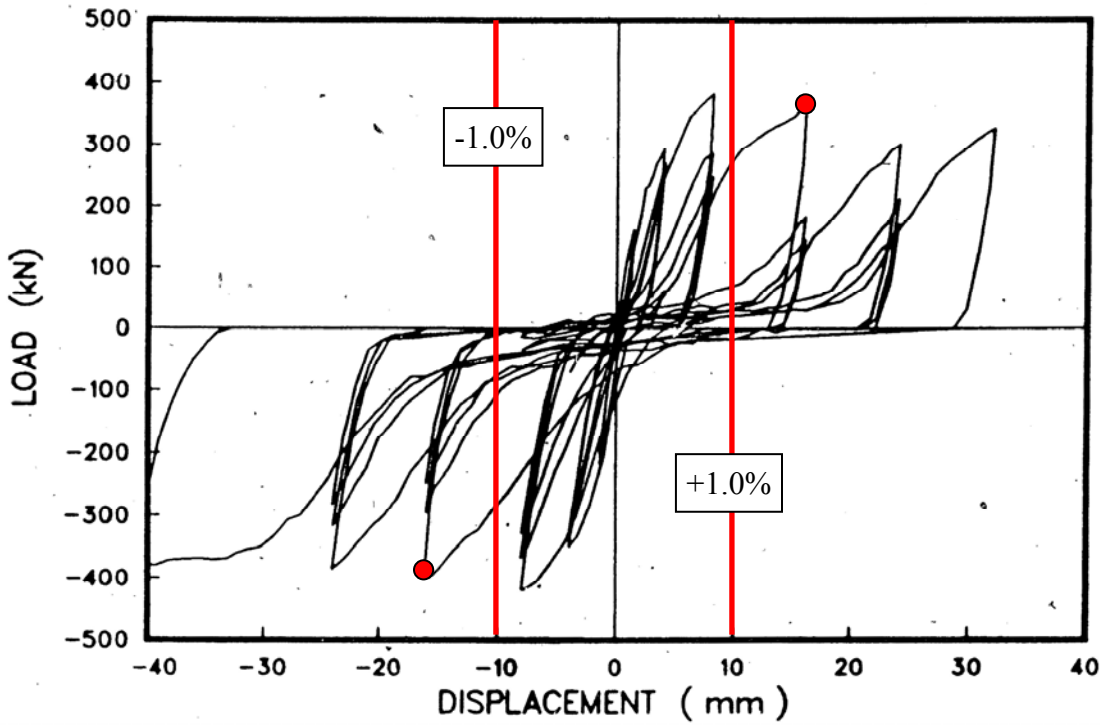


**Figure C-163 The load-displacement relationship for wall 4 [Pilette (1987)]**

### C.1.8.4.1 Wall 5

**Table C-32 Evaluation of damage data for wall 5 tested by Pilette**

| Wall ID | MoR | Damage State (DS) | Drift (%) | Comments |
|---|---|---|---|---|
| Wall 5 | 1 | 1.3 | 0.08 | The drifts for these damage states are provided by the researcher. |
| | 2a | 2.3 | 0.57 | |
| | | 2.5a | 0.68 | |
| | 2b | 2.5b | 0.68 | |
| | 4 | 4.1 | 1.14 | The researcher reported that the wall failed by sliding shear and so the supplemental criteria are invoked to obtain a drift associated with this damage state. |
| | 4* | $SC_1$ | 1.14 | The smaller of the two drifts is obtained from the 1st quadrant of the load-displacement relationship (see Figure C-164, red circle). The corresponding residual drift is slightly less than 1.0%. |
| | | $SC_2$ | 3.63 | The smaller of the two drifts is obtained from the 3rd quadrant of the load-displacement relationship (see Figure C-164). |

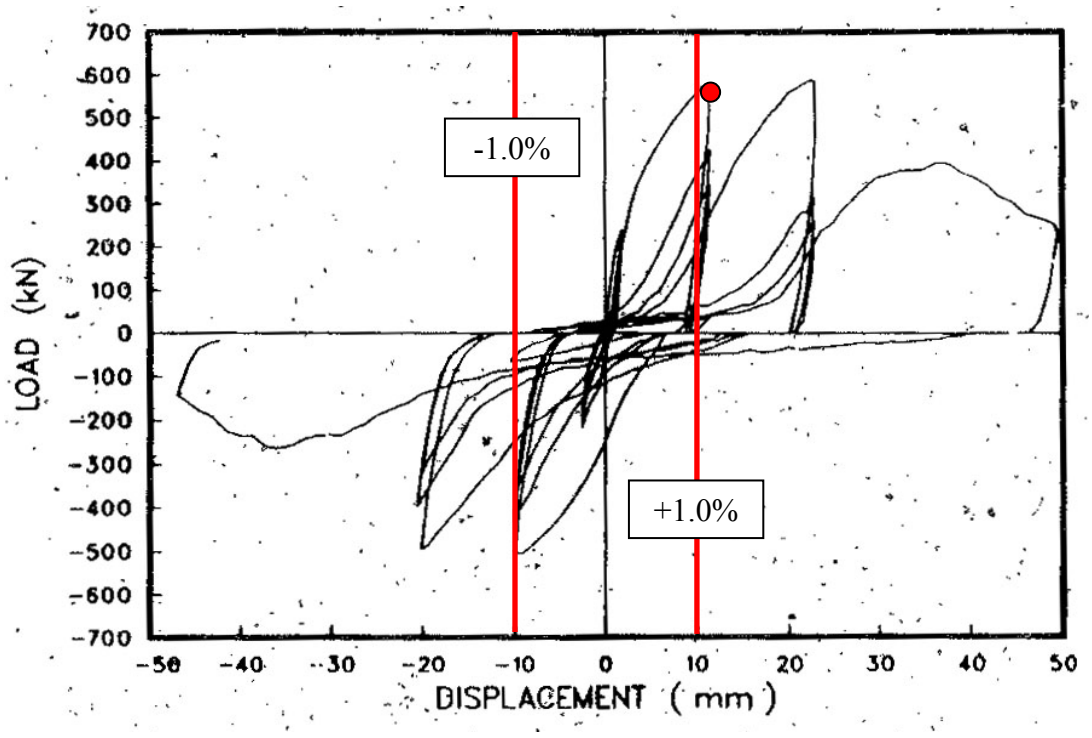


**Figure C-164 Load-displacement relationship for wall 5 [Pilette (1987)]**

## C.1.9 Mohammadi-Doostdar (1994) Walls

### C.1.9.1 Wall 7

**Table C-33 Evaluation of damage data for wall 7 tested by Mohammadi-Doostdar**

| Wall ID | MoR | Damage State (DS) | Drift (%) | Comments |
|---|---|---|---|---|
| Wall 7 | 1 | 1.2 | 0.07 | The drifts for these damage states are provided by the researcher. |
| | 2a | 2.3 | 0.33 | |
| | 3 | 3.1 | 1.02 | Based on the researcher's description of damage at this drift: "The concrete cover at the west end was badly damaged near the foundation and started to crush…" [Mohammadi-Doostdar (1994), page 50]. The damaged region requiring partial wall replacement is identified using a dashed box in Figure C-168. |
| | 4 | 4.1 | 1.68 | The researcher reported that the wall failed by sliding shear and so the supplemental criteria are invoked to obtain a drift associated with this damage state. |
| | | 4.3 | 2.34 | An image reported at this drift (Figure C-172) shows widespread crushing. |
| | 4* | $SC_1$ | 1.68 | The smaller of the two drifts is obtained from the 1st quadrant of the load-displacement relationship (see Figure C-165, red circle). |
| | | $SC_2$ | N/A | The post-peak resistance computed using the first cycle backbone curve did not drop to $0.5V_{peak}$ (see Figure C-165). |

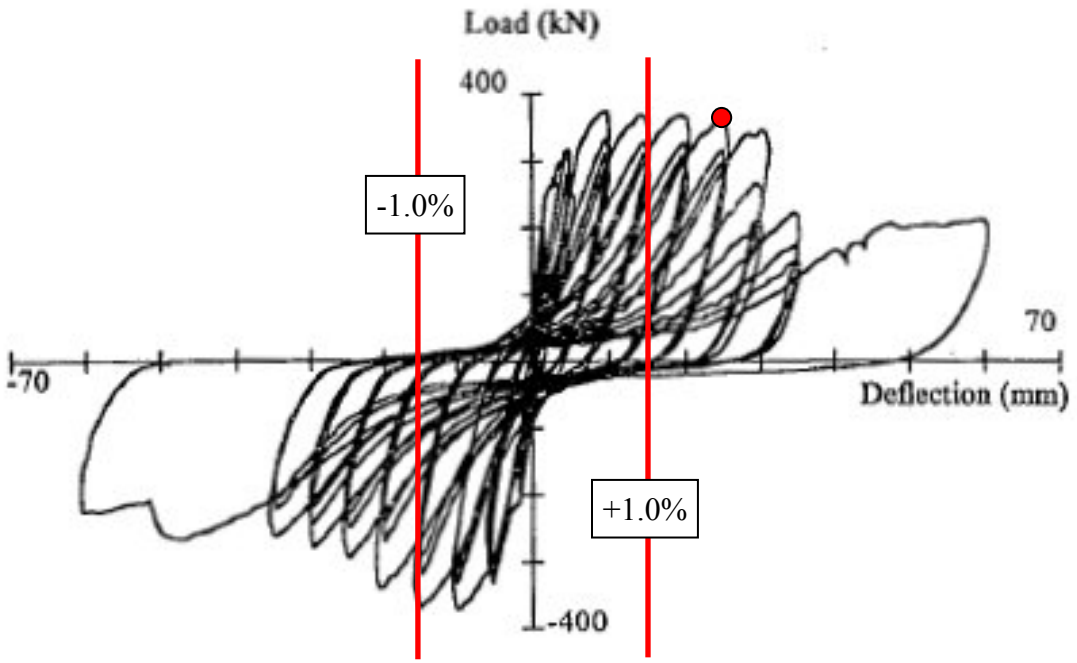


**Figure C-165 Load-displacement relationship for wall 7 [Mohammadi-Doostdar (1994)]**

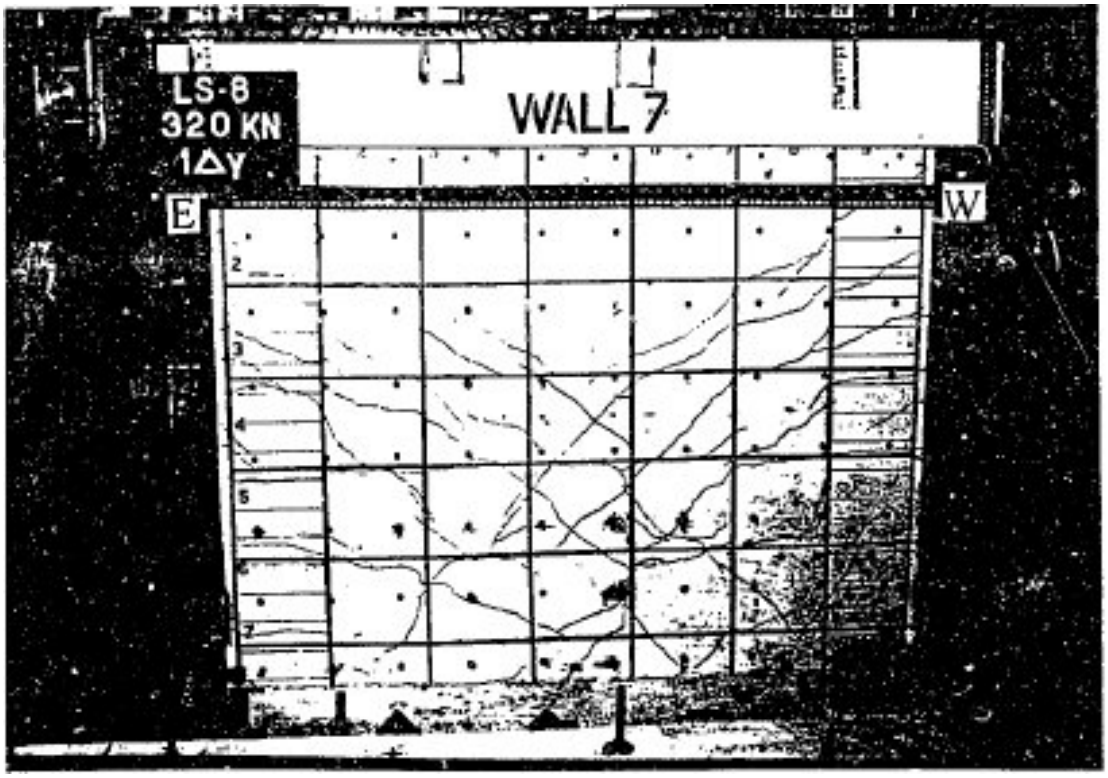


**Figure C-166 Condition of wall 7 at -0.37% drift [Mohammadi-Doostdar (1994)]**

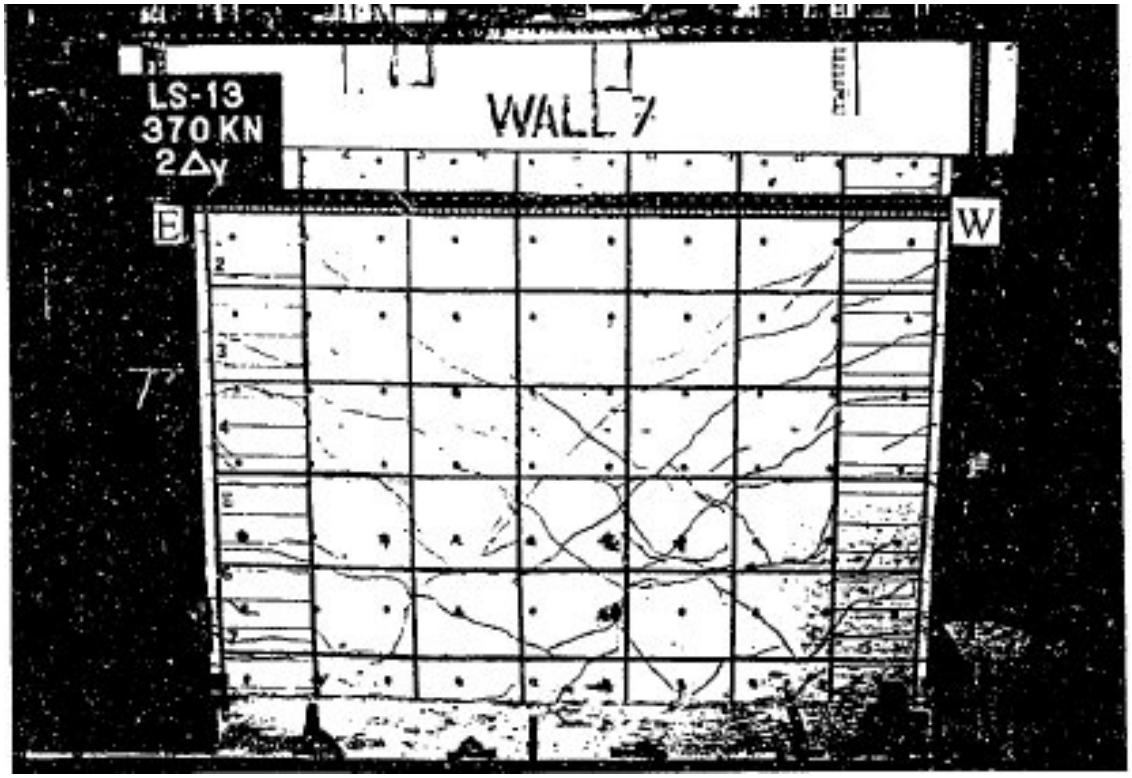


**Figure C-167 Condition of wall 7 at 0.61% drift [Mohammadi-Doostdar (1994)]**

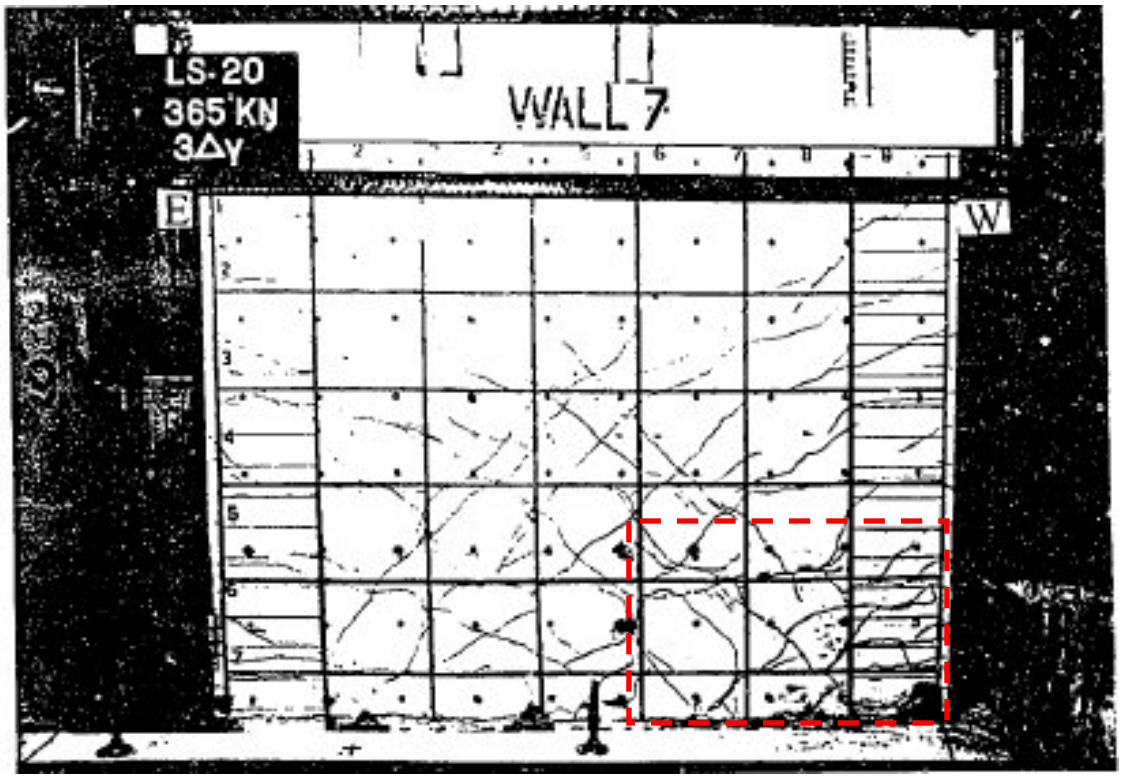


**Figure C-168 Condition of wall 7 at -1.02% drift [Mohammadi-Doostdar (1994)]**

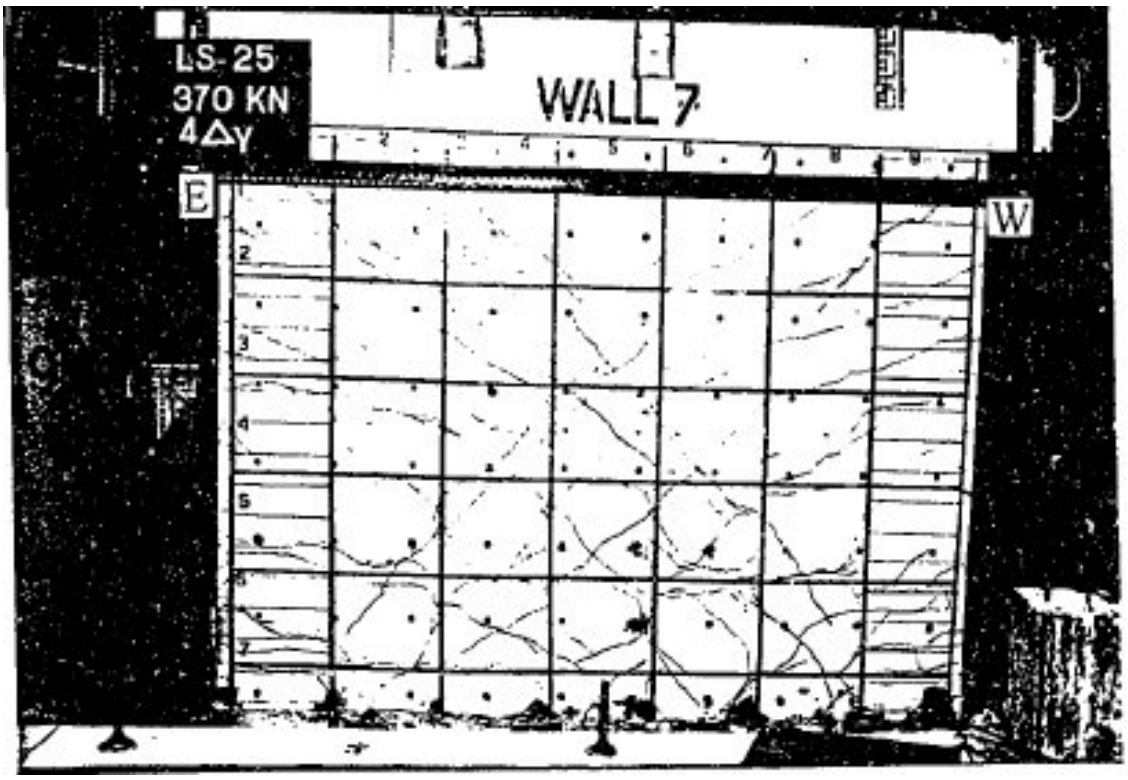


**Figure C-169 Condition of wall 7 at 1.34% drift [Mohammadi-Doostdar (1994)]**

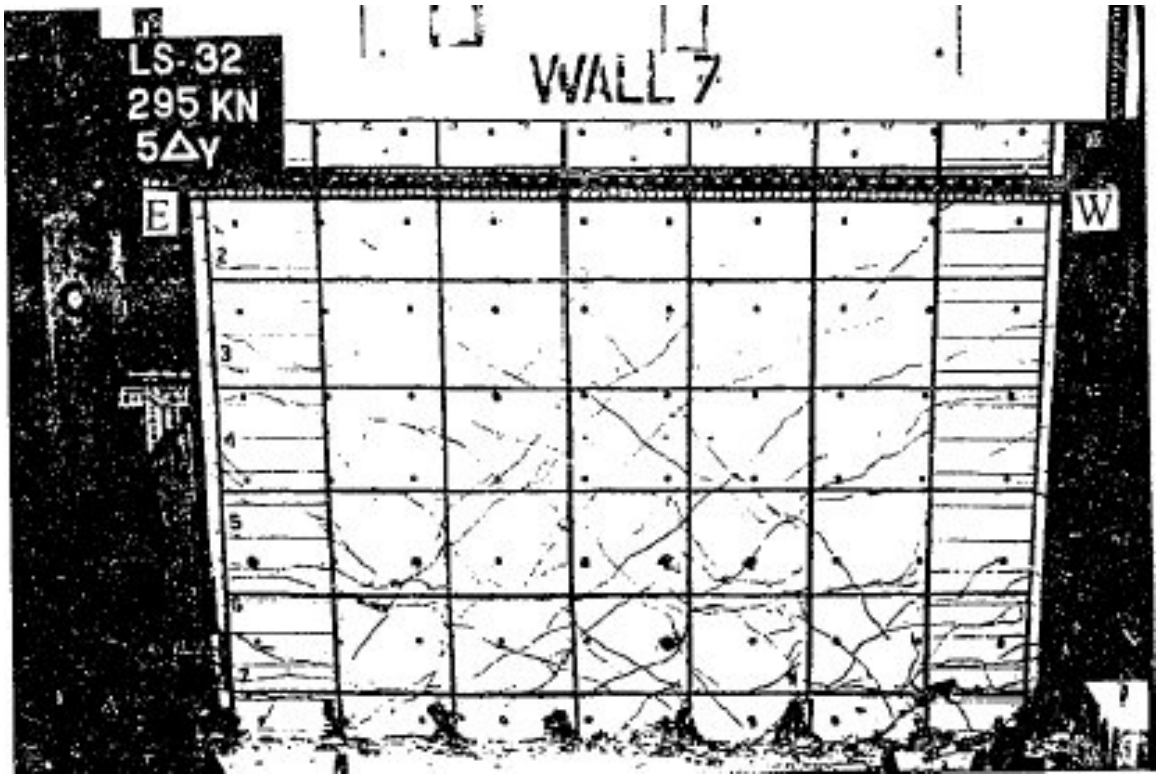


**Figure C-170 Condition of wall 7 at -1.64% drift [Mohammadi-Doostdar (1994)]**

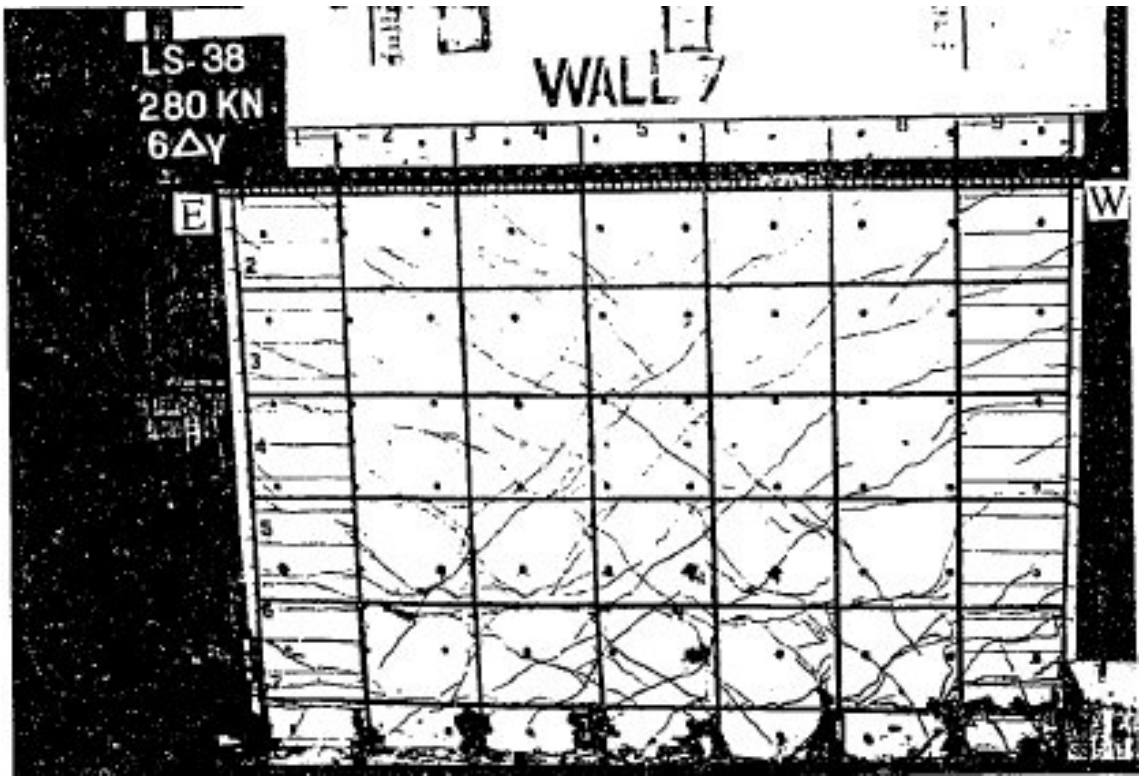


**Figure C-171 Condition of wall 7 at -1.98% drift [Mohammadi-Doostdar (1994)]**

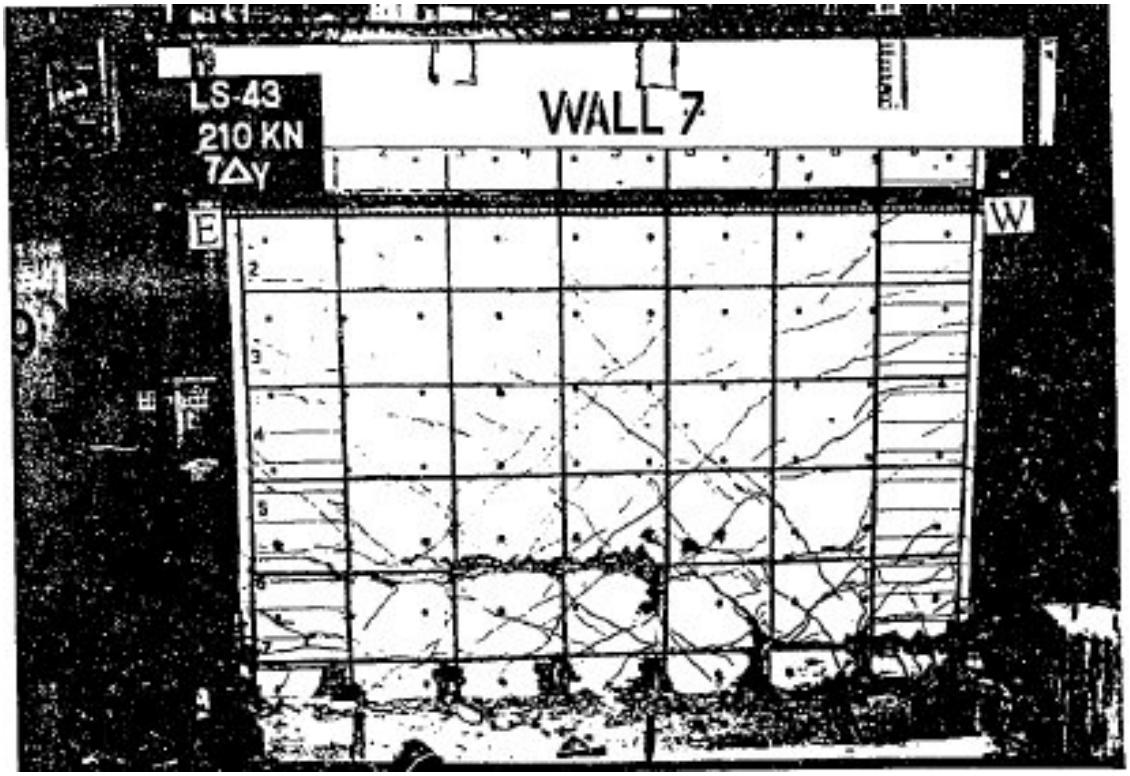


**Figure C-172 Condition of wall 7 at 2.34% drift [Mohammadi-Doostdar (1994)]**

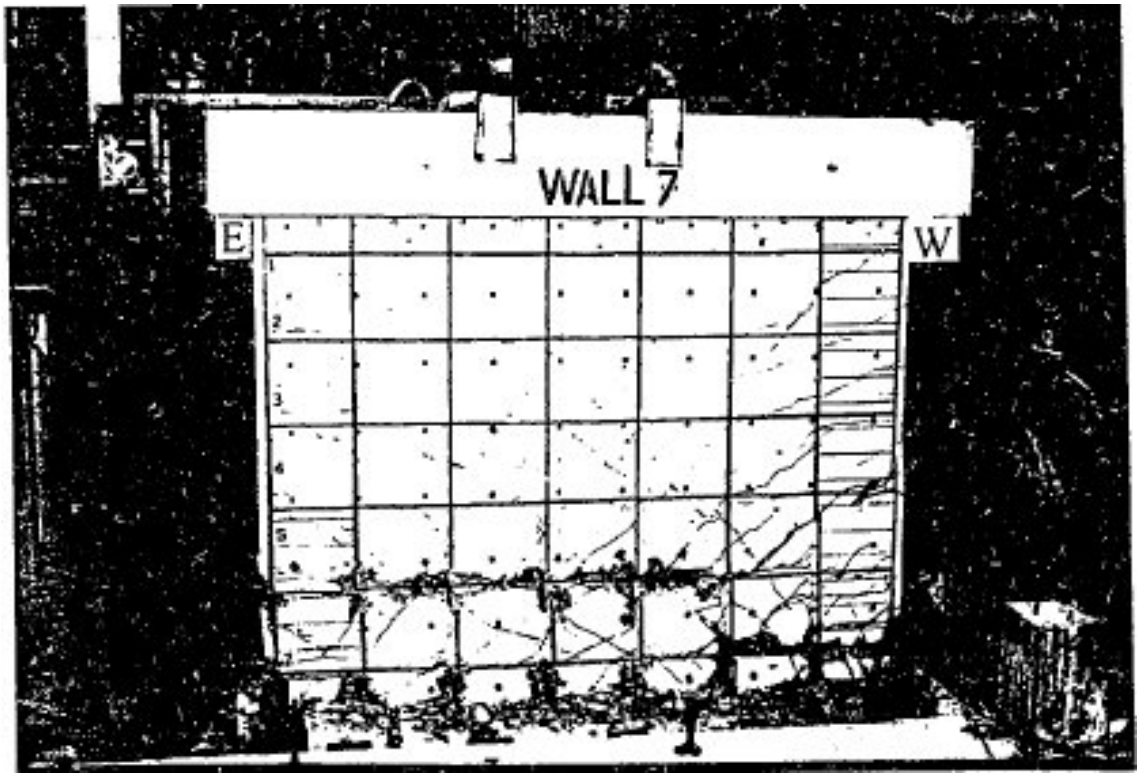


**Figure C-173 Condition of wall 7 at 4.03% drift [Mohammadi-Doostdar (1994)]**

### C.1.9.2 Wall 8

**Table C-34 Evaluation of damage data for wall 8 tested by Mohammadi-Doostdar**

| Wall ID | MoR | Damage State (DS) | Drift (%) | Comments |
|---|---|---|---|---|
| Wall 8 | 1 | 1.2 | 0.14 | The drift for this damage state is provided by the researcher. |
| | 3 | 3.1 | 1.46 | Based on the researcher's description of damage at this drift: "…the concrete cover at the west end was badly damaged near the foundation and started to crush…" [Mohammadi-Doostdar (1994), page 54]. The damaged region requiring partial wall replacement is identified using dashed boxes in Figure C-176. |
| | 4 | 4.1 | 1.46 | The researcher reported that the wall failed by sliding shear and so the supplemental criteria are invoked to obtain a drift associated with this damage state. |
| | | 4.4 | 2.47 | The drift for this damage state is provided by the researcher. |
| | 4* | $SC_1$ | 1.46 | The smaller of the two drifts is obtained from the 3rd quadrant of the load-displacement relationship (see Figure C-174, red circle). |
| | | $SC_2$ | N/A | The post-peak resistance computed using the first cycle backbone curve did not drop to $0.5V_{peak}$ (see Figure C-174). |

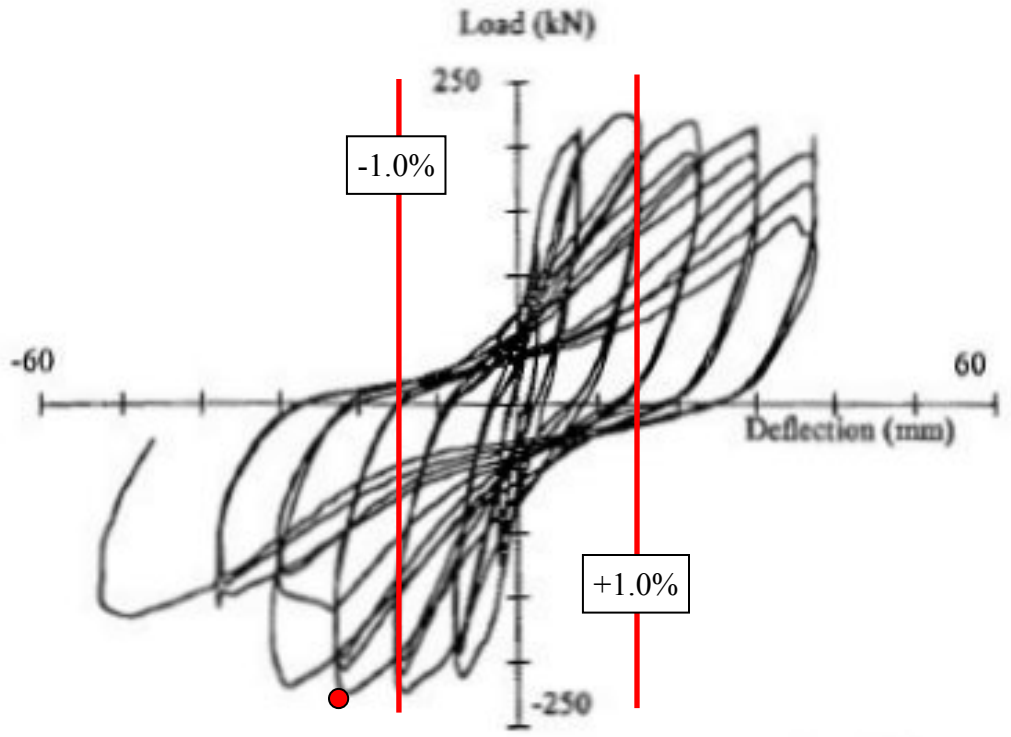


**Figure C-174 Load-displacement relationship for wall 8 [Mohammadi-Doostdar (1994)]**

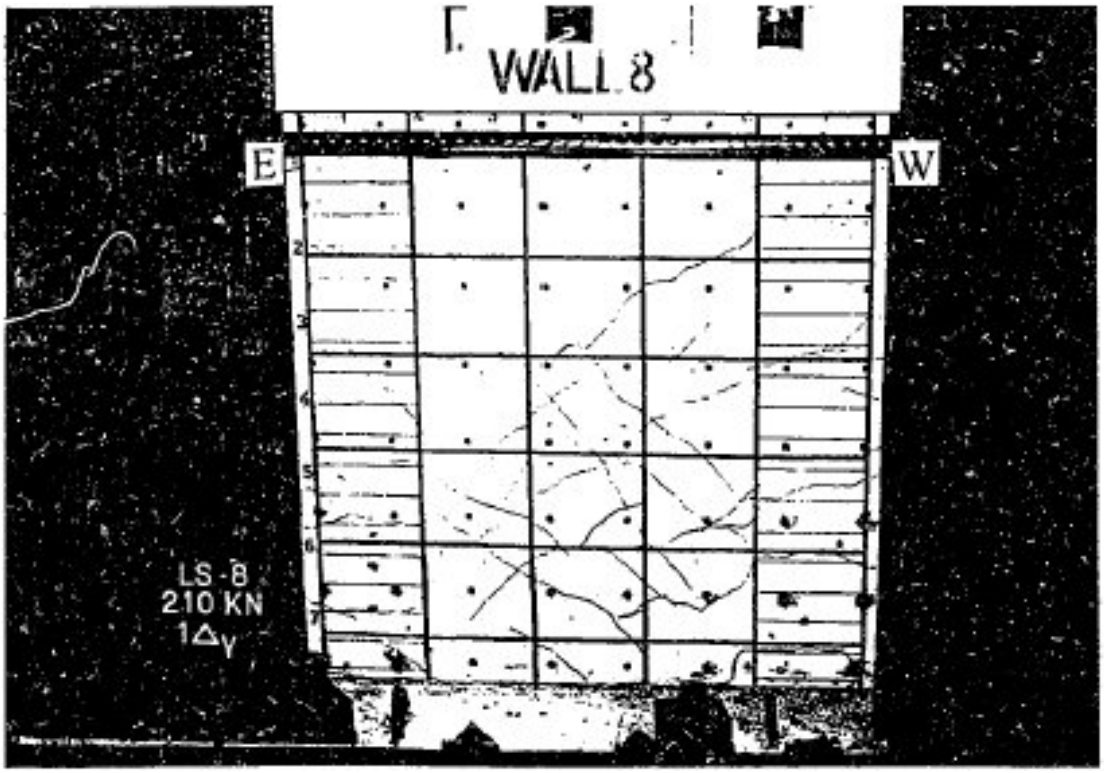


**Figure C-175 Condition of wall 8 at -0.48% drift [Mohammadi-Doostdar (1994)]**

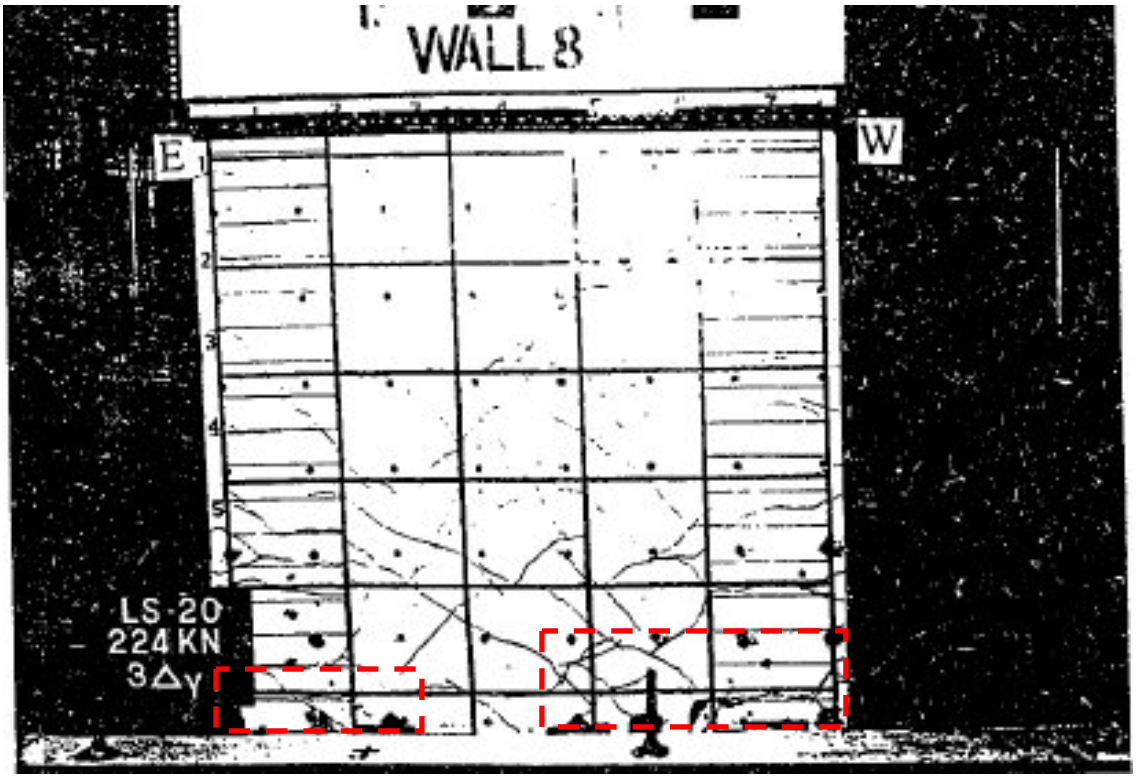


**Figure C-176 Condition of wall 8 at -1.46% drift [Mohammadi-Doostdar (1994)]**

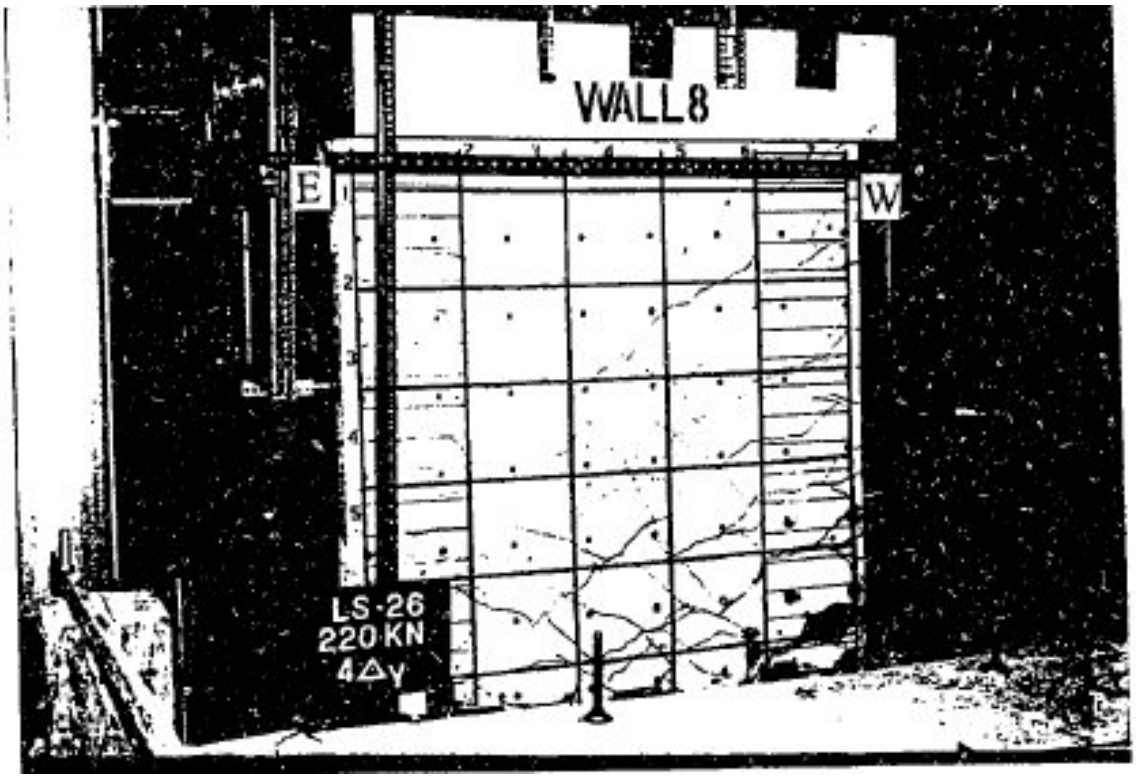


**Figure C-177 Condition of wall 8 at -1.95% drift [Mohammadi-Doostdar (1994)]**

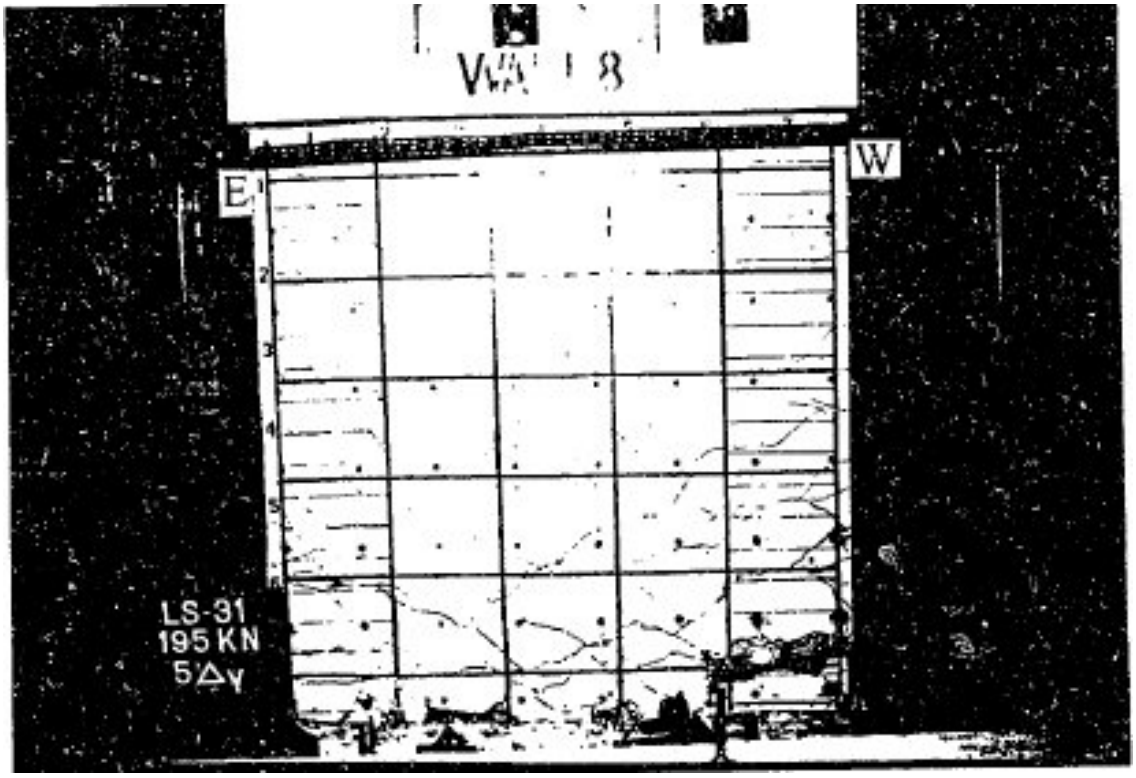


**Figure C-178 Condition of wall 8 at 2.47% drift [Mohammadi-Doostdar (1994)]**

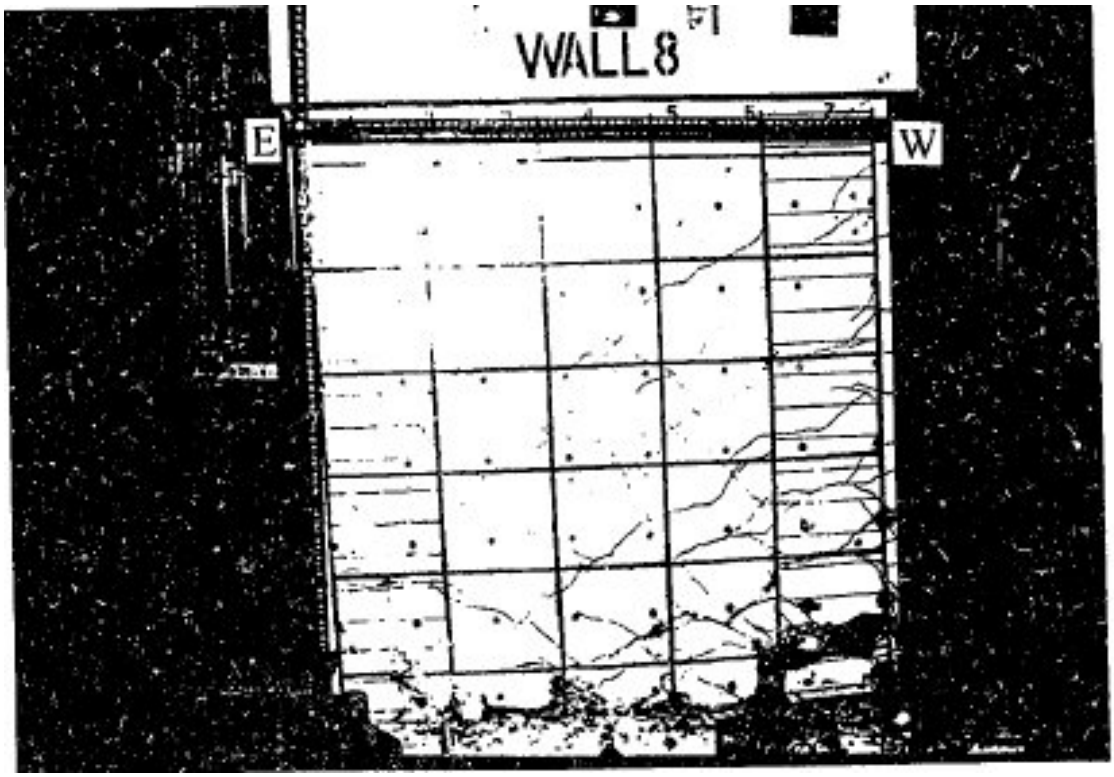


**Figure C-179 Condition of wall 8 at -3.36% drift [Mohammadi-Doostdar (1994)]**

## C.1.10 Salonikios et al. (1999) Walls

### C.1.10.1 Wall LSW3

| Wall ID | MoR | Damage State (DS) | Drift (%) | Comments |
|---|---|---|---|---|
| LSW3 | 4 | 4.1 | 1.43 | The researcher reported that the wall failed by sliding shear and so the supplemental criteria are invoked to obtain a drift associated with this damage state. |
| | 4* | $SC_1$ | 1.43 | The data point is obtained from the 3rd quadrant of the load-displacement relationship (see Figure C-180, red circle). A data point cannot be established in the 1st quadrant. |
| | | $SC_2$ | N/A | The post-peak resistance computed using the first cycle backbone curve did not drop to $0.5V_{peak}$ (see Figure C-180). |

**Table C-35 Evaluation of damage data for wall LSW3 tested by Salonikios**

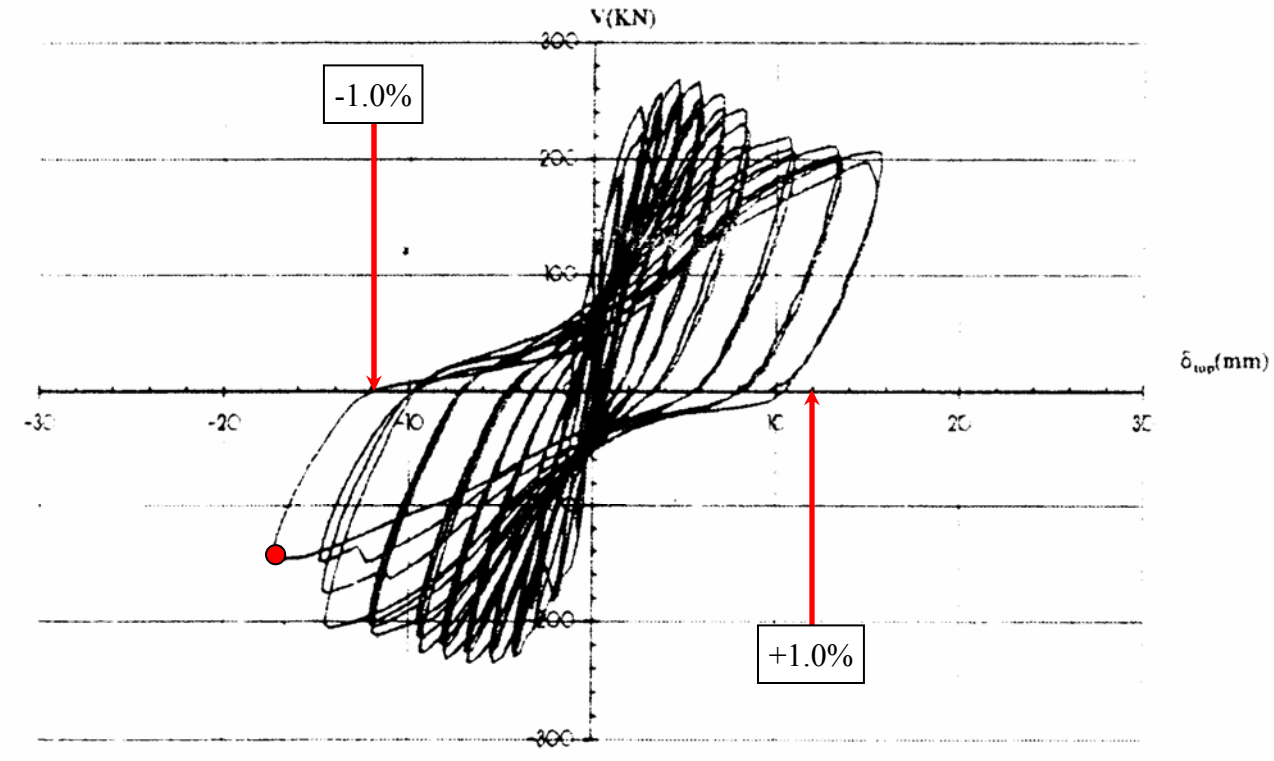


**Figure C-180 Load-displacement relationship for wall LSW3 [Salonikios et al. (1999)]**

**Figure C-181 Condition of wall LSW3 at the end of the test (maximum drift = 1.43%) [Salonikios et al. (1999)]**

### C.1.10.2 Wall MSW1

| Wall ID | MoR | Damage State (DS) | Drift (%) | Comments |
|---|---|---|---|---|
| MSW1 | 4 | 4.1 | 1.53 | The researcher reported that the wall failed by sliding shear and so the supplemental criteria are invoked to obtain a drift associated with this damage state. |
| | 4* | $SC_1$ | 1.53 | The data point is obtained from the 3rd quadrant of the load-displacement relationship (see Figure C-182, red circle). The corresponding residual drift is slightly less than 1.0%. A data point cannot be established in the 1st quadrant. |
| | | $SC_2$ | N/A | The post-peak resistance computed using the first cycle backbone curve did not drop to $0.5V_{peak}$ (see Figure C-182). |

**Table C-36 Evaluation of damage data for wall MSW1 tested by Salonikios**

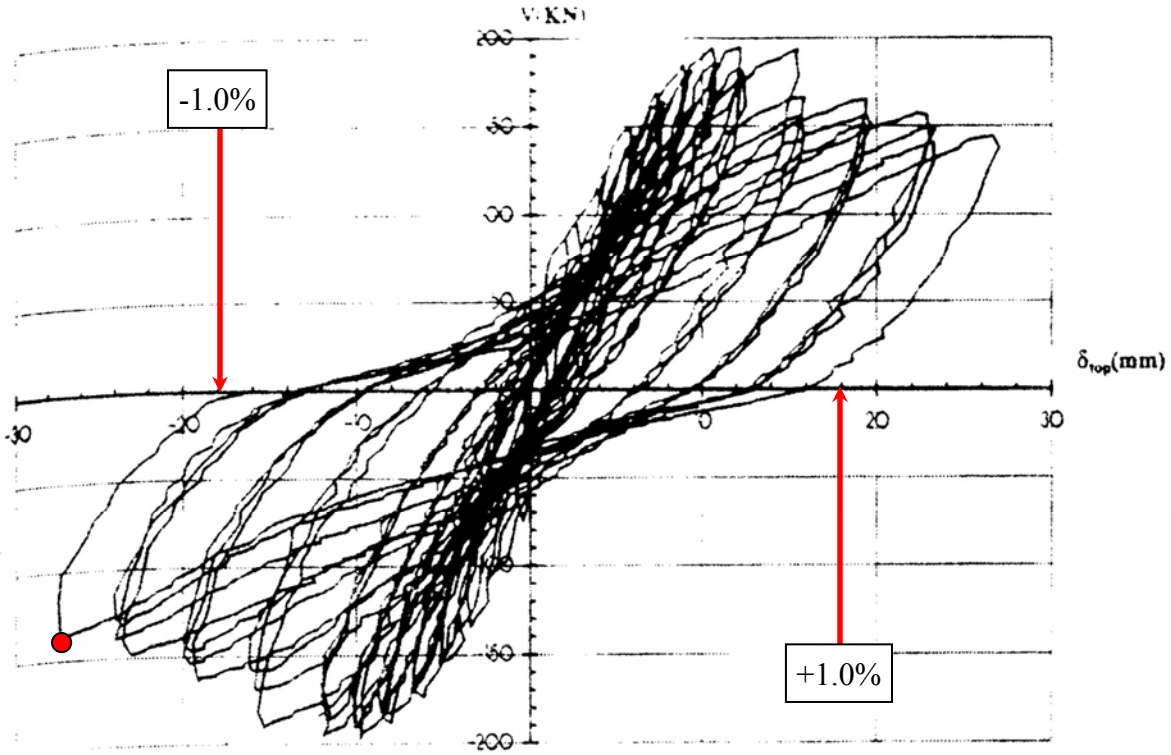


**Figure C-182 Load-displacement relationship for wall MSW1 [Salonikios et al. (1999)]**

**Figure C-183 Condition of wall MSW1 at the end of the test (maximum drift = 1.53%) [Salonikios et al. (1999)]**

### C.1.10.3 Wall MSW3

**Table C-37 Evaluation of damage data for wall MSW3 tested by Salonikios**

| Wall ID | MoR | Damage State (DS) | Drift (%) | Comments |
|---|---|---|---|---|
| MSW3 | 4 | 4.1 | 1.47 | The researcher reported that the wall failed by sliding shear and so the supplemental criteria are invoked to obtain a drift associated with this damage state. |
| | 4* | $SC_1$ | 1.47 | The data point is obtained from the 3rd quadrant of the load-displacement relationship (see Figure C-184, red circle). The corresponding residual drift is slightly less than 1.0%. A data point cannot be established in the 1st quadrant. |
| | | $SC_2$ | N/A | The post-peak resistance computed using the first cycle backbone curve did not drop to $0.5V_{peak}$ (see Figure C-184). |

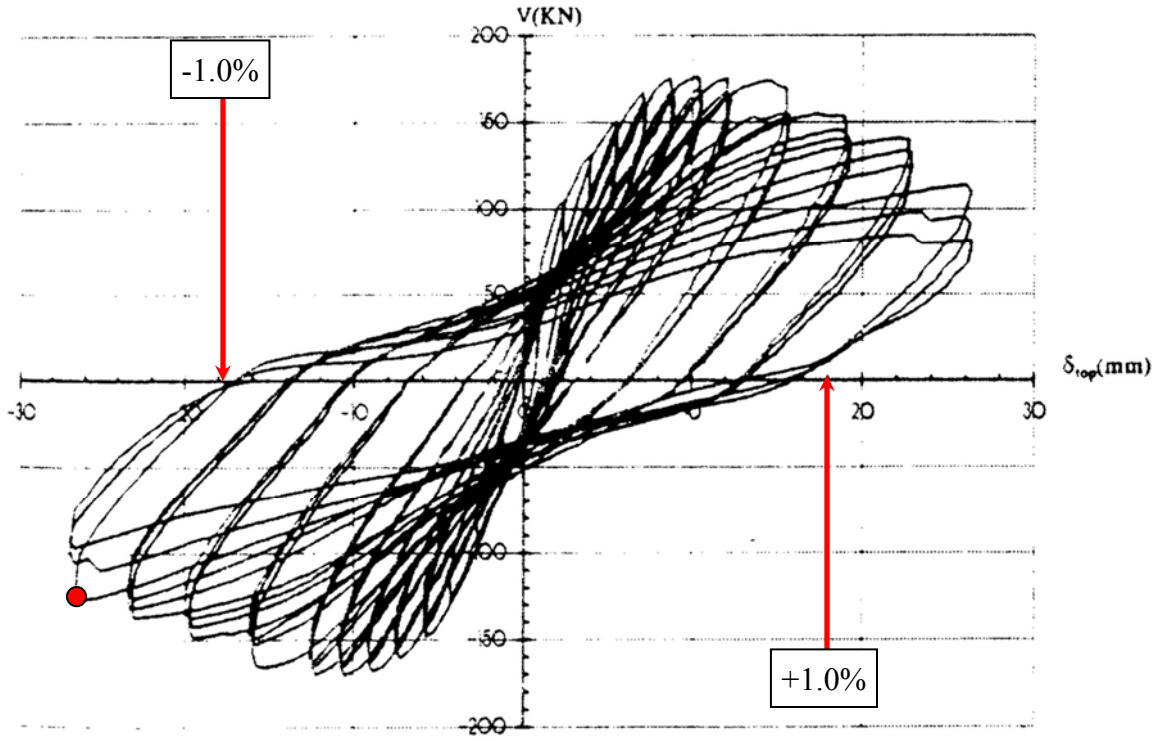


**Figure C-184 Load-displacement relationship for wall MSW3 [Salonikios et al. (1999)]**

**Figure C-185 Condition of wall MSW3 at the end of the test (maximum drift = 1.47%) [Salonikios et al. (1999)]**

### C.1.10.4 Wall MSW6

**Table C-38 Evaluation of damage data for wall MSW6 tested by Salonikios**

| Wall ID | MoR | Damage State (DS) | Drift (%) | Comments |
|---|---|---|---|---|
| MSW6 | 4 | 4.1 | 1.57 | The researcher reported that the wall failed by sliding shear and so the supplemental criteria are invoked to obtain a drift associated with this damage state. |
| | 4* | $SC_1$ | 1.57 | The smaller of the two drifts is obtained from the 3rd quadrant of the load-displacement relationship (see Figure C-186, red circle). |
| | | $SC_2$ | N/A | The post-peak resistance computed using the first cycle backbone curve did not drop to $0.5V_{peak}$ (see Figure C-186). |

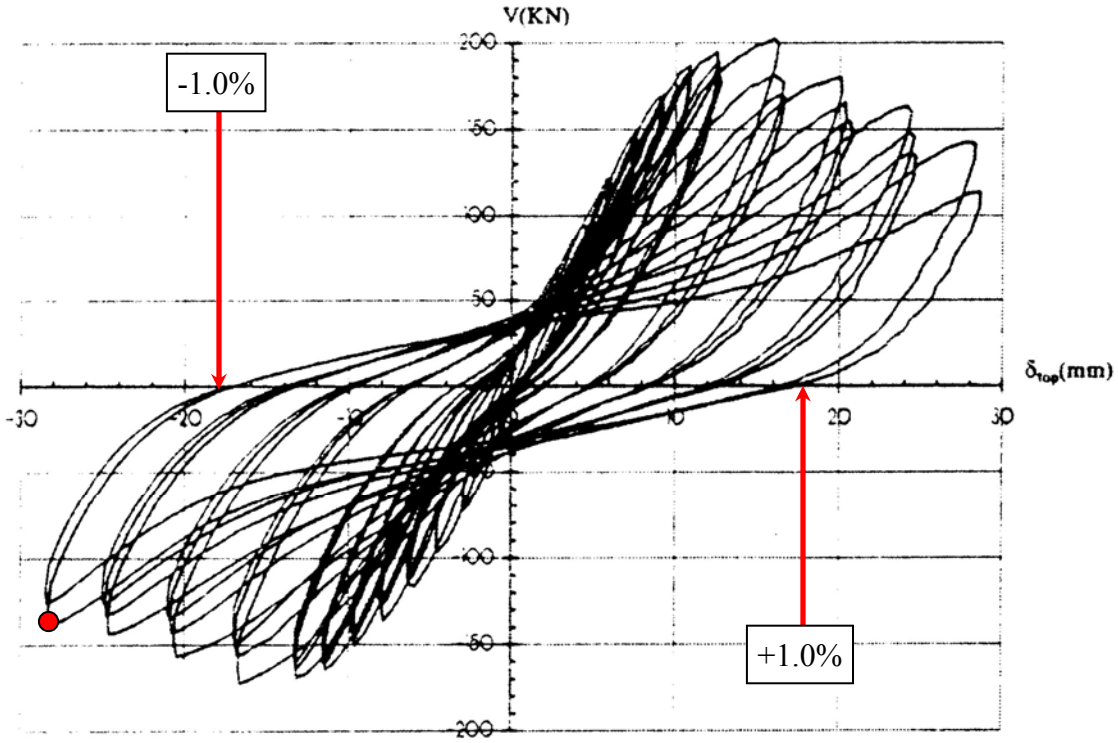


**Figure C-186 Load-displacement relationship for wall MSW6 [Salonikios et al. (1999)]**

**Figure C-187 Condition of wall MSW6 at the end of the test (maximum drift = 1.57%) [Salonikios et al. (1999)]**

## C.1.11 Hidalgo et al. (1998) Walls

### C.1.11.1 Specimen 23

**Table C-39 Evaluation of damage data for Specimen 23 tested by Hidalgo**

| Wall ID | MoR | Damage State (DS) | Drift (%) | Comments |
|---|---|---|---|---|
| Specimen 23 | 4 | 4.2 | 0.61 | The image reported at this drift (Figure C-189) shows major diagonal cracks that can be associated with diagonal tension failure. |

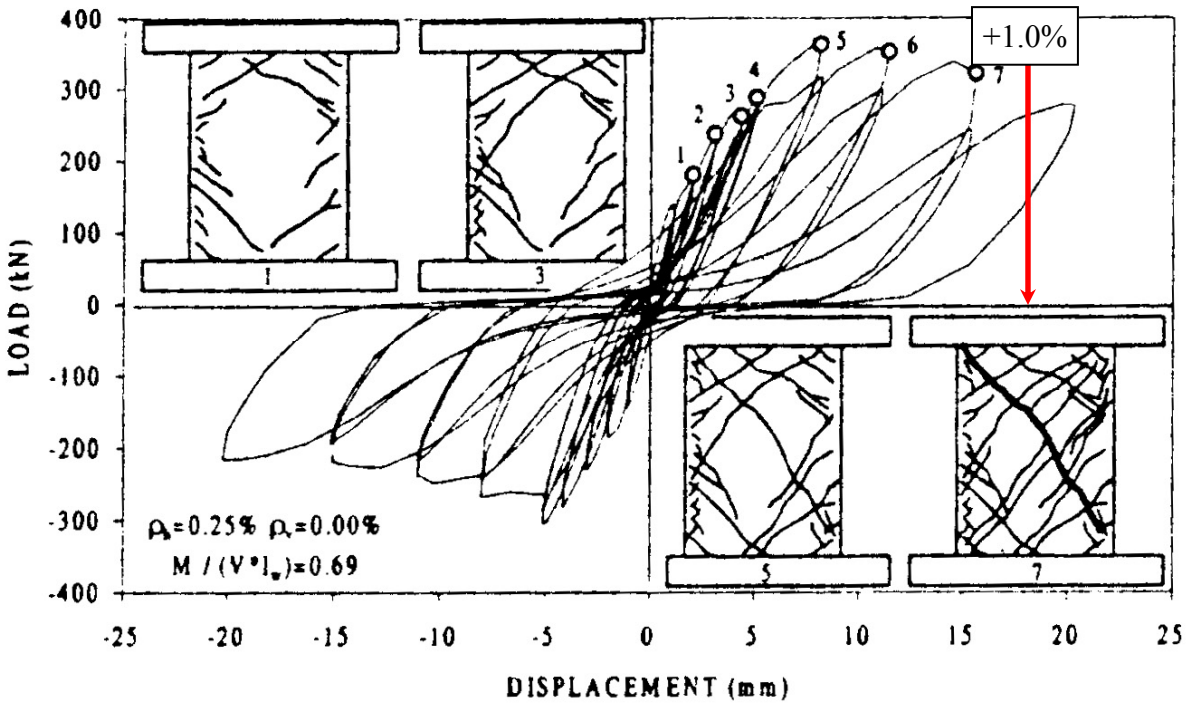


**Figure C-188 Load-displacement relationship for Specimen 23 [Hidalgo et al. (2002)]**

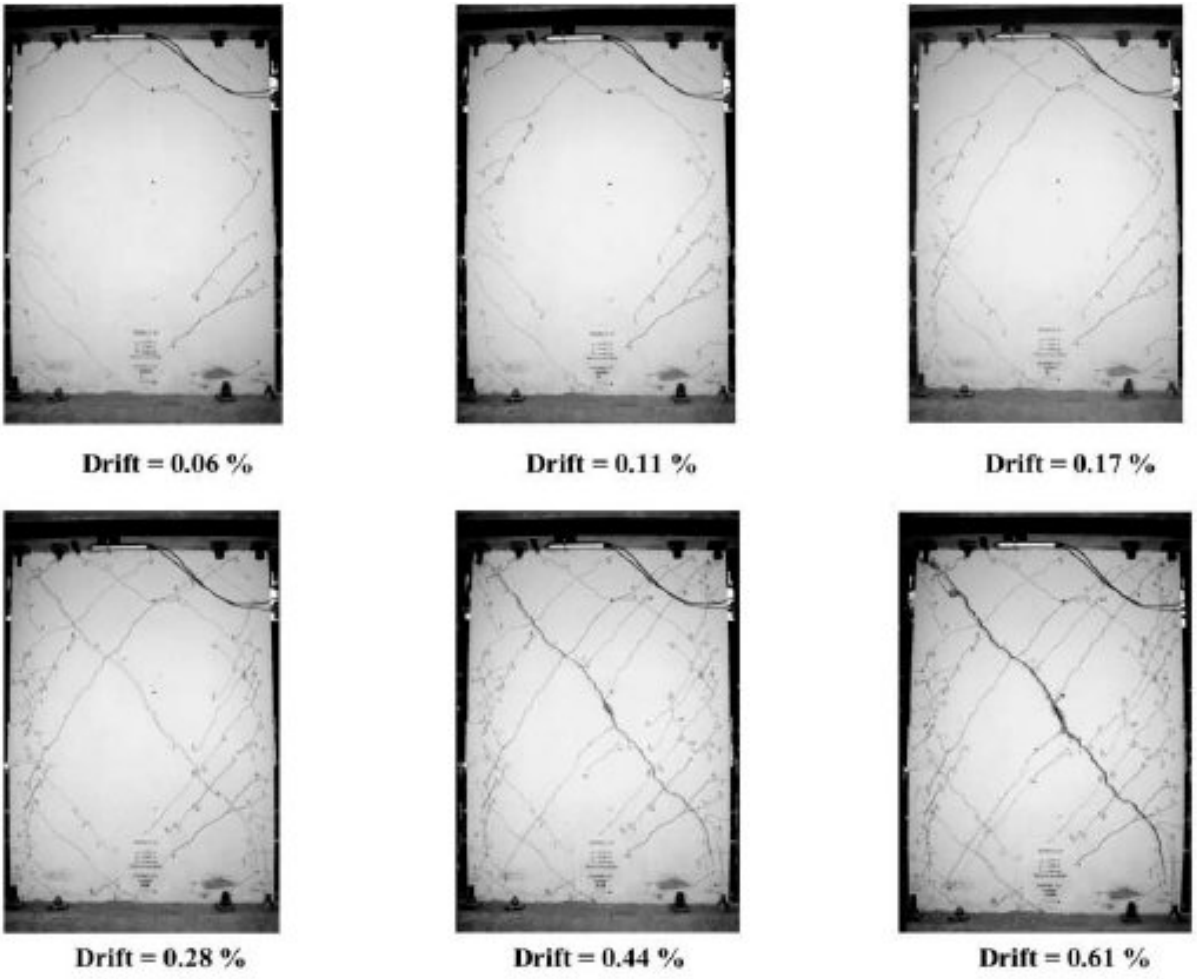


**Figure C-189 Progression of damage for Specimen 23 [Hidalgo et al. (2001)]**

### C.1.11.2 Specimen 27

**Table C-40 Evaluation of damage data for Specimen 27 tested by Hidalgo**

| Wall ID | MoR | Damage State (DS) | Drift (%) | Comments |
|---|---|---|---|---|
| Specimen 27 | 4 | 4.2 | 1.14 | The image reported at this drift (Figure C-191) shows major diagonal cracks that can be associated with diagonal tension failure. |

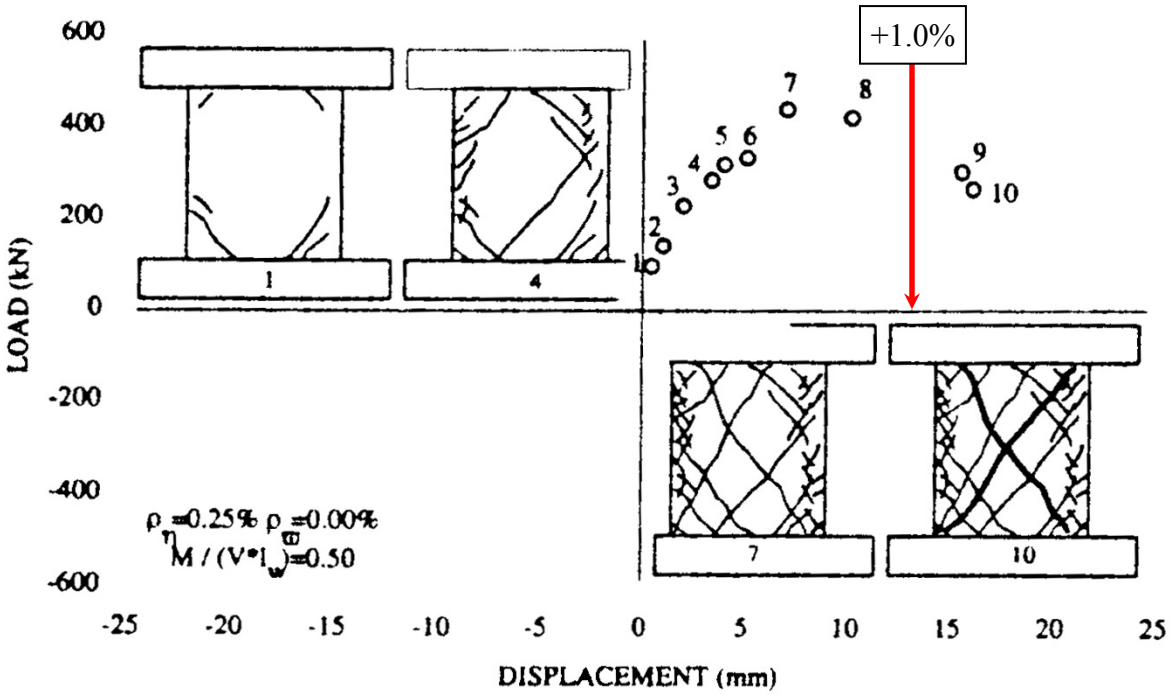


**Figure C-190 Load-displacement relationship for Specimen 27 [Hidalgo et al. (2002)]**

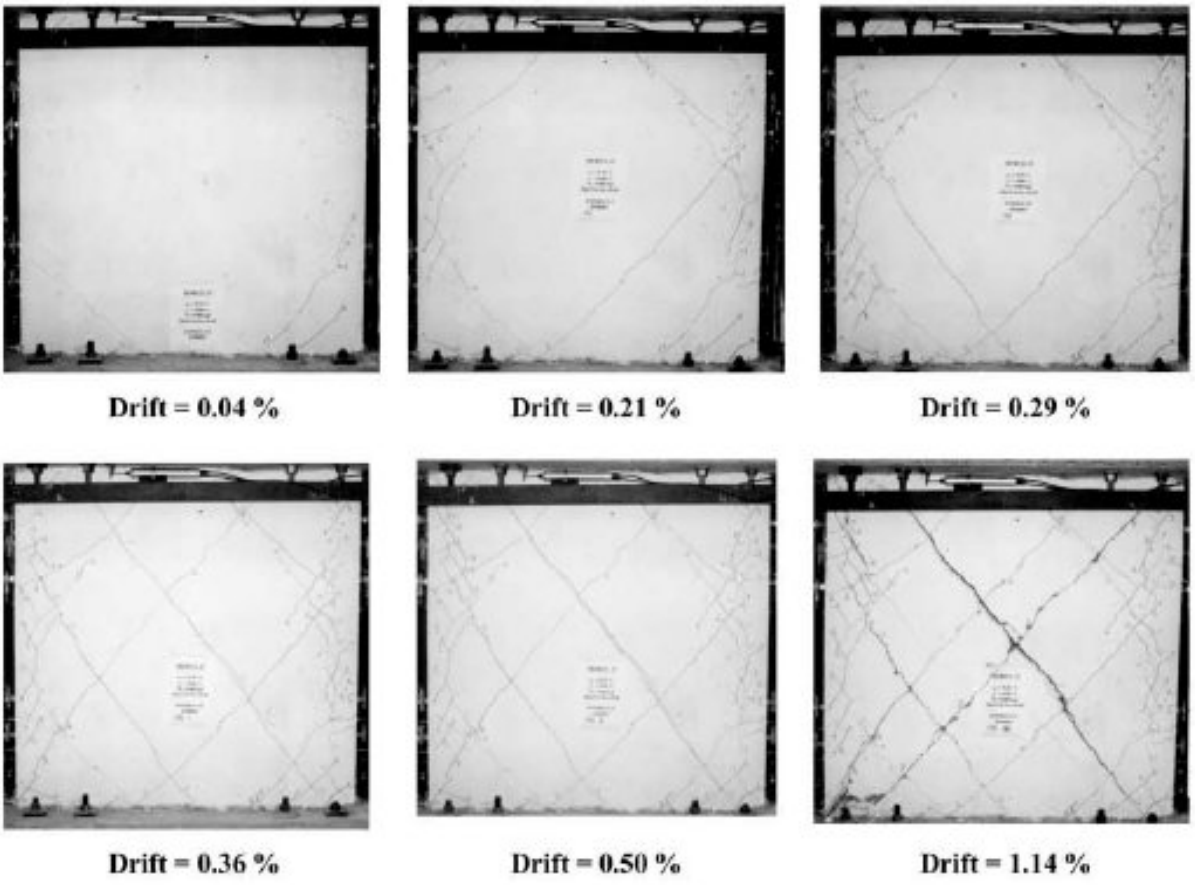


**Figure C-191 Progression of damage for Specimen 27 [Hidalgo et al. (2001)]**

## C.1.12 Xie and Xiao (2000) Wall

### C.1.12.1 Wall W1-A

**Table C-41 Evaluation of damage data for W1-A tested by Xie**

| Wall ID | MoR | Damage State (DS) | Drift (%) | Comments |
|---|---|---|---|---|
| W1-A | 1 | 1.2 | 0.02 | The drifts for these damage states are provided by the researcher. |
| | | 1.3 | 0.07 | |
| | 3 | 3.1 | 1.00 | Based on the researcher's description of damage at this drift: "The concrete crushing was more severe at the lower left corner than at the lower right corner…" [Xie and Xiao (2000), page 71]. |
| | 4 | 4.2 | 1.80 | The reported failure mode for the wall was diagonal tension. The drift associated with wall replacement is calculated using $SC_2$. |
| | 4* | $SC_2$ | 1.80 | The smaller of the two drifts is obtained from the 1st quadrant of the load-drift relationship (see Figure C-192). |

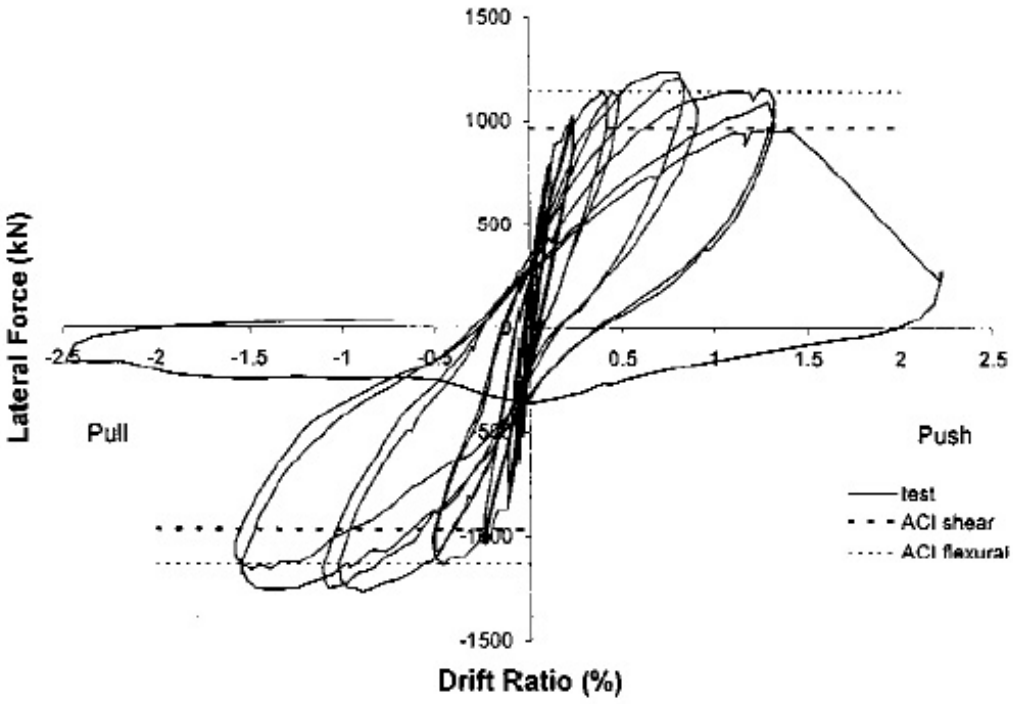


**Figure C-192 Load-displacement relationship for wall W1-A [Xie and Xiao (2000)]**

# C.2 Walls with Barbell Cross-Sections

## C.2.1 Chiba Walls [AIJ (1985b)]

### C.2.1.1 Wall No.1 (CW-0.6-1.2-20)

**Table C-42 Evaluation of damage data for wall No.1 tested by Chiba**

| Wall ID | MoR | Damage State (DS) | Drift (%) | Comments |
|---|---|---|---|---|
| No.1 | 1 | 1.3 | 0.03 | The drifts for these damage states are provided by the researcher. |
| | 2a | 2.4a | 0.69 | |
| | 4 | 4.3 | 0.91 | The image reported at this drift (Figure C-194) shows widespread crushing. |

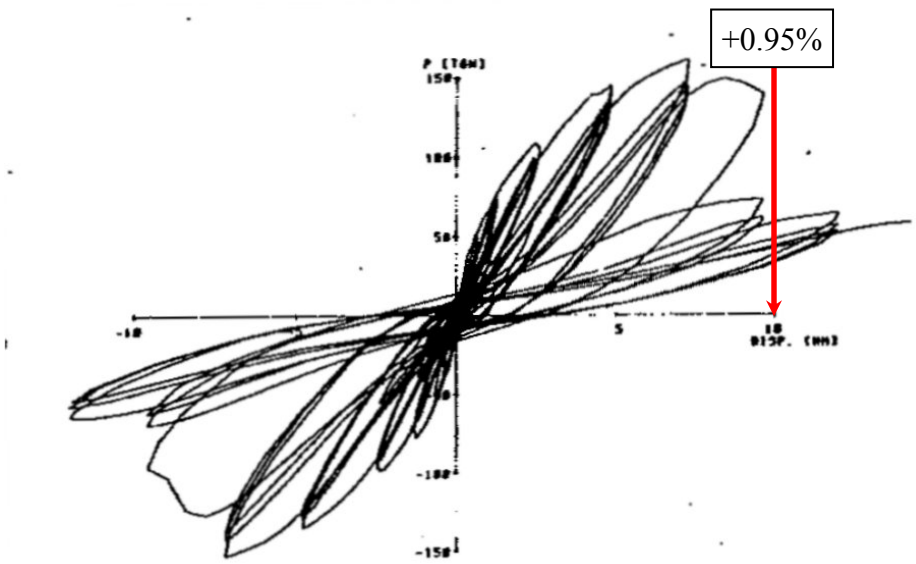


**Figure C-193 Load-displacement relationship for wall No.1 (CW-0.6-1.2-20) [AIJ (1985b)]**

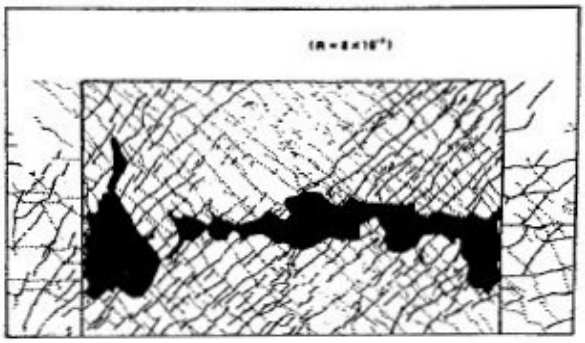

**Figure C-194 Condition of wall No.1 at 0.91% drift [AIJ (1985b)]**

### C.2.1.2 Wall No.2 (CW-0.6-0.6-20)

**Table C-43 Evaluation of damage data for wall No.2 tested by Chiba**

| Wall ID | MoR | Damage State (DS) | Drift (%) | Comments |
|---|---|---|---|---|
| No.2 | 1 | 1.3 | 0.04 | The drifts for these damage states are provided by the researcher. |
| | 2a | 2.4a | 0.43 | |
| | 4 | 4.3 | 0.46 | The image reported at this drift (Figure C-196) shows widespread crushing. |

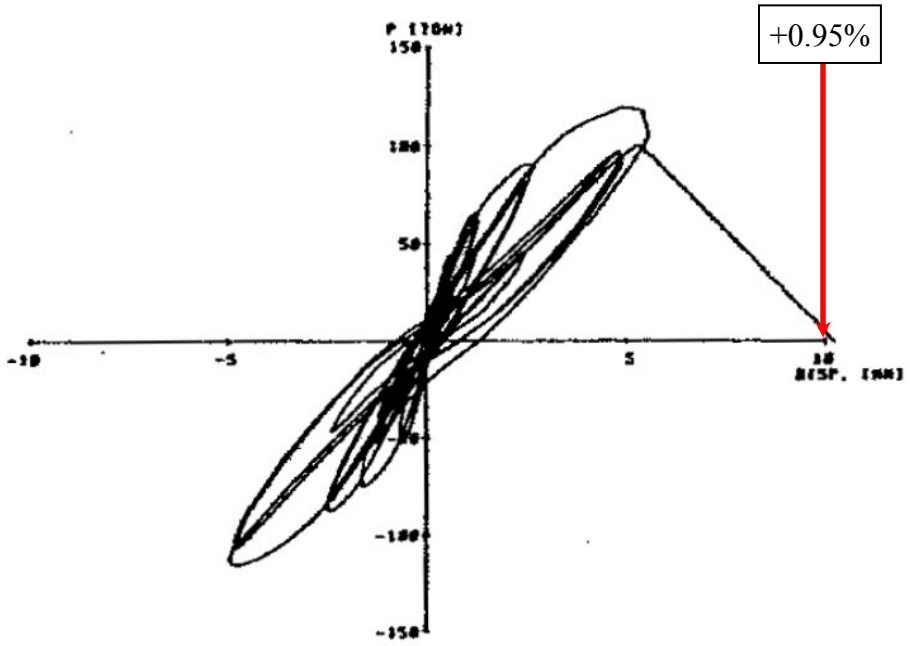


**Figure C-195 Load-displacement relationship for wall No.2 (CW-0.6-0.6-20) [AIJ (1985b)]**

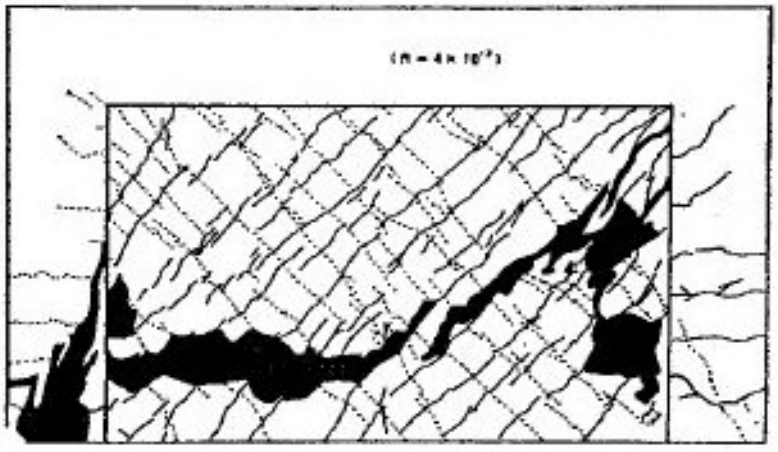

**Figure C-196 Condition of wall No.2 at 0.46% drift [AIJ (1985b)]**

### C.2.1.3 Wall No.3 (CW-0.6-0.8-20)

**Table C-44 Evaluation of damage data for wall No.3 tested by Chiba**

| Wall ID | MoR | Damage State (DS) | Drift (%) | Comments |
|---|---|---|---|---|
| No.3 | 1 | 1.3 | 0.04 | The drifts for these damage states are provided by the researcher. |
| | 2a | 2.4a | 0.34 | |
| | 2b | 2.4b | 0.64 | |
| | 4 | 4.3 | 0.91 | The image reported at this drift (Figure C-198) shows widespread crushing. |

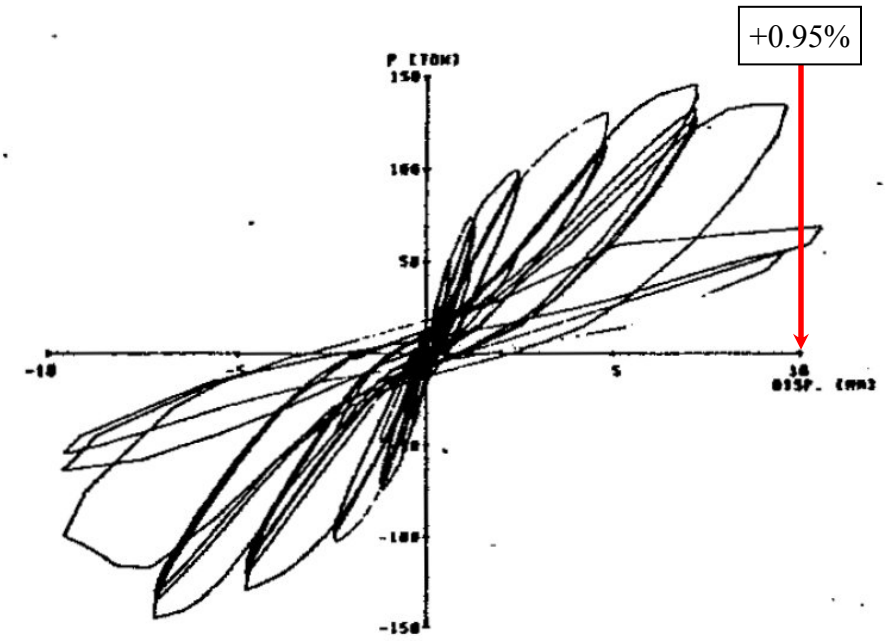


**Figure C-197 Load-displacement relationship for wall No.3 (CW-0.6-0.8-20) [AIJ (1985b)]**

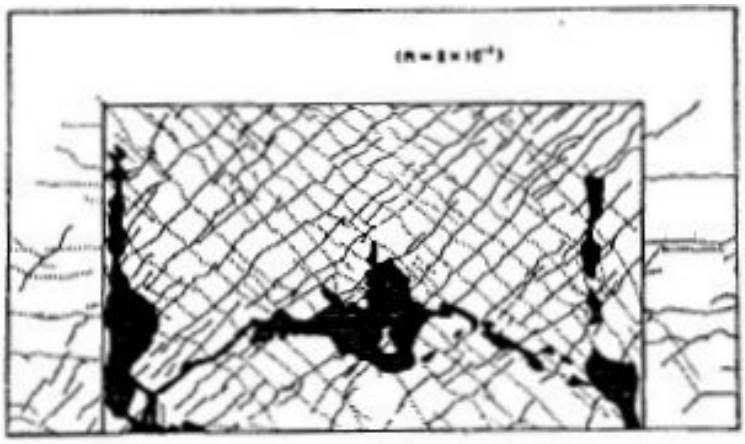

**Figure C-198 Condition of wall No.3 at 0.91% drift [AIJ (1985b)]**

### C.2.1.4 Wall No.4 (CW-0.6-1.6-20)

**Table C-45 Evaluation of damage data for wall No.4 tested by Chiba**

| Wall ID | MoR | Damage State (DS) | Drift (%) | Comments |
|---|---|---|---|---|
| No.4 | 1 | 1.3 | 0.06 | The drift for this damage state is provided by the researcher. |
| | 4 | 4.3 | 0.91 | The image reported at this drift (Figure C-200) shows widespread crushing. |

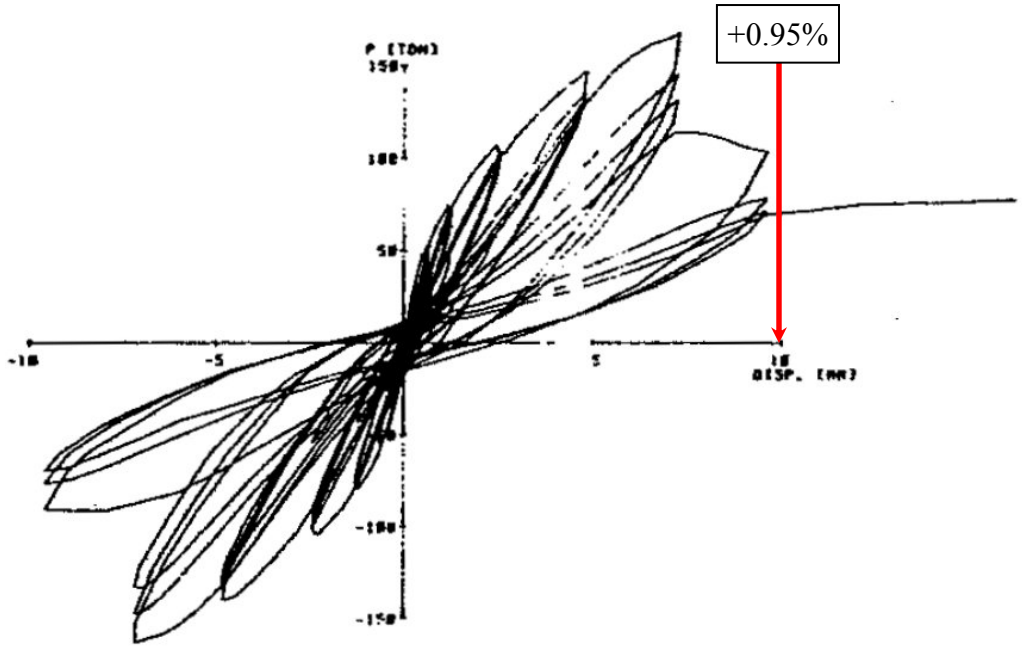


**Figure C-199 Load-displacement relationship for wall No.4 (CW-0.6-1.6-20) [AIJ (1985b)]**

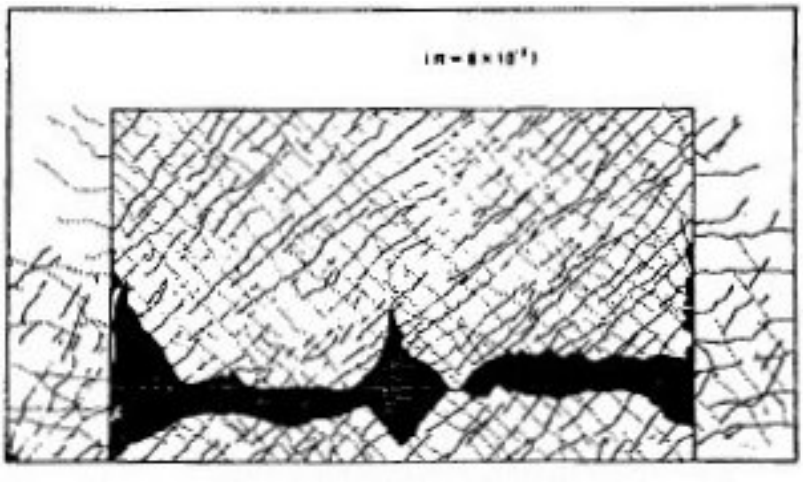

**Figure C-200 Condition of wall No.4 at 0.91% drift [AIJ (1985b)]**

### C.2.1.5 Wall No.5 (CW-0.6-2.0-20)

**Table C-46 Evaluation of damage data for wall No.5 tested by Chiba**

| Wall ID | MoR | Damage State (DS) | Drift (%) | Comments |
|---|---|---|---|---|
| No.5 | 1 | 1.3 | 0.04 | The drift for this damage state is provided by the researcher. |
| | 4 | 4.3 | 0.91 | The image reported at this drift (Figure C-202) shows widespread crushing. |

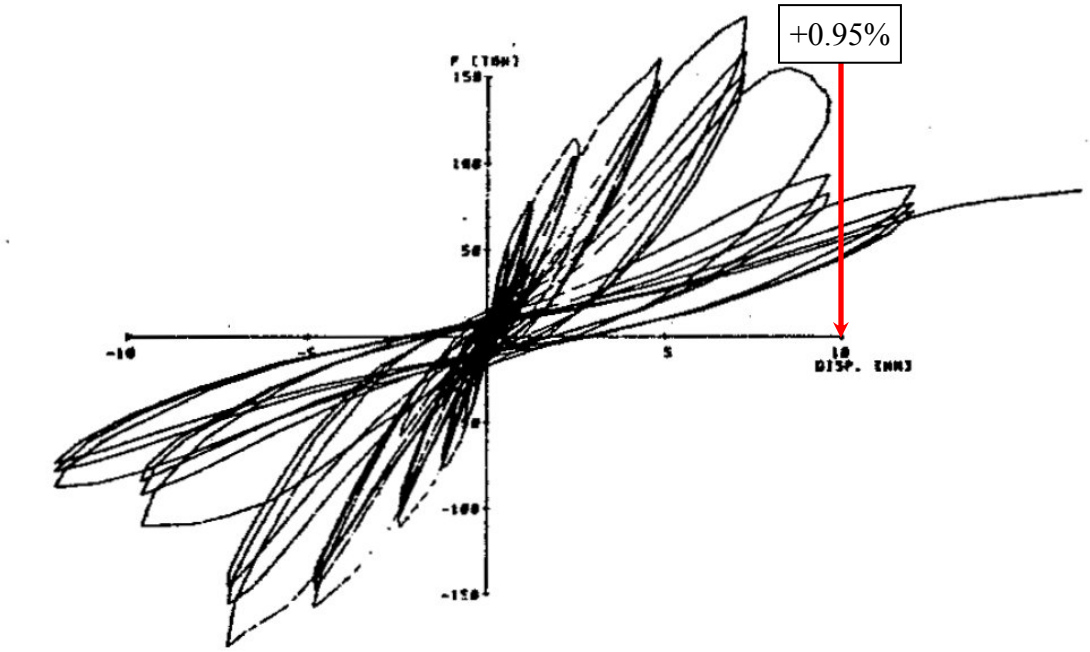


**Figure C-201 Load-displacement relationship for wall No.5 (CW-0.6-2.0-20) [AIJ (1985b)]**

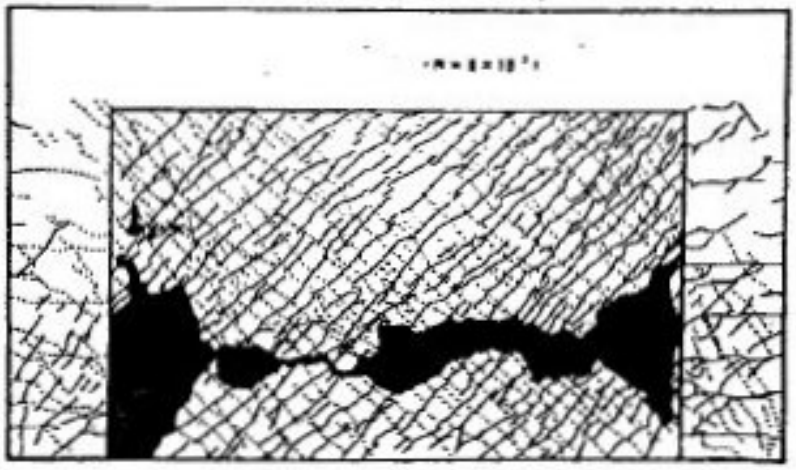

**Figure C-202 Condition of wall No.5 at 0.91% drift [AIJ (1985b)]**

### C.2.1.6 Wall No.6 (CW-0.6-1.2-40)

**Table C-47 Evaluation of damage data for wall No.6 tested by Chiba**

| Wall ID | MoR | Damage State (DS) | Drift (%) | Comments |
|---|---|---|---|---|
| No.6 | 1 | 1.3 | 0.03 | The drift for this damage state is provided by the researcher. |
| | 4 | 4.3 | 0.69 | The image reported at this drift (Figure C-204) shows widespread crushing. |

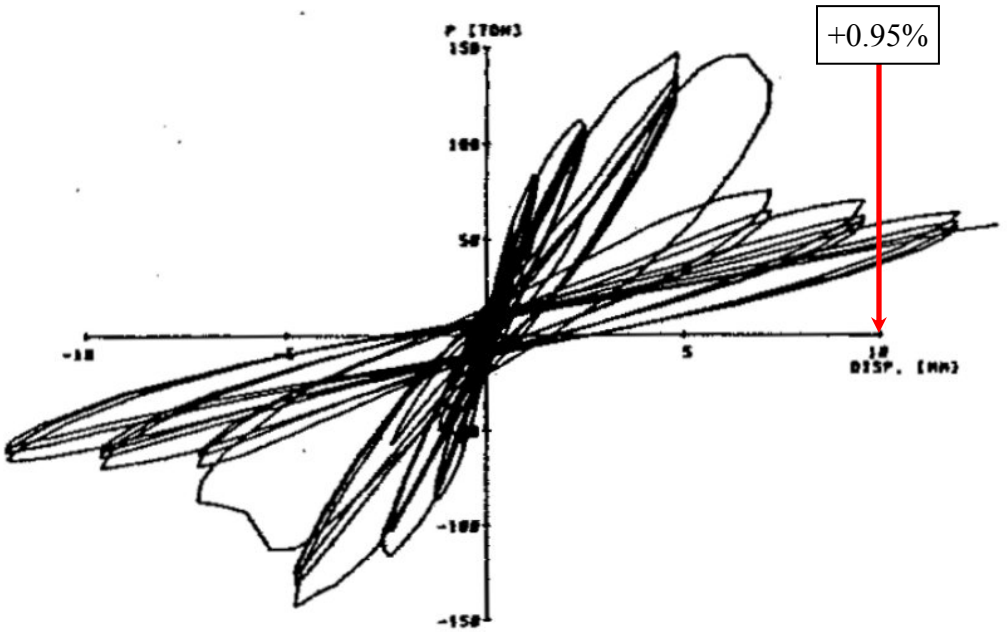


**Figure C-203 Load-displacement relationship for wall No.6 (CW-0.6-1.2-40) [AIJ (1985b)]**

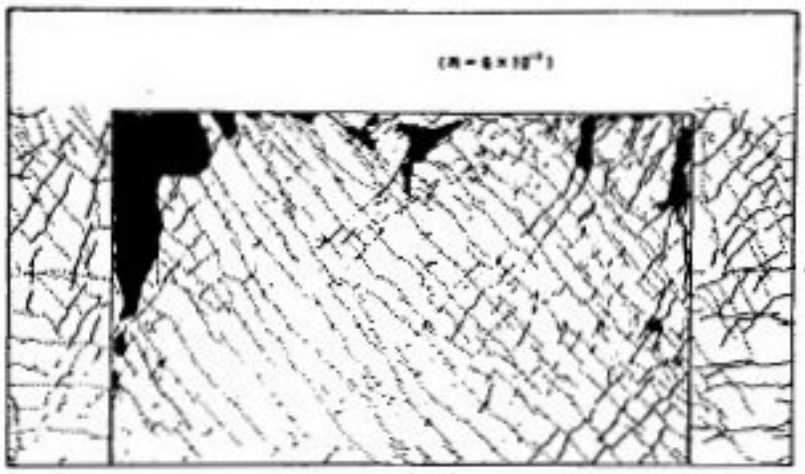

**Figure C-204 Condition of wall No.6 at 0.69% drift [AIJ (1985b)]**

### C.2.1.7 Wall No.7 (CW-0.4-1.2-20)

**Table C-48 Evaluation of damage data for wall No.7 tested by Chiba**

| Wall ID | MoR | Damage State (DS) | Drift (%) | Comments |
|---|---|---|---|---|
| No.7 | 1 | 1.3 | 0.04 | The drift for this damage state is provided by the researcher. |
| | 4 | 4.3 | 0.74 | The image reported at this drift (Figure C-206) shows widespread crushing. |

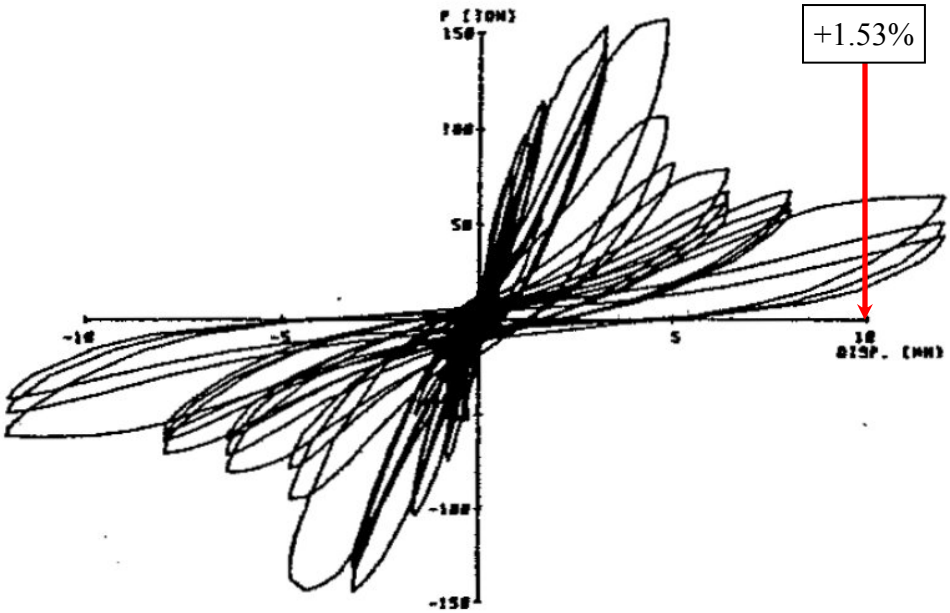


**Figure C-205 Load-displacement relationship for wall No.7 (CW-0.4-1.2-20) [AIJ (1985b)]**

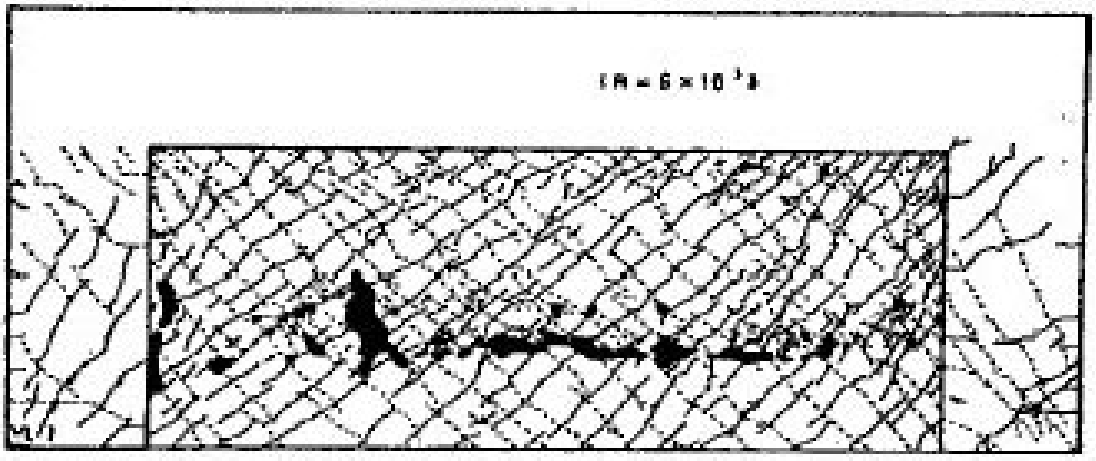

**Figure C-206 Condition of wall No.7 at 0.74% drift [AIJ (1985b)]**

### C.2.1.8 Wall No.8 (CW-0.8-1.2-20)

**Table C-49 Evaluation of damage data for wall No.8 tested by Chiba**

| Wall ID | MoR | Damage State (DS) | Drift (%) | Comments |
|---|---|---|---|---|
| No.8 | 1 | 1.3 | 0.03 | The drift for this damage state is provided by the researcher. |
| | 4 | 4.3 | 0.88 | The image reported at this drift (Figure C-208) shows widespread crushing. |

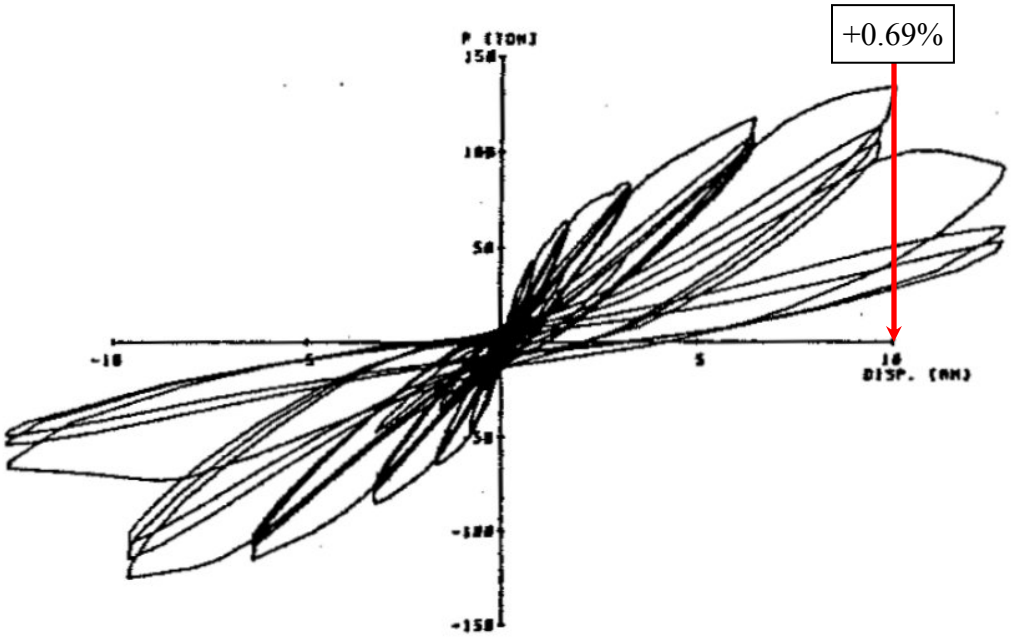


**Figure C-207 Load-displacement relationship for wall No.8 (CW-0.8-1.2-20) [AIJ (1985b)]**

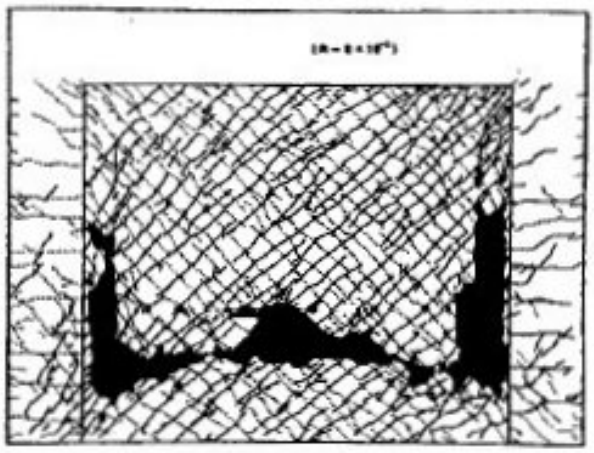

**Figure C-208 Condition of wall No.8 at 0.88% drift [AIJ (1985b)]**

## C.2.2 Fukuzawa Walls [AIJ (1985a)]

### C.2.2.1 Wall No.1 (CW-0.6-0-20)

**Table C-50 Evaluation of damage data for wall No.1 tested by Fukuzawa**

| Wall ID | MoR | Damage State (DS) | Drift (%) | Comments |
|---|---|---|---|---|
| No.1 | 1 | 1.2 | 0.11 | The drifts for these damage states are provided by the researcher. |
| | | 1.3 | 0.05 | |
| | 2a | 2.3 | 0.29 | |
| | 3 | 3.1 | 0.26 | |
| | 4 | 4.3 | 0.91 | The image reported at this drift (Figure C-210) shows widespread crushing. |

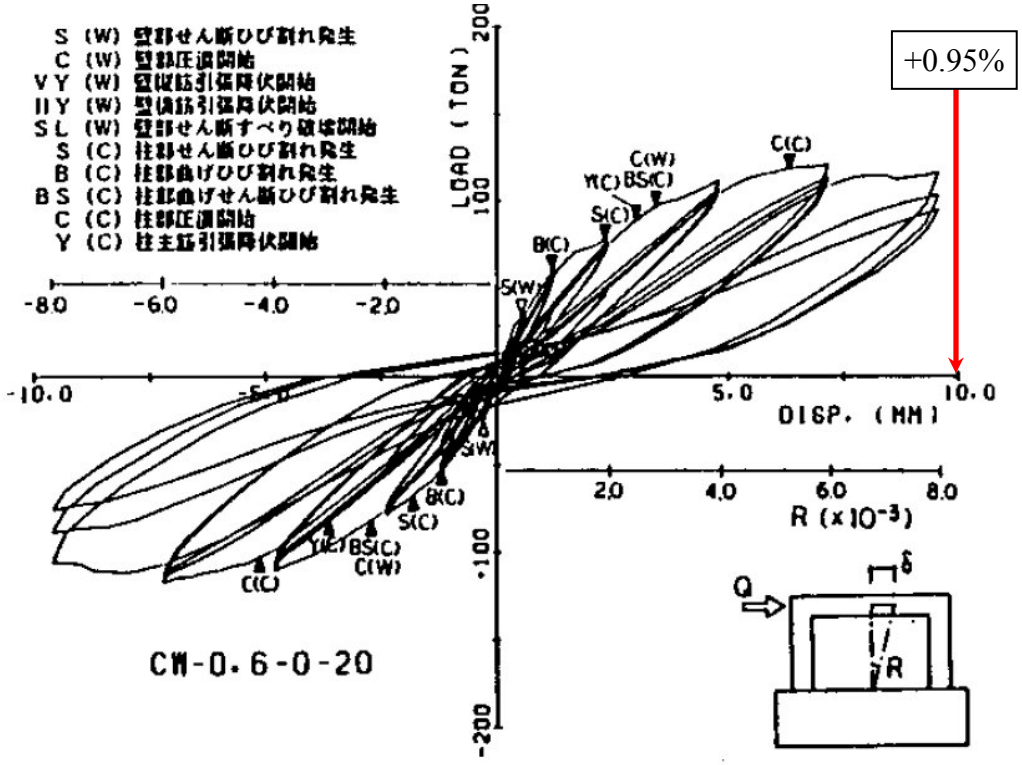


**Figure C-209 Load-displacement relationship for wall No.1 (CW-0.6-0-20) [AIJ (1985a)]**

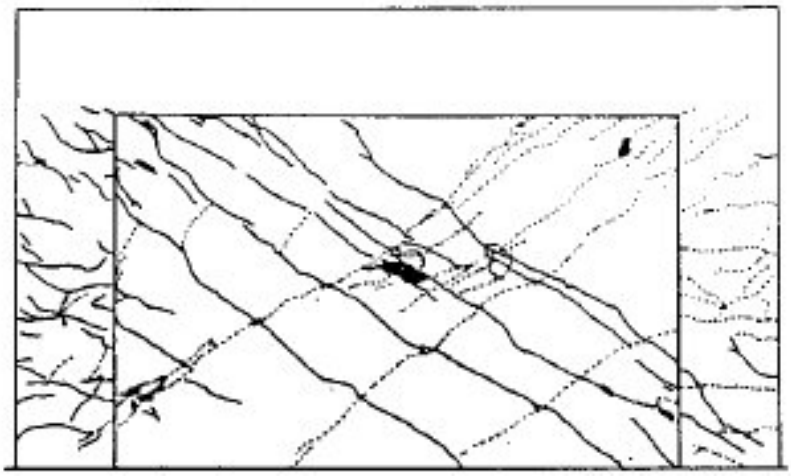

**Figure C-210 Condition of wall No.1 at 0.91% drift [AIJ (1985a)]**

**Figure C-211 Condition of wall No.1 at the end of testing (after 3 cycles at 0.91%) [AIJ (1985a)]**

### C.2.2.2 Wall No.2 (CW-0.6-0.3-20)

**Table C-51 Evaluation of damage data for wall No.2 tested by Fukuzawa**

| Wall ID | MoR | Damage State (DS) | Drift (%) | Comments |
|---|---|---|---|---|
| No.2 | 1 | 1.2 | 0.12 | The drifts for these damage states are provided by the researcher. |
| | | 1.3 | 0.03 | |
| | 2a | 2.1 | 0.12 | |
| | | 2.2 | 0.10 | |
| | | 2.3 | 0.34 | |
| | 3 | 3.1 | 0.29 | |
| | 4 | 4.3 | 0.91 | The image reported at this drift (Figure C-213) shows widespread crushing. |

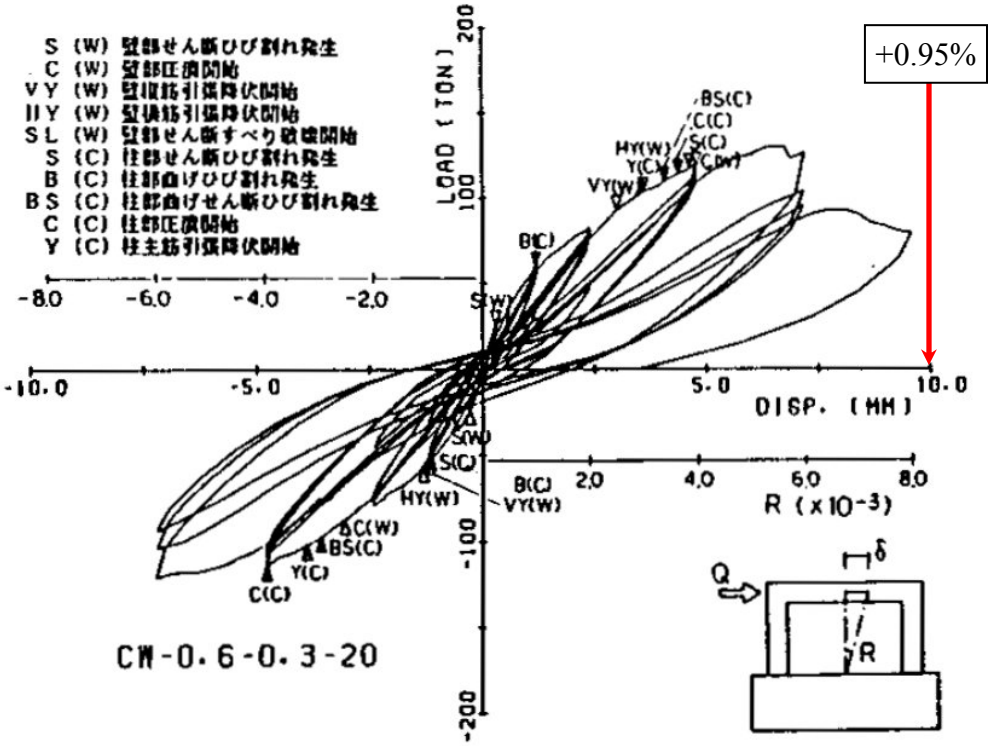


**Figure C-212 Load-displacement relationship for wall No.2 (CW-0.6-0.3-20) [AIJ (1985a)]**

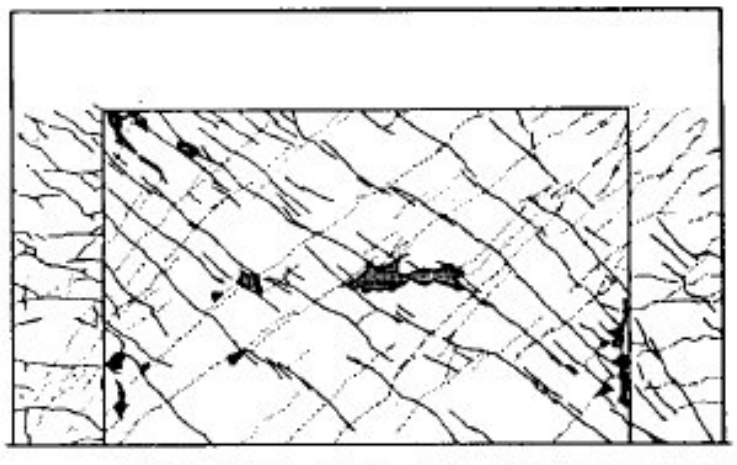

**Figure C-213 Condition of wall No.2 at 0.91% drift [AIJ (1985a)]**

### C.2.2.3 Wall No.3 (CW-0.6-2.4-20)

**Table C-52 Evaluation of damage data for wall No.3 tested by Fukuzawa**

| Wall ID | MoR | Damage State (DS) | Drift (%) | Comments |
|---|---|---|---|---|
| No.3 | 1 | 1.2 | 0.03 | The drifts for these damage states are provided by the researcher. The reported drift at sliding failure (shaded) is excluded from the fragility analysis because herein drift associated with sliding failure is calculated using the supplemental wall replacement criteria. No data associated with DS4.1 is registered since none could be obtained using the supplemental criteria. |
| | | 1.3 | 0.02 | |
| | 2a | 2.1 | 0.88 | |
| | | 2.3 | 0.54 | |
| | 3 | 3.1 | 0.46 | |
| | 4 | 4.1 | 0.83 | |
| | | 4.3 | 0.91 | The image reported at this drift (Figure C-215) shows widespread crushing. |
| | 4* | $SC_1$ | N/A | The residual drifts did not exceed 1.0% (Figure C-214). |
| | | $SC_2$ | N/A | The post-peak resistance computed using the first cycle backbone curve did not drop to $0.5V_{peak}$ (see Figure C-214). |

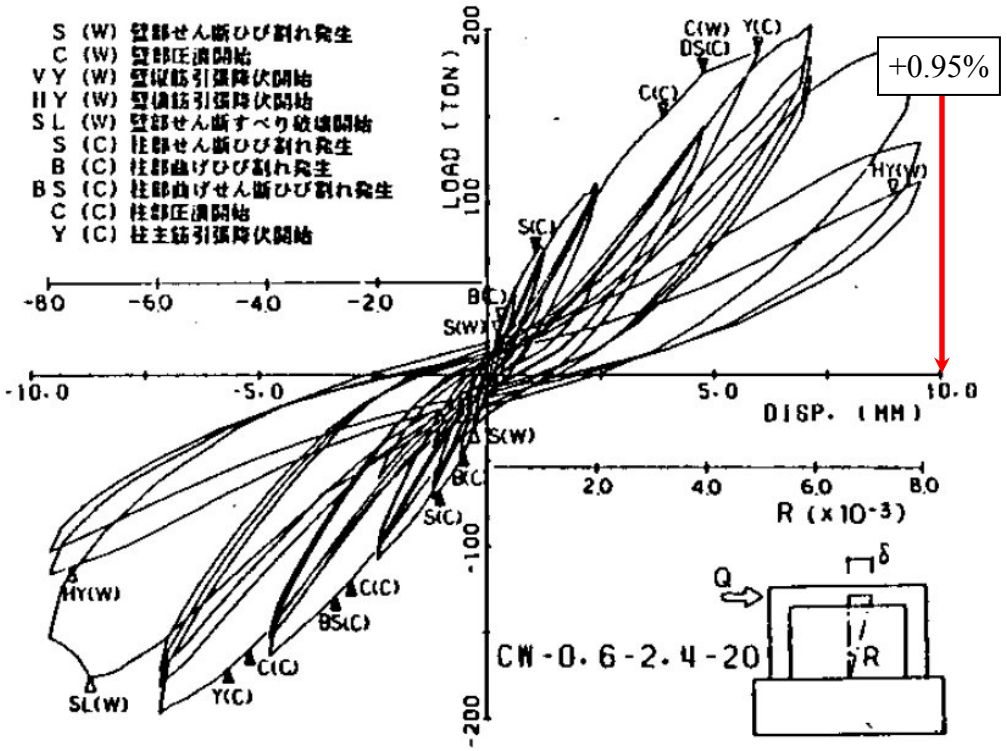


**Figure C-214 Load-displacement relationship for wall No.3 (CW-0.6-2.4-20) [AIJ (1985a)]**

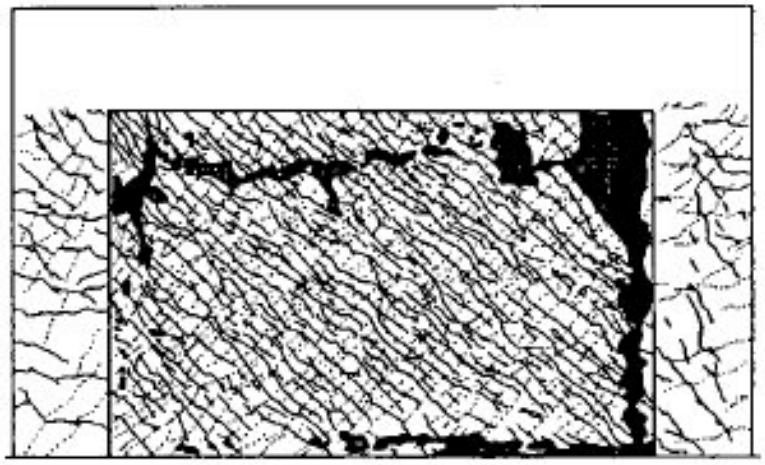

**Figure C-215 Condition of wall No.3 at 0.91% drift [AIJ (1985a)]**

### C.2.2.4 Wall No.4 (CW-0.6-2.8-20)

**Table C-53 Evaluation of damage data for wall No.4 tested by Fukuzawa**

| Wall ID | MoR | Damage State (DS) | Drift (%) | Comments |
|---|---|---|---|---|
| No.4 | 1 | 1.2 | 0.11 | The drifts for these damage states are provided by the researcher. |
| | | 1.3 | 0.05 | |
| | 2a | 2.3 | 0.80 | |
| | 3 | 3.1 | 0.69 | The image reported at this drift (Figure C-220) shows damage that can be repaired by partial wall replacement (MoR-3). The damaged region requiring partial wall replacement is identified using dashed boxes in Figure C-220. An author-reported drift for this damage state (0.43%) is excluded from the fragility analysis. |
| | 4 | 4.1 | 0.86 | The reported drift at sliding failure (shaded) is excluded from the fragility analysis because herein drift associated with sliding failure is calculated using the supplemental wall replacement criteria. No data associated with DS4.1 is registered since none could be obtained using the supplemental criteria. |
| | | 4.3 | 0.91 | The image reported at this drift (Figure C-221) shows widespread crushing. |
| | $4^*$ | $SC_1$ | N/A | The residual drifts did not exceed 1.0% (Figure C-216). |
| | | $SC_2$ | N/A | The post-peak resistance computed using the first cycle backbone curve did not drop to $0.5V_{peak}$ (see Figure C-216). |

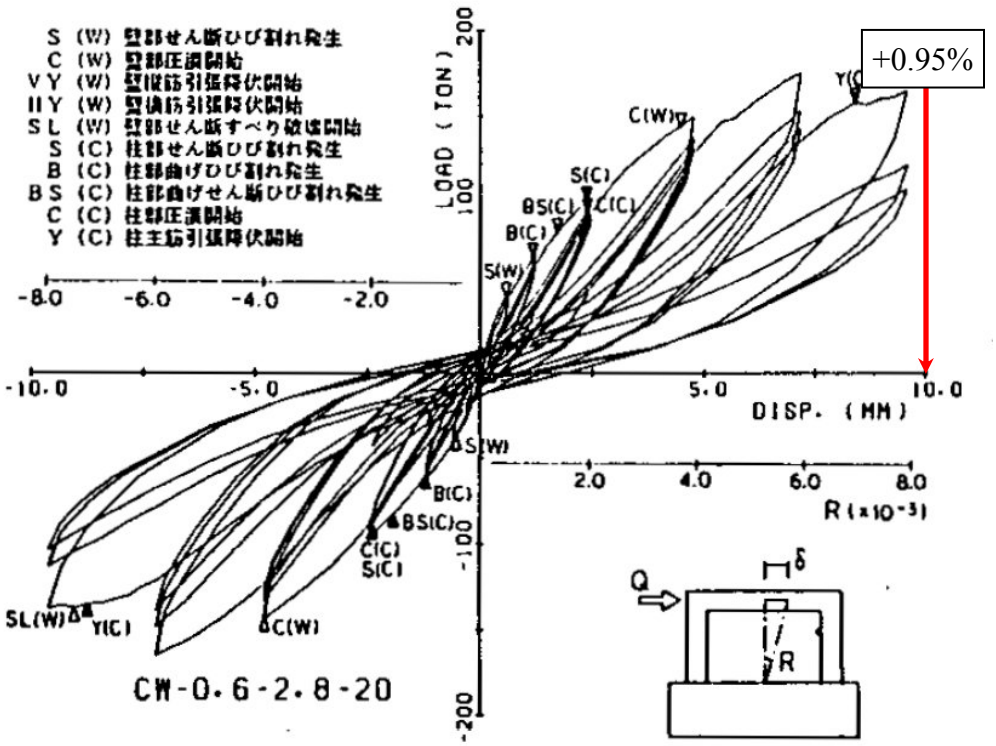


**Figure C-216 Load-displacement relationship for wall No.4 (CW-0.6-2.8-20) [AIJ (1985a)]**

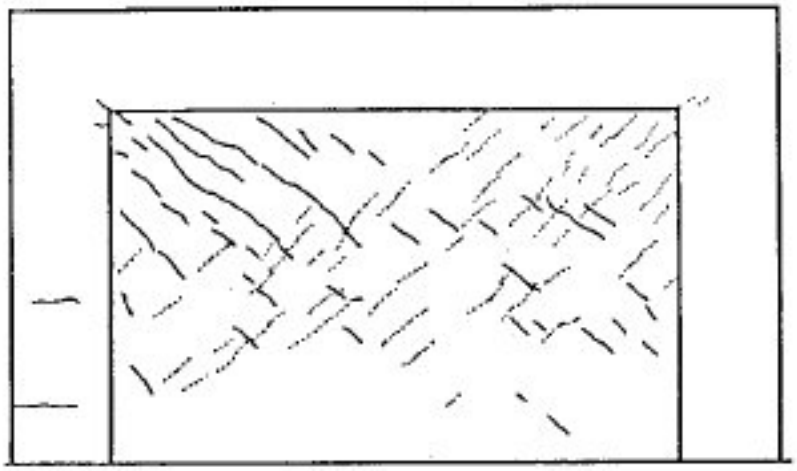

**Figure C-217 Condition of wall No.4 at 0.11% drift [AIJ (1985a)]**

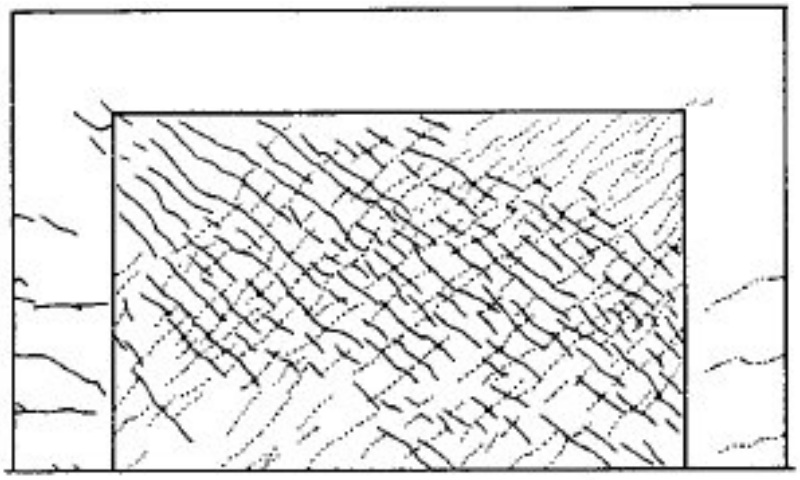

**Figure C-218 Condition of wall No.4 at 0.23% drift [AIJ (1985a)]**

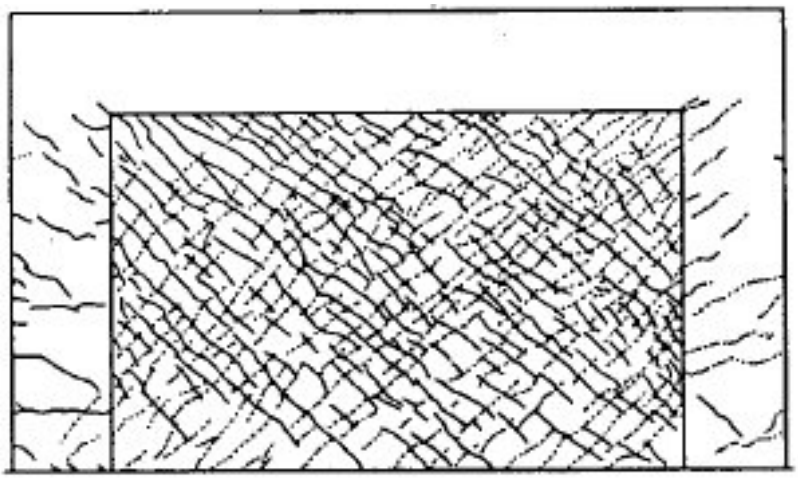

**Figure C-219 Condition of wall No.4 at 0.46% drift [AIJ (1985a)]**

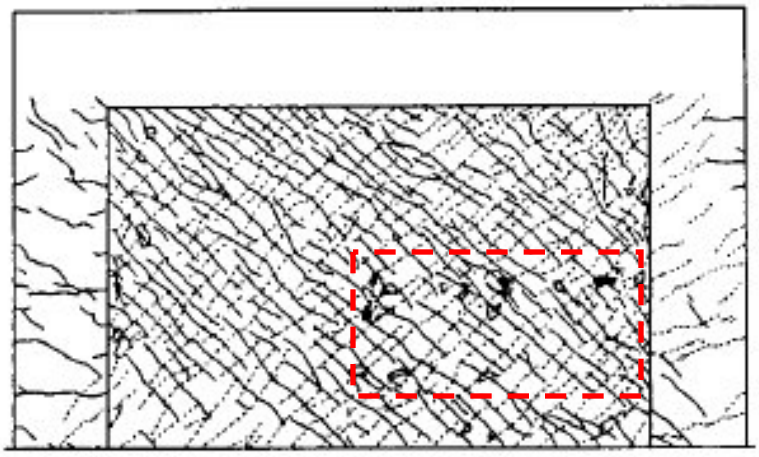

**Figure C-220 Condition of wall No.4 at 0.69% drift [AIJ (1985a)]**

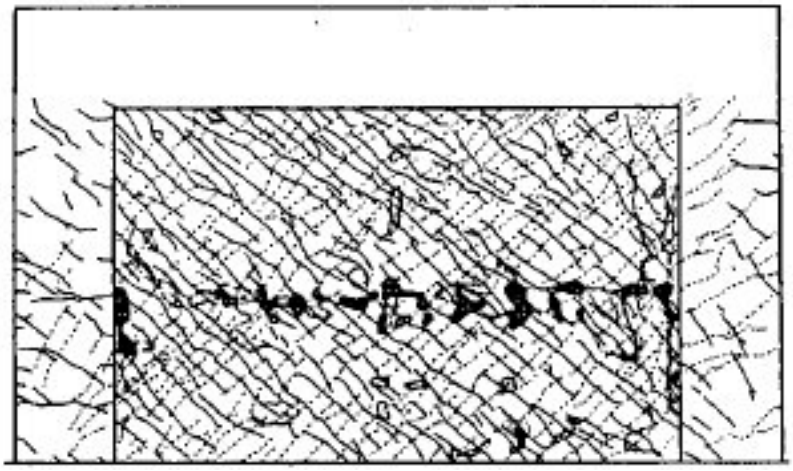

**Figure C-221 Condition of wall No.4 at 0.91% drift [AIJ (1985a)]**

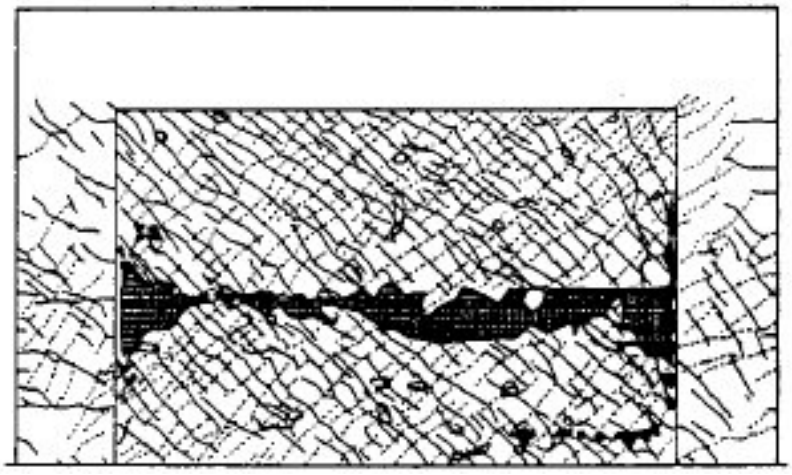

**Figure C-222 Condition of wall No.4 at the end of testing (after 3 cycles at 0.91%) [AIJ (1985a)]**

### C.2.2.5 Wall No.5 (CW-0.6-0-0)

**Table C-54 Evaluation of damage data for wall No.5 tested by Fukuzawa**

| Wall ID | MoR | Damage State (DS) | Drift (%) | Comments |
|---|---|---|---|---|
| No.5 | 1 | 1.2 | 0.04 | The drifts for these damage states are provided by the researcher. |
| | | 1.3 | 0.03 | |
| | 2a | 2.3 | 0.26 | |
| | 3 | 3.1 | 0.68 | |
| | 4 | 4.3 | 0.91 | The image reported at this drift (Figure C-224) shows widespread crushing. |

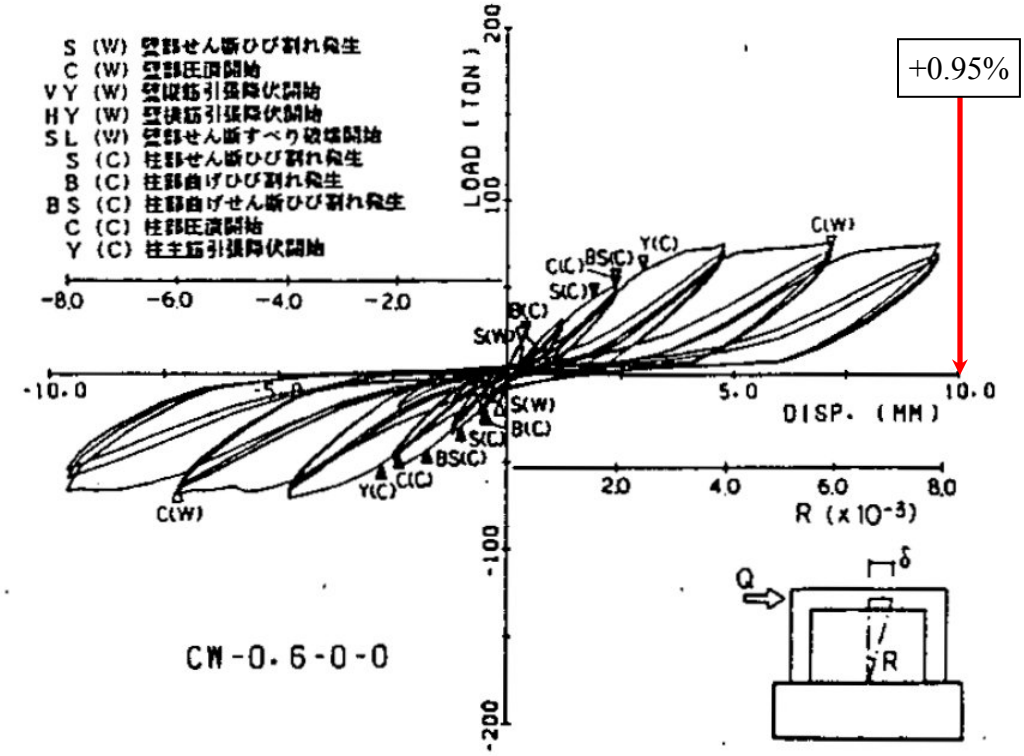


**Figure C-223 Load-displacement relationship for wall No.5 (CW-0.6-0-0) [AIJ (1985a)]**

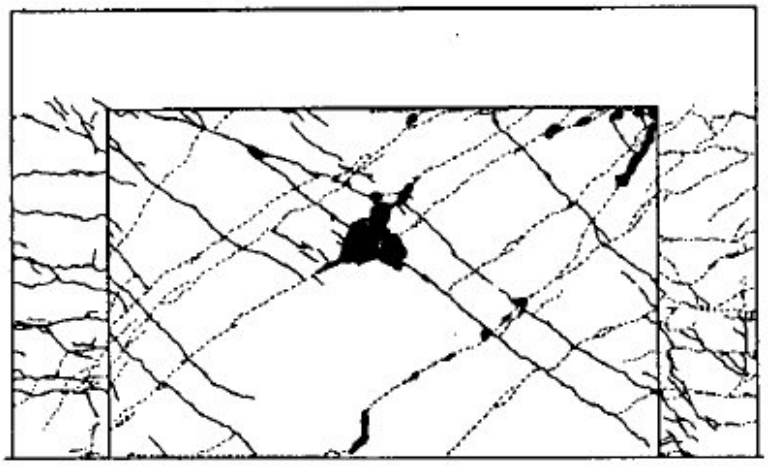

**Figure C-224 Condition of wall No.5 at 0.91% drift [AIJ (1985a)]**

### C.2.2.6 Wall No.6 (CW-0.6-0-40)

**Table C-55 Evaluation of damage data for wall No.6 tested by Fukuzawa**

| Wall ID | MoR | Damage State (DS) | Drift (%) | Comments |
|---|---|---|---|---|
| No.6 | 1 | 1.2 | 0.05 | The drifts for these damage states are provided by the researcher. The reported drift at sliding failure (shaded) is excluded from the fragility analysis because herein drift associated with sliding failure is calculated using the supplemental wall replacement criteria. No data associated with DS4.1 is registered since none could be obtained using the supplemental criteria. |
| | | 1.3 | 0.03 | |
| | 2a | 2.3 | 0.37 | |
| | 3 | 3.1 | 0.11 | |
| | 4 | 4.1 | 0.63 | |
| | | 4.3 | 0.69 | The image reported at this drift (Figure C-226) shows widespread crushing. |
| | 4* | $SC_1$ | N/A | The residual drifts did not exceed 1.0% (Figure C-225). |
| | | $SC_2$ | N/A | The post-peak resistance computed using the first cycle backbone curve did not drop to $0.5V_{peak}$ (see Figure C-225). |

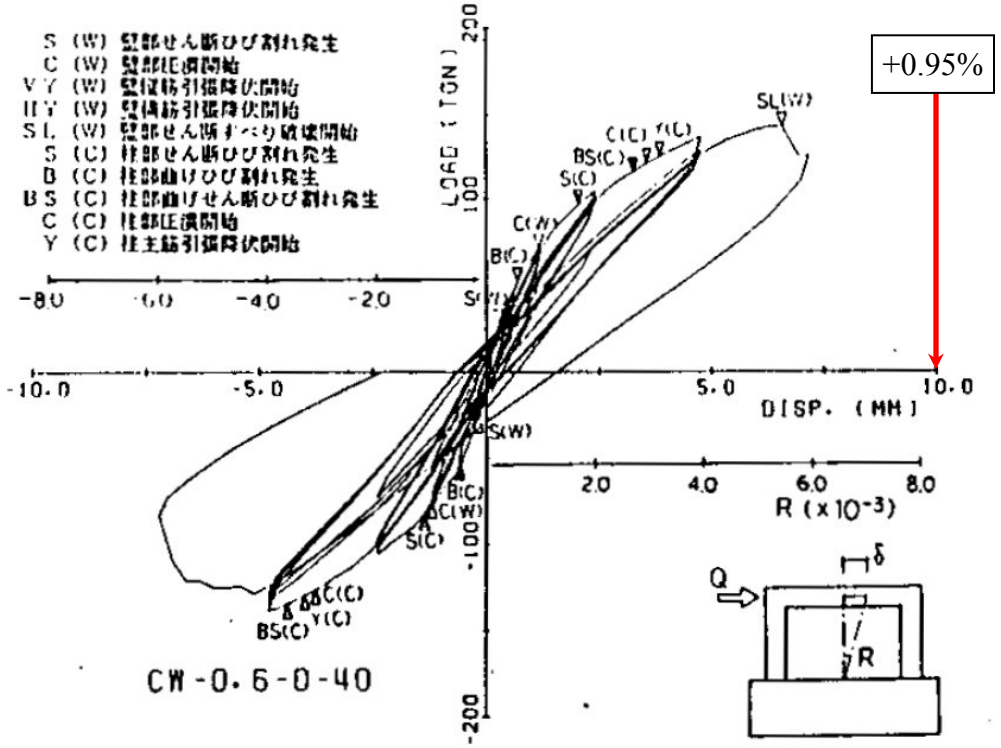


**Figure C-225 Load-displacement relationship for wall No.6 (CW-0.6-0-40) [AIJ (1985a)]**

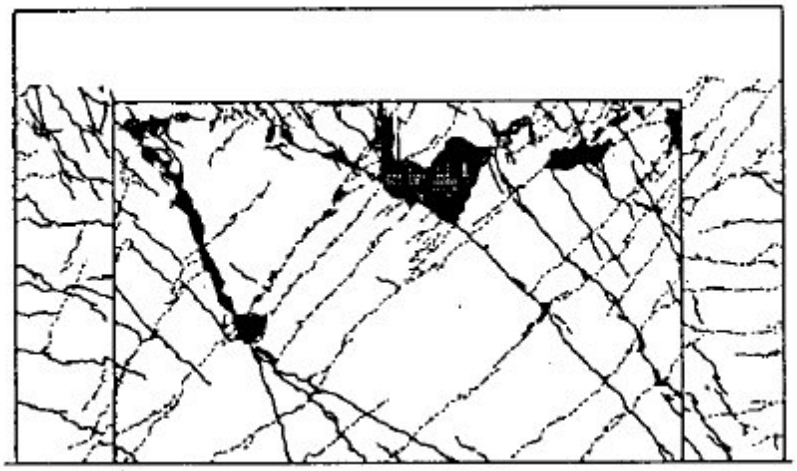

**Figure C-226 Condition of wall No.6 at 0.69% drift [AIJ (1985a)]**

### C.2.2.7 Wall No.7 (CW-0.6-0.6-0)

**Table C-56 Evaluation of damage data for wall No.7 tested by Fukuzawa**

| Wall ID | MoR | Damage State (DS) | Drift (%) | Comments |
|---|---|---|---|---|
| No.7 | 1 | 1.2 | 0.04 | The drifts for these damage states are provided by the researcher. |
| | | 1.3 | 0.02 | |
| | 2a | 2.1 | 0.46 | |
| | | 2.2 | 0.32 | |
| | | 2.3 | 0.22 | |
| | 3 | 3.1 | 0.22 | |
| | 4 | 4.3 | 0.91 | The image reported at this drift (Figure C-228) shows widespread crushing. |

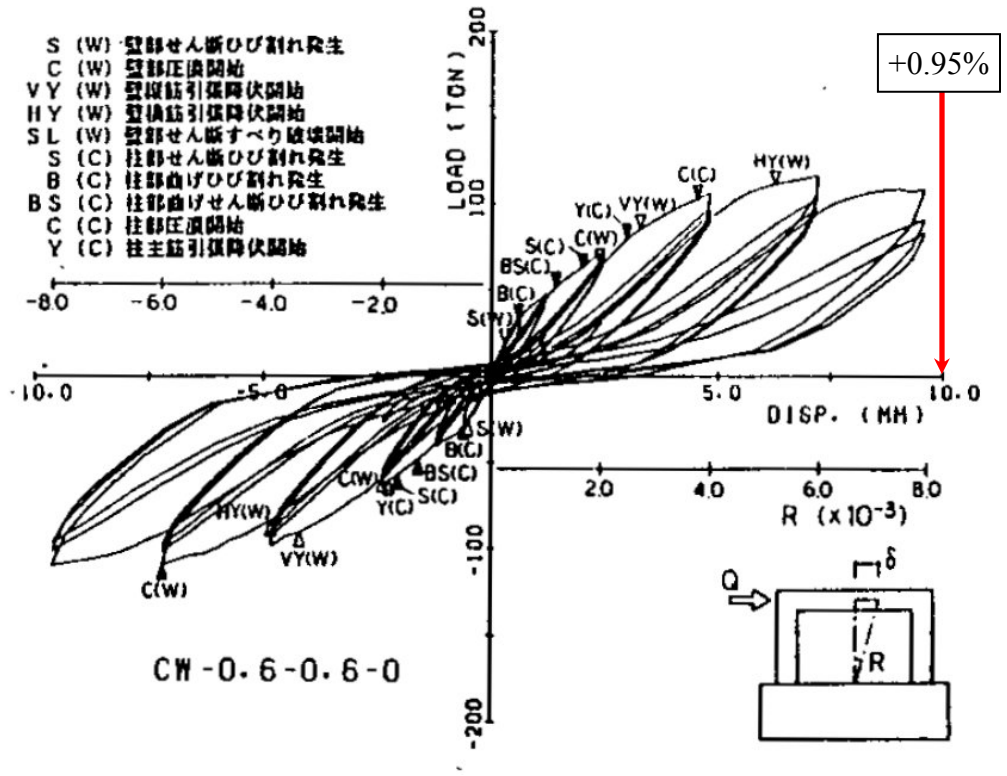


**Figure C-227 Load-displacement relationship for wall No.7 (CW-0.6-0.6-0) [AIJ (1985a)]**

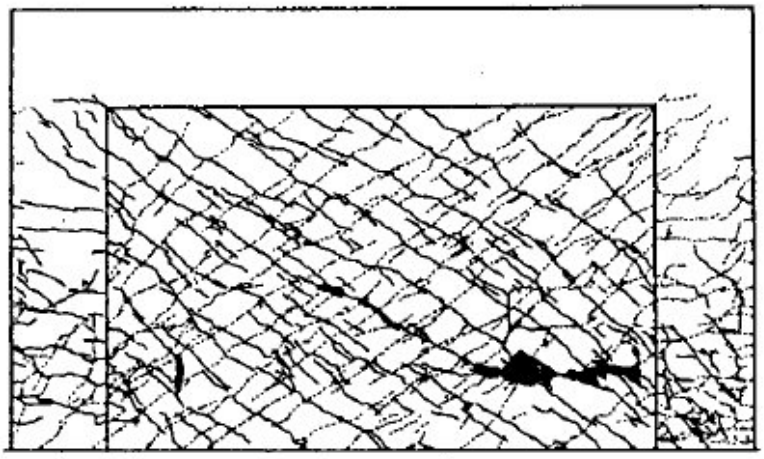

**Figure C-228 Condition of wall No.7 at 0.91% drift [AIJ (1985a)]**

### C.2.2.8 Wall No.8 (CW-0.6-0.6-40)

**Table C-57 Evaluation of damage data for wall No.8 tested by Fukuzawa**

| Wall ID | MoR | Damage State (DS) | Drift (%) | Comments |
|---|---|---|---|---|
| No.8 | 1 | 1.2 | 0.05 | The drifts for these damage states are provided by the researcher. The reported drift at sliding failure (shaded) is excluded from the fragility analysis because herein drift associated with sliding failure is calculated using the supplemental wall replacement criteria. No data associated with DS4.1 is registered since none could be obtained using the supplemental criteria. |
| | | 1.3 | 0.03 | |
| | 2a | 2.1 | 0.54 | |
| | | 2.2 | 0.57 | |
| | | 2.3 | 0.38 | |
| | 3 | 3.1 | 0.23 | |
| | 4 | 4.1 | 0.68 | |
| | | 4.3 | 0.69 | The image reported at this drift (Figure C-230) shows widespread crushing. |
| | 4* | $SC_1$ | N/A | The residual drifts did not exceed 1.0% (Figure C-229). |
| | | $SC_2$ | N/A | The post-peak resistance computed using the first cycle backbone curve did not drop to $0.5V_{peak}$ (see Figure C-229). |

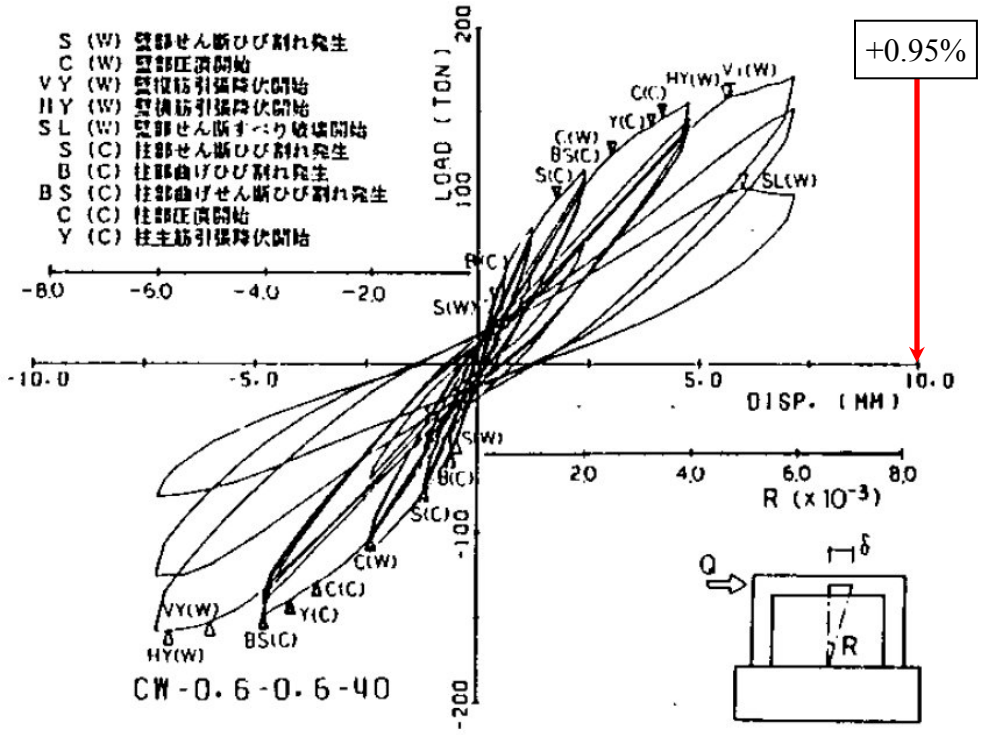


**Figure C-229 Load-displacement relationship for wall No.8 (CW-0.6-0.6-40) [AIJ (1985a)]**

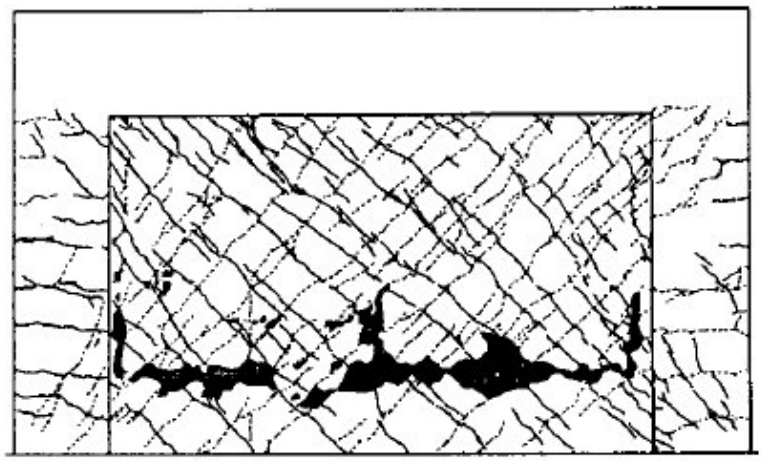

**Figure C-230 Condition of wall No.8 at 0.69% drift [AIJ (1985a)]**

### C.2.2.9 Wall No.9 (CW-0.4-0.6-20)

**Table C-58 Evaluation of damage data for wall No.9 tested by Fukuzawa**

| Wall ID | MoR | Damage State (DS) | Drift (%) | Comments |
|---|---|---|---|---|
| No.9 | 1 | 1.2 | 0.07 | The drifts for these damage states are provided by the researcher. The reported drift at sliding failure (DS4.1) is excluded from the fragility analysis because herein drift associated with sliding failure is calculated using the supplemental wall replacement criteria. No data associated with DS4.1 is registered since none could be obtained using the supplemental criteria. |
| | | 1.3 | 0.03 | |
| | 2a | 2.1 | 0.60 | |
| | | 2.2 | 0.24 | |
| | | 2.3 | 0.28 | |
| | 3 | 3.1 | 0.28 | |
| | 4 | 4.1 | 0.83 | |
| | | 4.3 | 0.98 | The image reported at this drift (Figure C-232) shows widespread crushing. |
| | 4* | $SC_1$ | N/A | The residual drifts did not exceed 1.0% (Figure C-231). |
| | | $SC_2$ | N/A | The post-peak resistance computed using the first cycle backbone curve did not drop to $0.5V_{peak}$ (see Figure C-231). |

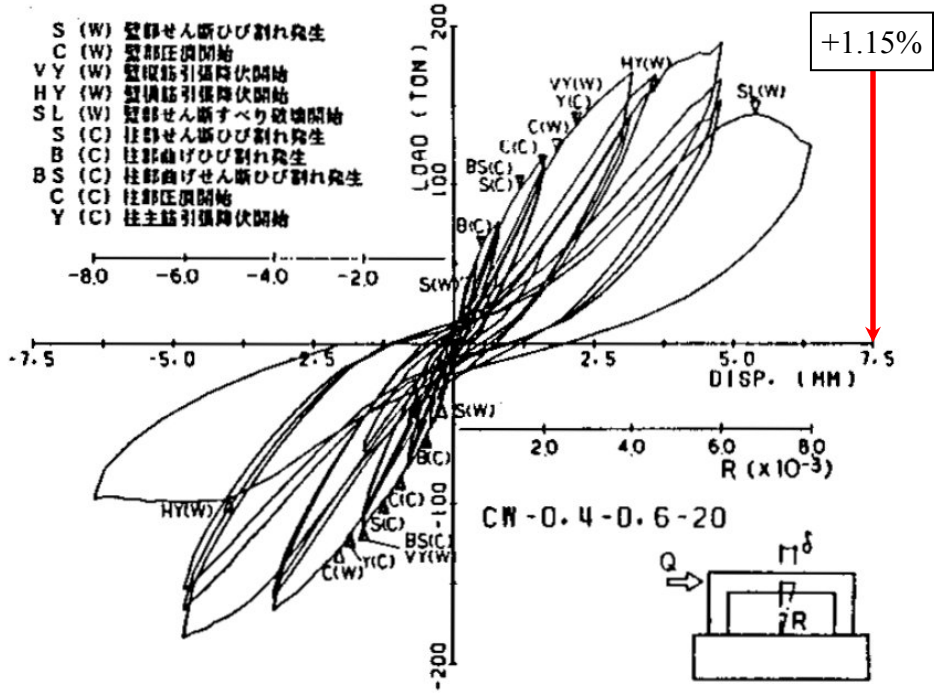


**Figure C-231 Load-displacement relationship for wall No.9 (CW-0.4-0.6-20) [AIJ (1985a)]**

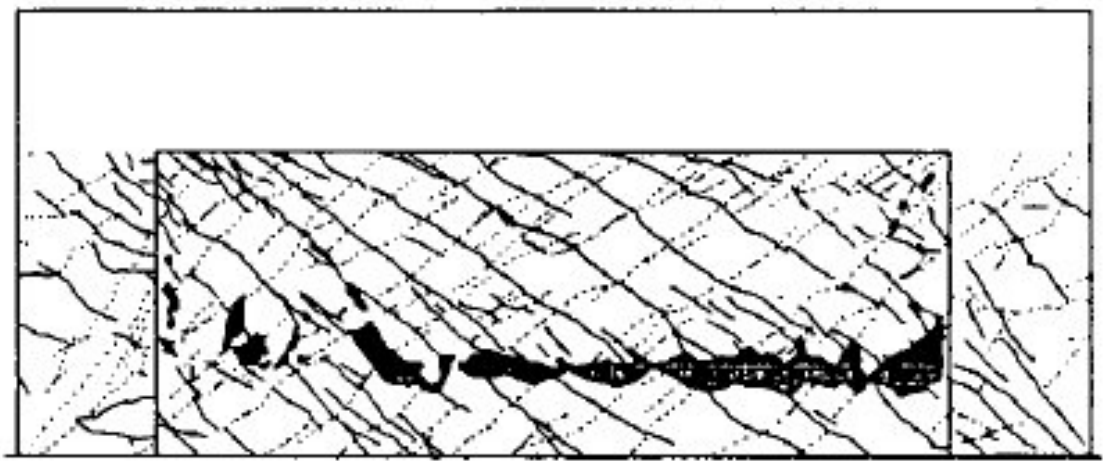

**Figure C-232 Condition of wall No.9 at 0.98% drift [AIJ (1985a)]**

### C.2.2.10 No.10 (CW-0.8-0.6-20)

**Table C-59 Evaluation of damage data for wall No.10 tested by Fukuzawa**

| Wall ID | MoR | Damage State (DS) | Drift (%) | Comments |
|---|---|---|---|---|
| No.10 | 1 | 1.2 | 0.05 | The drifts for these damage states are provided by the researcher. The reported drift at sliding failure (shaded) is excluded from the fragility analysis because herein drift associated with sliding failure is calculated using the supplemental wall replacement criteria. No data associated with DS4.1 is registered since none could be obtained using the supplemental criteria. |
| | | 1.3 | 0.02 | |
| | 2a | 2.1 | 0.39 | |
| | | 2.2 | 0.22 | |
| | | 2.3 | 0.29 | |
| | 3 | 3.1 | 0.31 | |
| | 4 | 4.1 | 0.94 | |
| | | 4.3 | 1.32 | The image reported at this drift (Figure C-234) shows widespread crushing. |
| | 4* | $SC_1$ | N/A | The residual drifts did not exceed 1.0% (Figure C-233). |
| | | $SC_2$ | N/A | The post-peak resistance computed using the first cycle backbone curve did not drop to $0.5V_{peak}$ (see Figure C-233). |

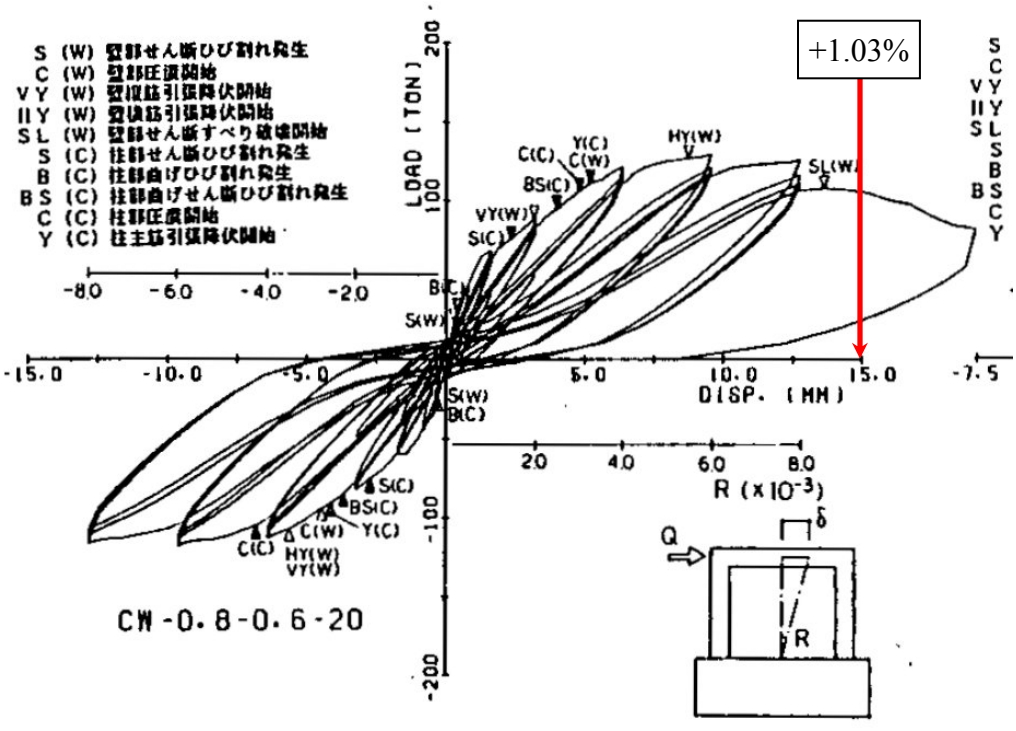


**Figure C-233 Load-displacement relationship for wall No.10 (CW-0.8-0.6-20) [AIJ (1985a)]**

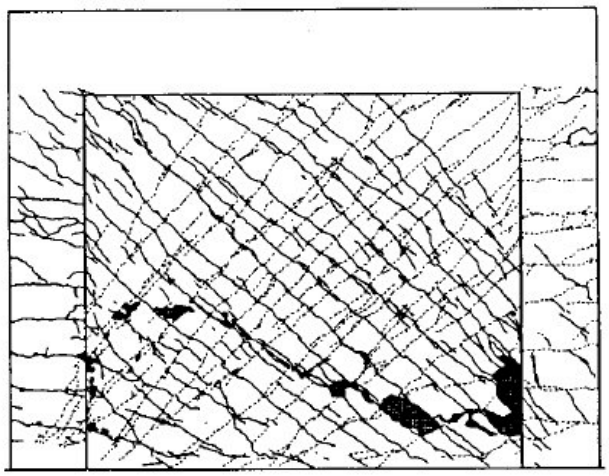

**Figure C-234 Condition of wall No.10 at 1.32% drift [AIJ (1985a)]**

### C.2.2.11 Wall No.11 (CW-0.4-2.0-20)

**Table C-60 Evaluation of damage data for wall No.11 tested by Fukuzawa**

| Wall ID | MoR | Damage State (DS) | Drift (%) | Comments |
|---|---|---|---|---|
| No.11 | 1 | 1.2 | 0.08 | The drifts for these damage states are provided by the researcher. |
| | | 1.3 | 0.03 | |
| | 2a | 2.3 | 0.65 | |
| | 3 | 3.1 | 0.45 | |
| | 4 | 4.3 | 0.74 | The image reported at this drift (Figure C-236) shows widespread crushing. |

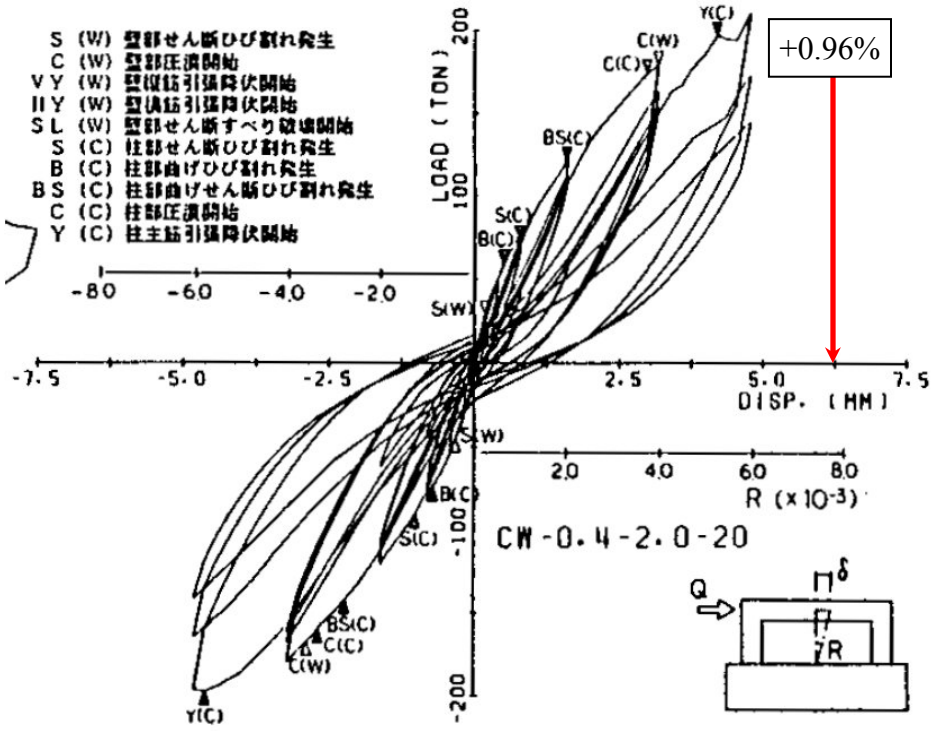


**Figure C-235 Load-displacement relationship for wall No.11 (CW-0.4-2.0-20) [AIJ (1985a)]**

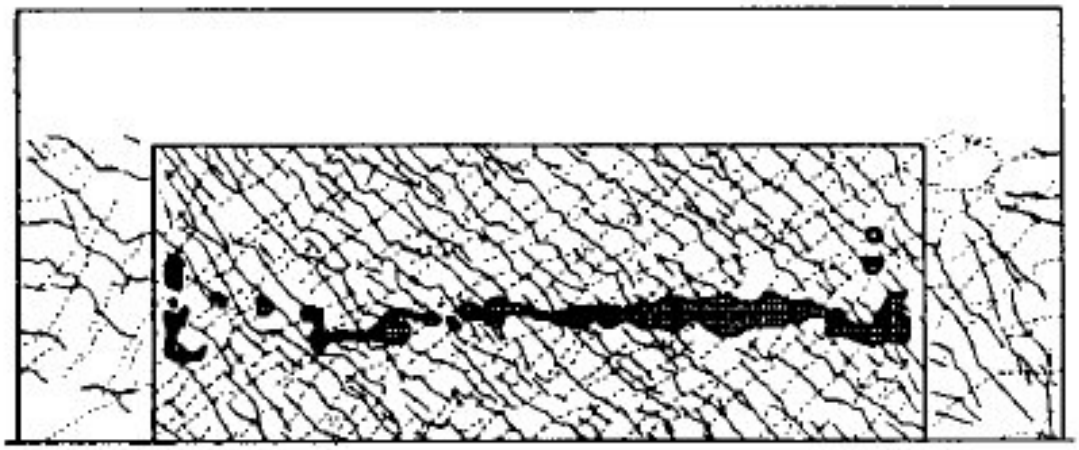

**Figure C-236 Condition of wall No.11 at 0.74% drift [AIJ (1985a)]**

### C.2.2.12 Wall No.12 (CW-0.8-2.0-20)

**Table C-61 Evaluation of damage data for wall No.12 tested by Fukuzawa**

| Wall ID | MoR | Damage State (DS) | Drift (%) | Comments |
|---|---|---|---|---|
| No.12 | 1 | 1.2 | 0.05 | The drifts for these damage states are provided by the researcher. The reported drift at sliding failure (shaded) is excluded from the fragility analysis because herein drift associated with sliding failure is calculated using the supplemental wall replacement criteria. No data associated with DS4.1 is registered since none could be obtained using the supplemental criteria. |
| | | 1.3 | 0.02 | |
| | 2a | 2.1 | 0.72 | |
| | | 2.2 | 0.74 | |
| | | 2.3 | 0.43 | |
| | 3 | 3.1 | 0.37 | |
| | 4 | 4.1 | 0.83 | |
| | | 4.3 | 0.88 | The image reported at this drift (Figure C-238) shows widespread crushing. |
| | 4* | $SC_1$ | N/A | The residual drifts did not exceed 1.0% (Figure C-237). |
| | | $SC_2$ | N/A | The post-peak resistance computed using the first cycle backbone curve did not drop to $0.5V_{peak}$ (see Figure C-237). |

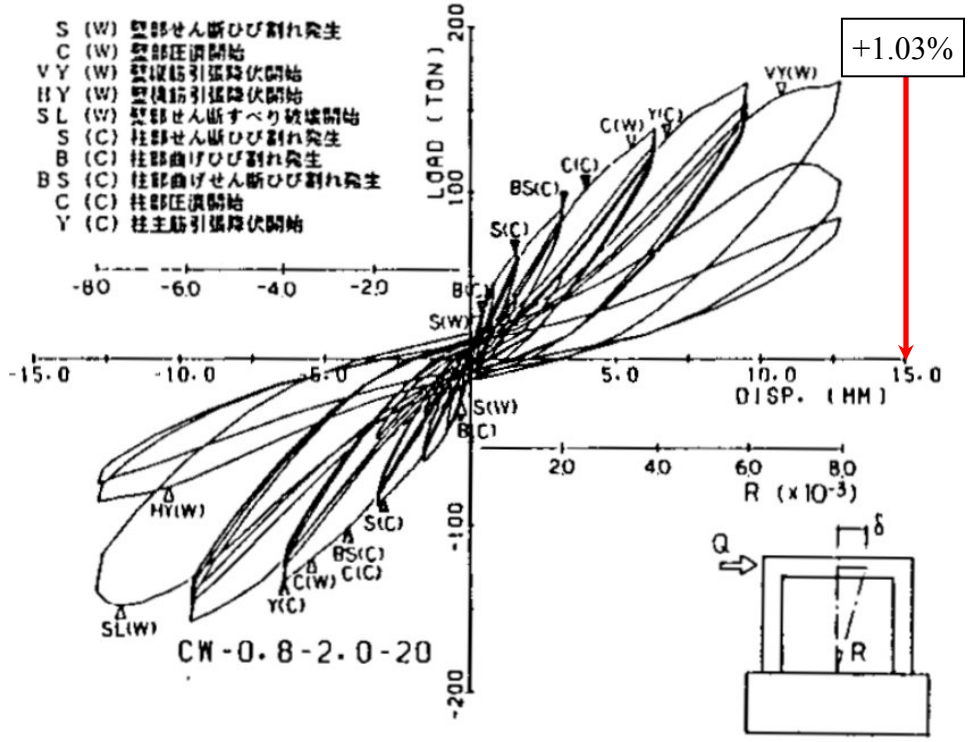


**Figure C-237 Load-displacement relationship for wall No.12 (CW-0.8-2.0-20) [AIJ (1985a)]**

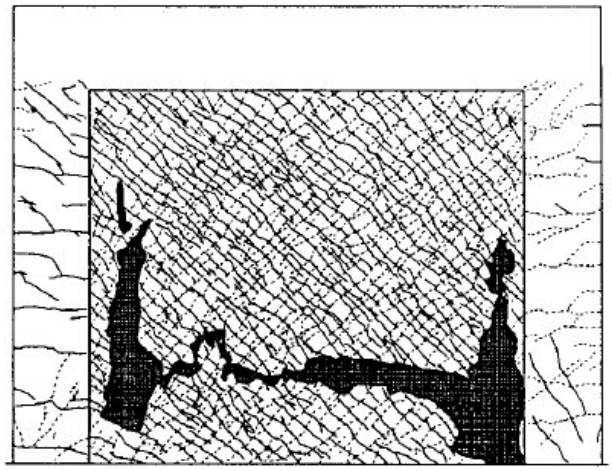

**Figure C-238 Condition of wall No.12 at 0.88% drift [AIJ (1985a)]**

## C.2.3 Hatori Walls [AIJ (1986b)]

### C.2.3.1 Wall No.1 (CW-0.6-2-0)

**Table C-62 Evaluation of damage data for wall No.1 tested by Hatori**

| Wall ID | MoR | Damage State (DS) | Drift (%) | Comments |
|---|---|---|---|---|
| No.1 | 1 | 1.3 | 0.03 | The drift for this damage state is provided by the researcher. |
| | 4 | 4.3 | 0.91 | The image reported at this drift (Figure C-240) shows widespread crushing. |

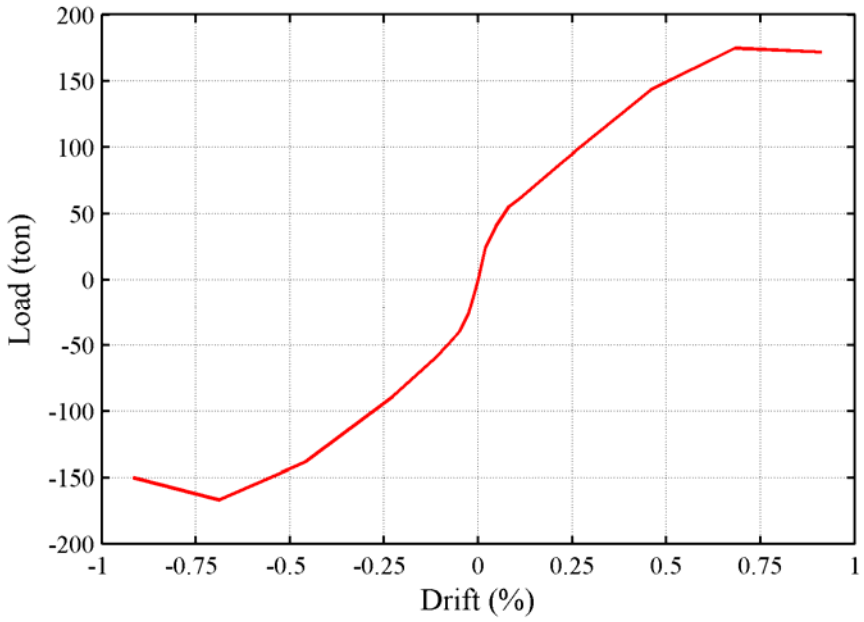


**Figure C-239 Backbone curve for wall No.1**

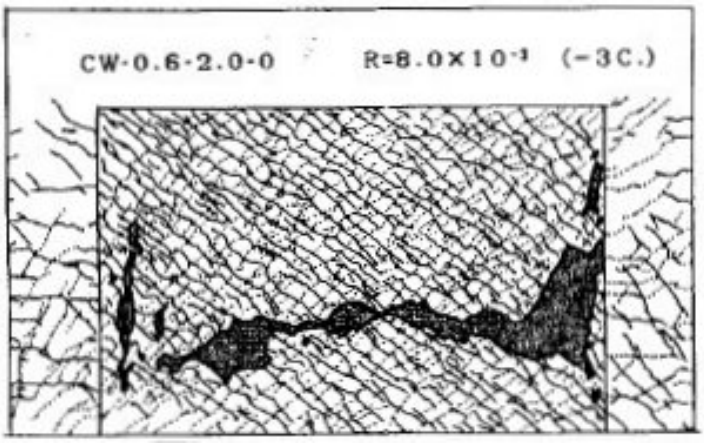


**Figure C-240 Condition of wall No.1 at 0.91% drift [AIJ (1986b)]**

## C.2.4 Wall No.2 (CW-0.6-2-40)

**Table C-63 Evaluation of damage data for wall No.2 tested by Hatori**

| Wall ID | MoR | Damage State (DS) | Drift (%) | Comments |
|---|---|---|---|---|
| No.2 | 1 | 1.3 | 0.05 | The drift for this damage state is provided by the researcher. |
| | 4 | 4.3 | 0.91 | The image reported at this drift (Figure C-242) shows widespread crushing. |

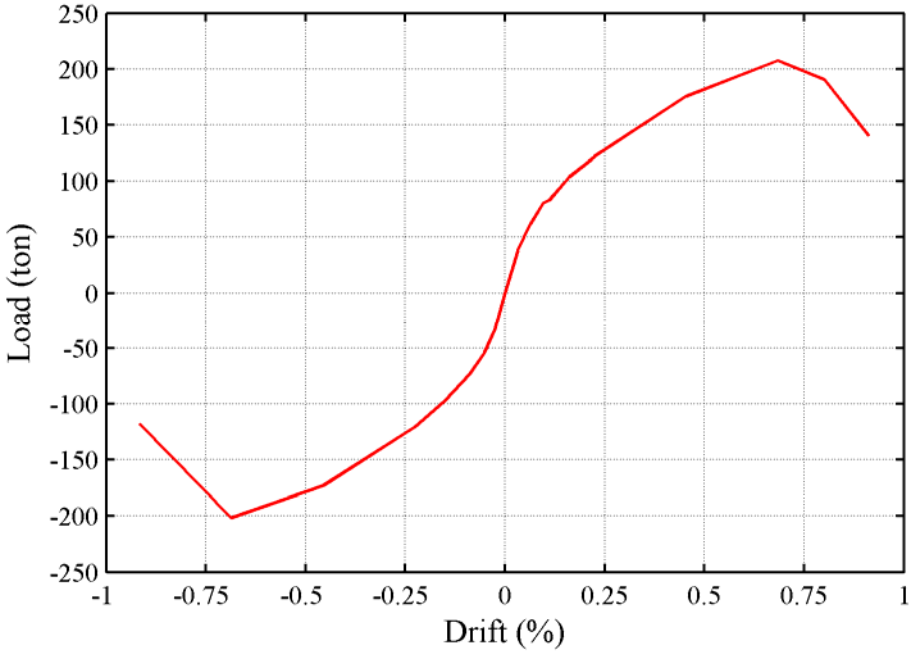


**Figure C-241 Backbone curve for wall No.2**

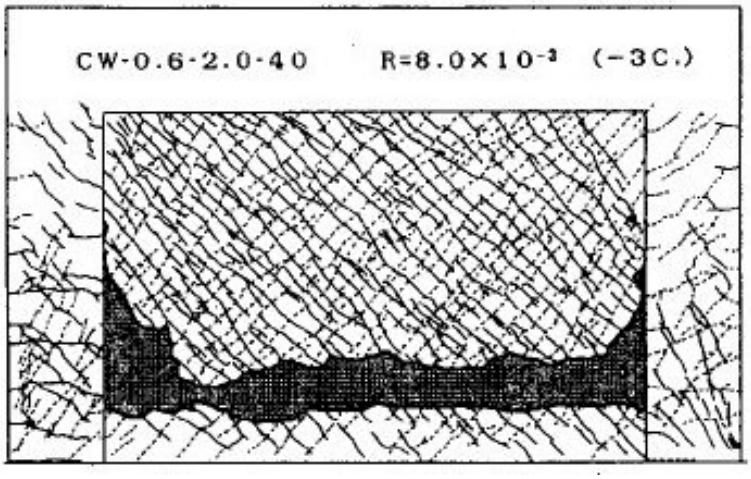


**Figure C-242 Condition of wall No.2 at 0.91% drift [AIJ (1986b)]**

### C.2.4.1 Wall No.3 (CW-0.6-2-20B)

**Table C-64 Evaluation of damage data for wall No.3 tested by Hatori**

| Wall ID | MoR | Damage State (DS) | Drift (%) | Comments |
|---|---|---|---|---|
| No.3 | 1 | 1.3 | 0.03 | The drift for this damage state is provided by the researcher. |
| | 4 | 4.3 | 0.91 | The image reported at this drift (Figure C-244) shows widespread crushing. |

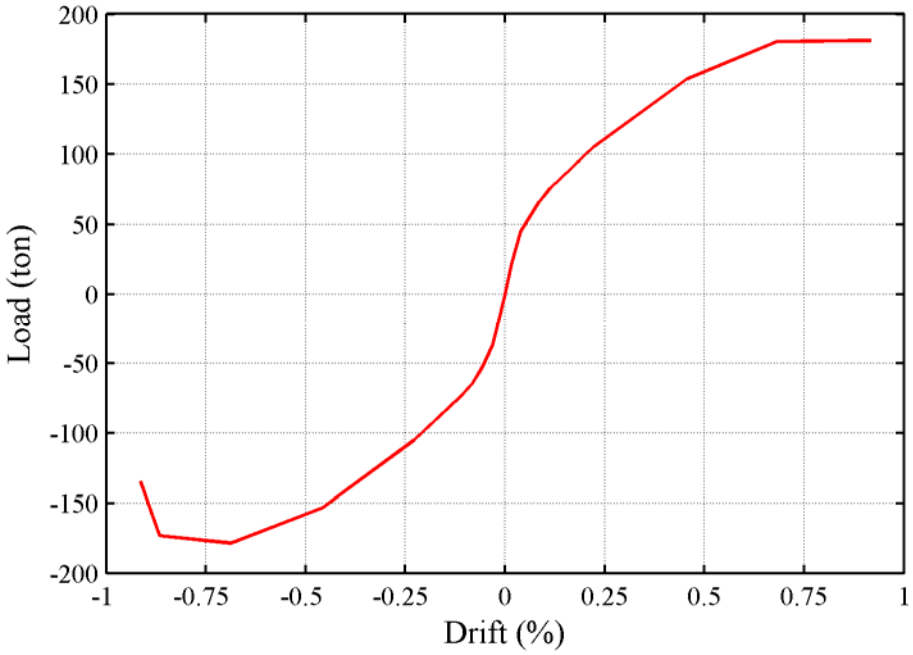


**Figure C-243 Backbone curve for wall No.3**

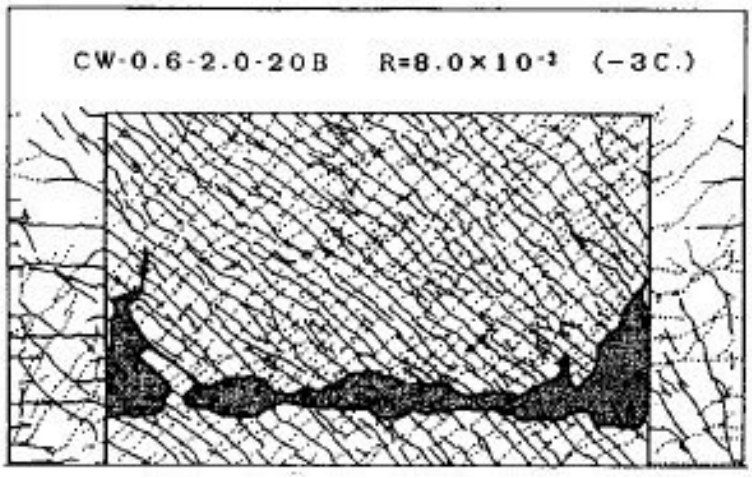


**Figure C-244 Condition of wall No.3 at 0.91% drift [AIJ (1986b)]**

## C.2.5 Wall No.4 (CW-0.6-0.6-20L)

**Table C-65 Evaluation of damage data for wall No.4 tested by Hatori**

| Wall ID | MoR | Damage State (DS) | Drift (%) | Comments |
|---|---|---|---|---|
| No.4 | 1 | 1.3 | 0.03 | The drift for this damage state is provided by the researcher. |
| | 4 | 4.3 | 0.91 | The image reported at this drift (Figure C-246) shows widespread crushing. |

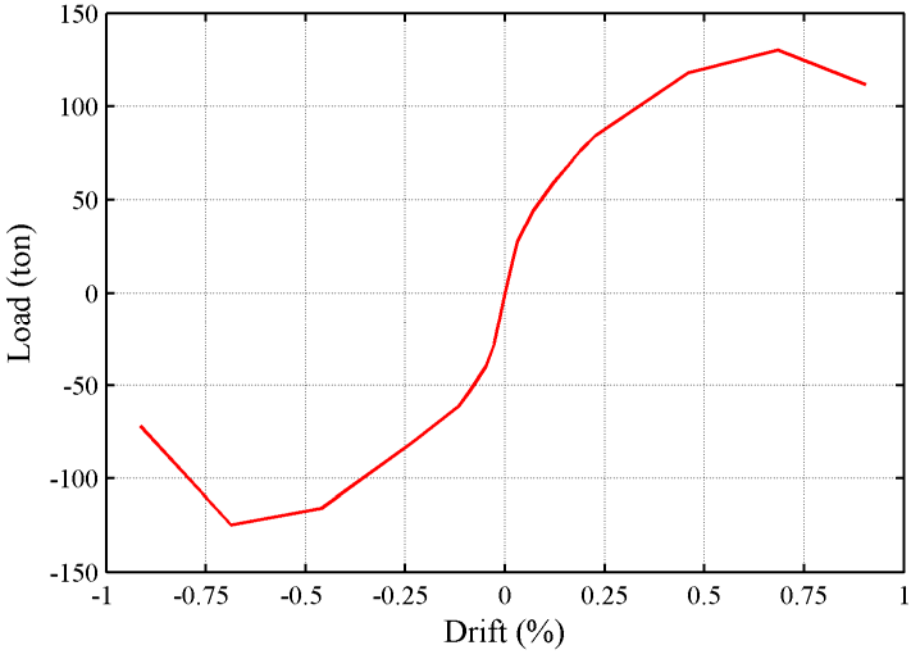


**Figure C-245 Backbone curve for wall No.4**

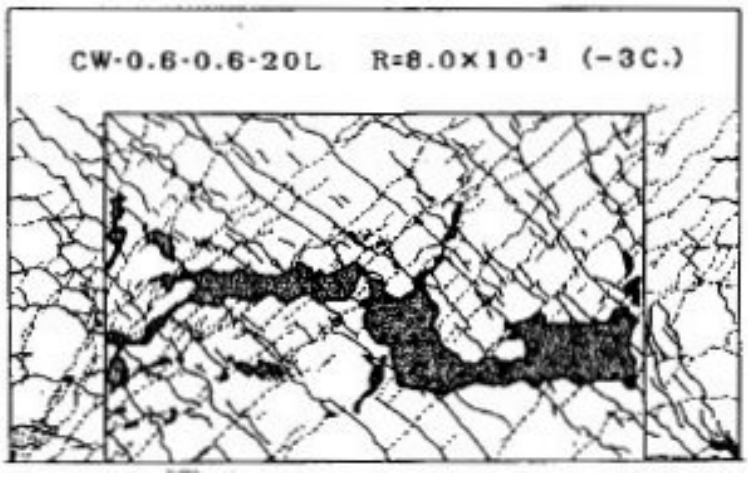


**Figure C-246 Condition of wall No.4 at 0.91% drift [AIJ (1986b)]**

### C.2.5.1 Wall No.5 (CW-0.6-1.2-20L)

**Table C-66 Evaluation of damage data for wall No.5 tested by Hatori**

| Wall ID | MoR | Damage State (DS) | Drift (%) | Comments |
|---|---|---|---|---|
| No.5 | 1 | 1.3 | 0.03 | The drift for this damage state is provided by the researcher. |
| | 4 | 4.3 | 0.91 | The image reported at this drift (Figure C-248) shows widespread crushing. |

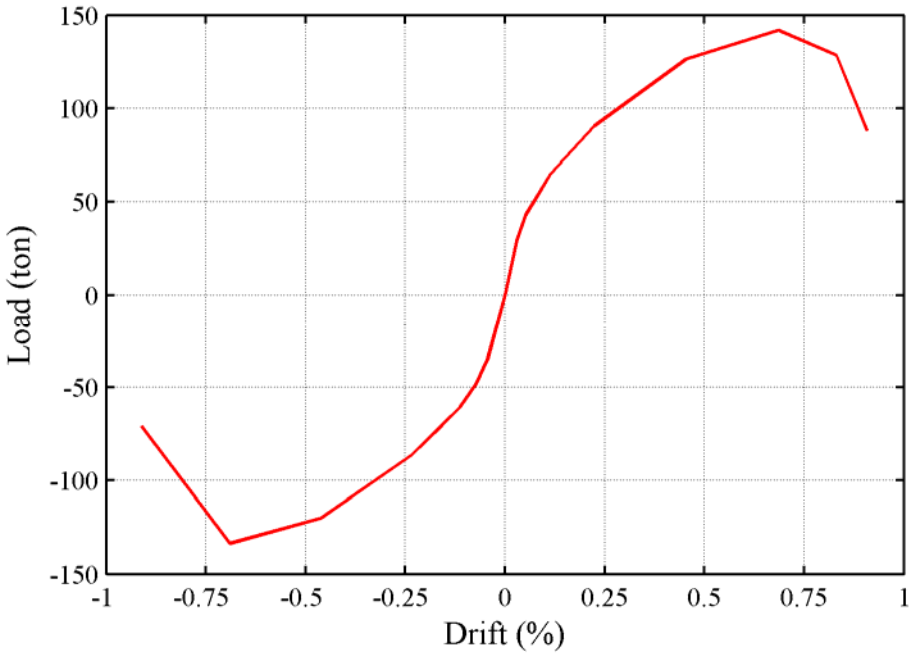


**Figure C-247 Backbone curve for wall No.5**

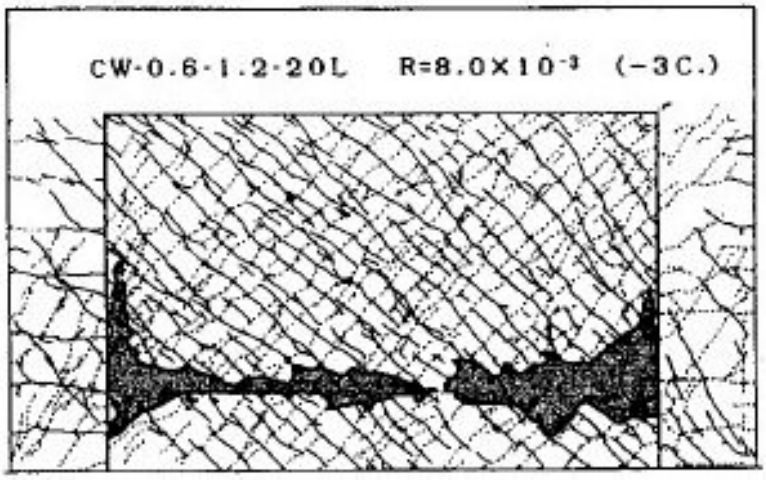


**Figure C-248 Condition of wall No.5 at 0.91% drift [AIJ (1986b)]**

### C.2.5.2 Wall No.6 (CW-0.6-2-20L)

**Table C-67 Evaluation of damage data for wall No.6 tested by Hatori**

| Wall ID | MoR | Damage State (DS) | Drift (%) | Comments |
|---|---|---|---|---|
| No.6 | 1 | 1.3 | 0.03 | The drift for this damage state is provided by the researcher. |
| | 4 | 4.3 | 0.91 | The image reported at this drift (Figure C-250) shows widespread crushing. |

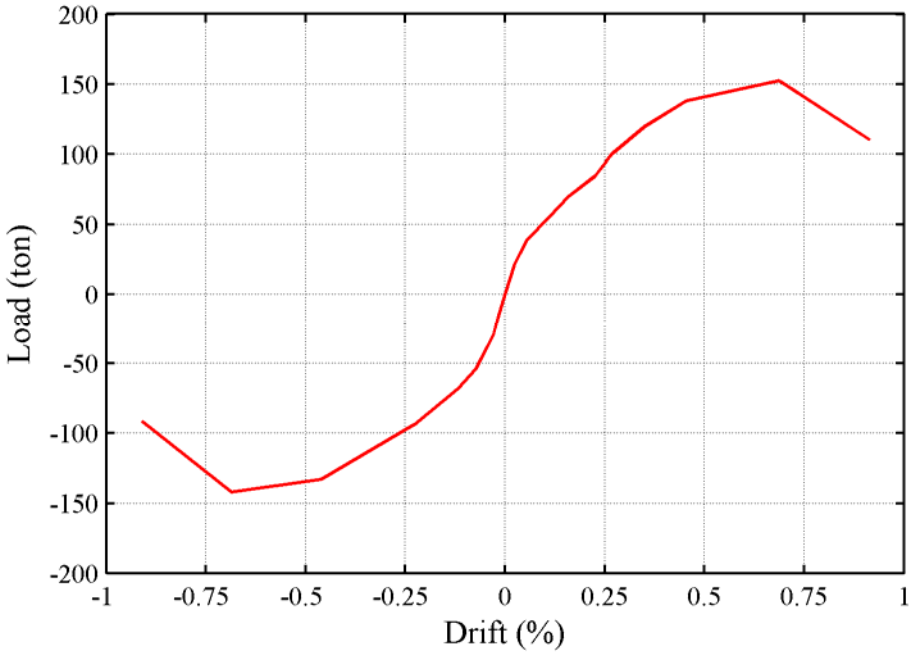


**Figure C-249 Backbone curve for wall No.6**

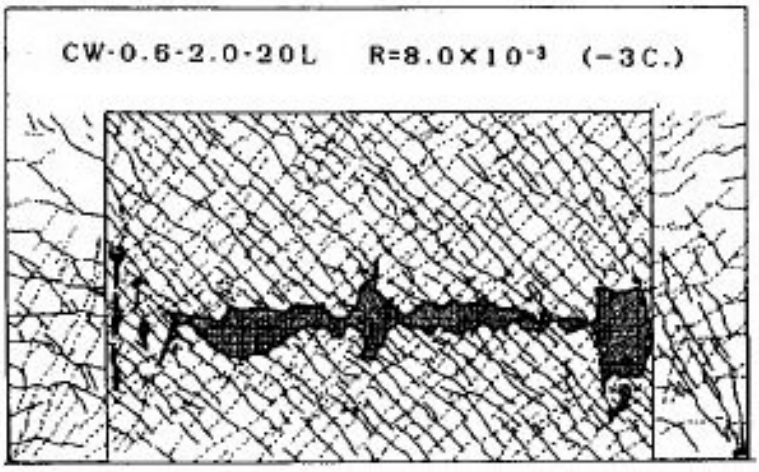


**Figure C-250 Condition of wall No.6 at 0.91% drift [AIJ (1986b)]**

## C.2.6 Yagishita Walls [AIJ (1986a)]

### C.2.6.1 No.2 (CW-0.6-0.6-20a)

**Table C-68 Evaluation of damage data for wall No.2 tested by Yagishita**

| Wall ID | MoR | Damage State (DS) | Drift (%) | Comments |
|---|---|---|---|---|
| No.2 | 1 | 1.2 | 0.02 | The drifts for these damage states are provided by the researcher. The reported drift at sliding failure (shaded) is excluded from the fragility analysis because herein drift at a sliding failure is associated with the supplemental wall replacement criteria. The drift obtained using the 2nd supplemental criterion (bolded) is used to replace the drift reported by the researcher. |
| | | 1.3 | 0.02 | |
| | 2a | 2.1 | 0.46 | |
| | | 2.3 | 0.33 | |
| | 3 | 3.1 | 0.29 | |
| | 4 | 4.1 | 0.52 | |
| | | 4.3 | 0.69 | The image reported at this drift (Figure C-252) shows widespread crushing. |
| | 4* | $SC_1$ | N/A | The residual drifts did not exceed 1.0% (Figure C-251). |
| | | $SC_2$ | **0.77** | The smaller of the two drifts is obtained from the 3rd quadrant of the load-displacement relationship (see Figure C-251). |

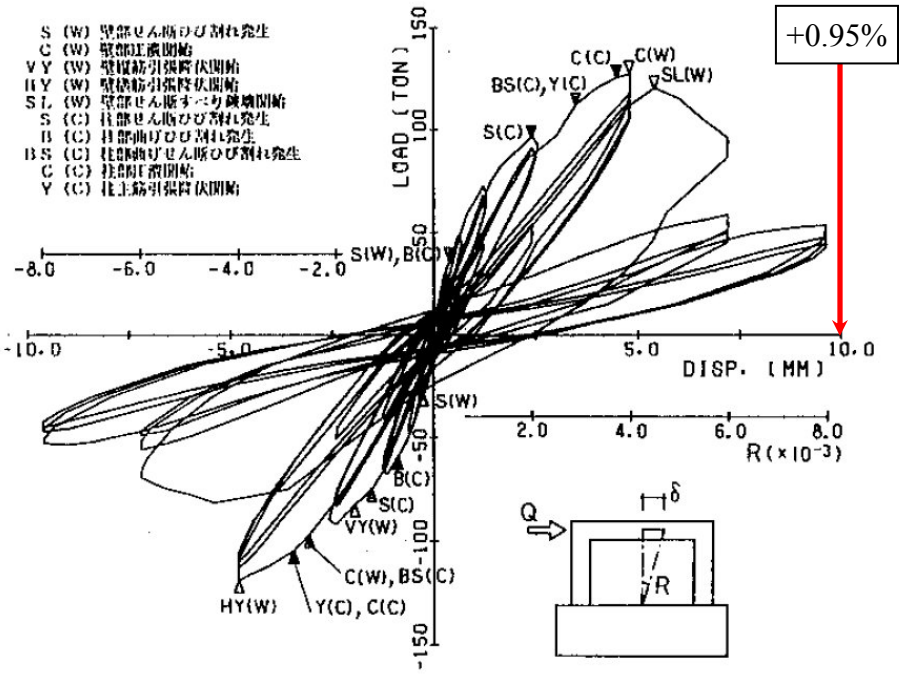


**Figure C-251 Load-displacement relationship for wall No.2 (CW-0.6-0.6-20a) [AIJ (1986a)]**

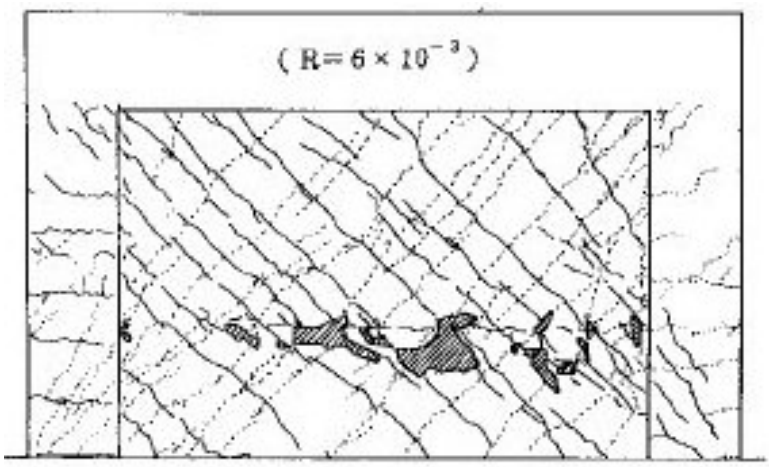


**Figure C-252 Condition of wall No.2 at 0.69% drift [AIJ (1986a)]**

### C.2.6.2 No.3 (CW-0.6-0.8-20a)

**Table C-69 Evaluation of damage data for wall No.3 tested by Yagishita**

| Wall ID | MoR | Damage State (DS) | Drift (%) | Comments |
|---|---|---|---|---|
| No.3 | 1 | 1.2 | 0.04 | The drifts for these damage states are provided by the researcher. |
| | | 1.3 | 0.02 | |
| | 2a | 2.1 | 0.56 | |
| | | 2.2 | 0.23 | |
| | | 2.3 | 0.38 | |
| | 3 | 3.1 | 0.23 | |
| | 4 | 4.3 | 0.91 | The image reported at this drift (Figure C-254) shows widespread crushing. |

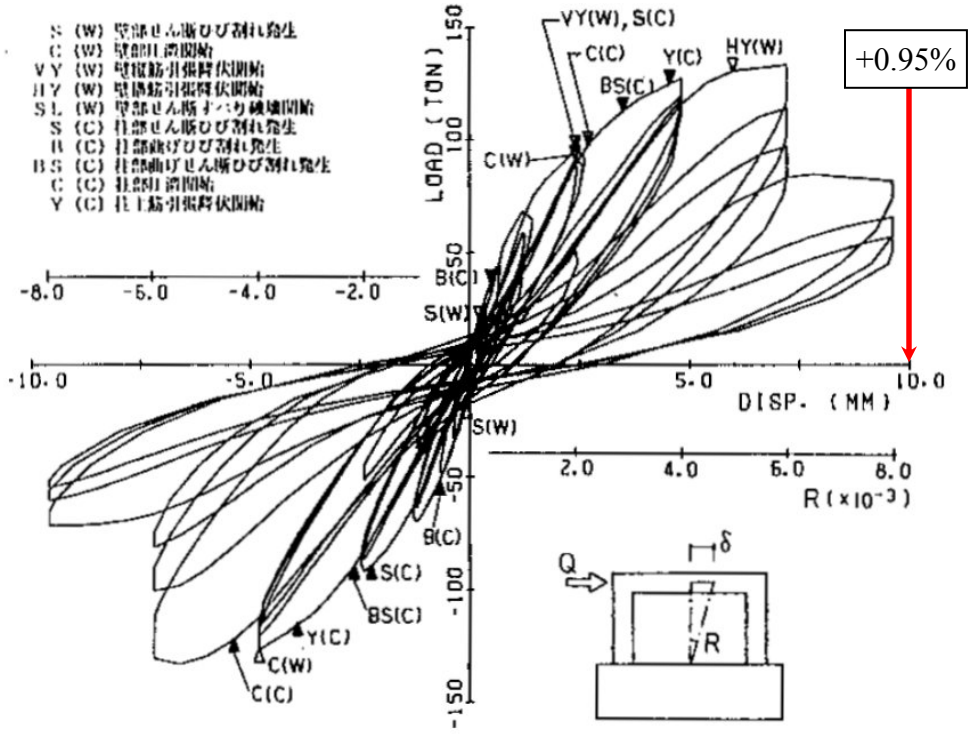


**Figure C-253 Load-displacement relationship for wall No.3 (CW-0.6-0.8-20a) [AIJ (1986a)]**

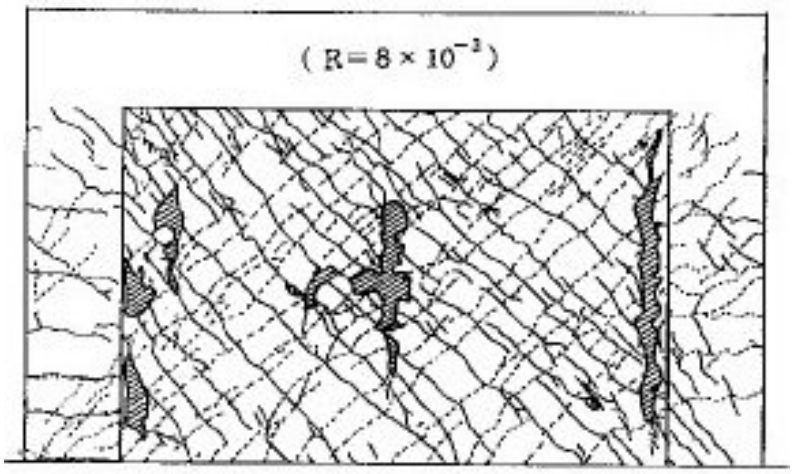


**Figure C-254 Condition of wall No.2 at 0.91% drift [AIJ (1986a)]**

### C.2.6.3 No.6 (CW-0.6-1.2-0)

**Table C-70 Evaluation of damage data for wall No.6 tested by Yagishita**

| Wall ID | MoR | Damage State (DS) | Drift (%) | Comments |
|---|---|---|---|---|
| No.6 | 1 | 1.2 | 0.05 | The drifts for these damage states are provided by the researcher. The reported drift at sliding failure (shaded) is excluded from the fragility analysis because herein drift associated with sliding failure is calculated using the supplemental wall replacement criteria. No data associated with DS4.1 is registered since none could be obtained using the supplemental criteria. |
| | | 1.3 | 0.02 | |
| | 2 | 2.1 | 0.68 | |
| | | 2.2 | 0.34 | |
| | | 2.3 | 0.23 | |
| | 3 | 3.1 | 0.40 | |
| | 4 | 4.1 | 0.80 | |
| | | 4.3 | 0.91 | The image reported at this drift (Figure C-256) shows widespread crushing. |
| | 4* | $SC_1$ | N/A | The residual drifts did not exceed 1.0% (see Figure C-255). |
| | | $SC_2$ | N/A | The post-peak resistance computed using the first cycle backbone curve did not drop to $0.5V_{peak}$ (see Figure C-255). |

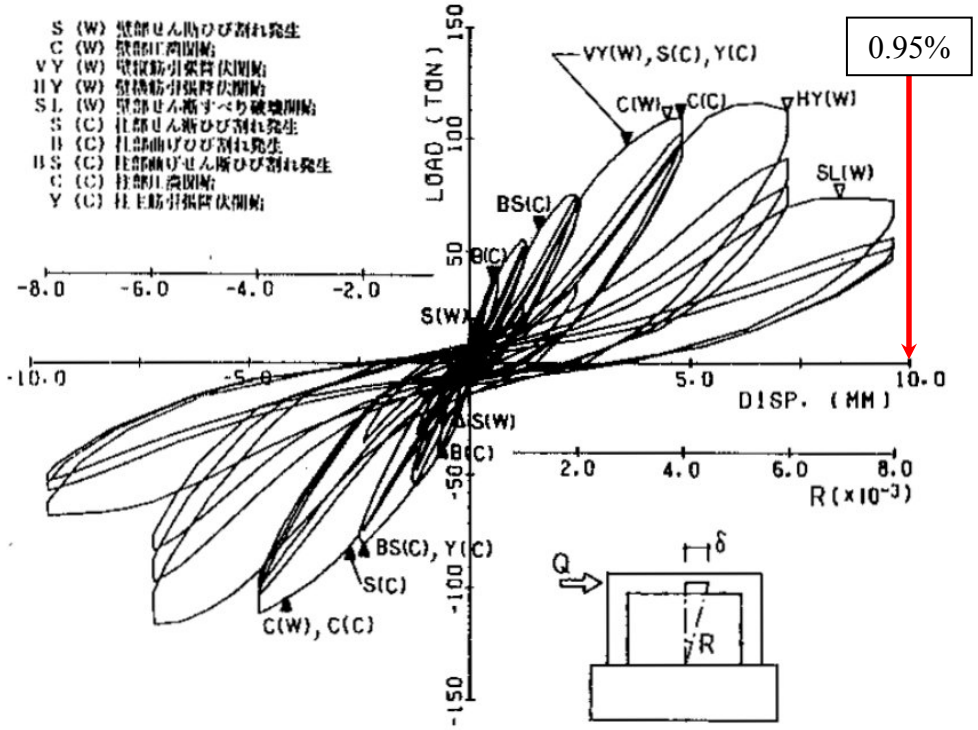


**Figure C-255 Load-displacement relationship for wall No.6 (CW-0.6-1.2-0) [AIJ (1986a)]**

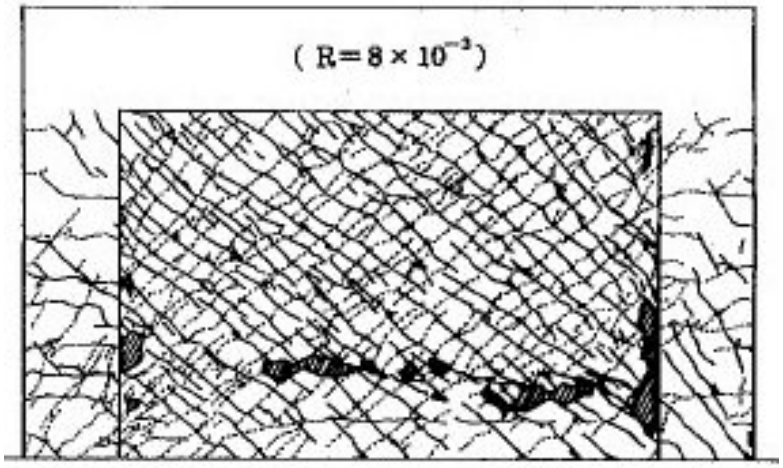


**Figure C-256 Condition of wall No.6 at 0.91% drift [AIJ (1986a)]**

## C.2.7 Taga Walls [AIJ (1986c)]

### C.2.7.1 Wall No.1

**Table C-71 Evaluation of damage data for wall No.1 tested by Taga**

| Wall ID | MoR | Damage State (DS) | Drift (%) | Comments |
|---|---|---|---|---|
| No.1 | 4 | 4.3 | 0.88 | The only damage image reported for this wall (Figure C-257) shows widespread crushing. However, the image corresponds to the condition of the wall at the end of the test. Therefore, $SC_2$ is invoked to obtain the drift associated with DS4.3. |
| | 4* | $SC_2$ | 0.88 | The smaller of the two drifts is obtained from the 3rd quadrant of the load-displacement relationship (see Figure C-259). |

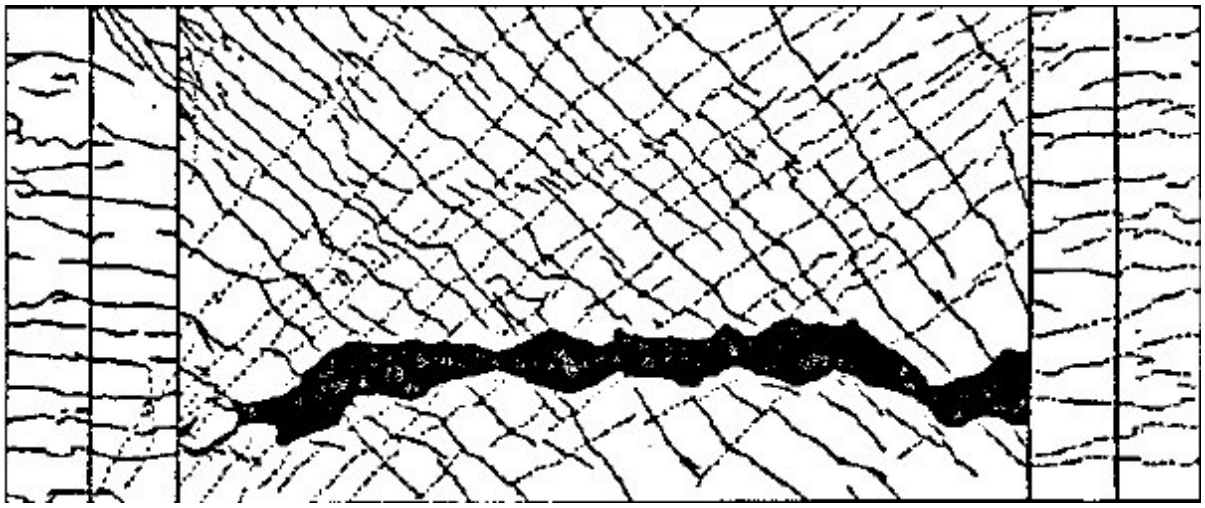

**Figure C-257 Condition of wall No.1 at the end of the test (maximum drift in the test = 1.21%) [AIJ (1986c)]**

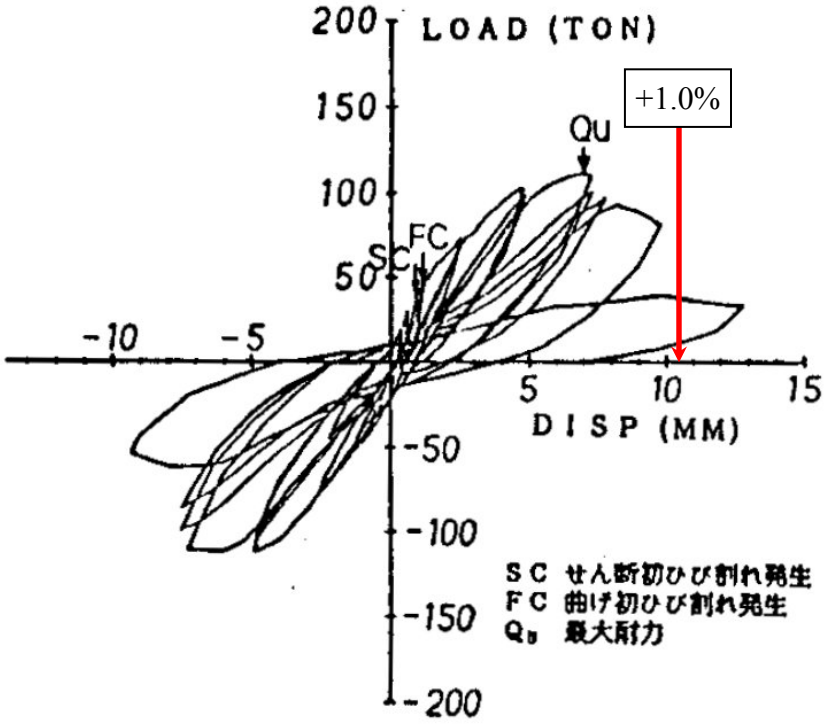


**Figure C-258 Load-displacement relationship for wall No.1 [AIJ (1986c)]**

## C.2.8 Wall No.2

**Table C-72 Evaluation of damage data for wall No.2 tested by Taga**

| Wall ID | MoR | Damage State (DS) | Drift (%) | Comments |
|---|---|---|---|---|
| No.2 | 4 | 4.3 | 1.07 | The only damage image reported for this wall (Figure C-259) shows widespread crushing. However, the image corresponds to the condition of the wall at the end of the test. Therefore, $SC_2$ is invoked to obtain the drift associated with DS4.3. |
| | 4* | $SC_2$ | 1.07 | The data point is obtained from the 1st quadrant of the load-displacement relationship (see Figure C-260). A data point cannot be established in the 3rd quadrant. |

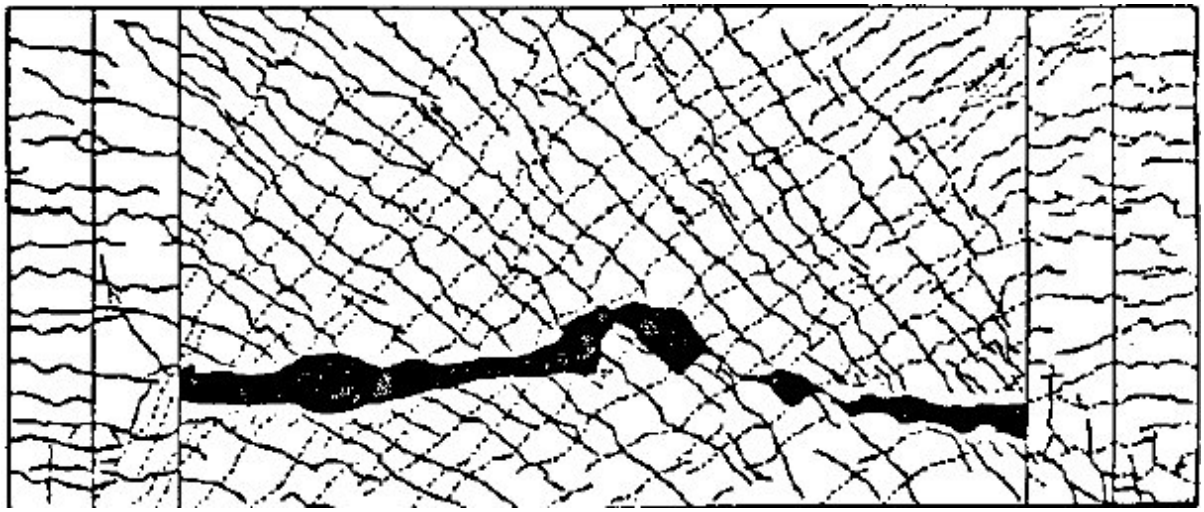

**Figure C-259 Condition of wall No.1 at the end of the test (maximum drift in the test = 1.18%) [AIJ (1986c)]**

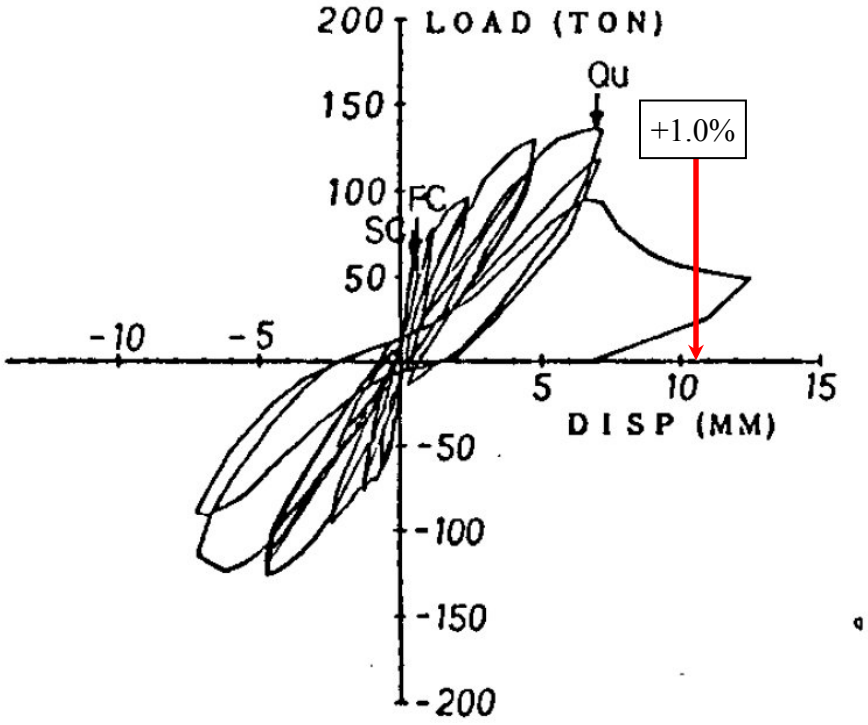


**Figure C-260 Load-displacement relationship for wall No.2 [AIJ (1986c)]**

### C.2.8.1 Wall No.3

**Table C-73 Evaluation of damage data for wall No.3 tested by Taga**

| Wall ID | MoR | Damage State (DS) | Drift (%) | Comments |
|---|---|---|---|---|
| No.3 | 4 | 4.3 | 0.93 | The only damage image reported for this wall (Figure C-261) shows widespread crushing. However, the image corresponds to the condition of the wall at the end of the test. Therefore, $SC_2$ is invoked to obtain a drift associated with MoR-4. Since no data could be obtained using $SC_2$, the maximum drift recorded in the test used. |
| | $4^*$ | $SC_2$ | N/A | The post-peak resistance computed using the first cycle backbone curve did not drop to $0.5V_{peak}$ (see Figure C-262). |

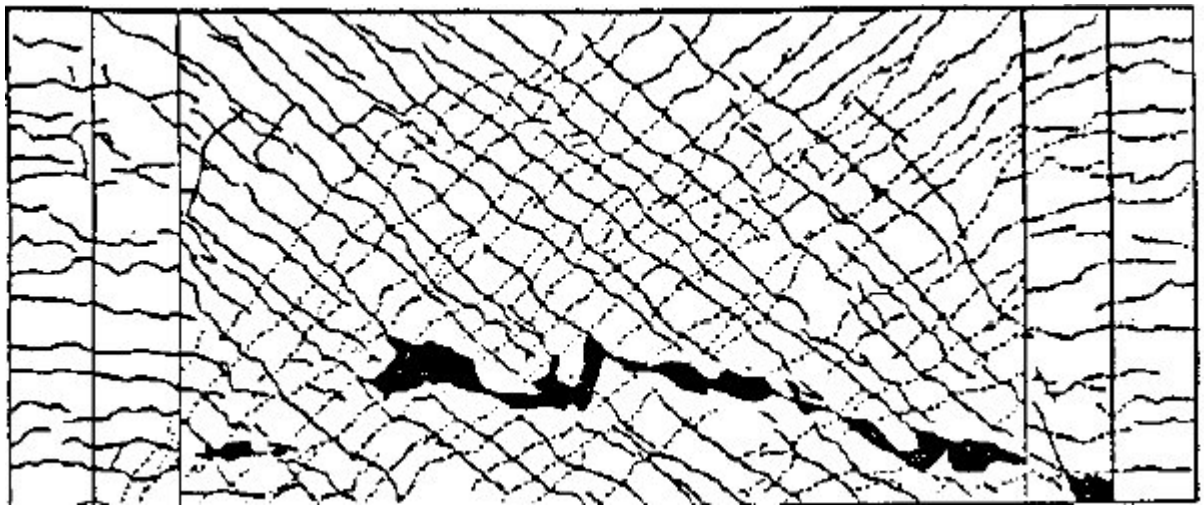

**Figure C-261 Condition of wall No.3 at the end of the test (maximum drift in the test = 0.93%) [AIJ (1986c)]**

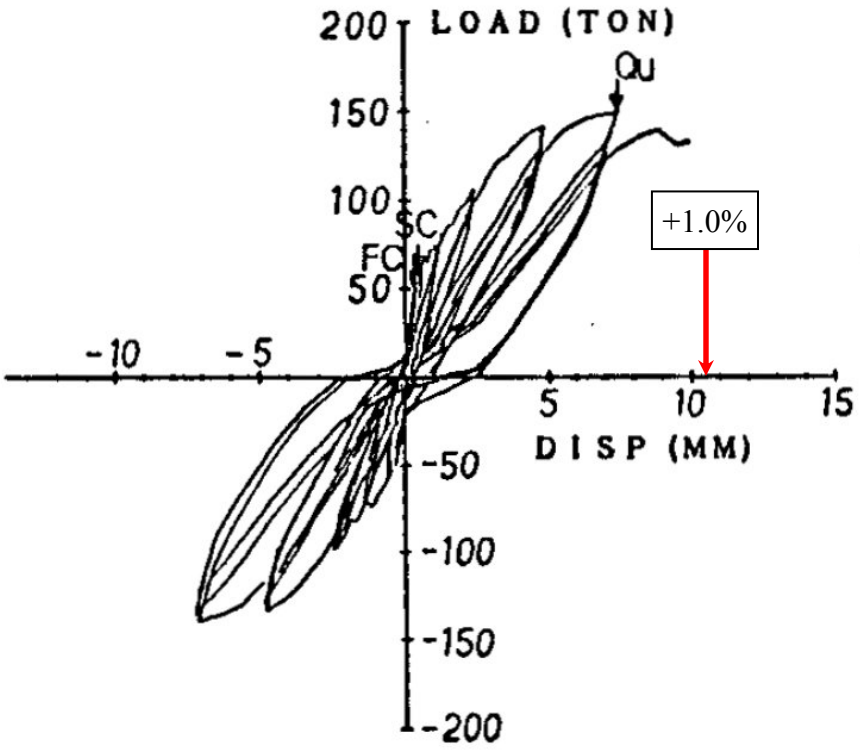


**Figure C-262 Load-displacement relationship for wall No.3 [AIJ (1986c)]**

# C.3 Walls with Flanges

## C.3.1 Barda (1972) Walls

### C.3.1.1 Wall B1-1

**Table C-74 Evaluation of damage data for wall B1-1 tested by Barda**

| Wall ID | MoR | Damage State (DS) | Drift (%) | Comments |
|---|---|---|---|---|
| B1-1 | 1 | 1.1 | 0.02 | The shear forces for these damage states are provided by the researcher. The corresponding drifts are obtained using the reported load-displacement relationship. |
| | | 1.2 | 0.03 | |
| | | 1.3 | 0.07 | |
| | | 1.4 | 0.36 | |
| | 2a | 2.1 | 0.45 | |
| | | 2.2 | 0.35 | |
| | 3 | 3.1 | 0.66 | The researcher stated that crushing initiated following the attainment of peak shear strength [Barda (1972), page 38]. A photograph at peak shear strength was presented (Figure C-264). In Figure C-264, the dashed box identifies the region of concrete requiring replacement. Note that this wall was tested under monotonic loading and so repair quantities were doubled to recognize the cyclic nature of earthquake loading. |
| | 4 | 4.3 | N/A | Wall B1-1 failed by crushing of the diagonal compression struts. However, based on the two damage images provided for this wall, the drift associated with DS4.3 could not be determined. In Figure C-264 (drift = 0.66%) crushing is not widespread whereas Figure C-265 shows gross damage at a drift of >8%, $SC_2$ is invoked to seek a drift for DS4.3. |
| | 4* | $SC_2$ | N/A | The reported load-displacement relationship (Figure C-263) is not complete. The drift for this criterion could not be determined. |

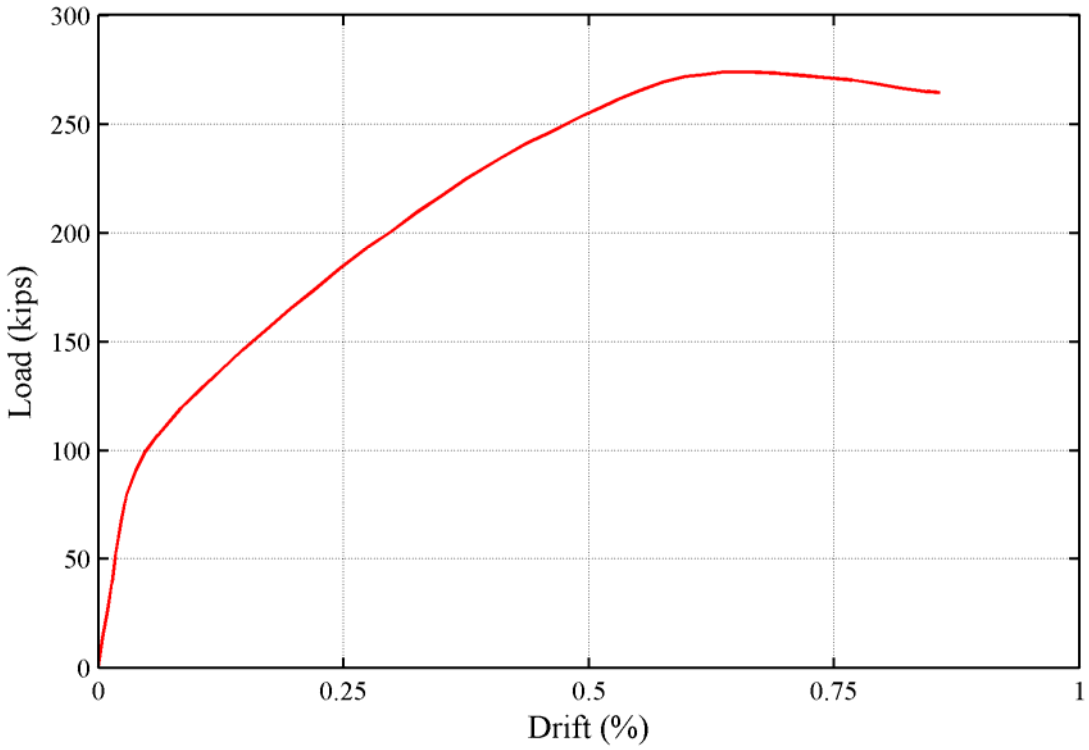


**Figure C-263 Load-drift relationship for wall B1-1**

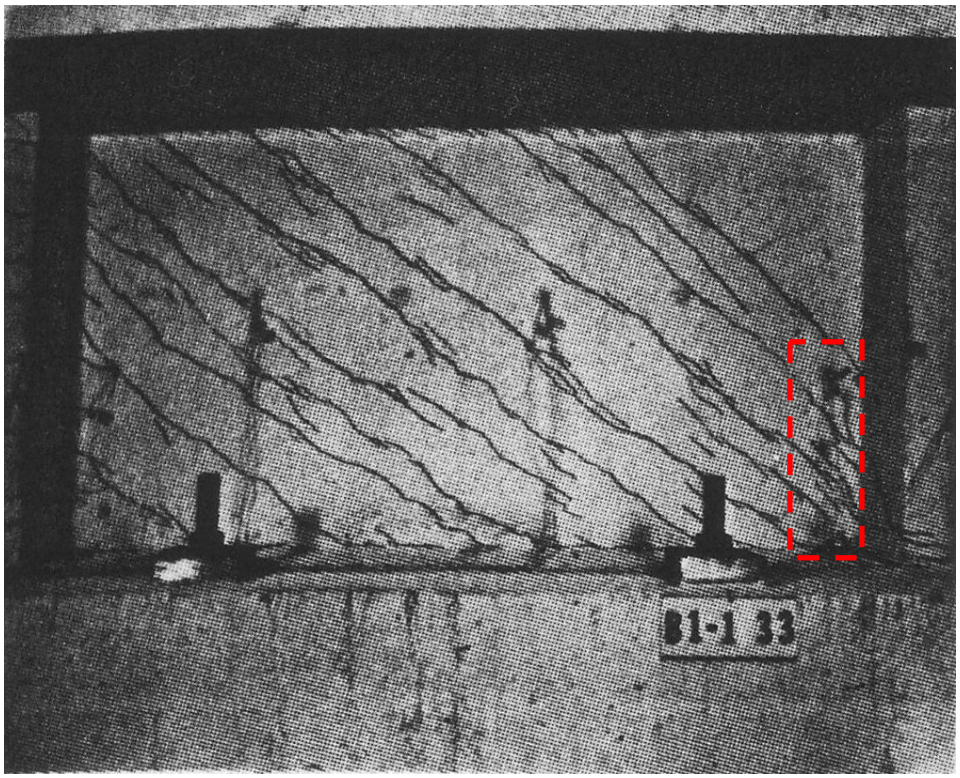


**Figure C-264 Condition of wall B1-1 at 0.66% drift [Barda et al. (1977)]**

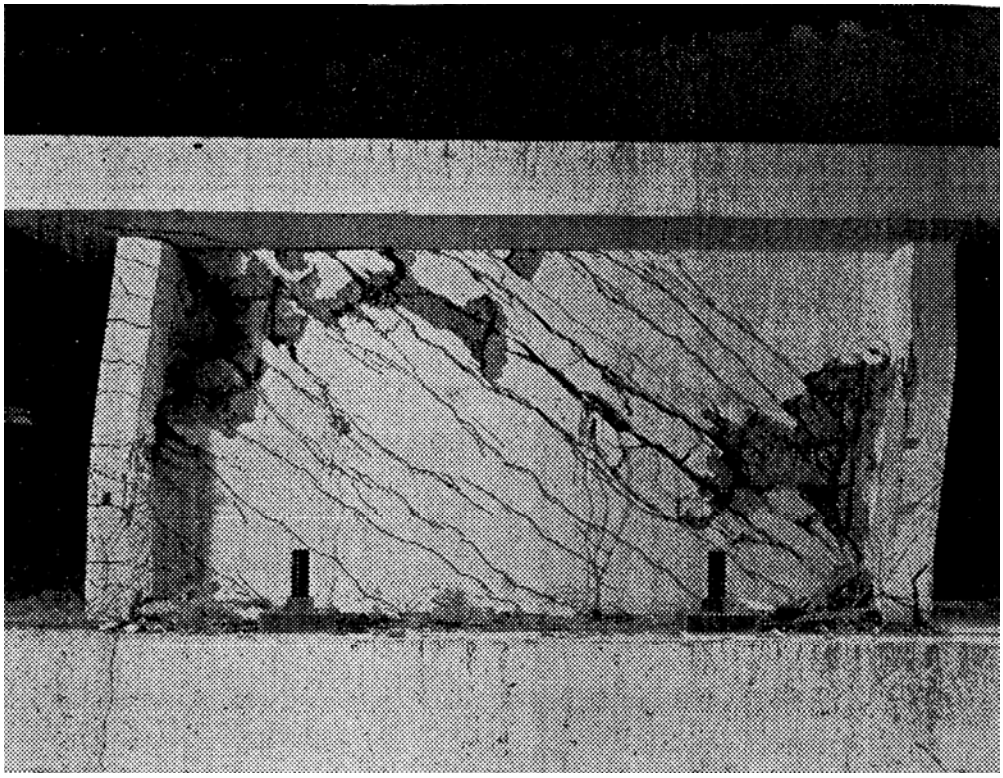

**Figure C-265 Condition of wall B1-1 at the end of the test (drift > 8%) [Barda et al. (1977)]**

### C.3.1.2 Wall B2-1

**Table C-75 Evaluation of damage data for wall B2-1 tested by Barda**

| Wall ID | MoR | Damage State (DS) | Drift (%) | Comments |
|---|---|---|---|---|
| B2-1 | 1 | 1.1 | 0.02 | The shear forces for these damage states are provided by the researcher. The corresponding drifts are obtained using the reported load-displacement relationship. |
| | | 1.2 | 0.06 | |
| | | 1.3 | 0.05 | |
| | | 1.4 | 0.40 | |
| | 2a | 2.1 | 0.26 | |
| | | 2.2 | 0.43 | |
| | 3 | 3.1 | 0.72 | The researcher stated that crushing initiated following the attainment of peak shear strength [Barda (1972), page 40]. A photograph at peak shear strength was presented (Figure C-267). In Figure C-267, the dashed box identifies the region of concrete requiring replacement. Note that this wall was tested under monotonic loading and so repair quantities were doubled to recognize the earthquake loading is cyclic in nature. |
| | 4 | 4.3 | 1.24 | Wall B2-1 failed by crushing of the diagonal compression struts. However, based on the two damage images provided for this wall, the drift for DS4.3 could not be determined. In Figure C-267 (drift = 0.72%) crushing is not widespread whereas Figure C-268 shows gross damage at a drift of >8%, $SC_2$ is invoked to obtain a drift for DS4.3. |
| | 4* | $SC_2$ | 1.24 | See Figure C-266. |

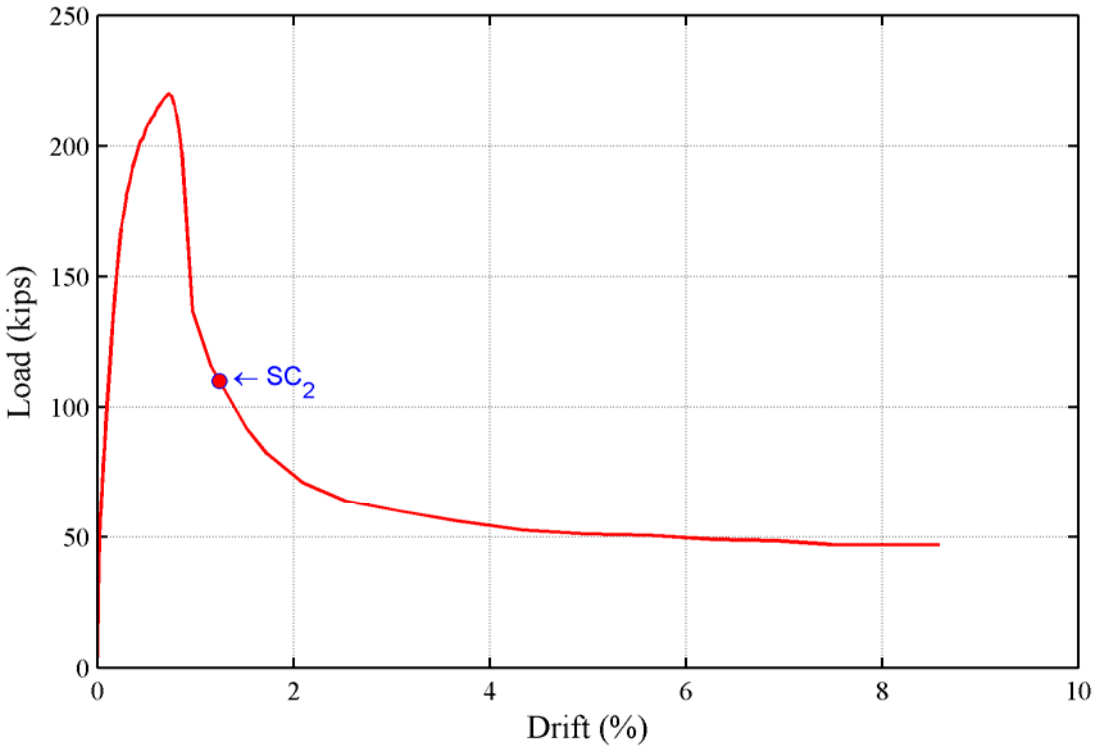


**Figure C-266 Load-drift relationship for wall B2-1**

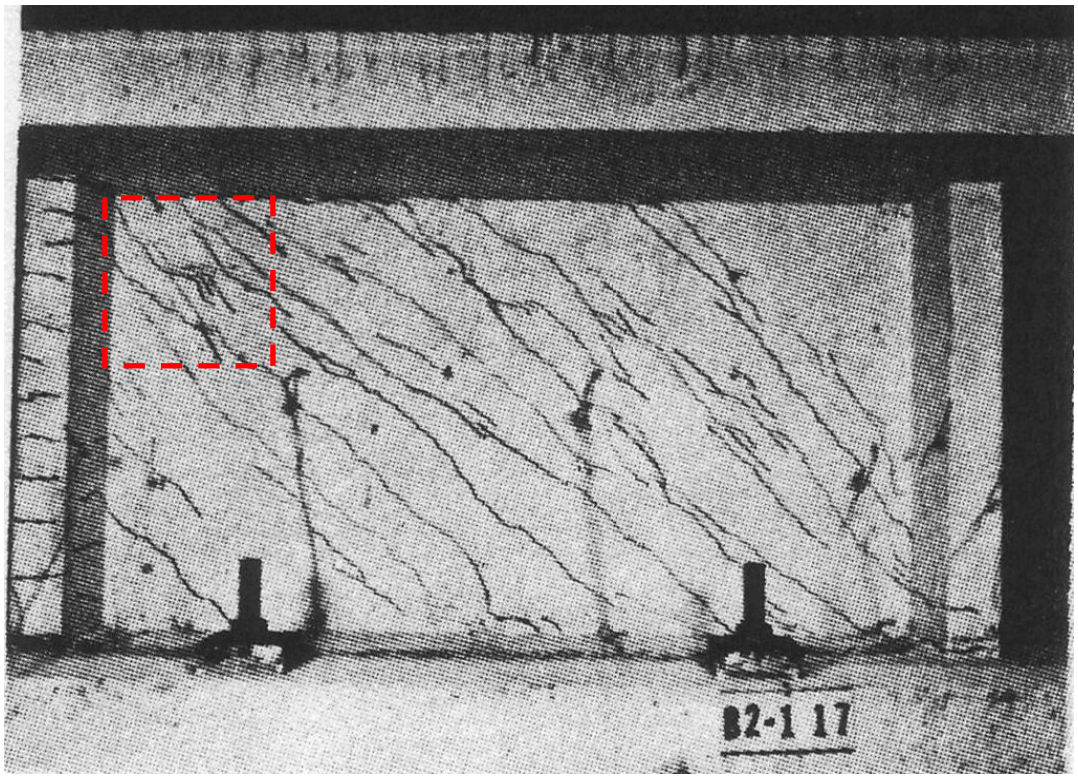


**Figure C-267 Condition of wall B2-1 at 0.72% drift [Barda et al. (1977)]**

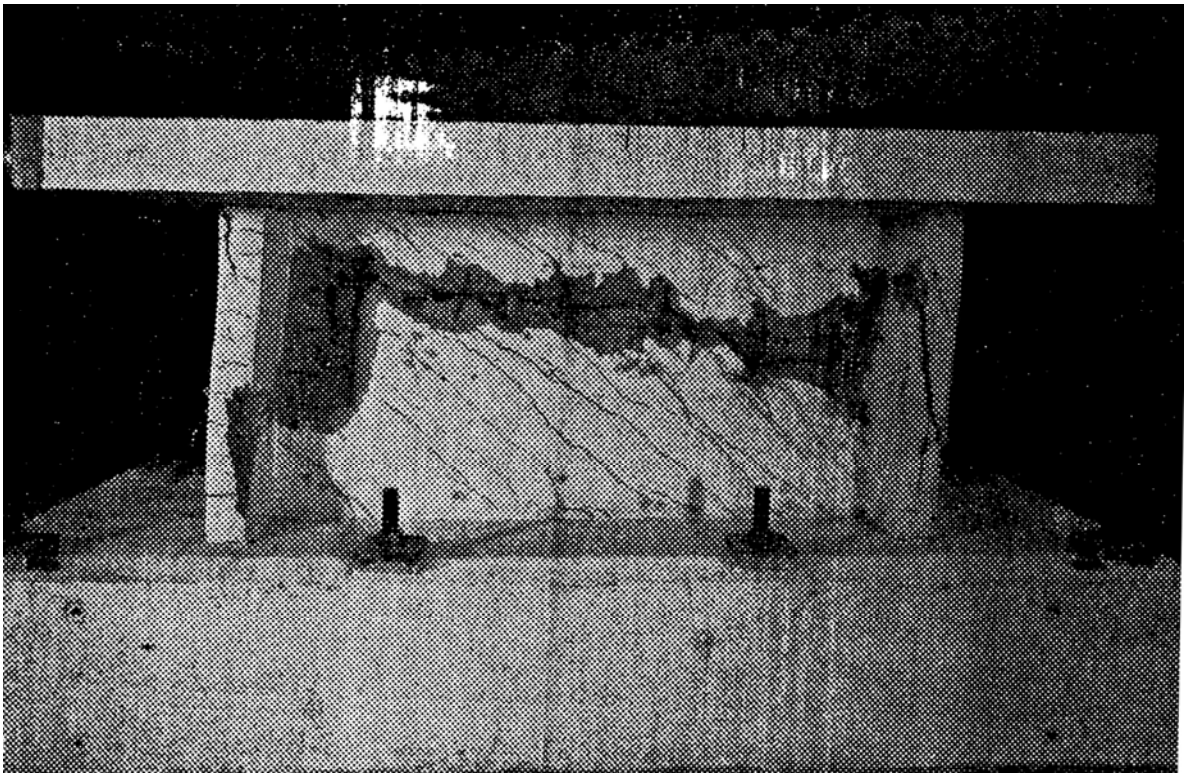

**Figure C-268 Condition of wall B2-1 at the end of the test (drift > 8%) [Barda et al. (1977)]**

### C.3.1.3 Wall B3-2

**Table C-76 Evaluation of damage data for wall B3-2 tested by Barda**

| Wall ID | MoR | Damage State (DS) | Drift (%) | Comments |
|---|---|---|---|---|
| B3-2 | 1 | 1.1 | 0.05 | The shear forces for these damage states are provided by the researcher. The corresponding drifts are obtained using the reported load-displacement relationship. |
| | | 1.2 | 0.08 | |
| | | 1.3 | 0.08 | |
| | | 1.4 | 0.29 | |
| | 2a | 2.2 | 0.23 | |
| | 3 | 3.1 | 0.59 | The researcher stated that crushing initiated following the attainment of peak shear strength [Barda (1972), page 47]. A photograph at peak shear strength was presented (Figure C-271). In Figure C-271, the dashed boxes identify the regions of concrete requiring replacement. |
| | 4 | 4.3 | 1.18 | Wall B3-2 failed by crushing of the diagonal compression struts. However, based on the damage images provided for this wall, the drift for DS4.3 could not be determined. In Figure C-271 (drift = 0.59%) crushing is not widespread whereas Figure C-272 shows gross damage at a drift of >8%, $SC_2$ is invoked to obtain a drift for DS4.3. |
| | 4* | $SC_2$ | 1.18 | The smaller of the two drifts is obtained from the 3rd quadrant of the load-drift relationship (see Figure C-269). |

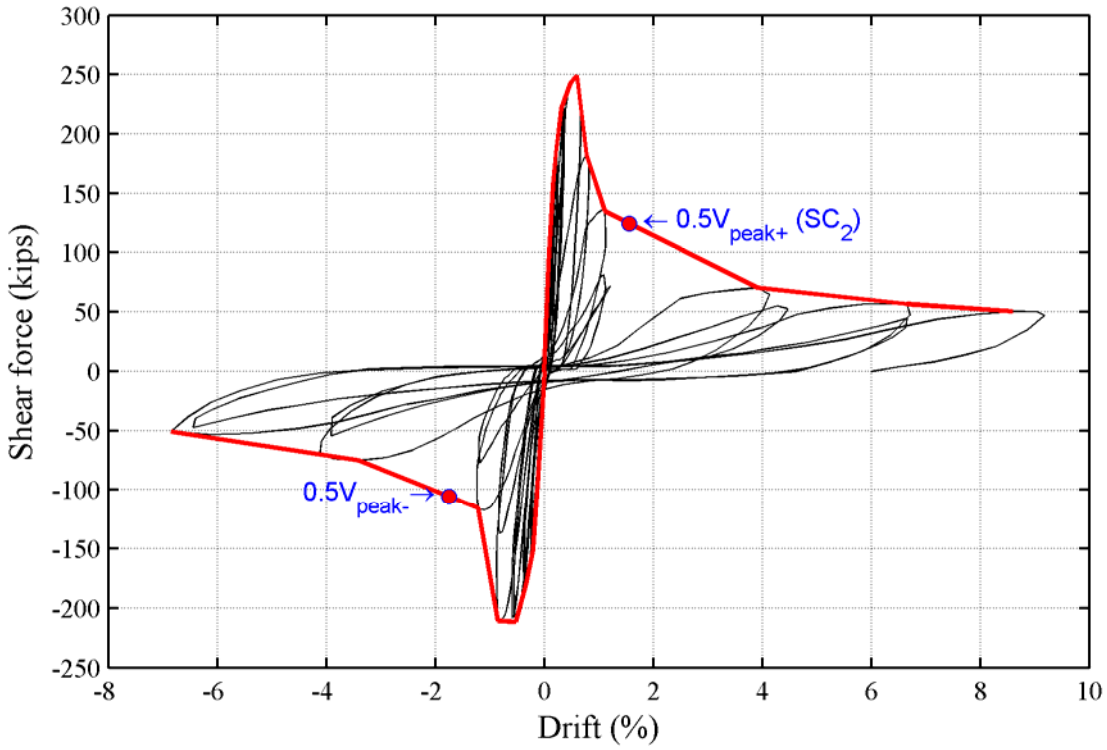


**Figure C-269 Load-drift relationship for wall B3-2**

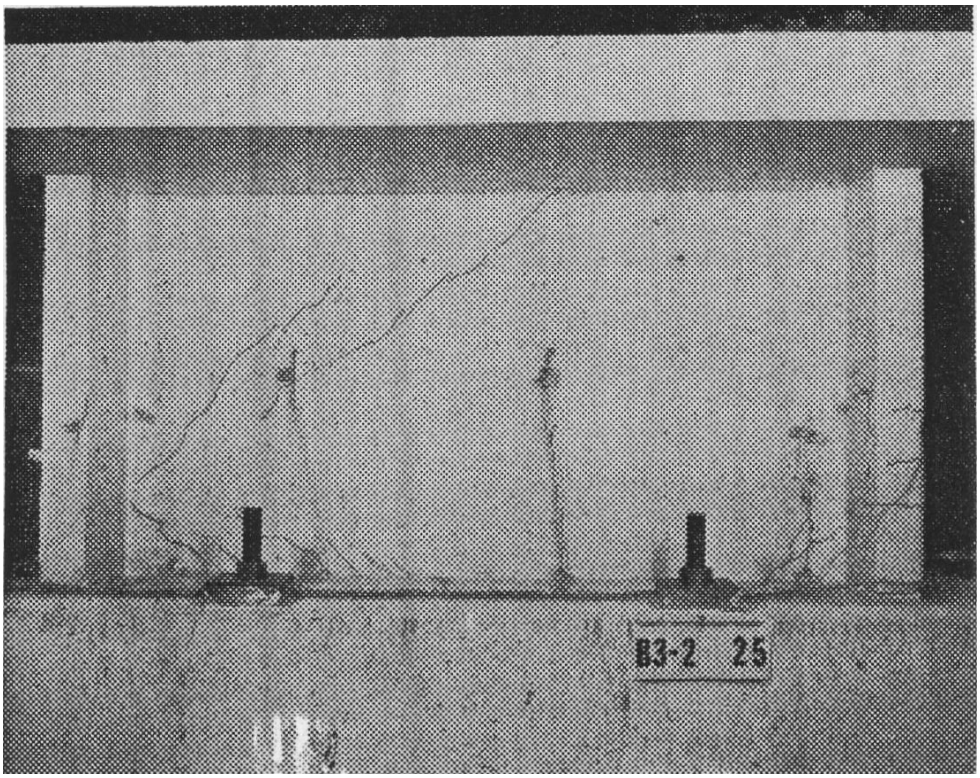


**Figure C-270 Condition of wall B3-2 at first shear cracking (drift = 0.08%) [Barda et al. (1977)]**

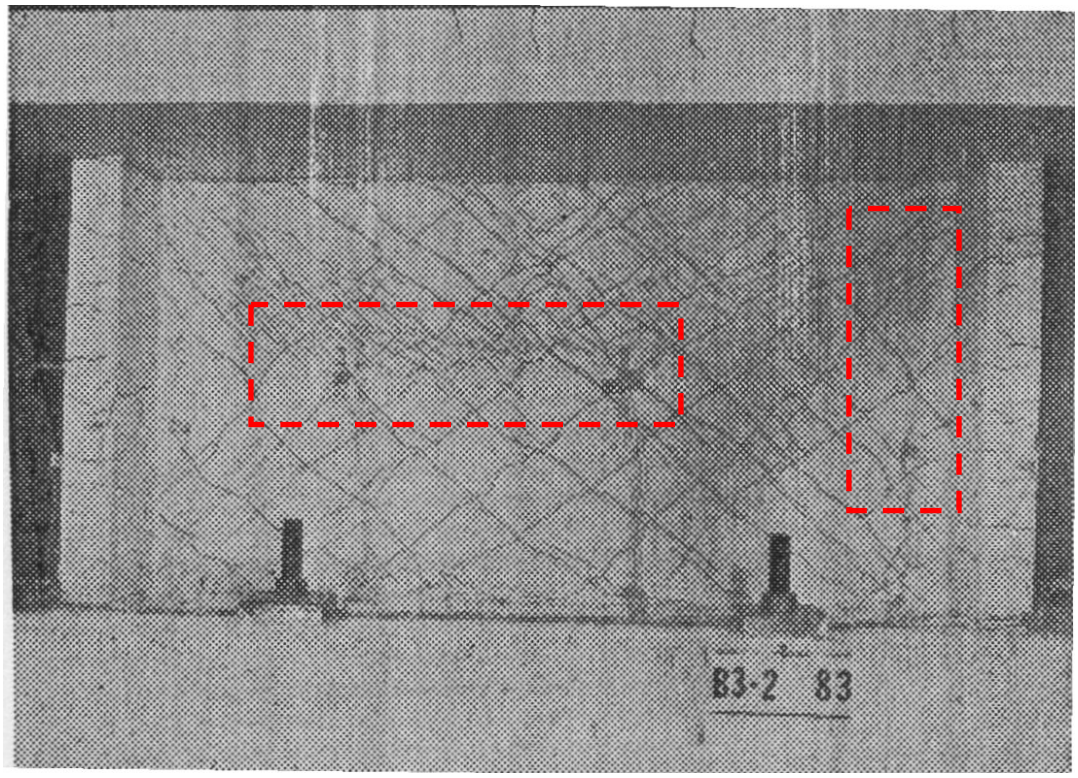


**Figure C-271 Condition of wall B3-2 at 0.59% drift [Barda et al. (1977)]**

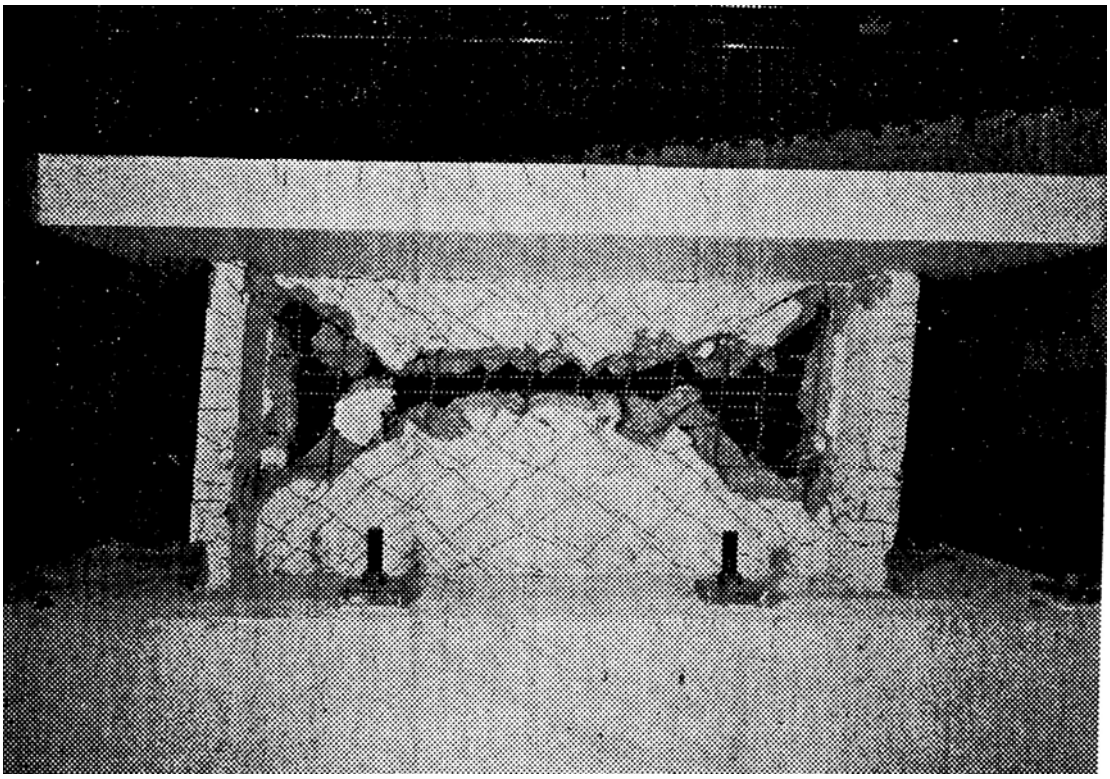

**Figure C-272 Condition of wall B3-2 at the end of the test (drift > 8%) [Barda et al. (1977)]**

### C.3.1.4 Wall B4-3

**Table C-77 Evaluation of damage data for wall B4-3 tested by Barda**

| Wall ID | MoR | Damage State (DS) | Drift (%) | Comments |
|---|---|---|---|---|
| B4-3 | 1 | 1.1 | 0.01 | The shear forces for these damage states are provided by the researcher. The corresponding drifts are obtained using the reported load-displacement relationship. Note that, although wall B4-3 was tested under cyclic loading, only a backbone curve was reported by the researcher. |
| | | 1.2 | 0.03 | |
| | | 1.3 | 0.05 | |
| | | 1.4 | 0.21 | |
| | 2a | 2.2 | 0.26 | |
| | | 2.4a | 0.31 | |
| | 3 | 3.1 | 0.58 | The researcher stated that crushing initiated following the attainment of peak shear strength [Barda (1972), page 60]. A photograph at peak shear strength was presented (Figure C-274). In Figure C-274, the dashed box identifies the region of concrete requiring replacement. |
| | 4 | 4.3 | 0.99 | Wall B4-3 failed by crushing of the diagonal compression struts. However, based on the damage images provided for this wall, the drift for DS4.3 could not be determined. In Figure C-274 (drift = 0.58%) crushing is not widespread whereas Figure C-275 shows gross damage at a drift of >8%, $SC_2$ is invoked to obtain a drift for DS4.3. |
| | 4* | $SC_2$ | 0.99 | See Figure C-273. |

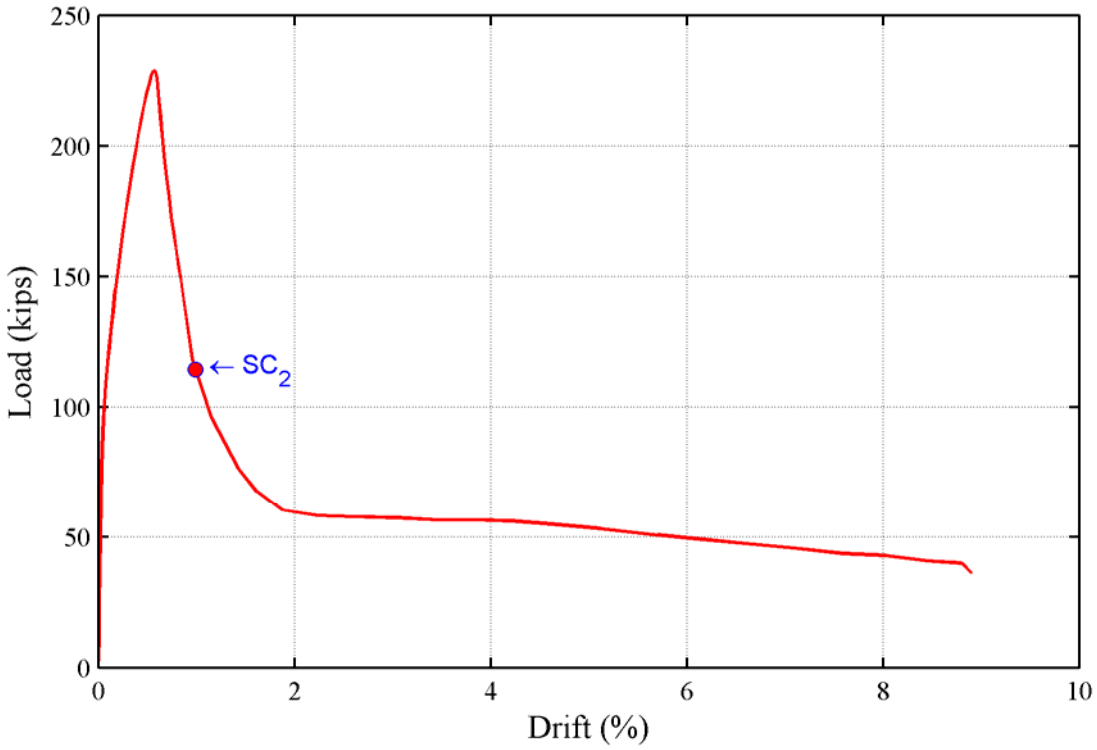


**Figure C-273 Backbone curve for wall B4-3**

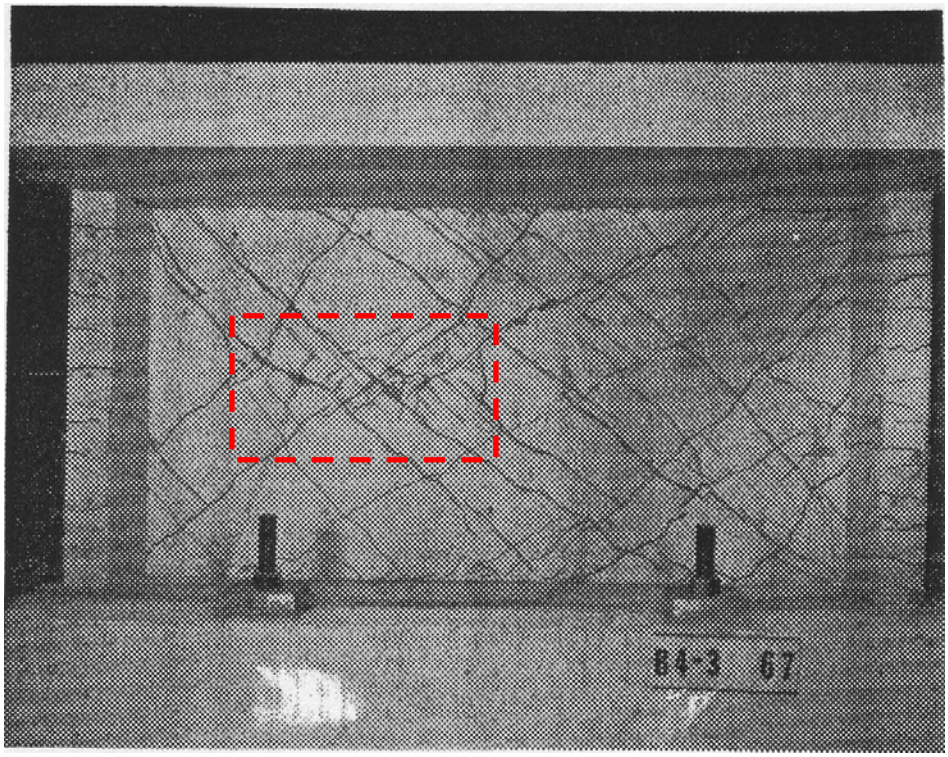


**Figure C-274 Condition of wall B4-3 at 0.58% drift [Barda et al. (1977)]**

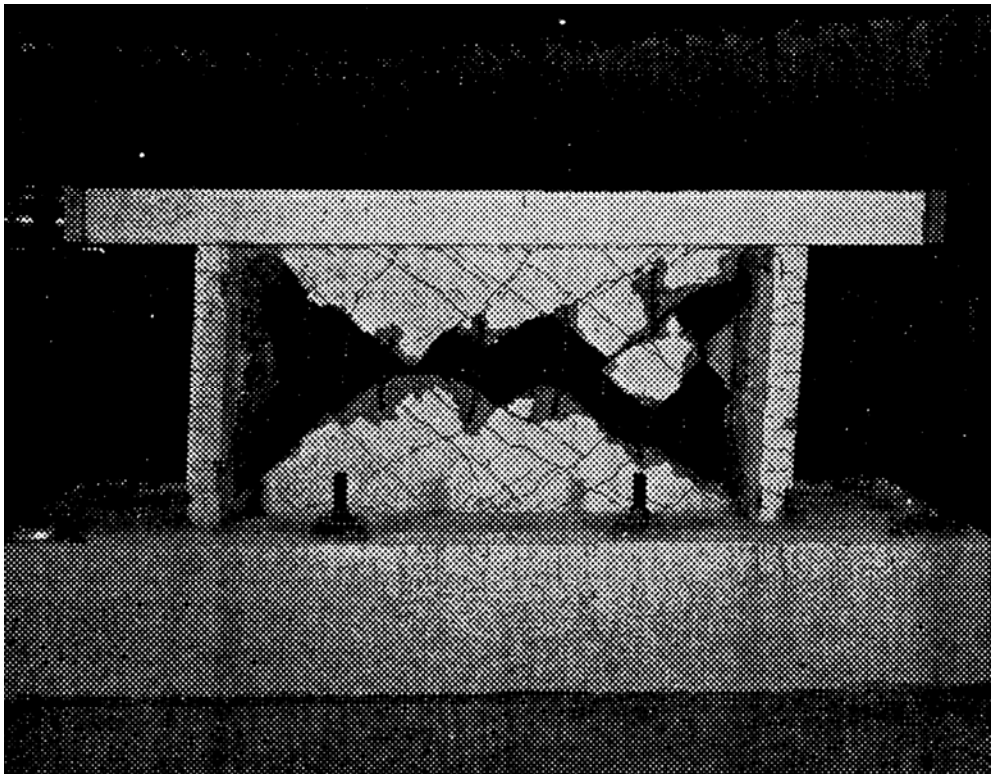

**Figure C-275 Condition of wall B4-3 at the end of the test (drift > 8%) [Barda et al. (1977)]**

### C.3.1.5 Wall B5-4

**Table C-78 Evaluation of damage data for wall B5-4 tested by Barda**

| Wall ID | MoR | Damage State (DS) | Drift (%) | Comments |
|---|---|---|---|---|
| B5-4 | 1 | 1.1 | 0.02 | The shear forces for these damage states are provided by the researcher. The corresponding drifts are obtained using the reported load-displacement relationship. Note that, although wall B5-4 was tested under cyclic loading, only a backbone curve was reported by the researcher. |
| | | 1.3 | 0.04 | |
| | 2a | 2.1 | 0.30 | |
| | | 2.4a | 0.05 | |
| | 3 | 3.1 | 0.68 | The researcher stated that crushing initiated following the attainment of peak shear strength [Barda (1972), page 65]. A photograph at peak shear strength was presented (Figure C-277). In Figure C-277, the dashed box identifies the region of concrete requiring replacement. |
| | 4 | 4.3 | N/A | Wall B5-4 failed by crushing of the diagonal compression struts. However, based on the two damage images provided for this wall, the drift for DS4.3 could not be determined. In Figure C-277 (drift = 0.66%) crushing is not widespread whereas Figure C-278 shows gross damage at a drift of >8%, $SC_2$ is invoked to seek a drift for DS4.3. |
| | $4^*$ | $SC_2$ | N/A | The post-peak resistance computed using the reported backbone curve did not drop to $0.5V_{peak}$. |

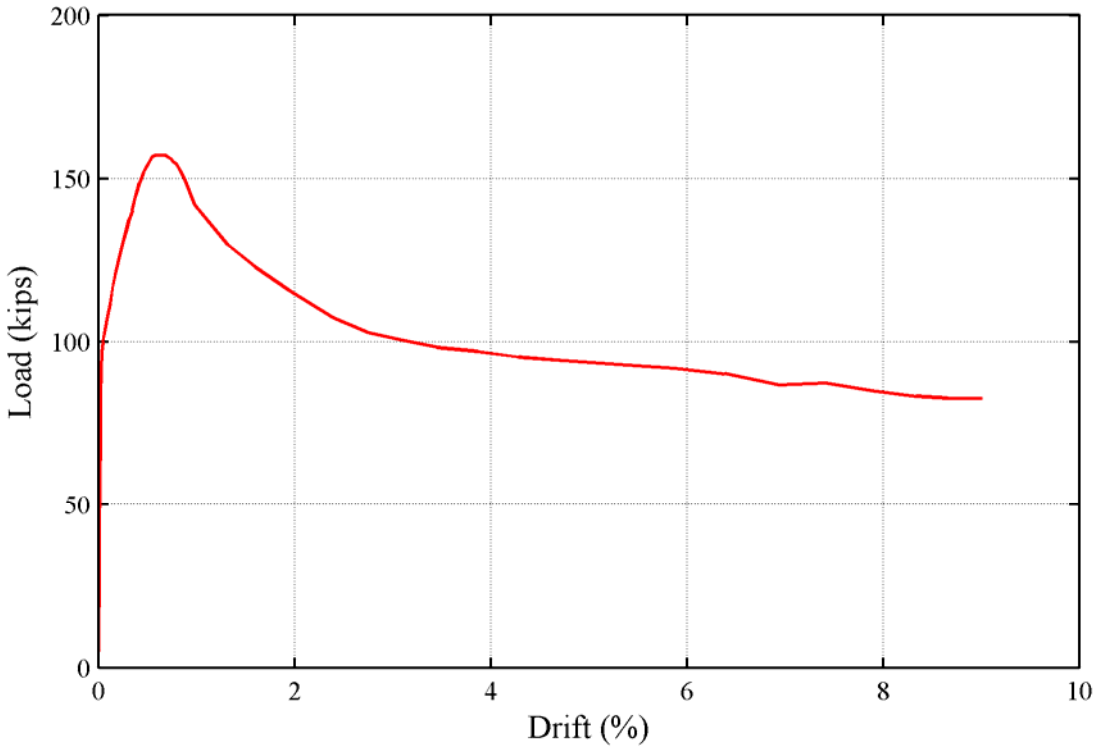


**Figure C-276 Backbone curve for wall B5-4**

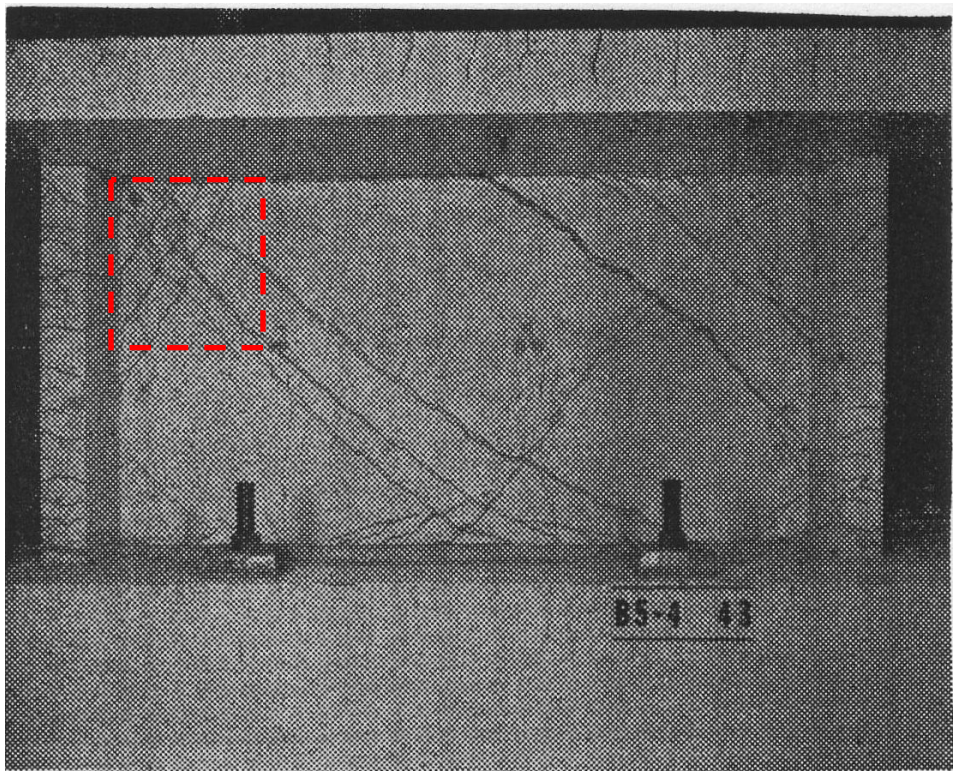


**Figure C-277 Condition of wall B5-4 at 0.68% drift [Barda et al. (1977)]**

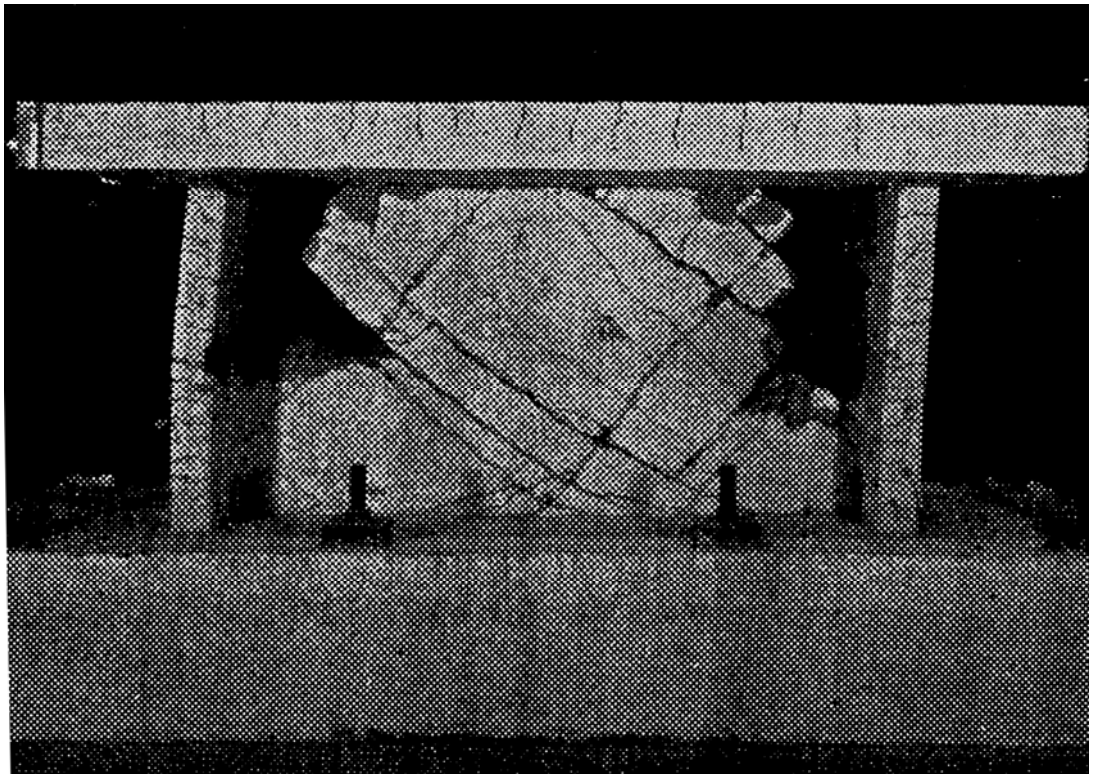

**Figure C-278 Condition of wall B5-4 at the end of the test (drift > 8%) [Barda et al. (1977)]**

### C.3.1.6 Wall B6-4

**Table C-79 Evaluation of damage data for wall B6-4 tested by Barda**

| Wall ID | MoR | Damage State (DS) | Drift (%) | Comments |
|---|---|---|---|---|
| B6-4 | 1 | 1.1 | 0.02 | The shear forces for these damage states are provided by the researcher. The corresponding drifts are obtained using the reported load-displacement relationship. Note that, although wall B6-4 was tested under cyclic loading, only a backbone curve was reported by the researcher. |
| | | 1.2 | 0.03 | |
| | | 1.3 | 0.03 | |
| | | 1.4 | 0.13 | |
| | 2a | 2.1 | 0.28 | |
| | | 2.2 | 0.28 | |
| | | 2.4a | 0.17 | |
| | 2b | 2.4b | 0.53 | |
| | 3 | 3.1 | 0.69 | The researcher stated that crushing initiated following the attainment of peak shear strength [Barda (1972), page 66]. A photograph at peak shear strength was reported (Figure C-280). In Figure C-280, the dashed box identifies the region of concrete requiring replacement. |
| | 4 | 4.3 | 2.19 | Wall B6-4 failed by crushing of the diagonal compression struts. However, based on the two damage images provided for this wall, the drift for DS4.3 could not be determined. In Figure C-280 (drift = 0.66%) crushing is not widespread whereas Figure C-281 shows gross damage at a drift of >8%, $SC_2$ is invoked to obtain a drift for DS4.3. |
| | 4* | $SC_2$ | 2.19 | See Figure C-279. |

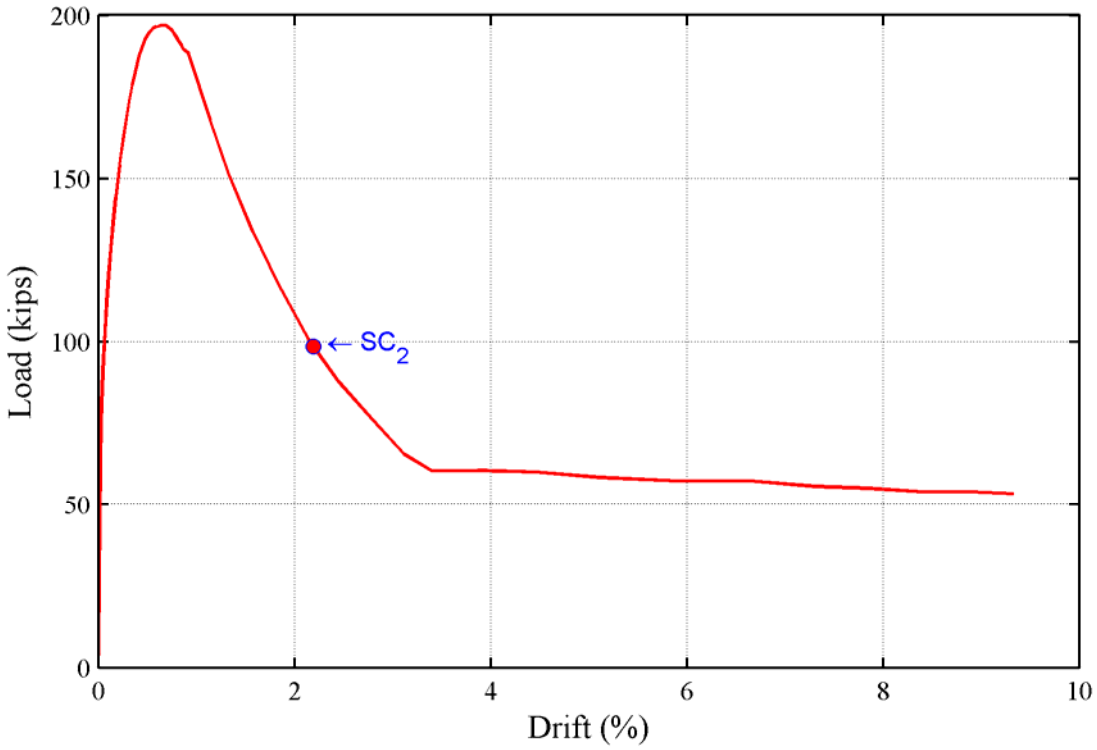


**Figure C-279 Backbone curve for wall B6-4**

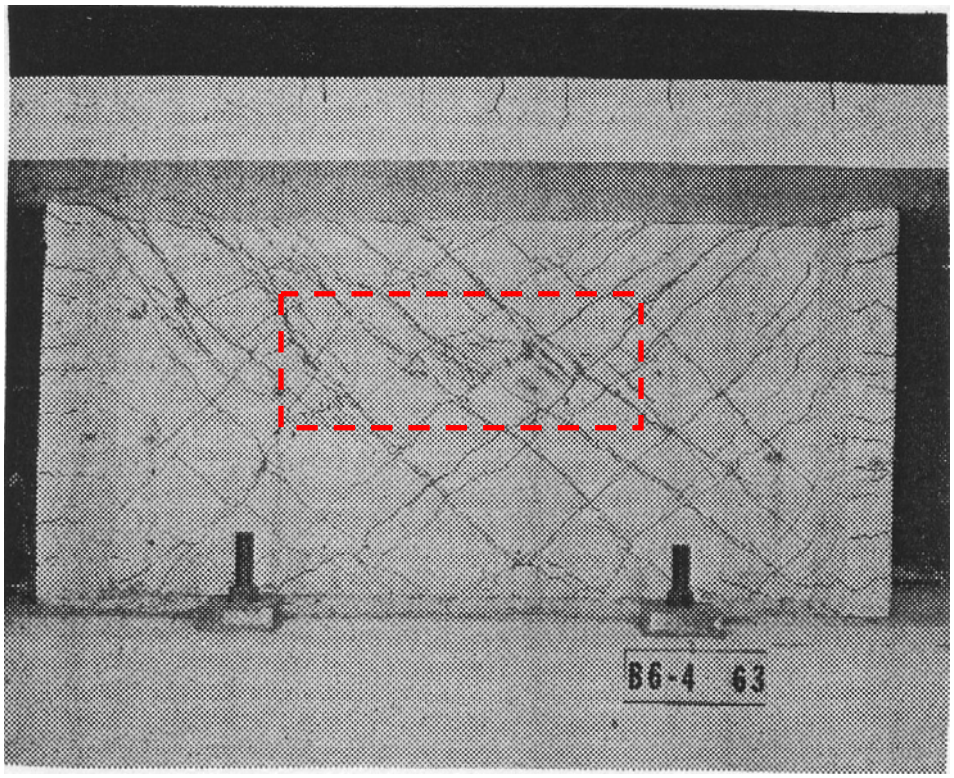


**Figure C-280 Condition of wall B6-4 at 0.69% drift [Barda et al. (1977)]**

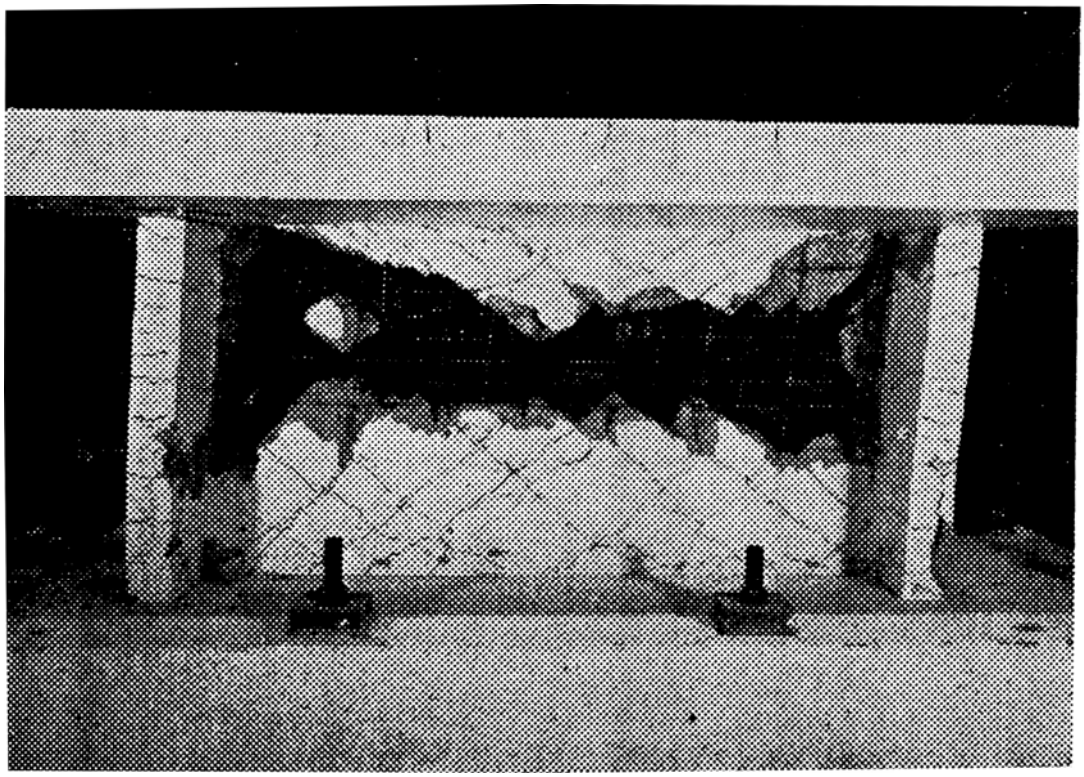

**Figure C-281 Condition of wall B6-4 at the end of the test (drift > 8%) [Barda et al. (1977)]**

### C.3.1.7 Wall B7-5

**Table C-80 Evaluation of damage data for wall B7-5 tested by Barda**

| Wall ID | MoR | Damage State (DS) | Drift (%) | Comments |
|---|---|---|---|---|
| B7-5 | 1 | 1.1 | 0.05 | The shear forces for these damage states are provided by the researcher. The corresponding drifts are obtained using the reported load-displacement relationship. |
| | | 1.3 | 0.05 | |
| | | 1.4 | 0.34 | |
| | 2a | 2.1 | 0.97 | |
| | | 2.2 | 0.29 | |
| | | 2.4a | 0.87 | |
| | 3 | 3.1 | 0.97 | A damage image reported at this drift level shows distress at the upper corners of the wall panel that require partial concrete replacement (Figure C-283). In Figure C-283, the dashed boxes identify the regions of concrete requiring replacement. |
| | 4 | 4.1 | 0.97 | The researcher stated that slipping initiated following the attainment of peak shear strength [Barda (1972), page 73]. A damage image at peak shear strength was reported (Figure C-283). However, sliding failure is not evident in this figure. Therefore, the drift obtained using the 1st supplemental criterion (bolded) is used to replace the drift reported by the researcher (shaded). |
| | 4* | $SC_1$ | **1.97** | The smaller of the two drifts is obtained from the 3rd quadrant of the load-drift relationship (see Figure C-282). |
| | | $SC_2$ | 9.10 | The data point is obtained from the 1st quadrant of the load-drift relationship (see Figure C-282). A data point cannot be established in the 3rd quadrant. |

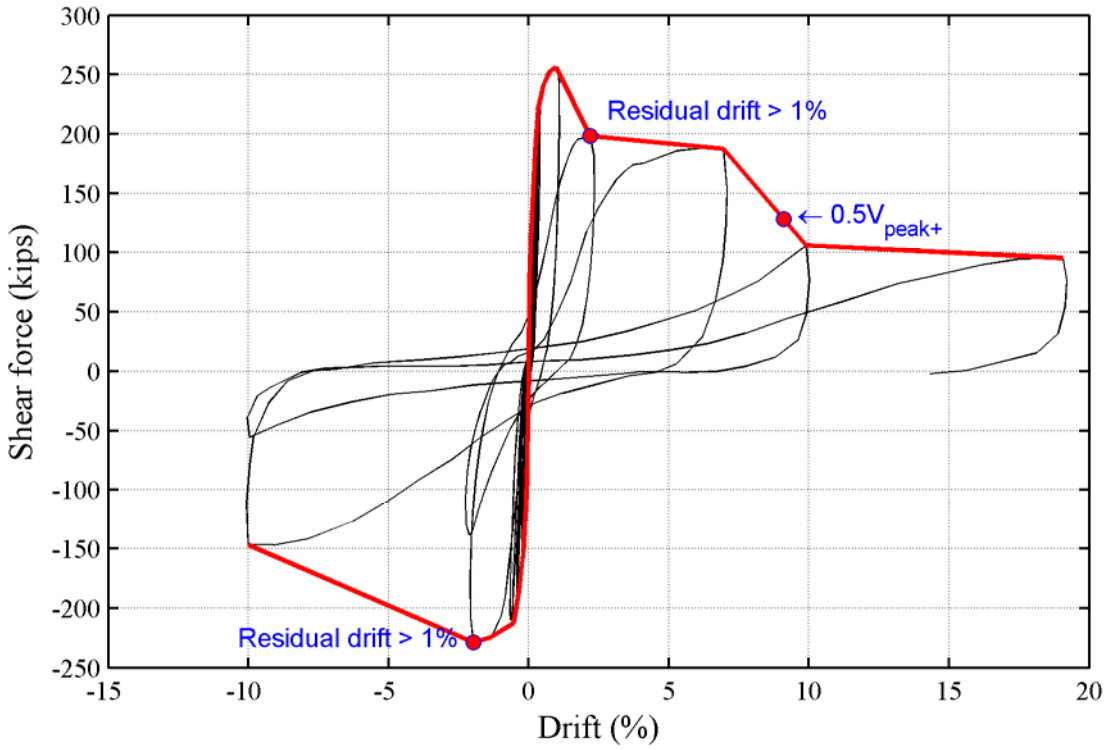


**Figure C-282 Load-drift relationship for wall B7-5**

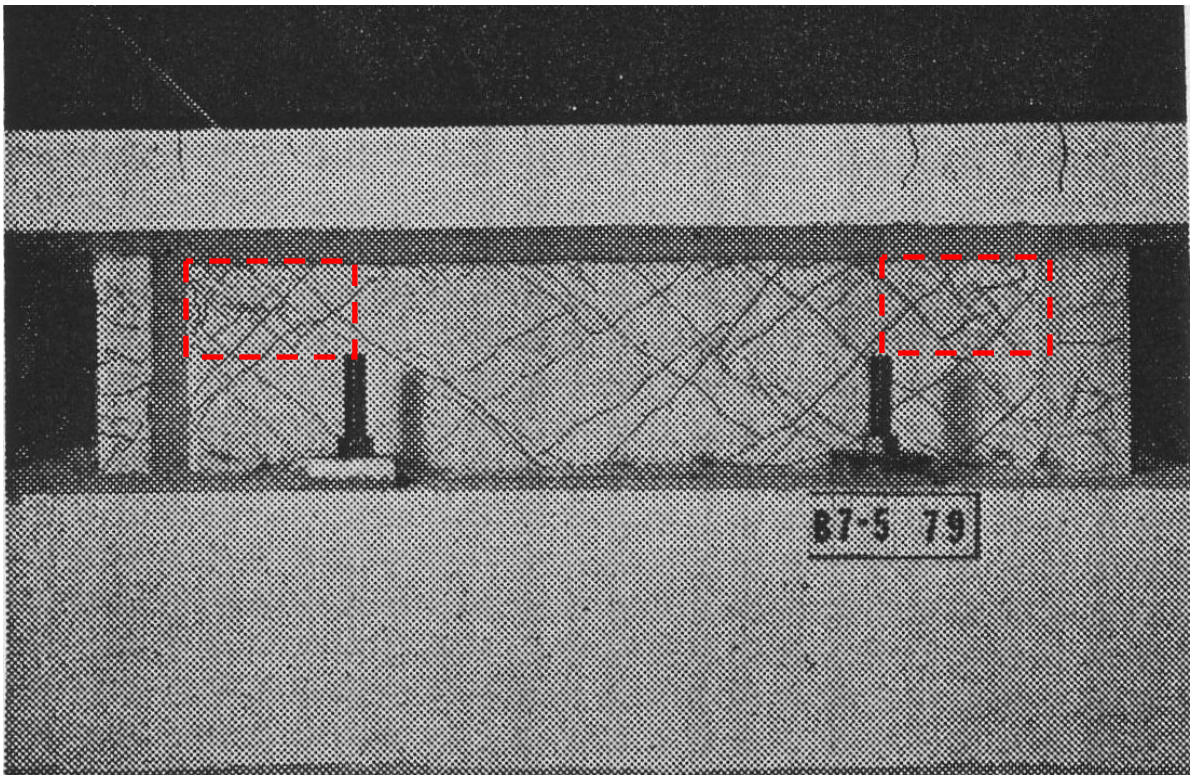


**Figure C-283 Condition of wall B7-5 at 0.97% drift [Barda et al. (1977)]**

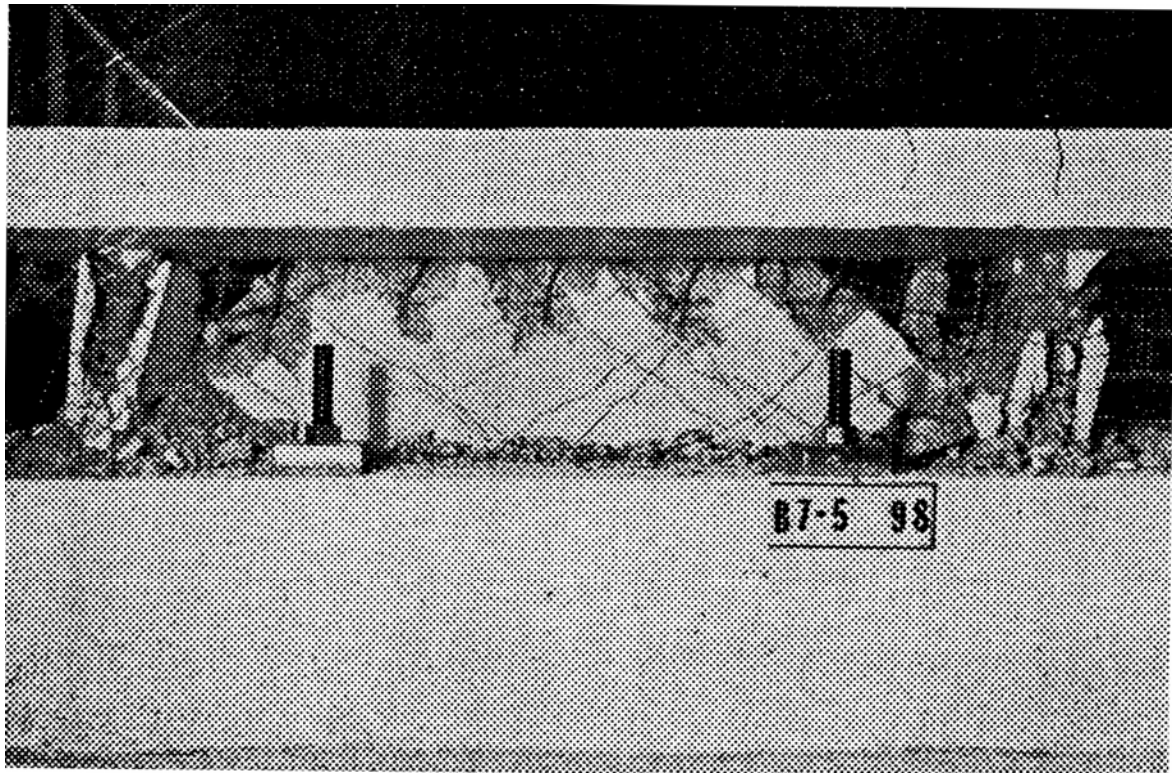


**Figure C-284 Condition of wall B7-5 at the end of the test (drift > 15%) [Barda et al. (1977)]**

### C.3.1.8 Wall B8-5

**Table C-81 Evaluation of damage data for wall B8-5 tested by Barda**

| Wall ID | MoR | Damage State (DS) | Drift (%) | Comments |
|---|---|---|---|---|
| B8-5 | 1 | 1.1 | 0.02 | The shear forces for these damage states are provided by the researcher. The corresponding drifts are obtained using the reported load-displacement relationship. |
| | | 1.3 | 0.02 | |
| | | 1.4 | 0.19 | |
| | 2a | 2.1 | 0.11 | |
| | | 2.2 | 0.57 | |
| | | 2.4a | 0.29 | |
| | 3 | 3.1 | 0.57 | The researcher stated that crushing initiated following the attainment of peak shear strength [Barda (1972), page 75]. A photograph at peak shear strength was reported (Figure C-286). In Figure C-286, the dashed box identifies the region of concrete requiring replacement. |
| | 4 | 4.3 | 1.46 | Wall B8-5 failed by crushing of the diagonal compression struts. However, based on the two damage images provided for this wall, the drift for DS4.3 could not be determined. In Figure C-286 (drift = 0.57%) crushing is not widespread whereas Figure C-287 shows gross damage at a drift of >4%, $SC_2$ is invoked to obtain a drift for DS4.3. |
| | $4^*$ | $SC_2$ | 1.46 | The smaller of the two drifts is obtained from the $1^{st}$ quadrant of the load-drift relationship (see Figure C-285). |

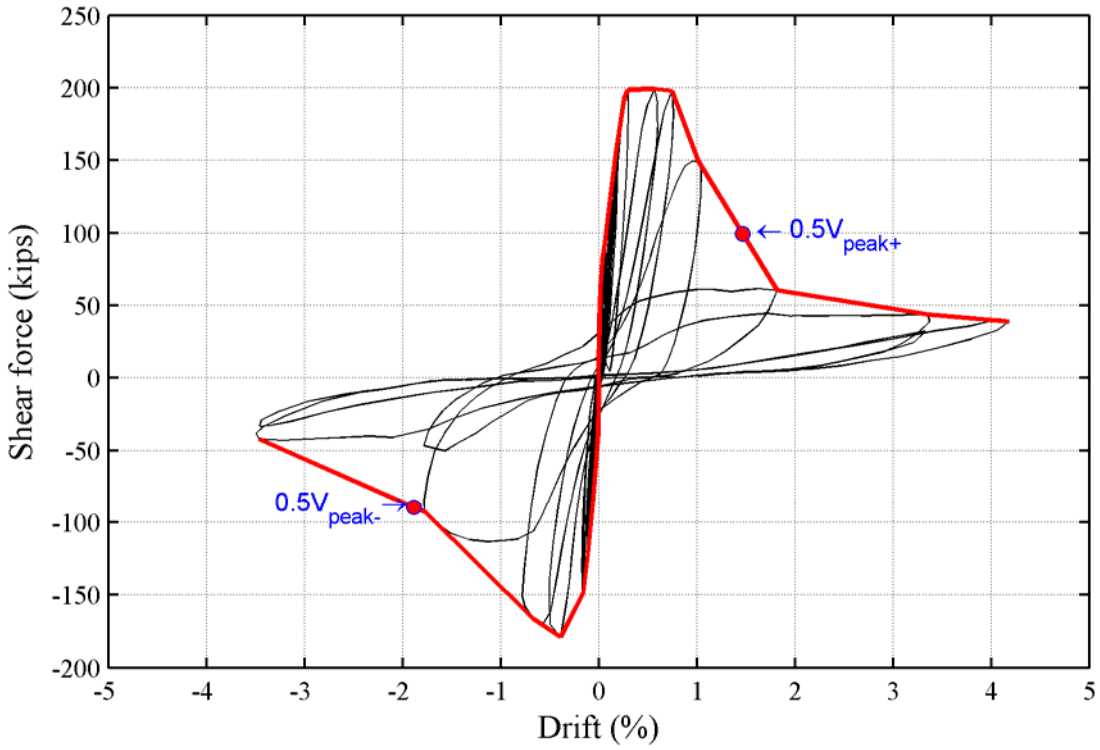


**Figure C-285 Load-drift relationship for wall B8-5**

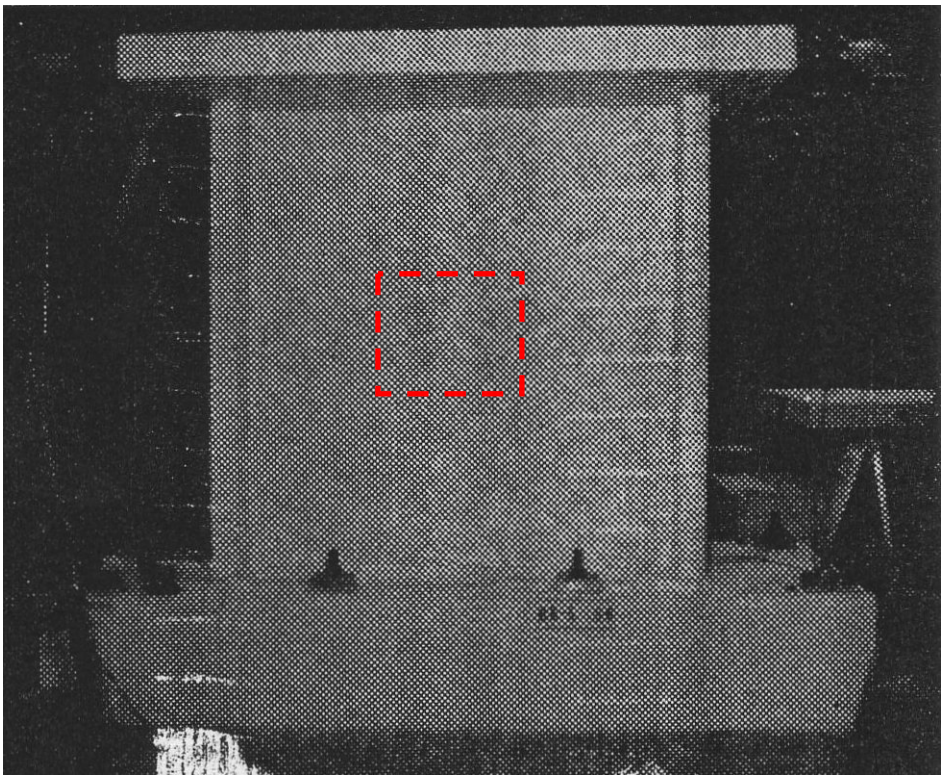

**Figure C-286 Condition of wall B8-5 at 0.57% drift [Barda et al. (1977)]**

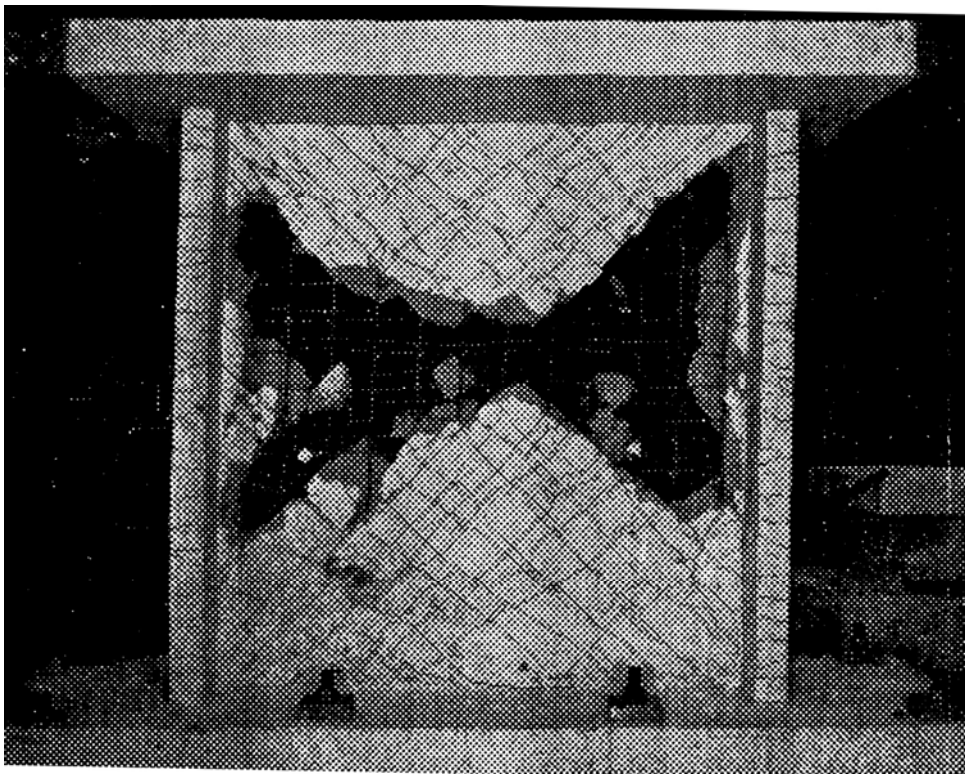

**Figure C-287 Condition of wall B8-5 at the end of the test (drift > 4%) [Barda et al. (1977)]**

## C.3.2 Palermo Walls [Palermo and Vecchio (2002)]

### C.3.2.1 Wall DP1

**Table C-82 Evaluation of damage data for wall DP1 tested by Palermo**

| Wall ID | MoR | Damage State (DS) | Drift (%) | Comments |
|---|---|---|---|---|
| DP1 | 1 | 1.2 | 0.14 | The drifts for these damage states are provided by the researcher. |
| | | 1.3 | 0.03 | |
| | | 1.4 | 0.35 | |
| | 2a | 2.1 | 0.57 | |
| | | 2.4a | 0.40 | |
| | | 2.5a | 0.40 | |
| | 2b | 2.4b | 0.64 | |
| | | 2.5b | 0.54 | |
| | 3 | 3.1 | 0.59 | The researcher reported a drift of 0.40% at initiation of concrete crushing at the compression toe of the web. Figure C-296 shows the condition of the wall at 0.40% drift. Based on the condition of extent of damage provided in this figure, it is concluded that the drift reported by the author is too small for MoR-3 since crushing is probably limited to a very small region. A drift of 0.59% is assumed for this damage state based on Figure C-300. In Figure C-300, the dashed boxes identify the regions of concrete requiring replacement. |
| | 4 | 4.3 | 0.64 | The image reported at this drift shows widespread crushing (Figure C-301). |

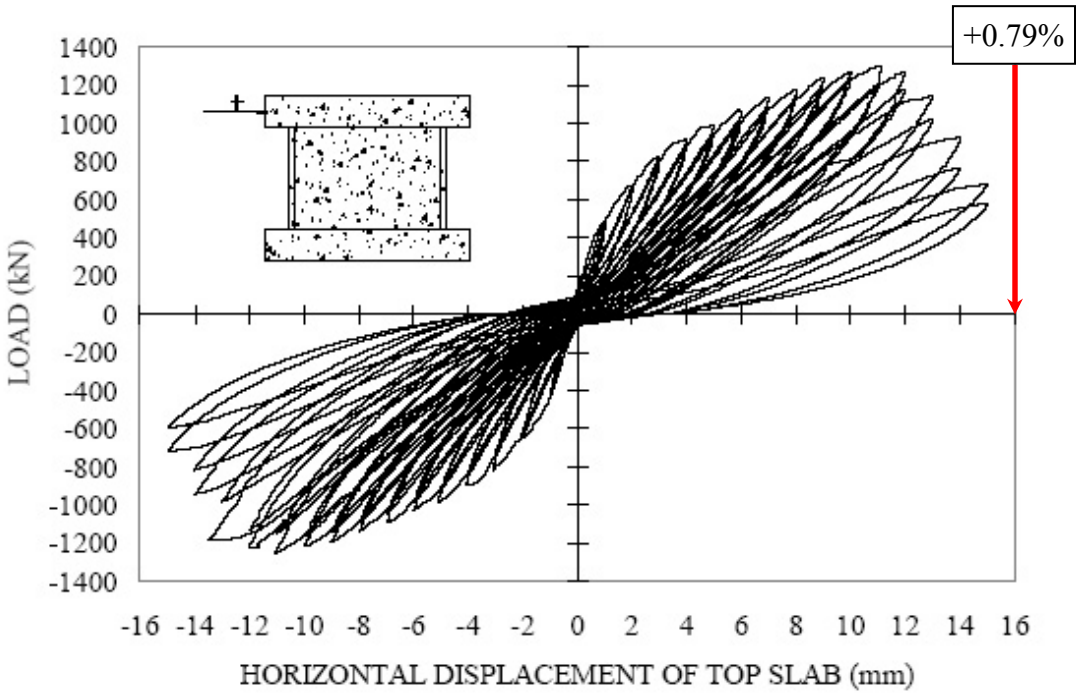


**Figure C-288 Load-displacement relationship for wall DP1 [Palermo and Vecchio (2002)]**

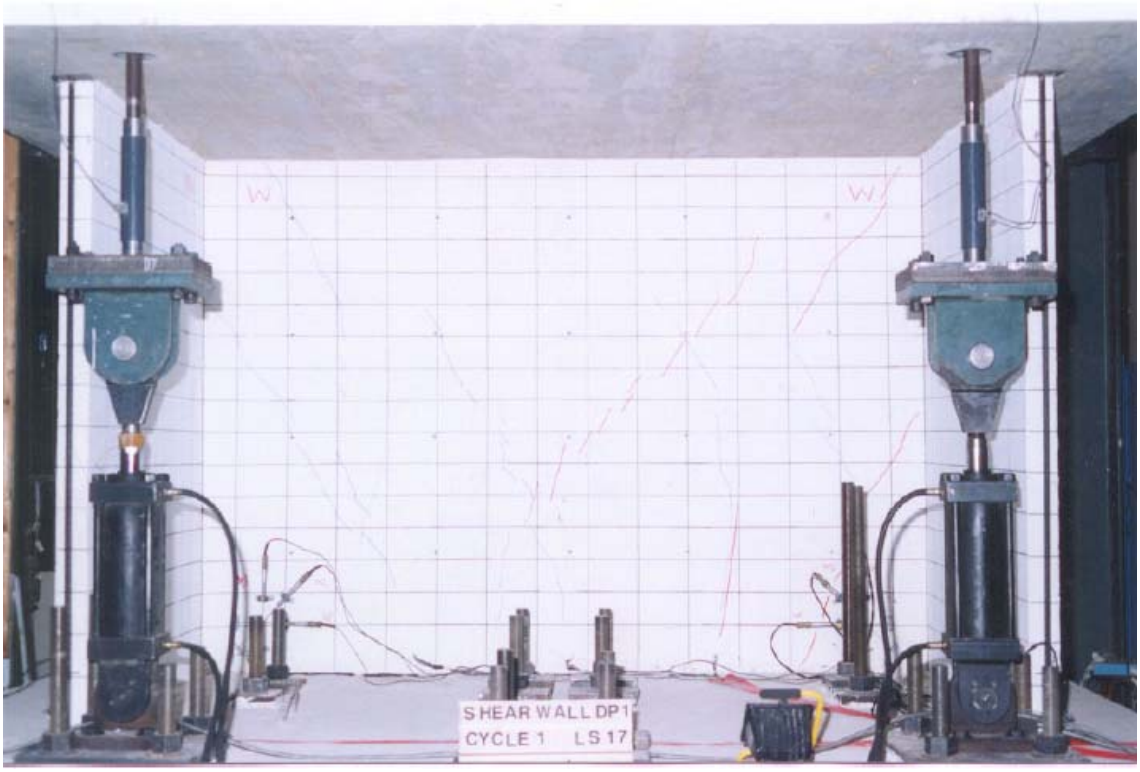


**Figure C-289 Condition of wall DP1 at 0.05% drift [Palermo and Vecchio (2002)]**

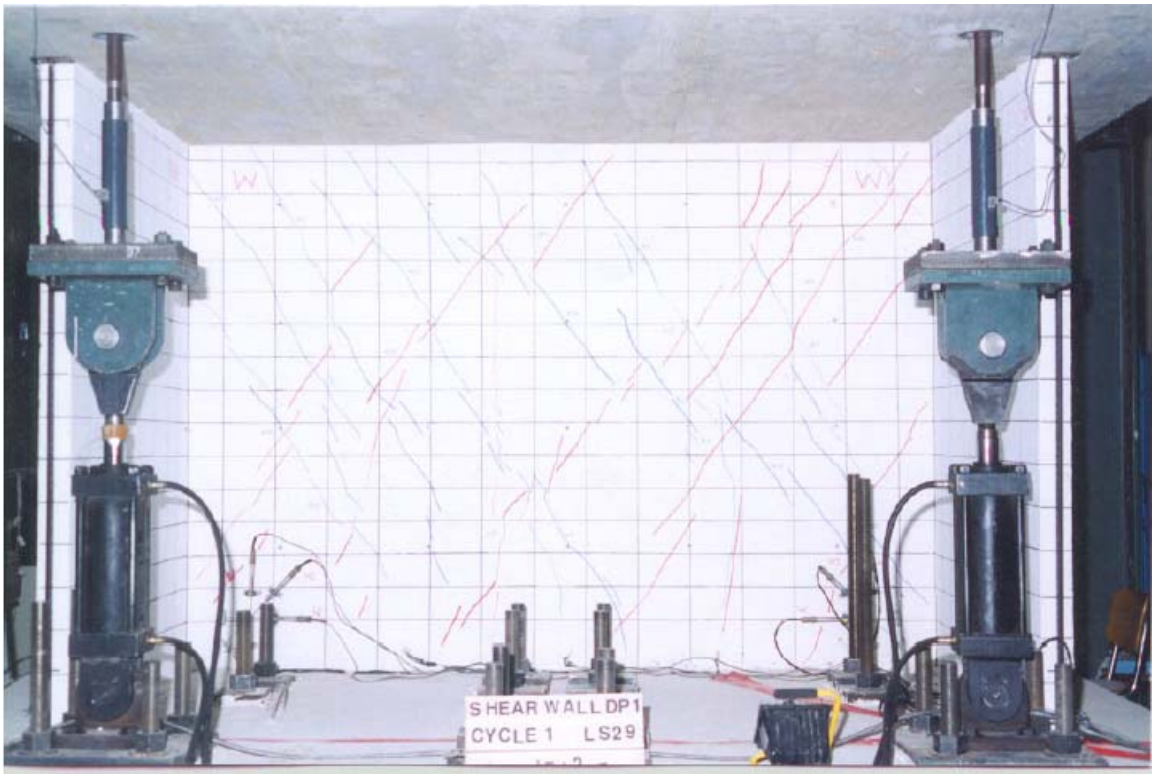


**Figure C-290 Condition of wall DP1 at 0.10% drift [Palermo and Vecchio (2002)]**

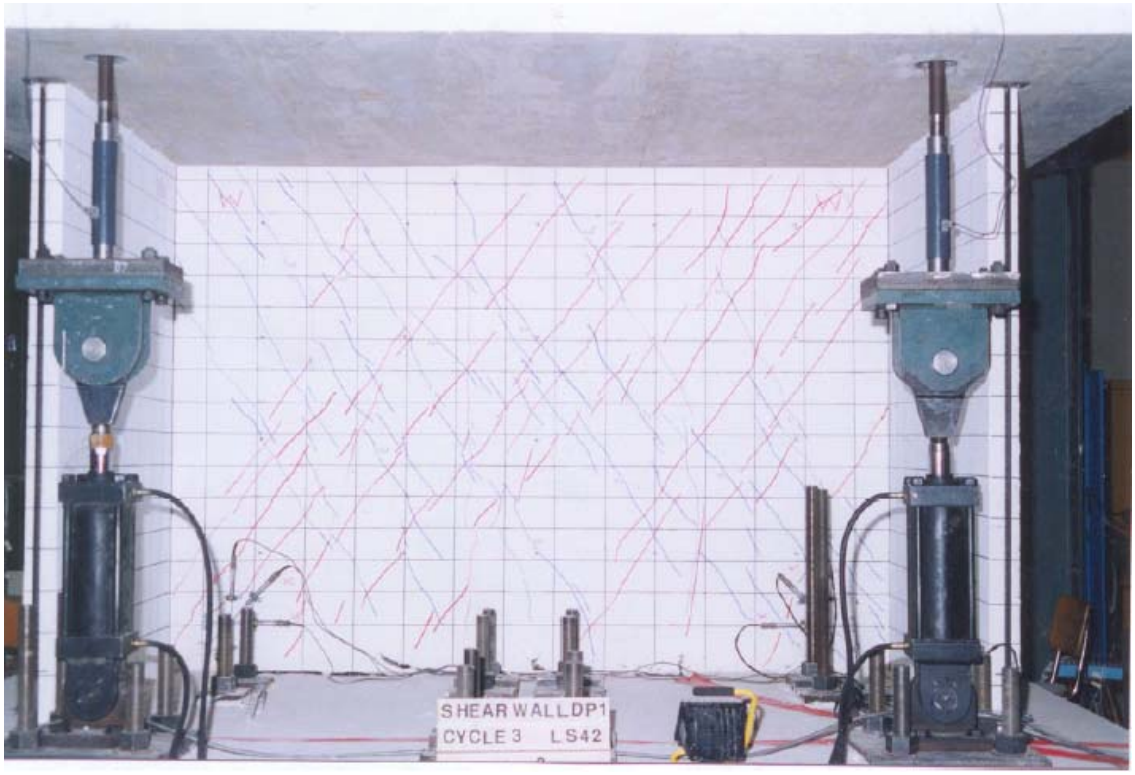


**Figure C-291 Condition of wall DP1 at 0.15% drift [Palermo and Vecchio (2002)]**

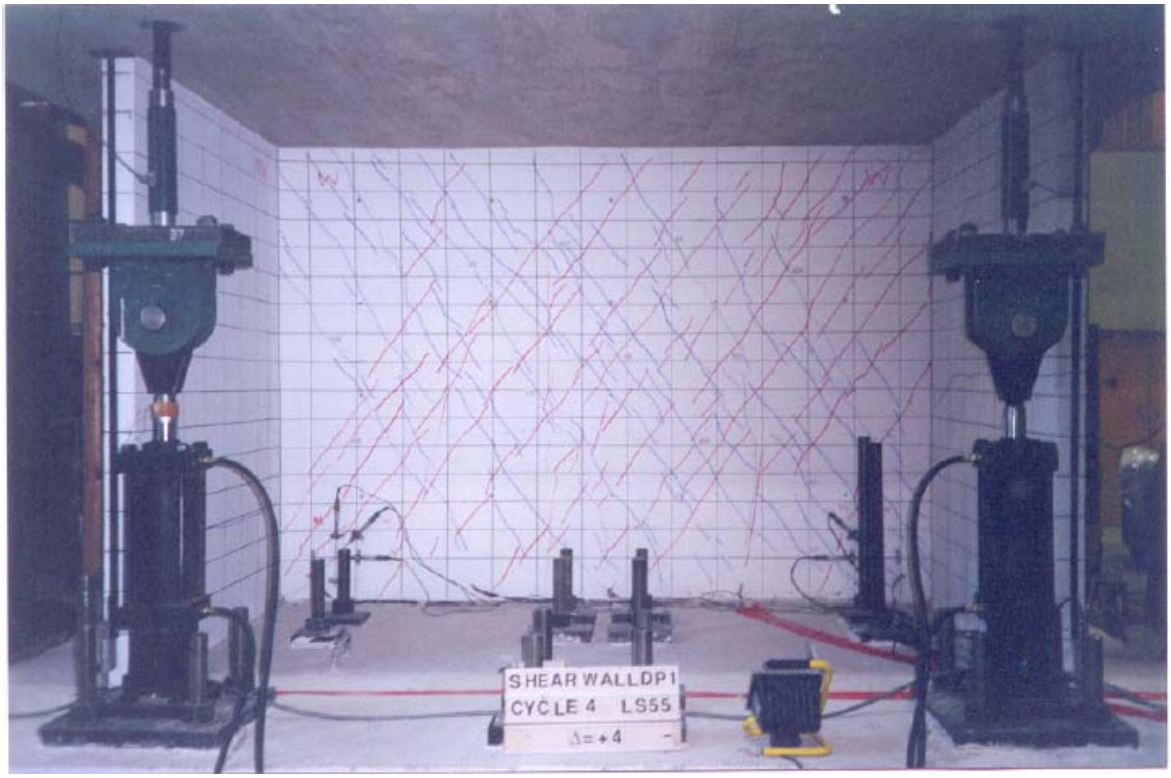


**Figure C-292 Condition of wall DP1 at 0.20% drift [Palermo and Vecchio (2002)]**

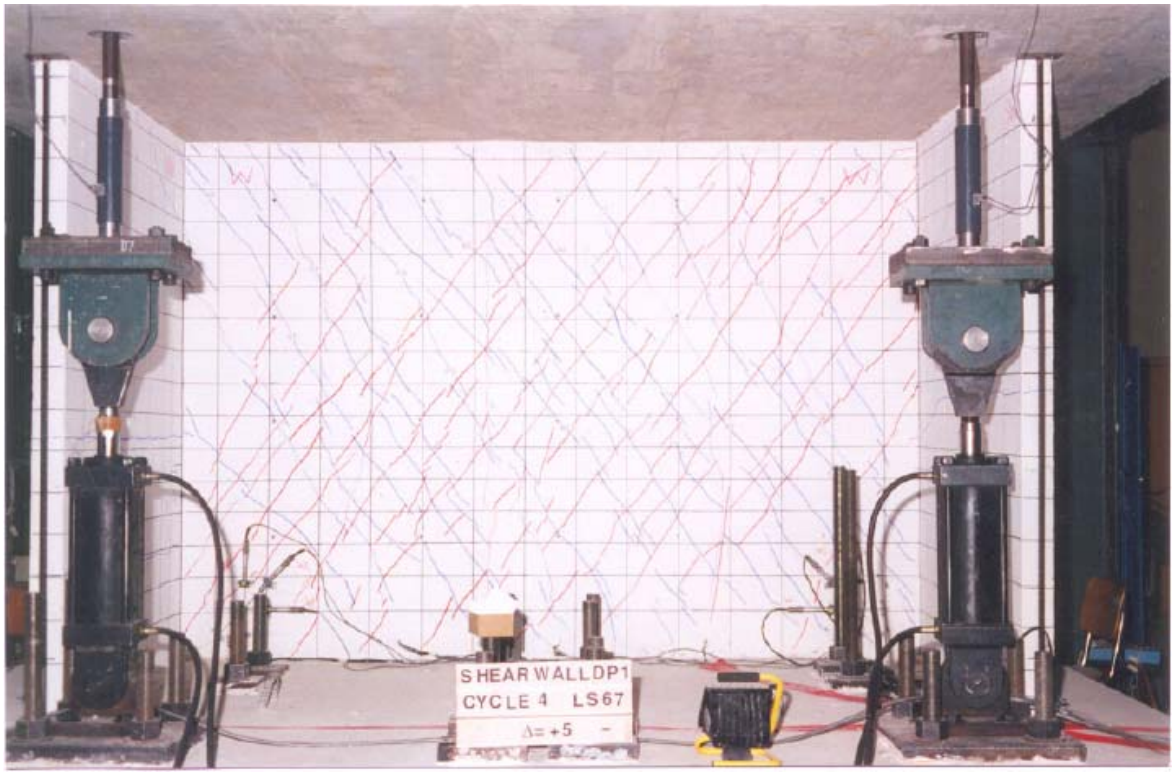


**Figure C-293 Condition of wall DP1 at 0.25% drift [Palermo and Vecchio (2002)]**

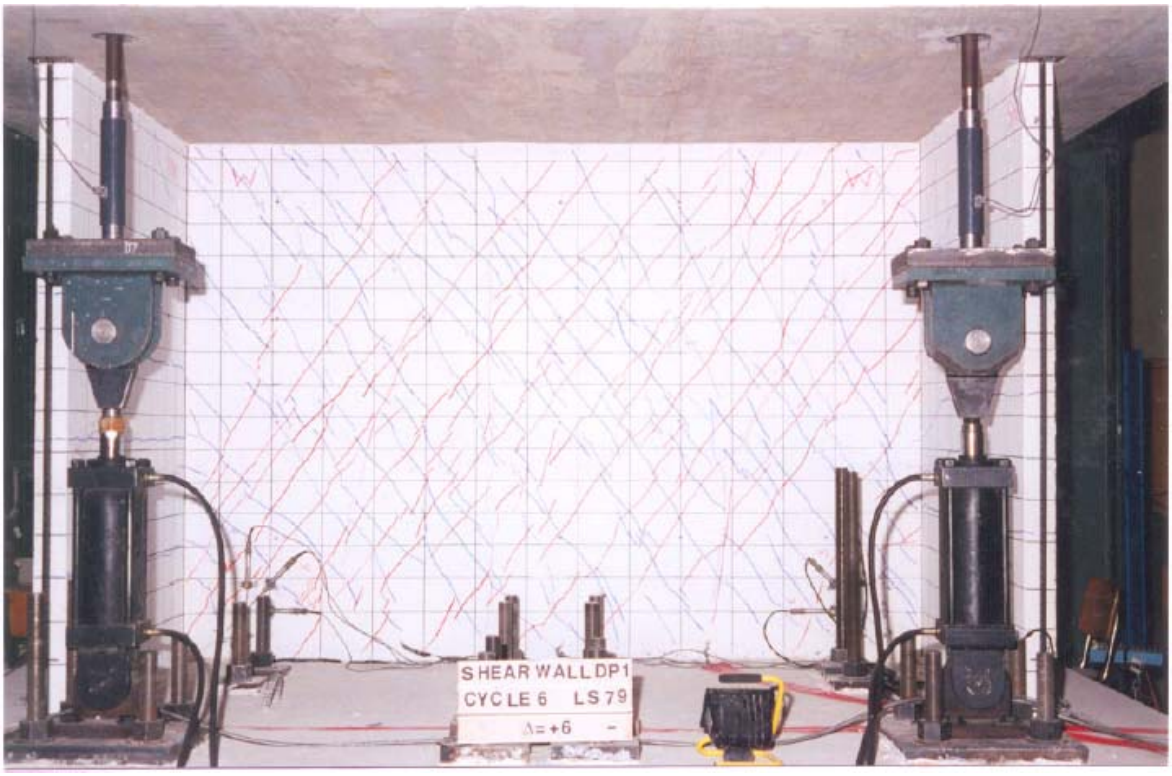


**Figure C-294 Condition of wall DP1 at 0.30% drift [Palermo and Vecchio (2002)]**

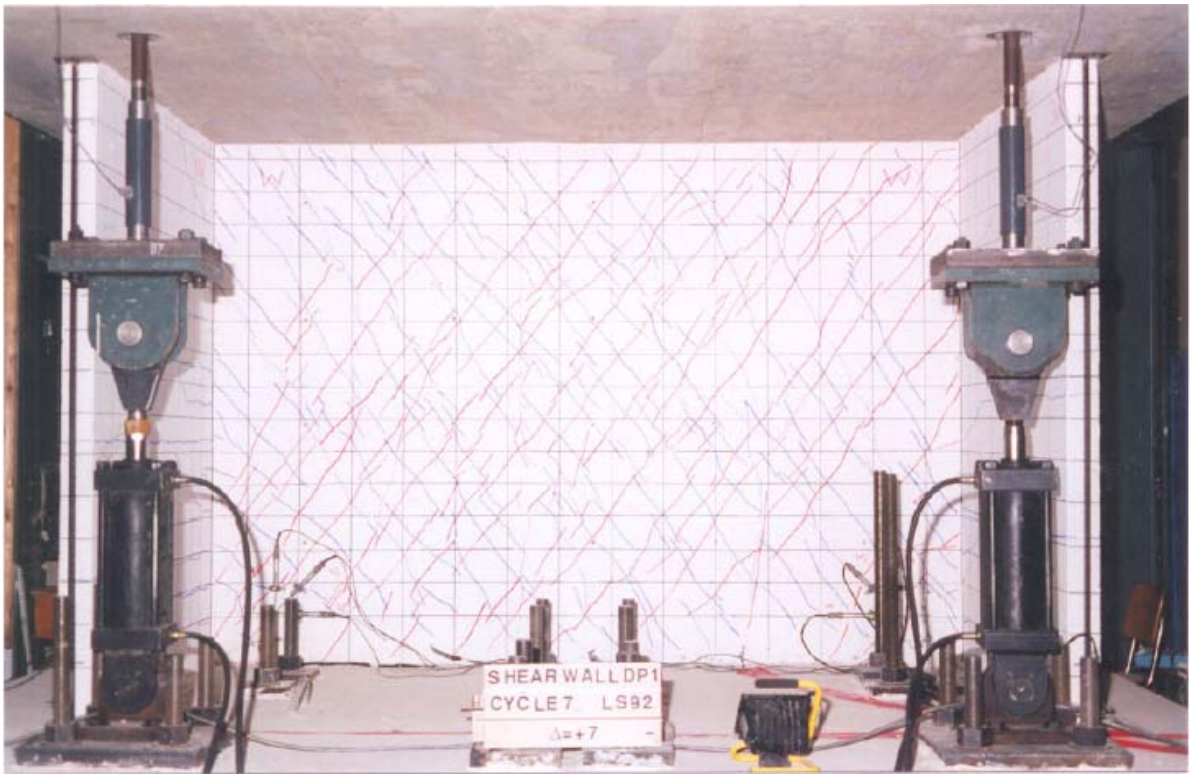


**Figure C-295 Condition of wall DP1 at 0.35% drift [Palermo and Vecchio (2002)]**

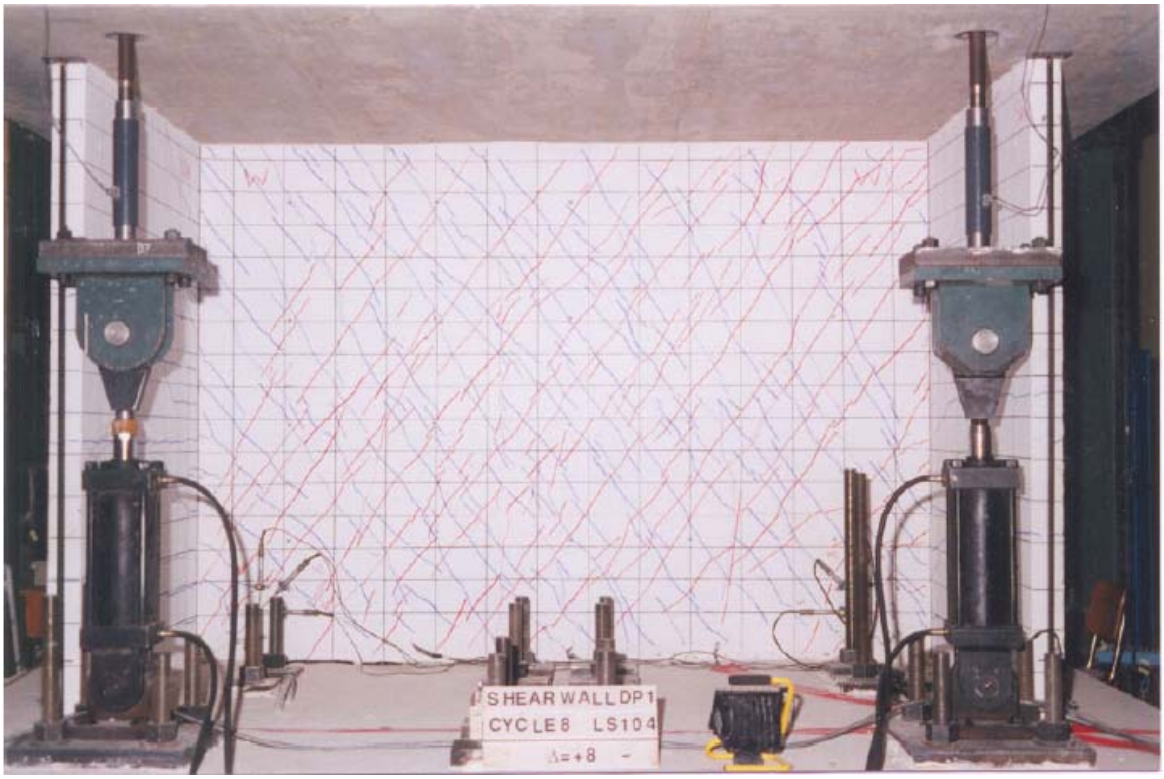


**Figure C-296 Condition of wall DP1 at 0.40% drift [Palermo and Vecchio (2002)]**

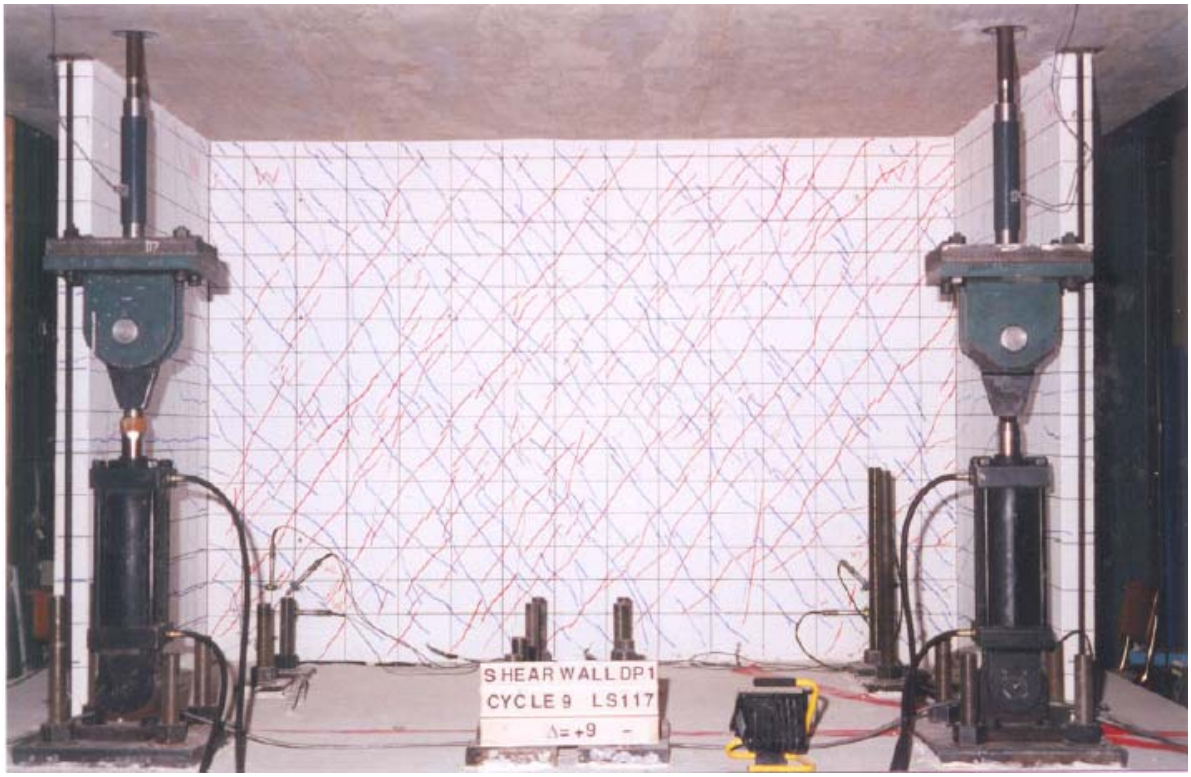


**Figure C-297 Condition of wall DP1 at 0.45% drift [Palermo and Vecchio (2002)]**

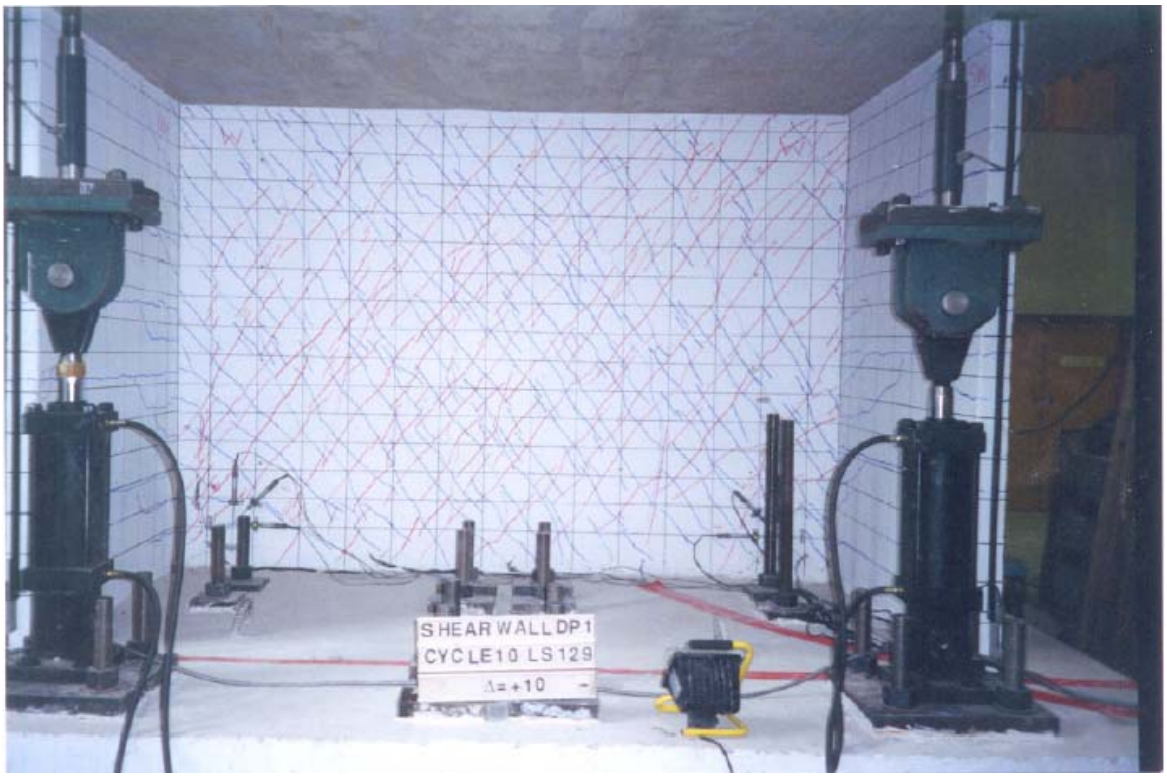


**Figure C-298 Condition of wall DP1 at 0.50% drift [Palermo and Vecchio (2002)]**

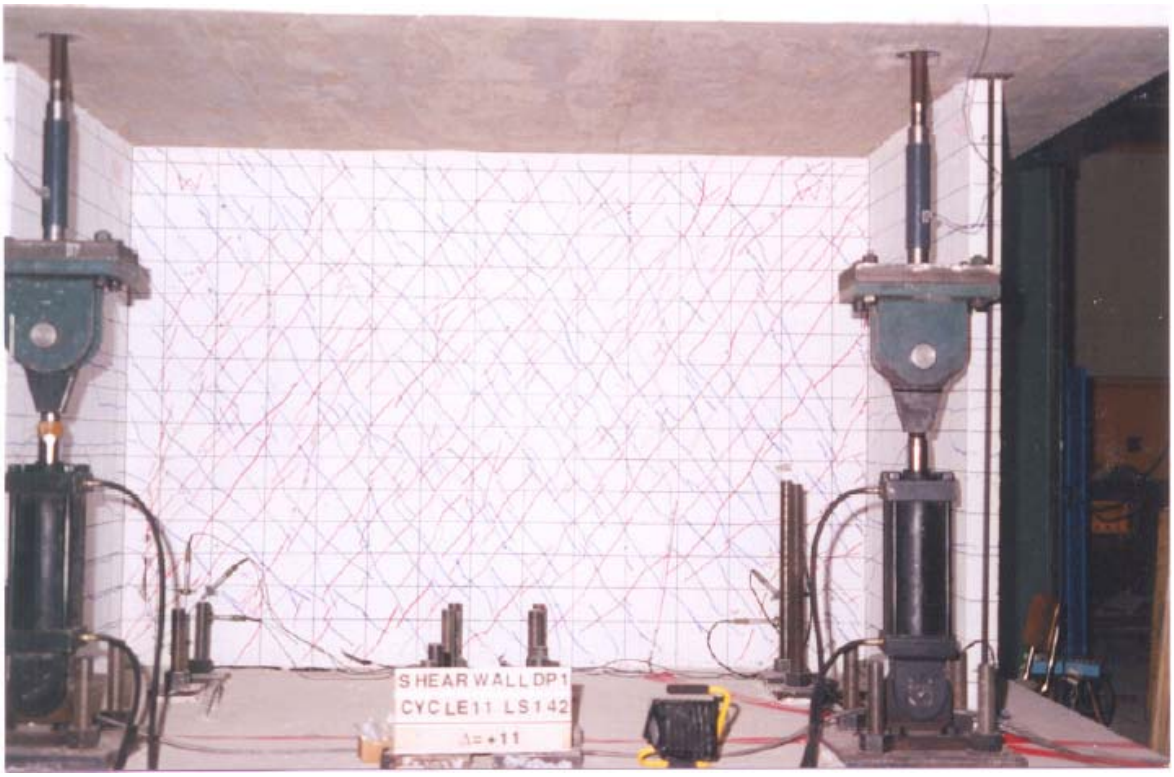


**Figure C-299 Condition of wall DP1 at 0.54% drift [Palermo and Vecchio (2002)]**

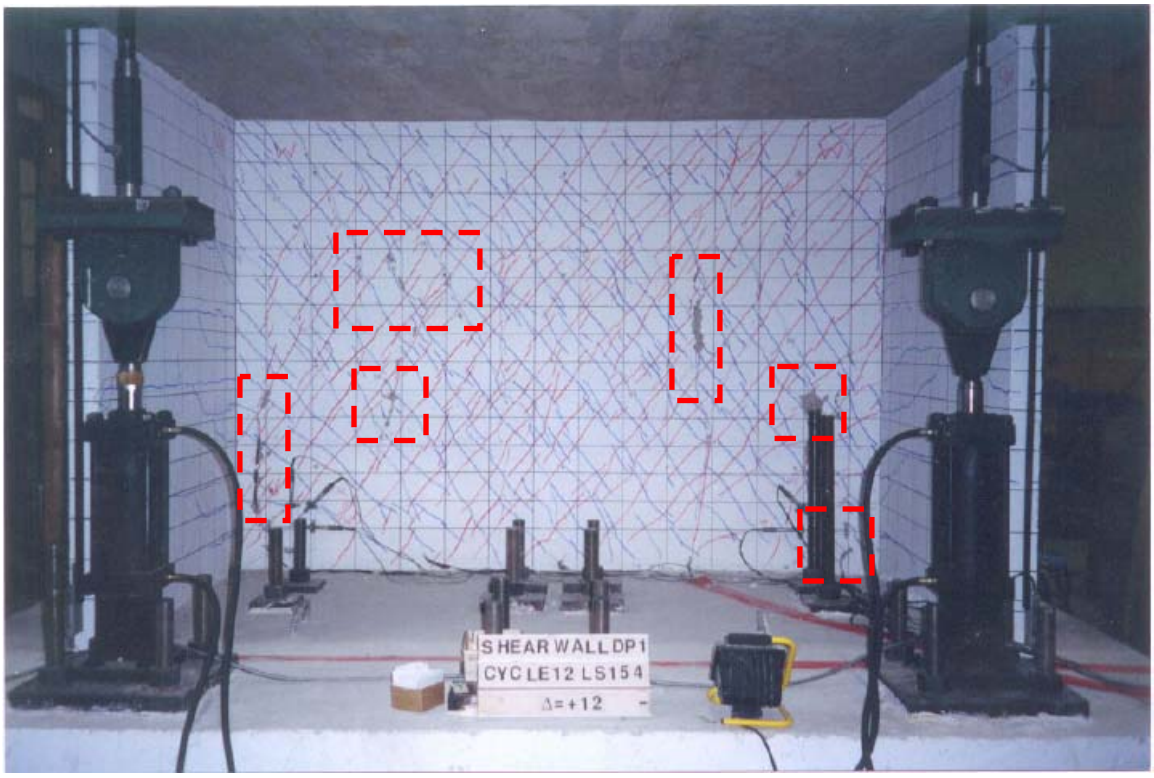


**Figure C-300 Condition of wall DP1 at 0.59% drift [Palermo and Vecchio (2002)]**

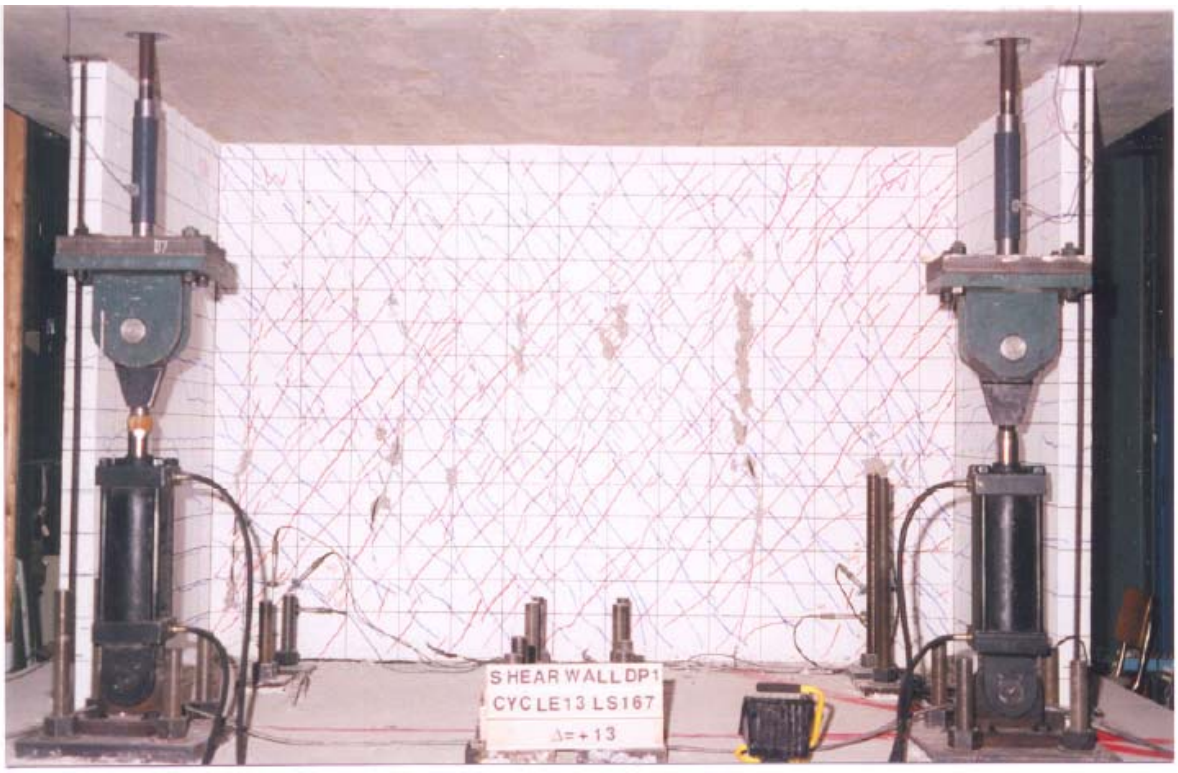


**Figure C-301 Condition of wall DP1 at 0.64% drift [Palermo and Vecchio (2002)]**

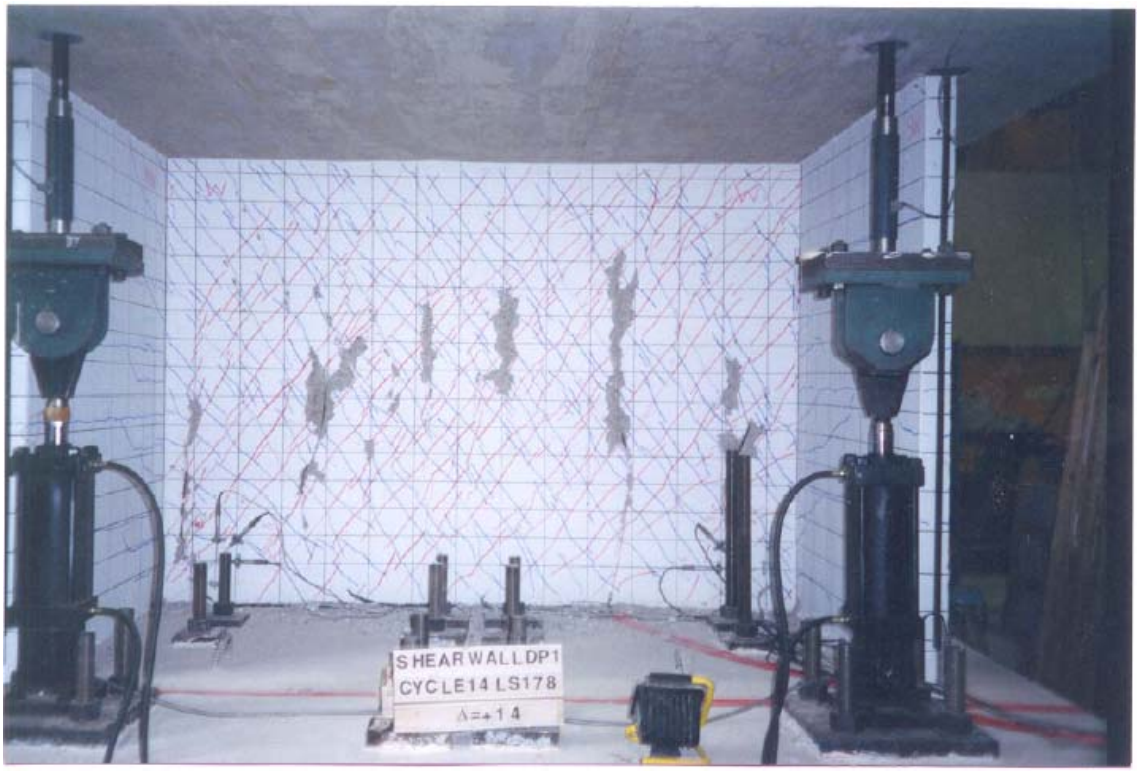


**Figure C-302 Condition of wall DP1 at 0.69% drift [Palermo and Vecchio (2002)]**

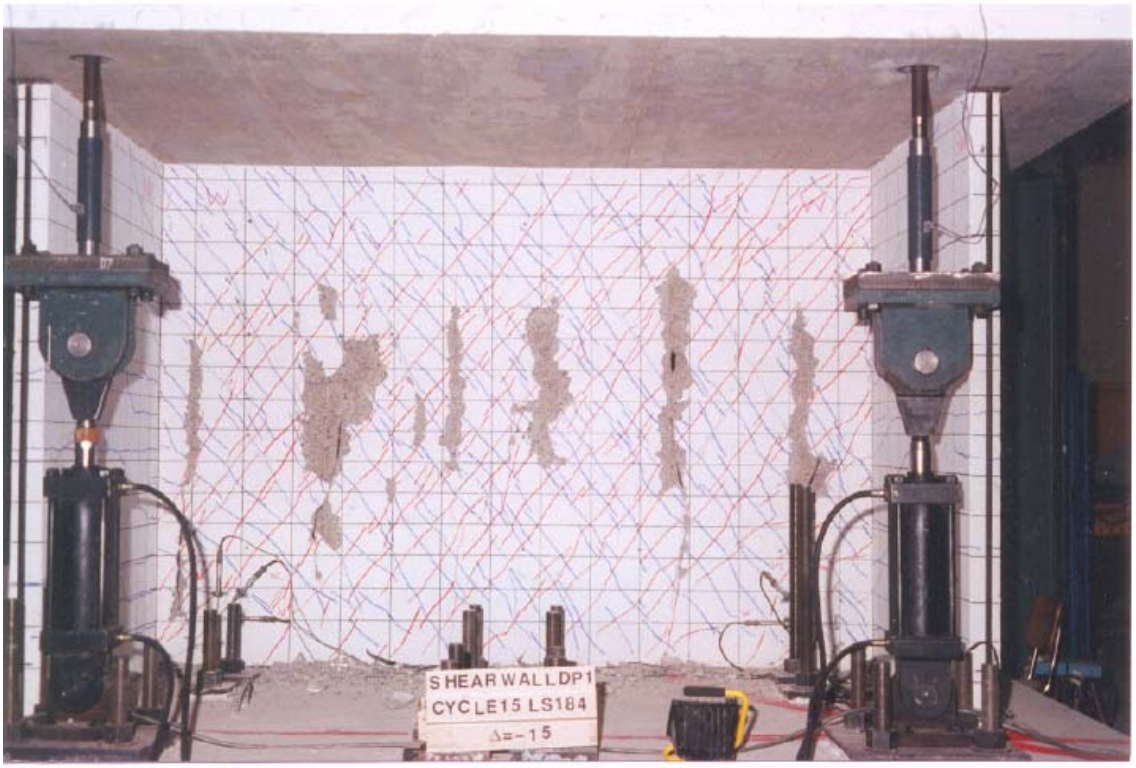


**Figure C-303 Condition of wall DP1 at 0.74% drift [Palermo and Vecchio (2002)]**

### C.3.2.2 Wall DP2

**Table C-83 Evaluation of damage data for wall DP2 tested by Palermo**

| Wall ID | MoR | Damage State (DS) | Drift (%) | Comments |
|---|---|---|---|---|
| DP2 | 1 | 1.2 | 0.06 | The drifts for these damage states are provided by the researcher. |
| | | 1.3 | 0.02 | |
| | | 1.4 | 0.25 | |
| | 2a | 2.4a | 0.35 | |
| | | 2.5a | 0.30 | |
| | 2b | 2.5b | 0.45 | |
| | 3 | 3.1 | 0.45 | The researcher reported a drift of 0.40% at initiation of concrete crushing at the compression toe of the web. Figure C-312 shows the condition of the wall at 0.40% drift. Based on the condition of extent of damage provided in this figure, it is concluded that the drift reported by the author is too small for MoR-3 since crushing is probably limited to a very small region. A drift of 0.45% is assumed for this damage state based on Figure C-313. In Figure C-313, the dashed boxes identify the regions of concrete requiring replacement. |
| | 4 | 4.1 | 0.50 | The image reported at this drift shows sliding damage (Figure C-314). |

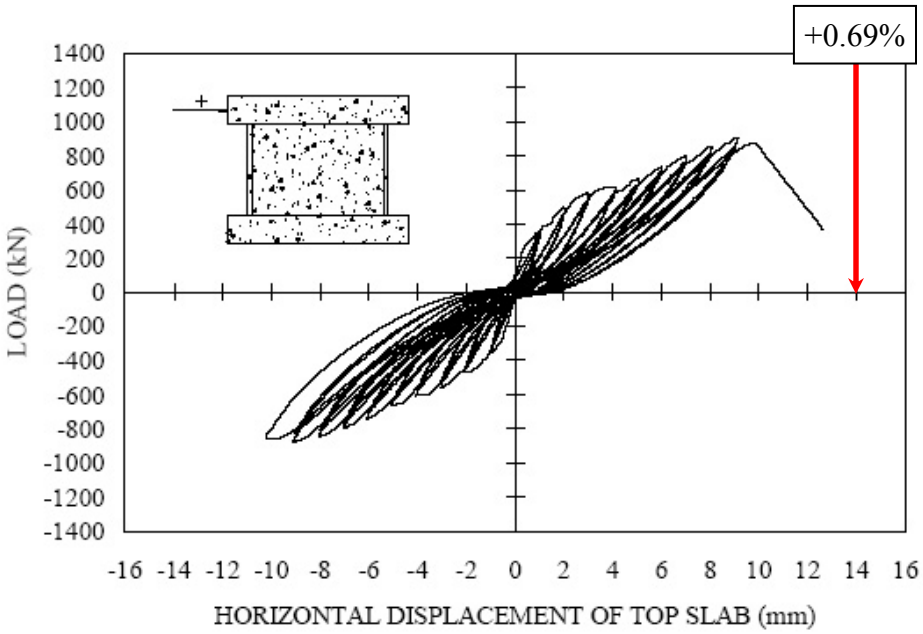


**Figure C-304 Load-displacement relationship for wall DP2 [Palermo and Vecchio (2002)]**

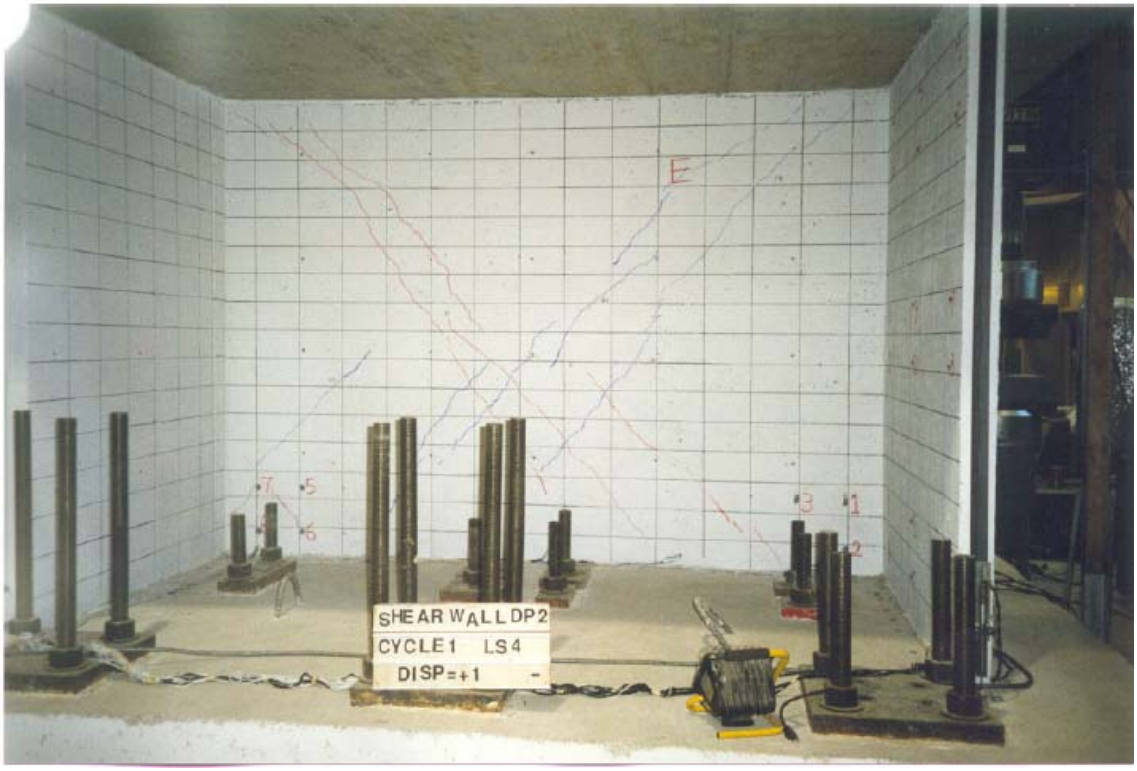


**Figure C-305 Condition of wall DP2 at 0.05% drift [Palermo and Vecchio (2002)]**

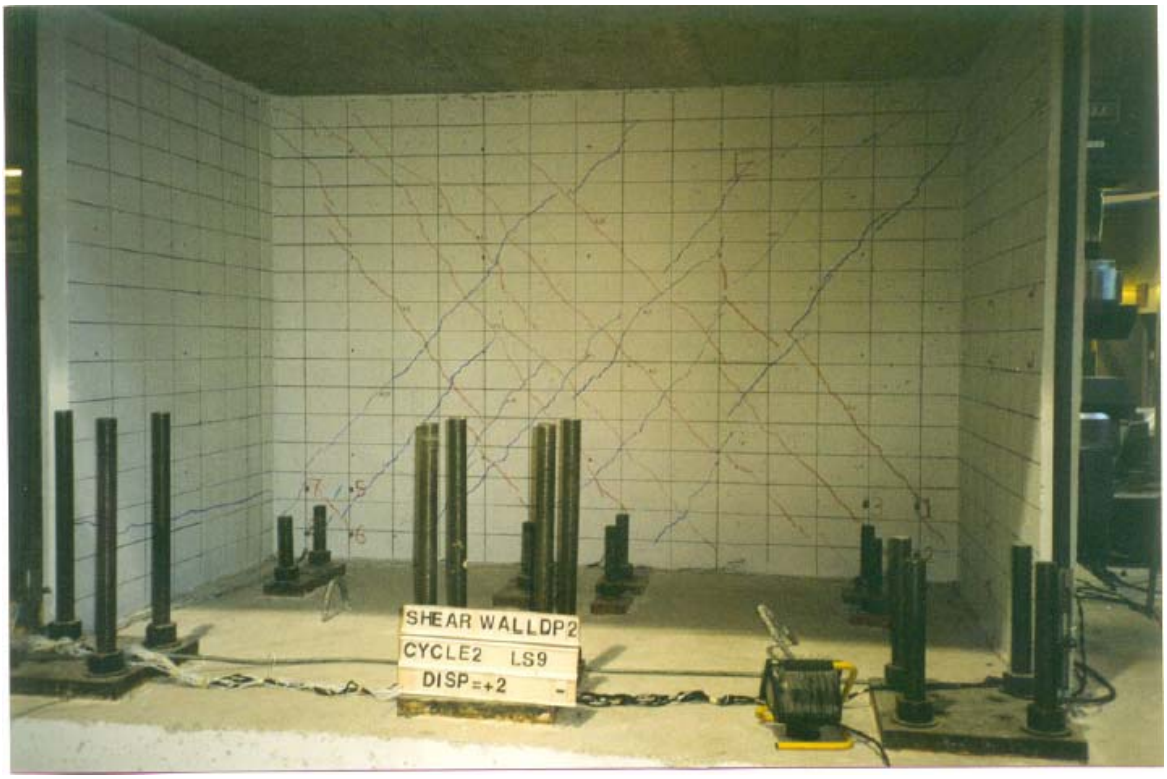


**Figure C-306 Condition of wall DP2 at 0.1% drift [Palermo and Vecchio (2002)]**

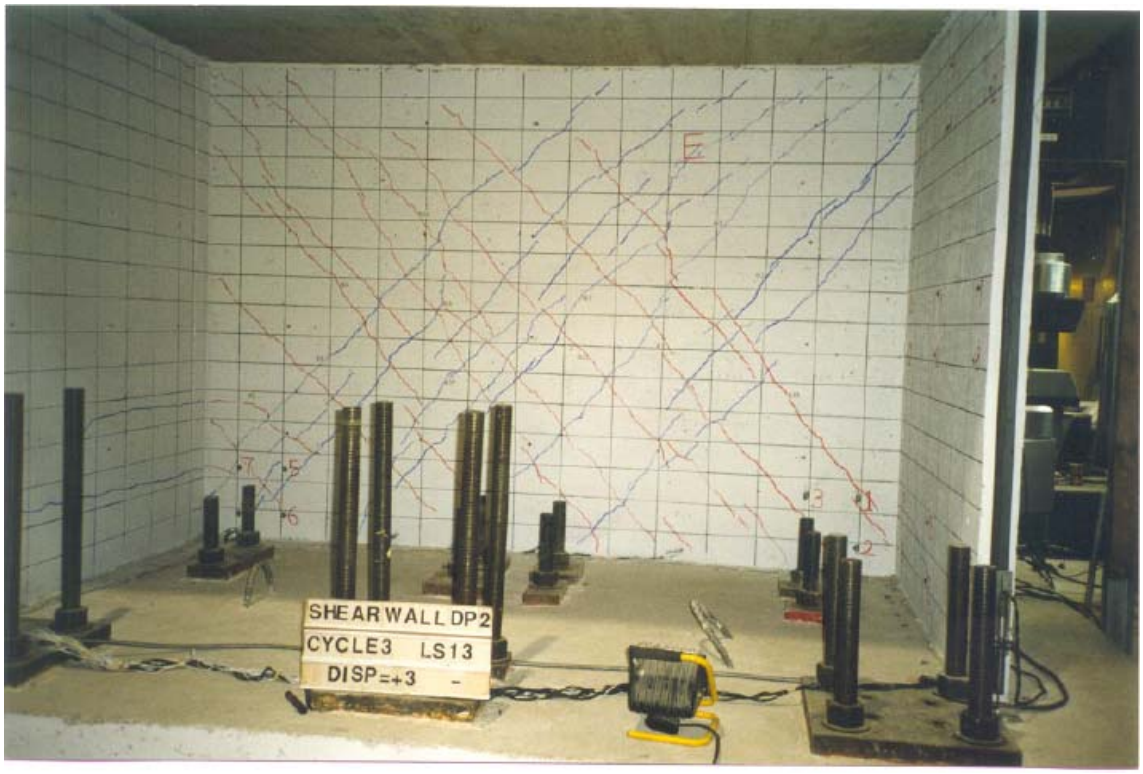


**Figure C-307 Condition of wall DP2 at 0.15% drift [Palermo and Vecchio (2002)]**

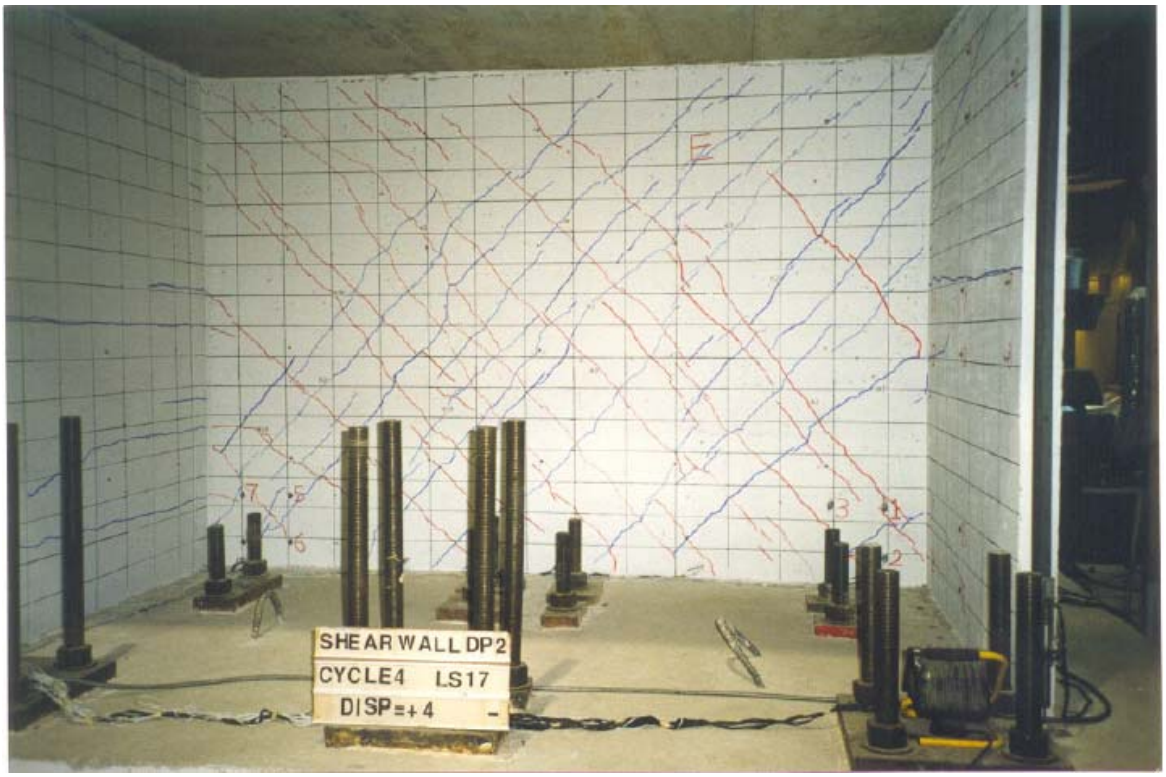


**Figure C-308 Condition of wall DP2 at 0.20% drift [Palermo and Vecchio (2002)]**

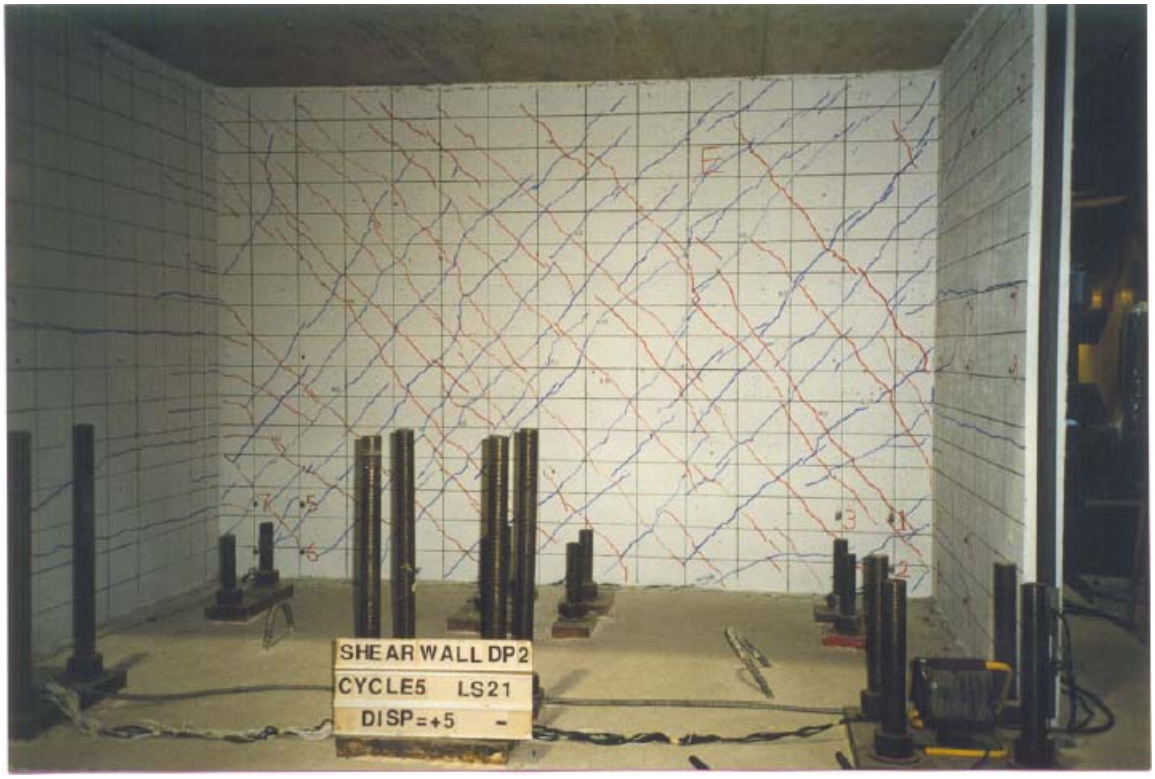


**Figure C-309 Condition of wall DP2 at 0.25% drift [Palermo and Vecchio (2002)]**

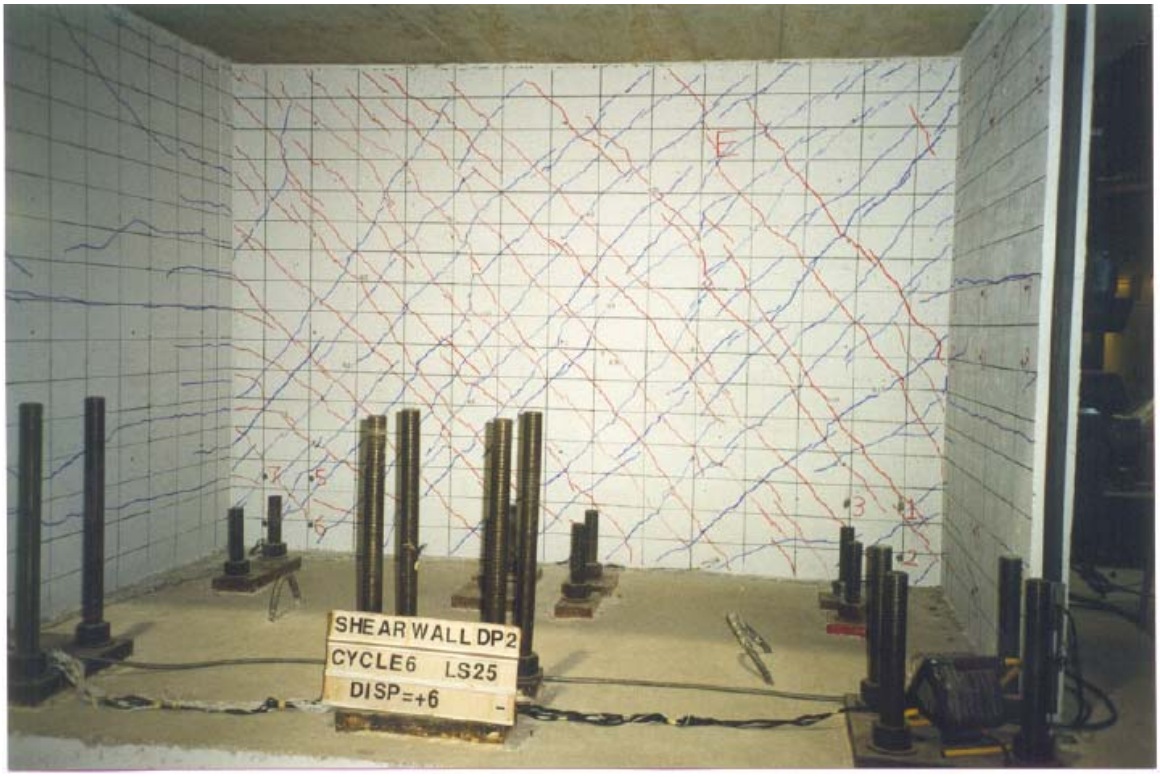


**Figure C-310 Condition of wall DP2 at 0.30% drift [Palermo and Vecchio (2002)]**

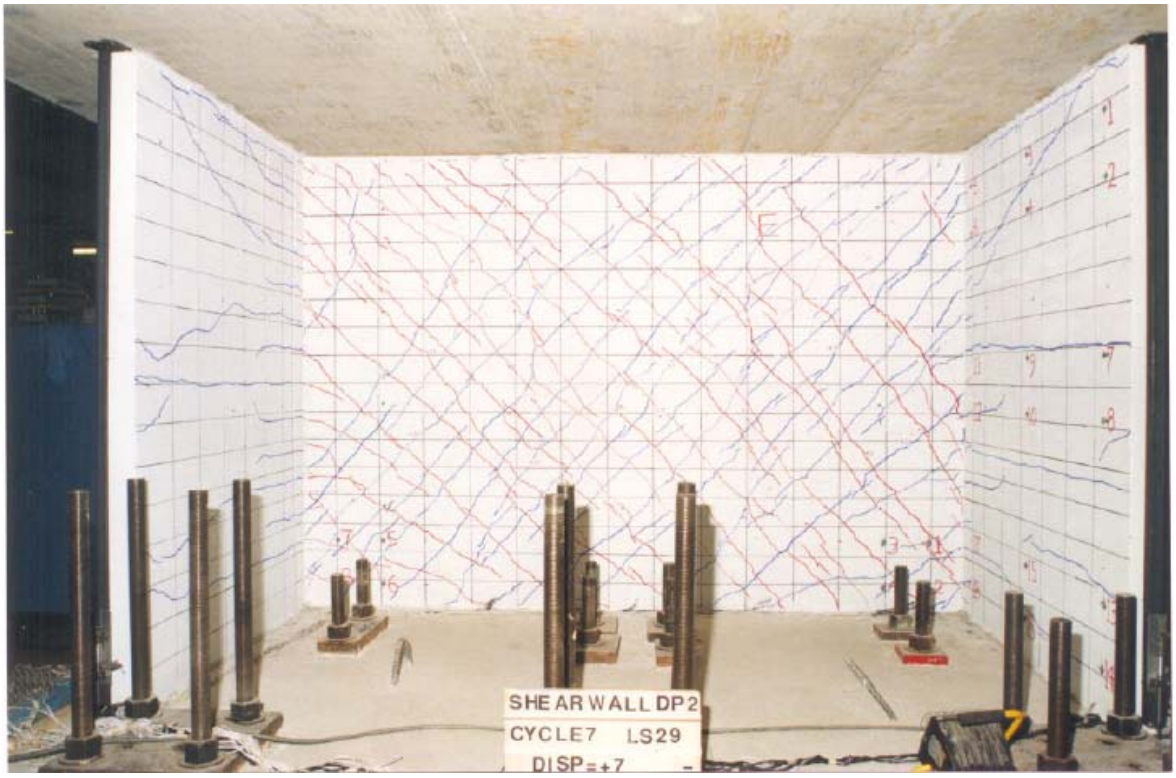


**Figure C-311 Condition of wall DP2 at 0.35% drift [Palermo and Vecchio (2002)]**

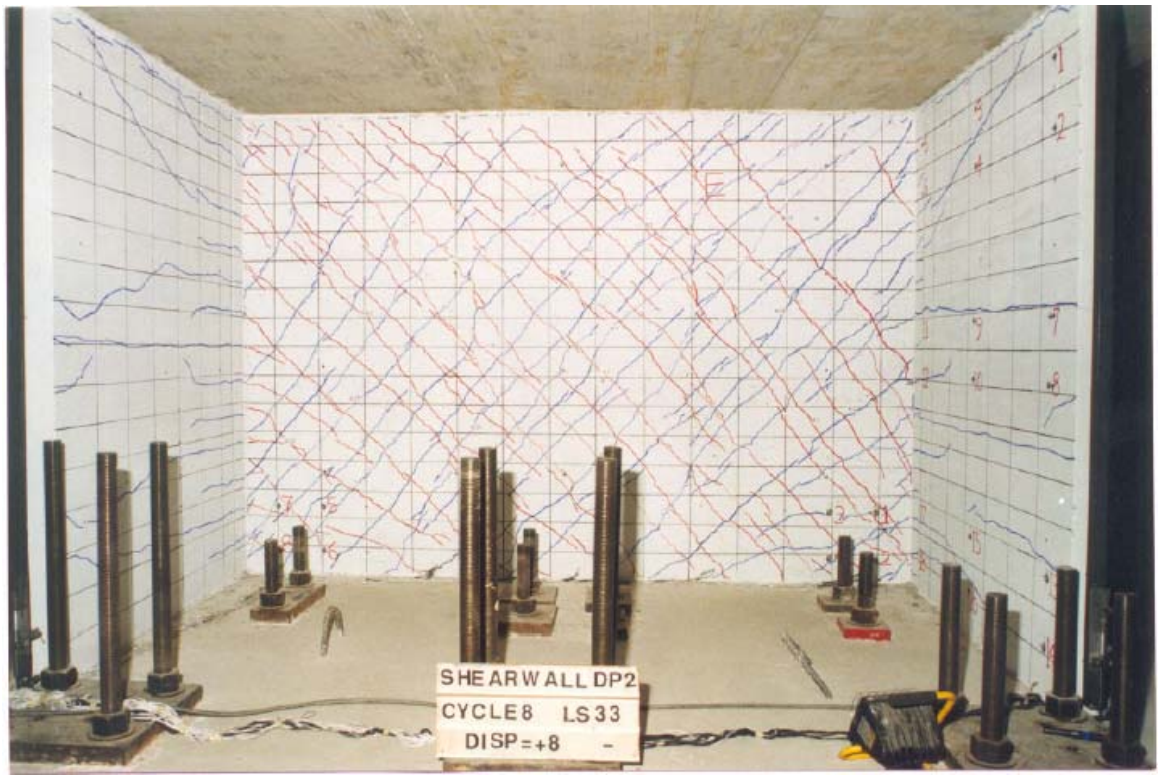


**Figure C-312 Condition of wall DP2 at 0.40% drift [Palermo and Vecchio (2002)]**

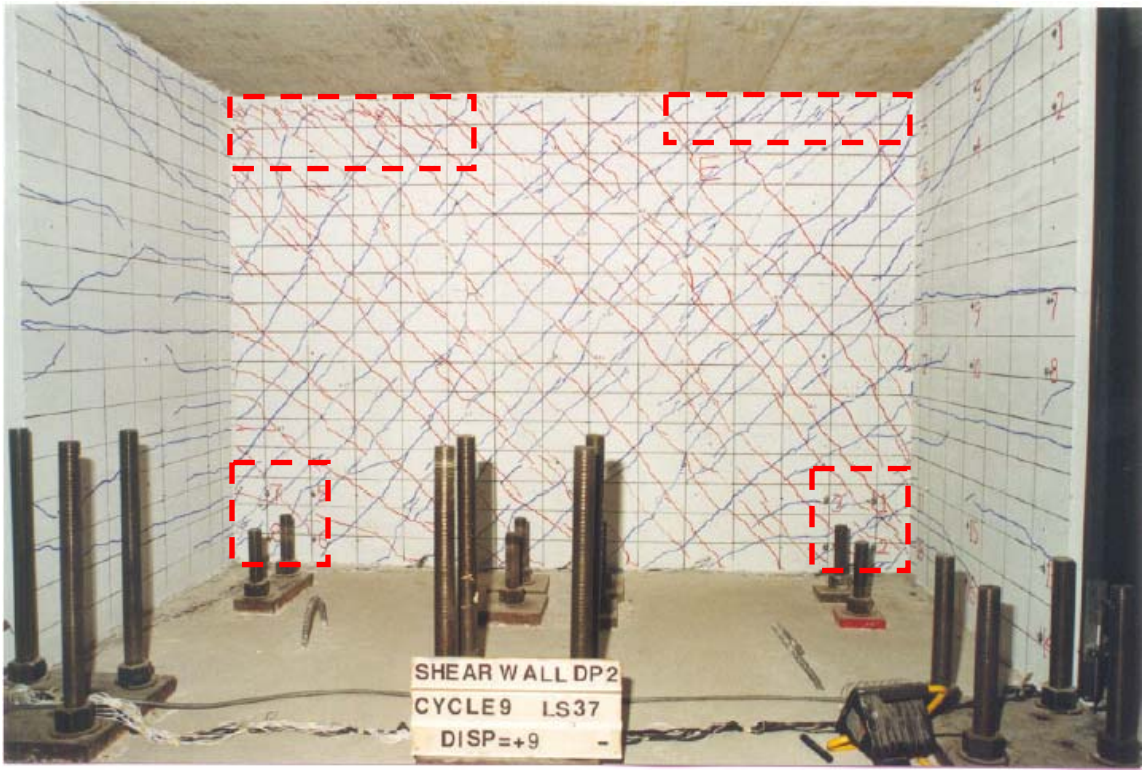


**Figure C-313 Condition of wall DP2 at 0.45% drift [Palermo and Vecchio (2002)]**

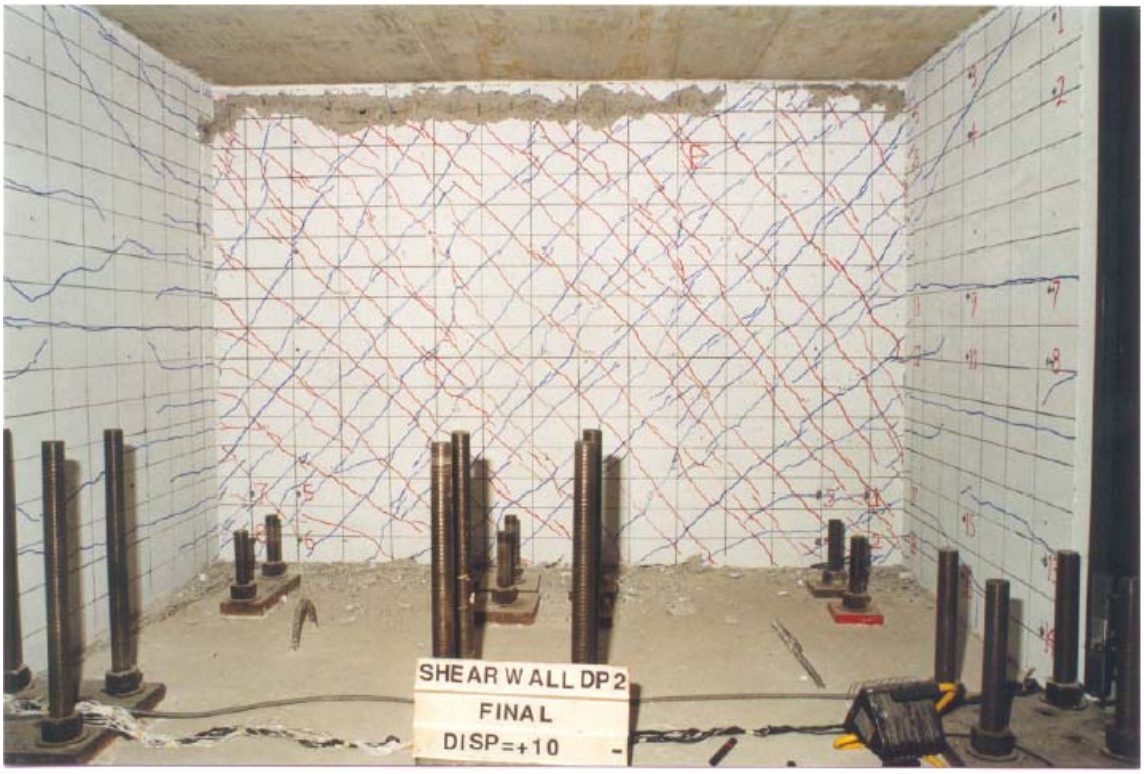


**Figure C-314 Condition of wall DP2 at 0.50% drift [Palermo and Vecchio (2002)]**

## C.3.3 NUPEC Wall [Kitada et al. (1997)]

### C.3.3.1 Wall U1

**Table C-84 Evaluation of damage data for wall U1 tested by NUPEC**

| Wall ID | MoR | Damage State (DS) | Drift (%) | Comments |
|---|---|---|---|---|
| U1 | 4 | 4.1 | 0.87 | The researcher reported that the wall failed by sliding shear and so the supplemental criteria are invoked to obtain a drift associated with this damage state. |
| | 4* | $SC_1$ | 0.87 | The smaller of the two drifts is obtained from the 1st quadrant of the load-displacement relationship (see Figure C-315, red circle). Note that wall U-1 was tested using an earthquake simulator therefore, the residual drift associated with $SC_1$ is 0.5%. |
| | | $SC_2$ | 0.83 | The data point is obtained from the 1st quadrant of the load-displacement relationship (see Figure C-315). A data point cannot be established in the 3rd quadrant. |

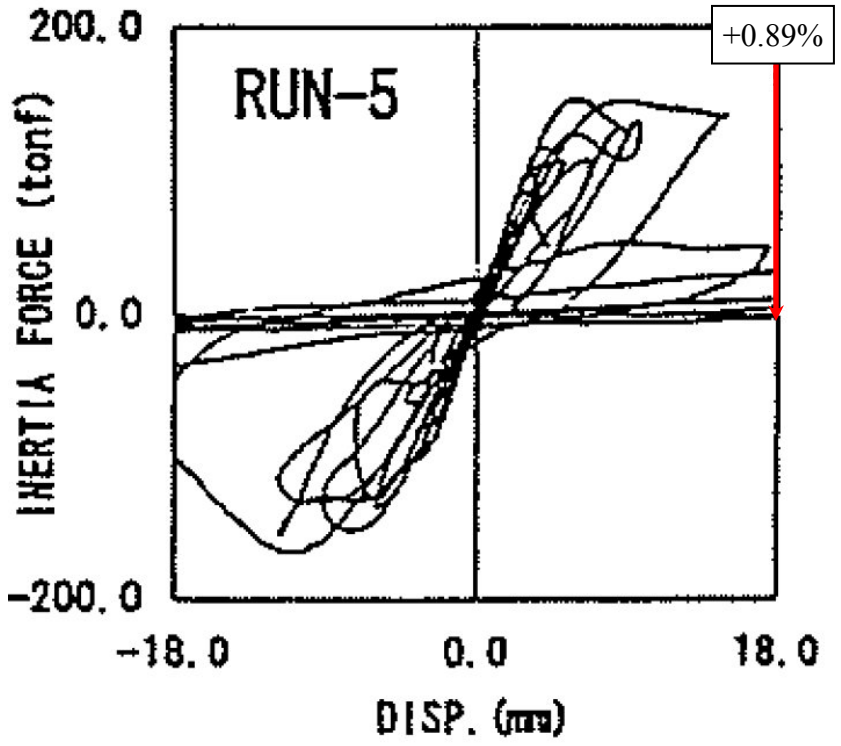


**Figure C-315 Load-displacement relationship for wall U1 [Kitada et al. (1997)]**

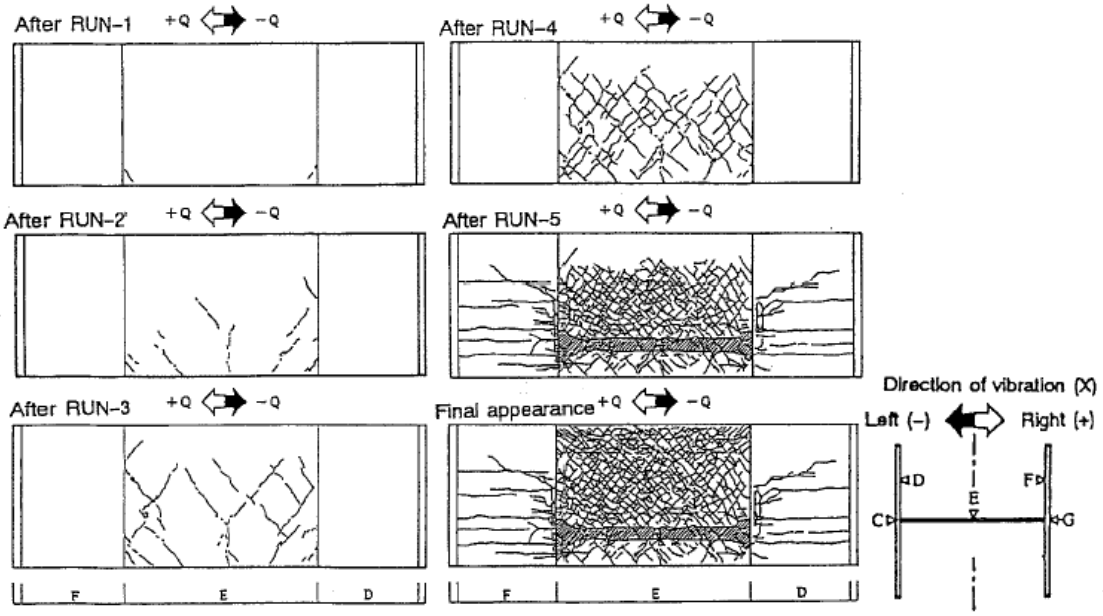


**Figure C-316 Progression of damage for wall U1 [Kitada et al. (1997)]**

## C.3.4 Sato et al. (1989) Walls

### C.3.4.1 Wall 24M8-30

**Table C-85 Evaluation of damage data for wall 24M8-30 tested by Sato**

| Wall ID | MoR | Damage State (DS) | Drift (%) | Comments |
|---|---|---|---|---|
| 24M8-30 | 2a | 2.3 | 0.47 | The shear forces for these damage states are provided by the researcher. The corresponding drifts are obtained using the reported backbone load-displacement relationship. |
| | 3 | 3.1 | 0.80 | |
| | 4 | N/A | N/A | The failure mode was not reported and so the supplemental criteria are invoked to seek a drift associated with this damage state. |
| | 4* | $SC_1$ | N/A | The wall was loaded cyclically, but only a backbone load-displacement relationship was reported. |
| | | $SC_2$ | N/A | The post-peak resistance computed using the reported backbone curve did not drop to $0.5V_{peak}$ (Figure C-317). |

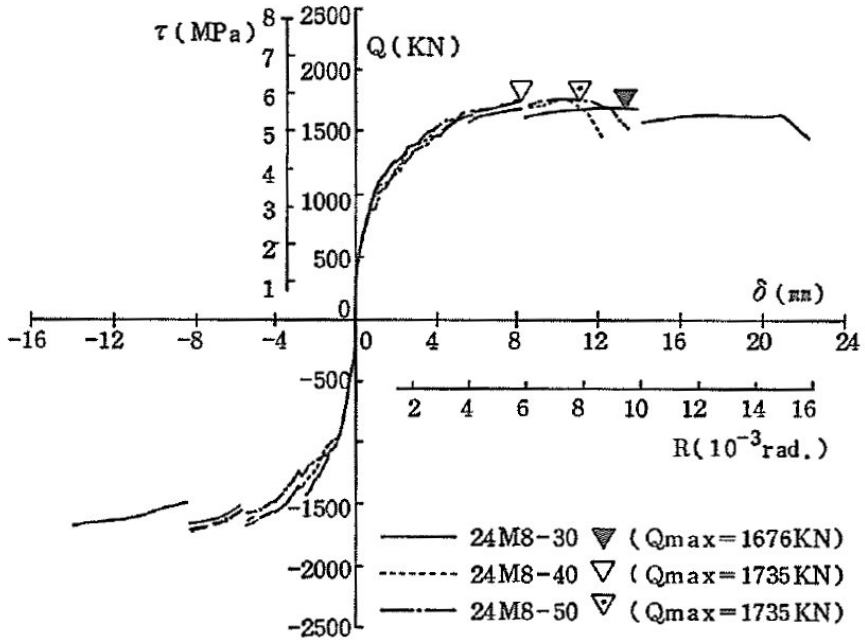


**Figure C-317 Backbone curves for walls 24M8-30, 24M8-40, and 24M8-50 [Sato et al. (1989)]**

### C.3.4.2 Wall 24M8-40

**Table C-86 Evaluation of damage data for wall 24M8-40 tested by Sato**

| Wall ID | MoR | Damage State (DS) | Drift (%) | Comments |
|---|---|---|---|---|
| 24M8-40 | 2a | 2.3 | 0.49 | The shear forces for these damage states are provided by the researcher. The corresponding drifts are obtained using the reported backbone load-displacement relationship. |
| | 3 | 3.1 | 0.54 | |
| | 4 | N/A | N/A | The failure mode was not reported and so the supplemental criteria are invoked to seek a drift associated with this damage state. |
| | 4* | $SC_1$ | N/A | The wall was loaded cyclically, but only a backbone load-displacement relationship was reported. |
| | | $SC_2$ | N/A | The post-peak resistance computed using the reported backbone curve did not drop to $0.5V_{peak}$ (Figure C-317). |

### C.3.4.3 Wall 24M8-50

**Table C-87 Evaluation of damage data for wall 24M8-50 tested by Sato**

| Wall ID | MoR | Damage State (DS) | Drift (%) | Comments |
|---|---|---|---|---|
| 24M8-50 | 2a | 2.3 | 0.37 | The shear forces for these damage states are provided by the researcher. The corresponding drifts are obtained using the reported backbone load-displacement relationship. |
| | 3 | 3.1 | 0.78 | |
| | 4 | N/A | N/A | The failure mode was not reported and so the supplemental criteria are invoked to seek a drift associated with this damage state. |
| | 4* | $SC_1$ | N/A | The wall was loaded cyclically, but only a backbone load-displacement relationship was reported. |
| | | $SC_2$ | N/A | The post-peak resistance computed using the reported backbone curve did not drop to $0.5V_{peak}$ (Figure C-317). |

### C.3.4.4 Wall 36M8-30

**Table C-88 Evaluation of damage data for wall 36M8-30 tested by Sato**

| Wall ID | MoR | Damage State (DS) | Drift (%) | Comments |
|---|---|---|---|---|
| 36M8-30 | 1 | 1.2 | 0.03 | The drifts for these damage states are provided by the researcher. |
| | | 1.3 | 0.06 | |
| | 2a | 2.1 | 1.32 | |
| | | 2.3 | 0.25 | |
| | 3 | 3.1 | 1.00 | |
| | 4 | 4.1 | 1.53 | The researcher reported that the wall failed by sliding shear and so the supplemental criteria are invoked to obtain a drift associated with this damage state. |
| | 4* | $SC_1$ | 1.53 | The residual drifts did not exceed 1.0%. However, the maximum recorded residual drift is judged to be close enough to 1.0% (see Figure C-318) and supports the use of 1.50% reported previously. |
| | | $SC_2$ | N/A | The post-peak resistance computed using the reported backbone curve did not drop to $0.5V_{peak}$ (Figure C-318). |

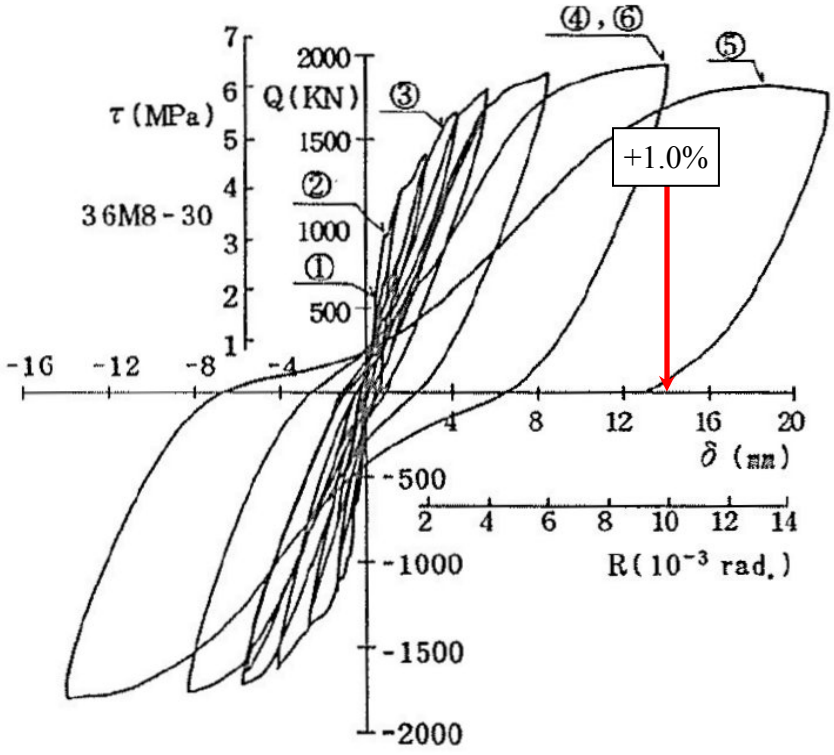


**Figure C-318 The load-displacement relationship for wall 36M8-30 [Sato et al. (1989)]**

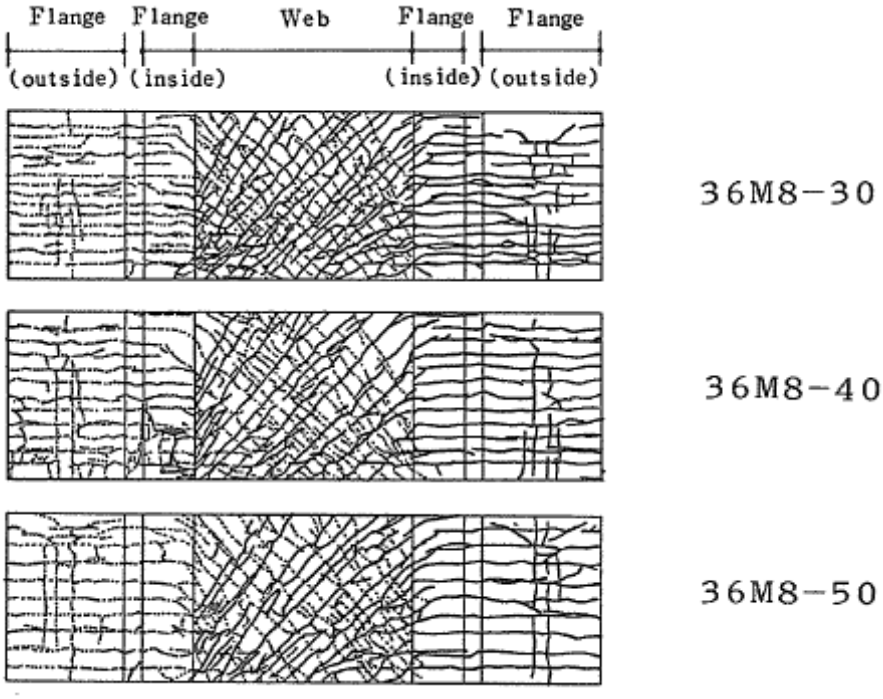


**Figure C-319 Conditions of walls 36M8-30, 36M8-40 and 36M8-50 at the end of the test [Sato et al. (1989)]**

### C.3.4.5 Wall 36M8-40

**Table C-89 Evaluation of damage data for wall 36M8-40 tested by Sato**

| Wall ID | MoR | Damage State (DS) | Drift (%) | Comments |
|---|---|---|---|---|
| 36M8-40 | 2a | 2.3 | 0.39 | The drifts for these damage states are provided by the researcher. |
| | 3 | 3.1 | 0.83 | |
| | 4 | 4.1 | 1.50 | The researcher reported sliding shear failure at a drift of 1.50%. The reported drift at sliding failure (DS4.1) is excluded from the fragility analysis because herein drift associated with sliding failure is calculated using the supplemental wall replacement criteria. No data associated with DS4.1 is registered since none could be obtained using the supplemental criteria. |
| | 4* | $SC_1$ | N/A | The wall was loaded cyclically, but only a backbone load-displacement relationship was reported. |
| | | $SC_2$ | N/A | The post-peak resistance computed using the reported backbone curve did not drop to $0.5V_{peak}$ (Figure C-320). |

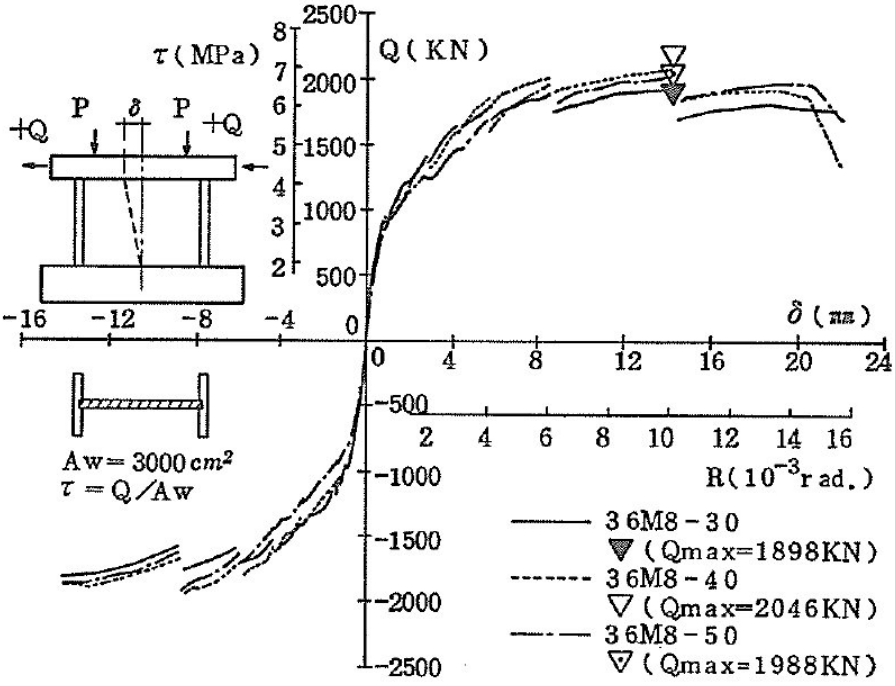


**Figure C-320 Backbone curves for walls 36M8-30, 36M8-40, and 36M8-50 [Sato et al. (1989)]**

### C.3.4.6 Wall 36M8-50

**Table C-90 Evaluation of damage data for wall 36M8-50 tested by Sato**

| Wall ID | MoR | Damage State (DS) | Drift (%) | Comments |
|---|---|---|---|---|
| 36M8-50 | 1 | 1.2 | 0.03 | The drift data for these damage states are provided by the researcher. |
| | | 1.3 | 0.05 | |
| | 2a | 2.1 | 1.55 | |
| | | 2.3 | 0.37 | |
| | 3 | 3.1 | 1.04 | |
| | 4 | 4.1 | 1.55 | The researcher reported that the wall failed by sliding shear and so the supplemental criteria are invoked to obtain a drift associated with this damage state. |
| | 4* | $SC_1$ | 1.55 | Residual drifts did not exceed 1.0%. However, the maximum recorded residual drift is judged to be close enough to 1.0% (Figure C-319) and supports the use of 1.50% reported previously. |
| | | $SC_2$ | N/A | The post-peak resistance computed using the reported backbone curve did not drop to $0.5V_{peak}$ (Figure C-321). |

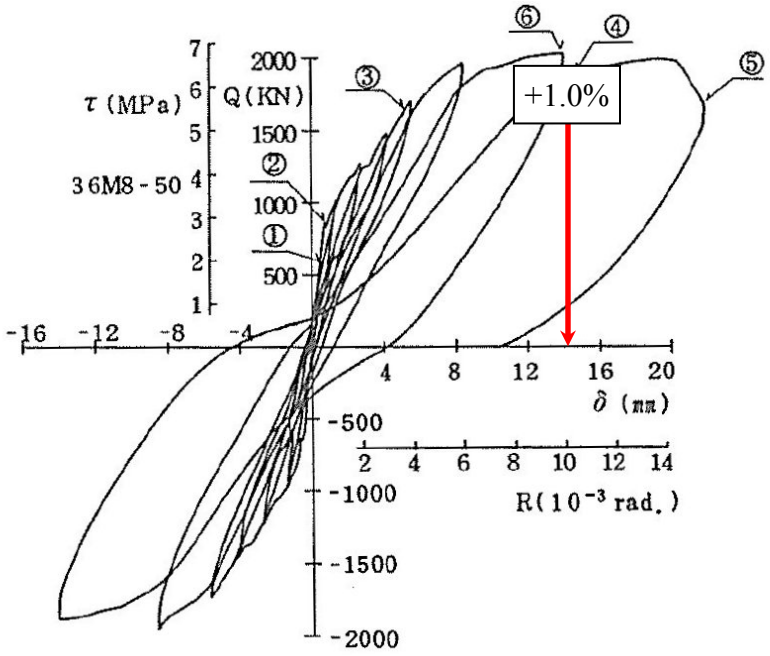


**Figure C-321 Load-displacement relationship for wall 36M8-50 [Sato et al. (1989)]**

### C.3.4.7 Wall 48M8-30

**Table C-91 Evaluation of damage data for wall 48M8-30 tested by Sato**

| Wall ID | MoR | Damage State (DS) | Drift (%) | Comments |
|---|---|---|---|---|
| 48M8-30 | 2a | 2.3 | 0.38 | The shear forces for these damage states are provided by the researcher. The corresponding drifts are obtained using the reported backbone load-displacement relationship. |
| | 3 | 3.1 | 0.59 | |
| | 4 | N/A | N/A | The failure mode was not reported and so the supplemental criteria are invoked to seek a drift associated with this damage state. |
| | 4* | $SC_1$ | N/A | The wall was loaded cyclically, but only a backbone load-displacement relationship was reported. |
| | | $SC_2$ | N/A | The post-peak resistance computed using the reported backbone curve did not drop to $0.5V_{peak}$ (Figure C-322). |

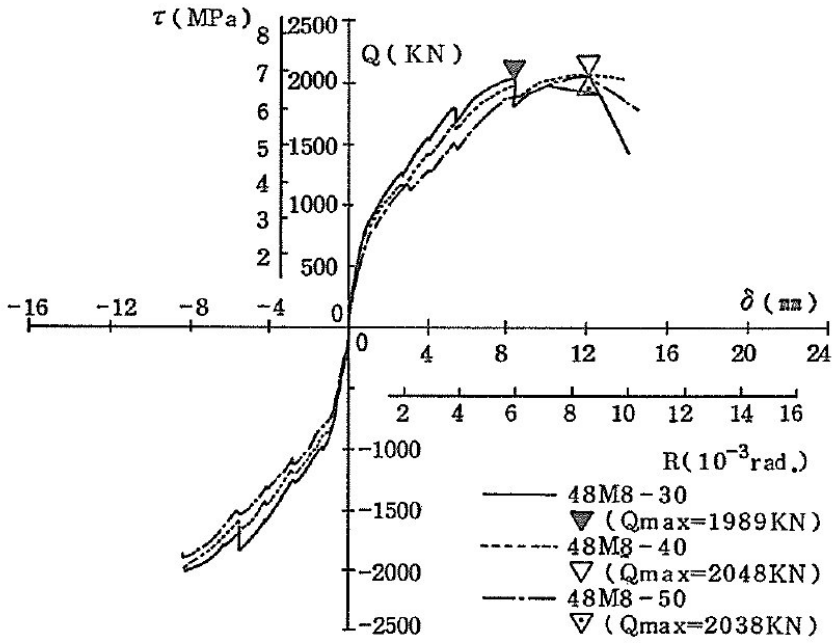


**Figure C-322 Backbone curves for walls 48M8-30, 48M8-40, and 48M8-50 [Sato et al. (1989)]**

### C.3.4.8 Wall 48M8-40

**Table C-92 Evaluation of damage data for wall 48M8-40 tested by Sato**

| Wall ID | MoR | Damage State (DS) | Drift (%) | Comments |
|---|---|---|---|---|
| 48M8-40 | 2a | 2.3 | 0.42 | The shear forces for these damage states are provided by the researcher. The corresponding drifts are obtained using the reported backbone load-displacement relationship. |
| | 3 | 3.1 | 0.66 | |
| | 4 | N/A | N/A | The failure mode was not reported and so the supplemental criteria are invoked to seek a drift associated with this damage state. |
| | 4* | $SC_1$ | N/A | The wall was loaded cyclically, but only a backbone load-displacement relationship was reported. |
| | | $SC_2$ | N/A | The post-peak resistance computed using the reported backbone curve did not drop to $0.5V_{peak}$ (Figure C-322). |

### C.3.4.9 Wall 48M8-50

**Table C-93 Evaluation of damage data for wall 48M8-50 tested by Sato**

| Wall ID | MoR | Damage State (DS) | Drift (%) | Comments |
|---|---|---|---|---|
| 48M8-50 | 2 | 2.3 | 0.55 | The shear forces for these damage states are provided by the researcher. The corresponding drifts are obtained using the reported backbone load-displacement relationship. |
| | 3 | 3.1 | 0.52 | |
| | 4 | N/A | N/A | The failure mode was not reported and so the supplemental criteria are invoked to seek a drift associated with this damage state. |
| | 4* | $SC_1$ | N/A | The wall was loaded cyclically, but only a backbone load-displacement relationship was reported. |
| | | $SC_2$ | N/A | The post-peak resistance computed using the reported backbone curve did not drop to $0.5V_{peak}$ (Figure C-322). |

## C.3.5 Synge Wall [Synge (1980)]

### C.3.5.1 Wall 3

**Table C-94 Evaluation of damage data for wall 3 tested by Synge**

| Wall ID | MoR | Damage State (DS) | Drift (%) | Comments |
|---|---|---|---|---|
| Wall 3 | 1 | 1.3 | 0.10 | The drifts for these damage states are provided by the researcher. For DS3.1, see Synge (1980), page 75. |
| | 2a | 2.2 | 0.20 | |
| | | 2.3 | 0.20 | |
| | 3 | 3.1 | 0.82 | |
| | | 3.4 | 0.82 | |
| | 4 | 4.1 | 1.19 | The researcher reported that the wall failed by sliding shear and so the supplemental criteria are invoked to obtain a drift associated with this damage state. |
| | 4* | $SC_1$ | 1.19 | The residual drift at a peak transient drift of 1.19% (3rd quadrant) is slightly lower than 1.0% but judged to be sufficiently close to 1.0% to produce a data point (see Figure C-323, red circle). |
| | | $SC_2$ | N/A | The post-peak resistance computed using the reported backbone curve did not drop to $0.5V_{peak}$ (Figure C-323). |

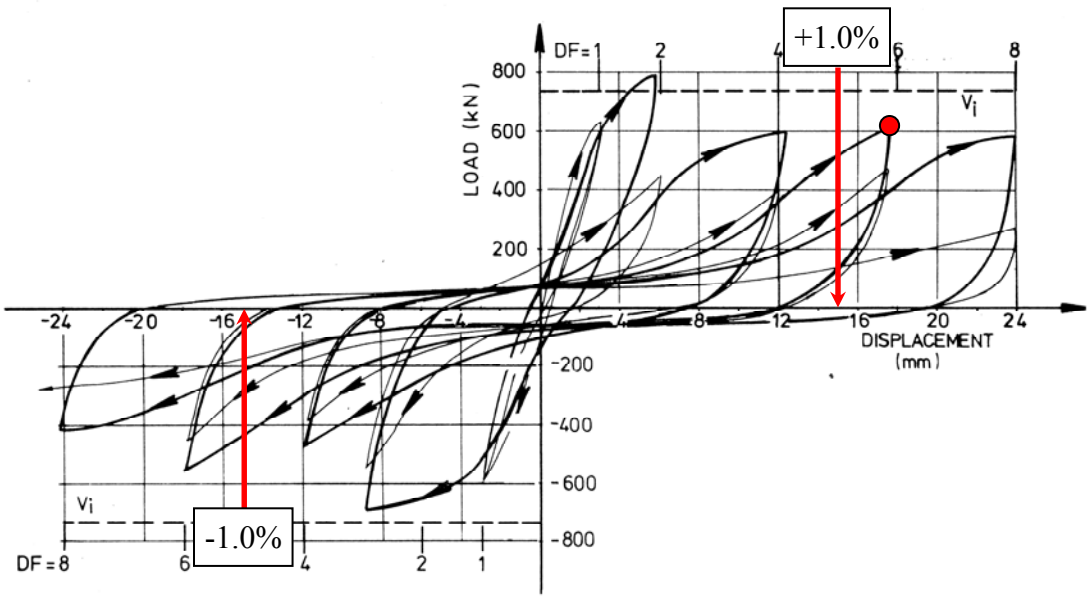


**Figure C-323 Load-displacement relationship for wall 3 [Synge (1980)]**

## C.3.6 Maier and Thürlimann (1985) Walls

### C.3.6.1 Wall S1

**Table C-95 Evaluation of damage data for wall S1 tested by Maier**

| Wall ID | MoR | Damage State (DS) | Drift (%) | Comments |
|---|---|---|---|---|
| S1 | 1 | 1.2 | 0.04 | The drifts for these damage states are provided by the researcher. |
| | 2a | 2.2 | 1.08 | |
| | | 2.3 | 0.67 | |
| | | 2.5a | 0.77 | |
| | 2b | 2.5b | 0.98 | |
| | 3 | 3.1 | 2.17 | The image reported at this drift (Figure C-328) shows damage that can be repaired by partial wall replacement (MoR-3). The damaged region requiring partial wall replacement is identified using dashed boxes in Figure C-328. Note that this wall was tested under monotonic loading. |
| | 4 | 4.3 | 2.89 | The image reported at this drift (Figure C-329) shows widespread crushing. |

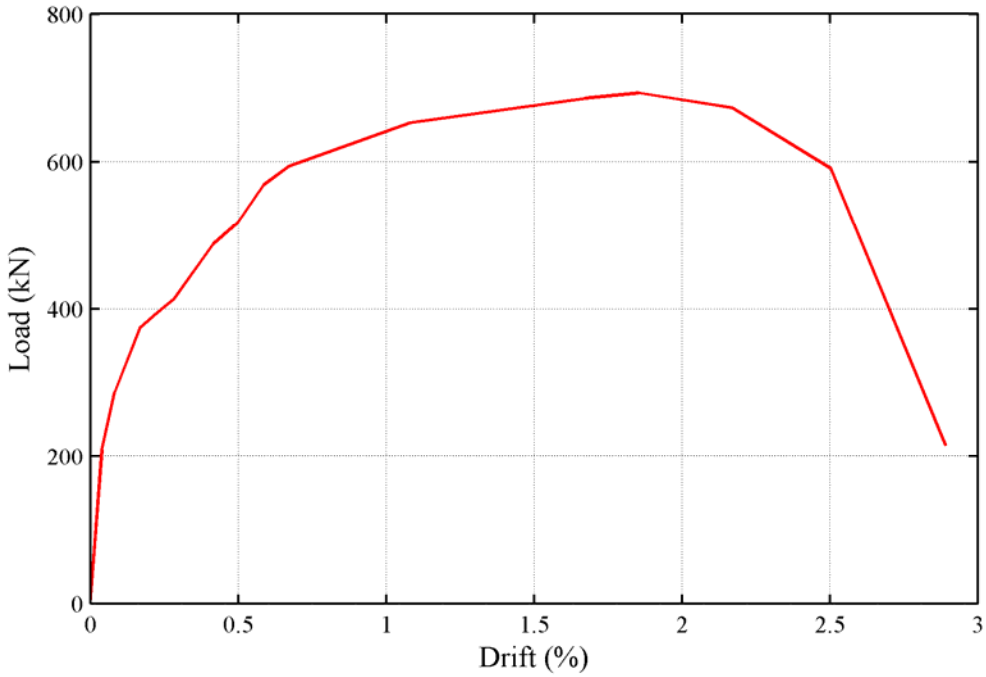


**Figure C-324 Load-drift relationship for wall S1**

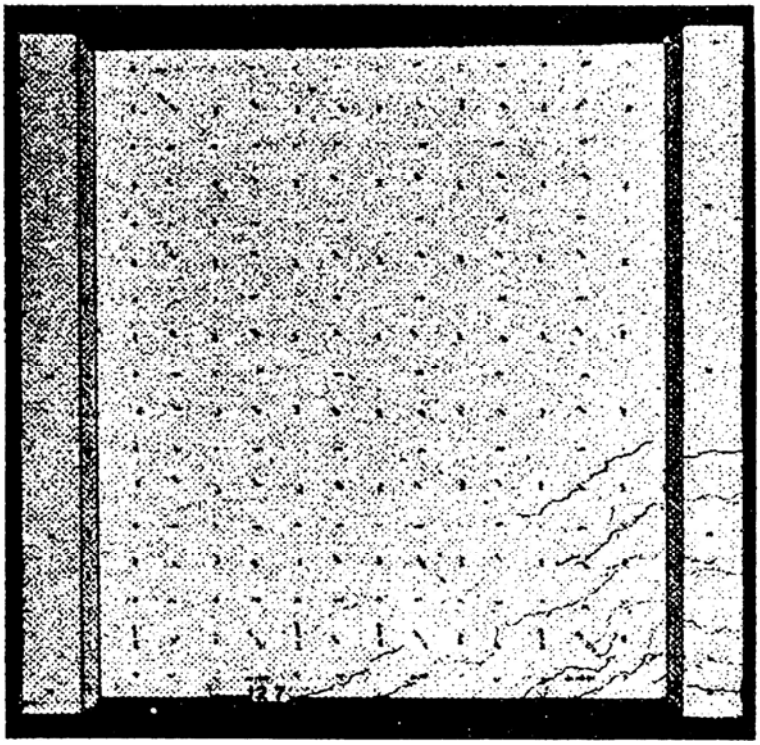

**Figure C-325 Condition of wall S1 at 0.17% drift [Maier and Thürlimann (1985)]**

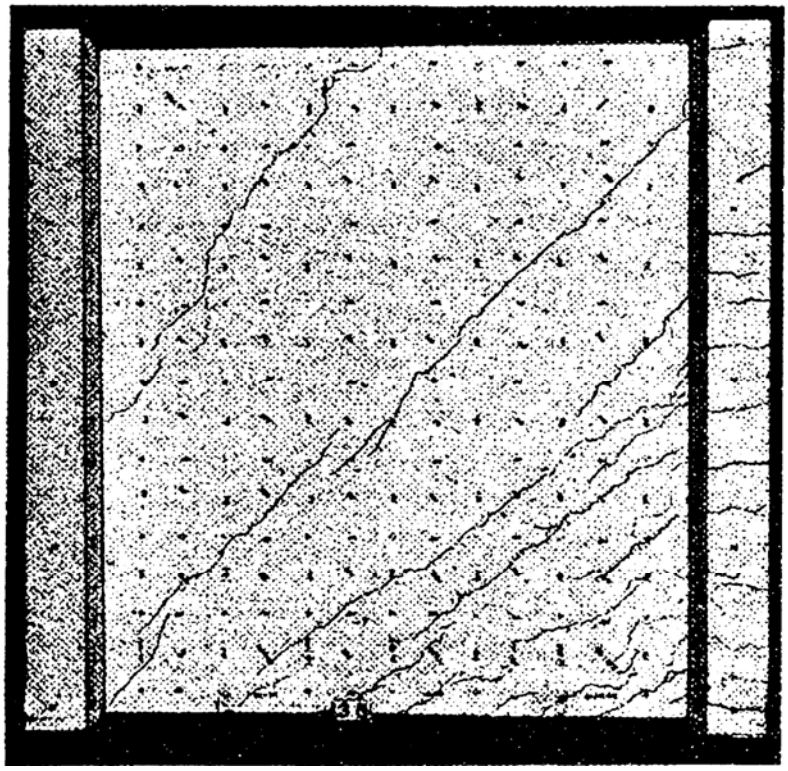

**Figure C-326 Condition of wall S1 at 0.28% drift [Maier and Thürlimann (1985)]**

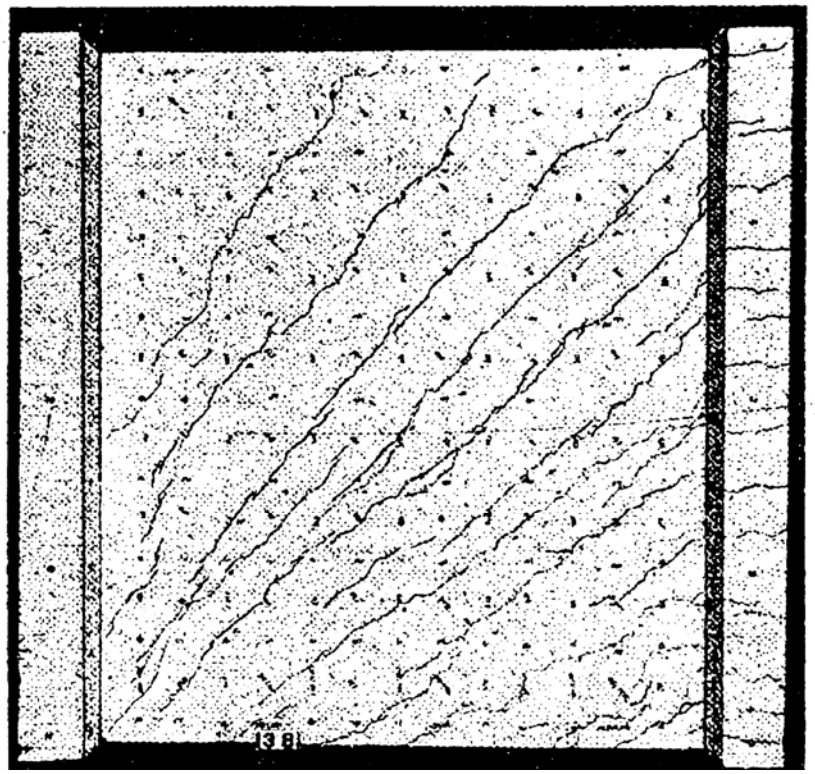

**Figure C-327 Condition of wall S1 at 0.42% drift [Maier and Thürlimann (1985)]**

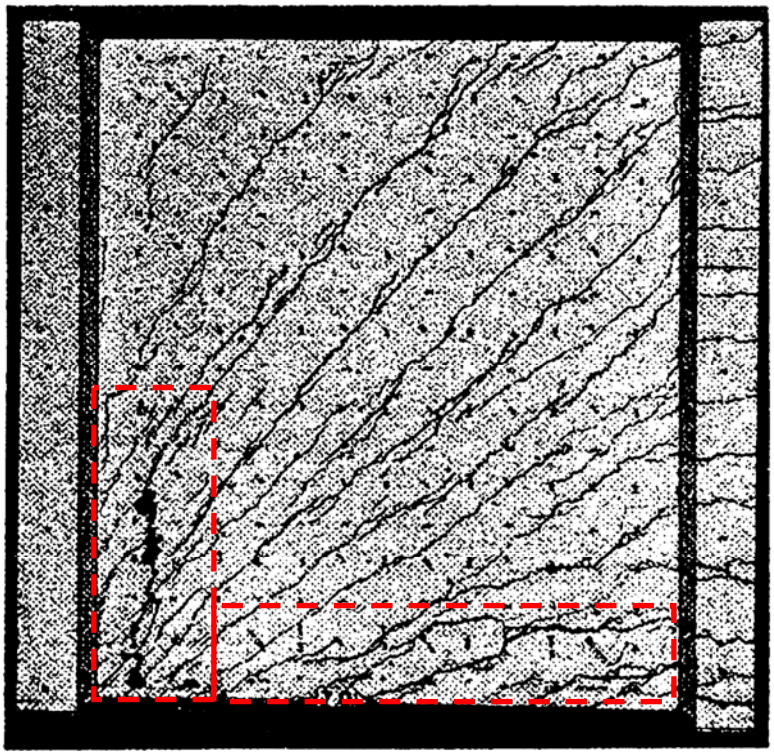

**Figure C-328 Condition of wall S1 at 2.17% drift [Maier and Thürlimann (1985)]**

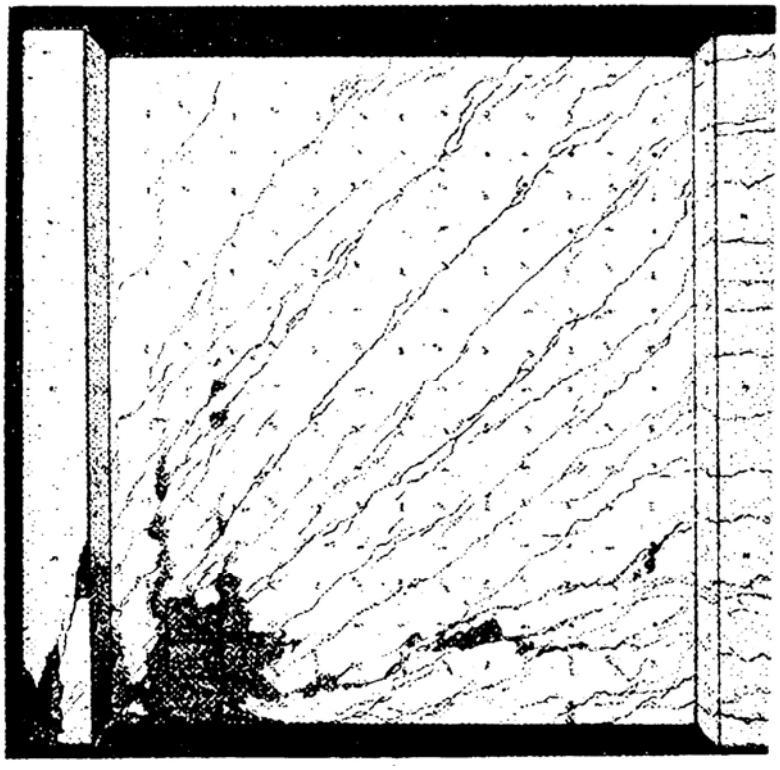

**Figure C-329 Condition of wall S1 at 2.89% drift [Maier and Thürlimann (1985)]**

### C.3.6.2 Wall S2

**Table C-96 Evaluation of damage data for wall S2 tested by Maier**

| Wall ID | MoR | Damage State (DS) | Drift (%) | Comments |
|---|---|---|---|---|
| S2 | 1 | 1.3 | 0.17 | The drifts for these damage states are provided by the researcher. For DS3.1, see Maier and Thürlimann (1985), page 12. |
| | | 1.4 | 0.72 | |
| | 2a | 2.3 | 0.80 | |
| | 3 | 3.1 | 0.89 | |
| | 4 | 4.3 | 1.03 | The image reported at this drift (Figure C-335) shows widespread crushing. |

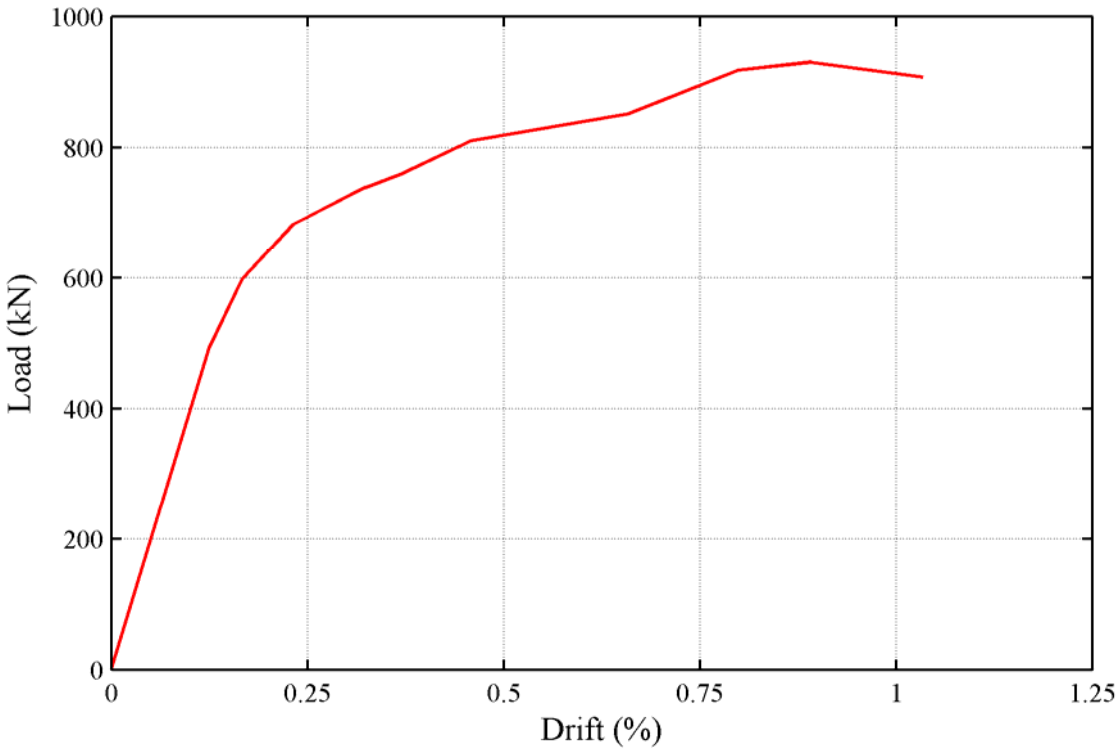


**Figure C-330 Load-drift relationship for wall S2**

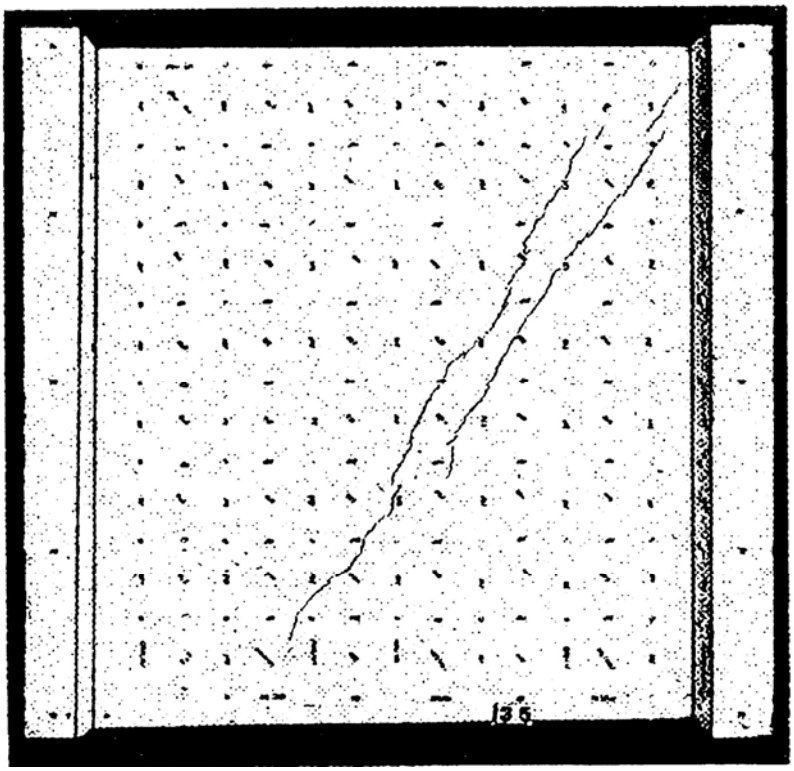

**Figure C-331 Condition of wall S2 at 0.17% drift [Maier and Thürlimann (1985)]**

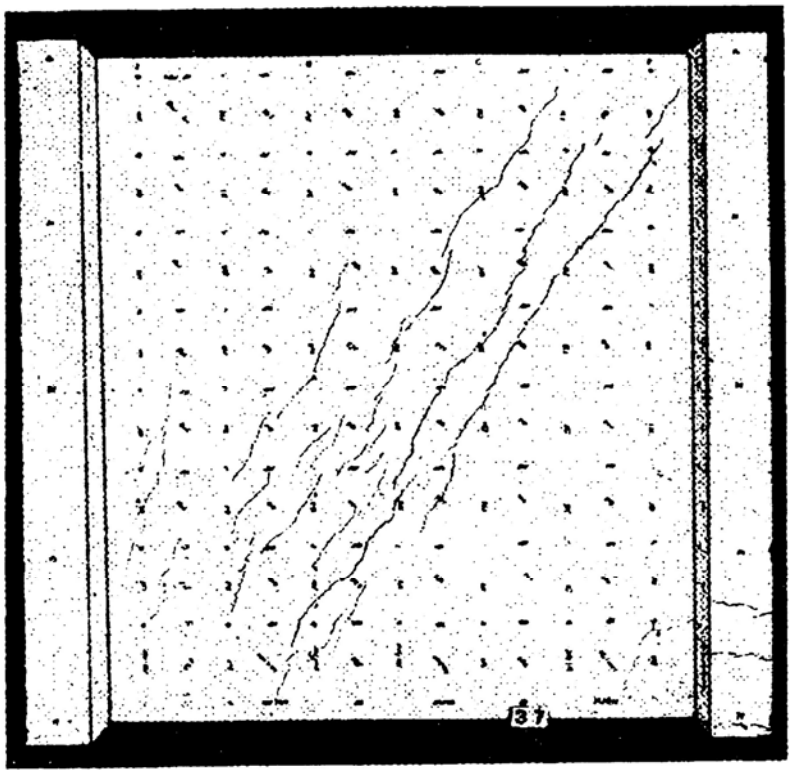

**Figure C-332 Condition of wall S2 at 0.23% drift [Maier and Thürlimann (1985)]**

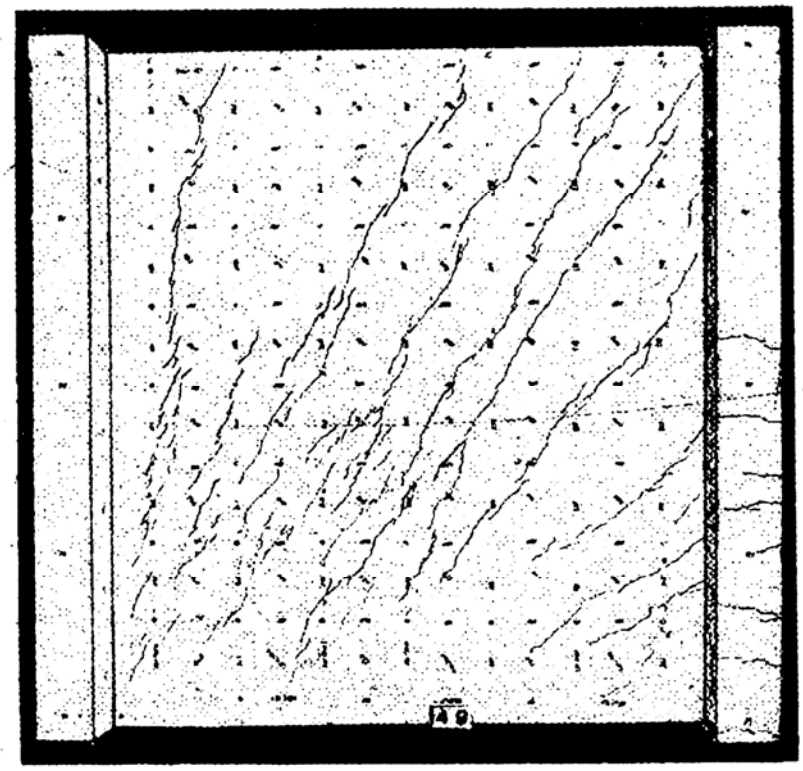

**Figure C-333 Condition of wall S2 at 0.37% drift [Maier and Thürlimann (1985)]**

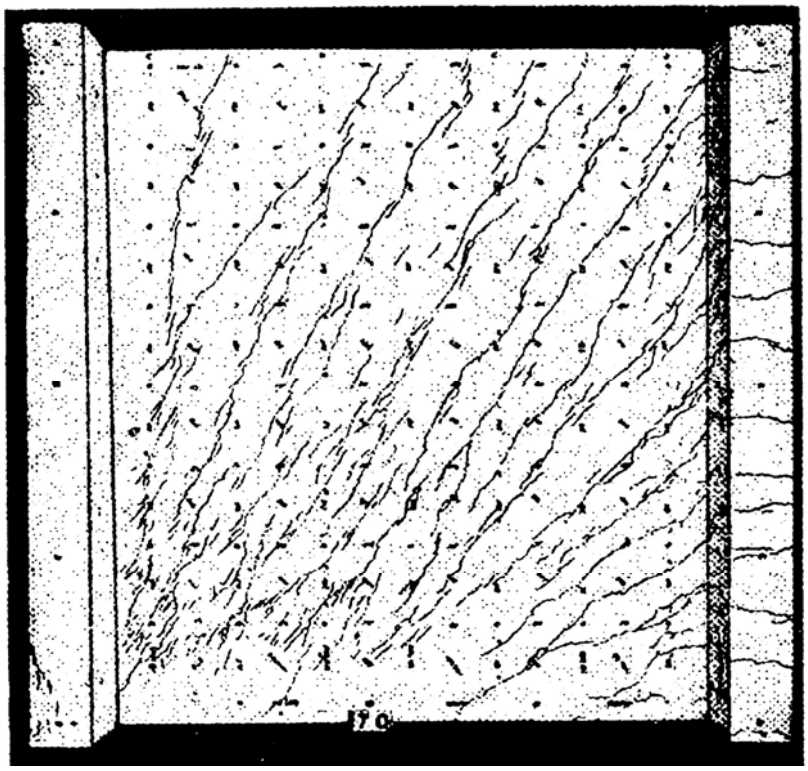

**Figure C-334 Condition of wall S2 at 0.80% drift [Maier and Thürlimann (1985)]**

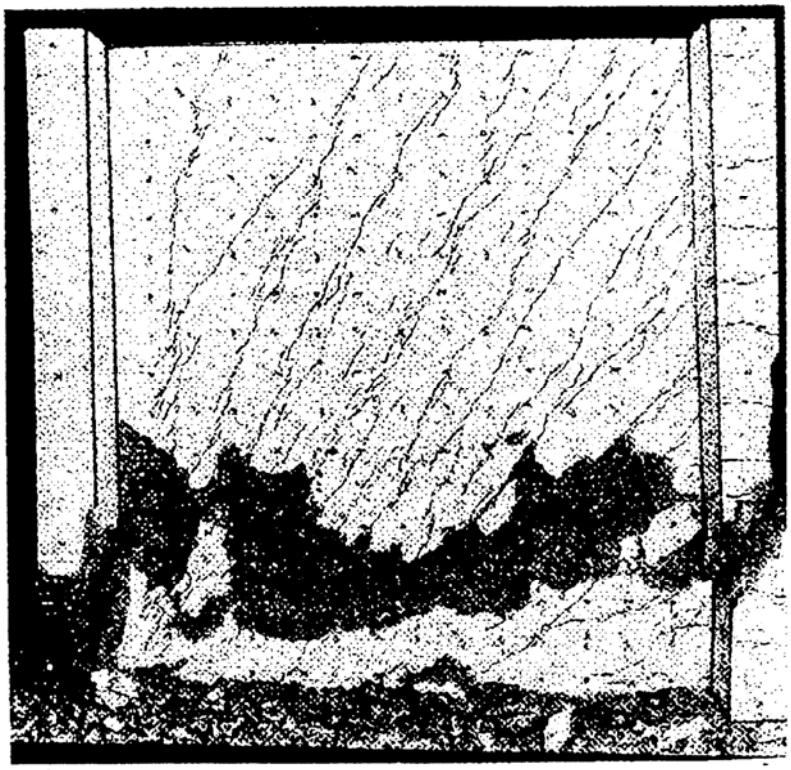

**Figure C-335 Condition of wall S2 at 1.03% drift [Maier and Thürlimann (1985)]**

### C.3.6.3 Wall S3

**Table C-97 Evaluation of damage data for wall S3 tested by Maier**

| Wall ID | MoR | Damage State (DS) | Drift (%) | Comments |
|---|---|---|---|---|
| S3 | 1 | 1.2 | 0.08 | The drifts for these damage states are provided by the researcher. |
| | 2a | 2.1 | 1.08 | |
| | | 2.3 | 1.08 | |
| | | 2.5a | 0.74 | |
| | 2b | 2.5b | 0.97 | |
| | 4 | 4.3 | 2.02 | The image reported at this drift (Figure C-342) shows widespread crushing. |

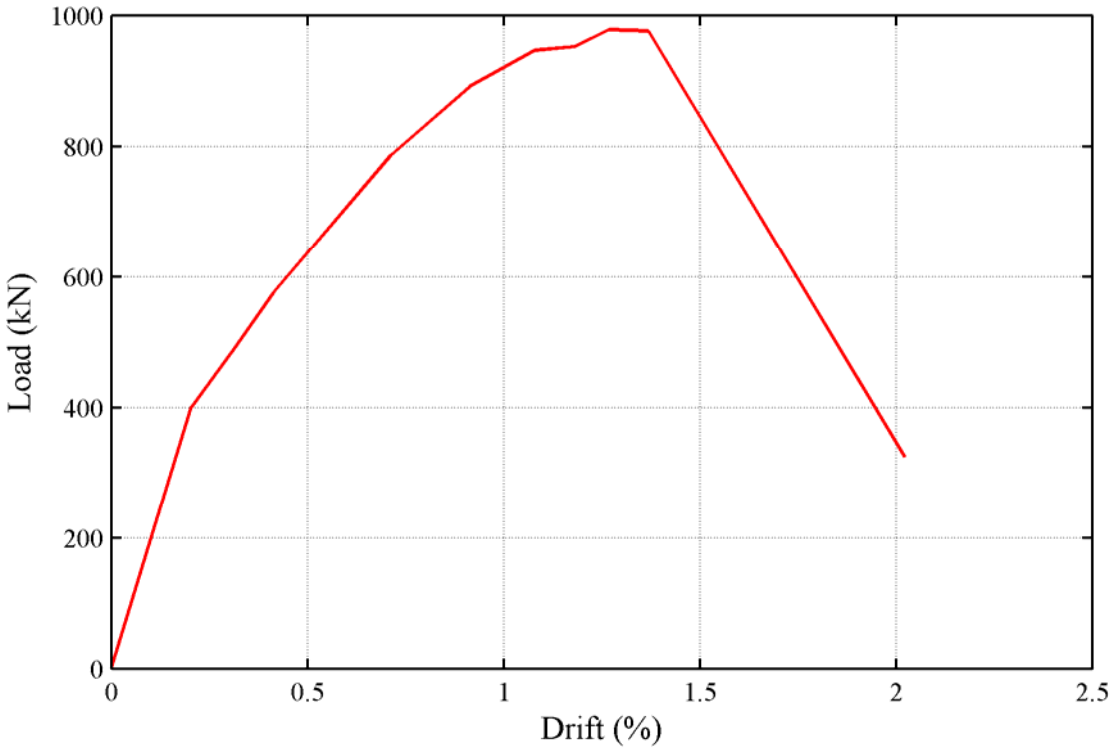


**Figure C-336 Load-drift relationship for wall S3**

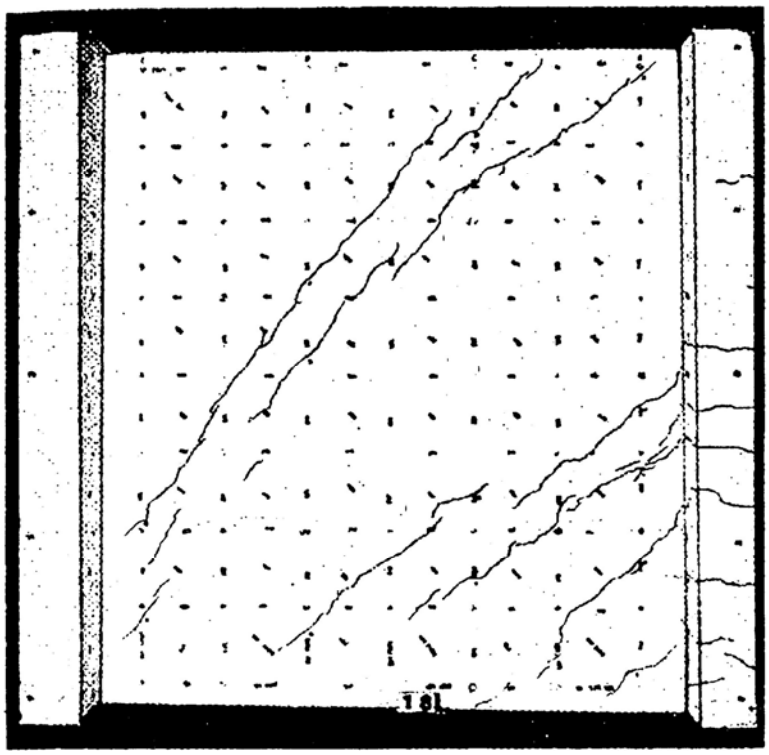

**Figure C-337 Condition of wall S3 at 0.20% drift [Maier and Thürlimann (1985)]**

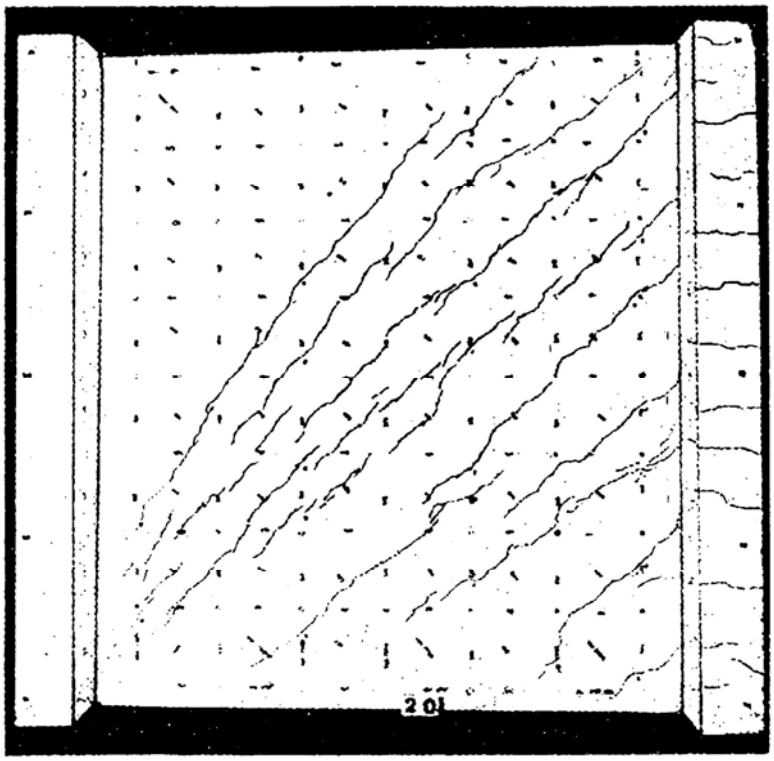

**Figure C-338 Condition of wall S3 at 0.31% drift [Maier and Thürlimann (1985)]**

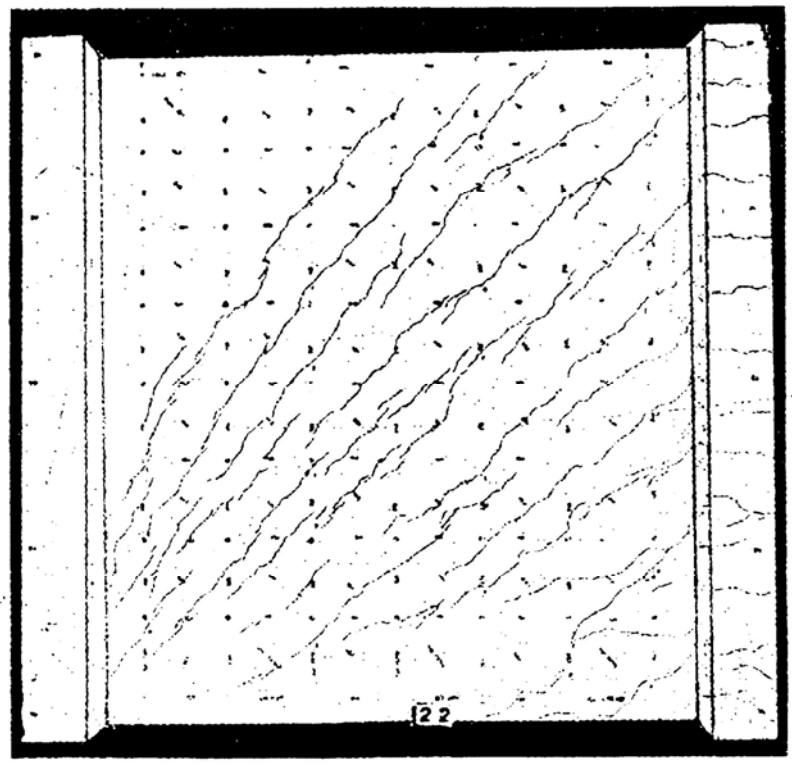

**Figure C-339 Condition of wall S3 at 0.41% drift [Maier and Thürlimann (1985)]**

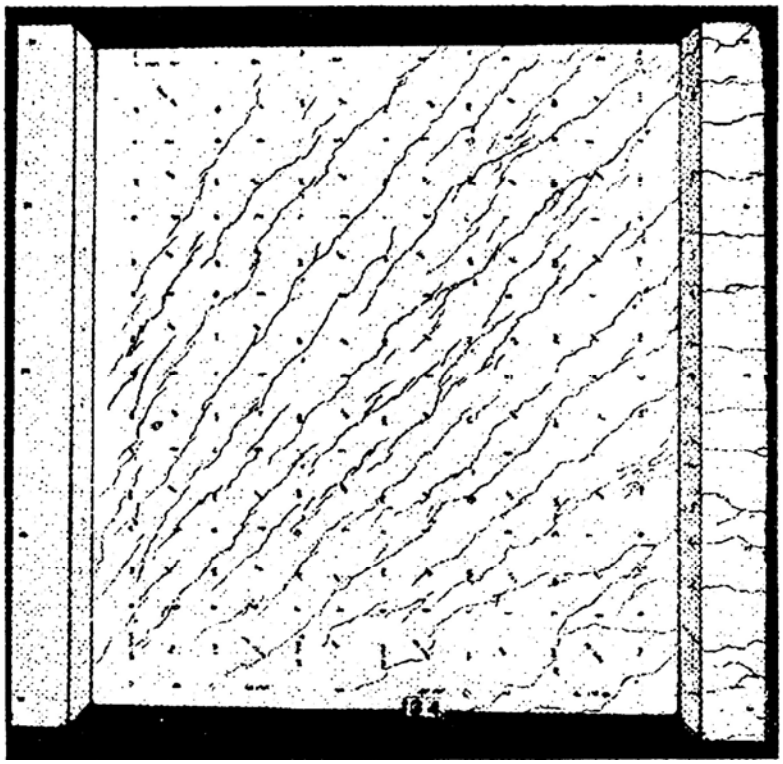

**Figure C-340 Condition of wall S3 at 0.71% drift [Maier and Thürlimann (1985)]**

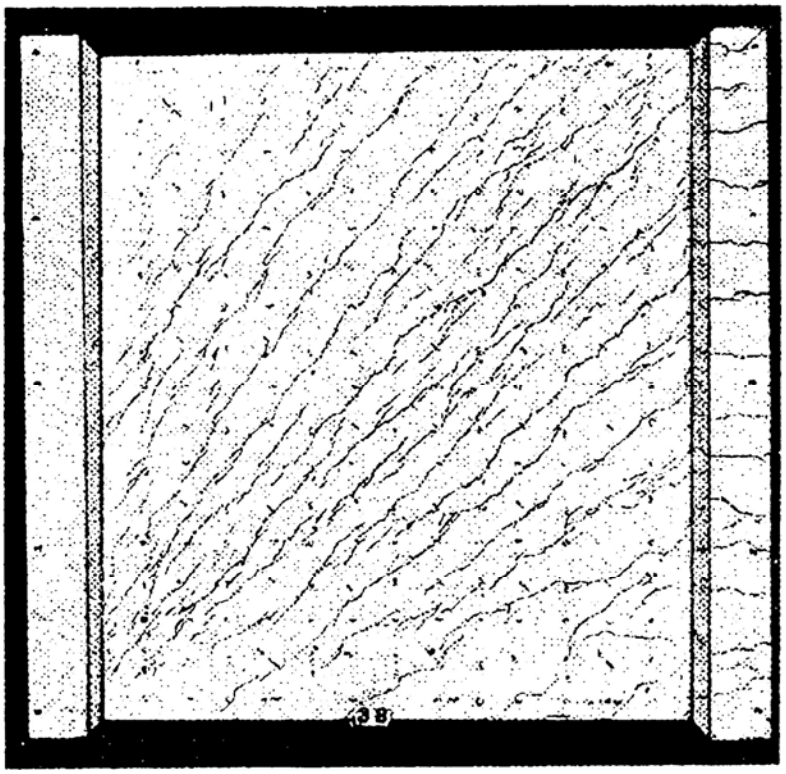

**Figure C-341 Condition of wall S3 at 1.08% drift [Maier and Thürlimann (1985)]**

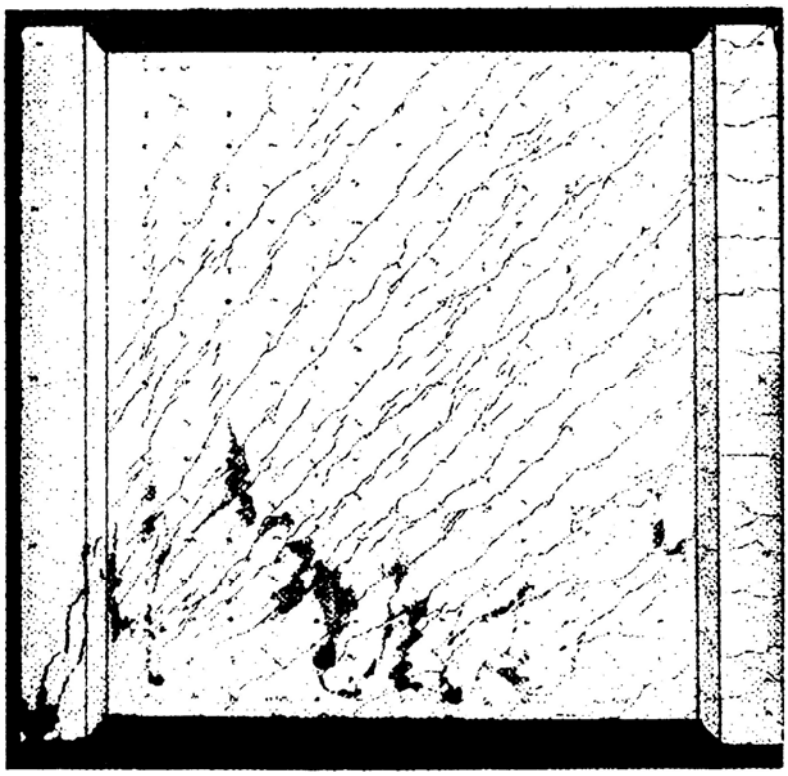

**Figure C-342 Condition of wall S3 at 2.02% drift [Maier and Thürlimann (1985)]**

### C.3.6.4 Wall S5

**Table C-98 Evaluation of damage data for wall S5 tested by Maier**

| Wall ID | MoR | Damage State (DS) | Drift (%) | Comments |
|---|---|---|---|---|
| S5 | 1 | 1.2 | 0.12 | The drifts for these damage states are provided by the researcher. |
| | 2a | 2.1 | 1.79 | |
| | | 2.2 | 0.94 | |
| | | 2.3 | 0.94 | |
| | | 2.4a | 0.95 | |
| | 2b | 2.4b | 1.14 | |
| | 3 | 3.1 | 0.94 | The image reported at this drift (Figure C-346) shows damage that can be repaired by partial wall replacement (MoR-3). The damaged region requiring partial wall replacement is identified using a dashed box in Figure C-346. |
| | 4 | 4.3 | 1.82 | The image reported at this drift (Figure C-347) shows widespread crushing. |

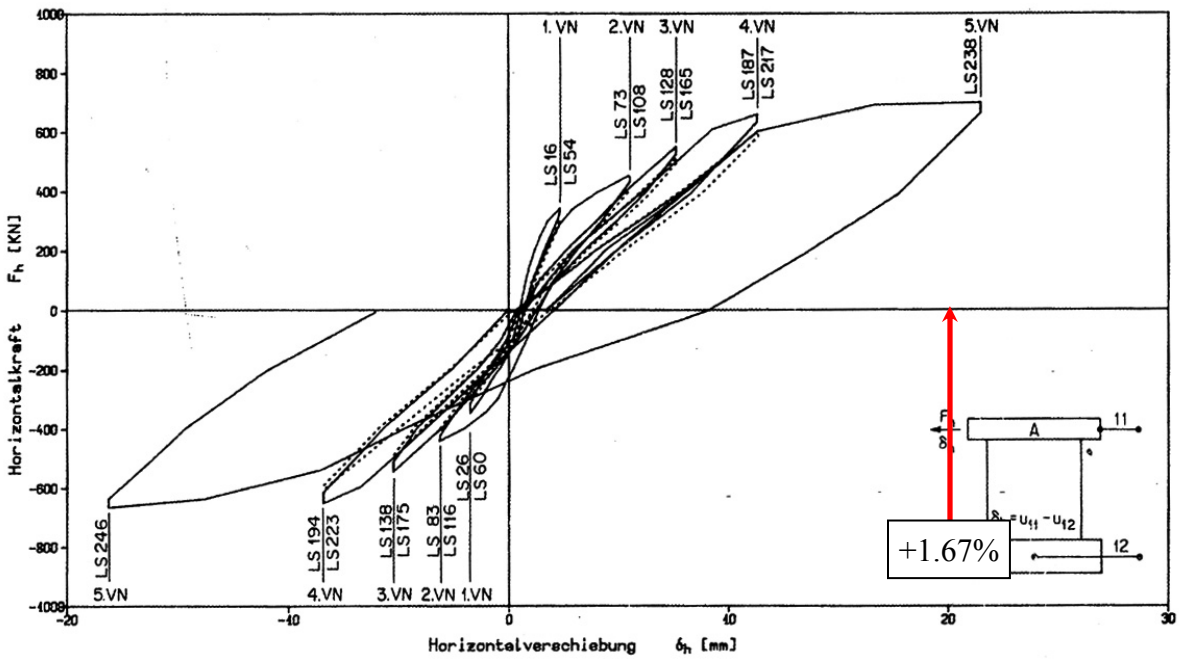


**Figure C-343 Load-displacement relationship for wall S5 [Maier and Thürlimann (1985)]**

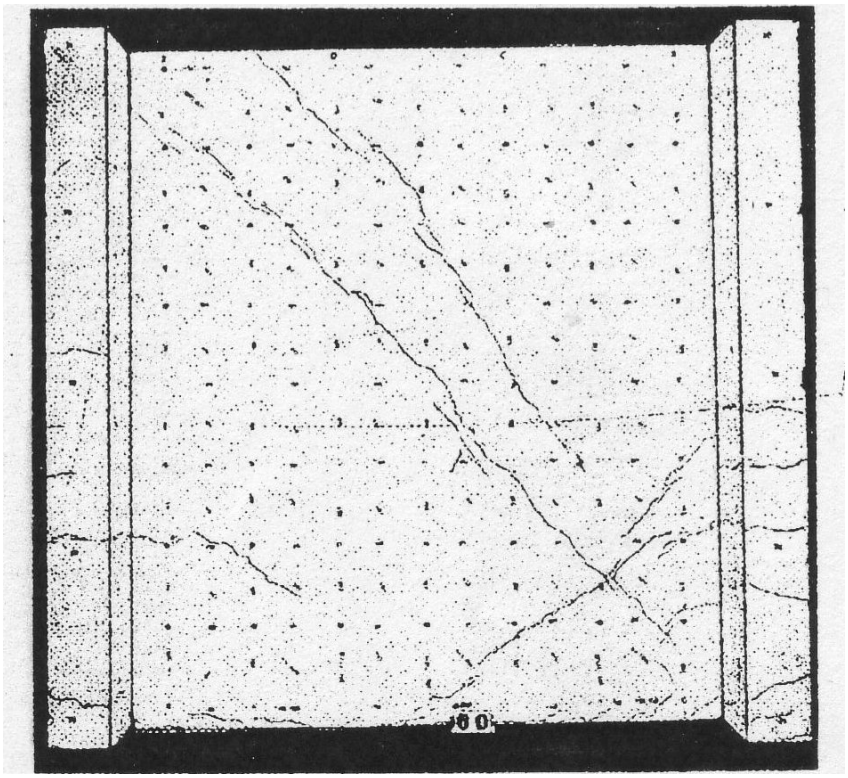

**Figure C-344 Condition of wall S5 at 0.20% drift [Maier and Thürlimann (1985)]**

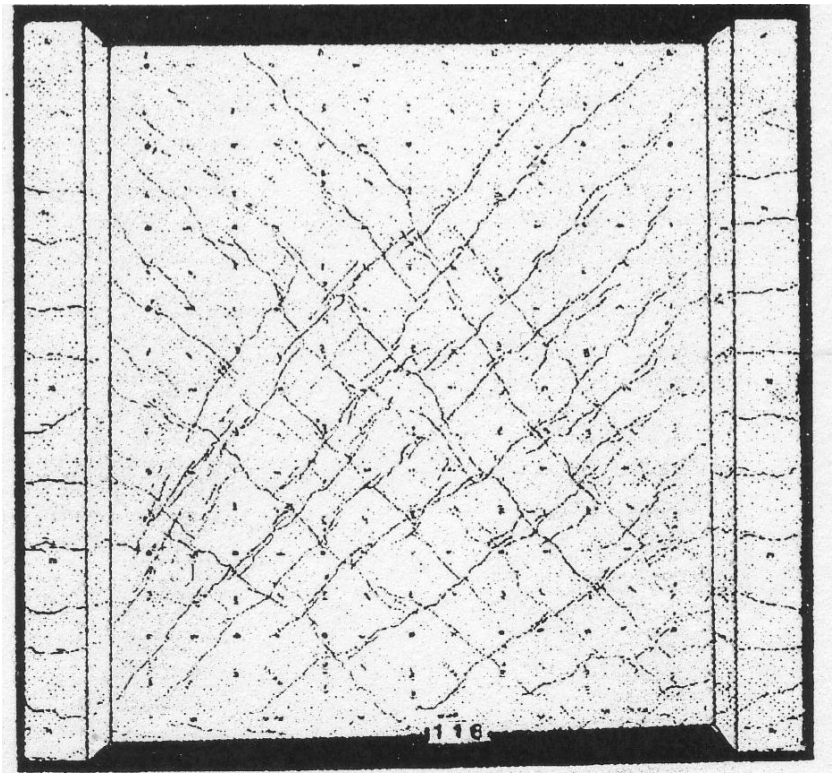

**Figure C-345 Condition of wall S5 at 0.46% drift [Maier and Thürlimann (1985)]**

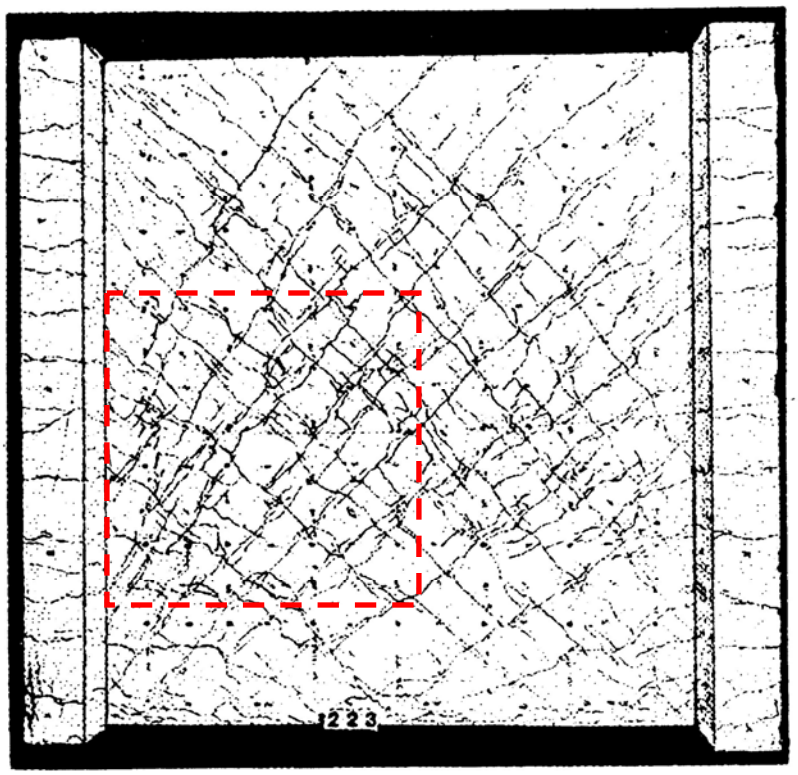


**Figure C-346 Condition of wall S5 at 0.94% drift [Maier and Thürlimann (1985)]**

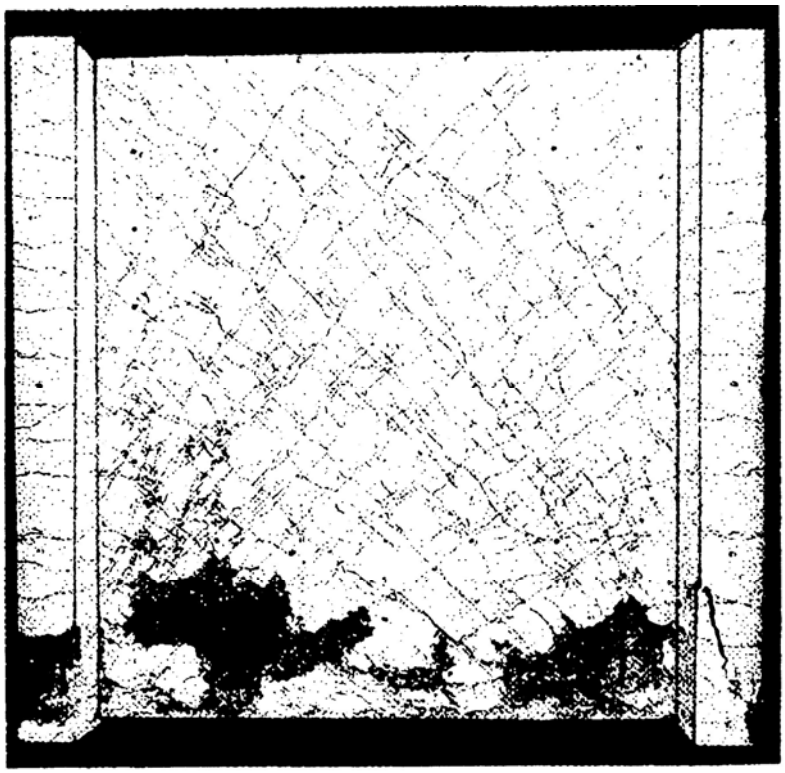

**Figure C-347 Condition of wall S5 at 1.82% drift [Maier and Thürlimann (1985)]**

### C.3.6.5 Wall S6

**Table C-99 Evaluation of damage data for wall S6 tested by Maier**

| Wall ID | MoR | Damage State (DS) | Drift (%) | Comments |
|---|---|---|---|---|
| S6 | 1 | 1.2 | 0.10 | The drifts for these damage states are provided by the researcher. |
| | 2a | 2.1 | 1.25 | |
| | | 2.2 | 0.75 | |
| | | 2.3 | 0.75 | |
| | | 2.4a | 0.88 | |
| | 3 | 3.1 | 1.09 | The image reported at this drift (Figure C-352) shows damage that can be repaired by partial wall replacement (MoR-3). The damaged region requiring partial wall replacement is identified using a dashed box in Figure C-352. |
| | 4 | 4.3 | 2.35 | The image reported at this drift (Figure C-353) shows widespread crushing. |

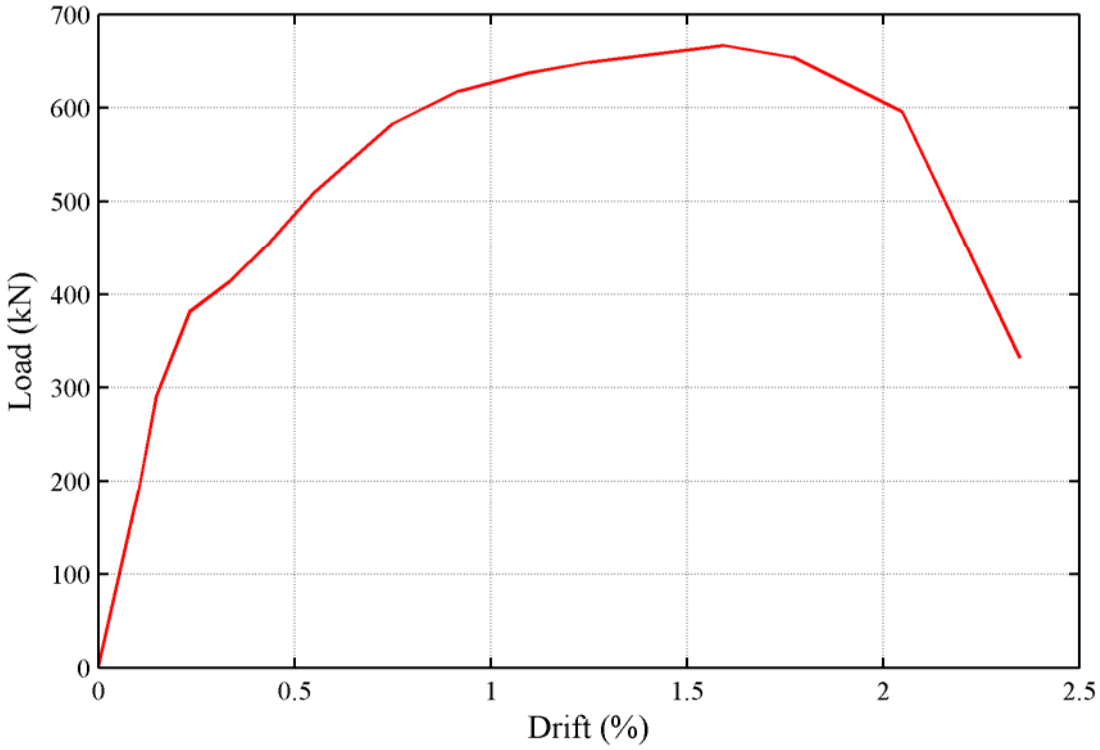


**Figure C-348 Load-drift relationship for wall S6**

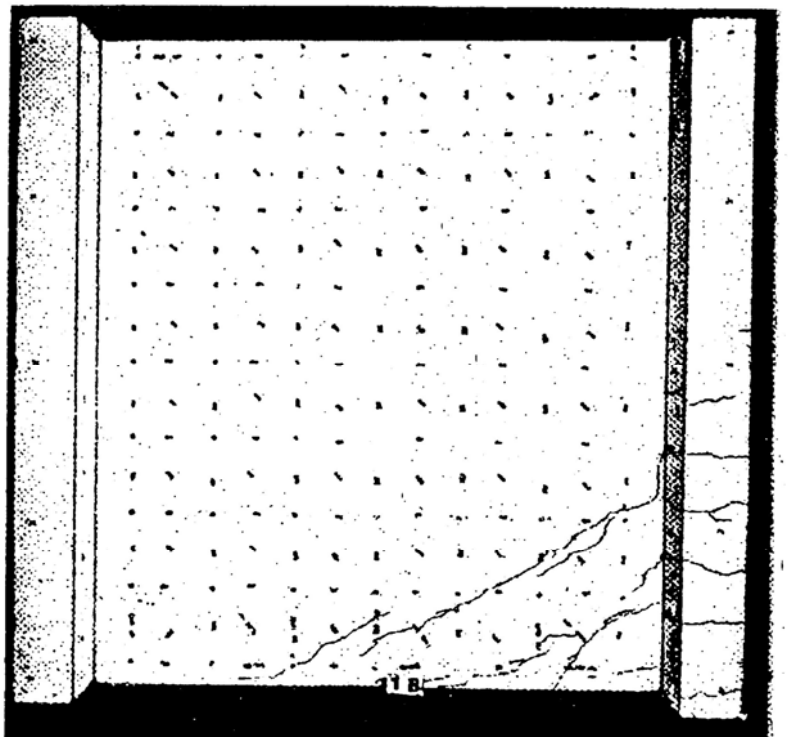

**Figure C-349 Condition of wall S6 at 0.23% drift [Maier and Thürlimann (1985)]**

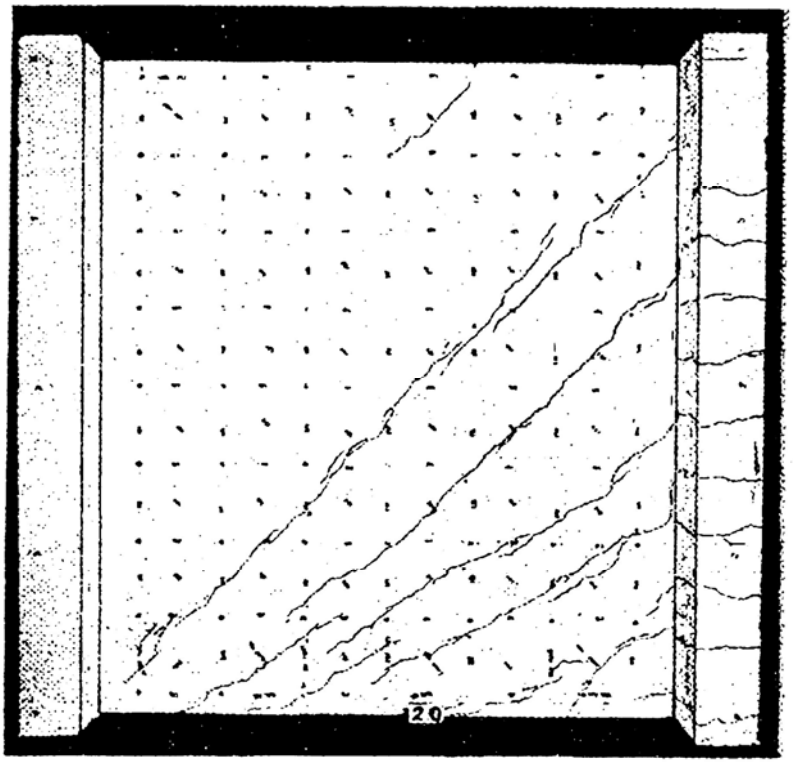

**Figure C-350 Condition of wall S6 at 0.34% drift [Maier and Thürlimann (1985)]**

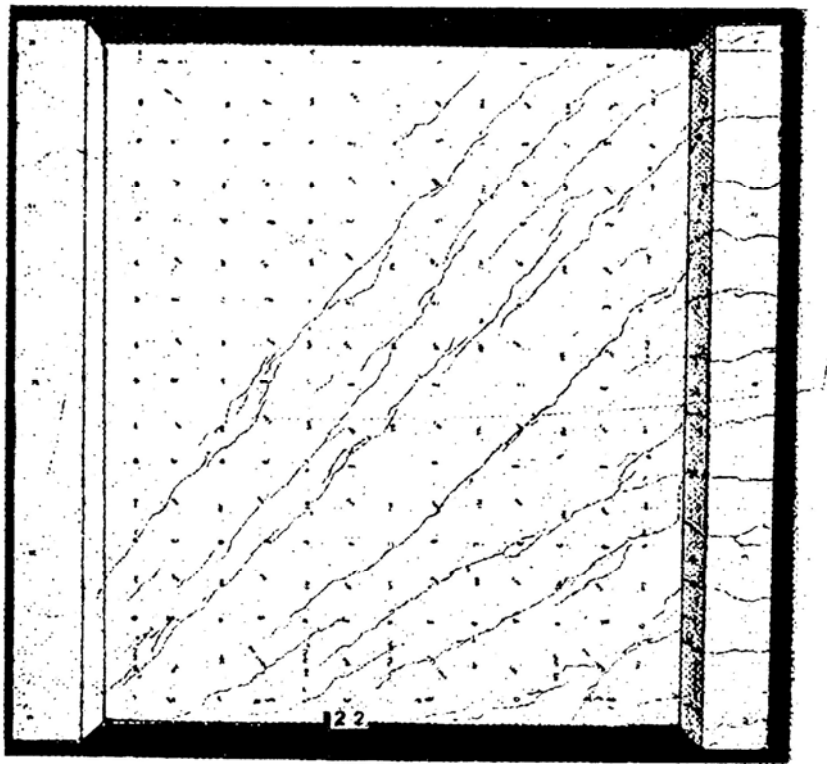

**Figure C-351 Condition of wall S6 at 0.43% drift [Maier and Thürlimann (1985)]**

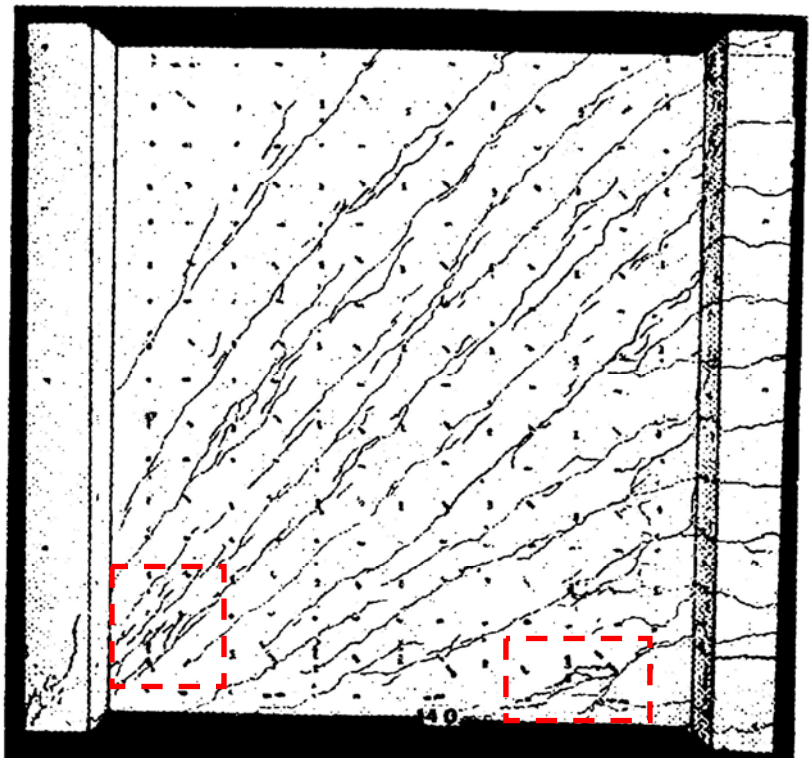

**Figure C-352 Condition of wall S6 at 1.09% drift [Maier and Thürlimann (1985)]**

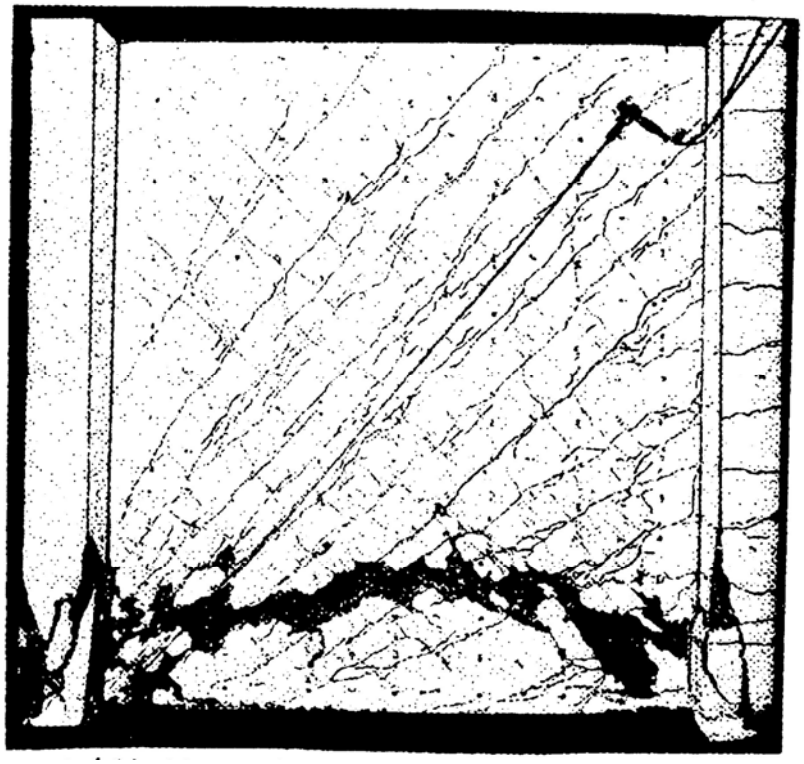

**Figure C-353 Condition of wall S6 at 2.35% drift [Maier and Thürlimann (1985)]**

### C.3.6.6 Wall S7

**Table C-100 Evaluation of damage data for wall S7 tested by Maier**

| Wall ID | MoR | Damage State (DS) | Drift (%) | Comments |
|---|---|---|---|---|
| S7 | 1 | 1.3 | 0.17 | The drifts for these damage states are provided by the researcher. |
| | | 1.4 | 0.62 | |
| | 2a | 2.1 | 0.67 | |
| | 4 | 4.3 | 0.84 | The image reported at this drift (Figure C-359) shows widespread crushing. Note that Figure C-358 at 0.68% drift also shows widespread crushing. But that data point is excluded since the damage requiring wall replacement (MoR-4) was attained at the 10th cycle to that drift. |

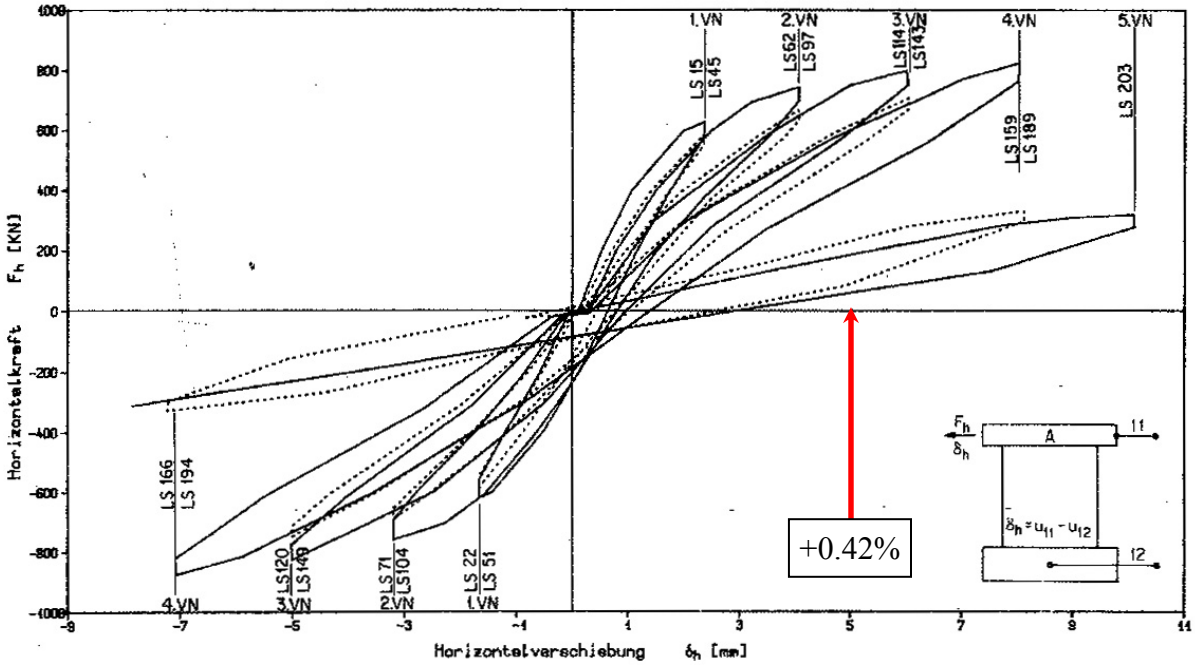


**Figure C-354 Load-displacement relationship for wall S7 [Maier and Thürlimann (1985)]**

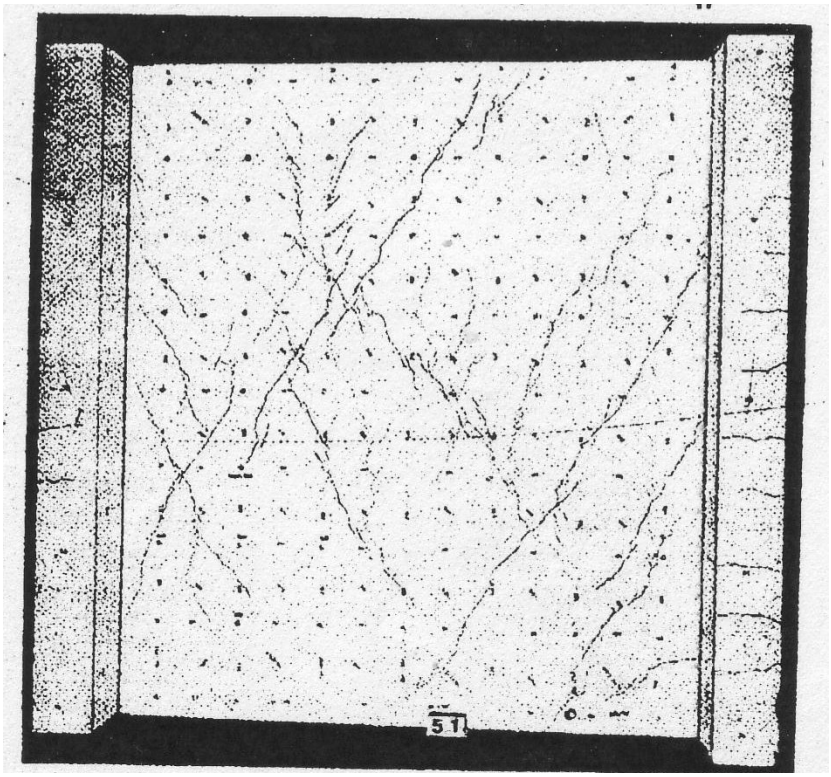


**Figure C-355 Condition of wall S7 at 0.20% drift [Maier and Thürlimann (1985)]**

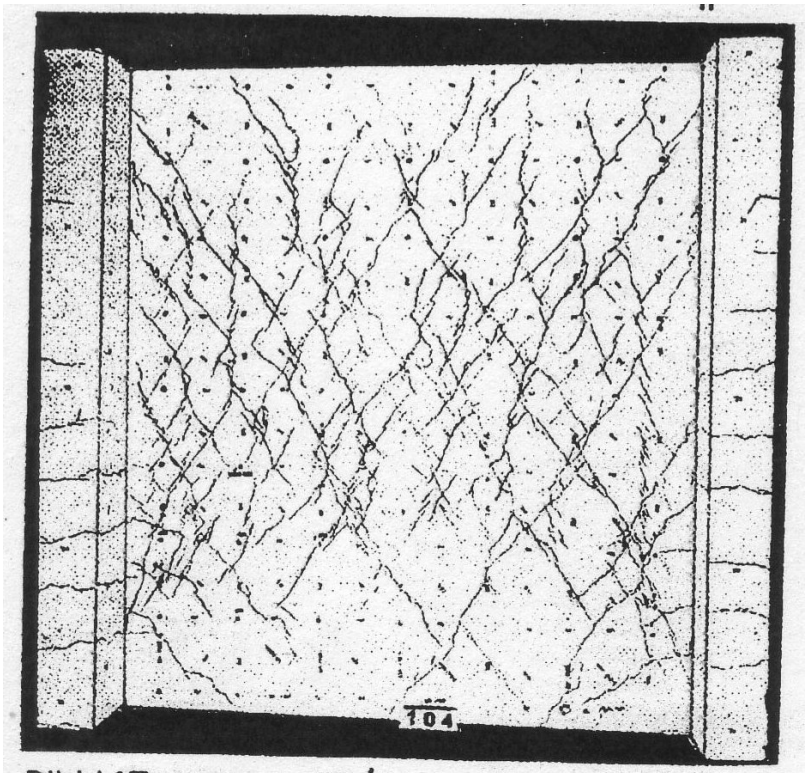


**Figure C-356 Condition of wall S7 at 0.34% drift [Maier and Thürlimann (1985)]**

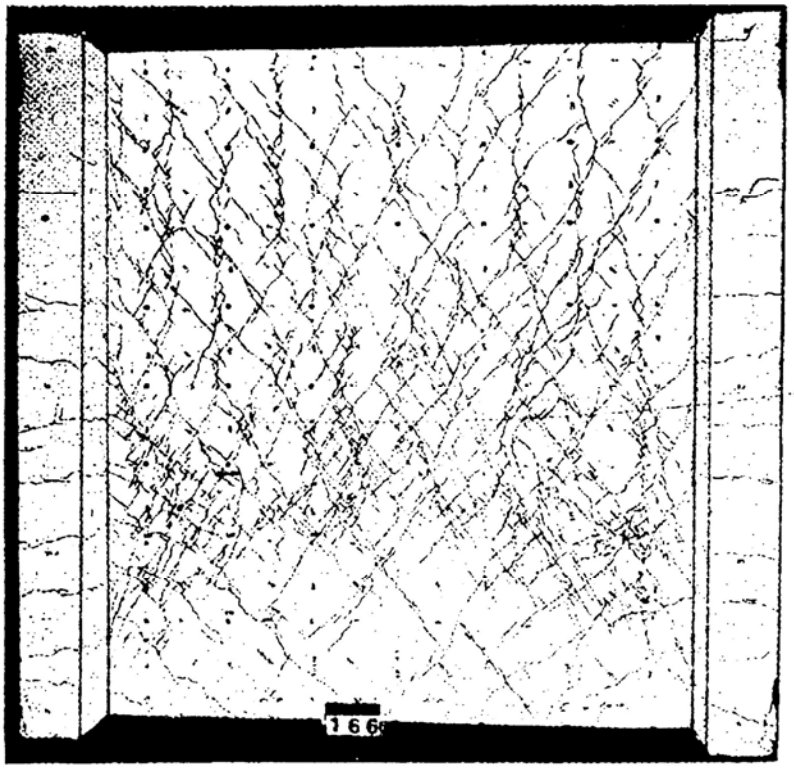

**Figure C-357 Condition of wall S7 at 0.67% drift (1st cycle around this drift level) [Maier and Thürlimann (1985)]**

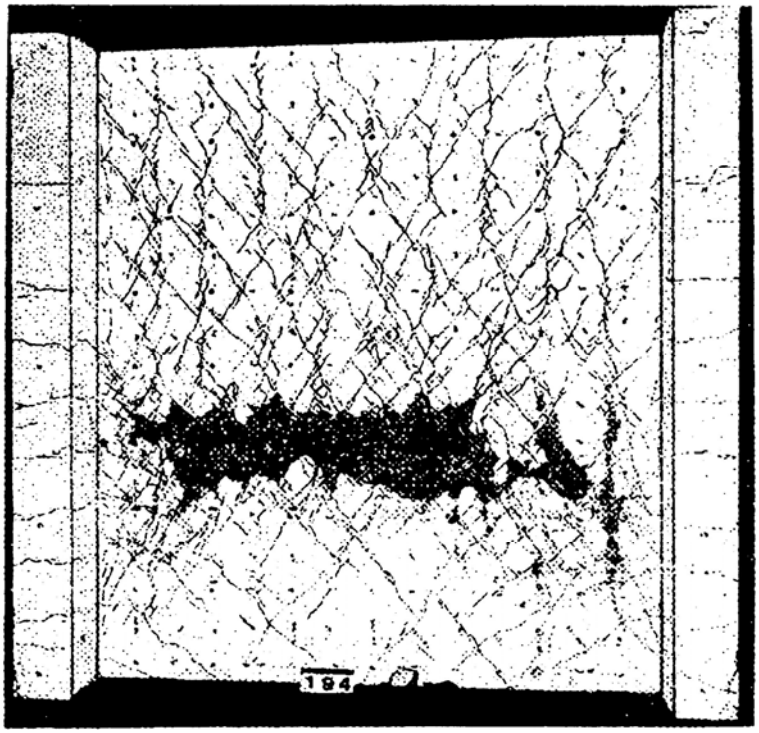

**Figure C-358 Condition of wall S7 at 0.68% drift (10th cycle around this drift level) [Maier and Thürlimann (1985)]**

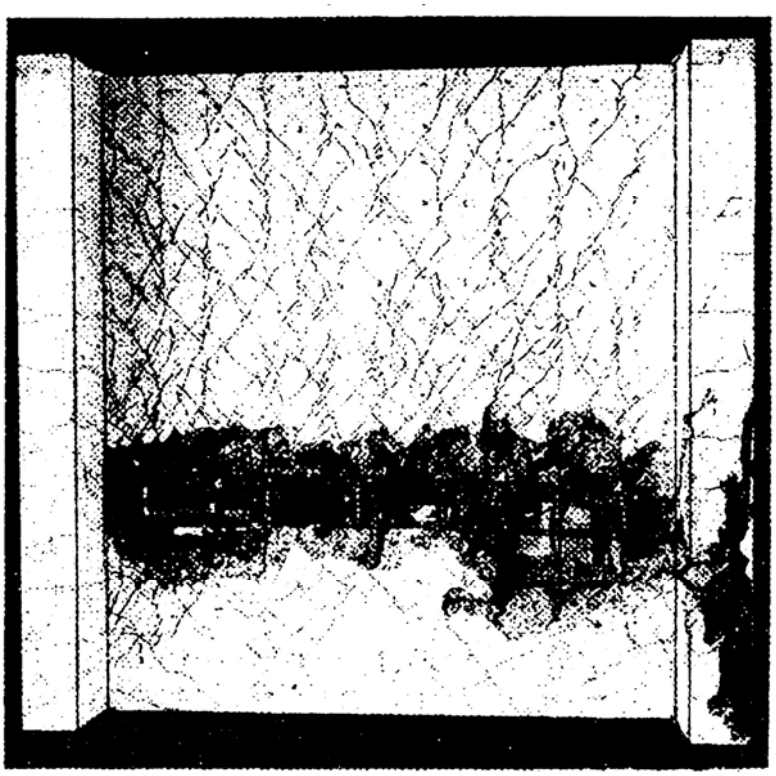

**Figure C-359 Condition of wall S7 at 0.84% drift [Maier and Thürlimann (1985)]**

### C.3.6.7 Saito et al. (1989) Wall

### C.3.6.8 Wall W-12-1

**Table C-101 Evaluation of damage data for wall W-12-1 tested by Saito**

| Wall ID | MoR | Damage State (DS) | Drift (%) | Comments |
|---|---|---|---|---|
| W-12-1 | 2 | 2.1 | 0.54 | The drift for this damage state is provided by the researcher. |
| | 4 | 4.3 | 1.32 | The failure mode was assumed to be diagonal compression because of the heavy wall reinforcement. The drift associated with wall replacement is calculated using $SC_2$. |
| | 4* | $SC_2$ | 1.32 | The data point is obtained from the 1st quadrant of the load-displacement relationship (see Figure C-360). A data point cannot be established in the 3rd quadrant. |

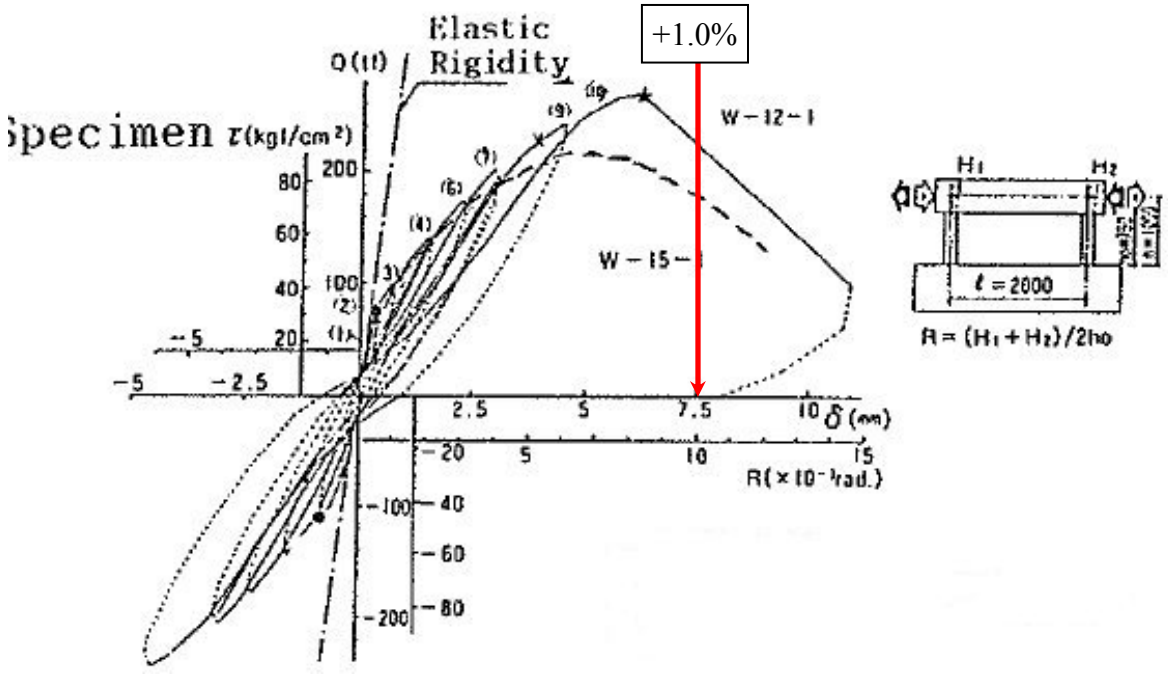


**Figure C-360 Load-displacement relationship for wall W-12-1 [Saito et al. (1989)]**

# Appendix D – Supplemental Information on Scope of Repair for MoR-2 and MoR-3

This appendix presents data to support the scopes of repair for MoR-2 and MoR-3 in Section 8: 1) the total length of cracks requiring epoxy injection for MoR-2 and MoR-3, and 2) percentage of wall panel requiring replacement for MoR-3.

## D.1 Total Crack Length for Epoxy Injection

The total length of cracks in a damaged wall that require epoxy injection for repair is calculated using author-reported images of damage.

Section D.1.1 presents calculations for walls that can be repaired by epoxy injection of cracks, namely, MoR-2a. The images of damage presented in Appendix C that were reported at or near the drifts associated with MoR-2a are used for these calculations. Such damage images with clearly visible crack patterns are available for 14 walls. In those cases where more than one damage image associated with MoR-2a was available for a given wall, the total crack length is measured using the image reported at the smaller drift. Only a single value of crack length is reported for each wall.

Section D.1.2 presents crack-length information for MoR-2b.

Section D.1.3 presents calculations for walls that require both partial wall replacement and epoxy injection of cracks, namely, MoR-3. Damage images at MoR-3 are available for 9 of the 14 walls of Section D.1.1.

### D.1.1 Crack lengths for MoR-2a

The crack length is calculated using the visible cracks resulting from loading in one direction and then multiplied by 2 to account for the cyclic nature of earthquake shaking. The resultant measured crack length is normalized by the area of the wall panel, presented as a crack length per 100 $ft^2$ of wall panel, and denoted $TCL_1$ for MoR-2a.

Table D-1 presents information for MoR-2a calculations. Figure ID identifies the figure in Appendix C that is used for the crack length calculation for each wall. The value of $TCL_1$ for each wall is listed in the table. However, only a fraction of all measured cracks require epoxy injection since the crack widths vary from crack to crack and within each crack. The percentage of the measured total crack length requiring epoxy injection (%EI) is identified based on evaluation of a) the reported damage images, and b) the web reinforcement ratios (see Table D-2), as described below. The variable $TCL_2$ is calculated as twice the product of $TCL_1$ and %EI because epoxy injection will likely be required on each face of the damaged wall.

Walls DP1 and DP2: Each wall had a similar crack pattern and the widths of the cracks appear to vary significantly. Considering the density of the cracks and the relatively high web reinforcement ratio, 50% of the measured cracks are assumed to require epoxy injection. Since high-resolution photographs are available for only these two walls, the Palermo walls are used to index other %EI estimates.

**Table D-1 Crack length data (per 100 ft$^2$) associated with MoR-2a**

| Researcher | Wall ID | Figure ID | $TCL_1$ (1/ft) | %EI | $TCL_2$ (1/ft) |
|---|---|---|---|---|---|
| Palermo | DP1 | Figure C-296 | 304 | 50% | 304 |
| Palermo | DP2 | Figure C-310 | 316 | 50% | 316 |
| Maier | S2 | Figure C-334 | 415 | 40% | 332 |
| Maier | S3 | Figure C-340 | 512 | 40% | 410 |
| Maier | S5 | Figure C-346 | 489 | 40% | 392 |
| Barda | B7-5 | Figure C-283 | 367 | 60% | 378 |
| Synge | Wall 1 | Figure C-15 | 125 | 90% | 225 |
| Pilakoutas | SW5 | Figure C-28 | 464 | 35% | 325 |
| Pilakoutas | SW7 | Figure C-42 | 361 | 40% | 289 |
| Pilakoutas | SW8 | Figure C-48 | 382 | 40% | 306 |
| Pilakoutas | SW9 | Figure C-55 | 452 | 40% | 361 |
| Maier | S4 | Figure C-7 | 278 | 50% | 278 |
| Maier | S9 | Figure C-12 | 247 | 50% | 247 |
| Doostdar | Wall 7 | Figure C-166 | 285 | 90% | 256 |

**Table D-2 Summary of walls used in crack length evaluation associated with MoR-2a**

| Researcher | Wall ID | Geometry | $h_w / l_w$ | $\rho_h$ | $\rho_v$ | $P / Af_c'$ |
|---|---|---|---|---|---|---|
| Palermo | DP1 | Flanged | 0.66 | 0.76 | 0.82 | 5.4 |
| Palermo | DP2 | Flanged | 0.65 | 0.76 | 0.82 | 0.0 |
| Maier | S2 | Flanged | 1.02 | 1.01 | 1.13 | 24.2 |
| Maier | S3 | Flanged | 1.02 | 1.01 | 2.54 | 6.5 |
| Maier | S5 | Flanged | 1.02 | 1.01 | 1.13 | 6.3 |
| Barda | B7-5 | Flanged | 0.21 | 0.49 | 0.50 | 0.0 |
| Synge | Wall 1 | Rectangular | 0.50 | 1.61 | 0.81 | 0.0 |
| Pilakoutas | SW5 | Rectangular | 2.00 | 0.31 | 0.59 | 0.0 |
| Pilakoutas | SW7 | Rectangular | 2.00 | 0.39 | 0.59 | 0.0 |
| Pilakoutas | SW8 | Rectangular | 2.00 | 0.28 | 0.50 | 0.0 |
| Pilakoutas | SW9 | Rectangular | 2.00 | 0.56 | 0.50 | 0.0 |
| Maier | S4 | Rectangular | 1.02 | 1.01 | 1.02 | 7.7 |
| Maier | S9 | Rectangular | 1.02 | 1.01 | 1.02 | 7.7 |
| Doostdar | Wall 7 | Rectangular | 0.75 | 0.80 | 0.59 | 0.0 |

Walls S2, S3 and S5: All three walls were tested under imposed axial load and had horizontal and vertical web reinforcement ratios greater than 1.0%. The percentage of cracks that require epoxy injection is estimated to be 40% because the Maier walls had higher web reinforcement ratios than the Palermo walls and thus finer cracks.

Wall B7-5: Although the web of the Barda wall was more lightly reinforced than the Palermo walls (an increase in %EI), it was reinforced at each end by heavily reinforced flanges and its aspect ratio was significantly smaller (a decrease in %EI). The percentage of cracks requiring epoxy injection is 60%.

Wall 1 and Wall 7: The damage images reported for these walls show only a few major cracks in each direction. Ninety percent of these cracks are assumed to require epoxy injection.

Walls SW5, SW7, SW8, and SW9: The damage images reported for these walls were hand drawn and it was not possible to identify whether the cracks were hairline or major, requiring grouting. The final condition of the walls was used to guide selection of %EI. For example, Figure C-29 shows the condition of wall SW5 at failure; there were two diagonal cracks in each direction that dominated the wall response. Therefore, it is reasonable to assume that for MoR-2, only these cracks will require epoxy injection and %EI is 35%. Using a similar procedure for SW7, %EI is 40%. Walls SW8 and SW9 failed by concrete crushing rather than diagonal tension and it was not possible to use the same approach to compute %EI and so 40% was chosen based on the result for SW7.

Walls S4 and S9: Both rectangular (S4 and S9) and flanged walls (S2, S3, and S5) tested by Maier generally included similar web reinforcement (see Table D-2). The major difference in the crack patterns of the rectangular and flanged walls is that the crack density for the rectangular walls is consistently less than that of the flanged walls. A lower crack density is associated with higher crack widths and %EI for flanged walls of Maier is increased from 40% (flanged walls) to 50% (rectangular walls).

Table D-3 presents a statistical summary of the results for $TCL_2$. On the basis of these results, total crack lengths requiring epoxy injection are 300 ft. and 350 ft. (per 100 $ft^2$ wall panel) for rectangular and flanged walls, respectively.

**Table D-3 Statistical summary of total crack length (per 100 $ft^2$) for epoxy injection ($TCL_2$ in Table D-1)**

| | Wall geometry | | |
|---|---|---|---|
| | **All** | **Rectangular** | **Flanged** |
| **Mean** | 316 | 286 | 355 |
| **Median** | 311 | 283 | 355 |
| **Standard Deviation** | 55 | 40 | 44 |
| **Coefficient of Variation** | 0.18 | 0.14 | 0.12 |

## D.1.2 Crack lengths for MoR-2b

As seen in Table 8-22 and Table 8-23, the fragility curves for MoR-2b for barbell and flanged walls are set aside since the corresponding medians equal or exceed those calculated for Method of Repair MoR-3. Crack length data for MoR-2b is not available for rectangular walls and the

normalized crack length for MoR-2a (300 ft. per 100 $ft^2$ wall panel) is adopted for MoR-2b since the calculated medians for MoR-2a (0.41) and MoR-2b (0.55) are comparable.

### D.1.3 Crack lengths for MoR-3

The MoR-3 crack length is calculated using the visible cracks resulting from loading in one direction and then multiplied by 2 to account for the cyclic nature of earthquake shaking. The resultant measured crack length is normalized by the area of the wall panel, presented as a crack length per 100 $ft^2$ of wall panel, and denoted $TCL_3$ for MoR-3.

Damage images at drifts associated with MoR-3 are available for 9 of the 14 walls considered in Section D.1.1. Table D-4 presents the normalized total crack lengths ($TCL_3$) measured from those images. The normalized crack lengths increase only modestly for flanged walls but significantly for rectangular walls as the damage progresses from MoR-2a to MoR-3. The ratio of $TCL_3$ to $TCL_1$ is 1.30 for rectangular walls and 1.05 for flanged walls.

**Table D-4 Comparison of measured crack lengths (per 100 $ft^2$) for MoR-2a and MoR-3**

| Researcher | Wall ID | Geometry | $TCL_1$ (1/ft) | $TCL_3$ (1/ft) | $TCL_3$ / $TCL_1$ | Figure |
|---|---|---|---|---|---|---|
| Palermo | DP1 | Flanged | 304 | 332 | 1.09 | Figure C-300 |
| Palermo | DP2 | Flanged | 316 | 334 | 1.06 | Figure C-313 |
| Maier | S5 | Flanged | 489 | 511 | 1.04 | Figure C-346 |
| Barda | B7-5 | Flanged | 315 | 315 | 1.00 | Figure C-283 |
| Synge | Wall 1 | Rectangular | 125 | 174 | 1.39 | Figure C-16 |
| Pilakoutas | SW8 | Rectangular | 382 | 482 | 1.26 | Figure C-50 |
| Pilakoutas | SW9 | Rectangular | 452 | 535 | 1.18 | Figure C-57 |
| Maier | S4 | Rectangular | 278 | 423 | 1.52 | Figure C-8 |
| Doostdar | Wall 7 | Rectangular | 142 | 156 | 1.10 | Figure C-168 |

Given that approximately 15% of the wall panel will be replaced for MoR-3 (see Section D.2 below), the normalized total crack length for MoR-3 and rectangular walls is 330 ($=0.85\times300\times1.3$) and for MoR-3 and flanged walls is 310 ($=0.85\times350\times1.05$). The normalized crack length for MoR-3 calculated for flanged walls (310 ft. per 100 $ft^2$ wall panel) is adopted for barbell walls for which data are unavailable.

## D.2 Percentage of Wall Replacement at MoR-3

If an image at or near the drift associated with MoR-3 was available for a given wall, the damaged region likely requiring replacement is identified using a dashed box. The ratio of the area of each dashed box to the total wall panel area ($A_d / A_{wp}$) is presented in Table D-5. In this table, the column labeled Figure ID provides the figure number used to calculate the percentage of the wall requiring replacement.

**Table D-5 Ratios of area of damaged region to total area of wall panel**

| Researcher | Wall ID | Section | Figure ID | $A_d / A_{wp}$ (%) |
|---|---|---|---|---|
| Fukuzawa | No4 | Barbell | Figure C-220 | 23 |
| Barda | B1-1 | Flanged | Figure C-264 | 10 |
| Barda | B2-1 | Flanged | Figure C-267 | 15 |
| Barda | B3-2 | Flanged | Figure C-271 | 24 |
| Barda | B4-3 | Flanged | Figure C-274 | 14 |
| Barda | B5-4 | Flanged | Figure C-277 | 10 |
| Barda | B6-4 | Flanged | Figure C-280 | 17 |
| Barda | B7-5 | Flanged | Figure C-283 | 17 |
| Barda | B8-5 | Flanged | Figure C-286 | 9 |
| Palermo | DP1 | Flanged | Figure C-300 | 15 |
| Palermo | DP2 | Flanged | Figure C-313 | 16 |
| Maier | S1 | Flanged | Figure C-328 | 21 |
| Maier | S5 | Flanged | Figure C-346 | 25 |
| Maier | S6 | Flanged | Figure C-352 | 7 |
| Lefas | Type I | Rectangular | Figure C-1 | 14 |
| Maier | S4 | Rectangular | Figure C-8 | 7 |
| Synge | Wall 1 | Rectangular | Figure C-16 | 8 |
| Pilakoutas | SW4 | Rectangular | Figure C-22 | 17 |
| Pilakoutas | SW6 | Rectangular | Figure C-36 | 26 |
| Pilakoutas | SW8 | Rectangular | Figure C-50 | 32 |
| Pilakoutas | SW9 | Rectangular | Figure C-57 | 14 |
| Greifenhagen | M3 | Rectangular | Figure C-84 | 15 |
| Lopes | SW13 | Rectangular | Figure C-115 | 15 |
| Lopes | SW14 | Rectangular | Figure C-123 | 8 |
| Lopes | SW17 | Rectangular | Figure C-146 | 23 |
| Wiradinata | Wall 1 | Rectangular | Figure C-155 | 12 |
| Doostdar | Wall 7 | Rectangular | Figure C-168 | 15 |
| Doostdar | Wall 8 | Rectangular | Figure C-176 | 11 |

Table D-6 presents a statistical summary of the $A_d / A_{wp}$ data presented in Table D-5. Damage associated with MoR-3 requires on average replacement of 15% of wall panel area for both rectangular and flanged walls. Only a single value of $A_d / A_{wp}$ (=23%) could be computed for barbell walls and so the average value for flanged walls of 15% is used instead.

**Table D-6 Statistical summary of $A_d / A_{wp}$**

| | Wall geometry | | |
|---|---|---|---|
| | **All** | **Flanged** | **Rectangular** |
| **Mean** | 16 | 15.4 | 15.4 |
| **Median** | 15 | 15.0 | 14.4 |
| **Standard Deviation** | 6.4 | 5.7 | 7.2 |
| **Coefficient of Variation** | 0.41 | 0.37 | 0.46 |

# Appendix E – Scopes of Repair for Squat Concrete Walls

## E.1 Introduction

This appendix presents the list of repair activities that are required for each method of repair, namely, MoR-1 through MoR-4, defined in Section 8 for squat reinforced concrete walls.

## E.2 MoR-1, Cosmetic Repair

Cosmetic repairs are made when the residual crack widths are relatively narrow and no structural repair is deemed necessary. The main scope of this method of repair is limited to the repair of surface finishes to restore the aesthetic appearance, maintain fire resistance and prevent water infiltration into the wall, [ATC (1998)]. A list of repair activities is not provided for MoR-1 because the repair is not structural.

## E.3 MoR-2, Epoxy Injection

Epoxy injection is widely used to restore the stiffness and strength of cracked concrete components. Structural repair using epoxy injection involves the following steps, which assume that the to-be-repaired wall is in a commercial office building.

1. Relocate all office equipment and furniture within 6 ft. of the wall, on both sides of the wall. Install protective covers on the floor finishes.
2. Remove architectural finishes over the height and length of the wall, on both sides of the wall.
3. Relocate mechanical, electrical, and plumbing (MEP) systems within 6 ft. of the damaged wall.
4. Prepare and injection grout 300 ft. of crack per 100 $ft^2$ of wall panel for rectangular cross sections. (See Appendix D for additional information on calculation of the suggested cracks lengths.)
5. Reinstall/return all office equipment, architectural finishes, furniture, and MEP systems.

## E.4 MoR-3, Partial Wall Replacement

Partial wall replacement (MoR-3) includes a) removal and replacement of damaged concrete and rebar, and b) epoxy injection of cracks to restore component strength and stiffness. Such repair involves the following steps that assume a) the wall is in a commercial office building, and b) wall replacement does not involve shoring of columns and floor slabs. The scope of repair is not additional to that of MoR-2.

1. Relocate all office equipment and furniture within 6 ft. of the wall, on both sides of the wall. Install protective covers on the floor finishes and adjacent curtain wall system (where occurs).

2. Remove architectural finishes over the height and length of the wall, on both sides of the wall.
3. Relocate MEP systems within 6 ft. of the damaged wall.
4. Prepare and injection grout 330 ft. of crack per 100 $ft^2$ of wall panel for walls with rectangular cross sections and 310 ft. of crack per 100 $ft^2$ of wall panel for walls with flanged or barbell cross sections. (See Appendix D for additional information on calculation of the suggested cracks lengths.)
5. Remove 15 $ft^2$ per 100 $ft^2$ of wall panel and 10 1-ft. long sections of #8 buckled rebar. (See Appendix D for additional information on the calculation of the area of wall panel to be removed.)
6. Replace buckled rebar with new rebar, attached to exposed ends of existing rebar with mechanical splices; provide 8 #4 seismic ties at 4 in. on center at each end of the wall; re-bend 16 horizontal rebar in the web of the wall around new rebar.
7. Install formwork and cast new 5000 psi concrete into the pockets cut in step 5.
8. Strip formwork, remove all construction equipment, and reinstall/return all office equipment, architectural finishes, furniture, and MEP systems.

## E.5 MoR-4, Wall Replacement

Method of repair MoR-4 includes replacement of the damaged wall panel and is similar to Structural Repair 5 (SR5) of FEMA 308 [ATC (1998)]. MoR-4 involves the following steps, which assume that a) the wall is in a commercial office building, and b) wall removal and replacement in 5-ft. increments such that shoring of columns and floor slabs above is not required.

1. Relocate all office equipment and furniture within 10 ft. of the wall, on both sides of the wall. Install protective covers on the floor finishes and adjacent curtain wall system (where occurs). Relocate MEP systems within 10 ft. of the damaged wall.
2. Remove architectural finishes over the height and length of the wall, on both sides of the wall.
3. Remove and replace the damaged reinforced concrete in 5-ft. segments along the length along the wall.
4. Install new reinforcement as follows:
    a. 12#9 A706 rebar in the boundary zone at each end of the wall; attach new rebar to existing using mechanical splices
    b. #4 A706 double sets of seismic ties at 4 in. on center in each boundary zone;
    c. #4 A706 rebar at 6 in. on center, each face, each way; lap splice new vertical bars to existing at the head of the wall; drill and epoxy grout #4 bars into wall/foundation below at 6 in. on center to match new rebar above. Horizontal rebar to be anchored in new boundary zones with seismic hooks or lapped 24 in. with horizontal bars in adjacent wall panels.

5. Form new wall panel and cast 5000 psi concrete in 3-ft. lifts; leave a 1-in. gap at the underside of the wall above for grouting 24 hours after the wall panel is cast. Strip formwork 48 hours after casting. Commence work on a new panel after concrete has achieved compressive strength of 3000 psi.
6. Remove all construction equipment and reinstall/return all office equipment, architectural finishes, furniture, and MEP systems.

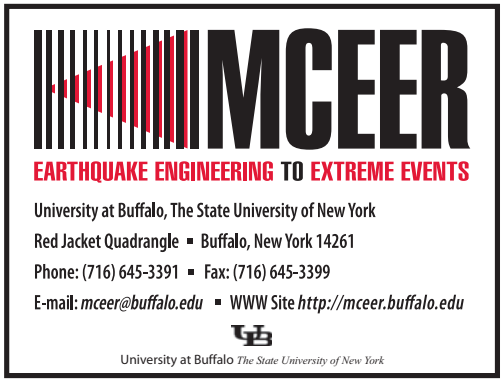


ISSN 1520-295X